Issues 1-4 2015 | Volume 11

The Journal on Advanced Studies in Theoretical and Experimental Physics, including Related Themes from Mathematics

PROGRESS IN PHYSICS

"All scientists shall have the right to present their scientific research results, in whole or in part, at relevant scientific conferences, and to publish the same in printed scientific journals, electronic archives, and any other media." — Declaration of Academic Freedom, Article 8

ISSN 1555-5534

The Journal on Advanced Studies in Theoretical and Experimental Physics, including Related Themes from Mathematics

PROGRESS IN PHYSICS

A quarterly issue scientific journal, registered with the Library of Congress (DC, USA). This journal is peer reviewed and included in the abstracting and indexing coverage of: Mathematical Reviews and MathSciNet (AMS, USA), DOAJ of Lund University (Sweden), Zentralblatt MATH (Germany), Scientific Commons of the University of St. Gallen (Switzerland), Open-J-Gate (India), Referativnyi Zhurnal VINITI (Russia), etc.

Electronic version of this journal:
http://www.ptep-online.com

Postal Address

Department of Mathematics and Science,
University of New Mexico,
705 Gurley Ave., Gallup, NM 87301, USA

ISSN: 1555-5534 (print)
ISSN: 1555-5615 (online)

Standard Address Number: 297-5092
Printed in the United States of America

January 2015 **Vol. 11, Issue 1**

CONTENTS

Information for Authors and Subscribers

Progress in Physics has been created for publications on advanced studies in theoretical and experimental physics, including related themes from mathematics and astronomy. All submitted papers should be professional, in good English, containing a brief review of a problem and obtained results.

All submissions should be designed in LaTeX format using *Progress in Physics* template. This template can be downloaded from *Progress in Physics* home page http://www.ptep-online.com. Abstract and the necessary information about author(s) should be included into the papers. To submit a paper, mail the file(s) to the Editor-in-Chief.

All submitted papers should be as brief as possible. Short articles are preferable. Large papers can also be considered in exceptional cases. Letters related to the publications in the journal or to the events among the science community can be applied to the section *Letters to Progress in Physics*.

All that has been accepted for the online issue of *Progress in Physics* is printed in the paper version of the journal. To order printed issues, contact the Editors.

This journal is non-commercial, academic edition. It is printed from private donations. (Look for the current author fee in the online version of the journal.)

EDITORIAL MESSAGE

Progress in Physics: 10 Years in Print

In January, 2015, we celebrate first 10 years of our journal *Progress in Physics*. This is a good time to remember what events led to the idea of the journal, and how the journal was founded.

Ten years ago, in the fall of 2004, CERN Document Server has changed its policy so that it closed its door for all future pre-prints submitted by non-CERN employee. All other persons were advised to submit their papers to Cornell E-Print Archive (known as arXiv.org).

The main problem of this change was that Cornell E-Print Archive only accept papers from people who have a scientific institute affiliation. This policy continues to this day, and is a necessary condition for consideration of papers in almost all modern scientific journals.

This was a serious impact to the scientific community, where so many researchers continue their studies in between short-term grants, or even continue their scientific activity as independent researchers. They all are not affiliated to any scientific institution. So, they all loose their fundamental right to be published in scientific journals.

But it was not always. In already the beginning of the 20th century, every person was able to submit a paper to any scientific journal. And this paper was considered according to its real scientific importance, not the formal degree or scientific institute affiliation of the submitter. Otherwise, many great scientists such as Einstein and others would never have published their scientific works.

However, in the early 20th century, science was a matter of a very few people. With the progress of democracy and improved living mass of the people, in the 1950–1960's, science has become a professional field of activity of hundreds of thousands and even millions of people in the world. Massive investment in research activities have led to the fact that the scientific community is filled with people who do not view science as a search for truth but as "employment". Many scientific workers speak frankly to each other that we went to the science just in order "to get good income" thus doing some formal activities in the field which is a hard to understand for investors who pay for it all. Such "research staff", not being burdened with a large intellectual tension of the solution of scientific problems were much more socially active than the real scientists. Therefore, they quickly and systematically took formal positions in the scientific community, including scientific journals. As a matter of fact that they considered real scientists as potentially dangerous persons, who may potentially qualify for their sure and well-paid job positions. To defend themselves, they built a complicate bureaucratic system, where, as Grisha Perelman said very well, no one researcher who is really busy with research will waste so much time and effort to fill out all the paperwork for a grant. Only familiarity in the editorial board of the scientific journal, or belonging to the "friendly" scientific group gives the opportunity to publish your article.

In this way, the scientific bureaucracy was born. This situation continues in the scientific community until this day.

In this background, CERN Document Server was the solely possibility to publish research papers for the scientists, who are not joined into "groups" or do not belong to "scientific clans". In the fall of 2004, this window was closed.

It is comical, but even papers authored by Brian Josephson (Nobel Prize in Physics, 1973) were refused by Cornell E-Print Archive. As was claimed the reason was that he has right only to submit articles on his very particular field of physics, and has not rights to submit articles on other field of physics where he "cannot be an expert".

Correspondence among Josephson and other researchers, who were thinking of the future of the scientific community, has began. In the course of correspondence with Josephson, I met Florentin Smarandache. We both were active CERN E-Print Server users. I looked for another possibility to publish a series of research papers authored by me and Larissa Borissova, my closest colleague and friend. In our common discussion with Florentin, I told him that we must establish a new journal of physics: it is better and easier than to fight for influence in existing journals. Do you like to see this journal in print? — Florentin replied. So, *Progress in Physics* was established by our common power. It was January, 2005.

Then I wrote *Declaration of Academic Freedom*, to fix the fundamental rights and freedoms allowed among the scientific community. This text, known also as *Academic Bill of Rights* is now published in ten languages. All that we do in our journal, is according to the articles of the Bill.

During the first year, we had no many authors and readers. Nevertheless, ten years later, i.e. now, the journal has grown very much. We now have a stable traffic in the range from 25,000 to 35,000 downloaded papers per month, with some peaks in the months when a hot research is published.

Despite some difficulties, the journal is now stable. We allow every person to submit a paper, with the warranty that the submission will be reviewed according only to scientific judgements, independent on the personality of the submitter. Our personnel works on voluntary basis, to keep the author's fee as low as possible. I hope that first 10 years of *Progress in Physics* will be the beginning of the long term life of the journal, among the other respected journal of physics.

Dmitri Rabounski, Editor-in-Chief

Trapping Regions for the Navier-Stokes Equations

Craig Alan Feinstein

2712 Willow Glen Drive, Baltimore, Maryland 21209. E-mail: cafeinst@msn.com

In 1999, J. C. Mattingly and Ya. G. Sinai used elementary methods to prove the existence and uniqueness of smooth solutions to the 2D Navier-Stokes equations with periodic boundary conditions. And they were almost successful in proving the existence and uniqueness of smooth solutions to the 3D Navier-Stokes equations using the same strategy. In this paper, we modify their technique to obtain a simpler proof of one of their results. We also argue that there is no logical reason why the 3D Navier-Stokes equations must always have solutions, even when the initial velocity vector field is smooth; if they do always have solutions, it is due to probability and not logic.

1 Introduction

In this paper, we examine the three-dimensional Navier-Stokes equations, which model the flow of incompressible fluids:

$$\left.\begin{aligned} &\frac{\partial u_i}{\partial t}+\sum_{j=1,2,3} u_j\frac{\partial u_i}{\partial x_j}=\nu\Delta u_i-\frac{\partial p}{\partial x_i} \qquad i=1,2,3\\ &\sum_{i=1,2,3}\frac{\partial u_i}{\partial x_i}=0 \end{aligned}\right\}, \quad (1)$$

where $\nu>0$ is viscosity, p is pressure, u is velocity, and $t>0$ is time. We shall assume that both u and p are periodic in x. For simplicity, we take the period to be one. The first equation is Newton's Second Law, force equals mass times acceleration, and the second equation is the assumption that the fluid is incompressible.

Mattingly and Sinai [5] attempted to show that smooth solutions to 3D Navier Stokes equations exist for all initial conditions $u(x,0)=u^0(x)\in C^\infty$ by dealing with an equivalent form of the Navier-Stokes equations for periodic boundary conditions:

$$\frac{\partial\omega_i}{\partial t}+\sum_{j=1,2,3} u_j\frac{\partial\omega_i}{\partial x_j}=\sum_{j=1,2,3}\omega_j\frac{\partial u_i}{\partial x_j}+\nu\Delta\omega_i \quad i=1,2,3, \quad (2)$$

where the vorticity $\omega(x,t)=(\frac{\partial u_2}{\partial x_3}-\frac{\partial u_3}{\partial x_2},\frac{\partial u_3}{\partial x_1}-\frac{\partial u_1}{\partial x_3},\frac{\partial u_1}{\partial x_2}-\frac{\partial u_2}{\partial x_1})$.

Their strategy was as follows: Represent the equations (2) as a Galerkin system in Fourier space with a basis $\{e^{2\pi ikx}\}_{k\in\mathbb{Z}^3}$. A finite dimensional approximation of this Galerkin system can be associated to any finite subset $\mathcal{Z}$ of $\mathbb{Z}^3$ by setting $u^{(k)}(t)=\omega^{(k)}(t)=0$ for all k outside of $\mathcal{Z}$. For each finite dimensional approximation of this Galerkin system, consider the system of coupled ODEs for the Fourier coefficients. Then construct a subset $\Omega(K)$ of the phase space (the set of possible configurations of the Fourier modes) so that all points in $\Omega(K)$ possess the desired decay properties. In addition, construct $\Omega(K)$ so that it contains the initial data. Then show that the dynamics never cause the sequence of Fourier modes to leave the subset $\Omega(K)$ by showing that the vector field on the boundary of $\Omega(K)$ points into the interior of $\Omega(K)$.

Unfortunately, their strategy only worked for the 3D Navier-Stokes equations when the Laplacian operator Δ in (2) was replaced by another similar linear operator. (Their strategy was in fact successful for the 2D Navier-Stokes equations.) In this paper, we attempt to apply their strategy to the original equations (1).

2 Navier-Stokes equations in Fourier space

Moving to Fourier space where

$$\left.\begin{aligned} u_i(x,t)&=\sum_{k\in\mathcal{Z}} u_i^{(k)}(t)e^{2\pi ikx}\\ p(x,t)&=\sum_{k\in\mathcal{Z}} p^{(k)}(t)e^{2\pi ikx}\\ |k|&=\sqrt{\sum_{j=1,2,3}k_j^2} \end{aligned}\right\}, \quad (3)$$

let us consider the system of coupled ODEs for a finite-dimensional approximation to the Galerkin-system corresponding to (1),

$$\frac{du_i^{(k)}}{dt}=\Big(\sum_{\substack{q+r=k\\ q,r\in\mathcal{Z}}}\sum_{j=1,2,3}-2\pi iq_ju_i^{(q)}u_j^{(r)}\Big)- -4\pi^2\nu|k|^2u_i^{(k)}-2\pi ik_ip^{(k)} \qquad i=1,2,3, \quad (4)$$

$$\sum_{i=1,2,3}k_iu_i^{(k)}=0\,, \quad (5)$$

where $\mathcal{Z}$ is a finite subset of $\mathbb{Z}^3$ in which $u^{(k)}(t)=p^{(k)}(t)==0$ for each $k\in\mathbb{Z}^3$ outside of $\mathcal{Z}$. Like the Mattingly and Sinai paper, in this paper, we consider a generalization of this Galerkin-system:

$$\frac{du_i^{(k)}}{dt}=\Big(\sum_{\substack{q+r=k\\ q,r\in\mathcal{Z}}}\sum_{j=1,2,3}-2\pi iq_ju_i^{(q)}u_j^{(r)}\Big)- -4\pi^2\nu|k|^\alpha u_i^{(k)}-2\pi ik_ip^{(k)} \qquad i=1,2,3, \quad (6)$$

$$\sum_{i=1,2,3}k_iu_i^{(k)}=0\,, \quad (7)$$

where $\alpha \geqslant 2$. Multiplying each of the first three equations by k_i for $i = 1, 2, 3$ and adding the resulting equations together, we obtain

$$\sum_{\substack{q+r=k \\ q,r\in\mathcal{Z}}} \sum_{\substack{j=1,2,3 \\ l=1,2,3}} -2\pi i k_l q_j u_l^{(q)} u_j^{(r)} = 2\pi i |k|^2 p^{(k)}, \tag{8}$$

since $\sum_{i=1,2,3} k_i \frac{du_i^{(k)}}{dt} = 0$ (by equation (7)). Then substituting the above calculated expression for $p^{(k)}$ in terms of u into (6) we obtain

$$\frac{du_i^{(k)}}{dt} = \Big[\sum_{\substack{q+r=k \\ q,r\in\mathcal{Z}}} \sum_{\substack{j=1,2,3 \\ l=1,2,3}} 2\pi i \left(\frac{k_i k_l}{|k|^2} - \delta_{il}\right) q_j u_l^{(q)} u_j^{(r)}\Big] - - 4\pi^2 \nu |k|^\alpha u_i^{(k)} \qquad i = 1, 2, 3. \tag{9}$$

And since $\sum_{j=1,2,3} r_j u_j^{(r)} = 0$ and $q_j + r_j = k_j$, we can substitute k_j for q_j:

$$\frac{du_i^{(k)}}{dt} = \Big[\sum_{\substack{q+r=k \\ q,r\in\mathcal{Z}}} \sum_{\substack{j=1,2,3 \\ l=1,2,3}} 2\pi i \left(\frac{k_i k_l}{|k|^2} - \delta_{il}\right) k_j u_l^{(q)} u_j^{(r)}\Big] - - 4\pi^2 \nu |k|^\alpha u_i^{(k)} \qquad i = 1, 2, 3. \tag{10}$$

3 A new theorem

Now, we state and prove the following theorem:

Theorem: *Let $\{u^{(k)}(t)\}$ satisfy (10), where $\alpha > 2.5$. And let $1.5 < s < \alpha - 1$. Suppose there exists a constant $C_0 > 0$ such that $|u^{(k)}(0)| \leqslant C_0 |k|^{-s}$, for all $k \in \mathbb{Z}^3$. Then there exists a constant $C > C_0$ such that $|u^{(k)}(t)| \leqslant C|k|^{-s}$, for all $k \in \mathbb{Z}^3$ and all $t > 0$. (The constants, C_0 and C, are independent of the set $\mathcal{Z}$ defining the Galerkin approximation.)*

Proof: By the basic energy estimate (see [1,2,7]), there exists a constant $E \geqslant 0$ such that for each $t \geqslant 0$ and for any finite-dimensional Galerkin approximation defined by $\mathcal{Z} \subset \mathbb{Z}^3$, we have $\sum_{k\in\mathcal{Z}} \sum_{i=1,2,3} |u_i^{(k)}(t)|^2 \leqslant E$. Hence, for any $K > 0$, we can find a $C > C_0$ such that $|\Re(u^{(k)})| \leqslant C|k|^{-s}$ and $|\Im(u^{(k)})| \leqslant C|k|^{-s}$, for all $t \geqslant 0$ and $k \in \mathbb{Z}^3$ with $|k| \leqslant K$. Now let us consider the set,

$$\Omega(K) = \Big\{\Big(\Re(u^{(k)}), \Im(u^{(k)})\Big)_{k\in\mathbb{Z}^3} : |k| > K\,, \quad |\Re(u^{(k)})| \leqslant C|k|^{-s}, \quad |\Im(u^{(k)})| \leqslant C|k|^{-s}\Big\}. \tag{11}$$

We will show that if K is chosen large enough, any point starting in $\Omega(K)$ cannot leave $\Omega(K)$, because the vector field along the boundary $\partial\Omega(K)$ is pointing inward, i.e., $\Omega(K)$ is a trapping region. Since the initial data begins in $\Omega(K)$, proving this would prove the theorem.

We pick a point on $\partial\Omega(K)$ where $\Re(u_i^{(\bar{k})})$ or $\Im(u_i^{(\bar{k})}) = \pm C|\bar{k}|^{-s}$ for some $\bar{k} \in \mathcal{Z}$ such that $|\bar{k}| > K$ and some $i \in \{1, 2, 3\}$. (For definiteness, we shall assume that $\Re(u_i^{(\bar{k})}) = C|\bar{k}|^{-s}$, but the same line of argument which follows also applies to the other possibilities.) Then the following inequalities hold when K is chosen large enough:

$$\Big|\sum_{\substack{q+r=\bar{k} \\ q,r\in\mathcal{Z}}} \sum_{\substack{j=1,2,3 \\ l=1,2,3}} 2\pi \left(\delta_{il} - \frac{\bar{k}_i \bar{k}_l}{|\bar{k}|^2}\right) \bar{k}_j \Im(u_l^{(q)} u_j^{(r)})\Big| \leqslant$$

$$\sum_{\substack{q+r=\bar{k} \\ q,r\in\mathcal{Z}}} \sum_{\substack{j=1,2,3 \\ l=1,2,3}} 4\pi |\bar{k}_j| |u_l^{(q)}| |u_j^{(r)}| \leqslant$$

$$\sum_{\substack{j=1,2,3 \\ l=1,2,3}} 4\pi |\bar{k}_j| \Big(\sum_{q\in\mathcal{Z}} |u_l^{(q)}|^2\Big)^{1/2} \Big(\sum_{r\in\mathcal{Z}} |u_j^{(r)}|^2\Big)^{1/2} \leqslant$$

$$\sum_{\substack{j=1,2,3 \\ l=1,2,3}} 4\pi |\bar{k}_j| E < 4\pi^2 \nu |\bar{k}|^\alpha \frac{C}{|\bar{k}|^s} = 4\pi^2 \nu |\bar{k}|^\alpha |\Re(u_i^{(\bar{k})})|. \tag{12}$$

This establishes that the vector field points inward along the boundary of $\Omega(K)$ for all $t > 0$. So the trajectory never at any time leaves $\Omega(K)$. Then we have the desired estimate that $|u^{(k)}(t)| \leqslant C|k|^{-s}$ for all $t > 0$. ■

4 Discussion

Just as in the 1999 paper by Mattingly and Sinai [5], an existence and uniqueness theorem for solutions follows from our theorem by standard considerations (see [1, 2, 7]). The line of argument is as follows: By the Sobolev embedding theorem, the Galerkin approximations are trapped in a compact subset of L^2 of the 3-torus. This guarantees the existence of a limit point which can be shown to satisfy (10), where $\mathcal{Z} = \mathbb{Z}^3$. Using the regularity inherited from the Galerkin approximations, one then shows that there exists a unique solution to the generalized 3D Navier-Stokes equations where $\alpha > 2.5$.

The inequality (12) in the proof of our Theorem is not necessarily true when $\alpha = 2$. Because of this, there is nothing preventing the solutions to (10) from escaping the region $\Omega(K)$ when $\alpha = 2$. Hence, there is no logical reason why the standard 3D Navier-Stokes equations must always have solutions, even when the initial velocity vector field is smooth; if they do always have solutions, it is due to probability (see [6]) and not logic, just like the Collatz $3n + 1$ Conjecture and the Riemann Hypothesis (see [3, 4]). Of course, it is also possible that there is a counterexample to the famous unresolved conjecture that the Navier-Stokes equations always have solutions when the initial velocity vector field is smooth. But as far as the author knows, nobody has ever found such a counterexample.

Submitted on October 15, 2014 / Accepted on October 22, 2014

References

1. Constantin P., Foiaş C. Navier-Stokes Equations. University of Chicago Press, Chicago, 1988.

2. Doering C., Gibbon J. Applied analysis of the Navier-Stokes equations. Cambridge Texts in Applied Mathematics. Cambridge University Press, Cambridge, 1995.
3. Feinstein C. Complexity Science for Simpletons. *Progress in Physics*, 2006, issue 3, 35–42.
4. Feinstein C. The Collatz $3n+1$ Conjecture is Unprovable. *Global Journal of Science Frontier Research, Mathematics & Decision Sciences*, 2012, v. 12, issue 8, 13–15.
5. Mattingly J., Sinai Y. An elementary proof of the existence and uniqueness theorem for the Navier-Stokes equations. *Commun. Contemp. Math. 1*, 1999, no. 4, 497–516.
6. Montgomery-Smith S., Pokorny M. A counterexample to the smoothness of the solution to an equation arising in fluid mechanics. *Commentationes Mathematicae Universitatis Carolinae*, 2002, v. 43, issue 1, 61–75.
7. Temam R. Navier-Stokes equations: Theory and numerical analysis. Volume 2 of *Studies in Mathematics and its Applications*, North-Holland Publishing Co., Amsterdam-New York, revised edition, 1979.

Majorana Particles: A Dialectical Necessity and not a Quantum Oddity

Abdul Malek

980 Rue Robert Brossard, Québec J4X 1C9, Canada. E-mail: abdulmalek@qc.aibn.com

The confirmation of the existence of Majorana particles is the strongest ever imperative for a dialectical perspective for physics; and may have implications for epistemology from the sub-nuclear to the cosmic scale. As the Majorana particle suggests matter at its most fundamental level must be viewed as a composite of the "unity of the opposites" — a contradiction, the resolution of which imparts "motion" to matter and hence the dialectical assertion that "there can be no matter without motion and no motion without matter". The existence of Majorana particles show that the anti- dialectical conception of matter as composed of distinctive and unitary particles like the fermions and the bosons at the most fundamental level, is faulty and is untenable. These types of sharp distinctions and categories of matter are indeed to be found in nature, but with relative and conditional validity.

For dialectics, any tangible material existence is a composite of the unity of the two opposites; or an "Absolute Identity of identity and non-identity" — a contradiction and a rationale for its change, motion, development, evolution and so on. At the most fundamental level this contradiction is the unity of the opposites of "being" and "nothing" — an interpenetration of the opposites and/or their inter-conversion to each other. Any synthesis to a different level is infected with this and its own peculiar new contradictions. The newly confirmed [1] existence of the Majorana particle is an affirmation of this dialectical law and at the same time it is a negation of the (artificial) division into the absolute and the unitary categories of the fundamental particles in nature as bosons and fermions. This differentiation is indeed possible from an anti-dialectical perspective, but only with relative and conditional validity. The three laws of dialectics, namely i) the unity or the interpenetration of the opposites, ii) the inter-conversion of quality and quantity and iii) the negation of the negation mediated by chance and necessity; provide an essential basis for an understanding of nature from the microcosm to the macrocosm [2]. Any attribute, characteristics, manifestation, developments, etc. of matter in dialectical epistemology, therefore, must be found primarily within matter itself and through its contradictions and not through any external agency.

Official physics continues to operate under the perspective of what Hegel termed as the "view of understanding" which roughly corresponds to causality. This view follows the rules of formal logic, and Aristotle's doctrine of "unity, opposition and the excluded middle" and with the mutual exclusion of the opposites. The opposites in this view stand in absolute opposition to each other and remain the same forever once brought into existence by an external agency. This "good old commonsense" view of the world though approximate and faulty at human scale; was in essence satisfactory enough to serve humanity and natural science reasonably well. But the advent of the idea of evolution in biology and the quantum phenomenon in physics fundamentally undermined the validity of the notions of the "view of understanding" in epistemology, particularly in modern physics.

Even before the discovery of the quantum phenomena; thinkers starting from Heraclitus through Epicurus, Hegel, Marx and Engels showed that dialectics offers a better epistemological tool for an understanding of nature, life, history, society and thought. The existence of polarity and the "unity of the opposites" and hence motion, was shown to manifest itself in all aspects of the world But of course, dialectics that denies the stability or the permanence of what exists is inimical to a class based social structure, which insists on permanence, continuity, certainty etc. Of necessity, and because of its very nature as the conservative, the resisting and the preserving side of what exists; the "view of understanding" historically became the dominant epistemological tool, including that of the natural sciences. The anti-dialectical notion of the unitary and the absolutely defined "fundamental building blocks" or fundamental elementary particles in nature and their classification into fermions and bosons as developed through the quantum field theories of modern particle physics is a case in point.

The Italian physicist Ettore Majorana in his 1937 paper [3] raised serious doubt about such absolute categorization and forced the dialectical perspective on modern particle physics; shortly after Paul Dirac gave the relativistic formulation of quantum mechanics for the electron [4] and conceived the theoretical basis for describing the spin 1/2 particles that would divide all possible matter particles into two mutually exclusive groups known as fermions and bosons, based on their spin properties. Following the mathematical logic and the symmetry rules of Dirac; Majorana in contradiction to Dirac, showed that such an absolute differentiation is not possible, because both the fermions and the boson can contain their opposites within themselves as the dialectical unity of

the opposites.

Paul Dirac ushered in the revolutionary idea of the anti-particles in nature as a dialectical necessity. Dirac's epoch making discovery that anti-particles must exist as part of the real world in the context of a real/virtual dialectical category and that the quantum vacuum is seething with virtual particles with momentary existence and which can turn into real particles through quantum tunnelling; for the first time gave validity to the dialectical speculation of Hegel's fundamental triad of "being-nothing-becoming" as the mode of "coming into being and passing out of existence" of matter as elementary particles in nature [5].

The developments in particle physics from the turn of the 20th century led to the discovery of multitude of so-called "elementary particles" of matter/energy. These were eventually rationalized based on their integral or fractional electric charge and fractional/integral spin values into two groups of matter particles, namely Dirac fermions with fractional spin values and bosons (named after the Indian physicist S. N. Bose) with integral spin values. In his attempt to develop a theoretical framework for describing spin 1/2 particles, Dirac thereby made a revolutionary discovery of hitherto unknown dialectical realm of the "unity of the opposites" of matter/antimatter. To describe the spin 1/2 particles, Dirac found it necessary to incorporate imaginary and complex quantities in his equations that gave rise to the complex-conjugate field ϕ^* of the real field ϕ, where the complex- conjugate fields ϕ^* can accommodate the antiparticles. This is a new aspect of reality brought forth by the developments in quantum mechanics. Physics previously only dealt with integral spins of 0, 1 and 2 in its equations namely, the Klein-Gordon, Maxwell (electromagnetism) and Einstein (general relativity) equations, respectively; which readily accommodate real fields.

The concept of antiparticles in nature means that, as a dialectical necessity all particles must have or be their own antiparticles. This "unity of the opposites" may manifest either in the same body like the two poles of a magnet or on separate bodies like the positive and negative electric charge or in the same body simultaneously containing the opposites continuously exchanging into their opposite polarity; depending on the nature of the exchange force that keep the two opposites together and the external circumstances under which this force operates. The latter case is manifested for example in positronium or meson where (though very unstable) matter and antimatter reside together as the unity of the opposites. Both positronium and mesons can exist even as their dimmers like the dipositronium and the mystery meson (X3872) respectively. Even the most pure and holy of all things in the world, namely the light photon has opposite characteristics of a particle and a wave and also is a composite of two matter — antimatter particles and can be resolved into a pair of the particles such as the electron-positron pair if the photon has enough energy equivalent of the mass of the particle pair. All these particles probably exist in Majorana type formation where the two opposites exist in the same body through rapid inter-conversion of the one opposite to the other.

The conundrum for anti-dialectical official physics is that the existence of antiparticle itself is problematic. In the narrative of the big bang theory all matter (and admittedly now antimatter) was created in one fell swoop. Any antimatter that was created was conveniently annihilated by reaction with matter, so that only matter (which arbitrarily was in relative excess) now prevails in the universe. Any new antimatter can now only be produced in negligible quantity through secondary processes; but the existence of any tangible amount (or even in large scale equivalent to matter); of antimatter is therefore, impossible. This author has previously challenged this contention of official physics; as many cosmic phenomena and the dynamics of the galaxies can be attributed to large-scale presence of antimatter in the universe [6].

The existence of anti-particle as such is not a big problem for anti-dialectical official physics. Because neutral and integer spin particles (like bosons) can be viewed as their own antiparticles, as they must be created by fields ϕ that obey $\phi = \phi^*$ — that is, real fields, like electromagnetism and gravity discussed above. What is "fundamentally confusing" (to use the term expressed by some famous physicists) for official physics is that some fermions with electric charge and spin 1/2 must also be their own antiparticles as Majorana (and dialectics) asserted. These fermions already have their anti-particles that exist separately. For example the neutron even with 0 charge and spin 1/2 has its antiparticle — the anti-neutron, as electron and proton have their antiparticles as positron and anti-proton respectively. Why then the Dirac fermions still should behave as their own antiparticle in one single body as the unity of the opposites under special circumstances like for example positronium or pion? It is simply that matter and antimatter in the Majorana particles has undergone a qualitative change and now reside in the same entity (instead of different ones) like the two opposites poles of a magnet or to take the analogy further, like a transgender person. The matter and antimatter characteristics in the Majorana particle did not vanish, but are maintained in a different way, probably through rapid inter-conversion of the one to the other through the exchange of some force particles. This is the same as in the case of positronium or meson (or even in the inter-conversion of nucleons in the atomic nucleus). In meson for example (a simpler case) the quark and the antiquark must undergo rapid interchange of identity into each other (through exchange of force particles) to remain in a stable form. This seems evident; for example in the case of pi-meson, an up and anti-down quark combination has a mass-energy of only 140 MeV; yet the same quark combination but only with different spin in a rho-meson has a mass-energy of 770 MeV!

How the Majorana particle emerges in the experimental setup of Ali Yazdani's group described in [1] is a matter of

speculation at this stage. It seems that the super-conducting magnet (two opposing factors) somehow polarizes the electron, probably through some new kind of unifying electomagneton coupling interaction, forming the end-to-end linear chain of the polarized electrons within the magnet, turning them into particles like the neutrinos, or mesons or even photons with the unbalanced opposite polarity emerging at the two ends of the magnet

The random and catastrophic gamma ray bursts (GRBs) observed in the cosmos can be attributed to the chance accumulated cosmic scale Majorana type formation of matter and anti-matter clusters, or somewhat like speculated boson stars [7]; probably mediated by the magnatic fields of the host galaxies and their instant annihilations as gigantic cosmic "fire-balls"; emmiting high energy gamma rays, triggered sponteneously or by some outside events [2]. GRBs are short duration (10 milliseconds to several minutes) intense flashes of high energy (from KeV to MeV to GeV range) gamma rays associated with extremely energetic events in distant galaxies that appear from random locations isotropically distributed in the celestial sphere. The progenitors of these astrophysical phenomena remain largely unknown [8]. These energetic events mostly emmiting gamma ray photons probably occur from various scale matter-antimatter annihilation processes. Indeed in the lower energy range, the most dominant peak centered around ~ 1 MeV probably corresponds to the mass equivalent of the elctron-positron pair.

Like the quantum phenomena itself, dialectics and the Majorana particle are counter-intuitive for anti-dialectical physics. The discovery of the Majarona particle represents another blow to the anti-dialectical perspective of modern physics and shows the futility of hunting for absolutely unitary fundamental constituents of matter in nature, like the magnetic monopole.

Submitted on October 21, 2014 / Accepted on October 23, 2014

References

1. Nadj-Perge S., et al. Observation of Majorana fermions in ferromagnetic atomic chains on a superconductor. *Science Express*, published online October 02, 2014; doi: 10.1126/science.1259327.
2. Malek A. The Dialectical Universe — Some Reflections on Cosmology. Agamee Prakashani Publishers, Dhaka, 2012.
3. Majorana E. *Nuovo Cimento*, 1937, v. 5, 171–184.
4. Dirac P. A. M. *Proc. Royal Soc. Lond.*, 1928, v. A117, 610–624.
5. Malek A. The real/virtual exchange of quantum particles. *Progress in Physics*, 2014, v. 10, issue 4, 209–211.
6. Malek A. Ambartsumian, Arp and the breeding galaxies. *Apeiron*, 2005, v. 12, no. 2, 256–271.
7. Shunck F. E. and Mielke E. W. General relativistic boson stars. *Class. & Quantum Grav.*, 2003, v. 20, R301–R356.
8. Goldstein A. et al. The BATSE 5B gamma-ray burst spectral catalog. arXiv: 1311.7135.

LETTERS TO PROGRESS IN PHYSICS

An Essay on Numerology of the Proton to Electron Mass Ratio

Alexander Kritov
E-mail: alex@kritov.ru

There are few mathematical expressions for calculation proton to electron mass ratio presented. Some of them are new and some are not. They have been analysed in terms of their simplicity, numerical significance and precision. Expressions are listed in the structured manner with comments. The close attention should be paid to a comparison of the formula similarity via their precision. A brief review of the different attempts in similar search is given.

1 Introduction

The founding of the analytical expression for fundamental dimensionless constant was a dream of a physical science for many years. There are many papers in literature trying to derive or explain fine structure constant from pure numerical theories. Such hypothetical theories can be divided into two types. The first one proposes that the dimensionless constants of the Nature are not actually constant and suggests using some close numbers which deviate from the original ones. This type of the theories requires further experimental research because deviations of the dimensionless constants are still unknown with good precision. For example G. Gamov following Eddington's belief explained the fine structure constant suggesting that it is equal to exactly 137 but it differs from exact number because of some small quantum perturbations similar to those in the case of the Lamb-Rutherford effect [1]. The second type of the theories is less common, it suggests exact relation for the dimensionless constants which is close to current experimental value. Usually such hypotheses derive huge and unnatural formulas that lack of elegance and explain-ability. Moreover physical justification for such expressions doesn't have enough arguments or the physical model is absent. However some of such recent theories may look interesting and promising in the view of the the presented material [2–4].

The part of the physics which involves dimensionless constants is very prone to invasion of numerology. However such cooperation has not been shown to be efficient yet. Though it is worth to notice that numerology itself stays very close to algebra and number theory of mathematics. Numerology itself can be considered as ancient prototype of the modern algebra (as well as alchemy was a base for a modern chemistry) and as it was said by I. J. Good: "At one time numerology meant divination by numbers, but during the last few decades it has been used in a sense that has nothing to do with the occult and is more fully called physical numerology" [5]. At this perspective, physical numerology seems to be a way through back-door which researches also try to enter and finding a key by trying to pickup right numbers. Such attempts should not be ignored as they may provide not only new clues for the researchers, but also in case of null-result they might be an evidence for another consistent principle which can be explored further.

2 Background

The search for mathematical expression for this dimensionless number motivated many serious scientists. A sufficient theory on particle masses and their ratios is not yet ready. The mass ratio of proton to electron ($\mu = m_p/m_e$) — two known stable particles which belong to two different types (leptons and hadrons) — still remains the mystery among other dimensionless numbers.

In 1929 Reinhold Fürth hypothesized that μ can be derived from the quadratic equation involving the fine structure constant [6]. Later on in 1935, A. Eddington who accepted some of Fürth's ideas presented the equation for proton to electron mass ratio calculation ($10\mu^2 - 136\mu + 1 = 0$) which appeared in his book "New Pathways in Science" [17]. However both approaches can not be used nowadays as they give very high deviation from the currently known experimental value of μ, so they are not reviewed in present work. Later on in 1951, it was Lenz [7] (but not Richard P. Feynman!) who noted that μ can be approximated by $6\pi^5$. In 1990, I.J. Good, a British mathematician assembled eight conjectures of numerology for the ratio of the rest masses of the proton and the electron.

Nowadays proton to electron mass ratio is known with much greater precision: $\mu = m_p/m_e = 1836.15267245(75)$, with uncertainty of 4.1×10^{-10} (CODATA 2010, [4]). Recently the professional approach to mathematically decode m_p/m_e ratio was done by Simon Plouffe [8]. He used a large database of mathematical constants and specialized program to directly find an expression. Alone with his main remarkable result for the expression for μ via Fibonacci and Lucas numbers and golden ratio he also noted that expression for μ using π can be improved as $6\pi^5 + 328/\pi^8$, but he concluded that this expression: "hardly can be explained in terms of primes and composites".

Expression	Value	Ref.
$\mu = \left(\frac{7}{2}\right)^6$	**183**8.2656 (1×10^{-3})	1.
$\mu = \sin\left(\frac{\pi}{5}\right) \cdot 5^5$	**1836**.8289 (4×10^{-4})	2.
$\mu = \frac{17}{4}\,432$	**1836**.0000 (8×10^{-5})	3.
$\mu = 150^{\frac{3}{2}} - 1$	**1836.1**173 (2×10^{-5})	4.
$\mu = 6\pi^5$	**1836.1**181 (2×10^{-5})	5.
$\mu = \frac{200^{300}}{7^{103}}$	**1836.1**179 (2×10^{-5})	6.
$\mu = \frac{22}{(5 \cdot 3 \cdot \alpha)^2}$	**1836.15**56 (2×10^{-6})	7.
$\mu = \frac{5 \cdot 7^3}{6 \cdot 67} 137\pi$	**1836.15**14 (6×10^{-7})	8.
$\mu = \frac{2^4 3^5}{5\alpha^{-1}} 103\pi$	**1836.152**20 (3×10^{-7})	9.
$\mu = \frac{e^8 - 10}{\phi}$	**1836.15**301 (2×10^{-7})	10.
$\mu = \frac{40}{3}\alpha^{-1} + \frac{800}{9\pi^2}$	**1836.152**98 (2×10^{-7})	11.
$\mu = \frac{86^4}{31^3}$	**1836.152**39 (2×10^{-7})	12.
$\mu = \frac{2267^2}{5 \cdot 7 \cdot 11 \cdot \alpha^{-1}} 6\pi$	**1836.152**5639 $(6 * 10^{-8})$	13.
$\mu = \frac{11^2 5^{\frac{4}{5}} 7^{\frac{2}{5}} e^3}{6 \cdot 2^{\frac{4}{5}}}$	**1836.15267**03 (1×10^{-9})	14.
$\mu = \frac{55 \cdot 5^{\frac{3}{2}} 11^{\frac{15}{32}}}{\phi^{\frac{1}{16}}}$	**1836.15267**48 (1×10^{-9})	15.
$\mu = \frac{3^{\frac{15}{4}} 5^{\frac{9}{4}} 14^{\frac{3}{2}}}{\pi^3 e^{\frac{3}{4}}}$	**1836.15267**19 (1×10^{-10})	16.

3 Variability

During the last decade a subject of variability of μ appeared under heavy debate and serious experimental verifications. The main experimental task is to distinguish cosmological red-shift of spectral lines from the shift caused by possible variation of μ. There is also proposed method to observe absorption spectra in the laboratory using the high precision atomic clocks.

Reinhold et al. [9] using the analysis of the molecular hydrogen absorption spectra of quasars Q0405-443 and Q0347-373 concluded that μ could have decreased in the past 12 Gyr and $\Delta\mu/\mu = (2.4 \pm 0.6) \times 10^{-5}$. This corresponds to entry value of μ= 1836.19674. King et al. [9] re-analysed the spectral data of Reinhold et al. and collected new data on another quasar, Q0528-250. They estimated that $\Delta\mu/\mu = (2.6 \pm 3.0) \times 10^{-6}$, different from the estimates of Reinhold et al. (2006). So the corresponding value for maximal deviated μ to be something around 1836.1574. The later results from Murphy et al. [15] and Bagdonaite et al. [2] gave a stringent limit $\Delta\mu/\mu < 1.8 \times 10^{-6}$ and $\Delta\mu/\mu = (0.0 \pm 1.0) \times 10^{-7}$ respectively. However these deviations could be valid only for the half of the Universe's current age or to the past of 7 Gyr which may not be enough for full understanding of the evolution of such variation. The results obtained by Planck gave $\Delta\alpha/\alpha = (3.6 \pm 3.7) \times 10^{-3}$ and $\Delta m_e/m_e = (4 \pm 11) \times 10^{-3}$ at the 68% confidence level [13] which provided not so strong limit comparing to found in [9] and [10].

At first sight the variation, if confirmed, may seem to make the numerical search for the mathematical expression meaningless. However possible variability of the μ should not prevent such search further, because the variation means one has to find a mean value of its oscillation or the beginning value from where it has started to change. And such variation would give a wider space for the further numerical sophistication because such value can not be verified immediately as we currently lack experimental verification of the amount of such change. If the fundamental constants are floating and the Nature is fine-tuned by slight the ratio changes from time to time, even so, there should be middle value as the best balance for such fluctuations. In this sense numerologists are free to use more relaxed conditions for their search, and current the precision for μ with uncertainty of 2×10^{-6} (as discussed above) may suffice for their numerical experiments. The formulas listed after number 7 in the table below do fall into this range.

4 Comments to the table

1. This expression is not very precise and given for its simple form. Also the number (7/2) definitely has certain numerological significance. The result actually better fits to the value of the m_n/m_e ratio (relative uncertainty is 2×10^{-4}). It is not trivial task to improve the formula accuracy, but why not, for example: $\mu = \left(\frac{7}{2}\right)^8 \frac{9 \cdot 13}{10\pi \cdot \alpha^{-1}}$ (relative error: 10^{-6}).
2. It is well known [8] that m_p/m_n ratio can be well approximated as $\cos\left(\frac{\pi}{60}\right)$ with relative uncertainty of 6×10^{-6}. So this is an attempt to build the formula for m_p/m_e ratio of similar form. Next more precise formula of the same form would be: $\mu = \frac{17^{43}}{19^{37}} \sin\left(\frac{\pi}{674}\right) =$

1836.1526661 (relative error is 3×10^{-9}). In the table it would be placed between number 13 and 14.

3. It was Werner Heisenberg in 1935 [14] who suggested to use number $2^4 3^3$ (which is equal to 432) to calculate alpha as $\alpha^{-1} = 432/\pi$, so m_p/m_e ratio can be also obtained approximately via 432. The expression can be rewritten as $1836 = 17 \cdot 108$ (the number 108 was considered to be sacred by ancients). There are other possible representations for the number 1836 which were noticed in the past, for example: $1836 = (136 \cdot 135)/10$ (see review in [5] and [22]).
4. This expression has some certain theoretical base related to original R. Fürth ideas [6], but it won't be discussed here. The precision has the same order as famous $6\pi^5$.
5. This is a Lenz's formula and it remains the favorite among the physicists. Recently Simon Plouffe also suggested yet another adjustment to this formula as following: $\mu = \dfrac{1}{5\cosh(\pi)} + 6\pi^5 + \dfrac{1}{5\sinh(\pi)}$ which looks remarkably symmetric and natural. The relative error is also extremely good: 4×10^{-9}. This formula has not been published before, it definitely has to attract further attention of the researchers.
6. The simplest way to approximate m_p/m_e ratio using powers of 2 and 7. Similar formula: $\mu = \dfrac{3^5 7^{16}}{2^{42}}$.
7. The elegant expression which uses almost 'kabalistic' numbers 22, 5, 3 and fine structure constant. Other possible expression with similar look and with the same precision: $\mu = \dfrac{5^{76}}{2^{127}3^{25}}$. Being combined together one can derive approximation for fine structure constant as 137.035999761 (with good relative deviation of 5×10^{-9}): $\alpha^{-2} = \dfrac{5^{78}}{11 \cdot 2^{127}3^{23}}$.
8. Parker-Rhodes in 1981, see [21] and review in [5]. McGoveran D.O. [20] claimed that this formula does not have anything in common with numerology as it was derived entirely from their discrete theory.
9. This elegant expression uses only the fine structure constant α, powers of 2, 3, 5 and the number 103. As J.I. Good said: "the favoured integers seem all to be of the form $2^a 3^b$ " [5].
10. By unknown source. No comment.
11. The expression can be also rewritten in more symmetric form: $\mu = 2\left(\dfrac{20}{3}\alpha^{-1} + \left(\dfrac{20}{3\pi}\right)^2\right)$. It can be noted that the number (20/3) appears in the author previous work [18] in the expression for the gravitational constant G.
12. One of the found expressions by author's specialized program. The search was performed for the expression of the view: $\mu = p_1^{n_1} p_2^{n_2} p_3^{n_3} p_4^{n_4}$, where p_i — some prime numbers, n_i — some natural numbers. Also: $\mu = \left(\dfrac{19}{5}\right)^{21} \dfrac{1}{13^8}$.
13. Number 2267 has many interesting properties; it is a prime of the form $(30n-13)$ and $(13n+5)$, it is congruent to 7 mod 20. It is father primes of order 4 and 10 etc. In the divisor of this formula there are sequential primes 5, 7, 11. There are other possible expressions of the similar form with such precision (10^{-8}), for example: $\mu = \dfrac{45 * 49 * 53^2}{8 * 29 * \alpha^{-1}} 5\pi$. It is also hard to justify why in expressions 9 and 13 α^{-1} stays opposite to π as by definition they supposed to be on the same side: $\alpha^{-1} = \hbar c/ke^2$ or $(2\pi\alpha^{-1}) = hc/ke^2$. But the author did not succeed in finding similar expressions with α and π on the same side with the same uncertainty. There are some few other nice looking formulas which the use of big prime numbers, for example: $\mu = \sqrt{4^3 \cdot 52679}$ (9×10^{-8}).
14. Another possible expression was found using web based program Wolframalpha [23]. The precision is the same as in next formula.
15. Simon Plouffe's approximation using Fibonacci and Lucas numbers [8] - slightly adjusted from its original look. Another elegant form for this expression is following: $\mu^{32} = \dfrac{11^{47}5^{80}}{\phi^2}$.
16. This formula has the best precision alone the listed. Though, powers of π and e seem to despoil its possible physical meaning.

5 Conclusions

At the present moment big attention is paid to experimental verification of possible proton-electron mass ratio variation. If experimental data will provide evidence for the ratio constancy then only few expressions (14-16 from the listed) may pretend to express proton-electron mass ratio as they fall closely into current experimental uncertainty range (4.1×10^{-10} as per CODATA 2010). Of course Simon Plouffe's formula (14) seems as a pure winner among them in terms of the balance between it simplicity and precision. However, some future hope for the other formulas remains if the variability of the proton to electron mass ratio is confirmed. Important to note that there could be unlimited numbers of numerical approximations for dimensionless constant. Some of them may look more simple and "natural" than others. It is easy to see that expression simplicity and explain-ability in opposite determines its precision. As all formulas with uncertainty 10^{-8} and better become obviously more complex. And at the end: "What is the chance that seemingly impressive formulae arise

purely by chance?" [15].

Remembering mentioning words said by Seth Lloyd [19] "not to follow in Dirac's footsteps and take such numerology too seriously" the author encourages the reader to continue such mathematical experiments and in order to extend the table of the formulas and submit your expressions to the author. Special attention will be brought to simple expressions with relations to: power of two (2^n), prime numbers and properties of Archimedean solids. Besides that it may be interesting mathematical exercise it may also reveal some hidden properties of the numbers. But how complexity of the mathematical expression can be connected to the complexity of the numbers? What is the origin of the Universe complexity? How much we can encode by one mathematical expression?

The mass ratio of proton to electron — two stable particles that define approximately 95% of the visible Universe's mass — can be related to the total value Computational capacity of the Universe (see [19]). So as a pure numbers they supposedly have to be connected to prime numbers, entropy, binary and complexity. So, possibly, their property should be investigated further by looking through the prism of the algorithmic information theory.

Let's hope that presented material can be a ground for someone in his future investigation of this area.

Acknowledgements

I would like to express my gratitude to Simon Plouffe for his valuable guideline and advises.

Submitted on October 17, 2014 / Accepted on October 20, 2014

References

1. Gamov G. Numerology of the constants of Nature. *Proc. Natl. Acad. Sci. USA*, Feb. 1968, v. 59(2), 313–318.
2. Ionescu L.M. Remarks on Physics as Number Theory, arXiv: 0309981, 2011.
3. Kocik J. The Koide Lepton Mass Formula and Geometry of Circles. arXiv: 1201.2067, 2012
4. Rhodes C. K. Unique Physically Anchored Cryptographic Theoretical Calculation of the Fine-Structure Constant α Matching both the g/2 and Interferometric High-Precision Measurements. arXiv: 1008.4537, 2012.
5. Good I.J. A quantal hypothesis for hadrons and the judging of physical numerology. In G. R. Grimmett (Editor), D.J.A. Welsh (Editor), Disorder in Physical Systems. Oxford University Press, 1990, p.141.
6. Fürth R. Über einen Zusammenhang zwischen quantenmechanischer Unscharfe und Struktur der Elementarteilchen und eine hierauf begründete Berechnung der Massen von Proton und Elektron. *Zeitschrift für Physik*, 1929, v. 57, 429–446.
7. Lenz F. The ratio of proton and electron masses. *Physical Review*, 1851, v. 82, 554.
8. Plouffe S. A search for a mathematical expression for mass ratios using a large database. viXra:1409.0099, 2014.
9. Reinhold E., Buning R., Hollenstein U., Ivanchik A., Petitjean P., Ubachs W. Indication of a cosmological variation of the proton-electron mass ratio based on laboratory measurement and reanalysis of H_2 spectra. *Physical Review Letters*, 2006, v. 96(15), 151101.
10. King J., Webb J., Murphy M., Carswell R. Stringent null constraint on cosmological evolution of the proton-to-electron mass ratio. *Physical Review Letters*, 2008, v. 101, 251304.
11. Murphy M. et al. Strong limit on a variable proton-to-electron mass ratio from molecules in the distant Universe. arXiv:0806.3081, 2008.
12. Bagdonaite J. A Stringent Limit on a Drifting Proton-to-Electron Mass Ratio from Alcohol in the Early Universe. *Science*, 4 January 2013, v. 339, no. 6115, 46–48.
13. Ade P.A.R. et al. Planck intermediate results. XXIV. Constraints on variation of fundamental constants. arXiv: 1406.7482, 2014.
14. Kragh H. Magic number: A partial history of the fine-structure constant. *Arch. Hist. Exact Sci.*, 2003, v. 57, 395–431.
15. Barrow D. John. The Constants of Nature. Vintage Books, 2004, p.93.
16. CODATA Value: proton-electron mass ratio. The NIST Reference on Constants, Units, and Uncertainty. US National Institute of Standards and Technology, June 2011.
17. Eddington A. New Pathways in Science. Cambridge University Press, 1935.
18. Kritov A. A new large number numerical coincidences. *Progress in Physics*, 2013, v. 10, issue 2, 25–28.
19. Lloyd S. Computational capacity of the universe. arXiv:quant-ph/0110141, 2001.
20. McGoveran D.O., Noyes H. P. Physical Numerology? Stanford University, 1987.
21. Parker-Rhodes A.F. The Theory of Indistinguishables: A Search for Explanatory Principles below the level of Physics. Springer, 1981.
22. Sirag S.P. A combination [combinatorial] derivation of the proton-electron mass ratio. *Nature*, 1977, v. 268, 294.
23. www.wolframalpha.com

Ives-Stilwell Time Dilation Li^+ ESR Darmstadt Experiment and neo-Lorentz Relativity

Reginald T. Cahill

School of Chemical and Physical Sciences, Flinders University, Adelaide 5001, Australia. Email: reg.cahill@flinders.edu.au

Botermann *et al* in *Test of Time Dilation Using Stored Li^+ Ions as Clocks at Relativistic Speed*, *Physical Review Letters*, 2014, 113, 120405, reported results from an Ives-Stilwell-type time dilation experiment using Li^+ ions at speed 0.338c in the ESR storage ring at Darmstadt, and concluded that the data verifies the Special Relativity time dilation effect. However numerous other experiments have shown that it is only neo-Lorentz Relativity that accounts for all data, and all detect a 3-space speed $V \approx 470$ km/s essentially from the south. Here we show that the ESR data confirms both Special Relativity and neo-Lorentz Relativity, but that a proposed different re-analysis of the ESR data should enable a test that could distinguish between these two theories.

1 Introduction

Botermann *et al* [1] reported results from an Ives-Stilwell [2, 3] time dilation experiment using Li^+ ions at speed $v = 0.338c$ in the ESR storage ring at Darmstadt, and concluded that the data verifies the Special Relativity time dilation effect, in (1). However numerous other experiments [4, 5] have shown that it is only neo-Lorentz Relativity that accounts for all of the data from various experiments, all detecting a 3-space speed $V \approx 470$ km/s approximately from the south, see Fig. 3. Here we show that the ESR data confirms neo-Lorentz Relativity, and that the ESR Darmstadt experimental data also gives $V \approx 470$ km/s.

2 Special or Lorentz Relativity?

The key assumption defining Special Relativity (SR) is that the speed of light in vacuum is invariant, namely the same for all observers in uniform relative motion. This assumption was based upon the unexpectedly small fringe shifts observed in the Michelson-Morley experiment (MM) 1887 experiment, that was designed to detect any anisotropy in the speed of light, and for which Newtonian physics was used to calibrate the instrument. Using SR, a Michelson interferometer should not reveal any fringe shifts on rotation. However using LR, a Michelson interferometer [4] can detect such anisotropy when operated in gas-mode, i.e. with a gas in the light paths, as was the case with air present in the MM 1887 experiment. The LR calibration uses the length contraction, from (4), of the interferometer arms. This results in the device being some 2000 times less sensitive than assumed by MM who used Newtonian physics. Reanalysis of the MM data then led to a significant light speed anisotropy indicating the existence of a flowing 3-space with a speed of some 500 km/s from the south. This result was confirmed by other experiments: Miller 1925/26 gas mode Michelson interferometer, DeWitte 1991 coaxial cable RF speeds, Cahill 2009 Satellite Earth-flyby Doppler shift NASA data [6], Cahill 2012 dual coaxial cable RF speed [7], Cahill 2013-2014 [8, 9] Zener diode 3-space quantum detectors. These and other experiments are reviewed in [4, 10]. All these experiments also revealed significant space flow turbulence, identified as gravitational waves in the 3-space flow [10]. However there are numerous experiments which are essentially vacuum-mode Michelson interferometers in the form of vacuum resonant optical cavities, see [11], which yield null results because there is no gas in the light paths. These flawed experimental designs are quoted as evidence of light speed invariance. So the experimental data refutes the key assumption of SR, and in recent years a neo-Lorentz Relativity (LR) reformulation of the foundations of fundamental physics has been underway, with numerous confirmations from experiments, astronomical and cosmological observations [12–14].

However of relevance here are the key differences between SR and LR regarding time dilations and length contractions. In SR, these are

$$\Delta t = \Delta t_0 / \sqrt{1 - v^2/c^2} \tag{1}$$

$$\Delta L = \Delta L_0 \sqrt{1 - v^2/c^2} \tag{2}$$

where v is the speed of a clock or rod with respect to the observer, c is the invariant speed of light, and subscript 0 denotes at rest time and space intervals. In SR, these expressions apply to all time and space intervals. However in LR, the corresponding expressions are

$$\Delta t = \Delta t_0 / \sqrt{1 - v_R^2/c^2} \tag{3}$$

$$\Delta L = \Delta L_0 \sqrt{1 - v_R^2/c^2} \tag{4}$$

where v_R is the speed of a clock or rod with respect to the dynamical 3-space, and where c is the speed of light with respect to the dynamical 3-space. In LR, these expressions only apply to physical clocks and rods, and so the so-called time dilation in SR becomes a clock slowing effect in LR, caused by the motion of clocks with respect to the dynamical 3-space. Only

by using (4) in place of (2) does the data from the Michelson-Morley and Miller gas-mode interferometers agree with the results from using other experimental techniques [5].

The interpretation of (1) and (3), relevant to the experiment discussed herein, is that if a time interval Δt_0 corresponds to 1 cycle of an oscillatory system at rest with respect to an observer in SR, or at rest with respect to space in LR, then $\nu_0 = 1/\Delta t_0$ is the frequency of the emitted photon. When the system is moving with speed v with respect to an observer, or with speed v_R with respect to space, then the time internal Δt_0 is increased, and the emitted photon frequency is decreased to $\nu = 1/\Delta t$.

Here the LR effects are applied to the frequencies of photons emitted by the moving Li^+ ions, to the Doppler shifts of these photons, and to the clock slowing of the two detectors that measure the detected photon frequencies.

Fig. 1 shows the direction of the 3-space flow as determined from NASA satellite Earth-flyby Doppler shifts [6], revealing that the flow direction is close to being South to North, which is relevant to the ESR Darmstadt experiment in which the Li^+ ions travel also from South to North.

Fig. 2 shows the simple circuit for the quantum detection of the 3-space velocity, The measured 3-space speeds are shown in Fig. 3, and follow from measuring the time delay between two such detectors, separated by 25 cm and orientated such that the maximum time delay is observed for the 3-space induced quantum tunnelling current fluctuations.

3 Special Relativity and Li$^+$ ESR Darmstadt experiment

The Li^+ ESR Darmstadt experiment measured the photon frequencies ν_N and ν_S at the two detectors, emitted by the ions moving North at speed $v = 0.338c$, see Fig. 4 Top. In SR, there are two effects: time dilation of the emitting source, giving emitted photons with frequency $\nu_0\sqrt{1 - v^2/c^2}$, from (1), where ν_0 is the frequency when the ions are at rest with respect to the two detectors. The second effect is the Doppler shift factors $1/(1 \pm v/c)$, giving the detected frequencies

$$\nu_N = \nu_0\sqrt{1 - v^2/c^2}/(1 - v/c) \tag{5}$$

$$\nu_S = \nu_0\sqrt{1 - v^2/c^2}/(1 + v/c). \tag{6}$$

Then

$$\nu_N\nu_S/\nu_0^2 = 1 \tag{7}$$

and this result was the key experimental test reported in [1], with the data giving

$$\sqrt{\nu_N\nu_S/\nu_0^2} - 1 = (1.5 \pm 2.3) \times 10^{-9}. \tag{8}$$

On the basis of this result it was claimed that the Special Relativity time dilation expression (1) was confirmed by the experiment.

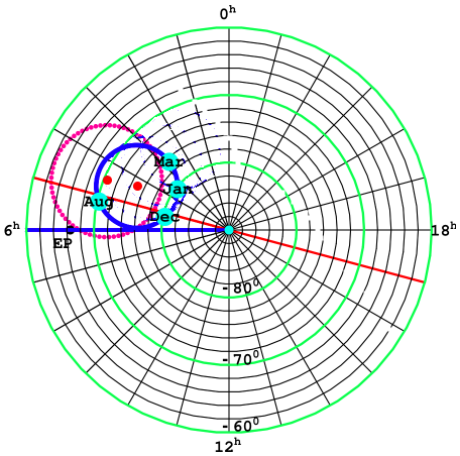

Fig. 1: South celestial pole region. The dot (red) at RA=4.3^h, Dec=75°S, and with speed 486 km/s, is the direction of motion of the solar system through space determined from NASA spacecraft Earth-flyby Doppler shifts [6], as revealed by the EM radiation speed anisotropy. The thick (blue) circle centred on this direction is the observed velocity direction for different months of the year, caused by Earth orbital motion and sun 3-space inflow. The corresponding results from the 1925/26 Miller gas-mode interferometer are shown by second dot (red) and its aberration circle (red dots). For December 8, 1992, the speed is 491km/s from direction RA=5.2^h, Dec=80°S, see Table 2 of [6]. EP is the pole direction of the plane of the ecliptic, and so the space flow is close to being perpendicular to the plane of the ecliptic.

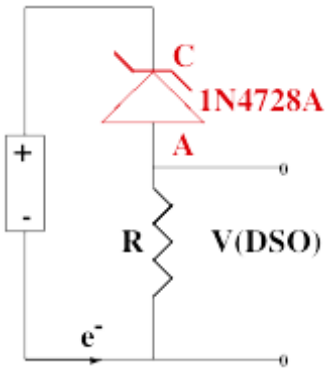

Fig. 2: Circuit of Zener Diode 3-Space Quantum Detector, showing 1.5 V AA battery, two 1N4728A Zener diodes operating in reverse bias mode, and having a Zener voltage of 3.3 V, and resistor R =10 KΩ. Voltage V across resistor is measured and used to determine the space driven fluctuating tunnelling current through the Zener diodes. Current fluctuations from two collocated detectors are shown to be the same, but when spatially separated there is a time delay effect, so the current fluctuations are caused by space speed fluctuations [8, 9]. Using more diodes in parallel increases S/N, as the measurement electronics has $1/f$ noise induced by the fluctuating space flow.

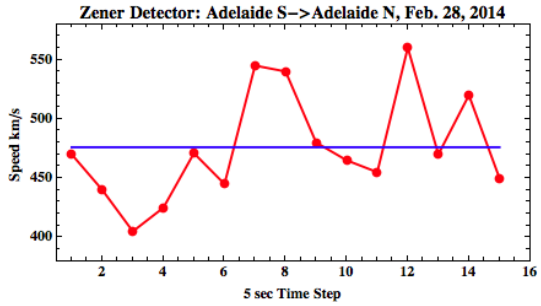

Fig. 3: Average speed, and speed every 5 sec, on February 28, 2014 at 12:20 hrs UTC, giving average speed = 476 ± 44 (RMS) km/s, from approximately S → N, using two Zener Diode detectors [9]. The speeds are effective projected speeds, and so do not distinguish between actual speed and direction effect changes. The projected speed = $V\cos\theta$, where θ is the angle between the space velocity V and the direction defined by the two detectors. V cannot be immediately determined with only two detectors. However by varying direction of detectors axis, and searching for maximum time delay, the average direction (RA and Dec) may be determined. As in previous experiments there are considerable fluctuations at all time scales, indicating a dynamical fractal structure to space.

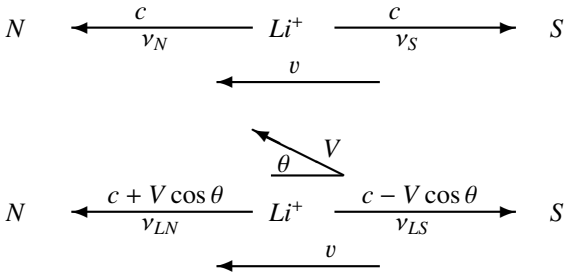

Fig. 4: **Top:** Special Relativity speed diagram with Li^+ ions travelling at speed v towards the North, emitting photons with speed c and frequency ν_N to the North, and speed c to the South with frequency ν_S, with all speeds relative to the detectors N and S frame of reference. The invariant speed of light is c. The photons are emitted with frequency ν_0 with respect to the rest frame of the ions.
Bottom: Neo-Lorentz Relativity speed diagram with space flow speed V at angle θ and Li^+ ions travelling at speed v towards the North, emitting photons with speed $c + V\cos\theta$ to the North and frequency ν_{LN}, and speed $c - V\cos\theta$ to the South and frequency ν_{LS}. $V\cos\theta$ is the projected space flow speed towards the North, with speeds relative to the detectors N and S frame of reference. The speed of light is c relative to the 3-space. The photons are emitted with frequency ν_0 with respect to the rest frame of the ions.

4 Lorentz Relativity and Li⁺ ESR Darmstadt experiment

In LR, expressions (5) and (6) are different, being

$$\nu_{LN} = \frac{\nu_0\sqrt{1-(v-V\cos\theta)^2/c^2-(V\sin\theta)^2/c^2}}{(1-v/(c+V\cos\theta))\sqrt{1-V^2/c^2}} \quad (9)$$

$$\nu_{LS} = \frac{\nu_0\sqrt{1-(v-V\cos\theta)^2/c^2-(V\sin\theta)^2/c^2}}{(1+v/(c-V\cos\theta))\sqrt{1-V^2/c^2}} \quad (10)$$

where $\nu_0\sqrt{1-(v-V\cos\theta)^2/c^2-(V\sin\theta)^2/c^2}$, from (3), is the expression for the lower emitted photon frequency with the ions moving at velocity

$$v_R = (v - V\cos\theta, -V\sin\theta) \quad (11)$$

with respect to the 3-space; with $1/(1-v/(c+V\cos\theta))$ and $1/(1+v/(c-V\cos\theta))$ being the Doppler shift factors as the photons have speed $c \pm V\cos\theta$ with respect to the detectors frame of reference; and $1/(1-V^2/c^2)$ being the time dilation effect for the clocks in the frequency measuring devices, as the slowing of these clocks, from (3), makes the detected frequency appear higher, as they have speed V with respect to the 3-space; see Fig. 4 Bottom. From (9) and (10) we obtain

$$\nu_{LN}\nu_{LS}/\nu_0^2 = 1 - \frac{v^2\sin^2\theta}{c^2(c^2-v^2)}V^2 + O[V^4] \quad (12)$$

which is identical to (7) to first order in V. We obtain

$$\sqrt{\nu_{LN}\nu_{LS}/\nu_0^2} - 1 = -\frac{v^2\sin^2\theta}{2c^2(c^2-v^2)}V^2 \quad (13)$$

and, for example, $V = 400$ km/s at an angle $\theta = 5°$, with $v = 0.338c$, gives

$$\sqrt{\nu_{LN}\nu_{LS}/\nu_0^2} - 1 = -0.9\times10^{-9} \quad (14)$$

which is nearly consistent with the result from [1] in (8). It is not clear from [1] whether the result in (8) is from the smallest values or whether it is from averaging data over several days, as the LR prediction varies with changing θ, as would be caused by the rotation of the earth. Here we have used $\theta = 5°$ which suggest the former interpretation of the data.

A more useful result follows when we examine the ratio ν_{LN}/ν_{LS} because we obtain a first order expression for V

$$V\cos\theta = \frac{c(c-v)^2}{2v^2}\left(\frac{c+v}{c-v} - \frac{\nu_{LN}}{\nu_{LS}}\right) \quad (15)$$

which will enable a more sensitive measurement of the projected $V\cos\theta$ value to be determined from the Li^+ ESR Darmstadt data. This result uses only the neo-Lorentz Doppler shift factors, and these have been confirmed by analysis of the Earth-flyby Doppler shift data [6]. $V\cos\theta$ will show space flow turbulence fluctuations and earth rotation effects, and over months a sidereal time dependence. The values are predicted to be like those in Fig. 3 from the 3-space quantum detectors. Indeed such a simple detection technique should be run at the same time as the Li^+ data collection. The data is predicted to give $V\cos\theta \approx 470$ km/s, as expected from Fig. 3. Then the Li^+ experiment will agree with results from other experiments [4–10].

Note that SR gives, from (5) and (6),

$$\left(\frac{c+v}{c-v}-\frac{\nu_N}{\nu_S}\right)=0 \qquad (16)$$

in contrast to (15).

5 Conclusions

The non-null experimental data, from 1887 to the present, all reveal the existence of a dynamical 3-space, with a speed $\approx$ 500 km/s with respect to the earth. Originally Lorentz proposed an aether moving through a static geometrical space. However the data and theory imply a different neo-Lorentz Relativity, with there being a dynamical fractal flowing 3-space, which possesses an approximate geometrical measure of distances and angles, which permits the geometrical description of relative locations of systems [5]. As well the dynamical theory for this 3-space has explained numerous gravitational effects, with gravity being an emergent quantum and EM wave refraction effect, so unifying gravity and the quantum [4, 10, 13–16]. An important aspect of Lorentz Relativity, which causes ongoing confusion, is that the so-called Lorentz transformation is an aspect of Special Relativity, but not Lorentz Relativity. The major result here is that the Li^+ ESR Darmstadt experimental data confirms the validity of both Special Relativity and neo-Lorentz Relativity, but only when the 3-space flow is nearly parallel to the NS orientation of the Li^+ beam. Then to distinguish between these two relativity theories one could use (15). This report is from the Flinders University Gravitational Wave Project.

Submitted on October 17, 2014 / Accepted on November 1, 2014

References

1. Botermann B., Bing D., Geppert C., Gwinner G., Hänsch T. W., Huber G., Karpuk S., Krieger A., Kühl T., Nörtershäuser W., Novotny C., Reinhardt S., Sánchez R., Schwalm D., Stöhlker T., Wolf A., and Saathoff G. Test of Time Dilation Using Stored Li^+ Ions as Clocks at Relativistic Speed. *Physical Review Letters*, 2014, v. 113, 120405
2. Ives H. E. and Stilwell G. R. An Experimental Study of the Rate of a Moving Atomic Clock. *Journal of the Optical Society of America*, 1938, v. 28, 215.
3. Ives H. E. and Stilwell G. R. An Experimental Study of the Rate of a Moving Atomic Clock II. *Journal of the Optical Society of America*, 1941, v. 31, 369.
4. Cahill R. T. Discovery of Dynamical 3-Space: Theory, Experiments and Observations - A Review. *American Journal of Space Science*, 2013, v. 1 (2), 77–93.
5. Cahill R. T. Dynamical 3-Space: Neo-Lorentz Relativity. *Physics International*, 2013, v. 4 (1), 60–72.
6. Cahill R. T. Combining NASA/JPL One-Way Optical-Fiber Light-Speed Data with Spacecraft Earth-Flyby Doppler-Shift Data to Characterise 3-Space Flow. *Progress in Physics*, 2009, v. 5 (4), 50–64.
7. Cahill R. T. Characterisation of Low Frequency Gravitational Waves from Dual RF Coaxial-Cable Detector: Fractal Textured Dynamical 3-Space. *Progress in Physics*, 2012, v. 8 (3), 3–10.
8. Cahill R. T. Nanotechnology Quantum Detectors for Gravitational Waves: Adelaide to London Correlations Observed. *Progress in Physics*, 2013, v. 9 (4), 57–62.
9. Cahill R. T. Gravitational Wave Experiments with Zener Diode Quantum Detectors: Fractal Dynamical Space and Universe Expansion with Inflation Epoch. *Progress in Physics*, 2014, v. 10 (3), 131–138.
10. Cahill R. T. Review of Gravitational Wave Detections: Dynamical Space, *Physics International*, 2014, v. 5 (1), 49–86.
11. Mueller H., Hermann S., Braxmaier C., Schiller S. and Peters A. Modern Michelson-Morley Experiment Using Cryogenic Optical Resonators *Physical Review Letters*, 2003, v. 91, 020401.
12. Cahill R. T. and Kerrigan D. Dynamical Space: Supermassive Black Holes and Cosmic Filaments. *Progress in Physics*, 2011, v. 7 (4), 79–82.
13. Cahill R. T. and Rothall D. P. Discovery of Uniformly Expanding Universe. *Progress in Physics*, 2012, v. 8 (1), 63–68.
14. Rothall D. P. and Cahill R. T. Dynamical 3-Space: Black Holes in an Expanding Universe. *Progress in Physics*, 2013, v. 9 (4), 25–31.
15. Cahill R. T. Dynamical Fractal 3-Space and the Generalised Schrödinger Equation: Equivalence Principle and Vorticity Effects. *Progress in Physics*, 2006, v. 2 (1), 27–34.
16. Cahill, R. T. Dynamical 3-Space: Emergent Gravity. In Should the Laws of Gravity be Reconsidered? Munera H. A., ed. Apeiron, Montreal, 2011, 363–376.

The Strong and Weak Forces and their Relationship to the Dirac Particles and the Vacuum State

William C. Daywitt

National Institute for Standards and Technology (retired), Boulder, Colorado. E-mail: wcdaywitt@me.com

This paper argues that the strong and weak forces arise from the proton and electron coupling to the Planck vacuum state. Thus they are not free space forces that act between free space particles, in contradistinction to the gravitational and electromagnetic forces. Results connect these four natural forces to the vacuum superforce.

1 Introduction

The Dirac particles (proton and electron) have been discussed in a number of previous papers [1] [2] [3] [4], where it is shown that they possess similar structures. Of interest here is the fact that they are both strongly coupled to the Planck vacuum (PV) state via a two-term coupling force that vanishes at their respective Compton radii. It is at these vanishing points where the strong and weak forces emerge. Consequently both forces are defined by the particle/PV coupling; i.e., they are not free space forces acting between free space particles.

What follows derives the strong and weak forces and calculates their relative strengths with respect to each other and with respect to the gravitational and electromagnetic forces. It is shown that these four forces are connected to the superforce associated with the PV (quasi-) continuum.

Strong Force

In its rest frame the proton core (e_*, m_p) exerts the following two-term coupling force (the Compton relations $r_e m_e c^2 = r_p m_p c^2 = r_* m_* c^2 = e_*^2$ are used throughout the calculations)

$$F_p(r) = \frac{(e_*)(-e_*)}{r^2} + \frac{m_p c^2}{r} = -F_s\left(\frac{r_p^2}{r^2} - \frac{r_p}{r}\right) \qquad (1)$$

on the PV continuum, where the proton Compton radius r_p ($= e_*^2/m_p c^2$) is the radius at which the force vanishes. The mass of the proton is m_p [3] and the bare charge e_* is massless. The radius r begins at the proton core and ends on any particular Planck-particle charge $(-e_*)$ at a radius r within the PV.

The strong force

$$F_s \equiv \left|\frac{(e_*)(-e_*)}{r_p^2}\right| = \frac{m_p c^2}{r_p} \qquad \left(= \frac{m_p m_* G}{r_p r_*}\right) \qquad (2)$$

is the magnitude of the two forces in the first sum of (1) where the sum vanishes. The (e_*) in (2) belongs to the free-space proton and the $(-e_*)$ to the separate Planck particles of the PV, where the first and second ratios in (2) are the vacuum polarization and curvature forces respectively. It follows that the strong force is a proton/PV force. The Planck particle mass m_* and Compton radius r_* are equal to the Planck Mass and Planck Length [5, p.1234].

Weak Force

The electron core $(-e_*, m_e)$ exerts the coupling force

$$F_e(r) = \frac{(-e_*)(-e_*)}{r^2} - \frac{m_e c^2}{r} = F_w\left(\frac{r_e^2}{r^2} - \frac{r_e}{r}\right) \qquad (3)$$

on the vacuum state and leads to the Compton radius r_e ($= e_*^2/m_e c^2$), where the first $(-e_*)$ in (3) belongs to the electron and the second to the separate Planck particles in the negative energy vacuum.

The weak force

$$F_w \equiv \frac{(-e_*)(-e_*)}{r_e^2} = \frac{m_e c^2}{r_e} \qquad \left(= \frac{m_e m_* G}{r_e r_*}\right) \qquad (4)$$

is the magnitude of the two forces in the first sum of (3) where the sum vanishes. Again, the first and second ratios in (4) are vacuum polarization and curvature forces. Thus the weak force is an electron/PV force.

2 Relative Strengths

The well known gravitational and electromagnetic forces of interest here are

$$F_g(r) = -\frac{m^2 G}{r^2} \qquad \text{and} \qquad F_{em}(r) = \pm\frac{e^2}{r^2} \qquad (5)$$

where r is the free-space radius from one mass (or charge) to the other.

The relative strengths of the four forces follow immediately from equations (2), (4), and (5):

$$\frac{F_w}{F_s} = \frac{r_p^2}{r_e^2} = \frac{m_e^2}{m_p^2} = \frac{1}{1836^2} \approx 3\times 10^{-7} \qquad (6)$$

$$\frac{|F_g(r_p)|}{F_s} = \frac{m_p^2 G/r_p^2}{e_*^2/r_p^2} = \frac{m_p^2(e_*^2/m_*^2)}{e_*^2} = \frac{m_p^2}{m_*^2} = \frac{r_*^2}{r_p^2} \approx 6\times 10^{-39} \qquad (7)$$

where $G = e_*^2/m_*^2$ [1] is used in the calculation, and

$$\frac{|F_{em}(r_p)|}{F_s} = \frac{e^2/r_p^2}{e_*^2/r_p^2} = \frac{e^2}{e_*^2} = \alpha \approx \frac{1}{137} \qquad (8)$$

where α is the fine structure constant.

3 Superforce

The relative strengths (6)–(8) agree with previous estimates and demonstrate that the free space forces

$$F_g(r_p) = -\frac{r_*^2}{r_p^2}\,F_s\,, \qquad F_g(r_e) = -\frac{r_*^2}{r_e^2}\,F_w \tag{9}$$

and

$$F_{em}(r_p) = \pm\alpha F_s\,, \qquad F_{em}(r_e) = \pm\alpha F_w \tag{10}$$

are related to the proton and electron coupling forces (1) and (3) through the strong and weak forces.

Equations (2) and (4) give precise definitions for the strong and weak forces, and are connected to the vacuum superforce via:

$$F_s = \left(\frac{r_*^2}{r_p^2}\right)\frac{e_*^2}{r_*^2} \qquad \text{and} \qquad F_w = \left(\frac{r_*^2}{r_e^2}\right)\frac{e_*^2}{r_*^2} \tag{11}$$

where

$$\text{superforce} \equiv \frac{e_*^2}{r_*^2} = \frac{m_* c^2}{r_*} \qquad \left(= \frac{m_*^2 G}{r_*^2}\right) \tag{12}$$

is the PV superforce to which Davies alludes [6, p.104]. The equality of the first and third ratios in (12) indicate that the degenerate vacuum state is held together by gravity-like forces.

The Newtonian force

$$-F_g(r) = \frac{m^2 G}{r^2} = \frac{(mc^2/r)^2}{c^4/G} =$$

$$= \frac{(mc^2/r)^2}{m_* c^2/r_*} = \left(\frac{mc^2/r}{m_* c^2/r_*}\right)^2 \frac{m_* c^2}{r_*} \tag{13}$$

is related to the superforce through the final expression, where $c^4/G\,(=\, m_* c^2/r_*)$ is the curvature superforce in the Einstein field equations [7]. The parenthetical ratio in the last expression is central to the Schwarzschild metrics [8] associated with the general theory.

Finally,

$$F_{em}(r) = \pm\frac{e^2}{r^2} = \pm\alpha\left(\frac{r_*^2}{r^2}\right)\frac{e_*^2}{r_*^2} \tag{14}$$

is the free space Coulomb force in terms of the vacuum polarization superforce.

Submitted on October 24, 2014 / Accepted on November 4, 2014

References

1. Daywitt W.C. The Planck Vacuum. *Progress in Physics*, v. 1, 20, 2009. See also www.planckvacuum.com.
2. Daywitt W.C. The Electron and Proton Planck-Vacuum Forces and the Dirac Equation. *Progress in Physics*, v. 2, 114, 2014.
3. Daywitt W.C. Why the Proton is Smaller and Heavier than the Electron. *Progress in Physics*, v. 10, 175, 2014.
4. Daywitt W.C. The Dirac Proton and its Structure. To be published in the International Journal of Advanced Research in Physical Science (IJARPS). See also www.planckvacuum.com.
5. Carroll B.W., Ostlie D.A. *An Introduction to Modern Astrophysics*. Addison-Wesley, San Francisco—Toronto, 2007.
6. Davies P. *Superforce: the Search for a Grand Unified Theory of Nature*. Simon and Schuster, Inc., New York, 1984.
7. Daywitt W.C. Limits to the Validity of the Einstein Field Equations and General Relativity from the Viewpoint of the Negative-Energy Planck Vacuum State. *Progress in Physics*, v. 3, 27, 2009.
8. Daywitt W.C. The Planck Vacuum and the Schwarzschild Metrics. *Progress in Physics*, v. 3, 30, 2009.

Lorentzian Type Force on a Charge at Rest. Part II

Rudolf Zelsacher

Infineon Technologies Austria AG, Siemensstrasse 2 A-9500 Villach. E-mail: Rudolf.zelsacher2@infineon.com

Some algebra and *seemingly* crystal clear arguments lead from the Coulomb force and the Lorentz transformation to the mathematical expression for the field of a moving charge. The field of a moving charge, applied to currents, has as consequences a magnetic force on a charge at rest, dubbed Lorentzian type force, and an electric field $\vec{E}$, the line integral of which, taken along a closed loop, is not equal to zero. Both consequences are falsified by experiment. Therefore we think that the arguments leading to the mathematical formulation of the field of a moving charge should be subject to a careful revision.

1 Citations

If someone asks me what time is, I do not know; if nobody asks me, I don't know either. [Rudolf Zelsacher]

2 Introduction

2.1 Miscellaneous

We will follow very closely the chain of thought taken by Edward Mills Purcell in [1]. We will use the Gaussian CGS units in order to underline the close relationship between electric field $\vec{E}$ and magnetic field $\vec{B}$.

Table 1: Definition of symbols

symbol	description
$j_x, \vec{J}$	current density
I	current
A, a	area
c	speed of light in vacuum
$v, \vec{v}$	speed, velocity
ϑ, α	angles
ω	anglular velocity
$N_e(x), n_e(x)$	current electron density, electron density
$\hat{R}$ etc.	unit vector in the direction of $\vec{R}$
$F(x, y, z, t)$, $F'(x', y', z', t')$	inertial systems in the usual sense as defined in e.g. [2]
β	$\frac{v}{c}$
$\vec{E}$	electric field
$\vec{B}$	magnetic field
q, Q, e, p	charge
h, a, r, R, s	distance
i, k, N, m	natural number variables
x, y, z	cartesian coordinates
t	time

2.2 The electric field $\vec{E}$ in F arising from a point charge q at rest in F′ and moving with $\vec{v}$ in F

The electric field $\vec{E}$ in F of a charge moving uniformly in F, at a given instant of time, is generally directed radially outward from its instantaneous position and given by [1]

$$\vec{E}(\vec{R}, \vartheta) = \frac{q(1-\beta^2)}{R^2(1-\beta^2 \sin^2 \vartheta)^{\frac{3}{2}}} \hat{R}. \tag{1}$$

R is the length of $\vec{R}$, the radius vector from the instantaneous position of the charge to the point of observation; ϑ is the angle between $\vec{v}\Delta t$, the direction of motion of charge q, and $\vec{R}$. Eq. 1, multiplied by Q, tells us the force on a charge Q at rest in F caused by a charge q moving in F (q is at rest in F').

3 Lorentzian type, i.e. magnetic like, force on a charge Q at rest

3.1 Boundary conditions that facilitate the estimation of the field characteristics

We have recently calculated the non-zero Lorentzian type force of a current in a wire on a stationary charge outside the wire by using conduction electrons all having the same speed [3]. We now expand the derivation given in [3] to systems with arbitrary conduction electron densities, i.e. to conduction electrons having a broader velocity range. Based on Eq. 1, describing the field of a moving charge, we derive geometric restrictions and velocity restrictions useful for our purposes. These boundary conditions allow the knowledge of important field characteristics, due to a non-uniform conduction electron density, at definite positions outside the wire.

3.1.1 The angular dependent characteristics of the field of a moving charge

For a given β, at one instant of time, the angle ϑ_c (theta change), between $\vec{R}$ and $\vec{v}\Delta t$, given by

$$\vartheta_c = \arcsin \frac{\left[1 - \left(1 - \beta^2\right)^{\frac{2}{3}}\right]^{\frac{1}{2}}}{\beta} \tag{2}$$

separates two regions: one where the absolute value of the field of the moving charge is less than $\frac{q}{R^2}$ and a second where the absolute value of the field of the moving charge is greater than $\frac{q}{R^2}$. For small velocities, e.g. $v = 2 \cdot 10^{-10}$ [cm/s], ϑ_c is $\approx \arcsin \sqrt{\frac{2}{3}}$ or about 54.7°. For $v = 2 \cdot 10^{10}$ [cm/s], ϑ_c is less than 60°. We will later need ϑ_c to estimate the effect of the field of conduction electrons at the position of a test charge Q. In Fig. 1 we have sketched in one quadrant the regions where the absolute value of the field of the moving charge is separated by ϑ_c. $2 \cdot 10^{10}$ cm/s or $2c/3$ is just an arbitrarily chosen and of course sufficiently high speed limit for conduction electrons to be used in our estimations.

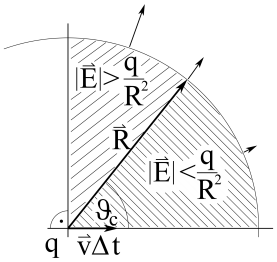

$$\vartheta_c = \arcsin \frac{\left(1 - \left(1 - \beta^2\right)^{\frac{2}{3}}\right)^{\frac{1}{2}}}{\beta}$$

for $v < c$

$$\vartheta_c \cong \arcsin\left(\sqrt{\frac{2}{3} + \frac{\beta^2}{9} + \frac{4\beta^4}{81} \cdots}\right)$$

(for $v = 2e^{10}[cms^{-1}]$ $\vartheta_c < 60°$)

(for $v \ll c$

$$\vartheta_c = \arcsin \frac{\sqrt{2}}{\sqrt{3}} \cong 54.7°$$

Fig. 1: The angle ϑ_c separates the region where the absolute value of the field of a moving charge is greater than $\frac{q}{R^2}$ from the region where the absolute value of the field of the moving charge is less than $\frac{q}{R^2}$.

3.1.2 The conduction electron density of a stationary current in a metal wire

We will use neutral wires and apply an electromotive force so that currents will flow in the wires. We also have in mind superconducting wires; at least we cool down the wires to near 0°[K] to reduce scattering. As in [1] we will restrict our investigation to a one dimensional current i.e. to velocities in one direction (v_x). A stationary current I, the number of electrons passing a point in a wire per unit of time, is then given by

$$I = \int \vec{j} d\vec{a} = A\,(-e)\,N_e\,(x)\,\bar{v}_x\,(x) \tag{3}$$

where A is the cross section of the wire, $\vec{j}$ or component j_x is the current density, $N_e(x)$ is the local conduction electron density and $\bar{v}_x(x)$ is the local mean velocity of the conduction electrons. For a stationary current $div\vec{j} = 0$. This indicates that there can be no permanent pile up of charges anywhere in the wire. From our discussion with regard to ϑ_c in section 3.1.1 we know that for restricted velocities v_x of the conduction electrons and restricted angles ϑ the absolute value of the field of the conduction electron $\frac{e(1-\beta^2)}{r^2(1-\beta^2 \sin^2 \vartheta)^{\frac{3}{2}}}$, at the position of the test charge Q, is either greater than $\frac{e}{r^2}$ or less than $\frac{e}{r^2}$.

3.1.3 The line integral of the field of a moving charge

The field of a moving charge at an instant t_0 cannot be compensated by any stationary distribution of charges. The reason is that for the field of a moving charge in general

$$\oint \vec{E} d\vec{s} \neq 0. \tag{4}$$

We will use this property to estimate whether a variable electron density $n_e(x)$ along a wire can compensate the field due to the moving conduction electrons. In addition we will use this fact to show that currents in initially neutral wires produce electric fields whose line integral along a closed loop is non-zero.

3.2 The force of a pair of moving charges on a resting charge

In Fig. 2 we show two charges q_n and q_p moving in lab and a test charge Q at rest in lab. The indices n & p were chosen to emphasize that we will later use a negative elementary charge and a positive elementary charge, and calculate the effect of such pairs, one moving and the other stationary, on a test charge Q at rest in lab.

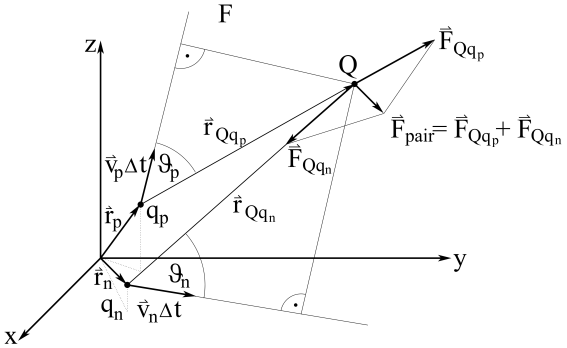

Fig. 2: The force $\vec{F}_{pair}$ on a resting charge Q caused by the two moving charges q_n and q_p. We assign the name $\vec{F}_{pair}$ to the result of the calculation of a force on a resting test charge Q, by at least two other charges having different velocities (including $\vec{v} = \vec{0}$).

The force $\vec{F}_{pair}$ exerted by this pair of charges, of q_n and

q_p, on the test charge Q is, according to Eq. 1, given by

$$\vec{F}_{pair} = \vec{F}_{Qq_p} + \vec{F}_{Qq_n} = \\ = \frac{q_p Q\left(1-\frac{\vec{v}_p^2}{c^2}\right)\hat{r}_{Qq_p}}{\vec{r}^2_{Qq_p}\left(1-\frac{\vec{v}_p^2}{c^2}\sin^2\vartheta_p\right)^{\frac{3}{2}}} + \frac{q_n Q\left(1-\frac{\vec{v}_n^2}{c^2}\right)\hat{r}_{Qq_n}}{\vec{r}^2_{Qq_n}\left(1-\frac{\vec{v}_n^2}{c^2}\sin^2\vartheta_n\right)^{\frac{3}{2}}}. \quad (5)$$

We are going to use such pairs of charges – specifically a conduction electron $(-e)$, and its partner, the nearest stationary proton (e) – in a current carrying wire and investigate the non vanishing field in lab produced by such pairs outside the wire. "Stationary" (or resting, or at rest) indicates that the "stationary charges" retain their mean position over time.

3.3 Lorentzian type force, part 1

We consider now two narrow wires isolated along their length, but connected at the ends, each having length 2a and lying in *lab* coaxial to the x-axis of F from $x = -a$ to $x = a$. In addition the system has a source of electromotive force applied so that a current I is flowing through the wires; in one of the wires I flows in the positive x direction and in the other wire I flows in the negative x direction. We also have in mind superconducting wires. On the z-axis of F fixed (stationary) at (0, 0, h) a test charge Q is located. The system is sketched in Fig. 3. We will now calculate the Lorentzian type force $\vec{F}_{Lt}$ on the stationary test charge Q fixed at (0, 0, h) exerted by the electrons of the current I and their nearest stationary protons at an instant t_0.

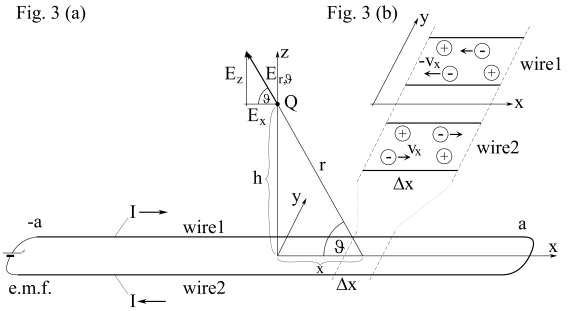

Fig. 3: (a) (b): We show in Fig. 3(a) the two wires carrying the current I extended along the x axis of F from $x = -a$ to $x = a$ and the charge Q at rest in F at (0, 0, h). Additionally on the right-hand side a magnification of a small element Δx containing the two wires and labeled Fig. 3(b) can be seen. Fig. 3(b) shows some moving electrons and for each of these the nearest neighboring proton situated in the tiny element. We calculate the force on Q by precisely these pairs of charges.

The two wires are electrically neutral before the current is switched on. Therefore after the current is switched on we have an equal number of N electrons and N protons in the system - the same number N, as with the current switched off. We look at the system at one instant of *lab* time t_0, after the current I is switched on and is constant. We consider the k electrons that make up the current I. For each of these k electrons e_i with $i = 1, 2, ..k$, having velocity $v_{x,i}$, we select the nearest neighboring stationary proton p_i with $i = 1, 2, ..k$. "Stationary" means that the charges labeled stationary retain their mean position over time. For each charge of the mobile electron-stationary proton pair, we use the same $\vec{r}_i$ as the vector from each of the two charges to Q. We use $\vartheta_i = \arcsin\frac{h}{r_i}$ as the angle between the x-axis and $\vec{r}_i$ for each pair of charges. As long as the velocity $v_{x,i}$ of a conduction electron is less than $2 \cdot 10^{10}[cm/s]$ and the angle $\vartheta_i = \arcsin\frac{h}{r_i}$, between the x-axis and the vector $\vec{r}_i$ from the current electron to test charge Q, is greater than 60°(and less than 120°), the contribution of the current electron to the absolute value of the field at (0,0,h) is, according to our discussion in section 3.1.1, greater than $\frac{e}{r_i^2}$. The contribution of the nearest proton that completes the pair is $\frac{e}{r_i^2}$. If we restrict ϑ_i to between 60°and 120°, we will have an electric field $\vec{E} \neq \vec{0}$ at the position of Q pointing towards the wire. The Lorentzian type force $\vec{F}_{Lt}$ on the stationary test charge Q is then given by

$$\vec{F}_{Lt} = Qe\sum_i\left\{\left|\frac{\cos\vartheta_i}{r_i^2}\right|(-1)^{m_i}\left(1-\frac{\left(1-\frac{v_{x,i}^2}{c^2}\right)}{\left(1-\frac{v_{x,i}^2}{c^2}\sin^2\vartheta_i\right)^{\frac{3}{2}}}\right)\hat{x}+ \right. \\ \left. +\frac{\sin\vartheta_i}{r_i^2}\left(1-\frac{\left(1-\frac{v_{x,i}^2}{c^2}\right)}{\left(1-\frac{v_{x,i}^2}{c^2}\sin^2\vartheta_i\right)^{\frac{3}{2}}}\right)\hat{z}\right\} = S_{Lt}\hat{S}. \quad (6)$$

The m_i ($m_i = 0$ if $x_{e_i} - x_Q < 0, m_i = 1$ if $x_{e_i} - x_Q > 0$) ensures the correct sign for the x-component of the force. Eq. 6 shows that an equal Number N of positive and negative elementary charges (the charges of the wire loop) produces a force on a stationary charge, when a current is flowing. This force can be written as

$$\vec{F}_{Lt} = F_{x,Lt}\hat{x} + F_{z,Lt}\hat{z} = \\ = \frac{\sqrt{F_{x,Lt}^2 + F_{z,Lt}^2}}{\sqrt{F_{x,Lt}^2 + F_{z,Lt}^2}}\left(F_{x,Lt}\hat{x} + F_{z,Lt}\hat{z}\right) = S_{Lt}\hat{S} \quad (7)$$

with the unit vector $\vec{\hat{S}}$ pointing from the position of the test charge $Q(0, 0, h)$ to a point $X(-a < X < a)$ on the x-axis. X will probably not be far from zero, but we leave this open as the resulting force vector $\vec{F}_{Lt} = S_{Lt}\vec{\hat{S}}$ depends on the local current electron density in the wire. Note that $\frac{\left(1-\frac{v_{x,i}^2}{c^2}\right)}{\left(1-\frac{v_{x,i}^2}{c^2}\sin^2\vartheta_i\right)^{\frac{3}{2}}}$ is greater than 1 as long as $v_{x,i} < 2 \cdot 10^{10}$ [cm/s] and 60°<

ϑ_i <120°, as was shown in section 3.1.1 This means the field at (0, 0, h) points to the wire.

3.4 Lorentzian type force, part 2

Next we place the stationary charge Q at the position $(b > a, 0, h)$, with $\vartheta_{max} = \arctan\frac{h}{b-a} < 54°$ (see Fig. 4).

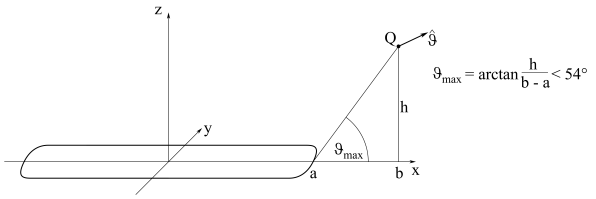

Fig. 4: If the test charge Q, is located at $(b, 0, h)$ as shown here, with $\vartheta_{max} = \arctan\frac{h}{b-a}$ <54°, then the absolute value of the field of each of the conduction electrons at $(b, 0, h)$ is less than that of a stationary charge for all velocities $0 < v_x < c$.

The force on the stationary test charge Q is given by Eq. 6. But now $\frac{\left(1-\frac{v_{x,i}^2}{c^2}\right)}{\left(1-\frac{v_{x,i}^2}{c^2}\sin^2\vartheta_i\right)^{\frac{3}{2}}}$ is less than 1 for $0 < v_{x,i} < 3\cdot 10^{10}$ [cm/s] and $0° < \vartheta_i < 54°$ or $136° < \vartheta_i < 180°$ as was shown in section 3.1.1. This means the field at $(b, 0, h)$ points away from the wire.

3.5 The line integral of the field of two parallel wires calculated at one instant t_0

We continue by estimating a specific line integral of the electric field outside the wire along the closed path shown in Fig. 5.

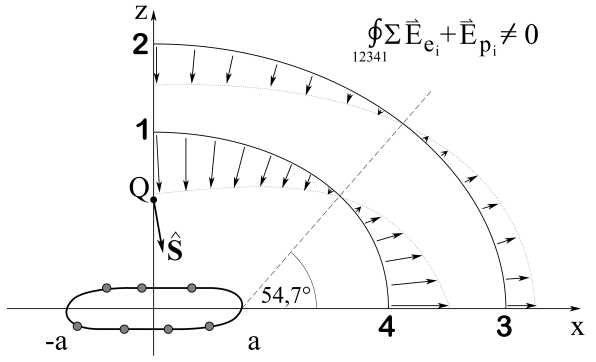

Fig. 5: Shows the electric field $\sum(\vec{E}_{e_i} + \vec{E}_{p_i})$ due to the moving conduction electrons and their partner protons of the system of Fig. 3. In addition the path 12341 is shown where the line integral of the electric field $\sum(\vec{E}_{e_i} + \vec{E}_{p_i})$ is estimated. $\vec{E}_s + \vec{E}_Q$, the field of the residual stationary charges of the system and the test charge Q, is not shown because the line integral of the field $\vec{E}_s + \vec{E}_Q$, along a closed path is zero.

The electric field of the system is a superposition of the field of the moving conduction electrons and their stationary partner protons $\sum(\vec{E}_{e_i} + \vec{E}_{p_i})$, the field $\vec{E}_s$ of the residual stationary electrons and protons of the wire and the field $\vec{E}_Q$ of the resting test charge Q. The line Integral of $\vec{E}_s + \vec{E}_Q$ along every closed path is zero. The line integral of the electric field $\sum(\vec{E}_{e_i} + \vec{E}_{p_i})$ due to the moving conduction electrons and their partner protons is, according to our discussion in section 3.1.1 and the results given by Eq. 6 at positions like (0, 0, h) and (b, 0, h), less than zero from 1 to 2, zero from 2 to 3 (because here we have chosen a path perpendicular to the field), less than zero from 3 to 4 and zero from 4 to 1 (because here we have again chosen a path perpendicular to the field).

$$\oint_{12341}\vec{E}d\vec{s} = \oint_{12341}\left(\sum\left(\vec{E}_{e_i}+\vec{E}_{p_i}\right)+\vec{E}_s+\vec{E}_Q\right)d\vec{s} = \\ = \left[\oint_1^2\left(\sum\vec{E}_{e_i}+\vec{E}_{p_i}\right)d\vec{s}+\oint_3^4\left(\sum\vec{E}_{e_i}+\vec{E}_{p_i}\right)d\vec{s}\right] < 0. \tag{8}$$

A wire bent like the loop 12341 might be a good device for the experimental detection of $\vec{F}_{Lt}$. As we have mentioned in section 3.1.2 we do not expect pile-up effects of charges in the wire because from experiment we know the extreme precision to which Ohm's Law, is obeyed in metals. But we expect a variable electron density $n_e(x)$ (not to be confused with the variable conduction electron density $N_e(x)$) on the wires resulting from capacitive and shielding effects, together with the field component of the moving conduction electrons directed along the wire. The estimation of the line integral of the electric field of the system, resulting in Eq. 8, shows, by being non-zero, that no "stationary" static charge distribution on the wires is able to compensate the field due to the moving conduction electrons.

3.6 The force on a charge at rest due to a superconducting ring

We consider now a superconducting current carrying ring, with radius a, and assume that one of its conduction electrons e_i at t_0, at rest in its local inertial frame, has constant velocity $\vec{v}_i = \vec{\omega}_i \times \vec{r}_i$. Then, according to Eq. 5 and Fig. 6 the Lorentzian type force on a charge Q at rest at $(0, 0, h)$ caused by this system is given by

$$\vec{F}_{Lt} = \sum_i \frac{Qe}{r_i^2+h^2}\left[1-\frac{1}{\left(1-\beta_i^2\right)^{\frac{1}{2}}}\right]\cos\arctan\frac{a}{h}\hat{z} \tag{9a}$$

or if $v \ll c$

$$\vec{F}_{Lt} \approx \sum_i \frac{Qe}{r_i^2+h^2}\left[1-1-\frac{\beta_i^2}{2}\right]\cos\arctan\frac{a}{h}\hat{z} = \\ = \sum_i -\frac{Qv_i}{c}\frac{ev_i}{2\left(r_i^2+h^2\right)c}\cos\arctan\frac{a}{h}\hat{z}. \tag{9b}$$

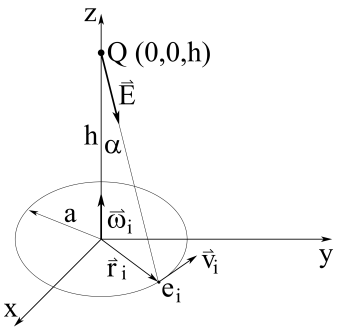

Fig. 6: The electrical field, at the position of a charge Q at rest, caused by one of the charges e_i of the current in a superconducting wire.

As stated above we assume that the current carriers are at rest in a succession of individual local inertial frames when circling in the loop; i.e. the movement of the charges is well described by a polygon, with as many line segments as you like it. This view is supported by the experimental fact that currents flow for years in such loops without weakening, showing that the passage from one inertial frame to the next happens without much radiation.

3.7 The Field due to a constant electron density in the parallel wires connected at the ends

We now proceed to the case where the current electron density $N_e(x)$ is constant along the wires *by definition* to get an analytic expression for the force $\vec{F}_{Lt}$ on a stationary charge. This was calculated in [3] and here we just rewrite the result. The Lorentzian type force on a charge Q at rest due to a system like that shown in Fig. 2 is, by assuming a constant current electron density, given by

$$\vec{F}_{Lt} = -\frac{Qv_x}{c}\frac{2I\cos\vartheta_{min}\sin^2\vartheta_{min}}{hc^2}\hat{z}. \qquad (10)$$

The force described by Eq. 10 is of the same order of magnitude as magnetic forces, as can be seen by comparing it to Eq. 11, the result of a similar derivation given in [1]

$$\vec{F} = \frac{qv_x}{c}\frac{2I}{rc^2}\hat{y}. \qquad (11)$$

4 Discussion

The one and only way to scientific truth is the comparison of theoretical conclusions with the experimental results. We have investigated the consequences of Eq. 1 - the elegant mathematical formulation of the field of a moving charge. By applying the field of a moving charge to currents in loops we derive a magnetic force on a charge at rest outside these loops. We have dubbed this force "Lorentzian type force" and state that such a force has never been observed in experiments. In addition such current-carrying systems, when investigated by using the mathematical expression for the field of a moving charge, show an electric field whose line integral along a closed loop is non-zero. Also this prediction has never been observed by experimental means. We find the example of the Lorentzian type, i.e. magnetic, force on a charge at rest due to the superconducting ring (as given in 3.6), which also has been never observed, to be especially instructive because nothing disturbs the intrinsic symmetry. The overall conclusion from our investigation is that the arguments leading to the formula for the field of a moving charge should be subject to a careful revision.

Acknowledgements

I am grateful to Thomas Ostermann for typesetting the equations and to Andrew Wood for correcting the English.

Submitted on November 20, 2014 / Accepted on November 22, 2014

References

1. Purcell E.M. Electricity and Magnetism, McGraw-Hill Book Company, New York, 1964.
2. Kittel C. et al, Mechanics 2^{nd} Edition, McGraw-Hill Book Company, New York, 1973.
3. Zelsacher R. Lorentzian Type Force on a Charge at Rest. *Progress in Physics*, 2014, v. 10(1), 45–48.

Gauge Freedom and Relativity: A Unified Treatment of Electromagnetism, Gravity and the Dirac Field

Clifford Chafin

Department of Physics, North Carolina State University, Raleigh, NC 27695. E-mail: cechafin@ncsu.edu

The geometric properties of General Relativity are reconsidered as a particular nonlinear interaction of fields on a flat background where the perceived geometry and coordinates are "physical" entities that are interpolated by a patchwork of observable bodies with a nonintuitive relationship to the underlying fields. This more general notion of gauge in physics opens an important door to put all fields on a similar standing but requires a careful reconsideration of tensors in physics and the conventional wisdom surrounding them. The meaning of the flat background and the induced conserved quantities are discussed and contrasted with the "observable" positive definite energy and probability density in terms of the induced physical coordinates. In this context, the Dirac matrices are promoted to dynamic proto-gravity fields and the keeper of "physical metric" information. Independent sister fields to the wavefunctions are utilized in a bilinear rather than a quadratic lagrangian in these fields. This construction greatly enlarges the gauge group so that now proving causal evolution, relative to the physical metric, for the gauge invariant functions of the fields requires both the stress-energy conservation and probability current conservation laws. Through a Higgs-like coupling term the proto-gravity fields generate a well defined physical metric structure and gives the usual distinguishing of gravity from electromagnetism at low energies relative to the Higgs-like coupling. The flat background induces a full set of conservation laws but results in the need to distinguish these quantities from those observed by recording devices and observers constructed from the fields.

1 Introduction

The theories (special and general) of relativity arose out of an extension of notions of geometry and invariance from the 19th century. Gauge freedom is an extension of such ideas to "internal" degrees of freedom. The gauge concept follow from the condition that quantities that are physically real and observable are generally not the best set of variables to describe nature. The observable reality is typically a function of the physical fields and coordinates in a fashion that makes the particular coordinates and some class of variations in the fields irrelevant. It is usually favored that such invariance be "manifest" in that the form of the equations of motion are evidently independent of the gauge. Implicit in this construction is the manifold-theory assumption that points have meaning and coordinate charts do not. We are interested in the largest possible extension of these ideas so that points themselves have no meaning and gauge equivalence is defined by mappings of one solution to another where the observers built of the underlying fields cannot detect any difference between solutions. This is the largest possible extension of the intuitive notion of relativity and gauge. It will be essential to find a mathematical criterion that distinguishes this condition rather than simply asserting some gauge transformation exists on the lagrangian and seeking the ones that preserve this. This leads us to consider a more general "intrinsic" reality than the one provided by manifold geometry but, to give a unified description of the gravitational fields and the fields that are seen to "live on top of" the manifold structure it induces requires we provide an underlying fixed coordinate structure. The physical relevance, persistence and uniqueness of this will be discussed, but the necessity of it seems unavoidable.

Initially we need to reconsider some aspects of the particular fields in our study: the metric, electromagnetic and Dirac fields. The Dirac equation is interesting as a spinor construction with no explicit metric but an algebra of gamma-matrices that induce the Minkowskii geometry and causal structure. There are many representations of this but the algebra is rigid. The general way to include spinors in spacetime is to use a nonholonomic tetrad structure and keep the algebra the same in each such defined space. We are going to suggest an initially radical alteration of this and abandon the spinor and group notions in these equations and derive something isomorphic but more flexible that does not require the vierbein construction. It is not obvious that this is possible. There are rigid results that would seem to indicate that curvature necessitates the use of vierbeins [1]. These are implicitly built on the need for ψ itself to evolve causally with respect to the physical metric (in distinction with the background metric). We will extend the lagrangian with auxiliary fields so that this is not necessary but only that the gauge invariant functions of the *collective* reality of these fields evolve causally. This is a subtle point and brings up questions on the necessity of the positive definiteness of energy, probability, etc. as defined by the underlying (but not directly observable) flat space.

Let us begin with a brief discussion of the Dirac equation and this modification. The Dirac equation is the fundamental description for electrons in quantum theory. It is typically derived in terms of causality arguments and the need for an equation of motion that is first order in time, as was Dirac's approach, or, more formally, in terms of representation theory of the Lorentz group. These arguments are discussed many places [2–4]. While this is a powerful description and has led to the first inclination of the existence of antiparticles, it has its own problems. Negative energy solutions have had to be reconciled by Dirac's original hole theory or through the second quantization operator formalism. Most are so steeped in this long established perspective and impressed by its successes that it gets little discussion.

A monumental problem today is that of "unification" of quantum theory and gravity. There are formal perturbative approaches to this and some string theory approaches as well. In quantum field theory we often start with a single particle picture as a "classical field theory" and then use canonical quantization or path integral methods. For this reason, it is good to have a thorough understanding of the classical theory to be built upon. We will show that, by making some rather formal changes in traditional lagrangians, some great simplifications can result. The cost is in abandoning the notions that the fields corresponding to nature are best thought of as evolving on the "intrinsic" geometry induced by a metric and that spacetime is a locally Lorentzian manifold. In place of this is a trivial topological background and a reality induced by fields which encodes the observable reality and apparent coordinates (induced by collections of objects) and metrical relationships in a non-obvious fashion. Usual objections to such a formalism in the case of a gravitational collapse are addressed by adherence to the time-frozen or continued collapse perspective.

A main purpose of this article is to illustrate an alternate interpretation of the Dirac equation. In the course of it, we will make gravity look much more like the other bosonic fields of nature and give a true global conservation law (that is generally elusive in GR). Our motivation begins with a reconsideration of the spinor transformation laws and the role of representation theory. This approach will greatly expand the gauge invariance of the system. In place of the metric $g_{\mu\nu}$ as the keeper of gravitational information, we will let the γ matrices become dynamic fields and evolve. Our motivation for this is that, for vector fields, the metric explicitly appears in each term and variation of it, gives the stress-energy tensor. The only object directly coupling to the free Dirac fields is γ. Additionally, γ^μ bears a superficial resemblance to A^μ and the other vector bosons. Since $g \sim \gamma\gamma$ we might anticipate that the spin of this particle is one rather than two as is for the graviton theories which are based explicitly on $g^{\mu\nu}$. It is because we only require our generalized gauge invariant functions to obey causality and that these conserved quantities, while exact, are not directly observable so do not have to obey positive definiteness constraints that this approach can be consistent.

We will be able to show that this construction can give GR evolution of packets in a suitable limit and obeys causal constraints of the physical metric. It is not claimed that the evolution of a delocalized packet in a gravitational field agrees with the spinor results in a curved spacetime. This will undoubtably be unsatisfactory to those who believe that such a theory is the correct one. In defense, I assert that we do not have any data for such a highly delocalized electron in a large nonuniform gravitational field and that the very concept of spinor may fail in this limit. As long as causality holds, this should be considered an alternate an viable alternative theory of the electron in gravity. The purely holonomic nature of the construction is pleasing and necessary for a theory built on a flat background. A unification of gravity in some analogous fashion to electroweak theory would benefit from having a its field be of the same type. One might naturally worry about the transformation properties of ψ_a and γ^μ_{ab} in this construction. Under coordinate transformations of the background, ψ_a behaves as a scalar not a spinor and γ^μ_{ab} is a vector. One should not try to assign to much physical meaning to this since these transformations of the structure are passive. Active transformations where we leave the reality of all the surrounding and weakly coupled fields the same but alter the electron of interest can be manifested by changes in both ψ and γ (and A) so that the local densities and currents describing it are boosted and those of the other fields are not. The usual active boost $\psi'_b = S(\Lambda)_{ba}\psi_a$ is included as a subset of this more general gauge change.

There has been work from the geometric algebra perspective before [5] in trying to reinterpret the Dirac and Pauli matrices as physically meaningful objects. Since the author has labored in isolation for many years searching for a physical meaning for the apparent geometric nature of physical quantities this did not come to his attention until recently. However, there are significant differences in the approach presented here and the easy unification with gravity that follows seems to depend on abandoning group representation theory in the formulation. Most importantly, one has a new notion of gauge freedom as it relates to the reality expressed by particle fields (i.e. the full gauge independent information associated with it). Coupling destroys the ability to associate the full "reality" of the electron with the wavefunction. We will see that this can get much more entangled when one includes gravity and, with the exception of phase information, the only consistent notion of a particle's reality comes from the locally conserved currents that can be associated with it. Here will involve multiple field functions not just ψ_a as in the free particle case.

The dominant approaches to fundamental physics has been strongly inspired by the mathematical theory of manifolds where a set of points is given a topology and local coordinate chart and metric structure. The points have a reality

in this construction and the charts are grouped into atlases so that coordinates are "pure guage" and no physical reality is associated with them. We frequently say that the invariance of the field's equations requires that we have a metric invariant action be a scalar. It can be shown somewhat easily [6] that this is not true and that most lagrangians that give many common (local) field equations are neither invariant nor local. In the following we enlarge the class of physically equivalent fields to the set of fields that evolve in such a fashion where the "observers" built from the fields cannot distinguish one description from another. This includes simple spacetime translations of a flat space of the entirety of fields and far more general deformations of the fields which do not preserve the underlying set of points.

The underlying space is chosen trivially flat with the $\eta^{\mu\nu}$ metric. This begs the question of how general curved coordinates resulting from the effective curvature induced by the field $g^{\mu\nu}(\gamma)$ relate to it and how the causally connected structure induced by the fields evolves through this flat background. In this picture the "physical coordinates" seen by observers are measures induced by "candles," specifically highly independent localized objects and radiators, that induce his perception of his surroundings. Clocks are induced by atomic oscillations and other local physical processes. Collective displacements and alterations of the fields on the underlying flat space that preserve the preserved reality are considered alternate representations of the same physical reality rather than an active transformation of it to a new and distinct one, as one would expect from the usual manifold founded perspective.

At the foundations of manifold inspired physics are tensors and their transformation rules under coordinate changes. In this case we have little interest in the transformations with respect to the underlying flat space and all fields are treated as trivial tensors with respect to it. The interesting case of apparent curvature must then be measured with respect to these local candles. The vector properties of functions of a field, like the current $j^{\mu}_{(0)} = \bar{\psi}_{(0)}\gamma^{\mu}\psi_{(0)}$, are then the collective result of active transformations of the $\psi_{(i)}$, γ and underlying coordinates that leave the nearby candles' (labelled by i) gauge invariant features unchanged and a transformation of the field $\psi_{(0)}$ so that the resulting current $j_{(0)}$ appears to move through a full set of Lorentz boosts and rotations relative to measurements using these candles.

This is a significant departure from the usual geometry inspired approach. Not surprisingly many formulas will appear (deceptively) similar to usual results despite having very different meaning since they will all be written with respect to the underlying flat structure not some "physical coordinates" with respect to some fixed point set induced by the candles. The mystery of how we arrive at a geometric seeming reality and at what energy scale we can expect this to fail is a main motivation for this article. Conservation laws follow from the usual ten Killing vectors of flat space but the meaning of these conservation laws (and their form in terms of observable quantities) is unclear. Even the positive definiteness of quantities like energy and mass density are not assured and failure of them do not carry the same consequences as in usual metric theories. The symmetry responsible for mass conservation is the same one as for probability so such a situation raises more questions that must be addressed along the way. We have been nonspecific about the details of what determines equivalent physical configurations. Aside from the geometry induced by candles the gauge invariant quantities that we presume are distinguishable by observers are those induced by conserved currents such as mass and stress-energy. It is not obvious why such should be the case. A working hypothesis is that all observers are made up of long lasting quasilocalized packets of fields that determine discrete state machines and these are distinguished by localized collections of mass, charge and other conserved quantities.

In this article we only discuss these as classical theories in a 4D spacetime. Of course, the motivation is for this to lead to a general quantum theory. There is a lot of work on reinterpretation of quantum theory as a deterministic one. Everyone who works on this has his favorite approach. The author here is no exception and has in mind a resolution that is consistent with the theory in [7] that gives QM statistics assuming that particular far-from-eigenstate wavefunctions describe classical matter that arise in an expanding universe with condensing solids. The motivations behind the following constructions is not just to get some insight on unification but to take steps to resolve some of the fundamental contradictions of quantum field theory, such as Haag's theorem, and to give a solid justification for the calculations of field theory that have been successful.

The structure of the article will be as follows. Invariance and the nature of causality are discussed and contrasted with the usual flat background approach in §2. This is especially subtle since the "physical" metric, reality and coordinate features are encoded in this construction in nonobvious ways, the gauge group is large and some conserved quantities and expected positive definiteness of quantities can change without altering the physically observable results. Next we will elaborate in §3 on the transformation properties of the fields and promotion of the gamma matrices to holonomically described proto-gravity fields in causally consistent manner and in §4 give a discussion on the "reality" induced by fields. In §5 we modify the Dirac lagrangian with an auxiliary field ϕ to replace the awkward $\bar{\psi} = \psi^*\gamma^0$ with its extra γ^0 factor uncontracted in any tensorial fashion, and demonstrate causality of the gauge invariant functions of the field.* In §6, a sister

*We typically vary ψ and ψ^* independently in the lagrangian to get equations of motion but then constrain them to be so related (though we should show this constraint is propagated as well). Here we make no such restriction and allow ψ and ϕ to be independent fields with no constraints on the initial data. In the flat space case, the case of $\phi = \gamma^0\psi^*$ gives the usual results and shows many other cases (i.e. ψ, ϕ initial data pairs) are gauge related to this.

field to γ is introduced that allows a similar lagrangian for the proto-gravity fields (when a Higgs-like construction is used) as for the electromagnetic field and that gives General Relativity in a suitable limit. This similarity suggests a pairing of the electromagnetic and proto-gravity fields in a manner reminiscent of the electroweak theory. §7 gives a discussion of the global conservation laws that arise due to symmetries of the flat background.

2 Roles of invariants in physics

The mathematical theory of invariants arose in the 19th century and the intuition derived from them made a physical appearance with the work of Mach [8] and Einstein [9]. Since then they have played a preeminent role both in formulating theory and solving particular problems. The geometrodynamic approach to General Relativity is to assume some underlying geometry that is locally special relativity and posit that this geometric structure and its associated transformation laws are the natural way to look at the world. "Flat background" approaches are generally to look at small post-Newtonian corrections to the universe for nearly flat spaces where gravity is playing a small role [10]. In more dramatic configurations this formalism seems hopelessly flawed. Wormholes are topologically forbidden from such a description. Black holes with their singularities have infinite metric curvature at the center and the interior of the event horizon causally decouples in one direction from the exterior.

There is an old and out-of-favor view of black holes that goes back to Oppenheimer [11] whereby the infalling matter gets redshifted to an effective asymptotic standstill so that no singularity or horizon ever forms. This is often called the "time-frozen" picture. For many this is considered equivalent to lagrangian evolution where the particles fall in finite proper time to the center. It is usually neglected that this implies a transfinite amount of external observer time must elapse for this to occur. This implies that we have assumed that in the entirety of external observer time, no collective action occurs to interfere with black hold formation before the event horizon forms. Furthermore, an infalling pair of charges on opposite nodes will be seen as a dipole field for all future time in the time-frozen case. The lagrangian approach would suggest that these fall to the center and form a spherically symmetric charge distribution as suggested by the "no-hair" conjecture. This latter picture has no physical relevance for the external observers, so the author is firmly in the time-frozen camp.

The importance of this point of view is that there are no exotic topologies to get in the way of assuming that one has a flat background. The "geometric" aspects of gravity are some yet to be explained feature of a field that evolves in an equivalent fashion to all the other fields of nature. Let us now take the point of view that there is a flat background and, rather that looking at perturbations of it as $g^{\mu\nu} = \eta^{\mu\nu} + \tilde{h}^{\mu\nu}$, the field h^{ab} sits on top of it and is coupled to the other fields, including the kinetic terms, in the fashion of a metric. Let this background have the flat space metric $\eta^{\mu\nu}$ so that coupling, for the electromagnetic case, is of the form

$$\mathcal{L} = \left(\partial_\alpha A_\beta - C^\gamma_{\alpha\beta} A_\gamma\right) h^{\alpha\alpha'} h^{\beta\beta'} \left(\partial_{\alpha'} A_{\beta'} - C^{\gamma'}_{\alpha'\beta'} A_{\gamma'}\right),$$

where the connection-like C tensor is yet to be defined. Importantly, these are *not* considered to be indices that transform as co and contravariant tensors under the metric h. All the objects here are flat space η-tensor objects. This seemingly bazaar construction gives causal cones for the evolution that are not the flat space cones defined by $\eta^{\mu\nu}$. The coordinate labels $\hat{t}, \hat{x}, \hat{y}, \hat{z}$ give coordinate directions. We expect that the (x, y, z) set are h-spacelike in the sense that $h^{ij}u_i u_j > 1$ for all u in the span of $\hat{x}, \hat{y}, \hat{z}$. The forward timelike direction has a positive projection on $\hat{t}$ even if the cone is so tilted that $h^{tt} > 0$. Thus it gives a positive evolution direction for a future on the background.

In general, any reasonable equation of motion for h should preserve this set of conditions and evolve in our coordinate time variable t for all values. In the case of black hole formation the metric tends to asymptotically converge on a degenerate state leading to a set of equations that are very ill-conditioned. How to treat this situation numerically is still unclear but the presence of a flat η-background means that we have a full set of conservation laws so these may provide an avenue to evolve without such problems [12]. We will not be answering the question of general persistence of evolution of the equations as it seems to be a very hard problem (as most nonlinear PDE solution existence problems are) but it is very important. Failure of this to hold would be destructive to such a theory. It is taken as an article of faith that such a set of initial data can be evolved for all coordinate time with time steps taken uniformly at all locations. In other words, cones may narrow and tilt but they will never intersect with our spatial coordinate slices.

The role of gauge invariance in physics is analogous to an equivalence class in mathematics. In mathematics we have some set of structures we wish to preserve and there can be classes of elements that act the same under them. In physics, we may have a set of fields that evolve under the equations of motion in such a way that there are classes that retain some set of properties under evolution. We usually describe the set by a gauge transformation that joins each subclass. It is not clear that nature is really blind to which element of the class we are choosing. One could choose a representative element and claim that this is the "correct" one and be no worse for it. In the case of the Dirac field ψ and the electromagnetic field A each has a set of gauge transformations as free fields. The Dirac field has only a global phase transformation however, when coupled to the electromagnetic field, it acquires some local gauge freedom $A \to A + \nabla\chi$ in that the phase $\varphi \to$

In the case of a nontrivial gravity field, we allow the possibility that no such mapping may exist.

$\varphi - \chi$. This is what we mean by "promoting" a global to a local symmetry.

In the following we will replace the quadratic lagrangian with a bilinear one by replacing $\bar{\psi} = \psi^* \gamma^0$ with a new field ϕ.* This is the motivation for the title. We are really only abandoning γ^0 in this sense as a factor in defining $\bar{\psi}$. The fields γ^μ are all retained as what might be loosely called a "spin 1" encoding of the gravitational field. We now need to ask what are the physically distinguishable states of the system. It is natural to argue that the conserved quantities give the only unambiguous physical quantities that we can distinguish. Phase is complicated in that it gives current and relative cancellation due to interference. One can define a ψ by the mass density ρ and the current j. When the density is over a compact set this is enough to fix the phase up to a constant. For our new set we will have conservation laws that depend on ψ, ϕ and γ. The γ^0 is still present but now a dynamical field. This trio of fields now collectively determines the conserved currents. Naturally this is a massive expansion of the gauge group. In the "flat space" case we can choose γ^μ to be the Dirac matrices in some representation and $\phi = \gamma^0 \psi^*$ and obtain the usual Dirac results.

The Noether charge symmetries here correspond to spacetime symmetries and phase transformations. When we consider the quantum analogs of such fields the importance of positive definite norm is important. This is because it is given the role of a probability for a measurement so must be positive definite and normalizable. This fails in the classical theory of Dirac particles but is "fixed up" in the quantum field theory by choices for the commutation relations of the operators and their action on the vacuum ground state (as with the Gupta-Bluer formalism [13]). In this classical theory we are not necessarily concerned with this for this reason but the same symmetry generates mass and charge conservation so it still is important. Interestingly, this symmetry holds in curved space as we propagate hyperbolic spacelike slices even when there is no spacetime symmetry.

One way the Dirac field is incorporated into curved spacetime is to fix γ^μ set to be a particular representation and use vierbein fields (tetrad formalism). This preserves the desired norm properties above and ensures local packets move correctly. There is little choice in this approach if one is to use wavefunction evolution from a quadratic lagrangian [1]. To be fair, no one knows what the evolution of an electron is on such scales. We expect packets to move along geodesics but if some negative norm or mass density entered we then must defer to experiment to validate or reject this. The probabilistic interpretation seems hopeless but consider that true "observers" as machines that measure the results are themselves built from such fields. If quantum evolution is a deterministic feature as decoherence advocates suggest, then the probability is unity by the evolution and a change in positive definite norm means that the action of our measurement devices must obey a modified rule that preserves this. This should be kept in mind when we consider questions about the conserved quantities. Negative energy and mass regions of quantum bodies in highly curved regions my not be forbidden by nature as much as we forbid it by our assumptions about the essential meaning of such quantities.

For evolution on such a flat η-background that mimics gravity, we must then ask what kinds of transformations correspond to the general coordinate transformations we are used to in GR. Firstly, just as information has come to be considered a physical state in quantum information theory, coordinates and time should be thought of as physical conditions given by the kinds of candles afforded by local atoms and clusters that triangulate our spacetime. We may as well think of "physical coordinates" (i.e. non η-background coordinate changes) as made of material bodies that are small enough to give insignificant perturbations to the general dynamics. To actively boost to another RF (reference frame) we consider a local current relative to some other standard currents that define the frame and choose the new current so the relative local motion matches. To passively boost to another RF we consider a transformation of the underlying η-background coordinates. Since the physically causal light cones induced by $h^{\mu\nu}$ in its coupling to the other fields A, ψ, etc. are not the cones induced by η we must take care to maintain the $\hat{t}$-forward direction of the cones under such changes. The tensor field constructions made with the usual forms $\bar{\psi}\gamma^\mu_D\psi$, etc. will now be of the form $j^\mu = \phi\gamma^\mu\psi$ so that their transformation properties under η-background coordinate changes are tensorial. This is, however, not very interesting because it does not relate to our physical observers and their physical coordinates that relate to the function $h^{\mu\nu}$. Many active transformation of the field trio ϕ, γ, ψ give the same boosted current. If we make the change purely with γ and assume our metric function $h^{\mu\nu}$ is built from them, this will change other terms in the equations of motion.

There remains the many possibilities of transforming the pair ψ, ϕ to give a new current function without altering the local observed geometry. Passive transformations based on allowable background coordinate changes can be done by changing the η-background coordinates or altering the fields ψ, ϕ in a manner that gives a shifted (on the background coordinates) set of currents and conserved densities that evolve in an isomorphic fashion to the original fields. The possibility of having shifted and deformed sets of fields on the background space with the same observable reality is a novel extension over the manifold approach where the points have reality and we assign and transform fields there based on coordinate changes and other gauges. It is analogous to having a set of fields on $\mathbb{R}^4$ and shifting the set by a 4-vector v^μ to give a new equivalent universe of solutions in the equivalence class; an obviously true equivalence that is not present by positing a

*Such a construction also introduces a large set set of nonlocal conservations laws. [6]

manifold with fields. We now allow this full set of equivalent representations of such a universe.

3 Transformation rules

The theory of spinors arose naturally out of Dirac's algebraic attempts to reconcile causality with the first order equations that seem to describe nonrelativistic electrons. Interestingly, Schrödinger originally attempted the, later named, Klein-Gordon equation to describe electrons but could not get the fine structure right [4]. He settled on a diffusion-like equation that was first order in time and second order in spatial derivatives. Pauli adapted it to include spin but, as for most such equations, signal propagation speeds diverge. Dirac introduced a pair of spinors and a linear first order operator that when "squared" gave the Klein-Gordon equation for each component, thus ensuring causality.

His treatment introduces a set of γ^{μ}_{ab} matrices that are considered fixed and constitute representations of the $SL(2,\mathbb{C})$ group which is a two-fold covering group of the $SO^{+}(3,1)$ group. More explicity, this gives a map of complex valued bi-spinors $\binom{a}{b}\binom{c}{d}$ to real 4-vectors so that each 4×4 complex matrix action corresponds to a Lorentz transformation and compositions among these is preserved by this mapping. In the humblest of terms, we can decompose a general free state ψ_a into a basis of free progressive wave solutions $e^{ik_\mu x^\mu}u_a(k)$ where we can define a general Lorentz transformation $\Lambda^{\mu'}_{\nu}$ through the coordinate *and* algebraic action $S(\Lambda)_{ab}\psi_b(\Lambda x)$. We define this action so that the current j^μ is transformed by a boost and interpret it as the actively boosted free plane wave of positive energy. Note that $S(\Lambda)_{ab}\psi_b(x) \neq \psi_a(\Lambda x)$.

The Dirac lagrangian has a (seemingly) symmetric form

$$\mathcal{L}_D = i\bar{\psi}\gamma^\mu\partial_\mu\psi - m\bar{\psi}\psi, \tag{1}$$

where $\bar{\psi} = \psi^*\gamma^0$. This inconvenient γ^0 is generally considered necessary to give Lorentz invariance. We can see that without it we would get inconsistent equations of motion for ψ and ψ^* if we vary them independently.

The operator $S(\Lambda)_{ab}$ performs a transformation of ψ_a so that the lagrangian is invariant and the resulting current is boosted as

$$\begin{aligned} j'^{\alpha}(x') &= \left(\psi'(x')^*\gamma^\alpha\psi'(x')\right) \\ &= \left((S\psi(x))^*\gamma^\alpha S\psi(x)\right) = \left(\psi(x)^*S^*\gamma^\alpha S\psi(x)\right) \\ &= \left(\psi(x)^*\gamma'^{\alpha}\psi(x)\right) = \Lambda^\alpha_\beta\left(\psi^*(x)\gamma^\beta\psi(x)\right) \\ &= \Lambda^\alpha_\beta j^\beta(x). \end{aligned} \tag{2}$$

The Dirac theory allows us to think of the complex 4-spinors ψ_a at each point as indicating the local direction of the local current of the particle corresponding to it. To achieve this it has been necessary to introduce negative energy solutions. The negative energy solutions are reinterpreted as positrons and given a positive mass through the details of canonical quantization since they are generally deemed undesirable. One reason to reconsider this point is that net positive energy initial data may maintain this property and negative energy states do not necessarily provide an avenue for some subset of the space to fall to negative infinite energy at the expense of heating the rest of the system. Such a result would depend on the details of the coupling and dynamics. Local net negative energy density in solutions arising from positive local energy physically arising states would produce problems but it is not clear that this ever arises except in extreme cases where pair production becomes available.

Other conservation laws such as the conservation of probability (which arise from the same global phase symmetry that give mass and charge conservation) have similar problems. In an "emergent" theory of quantum measurement we do not need a probability operator (or any operators at all). The probabilities arise from measurements with the kinds of macroscopic yet still quantum mechanical matter that constitutes the classical world [7]. In this approach, the initial data and evolution equations generate their dynamics in a deterministic fashion and the probabilistic features arise from the long lived partitioning of the classical world into subsets indexed by the delocalized objects that interact with it. Details of when this is a consistent procedure are discussed in ref. [7]. For this reason, we do not seek to validate or build upon arguments that start with an "interpretation" of particular expressions since we ultimately expect the evolution and interactions to independently determine the expressions that give all observable results.

One of the frustrating aspects of the Dirac equation as it stands is that it is not clear how we should alter its form in general coordinates. One can use the local frame approach and assume the Dirac matrices are members of the same representation in each one. A spinorial connection then indicates how nearby spinors are related as a consequence of geometry. If we allow the matrices to become functions of space and time with only the spacetime indices changing this gives a simple approach but then it is not clear how we recover local Klein-Gordon (KG) evolution of each component and what the locally boosted fields should be. If we continue with the spinor approach and let the $\gamma^\mu(x)$ matrices be fixed and alter the spinor fields instead then we need a transformation that is a kind of "square root" of the Lorentz vector transformation. This is how we get the actively boosted solutions in flat space. In curved spacetime, there is no global notion of a boost so the former perspective seems more valuable. Ultimately, we specify a configuration by the spacetime metric and the fields on it but the metric will be a function of the γ^μ matrix fields (and some associated dual fields) that only give geodesic motion below some energy bound.

In the early days of the Dirac equation, interpretations have evolved from a proposed theory of electrons and protons to that of electrons and positrons with positrons as "holes" in an infinitely full electron "sea" to that of electrons with

positrons as electrons moving "backwards in time." The first interpretation failed because the masses of the positive and negative energy parts are forced to be equal. The second was introduced out of fear that the negative energy solutions of the Dirac equations would allow a particle to fall to endlessly lower energies. The last was introduced as a computational tool. The negative mass solutions were to be reinterpreted as positive mass with negative charge. Necessary computational fixes associated with this idea are subtly introduced through the anticommutation relations used in the field theory approach to fermions and the properties of the supposed ground state [13]. If we are going to seek a classical field theory approach to this problem we need another mechanism.

For the moment, we assume the γ matrices are those of the Dirac representation. Standard treatments allow any selection of 4×4 matrices that represent the $SO^+(3,1)$ group. Here we choose a specific representation because we are going to let the γ's be fields and let these other choices be a kind of gauge freedom until some interaction restricts us to a specific subset. The Dirac lagrangian has a (seemingly) symmetric form

$$\mathcal{L}_D = i\bar{\psi}\gamma^\mu\partial_\mu\psi - m\bar{\psi}\psi \tag{3}$$

where $\bar{\psi} = \psi^*\gamma^0$. This is generally considered necessary to give Lorentz invariance. The Dirac matrices satisfy the condition

$$\{\gamma^\mu, \gamma^\nu\} = -2\eta^{\mu\nu}, \tag{4}$$

where η =Diag(−, +, +, +). This suggests that we could view the metrical properties of the space as encoded in γ rather than invoking a metric η. The metric has ten independent parameters at each point and γ has 4×10 or 4^3 parameters, depending on chosen symmetry constraints but we need to satisfy 4^4 equations. If we trace the suppressed spin indices then there are only 10 equations and a general metric can be encoded in the γ^μ set. However, eqn. 4 is the identity we require to convert the Dirac equation into a KG one that demonstrates causality in each component. This is a loose end in deriving geodesic motion for a packet to show that we get observed motion in the classical GR limit and an important consideration in what follows.

In anticipation of a future unification theory one cannot help but notice the greater similarity of $\gamma^\mu_{ab}(x)$ to $A^\mu(x)$ and the other vector boson fields than any of these to the metric $g_{\mu\nu}$. For now we simply leave this as constant but accept that it can have its own transformation properties as a one-vector. In contrast, all the "spinor" labels are considered as having only scalar transformation properties. The bispinors ψ_a now transform as scalars. To emphasize their new properties and that they still have a collective reality as a four-tuple of functions we term it a "spinplet." The mixed objects γ^μ_{ab} we consider a vector object with extra labels and, by analogy, label it a "vectorplet."

There are some surprising implications of this. The equations are unchanged but the transformation properties are now different. Since the γ^μ_{ab}'s can vary with position, we expect a much larger equivalence class of electron-gravity field pairs, $\{\psi, \gamma\}$, that correspond to the same underlying reality. We can boost the system by $\Lambda^\mu_\alpha\gamma^\alpha$. This gives the same ψ_a fields at every point but the physically measurable j^ν currents are altered. Of course we still have the traditionally boosted solutions $S(\Lambda)\psi^{(0)}(\Lambda x)$ that have this same current so we have a degeneracy in the pairs $(\Lambda\gamma, \psi^{(0)})$ and $e^{i\phi}(\gamma, S(\Lambda)\psi^{(0)})$ and all other states with the same current and net phase. This is not the result of a discrepancy in the active vs. passive coordinate transformations we observe in a fixed representation but an additional degeneracy in the equivalent physical descriptions. We have only used the current j^μ to distinguish states and we expect that there will be some other conserved quantities, like stress-energy, that will physically subdivide this set into distinct equivalence classes. Since there are so many degrees of freedom in the set of $\gamma^\mu_{ab}(x)$'s we anticipate that the set is still significantly enlarged.

4 Reality and gauge

The AB effect gives a simple example of how the "reality" of an electron is not sufficiently described by the wavefunction of the electron itself. In this case, the current is a function of both ψ and A as $J = i\hbar\nabla\psi + eA$. This construction is useful in sorting out various apparent contradictions in electromagnetism. If we want to investigate the radiation reaction or questions of "hidden momentum" [14, 15] one can build a packet that spreads slowly compared to the effects of external fields and see how the self field and lags contribute to the actual motion. The power of it is that there is no ambiguity in the gauge as for a hodge-podge lagrangian like $\frac{1}{2}mv^2 + jA - \frac{1}{4}FF$ [16] because the physical current of a packet is the gauge invariant J not the naive $j = mv$. The AB effect seems like a topological effect because it is viewed through the lens of ψ being the pure descriptor of the reality of the electron and as a stationary effect. In driving a solenoidal current to create a circulating A field we accelerate J with a transient circulating E field. Part of the current is made up of the phase gradient of ψ and part from A itself. The field and the acceleration moves outwards from the current source at the speed of light and the resulting equilibrated current becomes a function of the final magnetic flux. This circulating current must gain all of its curl from A. The ψ can only contribute to an irrotational flow so general charge packet motion requires a contribution from A. This suggests we might generally want a more nuanced distinction of particle reality than merely a function of each individual field in a lagrangian that has been nominally assigned to the particle type alone.

In flat space without gravity or interactions, we can consider packets of fields that are widely separated based on type. These can then evolve separately and the type of field and the reality implied by it are synonymous. There can still be some gauge freedom but the packets and any interesting properties

that one might observe are contained in the same support. The observables are, at best, the gauge invariant properties such as stress-energy or current. Allowing interactions, this reality gets complicated in two ways. Firstly, the conserved currents may now involve aspects of more than one kind of field and second, there are now constraints that must be obeyed. These are generally defined by elliptic PDEs such as $\nabla \cdot E = \rho$ that are propagated by the dynamic equations.*

If we now include gravity in the form of a γ_μ field that has some gauge freedom that mixes with the reality of the wavefuction ψ then we cannot make the above separation. The gravitational field is everywhere so no isolation of packets is possible. The reality of the electron is now a function of ψ and any γ-like fields that have global extent. This is in contrast with the case where the gravitational information is completely specified in the $g^{\mu\nu}$ field. Since this has no gauge freedom beyond that of coordinate changes, the packet motion of a wavefunction is affected by it yet the reality of the electron is still entirely determined by the values of ψ in the packet itself.

For the case where multiple fields determine a single reality, when is it really viable to call one set of quantities the "electron current" versus some combination of quantities that strictly depend on multiple types of fields? In the case of the Dirac and electromagnetic field (in flat space with constant γ matrices), the density of the field is only a function of ψ so that we have at least one component of the 4-current that is entirely specified by the wavefunction. This allows us a uniquely associate j^0 with the electron field ψ and so call it the "electron-density." The stress-energy terms similarly have T^{00} as a simple function of ψ alone. If every conserved quantity can be associated this way, we have a well-defined mapping between the fields and conserved quantities. If we are interested in more exotic lagrangians than can be formed by the "minimal" prescriptions from the free quadratic cases, we will need to be mindful of the possibility that the currents may not necessarily be so associated with one particular field.

Although this discussion may feel somewhat pedantic, it is important to make this distinction and not get trapped in the vague lore that sometimes accompanies discussions in physics. For example, it is often said that we must have "manifestly invariant" lagrangians to get relativistically consistent results. This is not true not only in the obvious sense that they can be rearranged in a nonobvious invariant form. One can conceivably write down a set of fields that gives a class of solutions whereby the degrees of freedom and invariance is with respect to the observers built of other physical fields. Here we can imagine inducing a set of "physical coordinates" based on local packets of long lasting separated objects that define a grid. With the right time evolution parameterization, we would expect the form of the equations to be invariant with respect to such a coordinate set. The overall class of equivalent solutions should allow for local field changes that induce independent observable current changes with the appropriate degrees of freedom for the observed dynamic freedom of the system. In general, we only need observers to see the world with such symmetry (such as Lorentz) but it need not hold with respect to the coordinates. As long as the constituent fields of the observers and the external reality "covary" together, then the observers see exactly the same thing. Allowing such dynamics can enlarge the equivalence classes at the cost of a more complicated relationship between coordinates and observable reality.

Generally we seek a quadratic free field lagrangian and then gauge and Lorentz invariant couplings between them. The Dirac lagrangian is usually presented in the superficially symmetric form

$$\mathcal{L}_D = i\bar{\psi}\gamma^\mu\partial_\mu\psi - m\bar{\psi}\psi. \tag{5}$$

The appearance of the γ^0 is displeasing if we are to interpret the μ indices as spacetime indices. This particular form is often considered important because it gives a positive definite probability density. In an "emergent" approach to quantum theory where the probabilities are defined by the evolution equations in a deterministic fashion, this is not important. Probability will automatically be conserved by the normalization over the resulting paths that bifurcate the histories of recording devices and observers as indexed by the delocalized particle's coordinates [7] regardless of whether there is a "nice" operator that describes it. More importantly, we need the eom of ψ and ψ^* to be consistent. This dictates that the γ^0 appear in this expression. By using a representation where $\gamma^0\gamma^\mu\gamma^0 = \gamma^\mu$ the variations of the action give equivalent equations of motion.

To achieve a lagrangian that is manifestly invariant using this "vector-plet" interpretation we introduce an auxiliary field ϕ that, in flat space, can be chosen to be $\psi^*\gamma^0$. For the usual Dirac equation this condition is propagated. One should wonder if this will give a true isomorphism with physical results. We are interested in the propagation of conserved quantities as mass, charge... and some local phase information. This brings us to a subtle point. Even in nonrelativistic quantum mechanics, the "reality" of interacting particles is not completely given by the corresponding fields themselves. This is most clearly observed in the AB effect. Often this is viewed as an important example of topology and gauge in

*This is purely a classical theory of delocalized fields so we do not have the problem of "self-energy" or the "particle not feeling its own fields." In the many body case, the fields presumably are made of many constituent ones with only the "center of mass" motion as visible to us. This allows us to have a wavefunction of a charged particle that does not spread under the influence of the field generated by it, as in the classical particle case [15]. However, the self force and momentum are subtle concepts in that such a composite charge must have both m_{bare} and m_{em} components. Only m_{bare} is localized and m_{em} is spread over the range the static fields. The contribution to the electromagnetic momentum in $Ma = (m_{bare} + m_{em})a = F_{ext}$ in the force law is actually provided by a self field of the radiation field traversing the support of the charge.

physics. It is more simply understood as an expression of the electron current being not simply a function of the electron wavefunction alone. A similar property is observed in the London skin depth in superconductors. The only way an electron current can obtain rotational flow is through the vector field $\vec{A}$ or through the appearance of discrete vortices. The moral here is that angular momentum, among other conserved quantities, is defined by a collective set of fields so it makes no sense to associate with one particular particle. "Spin" is now a kind of angular momentum that exists through the collective local reality of this new vector-plet graviton and two fermion spinplet fields. By abandoning this usual concept of a spinor we will obtain an isomorphic theory that has significant generalizations.

5 Bilinear modification

To resolve the complications arising from the hidden γ^0 in the usual Dirac lagrangian, let us replace $\bar{\psi}$ with an associated yet independent field ϕ and see when it evolves in a consistent fashion when we simplify to the Dirac representation. Consider the Dirac-limiting lagrangian density we can choose using only the complex valued ψ, ϕ and γ^α (with $g^{\mu\nu}$ an implicit function of it) is of the form

$$\mathcal{L} = i\left(\phi_a \gamma^\mu_{ab} \partial_\mu \psi_b - \partial_\mu \phi_a \gamma^\mu_{ab} \psi_b\right) - 2m\phi_a\psi_a. \tag{6}$$

For constant γ's chosen to be the Dirac representation, then variation $\delta\phi$ yields $i\gamma^\mu\partial_\mu\psi - m\psi = 0$. Variation by $\delta\psi$ yields $-i(\partial\phi)\gamma^\mu - m\phi = 0$. If we choose $\phi_a = \gamma^0_{ab}\psi^*_b$ then this is equivalent to the Dirac equation solution for ϕ.

When we consider the gauge equivalent states this introduces some additional considerations. For example, if the support of ψ and ϕ are disjoint then there is no net mass or current density. Such a state is evidently a vacuum despite the nontrivial values of the functions and evolution equations. Here we see that our notions of the physical meaning we attach to functions as describing the reality of a particle is less trivial than usual.

So far we have not explicitly included any measure or metric and the action of $\nabla_\mu\gamma^\nu$ is ambiguous without it. We can make formal definitions of these by using eqn. 4 as a guide. The pair of functions,

$$\left.\begin{aligned} g^{\mu\nu} &= -\frac{1}{4}\,\mathrm{Tr}_{ac}\gamma^{(\mu}_{ab}\gamma^{\nu)}_{bc} \\ g_{\mu\nu} &= \mathrm{Inv}\left(-\frac{1}{4}\,\mathrm{Tr}_{ac}\gamma^{(\mu}_{ab}\gamma^{\nu)}_{bc}\right) \end{aligned}\right\} \tag{7}$$

to define the metric in terms of γ are evidently complicated when explicitly constructed but they do give us trial definitions for $g^{\mu\nu}(\gamma)$ and its inverse in terms of γ^μ that can specify a completely general metric field. Another possible objections is that the form of γ^μ with indices raised as a contravariant object is opposite that of the covariant form that A_μ enters the lagrangian especially the interaction terms $q\bar{\psi}\gamma^\mu A_\mu\psi$ which gives us pause when considering the possibility of treating γ^μ and A_μ as analogous fields where no a priori metric exists.

Since we are interested in a theory that includes electrons, positrons, photons and gravity with the electromagnetic and gravitational fields on an equivalent footing we will will need to make a further modification. It will be convenient to let the natural form of γ be a lowered index object γ_μ and introduce a contravariant sister field λ^ν that generates $g^{\mu\nu}$ in the same fashion that γ_μ generates $g_{\mu\nu}$. It is not automatic that these be inverse functions despite the suggestive notation but we will show that they do so in sufficiently low energy cases for a particular lagrangian. We expect the following relations to be able hold in the flat space limit

$$\left.\begin{aligned} g^{\mu\nu}\delta_{ac} &= -\frac{1}{2}\{\lambda^\mu, \lambda^\nu\} = -\lambda^{(\mu}, \lambda^{\nu)} \\ g_{\mu\nu}\delta_{ac} &= -\frac{1}{2}\{\gamma_\mu, \gamma_\nu\} = -\gamma_{(\mu}, \gamma_{\nu)} \end{aligned}\right\}. \tag{8}$$

It is very important to distinguish between this case, which arises in deriving the Klein-Gordon results that demonstrate causality for the Dirac components and the traced result. The arbitrary metric field $g_{\mu\nu}(x) = -\frac{1}{8}\mathrm{Tr}\{\gamma_\mu(x), \gamma_\nu(x)\}$ can be defined in terms of $\gamma^\mu_{ab}(x)$'s but the untraced result for $g_{\mu\nu}(x)\delta_{ac}$ cannot. This will be central to what follows.

We like to have the metric appear explicitly in all the terms of the lagrangian for the reason it gives us something to vary in obtaining a conservation law for stress-energy. One way to do this is is to use the lagrangian

$$\mathcal{L}_e = i\left(g^{\mu\nu}\phi_a\gamma_{\mu:ab}\partial_\nu\psi_b - g^{\mu\nu}(\partial_\mu\phi_a)\gamma_{\nu:ab}\psi_b\right) - 2m\phi_a\psi_a, \tag{9}$$

where the colon separates spacetime from scalar indices. We define $g^{\mu\nu} = -\frac{1}{4}\mathrm{Tr}\lambda^{(\mu}, \lambda^{\nu)}$. The evolution equations are given by the variations $\delta\phi$

$$\left.\begin{aligned} &i\left(g^{\mu\nu}\gamma_{\mu:ab}\partial_\nu\psi_b + g^{\mu\nu}\nabla_\mu(\gamma_{\nu:ab}\psi_b)\right) - 2m\psi_a = 0 \\ &i g^{\mu\nu}\gamma_{\mu:ab}\partial_\nu\psi_b + \frac{1}{2}\,i g^{\mu\nu}(\nabla_\mu\gamma_{\nu:ab})\psi_b - m\psi_a = 0 \end{aligned}\right\} \tag{10}$$

and $\delta\psi$

$$i g^{\mu\nu}(\nabla_\mu\phi_b)\gamma_{\nu:ba} + \frac{1}{2}\,i g^{\mu\nu}\phi_b(\nabla_\mu\gamma_{\nu:ba}) + m\phi_a = 0 \tag{11}$$

so that ϕ evolves as ψ with $m \to -m$ and $\gamma \to \gamma^{\mathrm{T}}$.*

Since we are about to determine the motion of the conserved gauge invariant stress energy associated with the fields and it is deeply connected with geometry, we make a brief segue to derive this conserved quantity. A general action contains both a lagrangian and a measure that can be related to the metric

$$S = \int d^4x\,\mathcal{L}\sqrt{-g_{\cdot\cdot}}\,. \tag{12}$$

*Note that this does not mean that the energy of the rest field is m ($c = 1$). The energy is a function of the triple of fields (ψ, ϕ, γ) as we see next.

Incorporating general relativity, the lagrangian density is generally written

$$\mathcal{L} = \frac{1}{2\varkappa} R(g) + \mathcal{L}_{\text{fields}}, \tag{13}$$

where $\varkappa = 8\pi G$ and the first term gives the Riemann curvature and the second gives the field terms that do not depend only on the metric. The conservation laws arise from varying the metric $\delta g^{\mu\nu}$ from which we obtain

$$G^{\mu\nu} = 8\pi G T^{\mu\nu} = -\varkappa \frac{-2}{\sqrt{-g^{\cdot\cdot}})^{-1}} \frac{\delta \mathcal{L}_{\text{fields}}(\sqrt{-g^{\cdot\cdot}})^{-1}}{\delta g^{\mu\nu}}. \tag{14}$$

Since $\nabla_\mu G^{\mu\nu} = 0$ as an identity we have $\nabla_\mu T^{\mu\nu} = 0$. This is a local conservation law. To obtain a global one we need a spacetime with persistent Killing vectors corresponding to continuous symmetries. The action of gravity typically destroys these as global conservation laws, however, if $G \to 0$ *and* the initial data is chosen to be flat then these exist and persist so we have the usual global symmetric conservation laws. This justifies this as a general method of deriving conservation laws with symmetric stress-energy tensors for fields on flat space when all the fields present are tensorial. Of course, we expect any such conservation law to correspond to a symmetry. In this case, we can vary the coordinates locally and this leaves the quantity $\mathcal{L}\sqrt{g_{\cdot\cdot}}$ invariant. Since all the derivatives are covariant, we can replace a passive coordinate change on an open set with an active transformation of the metric field $g^{\mu\nu}$. Varying $g^{\mu\nu}$ is therefore equivalent to a general small variation in the local coordinates. Of course, we are considering these as fields on a flat background so that they change in a rather simple fashion relative to the coordinate changes and we should include a coordinate measure $\sqrt{-\eta}$ and this underlying space generates full set of ten conserved quantities (see §3).

The (symmetric) stress tensor is usually defined by*

$$\begin{aligned} T_{\mu\nu} = & -\frac{2}{(\sqrt{-g^{\cdot\cdot}})^{-1}} \frac{\delta\left(\mathcal{L}_{\text{fields}}\left(\sqrt{-g^{\cdot\cdot}}\right)^{-1}\right)}{\delta g^{\mu\nu}} \\ = & -2\frac{\delta(\mathcal{L}_{\text{fields}})}{\delta g^{\mu\nu}} + g_{\mu\nu}\mathcal{L}_{\text{fields}} \\ = & \; 2i\left(\phi_a \gamma_{(\mu:ab}\partial_{\nu)}\psi_b - (\partial_{(\mu}\phi_a)\gamma_{\nu):ab}\psi_b\right) \\ & + g_{\mu\nu}\Big[\, i\left(g^{\alpha\beta}\phi_a\gamma_{\alpha:ab}\partial_\beta\psi_b\right. \\ & \left. - g^{\alpha\beta}(\partial_\alpha\phi_a)\gamma_{\beta:ab}\psi_b\right) - 2m\phi_a\psi_a\Big] \\ = & \; 2i\left(\phi_a\gamma_{(\mu:ab}\partial_{\nu)}\psi_b - [\partial_{(\mu}\phi_a]\gamma_{\nu):ab}\psi_b\right), \end{aligned} \tag{15}$$

where we have varied with respect to $g^{\mu\nu}$ and assumed γ_μ is a field independent of it in anticipation of $g^{\mu\nu}$ being a function of λ^μ.

*Here we make the choice of taking the determinant with respect to the "contravariant" metric $g(\gamma^\mu)$ in anticipation of later work. This explains the power -1 this expression.

We can similarly examine the continuous symmetry given by the globally constant phase changes $\psi \to e^{i\theta}\psi$ and $\phi \to e^{-i\theta}\phi$ to get the conserved current

$$j^\nu = 2i g^{\mu\nu}\phi_a\gamma_{\mu:ab}\psi_b \tag{16}$$

so that $\nabla_\nu j^\nu = 0$. Here we see this current also depends on all three fields so that the vanishing of any one of them on a region necessitates the entirety of the physical reality vanish.

We will now consider the implications of packet motion given these two conservation laws. Firstly, when we say "packet" we are not referring to a packet of localized ψ or ϕ as much as a localized region where the reality associated with these fields through $T_{\mu\nu}$ and j^μ are nonzero. Let us also consider a packet that is devoid of internal stress and rotation and where the pressure is minimal. For such a packet with sufficiently uniform interior we can average over the current to give $\langle j^\mu\rangle \approx m v^\mu$ where m^2 is the averaged $g_{\mu\nu}j^\mu j^\nu$ density and, assuming the packet preserves its structure as it moves, v^i is the local coordinate velocity of the packet. We can then define v^0 by the relation $g_{\mu\nu}v^\mu v^\nu = -1$. The conservation law tells us that ρ is conserved. v^μ is well defined to the extent packet motion is so.

From $\langle T^{\mu 0}\rangle$ we can define a velocity u that carries the energy in a localized packet so that $\langle T^{\mu 0}\rangle \approx m' u^{(\mu}u^{0)}$. Since a vanishing of the current on a region implies vanishing of stress-energy as well we have that $v = u$ and that $\langle T^{\mu 0}\rangle \approx m'^{(\mu}v^{0)} = \alpha m^{(\mu}v^{0)}$. Since there are no internal stresses, $\langle T^{\mu\nu}\rangle \approx \alpha m v^\mu v^\nu$. By combining these expressions we derive that these "macroscopic" variables are

$$\left.\begin{aligned} v^\nu &= \frac{\langle T^{\mu\nu}\rangle}{\alpha\langle j^\mu\rangle} \\ m &= \alpha^2 \frac{\langle j^\mu\rangle\langle j^\nu\rangle}{\langle T^{\mu\nu}\rangle} \end{aligned}\right\}, \tag{17}$$

where these are actually several equations (repeated indices are not summed) that are all equal by the conditions above.

Now consider the parcel averaged stress-energy conservation law. Applying $\nabla_\mu j^\mu = 0$ we have

$$\begin{aligned} \langle \nabla_\mu T^{\mu\nu}\rangle &= \langle \nabla_\mu (j^\mu v^\nu)\rangle \\ &= \langle (\nabla_\mu j^\mu)v^\nu + j^\mu \nabla_\mu v^\nu\rangle \\ &= m' \langle \nabla_v v\rangle = 0, \end{aligned} \tag{18}$$

which indicates the gauge invariant aspects (i.e. the reality) of the parcel follows geodesic motion. This is not entirely surprising given that it is known that the conservation laws generally dictate that classical particles follow geodesics though the proofs are generally quite difficult [18]. The "geodesics" here are generally curved paths in our underlying coordinate space but appear as geodesics in the geometry most apparent to observers.

In the next section for a theory of "lepto-electro-gravity" we have two covariant gauge fields and one contravariant one.

These have trivial transformation laws in the flat background coordinates but we maintain this distinction because it seems more relevant for observers. In this sense we think of it as a "2+1" theory. One contravariant field is always necessary to match the covariant derivatives that must arise in any differential equation. The electron field is described by a (ϕ, ψ) pair of fields that embody its reality with a very large gauge group and the meaning of the reality they describe depends not only on the metric but the covariant gravity field γ_μ. We will see that these have properties that are distinct from the positive energy positrons so we will require another pair of fields for their description. Along the way we will introduce a lagrangian that exists as a purely polynomial expression and removes the need for complicated nonanalytic measures and rational inverse matrix functions.

6 Electro-gravity lagrangian

Here we seek a lagrangian that encompasses electrons, positrons, electromagnetism and gravity and seek to have equations that are polynomial rather than complicated rationals that arise from the operation of taking the inverse of the metric. For this reason we define the function $g : \mathcal{V} \to \mathcal{T}$ where $\mathcal{V}$ is the set of vector-plet objects λ^μ_{ab} and $\gamma_{\mu:ab}$ and $\mathcal{T}$ is the set of corresponding contravariant or covariant 2-tensors $g^{\mu\nu}$ and $g_{\mu\nu}$ respectively. Specifically,

$$g(A, B) = -\frac{1}{8}\,\mathrm{Tr}(AB + BA).$$

We will establish a lagrangian that gives Dirac particle motion in the flat space limit, electromagnetism and a form for GR that gives a simple parallel between the motion of the gravitational fields, γ_ν and the electromagnetic ones A_ν that allows gravity to obtain the nonlinear "geometric" features of GR.

Since we are interested predominantly in positive energy solutions we will need to introduce a separate action term Λ_p for positrons that have positive mass but a reversal of sign of the charge in the coupling. We can write the lagrangian for the covariant gravitational field γ by substitution into the Einstein-Hilbert lagrangian. Alternately, we can choose it to have a similar form of the action Λ'_g as the other vector potential Λ_A and the coupling terms $\Lambda_{e\lambda A}$, $\Lambda_{p\lambda A}$ will involve both the contravariant gravitational field λ and the vector potential. Finally, there will need to be some way for the covariant and contravariant gravitational fields to relate to one another. This will be accomplished by a Higgs-like interaction term Λ_c. The general action is then defined as

$$\begin{aligned} S &= \int d^4x \mathcal{L}\sqrt{-g} = \int d^4x\,\Lambda \\ &= \int d^4x\,(\Lambda_g + \Lambda_\lambda + \Lambda_A + \Lambda_e + \Lambda_p \\ &\qquad + \Lambda_{e\lambda A} + \Lambda_{p\lambda A} + \Lambda_c), \end{aligned} \tag{19}$$

where we will define Λ_λ shortly.

Since the measure is a nonanalytic function of the metric but this is not retained in the usual equations of motion. We will find that this is also true here. For reasons as above we use the λ fields in defining the measure.

The electron part of the action is given by the substitutions

$$\begin{aligned} \Lambda_e &= \mathcal{L}_e\left(\sqrt{g^{\cdot\cdot}(\lambda)}\right)^{-1} \\ &= \Big[\, i\left(g^{\mu\nu}(\lambda)\phi_a\gamma_{\mu:ab}\nabla_\nu\psi_b - g^{\mu\nu}(\lambda)(\nabla_\mu\phi_a)\gamma_{\nu:ab}\psi_b\right) \\ &\quad - 2m\phi_a\psi_a \,\Big]\left(\sqrt{g^{\cdot\cdot}(\lambda)}\right)^{-1} \end{aligned} \tag{20}$$

where we have, harmlessly, replaced the ordinary with covariant derivatives since the act on spinplet objects which are essentially scalars. Variation with the measure present allows their action on higher tensors to give the appropriate covariant connection terms. This is one indication of how the physics itself can generate the geometric aspects of gravity rather than imposing it by fiat in the formulation of the theory's foundations.

The positron portions of the lagrangian is of the same form as Λ_e but with a different pair of fields $\tilde\phi, \tilde\psi$. The distinction comes in the form of the interaction terms. The usual minimal coupling prescription gives

$$\left.\begin{aligned} \Lambda_{e\lambda A} &= -\,q\,\phi_a\lambda^\mu_{ab}A_\mu\psi_b \\ \Lambda_{p\lambda A} &= +\,q\,\tilde\phi_a\lambda^\mu_{ab}A_\mu\tilde\psi_b \end{aligned}\right\}. \tag{21}$$

It is only the sign of the charge in the interaction terms that distinguishes positrons from electrons and it only appears in the couplings.

The gravitational part of the action can be defined by a simple extension of the Einstein-Hilbert action

$$\Lambda_g = \frac{1}{2\varkappa}\,R\left(g_{\mu\nu}(\gamma), g^{\mu\nu}(\lambda)\right)\left(\sqrt{g^{\cdot\cdot}(\lambda)}\right)^{-1}. \tag{22}$$

R is defined in terms of $g_{\mu\nu}(\gamma)$, $g^{\mu\nu}(\lambda)$ and the connections implicit in the expression are defined by

$$\Gamma^\alpha_{\mu\nu} = \frac{1}{2}\,g^{\alpha\sigma}(\lambda)\left(g_{\mu\sigma,\nu}(\gamma) + g_{\sigma\nu,\mu}(\gamma) - g_{\mu\nu,\sigma}(\gamma)\right) \tag{23}$$

and their derivatives. We expect that some induced constraints force $g(\gamma)g(\lambda) = \delta$. To have this done as a result of field interactions we exploit a "Higgs-ish" mechanism with the coupling term

$$\Lambda_c = M\left|\, g_{\mu\nu}(\gamma)\, g^{\nu\rho}(\lambda) - \delta^\rho_\mu\right|^2 \tag{24}$$

for a sufficiently large mass M. When the energies in the other terms are much smaller this drives the relation between γ and λ to hold so that the solutions become "geometric." Specifically, while it is easy to enforce causality if all evolution fields obey some equation such as $g^{\mu\nu}\partial_\mu\partial_\nu\phi + \ldots$ where $g^{\mu\nu}$ is a metric with signature +2, the geometric case indicates that slowly spreading packets in regions of slowly varying spacetime move along geodesics. When such a relation holds

our lagrangian has a form that can be interpreted as coordinate invariant in that the derivatives act on the tensor fields with covariant derivatives with the Γs induced by the metric $g_{\mu\nu} = -4^{-1}\mathrm{Tr}\gamma_{(\mu}\gamma_{\nu)}$. In the next section we will see that we can also interpret the system to live on a flat background and derive global conservation laws.

The other gauge fields all come from lagrangians that have electromagnetic form $F^{\mu\nu}F_{\mu\nu}$ where $F_{\mu\nu} = \partial_\mu A_\nu - \partial_\nu A_\mu$. Specifically,

$$\begin{aligned}\Lambda_A = \; & g^{\mu\alpha}(\lambda)g^{\nu\beta}(\lambda)(\partial_\mu A_\nu - \partial_\nu A_\mu) \\ & \times (\partial_\alpha A_\beta - \partial_\beta A_\alpha)\left(\sqrt{-g^{\cdot\cdot}(\lambda)}\right)^{-1}.\end{aligned} \tag{25}$$

It is not necessary to use covariant derivatives here since antisymmetry cancels them. For example, we model the action contribution from the "dual field" λ as

$$\begin{aligned}\Lambda_\lambda = \; & \epsilon\, g^{\mu\alpha}(\lambda)\, g^{\nu\beta}(\lambda)\,\mathrm{Tr}(\partial_\mu\tilde{\lambda}_\nu - \partial_\nu\tilde{\lambda}_\mu) \\ & \times (\partial_\alpha\tilde{\lambda}_\beta - \partial_\beta\tilde{\lambda}_\alpha)\left(\sqrt{-g(\lambda)}\right)^{-1},\end{aligned} \tag{26}$$

where $\tilde{\lambda}_\mu = g_{\mu\nu}(\gamma)\lambda^\nu$.* where we have chosen the constant ϵ to be small so that the dynamics can be dominated by γ and the constraints induced by the Higgs-like term.

For a function $F_\mu(g_{\mu\nu}(\gamma))$ the variation under $\delta\gamma_\nu$ gives

$$\delta F_\mu = \frac{\delta F}{\delta g_{\mu\nu}}\,\delta\gamma_\nu \tag{27}$$

and similarly for $\delta\lambda$. Variation of Λ_g by $\delta\lambda$ gives

$$\frac{1}{2\varkappa}\left(R_{\mu\nu} - \frac{1}{2}\,R g_{\mu\nu}\right)\delta\lambda^\nu \tag{28}$$

or

$$G_{\mu\nu}\delta\lambda^\nu = \varkappa T_{\mu\nu}\delta\lambda^\nu, \tag{29}$$

where $T_{\mu\nu}$ is the stress-energy tensor for all the actions terms other that Λ_g. We have implicitly assumed that we are in a low enough energy regime and the initial data includes no "waves" of λ so that the contributions of Λ_λ can be ignored. Since the γ's contain gauge freedom that is independent of coordinate changes so that we can choose any γ_μ that give the same $g_{\mu\nu}(\gamma)$ field, this requires

$$G_{\mu\nu} = \varkappa T_{\mu\nu}\,. \tag{30}$$

7 Conservation laws

We can argue the whole structure exists on a flat background though this is just a convenient artifice among many. It is however a very convenient one. The appearance of geometric evolution via the additional Γ factors that make the derivatives seem "covariant" with respect to some induced geometry of these fields is an emergent byproduct of the kind of couplings present. It should be noted that these $\Gamma^\alpha_{\beta\gamma}$ factors are actual η-tensors on the background space instead of affine connections. Of course, we still need to know if our equations can be evolved for arbitrary times using this point of view. Some discussion of this, especially in the case of black hole formation is given in [12]. For now we assume that this is unlimited however, although other methods have attempted to justify working on a flat background [17] it is a delicate process to have this make sense as gravitational collapse ensues due to the trend of the equations to become ill conditioned here. One should not be overly comfortable with formalism in this case. A method to handle evolution on the large regions of nearly degenerate metric using conservation laws is proposed in [12]

The flat background has a natural set of Killing vectors that give global conservation laws. To elucidate this consider the lagrangian written in terms of ordinary derivatives and make the modification by defining $g(\gamma) = h(\gamma) \circ \eta$

$$\Lambda = \mathcal{L}\sqrt{-g} \to \Lambda\sqrt{h}\sqrt{-\eta}\,. \tag{31}$$

All actions on tensors induced by η-background coordinate transformations are of the form

$$\partial_\mu A^\alpha \to \nabla_\mu(\eta)A^\alpha = \partial_\mu A^\alpha - \Gamma^\alpha_{\mu\nu}(\eta)A^\nu \tag{32}$$

and so forth, where η is a metric (in any coordiates) that can be varied about the flat space case. Any covariant derivatives $\nabla_\mu(g)$ in terms of the metric induced connections are reinterpreted as formal couplings through $\Gamma(g)$ and the ∂_μ are converted by this prescription. We see a problem with eqn. 31 is that it is not invariant under general η-space coordinate transformations due to the factor $\sqrt{-g}$. It is, however, invariant under the isometries of flat spacetime that we use to generate global conservation laws.

Since the flat space contains a full set of ten Killing vectors we have a set of conserved global quantities that now includes the gravitational fields of the form

$$\partial_\mu T'^{\mu\nu} = 0 \tag{33}$$

with the Killing (co)vector fields $p_\nu = \hat{\omega}_\nu$, $M_{ijk} = \epsilon_{ijk}x_j\hat{\omega}_k$ and $b_i = x_0\hat{\omega}_i + x_i\hat{\omega}_0$. The globally conserved quantities in these coordinates are

$$\left.\begin{aligned} P^\nu &= \int d^3x\; p_\mu T'^{\mu\nu} \\ J^i &= \int d^3x\; M^i_{jk}T'^{ij} \\ C^j &= \int d^3x\; b_i T'^{ij} \end{aligned}\right\}. \tag{34}$$

8 Conclusions

The notions of invariance from differential geometry and invariance theory are imported into physics in a fashion that ranges from formal to ad hoc. Surprisingly, they have not

*We distinguish this field with a tilde because of the earlier convention that these are all tensor indices under the underlying flat space metric so that "lowering" an index with g must be new field to not be ambiguous.

been reconsidered from the more physical point of view that all configurations that are indistinguishable to observers built of the fields themselves should form the most general equivalence class of systems. This enlarged meaning of "gauge" requires some underlying structure. We have shown that many of the usual objections to a flat background can be overcome and that this allows the fields to have very simple transformation laws and a large set of conservation laws with respect to this flat background. The observers can then perceive a curved space with all its mathematical complexity as emerging from the nature of nonlinear and multilinear coupling among fields. Importantly, there is a classical lagrangian with a Higgs-like term that causes there to be such a strongly nonlinear and geometric theory of gravity to arise from the perspective of such observers at low energy.

An interesting by-product of this approach is that the apparent co and contravariant properties of the fields in the "physical coordinates" induced by objects for the observers obtain their transformation properties by the equations of motion not by a by-fiat assignment. This is another aspect of "geometry" that is determined by the physics itself. At high enough energies we expect this geometric association to fail and nonmetric features to become evident to the observers. In this case the induced constraints fail and evolution becomes potentially more difficult. One suggestion is that such a situation allows inconsistent light cone structures to be induced for different fields and that some intersection of these gives the proper causal structure for these fields when they are interacting.

The bilinear extension of the Dirac equation and promotion of the γ matrices to dynamical fields introduced a number of concerns related to positive definiteness of energy and probability and causality of the equations of motion. The latter has been verified for packets using gauge invariant functions of the fields. The former is seen to be not essential since these quantities, while rigidly conserved, are not necessarily the physical ones an observer perceives since they are derived from background coordinate symmetries. The probability function may be a nontrivial function of the fields in the case of gravity but normalization is assured in any theory of emergent measurement such as decoherence.

There are undoubtably many inequivalent such theories with the same low energy limit so we have presented only one of probably many such solutions. From here it is unclear how to extend this classical theory to a quantum one. The couplings are such that they determine the local notion of causality and it is not clear when or how well a perturbative scheme, which is generally built on free fields solutions, will work in the many body case. This is a direction for future work.

Submitted on November 4, 2014 / Accepted on November 24, 2014

References

1. Marquet P. Lichnierowicz's theory of spinors in General Relativity: the Zelmanov approach. *The Abraham Zelmanov Journal*, 2012 v. 5, 117–133.
2. Bjorken J.D., Drell S.D. Relativistic Quantum Mechanics and Relativistic Quantum Fields. McGraw-Hill, 1965.
3. Peskin M.E. and Schroeder D.V. An Introduction to Quantum Field Theory, Ed. Westview, Boulder, 1995.
4. Weinberg S. The Quantum Theory of Fields. Volumes I and II. Cambridge University Press, Cambridge, 1995.
5. Hestenes D. A unified language for Mathematics and Physics & Clifford algebra and the interpretation of quantum mechanics. In: Clifford Algebras and Their Applications in Mathematics and Physics. J.S.R. Chisholm & A.K. Common, eds., Reidel, Dordrecht, 1986, pp. 1–23 and pp. 321–346.
6. Chafin C. Automorphism Induced Nonlocal Conservation Laws. math-ph/arXiv: 1407.6782.
7. Chafin C. The Quantum State of Classical Matter I: Solids and Measurements. quant-ph/arXiv:1308.2305.
8. Mach E. The Science of Mechanics; a Critical and Historical Account of its Development. LaSalle, IL: Open Court Pub. Co., 1960.
9. Einstein A. On the electrodynamics of moving bodies. *Annalen der Physik*, 1905, v. 17, 891–921.
10. Misner C.W., Thorne K.S. and Wheeler J.A. Gravitation. Freeman, 1973.
11. Oppenheimer J.R. and Snyder H. On Continued Gravitational Contraction. *Physical Review*, 1939, v. 56(5), 455–459.
12. Chafin C. Globally Causal Solutions for Gravitational Collapse. gr-qc/arXiv:1402.1524.
13. Schweber S.S. An Introduction to Relativistic Quantum Field Theory. Harper and Row, 1962.
14. Jackson J. D. Classical Electrodynamics. Wiley, New York, 1962.
15. Rohrlich F. Classical Charged Particles. World Scientific, 2007.
16. Landau L. and Lifshitz E. M. The Classical Theory of Fields. Pergamon, Oxford, 1979.
17. Lasenby A. Doran C. and Gull S. Gravity, gauge theories and geometric algebra. *Philosophical Transactions of the Royal Society*, London, 1998, v. 356, 487.
18. Ehlers J. and Geroch R. Equation of motion of small bodies in relativity. *Annals of Physics*, 2004, v. 309, 232–239.

LETTERS TO PROGRESS IN PHYSICS

Bio-Precursors of Earthquakes and Their Possible Mechanism

Takhir R. Akhmedov

333 S. Webster Ave, Suite 4, Norman, OK 73069. E-mail: TakhirAkhmedov@yandex.com

People observed anomalous behavior of animals prior to powerful earthquakes since ancient times. Only in mid-20th century scientific community got interested in understanding what makes some animals "sensitive" to approaching earthquakes. Questions were raised of whether we are truly observing anomalous behavior or just interpreting it as such after the earthquake. Do animals actually "feel" the earthquakes? What are the stimuli impacting animal behavior? Scientists looked at chemical composition of ground water, release of some gases, sound booms and even electromagnetic activity as potential stimuli. With no comprehensive and systematic study of animal behavior prior to, during and after powerful earthquakes no plausible hypotheses explaining the sensitivity exist at this point. In this article, we propose a possible mechanism based on gravitational receptor, which each and every animal possess.

Accurate prediction of powerful earthquakes is one of the important problems faced by modern geophysics.

Rikitake (1979) presented extensive research data used for predicting earthquakes and tried to provide theoretical explanation [1]. While existing instrumental and statistical methods of predicting earthquakes allow identification of some patterns of future earthquakes, they do not answer the most important questions — the magnitude of future earthquake and its precise time. Geller (1997) states that "extensive searches have failed to find reliable precursors" [2]. He further notes that "theoretical work suggests that faulting is a non-linear process which is highly sensitive to unmeasurably fine details of the state of the Earth in a large volume, not just in the immediate vicinity of the hypocentre" [2].

Usually powerful earthquakes are accompanied with rapid increase in speed of vertical shift of Earth's crust in epicenter and adjacent areas. For example, after Ashkhabad, Turkmenistan, earthquake (October 5, 1948) as a result of leveling an increase in speed of vertical shift of Earth's crust with a maximum near Ashkhabad was identified. Similar observation made during Tashkent, Uzbekistan, earthquake (April 26, 1966).

Therefore, we can assume, that prior to powerful earthquakes an increase in speed of vertical shift of Earth's crust can be observed.

In recent years scientists got interested in the anomalous behavior of animals prior to powerful earthquakes. Even though anomalous behavior of animals is long known, scientific community only recently started researching this phenomenon. In late 1976, USA hosted the first conference on this subject.

The most important task facing scientists is identification of the physical nature of the processes, which lead to anomalous behavior of animals prior to powerful earthquakes.

Out of four types of forces (electromagnetic, gravitational, strong and weak) only electromagnetic and gravitational forces could be related to the mechanism of sensitivity of bio-precursors of earthquakes. Characteristics of Earth's electromagnetic field experience significant variations, which may impact sensitivity of the mechanism. Therefore, we will not consider electromagnetic force as the main force, which impacts the mechanism of sensitivity of bio-precursors of earthquakes. Let's consider gravitational force as the main force.

It is known that biological objects evolved within constant influence of gravitational field of the Earth. This lead to the creation of apparatus, gravitational receptor, allows biological objects to orient themselves in gravitational field [3]. Gravitational receptor basically consists of two main parts — "proof mass" with a mass m_p, which is capable of moving within the organ and around receptors that react to the changes of position of "proof mass".

One essential peculiarity of gravitational field is its constant presence and our inability to shield against its impact, i.e. all-pervading nature of the field.

One of the main characteristics of the gravitational field is free-fall acceleration g (analogous to the electric field intensity E). With changing characteristics of the field changes the force, which impacts the "proof mass" with the mass m_p. Such changes are possible prior to powerful earthquakes. However, there have not been successful measurements of such changes due to inadequate sensitivity of the instruments.

Biological objects, it seems, are able to react to the speed of changing free-fall acceleration parameter, which results from vertical shift of Earth's crust. If we consider the value of sensitivity of biological objects to such changes as m_p/M, where M is mass of the Earth, then biological objects are able to sense relative changes of the free-fall acceleration resulting from a vertical shift of Earth's crust, numerical value of

which exceeds m_p/M. Evaluations showed that speed of relative changes of free-fall acceleration, resulting from vertical shift of Earth's crust, exceeds maximum sensitivity of gravitational receptors of biological objects.

Thus, we conclude that biological objects, using signals from gravitational receptors, can react to the relative local changes of gravitational field prior to powerful earthquakes.

For experimental test of the proposed mechanism, we would suggest experiments with biological objects used as sensors of characteristics of gravitational field via continuous recording of bioelectric current from gravitational receptor during rapid increase in speed of vertical shift of Earth's crust in active seismic zones.

Submitted on December 1, 2014 / Accepted on December 4, 2014

References

1. Rikitake T. Prediction of Earthquakes. Mir Publishers, Moscow, 1979.
2. Geller R. J. Earthquake prediction: a critical review. *Geophys. J. Int.*, 1997, v. 131(3), 425–450.
3. Vinnikov Ya. A., Gazenko O. G., et al. Gravitational receptor. *Problems of Space Biology*, v. 12, Nauka, Leningrad, 1971.

Astrophysical Clock and Manned Mission to Mars

Takhir R. Akhmedov

333 S. Webster Ave, Suite 4, Norman, OK 73069. E-mail: TakhirAkhmedov@yandex.com

For many years scientists of different countries are engaged in research of biological processes, which have rhythms close to geophysical ones. The main objective of this research was finding the mechanism of time sensor, which leads to these rhythms. In the previous article (Akhmedov T.R. *Progress in Phys.*, 2014, v. 10, issue 1), based on the analysis of the known experimental data obtained from biological objects and in consideration of the original data obtained in Tashkent State University, we came to a conclusion that the time sensor of a biological clock is exogenous in nature. This means that clocks setting rhythms close to geophysical for biological processes exist outside of those biological objects. From this we conclude that there are no biological clocks, but rather there are astrophysical clocks (APhC), which form rhythms with periods close to geophysical within physical, chemical and biological processes.

1 Astrophysical Clocks (APhC)

Let us review the experimental data proving the existence of Astrophysical Clock. For this experiment we put assembled a system, schematics of which is plotted on Fig. 1.

Container (1) with distilled water was placed into the thermostated chamber (2), where stable temperature at $103 \pm 0.1^{\circ}$C was maintained. Water was boiling inside the container (1). The water vapor went through the cooling system (3) and precipitated into the container (4). The mass of the evaporated/precipitated water was measured every 15 min and a set of 4 measurements had been plotted on the Fig. 2 and Fig. 3. The experiments were carried out uninterruptedly by a number of series of 1 to 7 days of duration. In order to thoroughly investigate the rate of water vaporization power supply of the thermostat was carefully stabilized, all containers and tubes and connections were thermally insulated, mass was carefully measured and stability of the temperature was closely monitored. The data coming from the measurements strongly suggested the existence of CR in the physical process of distilled water evaporation from a thermostated container.

Initial experiments were carried out in 1974. During one of experiments it became necessary to obtain a stable flow of water vapor of low intensity (1.4×10^{-5} kg/s). This experimental data had been obtained in 1974 by a group of physicists conducted by Prof. M. A. Asimov. Author of the present article was a responsible head for the experiments.

2 Lunar rhythms

This study rises from my previous article [1], based on the analysis of the known experimental data obtained from biological objects and in consideration of the original data obtained in Tashkent State University. We came to a conclusion therein that the time sensor of a biological clock is exogenous in nature.

Scientific publications, dedicated to research of biological rhythms with periods close to geophysical ones, present much experimental data pointing at the existence of lunar

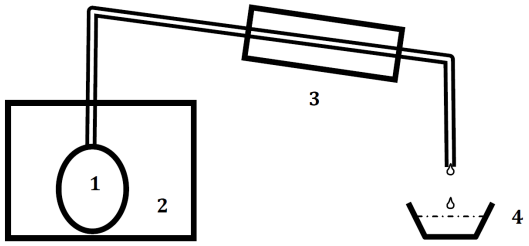

Fig. 1: (1) Container filled with distilled water; (2) Thermostated chamber with inside temperature of $103 \pm 0.1^{\circ}$C; (3) Cooling system; (4) Container where the water condensate was collected.

rhythms in biological processes [2, 3]. In 1974, a research group conducted by M. A. Azimov in Tashkent State University (Uzbekistan) identified lunar rhythms in chemical reaction of vapor conversion of methane at $T = 450^{\circ}$C. It is obvious that at such temperatures we can effectively exclude biological processes.

The stable vapor flow of low intensity was necessary for studying of chemical reaction of vapor conversion of methane. The reaction used in chemical industry to produce hydrogen is described by a formula:

$$CH_4 + 2H_2O \longrightarrow 450^{\circ}C \longrightarrow CO_2 + 4H_2 \,.$$

To investigate time dependence of the reaction speed there were provided stable flows of gaseous CH_4 and water vapor (deviations were $\pm 0.3\%$ and $\pm 3\%$, respectively). The experiment had been carried out for 540 hours in October and November of 1974.

In Fig. 3 the experimental measurements were plotted, y axis shows the fraction of residual methane in the converted dry gas at the output of the reactor.

Composition of the gas at the output was analyzed by the method of gas chromatography. Every 15 min three chromatographs were collected; results of 2-4 hour measurements were averaged and then plotted on the Fig. 3. Results of

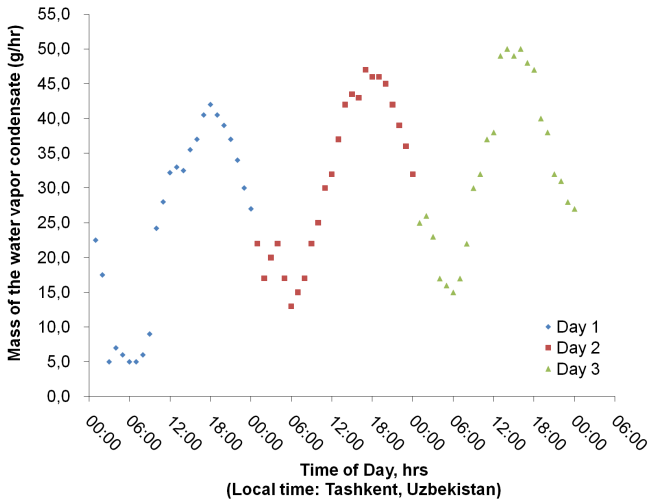

Fig. 2: Circadian periodicity of evaporation of water from a thermostated vessel at 103° (1974).

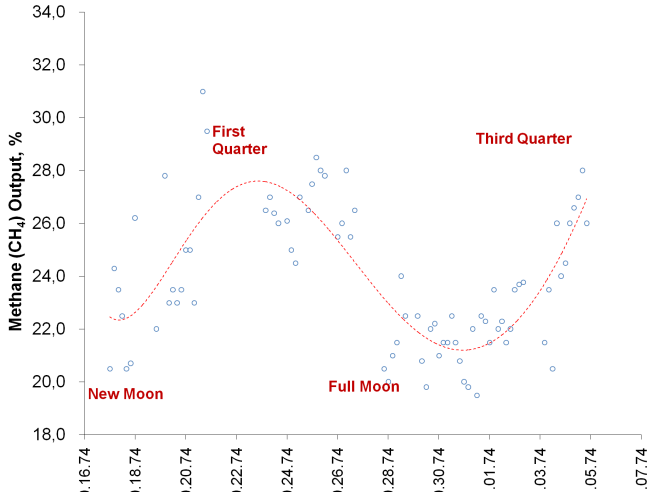

Fig. 3: Concentration of residual CH_4 in % in vapor conversion reaction output.†

these studies indicated on the existence of a lunar rhythm in the chemical reaction of vapor conversion of methane at $T = 450$°C. This temperature is noticeably higher than temperature of any known living organism.

3 Shnoll effect

One more argument in favor of existence of astrophysical clocks (APhC) is Shnoll Effect. It is shown that due to fluctuations, a sequence of discrete values is generated by successive measurement events whatever the type of the process measured. The corresponding histograms have much the same shape at any given time and for processes of a different nature and are very likely to change shape simultaneously for various processes and in widely distant laboratories. For a series of successive histograms, any given one is similar to its nearest neighbors and occurs repeatedly with a period of 24 hours, 27 days, and about 365 days, thus implying that the phenomenon has a very profound cosmophysical (or cosmogenic) origin [4, 5].

Substantial experimental material accumulated by biologists studying rhythms close to geophysical constitutes observations of the hands of astrophysical clock, which sets rhythms for biological processes. The rhythms for these processes are set by external forces.

Thus, from above described experimental data we conclude that rhythms close to geophysical, which occur in physical, chemical and biological processes, exist because of Astrophysical Clock (APhC).

4 How does Astrophysical Clock (APhC) work?

Let's analyze changing of kinetic and potential energy of atoms/molecule on the surface of the Earth. An atom/molecule on the surface of the Earth takes part in following motions:

1. Spinning of the Earth around its own axis with the surface speed $V_1 = 465 \cos\alpha$ m/s, where α is the geographic latitude;
2. Revolving with the Earth around the Sun with a linear speed of $V_2 = 3 \times 10^4$ m/s;
3. Moving with the Solar system around the center of the Galaxy with a linear speed of about $V_3 = 2.5 \times 10^5$ m/s;
4. Moving with the Galaxy from the center of the Universe with a linear speed of about $V_4 = 6 \times 10^5$ m/s.

It's known that total mechanical energy is the sum of kinetic energy E_K and potential energy U:

$$E_{\text{total}} = E_K + U(2).$$

And, if any of these components or both of them change according to a law, then the total energy will change according to the same law. And the change can be potentially affecting any physical, chemical or biological process. The factors 1-3 cause changing of kinetic energy of atoms/molecules on the surface of the Earth with periods, respectively, 24 hours (CR), a year (year rhythm), 180 million years (the Galaxy "year" rhythm). The existence of the rhythms has been mentioned above. Analysis of the kinetic energy changing leads us to the following formula:

$$E_{\max} - E_{\min} = 2m \times V_T \times V_E \cos\alpha\,,$$

where m is mass of an atom/molecule, V_T is thermodynamic speed of an atom/molecule, V_E is the orbital speed of the Earth's surface on the equator, α is the geographic latitude.

†Experimental data presented in this figure was obtained in 1972–1975, in Tashkent State University, Uzbekistan, by Azimov's group, headed by Takhir R. Akhmedov.

5 Conclusion

1. Experimental data on research of rhythmic processes with the periods close to geophysical (circadian rhythm — CR, lunar rhythm — LR, annual/year rhythm — YR) testify to existence of Astrophysical hours (APhC).

2. Rhythms with the periods close to the geophysical are experimentally observed in physical, chemical, and in biological processes. Furthermore, the circadian rhythm (CR) both in physical and in biological processes demonstrated a connection to local time.

3. Periods close to geophysical in all processes are formed Astrophysical Clock by change of a total energy (kinetic and potential) of atoms/ molecules located on the surface of Earth and moving with it in a space.

4. The Lunar Rhythm (LR) observed in chemical and biological processes is a result of a change of potential energy of atom (molecule), located on the surface of Earth. This change in potential energy is caused by movement of the Moon within the system Sun – Earth – Moon. All planets of the Solar System can have similar impact on processes taking place on Earth.

5. Biological objects (including humans) constantly have to receive signals of astrophysical clocks (APhC) for normal functioning. Thanks to APhC biological objects (almost closed systems) have an opportunity to exchange energy with environment, while maintaining their integrity.

6. During a long flight on low Earth orbit the time sensor of circadian rhythms is distorted for astronauts. This distortion could lead to imbalance of biochemical processes in astronaut's body, which could result in serious health issues. These issues may not manifest immediately.

7. During flight to Mars, human body stops receiving signals for setting circadian, lunar and yearly rhythms. This leads to total unbalancing of finely tuned biochemical reactions inside the body. At this point nobody knows what consequences this unbalancing may lead to. The difficulty of this problem is that experiments like Mars-500 cannot provide answers to these questions. One cannot turn off astrophysical clock during experiments on Earth.

8. To all those who desire and are able to carry out experiments studying the time dependence of water evaporation within a thermostatic vessel, further I provided the technical specifications:

- Thermostatic vessel to contain the liquid (8–10 litres of volume);
- Thermostatic liquid — motor or vegetable oil with temperature of 103±0.1°C;
- A system to distilled water, using typical chemical lab hardware;
- The flask with water to be evaporated should be located inside the thermostatic vessel;
- Cooling system for water vapor condensation;
- Water passing through the cooling system should be room temperature of 20°C with flow rate at 1 litre per minute;
- The frequency of measurements (time interval at which measurements are taken) is at the discretion of scientists setting up experiments (10 min, 15 min, etc.).

Objective: to plot the correlation of water vapor (condensate) with the time of day. Running experiment for 72 hrs is preferred. When publishing results of this experiment, the researcher needs to state geographical coordinates where experiment took place.

Submitted on December 1, 2014 / Accepted on December 4, 2014

References

1. Akhmedov T. R. Exogenous mechanism of the time sensor of biological clock. *Progress in Physics*. 2014, v. 10(1), 56–59.
2. Biological Clock. Transl. from Eng. with Introduction by S. E. Shnol, Mir Publishers, Moscow, 1964.
3. Biological Rhythms. Vols. 1-2, Ed. Achhoff J., Mir Publishers, Moscow, 1984.
4. Shnoll S. E., Kolombet V. A., Pozharskii E. V., Zenchenko T. A., Zvereva I. M., Konradov A. A. Realization of discrete states during fluctuations in macroscopic processes. *Physics Uspekhi*, 1998, v. 41, issue 10, 1025–1035.
5. Shnoll S. E. Cosmophysical Factors in Stochastic Processes. American Research Press, Rehoboth (NM), 2012.

Periodic Relativity: Deflection of Light, Acceleration, Rotation Curves

Vikram H. Zaveri

B-4/6, Avanti Apt., Harbanslal Marg, Sion, Mumbai 400022 INDIA. E-mail: zaverivik@hotmail.com

Vectorial analysis relating to derivation of deflection of light is presented. Curvilinear acceleration is distinguished from the Newtonian polar conic acceleration. The difference between the two is due to the curvature term. Lorentz invariant expression for acceleration is derived. A physical theory of rotation curves of galaxies based on second solution to Einstein's field equation is presented. Theory is applied to Milky Way, M31, NGC3198 and Solar system. Modified Kepler's third law yields correct orbital periods of stars in a galaxy. Deviation factor in the line element of the theory happens to be the ratio of the Newtonian gravitational acceleration to the measured acceleration of the star in the galaxy. Therefore this deviation factor can replace the MOND function.

1 Introduction

The article presented here is only a small element of a much larger formulation [1–6] proposed to arrive at a theory of quantum gravity and cosmology. Physicists have put in considerable efforts to unify general relativity and quantum mechanics but without success. The string theory and loop quantum gravity are still far from their goal.

Scientists are looking for a unified theory of creation. To achieve this objective, the physicists have set up two principal goals. First is the search for the fundamental building block of the universe. Second is the unification of four fundamental forces in nature. This constitutes the mainstream physics. The theory presented here regards these two principal goals as speculative and not plausible and hence the deviation from the mainstream physics.

Another feature of the mainstream physics is that most of the physicists if not all, consider consciousness [5, 6] as something outside the domain of physics and therefore when they talk about theory of everything, they really mean theory of everything excluding consciousness. As per the current understanding in the physical and life sciences, much of the scientific literature maintain strict distinction between consciousness and matter. The former is considered sentient and the later insentient. Many people are of the opinion that the existence of consciousness in this universe is a reality and the big bang theory could not be considered complete till it can account for the presence of consciousness along with the other forms of insentient matter.

Having rejected the two principal goals of the mainstream physics, this theory proposes that everything in the universe is reducible to energy. Therefore unity behind four forces (bosons), fermions and leptons should be sought in energy. Another point this theory makes is that the consciousness and energy are two states of one and the same thing which you may call the fundamental substance (Spirit) of the universe. Fundamental building block of the universe is assumed to be a micro entity, but the fundamental substance of the universe is all pervasive and ever remains undivided.

In this theory space and time does not have any physical existence, but they exist only in the human mind as imaginary artifacts. Comparatively, the energy has some real existence and it is found in myriads of forms. Again the energy is always associated with oscillations and motion, without exception. When these oscillation and motion of the energy subside, it gets transformed into the unmanifest which is not the energy and therefore does not gravitate. This unmanifest is motionless without any oscillations and therefore impossible to detect like empty space.

The idea of space-time arise in the human mind by way of delusion. When a particle wave is presented to a physicist, instead of seeing the oscillating energy, what he does is, superimposes the idea of wavelength and period on this wave and sees the space-time. All the geometrical theories in physics are founded upon such delusion. In periodic quantum gravity (PQG), the time does not flow in one direction, but one gets the sense of time by comparing one period of time with another. Hence time is a periodic phenomenon and periods are inverse of frequencies. Therefore in PQG, the Hubble parameter is associated with the frequency of the particle. Both have the same units. This eliminates the problem of time which plagues the Wheeler De Witt equation and its associated theories like loop quantum gravity, Hartle-Hawking wavefunction of the universe etc.

Advantage of Periodic relativity (PR) over general relativity can be seen in its use of revised principle of equivalence which states that the gravitational mass is equal to the relativistic mass. Application of this principle gives a very simple derivation for the orbital period derivative of the binary star [3]. And most important of all, allows the unification of periodic relativity with quantum mechanics. Because of this revised principle of equivalence, (modified) Newton's inverse square law of gravitation can be merged with the (modified) Schrodinger Wave equation which gives the basis for periodic quantum gravity and cosmology theory [4]. PR satisfies Einstein's field equations but does not utilize weak field approximation.

The reason general relativity (GR) got plagued with these two problems (the problem of time associated with Wheeler

De Witt equation and the inaccurate notion that the gravitational mass is equal to the inertial mass) is its dependence on the weak field approximation. The use of weak field approximation automatically locks the theory into having these two problems. When you depend on weak field approximation, you cannot treat time as a periodic phenomenon and you cannot introduce energy momentum invariant into Newton's inverse square law.

Another problem with GR is that the universe in this theory begins with a mixture of energy (radiation) and matter field. It doesn't even bother to explain where these two things come from. Another contradiction is that the equivalence of mass and energy is the biggest feature of GR at the same time they must have the universe begin with a mixture of energy (radiation) and the matter field. And all the physicists find it very comfortable to ignore the presence of life and consciousness in the universe. At the same time they must have a theory of everything.

Periodic quantum gravity and cosmology [4] is based on the idea that there is a connection between consciousness and energy [5]. Based on these ideas PQG proposes a unified field of consciousness (UFC) [6] underlying the entire universe from which comes the energy and matter fields of the big bang theory. In relating the consciousness and the energy the periodic nature of the time is the most essential factor. You don't need any clock operators of the Wheeler De Witt theory.

On the quantum mechanical side I don't think Dirac's linear representation of the wave function is very accurate because spin in that theory is not a part of the dynamics of motion but it is introduced as a perturbation just like in Darwin and Pauli theories. Also, the selection of the radial momentum operator is somewhat arbitrary and it isn't Hermitian as pointed out by several authors. These deficiencies are removed in the modified Schrodinger wave equation [2] in which spin is directly introduced in the Laplacian operator. This gives exactly same energy levels for hydrogen atom as in Dirac's theory and also it's application to heavy quarkonium spectra gives data which are spin dependent.

When these two theories, the periodic relativity and the relativistic wave mechanics are united, the result is the periodic quantum gravity and cosmology theory [4] which yields the entire table of standard model particles from a single formula. There is no other theory of quantum gravity that can do this.

Current article presents some corrections in previous article [1] and perfects the derivation for the deflection of light. It develops Lorentz invariant expression for the acceleration and provides solution for the rotation curves of galaxies which does not exist in GR. This solution does not have a discontinuity like the one in the MOND function. The transition from short distances to astronomical distances is continuous. This theory gives perfect fit for the rotation curves which MOND theory cannot give.

2 Curvilinear Gravity

In the earlier article "Periodic relativity: basic framework of the theory" [1], we obtained correct deflection of light in Newtonian theory by multiplying both sides of Newton's inverse square law of gravitation by the factor $(\cos\psi + \sin\psi)$. As shown in Figs. 1 and 2 of that article, ψ is the angle between the radial vector and the tangential velocity vector. Explanation given below makes it more clear that the theory is Lorentz invariant and factor $(\cos\psi + \sin\psi)$ introduces geodesic like trajectories. The details are as follows. After very elaborate analysis, we arrive at Newton's inverse square law given by

$$m_0 \frac{d^2\mathbf{r}}{dt^2} = -\frac{GM_0 m_0}{r^2}\,\hat{\mathbf{r}}, \tag{1}$$

where $GM_0 = \mu$. Here we introduce the dynamic weak equivalence principle which states that the gravitation mass is equal to the relativistic mass. Therefore Eq. 1 becomes

$$m \frac{d^2\mathbf{r}}{dt^2} = -\frac{\mu m}{r^2}\,\hat{\mathbf{r}}. \tag{2}$$

In classical mechanics, we have two different expressions for the acceleration acting on a body in motion. One is a general expression $d\mathbf{v}/dt$ in cartesian coordinates which include the curvature term, and another is for Newtonian gravity in polar coordinates $d^2\mathbf{r}/dt^2$ based on the angular momentum vector $\mathbf{h}$, which is supposed to be a constant in order to satisfy Kepler's third law of equal areas in equal times. In periodic relativity [1] we have shown that these two accelerations are not equal. At the same time we have maintained that the velocity vectors in both coordinate systems are equal, $\mathbf{v} = d\mathbf{r}/dt$. The reason for this is that the Newtonian gravity ignores the variation of angle ψ along the trajectory by assuming constant $\mathbf{h}$.

As shown in Fig. 1, this angle ψ is related to curvature through the expression

$$\phi = \theta + \psi, \tag{3}$$

where $d\phi/ds = \kappa$ is the curvature. Newtonian gravity ignores this curvature term by assuming constant $\psi = \pi/2$. This can be verified from following arguments.

$$\mathbf{h} = \frac{\mathbf{L}}{m} = \frac{\mathbf{p}\times\mathbf{r}}{m} \equiv \frac{|\mathbf{p}||\mathbf{r}|\sin\psi}{m}\,\hat{\mathbf{h}} = r^2\frac{d\theta}{dt}\sin\psi\,\hat{\mathbf{h}}. \tag{4}$$

From Eq. 4 we can see that $\mathbf{h}$ can be the desired constant only if $\sin\psi = 1$. This shows that the very foundation of Newtonian gravity ignores the curvature of the trajectory of the orbiting body. Hence in periodic relativity it is considered unreasonable to equate the cartesian acceleration $d\mathbf{v}/dt$ with the Newtonian polar acceleration $d^2\mathbf{r}/dt^2$.

In order to account for the variation of angle ψ along the trajectory, we propose that the absolute sum of vector and scalar products of $(\mu/r^2)\hat{\mathbf{r}}$ and $\hat{\mathbf{a}}$ is equal to magnitude

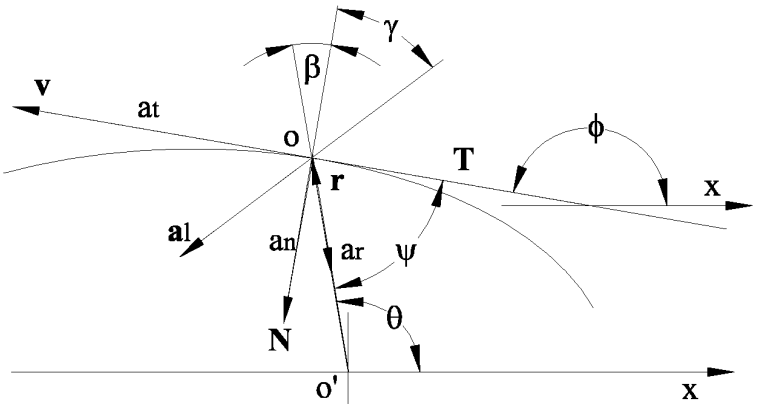

Fig. 1: Vectors in a two-body system.

of $d\mathbf{v}/dt$. The relation of these vectors to angle ψ is shown in Fig. 1

$$\left|\frac{d\mathbf{v}}{dt}\right| = \left|-\left|\hat{\mathbf{a}}\times\frac{\mu}{r^2}\hat{\mathbf{r}}\right| - \frac{\mu}{r^2}\hat{\mathbf{r}}\cdot\hat{\mathbf{a}}\right|, \tag{5}$$

$$\left|\frac{d\mathbf{v}}{dt}\right| = \left|\hat{\mathbf{a}}\right|\left|\frac{\mu}{r^2}\hat{\mathbf{r}}\right|\sin(\beta+\gamma)\hat{\mathbf{h}}\Big| + \left|\frac{\mu}{r^2}\hat{\mathbf{r}}\right|\left|\hat{\mathbf{a}}\right|\cos(\beta+\gamma), \tag{6}$$

where

$$\beta = \left(\frac{\pi}{2} - \psi\right), \tag{7}$$

$$\gamma = \tan^{-1}\left(\frac{a_t}{a_n}\right). \tag{8}$$

Various magnitudes of the parameters shown in Fig. 1 are as follows.

$$\mathbf{a}_l = \frac{d\mathbf{v}}{dt}, \tag{9}$$

$$a_t = \left(\frac{d^2s}{dt^2} + \frac{v}{\nu}\frac{d\nu}{dt}\right), \tag{10}$$

$$a_n = \kappa\left(\frac{ds}{dt}\right)^2, \tag{11}$$

$$a_r = -\frac{\mu}{r^2} = \left|\frac{d^2\mathbf{r}}{dt^2}\right|, \tag{12}$$

$$\mathbf{v} = \frac{d\mathbf{r}}{dt}. \tag{13}$$

Substitution of Eq. 7 in Eq. 6 gives

$$\left|\frac{d\mathbf{v}}{dt}\right| = \frac{\mu}{r^2}\left(\cos(\psi-\gamma) + \sin(\psi-\gamma)\right). \tag{14}$$

When the tangential component of the acceleration is absent then we have $a_t\widehat{\mathbf{T}} = 0$. This gives $\gamma = 0$ and Eq. 14 reduces to

$$\left|\frac{d\mathbf{v}}{dt}\right| = \frac{\mu}{r^2}\left(\cos\psi + \sin\psi\right). \tag{15}$$

Similarly we can show that

$$\left|\frac{d\mathbf{v}}{dt}\right| = \left|\frac{d^2\mathbf{r}}{dt^2}\right|\left(\cos(\psi-\gamma) + \sin(\psi-\gamma)\right). \tag{16}$$

The first term on the right of Eq. 14 can be interpreted as an angular acceleration vector with its axis perpendicular to the plane of motion. This could be the additional acceleration quantity responsible for the rotation of the velocity vector $\mathbf{v}$ about the coordinate origin o, causing the curvature of the trajectory.

2.1 Lorentz invariant acceleration

Little diversion here. In the earlier work [1], we introduced deviation to the flat Minkowski metric due to the gravitational field in the form,

$$\left(\frac{dt}{d\tau}\right)^2 = \gamma^{2n} = (1-\beta^2)^{-n}. \tag{17}$$

Here I propose a correction to our theory and change the method of introducing the deviation so that the deviation factor n is directly introduced in the Lorentz transformation equation as given below.

$$\left(\frac{d\tau}{dt}\right)^2 = \left(1 - n\beta^2\right), \tag{18}$$

where t is the coordinate time, τ the proper time of the orbiting body, n is a real number and $\beta = v/c$. The corresponding line element in polar coordinates is,

$$ds^2 = c^2dt^2 - ndr^2 - nr^2d\theta^2 - n(r^2\sin^2\theta)d\phi^2. \tag{19}$$

We showed [1] that the line element Eq. 19 satisfies Einstein's field equations for any constant value of n. For any constant value of n, metric 19 always remain flat. This is similar to the line element in Friedmann model when curvature factor $K = 0$. The change made in equation 18 does not alter any of the previous derivations.

Coming back to the main topic, in relativity we can either write our equations in terms of proper time or alternatively we can write them in terms of relativistic mass. Eq. 18 can be written as

$$\left(\frac{d\tau}{dt}\right)^2 = \left(1 - n\beta^2\right) = \left(\frac{m_0}{m}\right)^2 = \left(\frac{E_0}{E}\right)^2, \tag{20}$$

where $E = mc^2 = h\nu$. This gives

$$E = \left(E_0^2 + nE^2\beta^2\right)^{1/2}. \tag{21}$$

Differentiating w.r.t. time we get

$$\frac{dE}{dt} = \hat{\mathbf{v}}F = n\left(m\mathbf{a} + \frac{h\mathbf{v}}{c^2}\frac{d\nu}{dt}\right). \tag{22}$$

Here we arrive at the same relation that we described as true force in the previous article [1] except that now we have introduced the deviation factor n. I like to further point out a correction that this true force is same as the Lorentz force. Here we have used the relation $E = mc^2 = h\nu$. Therefore

$$\mathbf{F} = \frac{d\mathbf{p}}{dt} = \frac{dm\mathbf{v}}{dt} = n\left(m\mathbf{a} + \frac{h\mathbf{v}}{c^2}\frac{d\nu}{dt}\right), \tag{23}$$

where $\mathbf{F}$ is the Lorentz force and $\mathbf{v}$ the velocity vector and $\mathbf{a}$ is the classical acceleration of the particle given by

$$\mathbf{a} = \left(\frac{d^2s}{dt^2}\widehat{\mathbf{T}} + \kappa\left(\frac{ds}{dt}\right)^2\widehat{\mathbf{N}}\right). \tag{24}$$

Therefore, Lorentz force = Classical force + de Broglie force. From Eq. 23 we can define Lorentz invariant acceleration $\mathbf{a}_l$ as

$$n\mathbf{a}_l = n\left(\left(\frac{d^2s}{dt^2} + \frac{v}{\nu}\frac{d\nu}{dt}\right)\widehat{\mathbf{T}} + \kappa\left(\frac{ds}{dt}\right)^2\widehat{\mathbf{N}}\right). \tag{25}$$

The de Broglie force acts along the tangent vector. Now we equate Lorentz force with the gravitational force given by Eq. 14

$$\begin{aligned} |nm\,\mathbf{a}_l| &= \left|m\frac{d\mathbf{v}}{dt}\right| \\ &= nm\left(\left(\frac{d^2s}{dt^2} + \frac{v}{\nu}\frac{d\nu}{dt}\right)\widehat{\mathbf{T}} + \kappa\left(\frac{ds}{dt}\right)^2\widehat{\mathbf{N}}\right) \\ &= \frac{\mu m}{r^2}\left(\cos(\psi-\gamma) + \sin(\psi-\gamma)\right), \end{aligned} \tag{26}$$

$$\begin{aligned} |\mathbf{a}_l| &= \left|\frac{1}{n}\frac{d\mathbf{v}}{dt}\right| = \left(\left(\frac{d^2s}{dt^2} + \frac{v}{\nu}\frac{d\nu}{dt}\right)\widehat{\mathbf{T}} + \kappa\left(\frac{ds}{dt}\right)^2\widehat{\mathbf{N}}\right) \\ &= \frac{\mu}{nr^2}\left(\cos(\psi-\gamma) + \sin(\psi-\gamma)\right). \end{aligned} \tag{27}$$

2.2 Bending of light in periodic relativity

For the bending of light around the sun, we introduce light parameters $v = ds/dt = c$, $d^2s/dt^2 = 0$ and $cdt = ds$, along with $\kappa = d\phi/ds$ for the curvature of the trajectory in Eq. 27. In this case we will have $d\nu/dt = 0$ because the ray is equally blue shifted and then red shifted, and the frequency shift is 0 at the limb of the sun. This gives,

$$\left|\frac{c^2}{\nu}\frac{d\nu}{ds}\widehat{\mathbf{T}} + c^2\frac{d\phi}{ds}\widehat{\mathbf{N}}\right| = \frac{\mu}{nr^2}\left(\cos(\psi-\gamma) + \sin(\psi-\gamma)\right). \tag{28}$$

Multiplying both sides by $d\psi$, we get

$$\begin{aligned} &\left|\frac{1}{\nu}d\nu d\psi\widehat{\mathbf{T}} + d\phi d\psi\widehat{\mathbf{N}}\right| \\ &= \frac{\mu}{nc^2r^2}\left(\cos(\psi-\gamma) + \sin(\psi-\gamma)\right)ds d\psi. \end{aligned} \tag{29}$$

We integrate both sides with proper limits. For the star light approaching the sun we get,

$$\begin{aligned} &\left|\int_{\nu_1}^{\nu_2}\int_{\pi}^{\frac{\pi}{2}}\frac{1}{\nu}d\nu d\psi\widehat{\mathbf{T}} + \int_{-\phi}^{0}\int_{\pi}^{\frac{\pi}{2}}d\phi d\psi\widehat{\mathbf{N}}\right| \\ &= \frac{\mu}{nc^2}\int_{-\infty}^{0}\int_{\pi}^{\frac{\pi}{2}}\frac{1}{r^2}\left(\cos(\psi-\gamma) + \sin(\psi-\gamma)\right)d\psi ds. \end{aligned} \tag{30}$$

For the star light approaching earth from the limb of the sun we get,

$$\begin{aligned} &\left|\int_{\nu_2}^{\nu_1}\int_{\frac{\pi}{2}}^{0}\frac{1}{\nu}d\nu d\psi\widehat{\mathbf{T}} + \int_{0}^{-\phi}\int_{\frac{\pi}{2}}^{0}d\phi d\psi\widehat{\mathbf{N}}\right| \\ &= \frac{\mu}{nc^2}\int_{0}^{\infty}\int_{\frac{\pi}{2}}^{0}\frac{1}{r^2}\left(\cos(\psi-\gamma) + \sin(\psi-\gamma)\right)d\psi ds, \end{aligned} \tag{31}$$

$$\begin{aligned} &\left|(\ln\nu_2 - \ln\nu_1)\widehat{\mathbf{T}} + \phi\widehat{\mathbf{N}}\right| \\ &= \frac{\mu}{nc^2}\int_{-\infty}^{0}\int_{\pi}^{\frac{\pi}{2}}\frac{1}{r^2}\left(\cos(\psi-\gamma) + \sin(\psi-\gamma)\right)d\psi ds, \end{aligned} \tag{32}$$

$$\begin{aligned} &\left|(\ln\nu_1 - \ln\nu_2)\widehat{\mathbf{T}} + \phi\widehat{\mathbf{N}}\right| \\ &= \frac{\mu}{nc^2}\int_{0}^{\infty}\int_{\frac{\pi}{2}}^{0}\frac{1}{r^2}\left(\cos(\psi-\gamma) + \sin(\psi-\gamma)\right)d\psi ds. \end{aligned} \tag{33}$$

If we add l.h.s. of Eqs. 32 and 33 we get,

$$\text{l.h.s.} = \left|0.\widehat{\mathbf{T}} + 2\phi\widehat{\mathbf{N}}\right|. \tag{34}$$

From Eq. 34 we see that the magnitude of the tangential component is zero. Therefore $\gamma = 0$. Hence substituting $r^2 = s^2 + \Delta^2$ in Eqs. 32 and 33 we get

$$2\phi = \frac{4\mu}{nc^2\Delta}. \tag{35}$$

It is obvious from Eq. 35 that the value of constant n is 1 and not 0 as was assumed in earlier article [1]. $n = 1$ corresponds to the flat Minkowski metric therefore both the bending of light and the gravitational frequency shift can be explained corresponding to $n = 1$. Not only that, but no matter what gets measured in future experiments such as LATOR, the new measurement can easily be made to fit Eq. 35 by adjusting the constant n.

2.3 Curvic and conic gravity

Newtonian gravity is based on the constant vector **h** which yields the conic sections. Therefore we can distinguish the gravity that uses the Lorentz invariant acceleration as the curvilinear (or curvic) gravity and the Newtonian gravity with constant **h** as the conic gravity. Accelerations of the curvic and conic gravity are related by Eq. 16. It also needs to be understood that $d^2\mathbf{r}/dt^2$ is a radial vector but $d\mathbf{r}/dt$ is not a radial vector which acts along the velocity vector **v**. Moreover, the constant vector **h** does not play any role in defining the velocity vector **v**. Therefore factor $(\cos\psi + \sin\psi)$ does not appear in this expression of velocity $\mathbf{v} = d\mathbf{r}/dt$ which remains unaltered. This can be verified from following analysis. By definition we have

$$\cos\psi = \frac{dr}{ds}, \quad \text{and} \quad \sin\psi = \frac{rd\theta}{ds}, \tag{36}$$

$$\frac{d\mathbf{r}}{dt} = \left(\frac{dr}{dt}\hat{\mathbf{r}} + \frac{rd\theta}{dt}\hat{\theta}\right), \tag{37}$$

$$\frac{d\mathbf{r}}{dt} = \frac{ds}{dt}\left(\cos(\psi+\theta)\mathbf{i} + \sin(\psi+\theta)\mathbf{j}\right). \tag{38}$$

Substitution of Eq. 3 gives

$$\frac{d\mathbf{r}}{dt} = \frac{ds}{dt}\sqrt{\left(\cos^2\phi + \sin^2\phi\right)}\widehat{\mathbf{T}} = \frac{ds}{dt}\widehat{\mathbf{T}} = \mathbf{v}. \tag{39}$$

From Fig. 1 we can verify that the unit vector acting at an angle ϕ is $\widehat{\mathbf{T}}$. Therefore Eq. 39 is not influenced by the constant **h** assumption.

3 Rotation curves of galaxies

Earlier [1] we obtained two solutions to Einstein's field equations,

$$\left(\frac{r}{n}\frac{\partial n}{\partial r}\right) = 0 \qquad \text{and} \qquad \left(\frac{r}{n}\frac{\partial n}{\partial r}\right) = -4. \tag{40}$$

So far we have seen the application of the first solution which requires n to be any real number constant. Now we look at the second solution which we can write as

$$\int \frac{\partial n}{n} = -4\int \frac{\partial r}{r}, \tag{41}$$

$$\ln(nr^4) = C, \tag{42}$$

where C is a constant of integration. This gives

$$n = \frac{e^C}{r^4} = \frac{k}{r^4}, \tag{43}$$

where

$$k = e^C = \text{constant}. \tag{44}$$

In this second solution n need not be a constant. We make use of Eq. 27 in order to apply the second solution to rotation curves of a galaxies. Assuming circular orbit we substitute $\psi = \pi/2$ and $\gamma = 0$. This gives

$$|\mathbf{a}| = \frac{\mu}{nr^2} = \frac{\mu r^2}{k} = \frac{v^2}{r}, \tag{45}$$

$$k = \frac{\mu r^3}{v^2}. \tag{46}$$

We can write Eq. 45 as

$$v^2 = \frac{4\pi^2 r^2}{P^2} = \frac{\mu}{nr}, \tag{47}$$

$$P = \frac{2\pi r}{v}, \tag{48}$$

$$P^2 = \frac{4\pi^2 r^3 n}{\mu}. \tag{49}$$

For $n = 1$, Eq. 49 reduces to Kepler's third law, where P is the orbital period. Substituting Eq. 46 in Eq. 43 and Eq. 18 we can compute the ratio $d\tau/dt$. We can apply these equations of stellar motion to Blue Horizontal-Branch (BHB) halo stars of the Milky Way [8]. The circular velocity estimates are based on Naab's simulation [9]. To this data, one additional data point for solar radius of $8kpc$ [10] is added and the results obtained from Eqs. 46, 43 and 18 are shown in Table 1. Computed values are based on the stellar mass at the galactic center, which is $5.0924 \times 10^{10} M_\odot$ [11, 12]. Observed values of r and circular velocities constrain the integration constant k which provides a measure of non-uniform distribution of the galactic matter and the cold dark matter at a given radius. Hence it is appropriate to describe k as a galactic matter distribution constant. We also find that Eqs. 48 and 49 both yield exactly the same orbital period when velocity and deviation n along with the galactic stellar mass are used from the Tables. For the Sun, both yield 223.4 million years.

Table 1: Milky Way rotation curve based on proper time. r(kpc), v(km/s).

r	v	$k \times 10^{-81}$	n	$(1 - d\tau/dt)$
7.5	216	1.79546	0.62593	1.6246×10^{-7}
8.0	220	2.10050	0.56566	1.5231×10^{-7}
12.5	227	7, 52624	0.34004	9.748×10^{-8}
17.5	179	33.2129	0.39061	6.9628×10^{-8}
22.5	168	80.1362	0.34490	5.4155×10^{-8}
27.5	183	123.309	0.23782	4.43091×10^{-8}
32.5	143	333.332	0.32956	3.7492×10^{-8}
37.5	170	362.322	0.20210	3.2493×10^{-8}
42.5	183	455.160	0.15388	2.8670×10^{-8}
47.5	165	781.650	0.16936	2.5652×10^{-8}
55	183	986.474	0.11891	2.2154×10^{-8}

Table 2 shows solar system data from NASA planet fact sheets. Radial distance equal to semi major axis and mean

Table 2: Solar system rotation curve based on proper time. r(m), v(km/s).

Planet	$r \times 10^{-9}$	v	k	n
Mercury	57.91	47.87	1.12×10^{43}	1.000103
Venus	108.21	35.02	1.37×10^{44}	1.000059
Earth	149.6	29.78	5.01×10^{44}	1.000332
Mars	227.92	24.13	2.69×10^{45}	1.000065
Jupiter	778.57	13.07	3.66×10^{47}	0.997876
Saturn	1433.53	9.69	4.16×10^{48}	0.985986
Uranus	2872.46	6.81	6.78×10^{49}	0.99627
Neptune	4495.06	5.43	4.08×10^{50}	1.00136
Pluto	5869.66	4.72	1.20×10^{51}	1.014912
Moon	0.3844	1.023	2.16×10^{34}	0.990824

Table 3: M31 rotation curve. k in m^4, r(kpc), v(km/s), P in billions of yrs, $x = k \times 10^{-81}$.

r	v	x	n	$(1 - d\tau/dt)$	P
8.5	232	6.23	1.316	3.94×10^{-7}	0.225
12.5	251	16.89	0.763	2.68×10^{-7}	0.305
16.5	251	38.74	0.576	2.03×10^{-7}	0.402
20.5	227	90.94	0.568	1.63×10^{-7}	0.553
24.5	226	156.89	0.480	1.367×10^{-7}	0.665
28.5	218	263.96	0.441	1.175×10^{-7}	0.80
32.5	224	371.15	0.367	1.030×10^{-7}	0.888
36.5	240	460.47	0.286	9.178×10^{-8}	0.933

Table 4: NGC3198 rotation curve. k in m^4, r(kpc), v(km/s), P in billions of yrs, $x = k \times 10^{-79}$.

r	v	x	n	$(1 - d\tau/dt)$	P
0.68	55	0.202	10.45	1.76×10^{-7}	0.0759
1.36	92	0.579	1.868	8.79×10^{-8}	0.0908
2.72	123	2.593	0.522	4.39×10^{-8}	0.1358
5.44	147	14.52	0.183	2.2×10^{-8}	0.2273
8.16	156	43.52	0.108	1.466×10^{-8}	0.3213
13.6	154	206.78	0.066	8.79×10^{-9}	0.5425
19.04	148	614.36	0.0515	6.28×10^{-9}	0.7903
24.48	148	1305.7	0.040	4.88×10^{-9}	1.016
29.92	149	2352.1	0.0323	3.99×10^{-9}	1.233

orbital velocity are used. k and n are computed using Eqs. 46 and 43. $(1 - d\tau/dt)$ are of order 10^{-8} to 10^{-12} and not shown in the table. In case of moon, earth mass 5.9736×10^{24} Kg. is used. Value of n for Mercury shown in Table 2 should not be compared with that used in the derivation of perihelic precession [1] because here we have used second solution of Einstein's field equations with constant k, where as perihelic precession is derived from the first solution of Einstein's field equations with constant n. These two solutions are derived from two roots of a quadratic equation. The purpose of presenting the solar system data is only to show that there is no discontinuity like the MOND function. One should not look for precision in Table 2 because it is based on circular orbit approximation. It is sufficient to note that $n = 1$ for flat Minkowski metric is recovered at small distances.

We can also apply these equations of stellar motion to rotation curves of M31 [13] and NGC3198 [14]. The results obtained from Eqs. 46, 43 and 18 are shown in Tables 3 and 4. Computed values are based on the stellar mass at the galactic center, which is $1.4 \times 10^{11} M_\odot$ for M31 and $5.0 \times 10^9 M_\odot$ for NGC3198.

From Eq. 27, we can see that n is a ratio of Newtonian gravitational acceleration to the measured acceleration which is 1 for flat Minkowski metric. From Eq. 45 we get the same relation for circular orbits.

$$n = \frac{\mu/r^2}{v^2/r}. \tag{50}$$

Substitution of n in Eq. 18 gives

$$d\tau^2 = \left(1 - \frac{\mu}{rc^2}\right) dt^2. \tag{51}$$

Therefore metric 51 becomes singular for the limiting radius

$$r_l = \frac{\mu}{c^2}. \tag{52}$$

This is the same expression which we derived earlier [1] for a black hole.

4 Conclusion

We have presented derivation for the deflection of light from fundamentals by introducing vectors. Here we can relate the additional component of acceleration with the rotation of the velocity vector which causes the curvature of the trajectory. We have distinguished the cartesian curvilinear acceleration from the polar conic acceleration and explained why they are not equal even though they are derived from the same velocity vector. We have derived expression for the Lorentz invariant acceleration. We have presented a theory of rotation curves of galaxies which is based on the second solution of Einstein's field equations which yields much better results than the earlier one based on the first solution with constant n [7]. Deviation factor n appears in the expression for acceleration as well as the modified Kepler's third law which now yeilds correct orbital periods for the stars of galaxies. Deviation factor n plays the same role as the MOND function in the expression for acceleration. This kind of solution cannot be obtained in general relativity because of the weak field approximation, which is a different way of introducing deviation to the flat Minkowski metric.

Acknowledgments

Author is grateful to Robert Low, Gerard t'Hooft, Stam Nicolis, Christopher Eltschka, Bruce Rout and Thiago C. Junqueira for useful discussion and comments.

Submitted on November 24, 2014 / Accepted on November 28, 2014

References

1. Zaveri V.H. Periodic relativity: basic framework of the theory. *Gen. Relativ. Gravit.*, 2010, v. 42 (6), 1345–1374. https://www.researchgate.net/publication/225712819.
2. Zaveri V.H. Quarkonium and hydrogen spectra with spin dependent relativistic wave equation. *Pramana — J. Phys.* 2010, v. 75 (4), 579–598.
3. Zaveri V.H. Orbital period derivative of a binary system using an exact orbital energy equation. arXiv:0707.4544v3.
4. Zaveri V.H. Periodic quantum gravity and cosmology. Submitted, *Grav. Cosmol.* May 2014, https://www.researchgate.net/publication/262492889.
5. Zaveri V.H. Consciousness and energy. In: The Big Bang: Theory, Assumptions and Problems, eds. O'Connell J.R., Hale A.L. 275–284. Nova Science Publishers, New York, 2012, https://www.researchgate.net/publication/262494186.
6. Zaveri V.H. Unified field of consciousness. 2014. https://www.researchgate.net/publication/266618399.
7. Zaveri V.H. Rotation curves of galaxies in periodic relativity. arXiv: 0805.2233v4.
8. Xue X.-X., Rix H.-W., Zhao G., Fiorentin P.R., Naab T., Steinmetz M., Van den Bosch F.C., Beers T.C., Lee Y.S., Bell E.F., Rockosi C., Yanny B., Newberg H., Wilhelm R., Kang X., Smith M.C., Schneider D.P. The Milky Way's Rotation Curve to 60 kpc and an Estimate of the Dark Matter Halo Mass from Kinematics of 2500 SDSS Blue Horizontal Branch Stars. *Astrophys. J.*, 2008, v. 684, 1143–1158. arXiv:0801.1232v3[astro-ph].
9. Naab T., Johansson P.H., Ostriker J.P., Efstathiou G. Formation of Early-Type Galaxies from Cosmological Initial Conditions. *Astrophys. J.*, 2007, v. 658, 710N.
10. Eisenhauer F., Schoedel R., Genzel R., Ott T., Tecza M., Abuter R., Eckart A. Alexander T. A Geometric Determination of the Distance to the Galactic Center. *Astrophys. J. Lett.*, 2003, v. 597, L121–L124.
11. Wu X., Famaey B., Gentile G., Perets H., Zhao H.S. Milky Way potentials in CDM and MOND. Is the Large Magellanic Cloud on a bound orbit? *Mon. Not. R. Astron. Soc.*, 2008, v. 386 (4), 2199–2208. arXiv:0803.0977v1[astro-ph].
12. Robin A.C., Reyle C., Derriere S., Picaud S. A synthetic view on structure and evolution of the Milky Way. *Astron. Astrophys.*, 2003, v. 409 (2), 523.
13. Corbelli E., Lorenzoni S., Walterbos R., Braun R., Thilker D. A wide-field H I mosaic of Messier 31 — II. The disk warp, rotation, and the dark matter halo. *Astron. Astrophys.*, 2010, v. 511, A89.
14. Begeman K.G. H I rotation curves of spiral galaxies. I — NGC 3198. *Astron. Astrophys.*, 1989, v. 223, 47–60.

Motion-to-Motion Gauge for the Electroweak Interaction of Leptons

Felix Tselnik

Ben-Gurion University of the Negev, P.O.B. 653 Beer-Sheva 84105, Israel. E-mail: tselnik@ee.bgu.ac.il

Comprised of rods and clocks, a reference system is a mere intermediary between the motion that is of interest in the problem and the motions of auxiliary test bodies the reference system is to be gauged with. However, a theory based on such reference systems might hide some features of this actual motion-to-motion correspondence, thus leaving these features incomprehensible. It is therefore desirable to consider this correspondence explicitly, if only to substantiate a particular scheme. To this end, the very existence of a (local) top-speed signal is shown to be sufficient to explain some peculiarities of the weak interaction using symmetrical configurations of auxiliary trajectories as a means for the gauge. In particular, the unification of the electromagnetic and weak interactions, parity violation, $SU(2)_L \times U(1)$ group structure with the values of its coupling constants, and the intermediate vector boson are found to be a direct consequence of this gauge procedure.

1 Introduction

We shall apply a direct motion-to-motion gauge to the electroweak interactions. In so doing, our sole tool is the counting of the numbers of the top-speed signal oscillations in order to arrange test particles in special configurations of their trajectories possessing a particular symmetry. First we shortly review the basics of the motion-to-motion measurements (Sec. 1). Second we introduce compact symmetric configurations suitable for the gauge (Secs. 2, 3). Third we apply this gauge to construct a regular lattice suitable to unambiguously transport the (integer) value of the electric charge unit over the space-time and find that parity violating weak interaction is a necessary component of this (Sec. 4). In the Sec. 5, we describe some other applications of the gauge. The burden of the argument is as follows. The cube-star arrangement of electron and positron trajectories allows for the construction of a regular gauging lattice only under some conditions. In particular, it turns out that the particle charges must be altered, so as to let them leave the gauging cell intact notwithstanding the residual uncertainty pertinent to the gauge. Aiming at the finest lattice, we have found its minimal cell size required for the gauge. This size defines the range which is free to introduce an additional ("weak") interaction having no effect on the gauge itself. We can use this additional interaction to realize the necessary charge conversion (the electrons into the neutrinos). However, the top-speed signal oscillation numbers define not a single but two trajectories, and we have to provide the weak interaction with the property to select one of them. This interaction must depend on spin and contains parity violation as a necessary ingredient of electric charge gauge and transport.

2 Motion gauged with auxiliary motion

Ultimately, mechanics is based on comparing a trajectory of the body which is of interest in a problem to the trajectories of test bodies that are measuring force in the related points. Applications of the scheme also require a means to follow motions of the body. Otherwise, one could never be sure (in the absence of instant communication) that at a later moment it is the same body rather than a similar one. To this end, a top speed signal must exist in the scheme for not to loose the object upon its possible accelerations. In the conventional version, the required comparison is being carried out via an intermediate reference system comprised of rods and clocks. However, finally the real devices designed to measure the trajectories of bodies are to be gauged with the use of some standard motions. Thus, narrow light rays or free fall are used to determine whether or not the rod is rectilinear, and clock readings are to agree with astronomical and/or atomic processes. So, a reference system comprised of rods and clocks is just an intermediary in the comparison of one motion to another. One could guess that this intermediary might either add some features of its own to the gauge or, on the contrary, hide some important information in cases when the standard procedure is used beyond its traditional scope. It is therefore desirable to dispense with any intermediary so as to gauge motions directly, if only to obtain a criterion of suitability of the intermediary. To this end, many authors attempted to define the structure of space-time solely in terms of trajectories. In particular, natural topologies have been proposed to conform to the special role of the time axis [1-5]. A drawback of some of these approaches is the premise of a four-dimensional differentiable manifold for the space-time a topology to be introduced in. (However, the very idea to construct open subsets out of all trajectories, rather than of only free ones, and to deduce space-time properties, e.g., its dimension, out of their intersections was already considered [2].) Furthermore, topology is a too general structure, and practice requires more details. Thus, in order to define metrics based on a subset of trajectories, it was proposed to eliminate rigid rods (see, e.g., [6] and references therein); still clocks, at least in the form of affine parameters, seemed unavoidable.

But then, trajectories cannot be taken as primary entities in a theory to be developed from scratch, even though they might be considered directly observed (contrary to empty space-time!). It must be explained why just the trajectories of bodies are of particular interest rather than arbitrary changes in nature. Already in the Einstein's picture of the space-time, the event is defined as the intersection point of world lines of particles or of light pulses. This approach was further developed by Marzke and Wheeler [7]. In actual fact, primary definitions must be substantiated by the intended application of the theory, and therefore they must arise directly from the desirable statement of the problem, that is, to be axioms rather than hypotheses. Of course, a general uncertain concept of event cannot be basic for technical use that aims at a method to provide predictions, and therefore mechanics offers a particular kind of event, namely, contact (collision). The idea is to leave aside the question as to what results from the contact, assuming instead that nothing will happen, provided the contact does not occur. Whereas the notion "material point", i.e. "infinitesimal body", requires a preliminary concept of metric, the concept of contact is self-contained: the contact either exists or not. Only such problems are allowed for the analysis in mechanics. To this end, we define trajectories merely as a means to predict whether or not the contact of interest will occur in a particular problem upon detecting only some auxiliary contacts to be appropriately selected. Each trajectory possesses its own linear order, since it is introduced just for step-to-step predictions. This order introduces the topology of a simple arc on the trajectory to provide the basis for emerging structures. For this to be possible, we have to prepare a set of auxiliary (standard) trajectories in order to encode final, initial and intermediary states (contacts) solely in terms of these. Yet the choice of standard trajectories needs an explanation of its own. Can we dispense with geodesics? What properties of these are actually necessary for the scheme? Might these properties be deduced from meager information?

A reliable concept to begin with is the communication of bodies with a top speed signal (which is necessary anyway to follow motions of the body, while ensuring its unambiguous identification). Top speed signal can be defined independently of any general concept of speed. Consider two bodies A and B, the problem being stated of whether or not they will come into contact. Let A contact with an auxiliary body X which then contacts with B. Among these X's we look for the first to reach B, whatever ways they go. Only the order of these contacts matters, e.g., an X might put a mark on B, so that all the X's, except the first, find B already marked. It is this top-speed body that will serve as the signal. Let further there be a triple contact (B,X,Y), such that Y is, in turn, the first to meet A afterwards. If the contact (A,B) occurs, the number of these oscillations (multiple "echo") is infinite, corresponding to the so-called Zeno sequence. Otherwise, the last oscillation would occur before (A,B), and then this last oscillating body would not be a top-speed one. We could reverse this argument, suggesting that tending the number of oscillations to infinity could be used to predict the occurrence of (A,B), if in the absence of this contact the number of oscillations were not infinite as well. In conventional notions this implies infinite time of oscillations, but we cannot introduce space-time terms a priori aiming at a solution solely in terms of contacts. For this purpose, let us provide in our scheme some auxiliary X, such that (B,X) does occur. Then we can state that (A,B) occurs, provided the ratio of the (infinite) numbers of oscillations between A and B to that between B and X tends to a finite limit. For this to be actually used, one begins to count oscillation numbers at a moment, and the value of the ratio is determined as its limit when the number of oscillations as measured for the contacts of the signal with, e.g., A tends to infinity. This limit does not depend on the moment it starts from or on the reciprocal positions of the signals coming to A from B and X within one oscillation cycle [8]. We emphasize, that only local existence of the top speed signals is important (no cm/sec and no free trajectories to appear from the outset!). The counting of such ratios will be our sole tool in the sequel; however in some cases also finite oscillation numbers are suitable. (Finite numbers of top-speed signal oscillations were already used to compare distances [6, 7].)

We *define* space-time R not as something pre-existing but rather as an envelope of combination of all possible trajectories, the occurrence of contacts between which can be determined by means of top speed signal. In fact a (single!) reference system does exist in this approach, comprising an appropriate subset of trajectories – X's – chosen under the following conditions: i. Any pair of them either have no common contact or have only one (at least locally – with respect to their own topology); ii. If some trajectory A has a contact with some other trajectory B, there exists some X with the triple contact (A,B,X); iii. Although X's might have multiple contacts with trajectories not belonging to the subset, any pair of such contacts could be separated to insert a sequence of the top-speed signal oscillations for each of them. Moreover, just multiple contacts determine dynamics in terms of X's upon using an additional subset of "charged" test bodies, the trajectories of which are also encoded via X's. Under these conditions, infinite oscillation numbers provide the space-time with differential topology as a means to clearly separate possible contacts. Moreover, space-like hyper-surfaces S and the projections of trajectories thereon ("paths") might also be defined in these terms. The condition for a so defined contact scheme to represent any finite arrangement of the projections with their mutual intersections, while excluding any unnecessary for this purpose subsets, defines the topology of S. In the framework of traditional topology [1-5], dim R=ind R=1, but S is *not* a sub-space of R, though the set of its neighborhoods can be induced by trajectories from R: Each neighborhood of a point of the trajectory defines the corresponding neighbor-

hood of this point in S, consisting of all its points connected with top-speed signal to this neighborhood of the trajectory. However, S is not a topological image of R, and its dimension is to be defined independently of R.

Unlike the trajectory itself, its projection on S need not be a simple arc, and it might have various self-intersections. However, according to the Nöbeling-Pontryagin embedding theorem, any n-dimensional metrizable topological space with a countable base of open subsets can be embedded into the (2n+1)-dimensional Euclidean space. In fact, the theorem states that in this space its n-dimensional subspaces are free to intersect or not, while a space of a lower dimension might be too "dense" forcing some of them to intersect necessarily, and a space of a higher dimension would add nothing to this freedom. This is particularly clear for n=1: In only two dimensions a line cannot pass a closed boundary line without crossing it, whereas in three dimensions this is always possible (traffic interchange, say), while the fourth dimension would be redundant. For a finite (and even for a countable) array of trajectories its map in S has n=1, so dim S = 3. It follows that each contact might be encoded with only three X's. This fact could never be understood unless the space-time is defined as a union of actual trajectories [2] rather than being accepted in advance. In this version, the extension of bodies should itself be regarded just as their property to obstruct some trajectories or their paths.

Upon focusing in this presentation only on some features of motion-to-motion measurements relevant for weak interactions, further analysis of geometrical properties of the space-time that arise from this approach is left for discussion elsewhere.

3 Compact arrangements of trajectories

Consider a set of trajectories with their common contact. We can choose some triple of them to provide a basis, so that any other member of the set can be specified with its oscillation numbers ratios with those of the basis. *However, there exists the twin to any so defined trajectory.* Indeed, let us consider for the sake of visualization such decomposition in the rest frame of one of bodies of the basis. Then the other two define a surface, e.g., a plane, and the dual to a trajectory is its mirror image with respect to this plane. In order to specify the trajectory uniquely, we have to add some internal degree of freedom, a doublet, in close analogy to the spin variable.

Among all such sets we select a particular subset – *spheres* – that is defined as follows. It is convenient to introduce an additional body for the center of the sphere. The sphere is comprised of a finite number of trajectories with equal oscillation numbers with respect to the center body, that is, their ratio equals 1 for each pair of the sphere members. The sphere might be viewed as a compact arrangement of trajectories which are specified solely by their mutual angles. While the ratios of the oscillations numbers between the members themselves to those between them and the center are in general different, we can define for each trajectory its neighbors as those for which this ratio is maximal. The spheres might be used to specify a condition for forces that are permitted to act on bodies over their trajectories. If we accept that everything in sight must be described in terms of signals, we have to define forces in these terms as well. Such a rule must be independent of the space-time point, i.e. to require the force not to alter oscillation number ratios.

Let us take the sphere consisting of A, B, C and use conventional variables in order to reveal the familiar forces that satisfy this condition. The ratio ${}_A\Gamma_{BC}$ of the oscillation numbers between the bodies A and B to that of A and C is [8]:

$$ {}_A\Gamma_{BC} = \lim_{n_{AB}\to\infty} \frac{n_{AB}}{n_{AC}} = \frac{\ln\left(u_{Ai}u_{Bi} + \sqrt{(u_{Ai}u_{Bi})^2 - 1}\right)}{\ln\left(u_{Ai}u_{Ci} + \sqrt{(u_{Ai}u_{Ci})^2 - 1}\right)} \qquad (1) $$

where u_{Ai} and others are the four-velocities of the bodies, and summation over i is implied. Evidently the ratio ${}_A\Gamma_{BC}$ will not change under a force if the scalar products of the four-velocities do not.

Consider the electromagnetic force, F_{ik}. Then for velocity of light c, the charges and masses of the bodies e and m:

$$ du_{Ai} = \frac{e}{mc} F_{ik}u_{Ak}ds_A \,. \qquad (2) $$

Hence:

$$ d(u_{Ai}u_{Bi}) = \frac{e_A}{m_Ac} F_{ik}u_{Ak}u_{Bi}ds_A + \frac{e_B}{m_Bc} F_{ki}u_{Bi}u_{Ak}ds_B \,. \qquad (3) $$

But $ds_A = ds_B$ since A and B are the members of a sphere. Then, $d(u_{Ai}u_{Bi}) = 0$, if $F_{ik} = -F_{ki}$ and also $e_A/m_A = e_B/m_B$. Apart from electromagnetic field, anti-symmetry of which can be expressed, in the connected space-time manifold, via potentials as $F_{ik} = \partial A_i/\partial x_k - \partial A_k/\partial x_i$, a field might also include commutators $[A_i, A_k]$ if the components of the potential do not commute. (Quanta of these fields must be bosons, whereas fermions would require only anti-commutators.) We can then reverse the argument to state that only fields preserving the ratios of the oscillation numbers can appear in the theory as bosons. Moreover, propagation of the fields can also be expressed via appropriate contact schemes by means of Green functions [9]. To complete the method, we stay in need of a condition, in terms of contacts, for the constancy of charge and mass in (3) everywhere, and in order to find this condition we need a means to translate these values over the whole space- time. For this purpose consider a particular subset of spheres, in which the oscillation number ratios with its neighbors are the same for each member of the sphere. Such a sphere will be called a star. In three-dimensional space only five stars are possible. These are known as Platonic solids. Note that the definition of star doesn't imply that its bodies move uniformly.

4 Star-based gauge of electric charge

Eventually, all that is actually measured in experiments relates to motion under electromagnetic force of, e.g., particles, products of their interactions etc. It is therefore this force proportional to the electric charge of the particle it acts upon that must be gauged in the first place. The value of this charge is commonly accepted to be the same everywhere. Still a method is needed to detect this identity in terms of contacts. We want to use the stars for gauging electric charge without any intermediary. To this end, we have to specify the charge not only locally but also to develop some motion-to-motion gauge for its translation to any point the body of interest might occupy along its trajectory. This should be based on the symmetries of stars, which can easily be expressed in terms of equality of some oscillation numbers.

Suppose all the members of a star (in the gauge procedure we will call them particles) are electrically charged with equal e/m values and move only under mutual electromagnetic interaction. In any star comprised of identical particles they move along straight lines repelling each other, and the particles cannot reach the center. Moreover, the trajectories might become curved, provided some of the particles differ from others in charges or masses, and for this reason they miss the center as well. But in a symmetry-based charge gauging procedure, it is the disparity of charges and masses that is detected as a star symmetry breaking. If the particles miss the star center anyway, we cannot be sure that the symmetry is not broken just at the closer vicinity of the center, still being observed far from it. We must therefore use for the gauge only neutral as a whole stars with equal numbers of positive and negative particles. Of all Platonic solids, the center is reached only in the cube with opposite signs of the charges between the tetrahedrons the cube is comprised of. Although in the cube star the particles keep moving along straight lines (even if the absolute values of their charges differ between its two tetrahedrons, while being identical within each of them), the symmetry will be broken because the tetrahedrons are being differently accelerated by mutual attraction.

Starting the counting of the oscillation numbers between the particle and an introduced, for the sake of simplicity, imaginary central particle at a moment before the contact, we detect the symmetry breaking if these numbers, as measured at the center, differ at least by one oscillation. In the limit of the smallest star size, defining the highest precision of electromagnetic gauge, one tetrahedron nears the center over only one oscillation while another — over two oscillations. At a smaller initial radius the second oscillation has no time to occur. Since we detect only integer numbers of signal oscillations, the values of charge to be detected must be discrete. Indeed, suppose that the charges differ by some infinitesimal value. However close to the center the symmetry was detected, we cannot be sure that asymmetry could still be detected upon continuing the counting, since nothing is being registered in between the neighboring contacts. So, we are able to detect with our method only discrete values of charge (and/or mass), hence a minimum value of charge e can be registered, the next value being $2e$. Now, whereas in a given external field acceleration depends on e/m, for a case of interacting particles it depends on e^2/m, and in order to observe the symmetry of a star the masses and the absolute values of the charges of its particles are to be equal.

The particles of the tetrahedron having the charge $2e$ experience smaller acceleration as compared to the tetrahedron having the charge e. The related symmetry breaking gauge condition — one extra oscillation — is reached at some final radius r_{min}. Smaller radii are not involved in the gauge procedure, leaving this region free to introduce a new interaction under our general trend to regard possible in mechanics everything described with the motion-to-motion schemes. In the next section, we will find such an interaction to be necessary for the gauge itself.

5 Application to electroweak interactions

With the basic cube star at hand we proceed to develop the whole regular lattice, along which the value of the electric charge can be transported to a point of the trajectory in question. Along our general lines, the regular lattice must comprise elementary cube-star cells. For this purpose, we use some particles of one star, after they pass its center, as a seed for the next star. According to Sec. 2, just three stars are sufficient to completely define their next star. As a matter of fact, this simple picture cannot be trusted, because deviation of the charge at radii that are smaller than those involved in the gauge for the finest lattice might either prevent electrons and positrons from escaping the star against the exit potential barrier formed by the attraction of the other members of the star or to have a final energy differing from what is needed as the input energy of the next star. Even small charge deviation are important, since the energy near the minimal radius is typically much higher than the energies of the particles at the star entrance, and momentum conservation would yield large final fluctuations there; moreover, the deviation might be collected over a sequence of stars. In particular, even low level radiation that has a small effect on the matching of incoming to outgoing energies in a single star might cause large deviations over long sequences.

Radiation is negligible in stars comprising large bodies, and our gauge is quite feasible in this case. Long sequences might then be directly arranged, in which the outgoing bodies are directly used in the next star, since their velocity return to the initial values being decelerated after passing the star center. This is impossible in the limit of elementary particles. If, however, a new — "weak" — interaction converts the charge of the particles to zero at the smallest radius of the symmetry detection, the gauge becomes independent of radiation. Being constrained to radii that are smaller than those involved in the

electric charge gauge, such a conversion doesn't obstruct the gauge. Over a larger scale, one could consider stars consisting, e.g., of ions, which can change their charge via charge exchange or stripping. We, however consider the limiting case of the finest lattice comprised of stars having the smallest possible size, still allowing the motion-to-motion charge gauge. Then only elementary particles might participate in the lattice, and an elementary neutral particle must complete the collection. It is just in this extreme case the weak interaction with its parity violation appears.

In order to form the lattice, this newborn particle, the "neutrino", has then to be converted back into the electron of the next star. This can happen under the same weak interaction, provided the neutrino collides with the anti-neutrino to create the electron-positron pair. Though never observed in practice, such a limiting process, as well as the charged star itself — with its eight particles' simultaneous collision, should be considered a feature of our formal language to question nature, providing as concepts for theories so also rules for experiments. We need therefore to introduce intermediate cube stars made up of only neutrinos and anti-neutrinos and positioned at the corners of the charged cube. These neutral stars are "blind" in the sense that their symmetry cannot be detected electromagnetically. Still, suitability of the whole regular lattice might be detected, provided the following charged star is found to repeat the original symmetry. So, we need a doublet consisting of electrons and neutrinos to prepare a regular lattice. The doublet corresponds to two charge states that convert one into another at the vertices, suggesting the SU(2) group for transformations of the inner (charge) space in the gauge field theory, but now it appears as an indispensable mechanism to realize the regular lattice by means of the motion-to-motion gauge.

Our next step is to define all the members of the next star starting with the trajectories that are continuations of its three preceding stars. For any star, it is sufficient to take a basis of three trajectories to determine all the others. In order to visualize this construction, it is convenient to proceed using the conventional picture, that is, to imagine the cube star in its center-of-mass (CM) reference system as eight particles at its vertices moving toward the center with equal velocities v ($\beta = v/c$). Let us take, for example, the trajectory A and its neighbors B and C as the basis for the star to be constructed and choose the line of A for the x-axis, the line through the cube center parallel to the line between the vertices B and C for the y-axis, and the z-axis as orthogonal to these two. We have to find D as the third neighbor of A. In so chosen coordinates, the decomposition coefficients of the basis are:

$$\left.\begin{aligned} &\beta_{Ax} = \beta, \quad \beta_{Ay} = \beta_{Az} = 0 \\ &\beta_{Bx} = \beta_{Cx} = \frac{\beta}{3}, \quad \beta_{By} = -\beta_{Cy} = \beta\sqrt{\frac{2}{3}} \\ &\beta_{Bz} = \beta_{Cz} = \beta\,\frac{\sqrt{2}}{3} \end{aligned}\right\}, \qquad (4)$$

and those of D:

$$\beta_{Dx} = \frac{\beta}{3}, \quad \beta_{Dy} = 0, \quad \beta_{Dz} = -\beta\,\frac{2\sqrt{2}}{3}. \qquad (5)$$

But we know from Sec. 2 that via the oscillation number ratios counting — our sole means — the basis A, B, C defines actually two trajectories, that is, there exists another trajectory E besides D with the same ratios of the oscillations. In order to determine the coordinates of E, we transform (4) and (5) to the reference system, in which A is at rest, to find E there as the mirror image of D, and then to return to the CM system to find the coordinates of E there. From the relativistic transformation formulae for velocities, we find:

$$\left.\begin{aligned} &\beta'_{Ax} = \beta'_{Ay} = \beta'_{Az} = 0 \\ &\beta'_{Bx} = \beta'_{Cx} = -\beta\,\frac{2}{3-\beta^2} \\ &\beta'_{By} = -\beta'_{Cy} = \beta\,\frac{\sqrt{6(1-\beta^2)}}{3-\beta^2} \\ &\beta'_{Bz} = \beta'_{Cz} = \beta\,\frac{\sqrt{2(1-\beta^2)}}{3-\beta^2} \\ &\beta'_{Dx} = -\beta\,\frac{2}{3-\beta^2}, \quad \beta'_{Dy} = 0 \\ &\beta'_{Dz} = -\beta\,\frac{2\sqrt{2(1-\beta^2)}}{3-\beta^2} \end{aligned}\right\}. \qquad (6)$$

Using (6), we obtain the mirror image E of D trajectory with respect to the plane defined by the transformed B and C velocities as:

$$\left.\begin{aligned} &\beta'_{Ex} = -\beta\,\frac{2(3-5\beta^2)}{(3-\beta^2)^2} \\ &\beta'_{D'y} = 0 \\ &\beta'_{D'z} = \beta\,\frac{2\sqrt{2(1-\beta^2)}\,(3+\beta^2)}{(3-\beta^2)^2} \end{aligned}\right\}. \qquad (7)$$

Upon back transforming (7) to the laboratory reference frame, we find finally:

$$\left.\begin{aligned} \beta_{Ex} &= \frac{\beta\left((3-\beta^2)^2 - 2(3-5\beta^2)\right)}{(3-\beta^2)^2 - 2\beta^2(3-5\beta^2)} \\ \beta_{Ez} &= \frac{2\sqrt{2}\,\beta(1-\beta^2)(3+\beta^2)}{(3-\beta^2)^2 - 2\beta^2(3-5\beta^2)} \end{aligned}\right\}. \qquad (8)$$

Though in our example (D placed between B and C) E moves in the same xz plane as D, (8) does not define a vertex of the cube. Even the absolute values of the D and E velocities differ already in the order of β, though their oscillations numbers with respect to the basis are the same. So, upon constructing the next star we must introduce some additional — internal — degree of freedom, helicity, to define just D but not E by means of choosing a particular order in the basis A,

B, C. Mathematically, this is similar to the spin variable, the spin being directed either in the direction of the momentum of the particle or oppositely. So, parity violation turns out to be a necessary property of the motion-to-motion gauge, since only the projection of spin on the momentum direction conveys the necessary information to select the appropriate trajectory out of the two. In the electron/positron cube star, the opposite sense particles belong to different tetrahedrons, and of the two particles on each main diagonal of the cube one is the electron while another – the positron. Therefore the order of the basis for the electron is seen as reversed from its opposite positron, and the product of parity and charge conjugation is the same for both (CP conservation).

We are able now to use parity in the electric charge gauge as performed solely with photon oscillations counting. In the symmetric cube star magnetic field is zero on the trajectories, hence there is no orbital angular momentum, and only the spin of the particle defines its total angular momentum. Then our electric charge gauge fails to distinguish between particles with left and right orientations, letting both enter the weak interaction zone. In order to define the fourth trajectory, the neutrinos must be provided with a definite, e.g., left, helicity, and therefore the charged star must generate only these. To this end, the weak interaction must be spin-dependent to create only left-handed neutrinos (and right-handed antineutrinos) in the collision of the particles in the charged star. It is sufficient to consider only the electron and its neutrino, the argument being similar for their antiparticles. In the blind star the neutrino will turn into the electron with the same projection of its spin in virtue of the angular momentum conservation.

For the left-handed electrons in the charged star, the function of the weak interaction is dual. On the one hand, the weak interaction for the left-handed electrons possesses its own dynamics, since it should match the output and input energies in the sequence of charged stars over the whole lattice. On the other hand, its intensity defines charge conversion probability, scaling as $\gamma^2 = (1-\beta^2)^{-1}$ according to the general properties of all acceptable fields as satisfying the condition (1), and the same field should also accelerate the electrons to maximize the cross-section of charge conversion along with minimizing that of annihilation. (The latter scales as γ^{-2}; so the ratio of the related probabilities (however small) is proportional to γ^4.) This relationship of the dynamics and the charge conversion implies their common coupling constant. For the same reason charged particles created in the neutral star are to leave the weak interaction region avoiding annihilation.

When the left-handed electron passes the weak interaction region of the star, it has some probability either to turn into the neutrino or to annihilate or to cross this region intact. In the latter case this left-handed electron might be reflected by the exit potential to pass the star center in the opposite direction now as a right-handed one. Being reflected once again, this electron can turn into the neutrino becoming left-handed again, thus sharing the total neutrino flux. This cannot be allowed for the gauge, since the time moment of this electron would differ from that of the normally leaving star electron to result further on in the incorrect initial moment of the newborn electron in the next star. This unwanted process can be suppressed by annihilation of the electron-positron pair when the reflected particles flip their helicity. The related probabilities depend on the value of the weak coupling constant g_L, given the electromagnetic coupling constant e (the subscript L refers to the left-handed electron).

Let us first consider the energy matching dynamics ignoring radiation. In the charged star, the electron is being accelerated from γ_i at the radius r_i, as defined by the finest star cell still possible for the gauge of electron charge, up to some γ_f at $r_{min} \ll r_i$ [10]. As any field satisfying the general motion-to-motion condition (1), the weak field has to satisfy a wave equation [9]. In particular, the finite range weak interaction could be expressed via the Yukawa potential $gr^{-1}\exp(-r/r_{min})$ satisfying the wave equation with an additional "mass" term. For not to disturb the charge gauge, the weak potential should be at most of the order of the Coulomb potential e^2/r at the minimal gauge-defined radius r_{min}. Apart from the short range, parity violation and electric neutrality, the dynamical behavior of weak field should be quite similar to that of electric field, as prescribed by (1). For the estimations let us approximate the weak field Yukawa potential with its averaged factor g^2/r, analogous to the electromagnetic e^2/r, though defined only within the weak field range $r/r_{min} \sim 1$: For $r/r_{min} < 1$, the potential $gr^{-1}\exp(-r/r_{min}) \approx g/r - g/r_{min}$ constant second term being immaterial. We introduce therefore a combined radius r_L, $r_L = (e^2+g_L^2)/mc^2$ to write the following equation for γ in the CM reference system:

$$\gamma^3 = \gamma_f^3 + 3Ar_L\left(\frac{1}{r} - \frac{1}{r_{min}}\right) \tag{9}$$

where $A \approx 10$ represents the force created by all the other particles of the cube star together [10]. In dimensionless variables $\eta_L = 3Ar_L/r_{min}$ and $x = r/r_{min}$ (8) reads:

$$\gamma^3 = \gamma_f^3 + \eta_L\left(x^{-1} - 1\right). \tag{10}$$

In the transition from one star to the next, the electron starting with $\gamma = \gamma_f$ is accelerated by both the electromagnetic and weak forces from r_{min} down to some smaller r', where it turns into the neutrino, which moves to some r'' on the opposite end of the weak region under the weak force only, then this neutrino moves freely to start being accelerated by the weak field of the neutral star at r_{min}, where it turns into the new electron at r'', which finally decelerates by both the electromagnetic and weak fields to become a member of the next star, now at its own r_i, where it must have $\gamma = \gamma_i$. In this oversimplified scenario the total contribution of the weak field over the whole path from the output of one

charged star to the input of the next charged star is zero, and it is the sole electric field, which is active only over its parts, defines the final velocity. In order to obtain a non-zero result also for the weak field, we have to switch it on and off over some parts of the transition. A natural means to realize this switch is to include an intermediate particle with a different mass as its carrier. This is the typical situation for a random process (at least, for a local one [11]), e.g., for quantum mechanics: the described with the wave function particle can be found (with some probability) anywhere at the same moment, still remaining point-like. The required intermediate particle will then have some mass M, the value of which must be large, being defined only within the short weak field range $\Lambda = \hbar/Mc \sim r_{min}$, so describing the transition solely in terms of the charge gauge.

For the energies relevant in our gauge procedure such a massive particle can only be a virtual one, its sole role consisting in correctly transporting the momentum, charge and spin data. For this to be possible, this meson must possess its own charge and polarization, having the spin equal to 1 to preserve the total angular momentum in the charge conversion, since the two other particles — the electron and the neutrino — have spin 1/2. Similarly, transporting the value of momentum as encoded by means of the boson properties implies its motion. Then the moments of creation and decay of the boson must be separated by a time interval, however short due its small velocity for the large mass. The whole transition between the charged stars will now look as follows. In electron at r_{min} having $\gamma = \gamma_f$ is being accelerated to reach the energy $mc^2\gamma'$ at $r = r'$. Here the electron turns into the intermediate boson, non-relativistic because of its large mass, moving with the velocity $v = c(\gamma' 2m/M)^{1/2}$.

Over the characteristic time Λ/c the boson moves a distance of the order $\Lambda(\gamma' 2m/M)^{1/2} \sim r_{min}(\gamma' 2m/M)^{1/2}$ (neglecting acceleration due to its large mass) to turn into the neutrino, moving with the same energy the distance $\sim r_i$ with velocity c to turn back into the boson at $r = r''$ (now measured from the center of the neutral star). Here the newborn electron is being decelerated, again by the electromagnetic and weak forces to reach $\gamma = \gamma_i$ at $r = r_i$ as measured from the center of the next charged star. In order to get in the course of the transition to the required γ_i given γ_f, we put $r'' = r' - r_{min}(\gamma' 2m/M)^{1/2}$ to obtain for the whole transition:

$$\gamma_i^3 = \gamma_f^3 + \eta_L \left(x'^{-1} - \frac{1}{x' - \sqrt{2m/M\gamma'}} \right). \qquad (11)$$

This equation should be supported with the equation for $\gamma' = \gamma(x')$:

$$\gamma'^3 = \gamma_f^3 + \eta_L \left(x'^{-1} - 1 \right). \qquad (12)$$

We eliminate x' from the system of (11) and (12) to obtain:

$$\begin{aligned} F(\gamma', \eta_L) = {} & \gamma_f^3 - \gamma_i^3 \\ & - \frac{\left(\eta_L + \gamma'^3 - \gamma_f^3\right)\sqrt{2m/M\,\gamma'}}{\eta_L - \left(\eta_L + \gamma'^3 - \gamma_f^3\right)\sqrt{2m/M\,\gamma'}} \\ = {} & 0. \end{aligned} \qquad (13)$$

Still, the condition of reducing γ from γ_f to γ_i in the course of the whole transition doesn't define the points r' and r'' of the charge flips uniquely, unless the charge conversion is connected with the related dynamics (otherwise the flip might occur at any point within the weak interaction region), and we look for the maximum of γ' to achieve the maximal ratio (increasing as γ') of the charge conversion cross section to that of the dominating (two-photon) electron/positron annihilation.

The equation (13) implicitly defines $\gamma'(\eta)$ given γ_f and γ_i, and the condition for its maximum $d\gamma'(\eta_L)/d\eta_L = \partial F/\partial\eta_L = 0$ (provided $\partial F/\partial\gamma' \neq 0$ at $\eta_L = \eta_{L(max)}$) yields:

$$\eta_{max} = \left(\gamma'^3_{max} - \gamma_f^3\right)\frac{1 + \sqrt{2m/M\,\gamma'_{max}}}{1 - \sqrt{2m/M\,\gamma'_{max}}}. \qquad (14)$$

Substituting (14) in (13), we obtain the equation for γ'_{max}, given γ_f and γ_i:

$$\gamma'^3_{max} - \left(\gamma_f^3 - \gamma_i^3\right)\frac{\left(1 - \sqrt{2m/M\,\gamma'_{max}}\right)^2}{4\sqrt{2m/M\,\gamma'_{max}}} - \gamma_f^3 = 0. \qquad (15)$$

For the finest lattice as defined by the electron charge gauge, the equation for γ_f is similar to (9), in which, however, the electric force, introduced via $r_e = e/mc$, acts alone:

$$\gamma_f^3 = \gamma_i^3 + 3Ar_e\left(\frac{1}{r_{min}} - \frac{1}{r_i}\right). \qquad (16)$$

In the gauge procedure, the value of γ_i is of great importance, because it is this lowest velocity that mainly contributes to the sensitivity of asymmetry detection in the stars: Since $r_i \gg r_{min}$, it will be: $\gamma_f \gg \gamma_i$ and the exact value of γ_f (since β_f is very close to 1) is but of minor importance in the integration of the disparity between the tetrahedrons [10]. However, γ_f is important in equations (9)-(15).

With resulting from the gauge condition [10] $\gamma_i \sim 3$ and $r_{min} \sim 3\times10^{-3}r_e$, we find from (16): $\gamma_f \sim 30$. Then from (15) and (14): $\gamma'_{max} \sim 50$ and $\eta_{L(max)} \sim 10^5$. This value of $\eta_{L(max)}$ corresponds to $g \sim 2e$, in agreement with the experimental data: $\sin\theta_w \sim 0.5$.

Until now we ignored radiation, and we have to consider its importance. In the gauge process itself, i.e. for $r_i > r > r_{min}$, radiation decreases the value of γ_f, and in the weak field regions, $r_{min} > r > r'$ and $r'' < r < r_{min}$, radiation is active as well. Both effects decrease the related γ's and therefore the probability of the charge conversions.

Whereas only the mean values of mechanical variables (behaving classically) are important in our gauge, as based solely on the top-speed signal oscillations, the analysis of the role of radiation requires the full quantum theory. Indeed, it was shown [10] that in the classical limit, corresponding to multiple soft-photons emission [11], radiation restricts the size of the star for the finest lattice down to the order of r_e. But it is well known that the classical field theory is no longer valid at these distances. Instead, we are bound to calculate only the cross sections for the emission of single photons.

Contrary to the classical limit, single photon radiation in QED occurs only with some probability, i.e. there is also a finite probability for the absence of emission. Only this case is relevant for our gauge, since radiation decreasing the related γ accordingly decreases the proportional to γ ratio of charge conversion cross section to that of annihilation. If the radiation cross section is not too close to unity, the charge conversion events which are not accompanied by radiation might be isolated as providing correct γ_f to γ_i transitions in accord with (11).

In the close vicinity of the star center only some small central part of the wave packet can take a part in the interaction, which is the source of radiation. Therefore, only a small part of the infinite range Coulomb interaction is actually involved, behaving there like a short range interaction. A similar effect in scattering on (neutral) atoms is accounted for by means of "screening" the potential [11, 12]. When the particle interacts with atom, this screening appears as a form factor effectively reducing the range of Coulomb potential to the size of the atom. In the same way, the short range Yukawa potential could be regarded as a screened initially long range fictitious potential, and we consider also the electromagnetic interaction to be screened as well, because now the flux of incoming particles should be normalized for a wave packet of the relevant size rather than for a plane wave. We start with the ultra- relativistic case for the radiation cross section formula in the center-mass system [11]:

$$d\sigma_{rad} = 4\alpha r_e^2 \frac{df}{f}\left(1 - \frac{2}{3}(1-f) + (1-f)^2\right) \times \left(\ln 4\gamma_0^2\left(\frac{1}{f} - 1\right) - \frac{1}{2}\right), \tag{17}$$

where $\alpha = e^2/\hbar c \sim 1/137$ is the fine structure constant $f = \hbar\omega/\epsilon_0$ (ω is the frequency of the emitted photon, ϵ_0 is the energy of the incident electron in the CM system, $\gamma_0 = \epsilon_0/m$). Integrating (17), we find σ_{rad}. The integral diverges for small f. For a simple estimation let us replace $\ln(1/f - 1)$ with its average value Q. Integrating f from some f_{min}, (to be determined later) to 1:

$$\sigma_{rad} = 4\alpha r_e^2\left(Q - \frac{1}{2} + 2\ln 2\gamma_0\right) \times \left(\frac{5}{6} - \frac{4}{3}(\ln f_{min} - f_{min}) - \frac{1}{2}f_{min}^2\right). \tag{18}$$

In the scattering matrix theory, the analysis is carried out over the infinite distances from the interaction region both for initial and final states of the system, so that the incoming and outgoing wave functions are plain waves over the whole continuum, and in the derivation of (17), the integral for the Fourier component of the infinite range Coulomb potential is taken from 0 to ∞. In our case, only radiation events within the star are important, e.g., for $r_i > r > r'$ in the charged star and for $r'' < r < r_{min}$ in the neutral one. We shall therefore accept a model, in which the wave functions outside the interaction regions are still plain waves though bounded laterally to the interaction radii. These functions are given in advance, not taking care of how they were actually prepared. Then we can replace r_e^2 with r_i^2 for the gauge region in (17) and (18), so normalizing the plane wave spinors in the S-matrix element with one particle in r_i^3 rather than in the unit volume, in accord with the flux density of one electron per r_i^2. Similarly, r_{min} will replace r_e for the weak field region. We have also to modify α to account for the weak potential: $\alpha_L = e(e+g_L)/\hbar c$.

It will then be possible to use the Feynman diagram technique to calculate the radiation cross sections. Considering the interactions as existing only in these regions, we calculate the related interaction potential in the momentum representation. In particular, for the pure Coulomb potential $eA_0(q)$ (the time component of the four-vector eA_i) in the gauge region ($r_i > r > r_{min}$) we write (see, e.g., [11]):

$$\begin{aligned} A_0(q) &= -4\pi e\int_{r_{min}}^{r_i} dr\ \exp(iqr) \\ &= \frac{4\pi e}{q^2}\left(\cos(qr_i) - \cos(qr_{min})\right), \end{aligned} \tag{19}$$

where we put the boundary radii instead of usual ∞ and 0. (If r_i were to tend to infinity, the exponential factor with a negative real power should be included in the integrand (to be set zero at the end in order to cancel the first term in the parenthesis, while and the second term becomes unity). In the derivation of (17) (see, e.g., [11, 12]), the argument q has to be set equal to the absolute value of the recoil momentum according to the total four-momentum conservation. In the ultra-relativistic case $q \approx mc/\hbar$, so for the gauge region ($r_i \sim r_e \gg r_{min}$), $qr_i \sim e^2/\hbar c = \alpha \ll 1$, and it follows from (19):

$$A_0(q) = -\frac{2\pi e}{q^2}\alpha^2. \tag{20}$$

Since the S-matrix element is proportional to (20), the radiation cross section (17), proportional to the S-matrix element squared, becomes modified by the additional factor $\alpha \sim 10^{-9}$. In order to obtain the total probability w_{rad} of emission in the interval ($r_i > r > r_{min}$) of a single photon with $f_{min} < f < 1$, the modified according to (20) cross section (18) is to be multiplied by the flux $j = 2v/V$ ($v \approx c$ is the velocity in the CM system, and $V \sim r_i^3$ is the gauge region volume) to obtain the probability for unit time, and then multiplying by r_i/v to find the probability for this region. With all

these substitutions:

$$w_{rad} \approx 4\alpha^5 \left(Q - \frac{1}{2} + 2\ln 2\gamma_0 \right) \times \left(\frac{5}{6} - \frac{4}{3}\left(\ln f_{min} - f_{min}\right) - \frac{1}{2} f_{min}^2 \right). \quad (21)$$

Due to the factor α^5, this probability is very low, unless f_{min} is sufficiently small. For w_{rad} to be of the order of unity, it must be: $\ln(1/f_{min}) \sim \alpha^{-5}$, whatever all other factors in (21) might be. Evidently, such soft photons cannot bring about any changes in the value of γ_f in the gauge region. The same reasoning and with the same conclusion holds in the weak field region for γ'_{max} and η_{max}.

The factor α^4 in (21) suppresses radiation of the electron that does not pass the star center, the nearest vicinity of which provides main contribution to radiation. However, for the electron that passes the center without turning into the neutrino the full radiation cross section must be accounted for. As it follows from (18), the probability of emitting even rather high energy photons is of the order of unity, and it will be collected over a sequence of stars, since radiation can only decelerate the electron. Loosing even a small part of its final energy ($\geq mc^2\gamma_i$), this electron either reaches a lower value of γ_i than allowed for the next stars, or even fails to overcome the exit potential barrier of the last star of a short star sequence, so destroying the gauge lattice.

Although the right-handed electrons take no part in the charge conversion, they might ruin the charge gauge. Indeed, their helicity becomes opposite if they are reflected by the output electromagnetic barrier of the star, and the initially right-handed electron becomes a source of the left-handed neutrino as well. Such oppositely moving neutrinos would make uncertain the choice of the charge sign in the next star, being admixed to the proper antineutrinos generated by the positrons. The flux of these neutrinos could be somewhat suppressed by the electromagnetic electron-positron annihilation, provided the weak interaction acts against the electromagnetic acceleration. So, for the right-handed electron the weak interaction also receives some dynamical meaning.

In order to determine the value of the corresponding coupling constant g_R in the Yukawa potential, we have to find the probability w_{an} of the two-photon electron-positron annihilation when they are decelerated from $\gamma = \gamma_f$ down to $\gamma = 0$ at the turning point. We start with the well-known Dirac's formula for the annihilation cross section in the CM system. In our case it looks:

$$\sigma_{an} = \frac{2\pi r_{min}^2}{\gamma^4\sqrt{\gamma^2-1}}\left[\left(\gamma^4+\gamma^2-\frac{1}{2}\right)\ln\left(\gamma+\sqrt{\gamma^2-1}\right) - \frac{1}{2}\gamma\left(\gamma^2+1\right)\sqrt{\gamma^2-1}\right]. \quad (22)$$

The probability of annihilation w_{an}, increasing with deceleration, depends on the function $\gamma(r)$, which, in turn, depends on r:

$$\gamma^3 = \gamma_f^3 - \eta_R\left(\frac{1}{x} - 1\right) \quad (23)$$

where $\eta_R = 30r_R/r_{min}$, $r_R = (g_R^2 - e^2)/mc^2$, $x = r/r_{min}$. Annihilation probability dw an over the interval dx is:

$$dw_{an} = \sigma_{an}\frac{2v}{r_{min}^2}\,dx. \quad (24)$$

From (22), (23) and (24) we obtain:

$$w_{an} = 12\pi\eta_R\int_1^{\gamma_f} d\gamma \times \frac{\left(\gamma^4-\gamma^2-\frac{1}{2}\right)\ln\left(\gamma+\sqrt{\gamma^2-1}\right)-\frac{1}{2}\gamma\left(\gamma^2+1\right)\sqrt{\gamma^2-1}}{\gamma^2\sqrt{\gamma^2-1}\left(\gamma_f^3+\eta_R-\gamma^3\right)^2}. \quad (25)$$

Given γ_f, this equation defines a function $w_{an}(\eta_R)$, which possesses a maximum. A simple numerical calculation with $\gamma_f \approx 30$ gives: $w_{an}(max) = 0.12$ for $\eta_R(max) \approx 2500$. This value of $\eta_R(max)$ corresponds to $g_R \approx 1.15e$, again in close correspondence with the experimental value of $\cos\theta_w$. In a standard probabilistic approach, this 12% difference is sufficient to reliably discern between particles and antiparticles.

6 Conclusion

In summary, our argument goes as follows:

i. A direct gauge of electric charge using motion-to-motion measurements might be based on the very existence of a (local) top-speed signal, no matter how high this speed is in any units whatsoever.

ii. Letting this signal oscillate between test particles and counting the ratios of the (infinite) numbers of these oscillations, we are able to detect the symmetry of the stars arranged as Platonic solids.

iii. Of the five Platonic solids, only the neutral as a whole cube-symmetrical star, consisting of the two tetrahedrons – one for the electron and another for the positron – is suitable for the electric charge gauge, since it is the only symmetry in which the particles move under electrical interaction along straight lines to cross at their common center.

iv. In order for the electron charge to be gauged as having the same value everywhere, the stars must be arranged in a lattice extended over the whole space-time, in which the initial star arrangement gives rise to its followings by means of the same signal oscillations counting.

v. For this to be possible, the method must uniquely define the transitions in the star sequences; however, the oscillation ratios counting method defines two trajectories rather than only one, and some internal degree of freedom (spin) should be given the particle to make the choice unique.

vi. With our gauge confined to integer charge values and sensitive to deviation from these, however small, beyond the

gauge region, transitions between the stars in the lattice becomes uncertain; however, our charge gauge leaves free some vicinity of the star center, where an additional interaction not destroying the gauge might exist, and it could be used for charge conversion to make this uncertainty immaterial.

vii. The weak interaction realizes the necessary charge conversion with the neutrino that must also provide the necessary information to select a single trajectory out of the two in the next star, their spin projection onto the momentum direction being the sole source for this selection. The transition within the lattice also requires appropriate matching between the in and out energies of the electrons in the succeeding stars; this can be reached only with an intermediate vector boson.

viii. The design of the lattice requires only one conversion of the electric charge, so involving only two charge eigenstates (the SU(2) doublet).

ix. The charge gauge naturally combines the weak and electromagnetic interactions in a single interaction as pertaining to the common cube star, and the numerical relationships between the three coupling constants directly follow from this gauge.

It is fascinating that just the existence of top-speed signals is sufficient to predict the existence of the weak interactions with its range, parity violation and even the intermediate boson, basing solely on Platonic symmetries. The electroweak segment in the standard model suggesting $SU(2)_L \times U(1)$ group with adjusted coupling constants to account for the previously observed in experiments data including parity violation (while PC is still preserved for the leptons) provides good predictions as well. One should appreciate, however, the difference between a theory predicting these features from its own "first principles" and a developed ad hoc theory that only explains, however successfully, already known experimental results. Moreover in other applications, the existence of top-speed signal is sufficient to construct the non-singular part of the Green function (the so-called Huygens' tail) in general relativity [9]. Also, motion-to-motion measurements are relevant in stochastic approach to quantum mechanics [13], in which random scattering on the measuring device, that is realized as a set of macroscopic bodies moving so as to correspond on average to that of the particle in question, leads to the Schrodinger equation: In the form of the Madelung's fluid with its "quantum potential" depending on the same wave function, the external force vector corresponds to the total average acceleration of the particle, that is, the "scattering medium" itself depends also on the own motion of the particle under measurement. One more application of the motion-to-motion gauge helps to explain the existence and masses of the heavy μ- and τ-mesons [14]: In the cube cell, the same gauge regular lattice might occur if one (for the τ) or two (for the μ) electron/positron pairs are being replaced by the heavy mesons. These two sub-symmetries of the cube star may form the whole regular lattice, provided these "foreign" entries move under the mutual acceleration in the cell nearly identically to other electrons and positrons. This situation was found to exist only for some particular values of the mesons' masses, found to be close to experimental data.

We deduce therefore that the pure motion-to-motion gauge eliminating all artificial ingredients (even free falling bodies) and basing only on the (local) existence of top-speed signals provides not only its own interpretation of observations, but it can predict experimental results, otherwise hidden. This is not surprising, since such a gauge is based solely on the very statement of practical problems, and the attached theoretical scheme merely prescribes appropriate notions to address nature. Experiments, as carried out along these lines, can give then nothing but what these notions already imply, in accord with the viewpoint of I. Kant [15] (see also H. Bergson [16]).

Submitted on November 24, 2014 / Accepted on November 28, 2014

References

1. Zeeman E.C. *Topology*, 1967, issue 6, 161.
2. Tselnik F. *Sov. Math. Dokl.*, 1968, v. 9, 1151.
3. Hawking S.W., King A.R., McCarty P.J. *J. Math. Phys.*, 1976, v. 17, 174.
4. Gobel R. *Comm. Math. Phys.*, 1976, v. 46, 289.
5. Fullwood D.T. *J. Math. Phys.*, 1992, v. 33, 2232 and references therein.
6. Ehlers J., Pirani F.A.E. and Schild A. In: General Relativity, ed. by L. O'Raifeartaigh, 1972.
7. Marzke R.F., Wheeler J.A. In: Gravitation and Relativity, ed. by H.Y. Chiu and W.F. Hoffmann, New York, 1964.
8. Tselnik F. Preprint N89-166, Budker Institute of Nuclear Physics, Novosibirsk, 1989.
9. Tselnik F. *Nuovo Cimento*, 1995, v. 110B(12), 1435.
10. Tselnik F. *Communications in Nonlinear Science and Numerical Simulation*, 2005, v. 12(8), 1427.
11. Berestetskii V.B., Lifshitz E.M., Pitaevskii L.P. Relativistic Quantum Theory. Pergamon Press, 1971.
12. Gingrich D.M. Practical Quantum Electrodynamics. Taylor & Francis, 2006.
13. Tselnik F. *Sov. Phys. Dokl.*, 1989, v. 34(7), 634.
14. Tselnik F. Cube star gauge implies the three lepton families (to be published).
15. Kant I. Prolegomena to Any Future Methaphysics. New York, Bobbs-Merrill, 1950.
16. Bergson H. Creative Evolution. London Macmillan, 1911.

Mixed Ion-Electron Conductivity and Superconductivity in Ceramic Electrolytes

Sebastiano Tosto
Retired Physicist. E-mail: stosto44@gmail.com

The paper concerns a theoretical model on the transport mechanisms occurring when the charge carriers generated during the working conditions of a fuel cell interact with point and line defects in a real lattice of solid oxide electrolyte. The results of a model previously published on this topic are here extended to include the tunnelling of carriers within the stretched zone of edge dislocations. It is shown that at temperatures appropriately low the charge transport turns into a frictionless and diffusionless mechanism, which prospects the chance of solid oxide fuel cells working via a superconductive effect.

1 Introduction

The electric conductivity of ceramic electrolytes for solid oxide fuel cells (SOFC) has crucial importance for the science and technology of the next generation of electric power sources. Most of the recent literature on solid oxide electrolytes concerns the effort to increase the ion conductivity at temperatures as low as possible to reduce the costs and enhance the portability of the power cell. The efficiency of the ion and electron transport play a key role in this respect.

In general different charge transfer mechanisms are active during the working conditions of a fuel cell, depending on the kind of microstructure and temperature of the electrolyte. The ion migration in the electrolyte is consequence of the chemical reactions at the electrodes, whose global free energy change governs the charge flow inside the electrolyte and the related electron flow in the external circuit of the cell. Aliovalent and homovalent chemical doping of the oxides affects the enthalpy of defect formation, whose kind and amount in turn control the diffusivity of the charge carriers and thus their conductivity. Particularly interesting are for instance multi-ion [1] and super-ion [2] conduction mechanisms.

Yet in solid oxide electrolytes several reasons allow also the electronic conduction; are important in this respect the non-stoichiometric structures originated by appropriate heat treatments and chemical doping. In general an oxygen vacancy acts as a charge donor, because the two electrons related to O^{-2} can be excited and transferred throughout the lattice. Oxygen deficient oxides have better conductivity than stoichiometric oxides. Typical case is that of oxygen deficient oxides doped with lower valence cations, e.g. ZrO_2 with Y or Ca. As a possible alternative, even oxide doping with higher valence cations enables an increased amount of electrons while reducing the concentration of oxygen vacancies. Besides, an oxide in equilibrium with an atmosphere of gas containing hydrogen, e.g. H_2O, can dissolve neutral H or hydride H^- or proton H^+; consequently the reaction of hydrogen and hydrogen ions dissolved in the oxide with oxygen ions releases electrons to the lattice in addition to the proton conduction.

Mixed ionic–electronic conductors (MIECs) concern in general both ion, σ_i, and hole/electron, σ_{el},conductivities of the charge carriers. Usually the acronym indicates materials in which σ_i and σ_{el} do not differ by more than 2 orders of magnitude [3] or are not too low (e.g. $\sigma_i, \sigma_{el} \geq 10^{-5}$ S cm^{-1}). According to I. Riess [4], this definition can be extended to intend that MIEC is a material that conducts both ionic and electronic charges. A review of the main conduction mechanisms of interest for the SOFC science is reported in [5]. Anyway, regardless of the specific transport mechanism actually active in the electrolyte, during the work conditions of the cell the concentration profiles of the charges generated by the chemical reactions at the electrodes look like that qualitatively sketched in the figure 1.

It is intuitive that the concentration of each species is maximal at the electrode where it is generated. The con-

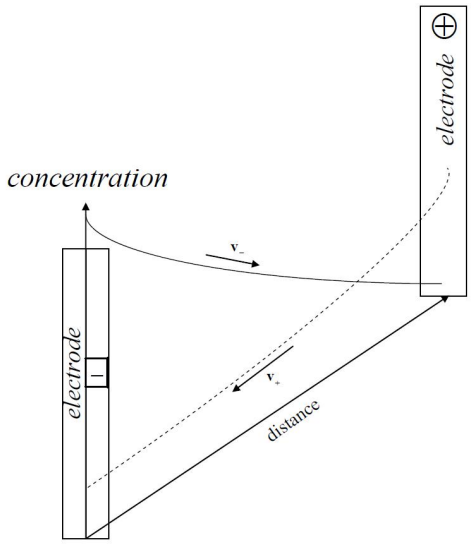

Fig. 1: Qualitative sketch of the concentration profiles of two carriers with opposite charges in the electrolyte as a function of their distance from the electrode where either of them was generated. The profiles represent average diffusion paths, regardless of the local microscopic lattice jumps around the average paths.

centration gradients are sustained by the free energy change of the global reaction in progress; so the charges are subjected to a diffusive driving force $\mathbf{F}_c$ and electric potential gradient driving force $\mathbf{F}_\phi$, the latter being related to the non-uniform distribution of charges at the electrodes. In general both forces control the dynamics of all charge carriers.

This picture is however too naive to be realistic. Dopant induced and native defects in the lattice of the electrolyte can interact together and merge to form more complex defects, in particular when the former and the latter have opposite charges, until an equilibrium concentration ratio of single to complex defects is attained in the lattice. Moreover, in addition to the vacancies and clusters of vacancies, at least two further crystal features are to be taken into account in a real material: the line defects and the grain boundaries, which act as potential barriers to be overcome in order that the ions perform their path between the electrodes. The former include edge and screw dislocations that perturb the motion of the charge carriers because of their stress field; the latter have a very complex local configuration because of the pile up of dislocations, which can result in a tangled dislocation structure that can even trap the incoming ions and polygonized dislocation structure via appropriate annealing heat treatments. For instance hydrogen trapping in tangled dislocations is reported in [6]. Modelling these effects is a hard task; exists in the literature a huge amount of microscopic [7] and macroscopic [8] models attempting to describe the transport mechanisms of the charge carriers through the electrolyte.

The former kind of models implements often quantum approaches to get detailed information on a short range scale of phenomena; their main problem is the difficulty of theoretical approach that often requires drastic approximations, with results hardly extrapolable to the macroscopic behaviour of a massive body and scarcely generalizable because of assumptions often too specific.

The latter kind of models regards the electrolyte as a continuous medium whose properties are described by statistical parameters like temperature, diffusion coefficient, electrical conductivity and so on, which average and summarize a great variety of microscopic phenomena; they typically have thermodynamic character that concerns by definition a whole body of material, and just for this reason are more easily generalized to various kinds of electrolytes and transport mechanisms.

A paper has been published to model realistically the electrical conductivity in ceramic lattices used as electrolytes for SOFCs [9]; the essential feature of the model was to introduce the interaction between charge carriers and lattice defects, in particular as concerns the presence of dislocations. It is known that the diffusion coefficient D of ions moving in a diffusion medium is affected not only by the intrinsic lattice properties, e.g. crystal spacing and orientation, presence of impurities and so on, but also by the interaction with point and line defects. The vacancies increase the lattice jump rate and decrease the related activation energy, thus enhancing the diffusion coefficient; this effect is modelled by increasing purposely the value of D, as the mechanism of displacement of the charge carriers by lattice jumps is simply enhanced but remains roughly the same. More complex is instead the interaction with the dislocation; thinking for simplicity one edge dislocation, for instance, the local lattice distortion due to stress field of the extra-plane affects the path of the ions between the electrodes depending on the orientation of the Burgers vector with respect to the applied electric field. Apart from the grain boundaries, where several dislocations pile up after having moved through the core grain along preferential crystal slip planes, the problem of the line defects deserves a simulation model that extends some relevant concepts of the dislocation science: are known in solid state physics phenomena like dislocation climb and jog, polygonization structures and so on.

From a theoretical point of view, the problem of ion diffusion in real lattices is so complex that simplifying assumptions are necessary. The most typical one introduces a homogeneous and isotropic ceramic lattice at constant and uniform temperature T; in this way D is given by a unique scalar value instead of a tensor matrix. Also, the dependence of D and related conductivity σ upon T are described regardless of their microscopic correlation to the microstructure, e.g. orientation and spacing of the crystal planes with respect to the average direction of drift speed of the charge carriers. Since the present paper represents an extension of the previous results, a short reminder of [9] is useful at this point. The starting points were the mass flow equations

$$\mathbf{J} = -D\nabla c = c\mathbf{v} : \tag{1}$$

the first equality is a phenomenological law that introduces the proportionality factor D, the latter is instead a definition consistent with the physical dimensions of matter flow i.e. $mass/(surface \times time)$. The second Fick law is straightforward consequence of the first one under the additional continuity condition, i.e. the absence of mass sinks or sources in the diffusion medium. Strictly speaking one should replace the concentration with the activity, yet for simplicity the symbol of concentration will be used in the following. The model focuses on a solid lattice of ceramic electrolyte, assumed for simplicity homogeneous and isotropic, where charge carriers are allowed to travel under concentration gradient and electric potential field. It is interesting in this respect the well known Nernst-Einstein equation linking σ to D/k_BT, which has general valence being inferred through elementary and straightforward thermodynamic considerations shortly commented below; so, in the case of mixed electronic-ionic conduction, it holds for ions and expectedly for electrons too, being in effect direct consequence of the Ohm law. Is known the dependence of D on T; the Arrhenius-like form $D = D_0 \exp(-\Delta G/kT)$ via the activation free energy ΔG is due not only to the direct T-dependence of the frequency of lattice jumps inherent D_0, but also to the fact that the temperature controls the amount

and kind of point defects that affect ΔG. The Nernst-Einstein equation has conceptual and practical importance, as it allows calculating how the electrolytes of SOFCs conduct at different temperatures; yet it also stimulates further considerations about the chance of describing the interactions of charges in a crystal lattice via the concept of "effective mass" and the concept of diffusion coefficient in agreement with the Fick laws. This point is shortly highlighted as follows.

It is known that the effective mass m^{eff} of an electron with energy E moving in a crystal lattice is defined by $m^{\text{eff}} = \hbar^2\left(\partial^2 E(k)/\partial k^2\right)^{-1}$, being $k = 2\pi/\lambda$ and λ the wavelength of its De Broglie momentum $p = h/\lambda = \hbar k$. The reason of this position is shortly justified considering the classical energy $E = p^2/2m + U$, which reads $E = \hbar^2 k^2/2m + U$ from the quantum standpoint; $U = U(k)$ is the electron interaction potential with the lattice. If in particular $U = 0$, then m^{eff} coincides with the ordinary free electron rest mass m. Instead the interacting electron is described by an effective mass $m^{\text{eff}} \neq m$; putting $U = \hbar^2 u(k)/m$ and replacing in E, one finds instead $m^{\text{eff}} = m(1 + \partial^2 u/\partial k^2)^{-1}$. In fact the deviation of m^{eff} from m measures the interaction strength of the electron with the lattice; it is also known that by introducing the effective mass, the electron can be regarded as a free particle with good approximation. Owing to the physical dimensions $length^2 \times time^{-1}$ of $\hbar/m$, the same as the diffusion coefficient, it is formally possible to put $D = \hbar q_m/m$ and $D^{\text{eff}} = \hbar q_{m^{\text{eff}}}/m^{\text{eff}}$ via appropriate coefficients q_m and q_m^{eff} able to fit the experimental values of D and D^{eff}.

Rewrite thus m^{eff}/m as

$$\frac{D^{\text{eff}}}{D^*} = 1 + \frac{\partial^2 u}{\partial k^2} \qquad D = \frac{\hbar q_m}{m} \qquad D^* = qD \qquad q = \frac{q_{m^{\text{eff}}}}{q_m}, \quad (2)$$

which calculate D^* and thus D^{eff} as a function of the physical D actually measurable. So, once taking into account the interaction of the electron with the lattice, one could think that the real and effective electron masses correspond to the actual D and effective D^{eff} related to its interaction with the electric field and lattice. Note that the first eq (2) reads

$$D^{\text{eff}} = D^* + D^{\S} \qquad D^{\S} = D^* \frac{\partial^2 u(k)}{\partial k^2}. \quad (3)$$

Clearly the contribution of $D^{\S}$ to the actual diffusion coefficient D^{eff} is due to the kind and strength of interaction of the charge carrier with the lattice; thus D^{eff}, and not the plain D, has physical valence to determine the electrical conductivity of the electrolyte during the operation conditions of the cell: the electron in the lattice is not a bare free particle, but a quasi-particle upon which depends in particular its conductivity. It is known indeed that electrons in a conductor should be uniformly accelerated by an applied electric field, but attain instead a steady flow rate because of their interaction with the lattice that opposes their motion; the resistivity is due to the electron-phonon scattering and interaction with lattice ions, impurities and defects, thermal vibrations. Any change of these mechanisms affects the resistivity; as a limit case, even the superconducting state with null resistivity is due itself to the formation of Cooper pairs mediated just by the interaction between electrons and lattice. Write thus the Nernst-Einstein equation as follows

$$\sigma^{\text{eff}} = \frac{1}{\rho^{\text{eff}}} = \frac{(ze)^2 c D^{\text{eff}}}{k_B T}. \quad (4)$$

The crucial conclusion is that all this holds in principle for any charge carrier, whatever U and m might be. To understand this point, suppose that the interaction potential U depends on some parameter, e.g. the temperature, such that $u = u(k, T)$ verifies the condition $\lim_{T \to T_c} \partial^2 u/\partial k^2 = \infty$ at a critical temperature $T = T_c$. Nothing excludes "a priori" such a chance, as this condition does not put any physical constrain on the macroscopic value of the diffusion coefficient D nor on the related D^*: likewise as this latter is simply D affected by the applied electric field via the finite factor q, the same holds for D^{eff} affected by the lattice interaction upon which depends m^{eff} as shown in the eq (2). Thus the limit $\lim_{T \to T_c} (D^{\text{eff}}/D) = \infty$ concerns $D^{\S}$ only. Being $q_m > 0$ and $q_m^{\text{eff}} > 0$ but anyway finite, the divergent limit is not unphysical, it merely means that at $T = T_c$ the related carrier/lattice interaction implies a new non-diffusive transport mechanism; this holds regardless of the actual value of D, which still represents the usual diffusion coefficient in the case of carriers ideally free or weakly interacting with the lattice in a different way, e.g. via vacancies only. In conclusion are possible two diverse consequences of the charge carrier/lattice defect interactions: one where $D^{\S} \neq D$, i.e. the presence of defects simply modifies the diffusion coefficient, another one where the usual high temperature diffusive mechanism is replaced by a different non-diffusive mechanism characterized by $D^{\S} \to \infty$, to which corresponds $\rho^{\text{eff}} \to 0$ at $T = T_c$. Two essential remarks in this respect, which motivate the present paper, concern:

(i) The quantum origin of both eqs (1) is inferred in [10]; this paper infers both equations as corollaries of the statistical formulation of quantum uncertainty. Has been contextually inferred also the statistical definition of entropy $S = -\sum_j \pi_j \log(\pi_j)$ in a very general way, i.e. without hypotheses about the possible gaseous, liquid or solid phase of the diffusion medium. It has been shown that the driving force of diffusion is related to the tendency of a thermodynamic system in non-equilibrium state because of the concentration gradients towards the equilibrium corresponding to the maximum entropy, whence the link between diffusion propensity and entropy increase.

(ii) The result $D^{\text{eff}} = D^{\S} + D^*$, actually inferred in [9]: the interaction of the charge carrier with the stress field of one edge dislocation defines an effective diffusion coefficient D^{eff} consisting of two terms, D^* related to its interaction with the

electric potential of the cell and $D^{\S}$ related to its chemical gradient and interaction with the stress field of the dislocation.

The concept of D^{eff} is further concerned in the next section to emphasize that the early ideas of Fick mass flow, which becomes now effective mass flow, and Einstein D^{eff}-dependent conductivity are extendible to and thus still compatible with the limit case $D^{\S} \to \infty$.

In summary $D_{id} \to D \to D^{*} \to D^{\text{eff}}$ are the possible diffusion coefficients of each charge carrier concerned in [9]: D_{id} is that in an ideal defect free lattice, D that in a lattice with point defects only, D^{*} in the given lattice with an applied electric potential, D^{eff} in a real lattice with dislocations under an applied electric potential. The chance of extrapolating the equation (4) to the superconducting state, despite this latter has seemingly nothing to do with the diffusion driven charge displacement, relies on two logical steps.
The first step is to acknowledge that $D^{\text{eff}} = D^{\S} + D$ is required by the presence of dislocations, because D^{eff} cannot be defined simply altering the value of the plain D; the reason of it has been explained in [9] and is also summarized in the next section for clarity.

To elucidate the second step, consider preliminarily $D \to D^{\text{eff}}$ simply because $D^{\S} \gg D$: in this case the finite contribution $D^{\S}$ due to the charge/dislocation interaction can be accepted without further problems.

Suppose that a valid physical reason allows a charge carrier to move as a free particle in the lattice, regardless of the concentration gradient or applied potential difference or force $\mathbf{F}$ of any physical nature; in this extreme case, the condition $\rho^{\text{eff}} \to 0$ necessarily results by consequence and requires itself straightforwardly $D^{\S} \to \infty$ in the Nernst-Einstein equation. In other words, the second step to acknowledge the divergent value of $D^{\S}$ is to identify the peculiar interaction mechanism such that the charge carrier behaves effectively in the lattice as a free particle at a critical temperature T_c: the existence of such a mechanism plainly extrapolates to the superconducting state the eq (4), which is thus generalized despite the link between σ and D is usually associated to a diffusive mechanism only.

The present paper aims to show that thanks to the fact of having introduced both point and line lattice defects in the diffusion problem, the previous model can be effectively extended to describe even the ion superconducting state in ceramic electrolytes. It is easy at this point to outline the organization of the present paper: the section 2 shortly summarizes the results exposed in [9], in order to make the exposition clearer and self-contained; the sections 3 and 4 concern the further elaboration of these early results according to the classical formalism. Eventually the section 5 reviews from the quantum standpoint the concepts elaborated in section 4. Thus the first part of the paper concerns in particular the usual mechanism of charge transport via ion carriers, next the results are extended to the possible superconductivity effect described in the section 5. A preliminary simulation test in the section 5.1 will show that the numerical results of the model in the particular case where the charge carrier is just the electron match well the concepts of the standard theory of superconductivity.

2 Physical background of the model

The model [9] assumes a homogeneous and isotropic electrolyte of ceramic matter at uniform and constant temperature everywhere; so any amount function of temperature can be regarded as a constant. The electrolyte is a parallelepiped, the electrodes are two layers deposited on two opposite surfaces of the parallelepiped. The following considerations hold for all charge carriers; for simplicity of notation, the subscript i that numbers the i-th species will be omitted. Some remarks, although well known, are shortly quoted here because useful to expose the next considerations in a self-contained way. Merging the flux definition $\mathbf{J} = c\mathbf{v}$ and the assumption $\mathbf{J} = -D\nabla c$ about the mass flux yields $\mathbf{v} = -D\nabla \log(c)$. Introduce then the definition $\mathbf{v} = \beta\mathbf{F}$ of mobility β of the charge carrier moving by effect of the force $\mathbf{F}$ acting on it; one infers both $D = k_B T\beta$ and $\mathbf{F} = -\nabla\mu$ together with $\mu = -k_B T \log(c/c_o)$. An expression useful later is

$$\mathbf{F} = \frac{k_B T}{D}\mathbf{v} = \frac{k_B T}{Dc}\mathbf{J}. \tag{5}$$

So the force is expressed through the gradient of the potential energy μ, the well known chemical potential of the charge carrier. The arbitrary constant c_o is usually defined as that of equilibrium; when c is uniform everywhere in the diffusion medium, the driving force of diffusion vanishes and the Fick law predicts a null flow of matter, which is consistent with $c \equiv c_o$. Another important equation is straightforward consequence of the link between mass flow and charge flow; since the former is proportional to the number of charged carriers, each one of which has charge ze, one concludes that $\mathbf{J}_{ch} = ze\mathbf{J}$ and so $\beta_{ch} = ze\beta$. Let the resistivity ρ be summarized macroscopically by Ohm's law $\rho\mathbf{J}_{ch} = -\nabla\phi = \mathbf{E}$; i.e. the charge carrier interacts with the lattice while moving by effect of the applied electric potential ϕ and electric field $\mathbf{E}$. The crucial eq (4) is inferred simply collecting together all statements just introduced in the following chain of equalities

$$\mathbf{J}_{ch} = \sigma\mathbf{E} = zec\mathbf{v} = zec\beta_{ch}\mathbf{E} =$$

$$= (ze)^2 c\beta\mathbf{E} = \frac{(ze)^2\mathbf{E}cD}{k_B T} = -\frac{cDze\nabla\phi}{k_B T}. \tag{6}$$

Moreover the effect of an electric field on the charge carriers moving in the electrolyte is calculated through the last sequence of equalities recalling that the electric and chemical forces are additive. Consider thus the identity

$$\mathbf{F}_{tot} = -\nabla\mu - \alpha ze\nabla\phi = -\frac{k_B T}{c}\left(\nabla c + \alpha\frac{zec\nabla\phi}{k_B T}\right)$$

where α is the so called self-correlation coefficient ranging between 0.5 to 1; although usually taken equal to 1 and omitted [11], it is quoted here by completeness only. Recalling the mobility equation $k_BT/c = D/\beta c$ and noting that $\mathbf{F}\beta c$ is just a mass flow, the result is

$$\mathbf{J}_{tot} = -D\left(\nabla c + \alpha\frac{zec}{k_BT}\nabla\phi\right) = \frac{cD}{k_BT}\left(\nabla\mu - \alpha ze\nabla\phi\right). \qquad (7)$$

So far D has been introduced without mentioning the diffusion medium, in particular as concerns its temperature and the presence of lattice defects of the ceramic crystal. As the point defects simply increase the frequency of lattice jumps [12] and thus the value of the diffusion coefficient, in these equations D is assumed to be just that already accounting for the vacancy driven enhancement. As concerns the presence of edge and screw dislocations also existing in any real crystal, the paper [9] has shown that in fact the dislocations modify significantly the diffusion mechanism in the electrolyte: their stress field hinders or promotes the charge transfer by creating preferential paths depending on the orientation of the dislocation stress field with respect to the electrode planes. In particular the dislocation affects the mobility of the charge carriers, as it is intuitive to expect: phenomena like the climbing, for instance, occur when a dislocation or isolated atoms/ions move perpendicularly to the extra plane of another dislocation to overcome the compression field due to the local lattice distortion. Moreover, in the case of edge dislocations the figure 2 shows the possibility of confinement of light atoms, e.g. typically C and N, along specific lattice directions perpendicular to the Burgers vector; this emphasizes the importance of the orientation of grains and dislocations with respect to the average path of the charges between the electrodes.

Assume first one lonely dislocation in a single crystal lattice; this case allows a preliminary assessment of the interaction between charge carriers travelling the lattice in the presence of an applied potential field. In the case of edge dislocation the shear stress component on a plane at distance y above the slip plane is known to be $\sigma_{xy} = [8\pi y(1-\nu)]^{-1}Gb\sin(4\theta)$, being ν the Poisson modulus, G the shear modulus, $b = |\mathbf{b}|$ and $\mathbf{b}$ the Burgers vector, θ is the lattice distortion angle induce by the extra plane on the neighbour crystal planes [13]. Moreover the modulus of the force per unit length of such dislocation is $F^{(d)} = b\sigma_{xy}$, where the superscript stands for dislocation. Hence, calling $l^{(d)}$ the length of the extra plane, the force field due to one dislocation is

$$\mathbf{F}^{(d)} = [8\pi y(1-\nu)]^{-1}Gb^2 l^{(d)}\sin(4\theta)\mathbf{u}_b$$

where $\mathbf{u}_b$ is a unit vector oriented along the Burger vector, i.e. normally to the dislocation extra plane. It is known that atom exchange is allowed between dislocations; the flow $\mathbf{J}$ of these atoms within a lattice volume Ω is reported in the literature to be

$$\mathbf{J} = D_L\nabla\mu/(\Omega k_BT) \qquad \mu = -kT\log(c_\Omega),$$

being μ the chemical potential and D_L the appropriate diffusion coefficient; for clarity are kept here the same notations of the original reference source [14]. Actually this flow is straightforward consequence of the Fick law, as it appears noting that the mass m_Ω of atoms within the volume Ω of lattice corresponds by definition to the average concentration $c_\Omega = m_\Omega/\Omega$; so the atom flow between dislocations at a mutual distance consistent with the given Ω is nothing else but the diffusion law $\mathbf{J}_\Omega = -D_L\nabla c_\Omega$ itself, as it is shown by the following steps

$$\begin{aligned}\mathbf{J}_\Omega &= -D_L\nabla c_\Omega = -c_\Omega D_L\nabla\log(c_\Omega)\\ &= \frac{c_\Omega D_L}{k_BT}\nabla\mu = \frac{m_\Omega}{\Omega}\frac{D_L}{k_BT}\nabla\mu.\end{aligned} \qquad (8)$$

Thus the flow $\mathbf{J} = \mathbf{J}_\Omega/m_\Omega$ reported in the literature describes the number of atoms corresponding to the pertinent diffusing mass. The key point of the reasoning is the appropriate definition of the diffusion coefficient D_L, which here is that of a cluster of atoms of total mass m_Ω rather than that of one atom in a given matrix. Once having introduced $\mathbf{F}^{(d)}$, it is easy to calculate how the flow of the charge carriers is influenced by this force field via the related quantities $D^{(d)} = k_BT\beta^{(d)}$ and $\mathbf{v}^{(d)} = \beta^{(d)}\mathbf{F}^{(d)}$; in metals, for instance, it is known that the typical interaction range of a dislocation is of the order of 10^{-4} cm [13]. The contribution of this exchange to the charge flow is reasonably described by $\mathbf{J}^{(d)} = \mathbf{F}^{(d)}D^{(d)}c/k_BT$ according to the eq (5). Consider now $\mathbf{F}^{(d)}$ as the average field due to several dislocations, while the same holds for $\beta^{(d)}$ and $D^{(d)}$, which are therefore related to the pertinent $\sigma^{(d)}$; omitting the superscript to simplify the notation, eq (7) reads thus

$$\mathbf{J}_{tot} = -D\left(\nabla c + \alpha\frac{zec}{k_BT}\nabla\phi - \frac{c\mathbf{F}}{k_BT}\right)$$

$$\mathbf{F} = <\mathbf{F}^{(d)}(G,\nu,l^{(d)},\mathbf{b})>. \qquad (9)$$

In this equation D has the usual statistical meaning in a real crystal lattice and includes the electric potential as well. Here the superscript has been omitted because also $\mathbf{F}$ denotes the statistical average of all the microscopic stress fields $\mathbf{F}^{(d)}$ existing in the crystal. One finds thus with the help of the continuity condition

$$\nabla\cdot\left[D\left(\nabla c + \alpha\frac{zec}{k_BT}\nabla\phi - \frac{c\mathbf{F}}{k_BT}\right)\right] = \frac{\partial c}{\partial t} \qquad D = D(T,c,t) \quad (10)$$

where c and $\mathbf{v}$ are the resulting concentration and drift velocity of the i-th charge carrier in the electrolyte. In general the diffusion coefficient depends on the local chemical composition and microstructure of the diffusion medium. Moreover the presence of $\mathbf{F}$ into the general diffusion equation is required to complete the description of the charge drift through a real ceramic lattice by introducing a generalized thermodynamic force, justified from a microscopic point of view and

thus to be regarded also as a statistical macroscopic parameter. This force, considered here as the average stress field resulting from the particular distribution of dislocation arrays in the lattice, accounts for the interaction of a charge carrier with the actual configuration of lattice defects and is expected to induce three main effects: (i) to modify the local velocity $\mathbf{v}$ of the charge carrier, (ii) to modify the local concentration of the carriers (recall for instance the "Cottrel atmospheres" that decorate the dislocation), (iii) to modify the local electric potential because altering the concentration of charged particles certainly modifies the local ϕ. Accordingly, considering again the average effects of several dislocations in a macroscopic crystal, it is reasonable to write

$$\frac{c\mathbf{F}}{k_BT} = \frac{mc\dot{\mathbf{v}}}{k_BT} + a\nabla c + \mathbf{\Gamma}$$
$$\dot{\mathbf{v}} = \dot{\mathbf{v}}(c) \qquad \mathbf{\Gamma} = \mathbf{\Gamma}(c, \phi_o) \qquad c = c(x, y, z, t, T)$$

being a a proportionality constant. The first addend at right hand side accounts for the effect (i), the second for the effect (ii), the vector $\mathbf{\Gamma}$ for the effect (iii) because it introduces the local potential ϕ_o due to the charges piled up around the dislocation; the dependence of these quantities on c of the pertinent carrier emphasizes the local character of the respective quantities depending on the time and space coordinates. The final step is to guess the form of $\mathbf{\Gamma}$ in order to introduce in the last equation the electrochemical potential $\alpha\phi + \mu/ze$ inferred from the eq (7) . As motivated in [9], $\mathbf{\Gamma}$ is defined as a local correction of ϕ because of the concentration of the charge carriers; with the positions

$$\mathbf{\Gamma} = \frac{c\alpha}{k_BT}\nabla(ze\phi + \mu) - \frac{ze\phi_o\alpha}{k_BT}\nabla c \qquad a = 1 - \alpha$$

eq (10) turns into

$$\nabla \cdot \left[\frac{m\mathbf{v}}{k_BT}\frac{\partial(cD)}{\partial t} + \frac{ze\phi_o\alpha}{k_BT}D\nabla c\right] = \frac{\partial C}{\partial t} \tag{11}$$

where

$$C = c + \frac{m}{k_BT}\nabla \cdot (cD\mathbf{v}) \qquad \phi_o = \phi_o(x, y, z, t).$$

The function ϕ_o has physical dimensions of electric potential. Eventually, owing to this definition of C, the last equation reads

$$\nabla \cdot \left[(D^* + D^{\S})\nabla C\right] = \frac{\partial C}{\partial t} \tag{12}$$

being

$$D^* = \frac{ze\phi_o}{k_BT}\alpha D \qquad \frac{m}{k_BT}\frac{\partial(cD)}{\partial t}\mathbf{v} = D^*\nabla(C - c) + D^{\S}\nabla C.$$

These considerations show that it is possible to define an effective diffusion coefficient in the presence of an applied potential ϕ and taking into account the presence of point and line defects

$$D^{\text{eff}} = D^* + D^{\S}. \tag{13}$$

This equation is equal to that inferred via the effective mass of the charge carrier interacting with the lattice, see the eq (3); $D^{\S}$ is defined by the last eq (12) accounting via C for the presence of dislocations in a real ceramic electrolyte. Accordingly, the equation (13) is modified as follows

$$\frac{D^{\text{eff}}}{D} = \alpha\frac{ze\phi_o}{k_BT} + \frac{D^{\S}}{D} \qquad \sigma^{\text{eff}} = \frac{1}{\rho^{\text{eff}}} = \frac{D^{\text{eff}}}{D}\sigma. \tag{14}$$

The solution of the eq (10) via the eq (12) to find the analytical form of the space and time profile of c is described in [9]; it is not repeated here because inessential for the purposes of the present paper. Have instead greater importance the result (13) and the following equations inferred from the eqs (11) and (12)

$$\nabla \cdot (cD\mathbf{v}) = 0, \qquad C \equiv c, \qquad \mathbf{v} = \frac{k_BT}{m}\frac{D^{\S}}{\partial(cD)/\partial t}\nabla c. \tag{15}$$

The consistency of the first equation with the eq (12) has been therein shown. This condition requires that the vector $cD\mathbf{v}$, having physical dimensions of energy per unit surface, is solenoidal i.e. the net flow of carriers crossing the volume enclosed by any surface is globally null; this holds for all carriers and means absence of source or sinks of carriers around any closed surface. Note that this condition is fulfilled by

$$\mathbf{v} = \frac{\mathbf{B}}{cD} \tag{16}$$

with

$$\mathbf{B} = \mathbf{i}B_x(y, z, t) + \mathbf{j}B_y(x, z, t) + \mathbf{k}B_z(x, y, t) \qquad |\mathbf{B}| \to \frac{energy}{surface}.$$

The vector $\mathbf{B}$ is defined by arbitrary functions whose arguments depend on the coordinate variables as shown here: at any time and local coordinates the functions expressing the components of $\mathbf{B}$ can be appropriately determined in order to fit the corresponding values of $\mathbf{v}cD$ resulting from the solution of the eq (10). Hence the positions (15) do not conflict with this solution, whatever the analytical form of $\mathbf{v}$ and c might be; the third equality (15) defines $D^{\S} = D^{\S}(c, D, \mathbf{v}, T)$. The central result to be implemented in the present model is

$$\mathbf{v} = \frac{k_BT}{\eta}D^{\S}\frac{\nabla c}{m} = \Omega D^{\S}\nabla n \tag{17}$$

where

$$\eta = \frac{\partial(cD)}{\partial t} \qquad n = \frac{c}{m} \qquad \Omega = \frac{k_BT}{\eta}$$

with n numerical density of the given carrier and η energy density corresponding to the time change of cD; the volume Ω results justified by dimensional reasons and agrees with the fact that the diffusion process is thermally activated. Moreover one finds

$$\mathbf{v} = \frac{\mathbf{B}}{cD} = \frac{\Omega}{m}D^{\S}\nabla c = D^{\S}\frac{\nabla c}{c} \qquad m = c\Omega. \tag{18}$$

Owing to the importance of the third eq (15) for the purposes of the present paper, it appears useful to verify its validity; this check is shortly sketched below by demonstrating its consistency with relevant literature results.

First of all, the eq (17) leads itself to the literature result (8); the key points are the definition of mobility β and its relationship to the diffusion coefficient $\beta = D/kT$ previously reported in the eq (5). Let the atom exchange between dislocations be thermally activated, so that holds the last eq (17). Being $\mathbf{v} = D^{\S}\nabla\mu/k_BT$ according to the eq (18), then $D_L\mathbf{F}/k_BT = -D^{\S}\nabla\mu/k_BT$ specifies $D_L \equiv D^{\S}$, i.e. the diffusion coefficient is that pertinent to the interaction of atoms with the concerned dislocations; moreover the force $\mathbf{F} \equiv -\nabla\mu$ acting on the atoms corresponds to the change of chemical potential related to the migration of the atoms themselves. Since these relationships are directly involved in the Fick equation inferred in section 1, it follows that the eq (15) fits well the model of concentration gradient driven diffusion process.

Furthermore let us show that eq (15) implies the link between $\nabla\mu$ and the stress τ that tends to move preferentially dislocations with Burgers vector favourably oriented in a crystal matrix, e.g. perpendicularly to a tilt boundary plane [14]; this stress produces thus a chemical potential gradient between adjacent dislocations having non-perpendicular component of the Burgers vector. Once more D to be implemented here is just the diffusion coefficient $D^{\S}$ pertinent to the interaction with the dislocation and thus appropriate to this specific task. Assuming again $k_BT/\eta \approx \Omega$, then $\mathbf{F} = -\nabla\mu$ yields $\mathbf{F}\Omega = -(k_BT/\eta)\nabla\mu$. If two dislocations are at a distance d apart, then $\Omega = Ad/2$ for each dislocation, being A the surface defined by the length L of the dislocations and the height of their extra-planes; so Ad is the total volume of matrix enclosed by them, whereas $Ad/2$ is the average volume defined by either extra-plane and its average distance from an equidistant atom, assumed $d/2$ apart from each dislocation. Being $2\mathbf{F}\Omega/(Ad) = -\nabla\mu$, the conclusion is that $2\tau\Omega/d = -\nabla\mu$ with $\tau = \mathbf{F}/A$, which is indeed the result reported in [14].

Finally let us calculate with the help of the eq (15) also the atom flux $\mathbf{I} = A\mathbf{J}/m$ between dislocations per length of boun-dary of cross section A in direction parallel to the tilt axis. The following chain of equations

$$\mathbf{I} = -\frac{AD_L\nabla c}{m} = -\frac{AD_L\nabla c}{c\Omega} = -\frac{AD_L\nabla\log(c)}{\Omega} =$$

$$= \frac{D_LA\nabla\mu}{k_BT\Omega} = -\frac{2D_L\mathbf{F}}{k_BTd} = -\frac{2D_LL\tau}{k_BT} \qquad \tau = \frac{\mathbf{F}}{Ld}$$

yields the literature result $-2D_L\tau/kT$ per unit length of dislocation [14].

All considerations carried out from now on are self-contained whatever the analytical form of c might be. In the following the working temperature T of the cell is always regarded as a constant throughout the electrolyte.

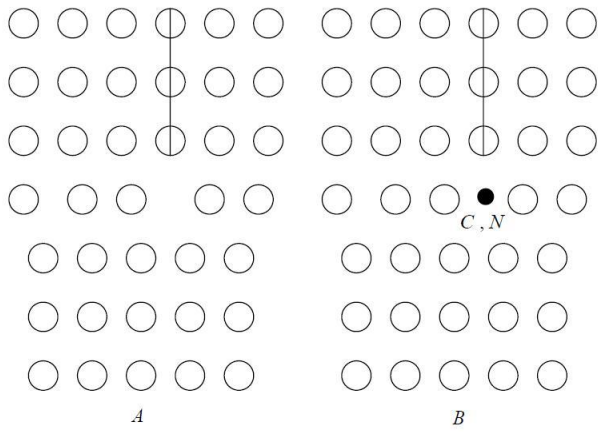

Fig. 2: A: Cross section of the stretched zone of an edge dislocation at the interface between the lower boundary of the extra plane and the perfect lattice. B: Equilibrium position of an atom, typically carbon or nitrogen, in the stretched zone after stress ageing.

3 Outline of the charge transport model

In general, the macroscopic charge flow within the electrolyte of a SOFC cell is statistically represented by average concentration profiles of all charges that migrate between the electrodes. The profiles of the ions during the working condition of the cell, qualitatively sketched in the fig. 1, are in effect well reproduced by that calculated solving the diffusion equation (12) [9]. The local steps of these paths consist actually of random lattice jumps dependent on orientation, structure and possible point and line defects of the crystal grains forming the electrolyte, of course under the condition that the displacement of the charge carriers must be anyway consistent with the overall formation of neutral reaction products. So $\mathbf{v}$ and ∇n of the eqs (17) are average vectors that consist actually of local jumps dependent on how the charge carriers interact each other and with lattice defects, grain boundaries and so on. The interaction of low sized light atoms and ions with the lattice distortion due to the extra plane of a dislocation has been concerned in several papers, e.g. [15]: the figure 2A shows the cross section of the stretched zone of an edge dislocation, the fig. 2B the location of a carbon atom in the typical configuration of the Cottrell atmosphere after strain ageing of bake hardenable steels. The segregation of N and C atoms, typically interstitials, on dislocations to form Cottrell atmospheres is a well known effect; it is also known that after forming these atmospheres, energy is required to unpin the dislocations: Luders bands and strain ageing are macroscopic evidences of the pinning/unpinning instability. These processes are usually activated by temperature and mechanical stresses.

Of course the stress induced redistribution and ordering of carbon atoms has 3D character and has been experimentally

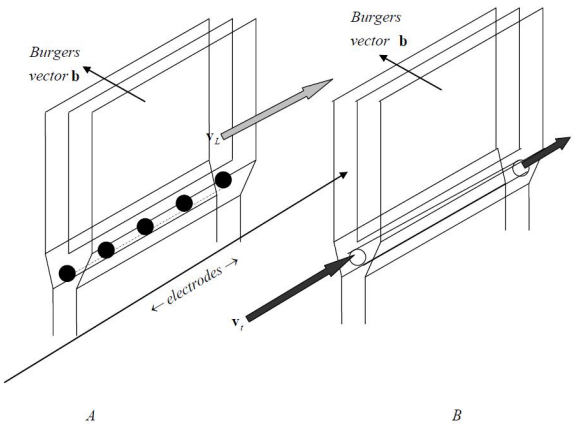

Fig. 3: 3D representation of the static Cottrell configuration of several carbon atoms after interaction with the stress field of an edge dislocation. B: dynamical flow of charge carriers that tunnel along the length of the extra plane of the dislocation.

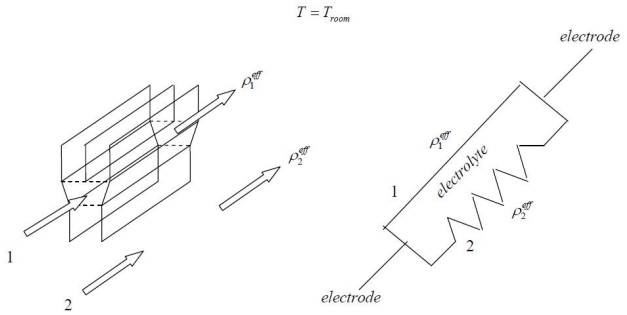

Fig. 4: Shunt effect of charge carriers between dislocation path and lattice path of different resistivity. On the left is sketched the possible path within and in proximity of the stretched zone of an edge dislocation; on the right is shown the corresponding electric circuit of the currents crossing the electrolyte.

verified in ultra low carbon steels; the configuration reported in the literature and redrawn in fig 3A explains the return to the sharp yield point of the stress-strain curve of iron [16].

The chance that light atoms line up into the strained zone of an edge dislocation is interesting for its implications in the case of mixed conductivity in ceramic electrolytes. It is reasonable to guess that the aligned configuration sketched in fig. 3A is in principle also compatible with the path of mobile charge carriers displacing along this transit trail, as represented in the fig. 3B. Among all possible paths, the next section concerns in particular the conduction mechanism that occurs when low atomic number ions tunnel along the stretched zone at the interface between the extra-plane of an edge dislocation and the underlying perfect lattice. The mechanism related to this specific configuration of charges involves directly the interaction of the carriers with the dislocation and thus is described by the eq (15), which indeed depends explicitly upon $D^{\S}$. From a classical point of view, is conceivable in principle an ideal fuel cell whose electrolyte is a ceramic single crystal with one edge dislocation spanning the entire distance between the electrodes; in this particular case, therefore, is physically admissible a double conduction mechanism based on the standard diffusive process introduced in [9] plus that of ion tunnelling throughout the whole electrolyte size. Regarding the tunnel path and the whole lattice path as two parallel resistances, the Kirchhoff laws indicate how the current of charge carriers generated at the electrodes shunts between either of them. This is schematically sketched in the figure 4.

The tunnel mechanism appears reasonable in this context considering the estimated electron and proton classical radii, both of the order of 10^{-15} m, in comparison with the lattice spacing, of the order of some 10^{-10} m. A short digression about the atom and ion sizes with respect to the crystal cell parameter deserves attention. Despite neither atoms nor ions have definite sizes because of their electron clouds lack sharp boundaries, their size estimate allowed by the rigid sphere model is useful for comparison purposes; as indeed the Cottrel atmospheres of C and N atoms have been experimentally verified, the sketch of the fig. 3A suggests by size comparison a qualitative evaluation about the chance of an analogous behaviour of ions of interest for the fuel cells. The atomic radius is known to be in general about 10^4 times that of the nucleus, the radii of low atomic number elements typically fall in the range $1 \div 100$ pm [17]. Specifically, the covalent values for C, N and O atoms are 70, 65 and 60 pm respectively; it is known that they decrease across a period. The ionic radii of low atomic number elements are typically of the order of 100 pm [18]; they are estimated to be 0.1 and 0.14 nm for Na^+ and $O^=$. It is known that the average lattice parameters of solid oxides increase about linearly with cationic radii [19]; typical values of lattice average spacing are of the order of 0.5-0.6 nm. As the stretched zone of a dislocation has size necessarily greater than the unstrained spacing, one reasonably concludes that, at least in principle, not only the proton and nitrogen and carbon atoms but even oxygen ions have sizes compatible with the chance of being accommodated in the stretched zone underlying the dislocation extra-plane. These estimates suggest by consequence that even low atomic number ion conduction via channelling mechanism along the stretched zone of the dislocation is reasonably possible. It is known that proton conducting fuel cells typically work with protons crossing of polymer membranes from anode to cathode, whereas in-SOFCs oxygen ions migrate through the ceramic electrolyte from cathode to anode; yet the tunnelling mechanism seems in principle consistent with both kinds of charge carriers in typical SOFC electrolytes.

Consider now the case where the driving energy of the segregation process of atoms to dislocations is not only the lattice strain of the ceramic electrolyte but, during the working cycle of a fuel cell, also the free energy that generates ions at the electrodes and compels them migrating by effect of the electric potential; the alignment of several ions confined along the dislocation length sketched in fig. 3A has thus a dynamical valence, i.e. it suggests the specific displacement mechanism that involves the tunnelling of ions throughout the stretched zone of an edge dislocation at its boundary with the perfect lattice. In other words, one can think that the line of foreign light ions along this zone is also compatible with the particular migration path of such ions generated at either electrode; certainly the proton is a reasonable example of carrier compliant with such particular charge transport mechanism, as qualitatively sketched in fig. 3B. These considerations explain the difference between D, the usual diffusion coefficient of a given ion in a given lattice with or without point defects, and D^{eff}, which in this case is the effective diffusion coefficient of the same ion that moves confined in the stretched zone of the dislocation. This conclusion agrees with and confirms the idea that the electric conductivity is related to D^{eff} and not to D, because the former only accounts for this particular kind of interaction between charge carrier and dislocation. Also, just for this reason in the fig. 4 the resistivity of ions with different kind of interaction with the dislocation, i.e. inside it along the stretched zone and outside it in the lattice compression zone, have been labelled respectively ρ_1^{eff} and ρ_2^{eff}. Despite D^{eff} is related generically to any interaction mechanism possible when charge carriers move in the presence of dislocations, it will be regarded in the following with particular reference to the charge tunnelling mechanism just introduced.

4 Classical approach to elaborate the early results [9]

The experimental situation described in this section, in principle possible, is the one of a unique edge dislocation crossing throughout the single crystal ceramic electrolyte and arbitrarily inclined with respect to plane parallel electrodes. The following discussion concerns the eq (17) and consists of two parts: the first part has general character, i.e. it holds at any point of the ceramic lattice, in which case the presence of the dislocation merely provides a reference direction to define specific components of $\mathbf{v}$; the second part aims to describe the particular mechanism of transport of charges that tunnel along the stretched zone of the dislocation, which in fact is the specific case of major interest for the present model.

4.1 Charge transport in the electrolyte lattice

Regard in general the drift velocity $\mathbf{v}$ of a charge carrier as due to a component $\mathbf{v}_\parallel$ parallel to the tunnelling direction and a component $\mathbf{v}_\perp$ perpendicular to $\mathbf{v}_\parallel$; so the eq (17) yields

$$\mathbf{v} = \mathbf{v}_\parallel + \mathbf{v}_\perp \qquad \mathbf{v}_\parallel \eta = k_B T D_\parallel^{\S} \nabla n \pm \eta' \mathbf{v}_a \tag{19}$$

$$\mathbf{v}_\perp \eta = k_B T D_\perp^{\S} \nabla n \mp \eta' \mathbf{v}_a \qquad D_\parallel^{\S} + D_\perp^{\S} = D^{\S}$$

where η' has physical dimensions of energy per unit volume and $\mathbf{v}_a$ is an arbitrary velocity vector: with the given signs, the third equation is fulfilled whatever $\mathbf{v}_a$ and η' might be. Of course the components of $\mathbf{v}$ are linked by

$$\mathrm{v} = \sqrt{\mathrm{v}_\parallel^2 + \mathrm{v}_\perp^2} \qquad \mathbf{v}_\perp = \left(\mathbf{u}_\parallel - \frac{\mathbf{u}_o}{\mathbf{u}_o \cdot \mathbf{u}_\parallel}\right)\mathrm{v}_\parallel \qquad \mathbf{u}_\parallel = \frac{\mathbf{v}_\parallel}{\mathrm{v}_\parallel} \tag{20}$$

with $\mathrm{v} = |\mathbf{v}|$ given by the solution of the set (12) of diffusion equations; the same notation holds for the moduli $\mathrm{v}_\parallel$ and $\mathrm{v}_\perp$. The arbitrary unit vector $\mathbf{u}_o$ is determined in order to satisfy the first equation; trivial manipulations yield indeed

$$\mathrm{v} = \frac{\mathrm{v}_\parallel}{\cos\varphi} \qquad \mathrm{v}_\perp^2 = \mathrm{v}_\parallel^2 \left(\frac{1}{\cos^2\varphi} - 1\right) \qquad \mathbf{u}_o \cdot \mathbf{u}_\parallel = \cos\varphi, \tag{21}$$

which fits v^2 via an appropriate value of $\cos\varphi$. Moreover the eq (17) yields

$$\mathrm{v}_\parallel = \Omega D^{\S} \mathbf{u}_\parallel \cdot \nabla n, \tag{22}$$

which in principle is fulfilled by an appropriate value of Ω whatever the actual orientation of $\mathbf{u}_o$ and related value of $\cos\varphi$ in the eqs (21) might be. Consider now that also the thermal energy $k_B T = m\mathrm{v}_T^2/2$ contributes to the velocity of the carriers crossing the electrolyte, and thus must someway appear in the model; v_T defined in this way is the average modulus of the velocity vector $\mathbf{v}_T$, whose orientation is by definition arbitrary and random. During the working conditions of the cell it is reasonable to expect that the actual dynamics of charge transport is described combining $\mathbf{v}_T$, due to the heat energy of the carrier in the electrolyte, with $\mathbf{v}$, due to its electric and concentration gradient driving forces. Let us exploit $\mathbf{v}_a$ of the eqs (19) to introduce into the problem just the vector $\mathbf{v}_T$ of the carriers; hence

$$\mathbf{v}_\parallel = \frac{D_\parallel^{\S}}{D^{\S}}\mathbf{v} \pm \frac{\eta'}{\eta}\mathbf{v}_T \qquad \mathbf{v}_\perp = \frac{D_\perp^{\S}}{D^{\S}}\mathbf{v} \mp \frac{\eta'}{\eta}\mathbf{v}_T \qquad \mathbf{v}_a \equiv \mathbf{v}_T. \tag{23}$$

These equations express the components of $\mathbf{v}$ along the tunnel direction and perpendicularly to it. Of course $\mathbf{v}$ is the actual velocity of the charge carrier resulting from the solution of the eq (12), $\mathbf{v}_\parallel$ and $\mathbf{v}_\perp$ are the components of $\mathbf{v}$ affected by the thermal perturbation consequently to either sign of $\mathbf{v}_T$; the notations $\mathbf{v}_\parallel^{\pm}$ and $\mathbf{v}_\perp^{\mp}$, in principle more appropriate, are implied and omitted for simplicity. So in general

$$\mathbf{v}_\parallel = r_\parallel \mathbf{v} \pm r\mathbf{v}_T \qquad \mathbf{v}_\perp = r_\perp \mathbf{v} \mp r\mathbf{v}_T \qquad r = \frac{\eta'}{\eta} \qquad r_\parallel = \frac{D_\parallel^{\S}}{D^{\S}} \tag{24}$$

$$r_\perp = \frac{D_\perp^{\S}}{D^{\S}} \qquad r_\parallel + r_\perp = 1.$$

As expected, the velocity components result given by the respective linear combinations of $\mathbf{v}$ and $\mathbf{v}_T$. Here it is reasonable to put $r = 1$ in order that $\mathbf{v}_\parallel \to \pm\mathbf{v}_T$ and $\mathbf{v}_\perp \to \mp\mathbf{v}_T$ for

$\mathbf{v} \to 0$; as this reasonably occurs for $T \to 0$, it means that both components of $\mathbf{v}$ tend to the respective values consistent with the zero point energy of the charge carrier. Note in particular that the second eq (24) $\mathbf{v}_T = \pm(r_\perp \mathbf{v} - \mathbf{v}_\perp)$ yields thanks to the eqs (21) $\mathrm{v}_T^2 = (r_\perp \mathrm{v})^2 + \mathrm{v}_\perp^2 - 2r_\perp \mathbf{v} \cdot \mathbf{v}_\perp$, i.e.

$$\mathrm{v}_T^2 = r_\perp^2 \frac{\mathrm{v}_\parallel^2}{\cos^2\varphi} + \mathrm{v}_\parallel^2 \tan^2\varphi - 2r_\perp \mathrm{v}_\perp^2 = \qquad (25)$$

$$= \left(\frac{r_\perp^2}{\cos^2\varphi} + (1 - 2r_\perp)\tan^2\varphi \right) \mathrm{v}_\parallel^2 \qquad \mathbf{v} \cdot \mathbf{v}_\perp = \mathrm{v}_\perp^2$$

Let us specify now the considerations hitherto carried out to describe the behaviour of a charge carrier moving inside the stretched zone of the dislocation; the next part of this section concerns in particular just the charge transport via tunnelling mechanism.

4.2 Charge transport along the stretched zone of the dislocation

Both possible chances $r_\parallel \mathbf{v}_\parallel + \mathbf{v}_T$ and $r_\parallel \mathbf{v}_\parallel - \mathbf{v}_T$ of the first equation (24) yield an average velocity vector still consistent with the possible tunnelling of the ion. The corresponding chances of the second equation, where instead the vector $\mathbf{v}_T$ sums and subtracts to $r_\perp \mathbf{v}_\perp$, are more interesting and critical. The components $r_\perp \mathbf{v}_\perp \mp \mathbf{v}_T$ of $\mathbf{v}$ show indeed that the thermal agitation summed up to the transverse component of ion velocity could possibly avert the tunnelling conduction mechanism; this linear combination implies the possibility for the ion path to deviate from the tunnel direction and flow outwards the tunnel. Moreover, even the Coulomb interaction of the carriers with the charged cores of the lattice closely surrounding the tunnel is to be considered: as the cores are in general electrically charged, their interaction with the flow of mobile carriers is expectable. The second condition for a successful tunnelling path of the carriers concerns just this interaction: if for instance the charge carrier is an electron, it is likely attracted to and thus neutralizes with the positive cores; so the tunnel path through the whole distance L is in practice impossible. If instead the carrier is a proton, its Coulomb repulsion with the positive cores is consistent with the chance of travelling through L and coming out from the dislocation tunnel: in the case of a ceramic single crystal and dislocations crossing throughout it, the charge carrier would start from one electrode and would reach the other electrode entirely in the confined state. This tunnel transport mechanism is coupled with the usual lattice transport mechanism. This situation is represented in the figure 5.

Let us analyze both effects. Let $\delta t = L/\mathrm{v}_\parallel$ be the time necessary for the carrier to tunnel throughout the length L of the stretched zone. Then, as schematically sketched in fig. 6, all possible trajectories are included in a cone centred on the entrance point of the carrier whose basis has maximum total size $2\delta r = 2(r_\perp \mathrm{v}_\perp + \mathrm{v}_T)\delta t$.

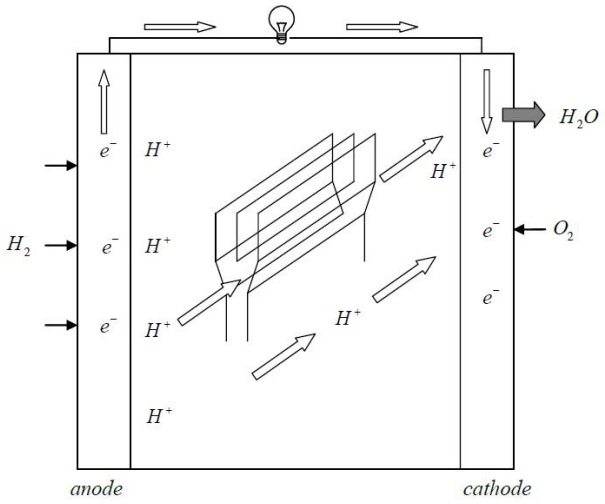

Fig. 5: Schematic sketch of a cell where is operating the proton conduction mechanisms.

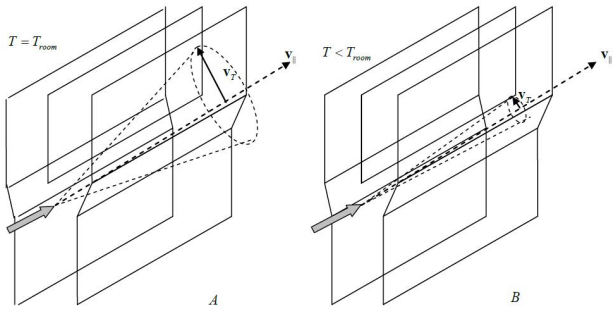

Fig. 6: The figure shows qualitatively the effect of the thermal velocity, solid arrow, on the tunnelling of a charge carrier that travels within the stretched zone of an edge dislocation. In A the vector sum of $\mathbf{v}_\parallel$ and $\mathbf{v}_T$ occurs at a temperature preventing the chance for the carrier to tunnel throughout the dislocation length; in B the reduced value of $\mathbf{v}_T$ at lower T allows the tunnelling effect.

As $\mathbf{v}_T$ has by definition random orientation, here has been considered the most unfavourable case where $\mathbf{v}_T$ is oriented just transversally to $\mathbf{v}_\parallel$ in assessing the actual chance of confinement of the carrier within the stretched zone of the dislocation. In general the tunnel effect is expectable at temperatures appropriately low only, in order that the width of the cone basis be consistent with the average size δl of the stretched zone: during δt the total lateral deviation $2\delta r$ of the ion path with respect to $\mathbf{v}_\parallel$ must not exceed δl, otherwise the ion would overflow in the surrounding lattice. In other words, the charge effectively tunnels if $\mathrm{v}_\parallel$ is such to verify the condition $(r_\perp \mathrm{v}_\perp + \mathrm{v}_T)L/\mathrm{v}_\parallel \leq \delta l$ only.
In conclusion, considering the worst case with the plus sign where $\mathbf{v}_T$ and $r_\perp \mathbf{v}_\perp$ sum up correspondingly to the maximum

deviation of the charge, it must be true that, whatever the component $\mathrm{v}_\parallel$ of the actual ion displacement velocity might be,

$$T \leq \frac{m}{2k_B}\left(\mathrm{v}_\parallel \frac{\delta l}{L} - r_\perp \mathrm{v}_\perp\right)^2 \qquad k_B T = \frac{m\mathrm{v}_T^2}{2}. \tag{26}$$

Two interesting equations are obtained merging the general eq (5) and the eqs (24). Specifying for instance that the modulus of velocity is $\mathrm{v}_\perp$ and D is actually $D^{\S}_\perp$, one finds $D^{\S}_\perp = \mathrm{v}_\perp k_B T/F_\perp$; so, multiplying both sides by $\mathrm{v}_\perp/D^{\S}$ and repeating identical steps also for $\mathrm{v}_\parallel$, the results are

$$r_\perp \mathrm{v}_\perp = \frac{k_B T}{F_\perp D^{\S}}\mathrm{v}_\perp^2 \qquad r_\parallel \mathrm{v}_\parallel = \frac{k_B T}{F_\parallel D^{\S}}\mathrm{v}_\parallel^2. \tag{27}$$

These equations introduce the confinement forces $F_\perp$ and $F_\parallel$ that constrain the carrier path within the tunnel and correspond to the interaction of the charge carrier with the neighbours lattice cores surrounding the stretched zone of the dislocation. Also, as the eqs (21) yield $\mathrm{v}_\perp = \pm \mathrm{v}_\parallel \tan\varphi$, one finds

$$T \leq \frac{m\mathrm{v}_\parallel^2}{2k_B}\left(\frac{\delta l}{L} - \frac{k_B T \mathrm{v}_\parallel}{F_\perp D^{\S}}\tan^2\varphi\right)^2$$

which is more conveniently rewritten as follows

$$\frac{T}{T_c} \leq \frac{m\mathrm{v}_\parallel^2}{2k_B T_c}\left(\frac{\delta l}{L} - \frac{T}{T_c}\frac{\mathrm{v}_\parallel}{\mathrm{v}_c} w\left(\frac{\delta l}{L}\right)^2\right)^2 \tag{28}$$

$$F_\perp D^{\S} = \mathrm{v}_c k_B T_c \qquad \tan\varphi = \pm w\frac{\delta l}{L} + \ldots .$$

The meaning of the second equation is at the moment merely formal, aimed to obtain an expression function of T/T_c and $\mathrm{v}_\parallel/\mathrm{v}_c$; as concerns the third position, is attracting the idea of writing the expression in parenthesis as a power series expansion of $\delta l/L$ truncated at the second order, in which case the proportionality constant w defines the series coefficient $T\mathrm{v}_\parallel w/(T_c \mathrm{v}_c)$. Note that this coefficient should expectably be of the order of the unity, in order that the series could converge; indeed this conclusion will be verified in the next subsection 5.2. Clearly v_c is definable as the transit critical velocity of the charge carrier making equal to 1 the right hand side of the first eq (28). Anyway both positions are acceptable because neither of them needs special hypotheses, being mere formal ways to rewrite the initial eq (26). This equation emphasizes that even when $\mathbf{v}_\perp = 0$, i.e. in the particular case where the entrance path of the charge carrier is exactly aligned along $\mathbf{v}_\parallel$, the mere thermal agitation must be consistent itself with the available tunnel cross section: the greater the latter, the higher the critical temperature below which the tunnelling is in fact allowed to occur. This equation links the lattice features δl and L to the operating conditions of the cell, here represented by the ion properties m and $\mathrm{v}_\parallel$. Hence it is reasonable to expect that v_T and thus T must not exceed a critical upper value in order to allow the tunnelling mechanism. If T and m, and thus v_T, are such that $\mathrm{v}_\parallel \delta t$ really corresponds to the whole length L of the dislocation, then the eqs (17) describe the flow of ions that effectively tunnel in the stretched zone of the dislocation.

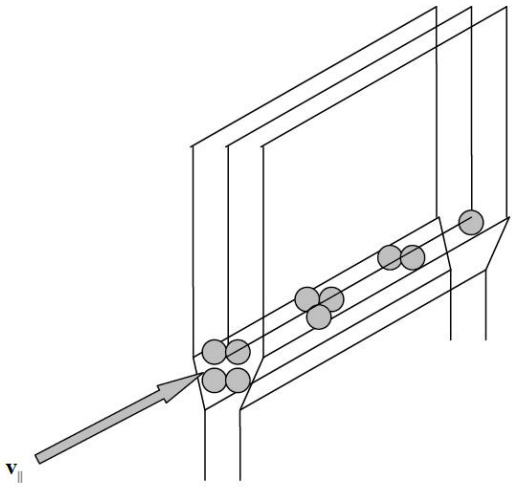

Fig. 7: The figure highlights that the arising of a concentration gradient along the tunnel is hindered by the size of the stretched zone of the dislocation.

4.3 The superconducting charge flow

The main feature of these results is that $D^{\S}$ and ∇n characterize the charge tunnelling path. In general the occurring of concentration gradient requires by definition a volume of electrolyte so large to allow the non-equilibrium distribution of a statistically significant number of charge carriers unevenly distributed among the respective lattice sites. Yet $\nabla n \neq 0$ is in fact inconsistent with the size of the dislocation stretched zone here concerned; in particular, the existence of the component $\mathbf{u}_\parallel \cdot \nabla n$ of this gradient would require a configuration of charges like that qualitatively sketched in fig. 7.

This chance seems however rather improbable because of the mutual repulsion between charges of the same sign in the small channel available below the dislocation extra plane. So the gradient term at right hand side of the eq (22) should intuitively vanish inside the tunnel. Assume thus the component $\mathbf{u}_\parallel \cdot \nabla n = 0$, i.e the carriers travel the stretched zone with null gradient within the tunnel path. To better understand this point, note that in the eq (22) appears the product $D^{\S}\nabla n$; moreover, in the eqs (27) appear the products $F_\perp D^{\S}$ and $F_\parallel D^{\S}$. These results in turn suggest two chances allowed at left hand side of eq (22):

(i) $\mathrm{v}_\parallel = 0$, i.e. all charges are statistically at rest in the stretched zone; the eq (22) trivially consisting of null terms at both sides is nothing else but the particular case of the Cottrell

atmosphere sketched in fig. 3A. The ions that decorate the dislocation prevent the tunnelling of further ions provided by the lattice. The charge flow in the cell is merely that described by the usual bulk lattice ion transport under concentration and electric potential gradients, already concerned in [9].

(ii) The left hand side of the eq (22) is non-vanishing: $\mathrm{v}_{\|} \neq 0$ reveals actual dynamics of charges transiting within the tunnel zone. This is closely related to the previous statement of the section 1 according which, for instance, a bare electron of mass m_e interacting with the dislocation can be described by a free electron of effective mass m_e^{eff}: owing to the eqs (2), this reasoning is identically expressed in general via D^{eff} instead of m^{eff} of any charge carrier.

The latter case is interesting, because the finite value of $\mathrm{v}_{\|} \neq 0$ requires that $D^{\S} \to \infty$ in order that the undetermined form $\infty \times 0$ makes finite the corresponding limit value of $D^{\S}\mathbf{u} \cdot \nabla n$. This also means that $D^{\mathrm{eff}} = D^{*} + D^{\S}$ tends to infinity as well, which compels the resistivity $\rho^{\mathrm{eff}} \to 0$ according to eq (4). Moreover, for the same reason this mechanisms implies both $F_{\perp} \to 0$ and $F_{\|} \to 0$ for $D^{\S} \to \infty$, which implies $D^{\S}_{\perp} \to \infty$ and $D^{\S}_{\|} \to \infty$; this in turn means null interaction of the charge carrier with the lattice surrounding the tunnel zone. Hence the eqs (28) and (27) yield

$$\frac{T}{T_c} = \frac{m\mathrm{v}_{\|}^2}{2k_B T_c}\left(\frac{\delta l}{L} - \frac{T}{T_c}\frac{\mathrm{v}_{\|}}{\mathrm{v}_c} w\left(\frac{\delta l}{L}\right)^2\right)^2 \qquad (29)$$

$$\lim_{\substack{D^{\S}\to\infty \\ F_{\perp}\to 0}} \frac{F_{\perp} D^{\S}}{k_B} = \mathrm{v}_c T_c \qquad \lim_{\substack{D^{\S}\to\infty \\ F_{\|}\to 0}} \frac{F_{\|} D^{\S}}{k_B} = \mathrm{v}'_c T_c .$$

In the eqs (28) T_c and v_c were in general arbitrary variables; here instead they are fixed values uniquely defined by the limit of the second and third equations; the same holds for v'_c related to $\mathrm{v}_{\|}$. So the transport mechanism in the stretched boundary zone of the dislocation extra plane is different from that in other zones of the ceramic crystal: clearly the former has nothing to do with the usual charge displacement throughout the lattice concerned by the latter. While the concentration gradient is no longer the driving force governing the charge transport, $F_{\perp} \to 0$ and $F_{\|} \to 0$ consequently obtained mean that the charge carrier moves within the tunnel as a free particle: the lack of friction force, i.e. electrical resistance, prevents dissipating their initial access energy into the dislocation stretched zone. This appears even more evident in the eq (5), where $D \equiv D^{\S}$ at $T = T_c$ yields $\mathbf{J} \neq 0$ compatible with $\mathbf{F} = 0$.

Simple considerations with the help of fig. 8, inferred from the fig. 4 but containing the information $\rho^{\mathrm{eff}} \to 0$, show the electric shunt between zones of different electrical resistivity and highlight why the charge carriers tend to privilege the zero resistance tunnel path: this answers the possible question about the preferential character of this conduction mechanism of the charge carriers. Further quantum considerations are necessary to complete the picture essentially classical so far carried out. On the one hand the expectation of a superconducting flow of charges cannot be certainly regarded as an unphysical result, despite its derivation has surprisingly the classical basis hitherto exposed. In this respect however it is worth recalling the quantum nature of both eqs (1), which indeed have been obtained as corollaries of the statistical formulation of the quantum uncertainty [10]; the fact that the Fick equations have been obtained themselves as corollaries of a quantum approach to the gradient driven diffusion force, shows that actually all results have inherently quantum physical meaning. Then, by definition, even a classical approach inferred from these equations has intrinsic quantum foundation. On the other hand, the heuristic character of this section requires being completed with further concepts more specifically belonging to the quantum world.

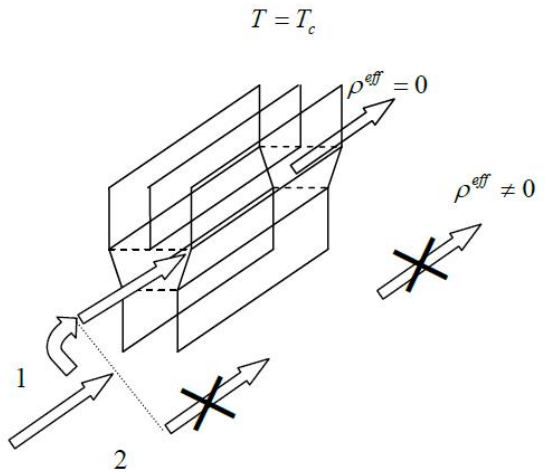

Fig. 8: Schematic sketch showing that at the ion current shunts to the zero resistivity path inside the tunnel with electrical resistivity $\rho^{\mathrm{eff}} = 0$ rather than to any lattice path with $\rho^{\mathrm{eff}} \neq 0$.

5 Quantum approach

This section aims to understand why the results of the classical model of a unique dislocation crossing through one single grain are actually extendible to a real grain with several disconnected dislocations of different orientations and to the grain boundaries consisting of several tangled dislocations inordinately piled up at the interface with other grains.

5.1 Grain bulk superconductivity

Define $\delta\varepsilon = \varepsilon_{tu} - \varepsilon_{la}$, being ε_{tu} the energy of the ion travelling the tunnel along the stretched zone of the edge dislocation and ε_{la} that of the ions randomly moving in the lattice before entering the tunnel; $\delta\varepsilon$ represents thus the gap between the energy of the ion in either location, which in turn suggests

the existence of an energy gap for a charge carrier in the superconducting and non-superconducting state. This conclusion is confirmed below. The fact of having introduced the tunnelling velocity components $\mathbf{v}_\perp$ and $\mathbf{v}_\parallel$, suggests introducing the respective components of De Broglie momentum of the ion corresponding to ε_{tu}. Being $p_\parallel = h/\lambda_\parallel$ and $p_\perp = h/\lambda_\perp$ these components, then $|\mathbf{p}| = h\sqrt{\lambda_\perp^{-2} + \lambda_\parallel^{-2}}$ in the tunnel state; $\lambda_\perp$ and $\lambda_\parallel$ are the wavelengths corresponding to the respective velocity components. Let us specify $n_\perp\lambda_\perp = \delta l$ and $n_\parallel\lambda_\parallel = L$, in order to describe steady waves with $n_\perp$ and $n_\parallel$ nodes along both tunnel sizes; then, with $n_\perp = 1$ and $n_\parallel = 1$,

$$p_{tu} = |\mathbf{p}| = \gamma h/\delta l \qquad \gamma = \sqrt{1 + (\delta l/L)^2}.$$

Note that $\gamma \approx 1$ approximates well p_{tu} even if L corresponds to just a few lattice sites aligned to form the extra-plane of the edge dislocation, i.e. even in the case of an extra-plane extent short with respect to the lattice spacing stretched to δl: indeed $(\gamma h/\delta l - h/\delta l)/(\gamma h/\delta l) \approx (\delta l/L)^2/2$ yields $\gamma \approx 1$ even for values $L \gtrsim \delta l$. Anyway with $p_{tu} = \gamma h/\delta l$ one finds $\varepsilon_{tu} = (h\gamma)^2/2m\delta l^2$. According to this result, the momentum is essentially due to the small cross section of the stretched zone that constrains the transverse velocity component $\mathbf{v}_\perp$ of the ion in the tunnel with respect to that of the ion randomly moving in the lattice; this means that remains instead approximately unchanged the component $\mathbf{v}_\parallel$ of velocity along the tunnel. Put now $\varepsilon_{la} = \vartheta\varepsilon_{tu}$, being θ an appropriate numerical coefficient such that $\delta\varepsilon = (\vartheta - 1)\varepsilon_{tu}$. In principle both chances $\vartheta \gtrless 1$ are possible, depending on whether $\varepsilon_{la} \gtrless \varepsilon_{tu}$: as neither chance can be excluded "a priori" for an ion in the two different environments, this means admitting that in general to the unique ε_{la} in the lattice correspond two energy levels spaced $\pm\delta\varepsilon$ around ε_{tu}, one of which is actually empty depending on either situation energetically more favourable. This is easily shown as the eqs (24) yield two chances for the energy of the charge carrier in the tunnel, depending on how $\mathbf{v}_T$ combines with $\mathbf{v}_\parallel$ and $\mathbf{v}_\perp$. These equations yield $\varepsilon_2 = \left((r_\parallel\mathbf{v} + \mathbf{v}_T)^2 + (r_\perp\mathbf{v} - \mathbf{v}_T)^2\right)m/2$ and $\varepsilon_1 = \left((r_\parallel\mathbf{v} - \mathbf{v}_T)^2 + (r_\perp\mathbf{v} + \mathbf{v}_T)^2\right)m/2$; trivial manipulations via the eqs (21) yield thus $\delta\varepsilon = \varepsilon_2 - \varepsilon_1 = 2m\mathbf{v}\cdot\mathbf{v}_T(r_\parallel - r_\perp)$ showing indeed a gap between the levels $\varepsilon_2 = \varepsilon_0 + m\mathbf{v}\cdot\mathbf{v}_T(r_\parallel - r_\perp)$ and $\varepsilon_1 = \varepsilon_0 - m\mathbf{v}\cdot\mathbf{v}_T(r_\parallel - r_\perp)$ with $\varepsilon_0 = \left((r_\parallel^2 + r_\perp^2)\mathrm{v}^2/2 + \mathrm{v}_T^2\right)m$: this latter corresponds thus to the Fermi level between the occupied and unoccupied superconducting levels defining the gap. As the ion dwell time δt in the tunnel is of the order of

$$\delta t = \frac{\hbar}{|\delta\varepsilon|} = 2\frac{m\delta l^2\hbar}{|\vartheta - 1|\,(\gamma h)^2},$$

the extent L of the extra-plane controlling the time range of ion transit at velocity $\mathrm{v}_\parallel$ requires

$$L = \mathrm{v}_\parallel\delta t = \frac{m\mathrm{v}_\parallel\delta l^2}{|\vartheta - 1|\,\pi h\gamma^2}.$$

So, supposing that n_{tu} electrons ξ apart each other transit simultaneously within the tunnel,

$$L = \frac{\mathrm{v}_\parallel\hbar}{|\delta\varepsilon|} = \frac{\mathrm{v}_\parallel\hbar}{|\vartheta - 1|\,\varepsilon_{tu}} \qquad L = (n_{tu} - 1)\xi \qquad \mathrm{v}_\parallel = \frac{\gamma h}{m\delta l}$$

suggest that

$$\xi = \frac{\mathrm{v}_\parallel\hbar}{(n_{tu} - 1)\,|\delta\varepsilon|} = \frac{\mathrm{v}_\parallel\hbar}{|\vartheta - 1|\,(n_{tu} - 1)\varepsilon_{tu}}.$$

Define now the tunnel volume V available to the transit of the ions as $V = \chi L\delta l^2$, being χ a proportionality constant of the order of the unity related to the actual shape of the stretched zone; if for instance the tunnel would be simulated by a cylinder of radius $\delta l/2$, then $\chi = \pi/4$. Hence

$$V = \chi\delta l^2\mathrm{v}_\parallel\delta t = \frac{\chi}{|\vartheta - 1|\,\pi}\frac{m}{h}\frac{\mathrm{v}_\parallel\delta l}{\gamma^2}\delta l^3.$$

Note that $\mathrm{v}_\parallel\delta l$ has the same physical dimensions of a diffusion coefficient; so it is possible to write $\mathrm{v}_\parallel\delta l = \psi D_\parallel$, being ψ an appropriate proportionality constant. Moreover recall that the diffusion coefficient has been also related in the section 1 to h/m via a proportionality constant, once more because of dimensional reasons; so put $D_m = q_m h/m$ via the proportionality factor q_m, as done in the section 1, whereas the subscript emphasizes that the diffusion coefficient is by definition that related to the mass of an ion or electron tunnelling in the stretched zone of the dislocation. So one finds

$$V = \frac{\chi\psi}{|\vartheta - 1|\,\pi\gamma^2}\frac{D_\parallel}{q_m D_m}\delta l^3.$$

Note eventually that it is certainly possible to write $V/\delta l^3 = \theta(1 + \zeta)$ with $\zeta > 1$ appropriate function and θ proportionality constant: indeed the tunnel can be envisaged as a series of cells of elementary volumes $L_0\delta l^2$, where L_0 corresponds to the lattice spacing of atoms aligned along the dislocation extra plane. Replacing these positions in the equation of V one finds

$$\frac{D_\parallel}{qD_m} = 1 + \zeta \qquad q = \frac{|\vartheta - 1|\,\theta\pi q_m}{\chi\psi}\gamma^2.$$

This result compares well with the eq (2) previously obtained in an independent way, simply identifying $\zeta = \partial^2 u(k)/\partial k^2$ and all constants with q; as expected here $D_\parallel$ plays at $T = T_c$ the role of $D^\S$ introduced in the section 1, whereas qD_m is just D^* previously obtained as electric potential driven enhancement of the plain diffusion coefficient $D \equiv D_m$. This agreement supports the present approach. This also suggests some more considerations about the nature of the superconducting charge wave propagating along the tunnel zone. It is intuitive that the quantum states of the charge carriers within the tunnel must correspond to an ordered flow of particles, all travelling the tunnel with the same velocity $\mathrm{v}_\parallel$; any perturbation of the motion of these charges would increase the total

Coulomb energy of the flow and could even spoil the flow; the low temperature helps in this respect. This requires in turn a sort of coupling between the carriers, because several fermions cannot have the same quantum state; in effect it is known that a small contraction of positive charges of the lattice cores around the transient electrons in fact couples two electrons. Actually, in this case the contraction is that of the lines of lattice cores delimiting the tunnel stretched by the dislocation plane around the transient charges. In other words, electron pairs or proton pairs travel through the tunnel as bosons with a unique quantum state.

5.2 Computer simulation

Some estimates are also possible considering a ceramic lattice whose average spacing is a; this is therefore also the order of magnitude expected for the size $\delta l \gtrsim a$ of the stretched zone. Consider first the case where the charge carrier is an electron, which requires negatively charged ion cores delimiting the tunnel cross section; this assumption reminds the familiar case of electron super-conduction and thus helps to check reliability and rationality of the estimates. To assess the previous results, put $m = 9 \times 10^{-28}$ g and consider the reasonable simulation value $\delta l = 5 \times 10^{-8}$ cm, consistent with a typical lattice spacing quoted in the section 3; one finds $\mathrm{v}_\parallel \approx 1.5 \times 10^8$ cm/s with the approximation $\gamma = 1$. Moreover putting $L = 10^{-4}$ cm, i.e. considering an edge dislocation that crosses through a test grain average size of the typical order of 1 μm, one finds a gap $\delta\varepsilon = \mathrm{v}_\parallel \hbar / L = 10^{-3}$ eV between the ion energies in the tunnel and in the lattice. Note that the zero point energy of a free ion in such a test lattice would be of the order of $\varepsilon_{la} \approx 3\hbar^2/2ma^2 \approx 0.3$ eV, quite small with respect to the definition value 1 eV of one electron or unit charge ion in a ceramic electrolyte of a cell operating with 1 V. To ε_{la} corresponds the zero point vibrational frequency $\nu = 2\varepsilon_{la}/h$, i.e. $\nu \approx 2 \times 10^{14}$ s^{-1}; with such a frequency the wavelength $\lambda_\parallel = L$ corresponds to a total charge wave due to $L\nu/\mathrm{v}_\parallel$ electrons. So one finds $\approx 10^2$ electrons, whose mean mutual distance is thus 10 nm about. Eventually the critical temperature compatible with the arising of the superconducting state given by the eq (26) is 0.02 K with $\mathrm{v}_\perp = 0$ or even smaller for $\mathrm{v}_\perp \neq 0$. Compare now this result obtained via the eq (26) with that obtainable directly through the eq (25)

$$\mathrm{v}_T^2 = \left(\frac{r_\perp^2}{\cos^2\varphi} + (1 - 2r_\perp)\tan^2\varphi \right) \mathrm{v}_\parallel^2 .$$

Note that v_T^2 has a minimum as a function of $r_\perp$. If $\varphi = \pi/2$ this minimum corresponds to $r_\perp^{\min} = 1$, to be rejected because it would imply $D_\perp^{\S} = D^{\S}$ and $D_\parallel^{\S} = 0$. If instead $\varphi \neq \pi/2$, then the minimum corresponds to $r_\perp^{\min} = \sin^2\varphi$, which yields in turn $\mathrm{v}_T^2 = \mathrm{v}_\parallel^2 \sin^2\varphi$; hence $k_B T_c = m\mathrm{v}_T^2/2$ yields

$$T_c = \frac{m}{2k_B} \mathrm{v}_\parallel^2 \sin^2\varphi .$$

With $\mathrm{v}_\parallel = 1.5 \times 10^8$ cm/s the electron mass would yield $T = 6.2 \times 10^6 \sin^2\varphi$ K. Comparing with the previous result, one infers that $10^{-8} \gtrsim \sin^2\varphi$; so being $\sin^2\varphi \approx \tan^2\varphi$ with good approximation, one also infers that the second position (28) is verified with w such that $T\mathrm{v}_\parallel w/(T_c \mathrm{v}_c)$ is of the order of unity for $\delta l/L = 10^{-4}$, as in fact it has been anticipated in the previous subsection 4.3. Of course the actual values of these order of magnitude estimates depend on the real microstructure of the ceramic lattice; yet the aim of this short digression concerning the electron is to emphasize that the typical properties of the test material used for this simulation are consistent with the known results of electron superconduction theory. The simulation can be repeated for the proton, considering that the proton velocity $\mathrm{v}_\parallel$ is now m_e/m_{prot} times lower than before; so, despite m is m_{prot}/m_e larger than before, $m\mathrm{v}_\parallel^2$ of the eq (26) predicts a critical T smaller than that of the electron by a factor m_e/m_{prot} for $r_\perp \mathrm{v}_\perp \ll \mathrm{v}_\parallel \delta l/L$.

5.3 Grain bulk and grain boundary superconductivity

As concerns the chance of superconduction in the grain bulk with several disconnected dislocations at the grain boundaries, it is necessary to recall the Josephson effect concurrently with the presence of tangled dislocations and pile up of dislocations. The former concerns the transfer of superconducting Cooper pairs existing at the Fermi energy via quantum tunnelling through a thin thickness of insulating material: it is known that the tunnelling current of a quasi-electron occurs when the terminals of two dislocations, e.g. piled up or tangled, are so close to allow the Josephson Effect. If some terminals are a few nanometers apart, then superconduction current is still allowed to occur even though the dislocation break produces a thin layer of ceramic insulator. In other words, the terminal of the superconducting channel of one dislocation transfers the pair to the doorway of another dislocation and so on: in this way a superconduction current can tunnel across the whole grain. An analogous idea holds also at the grain boundary. Of course the chance that this event be actually allowed to occur has statistical basis: due to the high number of dislocations that migrate and accumulate at the grain boundaries after displacement along favourable slip planes of the bulk crystal lattice, the condition favourable to the Josephson Effect is effectively likely to occur. As the same holds also within the grain bulk between two different dislocations close enough each other, e.g. because they glide preferentially along equal slip planes and pile up on bulk precipitates, the conclusion is that the pair tunnelling allows macroscopic superconduction even without necessarily requiring the classical case of a unique dislocation spanning throughout a single crystal electrolyte.

6 Discussion

It is commonly taken for granted that the way of working of the fuel cells needs inevitably high temperatures, of the or-

der of some hundreds C degrees, so as to promote adequately the ion conductivity; great efforts are addressed to reduce as much as possible this temperature, down to a few hundreds C degrees, yet still preserving an acceptable efficiency of the cell compatibly with the standard mechanisms of ion conduction.

The present paper proposes however a new approach to the problem of the electric conduction in solid oxide electrolytes: reducing the operating temperature of SOFCs down to a few K degrees, in order to promote a superconducting mechanism.

Today the superconductivity is tacitly conceived as that of the electrons only; the present results suggest however that at sufficiently low temperatures, even the low atomic number ions are allowed to provide an interaction free conduction thanks to their chance of tunnelling in the stretched zone of edge dislocations. Note that although the electron and ion superconduction occur at different temperatures, as it is reasonable to expect, the nature of the lattice cores appears able to filter either kind of mechanism during the working conditions of the cell for the reasons previously remarked: for instance positively charged cores hinder the electron superconduction by attractive Coulomb effect, while promoting instead the proton superconduction via the repulsive effect that keeps the proton trajectory in the middle of the stretched channel. The results obtained in this paper support reasonably the chance that, at least in principle, this idea is practicable. Of course other problems, like for instance the catalysis at the electrodes, should be carefully investigated at the very low temperatures necessary to allow the ion superconduction. However this side problem, although crucial, has been deliberately waived in the present paper: both because of its different physicochemical nature and because the foremost aim of the model was (i) to assess the chance of exploiting the superconductivity not only for the electric energy transmission but also for the electric energy production and (ii) to bring this intriguing topic of the quantum physics deeply into the heart of the fuel cell science.

Moreover other typical topics like the penetration depth of the magnetic field and the critical current have been skipped because well known; the purpose of the paper was not that of elaborating a new theory of superconductivity, but to ascertain the feasibility of an ion transport mechanism able to bypass the difficulties of the high temperature conductivity. Two considerations deserve attention in this respect. The first one concerns the requirement $\mathbf{u}_{\|} \cdot \nabla n = 0$ characterizing the superconductive state with $D \to \infty$. At first sight one could naively think that the eq (4) should exclude a divergent diffusion coefficient. Yet the implications of a mathematical formula cannot be rejected without a good physical reason. Actually neither the chain of equations (6) nor the eq (19) exclude $D \to \infty$: the former because it is enough to put the lattice-charge interaction force $\mathbf{F} \to 0$ whatever $\mathbf{v}$ and $k_B T$ might be, the latter provided putting concurrently $\nabla\phi = -\mathbf{E}e \to 0$. The product $\infty \times 0$ is in principle not necessarily unphysical despite D diverges, because this divergence is always counterbalanced by some force or energy or concentration gradient concurrently tending to zero; rather it is a matter of experience to verify whether the finite outcomes of these products, see for instance the eqs (29), have experimental significance or not. In this respect, however, this worth is recognized since the times of Onnes (1913). In fact, the electron superconductivity is nothing else but a frictionless motion of charges, somehow similar to the superfluidity. Coherently, both equations (29) and (10) suggest simply a free charge carrier moving without need of concentration gradient or applied potential difference or electric field or force $\mathbf{F}$ of any physical nature. The essence of the divergent diffusion coefficient is thus the lack of interaction between lattice and charge carrier. In this sense the Nernst-Einstein equation is fully compatible even with $D^{eff} \to \infty$: in fact is hidden in this limit, and thus in the eq (4) itself, the concept of superconductivity, regarded as a peculiar charge transport mechanism that lacks their interactions and thus does not need any activation energy or driving force.

These results disclose new horizons of research as concerns the solid oxides candidate for fuel cell electrolytes. The choice of the best oxides and their heat treatments is today conceived having in mind the best high temperature conductivity only. But besides this practical consideration, nothing hinders in principle exploring the chance of a fuel cell realized with MIEC solid oxides designed to optimize the ion superconducting mechanism. The prospective is that MIECS with poor ionic conductivity at some hundreds degrees could have excellent superconductors at low temperatures. It seems rational to expect that the optimization of the electrolytes for a next generation of fuel cells compels the future research not to lower as much as possible the high temperatures but to rise as much as possible the low temperatures.

7 Conclusion

The model has prospected the possibility of SOFCs working at very low temperatures, where superconduction effects are allowed to occur. Besides the attracting importance of the basic and technological research aimed to investigate and develop high temperature superconductors for the transport of electricity, the present results open new scenarios as they concern the production itself of electric power via zero resistivity electrolytes. Of course the chance of efficient fuel cells operating according to these expectations must be verified by the experimental activity; if the theoretical previsions are confirmed at least in the frame of a preliminary laboratory activity, as it is legitimate to guess since no ad hoc hypothesis has been introduced in the model, then the race towards high Tc electrolytes could allow new goals of scientific and applicative interest.

Submitted on December 9, 2014 / Accepted on December 12, 2014

References

1. Murch G.E. Atomic diffusion theory in highly defective solids. Trans Tech Publications, Limited, 1980
2. Kontturi K., Murtomäki L., Manzanares J.A. Ionic Transport Processes in Electrochemistry and Membrane Science, 2008, Oxford University Press, Oxford, UK.
3. Gellings P.J., Bouwmeester H.J.M. (Eds.), CRC Handbook of Solid State Electrochemistry, CRC Press, 1997.
4. Riess I. Mixed ionic–electronic conductors - material properties and applications. *Solid State Ionics*, 157, (2003).
5. Eoin M. NMR studies of conduction mechanisms in electrolyte materials for fuel cells. PhD Thesis, University of Dublin, School of chemical Sciences, 2007.
6. Hong G.W., Lee J.Y. The interaction of hydrogen with dislocations in iron. *Acta Metallurgica*, 1984, v. 32(10), p. 1581.
7. Rice M.J., Roth W.L. Ionic transport in super ionic conductors: a theoretical model. *Journal of Solid State Chemistry*, 1972, v. 4(2), p. 294.
8. Boris B., Bokshtein S., Zhukhovitskii A. Thermodynamics and kinetics of diffusion in solids, 1985, Oxonian Press, NY.
9. Tosto S. Correlation model of mixed ionic-electronic conductivity in solid oxide lattices in the presence of point and line defects for solid oxides fuel cells *International Journal of Energy Research*, 2011, v. 35(12), p. 1056.
10. Tosto S. Fundamentals of diffusion for optimized applications, 2012, ENEA Ambiente Innovazione, p. 94.
11. Freemann S.A., Booske J.H., Cooper R.F., Modeling and numerical simulations of microwave induced ion transport. Journal of Applied Physics, 1998, v. 83(11), 2979.
12. Karger J., Heitjans P., Haberlandt R. Diffusion in Condensed Matter, 1998, Friedr. Vieweg and Sohn Verlagsgesell. mbH Braunschweig.
13. Kittel C. Introduction to solid state physics, 2005, J. Wiley and Sons, Hoboken, NJ, USA.
14. Sutton A.P. and Balluffi R.W. Interfaces in Crystalline Materials. 1995 Clarendon Press, Oxford, UK.
15. Zhao J.Z., De A.K., De Cooman B.C. Formation of the Cottrell Atmosphere during Strain Ageing of Bake-Hardenable Steels, *Metallurgical and Materials Transactions*, 2001, v. 32A, p. 417.
16. Conrad H., Schoeck G. Cottrell locking and the flow stress in iron. *Acta Metallurgica*, 1960, v. 8(11), 791–796.
17. Slater J.C. Atomic Radii in Crystals. *Journal of Chemical Physics*, 1964, v. 41(10), 3199–3205.
18. Lande A. *Zeitschrift fur Physik*, 1920, v. 1(3), p. 191.
19. Otobe H. and Nakamura A. Lattice Parameters and Defect Structure of the Fluorite and C-Type Oxide Solid Solutions between MO2 and M2O3, in Solid Oxide Fuel Cells (SOFCs VI): Proc. Of the Sixth International Congress, S.C. Singhal and M. Dokiya Eds, 1999, p. 463, The Electrochemical Society, Pennington, N.J., USA.

Weinberg Angle Derivation from Discrete Subgroups of SU(2) and All That

Franklin Potter

Sciencegems.com, 8642 Marvale Drive, Huntington Beach, CA 92646 USA. E-mail: frank11hb@yahoo.com

The Weinberg angle θ_W of the Standard Model of leptons and quarks is derived from specific discrete (i.e., finite) subgroups of the electroweak local gauge group $SU(2)_L \times U(1)_Y$. In addition, the cancellation of the triangle anomaly is achieved even when there are four quark families and three lepton families!

1 Introduction

The weak mixing angle θ_W, or Weinberg angle, in the successful theory called the Standard Model (SM) of leptons and quarks is considered traditionally as an unfixed parameter of the Weinberg-Salam theory of the electroweak interaction. Its value of ~30° is currently determined empirically.

I provide the only first principles derivation of the Weinberg angle as a further application of the discrete symmetry subgroups of SU(2) that I used for the first principles derivation of the mixing angles for the neutrino mixing matrix PMNS [1] in 2013 and of the CKM quark mixing matrix [2] in 2014. An important reminder here is that these derivations are all done within the realm of the SM and no alternative theoretical framework beyond the SM is required.

2 Brief review of neutrino mixing angle derivation

The electroweak component of the SM is based upon the local gauge group $SU(2)_L$ x $U(1)_Y$ acting on the two SU(2) weak isospin flavor states $\pm\frac{1}{2}$ in each lepton family and each quark family. Its chiral action, i.e., involving LH doublets and RH singlets, is dictated by the mathematics of quaternions acting on quaternions, verified by the empirically determined maximum parity violation. Consequently, instead of using SU(2) generators acting on SU(2) weak isospin states, one can equivalently use the group of unit quaternions defined by q = a + bi + cj + dk, for a, b, c, d real and $i^2 = j^2 = k^2 =$ ijk = −1. The three familiar Pauli SU(2) generators σ_x, σ_y, σ_z, when multiplied by i, become the three generators k, j, i, respectively, for this unit quaternion group.

In a series of articles [3–5] I assigned three discrete (i.e., finite) quaternion subgroups (i.e., SU(2) subgroups), specifically 2T, 2O, 2I, to the three lepton families, one to each family (ν_e, e), (ν_μ, μ), (ν_τ, τ). These three groups permeate all areas of mathematics and have many alternative labelings, such as [3,3,2], [4,3,2], [5,3,2], respectively. Each of these three subgroups has three generators, $R_s = iU_s$ (s = 1,2,3), two of which match the two SU(2) generators, U_1 = j and U_3 = i, but the third generator U_2 for each subgroup is not k [6]. This difference between the third generators and k is the true source [1] of the neutrino mixing angles. All three families must act together to equal the third SU(2) generator k.

The three generators U_2 are given in Table 1, with $\phi = (\sqrt{5}+1)/2$, the golden ratio. The three generators must add to make the generator k, so there are three equations for three unknown factors. The arccosines of these three normalized factors determine the quaternion angles 105.337°, 36.755°, and 122.459°. Quaternion angles are double angle rotations, so one uses their half-values for rotations in R^3, as assumed for the PMNS matrix. Then subtract one from the other to produce the three neutrino mixing angles $\theta_{12} = 34.29°$, $\theta_{23} = -42.85°$, and $\theta_{13} = -8.56°$. These calculated angles match their empirical values $\theta_{12} = \pm 34.47°$, $\theta_{23} = \pm(38.39° - 45.81°)$, and $\theta_{13} = \pm 8.5°$ extremely well.

Table 1: Lepton Family Quaternion Generators U_2

Fam.	Grp.	Generator	Factor	Angle°
ν_e, e	332	$-\frac{1}{2}\,i - \frac{1}{2}\,j + \frac{1}{\sqrt{2}}\,k$	−0.2645	105.337
ν_μ, μ	432	$-\frac{1}{2}\,i - \frac{1}{\sqrt{2}}\,j + \frac{1}{2}\,k$	0.8012	36.755
ν_τ, τ	532	$-\frac{1}{2}\,i - \frac{\phi}{2}\,j + \frac{\phi^{-1}}{2}\,k$	−0.5367	122.459

Thus, the three mixing angles originate from the three U_2 generators acting together to become the k generator of SU(2). Note that I assume the charged lepton mixing matrix is the identity. Therefore, any discrepancy between these derived angles and the empirical angles could be an indication that the charged lepton mixing matrix has off-diagonal terms.

The quark mixing matrix CKM is worked out the same way [2] by using four discrete rotational groups in R^4, [3,3,3], [4,3,3], [3,4,3], [5,3,3], the [5,3,3] being equivalent to $2I \times 2I$. The mismatch of the third generators again requires the linear superposition of these four quark groups. The 3×3 CKM matrix is a submatrix of a 4×4 matrix. However, the mismatch of 3 lepton families to 4 quark families indicates a triangle anomaly problem resolved favorably in a later section by applying the results of this section.

3 Derivation of the Weinberg angle

The four electroweak generators of the SM local gauge group $SU(2)_L \times U(1)_Y$ are typically labeled W^+, W^0, W^-, and B^0, but they can be defined equivalently as the quaternion generators i, j, k and b. But we do not require the full SU(2) to act upon the flavor states $\pm\frac{1}{2}$ for discrete rotations in the unitary plane C^2 because the lepton and quark families represent specific discrete binary rotational symmetry subgroups of SU(2).

That is, we require just a discrete subgroup of $SU(2)_L \times U(1)_Y$. In fact, one might suspect that the 2I subgroup would be able to perform all the discrete symmetry rotations, but 2I omits some of the rotations in 2O. Instead, one finds that $2I \times 2I'$ works, where 2I′ provides the "reciprocal" rotations, i.e., the third generator U_2 of 2I becomes the third generator U_2' for 2I′ by interchanging ϕ and ϕ^{-1}:

$$U_2 = -\frac{1}{2}\, i - \frac{\phi}{2}\, j + \frac{\phi^{-1}}{2}\, k, \quad U_2' = -\frac{1}{2}\, i - \frac{\phi^{-1}}{2}\, j + \frac{\phi}{2}\, k. \quad (1)$$

Consider the three SU(2) generators i, j, k and their three simplest products: $i \times i = -1$, $j \times j = -1$, and $k \times k = -1$. Now compare the three corresponding $2I \times 2I'$ discrete generator products: $i \times i = -1$, $j \times j = -1$, and

$$U_2\, U_2' = -0.75 + 0.559i - 0.25\, j + 0.25k, \quad (2)$$

definitely not equal to -1. The reverse product $U_2' U_2$ just interchanges signs on the i, j, k, terms.

One needs to multiply this product quaternion $U_2 U_2'$ by

$$P = 0.75 + 0.559i - 0.25\, j + 0.25k \quad (3)$$

to make the result -1. Again, P′ has opposite signs for the i, j, k, terms only.

Given any unit quaternion $q = \cos\theta + \hat{n} \sin\theta$, its power can be written as $q^\alpha = \cos\alpha\theta + \hat{n} \sin\alpha\theta$. Consider P to be a squared quaternion $P = \cos 2\theta + \hat{n} \sin 2\theta$ because we have the product of two quaternions U_2 and U_2'. Therefore, the *quaternion* square root of P has $\cos\theta = \sqrt{0.75} = 0.866$, rotating the U_2 (and U_2') in the unitary plane C^2 by the quaternion angle of 30° so that each third generator becomes k. Thus the Weinberg angle, i.e., the weak mixing angle,

$$\theta_W = 30^\circ. \quad (4)$$

Therefore, the Weinberg angle derives from the mismatch of the third generator of $2I \times 2I'$ to the SU(2) third generator k.

The empirical value of θ_W ranges from 28.1° to 28.8°, values less than the predicted 30°. The reason for the discrepancy is unknown (but see [7]), although one can surmise either (1) that in determining the Weinberg angle from the empirical data perhaps some contributions have been left out, or (2) the calculated θ_W is its value at the Planck scale at which the internal symmetry space and spacetime could be discrete instead of continuous.

4 Anomaly cancellation

My introduction of a fourth quark family raises immediate suspicions regarding the cancellation of the triangle anomaly. The traditional cancellation procedure of matching each lepton family with a quark family "generation by generation" does produce the triangle anomaly cancellation by summing the appropriate $U(1)_Y$, $SU(2)_L$, and $SU(3)_C$ generators, producing the "generation" cancellation.

However, we now know that this "generation" conjecture is incorrect, because the derivation of the lepton and quark mixing matrices from the U_2 generators of the discrete binary subgroups of SU(2) above dictates that the 3 lepton families act as one collective lepton family for $SU(2)_L \times U(1)_Y$ and that the 4 quark families act as one collective quark family.

We have now created an effective single "generation" with one effective quark family matching one effective lepton family, so there is now the previously heralded "generation cancellation" of the triangle anomalies with the traditional summation of generator eigenvalues [8]. In the SU(3) representations the quark and antiquark contributions cancel. Therefore, there are no $SU(3) \times SU(3) \times U(1)$, $SU(2) \times SU(2) \times U(1)$, $U(1) \times U(1) \times U(1)$, or mixed U(1)-gravitational anomalies remaining.

There was always the suspicion that the traditional "generation" labeling was fortuitous because there was no specific reason for dictating the particular pairings of the lepton families to the quark families within the SM. Now, with the leptons and quarks representing the specific discrete binary rotation groups I have listed, a better understanding of how the families are related within the SM is possible.

5 Summary

The Weinberg angle derives ultimately from the third generator mismatch of specific discrete subgroups of SU(2) with the SU(2) quaternion generator k. The triangle anomaly cancellation occurs because 3 lepton families act collectively to cancel the contribution from 4 quark families acting collectively. Consequently, the SM may be an excellent approximation to the behavior of Nature down to the Planck scale.

Acknowledgements

The author thanks Sciencegems.com for generous support.

Submitted on December 17, 2014 / Accepted on December 18, 2014

References

1. Potter F. Geometrical Derivation of the Lepton PMNS Matrix Values. *Progress in Physics*, 2013, v. 9 (3), 29–30.
2. Potter F. CKM and PMNS mixing matrices from discrete subgroups of SU(2). *Progress in Physics*, 2014, v. 10 (1), 1–5.
3. Potter F. Our Mathematical Universe: I. How the Monster Group Dictates All of Physics. *Progress in Physics*, 2011, v. 7 (4), 47–54.
4. Potter F. Unification of Interactions in Discrete Spacetime. *Progress in Physics*, 2006, v. 2 (1), 3–9.
5. Potter F. Geometrical Basis for the Standard Model. *International Journal of Theoretical Physics*, 1994, v. 33, 279–305.
6. Coxeter H. S. M. Regular Complex Polytopes. Cambridge University Press, Cambridge, 1974.
7. Faessler M. A. Weinberg Angle and Integer Electric Charges of Quarks. arXiv: 1308.5900.
8. Bilal A. Lectures on Anomalies. arXiv: 0802.0634v1.

Can the Emdrive Be Explained by Quantised Inertia?

Michael Edward McCulloch

University of Plymouth, Plymouth, PL4 8AA, UK. E-mail: mike.mcculloch@plymouth.ac.uk

It has been shown that cone-shaped cavities with microwaves resonating within them move slightly towards their narrow ends (the emdrive). There is no accepted explanation for this. Here it is shown that this effect can be predicted by assuming that the inertial mass of the photons in the cavity is caused by Unruh radiation whose wavelengths must fit exactly within the cavity, using a theory already applied with some success to astrophysical anomalies where the cavity is the Hubble volume. For the emdrive this means that more Unruh waves are "allowed" at the wide end, leading to a greater inertial mass for the photons there. The gain of inertia of the photons when they move from the narrow to the wide end, and the conservation of momentum, predicts that the cavity must then move towards the narrow end, as observed. This model predicts the available observations quite well, although the observational uncertainties are not well known.

1 Introduction

It was first demonstrated by Shawyer (2008) that when microwaves are made to resonate within a truncated cone-shaped cavity a small, unexplained acceleration occurs towards the narrow end. In one example when 850 W of power was put into such a cavity with end diameters of 16 and 12 cm, and which had a Q value (dissipation constant) of 5900 the thrust measured was 16 mN towards the narrow end. The results from two of Shawyer's experiments are shown in Table 1 (rows 1-2). There is no explanation for this behaviour in standard physics, and it also violates the conservation of momentum, and Shawyer's own attempt to explain it using special relativity is not convincing, as this theory also should obey the conservation of momentum (Mullins, 2006).

Nethertheless, this anomaly was confirmed by a Chinese team (Juan et al., 2012) who put 80-2500 W of power into a similar cavity at a frequency of 2.45 GHz and measured a thrust of between 70 mN and 720 mN. Their result cannot however be fully utilised for testing here since they did not specify their cavity's Q factor or its geometry.

A further positive result was recently obtained by a NASA team (Brady et al., 2014) and three of their results are also shown in Table 1 (rows 3 to 5). They did provide details of their Q factor and some details of their cavity's geometry. The experiment has not yet been tried in a vacuum, but the abrupt termination of the anomaly when the power was switched off has been taken to show the phenomenon is not due to moving air.

McCulloch (2007) has proposed a new model for inertial mass that assumes that the inertia of an object is due to the Unruh radiation it sees when it accelerates, radiation which is also subject to a Hubble-scale Casimir effect. In this model only Unruh wavelengths that fit exactly into twice the Hubble diameter are allowed, so that a greater proportion of the waves are disallowed for low accelerations (which see longer Unruh waves) leading to a gradual new loss of inertia as accelerations become tiny, of order 10^{-10} m/s^2. This model, called MiHsC (Modified inertia by a Hubble-scale Casimir effect) modifies the standard inertial mass (m) as follows:

$$m_i = m\left(1 - \frac{2c^2}{|a|\Theta}\right) = m\left(1 - \frac{\lambda}{4\Theta}\right) \quad (1)$$

where c is the speed of light, Θ is twice the Hubble distance, a is the magnitude of the relative acceleration of the object relative to surrounding matter and λ is the wavelength of the Unruh radiation it sees. Eq. 1 predicts that for terrestrial accelerations (eg: 9.8 m/s^2) the second term in the bracket is tiny and standard inertia is recovered, but in low acceleration environments, for example at the edges of galaxies or in deep space (when a is small and λ is large) the second term in the bracket becomes larger and the inertial mass decreases in a new way.

In this way, MiHsC can explain galaxy rotation without the need for dark matter (McCulloch, 2012) and cosmic acceleration without the need for dark energy (McCulloch, 2007, 2010), but astrophysical tests like these can be ambiguous, since more flexible theories like dark matter can be fitted to the data, and so a controlled laboratory test like the EmDrive is useful.

Further, the difficulty of demonstrating MiHsC on Earth is the huge size of Θ in Eq. 1 which makes the effect very small unless the acceleration is tiny, as in deep space. One way to make the effect more obvious is to reduce the distance to the horizon Θ (as suggested by McCulloch, 2008) and this is what the emdrive may be doing since the radiation within it is accelerating so fast that the Unruh waves it sees will be short enough to be limited by the cavity walls in a MiHsC-like manner.

2 Method

The setup is a radio-frequency resonant cavity shaped like a truncated cone, with one round end then larger than the other. When the electromagnetic field is input in the cavity the microwaves resonate and we can consider the conservation of

momentum for the light

$$\frac{\partial(mv)}{\partial t} = 0 = m\frac{\partial v}{\partial t} + v\frac{\partial m}{\partial t}. \quad (2)$$

Interpreting the first term on the right hand side as the force (mass times acceleration) that must be exerted on the light to conserve its momentum, leads to

$$F = -c\frac{\partial m}{\partial t}. \quad (3)$$

So that

$$F = -c\frac{\partial m}{\partial x}\frac{\partial x}{\partial t} = -c^2\frac{\partial m}{\partial x}. \quad (4)$$

Normally, of course, photons are not supposed to have mass in this way, but supposing we consider this? We assume the inertial mass of the microwave photons (whatever its absolute value) is affected by MiHsC, but instead of the horizon being the far-off and spherically symmetric Hubble horizon as before, the horizon is now made by the asymmetric walls of the cavity. This is possible because the photons involved are travelling at the speed of light and are bouncing very fast between the two ends of seperation s and their acceleration ($a \sim v^2/s$) is so large that the Unruh waves that are assumed to produce their inertial mass are about the same size as the cavity, so they can be affected by it, unlike the Unruh waves for a terrestrial acceleration which would be far to long to be affected by the cavity. This dependence of the inertial mass on the width of the cavity means that the inertial mass is corrected by a MiHsC-like factor (Eq. 1). Using Eq. 4, the force is modified as follows

$$F = -c^2\left(\frac{m_{bigend} - m_{smallend}}{l}\right) \quad (5)$$

where l is the axial length of the cavity. Now using eq. 1 for the inertial masses and replacing the Hubble scale with the cavity width (W) assuming for simplicity the waves only have to fit laterally, and with subscripts to refer to the big and small ends, we get

$$F = \frac{-c^2 m}{l}\left(\frac{\lambda}{4W_{big}} - \frac{\lambda}{4W_{small}}\right) \quad (6)$$

where λ is the wavelength of the Unruh radiation seen by the photons because they are being reflected back and forth by the cavity$\lambda = 8c^2/a = 8c^2/(2c/(l/c)) = 4l$ so that

$$F = -4c^2 m\left(\frac{1}{4W_{big}} - \frac{1}{4W_{small}}\right). \quad (7)$$

Using $E = mc^2$ and $E = \int Pdt$ where P is the power, gives

$$F = -\int Pdt\left(\frac{1}{W_{big}} - \frac{1}{W_{small}}\right). \quad (8)$$

Table 1: Summary of EmDrive experimental data published so far, and the predicted (Eq. 10) and observed anomalous thrust.

Expt.	P	Q	l	w_{big}/w_{small}	F_{Pred}	F_{Obs}
	W	/1000	m	metres	mN	mN
S1	850	5.9	0.156	0.16/0.1275	4.2	16
S2	1000	45	0.345	0.28/0.1289	216	80-214
B1	16.9	7.32	0.332	0.397/0.244	0.22	0.091
B2	16.7	18.1	0.332	0.397/0.244	0.53	0.05
B3	2.6	22	0.332	0.397/0.244	0.1	0.055

Integrating P over one cycle (one trip of the photons from end to end) gives Pt where t is the time taken for the trip, which is l/c, so

$$F = \frac{-Pl}{c}\left(\frac{1}{W_{big}} - \frac{1}{W_{small}}\right). \quad (9)$$

This is for one trip along the cavity, but the Q factor quantifies how many trips there are before the power dissipates so we need to multiply by Q

$$F = \frac{-PQl}{c}\left(\frac{1}{W_{big}} - \frac{1}{W_{small}}\right) \quad (10)$$

where P is the power input as microwaves (Watts), Q is the Q factor measured for the cavity, l is the length of the cavity and W_{big} and W_{small} are the diameters of the wide and narrow ends of the cavity. MiHsC then predicts that a new force will appear acting towards the narrow end of the cavity.

3 Results

We can now try this formula on the results from Shawyer (2008) (from section 6 of their paper). This EmDrive had a cavity length of 15.6 cm, end diameters of 16 cm and 12.75 cm, a power input of 850 W and a Q factor of 5900, so

$$F = \frac{850 \times 5900 \times 0.156}{3 \times 10^8}\left(\frac{1}{0.16} - \frac{1}{0.1275}\right) = 4.2 \text{ mN}. \quad (11)$$

This predicts an anomalous force of 4.2 mN towards the narrow end, which is about a third of the 16 mN towards the narrow end measured by Shawyer (2008).

We can also try values for the demonstrator engine from section 7 of Shawyer (2008) which had a cavity length of 32.5 cm, end diameters of 28 cm and 12.89 cm, a power input of 1000 W and a Q factor of 45000. So we have

$$\begin{aligned} F &= \frac{1000 \times 45000 \times 0.325}{3 \times 10^8}\left(\frac{1}{0.28} - \frac{1}{0.1289}\right) \quad (12) \\ &= 216 \text{ mN}. \end{aligned}$$

This agrees with the observed anomalous force which was between 80 and 214 mN/kW (2008) (if we also take into account the uncertainties in the model due to the simplified 1-dimensional approach used).

Table 1 is a summary of various results from Shawyer (2008) in rows 1 and 2 and Brady et al. (2014) (see the Table on their page 18) in rows 3, 4 and 5. The Juan et al. (2012) data is excluded because they did not specify their Q factor or the exact geometry in their paper. Column 1 shows the experiment (S for Shawyer (2008) and B for Brady et al. (2014)). Column 2 shows the input power (in Watts). Column 3 shows the Q factor (dimensionless, divided by 1000). Column 4 shows the axial length of the cavity. Column 5 shows the width of the big and small ends (metres). Column 6 shows the thrust predicted by MiHsC and column 7 shows the thrust observed (both in milli-Newtons).

It is unclear what the error bars on the observations are, but they are likely to be wide, looking for example at the range of values for the case S2. MiHsC predicts the correct order of magnitude for cases S1, S2, B1 and B3 which is interesting given the simplicity of the model and its lack of adjustable parameters. The anomaly is case B2 where MiHsC overpredicts by a factor of ten. This case is anomalous in other ways since the Q factor in B2 was more than doubled from that in B1 but the output thrust almost halved.

More data is needed for testing, and a more accurate modelling of the effects of MiHsC will be needed. This analysis for simplicity, assumed the microwaves only travelled along the axis and the Unruh waves only had to fit into the lateral "width" dimension, but in fact the microwaves will bounce around in 3-dimensions so a 3-d model will be needed. This approximation would become a problem for a pointed cone shape where the second term in Eq. 10 would involve a division by zero, but it is a better approximation for a truncated cone, as in these experiments.

So far, it has been assumed that as the acceleration reduces, the number of allowed Unruh waves decreases linearly, but even a small change of frequency can make the difference between the Unruh waves fitting within a cavity, and not fitting and this could explain the variation in the observations, particularly in case B2.

4 Discussion

If confirmed, Equation 10 suggests that the anomalous force can be increased by increasing the power input, or the quality factor of the cavity (the number of times the microwaves bounce between the two ends). It could also be increased by boosting the length of the cavity and narrowing it. The effect could be increased by increasing the degree of taper, for example using a pointed cone. The speed of light on the denominator of Eq. 10 implies that if the value of c was decreased by use of a dielectric the effect would be enhanced (such an effect has recently been seen).

This proposal makes a number of controversial assumptions. For example that the inertial mass of photons is finite and varies in line with MiHsC. It is difficult to provide more backing for this beyond the conclusion that it is supported by the partial success of MiHsC in predicting the EmDrive with a very simple formula.

5 Conclusions

Three independent experiments have shown that when microwaves resonate within an asymmetric cavity an anomalous force is generated pushing the cavity towards its narrow end.

This force can be predicted to some extent using a new model for inertia that has been applied quite successfully to predict galaxy rotation and cosmic acceleration, and which assumes in this case that the inertial mass of photons is caused by Unruh radiation and these have to fit exactly between the cavity walls so that the inertial mass is greater at the wide end of the cavity. To conserve momentum the cavity is predicted to move towards its narrow end, as seen.

This model predicts the published EmDrive results fairly well with a very simple formula and suggests that the thrust can be increased by increasing the input power, Q factor, or by increasing the degree of taper in the cavity or using a dielectric.

Acknowledgements

Thanks to Dr Jose Rodal and others on an NSF forum for estimating from photographs some of the emdrives' dimensions.

Submitted on December 18, 2014 / Accepted on December 19, 2014

References

1. Brady D.A., White H.G., March P., Lawrence J.T. and Davies F.J. Anomalous thrust production from an RF test device measured on a low-thrust torsion pendulum. 50th AIAA/ASME/SAE/ASEE Joint Propulsion conference, 2014.
2. Juan Y. Net thrust measurement of propellantless microwave thrusters. *Acta Physica Sinica*, 2012, v. 61, 11.
3. McCulloch M.E. The Pioneer anomaly as modified inertia. *MNRAS*, 2007, v. 376, 338–342.
4. McCulloch M.E. Can the flyby anomaly be explained by a modification of inertia? *J. Brit. Interplanet. Soc.*, 2008, v. 61, 373–378.
5. McCulloch M.E. Minimum accelerations from quantised inertia. *EPL*, 2010, v. 90, 29001.
6. McCulloch M.E. Testing quantised inertia on galactic scales. *Astro. & Space Sci.*, 2012, v. 342, 575–578.
7. Mullins J. Relativity drive: the end of wings and wheels? *New Scientist*, 2006, no. 2568, 30–34.
8. Shawyer R. Microwave propulsion — progress in the emdrive programme. 59th International Astronautical conference (IAC-2008). Glasgow, UK.

Structures of Superdeforemed States in Nuclei with A ∼ 60 Using Two-Parameter Collective Model

N. Gaballah

Physics Department, Faculty of Science (Girls branch), Al-Azhar University, Cairo, Egypt. E-mail: nermgaballah@yahoo.com

Superdeformed (SD) states in nuclei in mass region $A \sim 60-90$ are investigated within the framework of two-parameter formula of Bohr and Motelson model. The concept of γ-ray transition energy E_γ over spin (EGOS) is used to assign the first order estimation of the bandhead spin. The model parameters and the true spin of bandhead have been obtained by adopted best fit method in order to obtain a minimum root-mean-square deviation between the calculated and the experimental γ-ray transition energies. The transition energies E_γ and the dynamical moment of inertia $J^{(2)}$ for data set include thirteen SD bands in even-even nuclei are calculated. The results agree with experimental data well. The behavior of $J^{(2)}$ as a function of rotational frequency $\hbar\omega$ are discussed. By using the calculated bandhead moment of inertia, the predicted quadrupole moments of the studied yrast SD bands are calculated and agree well with the observed data.

1 Introduction

Since the initial discovery of a superdeformed (SD) rotational band in ^{152}Dy [1], several SD bands were identified in different mass region [2]. The SD 60, 80 and 90 regions are of particular interest because they showed exciting new aspects of their large rotational frequency and they present experimental difficulties due to the increased doppler broading of γ-ray peaks and the decreased detection efficiency at large γ-ray transition energies. In $A \sim 60$, the negative-parity SD1 in ^{62}Zn was the first SD band [3], it assigned to configurations with two $ig_{9/2}$ protons (π) and three $ig_{9/2}$ neutrons (ν). It is formed in the $Z = 30$ deformed gap i.e with two $f_{7/2}$ proton holes [4,5]. The SD bands in $A \sim 60$ region are characterized by very large transition energies reaching 3.2 MeV or more. The yrast SD band in Sr was interpreted [6,7] as having the $\nu\, 5^2\pi 5^1$ configuration, i.e the excitation of two $N = 5$, $h_{11/2}$ intruder neutrons, which corresponding to the $N = 44$ shell gap with a large deformation, and a single proton excitation of the $N = 5$, $h_{11/2}$ intruder orbital. The predicted deformation for this band was $\beta_2 \simeq 0.55$ [6]. A systematic analysis on Sr nuclei shows that the quadrupole moment of the SD band in ^{82}Sr is the largest among these Sr isotopes. This may be an indication of the important role of $N = 44$ SD shell gap. For the region $A \sim 90$ SD states with large deformation $\beta_2 \simeq 0.6$ in ^{88}Mo were identified [8]. These findings were in agreement with cranked Woods-Saxon-Strutinsky calculations, which predicted $Z = 42$ and $Z = 43$ to be favored particle numbers at SD shapes in $A \sim 90$ nuclei [8,9].

As it is well known, the experimental data on SD bands consist only in a series of γ-ray transition energies linking levels of unknown spins. Spin assignment is one of the most difficult and unsolved problem in the study of superdeformation.This is due to the difficulty of establishing the deexcitation of a SD band into known yrast states of normal deformed band. Several approaches to assign the spins of SD bands were proposed [10–16]. For all such approaches an extrapolation fitting procedures was used. The purpose of the present paper is to predict the spins of the SD nuclear states in the $A \sim 60-90$ region and to study their properties by using the one-parameter and two-parameters Bohr-Mottelson model. The theoretical formalism is presented in section 2. The theoretical results and a comparison with experimental data are discussed in section 3. Finally a brief conclusion is given in section 4.

2 The formalism

For the strongly deformed nuclei, the collective excitations exhibit a spectrum of rotational character. In even-even nuclei, the spectrum is given by:

$$E(I) = A\,[I(I+1)] \tag{1}$$

where A is the inertial parameter $A = \hbar^2/2J$, with J denoting the effective moment of inertia, which is proportional to the square of the nuclear deformation, and expected to vary slowly with the mass number A. The γ-ray transition energies with the band are given by:

$$\begin{aligned} E_\gamma(I) &= E(I) - E(I-2) \\ &= 4A\left(I - \tfrac{1}{2}\right). \end{aligned} \tag{2}$$

It is interesting to discuss the energy levels by plotting the ratio $E_\gamma(I)$ to spin $(I-\frac{1}{2})$(EGOS)($E-Gamma$ Over Spin) [17] against spin. Therefore, the EGOS for rotational formula (2) can be written as:

$$EGOS = \frac{E_\gamma(I)}{\left(I - \frac{1}{2}\right)} = 4A. \tag{3}$$

Even in a first note on deformed nuclei, Bohr and Mottelson [18] remarked that the simple rotational formula equation (1) gives deviations from experimental data. They pointed out

Table 1: The calculated E Gamma Over Spin (EGOS) for $^{62}Z_n(\mathrm{SD}_1)$ compared to the experimental ones at three bandhead spins $I_0, I_0 \pm 2$ using the one-parameter formula.

$I(\hbar)$	$I_0 = 14.5$ $EGOS\,(\mathrm{keV}/\hbar)$		$I_0 = 16.5$ $EGOS\,(\mathrm{keV}/\hbar)$		$I_0 = 18.5$ $EGOS\,(\mathrm{keV}/\hbar)$	
	exp.	cal.	exp.	cal.	exp.	cal.
16.5	124.562	124.560				
18.5	123.055	124.560	110.722	110.720		
20.5	122.000	124.560	110.750	110.700	99.650	99.648
22.5	122.272	124.560	110.909	110.720	100.681	99.648
24.5	122.458	124.560	112.083	110.720	101.666	99.648
26.5	124.461	124.560	113.038	110.720	103.461	99.648
28.5			115.571	110.720	104.964	99.648
30.5					107.866	99.648

Table 2: The calculated E Gamma Over Spin(EGOS) for $^{62}Z_n(S\,D_1)$ compared to the experimental ones at three bandhead spins $I_0, I_0 \pm 2$ using the two-parameter formula.

$I(\hbar)$	$I_0 = 18$ $EGOS\,(\mathrm{keV}/\hbar)$		$I_0 = 20$ $EGOS\,(\mathrm{keV}/\hbar)$		$I_0 = 22$ $EGOS\,(\mathrm{keV}/\hbar)$	
	exp.	cal.	exp.	cal.	exp.	cal.
20	102.205	101.692				
22	103.023	102.901	92.697	92.477		
24	103.829	104.124	94.255	94.143	84.808	84.607
26	105.490	105.599	95.686	95.957	86.862	86.759
28	106.872	107.304	97.818	97.919	88.727	88.978
30	109.694	109.221	99.627	100.019	91.186	91.280
32			102.730	102.287	93.301	93.678
34					96.597	96.180

that agreement was improved by adding to it a second term (The Bohr-Mottelson two-term formula)

$$E(I) = A[I(I+1)] + B[I(I+1)]^2. \tag{4}$$

The new parameter B is almost negative and is 10^3 times less than that value of A.

$$E_\gamma(I) = A(4I-2) + B\left[2(4I-2)\left(I^2 - I + 1\right)\right], \tag{5}$$

and the EGOS can be written as:

$$\begin{aligned} EGOS &= \frac{E_\gamma(I)}{\left(I - \frac{1}{2}\right)} \\ &= 4A + 8B\left(I^2 - I + 1\right). \end{aligned} \tag{6}$$

For SD bands, one can determine the first-order estimation of the bandhead spin I_0 using equation (2) by calculating the ratio

$$\frac{E_\gamma(I_0+4)}{E_\gamma(I_0+2)} = \frac{E(I_0+4) - E(I_0+2)}{E(I_0+2) - E(I_0)} = \frac{2I_0+7}{2I_0+3}. \tag{7}$$

Let

$$E_{\gamma_1} = E_\gamma(I+2), \tag{8}$$

$$E_{\gamma_2} = E_\gamma(I+4), \tag{9}$$

$$J_0^2 = \frac{4}{E_{\gamma_2} - E_{\gamma_1}}, \tag{10}$$

we can find the bandhead spin I_0 as:

$$I_0 = \frac{1}{2}\left[E_{\gamma_1} J_0^2 - 3\right]. \tag{11}$$

Now, let us define the angular velocity ω as the derivative of the energy E with respect to the spin I

$$\omega = \hbar^{-1}\frac{dE}{d\hat{I}}; \quad \hat{I} = [I(I+1)]^{\frac{1}{2}}. \tag{12}$$

Two possible types of moments of inertia were suggested by Bohr and Mottleson [18] reflecting two different aspects of nuclear dynamics. The kinematic moment of inertia $J^{(1)}$ and the dynamic moment of inertia $J^{(2)}$:

$$J^{(1)} = \frac{\hbar^2}{2}\left[\frac{dE}{d[I(I+1)]}\right]^{-1} = \frac{\hbar}{\omega}[I(I+1)]^{\frac{1}{2}}, \tag{13}$$

Table 3: The bandhead spin proposition and the model parameters A and B adopted from the best fit procedures for the studied SD bands in the $A = 62 - 88$ mass region. The experimental bandhead moment of inertia are also given.

Z	N	Nuclear and the SD band	$E_\gamma(I_0+2\rightarrow I_0)$ (keV)	I_0 ($\hbar$)	A (keV)	B (keV)
30	32	^{62}Zn(SD1)	1993	20	20.997	2.313×10^{-3}
38	42	^{80}Sr(SD1)	1443	16	20.881	-1.873×10^{-4}
		^{80}Sr(SD2)	1688	18	22.106	-1.041×10^{-3}
		^{80}Sr(SD3)	1846	18	24.056	-4.466×10^{-4}
		^{80}Sr(SD4)	2140	20	26.371	-1.705×10^{-3}
38	44	^{82}Sr(SD1)	1429.8	17	19.292	1.770×10^{-4}
40	46	^{86}Zr(SD1)	1518	23	14.732	5.881×10^{-4}
		^{86}Zr(SD2)	1577	16	23.390	-1.354×10^{-3}
		^{86}Zr(SD3)	1866	25	19.082	-1.146×10^{-3}
		^{86}Zr(SD4)	1648	18	22.037	-1.021×10^{-3}
42	46	^{88}Mo(SD1)	1238.6	33	5.788	1.308×10^{-3}
		^{88}Mo(SD2)	1458.6	33	7.676	1.219×10^{-3}
		^{88}Mo(SD3)	1259.1	23	11.406	1.202×10^{-3}

$$J^{(2)} = \hbar^2 \left[\frac{d^2E}{d\left[[I(I+1)]^{\frac{1}{2}}\right]^2} \right] = \hbar \frac{d[I(I+1)]^{\frac{1}{2}}}{d\omega}. \quad (14)$$

$J^{(1)}$ is equal to the inverse of the slope of the curve of energy E versus $\hat{I}^2$ times $(\hbar^2/2)$, while $J^{(2)}$ is related to the curvature in the curve of E versus $\hat{I}$.

In terms of our two-parameter Bohr-Mottleson formula equation (4), yield

$$\hbar\omega(I) = 2\hat{I}\left(A + 2B\hat{I}^2\right), \quad (15)$$

$$J^{(1)}(I) = J_0\left(1 + \frac{2B}{A}\hat{I}^2\right)^{-1}, \quad (16)$$

$$J^{(2)}(I) = J_0\left(1 + \frac{6B}{A}\hat{I}^2\right)^{-1}, \quad (17)$$

with

$$J_0 = \frac{\hbar^2}{2A}. \quad (18)$$

Experimentally the dynamic moment of inertia $J^{(2)}$ is related to the difference ΔE_γ in consecutive transition energies E_γ along a band in the following way

$$\begin{aligned} J^{(2)} &= \frac{dI}{d\omega} \simeq \frac{\Delta I}{\Delta\omega} \simeq \frac{2}{\Delta\left(\frac{E_\gamma}{2}\right)} = \frac{4}{\Delta E_\gamma} \\ &= \frac{4}{E_\gamma(I+2\rightarrow I) - E_\gamma(I\rightarrow I-2)} \end{aligned} \quad (19)$$

remembering that $\omega \simeq E_\gamma/2$. Hence equal ΔE_γ's imply equal $J^{(2)}$'s.

The quadrupole deformation parameter β_2 are derived from the electric quadrupole transition probabilities $B(E_2)$. For this purpose, the well formula [18]

$$B(E_2, I\rightarrow I-2) = \frac{5}{16\pi} Q_0^2 \langle 2020|00\rangle^2, \quad (20)$$

was first applied to extract the intrinsic quadrupole moment Q_0. Then the deformation β_2 of the nuclear charge distribution was derived with the expression [19]

$$Q_0 = \frac{3}{\sqrt{5\pi}} ZR^2\beta_2(1 + 0.36\beta_2) \times 10^{-2}\text{eb} \quad (21)$$

where $R = 1.2\, A^{\frac{1}{3}}$ fm, and Z is the number of protons and A is the number of nucleons.

If X represents the ratio between the major to minor axis of an ellipsoid, then X can be deduced from Q by using the following formula [19]

$$Q = \frac{2}{5} ZR^2 \frac{X^2-1}{X^{\frac{2}{3}}} \times 10^{-2}\text{eb}. \quad (22)$$

The bandhead moment of inertia J_0 is related to the quadrupole deformation β_2 by the Grodzins formula [20]

$$J_0 = c(Z)A^{\frac{5}{3}}\beta_2^2. \quad (23)$$

c(Z) describes the calibration of this relationship between J_0 and β_2.

3 Results and discussions

For each SD band, we used the EGOS concepts of the one-parameter and the two-parameter models equations(3,6) to assign the bandhead spin I_0. Tables (1, 2) and Figure(1) presents

Table 4: Level spin I, γ-ray transition energies E_γ and the dynamical moment of inertia $J^{(2)}$ calculated by using the optimized best parameters listed in Table(3). The experimental γ-ray transition energies are also listed.

^{62}Zn(SD1)				^{80}Sr(SD3)			
E_γ^{exp}(keV)	$I(\hbar)$	E_γ^{cal}(keV)	$J^{(2)}(\hbar^2\text{MeV})^{-1}$	E_γ^{exp}(keV)	$I(\hbar)$	E_γ^{cal}(keV)	$J^{(2)}(\hbar^2\text{MeV})^{-1}$
1993	22	1988.275	17.849	1846	20	1849.857	21.806
2215	24	2212.375	17.054	2039	22	2033.287	22.028
2440	26	2446.915	16.269	2216	24	2214.874	22.275
2690	28	2692.781	15.499	2391	26	2394.445	22.549
2939	30	2950.862	14.750	2572	28	2571.830	22.853
3236	32	3222.048		2747	30	2746.857	
^{82}Sr(SD1)				^{86}Zr(SD1)			
E_γ^{exp}(keV)	$I(\hbar)$	E_γ^{cal}(keV)	$J^{(2)}(\hbar^2\text{MeV})^{-1}$	E_γ^{exp}(keV)	$I(\hbar)$	E_γ^{cal}(keV)	$J^{(2)}(\hbar^2\text{MeV})^{-1}$
1429.8	19	1436.598	25.385	1518	15	1513.088	29.361
1596.6	21	1594.170	25.273	1646	17	1649.323	28.729
1757.7	23	1752.439	25.151	1785	19	1788.551	28.081
1918.6	25	1911.473	25.020	1929	21	1930.996	27.417
2076.6	27	2071.340	24.880	2077	23	2076.886	26.745
2228.6	29	2232.107	24.731	2228	25	2226.446	26.066
2380.7	31	2393.844	24.574	2383	27	2379.901	25.384
2544.6	33	2556.616	24.408	2540	29	2537.478	24.702
2736	35	2720.494		2696	31	2699.403	
^{86}Zr(SD3)				^{86}Zr(SD4)			
E_γ^{exp}(keV)	$I(\hbar)$	E_γ^{cal}(keV)	$J^{(2)}(\hbar^2\text{MeV})^{-1}$	E_γ^{exp}(keV)	$I(\hbar)$	E_γ^{cal}(keV)	$J^{(2)}(\hbar^2\text{MeV})^{-1}$
1866	27	1851.803	36.037	1648	20	1658.218	25.696
1959	29	1962.798	38.197	1811	22	1813.881	26.412
2062	31	2067.518	40.815	1967	24	1965.327	27.241
2155	33	2165.521	44.030	2123	26	2112.163	28.202
2244	35	2256.368	48.048	2273	28	2253.996	29.317
2343	37	2339.618	53.181	2403	30	2390.435	30.615
2429	39	2414.832		2491	32	2521.086	
^{80}Sr(SD4)				^{88}Mo(SD2)			
E_γ^{exp}(keV)	$I(\hbar)$	E_γ^{cal}(keV)	$J^{(2)}(\hbar^2\text{MeV})^{-1}$	E_γ^{exp}(keV)	$I(\hbar)$	E_γ^{cal}(keV)	$J^{(2)}(\hbar^2\text{MeV})^{-1}$
2140	22	2132.134	23.600	1458.6	35	1460.250	29.582
2292.1	24	2301.619	24.723	1595.6	37	1595.465	27.823
2459	26	2463.411	26.068	1740.1	39	1739.226	26.182
2621.1	28	2616.854	27.693	1894.9	41	1892.002	24.652
2763	30	2761.294		2054.2	43	2054.260	23.227
				2224.3	45	2226.469	
^{80}Sr(SD2)				^{88}Mo(SD1)			
E_γ^{exp}(keV)	$I(\hbar)$	E_γ^{cal}(keV)	$J^{(2)}(\hbar^2\text{MeV})^{-1}$	E_γ^{exp}(keV)	$I(\hbar)$	E_γ^{cal}(keV)	$J^{(2)}(\hbar^2\text{MeV})^{-1}$
1688	20	1662.433	25.670	1238.6	35	1228.823	31.877
1821.1	22	1818.252	26.399	1342.1	37	1354.302	29.707
1950	24	1969.772	27.244	1480.7	39	1488.949	27.716
2090	26	2119.593	28.224	1633.5	41	1633.266	25.891
2256	28	2258.315	29.363	1795.5	43	1787.756	24.218
2364.1	30	2394.540	30.692	1962.2	45	1952.921	22.683
2573.9	32	2524.865		2133.4	47	2129.269	21.274
				2306.6	49	2317.284	

Table 6: The calculated quuadrupole deformation parameter β_2 and the major to minor axis ratio X in the yrast SD bands for even-even ^{62}Zn, ^{80,82}Sr, ^{86}Zn and ^{88}Mo nuclei. The experimental quadrupole moments Q^{exp} are also given for comparison.

	J_0 ($\hbar^2$MeV^{-1})	C(Z)	β_2	Q eb	X	Q^{exp} eb
^{62}Zn(SD1)	23.835	0.1261	0.4410	2.6178	1.52	2.70
^{80}Sr(SD1)	24.002	0.1106	0.3822	3.3438	1.44	3.42
^{82}Sr(SD1)	25.917	0.1089	0.3920	3.4973	1.45	3.54
^{86}Zr(SD1)	33.939	0.0996	0.4508	4.4512	1.54	4.60
^{88}Mo(SD1)	86.385	0.1707	0.5390	5.8295	1.66	6.00

Table 5: Level spin I, γ-ray transition energies E_γ and the dynamical moment of inertia $J^{(2)}$ calculated by using the optimized best parameters listed in Table(3). The experimental γ-ray transition energies are also listed.

^{80}Sr(SD1)			
E_γ^{exp}(keV)	$I(\hbar)$	E_γ^{cal}(keV)	$J^{(2)}(\hbar^2\text{MeV})^{-1}$
1443	18	1453.619	24.395
1611	20	1617.584	24.500
1775.1	22	1780.848	24.616
1948	24	1943.338	24.745
2118	26	2104.983	24.886
2284	28	2265.711	25.041
2440.9	30	2425.449	25.208
2595	32	2584.127	25.389
2743	34	2741.672	25.585
2680	36	2898.011	
^{86}Zr(SD3)			
E_γ^{exp}(keV)	$I(\hbar)$	E_γ^{cal}(keV)	$J^{(2)}(\hbar^2\text{MeV})^{-1}$
1577	18	1579.123	24.266
1730	20	1743.961	25.036
1890	22	1903.730	25.944
2056	24	2057.908	27.014
2227	26	2205.976	28.280
2392	28	2347.414	29.786
2514	30	2481.702	31.591
2562	32	2608.320	33.776
2708	34	2726.748	
^{88}Mo(SD3)			
E_γ^{exp}(keV)	$I(\hbar)$	E_γ^{cal}(keV)	$J^{(2)}(\hbar^2\text{MeV})^{-1}$
1259.1	25	1259.498	31.051
1382.6	27	1388.315	29.644
1522.9	29	1523.249	28.265
1669.4	31	1664.763	26.926
1817.0	33	1813.317	25.631
1976.0	35	1969.375	24.386
2134.0	37	2133.397	23.195
2297.0	39	2305.846	

the numerical values and graph of EGOS at three different values of bandhead spins I_0, $I_0 \pm 2$ for the yrast SD band in ^{62}Zn as example for our calculations. The model parameters

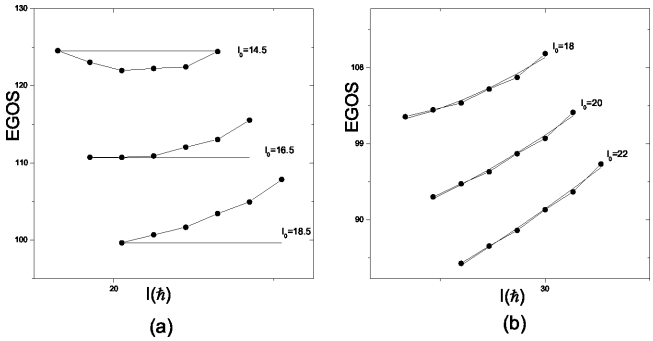

Fig. 1: Calculated (solid lines) and experimental (closed circles) EGOS against spin I for these different values of bandhead spin $I_0, I_0 \pm 2$. (a) for first order estimation of I_0 (b) for second order estimation of I_0.

A and B are then fitted to reproduce the observed transition energies E_γ. The procedure is repeated for several trail values of A and B and recalculate the true spin of the lowest observed level. In order to illustrate the sensitivity of the root mean square deviation, we employed the common definition of the chi squared

$$\chi^2 = \frac{1}{N}\sum_i \left[\frac{E_\gamma^{exp}(I_i) - E_\gamma^{cal}(I_i)}{\Delta E_\gamma^{exp}(I_i)}\right]^2 \qquad (24)$$

where N is the number of data points and ΔE_γ^{exp} is the experimental error in γ-ray transition energies. The experimental data are taken from the evaluated nuclear structure data file ENSDF [2]. Table (3) lists the bandhead spin proposition and the adopted model parameters. Using the best fitted parameters, the spins I, the γ-ray transition energies E_γ, the rotational frequency $\hbar\omega$ and the dynamical moment of inertia $J^{(2)}$ are calculated and listed in Table(4) compared to the observed E_γ.

Figures (2, 3, 4) shows the experimental and calculated dynamical moment of inertia $J^{(2)}$ as a function of rotational frequency $\hbar\omega$ for the SD bands in our even-even nuclei. The experimental and calculated values are denoted by solid circles and solid lines respectively.

By substituting the calculated bandhead moment of inertia J_0 in Grodzins formula equation (23), we adjusted the pro-

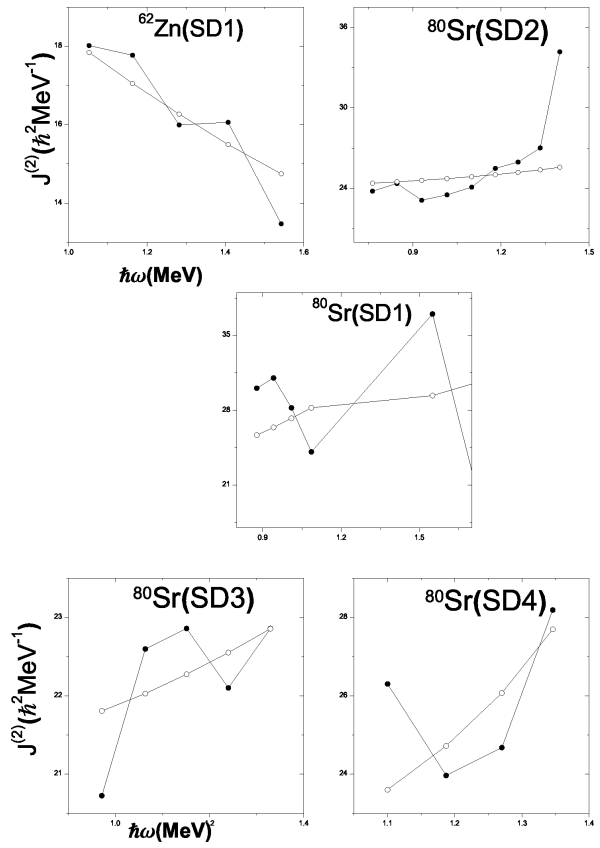

Fig. 2: Shows the experimental and calculated dynamical moment of inertia $J^{(2)}$ as a function of rotational frequency $\hbar\omega$ for even-even ^{62}Zn(SD1) and ^{80}Sr(SD1, SD2, SD3 and SD4). The experimental and calculated values are denoted by solid circles and solid lines respectively.

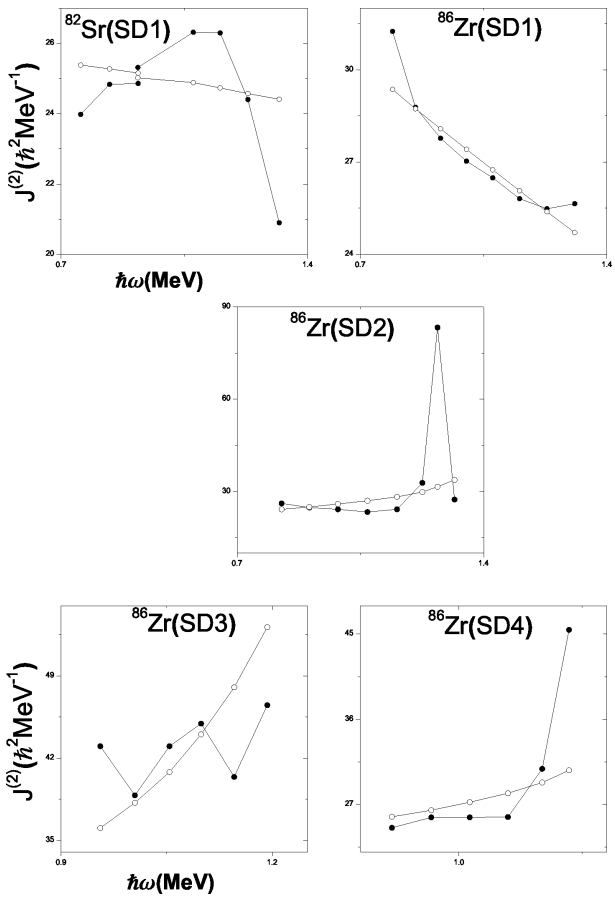

Fig. 3: Shows the experimental and calculated dynamical moment of inertia $J^{(2)}$ as a function of rotational frequency $\hbar\omega$ for even-even ^{82}Sr(SD1) and ^{86}Zn(SD1, SD2, SD3 and SD4). The experimental and calculated values are denoted by solid circles and solid lines respectively.

portional constant c(Z) for each yrast SD band and extracted the deformation parameter β_2 and then calculated the transition quadrupole moment Q which is related to the ratio X of the major to minor axis. The results are given in Table (5).

4 Conclusion

The structure of the SD bands in the mass region $A \sim 60-90$ have been investigated in the framework of two-parameter Bohr-Mottelson model. The bandhead spins have been extracted by using first order estimation method using the concept of EGOS. The model parameters have been determined by using a best fit method between the calculated and the experimental transition energies. The calculated transition energies E_γ, rotational frequency $\hbar\omega$ and dynamic moments of inertia $J^{(2)}$ are all well agreement with the experimental ones. This confirm that our model is a particular tool in studying the SD rotational bands. The behavior of $J^{(2)}$ as a function of $\hbar\omega$ have been discussed. The quadrupole deformation parameters are also calculated.

Submitted on December 5, 2014 / Accepted on December 12, 2014

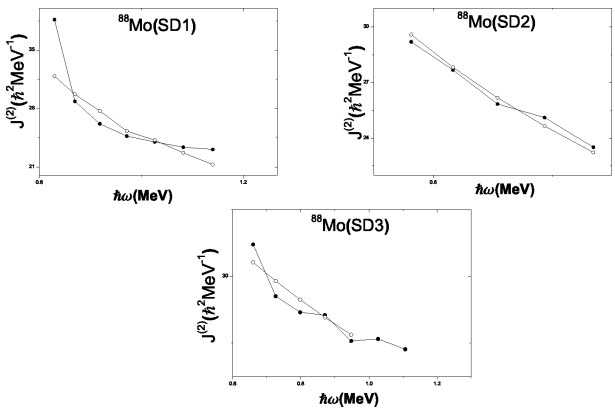

Fig. 4: Shows the experimental and calculated dynamical moment of inertia $J^{(2)}$ as a function of rotational frequency $\hbar\omega$ for even-even ^{88}Mo(SD1, SD2 and SD3). The experimental and calculated values are denoted by solid circles and solid lines respectively.

References

1. Twin P. J. , Nyak B. M. Observation of a Discrete Line Superdeformed Band up to $60\hbar$ in ^{152}Dy. *Physical Reveiw Letters*, 1986, v. 57, 811–814.
2. National Nuclear Data Center NNDC, Brookhaven National Laboratory, http.//www.nndc.bnl.gov/chart/
3. Svenssan C.E. et al. Observation and Quadrupole-Moment Measurement of the First Superdeformed Band in the $A \sim 60$ Mass Region. *Phys. Rev. Lett.*, 1997, v. 79, 1233.
4. C. H. Yu et al, Comparison of Superdeformation Bands in ^{61}Zn and ^{60}Zn: Possible evidence for $T = 0$ Pairing. *Phys. Rev.* 1999, v. 60C, 031305.
5. Johnasson E.K. et al. *Phys. Rev.*, 2008, v. C77, 064316.
6. Smith A.G. et al. Observation of Superdeformation in ^{82}Sr. *Phys. Lett.*, 1995, v. 355B, 32.
7. Yu C.H. et al. Lifetime Measurements of Normally Deformed and Superdeformed States in ^{82}Sr. *Phys. Rev.*, 1998, v. 57C, 113.
8. Bäck T. et al. Observation of Superdeformed States in ^{88}Mo. *Eur. Phys. J.*, 1999, v. 6A, 391.
9. Cederwall B. et al. Favoured Superdeformed States in ^{89}Tc. *Eur. Phys. J.*, 1999, v. 6A, 251.
10. Becker J.A. et al. Level Spin and Moment of Inertia in Superdeformed Nuclei Near $A = 194$. *Nucl. Phys.*, 1990, v. A520, C187–C194.
11. Droper J.E. et al. Spins in Superdeformed Bands in the Mass 190 region. *Phys. Rev.*, 1990, v. C42, R1791–R1795.
12. Zeng J.Z. et al. Critical of the spin Assignement of Rational Band. *Commun Theor. Phys.*, 1995, v. 24, 425.
13. Goel A. *Int. J. Scientific Research*, 2013, v. 21, 2277.
14. Hegazi A.M., Ghoniem M.H. and Khalaf A.M. Theoretical Spin Assignment for Superdeformed Rotational Bands in Mercury and Lead Nuclei. *Egyptian Journal of Physics*, 1999, v. 30, 293–303.
15. Khalaf A.M. et al. Description of Rotational Bands in Superdeformed Nuclei by Using Two-Parameter Empirical Formula. *Egyptian Journal of Physics*, 2003, v. 34, 159–177.
16. Khalaf A.M., Sirag M.M. and Taha M. Spin Assignement and Behavior of Superdeformed Bands in $A \sim 150$ Mass Region, *Turkish Journal of Physics*, 2013, v. 37, 49–63.
17. Khalaf A. and Okasha M. Properties of Nuclear Superdeformed Rotational Bands in $A \sim 190$ Mass Region. *Progress in Physics*, 2014, v. 10, 246–252.
18. Bohr A. and Mottelson B. Nuclear Structure v.2, Benjamin Inc, New York, 1975.
19. Clark R.M. et al. Very Extended Shapes in the $A \sim 110$ Region. *Phys. Rev. Lett.*, 2001, v. 87, 202502.
20. Grodzins I. *Phys. Lett.*, 1962, v. 2, 88.

ERRATA. NOTICE OF REVISION

Notice of Revision: "On the Equation which Governs Cavity Radiation I, II", by Pierre-Marie Robitaille

Pierre-Marie Robitaille
Department of Radiology, The Ohio State University, 395 W. 12th Ave, Columbus, Ohio 43210, USA
E-mail: robitaille.1@osu.edu

Professor Pierre-Marie Robitaille wishes to inform the readership of *Progress in Physics* that revisions were made on December 26, 2014 to the following two papers:

1. On the Equation which Governs Cavity Radiation I, *Progress in Physics*, 2014, v. 10, issue 2, 126–127.
2. On the Equation which Governs Cavity Radiation II, *Progress in Physics*, 2014, v. 10, issue 3, 157–162.

In addition to *Progress in Physics*, the electronic versions of these works have been archived on viXra.org and ResearchGate.

Submitted on December 29, 2014 / Accepted on December 29, 2014

Nuclear Power and the Structure of a Nucleus According to J. Wheeler's Geometrodynamic Concept

Anatoly V. Belyakov

E-mail: belyakov.lih@gmail.com

In this paper on a unified basis in terms of mechanistic interpretation of J. Wheeler's geometrodynamic concept the attempt to explain the nature of nuclear forces as the result of the complex nucleons structure and to submit the model of the structure of atomic nuclei is done. It is shown that the assumption of the existence of closed contours, including electron and proton quarks leads to a conclusion about the existence of W, Z-bosons and also the Higgs boson whose mass is calculated. Values of the coupling constants in the strong and weak interactions are calculated, and it is shown that they do not indicate the strength of the interaction, but indicate only the strength of bonds between the elements of nucleon structure. The binding energy of the deuteron, triton and alpha particles are defined. Dependence of the nucleon-nucleon interaction of the distance is explained. The structural scheme of nuclei is proposed, the inevitability of presence of envelopes in nuclei is proved, the formulas allowing to estimate the features of nuclear structure, as well as correctly to assess the binding energy of nuclei and their mass numbers are obtained. The results of calculations at the level of the model suggest the possibility to use this model for the construction of an appropriate theory.

1 Introduction

At present there is no a complete theory of the nuclear structure, which would explain all properties of atomic nuclei. To describe properties and behavior of atomic nuclei, different models are used, each of which is based on various experimental facts and explains some allocated properties of the nucleus. One reason for this is that the analytical dependences for the interaction forces between nucleons are until now not derived.

In the quantum theory, the interaction between the microparticles is described as an exchange of specific quanta (photons, pions, gluons, and vector bosons) associated with these types of interactions. The dimensionless parameter determining the relative strength of any interaction (an interaction constant or coupling constant α) is assumed proportional to the source interaction charge by analogy with the charge of an electron in the electromagnetic interaction:

$$\alpha_e = \frac{e^2}{\hbar c} = \frac{1}{137}, \qquad (1)$$

where e is the electron charge (in the CGSE).

But the problem consists in that for both strong and weak interactions the mechanism of interaction and, accordingly, a coupling constant strongly depend on the interaction energy (distance) and are determined experimentally.

In terms of the developed model based on the mechanistic interpretation of J. Wheeler's geometrodynamic concept [1], such a variety of types and mechanisms of interaction seems strange and unreasonable. In contrast to the quantum theory, which states that microphenomena in no way can be understood in the terms of our world scale, the mechanistic interpretation of Wheeler's idea above all assumes the existence of common or similar natural laws, which are reproduced at the different scale levels of matter that, in particular, allows using of macroscopic analogies in relation to the objects of microworld.

The proposed model of nuclear forces and nuclear structure as well as previous works [2–5] is based on the general conservation laws and balances between main interactions: electrical, magnetic, gravitational and inertial — with no additional coefficients or any arbitrary parameters introduced. Without using complicated mathematical apparatus, this work is not physical and mathematical one, but rather is the physical and logical model. However, application of Wheeler's ideas to this area of microphenomena gives the opportunity to clarify the cause and nature of nuclear forces and give a reasonable scheme of nuclear structure, which is confirmed by some of the examples of successful calculations made on the basis of the model.

2 Initial conditions

Recall that in this article, as well as in the earlier works, the charges in accordance with Wheeler's idea treated as singular points on the three-dimensional surface, connected by a "worm-hole" or vortical current tube similar to the source-drain principle, but in an additional dimension of space, constituting a closed contour as a whole.

The closest analogy to this model, in the scale of our world, could be the surface of ideal liquid, vortical structures in it and their interactions which form both relief of the surface and sub-surface structures (vortex threads and current tubes).

In this model, there is no place for a *charge* as a specific matter, it only manifests the degree of the nonequilibrium

state of physical vacuum; it is proportional to the momentum of physical vacuum in its motion along the contour of the vortical current tube. Respectively, the *spin* is proportional to the angular momentum of the physical vacuum with respect to the longitudinal axis of the contour, while the *magnetic interaction* of the conductors is analogous to the forces acting among the current tubes.

In such a formulation the electric constant ε_0 makes sense the linear density of the vortex current tube

$$\varepsilon_0 = \frac{m_e}{r_e} = 3.233 \times 10^{-16}\ \text{kg/m}, \tag{2}$$

and the value of *inverse magnetic constant* makes sense the centrifugal force

$$\frac{1}{\mu_0} = c^2\varepsilon_0 = 29.06\ \text{n}, \tag{3}$$

appearing by the rotation of a element of the vortex tube of the mass m_e and of the radius r_e with the light velocity c; this force is equivalent to the force acting between two elementary charges by the given radius, and electron charge makes sense the momentum of the vortex current tube (counter) with a mass of $m_e c_0^{2/3}$ and with velocity of $c_0^{2/3} \times [\text{m/sec}]$, the energy of which is equal to the maximum energy of the electron $m_e c^2$, i.e.

$$e = m_e c_0^{4/3} \cos q_w \times [\text{m/sec}] = 1.603 \times 10^{-19}\ \text{kg m/sec}, \tag{4}$$

where c_0 is the dimensionless light velocity $c \times [\text{m/sec}]^{-1}$, q_w is the Weinberg angle of mixing of the weak interaction, it equals 28.7°.

Vortex formations in the liquid can stay in two extreme forms — the vortex *at the surface* along the X-axis (let it be the analog of a fermion of the mass m_x) and the vortical current tube *under the surface* of the angular velocity v, the radius r and the length l_y along the Y-axis (let it be the analog of a boson of the mass m_y). These structures oscillate inside a real medium, passing through one another (forming an oscillation of oscillations). Probably, fermions conserve their boson counterpart with half spin, thereby determining their magnetic and spin properties, but the spin is regenerated up to the whole value while fermions passing through boson form. The vortex thread, twisting into a spiral, is able to form subsequent structures (current tubes). The possibility of reciprocal transformations of fermions and bosons forms shows that a mass (an energy) can have two states and pass from one form to another.

In paper [2] proceeding from conditions of conservation of charge and constancy parameters μ_0 and ε_0, parameters of the vortex thread m_y, v, r, for an arbitrary $p^+ - e^-$-contour defined as a proportion of the speed of light and electron radius as:

$$m_y = (an)^2, \tag{5}$$

$$v = \frac{c_0^{1/3}}{(an)^2}, \tag{6}$$

$$r = \frac{c_0^{2/3}}{(an)^4}, \tag{7}$$

where n is quantum number, a is inverse fine structure constant.

Wherein, referring to the constancy ε_0 (linear density), it is clear that the relative length of the tube current in the units of r_e is equal boson mass m_y in the units of m_e, i.e.

$$l_y = m_y = (an)^2. \tag{8}$$

In the model the particles themselves are a kind of a contour of subsequent order, formed by the intersection of the X-surface with the current tube, and they have their own quantum numbers defining the zone of influence of these microparticles. In [3] determined that for the proton

$$n_p = \left(\frac{2c_0}{a^5}\right)^{1/4} = 0.3338, \tag{9}$$

for an electron $n_e = \sqrt{n_p} = 0.5777$, and for the critical contour, when $r \to r_e$ and $v \to c$, $n_c = c_0^{1/6}/a = 0.189$.

Hereinafter all the numerical values of the mass, size and speed are given in dimensionless units: as a proportion of mass of the electron m_e, its radius r_e and speed of light c.

It is important to note that the contour or vortex tube, which the vortex thread fills helically, can be regarded as completely "stretched", i.e. elongated proportional to $1/r$ or, on the contrary, extremely "compressed", i.e. shortened proportional to $1/r$ and filling all the vortex tube of radius r_e. In the latter case its compressed length $L_p = l_y r$ is numerically equal to the energy of the contour boson mass in units of mass-energy.

Indeed, since $r = v^2$, then the above quantities values in dimensionless units are in all cases identical:

$$L_p = l_y r = m_y r = m_y v^2 = \frac{c_0^{2/3}}{(an)^2}. \tag{10}$$

It is obvious that an arbitrary boson mass in the units of mass-energy will match of its own value m_y only in the case of ultimate excitation of the vortex tube when $r \to r_e$ and $v \to c$.

Here are some of the parameters for mentioned three particular contours. Substituting in the formula (7) and (8) the parameters n_e, n_p, and n_c one can find the characteristic sizes of the vortex tubes: for an electron vortex thread radius $r = 0.0114$, the length of the vortex thread $l_y = 6267$, for the proton $r = 0.1024$, $l_y = 2092$, for a critical contour $r = 1$, $l_y = 670$.

As for the accepted *scheme of the nucleons structure*, in [3] it is shown that the proton has a complex structure, which

is revealed in process of transition to smaller scales with increasing the interaction energy, i.e., as if its "deepening" along the Y-axis; so to the outside observer the nuclear forces manifest themselves in a complex manner.

In the *inner area of the proton* there are three critical section (quarks), each of which is crossed by three force lines (charges 1, 1, −1). The presence of inverse circulation currents forming three closed contours leads to the fact that the intersection of the critical section by the lines of force inside the proton will for an outside observer be projected on the *outer proton surface* in the form of $\frac{2}{3}$, $\frac{2}{3}$, $-\frac{1}{3}$ of the total charge.

Along the Y-axis the proton boson vortex tube is located having parameters $m_{py} = 2092$ and $r_p = 0.1024$. The most "deep" along the Y-axis the quark vortex tubes are located with the parameters defined in [3]: the quantum number $n_k = 0.480$, the total fermion mass $m_{kx} = 12.9$, the total boson mass $m_{ky} = 4324$, the radius of the vortex tube $r_k = 0.024$.

It should be noted that the value of the parameter r_k is confirmed by works on studying of *neutron polarizability*. In [6] the lower limit the polarizability coefficient is specified of $a_p = 0.4\times10^{-42}\,\mathrm{cm}^3$. This means that the linear inhomogeneity parameter in the structure of the neutron coincides with the radius of the quark vortex tube as $(a_p)^{1/3} = 7.37\times10^{-15}$ cm or $0.026\,r_e$.

Neutron has three closed contour, i.e. six force lines instead of nine ones, which a proton has, and, therefore, the total neutron quark mass has the value of $12.9\times2/3 = 8.6$. Having in mind adopted direction and the possible distribution of the force lines in the neutron [3], one can expect that in the case of neutron polarization neutron may have the charges in the inner region of 1, −1, or −1, $\frac{2}{3}$, $\frac{1}{3}$, and in the projection of the outer surface of $-\frac{2}{3}$, $\frac{1}{3}$, $\frac{1}{3}$.

In the contour connecting the charged particles, the quarks are involved in the circulation and become an active part of the nucleon mass. It is assumed that in the critical section circulation velocity reaches the velocity of light, so quarks are actually dark matter, which is equivalent to the mass defect, reflecting the energy of bonds within nucleons or nuclei; the nominal mass-energy of a quark is $0.511\times\frac{12.9}{3} = 2.2$ MeV.

When considering the closed contour having contradirectional currents, from the balance of magnetic and gravitational forces recorded in a "Coulombless" form the characteristic size of a contour as a *geometrical mean* of two linear values is obtained:

$$l_k = \sqrt{l_i\, r_i} = \sqrt{\frac{z_{g_1} z_{g_2}}{z_{e_1} z_{e_2}}}\,\sqrt{2\pi\gamma\,\varepsilon_0}\;\times[\mathrm{sec}]\,, \qquad (11)$$

where z_{g_1}, z_{g_2}, z_{e_1}, z_{e_2}, r_i, l_i are gravitational masses and charges expressed through masses and charges of an electron, a distance between current tubes and theirs length.

Number of vortex thread constituting contour reflects the difference of material medium from vacuum, and their greatest value corresponds to the ratio of electrical forces to gravitational forces, i.e. value:

$$f = \frac{c^2}{\varepsilon_0\,\gamma} = 4.16\times10^{42}, \qquad (12)$$

where γ is the gravitational constant.

The contour can be considered located both in the X-area (for example, $p^+ - e^-$-contour in atom) and in the Y-area (vortex tube inside an atomic nucleus). When a proton and an electron come together (for example, when its contraction by the e-capture) a deformation of the contour takes place, energy and the fermion mass increase, while the boson mass decreases, but the impulse (charge) is conserved.

Formula (11) for unit charge taking $z_{g_2} = 1$ and after calculating the constants gets the form in the units of r_e and m_e:

$$m_k = z_{g_1} = b\,l_k^2\,, \qquad (13)$$

where m_k is the proton quark mass involved in the circulation contour, $b = 5.86\times10^{-5}$.

Parameter l_k is composite. If the contour (vortex tubes) is directed along the Y-axis, then $r_i = r$, $l_i = l_y$, if the contour is directed along the X-axis, then in calculating parameters are replaced, i.e. $r_i = l_y$, $l_i = r$. Having in mind (7), (8), (11), and (13)), replacing arbitrary parameters r_i and l_i by the sizes of short and long axes of the contour and calculating constants, we obtain the formulas relating the quark mass and the contour linear parameters:

$$m_k = \frac{26.25}{r} = 0.0392\,\sqrt{l_y}\,, \qquad (14)$$

and also

$$r\,\sqrt{l_y} = c_0^{1/3}. \qquad (15)$$

3 On boson masses

The circuit parameters in X-region and Y-region in the general case do not match, but both include the quark mass, which depends on the size of the contour. Let us compare the parameters of these contours for some specific cases.

Let us consider X-contour of own electron at $n_e = 0.5777$. Its size along the X-axis, as follows from (8), $r_i = l_y = 6267$. From (14) we find the quark mass $m_k = 3.10$. For having of the same value of mass-energy L_p, Y-contour, as follows from (10), should have a quantum number $n = 2.77$. The boson mass of such a contour according to (5) $m_y = 1.44\times10^5$, that is close to the mass of W-bosons.

Let us consider the contour of own proton at $n_p = 0.3338$. Its size along the X-axis $r_i = l_y = 2092$ and the quark mass $m_k = 1.795$. Y-contour having the same value of mass-energy has $n = 3.645$. Boson mass of such a contour $m_y = 2.494\times10^5$, that is almost exactly ***corresponds to the mass of the Higgs boson*** (125 GeV).

Let us consider the critical contour at $n_c = 0.189$. Its size along the X-axis $r_i = l_y = 672$ and the quark mass $m_k = 1.02$. That is, in the limiting case the ***quark mass becomes equal to the mass of an electron***. Y-contour having the same value of mass-energy has $n = 4.884$, i.e. it is a standard contour [2]. The boson mass of such a contour $m_y = 4.48 \times 10^5$, that is close to the total mass of W, Z-bosons.

Thus, these relations between the masses of the particles taking part in the weak interaction (quarks, bosons, protons, and electrons) to some extent clarify the nature of the weak interaction and the physical meaning of its interpretation as "the exchange of bosons". It turns out that W, Z-bosons and the Higgs boson are the vortex tube having the value of mass-energy equal to mass-energy of the quarks included in the circulation contours corresponding to their own electron, proton, and critical contours. And in the course of the weak interaction X-contour is reduced and when performing this condition, it is reoriented to Y-region, transmitting momentum (charge) to the proton while keeping the angular momentum (spin, in the case of e-capture, for example); then it is extracted as a neutrino [3]. From the above it implies that the *Higgs boson is not a unique particle in microcosm*.

4 The coupling constants

In [5] a formula is obtained, from which it follows that the unit contour or vortex tube having a *momentum equivalent to the electron charge* consist of three unit vortex threads. After transformation this formula can be written as:

$$n_i^3 = \frac{\frac{m_e c_0^{2/3} r_e}{\sqrt{2\pi} \times [\sec^2]}}{\frac{2\pi\gamma m_e^2}{r_e^2}} = 26.25. \qquad (16)$$

This formula represents the ratio of inertial forces occurring during acceleration of the standard contour boson mass and acting toward to periphery (as the value $\frac{r_e}{\sqrt{2\pi} \times [\sec]}$ is the rotational speed of the vortex thread relative to the longitudinal axis of the contour [3]) to the gravity forces acting between the masses of m_e at a distance of r_e. The numerator is constant, so the formula depends only on the force of gravity, i.e. from interacting masses and distances between them. This ratio (or its modification for arbitrary m_i and r_i) can be the equivalent of the coupling constant, as indicates the strength of the bonds between the elements of the proton structure (quarks).

4.1 Strong interaction

Suppose that quarks are located at the corners of an equilateral triangle at a distance r_e. In this case each of them is exposed of the sum of two projections forces, therefore the denominator into (16) should be corrected by multiplier $2 \sin 60°$. As a result, the formula (16) in the relative units of r_e and m_e after calculating of constants takes the form:

$$a_s = 15.15 \left(\frac{r_i}{m_i} \right)^2 . \qquad (17)$$

Consider the case of the strong interaction at low energies where the parameter r_i is greater than the nucleon size r_n. Let the mass of the proton quark takes a minimum value m_e (section 3), the distance between the quarks is r_e; substituting $r_i = 1$, $m_i = 1$ into (17), we obtain $a_s = 15.15$, which coincides with the known value determined at low energies $a_s \sim 15$.

It should be expected that at $a_s = 1$, there is a balance between the forces of gravity and peripheral inertia forces, which the nominal size of the proton can be determined from. Indeed, under this condition (17) it follows $r_i = 0.257$, and the size of the vortex tube, accordingly, is $0.257 / \sin 60° = 0.297$ or 0.84 fm, which coincides with the proton radius.

Consider the case of the strong interaction with $r_i < r_n$, where the energy of the interacting particles is high (about 100 GeV), and they approach each other at the minimum distance of the vortex proton tube $r_p = 0.1023$ (section 2). In this case, the distance between the quarks inscribed in the vortex proton tube is $r_i = r_p \sin 60° = 0.0887$. Substituting r_i and $m_i = 1$ into (17), we obtain $a_s = 0.119$. This calculated value coincides with the experimental data. Indeed, in [7] it was found that at the given energy $a_s = 0.1176 \pm 0.0024$.

Now it becomes clear physical meaning of the great difference in magnitudes of this type interaction. At low energies of the interacting particles affecting only the outer structure of nucleons ($r_i > r_n$, low "depth" along Y-axis) the peripheral inertial forces exceed the forces of gravity, so the elements of the structure (quarks) are weakly bonded to each other, can move away from the starting position and interact with nearby nucleon quarks. At high energies ($r_i < r_n$, more "depth" along Y-axis) interaction occurs at the level where the forces of mutual attraction holds the quarks in the bound state within the nucleon size, that leads to a decrease in the efficiency of the interaction of microparticles as a whole.

Note, that in the atoms nuclei quarks may also be in a bound state due to their large masses, which they acquire when entering into the $p^+ - e^-$-contours.

4.2 Weak interaction

When the weak interaction (such as in the case of e-capture, for example) the bosonic part of the proton quark or vortex tubes take part (section 3).

Let us assume that the mass of each of three quark tubes $m_i = m_{ky} = 4324/3 = 1441$ (section 2). Substituting m_i and $r_i = 1$ into (17), we find $a_w = 0.73 \times 10^{-5}$. This value agrees with the value of a_w, defined through Fermi constant (1×10^{-5}). At high interaction energies (about 100 GeV) the constant a_w increases to $\sim \frac{1}{40}$. In our model this increase can also be explained.

At the limit excitation of the contour vortex tube at the quarks level when $v \to c$ and $r \to r_e$ boson mass becomes equivalent to its mass-energy, but because the parameters ε_0 and μ_0 are constant then the radius of the vortex tube increases proportional to the ratio r_e/r_k. Since $r_e/r_k = 41.7$, then in this case $r_i = 41.7$, and the parameter a_w increases proportionally to the square of this ratio, i.e. $a_w = 0.73\times10^{-5}\times41.72^2 = \frac{1}{78}$, which is in agreement with the value of a_w determined at high energies.

4.3 On the electron

Suppose that the formula (17) is applied to the electron itself. Electron contains three vortex threads. Assuming $r_i = r_e$ and considering that the boson mass of an electron vortex threads is $m_i = \frac{1}{3}(an_e)^2 = 2089$, and it coincides with the proton boson mass, it is obvious that the *coupling constant for the electron in the weak interaction is identical to that of the proton*.

As for the strong interaction then in this case $m_i = \frac{1}{3}m_e$. Substituting into (17) $r_i = 1$ and $m_i = \frac{1}{3}$, we find $a_s = 136.4$, which almost coincides with the value of the reciprocal fine structure. Proceeding from the enormous value of the coupling constant a_s the electron structure cannot be in a bound state, and in equilibrium at $a_s = 1$ the size of the electron would be very small at $r_i = 0.086$. But having such a small radius the electron charge cannot place itself according to the classical definition, by which the potential energy of the electrostatic field is completely equivalent to the rest mass of an electron.

Thus, the electron to resolve this contradiction and be able to exist itself shall continuously oscillate between these states. Its pulsations provide the motion of medium along the p^+-e^--contours thereby confirming definition of the charge as the momentum.

Summing up the results of Chapter 4 one can say that the coupling constant defines neither the nature of nuclear forces, nor the interaction force, but only *indicates the strength of the bonds within the complex structure of nucleons*.

5 The nucleus

When considering nuclear forces hereinafter to take into account the Coulomb interaction at various energy levels (distances) proved sufficient, from which it can be concluded that the *introduction of any special nuclear forces is not required*, at least within the limits of this model.

As for scheme of nuclear structure, then the proposed scheme is, to a certain extent, associated with collective model (J. Rainwater, 1959, A. Bohr, and B. Mottelson, 1952). This model combines the provisions of the hydrodynamic and the envelope model and suggests that the nucleus consists of the inner stable part — the core formed the nucleons of filled envelopes and the outer nucleons moving in the field generated by the core nucleons.

5.1 Nuclear forces

Are there any special nuclear forces at all?

At high energies and short distances, i.e. when approaching nucleons to their radius $r_n = 0.842$ fm and overlapping of their *internal structures*, the interaction between nucleons occurs inside their total "quark bag" between oppositely quarks having inside the nucleon structure the charges of 1 and -1 at the distance of its vortex tube. Let us assume that the quark mass is minimal and equal to m_e, i.e. it is identical to an electron, then its vortex tube size is equal to the electron vortex tube size $r_k = 0.0114$ (section 2).

Write the formula for the potential in the units of MeV and the fractions of r_e. The depth of the attractive potential at the minimum distance for unit charges is

$$V = -\frac{0.511}{r_k}, \tag{18}$$

which gives -44.8 MeV (see Figure 1).

With further approach of nucleons at even higher energies (greater "depth" along Y-axis) the interaction at the level of boson vortex nucleons tubes is added. It is understood that the unidirectional vortex tubes are repelled, and as far as "deepening" along Y-axis their radius r decreases (here the role of magnetic attraction forces is negligible). Since the mass per unit length is reduced in proportion to the square of the radius, the local value of the electrical constant (linear density) ε_0 is reduced proportional to the ratio r/r_e. Thus repulsive potential as a result increases in inverse proportion to the square of the distance, and the resulting potential-distance dependence receives the form below:

$$V = 0.511\left(-\frac{1}{r_k} + \frac{1}{r^2}\right) \text{ MeV}. \tag{19}$$

Beyond "quark bag", at the distance of the nucleon diameter, the Coulomb interaction occurs between the fractional

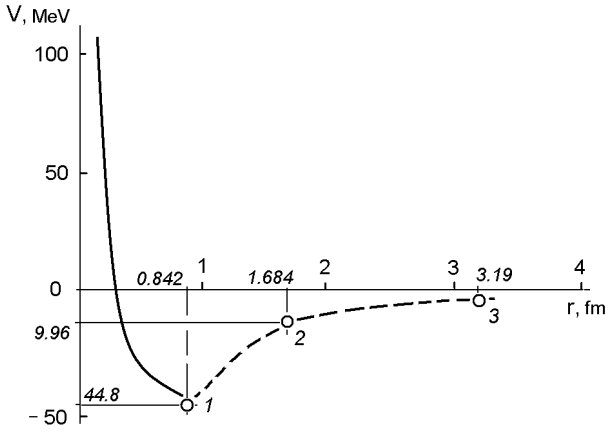

Fig. 1: Dependence of the nucleon-nucleon interaction on the distance between them.

charges of different signs, located on the *outer surface* of protons. Thus, attractive potential sharply decreases, for protons it is in proportion to the product of $\frac{1}{3} \times \frac{2}{3} = \frac{2}{9}$. Namely, at the distance $2r_n = 1.684$ fm attractive potential decreases to a value $\frac{2}{9} \times 44.8 = 9.96$ MeV.

Another reference point for plotting the dependence $V(r)$ can be found by equating the Coulomb repulsive forces between two protons at the distance between their centers to the residual attractive forces acting between the fractional charges located on the outer surface of the protons. In this case we have:

$$\frac{e^2}{\varepsilon_0 r^2} = \frac{2}{9} \frac{e^2}{\varepsilon_0 (r - 2r_n)^2}, \qquad (20)$$

from which we obtain $r = 2r_n \left(1 - \sqrt{\frac{2}{9}}\right)^{-1} = 3.78 r_n = 3.19$ fm, i.e. distance where the attractive forces between the nucleons can be neglected. The resulting dependence $V(r)$ is shown in Figure 1 and it as a whole corresponds to actual dependence.

Thus, it may be concluded that any special nuclear forces do not exist, and complex nuclear interaction is explained by the forces of unified nature (electrical) acting between the elements of the complex structure of nucleons at different levels (the "depths" along Y-axis), which are determined by the interaction energy.

5.2 The binding energy of deuterium, tritium and alpha particles

A deuterium nucleus — the deuteron is a rather loose formation, and therefore it can be assumed that the bond of two nucleons due to Coulomb forces between the proton having on its outer surface fractional charges of $\frac{2}{3}$, $\frac{2}{3}$, $-\frac{1}{3}$ and the polarized neutron with charges on the surface of $-\frac{2}{3}$, $\frac{1}{3}$, $\frac{1}{3}$. Let us assume that the nucleons form its own contour having at $n = n_p$ the parameters $l_y = 2092$ and $r = 0.1024$ (section 2). When substituting r into (18), we obtain the binding energy (potential) in the units of MeV bonding the nucleons in the deuteron: $E_d = 0.511 \times (\frac{2}{3} \times \frac{2}{3})/0.1024 = 2.22$ MeV that corresponds exactly to the actual binding energy of the deuteron.

Could this be an accidental coincidence? It is known that the good description of the characteristics of the deuteron provides the selection of the nucleon-nucleon n-p potential in the form of a rectangular pit of depth $V \sim 35$ MeV and of width $d = 2$ fm [8]. Assuming that d is the distance between the centers of nucleons, one can find that the distance between the fractional charges on the nucleon periphery is $d - 2r_n = 0.316$ fm or $0.112\, r_e$. The result is in good agreement with the proton vortex tube size, i.e. with parameter r, that confirms the correctness of calculation.

The tritium nucleus — triton consists of a proton and two neutrons attached. The mean square charge radius of the triton is 1.63 fm, so, obviously, the nucleons are in contact. Let us assume that the neutrons are polarized with charges of 1, -1. Binding energy can be determined by summing the mass-energy of the four quarks involved in creating bonds. As a result, we get $E_d = 2.2 \times 4 = 8.8$ MeV that is close to the actual triton binding energy (8.48 MeV).

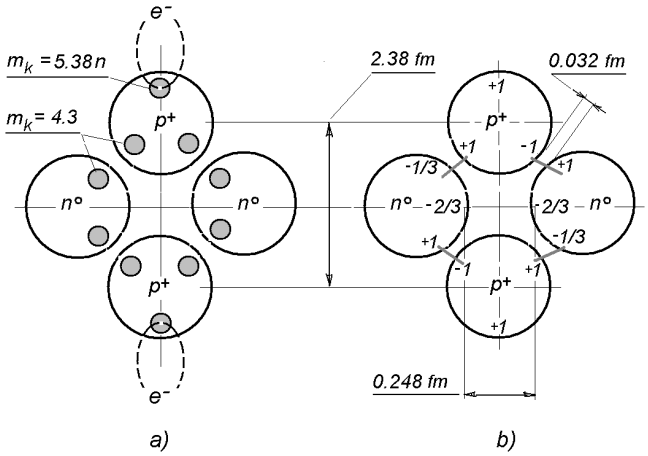

Fig. 2: Settlement scheme of the alpha particle: a — on the basis of the quark masses, b — on the basis of energy of the quarks.

An alpha-particle is a spherically symmetric object with radius of about 2 Fermi, and it is the most stable and compact structure (cluster) that can occur inside the atomic nucleus. If we assume that nucleons are in contact with each other, then for symmetrical arrangement of four nucleons having radii $r_n = 0.842$ fm and forming a closed system as a whole, in fact, the alpha-particles radius will be 2.04 fm, Figure 2.

The alpha particle emitted from a nucleus overcomes the potential barrier and, in addition, is a surplus energy in different ranges. Apparently, in addition to the mass-energy of eight quarks involved in the interaction, there is a necessity to take into account also the mass-energy of the two protons quarks included in $p^+ - e^-$-contours; this mass-energy depends on the quantum number of the contour, Figure 2a. It was revealed that alpha-clustering is most probable in the nucleus surface region where the density of nuclear matter is reduced to about one-third of density in the nucleus central part [9]. Therefore, we can assume that the protons of alpha-particles leaving the nucleus are associated with the second electron shell (the first one has only two electrons).

From (8), (13), and (14) it follows that the masses of quarks that are constituents in a $p^+ - e^-$-contour are proportional to the quantum number:

$$m_k = b\, a\, c_0^{1/3} n = 5.377\, n, \qquad (21)$$

i.e. for the second shell the quark mass is equal to 10.75. As a result, given the potential repulsion of two protons (~ 0.6 MeV at a specified distance 2.38 fm on the scheme), we obtain: $E_a = 0.511 \times (4.3 \times 8 + 10.75 \times 2) - 0.6 = 28.0$ MeV, which corresponds well to the actual alpha particles binding

energy (28.2 MeV).

One can determine the binding energy from another considerations by summing the energy of bonded opposite charges, assuming that the distance between them is equal to the radius of the electron vortex tube $r = 0.0114 = 0.032$ fm, Figure 2b. Other positive charges of the protons quarks are associated with the atom electrons, and the unaccounted negative neutrons charges create the repulsive potential. The bonds form a closed system, so one can assume that the alpha particle binding energy is the averaged binding energy of a link, since at destruction of a link the particle splits as a whole. Indeed, it is known that to remove of only a nucleon from alpha particles the energy about 20 MeV is required [9].

Given the above, referring to the adopted charges layout, the alpha particles geometry, and specified dimensions, one can write the final formula for the binding energy as the average energy per bond at subtracting the repulsive potentials of protons as whole units and the fractional charge repulsion potentials of neutrons:

$$E_a = \frac{1}{4}\left(1\times 1 + \frac{1}{3}\times 1 + 1\times 1 + \frac{1}{3}\times 1\right)\frac{0.511}{r} - \\ - 1\times 1\times\frac{0.511}{b} - \left(\frac{2}{3}\times\frac{2}{3}\right)\frac{0.511}{c}, \qquad (22)$$

where b and c are calculated from geometrical considerations: $b = 2r_n\sqrt{2} = 2.38$ fm or 0.845, $c = 2r_n(\sqrt{2}-1) = 0.697$ fm or 0.248. Substituting the values, we obtain $E_a = 28.3$ MeV, which coincides with the actual value.

It is known that the nuclei can be seen as the system of nucleons and at the same time as the system of the large number of clusters of different nature, which are in dynamic equilibrium, i.e. they disintegrate, are again formed and exchanged both nucleons and energy [10]. The closer to the nucleus center are protons, the higher energy they have, since the proton quarks mass-energy included in the $p^+ - e^-$-contours increases in proportion to the quantum number. When the transfer of energy from the center and from the inner envelopes to the periphery occurs, alpha-particles leaving the nucleus surface have the energy excess equal to the energy difference between the corresponding levels, i.e. referring to (22) and at changing to energy units $E_a = 2.75(n_2 - n_1)$ MeV.

Thus, when the excitation transfer from the third to the second envelope the energy of alpha-particles having two protons may be not more than $2\times 2.75 = 5.5$ MeV, and when the excitation transfer from the fourth to the second envelope — twice as much, not more than 11 MeV.

Indeed, for the emitted alpha particles there are two energy ranges: with the upper limit of 2–4 MeV for rare earth elements and 4–9 MeV for the elements heavier than lead [11]. Not numerous long-range alpha particles with higher energy get this energy after series of collisions with protons in the center of the nucleus, which are associated with the fifth, sixth, and seventh envelopes; accordingly, their maximum energy can reach $2\times 2.75(7-2) = 27.5$ MeV. The resulting value matches exactly the value of the maximum alpha particles energy, defined in during the study of heavy nucleus fission accompanied by the formation of three charged particles [12]. Moreover, in these particles energy spectrum there is no fine structure, which is understandable, since the energy of such particles is derived from protons homogeneously packed in the "quark bag" in the nucleus core, but not from the structural units in the nuclear envelopes composition having certain specificities.

It should be noted that the binding energies differences between neighboring isotopes for the nuclei of almost all elements are in the range of 20 MeV (for isotopes with the least number of neutrons) to 2 MeV (for isotopes with the greatest number of neutrons). That is, in the most cases these energy differences lie in the range from the nominal mass-energy of a cluster $2.2\times 8 = 17.6$ MeV to the mass-energy of a quark 2.2 MeV. This means that in the first case, with the excess of protons, addition of a neutron leads to the formation of an entire cluster (alpha-particles) and in the second case, with the excess of neutrons, — to another quark be only involved in a common bound nucleus structure.

Another fact confirming that clusters are only formed in the envelopes from the first to the fourth is the amount of isotopes depleted by neutrons. Typically, for most of elements (except radioactive ones) it is close to the number of clusters. The maximum amount of such isotopes Platinum has ($Pt^{195}\ldots Pt^{166}$), it is equal to the number of clusters in all four envelopes (30).

5.3 On the nucleus structure

In accordance with the model the packing density of alpha-clusters and of protons in particular increases toward the center of the nucleus, as the distance between the vortex tubes of $p^+ - e^-$- contours is reduced and the vortex tubes length increases. Therefore, the electrons located at the more distant orbits are associated with the protons located at the deeper nucleus levels; thus the *layers or envelopes are formed in the nucleus* that similarly to the electronic shells.

Suppose that the distance r_i between the vortex tubes cannot be less than the size of alpha-particles (4 Fermi). This condition limits the number of the electronic shell whose electrons can associate with the protons belonging to alpha-clusters and, accordingly, the nucleus envelope which deeper alpha-clusters are not formed. From (14) and (8) implies $n \geqslant 3.44$. Even if the diameter of the equivalent sphere equal to the volume of four alpha-particles nucleons ($\sim r_e$) to accept for limiting size, and even then $n < 5$. That is the electrons of the fifth and subsequent atom shells are associated with protons in the center of the nucleus; these protons are here not part of the alpha-clusters. Thus, the fourth layer (envelope) is the last in the nucleus.

It should be noted that a similar condition for the nu-

cleon size also determines the maximum possible number of the atom electron shell. Indeed, assuming $r_i \geqslant 2r_n$, we find $n_{max} \leqslant 8.1$.

Consider the heavy atom nucleus, for example, $_{82}Pb^{207}$, wherein there is a fourth filled electron shell with 32 electrons and, accordingly, the fourth layer of 16 clusters in the nucleus. It is not difficult calculate the outer and inner radii of the layer, assuming that one alpha-cluster has a volume equivalent to the volume of four nucleons, i.e. $4 \times (2r_n)^3 = 19.1$ fm^3. The inner radius is 2.93 fm. The remaining 22 protons are not part of the proton clusters; they are located in the center of the nucleus and have the volume equivalent to the sphere of exactly the same radius 2.93 fm. The outer diameter of the nucleus as a whole in the summation of the thickness of the four envelopes is $2.93 + 4 \times 2r_n = 9.66$ fm, which corresponds to the size of heavy nuclei.

Thus, it appears that for the elements heavier than lead, the protons taking part in the contours where electrons belong to the fifth and subsequent shells no longer completely go in the core of the nucleus. With increasing the number of protons the fourth nuclear envelope expands, additional neutrons are included in it, and radius of the nucleus increases.

Neutrons are not included in the cluster (for $_{82}Pb^{207}$ of such neutrons are 65) are placed in the free volume being forced out into the outer envelopes. One can assume that the average distance between them is not less r_e, accordingly, the average volume per a neutron exceeds 22.4 fm^3 that provides the nuclear attraction forces between neutrons to be absent and neutrons to move freely. Now it is possible to calculate the number of neutrons in the void volume (excluding the first envelope, which is the transition boundary structure, where the nuclear and charge density fall sharply down) and then the mass number. For lead the outer radius of the second envelope is $9.66 - 2r_n = 7.98$ fm, its volume is 2130 fm^3. Subtracting from this volume the volume of 30 clusters (120 nucleons) and subtracting the volume of 22 nucleons in the center of the nucleus, we obtain the volume 1452 fm^3, which can accommodate 65 neutrons. As a result, adding the number of protons (82) and neutrons in clusters (60), we obtain the exact mass number for the stable isotope of lead $A = 207$.

The highest density of nuclear matter exists in the nucleus center and in the inner envelopes. Assuming that the nucleons packing density in the nuclear core and in the adjoining envelope are identical, i.e. their nuclear density is the same, and on the basis of the above geometrical considerations, it is possible derive the relation between the number of nucleons in the nucleus core z_{cor} and their number in the adjoining envelope z_{env}, which provides this homogeneity condition:

$$z_{env} = c\left(1 + (\frac{z_{cor}}{c})^{1/3}\right)^3 - z_{cor}\,, \qquad (23)$$

were $c = \frac{4\pi}{3}$.

Equation (23) observed for the lead very precisely: 22 nucleons in the center correspond to 64 nucleons in the 4th

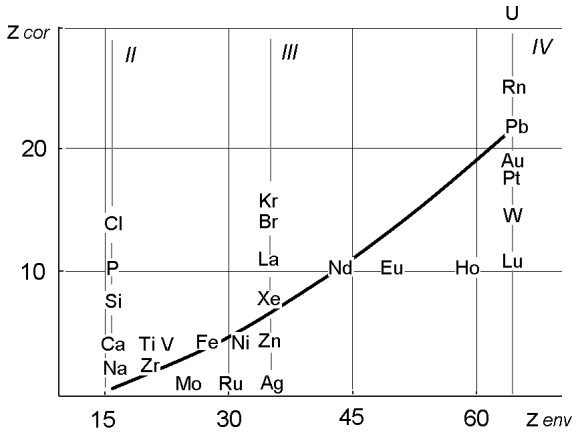

Fig. 3: Condition of the nucleus central part homogeneity with respect to the initial number of nucleons for the stable isotopes of some elements.

envelope (32 protons and 32 neutrons), so it turns out that in the nucleus core neutrons are absent. For the lighter nuclei the inner envelope volume including protons and neutrons can be considered as the core. Condition (23) is also satisfied of about for iron (4 nucleons in 4th envelope, 28 nucleons in 3d envelope), xenon (8 nucleons in the core 36 nucleons in 4th envelope) and for a few other elements. At that, for the nuclei of these elements the observed electric quadrupole moments are close to zero. For most other elements situation may be different; in the general case part of the neutrons or go in the nucleus core, or go in the adjacent envelope, and such nuclei may take a non-spherical shape.

Thus, for the condition (23) to be satisfied, it is necessary (for the metals heavier than iron having one or two electron at the fourth electronic shell) for the additional neutrons that are outside clusters to replenish the fourth inner nucleus envelope and (for the metals with $Z = 37 \ldots 52$, many of lanthanides, and heavy metals before lead) to instil into the nucleus core. For others, mainly non-metals and the elements heavier than lead, the neutrons must replenish the envelope adjoining to the nucleus inner part. Figure 3 shows the position of the curve $z_{cor}(z_{env})$ respect to the initial number of nucleons for stable isotopes of some elements.

Thus, knowing the structure of the atom electron shell and, accordingly, the number of protons in nucleus envelopes and its core, specifying the number of neutrons and having in mind the condition (23), one can try to reproduce the nucleus structure for different atoms and their isotopes. There is a question, how exactly the condition (23) should be satisfy during of additional neutrons distribution? That is whether equation (23) can be solved in integers, as it is done for lead? Perhaps this peculiarity defines some properties of the isotopes: lifetime and others.

To fill the outer nuclear envelopes neutrons there is usually no in enough. Therefore, for some nuclei its outer en-

Even numbered elements

Elements	$_4Be^9$	$_8O^{16}$	$_{14}Si^{28}$	$_{26}Fe^{56}$	$_{30}Zn^{65}$	$_{42}Mo^{96}$	$_{62}Sm^{150}$	$_{74}W^{184}$	$_{92}U^{238}$
Actual, MeV	58.2	128	237	492	567	831	1239	1473	1802
Calculated, MeV	62.6	131	244	487	566	822	1232	1479	1806
Calculated A	9	16	28	56	65	99	151	184	236

Odd numbered elements

Elements	$_5B^{11}$	$_{17}C^{l35}$	$_{21}Sc^{45}$	$_{29}Cu_{64}$	$_{39}Y^{89}$	$_{51}Sb^{122}$	$_{67}Ho^{165}$	$_{83}Bi^{209}$	$_{93}Np^{237}$
Actual, MeV	76.4	298	388	559	775	1033	1344	1640	1795
Calculated, MeV	79.7	303	388	544	757	1009	1344	1636	1821
Calculated A	11	35	45	63	90	123	165	208	238

velope must be squeezed, lose shape of a spherical layer and take the form of a polyhedron, in the corners of which alpha-clusters are. A similar phenomenon is starting to get a confirmation, for example, in [13].

5.4 The nuclei binding energies and the mass numbers

It is well known that nuclear binding energy E_n is calculated by the Weizsäcker semiempirical formula, based on the liquid drop model and consists of five members and empirical coefficients reflecting the contribution of various components in the total binding energy.

Presented above model allows calculating the nucleus binding energy without having to empirical coefficients. As mentioned in section 5.2, the nucleus energy is ultimately determined by the mass-energy of nucleon quarks. Represent this energy as the sum of the nominal energy of eight quarks in all clusters (Figure 2a), included in the envelopes from the first to the fourth as $8 \times 2.2\, z_{kl}$, the total energy of the proton quarks belonging to $p^+{-}e^-$-contour as $2.75(m_1 + 2m_2 + 3m_3 + \ldots)$, and the base energy of the first envelope as $2.75\, z$. The latter may be associated with a potential barrier.

Here it is denoted: z_{kl} is the clusters number, z is the protons total number, m_i is the electrons number in the i-th atom shell.

The final amount when changing the clusters number by the protons number in clusters has the form:

$$E_n = 8.8\, z_{pkl} + 2.75\,(m_1 + 2m_2 + 3m_3 + \ldots + z)\,,\ \text{MeV} \quad (24)$$

where z_{pkl} is the total protons number in the first — the fourth envelopes.

Formula (23) for the binding energy does not depend on the neutrons number; this indicates that for stable isotopes a certain optimum amount of neutrons are in accordance with protons. It turns out that it is possible to calculate the neutrons number based on energy balance considerations, using the dependences previously obtained.

It is considered that the neutrons and protons are different states of nucleons. This is true for the nominal quark masses of nucleons, since their mass-energies are identical and equal to $2 \times 2.2 = 4.4$ MeV. However, the mass-energy of neutron quarks must also comply with the mass-energy of proton quarks, which are included in the circulating $p^+{-}e^-$-contour $2.75(m_1 + 2m_2 + 3m_3 + \ldots)$, net of the basic energy of the unfilled first shell $2.75\, z$ and minus the nominal mass-energy of proton quarks, located in the nucleus center and not connected with neutrons $4.4(z{-}z_{pkl})$.

That is the balance of energy must be from which the neutrons number N and further the mass number $A = N + z$ can be determined:

$$2.75\,(m_1 + 2m_2 + 3m_3 + \ldots) - 2.75\, z - 4.4\left(z{-}z_{pkl}\right) = \\ = 4.4\, N\ \text{MeV}, \quad (25)$$

$$A = z_{pkl} + 0.625\,(m_1 + 2m_2 + 3m_3 + \ldots {-} z) + (4)_{A<140}\,. \quad (26)$$

For the mass number an amendment is necessary in some cases, which, it may be supposed, is the consequence of the presence of alpha-cluster four nucleons in the first envelope, which are split off when the nucleus reaches a certain mass. Thus, for light and medium nuclei the result of formula (26) should be increased by 4. For the heavier nuclei with $A > 140$, the amendment is not necessary, that seems to be due to their natural alpha decay. For the transuranic elements nuclei, as calculations are shown, their binding energy should also be reduced by the amount of the alpha particle binding energy.

Table 1 show the actual and calculated data of the binding energy and mass number rounded to the integer for the stable isotopes of certain elements according to the formulas (24) and (26). These formulas are obtained under the condition that the nuclei structure satisfies the condition (23). Existing slight variations in binding energy to the lower side for medium nuclei can be eliminated by considering their individual features, for example, with taking into account the energy bonds of additional neutrons, which replenish the core or adjoining nucleus envelope.

6 Conclusion

It seems surprising that the complex nature of nuclear forces and the structure of atomic nuclei proved possible to be largely understood without involving actual quantum concepts and complex mathematical apparatus.

The mass of equivalent to the Higgs boson mass are obtained, the coupling constants in different types of interactions, the binding energy of the deuteron, triton, and alpha particles are defined, the possible ranges of alpha particles energies are identified, and dependence of the nucleon-nucleon interaction from a distance is explained. Based only on the composition of the atom electron shells, it was possible to determine the nuclei binding energies, the nucleus neutron numbers, to reveal the important features of nuclei.

Obviously, these results indicate that the model adequately reflects the fundamental features of the atomic nucleus structure. These results give reason to believe that the foregoing model can become the basis of further theoretical developments for detailed describing the properties of nuclei and their behavior in nuclear reactions.

Submitted on December 19, 2014 / Accepted on December 25, 2014

References

1. DeWitt B.S. Quantum gravity. *Scientific American*, v. 249, December 1983, 112–129.
2. Belyakov A.V. Charge of the electron, and the constants of radiation according to J. A. Wheeler's geometrodynamic model. *Progress in Physics*, 2010, v. 4, 90–94.
3. Belyakov A.V. Macro-analogies and gravitation in the micro-world: further elaboration of Wheeler's model of geometrodynamics. *Progress in Physics*, 2012, v. 2, 47–57.
4. Belyakov A.V. On the independent determination of the ultimate density of physical vacuum. *Progress in Physics*, 2011, v. 2, 27–29.
5. Belyakov A.V. On materiality and dimensionality of the space. Is there some unit of the field? *Progress in Physics*, 2014, v. 10, 203–206.
6. Alexandrov Y.A. Polarizability of the neutron. The possibility of its determination of the neutron experiments. *Particle Physics and Nuclear Physics*, 2001, v. 2, issue 6.
7. Krivokhizhin V.G., Kotikov A.V. The structure functions of nucleons and the definition of the coupling constant of the strong interaction. *Particle Physics and Nuclear Physics*, 2009, v. 40, issue 7.
8. Ishkhanov B.S., Cabin E.I. Nuclear and Particle Physics. The Twentieth Century. Moscow University Publishers, Moscow, 2000.
9. Berezhnoy Y.A., Mikhailyuk V.P. Alpha-clustering in the scattering particles and light nuclei by nuclei. *Particle Physics and Nuclear Physics*, 2008, v. 39, issue 2.
10. Kadmensky S.G. Clusters in the Nucleus. *Soros Educational Journal*, 2000, issue 3.
11. Dulov E.N., Vagizov F.G., Bikchantaev M.M., Pyataev A.V. Gainov R.R. Spectra of Alpha-Particles, Semiconductor Detectors. Kazan State University, Institute of Physics, Kazan, 2013.
12. Perfilov N.A., Romanov Y.F., Solovyov Z.I. Fission of heavy nuclei with the emission of long-range α-particles. *Physics-Uspekhi*, July I960, v. LXXI, issue 3.
13. Dudek J., Curien D., Dubray N., Dobaczewski J., Pangon V., Olbratowski P., and Schunck N. Island of rare-Earth nuclei with tetrahedral and octahedral symmetries: possible experimental evidence. *Phys. Rev. Lett.*, 2006, v. 97, 072501.

Motion-to-Motion Gauge Entails the Flavor Families

Felix Tselnik
Ben-Gurion University of the Negev, P.O.B. 653, Beer-Sheva 84105, Israel
E-mail: tselnik@ee.bgu.ac.il

Charge and mass gauging procedure is carried out by means of counting the oscillation numbers of an auxiliary top-speed signal ("photons") between the appropriately ordered electrons and positrons, moving under their interaction along the diagonals of the cube toward its center (the "cube star"). Regular lattices composed of such stars transport the values of charge and mass over space-time regions. The gauge consists in detection of the cube symmetry in each star. However, the detected symmetry can also be observed, even if some particles of the basic electron/positron star are replaced with heavy mesons. These become an unavoidable byproduct of the gauge procedure. Two possible subsymmetries of the cube realizing such replacement correspond to two mesons, but the regularity of the whole lattice holds only for some particular values of their masses. Numerical solutions to the non-linear ODE systems describing this situation yield these masses in terms of electron mass, which are close to those of the μ- and τ-mesons.

1 Introduction

The existence of the three flavor families remains a mystery, and it appears rather artificial in the otherwise self-contained structure of the standard model of particle physics (see, for instance, [1]). As in all basic structures of physics, theories must agree with experimental facts, and, in turn, the performance of experiments depends on existing theoretical conceptions. The design of measuring devices includes their gauge, which is an intermediary between the measurement of interest and some standard test measurements. In order to eliminate clocks and rods in the gauge, which might hide some features of the desired correspondence, we suggested a direct motion-to-motion gauge [2, 3]. We shall show that the flavor families naturally arise from the particular way this gauge could be carried out. Since all related experiments are ultimately based on the observation of the trajectories of charged particles in external electromagnetic fields, the gauge of electric charges and masses of particles is at the heart of any measurement. A relevant gauge procedure could use a regular lattice comprised of elementary cells ("stars"), each one being a standard configuration of the trajectories of test particles that are identical, apart from the sign of their charges [2, 3]. Starting with the stars that are primary for the gauge lattice, the whole lattice is constructed in such a way that the primary stars completely define secondary ones. The resulting relay races make it possible to transport the initial values of charge and mass over a chosen space-time region. In an appropriate construction of the lattice, each star could be connected to a previous star along various sequences of intermediate stars. The preservation of charge and mass over such transports might be detected, provided various paths connecting a pair of stars reveal the same symmetry at both ends according to the dynamics of involved particles.

In order to realize this program one needs a method to construct standard stars unambiguously. For this purpose, it was proposed to count top signal oscillations between the particles of the star [2]. No rods or clocks are then needed, provided the elementary stars possess some symmetry belonging to the Platonic solids. In this communication, we confine ourselves to the lepton sector of elementary particles, corresponding to the cube subsystem of the full dodecahedron structure. To this end, consider electrons and positrons moving along the diagonals of the cube toward its center under mutual attraction — the "cube star". The cube consists of two interlaced tetrahedrons — one for electrons, another for positrons, and the star is thus electrically neutral as a whole. Charge is being gauged by means of detecting the cube symmetry as being seen in the equality of the related numbers of photon oscillations, so that the detection of even one extra oscillation is sufficient to find this symmetry broken. (It is convenient to replace formally the counting of inter-particle oscillations with that between the particle and an imaginary central body; the translation is straightforward.) Of particular interest is the limiting case of the finest lattice, in which only one photon oscillation is sufficient to detect the symmetry of the star. Just this finest star will be considered in what follows.

The regular lattice comprises the stars as elementary cells to form a whole charge gauging structure. For this to be possible, the electrons/positrons are bound to turn into neutrinos at the center: Otherwise, the exit potential together with the radiation reaction force would prevent their leaving the star, so destroying the lattice forming connections. We regard neutrinos massless (or having a mass that is negligible as compared to that of other involved particles), hence moving practically with the velocity of light independently of their kinetic energy.

Only the simplest case of cube star symmetry breaking was considered in the charge gauging procedure [2, 3], i.e. that in which asymmetry may occur only between the two opposite-charge tetrahedrons of the cube. The breaking of

cube symmetry in this case consists in this that particles belonging to different tetrahedrons have dissimilar masses m and/or absolute values of charge e, while these parameters remain identical within each tetrahedron. Perfect symmetry will be observed, provided all the involved particles have the same values of *both* m and $|e|$. In this case, the asymmetry to be detected is, in a sense, the weakest, and we assign it to the first flavor family, i.e. to that of the electron. We regard this — electron/positron — star as the basic one and ask whether or not our photon oscillations counting procedure might detect the symmetry as observed, even if some electrons/positrons in the star are being replaced with different particles. Detection of a perfect star with our method requires both charges and masses of the involved particles to be identical. Upon assuming the charges to remain equal, let us consider the lattice, in which some particles have a different mass. While electrons must turn into neutrinos in each star, these foreign particles ("mesons") are able to pass the center intact, since the exit barrier decreases there. They can then take part in the secondary stars. For this to be possible, they must satisfy three following requirements:

i. Preserve proper charge distribution in each star;

ii. Pass successfully the symmetry detection in the stars as carried out by counting photon oscillations;

iii. Yield the definite output velocity (e.g., equal to the input velocity) to be suitable over a long line of successive stars.

To fulfill these requirements, we have only two parameters at our disposal to be controlled over the whole lattice, that is, the mass and the velocity of the meson at the star entrance. We guess only much heavier mesons to be met with. Since the lattice is a ready structure and the slower mesons are just "impurities" in it, they will enter the next star with some time lag.

Besides the basic star, there exist only two configurations having weaker sub-symmetries. Depending on the mass found for the related foreign particle, one of the sub-symmetries will be ascribed to the τ-meson, and another to the μ-meson.

In the first sub-symmetry, only one pair of opposite electron and positron is replaced by the meson/anti-meson pair. Their diagonal is the natural axis of the star symmetry, since under the interaction in the star the mesons keep moving along this axis. The trajectories of the remaining three electrons and three positrons are curvilinear, though confined pair-wise to three planes (the members of each pair don't belong to a common diagonal of the cube). Then the absolute values of the Cartesian coordinates of all six electrons/positrons, both along and transverse the axis, will be the same. We refer to this case as (6:2) sub-symmetry. (In this notation, the electron/positron star is (8:0) sub-symmetry.) Contrary to the basic (8:0) case, magnetic part of the interaction is no longer cancelled on the curved trajectories in stars possessing only sub-symmetries, though the total resulting interaction still leaves the particles on the same planes they would move under the electric force alone.

In the second sub-symmetry, two identical meson/anti-meson pairs replace electron-positron pairs. Now all eight trajectories are curved though confined to the two mutually orthogonal planes, one of which carries only electrons and positrons, while another — only mesons and anti-mesons. Within each of these planes, the absolute values of the appropriately chosen Cartesian coordinates of its particles will be the same. We refer to this case as (4:4) sub-symmetry. Following the previous argument [2], we ignore the terms with retarded interaction in the equations describing the motion of the particles in the star, but radiation reaction of the accelerated particles may be important. However, even rough estimation of this multiple soft photons radiation will be sufficient to distinguish flavor families, provided the mesons are much heavier than the electron, and the mesons related to the two possible sub-symmetries strongly differ in their masses. As was found [2], the radius of the star is much smaller than the classical electron radius, still the smallest radius down to which the photon oscillations are being counted might be of the order or even larger than the classical radius r_0 of the meson. Therefore, the effect of radiation on the motion of the star particles should be estimated for the electrons and the mesons differently though the very motion of the center of the electron wave packet, which only matters in the photon oscillations counting procedure, might be described classically in virtue of the Ehrenfest theorem. In so complicated systems as the stars containing several interacting particles, accurate calculation of radiation would be rather complicated, and, moreover, it is well known [4] that r_0 is the limit of validity of the electrodynamics, while the trajectories for the finest star lie well deeper this value. Therefore, QED is needed to determine single photon radiation of electrons, pair production etc. in the very strong (even vacuum violating) electric field [5]. However, the motion of the electrons is of interest here only inasmuch as it influences that of the mesons, and we need not go into fine details for the electron component of the star. We thus choose to model radiation of the electrons with an appropriate functional factor S that tempers the energy increase of the accelerated electrons. This factor will depend on a parameter q, varying which one can match a solution for the mesons according to the threshold where the quantum single photon radiation reaction exceeds the driving force in the star. We assume that S depends only on the kinetic energy of the electron via the relativistic factor γ_e: $S = \exp[-(\gamma_e^{-2} - \gamma_{ei}^{-2})/q^2]$, where γ_{ei} is the initial value γ_e of in the star. So, $S = 1$ at the initial moment, while for appropriate solutions the value of q must be so chosen that its final value $\gamma_{e,f} \cong 5$, in accordance with the charge gauge [2] in the basic (8:0) star unperturbed by mesons.

The mesons are expected to move unchanged over many successive stars. Their motion should be analyzed in respect of the possibility to sustain a regular lattice, that is, of the

$$
\left.
\begin{aligned}
S^{-1}\frac{d\beta_{eu}}{d\chi} &= -4u_e\gamma_e^{-5}\left[4u_e^2+v_e^2-(2u_e\beta_{ev}+v_e\beta_{eu})^2\right]^{-\frac{3}{2}}-\frac{1}{4}u_e\gamma_e^{-5}\left[u_e^2+v_e^2-(u_e\beta_{ev}-v_e\beta_{eu})^2\right]^{-\frac{3}{2}}+\\
&+\left[(u_M-u_e)\left(1-\beta_{eu}^2\right)-v_e\beta_{ev}(\beta_M-\beta_{eu})\right]\gamma_M^{-2}\gamma_e^{-1}\left[(u_M-u_e)^2+v_e^2\gamma_M^{-2}\right]^{-\frac{3}{2}}+\\
&+\left[(u_M+u_e)\left(1-\beta_{eu}^2\right)+v_e\beta_{ev}(\beta_M-\beta_{eu})\right]\gamma_M^{-2}\gamma_e^{-1}\left[(u_M+u_e)^2+v_e^2\gamma_M^{-2}\right]^{-\frac{3}{2}}\\
S^{-1}\frac{d\beta_{ev}}{d\chi} &= -v_e\gamma_e^{-5}\left[4u_e^2+v_e^2-(2u_e\beta_{ev}+v_e\beta_{eu})^2\right]^{-\frac{3}{2}}-\frac{1}{4}v_e\gamma_e^{-5}\left[u_e^2+v_e^2-(u_e\beta_{ev}-v_e\beta_{eu})^2\right]^{-\frac{3}{2}}+\\
&+3^{-\frac{1}{2}}v_e^{-2}\gamma_e^{-5}\left(1-\beta_{eu}^2-\frac{1}{4}\beta_{ev}^2\right)^{-\frac{3}{2}}-\left[(u_M-u_e)\beta_{eu}\beta_{ev}+v_e\left(1-\beta_M\beta_{eu}-\beta_{ev}^2\right)\right]\gamma_M^{-2}\gamma_e^{-1}\times\\
&\times\left[(u_M-u_e)^2+v_e^2\gamma_M^{-2}\right]^{-\frac{3}{2}}-\left[(u_M+u_e)\beta_{eu}\beta_{ev}-v_e\left(1-\beta_M\beta_{eu}-\beta_{ev}^2\right)\right]\gamma_M^{-2}\gamma_e^{-1}\left[(u_M+u_e)^2+v_e^2\gamma_M^{-2}\right]^{-\frac{3}{2}}\\
\eta^{-1}\frac{d\beta_M}{d\chi} &= -3(u_M-u_e)\gamma_M^{-3}\gamma_e^{-2}\left[(u_M-u_e)^2+v_e^2\gamma_e^{-2}\right]^{-\frac{3}{2}}+\\
&+3(u_M+u_e)\gamma_M^{-3}\gamma_e^{-2}\left[(u_M+u_e)^2+v_e^2\gamma_e^{-2}\right]^{-\frac{3}{2}}-\frac{1}{4}u_M^{-2}\gamma_M^{-5}
\end{aligned}
\right\}. \quad (1)
$$

repeatability of their initial and final velocities either in each star or, at least, for a long sequence of successive stars. For each of the sub-symmetries this possibility depends on the mass of the related meson. Interaction of the electrons and the mesons results in that that the motion of the electrons depends on the meson mass as well, hence the ratio of electron to meson masses might be obtained from our condition of the whole lattice regularity. Motion of heavy mesons might be described classically.

Strictly speaking, one has to include explicitly the meson radiation reaction term in the equation of motion. It would be convenient however to use, wherever possible, perturbation methods to determine the radiation reaction, provided it is much less than the driving force: The equation of motion could be solved for the driving force alone, and then the radiated energy is found using this solution. The final kinetic energy of the meson is determined by subtracting the radiation loss from its value as obtained before (see, e.g., [4]). This estimation is certainly valid for a large enough mass, since the radiation cross section contains inverse square of the mass value. For this reason, we may use classical, that is, multiple soft photon emission value for the radiation of heavy mesons.

2 (6:2) sub-symmetry

In this case, the meson/anti-meson pair still moves along a straight line, whereas the curved trajectories of the three electron family pairs confine to three planes intersecting over the meson axis with the relative angles $\frac{2\pi}{3}$. It is convenient therefore to measure the z coordinate along the meson axis, and to choose the second coordinate ρ at each electron plane as the distance from this axis. Then the values of ρ for each particle of the electron family (each one measured in its own plane) are equal, and the absolute values of z are the same for all electrons. In dimensionless variables:

$$
\chi=\frac{ct}{r_0},\quad u_e=\frac{z_e}{r_0},\quad v_e=\frac{\rho}{r_0},\quad \beta_{eu}=\frac{du_e}{d\chi},
$$

$$
\beta_{ev}=\frac{du_v}{d\chi},\quad u_M=\frac{z_M}{r_0},\quad \beta_M=\frac{du_M}{d\chi},\quad \eta=\frac{m_e}{m_M},
$$

$$
\gamma_e=\left(1-\beta_{eu}^2-\beta_{ev}^2\right)^{-\frac{1}{2}},\quad \gamma_M=\left(1-\beta_M^2\right)^{-\frac{1}{2}},
$$

where the subscript e marks electrons, M means mesons, c is the speed of light. The system of three ODEs describes the motion of the electrons and the mesons in the star under their interaction. Using the well-known expression for the field of a fast moving charge [4], this system can be written as shown in Eqs. 1 on top of this Page 101.

This system should be numerically solved under the initial conditions taken from the solution for the basic electron family [2]: the initial radius of the electrons $r_{e,i}=0.24r_0$, and $\gamma_{e,i}=3.2$. In our variables, these correspond to:

$$
\left.
\begin{aligned}
&\chi_i=0,\quad u_{e,i}=\frac{r_i}{3r_0},\quad v_{e,i}=\frac{2\sqrt{2}r_i}{3r_0}\\
&\beta_{eu,i}=\frac{1}{3}\beta_{e,i},\beta_{ev,i}=\frac{2\sqrt{2}}{3}\beta_{e,i}\\
&\beta_{e,i}=\left(1-\gamma_{e,i}^{-2}\right)^{\frac{1}{2}},\quad \beta_{M,i}=\left(1-\gamma_{M,i}^{-2}\right)^{\frac{1}{2}}
\end{aligned}
\right\}. \quad (2)
$$

In the perturbation approach, the value of $\gamma_{M,i}$ for the regular lattice should be equal to the final $\gamma_{M,f}$ at the exit of the preceding star (or a group of stars) as obtained by subtracting the radiation term $\gamma_{M,rad}$ and the term of the exit potential barrier $\gamma_{M,ex}$ from the final value of the solution to the system (1). These terms are:

$$
\gamma_{M,rad}=\frac{2}{3}\eta\int_0^{\chi_f}d\chi\left(\frac{d\beta_M}{d\chi}\right)^2\gamma_M^3, \quad (3)
$$

$$\gamma_{M,ex} \cong 12^{-1}\eta u_{M,f}^{-1}\gamma_{M,i}^{-2}. \quad (4)$$

It is assumed in (4) that $\gamma_{M,ex} \ll \gamma_{M,f} - \gamma_{M,i}$, and $u_{M,f} \ll u_{M,i}$. (The first inequality holds since the deceleration from the opposite meson is at least an order of magnitude less than the acceleration from the electrons because of the relativistic anisotropy of the electric field of fast moving charges.)

Then the value of $u_{M,i}$ is: $u_{M,i} = \frac{r_i}{r_0}(2-\beta_{M,f})$, where $\beta_{M,f} = (1-\gamma_{M,f}^{-2})^{1/2}$.

The solution for (1) goes down to the final value $r_{e,2} = 0.002 r_0$, that is, $(u_{e,2}^2 + v_{e,2}^2 = 0.002)^{1/2}$. This value of $r_{e,2}$ corresponds to the average value of the weak Yukawa-type potential (instead of $r_{e,2} = 0.003 r_0$ found in the charge gauge procedure for (8:0) case [2]). We assume that the electrons and positrons disappear at $r < r_{e,2}$. The value of χ_f in (3) should be defined by the condition that the function $r_e(\chi_f) = r_{e,2}$ for the first time.

The solution must meet the requirement for the meson to be unrecognized with our method of symmetry detection, i.e., that the numbers of the photon oscillations remain equal for the electron and the meson. To this end, consider the photon emitted at $r_e(0) = r_i$ and reaching $r_{e,1} = r_e(\chi_{e,1})$ after being reflected at the star center. Then, $\chi_{e,1} = (u_{e,i}^2 + v_{e,i}^2)^{1/2} + (u_{e,1}^2 + v_{e,1}^2)^{1/2}$, where the last member should be taken from (1). Similarly for the meson: $\chi_{M,1} = u_{M,i} + u_{M,1}$. Neglecting the small (because $r_{M,1} \gg r_{M,2} \approx r_{M,i} - r_{e,i}$) difference in the initial positions, we write the condition for the second photon not to have enough time to oscillate between the electron and the center over the first oscillation of the meson as:

$$\left(u_{e,1}^2 + v_{e,1}^2\right)^{\frac{1}{2}} + 0.002 > u_{M,1}. \quad (5)$$

This inequality ensures that the electron annihilates within the time of the first oscillation for the meson. Since the meson doesn't annihilate, the opposite inequality preventing the second photon oscillation for the meson within the time of the first photon oscillation for the electron is:

$$u_{M,1} > \left(u_{e,1}^2 + v_{e,1}^2\right)^{\frac{1}{2}}. \quad (6)$$

Upon solving the system (1) with $q = 2$, it was found that only for $\eta = 0.0003$ there exists an "equilibrium cycle" that repeats itself over the series of the stars (possibly with small shift of $\gamma_{M,f}$ from a mean value in a star to be compensated with some opposite shift in the next star) under the conditions (5) and (6) for some particular value of $\gamma_{M,i}$. For $\gamma_{M,i} = 5.150408$, and $u_{M,i} = 0.244567$, the system (1) yields $\gamma_{M,f} = 5.248322 \neq \gamma_{M,i}$, but already in the next star with $u_{M,i}$, following from this $\gamma_{M,f} : u_{M,i} = 0.244397$ ($\gamma_{M,i} = 5.248322$), we obtain $\gamma_{M,f} = 5.150408$, and the solution for the whole trajectory of the meson repeats itself infinitely. For these two consecutive stars: $(u_{e,1}^2 + v_{e,1}^2)^{1/2} = 0.00437$ and 0.003782, $u_{M,1} = 0.004815$ and 0.003785 respectively, so both (5) and (6) are fulfilled for each of them; $u_{M,f} = u_{M,2} = 0.00214$, $(u_{e,1}^2 + v_{e,1}^2)^{1/2} = 0.002$, $\gamma_{e,f} = 5.280387$. According to (3) and (4), radiation decreases $\gamma_{M,f}$ by only $\gamma_{M,rad} \approx 10^{-4}$, and the exit potential by $\gamma_{M,ex} \approx 10^{-3}$. Both are small as compared to the variation in the energy of the meson along its trajectory: $\left|\gamma_{M,f} - \gamma_{M,i}\right| \approx 0.05$. Hence, our assumption for deceleration from the exit potential barrier to be negligible for (6:2) sub-symmetry is reasonable. No acceptable solutions exist for other values of η. Although at each η there is a value of $\gamma_{M,i}$, for which the electrons and the mesons meet at $(u_{e,2}^2 + v_{e,2}^2)^{1/2} \approx u_{M,2} \leqslant 0.002$, but $\gamma_{M,f} \neq \gamma_{M,i}$, tending to increase monotonously, when extended over the next stars. Eventually the electron radius $(u_{e,2}^2 + v_{e,2}^2)^{1/2}$ becomes larger than the weak interaction threshold 0.002 everywhere on the trajectory. E.g., for $\eta = 0.00015$ this happens at $\gamma_{M,i} \approx 5.46$, while for $\eta = 0.0004$ at $\gamma_{M,i} \approx 5.48$. (For $\eta = 0.0002$, only (6) is broken.) Then the annihilation of the electrons becomes impossible, and our lattice will be ruined.

This behavior of the solutions to (1) can be explained as follows. If in the immediate vicinity of the star center the positive, say, meson lags with respect to the three nearest electrons, it is accelerated, while the electrons are decelerated to be overtaken by the meson and vice versa. Which case is realized depends on η and on $\gamma_{M,i}$. The equilibrium along the whole series comes from balance in the interaction. If situation is far from the balance, the meson will move much ahead or behind the electrons. Then its attraction will not be able to compensate for the reciprocal repulsion of the electrons, resulting in the increase of $(u_{e,2}^2 + v_{e,2}^2)^{1/2}$, and this quantity becomes eventually larger than 0.002.

3 (4:4) sub-symmetry

In this case, electrons and mesons move in two orthogonal planes intersecting at some axis of the cube (z) that connects the centers of the pair of its opposite faces. In each of these planes, the absolute values of the two Cartesian coordinates of the particles are the same for its four particles — electrons or mesons — due to the (4:4) symmetry. It is convenient therefore to choose a coordinate frame with the (x) axis in the electron plane and the (y)axis in the meson plane.

We guess in this case $\eta \gg 0.0003$, since the effect of four electrons on four mesons is smaller than that of six electrons on two mesons. Hence, radiation is expected to be important, since the meson must radiate much more energy with main contribution coming from the close neighborhood of the star center. This effect owes to the smaller meson mass as well as to the curvature of the trajectory, since, given force, transverse acceleration scales as γ^{-1} while longitudinal one only as γ^{-3}. Although it was long shown [4, 6] that, in the relativistic case, the energy radiated by the particle might be even larger than that received under external acceleration, we cannot use this result directly. In these references, the accelerating field was considered given in advance, i.e. independent of the particle's motion, whereas in our case back influence of radiation

$$
\left.
\begin{aligned}
S^{-1}\frac{d\beta_{eu}}{d\chi} = &-\frac{1}{4}\left(1-\beta_{ev}^2\right)^{-\frac{1}{2}}\left(1-\beta_{eu}^2\right)\gamma_e^{-3}u_e^{-2}-\frac{1}{4}\left(1-\beta_{eu}^2\right)^{-\frac{1}{2}}\beta_{eu}\beta_{ev}\gamma_e^{-3}v_e^{-2}-\\
&-\frac{1}{4}\left[u_e\left(\gamma_e^{-2}+\beta_{eu}^2\beta_{ev}^2+\beta_{eu}\beta_{ev}^3\right)-v_e\left(2\beta_{eu}\beta_{ev}-\beta_{eu}^3\beta_{ev}^2-\beta_{eu}^2\beta_{ev}^2\right)\right]\gamma_e^{-3}\left[u_e^2+v_e^2-(u_e\beta_{ev}-v_e\beta_{eu})^2\right]^{-\frac{3}{2}}+\\
&+2\left[(u_M+u_e)\left(1-\beta_{ev}\beta_{Mu}\right)\left(1-\beta_{eu}^2\right)-v_e\left(1-\beta_{eu}\beta_{Mu}\right)\beta_{eu}\beta_{ev}\right]\gamma_e^{-1}\gamma_M^{-2}+\\
&+\left\{v_e^2\gamma_M^{-2}+w_M^2+(u_M+u_e)^2-\left[(u_M+u_e)\beta_{Mw}-w_M\beta_{Mu}\right]^2\right\}^{-\frac{3}{2}}+\\
&+2\left[(u_M-u_e)\left(1-\beta_{ev}\beta_{Mu}\right)\left(1-\beta_{eu}^2\right)-v_e\left(1-\beta_{eu}\beta_{Mu}\right)\beta_{eu}\beta_{ev}\right]\times\\
&\times\gamma_e^{-1}\gamma_M^{-2}\left\{v_e^2\gamma_M^{-2}+w_M^2+(u_M-u_e)^2-\left[(u_M-u_e)\beta_{Mw}-w_M\beta_{Mu}\right]^2\right\}^{-\frac{3}{2}}\\
S^{-1}\frac{d\beta_{ev}}{d\chi} = &-\frac{1}{4}\left\{u_e\beta_{ev}\left(\beta_{eu}+\beta_{ev}\right)\left(1-\beta_{ev}^2\right)+v_e\left[1-\beta_{ev}\left(\beta_{eu}+\beta_{ev}\right)\left(1-\beta_{eu}\beta_{ev}\right)\right]\right\}\gamma_e^{-3}\times\\
&\times\left[u_e^2+v_e^2-(u_e\beta_{ev}-v_e\beta_{eu})^2\right]^{-\frac{3}{2}}+\frac{1}{4}\left(1-\beta_{eu}^2\right)^{\frac{1}{2}}\left(1-\beta_{ev}^2\right)\gamma_e^{-3}v_e^{-2}+\frac{1}{4}\left(1-\beta_{eu}^2\right)^{-\frac{1}{2}}\beta_{eu}\beta_{ev}\gamma_e^{-1}u_e^{-2}+\\
&+2\left[(u_M+u_e)\left(1-\beta_{ev}\beta_{Mu}\right)\beta_{eu}\beta_{ev}-v_e\left(1-\beta_{eu}\beta_{Mu}\right)\left(1-\beta_{ev}^2\right)\right]\times\\
&\times\gamma_M^{-2}\gamma_e^{-1}\left\{v_e^2\gamma_M^{-2}+w_M^2+(u_M+u_e)^2-\left[(u_M+u_e)\beta_{Mw}-w_M\beta_{Mu}\right]^2\right\}^{-\frac{3}{2}}-\\
&-2\left[(u_M-u_e)\left(1-\beta_{ev}\beta_{Mu}\right)\beta_{eu}\beta_{ev}-v_e\left(1-\beta_{eu}\beta_{Mu}\right)\left(1-\beta_{ev}^2\right)\right]\gamma_M^{-2}\gamma_e^{-1}\times\\
&\times\left\{v_e^2\gamma_M^{-2}+w_M^2+(u_M-u_e)^2-\left[(u_M-u_e)\beta_{Mw}-w_M\beta_{Mu}\right]^2\right\}^{-\frac{3}{2}}\\
\frac{d^2\beta_{Mu}}{d\chi^2} = &\frac{3}{2}\left(\eta^{-1}\frac{d\beta_{Mu}}{d\chi}-U\right)\gamma_M^{-1}-2\left(\beta_{Mu}\frac{d\beta_{Mu}}{d\chi}+\beta_{Mw}\frac{d\beta_{Mw}}{d\chi}\right)\times\\
&\times\left[\frac{d\beta_{Mu}}{d\chi}-\gamma_M^{-2}\beta_{Mw}\left(\beta_{Mu}\frac{d\beta_{Mw}}{d\chi}-\beta_{Mw}\frac{d\beta_{Mu}}{d\chi}\right)\right]-2\gamma_M^{-2}\beta_{Mu}\left(\beta_{Mu}\frac{d\beta_{Mu}}{d\chi}+\beta_{Mw}\frac{d\beta_{Mw}}{d\chi}\right)^2\\
\frac{d^2\beta_{Mw}}{d\chi^2} = &\frac{3}{2}\left(\eta^{-1}\frac{d\beta_{Mw}}{d\chi}-W\right)\gamma_M^{-1}-2\left(\beta_{Mu}\frac{d\beta_{Mu}}{d\chi}+\beta_{Mw}\frac{d\beta_{Mw}}{d\chi}\right)\times\\
&\times\left[\frac{d\beta_{Mw}}{d\chi}+\gamma_M^{-2}\beta_{Mu}\left(\beta_{Mu}\frac{d\beta_{Mw}}{d\chi}-\beta_{Mw}\frac{d\beta_{Mu}}{d\chi}\right)\right]-2\gamma_M^{-2}\beta_{Mu}\left(\beta_{Mu}\frac{d\beta_{Mu}}{d\chi}+\beta_{Mw}\frac{d\beta_{Mw}}{d\chi}\right)^2
\end{aligned}
\right\},\quad (7)
$$

where the functions U and W are expressed as follows

$$
\begin{aligned}
U = &-\frac{1}{4}\left(1-\beta_{Mw}^2\right)^{-\frac{1}{2}}\left(1-\beta_{Mu}^2\right)\gamma_M^{-3}u_M^{-2}-\frac{1}{4}\left(1-\beta_{Mu}^2\right)^{-\frac{1}{2}}\beta_{Mu}\beta_{Mw}\gamma_{Mw}^{-3}w_M^{-2}-\\
&-\frac{1}{4}\left[u_M\left(\gamma_M^{-2}+\beta_{Mu}^2\beta_{Mw}^2+\beta_{Mu}\beta_{Mw}^3\right)-w_M\left(2\beta_{Mu}\beta_{Mw}-\beta_{Mu}^3\beta_{Mw}^2\right)\right]\gamma_M^{-3}\times\\
&\times\left[u_M^2+w_M^2-(u_M\beta_{Mw}-w_M\beta_{Mu})^2\right]^{-\frac{3}{2}}+2\left[(u_M+u_e)\left(1-\beta_{Mw}\beta_{eu}\right)\left(1-\beta_{Mu}^2\right)-w_M\left(1-\beta_{Mu}\beta_{eu}\right)\beta_{Mu}\beta_{Mw}\right]\times\\
&\times\gamma_M^{-1}\gamma_e^{-2}\left\{w_M^{-2}\gamma_e^{-2}+v_e^2+(u_M+u_e)^2-\left[(u_M+u_e)\beta_{ev}-v_e\beta_{eu}\right]^2\right\}^{-\frac{3}{2}}-\\
&-2\left[(u_M-u_e)\left(1-\beta_{Mw}\beta_{eu}\right)\left(1-\beta_{Mu}^2\right)-w_M\left(1-\beta_{Mu}\beta_{eu}\right)\beta_{Mu}\beta_{Mw}\right]\gamma_M^{-3}\times\\
&\times\left\{w_M^2\gamma_e^{-2}+v_e^2+(u_M-u_e)^2-\left[(u_e-u_M)\beta_{ev}-v_e\beta_{eu}\right]^2\right\}^{-\frac{3}{2}},
\end{aligned}
$$

$$W = -\frac{1}{4}\left\{u_M\beta_{Mw}\left(\beta_{Mu}+\beta_{Mw}\right)\left(1-\beta_{Mw}^2\right)+w_M\left[1-\beta_{Mw}\left(\beta_{Mu}+\beta_{Mw}\right)\left(1-\beta_{Mu}\beta_{Mw}\right)\right]\right\}\times$$
$$\times\ \gamma_M^{-3}\left[u_M^2+w_M^2-\left(u_M\beta_{Mw}-w_M\beta_{Mu}\right)^2\right]^{-\frac{3}{2}}+\frac{1}{4}\left(1-\beta_{Mu}^2\right)^{\frac{1}{2}}\left(1-\beta_{Mw}^2\right)\gamma_M^{-3}w_M^{-2}+$$
$$+\ \frac{1}{4}\left(1-\beta_{Mu}^2\right)^{-\frac{1}{2}}\beta_{Mu}\beta_{Mw}\gamma_M^{-1}u_M^{-2}+2\left[\left(u_M+u_e\right)\left(1-\beta_{Mw}\beta_{eu}\right)\beta_{Mu}\beta_{Mw}-w_M\left(1-\beta_{Mu}\beta_{eu}\right)\left(1-\beta_{Mw}^2\right)\right]\times$$
$$\times\ \gamma_e^{-2}\gamma_M^{-1}\left\{w_M^2\gamma_e^{-2}+v_e^2+\left(u_M+u_e\right)^2-\left[\left(u_M+u_e\right)\beta_{ev}-v_e\beta_{eu}\right]^2\right\}^{-\frac{3}{2}}+$$
$$+\ 2\left[\left(u_M-u_e\right)\left(1-\beta_{Mw}\beta_{eu}\right)\beta_{Mu}\beta_{Mw}-w_M\left(1-\beta_{Mu}\beta_{eu}\right)\left(1-\beta_{Mw}^2\right)\right]\times$$
$$\times\ \gamma_e^{-2}\gamma_M^{-1}\left\{w_M^2\gamma_e^{-2}+v_e^2+\left(u_M-u_e\right)^2-\left[\left(u_M-u_e\right)\beta_{ev}-v_e\beta_{eu}\right]^2\right\}^{-\frac{3}{2}}.$$

on the field-generating particles is important. We have thus to include the radiation reaction term explicitly in the equation of motion. But the value $\eta \approx 0.005$ is just at the boundary of self-contradiction of electrodynamics for the meson at the weak interaction threshold. Also quantum effects, however weaker than those for the electron, might alter radiation there. Moreover, deceleration of the meson at the exit potential barrier coming from other mesons as well as radiation accompanying this deceleration cannot be neglected now.

However, it would be inadequate merely to introduce a functional factor like that used above for the electron, because details of the meson trajectory are now in question. In order to trace the tendency, we shall instead try to approach the value $\eta = 0.005$ from below, i.e. from larger meson mass.

Again, in dimensionless variables

$$\chi=\frac{ct}{r_0},\quad u_e=\frac{z_e}{r_0},\quad v_e=\frac{x_e}{r_0},\quad \beta_{eu}=\frac{du_e}{d\chi},\quad \beta_{ev}=\frac{dv_e}{d\chi},$$
$$\gamma_e=\left(1-\beta_{eu}^2-\beta_{ev}^2\right)^{-\frac{1}{2}},$$
$$u_M=\frac{z_M}{r_0},\quad w_M=\frac{y_M}{r_0},\quad \beta_{Mu}=\frac{du_M}{d\chi},\quad \beta_{Mw}=\frac{dw_M}{d\chi},$$
$$\gamma_M=\left(1-\beta_{Mu}^2-\beta_{Mw}^2\right)^{-\frac{1}{2}},$$

the system of four ODE equations — Eqs. 7 shown in the previous Page 103, with the functions U and W explained on the same Page Page 103 and on top of this Page 104 — describes the relativistic motion of electrons and mesons in the (4:4) cubic star under their interaction.

This system will be numerically solved under following initial conditions:

$$u_{e,i}=u_{M,i}=\frac{r_i}{\sqrt{3}r_0},\quad v_{e,i}=w_{M,i}=\sqrt{\frac{2}{3}}\,\frac{r_i}{r_0},$$
$$\beta_{eu,i}=\frac{1}{\sqrt{3}}\,\beta_{e,i},\quad \beta_{Mu,i}=\frac{1}{\sqrt{3}}\,\beta_{M,i},\quad \beta_{ev,i}=\sqrt{\frac{2}{3}}\,\beta_{e,i},$$
$$\beta_{Mw,i}=\sqrt{\frac{2}{3}}\beta_{M,i},\quad \beta_{e,i}=\left(1-\gamma_{e,i}^{-2}\right)^{\frac{1}{2}},$$
$$\gamma_{e,i}=3.2,\quad \beta_{M,i}=\left(1-\gamma_{M,i}^{-2}\right)^{\frac{1}{2}}.$$

At the star exit, the contribution of radiation coming from meson-meson interaction is expected to be rather low. It is thus convenient to follow the method used in the previous section in order to separate the radiation part in the total decrease of kinetic energy there. So, we solve first the equations of motion ignoring radiation, and then compute $\gamma_{M,rad}$ over the confined to a plane meson trajectory corresponding to this solution:

$$\gamma_{M,rad}=\frac{2}{3}\,\eta\int_0^{\chi_f}d\chi\left[\left(\frac{d\beta_{Mu}}{d\chi}\right)^2+\left(\frac{d\beta_{Mw}}{d\chi}\right)^2-\right.$$
$$\left.-\left(\beta_{Mw}\frac{d\beta_{Mu}}{d\chi}-\beta_{Mu}\frac{d\beta_{Mw}}{d\chi}\right)^2\right]\gamma_M^3. \qquad (8)$$

The related ODE system is shown in Eqs. 9 on top of the next Page 104.

Since the lateral displacement of the heavy meson in a single star is expected to be small, the system (9) should be solved under the initial condition:

$$u_{Mi}=\frac{r_{M2}}{\sqrt{3}},\quad w_{Mi}=r_{M2}\sqrt{\frac{2}{3}},\quad r_{M2}=\left(u_{M2}^2+w_{M2}^2\right)^{\frac{1}{2}}, \qquad (10)$$

where r_{M2} is the final radius of the meson in the accelerating phase of the star. It was found that the condition (6) holds only for $\eta \geqslant 0.005$. With $\eta = 0.005$, the equilibrium cycle looks as follows. (We have to choose $q = 1.3$ to agree with the charge gauge condition $\gamma_{e,f} \approx 5$ as in [2]). Unlike (6:2) case, in which the full cycle of returning to the initial state takes two neighboring stars, now it takes four.

On the accelerating phase of the first star of the cycle: $r_{M,i} = 0.244912$; $r_{M,2} = 0.001923$; $\gamma_{M,i} = 4.927011$; $\gamma_{M,f} = 5.090523$; $\gamma_{e,f} = 5.353761$. On the decelerating phase: $\gamma_{M,f} = 4.925161$; $\gamma_{M,rad} = 0.014866$. Radiation energy decrease (8) is less than 0.1 of that from the exit potential barrier as found by subtraction the final energy for the deceleration phase (9) from that for the acceleration phase (7), the second being initial for the first. Hence, our approximation is appropriate. On the accelerating phase of the last star of the cycle: $r_{M,i} = 0.244921$; $r_{M,2} = 0.001934$; $\gamma_{M,i} = 4.926057$;

$$\left.\begin{aligned}
\eta^{-1}\frac{d\beta_{Mu}}{d\chi} &= \frac{1}{4}\left(1-\beta_{Mw}^2\right)^{-\frac{1}{2}}\left(1-\beta_{Mu}^2\right)\gamma_M^{-3}u_M^{-2} - \frac{1}{4}\left(1-\beta_{Mu}^2\right)^{-\frac{1}{2}}\beta_{Mu}\beta_{Mw}\gamma_M^{-3}w_M^{-2} - \\
&- \frac{1}{4}\left[u_M\left(\gamma_M^{-3}+\beta_{Mu}^2\beta_{Mw}^2+\beta_{Mu}\beta_{Mw}^3\right) - w_M\left(2\beta_{Mu}\beta_{Mw}-\beta_{Mu}^3\beta_{Mw}^2-\beta_{Mu}^2\beta_{Mw}^2\right)\right]\times \\
&\times\ \gamma_M^{-3}\left[u_M^2+w_M^2-(u_M\beta_{Mw}-w_M\beta_{Mu})^2\right]^{-\frac{3}{2}} \\
\eta^{-1}\frac{d\beta_{Mw}}{d\chi} &= -\frac{1}{4}\left\{u_M\beta_{Mw}\left(\beta_{Mu}+\beta_{Mw}\right)\left(1-\beta_{Mw}^2\right)+w_M\left[1-\beta_{Mw}\left(\beta_{Mu}+\beta_{Mw}\right)\left(1-\beta_{Mu}\beta_{Mw}\right)\right]\gamma_M^{-3}\times\right. \\
&\left.\times\left[u_M^2+w_M^2-(u_M\beta_{Mw}-w_M\beta_{Mu})^2\right]^{-\frac{3}{2}}+\frac{1}{4}\left(1-\beta_{Mu}^2\right)^{\frac{1}{2}}\left(1-\beta_{Mw}^2\right)\gamma_M^{-3}w_M^{-2}+\frac{1}{4}\left(1-\beta_{Mu}^2\right)^{-\frac{1}{2}}\beta_{Mu}\beta_{Mw}\gamma_M^{-1}u_M^{-2}\right.
\end{aligned}\right\}. \quad (9)$$

$\gamma_{M,f} = 5.089923$; $\gamma_{e,f} = 5.411567$. On its decelerating phase again: $\gamma_{M,f} = 4.927011$. The conditions (5) and (6) are satisfied in all four stars of the equilibrium cycle.

Contrary to the (6:2) case, both electron and meson energies have been found to increase in the close vicinity of the star center on the acceleration phase. Therefore, for (4:4) symmetry it is just meson radiation that dominates the mechanism to support equilibrium. An equilibrium cycle satisfying both (5) and (6) exists also for $\eta > 0.005$. Formal solution gives that only for $\eta > 0.02$ the condition (5) is broken. QED estimation with averaged Coulomb field [5] shows that for heavy meson ($\eta < 0.02$) quantum single photon corrections for radiation are small. However, classical electrodynamics is invalid for $\eta < 0.005$. Therefore $\eta = 0.005$ could only be accepted as the lowest value compatible with the above equations. This result by no means undermines the very fact of correspondence between the lepton families and the cube star sub-symmetries as detected with photon oscillation counting, which possesses its own meaning, independent of a particular theory to specify trajectories.

4 Concluding remarks

However imprecise, the obtained values for η strongly suggest the (6:2) and (4:4) sub-symmetries to be associated accordingly with the $\tau-$meson ($\approx 1.5\,\mathrm{GeV}/c^2$, $\eta = 0.0003$) and the meson ($\approx 100\,\mathrm{MeV}/c^2$, $\eta = 0.005$). Our estimations are reliable because of sufficiently big differences in mass values between the leptons. In order to find precise values, more complicated calculations of bremsstrahlung [5] are required for the star involving many Feynman diagrams for the mesons, interacting between themselves and with the electrons. Another approximation relates to the assumed sharp cut-off in the electroweak interaction at $r_{e,2}$.

We point out that the similar analysis might be carried out for quarks, which correspond to the three subsets of the complementary to the cube 12-particle part of the dodecahedron star in the full gauge lattice [2].

Although being presented here in the conventional form, the motion-to-motion gauge is actually coordinate-less, basing solely on the existence of the top velocity signal and symmetrical patterns of particles' trajectories. The existence of the flavor families could never be comprehended, unless the direct motion-to-motion gauge of charge is used, because the intermediary involving reference systems comprised of clocks and rods hides some important features of actual measurements. Just the same situation comes about in the weak interaction [3], where the obstructive role of reference systems stimulates the appearance of auxiliary "principles" like gauge invariance with its artificial group structure that can only explain the already known results of experiments rather than predict them. As a matter of fact, the very statement of the basic problem in mechanics, i.e. the contact problem, must be sufficient to substantiate all principles, including Lorentz covariance, gauge invariance and so on [7].

Submitted on December 23, 2014 / Accepted on December 28, 2014

References

1. Guidry M. Gauge Field Theories. A Wiley-Interscience Publication, 1991.
2. Tselnik F. *Communications in Nonlinear Science and Numerical Simulations*, 2007, v. 12, 1427.
3. Tselnik F. *Progress in Physics*, 2015, v. 1(1), 50.
4. Landau L.D., Lifshitz E.M. The Classical Theory of Fields. Oxford, Pergamon Press, 1962.
5. Akhiezer A.I, Berestetskii V.B. Quantum Electrodynamics. New York, Interscience Publishers, 1965.
6. Pomeranchuk I.Ya. Maximum energy that primary cosmic-ray electrons can acquire on the surface of the Earth as a result of radiation in the Earth's magnetic field. *JETP*, 1939, v. 9, 915; *J. Phys. USSR*, 1940, v. 2, 65.
7. Tselnik F. Preprint No. 89-166. Budker Institute of Nuclear Physics, Novosibirsk, 1989.

The Journal on Advanced Studies in Theoretical and Experimental Physics, including Related Themes from Mathematics

PROGRESS IN PHYSICS

A quarterly issue scientific journal, registered with the Library of Congress (DC, USA). This journal is peer reviewed and included in the abstracting and indexing coverage of: Mathematical Reviews and MathSciNet (AMS, USA), DOAJ of Lund University (Sweden), Zentralblatt MATH (Germany), Scientific Commons of the University of St. Gallen (Switzerland), Open-J-Gate (India), Referativnyi Zhurnal VINITI (Russia), etc.

Electronic version of this journal:
http://www.ptep-online.com

Postal Address

Department of Mathematics and Science,
University of New Mexico,
705 Gurley Ave., Gallup, NM 87301, USA

ISSN: 1555-5534 (print)
ISSN: 1555-5615 (online)

Standard Address Number: 297-5092
Printed in the United States of America

April 2015 **Vol. 11, Issue 2**

CONTENTS

Information for Authors and Subscribers

Progress in Physics has been created for publications on advanced studies in theoretical and experimental physics, including related themes from mathematics and astronomy. All submitted papers should be professional, in good English, containing a brief review of a problem and obtained results.

All submissions should be designed in LaTeX format using *Progress in Physics* template. This template can be downloaded from *Progress in Physics* home page http://www.ptep-online.com. Abstract and the necessary information about author(s) should be included into the papers. To submit a paper, mail the file(s) to the Editor-in-Chief.

All submitted papers should be as brief as possible. Short articles are preferable. Large papers can also be considered in exceptional cases. Letters related to the publications in the journal or to the events among the science community can be applied to the section *Letters to Progress in Physics*.

All that has been accepted for the online issue of *Progress in Physics* is printed in the paper version of the journal. To order printed issues, contact the Editors.

This journal is non-commercial, academic edition. It is printed from private donations. (Look for the current author fee in the online version of the journal.)

EDITORIAL MESSAGE

Celebrating the 60th Anniversary of Florentin Smarandache

December 10, 2014, marked the 60th anniverssay of Florentin Smarandache's birth. Through great personal sacrifice, our friend and colleague became one of the co-founders, and Executive Editor of our journal *Progress in Physics*. He is a mathematician of international renown, and a Professor in the Department of Mathematics and Science at the University of New Mexico, where he was Department Chair for many years. His detailed biography was previously published one year ago, in our journal.*

We, the colleagues and friends who have been privileged to know Florentin closely, wish him a happy life for many decades to come, good health, prosperity, and enthusiasm for his further research.

Dmitri Rabounski, Larissa Borissova, Andreas Ries,
Pierre Millette, Ebenezer Chifu, Gunn Quznetsov

Prof. Florentin Smarandache,
Executive Editor of *Progress in Physics*

*Rabounski D. Florentin Smarandache: A Celebration. *Progress in Physics*, 2014, issue 1, 25–27.

A Physical Model of Pulsars as Gravitational Shielding and Oscillating Neutron Stars

T. X. Zhang

Department of Physics, Alabama A & M University, Normal, Alabama 35762. E-mail: tianxi.zhang@aamu.edu

Pulsars are thought to be fast rotating neutron stars, synchronously emitting periodic Dirac-delta-shape radio-frequency pulses and Lorentzian-shape oscillating X-rays. The acceleration of charged particles along the magnetic field lines of neutron stars above the magnetic poles that deviate from the rotating axis initiates coherent beams of radio emissions, which are viewed as pulses of radiation whenever the magnetic poles sweep the viewers. However, the conventional lighthouse model of pulsars is only conceptual. The mechanism through which particles are accelerated to produce coherent beams is still not fully understood. The process for periodically oscillating X-rays to emit from hot spots at the inner edge of accretion disks remains a mystery. In addition, a lack of reflecting X-rays of the pulsar by the Crab Nebula in the OFF phase does not support the lighthouse model as expected. In this study, we develop a physical model of pulsars to quantitatively interpret the emission characteristics of pulsars, in accordance with the author's well-developed five-dimensional fully covariant Kaluza-Klein gravitational shielding theory and the physics of thermal and accelerating charged particle radiation. The results obtained from this study indicate that, with the significant gravitational shielding by scalar field, a neutron star nonlinearly oscillates and produces synchronous periodically Dirac-delta-shape radio-frequency pulses (emitted by the oscillating or accelerating charged particles) as well as periodically Lorentzian-shape oscillating X-rays (as the thermal radiation of neutron stars whose temperature varies due to the oscillation). This physical model of pulsars broadens our understanding of neutron stars and develops an innovative mechanism to model the emissions of pulsars.

1 Introduction

Neutron stars are extremely compact objects, resulting from supernova explosions of dying massive stars with 8 to 20 solar masses. The theoretical prediction for the existence of neutron stars in nature was proposed eight decades ago [1]. But the observational discovery of these compact objects was only done in the middle of the 1960s from the measurement of an unusual Dirac-delta-shape pulse-like radio emission from the Crab Nebula [2,3] first observed by Chinese astronomers in 1054. The mass and radius of neutron stars are mostly around 1.4 solar masses and 10 to 20 km, respectively. The recent measurement for the Shapiro delay of light from a binary millisecond pulsar has discovered a neutron star with a mass of about two solar masses [4]; and other measurements have found the radii of some neutron stars to be less than 10 km [5–7]. The mass-radius relation of these unusual neutron stars has been modeled recently by [8].

The conventional interpretation for the observed Dirac-delta-shape pulse-like radio emission was based on the lighthouse model of pulsars as fast rotating neutron stars [9–12]. Figure 1 sketches a diagram for the lighthouse model of pulsars. Charged particles that are accelerated along the magnetic field lines of neutron stars above the magnetic poles produce or give off coherent beams of radio emissions, through mechanisms which are, however, not yet entirely understood. These beams are viewed as pulsing radio-frequency radiation

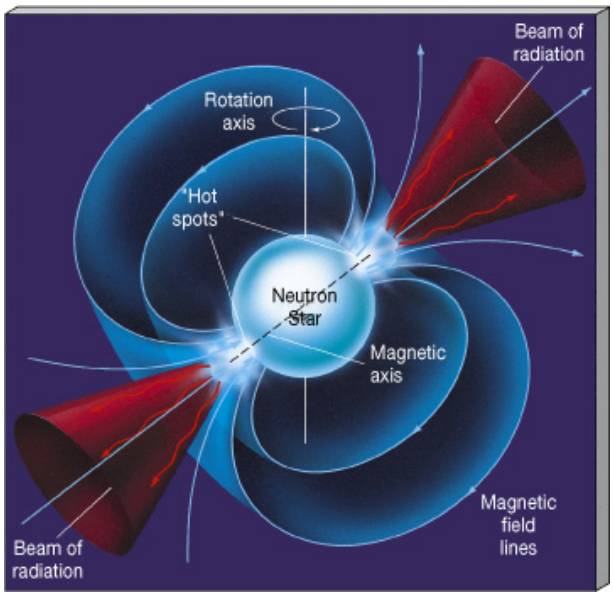

Fig. 1: A sketched diagram for the lighthouse model of pulsars as fast rotating neutron stars (Credit: www.pas.rochester.edu/afrank/A105). Charged particles, accelerated by the magnetism of the neutron star, flow along the magnetic field lines, producing radio radiation that beams outward.

Fig. 2: A flashlight beam through the air (Credit: www.youtube.com/watch?v=ggr5YQYqD0I). One can see the beam, even if it does not point to the viewer, because the air reflects the beam of the flashlight.

when the magnetic poles sweep the viewers. Twenty years after the discovery of neutron stars, quasi-periodic oscillations (QPOs) of X-rays were observed first from white dwarfs and then from neutron stars [13–14]. The recent observations of pulsar PSR B0943+10 by combining the X-ray telescope XMM-Newton and the radio telescope LOFAR have shown that this pulsar synchronously emits periodic Dirac-delta-shape pulses of radio-frequency radiation and Lorentzian shape oscillating X-rays [15]. At present, pulsar quasi-periodically oscillating X-rays are believed to come from inner edges of the accretion disks of white dwarfs, neutron stars, and black holes, but the physical cause still remains unsolved and a detailed consistent theory of how these fascinating stars work remains elusive.

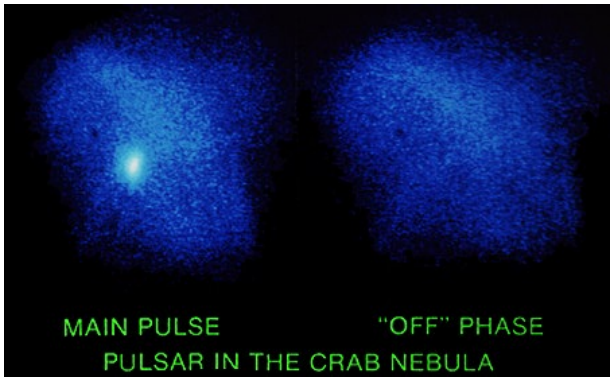

Fig. 3: X-ray images of the Crab Nebula. The left panel is the case when the pulsar turns on and the right panel is the case when the pulsar turns off. When the beam of X-rays points away, why we cannot see the radiation beam formed by the nebula reflection (Einstein Observatory image, Smithsonian Institution Photo No. 80-16234).

It is well known or experienced that a beam of flashlight is visible from the side because part of the light is scattered by the tiny particles like dust in the air (Figure 2). A beam of radio waves can bend or change the direction of propagation due to ionospheric reflections and refractions. However, the similar case does not happen for the beam of emissions (including radio waves through gamma rays) from the pulsar in the Crab Nebula. In visible light, the Crab Nebula consists largely of filaments with ionized gases of temperature $\sim 10-100$ times higher than ionosphere and density $\sim 1-1000$ times lower than ionosphere. The Crab Nebula, though behaving unlike the air or ionosphere, should be able to reflect or scatter the beams of radio waves or X-rays from the pulsar. But the observations have not shown such events occurring when the pulsar is in the OFF phase (see the right image of Figure 3). Figure 3 shows the X-ray images of the Crab Nebula taken by the Einstein Observatory when the pulsar is in the ON (the left panel) and OFF (the right panel) phases. According to the lighthouse model, the ON phase of the pulsar refers to the beam of radiation pointing to the Earth or the viewer; while the OFF phase refers to the beam of radiation pointing to other directions. The X-ray image of the entire Crab Nebula in the ON phase is significantly brighter than that in the OFF phase, especially the region above the lighting pulsar. This indicates that the Crab Nebula does reflect/scatter some X-rays of the pulsar when the pulsar is ON. However, there is not any reflection/scattering happened and perceived when the beam points to other directions through the Nebula in the OFF phase. This fact strongly implies that our conventional lighthouse model may not work. The lack of reflecting/scattering X-rays of the pulsar by the Crab Nebula in the OFF phase does not support the lighthouse model as expected. In the OFF phase, the pulsar is more likely to turn the radiation off entirely rather than just to direct the radiation away from the Earth or the viewer. In addition, the lighthouse model may not be able to theoretically form, except for when the deviation of the rotating axis from the magnetic poles is negligible, a stable accretion disk and jets, which were clearly seen in the X-ray images recently captured by the Chandra Observatory. It is also hard to explain why some pulsars are gamma rays only [16,17].

Recently, the author has developed a new mechanism for supernova explosion caused by gravitational field shielding [18], in accordance with his five-dimensional (5D) fully covariant Kaluza-Klein theory with a scalar field [8,19,20]. According to the gravitational field shielding theory, a supernova explosion takes place when its core collapses to a critical density where the gravitational field suddenly disappears or is shielded by the strong scalar field. At this moment, the extremely large pressure of matter immediately stops the core from collapsing and then the core quickly expands to powerfully push the mantle part of the supernova moving radially outward as a supernova explosion. As the core expands, the gravity resumes. After the mantle explodes out of the super-

nova, the core is left as a neutron star and starts to oscillate about its equilibrium of gravity and pressure. Rather than the rotation, acoustic wave and neutrino driven mechanisms of supernova explosions, this new mechanism is driven by the extreme pressure of the core when the gravitational field is suddenly weakened by the strong scalar field.

In this paper, we develop a physical model of pulsars, through which we propose an alternative explanation for neutron stars to emit the Dirac-delta-shape pulse-like radio frequency radiation and the Lorentzian shape oscillating X-rays, in terms of the 5D gravitational field shielding theory and the self-gravitating oscillations of neutron stars. We will also discuss how the frequency of emissions depends on the mass of the neutron star, the initial conditions, the equation of state, and the frozen magnetic field. In contrast to the conceptual lighthouse model, this physical oscillating model is based on the simple physics of thermal and accelerating charged particle radiation and the 5D gravity, and predicts power-time profiles of pulsars that are highly consistent with the measurements and observations.

2 Emissions of oscillating neutron stars

As described above, a neutron star starts to oscillate about its equilibrium of gravity and pressure once the mantle is exploded out of the supernova. The oscillation of the neutron star oscillates or accelerates inside particles. At the surface or in the crust, the acceleration of particles can be simply given by the following equation of motion,

$$a(t) \equiv \frac{d^2R(t)}{dt^2} = -g(R) - \frac{1}{\rho(R)}\frac{dP(\rho)}{dR}, \quad (1)$$

where $a(t)$ is the acceleration of the particle; $R(t)$ is the radial distance of the particle or simply the radius of the neutron star; $\rho(R)$ is the density of neutron star; $P(\rho)$ is the pressure of neutron star, which in this study is given by the Skyrme model for the Equation of State (EOS) of neutron stars [21,22],

$$P = 5.32\times10^{9}\rho^{5/3} + 1.632\times10^{-5}\rho^{8/3} - 1.381\times10^{5}\rho^{2}, \quad (2)$$

in the cgs unit system; and $g(R)$ is the gravitational field or acceleration, which in this study is determined according to the five-dimensional fully covariant Kaluza-Klein gravitational shielding theory with a scalar field that the author previously developed [18],

$$g = \frac{c^2}{2\phi^2}\left(\frac{d\phi}{dr} + \phi\frac{d\nu}{dr}\right)e^{-\lambda}, \quad (3)$$

in the Einstein frame. Here the scalar field ϕ, the metric 00- and 11-components e^{ν} and e^{λ} were solved as ([19] and references therein)

$$\phi^2 = -\alpha^2\psi^4 + (1+\alpha^2)\psi^{-2}, \quad (4)$$

$$e^{\nu} = \psi^2\phi^{-2}, \quad (5)$$

$$e^{\lambda} = \left(1 - \frac{B^2}{r^2}\right)^2\psi^{-2}, \quad (6)$$

in the Jordan frame, where ψ, B, and α are given by

$$\psi = \left(\frac{r-B}{r+B}\right)^{1/\sqrt{3}}, \quad (7)$$

$$B = \frac{GM}{\sqrt{3(1+\alpha^2)}\,c^2}, \quad (8)$$

$$\alpha = \frac{Q}{2\sqrt{GM}}. \quad (9)$$

This solution does not have an unknown parameter and reduces to the Schwarzschild solution in the Einstein frame when fields are weak and matter that generates the fields is neutral [8,18,23]. The weak field tests of general relativity are also the tests of this 5D gravity. In the case of strong fields, especially charged, the 5D gravity gives new effects such as the space polarization [24,25], electric redshift [19], gravitational field shielding or spacetime flattening [18], gravitationless black hole [23], and so on. The new effects are results of the strong scalar field, which significantly reduces the local gravity or, in other words, decreases the equivalent gravitational constant [20].

Figure 4a plots the radial distance as a function of time that is obtained from numerically solving (1). The result indicates that the neutron star nonlinear periodically oscillates, non-uniformly with quick stop and bounce by the pressure force when the gravity loses its dominance. It is in a dynamic equilibrium state rather than a static one. According to the gravitational shielding model [18], a supernova explosion takes place, due to the extremely large pressure pushing outward, when its core collapses to a critical density, at which the gravitational field suddenly disappears or is shed by the strong scalar field. Once a supernova or a dying star has exploded its mantle, the core as a stellar remnant forms a neutron star, located at the center of the supernova progenitor, with a relative large initial radius where the gravity is resumed. Then, the formed neutron star starts to gravitationally compress from its initial state. As it squeezes, the scalar field increases and reduces the gravitational field or flattens the spacetime again. To about the critical density, the gravitational field is disappeared or shed again by the strong scalar field. At this moment, the extensive pressure immediately stops the neutron star from the further collapse and extremely drives the neutron star to rapidly expand. Particles are extremely accelerated by the extensive pressure when the gravitational field is shed. After the neutron star is sufficiently expanded, the gravity resumes because the scalar field is weakened. When the gravity becomes dominant, the neutron star collapses again. This periodic switching of the dominance between the gravity and the pressure force leads to a nonlinear oscillation of the neutron star. Here in Figure 4 as an example we have chosen the mass of the neutron star to be about 1.5

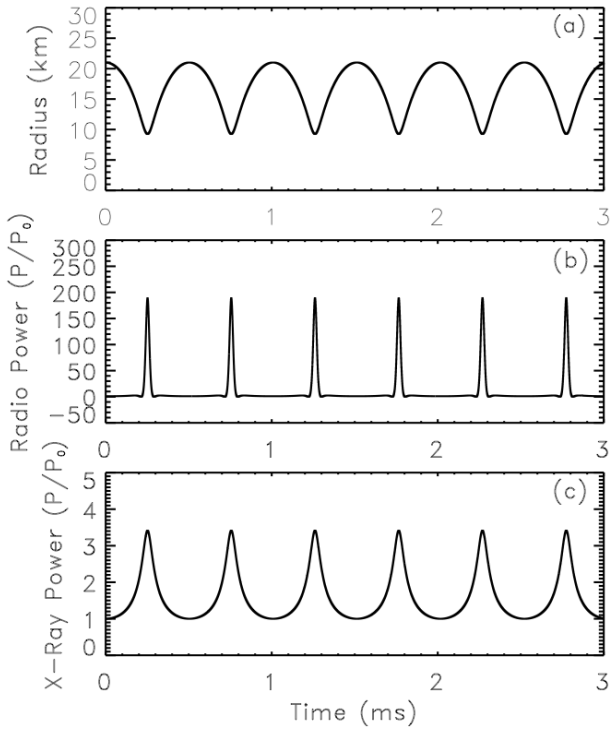

Fig. 4: Oscillation of a neutron star with 1.5 solar masses versus synchronous emissions of the Dirac Delta shape radio pulses and the Lorentzian shape X-ray oscillations. The radial distance (a), the power of radio emission (b), and the power of X-ray emission (c) are plotted as functions of time. The initial conditions for the radial distance and velocity of oscillation are chosen to be $R_0 = 22$ km and $v_0 = 0$.

solar masses; and the initial radial distance and velocity to be about $R_0 = 22$ km and $v_0 = 0$, respectively.

The accelerating particles, if electrically charged, generate radio emissions. According to the Larmor equation [26], the power of radio emissions generated by the accelerating charged particle is proportional to the square of the magnitude of the acceleration,

$$P_r(t) = \frac{q^2 a^2(t)}{6\pi\epsilon_0 c^3} \propto a^2(t), \tag{10}$$

where q is the particle charge; ϵ_0 is the dielectric constant in the free space; and c is the speed of light in free space. Figure 4b plots the power of radio emissions normalized to the power at the initial state, in terms of the Larmor equation (10) and the acceleration (1). The result indicates that the radio emissions by the nonlinearly oscillating neutron star are periodically pulse-like radiation with the Dirac delta shape, which is consistent with the general observations of pulsars. A neutron star could be possibly charged as a consequence of holding some certain amount of net protons or nuclei. The fraction and effect of protons in neutron stars have been considered for years [27,28]. To explain the observations of Geminga, a model of a dense neutron star with localized protons was proposed [29,30]. In [28], the maximum amount of charge in a compact star can be $\sim \sqrt{GM}$, which is $\sim 2.5 \times 10^{20}$ C for a neutron star with 1.5 solar masses.

On the other hand, a hot neutron star can emit thermal or blackbody radiation in the frequency range of X-rays. For instance, according to Wien's law, the frequency of blackbody radiation at the maximum or at the peak of the power by a hot body with surface temperature of 100 million Kelvins is about 10^{19} Hz, which is in the frequency range of X-rays. The total power of X-rays emitted by a hot neutron star can be given by

$$P_X(t) = 4\pi R^2(t)\,\sigma T^4(t) \propto R^{-\delta}(t), \tag{11}$$

where σ is the Stefan-Boltzmann constant. Here we have also considered that the surface temperature of the neutron star varies as the neutron star oscillates, or in other words, the temperature is a function of the radius or density. Figure 4c plots the power of X-rays normalized to the initial power, in terms of the blackbody radiation or (11). Here we have chosen the index $\delta = 3/2$, which corresponds to $T \propto R^{-(\delta+2)/4} = R^{-7/8}$. Choosing a larger δ does not alter the shape of the radiation, but can lead to a more significant oscillation of X-ray emissions, because the variation of temperature responding to the oscillation of neutron star increases with the index δ. The result shown in Figure 1c indicates that the X-rays emitted by the nonlinearly oscillating neutron star are synchronous periodically oscillating blackbody radiation with the Lorentzian shape, which is also consistent with the general observations of pulsars.

A neutron star may have a temperature as high as thousand billion degrees (10^{12} K) at the moment of its birth by an explosion of a supernova and then quickly cools down to a hundred million degrees (10^8 K) because of its strong radiation and neutrino emissions [31]. Therefore, for an early-aged neutron star, if the temperature is above 10^{10} K, the dominant thermal or blackbody radiation can be gamma rays. In other words, a younger pulsar as a hotter neutron star can emit gamma-rays mainly, which may explain the gamma ray only pulsars recently measured by NASA's Fermi Gamma Ray Telescope [32,33].

The frequency of the pulses shown in Figure 4 is about 2000 Hz (with a period of about 0.5 milliseconds), which depends on (1) the mass of the neutron star, (2) the initial kinetic and potential energy of the neutron star (or initial conditions of R_0 and v_0), and (3) the applied EOS. In general, at the same initial conditions with the same applied EOS, the pulse frequency is higher if the mass of the neutron star is greater because a larger mass, and thus larger gravity, collapses the neutron star quicker. Figures 5 and 6 show, respectively, the radial distance and the radio emission power for oscillating neutron stars with four different masses under the same initial conditions and the same applied EOS. It is seen that the frequency decreases with decreasing neutron star mass. For a

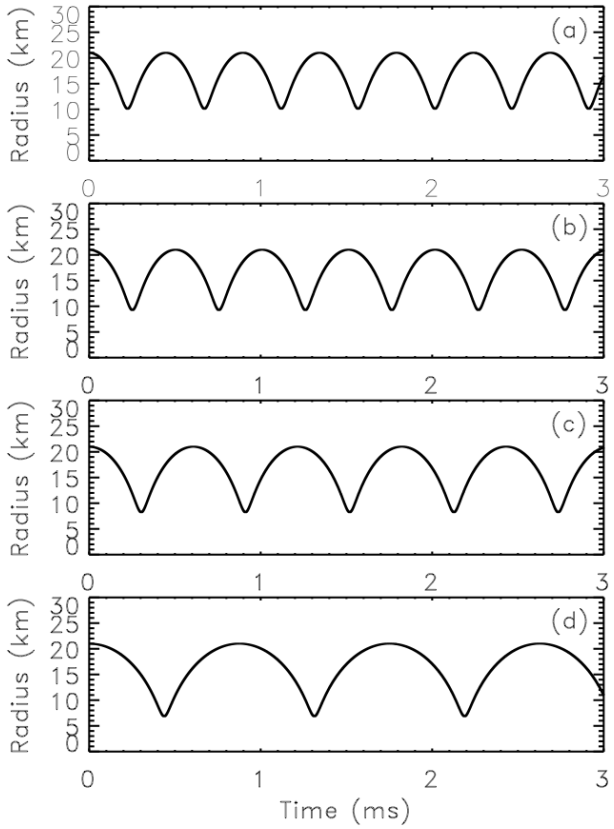

Fig. 5: Oscillations of neutron stars. The radial distance is plotted as a function of time for neutron stars with mass equal to 2, 1.5, 1, and 0.5 solar masses, respectively, from (a) through (d). The initial conditions and applied EOS are the same as in Figure 4.

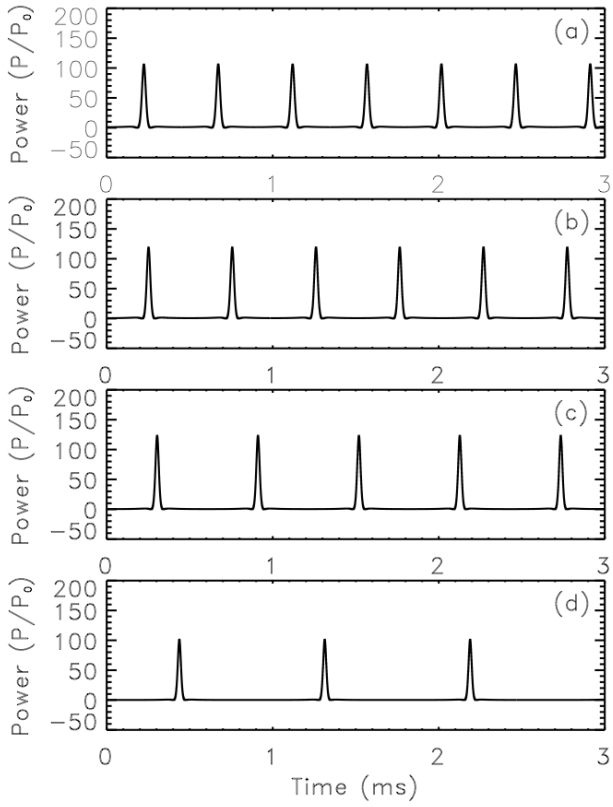

Fig. 6: Radio emissions of oscillating neutron stars. The power of radio emissions for neutron stars with mass equal to 2, 1.5, 1, and 0.5 solar masses, respectively, from (a) through (d). The initial conditions and applied EOS are the same as in Figure 5. The powers for all cases are normalized.

neutron star with mass four times smaller, the pulse frequency will be twice lower. The oscillation model of pulsars also gives very precise intervals between pulses as shown in Figures 3 to 5. Different pulsars can have quite different periods of pulses because they have different masses and start their oscillations from different initial states. Given a neutron star, the periodic switch between gravity and pressure dominant forces does not vary the period or frequency of oscillation.

3 Discussions and conclusions

For neutron stars with the same mass and the same applied EOS, the frequency of pulses is lower if the initial R_0 or v_0 is greater, because it takes a longer time to make one oscillation not only due to the longer course for the oscillation but also due to the weaker initial gravity. For neutron stars with the same mass and at the same initial state of motion, the frequency is greater if the density dependence of the pressure determined by the EOS is harder, because the pressure gradient push is greater and thus the oscillation is faster. On the other hand, the oscillation of the neutron star compresses and relaxes the frozen magnetic field of the neutron star as well as varies the particle radial speed of motion. The magnetic pressure and speed gradients also play some role in resisting the oscillations and thus decreasing the frequency of the oscillations, but not changing the emission characteristics. Therefore, oscillation periods of neutron stars can be in a wide range [34,35], when all these effects are considered. Details on these effects will be studied next.

The oscillation of a neutron star will be damped and thus slowed down due to the loss of energy or mass. Neutron stars can speed up their oscillations when they accrete more energy or mass than they lose. They may also twitch or glitch their pulses when their states of matter suddenly change [36,37]. Very hot neutron stars (e.g. 10^{10} K) may emit oscillating gamma rays [38,39]. Sufficiently cooled down neutron stars (e.g. 10^6 K) can emit oscillating ultraviolet radiation [40]. All the temperature-related emissions are periodically oscillating with the Lorentzian shape. Only the acceleration-related radio frequency emissions are pulse-like with the Dirac delta shape. Since electrons have much smaller inertia than nuclei, the pressure gradient buoyant forces accelerate them in different strengths with time lag. Therefore, the radio emissions from electrons and nuclei in the neutral crust of an oscillating neutron star are not completely destructed. Net ra-

dio emissions from the electrons and nuclei in the neutral crust of a neutron star can be generated by the self-gravitating oscillating neutron star. Due to the time lag, each primary pulse, which is produced by electrons, may follow a secondary pulse, which is produced by nuclei.

The sudden disappearance of gravitational field due to the shielding by the strong scalar field is significant for the radio emissions of neutron stars to be pulses with the Dirac delta shape. Under the Newtonian and Einsteinian gravitational theories, the gravitational oscillations of neutron stars may also produce the observed Dirac delta shape radio emissions, but need the neutron star to be over compressed in order for the pressure gradient push to dominate the non-shielding strong gravity. On the other hand, it should be noted that (1) and (2) are valid only for non-relativistic motion. According to the calculation done in Figure 1, we can see that the maximum speed of the oscillation is less than about one third of the light speed in vacuum. In this case, we have a relativistic factor $\gamma < 1.1$, which means that the relativistic effect is not significant and thus negligible. The shape of radio emissions depends on the acceleration of charged particles and the shape of X-ray emissions depends on the surface temperature or radius of the neutron star. This physical model quantitatively explains the emission characteristics of pulsars.

The energy dissipation deficiently decreases the neutron star's total energy, mass, amplitude of oscillation, EOS (or the bounce of the neutron star), magnetic field strength, and thus slightly changes or reduces both the power and frequency of pulses. The small energy dissipation or loss due to radiation (or damping) can only weakly slow down the pulses. The measured polarizations of pulsars can be considered as the causes of particles flowing, electromagnetic activities, and unevenly distributed surface temperatures. This paper has only addressed the radio emission of charged particles that are accelerated due to the oscillation of the neutron star. If we also consider the radio emission of charged particles that are accelerated due to particle flowing and electromagnetic activities, the pulse profiles should be polarized with multiple components [41–43] and complicated pulse profiles. The Dirac-delta shape and Lorentzian shape are only the main characteristics (i.e. periodicities) of radio pulses and X-ray emissions. The emissions of pulsars are gravitation-powered with effects of rotation, accretion, and/or magnetism, respectively. The gravitational (or oscillatory) energy dissipation provides the power for the pulsar-nebula system. The radio emissions are coherent with high brightness temperature because charged particles are coherently accelerated along with the oscillation of neutron stars. The X-ray emission of a pulsar is thermal but with the temperature varying in a range rather than a single temperature. To obtain the energy spectra of X-rays, we must integrate the flux of emission over a temperature range. The result of integration should be non-thermal as measured. All these aspects will be explored in details in future.

As a summary, we have developed a physical model of pulsars to quantitatively interpret the emission characteristics of pulsars, in accordance with the five-dimensional fully covariant Kaluza-Klein gravitational shielding theory and the physics of thermal and accelerating charged particle radiation. With the significant gravitational shielding by the strong scalar field, a neutron star nonlinearly oscillates and produces synchronous periodically Dirac-delta-shape pulse-like radio-frequency radiation as well as periodically Lorentzian shape oscillating X-rays. The oscillating or accelerating charged particles produce the Dirac-delta-shape pulse-like radio frequency radiation, while the thermal/blackbody radiation of neutron stars that oscillate and thus vary the temperature produces the Lorentzian shape X-rays. This physical model of pulsars as gravitational shielding and oscillating neutron stars broadens our understanding of neutron stars and develops an innovative mechanism to disclose the mystery of pulsars.

Acknowledgements

This work was supported by NASA EPSCoR, AAMU Title III, and Natural Science Foundation of China. The author also acknowledges B. J. Zhang for his numerical assistance.

Submitted on December 20, 2014 / Accepted on January 8, 2015

References

1. Baade W., Zwicky F. Remarks on supernovae and cosmic rays. *Physical Review*, 1934, v. 46, 76–77.
2. Hewish A., Okoye S. E. Evidence for an unusual source of high radio brightness temperature in the Crab Nebula. *Nature*, 1965, v. 207, 59–60.
3. Hewish A., Bell S. J., Pilkington J. D. H., Scott P. F., Collings R. A. Observation of a rapidly pulsating radio source. *Nature*, 1968, v. 217, 709–713.
4. Demorest P. B., Pennucci T., Ransom S. M., Roberts M. S. E., Hessels J. W. T. A two-solar-mass neutron star measured using Shapiro delay. *Nature*, 2010, v. 467, 1081–1083.
5. Guillot S., Rutledge R. E., Brown E. F. Neutron star radius measurement with the quiescent low-mass X-ray binary U24 in NGC 6397. *Astrophysical Journal*, 2011, v. 732, id. 88.
6. Güver T., Wroblewski P., Camarota L., Ozel F. The mass and radius of the neutron star in 4U 1820-30. *Astrophysical Journal*, 2010, v. 719, 1807–1812.
7. Güver T., Ozel P., Cabrera-Lavers A. The distance, mass, and radius of the Neutron Star in 4U 1608-52. *Astrophysical Journal*, 2010, v. 712, 964–973.
8. Zhang B. J., Zhang, T. X., Guggila P., Dokhanian M. Neutron star mass-radius relation with gravitational field shielding by a scalar field. *Research in Astronomy and Astrophysics*, 2013, v. 13, 571–578.
9. Pacini F. Energy emission from a neutron star. *Nature*, 1967, v. 216, 567–568.
10. Gold T. Rotating Neutron Stars as the Origin of the Pulsating Radio Sources. *Nature*, 1968, v. 218, 731–732.
11. Goldreich P., Julian W. H. Pulsar electrodynamics. *Astrophysical Journal*, 1969, v. 157, 869–880.
12. Lyne A. G., Graham-Smith F. Pulsar Astronomy. Cambridge Univ. Press, Cambridge, 2012.

13. van der Klis M., Jansen F., van Paradijs, Lewin, W. H. G., van der Heuve, E. P. J. Intensity-dependent quasi-periodic oscillations in the X-ray flux of GX5 – 1. *Nature*, 1985, v. 316, 225–230.
14. Middleditch J., Priedhorsky W. C. Discovery of rapid quasi-periodic oscillations in Scorpius X-1. *Astrophysical Journal*, 1986, v. 306, 230–237.
15. Hermsen W. *et al.* Synchronous X-ray and radio mode switches: A rapid global transformation of the pulsar magnetosphere. *Science*, 2013, v. 339, 436–439.
16. Abdo A. *et al.* A population of gamma-ray millisecond pulsars seen with the Fermi Large Area Telescope. *Science*, 2009, v. 325, 848–852.
17. Abdo A. *et al.* The First Fermi Large Area Telescope catalog of gamma-ray pulsars. *Astrophysical Journal Supplement*, 2010, v. 187, 460–494.
18. Zhang T. X. Gravitational field shielding and supernova explosions. *Astrophysical Journal Letters*, 2010, v. 725, L117–L121.
19. Zhang T. X. Electric redshift and quasars. *Astrophysical Journal Letters*, 2006, v. 636, L61–L64.
20. Zhang B. J., Zhang T. X., Guggilla P., Dokhanian M. Gravitational field shielding by scalar field and type II superconductors. *Progress in Physics*, 2013, v. 9 (1), 69–73.
21. Skyrme T. H. R. The effective nuclear potential *Nuclear Physics*, 1959, v. 9, 615–634.
22. Cameron A. G. W. Neutron star models. Astrophysical Journal, 1959, v. 130, 884–894.
23. Zhang T. X. Gravitationless black hole. *Astrophysics and Space Science*, 2011, v. 334, 311–316.
24. Nodvik J. S. Suppression of singularities by the g^{55} field with mass and classical vacuum polarization in a classical Kaluza-Klein theory. *Physical Review Letters*, 1985, v. 55, L2519–L2522.
25. Dragilev V. M. Vacuum polarization of a scalar field in anisotropic multidimensional cosmology. *Theoretical Mathematics in Physics*, 1990, v. 84, 887–893.
26. Jackson J. D. Classical Electrodynamics, 3rd Edition. John Wiley and Sons, 1999, p. 665.
27. Whinnett A. W., Torres D. F. Charged scalar-tensor boson stars: Equilibrium, stability, and evolution. *Physical Review D*, 1999, v. 60, id. 104050.
28. Ray S., Espindola A. L., Malheiro M., Lemos J. P. S., Zanchin V. T. Electrically charged compact stars and formation of charged black holes. *Physical Review D*, 2003, v. 68, id. 084004.
29. Kutschera M., Wojcik W. Proton impurity in the neutron matter: A nuclear polaron problem. *Physical Review C*, 1993, v. 47, 1077–1085.
30. Baiko D. A., Haensel P. Cooling neutron stars with localized protons. *Astronomy and Astrophysics*, 2000, v. 356, 171–174.
31. Yakovlev D. G., Gnedin O. Y., Kaminker A. D., Levenfish K. P., Potekhin A. Y. Neutron star cooling: Theoretical aspects and observational constraints. *Advances in Space Research*, 2004, v. 33, 523–530.
32. Atkinson N. Molecules in gamma-ray bursts detected. *Universe Today*, 2009, January 6.
33. Caraveo P. A. Gamma-ray pulsar revolution. *Annual Review of Astronomy and Astrophysics*, 2014, v. 52, 211–250.
34. Tsuruta S., Wright J. P. Oscillation periods of neutron stars. *Nature*, 1965, v. 206, 1137–1138.
35. Glass E. N., Lindblom L. The radial oscillations of neutron stars. *Astrophysical Journal Supplement*, 1983, v. 53, 93–103.
36. Anderson P. W., Itoh N. Pulsar glitches and restlessness as a hard superfluidity phenomenon. *Nature*, 1975, v. 256, 25–27.
37. Shemar S. L., Lyne A. G. Observations of pulsar glitches. *Monthly Notices of the Royal Astronomical Society*, 1996, v. 282, 677–690.
38. Harding A. K. Pulsar gamma-rays - Spectra, luminosities, and efficiencies. *Astrophysical Journal*,1981, v. 245, 267–273.
39. Romani R. W., Yadigaroglu I. A. Gamma-ray pulsars: Emission zones and viewing geometries. *Astrophysical Journal*, 1995, v. 438, 314–321.
40. Romani R. W., Kargaltsev O., Pavlov G. G. The Vela pulsar in the ultraviolet. *Astrophysical Journal*, 2005, v. 627, 383–389.
41. Lyne A. G., Smith F. G. Linear polarization in pulsating radio sources. *Nature*, 1968, v. 218, 124–126.
42. Han J. L., Demorest P. B., van Straten W., Lyne A. G. Polarization observations of 100 pulsars at 774 MHz by the Green Bank Telescope. *Astrophysical Journal Supplement*, 2009, v. 181, 557–571.
43. Yan W. M. *et al.* Polarization observations of 20 millisecond pulsars. *Monthly Notices of the Royal Astronomical Society*, 2011, v. 414, 2087–2100.

The Structured Proton and the Structureless Electron as Viewed in the Planck Vacuum Theory

William C. Daywitt

National Institute for Standards and Technology (retired), Boulder, Colorado. E-mail: wcdaywitt@me.com

This paper argues that the proton possesses structure because the positive proton charge attracts the negative-energy vacuum toward the massive proton core, exposing a small spherical portion of that vacuum to free-space perturbations. Calculations indicate that the apparent charge spread of the proton is due to this structure.

1 Introduction

The proton and electron are Dirac particles in the sense that they both possess a Compton radius and they both obey the Dirac equation, but the positive and negative charge of the proton and electron make their characteristics radically different. For example, the proton is smaller and more massive than the electron because of this charge difference [1]. It is shown below that this difference also accounts for the proton structure and its apparent charge spread. The structure is the result of the perturbed Planck vacuum (PV) state [2] in the vicinity of the massive proton core.

In its rest frame the proton core (e_*, m_p) exerts the following two-term coupling force [3] [4]

$$F_p(r) = \frac{(e_*)(-e_*)}{r^2} + \frac{m_p c^2}{r} = -F_s\left(\frac{r_p^2}{r^2} - \frac{r_p}{r}\right) \qquad (1)$$

on the PV negative-energy continuum, where the proton Compton radius $r_p\,(= e_*^2/m_p c^2)$ is the radius at which the force vanishes. The mass of the proton is m_p and the bare charge e_* is massless. The radius r begins at the proton core and ends on any particular Planck-particle charge $(-e_*)$ at a radius r within the PV. The strong force

$$F_s \equiv \left|\frac{(e_*)(-e_*)}{r_p^2}\right| = \frac{m_p c^2}{r_p} \qquad (2)$$

is the magnitude of the two forces in the first sum of (1) where the sum vanishes. The (e_*) in (1) and (2) belongs to the free-space proton and the $(-e_*)$ to the separate Planck particles of the PV, where the first and second ratios in (1) and (2) are vacuum polarization and curvature forces respectively. It follows that the strong force is a proton/PV force (rather than a free-space/free-space force). The Planck particle mass m_* and Compton radius r_* are equal to the Planck Mass and Planck Length [5, p. 1234]. (The three Compton relations $r_e m_e c^2 = r_p m_p c^2 = r_* m_* c^2 = e_*^2$ and $c\hbar = e_*^2$ are used throughout the preceding and the following calculations.)

The massive electron core $(-e_*, m_e)$ exerts the coupling force

$$F_e(r) = \frac{(-e_*)(-e_*)}{r^2} - \frac{m_e c^2}{r} = F_w\left(\frac{r_e^2}{r^2} - \frac{r_e}{r}\right) \qquad (3)$$

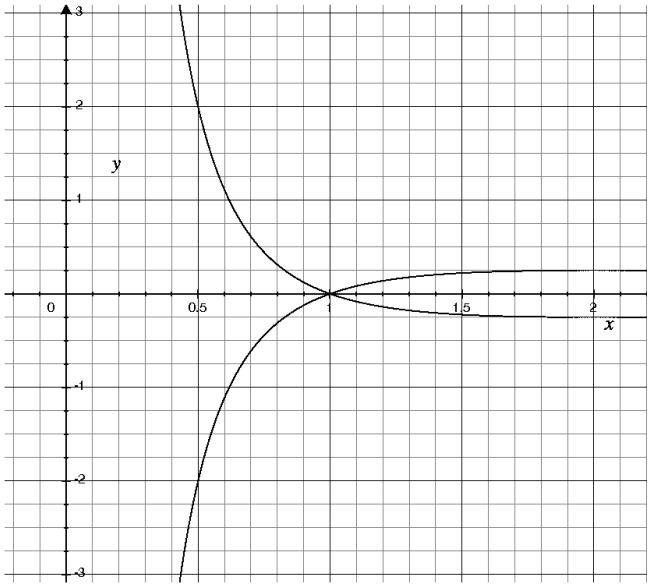

Fig. 1: Graphs of the normalized coupling forces $F_p(r)/F_s$ with $r_p = 1$ (negative to the left), and $F_e(r)/F_w$ with $r_e = 1$ (positive to the left). $(r_e/r_p = 1836)$

on the vacuum state and leads to the Compton radius $r_e\,(= e_*^2/m_e c^2)$, where the first $(-e_*)$ in (3) belongs to the electron. The weak force

$$F_w \equiv \frac{(-e_*)(-e_*)}{r_e^2} = \frac{m_e c^2}{r_e} \qquad (4)$$

is the magnitude of the two forces in the first sum of (3) where the sum vanishes. Again, the first and second ratios in (3) and (4) are vacuum polarization and curvature forces respectively. Thus the weak force, like the strong force, is an electron/PV force.

It is important to note that, for $r < r_p \ll r_e$, $F_p(r)$ and $F_e(r)$ are negative and positive respectively (Figure 1). That is, the proton and electron cores attract and repel respectively the Planck particles $(-e_*, m_*)$ within the PV. This is the phenomenon that gives the proton structure, while denying structure to the electron.

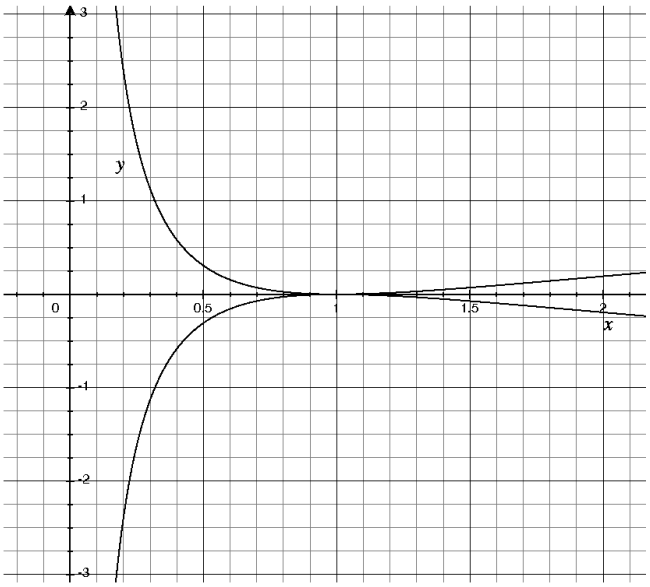

Fig. 2: Graphs of the normalized coupling potentials $V_p(r)/m_pc^2$ with $r_p = 1$ (upper curve), and $V_e(r)/m_ec^2$ with $r_e = 1$ (lower curve). ($r_e/r_p = 1836$)

2 Proton structure

The potential energy associated with the coupling forces (1) and (3) is defined as

$$V(r) = \int F(r)dr + V_0 \tag{5}$$

so that $dV/dr = F$ and $V(r_c) = 0$, where $r_c = e_*^2/mc^2$ is the force's Compton radius. For the proton and electron this definition leads to

$$\frac{V_p(r)}{m_pc^2} = \frac{r_p}{r} - 1 - \ln\left(\frac{r_p}{r}\right) \tag{6}$$

and

$$\frac{V_e(r)}{m_ec^2} = 1 - \frac{r_e}{r} + \ln\left(\frac{r_e}{r}\right) \tag{7}$$

where (6) and (7) yield $V_p(r) \geq 0$ and $V_e(r) \leq 0$ over the entire range of the radius r (Figure 2).

The spirit of the Klein Paradox discussed in Appendix A is that, if a region of free space is subjected to a sufficiently large *positive* potential, then an electron impinging on that region can extract energy from the negative-energy vacuum state. The following assumes that this paradox reflects a real physical phenomenon, implying that the positive charge of the proton core (but not the negative charge of the electron core) can expose a small region of the PV to perturbations from free-space particles. This conclusion leads to a structured proton and a structureless electron.

Equation (6) yields the quadrature formula

$$x = 1 + \frac{V_p}{m_pc^2} + \ln x \qquad \text{with} \qquad x \equiv r_p/r \tag{8}$$

from which the proton structure can be derived, where x is defined in the open interval $(0, \infty)$. The proton-proton (p-p) overlap radius (Appendix A) is determined by setting $V_p = 2m_pc^2$ in (8) and results in

$$x = 3 + \ln x \tag{9}$$

which leads to $x = 4.50$ and the p-p overlap radius r_1 ($\equiv r_p/4.50$). This is the radius where the negative-energy level $-m_pc^2$ of the vacuum state just enters the positive-energy level m_pc^2 of the free-space proton in its rest frame.

The negative energy maximum associated with the PV is $-m_ec^2$. Thus the proton electron-proton (e-p) overlap radius results from $V_p = m_pc^2 + m_ec^2$ and yields

$$\begin{aligned} x &= 1 + \frac{(m_pc^2 + m_ec^2)}{m_pc^2} + \ln x \\ &= 2 + \frac{r_p}{r_e} + \ln x \approx 2 + \ln x \end{aligned} \tag{10}$$

where $m_e/m_p = r_p/r_e = 1/1836$. Solving (10) leads to $x = 3.15$ and r_2 ($\equiv r_p/3.15$) for the e-p overlap radius. The sphere within the outer overlap radius r_2 ($> r_1$) represents the total exposed portion of the PV, and the surface of that sphere takes on a positive polarization charge due to the proton-core charge.

The size of the core $(-e_*, m_e)$ in the Dirac electron is no larger than $r_e/39,000$ [6] [7, pp. 402-403]; so it is reasonable to conclude that the proton core is similarly reduced in size below r_p. From the preceding the following picture of the proton structure emerges: the "point charge" proton core has a radius r_0 ($< r_p/39,000$); the p-p overlap radius is r_1; and the e-p overlap radius is r_2. The e-p surface at r_2 sustains a polarization charge caused by the core polarizing the exposed PV within that radius.

3 Charge spread

The core-charge polarization of the PV in the proton case leads to an apparent spread in the proton charge that can be roughly expressed in the proton electric field as

$$E(r) = \frac{e(r)}{r^2} \tag{11}$$

where the spread is

$$e(r) = \begin{cases} e_*\,, & r < r_0 \\ < e_*\,, & r_0 < r < r_2 \\ \sim e\,, & r_2 < r < r_p \\ e = \alpha^{1/2}e_*\,, & r_p < r \end{cases} \tag{12}$$

and α ($\approx 1/137$) is the fine structure constant. An important characteristic of this result is the large charge gradient

$$\frac{\Delta e}{\Delta r} = \frac{e_* - e}{r_2 - r_0} \approx \frac{e_*(1 - \sqrt{\alpha})}{r_p/3.15} \approx \frac{2.9e_*}{r_p} \tag{13}$$

between the core charge e_* and the polarization charge at r_2. This result explains a similar gradient in the QED spread depicted in Figure 11.6 of [8, p. 319].

Appendix A: Overlap radii

In the Klein Paradox [9, p. 127], a free electron propagates in the positive z-direction until it collides with the free-space region II in which the negative energy vacuum has been distorted by the *positive* step-potential

$$e\phi = \begin{cases} 0 & \text{for } z < 0 \text{ (region I)} \\ V_0 & \text{for } z > 0 \text{ (region II)} \end{cases} \qquad \text{(A1)}$$

that is externally applied to the half-space $z > 0$. The Klein Paradox demonstrates that a sufficiently strong positive free-space potential can expose a portion of the vacuum state to "attack" by free-space particles.

For $V_0 = 0$, the positive energy continuum for an electron in regions I and II increases from $m_e c^2$ in the positive energy direction, while the negative-energy vacuum continuum decreases from $-m_e c^2$ in the negative-energy direction. When the positive step-potential is imposed on the $z > 0$ half-space, however, the negative energy continuum in region II is increased as a whole by V_0. The electron positive energy continuum and the vacuum negative energy continuum can then overlap in region II. The plane at $z = 0$ is referred to in the present paper as an overlap boundary, and region II as the corresponding overlap region.

Upon collision with the step, the electron excites electron-positron pairs, the electrons and positrons propagating in the negative and positive z-directions respectively. In order for there to be pair excitation, the perturbing potential V_0 must satisfy the inequality

$$V_0 > E + m_e c^2 = (m_e^2 c^4 + c^2 p^2)^{1/2} + m_e c^2 \qquad \text{(A2)}$$

where E and p are the relativistic energy and momentum of the incident electron.

In the proton rest frame, the proton core (e_*, m_p) is responsible (via the coupling force (1)) for distorting the PV and for exposing the negative energy continuum to the free space around the core. The free-space spherical surfaces where the various positive and negative energy continua begin to overlap are defined in the present paper as *overlap radii*. The surface at the e-p overlap radius develops a positive polarization charge due to the polarizing effect of the positive core charge.

Submitted on January 7, 2015 / Accepted on January 12, 2015

References

1. Daywitt W. C. Why the proton is smaller and heaver than the electron. *Progress in Physics*, 2014, v. 10 (3), 175.
2. Daywitt W. C. The Planck vacuum. *Progress in Physics*, 2009, v. 5 (1), 20. See also www.planckvacuum.com.
3. Daywitt W. C. The electron and proton Planck-vacuum coupling forces and the Dirac equation. *Progress in Physics*, 2014, v. 10 (2), 114. The minus sign in equation (17) of this paper should be replaced by a positive sign.
4. Daywitt W. C. The strong and weak forces and their relationship to the Dirac particles and the vacuum state. *Progress in Physics*, 2015, v. 11 (1), 18.
5. Carroll B. W., Ostlie D. A. An Introduction to Modern Astrophysics. Addison-Wesley, San Francisco-Toronto, 2007.
6. Daywitt W. C. The source of the quantum vacuum. *Progress in Physics*, v. 5 (1), 27. There is a error in Appendix A of this paper: in the first line of the last paragraph "$p = \hbar/r_L$" should read "$m\gamma c = \hbar/r_L$".
7. Milonni P. W. The Quantum Vacuum – an Introduction to Quantum Electrodynamics. Academic Press, New York, 1994.
8. Aitchison I. J. R., Hey A. J. G. Gauge Theories in Particle Physics, Vol. 1. Taylor & Francis, New York, London, 2003.
9. Gingrich D. M. Practical Quantum Electrodynamics. CRC, The Taylor & Francis Group, Boca Raton, London, New York, 2006. – In the Klein Paradox V_0 is assumed to be a positive electrostatic potential, whereas the nonnegative potential $V_p(r)$ includes both charge (e_*) and mass (m_p). The difference between the two potentials is of no interest to the present paper, the salient point being the positive nature of both potentials.

"The Theory of Heat Radiation" Revisited: A Commentary on the Validity of Kirchhoff's Law of Thermal Emission and Max Planck's Claim of Universality

Pierre-Marie Robitaille[1] and Stephen J. Crothers[2]

[1]Department of Radiology, The Ohio State University, 395 W. 12th Ave, Columbus, Ohio 43210, USA
[2]Queensland, Australia
E-mails: robitaille.1@osu.edu, steve@plasmaresources.com

Affirming Kirchhoff's Law of thermal emission, Max Planck conferred upon his own equation and its constants, h and k, universal significance. All arbitrary cavities were said to behave as blackbodies. They were thought to contain black, or normal radiation, which depended only upon temperature and frequency of observation, irrespective of the nature of the cavity walls. Today, laboratory blackbodies are specialized, heated devices whose interior walls are lined with highly absorptive surfaces, such as graphite, soot, or other sophisticated materials. Such evidence repeatedly calls into question Kirchhoff's Law, as nothing in the laboratory is independent of the nature of the walls. By focusing on Max Planck's classic text, "*The Theory of Heat Radiation*', it can be demonstrated that the German physicist was unable to properly justify Kirchhoff's Law. At every turn, he was confronted with the fact that materials possess frequency dependent reflectivity and absorptivity, but he often chose to sidestep these realities. He used polarized light to derive Kirchhoff's Law, when it is well known that blackbody radiation is never polarized. Through the use of an element, $d\sigma$, at the bounding surface between two media, he reached the untenable position that arbitrary materials have the same reflective properties. His Eq. 40 ($\rho = \rho'$), constituted a dismissal of experimental reality. It is evident that if one neglects reflection, then all cavities must be black. Unable to ensure that perfectly reflecting cavities can be filled with black radiation, Planck inserted a minute carbon particle, which he qualified as a "catalyst". In fact, it was acting as a perfect absorber, fully able to provide, on its own, the radiation sought. In 1858, Balfour Stewart had outlined that the proper treatment of cavity radiation must include reflection. Yet, Max Planck did not cite the Scottish scientist. He also did not correctly address real materials, especially metals, from which reflectors would be constructed. These shortcomings led to universality, an incorrect conclusion. Arbitrary cavities do not contain black radiation. Kirchhoff's formulation is invalid. As a direct consequence, the constants h and k do not have fundamental meaning and along with "Planck length", "Planck time", "Planck mass", and "Planck temperature", lose the privileged position they once held in physics.

... That the absorption of a particle is equal to its radiation, and that for every description of heat.

Balfour Stewart, 1858 [1]

1 Introduction

Seldom does discovery bring forth scientific revolution [2]. In this regard, there can be no greater exception than Max Planck's [3] introduction of the quantum of action, at the beginning of the twentieth century [4, 5]. Within "*The Theory of Heat Radiation*" [5] Planck outlined the ideas which gave life both to this revolution and to the concept that fundamental constants existed which had universal significance throughout nature. The pillars which supported his ideas included: 1) Kirchhoff's Law of thermal emission [6, 7], 2) the irreversability of heat radiation, and 3) the adoption of discrete states.* He utilized Kirchhoff's Law not only to assist in the derivation of his equation, but to infer universality. Max Planck concluded that all cavities, irrespective of experimental evidence, would eventually become filled with blackbody, or normal, radiation. He argued that, if a cavity did not contain black radiation, the cause was a lack of thermal equilibrium, which could be easily rectified by the introduction of a minute particle of carbon [8]. For Max Planck, as for his teacher Gustav Kirchhoff [9], cavity radiation was independent of the nature of the enclosure. In reality, such ideas were not supported by experiment, as arbitrary cavities do not contain black, or normal, radiation. By applying his law to all cavities, the father of quantum theory detached his equation from physical reality itself. In truth, Planck's equation was only valid for laboratory blackbodies constructed from highly

**The Theory of Heat Radiation* is readily available online [5].

absorbing materials.

As a direct consequence, Planck's equation was never linked to a particular physical process and he did not provide physics with a cause for thermal emission. In fact, Kirchhoff's Law prevented him from advancing such a link [8, 10]. The exact nature of the oscillators responsible for thermal radiation could not be identified. Planck emphasized that [5, § 111],

> "*... to attempt to draw conclusions concerning the special properties of the particles emitting the rays from the elementary vibrations in the rays of the normal spectrum would be a hopeless undertaking*".

Studying Planck's classic text, the reader is eventually brought to the equation which governs specific intensity $\mathbf{K}_\nu$ [5, Eq. 300],

$$\mathbf{K}_\nu = \frac{h\nu^3}{c^2}\frac{1}{e^{\frac{h\nu}{kT}}-1}, \qquad (1)$$

wherein ν, c, h, k and T represent the frequency of interest, the speed of light,* Planck's constant, Boltzmann's constant, and absolute temperature, respectively. The validity of this equation appears to have been established for blackbodies; namely those specialized heated cavities whose interior is always lined with good absorbers over the frequency of interest, such as graphite, soot, carbon black, or other specialized materials (see [8] and references therein). Max Planck recognized that blackbodies were complex devices, as the data provided for his analysis had been obtained by some of the premier experimentalists in Germany [11–13].

He relied on the work of Rubens and Kurlbaum [11, 13] to secure the data which led to Eq. 1. In this regard, it is important to note the elaborate experimental setup used [11, 13]. It was very far from a simple cavity. These results made use of "the method of residual rays", a process which actually took place well beyond the confines of the cavity [11, 13]. Repeated reflections were supported by using crystals of quartz, fluorite, rocksalt, and sylvine, each for a given frequency of interest [11, 13]. The desired data points could only be obtained with an apparatus used to select the frequency of interest at the proper intensity.

In themselves, such extreme experimental methods confirmed that not all enclosures were filled with black radiation. Surely, if arbitrary cavities contained black radiation, there should have been no need for the use of these sophisticated approaches [13].

In this regard, it is also interesting to note that when faced with non-compliant experimental facts, scientists often invoke the inability to reach thermal equilibrium. This is especially true when cavities are constructed from materials with a low emissivity. Such arguments are not reasonable, given the speed of light and the relative ease of maintaining temperature equilibrium in metallic objects through conductive processes. Laboratory findings do not support Planck's position relative to Kirchhoff's Law.

Clearly, real blackbodies were much more than simple arbitrary cavities [11–13]. Yet, Max Planck believed with certainty in the universality of Kirchhoff's Law. It is this aspect of Planck's work which must be carefully considered. For if it holds true, then Eq. 1 continues to have far-reaching consequences. It can be applied to any thermal spectrum, whether on Earth in the laboratory, or within any astrophysical context, provided of course, that thermal equilibrium can be demonstrated.† However, if Kirchhoff's Law can be shown to be false, then Planck's equation, while still valid for laboratory blackbodies, loses all universal significance [8, 10, 14–19].

It could no longer be used indiscriminately outside of the laboratory, at least if the observer could not ensure that the source of the observed spectrum originated from a known solid. Hence, all applications of Planck's law in astronomy would very likely constitute violations of its required setting. In addition, the fundamental nature of Planck's constant, Boltzmann's constant, and of "Planck length", "Planck time", "Planck mass", and "Planck temperature" would forever be lost. All would have ordinary significance. They would be no more fundamental for physics than the mile versus the kilometer. Everything simply becomes a question of the scale physics chooses to select, rather than scales being imposed upon mankind by nature itself. Consequently, Max Planck's conclusion that Eq. 1 could be applied to all arbitrary cavities had great implications.

It remains an experimental fact that good reflectors, such as silver, are never utilized to construct blackbodies, in direct contradiction to Kirchhoff's claim that cavity radiation is independent of the nature of the walls from which it is comprised. Silver walls would prefer to increase their temperature when confronted with an influx of heat, such as that typically used to drive blackbodies in the laboratory (see [8] and references therein). They would not easily maintain their temperature while building a radiation field within a cavity using reflection (see [19] for a discussion). It has also not been established that cavities constructed from walls of low emissivity can contain Lambertian emission. These are some of the reasons why Kirchhoff's Law fails.

As such, how could this law have survived for so long? In order to answer this question, it is important to revisit both the experimental and theoretical foundations which brought forth Kirchhoff's Law. For this exposition, the journey will begin with the experiments of Balfour Stewart [1] in keeping with the reality that experiments [10], not solely theory, govern the laws of physics. At this point, the work of Gus-

*The United Nations has declared that 2015 will be the "Year of Light".

†There must be radiative equilibrium, no temperature changes, and no conduction or convection taking place in the system of interest.

tav Kirchhoff [6,7] must be discussed, especially as related to his treatment of reflection. Then, finally, a detailed analysis of Max Planck's derivation of Kirchhoff's Law, as outlined in "*The Theory of Heat Radiation*" [5], will be presented. It will be demonstrated that Planck's derivation suffers, not only with minor problems, but with significant departures from experimental reality.

2 Balfour Stewart and the Law of Equivalence

Balfour Stewart was a Scottish physicist. In 1858, one year before Kirchhoff's Law was proposed [6, 7], Stewart published what can be considered one of the most important works in the history of thermal emission [1]. His analysis of radiation was entirely based on experimental grounds. Hence, he never claimed, as law, principles which could not be proven experimentally [1]. Using actual measurements with material plates made of various substances, Stewart formulated the Law of Equivalence, first in §19 of his work [1],

> "*The absorption of a plate equals its radiation, and that for every description of heat*",

and then in §33 [1],

> *"That the absorption of a particle is equal to its radiation, and that for every description of heat*".

At the same time, he addressed cavity radiation, arriving at a general principle by considering a single theoretical argument. For Stewart, this principle did not rise to the level of a law, precisely because the conclusion had not been experimentally verified. He treated cavity radiation purely from a theoretical perspective and highlighted that the radiation which should come to fill the cavity resulted from the radiation emitted, in addition to the radiation which had been built up by reflection. The arguments advanced, being theoretical and not experimental, prevented him from formally proposing a new law with respect to cavity radiation. Rather, he spoke of a general principle [1],

> "*Although we have considered only one particular case, yet this is quite sufficient to make the general principle plain. Let us suppose we have an enclosure whose walls are of any shape, or any variety of substances (all at a uniform temperature), the normal or statical condition will be, that the heat radiated and reflected together, which leaves any portion of the surface, shall be equal to the radiated heat which would have left that same portion of the surface, if it had been composed of lampblack... Let us suppose, for instance, that the walls of this enclosure were of polished metal, then only a very small quantity of heat would be radiated; but this heat would be bandied backwards and forwards between surfaces, until the total amount of radiated and reflected heat together became equal to the radiation of lampblack*".

The problem is that good reflectors do not readily emit radiation. As such, in order to drive the reflection term, one must try to inject heat into the walls of these cavities, while hoping that additional photons will be produced. But, if one attempts to pump heat into their walls using conduction, for instance, the temperature of the walls can simply increase [18, 19]. Nothing dictates that new photons can become available for the buildup of the reflective term, while maintaining the cavity at the same temperature. One can infer that good reflectors can easily move away from the temperature of interest and fall out of thermal equilibrium. As a result, they cannot easily be filled with the desired radiation, even if theoretical arguments suggest otherwise. In the real world, nothing is independent of the nature of the materials utilized.

Stewart recognized that, if one could "drive the radiation" in a cavity made from arbitrary materials, by permitting the slow buildup of reflected radiation, the interior could eventually contain black radiation. The argument was true in theory, but not demonstrated in practice. Stewart remained constrained by experimental evidence. The situation could not be fully extended in the laboratory.

From Balfour Stewart, we gain three important lessons. First, he correctly supplied the Law of Equivalence: *Given thermal equilibrium, the emission of an object is equal to its absorption*. Second, he outlined the principle that cavity radiation can become black, in theory, in the event that the reflective term can be driven. Third, and most importantly, he did not advance a new law of physics without experimental confirmation.

3 Gustav Kirchhoff: Physics from Theory Alone

Soon after Balfour Stewart formulated the Law of Equivalence [1], Gustav Kirchhoff published his law of thermal emission [6, 7]. Almost immediately, the work was translated into English by F. Guthrie [7] and Kirchhoff's paper was then re-published in the same journal where Stewart had presented his law the year before. At this point, a battle ensued between Kirchhoff and Stewart.* The problem centered on Kirchhoff's attempt to dismiss Stewart's priority claims for the Law of Equivalence. Kirchhoff did so by arguing that Stewart had not brought forth sufficient theoretical support for his law. As for Stewart, he believed that the law had been experimentally proven, even if his mathematical treatment might have lacked sophistication.

In any event, Kirchhoff's paper went much beyond the Law of Equivalence. Thus, Stewart, who had outlined the principle that arbitrary cavities might come to hold black radiation, did not insist that this was always true [1]. Conversely, Kirchhoff formulated this conclusion as a law of physics, but

*An excellent treatment of this incident has already been published [20] and one of the authors has also addressed the issue [8].

he did so without recourse to a single experiment. Both of his proofs were theoretical [6, 7].

To begin his investigation, Kirchhoff, in the first section of his text, defined a blackbody as follows [7, § 1]:

> "*This investigation will be much simplified if we imagine the enclosure to be composed, wholly or in great part, of bodies which, for infinitely small thickness, completely absorb all rays which fall upon them*".

Note the emphasis on the absorption by an element of infinitely small thickness. The contrast between Kirchhoff's definition of a blackbody and that adopted by Max Planck was profound [5], as will be discovered below. In any event, in §3 of his classic paper [7] Kirchhoff presented his law as follows,

> "*The ratio between the emissive power and the absorptive power is the same for all bodies at the same temperature*".

In § 13, he explicitly wrote the following form,

$$\frac{E}{A} = e. \tag{2}$$

Kirchhoff eventually set $A = 1$ [7, § 3]. In modern notation,* one could express Kirchhoff's Law as follows:

$$\frac{E_\nu}{\alpha_\nu} = f(T, \nu), \tag{3}$$

where $f(T, \nu)$ corresponds to the right side of Eq. 1 above, as first defined by Max Planck [4, 5]. In §17 of his classic paper [7], Kirchhoff outlined his law as follows,

> "*When a space is surrounded by bodies of the same temperature, and no rays can penetrate through these bodies, every pencil in the interior of the space is so constituted, with respect to its quality and intensity, as if it proceeded from a perfectly black body of the same temperature, and is therefore independent of the nature and form of the bodies, and only determined by the temperature. The truth of this statement is evident if we consider that a pencil of rays, which has the same form but the reverse direction to that chosen, is completely absorbed by the infinite number of reflections which it successively experiences at the assumed bodies. In the interior of an opaque glowing hollow body of given temperature there is, consequently, always the same brightness whatever its nature may be in other respects.*"

*Though Kirchhoff speaks of absorptive power, A, he was actually referring to the unitless absorptivity, α_ν. Conversely, when referring to emissive power, E, he was, in fact, referring to this quantity, even in modern terms. That is, Kirchhoff's "E" has the same units as his "e" and neither is equal to 1. Kirchhoff, stated that "e" was a universal function and believed that its elucidation was a matter of great scientific importance.

Relative to Kirchhoff's formulation, three important concerns must be raised. First, the law becomes undefined in the perfect reflector, as $\alpha_\nu = 0$ under that condition. Planck himself recognized this fact [5, § 48], but might not have exercised proper care relative to its consequences. Second, it is clear that Kirchhoff lacked an accurate understanding of what was happening within his cavity, as an "infinite number" of reflections will never amount to absorption. An "infinite number" of reflections does not involve the exchange of energy. Conversely, when absorption occurs, energy is exchanged between the field in the interior of the cavity and the walls. Third, and the most serious objection to Kirchhoff's Law, centers upon his improper treatment of reflection. One of the authors has previously addressed these problems in detail [16].

In brief, within his first proof, Kirchhoff utilized transmissive plates to accomplish the proof, even if blackbody cavities must always be opaque. He addressed transmission by positioning mirrors behind his plates. In so doing, it appeared that Kirchhoff had properly treated reflection, because the mirrors did, in fact, reflect radiation. However, he had dismissed the possibility that the plates considered could possess differing surface reflection [16]. As shall be discovered below, Max Planck committed the same error, when he attempted to formulate Kirchhoff's Law [5, § 36–38]. In his second proof, Kirchhoff unknowingly permitted the cavity to fall out of thermal equilibrium, depending on the order in which operations were performed (see [16] for a detailed presentation).

It is evident that no valid theoretical proof of Kirchhoff's Law existed before Max Planck formulated his law of emission (see [21] for an excellent presentation). In fact, physicists continued to argue about a proper theoretical proof for Kirchhoff's Law until well after Planck's ideas became accepted [21]. Thus, in search of a proof, those provided by Planck, Hilbert, or Pringsheim may be the most relevant [21]. Yet, the proofs provided by Pringsheim and Hilbert have their own shortcomings [21].† It has even been claimed that, by applying Einstein coefficients to arrive at Planck's law, physics could dispense with the proof of Kirchhoff's Law [21]. However, Einstein's derivation utilized the energy density associated with a Wien radiation field, something which could only be found within a blackbody. Surely, Wien had not dispensed with Kirchhoff. In truth, it appears that those concerned with bringing forth a proper proof for Kirchhoff's Law were never able to reach their goal. The problem of finding a valid proof, seems to have simply been displaced by "more exciting physics", as the long sought definitive formulation of Kirchhoff's Law could no longer provide sufficient interest. The entire issue appears to have come to a slow death, without proper resolution.

It is certain that all theoretical proofs of Kirchhoff's Law

†The authors have not been able to locate an analysis of the proof advanced by Max Planck within "*The Theory of Heat Radiation*".

will be found to contain significant misapplications of experimental facts. The inability to provide a proper proof before the days of Planck [21], has not been easily overcome by some new insight into the nature of materials, after Planck. It remains true that all theoretical proofs of Kirchhoff's Law suffer from one or more of the following: 1) an improper treatment of reflection, absorption, or transmission; 2) the invocation of polarized light, when heat radiation is always unpolarized; 3) the use of transmissive materials, when Kirchhoff's Law refers to opaque enclosures; and 4) the existence of hypothetical objects which can have no place in the physical world.

However, the central proof of Kirchhoff's Law must always be the one outlined by Max Planck himself (see [5, § 1–51]), forty years after Kirchhoff [6,7]. For it is upon this proof (see [5, § 1–51]) that Eq. 1 was derived and through which Planck would ultimately attempt to lay the foundation for universality. Hence, it is best to forgo Kirchhoff's own derivations, as the theoretical validity of Kirchhoff's Law now rests with Max Planck [5, § 1–51].

4 Max Planck and Departure from Objective Reality

Having held such reverence for Max Planck over the years [3], it is with some regret that the following sections must be composed, outlining his sidestep of known experimental physics in the derivation of Kirchhoff's Law. Fortunately, in Planck's case, the validity of his equation is preserved, but only within the strict confines of the laboratory blackbody. The quantum of action continues to hold an important place in physics. Yet, the loss of universality cannot be taken lightly, as this aspect of Planck's work was the pinnacle of his career. In fact, above all else, it was universality which Planck sought, believing that he had discovered some great hidden treasure in nature [5, § 164],

> "*Hence it is quite conceivable that at some other time, under changed external conditions, every one of the systems of units which have so far been adopted for use might lose, in part or wholly, its original natural significance. In contrast with this it might be of interest to note that, with the aid of the two constants h and k which appear in the universal law of radiation, we have the means of establishing units of length, mass, time, and temperature, which are independent of special bodies or substances, which necessarily retain their significance for all times and for all environments, terrestrial and human or otherwise, and which may, therefore, be described as 'natural units'* ".

This was an illusion. With the collapse of Kirchhoff's Law, there are no "natural units" and all the constants of physics become a manifestation of the scales which the scientific community chooses.

4.1 Planck's Derivation of Kirchhoff's Law: Part I

Throughout his derivation of Kirchhoff's Law (see [5, § 1–51]), Max Planck sub-optimally addressed reflection, transmission, and absorption. This can be seen in the manner in which he redefined a blackbody, in an array of quotations [5, § 4],

> "*Strictly speaking, the surface of a body never emits rays, but rather it allows part of the rays coming from the interior to pass through. The other part is reflected inward and according as the fraction transmitted is larger or smaller, the surface seems to emit more or less intense radiation*".

For Planck, photons were being released from an object, not because they were emitted by its surface, but simply because they managed to be transmitted throughout, or beyond, its interior. The blackbody became a sieve. Planck stated [5, § 10],

> "*A rough surface having the property of completely transmitting the incident radiation is described as 'black'* ".

Planck continued [5, § 12],

> "*Thus only material particles can absorb heat rays, not elements of surfaces, although sometimes for the sake of brevity, the expression absorbing surfaces is used*.

Note the contrast, with Kirchhoff, which can be repeated for convenience [7, § 1],

> "*This investigation will be much simplified if we imagine the enclosure to be composed, wholly or in great part, of bodies which, for infinitely small thickness, completely absorb all rays which fall upon them*".

Planck acknowledged in a footnote that Kirchhoff considered a blackbody as absorbing over an infinitely thin element. He stated [5, § 10],

> "*In defining a blackbody Kirchhoff also assumes that the absorption of incident rays takes place in a layer 'infinitely thin'. We do not include this in our definition.*"

With his words, Planck redefined the meaning of a blackbody. The step, once again, was vital to his derivation of Kirchhoff's Law, as he relied on transmissive arguments to arrive at its proof. Yet, blackbody radiation relates to opaque objects and this is the first indication that the proofs of Kirchhoff's Law must not be centered on arguments which rely upon transmission. Planck ignored that real surface elements must possess absorption, in apparent contrast with Kirchhoff and without any experimental justification. Planck would expand on his new concept for a blackbody with these words [5, § 10],

> "*. . . the blackbody must have a certain minimum thickness depending on its absorbing power, in order to insure that the rays after passing into the body shall not be able to leave it again at a different point of the surface. The more absorbing a body is, the smaller the value of this minimum thickness, while in the case of bodies with vanishingly small absorbing power only a layer of infinite thickness may be regarded as black.*"

Now, he explicitly stated that bodies which are poor absorbers can still be blackbodies. Yet, we do not make blackbodies from materials which have low absorptivities, because these objects have elevated reflectivities, not because they are not infinite. Planck had neglected the important effects of absorption and reflection when formulating his new definition for a blackbody. This may have consequences throughout physics and astronomy [8, 17, 22].

In the end, Planck's surface elements must be composed of material particles. Since Planck was a theoretical physicist, he cannot work solely in the vacuum of a mathematical world. His derivations and conclusions must be related to physical reality. Yet, Planck's treatment had moved away from laboratory experiments with thin plates. These experiments were vital to the development of blackbody radiation science from the days long before Balfour Stewart [1]. Planck stated that [5, § 12],

> "*Whenever absorption takes place, the heat ray passing through the medium under consideration is weakened by a certain fraction of its intensity for every element of path traversed.*"

Clearly, Planck's element at the "bounding surface", as will soon be discovered, was an "element of path traversed". He therefore cannot neglect its absorption. Planck was well aware of this fact [5, § 12]:

> "*We shall, however, consider only homogeneous isotropic substances, and shall therefore suppose that α_ν has the same value at all points and in all directions in the medium, and depends on nothing but the frequency ν, the temperature T, and the nature of the medium.*"

and again [5, § 32],

> "*Consider then any ray coming from the surface of the medium and directed inward; it must have the same intensity as the opposite ray coming from the interior. A further immediate consequence of this is that the total state of radiation of the medium is the same on the surface as in the interior.*"

Still, at every turn, he attempted to include the effect of transmission, when it had no proper place in the treatment of blackbody radiation, as found in opaque bodies [5, § 14],

> "*Let $d\sigma$ be an arbitrarily chosen, infinitely small element of area in the interior of a medium through which radiation passes.*"

Planck thereby included the transmissive properties of the element, $d\sigma$, though he should have avoided such an extension. In the end, his definition of a blackbody was opposed to all that was known in the laboratory. Blackbodies are opaque objects without transmission, by definition. By focusing on transmission, Planck prepared for his move to universality, as will now be discussed in detail.

4.2 Planck's Derivation of Kirchhoff's Law: Part II

In the first section of his text, leading to his Eq. 27, [5, Eq. 27], Planck chose to formally neglect reflection, even though the total energy of the system included those rays which are both emitted/absorbed and those which would have been maintained by driving reflection [18, 19]. Such an approach was suboptimal. Planck must have recognized that the reflective contributions could eventually be canceled. Perhaps, that is why he simply neglected these terms, but the consequence was that insight was lost. In addition, by adopting this approach, Max Planck explicitly prevented the newcomer to the field of thermal radiation from appreciating the crucial importance of reflection within cavity radiation, as Balfour Stewart had well demonstrated [1, 18, 19].

In order to properly follow Planck's work, it is important to recognize his unusual conventions with respect to symbols. Dimensional analysis reveals that even though he spoke of a coefficient of emission (Emissionskoeffizienten) and utilized the symbol now reserved for emissivity, ϵ_ν, he was not referring to the emissivity in this instance. Rather, he was invoking the emissive power, $\mathbf{E}$, an entity with units. Conversely, when he spoke of the coefficient of absorption (Absorptionkoeffizienten), α_ν, he was truly referring to the dimensionless absorptivity, as we know it today. Insufficient attention relative to Planck's notation has, in fact, caused one of the authors to revise some of his previous works [18, 19]. Suffice it to note for the time being that, in order to remain consistent with Planck's notation, the following conventions will now be adopted: The symbol ϵ_ν, will represent emissive power, $\mathbf{E}$, and not emissivity. The symbols α_ν and ρ_ν will retain their modern meaning and represent dimensionless absorptivity and reflectivity, respectively. This is in keeping with Planck's notation. At the same time, we shall add the symbol η_ν, in order to deal with dimensionless emissivity, since Max Planck had already utilized the needed symbol when expressing emissive power.*

*In § 44, Planck presented Kirchhoff's Law in the following form [5, Eq. 48],

$$\frac{E}{A} = I = d\sigma \cos\theta \, d\Omega \, \mathbf{K}_\nu \, d\nu,$$

where A is actually the unitless absorptivity. Then, in § 45, Planck set $A = 1$. But, he also set, $E = A$. In so doing, he removed dimensionality from the emissive power, E.

At the outset, Max Planck considered the radiation within the interior of an isotropic medium. Inside this material, the total energy emitted from a volume element, $d\tau$, in frequency range of interest, $\nu + d\nu$, and in time, dt, in the direction of a conical element, $d\Omega$, was given by [5, Eq. 1],

$$dt\, d\tau\, d\Omega\, d\nu\, 2\epsilon_\nu, \tag{4}$$

from which Planck immediately surmised, by integrating over all directions and frequencies, that the total energy emitted corresponded to [5, Eq. 2],

$$dt\, d\tau\, 8\pi \int_0^\infty \epsilon_\nu\, d\nu. \tag{5}$$

He then moved to present the same equation, in slightly modified form in § 25 as,

$$dt\, v\, 8\pi \int_0^\infty \epsilon_\nu\, d\nu, \tag{6}$$

where v now corresponded to the volume element.

But since this element was contained within the medium of interest, it must also be reflecting radiation from other elements within the medium. That is because, as Balfour Stewart correctly highlighted, the total radiated power measured from a particle is to that portion which was emitted by the particle itself and that portion which it reflected [1]. This reflective component corresponds to the reflection coefficient, ρ_ν, multiplied by the specific intensity, $\mathbf{K}_\nu$, of the radiation leaving the second element, $d\tau'$, positioned at the end of Planck's conical section. The proper form of Eq. 4 [5, Eq. 1], including all of the radiation which leaves the particle, becomes,

$$dt\, d\tau\, d\Omega\, d\nu\, 2\left(\epsilon_\nu + \rho_\nu \mathbf{K}_\nu\right). \tag{7}$$

This expression, rather than leading to Eq. 6, results in,

$$dt\, v\, 8\pi \int_0^\infty \left(\epsilon_\nu + \rho_\nu \mathbf{K}_\nu\right)\, d\nu. \tag{8}$$

Similarly, Planck characterized the fate of the radiation which strikes the volume element, by including only absorption [5, Eq. 25],

$$dt\, v\, 8\pi \int_0^\infty \alpha_\nu\, \mathbf{K}_\nu\, d\nu. \tag{9}$$

If however, one considers that the radiation incident to the volume element, v, can be either absorbed or reflected, then Eq. 9 [5, Eq. 25] becomes,

$$dt\, v\, 8\pi \int_0^\infty \left(\alpha_\nu + \rho_\nu\right)\, \mathbf{K}_\nu\, d\nu. \tag{10}$$

Equating Eqs. 6 and 9, Planck obtained,

$$dt\, v\, 8\pi \int_0^\infty \epsilon_\nu\, d\nu = dt\, v\, 8\pi \int_0^\infty \alpha_\nu\, \mathbf{K}_\nu\, d\nu, \tag{11}$$

which led to [5, Eq. 27],

$$\mathbf{K}_\nu = \frac{\epsilon_\nu}{\alpha_\nu}. \tag{12}$$

Note that in this expression, Planck, like Kirchhoff, removed all consideration of reflection. Conversely, by combining Eqs. 8 and 10, we obtain that,

$$dt\, v\, 8\pi \int_0^\infty \left(\epsilon_\nu + \rho_\nu \mathbf{K}_\nu\right) d\nu = dt\, v\, 8\pi \int_0^\infty \left(\alpha_\nu + \rho_\nu\right) \mathbf{K}_\nu d\nu. \tag{13}$$

This expression leads to the following relation,

$$\epsilon_\nu + \rho_\nu \mathbf{K}_\nu = \alpha_\nu \mathbf{K}_\nu + \rho_\nu \mathbf{K}_\nu. \tag{14}$$

If one eliminates the terms involving reflection, this expression immediately leads to Eq. 12 [5, Eq. 27]. More importantly, since $\alpha_\nu + \rho_\nu = 1$ at thermal equilibrium, then a second expression, which retains the importance of reflectivity, is obtained,

$$\epsilon_\nu = \left(1 - \rho_\nu\right) \mathbf{K}_\nu. \tag{15}$$

Since Eq. 14 leads directly to Eq. 12, it now becomes clear why Max Planck chose to ignore the contribution of reflection in his derivation. He adopted a physically incomplete picture, but without mathematical consequence, at least in this instance. It could also be argued that Eq. 12 and Eq. 15 do not differ from one another, since at thermal equilibrium $1 - \rho_\nu = \alpha_\nu$. However, mathematically this is not the case. Eq. 12 becomes undefined when the absorptivity, α_ν, is set to zero. This is precisely what happens in the perfect reflector. Conversely, Eq. 15 is never undefined, as long as the reflective term is retained. As such, the prudent course of action for Max Planck might have been to adopt Eq. 15.

At this point, a trivial observation can be easily advanced. As mentioned above, given thermal equilibrium, then $1 - \rho_\nu = \alpha_\nu$. But at the same time, $\alpha_\nu = \eta_\nu$. This is the Law of Equivalence, first presented by Balfour Stewart [1]. As a result, it can be readily noted that Eq. 15 can be expressed as,

$$\epsilon_\nu = \eta_\nu\, \mathbf{K}_\nu \quad \text{or} \quad \mathbf{E}_\nu = \eta_\nu\, \mathbf{K}_\nu, \tag{16}$$

which is similar to Planck's Eq. 26 [5, Eq. 26]. In this case, $\mathbf{K}_\nu$ is given by Planck [5, Eq. 300]. It corresponds to a Planck function multiplied by the square of the index of refraction of the medium. Note what Eq. 16 is stating: *The emissive power of an arbitrary cavity at thermal equilibrium is equal to the emissivity of the material which makes up the cavity multiplied by a function*. This constitutes a proper and direct contradiction of universality. The nature of the radiation within the cavity becomes dependent on the nature of the cavity itself.

Thus, if the derivation is accomplished while including reflection, additional insight is gained. If given the choice, a function which is never undefined, like Eq. 15, must always take precedence over a function which can become undefined,

like Eq. 12. Then, consider Eq. 16. This relationship is important, because, like the form presented by Kirchhoff (Eq. 2) and Planck (Eq. 12), it is devoid of the consideration of reflection. But, when confronted with Eq. 16, it is impossible to conclude that arbitrary cavities contain black radiation.

In this initial treatment, Planck had not yet formally introduced Kirchhoff's Law. In order to accomplish this feat, he had to explore more than one medium at a time. Nonetheless, in this initial exposition of Planck's derivation, an important lesson has been learned: it is vital to recognize that the manner in which a result is presented can have a great deal of influence on its interpretation. Nowhere is this more applicable than in Planck's formal presentation of Kirchhoff's Law, as he leads the reader from Eq. 27 to Eq. 42 [5, Eq. 27–42]. It is here that Planck sidestepped experimental reality.

4.3 Planck's Derivation of Kirchhoff's Law: Part III

Heat radiation is unpolarized, by definition [23, p. 450]. In § 4 of *The Theory of Heat Radiation* [5], Planck considered a homogeneous isotropic emitting substance. Any volume element of such a material necessarily emits heat radiation uniformly in all directions. In § 5 Planck admitted that homogeneous isotropic media emit only natural or normal, i.e. unpolarized, radiation [5, § 5]:

> "*Since the medium was assumed to be isotropic the emitted rays are unpolarized.*"

This statement alone, was sufficient to counter all of the arguments which Planck later utilized to arrive at Kirchhoff's Law [5, Eq. 42]. That is because the important sections of Planck's derivation, namely § 35–37 make use of plane-polarized light. These steps were detached from experimental reality, relative to heat radiation [5, § 35],

> "*Let the specific intensity of radiation of frequency ν polarized in an arbitrary plane be $\mathbf{K}_\nu$ in the first substance ... and $\mathbf{K}'_\nu$ in the second substance ...*"

Planck also stated [5, § 36],

> "*... we have for the monochromatic plane-polarized radiation...*"

As such, to prepare for his use of polarized light in later sections, Planck resolved, in § 17, the radiation into its two polarized components. However, note that he could have arrived at Eq. 12 [5, Eq. 27] without ever resolving the radiation into its components. Nonetheless, his proof for the universality of Kirchhoff's Law [5, Eqs. 27–42] depended upon the use of polarized light [5, § 35–37]. Planck utilized polarized light in an isotropic medium, even though he had already recognized in § 5, that such radiation must be unpolarized. He clearly remarked in § 107,

> "*For a plane wave, even though it be periodic with a wave lying within the optical or thermal spectrum, can never be interpreted as heat radiation.*"

In order to arrive at Kirchhoff's Law, in § 35–37, Planck placed two different homogeneous isotropic media in contact with one another, as illustrated in Figure 1. The whole system was "*enclosed by a rigid cover impermeable to heat*". He then considered two arbitrary plane-polarized waves, one from each of the media, incident upon an element of area $d\sigma$ at the *bounding surface* of the two media. It can be seen in § 38, that Planck initially endowed this element with differing reflectivities, depending on whether the incident rays approached from medium 1 or medium 2. For Planck, both waves underwent reflection and refraction. He sidestepped that the ray could be absorbed, a decision vital to his ability to derive Kirchhoff's law [5, § 9],

> "*... a discontinuous change in both the direction and the intensity of a ray occurs when it reaches the boundary of a medium and meets the surface of a second medium. The latter, like the former, will be assumed to be homogeneous and isotropic. In this case, the ray is in general partly reflected and partly transmitted.*"

Planck invoked a small element of area $d\sigma$ at the boundary of his two contiguous media. This element had no consistent meaning in Planck's analysis. First, in § 36 and § 42 Planck placed this element in the *bounding surface* and, in so doing, allocated it properties characteristic of medium 1 on one half and medium 2 on the other. However, in § 43, he placed the element firmly within the surface of medium 2,

> "*... and falls on the surface element $d\sigma$ of the second medium.*"

Note that Planck had already introduced three causes for objection. First, what exactly was the location of $d\sigma$? In reality it must rest in one of the two media. Second, Planck neglected the fact that real materials can possess finite and differing absorptivities. While these can be ignored within the medium when treating propagation, because of the counter effect of emissivity, they cannot be dismissed at the boundary. Third, the simplest means of nullifying the proof leading to Planck's Eq. 42, is to use a perfect reflector as the second medium. In that case, a refractive wave could never enter the second medium and Planck's proof fails. The same objection can be raised using any fully opaque material for the second medium (i.e. $\alpha_\nu + \rho_\nu = 1$), as for all of them, τ_ν=0. This would include many materials typically used to construct real blackbodies in the laboratory. Consequently, for his proof of Kirchhoff's Law, Planck eliminated, by definition, virtually all materials of interest. In fact, he even excluded the perfect reflector, the very material he had chosen to consider throughout much of his text [5].

In § 36 Planck considered a monochromatic plane-polarized ray of frequency ν, emitted in time dt. In order to

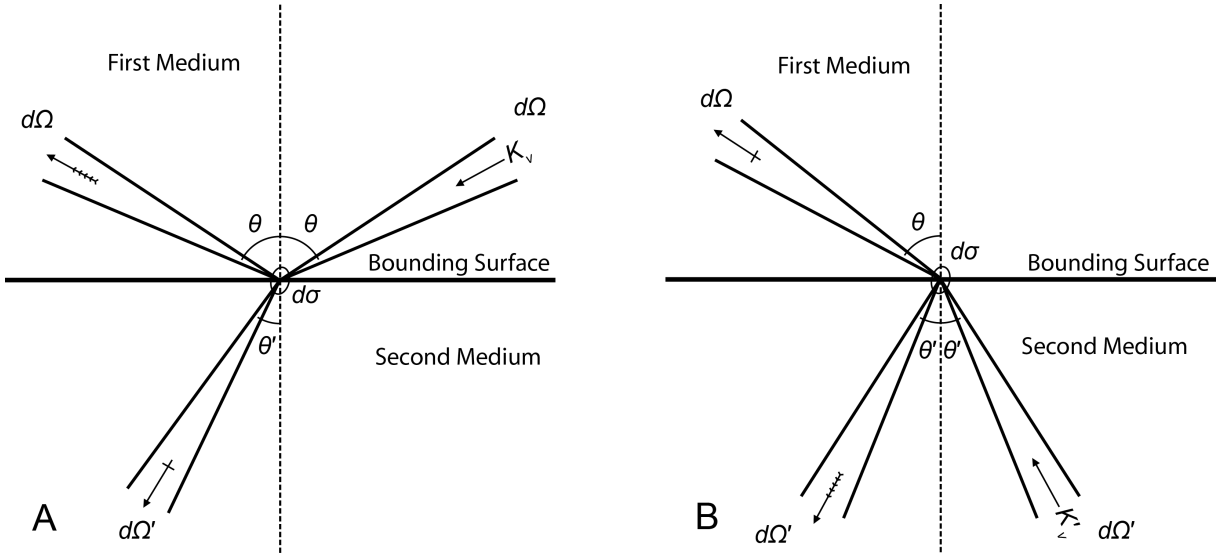

Fig. 1: Expansion of Figure 3 in "The Theory of Heat Radiation" [5] depicting the full complement of rays involved in treating the interaction between two media separated by a "bounding surface" which contained a hypothetical element of interest, $d\sigma$. Planck considered the reflective nature of $d\sigma$ to ascertain whether its reflection coefficients were identical depending on whether the incident ray originated from medium 1, (A), or medium 2, (B). A) Schematic representation of the incident specific intensity, $\mathbf{K}_\nu$ (plain arrow), at an angle θ, contained in the conical section, $d\Omega$, of the first medium (upper right quadrant) which is reflected by the bounding surface into the conical section $d\Omega$ in the upper left quadrant and refracted into the conical section $d\Omega'$ of the second medium, at an angle θ', in the lower left quadrant. Note that in order to preserve the proper specific intensities, $\mathbf{K}_\nu$, in the upper left quadrant, Planck must sum the reflected portion of the incident specific intensity of medium 1, $\rho_\nu \mathbf{K}_\nu$, with the refracted portion of the incident specific intensity of medium 2, $(1-\alpha'_\nu-\rho'_\nu)\mathbf{K}'_\nu$, depicted in B. This fact is represented by the feathered arrow. However, he neglected to include that part of the specific intensity in the upper left quadrant was being produced by emission in that direction, η_ν, by $d\sigma$. B) Schematic representation of the incident specific intensity, $\mathbf{K}'_\nu$ (plain arrow), at an angle θ',contained in the conical section, $d\Omega'$, of the second medium (lower right quadrant) which is reflected by the bounding surface into the conical section, $d\Omega'$, in the lower left quadrant and refracted into the conical section, $d\Omega$, of the first medium, at an angle θ, in the upper left quadrant. Note that, in order to preserve the proper specific intensities, $\mathbf{K}'_\nu$, in the lower left quadrant, Planck must sum the reflected portion of the incident specific intensity of medium 2, $\rho'_\nu \mathbf{K}'_\nu$, with the refracted portion of the incident specific intensity of medium 1, $(1-\alpha_\nu-\rho_\nu)\mathbf{K}_\nu$, as depicted in A. This fact is represented by the feathered arrow. However, he neglected to include that part of the specific intensity in the lower left quadrant was being produced by emission in that direction, η'_ν, by $d\sigma$.

address absorption at the "bounding surface", as mentioned under the second objection above, the total radiation which was both emitted and reflected by an element within the medium of interest (i.e. the incident ray) towards the "bounding surface" must be considered, as illustrated in Figure 2.

Note in this case, that the ray which is approaching the bounding surface will be transformed into three components: 1) that which will be absorbed at the "bounding surface" and then re-emitted in the direction of reflection; 2) that which will be reflected into the same medium; and 3) that which will be refracted into the other medium. The distinction is important, for Planck inferred that $\rho_\nu + \tau_\nu = 1$, whereas the correct expression involves $\rho_\nu+\tau_\nu+\alpha_\nu = 1$.* Planck permitted himself to state that $\tau_\nu = 1-\rho_\nu$, whereas he should have obtained $\tau_\nu = 1-\rho_\nu-\alpha_\nu$. Again, this completely prevents further progress towards Kirchhoff's Law [5, Eq. 42].

Planck considered the reflected rays in the first medium, of specific intensity $\mathbf{K}_\nu$ at incidence [5, Eq. 38],

$$\rho_\nu \, dt \, d\sigma \, \cos\theta \, d\Omega \, \mathbf{K}_\nu \, d\nu, \tag{17}$$

which were augmented by rays of incident specific intensity $\mathbf{K}'_\nu$ refracted from the second medium [5, Eq. 39],

$$(1-\rho'_\nu) \, dt \, d\sigma \, \cos\theta' \, d\Omega' \, \mathbf{K}'_\nu \, d\nu. \tag{18}$$

In this setting, the resultant rays in medium 1 consist of components from both media, the reflected and the refracted rays. Planck then obtained the following equation, at the end of his § 36,

$$\frac{\mathbf{K}_\nu}{\mathbf{K}'_\nu} \cdot \frac{q^2}{q'^2} = \frac{1-\rho'_\nu}{1-\rho_\nu}, \tag{19}$$

where q and q' correspond to speeds of light in first and second media, respectively. He rapidly moved to [5, Eq. 40],

$$\rho_\nu = \rho'_\nu, \tag{20}$$

*Note that in §36 Planck referred to frequency dependent reflectivity, ρ_ν, but chose to write it simply as ρ. In this case, since he was dealing with the frequency dependent value, the subscripted form will be utilized throughout the presentation which follows. As such, the equations presented by Max Planck will be modified such that ρ is replaced with ρ_ν in accordance with his description that the term was frequency dependent.

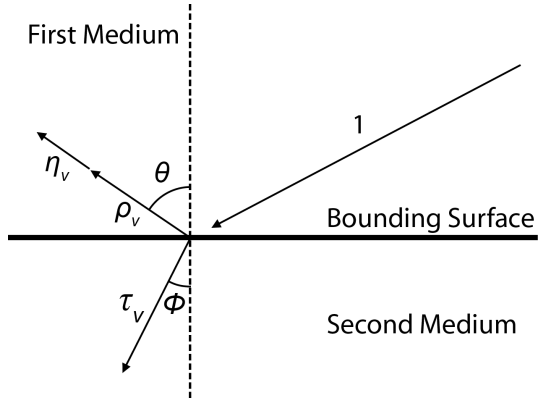

Fig. 2: Schematic representation of the fate of an incident ray, 1, which strikes a bounding surface. The ray will be split into three components: 1) the reflected ray, ρ_ν; 2) the refracted ray, τ_ν; and 3) that portion of the ray which is first absorbed, α_ν, then immediately re-emitted, η_ν, in order to preserve energy balance, in the direction of the reflected ray ($\alpha_\nu = \eta_\nu$). Thus, it is possible to describe this problem mathematically as $1 = \rho_\nu + \tau_\nu + \alpha_\nu$.

The result was stunning. Max Planck had determined that the reflectivities of all arbitrary media were equal. Yet, he attempted to dismiss such a conclusion by stating relative to Eq. 20 [5, Eq. 40]:

> "*The first of these two relations, which states that the coefficient of reflection of the bounding surface is the same on both sides, is a special case of a general rule of reciprocity first stated by Helmholtz.*"

Planck provided for the element of the bounding surface two separate coefficients of reflection. These must, in fact, correspond to those of the media utilized. Planck has already stated in § 35 that

> "*. . . let all quantities referring to the second substance be indicated by the addition of an accent.*"

Consequently, ρ and ρ' can only take meaning with respect to the media under consideration. Thus, how did Planck possibly reach the conclusion that these values must be equal? At the onset in Eq. 19 [5, § 35], Planck sought to force $\rho_\nu = \rho'_\nu$, in general, by first making $\rho_\nu = \rho'_\nu = 0$, in particular. To accomplish this feat, he considered rays that were,

> "*polarized at right angles to the plane of incidence and strike the bounding surface at the angle of polarization*" [5, § 37].

Again, such rays could never exist in the context of heat radiation [23, p. 450].

The "plane of incidence" is that containing the unit normal vector from the surface of incidence and the direction of the incident ray. There are two natural ways by which the orientation of an electromagnetic wave can be fixed; by the electric vector $\overline{\mathbf{E}}$ or the magnetic vector $\overline{\mathbf{B}}$. Contemporary convention is to use the electric vector $\overline{\mathbf{E}}$ [24, § 1.4.2]. Planck used the erstwhile magnetic vector convention.

The "angle of polarization" is Brewster's angle [23, p. 450]. The angle between reflected and refracted rays resulting from a given incident ray is then 90°. The reflected wave is entirely plane-polarized*, as shown in Figure 3,

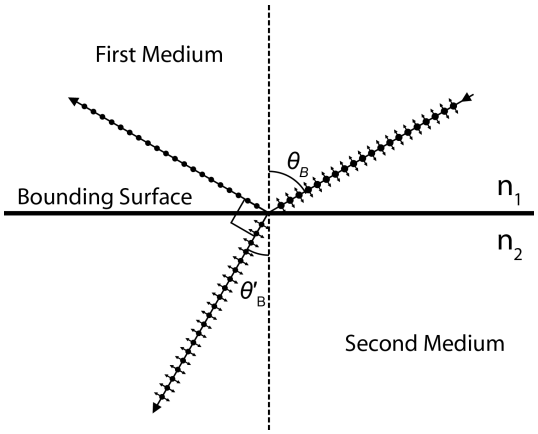

Fig. 3: Schematic representation of Brewster's Law. The dots correspond to the electric vector perpendicular to the page, whereas the double-headed arrows represent the electric vector in the plane of the page. An unpolarized, or arbitrarily plane-polarized, incident ray (upper right quadrant), strikes a surface at an angle of incidence, θ_B, corresponding to the Brewster's angle, or the angle of polarization. The reflected ray, depicted in the upper left quadrant will be entirely plane-polarized in such a way that it has no component of its electric vector in the plane of incidence. The transmitted ray produced at the angle of refraction, θ'_B, depicted in the lower left quadrant, will be partially polarized. The angle between the reflected and refracted rays is 90°. The angles, θ_B and θ'_B are complementary $\left(\theta + \theta'_B = 90^\circ\right)$. This process depends on the refractive indices of the two media involved, n_1 and n_2, such that the process is defined by Snell's Law, $n_1 \sin\theta_B = n_2 \sin(90^\circ - \theta_B)$, which in turn becomes $n_1 \sin\theta_B = n_2 \cos\theta_B$, or $\tan\theta_B = n_2/n_1$.

Planck's medium 2 has a Brewster's angle complementary to the Brewster's angle of his medium 1 ($\theta_B + \theta'_B = 90^\circ$). Brewster's angle is defined in terms of a reflected and a refracted beam. Unpolarized light, and plane-polarized light that is not "*at right angles to the plane of incidence*", produce reflected and refracted beams, in accordance with Brewster's Law. Planck invoked Brewster's Law [23, p. 450] with the special condition that incident rays are orthogonal to the plane of incidence. In this case, there could be no reflection, but only refraction, in accordance with Snell's Law. He simultaneously applied these same restricted conditions to medium 2.

> "*Now in the special case when the rays are polarized at right angles to the plane of incidence and strike the bounding surface at the angle of polarization,* $\rho = 0$*, and* $\rho' = 0$."

*The reflected ray has no $\overline{\mathbf{E}}$ component in the plane of incidence.

However, Planck's two contiguous media were homogeneous and isotropic. They could only emit unpolarized light and not plane-polarized light. Since the entire system was enclosed by a barrier impermeable to heat, there was no external source of any incident plane-polarized rays. All incident rays considered must be unpolarized and all resultant composite rays, at best, partially polarized. This implied that the reflectivities of both media were never zero. Yet, Planck made all rays plane-polarized and, in this special case, orthogonal to the plane of incidence (magnetic vector convention). Since plane-polarized rays in both media were chosen orthogonal to their common plane of incidence, they had no components which could be reflected. The conclusion that the reflectivities were equal was therefore never properly tested, as Planck had offered no possibility of any reflection taking place. Consequently, Planck's conclusion, that $\rho_\nu = 0$, and $\rho'_\nu = 0$ cannot be true. Thus, Planck becomes unable to move to Kirchhoff's Law, as presented in his Eq. 42 [5, Eq. 42].

The situation was actually more complex, as Planck did not provide the proper form for Eqs. 17, 18, and 19. In reality, he neglected the contribution from emission or absorption in Eqs. 17 and 18. He had already redefined the blackbody as possessing a purely transmissive surface, in contradiction to Kirchhoff, as seen above. This was a critical error. The proper form of Eq. 17 [5, Eq. 38] must also include a term for emissivity, η_ν, in the direction of the conical element,

$$(\eta_\nu + \rho_\nu)\ dt\, d\sigma\, \cos\theta\, d\Omega\, \mathbf{K}_\nu\, d\nu. \tag{21}$$

The proper form of Eq. 18 [5, Eq. 39] must also include a term for absorptivity of the second medium, α'_ν,

$$(1 - \rho'_\nu - \alpha'_\nu)\ dt\, d\sigma\, \cos\theta'\, d\Omega'\, \mathbf{K'}_\nu\, d\nu. \tag{22}$$

That is because the intensity of the ray from medium 2 which is refracted into medium 1 corresponds to the transmissivity ($\tau'_\nu = 1 - \rho'_\nu - \alpha'_\nu$). Clearly, the intensity of the transmitted ray must account for the reduction of the incident ray within medium 2 as a result of *both* reflection and absorption. Planck cannot ignore the absorption of the surface. Consequently, Eq. 19 should have included the emissivity of the first medium, η_ν, and the absorptivity of the second medium, α'_ν. If one considers that the emissivity of the first medium, η_ν, is equal to its absorptivity, α_ν, then Eq. 19 becomes,

$$\frac{\mathbf{K}_\nu}{\mathbf{K}'_\nu} \cdot \frac{q^2}{q'^2} = \frac{1 - \rho'_\nu - \alpha'_\nu}{1 - \rho_\nu - \alpha_\nu}. \tag{23}$$

This equation can never lead to Kirchhoff's Law [5, Eq. 42].

As a consequence, it is readily apparent that Planck, through Eqs. 17-20, adopted a presentation which selectively applied the rules of reflection and refraction to polarized rays, irrelevant to the discussion of heat radiation. Furthermore, he then arbitrarily chose the plane of polarization such that when the waves were incident at Brewster's angle, there would be no reflection. Nonetheless, if there could be no reflection, then Brewster's angle, or the angle of polarization, could have no meaning. That is because such an angle depends on the reflected and refracted rays being at 90° to one another. But since Planck insisted that no reflection occurred, then clearly the reflected and refracted rays could not form a 90° angle. Importantly, not only did Planck advance Eq. 20 (i.e. Planck's Eq. 40) by neglecting absorptivity and emissivity, he thereby selected materials which have little or no relevance to heat radiation. Planck could not neglect absorption and emission, treating only transmission and reflection, if he wished to have any relevance to actual blackbodies. In addition, he hypothesized a *bounding surface* without any true physical meaning. Given this array of shortcomings, this derivation of Kirchhoff's law can never be salvaged. Planck's claims for universality were without proper theoretical confirmation.

5 Planck's Perfectly Reflecting Cavities and the Carbon Particle

Throughout "*The Theory of Heat Radiation*", Planck had recourse to a perfectly reflecting cavity, in which he placed a minute carbon particle (see [8] for a detailed treatment). Obviously, cavities comprised solely of perfectly reflecting surfaces, can never contain black radiation, as such materials cannot emit photons [16]. Nonetheless, Planck believed that these cavities contained radiation. He was careful however, not to state that this radiation was black [5, § 51],

> "*... in a vacuum bounded by totally reflecting walls any state of radiation may persist.*"

This statement, by itself, was a violation of Kirchhoff's Law. Nonetheless, Planck believed that he could transform the radiation contained in all cavities into the thermodynamically stable radiation by inserting a carbon particle [5, § 51],

> "*If the substance introduced is not diathermanous for any color, e.g., a piece of carbon however small, there exists at the stationary state in the whole vacuum for all colors the intensity* $\mathbf{K}_\nu$ *of black radiation corresponding to the temperature of the substance*".

and later [5, § 52],

> "*It is therefore possible to change a perfectly arbitrary radiation, which exists at the start in the evacuated cavity with perfectly reflecting walls under consideration, into black radiation by the introduction of a minute particle of carbon. The characteristic feature of this process is that the heat of the carbon particle may be just as small as we please, compared with the energy of radiation contained in the cavity of arbitrary magnitude. Hence, according to the principle of the conservation of energy, the total energy of radiation remains essentially constant during the*

change that takes place, because the changes in the heat of the carbon particle can be entirely neglected, even if its changes in temperature should be finite. Herein the carbon particle exerts only a releasing (auslösend) action" .

Recall however, that Stewart's law insisted that [1],

"*. . . That the absorption of a particle is equal to its radiation, and that for every description of heat.*"

When Planck moved the carbon particle into the cavity, clearly the emissive field of the particle also entered the cavity provided the former had some real temperature. However, if one assumes that the particle was at T=0K, then no radiation from the carbon particle could enter the cavity. At the same time, if the particle was allowed to come into physical contact with the walls of the cavity, then energy could flow from the walls into the particle by conduction. Hence the particle, being perfectly emitting, would fill the entire cavity with black radiation. Alternatively, if the carbon particle could be suspended within the cavity, with no thermal contact to its walls, then the only radiation entering the system, would be that which accompanied the carbon particle itself [16]. That is because the walls of the cavity would not be able to "drive" the carbon particle, since they could emit no radiation. In that case, the radiation density within the cavity would remain too low and characterized only by the carbon particle. Unlike what Planck believed, the carbon particle could never be a simple catalyst, as this would constitute a violation of Stewart's law [1]. Catalysts cannot generate, by themselves, the product sought in a reaction. They require the reactants. Yet, the carbon particle was always able to produce black radiation, in accordance with Stewart's findings [1]. This was evidence that it could not be treated as a catalyst.

6 Planck's Treatment of Two Cavities

Planck's suboptimal treatment of the laws of emission continued [5, § 69],

"*Let us finally, as a further example, consider a simple case of a irreversible process. Let the cavity of volume V, which is everywhere enclosed by absolutely reflecting walls, be uniformly filled with black radiation. Now let us make a small hole through any part of the walls, e.g., by opening a stopcock, so that the radiation may escape into another completely evacuated space, which may also be surrounded by rigid, absolutely reflecting walls. The radiation will at first be of a very irregular character; after some time, however, it will assume a stationary condition and will fill both communicating spaces uniformly, its total volume being, say, V′. The presence of a carbon particle will cause all conditions of black radiation to be satisfied in the new state. Then, since there is neither external work nor addition of heat from the outside, the energy of the new state is, according to the first principle, equal to that of the original one, or U′ = U and hence from (78)*

$$T'^4 V' = T^4 V$$

$$\frac{T'}{T} = \sqrt[4]{\frac{V}{V'}}$$

which defines completely the new state of equilibrium. Since V′ > V the temperature of the radiation has been lowered by the process."

This thought experiment was unsound. First, both cavities were made of perfectly reflecting walls. As such, Planck could not assume that the second cavity contained no radiation. To do so, constituted a violation of the very law he wished to prove. Kirchhoff's Law stated that the second cavity could not be empty. Therefore, Planck could not surmise that the temperature had dropped.

If one accepted that Kirchhoff's Law was false, as has been demonstrated above, then both cavities must be viewed as empty, other than the minute contribution made by the carbon particle. Here again, Max Planck had moved beyond the confines of reality, for he advanced a result which could not be correct, whether or not Kirchhoff's Law was true. The cavities were either both empty (i.e. Kirchhoff's Law was not valid), or both filled with radiation (i.e. Kirchhoff's Law was valid). One could not be filled, while the other was empty. Planck's equation, in the quote above, was incorrect.

7 Conclusion

Throughout "*The Theory of Heat Radiation*' [5] Planck employed extreme measures to arrive at Kirchhoff's Law. First, he redefined the nature of blackbodies, by adopting transmission as a central element of his derivation. Second, he neglected the role of absorption at the surface of such objects, in direct contradiction to experimental findings and Kirchhoff's understanding of blackbodies. While it could be argued that absorption does not take place entirely at the surface, Planck could not assume that no absorption took place in this region. He was bound to include its contribution, but failed to meet this requirement. Third, he sidestepped reflection, by neglecting its presence in arriving at Eq. 12 [5, Eq. 27]. Nonetheless, the energy of the system under investigation included both that which was involved in emission/ absorption and that associated with the reflection terms. Stewart has well highlighted that such terms are central to the nature of the radiation within arbitrary cavities [1] and the concept has recently been re-emphasized [18, 19]. Fourth, Planck had recourse to plane-polarized light, whereas blackbody radiation is never polarized.

In the end, Planck's presentation of Kirchhoff's Law did not properly account for the behavior of nature. Arbitrary

cavities are not always black and blackbodies are highly specialized heated objects. Planck's characterization of the carbon particle as a simple "catalyst" constituted a dismissal of Stewart's Law [1]:

> "*. . . That the absorption of a particle is equal to its radiation, and that for every description of heat.*"

Planck could not transform a perfect absorber into a catalyst. Yet, without the carbon particle [8], the perfectly reflecting cavities, which he utilized throughout "*The Theory of Heat Radiation*" for the derivation of his famous Eq. 1 [4, 5], remained devoid of radiation. Perfectly reflecting cavities are incapable of producing radiation, precisely because their emissivity is 0 by definition. Planck can only properly arrive at Eq. 1 by having recourse to perfectly absorbing materials, a truth which he did not acknowledge. The presence of reflection must always be viewed as suboptimal to the creation of a blackbody, since significant reflection acts as a hindrance to the generation of photons through emission. It is never clear that the reflection term can easily be driven to arrive at the desired radiation, since thermal equilibrium, under these circumstances, can easily be violated, as the temperature of the cavity increases.

Planck's detachment from experimental findings relative to Kirchhoff's Law was evident in his presentation of Eq. 20 [5, Eq. 40]. His conclusion, with respect to the equivalence of the reflection in arbitrary materials, was false. Obviously, if reflection was always the same, then all opaque cavities would become identical. Eq. 20 [5, Eq. 40] became the vital result in Planck's derivation of Kirchhoff's Law. Unfortunately, the conclusion that $\rho{=}\rho'$ [5, Eq. 40] constituted a distortion of known physics and, by extension, so did Kirchhoff's formulation.

Without a proper proof of Kirchhoff's Law, Planck's claim for universality loses the role it plays in science. This has significant consequences in both physics and astronomy [8, 17, 24]. The constants h and k do not have fundamental meaning. Along with "Planck length", "Planck time", "Planck mass", and "Planck temperature", they are to be relegated to the role of ordinary and arbitrary constants. Their value has been defined by our own selection of scales, not by nature itself.

Dedication

This work is dedicated to the memory of Balfour Stewart [1].

Submitted on: January 24, 2015 / Accepted on: January 25, 2015
First published online on: January 28, 2015

References

1. Stewart B. An account of some experiments on radiant heat, involving an extension of Prévost's theory of exchanges. *Trans. Royal Soc. Edinburgh*, 1858, v. 22, no. 1, 1–20.
2. Kuhn T.S. The Structure of Scientific Revolutions. University of Chicago Press, Chicago, Il, 1962.
3. Robitaille P.-M. Max Karl Ernst Ludwig Planck: (1858–1947). *Progr. Phys.*, 2007, v. 4, 117–120.
4. Planck M. Über das Gesetz der Energieverteilung im Normalspektrum. *Annalen der Physik*, 1901, v. 4, 553–563.
5. Planck M. The theory of heat radiation. P. Blakiston's Son & Co., Philadelphia, PA, 1914, http://gutenberg.org/ebooks/40030.
6. Kirchhoff G. Über den Zusammenhang zwischen Emission und Absorption von Licht und. Wärme. *Monatsberichte der Akademie der Wissenschaften zu Berlin*, sessions of Dec. 1859, 1860, 783–787.
7. Kirchhoff G. Über das Verhältnis zwischen dem Emissionsvermögen und dem Absorptionsvermogen. der Körper fur Wärme und Licht. *Poggendorfs Annalen der Physik und Chemie*, 1860, v. 109, 275–301.
8. Robitaille P.-M. Blackbody radiation and the carbon particle. *Progr. Phys.*, 2008, v. 3, 36–55.
9. Agassi J. The Kirchhoff–Planck radiation law. *Science*, 1967, v. 156(3771), 30–37.
10. Robitaille P.-M. Kirchhoff's Law of thermal emission: 150 Years. *Progr. Phys.*, 2009, v. 4, 3–13.
11. Hoffmann D. On the experimental context of Planck's foundation of quantum theory. In: Revisiting the Quantum Discontinuity, Max Planck Institute for the History of Science, Preprint 150, 2000, 47–68.
12. Lummer O. and Pringsheim E. Kritisches zur schwarzen Strahlung. Annalen der Physik, 1901, v. 6, 192–210.
13. Rubens H. and Kurlbaum F. Anwendung der Methode der Reststrahlen zur Prüfung der Strahlungsgesetzes. *Annalen der Physik*, 1901, v. 2, 649–666; Rubens H. and Kurlbaum F. On the heat radiation of long wave-length emitted by black bodies at different temperatures. *Astrophys. J.*, 1901, v. 74, 335–348.
14. Robitaille P.M. On the validity of Kirchhoff's Law of thermal emission. *IEEE Trans. Plasma Sci.*, 2003, v. 31, no. 6, 1263–1267.
15. Robitaille P. M. L. An analysis of universality in blackbody radiation. *Progr. Phys.*, 2006, v. 2, 22–23; arXiv: physics/0507007.
16. Robitaille P.-M. A critical analysis of universality and Kirchhoff's Law: A return to Stewart's law of thermal emission. *Progr. Phys.*, 2008, v. 3, 30–35 (also in arXiv: 0805.1625).
17. Robitaille P.-M. Blackbody Radiation and the Loss of Universality: Implications for Planck's Formulation and Boltzmann's Constant. *Progr. Phys.*, 2009, v. 4, 14–16.
18. Robitaille P.-M. On the equation which governs cavity radiation. *Progr. Phys.*, 2014, v. 10, no. 2, 126–127; (see also Errata – Notice of Revision. *Progr. Phys.*, 2015, v. 11, no. 1, 88.)
19. Robitaille P.M. On the equation which governs cavity radiation II. *Progr. Phys.*, 2014, v. 10, no. 3, 157-162; (see also Errata – Notice of Revision. *Progr. Phys.*, 2015, v. 11, no. 1, 88.)
20. Siegel D.M. Balfour Stewart and Gustav Robert Kirchhoff: Two independent approaches to Kirchhoff's Law. *Isis*, 1976, v. 67, no. 4, 565–600.
21. Schirrmacher A. Experimenting theory: the proofs of Kirchhoff's radiation law before and after Planck. *Hist. Stud. Phys. Biol. Sci.*, 2003, v. 33, 299–335.
22. Robitaille P.M. Forty lines of evidence for condensed matter – The Sun on trial: Liquid metallic hydrogen as a solar building block. *Progr. Phys.*, 2013, v. 4, 90–142.
23. Jenkins F.A. and White H.E. Fundamentals of Optics (4th Edition), McGraw-Hill, Inc, New York, 1976.
24. Born M. and Wolf E. Principles of Optics (6th edition), Cambridge University Press, 1980.

Scaling of Body Masses and Orbital Periods in the Solar System

Hartmut Müller
Advanced Natural Research Institute in memoriam Leonhard Euler, Munich, Germany
E-mail: admin@anr-institute.com

The paper shows that the sequence of sorted by value body masses of planets and largest planetoids is connected by a constant scaling exponent with the sequence of their sorted by value orbital periods.

1 Introduction

In [1] we have shown that the observable mass distribution of large celestial bodies in the Solar system continues the mass distribution of elementary particles that can be understood as contribution to the fundamental link between quantum- and astrophysics via scaling.

Within the last ten years several articles [2–6] were published which confirm our statement that scaling is a widely distributed phenomenon. Possibly, natural oscillations of matter generate fractal distributions of physical properties in very different processes. Fractal scaling models [7] of oscillation processes in chain systems are not based on any statements about the nature of the link or interaction between the elements of the oscillating system. Therefore, the model statements are quite general, that opens a wide field of possible applications.

In this paper we will show, that the connection between the body mass distribution and the distribution of orbital periods of planets and largest planetoids in the solar system can be described by the scaling law (1):

$$M = \mu \cdot T^{\mathrm{D}}, \tag{1}$$

where M is a celestial body mass, T is a celestial body orbital period and μ and D are constants.

We will show, that for sorted by value couples of a body mass M and an orbital period T the exponent D is quite constant and is closed to 3/2. Furthermore, for M in units of the proton rest mass $m_p \approx 1.67 \times 10^{-27}$ kg [8] and T in units of the proton oscillation period $\tau_p = \hbar / m_p c^2 \approx 7.02 \times 10^{-25}$ s [9], the constant $\mu = 1$.

2 Methods

Already in the eighties the scaling exponent 3/2 was found in the distribution of particle masses [10]. In [11] we have shown that the scaling exponent 3/2 arises as consequence of natural oscillations in chain systems of harmonic oscillators.

Within our fractal model [1] of matter as a chain system of oscillating protons and under the consideration of quantum oscillations as model mechanism of mass generation [9], we interpret the exponent D in (1) as a Hausdorff [12] fractal dimension of similarity (2):

$$D = \frac{\ln M/m_p}{\ln T/\tau_p}. \tag{2}$$

The ratio M/m_p is the number of model protons, the ratio T/τ_p is the number of model proton oscillation cycles.

3 Results

If we sort by value the body masses and the orbital periods of planets and largest planetoids of the Solar system, then we can see that for sequently following couples of a body mass M and an orbital period T the fractal dimension D is quite constant and closed to the model value of 3/2.

Table 1 contains properties of planets and of the most massive planetoids in the Solar system. On the left side the bodies are sorted by their masses, on the right side the bodies are sorted by their orbital periods. Within the Solar system the average empiric value $\mathrm{D} \approx 1.527$ is a little bit larger then the model value of 3/2.

Based on the empiric value $\mathrm{D} \approx 1.527$, Table 2 continues the Table 1 until the Jupiter body mass. The orbital period of Eris corresponds well to the Uranus body mass, but the smaller transneptunian orbits, occupied by Pluto, Haumea and Makemake, ask for additional bodies. Possibly, the three vacant body masses and the three vacant orbital periods in Table 2 are properties of bodies which are still to be discover.

4 Resume

Celestial bodies are compressed matter which consist of nucleons over 99%. Possibly, the model approximation of $\mathrm{D} = 3/2$ and $\mu = 1$ in (1) for proton units is a macroscopic quantum physical property, which is based on the baryon nature of normal matter, because $\mu = 1$ means that $M/T^{\mathrm{D}} = m_p/\tau^{\mathrm{D}}$.

The scaling law (1) seems a true system property, because it describes a connection between masses and orbital periods of different celestial bodies (Mercury and Jupiter, Earth and Neptune, etc.) within the Solar system.

5 Acknowledgements

I'm thankful to my friend Victor Panchelyuga, my son Erwin and my partner Leili for the great experience to work with them, for the deep discussions and permanent support. I'm thankful to my teacher Simon Shnoll.

Submitted on January 26, 2015 / Accepted on January 27, 2015

Bodies, sorted by M	Body mass M, kg	$\ln(M/m_p)$	D	$\ln(T/\tau_p)$	Orbital period T, years	Bodies, sorted by T
Ceres	9.5000×10^{20}	109.9584	1.5387	71.4603	0.2408	Mercury
Makemake	2.1000×10^{21}	110.7516	1.5298	72.3980	0.6152	Venus
Haumea	4.0100×10^{21}	111.3985	1.5284	72.8839	1.0000	Earth
Pluto	1.3000×10^{22}	112.5746	1.5313	73.5156	1.8808	Mars
Eris	1.7000×10^{22}	112.8429	1.5165	74.4099	4.6000	Ceres
Mercury	3.3020×10^{23}	115.8094	1.5368	75.3573	11.8626	Jupiter
Mars	6.4191×10^{23}	116.4741	1.5272	76.2665	29.4475	Saturn
Venus	4.8690×10^{24}	118.5003	1.5327	77.3149	84.0168	Uranus
Earth	5.9742×10^{24}	118.7049	1.5221	77.9885	164.7913	Neptune

Table 1: For sorted by value couples of a body mass M and an orbital period T the fractal dimension D(2) is quite constant and closed to the model value 3/2. Data come from [8, 13–16].

Bodies, sorted by M	Body mass M, kg	$\ln(M/m_p)$	D2	$\ln(T/\tau_p)$	Orbital period T, years	Bodies, sorted by T
vacant	1.6358×10^{25}	119.7122	1.5270	78.3970	247.9207	Pluto
vacant	2.0281×10^{25}	119.9271	1.5270	78.5378	285.4000	Haumea
vacant	2.2999×10^{25}	120.0529	1.5270	78.6201	309.9000	Makemake
Uranus	8.6849×10^{25}	121.3816	1.5325	79.2064	557.0000	Eris
Neptun	1.0244×10^{26}	121.5467	1.5270	79.5984	824.2881	vacant
Saturn	5.6851×10^{26}	123.2605	1.5270	80.7207	2532.1227	vacant
Jupiter	1.8987×10^{27}	124.4664	1.5270	81.5104	5577.7204	vacant

Table 2: Continues Table 1 until the Jupiter body mass. The masses and orbital periods for vacant bodies are calculated, based on the empiric average value $D \approx 1.527$.

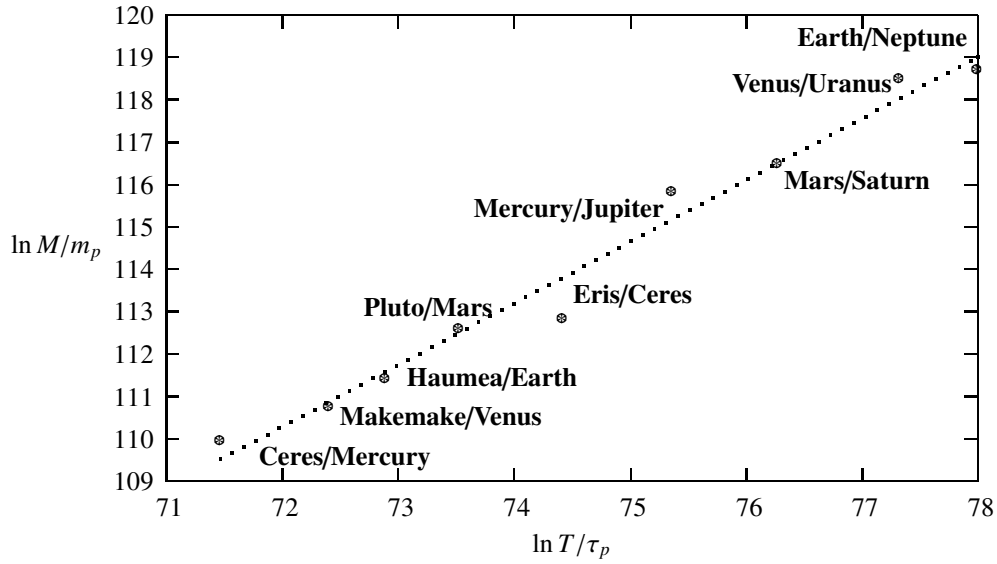

Fig. 1: Graphic representation of Table 1. For sorted by value couples of a body mass M and an orbital period T the fractal dimension D is quite constant. The doted line is drawed for the average $D \approx 1.527$.

References

1. Müller H. Fractal scaling models of natural oscillations in chain systems and the mass distribution of the celestial bodies in the Solar System. *Progress in Physics*, 2010, issue 3, 61–66.
2. Fook M.V.L., Ries A. Fractal Structure of Nature's Preferred Masses: Application of the Model of Oscillations in a Chain System. *Progress in Physics*, 2010, issue 4, 82–89.
3. Fook M.V.L., Ries A. Application of the Model of Oscillations in a Chain System to the Solar System. *Progress in Physics*, 2011, issue 1, 103–111.
4. Wu K.K.S., Lahav O., Rees M.J. The large-scale smoothness of the Universe. *Nature*, 1999, v. 397.
5. Barenblatt G.I. Scaling. Cambridge University Press, 2003.
6. Tatischeff B. Fractals and log-periodic corrections applied to masses and energy levels of several nuclei. arXiv: 1107.1976v1, 2011.
7. Müller H. Fractal scaling models of resonant oscillations in chain systems of harmonic oscillators. *Progress in Physics*, 2009, issue 2, 72–76.
8. Physical constants. Particle Data Group. www.pdg.lbl.gov
9. Müller H. Emergence of Particle Masses in Fractal Scaling Models of Matter. *Progress in Physics*, 2012, issue 4, 44-47.
10. Kolombet V. Macroscopic fluctuations, masses of particles and discrete space-time. *Biofizika*, 1992, v. 36, 492–499.
11. Müller H. Fractal Scaling Models of Natural Oscillations in Chain Systems and the Mass Distribution of Particles. *Progress in Physics*, 2010, issue 3, 61–66.
12. Hausdorff F. Dimension und äußeres Maß, 1919, v. 79.
13. Ragozzine D., Brown M. Orbits and Masses of the Satellites of the Dwarf Planet Haumea = 2003 EL61. *Astronomical Journal*, 2009. arXiv: 0903.4213v1.
14. Brown M, Schaller E. The Mass of Dwarf Planet Eris. *Science*, 2007, v. 316 (5831), p. 1585.
15. Neptune System Nomenclature Table Of Contents. Gazetteer of Planetary Nomenclature. USGS Astrogeology, 2009.
16. Malhotra R., Showman A. The Galilean Satellites. *Science*, 1999, v. 286, 77–84.

EDITORIAL MESSAGE

In Memoriam of Joseph C. Hafele (1933–2014)

Joseph Carl Hafele was born on July 25, 1933, in Peoria, Illinois, in the large family of Carl Louis Hafele and Thelma Loeb Hafele. He grew up among his many brothers and sisters.

In 1951, after serving in the US Army, he attended the University of Illinois at Urbana-Champaign. At the University, he got a BSc in engineering physics in 1959, and was bestowed the PhD degree in nuclear physics in 1962. After the graduation, during 1964–1966, he worked at the Los Alamos National Laboratory, wherein he conducted research in particle physics. After that, during 1966–1972, he worked within the Physics Faculty of Washington University at St. Louis, Missouri.

In 1958, he married Carol Hessling, and they raised four daughters.

In October 1971, Joseph C. Hafele commonly with Richard E. Keating, an astronomer from the US Naval Observatory, conducted the around-the-world-clock experiment which is one of the main experimental tests of the Theory of Relativity. Four Cesium atomic clocks were transported on board of a jet plane around the Globe twice, toward and against the direction of the Earth's rotation. The around-the-world-clock experiment showed, with high measurement precision, both gravitational and relativistic effects of Einstein's theory in the local space of the Earth. This experiment gave both of them world fame. Later, it became known as *Hafele-Keating experiment*.

Commencing in 1972, Joseph C. Hafele worked in different positions. He conducted some developments for Caterpillar Inc., lectured at Eureca College (1985–1991), was a visiting researcher for NASA at Langley AFB in Hampton, Virginia, lectured at Christopher Newport University in Newport News, Virginia. He retired in 1996, and settled in common with his wife Carol in Laramie, Wyoming.

Upon retirement, Joseph C. Hafele did not cease his scientific activity. Having no longer a physics laboratory for conducting experiments, he undertook deep theoretical research studies of the anomalous experiments which were unexplained in the frameworks of both modern classical mechanics and relativistic mechanics. He published a number of excellent papers in scientific journals, including our journal. It was a great honour for us to communicate with him and publish his research papers. Many of his scientific ideas still remain undeveloped until now.

In Laramie, Wyoming, he lived a modest life in common with his wife Carol, in their home where he grew tomatoes in his garden, and spent some astronomical observations at the telescope installed in his home observatory at the back yard.

Joseph C. Hafele and Richard E. Keating on board of a jet plane while performing the around-the-word-clock experiment (1971).

Joseph C. Hafele passed away in November 15, 2014, being 81 years old. His heart suddenly stopped during surgery for an aortic aneurism at the Medical Center of the Rockies in Loveland, Colorado.

Let his memory live for ever!

Dmitri Rabounski and Larissa Borissova

LETTERS TO PROGRESS IN PHYSICS

Solar-Time or Sidereal-Time Dependent? The Diurnal Variation in the Anisotropy of Diffusion Patterns Observed by J. Dai (2014, Nat. Sci.)

Felix Scholkmann

Bellariarain 10, 8038 Zürich, Switzerland. E-mail: felix.scholkmann@gmail.com

In this correspondence an additional analysis is reported about the anisotropic diffusion patterns of a toluidine blue colloid solution in water measured by J. Dai (*Nat. Sci.*, 2014, v. 6 (2), 54–58). In the previous analysis (Scholkmann, *Prog. in Phys.*, 2014, v. 10 (4), 232–235) it could be shown that the anisotropy data contain a diurnal and annual periodicity. This novel analysis investigated whether this periodicity is also present when the data were analyzed according to the sidereal time. The analysis revealed that the daily periodicity is present in the data scaled with the solar as well the sidereal time. When using solar time an oscillation with a diurnal period appears, when using sidereal time the oscillation is semidiurnal. In addition, the novel analysis revealed that the data of the maximum diffusion trend show a quantization of unknown origin.

Recently in this journal (v. 10 (4), [1]), I present a reanalysis of the data of J. Dai [2] that investigated fluctuations in anisotropic diffusion patterns of a toluidine blue colloid solution in water. It could be shown that the fluctuation of anisotropy, i.e. the maximum diffusion trend (MDT), clearly exhibits a diurnal and annual periodicity. Responding to this article, Prof. R. Cahill (Flinders University, Adelaide, Australia) suggested that it would be interesting to analyse if the observed periodicity is associated with the solar or the sidereal time (i. e. the time based on the Earth's rotation with respect to the fixed stars). In order to investigate this issue, the following new analysis was performed: (i) The time information given in the data of Dai was converted from the local solar time to the local sidereal time using the information of the location where the experiment was conducted (Wuhan City, China, latitude: N $\sim$ 30°35′35.1168″, longitude: E $\sim$ 114°18′18.6192″). (2) The data were analyzed by calculating the median and the median absolute deviation (MAD) for every hourly time interval (24 in total). (3) The function $f(\mathrm{MDT}) = \alpha_0 + \alpha_1 \cos(\mathrm{MDT}\ \omega)$ (with the free parameters α_0, α_1 and ω) was fitted to the daily grouped data using the Trust-Region-Reflective Least Squares Algorithm. For the fitting, the MAD values were taken into account to increase the precision of the fit (which is an improvement to the fitting approach used in the previous analysis [2]).

The individual MDT values plotted against the solar time and sidereal time are shown in Figure 1(a) and (e), respectively. Fitting the periodic (sinusoidal) function to the MDT data showed that the fit functions differ depending on the time scaling (solar vs. sidereal) used. When using the solar time the best fit is a function with a diurnal periodicity (see Figure 1(b)) whereas when using the sidereal time the best fit has a semidiurnal periodicity (See Figure 1(f)). The goodness-of-fit (quantified by the squared Pearson correlation coefficient, r^2, and the root-mean-square error, RMSE) for both cases were: (i) MDT data with solar time: $r^2 = 0.5028$, RMSE = 3.191, and (ii) MDT data with sidereal time: $r^2 = 0.4838$, RMSE = 3.04. A visualization of the r^2 and RMSE values for both cases is shown in Figure 1(d) and Figure 1(h). To visualize the density distribution of the MDT values the density at each point of the grid was calculated as $1/z$ with z the sum of squared distance from each point. For this the Matlab function "DataDensityPlot" written by M. McLean was used. The density plots are shown in Figure1(c) and Figure 1(g).

From this new analysis results we can conclude that (i) in both cases (solar and sidereal time scaling) the MDT data show a periodicity, (ii) the periodicity has a frequency depending on the time scaling: diurnal for solar time (oscillation maximum: at approx. 0.00 a.m.) and semidiurnal for sidereal time (oscillation maxima: at approx. 0.00 a.m. and 12.00–1.00 p.m.), (iii) the goodness-of-fit of the fitted function for both data sets (MDT vs. solar or sidereal time) is similar. The correlation is higher for the solar time scaling but the RMSE value lower for the sidereal time scaling. This can be interpreted as meaning that the MDT values contain an oscillation correlated with the solar as well as with the sidereal time. A related observation was obtained by Shnoll who found a solar and sidereal oscillation in the similarity of histograms of radioactive decay of ^{239}Pu [3, 4].

The detected oscillations indicate that there is possibly cosmophysical factor influencing the diffusion process. This factor might be influencing the process from a preferred direction in space such as determined for example by Miller (right ascension, $\alpha = 4^{\mathrm{hr}}\ 54^{\mathrm{min}}$, declination, $\delta = -70°\ 33'$ [5]; $\alpha = 4^{\mathrm{hr}}\ 56^{\mathrm{min}}$, $\delta = -70°\ 33'$ [6]), Cahill ($\alpha = 4.92^{\mathrm{hr}}$, $\delta = -75.0°$) [7], Múnera et al. ($\alpha = 16^{\mathrm{hr}}\ 40^{\mathrm{min}}$, $\delta = -75°$ [8]; $\alpha = 5^{\mathrm{hr}}\ 24^{\mathrm{min}}$, $\delta = +79°$ [9]), and Baurov ($\alpha = 19^{\mathrm{hr}}\ 32^{\mathrm{min}} \pm 40^{\mathrm{min}}$, $\delta = 36° \pm 10°$) [10].*

*The value for the right ascension is originally given by Baurov as $\alpha =$

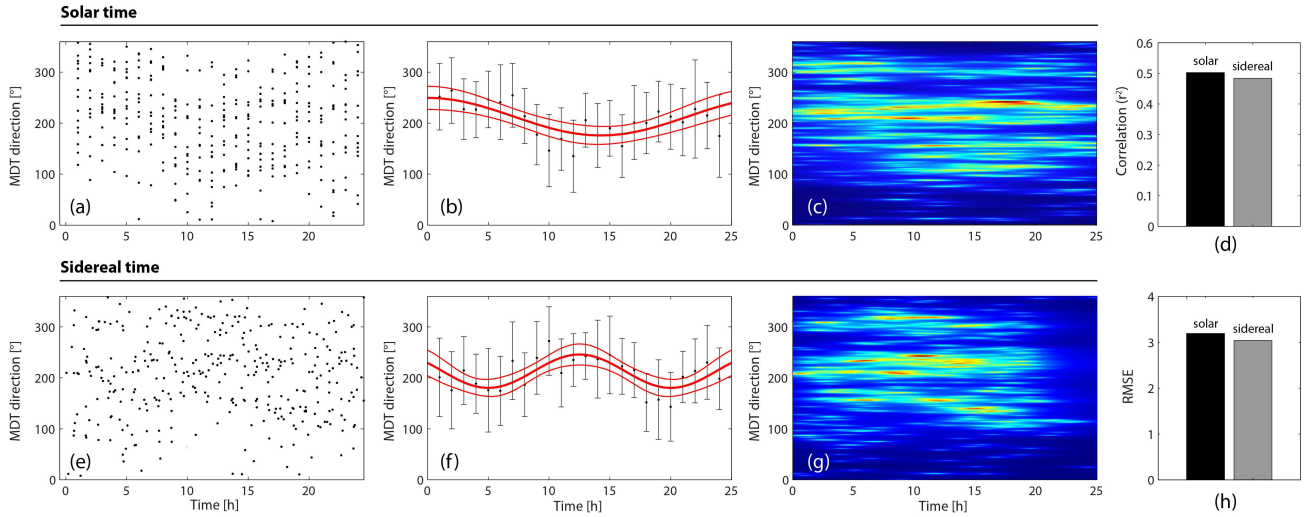

Fig. 1: Raw data plotted against solar (a) or sidereal (e) time. Fitted sinusoidal function to the MDT scaled using the solar (b) or sidereal (f) time. Density plot of the MDT values plotted against solar (c) or sidereal (g) time. The values for the correlation and RMSE value of the fit are shown in (d) and (h).

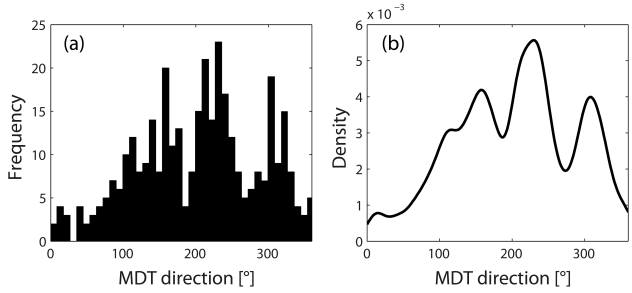

Fig. 2: (a) Histogram and Kernal density (b) of the MDT values.

As an additional analysis the characteristics of the distribution of the MDT from all 15 days were investigated by computing the histogram (number of bins: 40) and the Kernal density according to the method of Shimazaki & Shinomoto [5]. This analysis revealed an interesting pattern: the occurrence of MDT values shows three distinct peaks. The strongest peak is at 230°, the second at 158° and the third at 303° (see Figure 2). This quantization of diffusion anisotropy is another interesting feature of Dai's data that awaits explanation.

In conclusion, the new analysis performed shows novel features of the MDT data of Dai. Further MDT measurements and investigations into the cause of the observed effects would be an interesting next step in this area of research.

Submitted on January 28, 2015 / Accepted on February 5, 2015

293° ± 10° and was converted to $\alpha = 19^{\text{hr}}\ 32^{\text{min}}$ by the author using the equality 360° = 24 h.

References

1. Scholkmann F. Indications for a diurnal and annual variation in the anisotropy of diffusion patterns – A reanalysis of data presented by J. Dai (2014, Nat. Sci.). *Progress in Physics*, 2014, v. 10 (4), 232–235.
2. Dai J. Macroscopic anisotropic Brownian motion is related to the directional movement of a "Universe field". *Natural Science*, 2014, v. 6 (2), 54–58.
3. Shnoll S. E., Rubinstein I. A. Regular changes in the fine structure of histograms revealed in the experiments with collimators which isolate beams of alpha-particles flying at certain directions. *Progress in Physics*, 2009, v. 2, 83–95.
4. Shnoll S. E., Astashev M. E., Rubinstein I. A., Kolombet V. A., Shapovalov S. N., Bokalenko B. I., Andreeva A. A., Kharakoz D. P., Melnikov I. A. Synchronous measurements of alpha-decay of 239 Pu carried out at north pole, antarctic, and in Puschino confirm that the shapes of the respective histograms depend on the diurnal rotation of the earth and on the direction of the alpha-particle beam. *Progress in Physics*, 2009, v. 3, 11–16.
5. Miller D. C. The ether-drift experiment and the determination of the absolute motion of the earth. *Reviews of Modern Physics*, 1933, v. 5 (3), 203–242.
6. Miller D. C. The ether-drift experiment and the determination of the absolute motion of the earth. *Nature*, v. 133, 162–164.
7. Cahill R. T. Combining NASA/JPL one-way optical-fiber light-speed data with spacecraft Earth-flyby Doppler-shift data to characterise 3-space flow. *Progress in Physics*, v. 5 (4), 50–64.
8. Múnera H. A., Hernández-Deckers D., Arenas G., Alfonso E. Observation of a significant influence of Earth's motion on the velocity of photons in our terrestrial laboratory. *Proceedings of the SPIE, The Nature of Light: What Are Photons?*, v. 6664.
9. Múnera H. A., Hernándes-Deckers D., Arenas G, Alfonso E., López I. Observation of a non-conventional influence of earth's motion on the velocity of photons, and calculation of the velocity of our galaxy. *PIERS Proceedings, Beijing, China, 2009, March 23–27.*
10. Baurov Yu. A. Global Anisotropy of Physical Space. Nova Science Publishers, New York (USA), 2004.

Energy from Swastika-Shaped Rotors

Michael Edward McCulloch
University of Plymouth, Plymouth, PL4 8AA, UK
E-mail: mike.mcculloch@plymouth.ac.uk

It is suggested here that a swastika-shaped rotor exposed to waves will rotate in the direction its arms are pointing (towards the arm-tips) due to a sheltering effect. A formula is derived to predict the motion obtainable from swastika rotors of different sizes given the ocean wave height and phase speed and it is suggested that the rotor could provide a new, simpler method of wave energy generation. It is also proposed that the swastika rotor could generate energy on a smaller scale from sound waves and Brownian motion, and potentially the zero point field.

1 Introduction

With the recent awareness of the environmental damage caused by fossil fuels, there is a need to find renewable sources of energy. There are many possible sources of energy: sunlight, the wind, ocean tides and also the energy stored in ocean surface waves, and other types of waves. Ocean waves are particularly relevent for the island of Great Britain. It has been estimated that between 7 and 10 GW of energy might be extractable from the waves in UK waters by Wave Energy Converters (WECs), compared with the UK peak demand estimated at 65 GW, so that 15% of UK peak demand could be met by wave power [1].

One of the first viable techniques for the generation of ocean wave power was Salter's Duck which rotated along a horizontal axis under the undulation of waves and generated energy using dynamos. The result was an 81% conversion of wave energy into power [2], but this method extracts energy from waves only in one direction.

Another problem with Salter's duck and other wave energy converters is that they have many moving parts which can degrade with time. The new wave energy generation method proposed here is far simpler in structure and has only one moving part: the rotor. It can also be deployed far from the coast, and, as discussed later in the paper, is applicable to all kinds of waves or fluctuations and not just ocean waves, maybe also the zero point field.

Part of the inspiration for this paper was the proposal of Boersma [3] that two ships at sea will produce a wave shadow zone between them, so that more waves will hit the ships from outside than from between them and so the ships will tend to move together. This is an analogy to the well-known Casimir effect in quantum physics [4] which involves the suppression of the zero point field between two parallel conducting plates which are then forced together. The Casimir force has been measured [5]. The effect due to ocean waves is predicted to be small, but has recently also been measured by [6].

2 Method & results

This proposal uses a swastika, or Greek letter Chi, see Figure 1. The idea is that if waves arrive from all directions, more waves hit the outer sides of the swastika's arms, then hit the sheltered inner-facing sides of the arms, producing a torque that rotates the swastika about its axis.

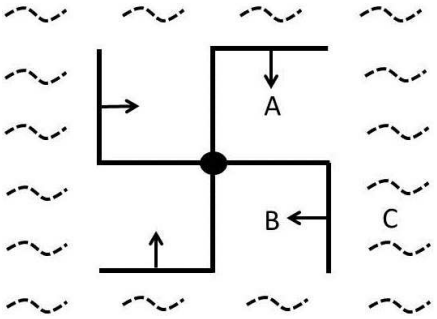

Fig. 1: Schematic showing the swastika rotor, the surrounding wave field (dashed lines) and the resulting forces (arrows).

To explain this more clearly and estimate the force that can be extracted from this shape we can consider three square areas that interact with the southeast arm: areas A, B and C as shown in Fig. 1. The assumption is that the areas A and B are sheltered zones rather like harbours and that only certain waves can exist between the walls, those with a wavelength that has nodes at the walls. If we then assume that the particular wavelength in the ocean does not fit, then there will be fewer waves in areas A and B, but there will of course be waves in area C since there is no closed boundary, it is open to the ocean. The maximum force obtainable from this shape can be found by looking at the net force on the southeast arm of the swastika and multiplying it by four. For the inner half of the southeast arm, between areas A and B, there is no net force since there are either no waves, or more likely the same intensity of waves, on either side, but for the outer half of the arm between B and C there will be a force on the arm pushing it westward because there are waves on the open east side, but not on the enclosed west side.

According to [7, 8] the impact pressure or slamming force (P) due to wave impacts is

$$P = \frac{F}{A} = K\rho C^2, \tag{1}$$

where A is the area of impact, K is an empirical constant between 3 and 10, ρ is the water density and C is the wave phase speed. For the southeast arm of the swastika this is

$$F = KA\rho C^2 \quad (2)$$

and A is the area hit by the waves which is the half-length of the arm (D) times the wave height h

$$F = KDh\rho C^2. \quad (3)$$

The force and resulting rotation will be clockwise, towards the arm-tips. Since $F = ma$, then the acceleration of the arm will be

$$a = \frac{KDh\rho C^2}{m}. \quad (4)$$

Equation 4 predicts the maximum acceleration obtainable from the swastika, neglecting friction, if its dimensions are such that it cancels the waves in areas A and B completely. The acceleration increases as a function of the wave height (h), length of the arms (D) and the phase speed (C). The acceleration, of course, decreases as the mass increases (m). The effect missing here is friction, which will slow the rotational acceleration as soon as it begins.

3 Discussion

This rotor is only a proposal at this stage. It requires testing in a wave tank big enough so that interactions between the swastika and the wave tank's walls are reduced and also so that the waves in area C are not damped. The waves should be a similar wavelength to the width of the arms of the swastika or shorter. Longer waves than this will not be able to resolve the shape of the arms so there will be no rotation. Eqs. 3 and 4 imply that to get the maximum rotation, the test should use a light rotor with arms projecting enough from the water to intercept the waves, subject to high waves with a large phase speed. Since the effect may be subtle, care will have to be taken to reduce the effects of residual rotational flows.

The swastika rotor has advantages over current wave energy devices in that it is simple and has only one moving part: the axle, it does not require wave impacts from any particular direction and can work just as well with isotropic random waves, and it will also rotate if a surface ocean current exists, but the opposite way, since it is then similar in design to an anenometer.

One intriguing possibility is that the rotation of the swastika shape in a wave field could also be applied at a much smaller scale. A smaller-scale swastika may be spun by sound waves, Brownian motion or even on the nanoscale by the zero-point field allowing perhaps that source of energy to be tapped for the first time.

On the Brownian scale [9] have shown that boomerang-shaped colloidal particles move towards their concave sides when subjected to Brownian motion: random collisions with atoms or molecules. A sheltering process similar to that described in this paper, might explain their results since, due to sheltering, these boomerang particles would see fewer impacts from atoms in the concave gap between their arms and more impacts on their convex side, so they should move towards their concave side, or towards their arm-tips, just as observed.

A light-driven swastika-shaped rotor on the nanoscale has already been demonstrated. It does not utilise the zero point field, but is driven by an applied beam of light and works in a different manner since the light photons interact with the electrons in the conducting shape [10].

4 Conclusions

It is predicted that a rotor in the shape of a swastika will rotate in the direction its arms are pointing, i.e.: towards the arm-tips, in the presence of isotropic waves, due to the sheltering effect of the arms.

It is proposed that such a rotor can be used to convert wave energy to electricity by using its axle to drive a dynamo. Its advantage over existing wave energy generating devices is its simplicity, its response to isotropic waves and its (reversed) response to surface currents. It now needs to be tested experimentally.

The swastika shape could also be used on smaller scales to generate energy from sound waves or Brownian motion: for example it may explain the observed motion of Boomerang-shaped particles. It may be possible to use nanoscale swastika rotors to extract energy from the hitherto untapped zero point field.

Submitted on February 1, 2015 / Accepted on February 4, 2015

References

1. Drew B., Plummer A.R., Sahinkaya M.N. A review of wave energy converter technology. *Proc. Inst. Mechanical Engineers, Part A: Journal of Power and Energy*, 2009, v. 223, no. 8, 887–902.
2. Falnes J. A review of wave-energy extraction. *Marine Structures*, 2007, v. 20(4), 185–201.
3. Boersma S.L. A maritime analogy of the Casimir effect. *Am. J. Phys.*, 1996, v. 64(5).
4. Casimir H.B.G. On the attraction between two perfectly conducting plates. *Proc. Kon. Nederland Akad. Wetensch.*, 1948, v. B51, 793.
5. Lamoreaux S.K. Demonstration of the Casimir force in the 0.6 to 6 μm range. *Phys. Rev. Lett.*, 1997, v. 78, 5–8.
6. Denardo B.C., Puda J.J. and Larazza A. A water wave analog of the Casimir effect. *Am. J. Phys.*, 2009, v. 77(12).
7. Bea R.G., Xu T., Stear J., Ramos R. Wave forces on decks of offshore platforms. *Journal of Waterway, Coastal and Ocean Engineering*, May/June 1999, 136–144.
8. Chen E.S and Melville W.K. Deep-water plunging wave pressure on a vertical plane wall. *Proc. R. Soc. Lond.*, 1988, v. A417, 95–131.
9. Chakrabarty A., Konya A., Wang F., Selinger J.V., Sun K., Wie Q.-H. Brownian motion of boomerang colloidal particles. *Phys. Rev. Lett.*, 2013, v. 111, 160603.
10. Liu M., Zentgraf T., Liu Y., Bartal G., Zhang X. Light-driven nanoscale plasmonic motors. *Nature Nanotechnology*, 2010, v. 5, 570–573.

Nuclear Phase Transition from Spherical to Axially Symmetric Deformed Shapes Using Interacting Boson Model

A. M. Khalaf[1], N. Gaballah[2], M. F. Elgabry[3] and H. A. Ghanim[1]

[1]Physics Department, Faculty of Science, Al-Azhar University, Nasr City 11884, Cairo, Egypt.
E-mail: ali_khalaf43@hotmail.com hussein00848@gmail.com

[2]Physics Department, Faculty of Science (Girls branch), Al-Azhar University, Nasr City 11884, Cairo, Egypt.
E-mail: nermgaballah@yahoo.com

[3]Mathematics and Physics Department, Faculty of Engineering, Al-Azhar University, Nasr City 11884, Cairo, Egypt.
E-mail: erereg@yahoo.com

The interacting boson model (sd-IBM1) with intrinsic coherent state is used to study the shape phase transitions from spherical U(5) to prolate deformed SU(3) shapes in Nd-Sm isotopic chains. The Hamiltonian is written in the creation and annihilation form with one and two body terms.For each nucleus a fitting procedure is adopted to get the best model parameters by fitting selected experimental energy levels, B(E2) transition rates and two-neutron separation energies with the calculated ones.The U(5)-SU(3) IBM potential energy surfaces (PES's) are analyzed and the critical phase transition points are identified in the space of model parameters.In Nd-Sm isotopic chains nuclei evolve from spherical to deformed shapes by increasing the boson number. The nuclei ^{150}Nd and ^{152}Sm have been found to be close to critical points.We have also studied the energy ratios and the B(E2) values for yrast band at the critical points.

1 Introduction

The interacting boson model (IBM) [1] describes the low energy quadruple collective states of even-even nuclei in terms of bosons with angular momentum 0 and 2 so called s and d bosons. The bosonic Hamiltonian is assumed to have a general form with one- and two-body terms and must be invariant under some fundamental symmetries. The algebraic formulation of the IBM allows one to find analytical solutions associated with breaking the U(6) into three dynamical symmetries called U(5), SU(3) and O(6) limits of the model, corresponding to spherical (vibrational), axially symmetric prolate deformed (rotational)and soft with respect to axial symmetric (γ-unstable) shapes respectively.

Phase transitions between the three shapes of nuclei are one of the most significant topics in nuclear structure research [2-11]. These shape phase transitions were considered in the framework of the geometric collective model [12], resulting in the introduction of the critical point symmetries E(5) [13] X(5) [14]. Y(5) [15], Z(5) [16] and E(5/4) [17]. The E(5) corresponds to the second order transition between U(5) and O(6), while X(5) corresponds to the first order transition between U(5) and SU(3). The symmetry at the critical point is a new concept in the phase transition theory, especially for a first order transition. From the classical point of view, in a first order transition, the state of the system changed discontinuously and a sudden rearrangement happens, which means that there involves an irregularity at critical point [18].

Empirical evidence of these transitional symmetries at the critical points has been observed in several isotopes.
The study of the shape phase transitions in nuclei can be best done in the IBM, which reproduces well the data in several transitional regions [8, 11].

In this paper we use the IBM with intrinsic coherent states to study the spherical to prolate deformed shape transition in the Nd-Sm isotopic chains. Section 2 outlines the theoretical approach and the main features of the U(5)-SU(3) model, the model Hamiltonian under study is introduced in subsection 2.1. In subsection 2.2 the intrinsic coherent states are given as energy states of the model Hamiltonian.In section 3 we present the numerical results of PES's for Nd-Sm isotopic chains and gives some discussions. Finally a conclusion is given in section 4.

2 Outline of the theoretical approach

2.1 The general Hamiltonian of the sd-IBM

In order to study the geometric shapes associated with the sd-IBM, we consider the most standard one and two body IBM Hamiltonian [1]

$$\begin{aligned} H &= \epsilon_s \hat{n}_s + \epsilon_d \hat{n}_d \\ &+ \sum_L \frac{1}{2}\sqrt{2L+1}\, C_L \Big[[d^\dagger \times d^\dagger]^{(L)} \times [\tilde{d} \times \tilde{d}]^{(L)}\Big]^{(0)} \\ &+ \frac{1}{\sqrt{2}} v_2 \left(\Big[[d^\dagger \times d^\dagger]^{(2)} \times \tilde{d}s\Big]^{(0)} + \Big[s^\dagger d^\dagger \times [\tilde{d} \times \tilde{d}]^{(2)}\Big]^{(0)}\right) \\ &+ \frac{1}{2} v_0 \left(\Big[[d^\dagger \times d^\dagger]^{(0)} \times ss\Big]^{(0)} + \Big[s^\dagger s^\dagger \times [\tilde{d} \times \tilde{d}]^{(0)}\Big]^{(0)}\right) \\ &+ u_2 [d^\dagger s^\dagger \times \tilde{d}s]^{(0)} + \frac{1}{2} u_0 [d^\dagger s^\dagger \times ss]^{(0)} \end{aligned} \quad (1)$$

with

$$C_L = \langle ddL|v|ddL\rangle, \tag{2}$$

$$v_2 = \sqrt{\frac{5}{2}}\,\langle dd2|v|ds2\rangle, \tag{3}$$

$$v_0 = \langle dd0|v|ss0\rangle, \tag{4}$$

$$u_2 = 2\sqrt{5}\,\langle ds2|v|ds2\rangle, \tag{5}$$

$$u_0 = \langle ss0|v|ss0\rangle, \tag{6}$$

where $s^\dagger(s)$ and $d^\dagger(\tilde{d})$ are the creation and annihilation operators of the s and d bosons. $\tilde{d}$ is the annihilation operator of the d boson with the time reversal phase relation $\tilde{d}_{2k} = (-1)^{2+k} d_{2,-k}$.

2.2 The intrinsic coherent state

The geometric picture of the IBM can be investigated by introducing the intrinsic coherent state which is expressed as a boson condensate [19]:

$$|N\beta\gamma\rangle = \frac{1}{\sqrt{N!}}({b_c}^\dagger)^N|0\rangle, \tag{7}$$

$${b_c}^\dagger = \frac{1}{\sqrt{1+\beta^2}}\left[s^\dagger + {d_0}^\dagger\,\beta\cos\gamma + \frac{1}{\sqrt{2}}({d_2}^\dagger + {d_{-2}}^\dagger)\beta\sin\gamma\right], \tag{8}$$

where N is the boson number, β and γ are the intrinsic deformation parameters which determine the geometrical shape of the nucleus.$|0\rangle$ is the boson vacuum. Here $\beta \geq 0$, $0 \leq \gamma \leq \frac{\pi}{3}$.

2.3 The Potential Eneryg Surface (PES)

The PES associated with the classical limit of IBM Hamiltonian (1) is given by its expectation value in the intrinsic coherent state (7)

$$\begin{aligned} E(N,\beta,\gamma) &= \langle N\beta\gamma|H|N\beta\gamma\rangle = \epsilon_s\frac{N}{1+\beta^2} + \epsilon_d\frac{N\beta^2}{1+\beta^2} + \\ &\left(\frac{1}{10}C_0 + \frac{1}{7}C_2 + \frac{9}{35}C_4\right) N(N-1)\frac{\beta^4}{(1+\beta^2)^2} - \\ &\frac{2}{\sqrt{35}}v_2 N(N-1)\frac{\beta^3\cos 3\gamma}{(1+\beta^2)^2} + \frac{1}{\sqrt{5}}(v_0+u_2)N(N-1) \\ &\frac{\beta^2}{(1+\beta^2)^2} + \frac{1}{2}u_0 N(N-1)\frac{1}{(1+\beta^2)^2}. \end{aligned} \tag{9}$$

If the parameter $v_2 = 0$, then the PES is independent of γ. If $v_2 \neq 0$ then for every $\beta > 0$ the PES has a minimum at $\gamma = 0$, if $v_2 > 0$ (axially symmetric case with prolate shape) or $\gamma = \frac{\pi}{3}$ if $v_2 < 0$ (oblate shape).

The PES equation (9) can be written in another form as:

$$\frac{E(N,\beta,\gamma)}{N} = \frac{A_2\beta^2 + A_3\beta^3\cos 3\gamma + A_4\beta^4}{(1+\beta^2)^2} + A_0 \tag{10}$$

Table 1: Equilibrium values of the parameters A_2, A_3, A_4 in the large N limit for transition from dynamical symmetry limit U(5) to dynamical symmetry limit SU(3) as an illustrative example.

Set	A_2	A_3	A_4
a	500	-283	850
b	102	-508	703
c	91	-514	727
d	0	-566	700
e	-250	-707	625
f	95	-512	728
g	85	-517	725

with

$$A_2 = \epsilon_d - \epsilon_s - u_0 + (N-1)\frac{1}{\sqrt{5}}(u_2 + v_0), \tag{11}$$

$$A_3 = -\frac{2}{\sqrt{35}}(N-1)v_2, \tag{12}$$

$$A_4 = \epsilon_d - \epsilon_s - \frac{1}{2}u_0 + (N-1)\left(\frac{1}{10}C_0 + \frac{1}{7}C_2 + \frac{9}{35}C_4\right), \tag{13}$$

$$A_0 = \frac{1}{2}u_0. \tag{14}$$

To determine the critical values of the order parameters of the system, one needs to determine the locus of points for which the conditions $\frac{\partial E}{\partial \beta} = 0$ and $\frac{\partial^2 E}{\partial \beta^2} = 0$ are fulfilled.

The equilibrium value of β is determined by:

$$\frac{\partial E(N,\beta)}{\partial \beta} = 0, \tag{15}$$

leading to

$$\beta\left[2A_2 + 3A_3\beta + (4A_4 - 2A_2)\beta^2 - A_3\beta^3\right] = 0. \tag{16}$$

Figure (1) (with the parameters listed in table (1)) illustrates the critical points: For $A_2 = 1, A_3 = A_4 = 0$, the nucleus is in the symmetric phase since the PES has a unique minimum at $\beta = 0$ when A_3 and A_4 not vanish and A_2 decreases, a second nonsymmetric minimum arises (set b) at $\beta \neq 0$. This non symmetric minimum take the same depth of the symmetric one at the critical point (set c). Beyond this value, the symmetric minimum at $\beta = 0$ becomes unstable point (set d). (Sets g, h) show two cases in the coexistence region.

3 Application to Nd–Sm isotopic chains

Nuclei in rare-earth region are well-known examples of the U(5)-SU(3). The validity of the present technique is examined for the rare earth isotopic chains $^{144-154}$Nd and $^{146-162}$Sm. The optimized values of the nine parameters of the Hamiltonian $\epsilon_s, \epsilon_d, c_0, c_2, c_4, u_0, u_2, v_0, v_2$ which are truncated to four parameters A_2, A_3, A_4, A_0 are adjusted by fitting

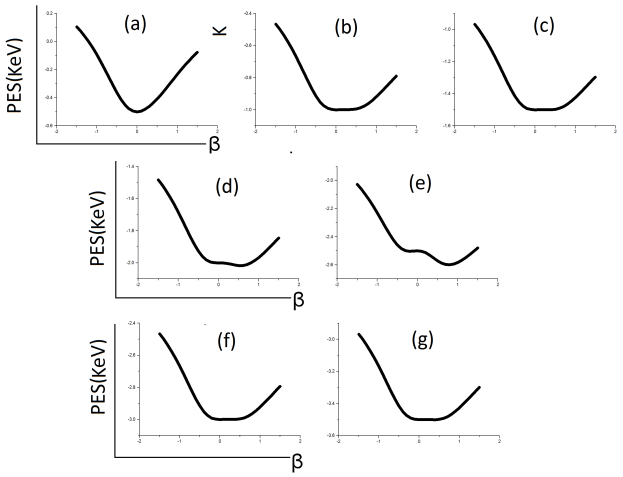

Fig. 1: The scaled PES's as a function of the deformation parameter β for the model parameters listed in table (1). The curves (b, c, d) represents the spinodal, critical and antispinodal points respectively. The curves (f, g) show two cases on the coexistence region.

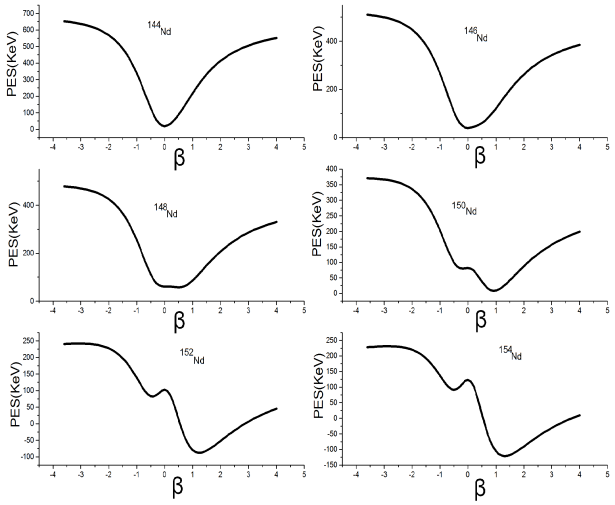

Fig. 2: The PES's (in the $\gamma = 0$ plane given by the IBM as a function of deformation parameter β , to describe the U(5)-SU(3) transition in $^{144-154}$Nd isotopic chain. The calculations are for $\chi = -\sqrt{7}/2$.

procedure using a computer simulated search program in order to describe the gradual change in the structure as neutron number varied (number of bosons) and to reproduce ten positive parity experimental levels namely ($2_1{}^\dagger$, $4_1{}^\dagger$, $6_1{}^\dagger$, $8_1{}^\dagger$, $0_2{}^\dagger$, $2_3{}^\dagger$, $4_3{}^\dagger$, $2_2{}^\dagger$, $3_1{}^\dagger$ and $4_2{}^\dagger$), the B(E2) values and the two neutron separation energies for each nucleus in each isotopic chain. The effect of ϵ_s be ignored also the parameter u_0 is kept zero because it can be absorbed in the three parameters. The resulting model parameters are listed explicitly in Table (2). The PES's $E(N,\beta)$ as a function of the deformation parameter $\beta$for our Nd-Sm isotopic chains evolving from spherical to axially symmetric well deformed nuclei are illustrated in the Figures 2, 3. At the critical points (^{150}Nd, ^{152}Sm) the spherical and deformed minima must coexist and be degenerated in order to obtain a first order phase shape transition. To identify the shape phases and their transition it is helpful to examine the correspondence between the interaction strengths in the microscopic model and the dynamical symmetry in the IBM.

Phase transitions in nuclei can be tested by calculating the energy ratios

$$R_{I/2} = E(I_1^+)/E(2_1^+). \tag{17}$$

For $I = 4$, the ratio $R_{4/2}$ varied from the values which correspond to vibrations around a spherical shape$R_{4/2} = 2$ to the characteristic value for excitations of a well deformed rotor $R_{4/2} = 3.33$. Figure (4) shows the $R_{I/2}$ for ^{150}Nd and ^{152}Sm compared to U(5) and SU(3) prediction.

Now, we discuss the electric quadruple transition probabilities. The general form of the E2 operator was used

$$T^{(E2)} = \alpha\left(\left[d^\dagger \times \tilde{s} + s^\dagger \times d^\dagger\right]^{(2)} + \beta\left[\tilde{d} \times \tilde{d}\right]^{(2)}\right) \tag{18}$$

where α is the boson effective charge and β is the structure

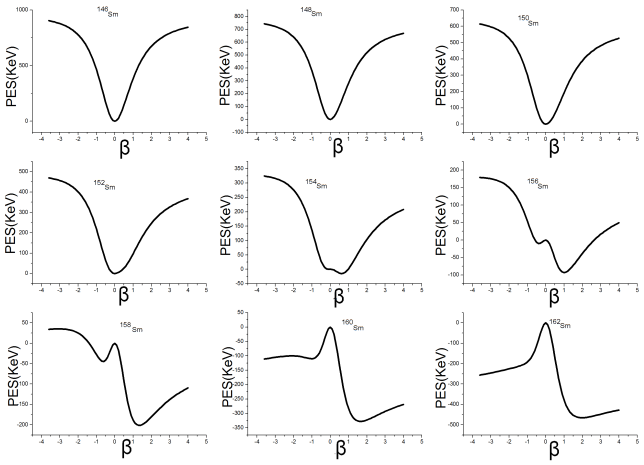

Fig. 3: The same as Fig.2 but for $^{146-162}$Sm isotopic chain.

parameter. The parameters α and β have been determined directly from the least square fitting to the observed $\beta(E2)$. $\alpha = 0.135$ and $\beta = -0.115$. The ratios of the E2 transition rates for the U(5) and SU(3) are given by

$$\begin{aligned} B_{(I+2)/2} &= B(E2, I+2 \to I)/B(E2, 2_1^+ \to 0_1^+), \\ &= \frac{1}{2}(I+2)\left(1 - \frac{I}{2N}\right) \qquad \text{for U(5)}, \\ &= \frac{15}{2}\frac{(I+2)(I+1)}{(2I+3)(2I+5)}\left(1 - \frac{I}{2N}\right)\left(1 + \frac{I}{2N+3}\right) \\ &\quad \text{for SU(3)}. \end{aligned} \tag{19}$$

In Figure (5), the $B_{(I+2)/2}$ ratios are shown for the best candi-

Table 2: The adopted best model parameters in (keV) for our selected Nd-Sm isotopic chains.

	N_B	A_2	A_3	A_4	A_0
^{144}Nd	6	400.132	-242.551	636.717	18.936
^{146}Nd	7	168.175	-291.061	452.077	39.874
^{148}Nd	8	54.518	-339.571	385.737	60.812
^{150}Nd	9	-140.338	-388.081	238.197	81.751
^{152}Nd	10	-359.495	-436.591	66.357	102.689
^{154}Nd	11	-452.052	-485.102	21.117	123.627
^{146}Sm	7	748.245	-160.541	946.905	0.0
^{148}Sm	8	554.405	-187.298	786.175	0.0
^{150}Sm	9	360.565	-214.055	625.445	0.0
^{152}Sm	10	166.725	-240.812	464.715	0.0
^{154}Sm	11	-27.115	-267.569	303.985	0.0
^{156}Sm	12	-220.955	-294.326	143.255	0.0
^{158}Sm	13	-414.795	-321.083	-17.475	0.0
^{160}Sm	14	-608.635	-347.839	-178.205	0.0
^{162}Sm	15	-802.475	-374.596	-338.935	0.0

date ^{152}Sm compared to the U(5) and SU(3) predictions and the experimental data.

4 Conclusion

The shape transition U(5)-SU(3) in $^{144-154}$Nd and $^{146-162}$Sm isotopic chains in the rare earth region is studied in the framework of sd IBM1 using the most general Hamiltonian in terms of creation and annihilation operators using the method of the intrinsic states.

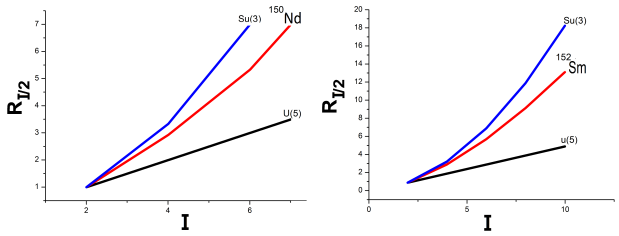

Fig. 4: Normalized excitation energies $R_{I/2} = E((I_1{}^{\dagger})/E((I_2{}^{\dagger})$ for ^{150}Nd and ^{152}Sm nuclei compared to U(5) and SU(3) predictions.

The optimized model parameters have been deduced by using a computer simulated search program in order to obtain a minimum root mean square deviation of the calculated some excitation energies, the two neutron separation energies and some B(E2) values from the measured ones. The PES's are analyzed and the location of the critical points are obtained. In our Nd and Sm chains, nuclei evolve from spherical to prolate deformed shape transition. The lighter nuclei are spherical and the heavier are well deformed. The ^{150}Nd and the ^{152}Sm have been found to be critical point nuclei, that is the

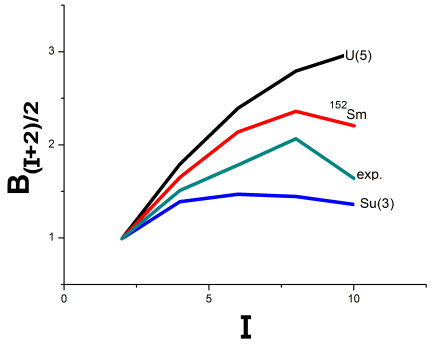

Fig. 5: Comparison of the $B_{I+2/2} = B(E2, I+2 : I)/B(E2, (2_1{}^{\dagger}, 0_1{}^{\dagger})$ ratios of the ground state band in ^{152}Sm (N=11) compared to the U(5) and SU(3) predictions and the experimental ratio.

transition from the spherical to deformed occurs between boson number N=9 and N=10. The energy ratios and the B(E2) values are also studied.

Submitted on January 18, 2015 / Accepted on February 2, 2015

References

1. Iachello F. & Arima A. The Interacting Boson Model. Cambridge University Press, Cambridge, (1987).
2. Liu Y.X., Mu L.Z. and Wei H. Approach to the Relation Driven Vibrational to Axially Rotational Shape Phase Transition along the yrast line of a Nucleus. *Phys. Lett.* 2006, v. 633 B, 49–53.
3. Rowe D.J. *Nuc. Phys.* 2004, v. A745, 47; Rosenstell G. and Rowe D.J. Nuc. Phys. 2005, v. A759, 92.
4. S.Heinze et al. Evolution of spectral properties along the O(6)-U(5) transition in the interacting boson model. I. Level dynamics – Heinze, Stefan et al. *Phys. Rev.*, 2006, v. C73, 014306.
5. Zhang J.F., Lü L.J. and Bai H.B. Critical behaviour in nuclear structure from spherical to axially symmetric deformed shape in IBM. *Chinese Physics*, 2007, v. 16, 1941–2006.
6. Hellemans v. et al. Phase Transition in the Configuration Mixed Interacting Boson Model u(5)-O(6) Mixing. *Acta Physica Palonica*, 2007, v. 38B, 1599.
7. Casten R.F. *Nucl. Phys.* 2009, v. A62, 183.
8. Khalaf A.M. and Awwad T.M. A Theoritical description of U(5)-SU(3)Nuclear Shape Transitions in the Interacting Boson Model. *Progress In Physics*, 2013, v. 1, 7–11.
9. Khalaf A.M. and Ismail A.M.,The Nuclear Shape Phase Transition Studied within the Geometric Collective Model. *Progress in Physics*, 2013, v. 2, 51–55; Structure Shape Evaluation in Lanthenide and Actinaide Nuclei,*Prgress in Physics*, 2013, v. 2, 98–104.
10. Khalaf A.M. et al,Nuclear Potential Enrgy Surfaces and Critical Point Symmetry withen the Geometric Collective Model. *Progress in Physics*, 2014, v. 10, 12–15.
11. Khalaf A.M., Hamdy H.S. and El-Sawy M.M. Nuclear Shape Transition using Interacting Boson Model with the Intrinsic Coherent State. *Progress in Physics*, 2013, v. 3, 44–51.
12. Bohr A. and Mottelson B. Nuclear Structures Benjamin, New York, 1975, Vol.2.

13. Iachello F. Dynamic Symmetries at the Critical point. *Phys. Rev. Lett.*, 2000, v. 85, 3580–3583.

14. Iachello F. Analytic Prescription of Critical Point Nuclei in a Spherical Axially Deformed Shape Phase Transition. *Phys. Rev. Lett.*, 2001, v. 87, 052502–052506.

15. Iachello F. Phase Transition on Angle variables. *Phys. Rev. Lett.*, 2003, v. 91, 132502–132507.

16. Bonatsos O. et al. Z(5): Critical Point Symmetry for the Prolate to Oblate Nuclear Shape Phase Transition. *Phys. Lett.*, 2004, v. 588B, 172–179.

17. Iachello F. *Phys. Rev. Lett.*, 2005, v. 95, 0525203.

18. Landau L.D. and Lifshitz F.M. Statistical Physics, Butterworth-Heinemann, Oxford, 2001, Part 1.

19. Dieprink A.E.L., Soholten O. and Iachello F. Classical Limit of the Interacting Boson Model. *Phys. Rev. Lett.*, 1980, v. 44, 1747–1750.

Planck's Radiation Law: Thermal Excitations of Vacuum Induced Fluctuations

Fernando Ogiba
E-mail: ogiba@cpovo.net

The second Planck's radiation law is derived considering that "resonators" induced by the vacuum absorb thermal excitations as additional fluctuations. The maximum energy transfer, as required by the maximum entropy equilibrium, occurs when the frequencies of these two kind of vibrations are equal. The motion resembles that of the coherent states of the quantum oscillator, as originally pointed by Schrödinger [1]. The resulting variance, due to random phases, coincides with that used by Einstein to reproduce the first Planck's radiation law from his thermal fluctuation equation [2].

1 Introduction

In 1901, Planck derived the spectral distribution of radiant heat, simply calculating entropy from the number of ways that thermal energy can be distributed among all blackbody resonators (maximum entropy). This forced him to interpret the possible energies of the resonators, for a given mode and temperature, as multiples of a fixed energy; the quantum of electromagnetic energy [3]. In such approach, the appearance of a collection of resonators — with all sort of frequencies — depends only on thermal excitations, that is, for $T = 0$ they do not exist. However, in 1912 Planck realized that *thermal equilibrium with radiation* would make sense only if the resonators remain even for $T = 0$ [4]. In this new approach the quantization of the first Law was preserved, but only in the emissions, that is, oscillators in equilibrium with radiation absorbs continuously until a certain $nh\nu$ is reached, and then they emit or continues absorbing. From this semi-classical derivation, one concludes that exists vibrations not induced by thermal excitations. In this way, arose the concept of zero-point energy (ZPE), which is a term of the second Planck's radiation law, i.e.

$$\langle E \rangle = \frac{1}{2}\,\hbar\omega + \frac{\hbar\omega}{e^{\hbar\omega/k_B T} - 1}. \tag{1}$$

At the time, the ZPE was a controversial concept; at best, it was accepted as "virtual photons due to nearby matter". The concept of a radiation field permeating the vacuum, and then inducing "matter-oscillators" with an energy given by the first term of Eq. (1), only gained credibility after the predictions of the quantum field theory (quantum vacuum states) and the experimental proof of the Casimir's force [5]. In fact, around the middle of the last century they begin appear works that assume explicitly that the matter (elementary electrical charges or agglomerates of them) are in permanent interaction with a zero-point radiation field (ZPF); absorbing and emitting electromagnetic radiation in a conservative way, independently of temperature.

In accordance with the experimentally proved work of Casimir [6] and the proponents of the stochastic electrodynamics [7], the ZPF is a homogeneous and isotropic distribution of electromagnetic plane waves pervading all space; each one carrying energy proportional to its frequency (ranging from zero to infinite, or a big cutoff value), $\hbar\omega/2$. Moreover, its spectral energy density is proved to be a Lorentz invariant. As the phases of such waves are randomically distributed in the range $[0, 2\pi]$, then electrical charges (or any agglomerate of them) are permanently receiving unpredictable impulses with the following features: First, the ZPF isotropy ensures zero net momentum transfer. Second, the emitted radiation, due to non uniform acceleration, responds by the local energy conservation. Third, the symmetric distribution of emissions ensures zero net self-momentum (no liquid radiation reaction). Fourth, the permanent nature of the absorption-emission process imply a remnant random trembling motion, whose energy in the particle-bound reference frame, in the case of a free electron, is the well-known rest energy

$$m_0 c^2 = \frac{\hbar\omega_Z}{2}, \tag{2}$$

where ω_Z is the zitterbewegung frequency [8, 9].

This zitterbewegung, strongly correlated with the translational motion trough the de Broglie's periodicity, prevent such particles to follow predictable paths (quantum randomness). Even so, the overall motion obeys the dynamical principle founded on trajectories. Non relativistically, this obedience means that the center of mass of the particle's vibrations can be found — instantly — over any one of the trajectories dictated by the stochastic Hamilton-Jacobi-Bohm equation, which is implicit in the Schrödinger's equation [10].

What follows is a derivation of Planck distribution, which replaces the quantization a priori by the presence of the ZPF, which, therefore, is the responsible by "resident blackbody resonators". Nevertheless, quantization is implied. Indeed, the zero-point energy ε_0, besides being a fixed quantity for each mode, is indispensable to get a discrete Boltzmann's distribution from a continuous one [12].

2 Thermal excitations of vacuum induced fluctuations

The energy absorbed (emitted) from (to) the ZPF in order to form temperature independent primordial matter-oscillators (or "Blackbody resonators") is

$$\varepsilon_0(\omega) = \frac{1}{2}\,\hbar\omega. \tag{3}$$

When particles absorbs such vibrant energy, conservatively, it is expected that its coordinates fluctuates as

$$q_0(t,\phi) = \sqrt{\frac{2\varepsilon_0(\omega)}{m\omega^2}}\cos(\omega t+\phi), \tag{4}$$

which differs from a typical classical oscillation only by the presence of random phases ϕ (ZPF randomness), which imply that this equation does not describe the actual path followed by particles, but simply obedience to the dynamic principle at each occupied position. Indeed, this is the main feature of the Schrödinger's equation, as argued elsewhere.

Notice, now $\varepsilon_0(\omega)$ is the energy of the matter-oscillator (the zero-point energy), which, as can be seen by simple substitution of Eq. (4), obey the equality

$$\varepsilon_0(\omega) = \frac{1}{2\pi}\int_0^{2\pi}\left[(2)\frac{2\pi}{\omega}\int_0^{2\pi/\omega}\frac{1}{2}\,m\left(\frac{dq_0(t,\phi)}{dt}\right)^2 dt\right]d\phi, \tag{5}$$

where the factor (2) refers to equal contributions from kinetic and potential energies of the harmonic oscillator, ω is the angular frequency of the absorbed radiation, the integral in t is an average over the radiation period, and the integral in ϕ is an average over random phases.

Given the permanent nature of the interactions, the ZPE must be viewed as a remnant energy. It is indispensable to compose the ground state energy of quantum systems. The exact shape, as it should be, only appears in the case of the harmonic oscillator.

For $T \neq 0$, there are thermal excitations, which manifest as additional vibrations that increase the amplitude of existing fluctuations. In a sense, this can be inferred from the thermal dilatation of bodies. In other words, the center of mass of the matter-fluctuations, as expressed by Eq. (4), fluctuates due to thermal excitations. This implies the superposition

$$q_{\phi,\Phi}(t) = \sqrt{\frac{2\varepsilon_0(\omega)}{m\omega^2}}\cos(\omega t+\phi)+\sqrt{\frac{2\mathcal{E}_T(\Omega)}{m\Omega^2}}\cos(\Omega t+\Phi), \tag{6}$$

where $\mathcal{E}_T(\Omega)$ is the vibrational energy induced be thermal excitations at the temperature T, Φ is a random phase, and, for the sake of generality, Ω is an arbitrary frequency.

It is worth informing, the assumption of the last paragraph is in full agreement with what is inferred from the coherent states of the quantum harmonic oscillator (the perfect framework to derive the Planck's law); that is, the statistical Gaussian of the ground state (here, the primordial oscillator) is moved, as a whole, by classical oscillations [11, see p. 104].

Averaging the energy

$$(2)\times\frac{\omega}{2\pi}\int_0^{2\pi/\omega}\frac{1}{2}\,m\left(\frac{dq_{\phi,\Phi}(t)}{dt}\right)^2 dt$$

over random phases, both ϕ and Φ, yields the energy absorbed (emitted) by this superposition of vibrations, i.e.

$$E(\omega,\Omega) = \varepsilon_0(\omega)+\mathcal{E}_T(\Omega), \tag{7}$$

where Ω still continues unknown.

Now, averaging the square deviation from $\varepsilon_0(\omega)$,

$$\left[(2)\times\frac{2\pi}{\omega}\int_0^{2\pi/\omega}\frac{1}{2}m\left(\frac{dq_{\phi,\Phi}(t)}{dt}\right)^2 dt-\varepsilon_0(\omega)\right]^2,$$

over both random phases, emerges the variance

$$\sigma^2_{\omega,\Omega} = \frac{2\hbar\omega^3\left(\omega^2+\Omega^2\right)\sin^2(\pi\Omega/\omega)\,E_T(\Omega)}{\pi^2\left(\omega^2-\Omega^2\right)}+$$
$$+\frac{\left[\omega^2+16\pi^2\Omega^2-\omega^2\cos^2(4\pi\Omega/\omega)\,E_T(\Omega)\right]E_T(\Omega)}{16\pi^2\Omega^2} \tag{8}$$

which seems to diverges when $\Omega\to\omega$. In true, there is the maximum variance

$$\sigma^2 = \lim_{\Omega\to\omega}\sigma^2_{\omega,\Omega} = E_T^2(\omega)+\hbar\omega E_T(\omega), \tag{9}$$

which can also be obtained replacing Ω by ω in the starting Eq. (6), and then performing the indicated operations.

Maximum variance implies maximum entropy (or thermodynamical equilibrium). Indeed, calculating entropy form Gaussian or exponential distribution (like Boltzmann's distribution) one find that entropy is proportional to $[\ln(\sigma^2)+cte]$.

From another point of view, the Eq. (9) also means that maximum energy transfer occurs when thermal vibrations are tuned with that induced by the ZPF, in full agreement with a well-known result of the theory of oscillations; that is, maximum energy transfer occurs at the natural frequency of the absorbing oscillator.

Therefore, from this tuned behavior — thermodynamical equilibrium — it follows that each possible energy, considering Eq. (7), obey

$$E = \frac{\hbar\omega}{2}+E_T(\omega), \tag{10}$$

and are distributed in such a way that the corresponding distribution has the variance σ^2.

It is crucial emphasizing, such ensemble of random energies is justified by a variance arising from random phases, ϕ and Φ. The first is a well-known feature of the ZPF (masterfully interpreted in the quantum mechanics framework), and the second is related to the myriad of ways that thermal excitations can move an elementary constituent of a body.

3 Thermal fluctuations and the Planck's radiation law

The variance expressed by Eq. (9) ensures that for each ω-mode at the remperature T there is a collection of random energies E, Eq. (10). From a thermodynamical point of view, the equilibrium involving such energy fluctuations must be treated in terms of the Boltzmann's statistics.

Deriving the moments of such distribution,

$$\langle E^r\rangle = \frac{\int_0^\infty dE E^r e^{-\beta E}}{\int_0^\infty dE e^{-\beta E}} = r!\langle E\rangle^r,$$

with respect to $\beta = 1/k_B T$, we obtain the Einstein's thermal fluctuation equation

$$\sigma_E^2 = k_B T^2 \frac{d\langle E\rangle}{dT}, \tag{11}$$

where, in the present calculations, $\langle E\rangle$ is the thermal average of the energies expressed by Eq. (10), i.e.

$$\langle E\rangle = \frac{\hbar\omega}{2} + \langle E_T\rangle, \tag{12}$$

and the thermal variance (thermal fluctuation) σ_E^2 is, therefore, the thermal average of Eq. (9):

$$\sigma_E^2 = \langle E_T\rangle^2 + \hbar\omega\langle E_T\rangle. \tag{13}$$

Combining the last three equations, we get the differential equation

$$k_B T^2 \frac{d\langle E_T\rangle}{dT} = \langle E_T\rangle^2 + \hbar\omega\langle E_T\rangle, \tag{14}$$

whose solution, considering $\langle E_T\rangle = 0$ for $T = 0$, is

$$\langle E_T\rangle = \frac{\hbar\omega}{e^{\hbar\omega/k_B T} - 1}. \tag{15}$$

Therefore,

$$\langle E\rangle = \frac{\hbar\omega}{2} + \frac{\hbar\omega}{e^{\hbar\omega/k_B T} - 1}. \tag{16}$$

Submitted on February 10, 2015 / Accepted on February 14, 2015

References

1. Schrödinger E. Collected Papers on Wave Mechanics, Blackie Son Limited, 1929
2. Einstein A. Zum gegenwartgen Stand des Strahlungs-problems. *Physikalische Zeitschift*, 1900, v. 10, 185–193. Published in The Collected Papers of Albert Einstein,v. 2: The Swiss Years: Writings, 1900-1909 (English translation supplement), Princeton University Press, 1989, 357–369.
3. Planck M. The Theory of Heat Radiation, Dover, New York, 1959.
4. Milonni P. W. The Quantum Vacuum: An Introduction to Quantum Electrodynamics, Academic Press, 1994.
5. Casimir H. B. G. On the attraction between two perfectly conducting plates. *Proceedings of the Royal Netherlands Academy of Arts and Sciences*, 1948, v. B51, 793–795.
6. Lamoraux S. K. Demonstration of the Casimir Force in the 0.6 to 6m Range. *Physical Review Letters*, 1997, v. 78, n. 1, 5–8.
7. Boyer T. H. Random electrodynamics: The theory of classical electrodynamics with classical electromagnetic zero-point radiation. *Physical Review D*. 1975, v. 11, n. 4, 790–808.
8. Dirac P. A. M. The Principles of Quantum Mechanics, 4ed. Oxford University Press, 1999.
9. Sidharth B. G. Revisiting Zitterbewegung. *International Journal of Theoretical Physics*, 2009, v. 48, 497–506.
10. Ogiba F. Addendum to Phenomenological Derivation of the Schrödinger Equation. *Progress in Physics*, 2014, v. 1, 108–110.
11. Burkhardt C. E., Leventhal J. J. Foundations of Quantum Physics, Springer, 2008.
12. de la Peña L., Ceto A. M. The Quantum Dice: An Introduction to the Stochastic Electrodynamics, Kluwer Academic, Dordrecht, 1996

Diffusion Equations, Quantum Fields and Fundamental Interactions

Sebastiano Tosto

Retired physicist. E-mail: stosto44@gmail.com, stosto@inwind.it

The paper concerns an "ab initio" theoretical model based on the space-time quantum uncertainty and aimed to identify the conceptual root common to all four fundamental interactions known in nature. The essential information that identifies unambiguously each kind of interaction is inferred in a straightforward way via simple considerations involving the diffusion laws. The conceptual frame of the model is still that introduced in previous papers, where the basic statements of the relativity and wave mechanics have been contextually obtained as corollaries of the quantum uncertainty.

1 Introduction

Understanding the fundamental interactions of nature is certainly one among the most challenging topics of the modern physics; a unified theory able to account for the fundamental forces is a dream of the physicists since a long time [1, 2]. The science of the fundamental interactions progressed with the advancement of the physics of the elementary particles [3], whose properties could be tested by examining their way of interacting with other particles. The theoretical models bridging quantum and relativistic theories [4, 5] progressed along with the merging of the physics of the elementary particles and quantum fields [6] with that of the fundamental interactions. All this culminated with the formulation of the standard model [7] and with the superstring theory [8]. The way the particles interact involves significantly even the cosmology [9, 10]. The GU theories [11, 12] share some general concepts about the four fundamental interactions, their basic idea to model the force between quantum particles is in principle simple: to exchange appropriate elementary particles that transfer momentum and energy between the interacting partners. The vector bosons are acknowledged to mediate the forces between particles according to their characteristic features of lifetime and action range [13]. These messenger particles, quanta of the respective fields, are said to mediate the interaction that propagates with finite velocity and perturbs the space-time properties. This way of thinking suggests reasonably the key role of the displacement mechanism of the particles that propagate the interaction, e.g. the different transport rates of massive or massless messengers; this means, in particular, that the space in between a set of interacting particles is filled with the vector bosons mutually exchanged. As clouds of these latter flow throughout the space-time, it is reasonable to expect that the global properties of the resulting interaction should depend on the ability of the messengers to spread around the respective partners. Eventually, since the mutual positions of each particle in the set are in general functions of time, even random local density gradients of these messengers are expectedly allowed to form throughout the space-time.

These preliminary considerations feed the idea of implementing a model of fundamental interactions based on a appropriate mechanism of transport of matter/energy, sufficiently general to be suitably extended from sub-nuclear to infinite range interactions. Among the possible transport mechanisms deserves attention the particle diffusion, driven by a gradient law originated by a non-equilibrium situation; as it has been shown in a previous paper [14], this law is strictly connected with the global entropy increase of an isolated thermodynamic system, the diffusion medium plus the diffusing species both tending to the equilibrium configuration in the state of maximum disorder. So the driving force of the diffusion process is actually the second principle of thermodynamics, i.e. a law so general to hold at the nano-micro-macro scales of interest in the present context. As a matter of fact, it has been found that this law allows describing not only the concentration gradient driven mass transport but also other important laws of physics: for instance Ohm's electric conductivity or Fourier's heat conductivity or Poiseuille pressure laws [14]. So, in agreement with the quantum character of the approach therein introduced, appears stimulating in principle the idea of testing via the diffusion laws even the exchange of vector bosons to describe the fundamental interactions. This hint leads in a natural way to the idea of dynamical flux of messenger particles, by consequence of which are exchanged momentum and energy of the interacting partners. This assumption merely requires that the messengers of the forces are exchanged as clusters of particles randomly flowing through the space-time and thus characterized in general by local concentration gradients. The physics of the four fundamental interactions has been already concerned in a dedicated paper [15]; in that paper the interactions have been described starting directly from the concept of space-time uncertainty. Here this problem is reformulated via the diffusion laws only in a surprisingly simple way. This paper aims to show that the key features of the fundamental forces are obtained by elaborating purposely the diffusion laws; it will be emphasized that these laws provide interesting hints also for relativistic and thermodynamic considerations. Of course the purpose of the paper is not that of providing an exhaustive description of the fundamental interactions, which would require a much longer review of the huge amount of literature

existing about each one of them; the paper intends instead to emphasize an even more crucial aspect of this topic, i.e. how to infer the essential features of all known interactions from a unique fundamental principle; in other words, the aim is to focus on a unique conceptual root from which follow contextually as corollaries all fundamental interactions. The paper introduces an "ab initio" model via considerations limited to the minimum necessary to infer the distinctive features of the various forms of interaction that identify unambiguously each one of them. Despite this topic is usually tackled via heavy computational ways, the present theoretical model is conceptual only but surprisingly straightforward. While the idea of interactions due to a diffusion-like flux of vector bosons has been early introduced [16], in the present paper this hint is further implemented. The model concerned in this paper exploits first the quantum origin of the diffusion laws, shortly reported for completeness of exposition, to infer next the interactions directly via the diffusion laws. Some concepts already published [14, 15, 16] are enriched here with further considerations in order to make this paper as self-contained as possible. It is clear the organization of the paper: the section 2 introduces the quantum background of the model and both Fick diffusion laws, plus ancillary information useful in the remainder sections; the section 3 introduces some thermodynamic considerations; the section 4 concerns the fundamental interactions, whereas the section 5 concerns a few additional remarks on the gravity force.

2 Physical background

The statistical formulation of the quantum uncertainty reads in one dimension

$$\Delta x \Delta p_x = n\hbar = \Delta\varepsilon\Delta t, \qquad \Delta\varepsilon = \mathrm{v}_x \Delta p_x, \qquad \mathrm{v}_x = \Delta x/\Delta t. \quad (1)$$

The subscript indicates the component of momentum range along an arbitrary x-axis. The second equality is actually consequence of the former merely rewritten as $(\Delta x/\mathrm{v}_x)(\Delta p_x \mathrm{v}_x)$, being Δt the delocalization time lapse necessary for the particle to travel throughout Δx; so this definition leaves unchanged the number n of quantum states allowed to the concerned system. Since the local coordinates are waived "a priori", i.e. conceptually and not as a sort of approximation aimed to simplify some calculation, these equations focus the physical interest on the region of the phase space accessible to the particle rather than on the particle itself. As these equations link the space range Δx to the time range Δt via n, any approach based on these equations is inherently four-dimensio-nal by definition. The sizes of the uncertainty ranges are arbitrary, unknown and unknowable; it has been shown that they do not play any role in determining the eigenvalues of the physical observables [17], as in effect it is known from the operator formalism of the wave mechanics. Actually it is possible to show that the wave formalism can be inferred as a corollary of the Eqs. (1) [17], coherently with the fact that n plays just the role of the quantum number in the eigenvalues inferable via these equations only [18, 19]. The Eqs. (1), early introduced in these papers to provide a possible way to describe the quantum systems in alternative to the solution of the pertinent wave equations, have been subsequently extended to the special and general relativity [20]. It has been shown for instance that a straightforward consequence of the space time uncertainty is

$$c^2 \Delta p_x = \mathrm{v}_x \Delta\varepsilon. \quad (2)$$

The demonstration is so short and simple to deserve of being mentioned here for completeness: this equation and the next Eq. (3) are enough for the purposes of the present paper. Consider a free particle delocalized in Δx. If this particle is a photon in the vacuum, then $\Delta x/\Delta t = c$; i.e. the time range Δt is necessary by definition for the photon to travel Δx. Yet, trusting to the generality of the concept of uncertainty, the Eqs. (1) must be able to describe even the delocalization of a massive particle moving at slower rate $\mathrm{v}_x = \Delta x/\Delta t < c$. Let us examine now this problem according to the Eqs. (1), i.e. starting from $\Delta x \Delta p_x = \Delta\varepsilon\Delta t$ to infer $\Delta\varepsilon/\Delta p_x = \Delta x/\Delta t$; as c represents the maximum velocity allowed to any particle, it must be true that $\Delta x/\Delta t \leq c$, whence $\Delta\varepsilon/\Delta p_x \geq c$. The inequality therefore constrains the ratio of the range sizes $\Delta\varepsilon$ and Δp_x depending on whether the delocalized particles are massive or not. Anyway both chances are considered writing $\Delta\varepsilon/\Delta p_x = (c/\mathrm{v}_x)c$. One finds thus the sought Eq. (2), which implies the local functional dependence $c^2 p_x = \mathrm{v}_x\varepsilon$ between energy and momentum and velocity components of the massive particles. Also note that the Eq. (2) implies the concept of mass simply introducing the limit

$$\lim_{\mathrm{v}_x \to 0} \frac{\Delta p_x}{\mathrm{v}_x} = \frac{\Delta\varepsilon_{rest}}{c^2} = m. \quad (3)$$

As there is no compelling reason to expect a vanishing $\Delta\varepsilon_{rest}$ for $\mathrm{v}_x \to 0$, one concludes that the left hand side is in general finite and corresponds to the definition of mass. Both signs are allowed in principle to v_x and thus to Δp_x; yet squaring $c^4\Delta p_x^2 = \mathrm{v}_x^2\Delta\varepsilon^2$ and implementing again $\mathrm{v}_x < c$, one finds $c^2\Delta p_x^2 < \Delta\varepsilon^2$ i.e. $\Delta\varepsilon^2 = c^2\Delta p_x^2 + \Delta\varepsilon_o^2$; thus the local functional dependence $\varepsilon^2 = c^2 p_x^2 + \varepsilon_o^2$, well known, combined with the Eq. (3) yields $\varepsilon_o = mc^2$ and also the explicit expressions of ε and p_x compliant with the respective Lorentz transformations.

2.1 Quantum basis of the diffusion laws

This subsection assumes that the diffusion medium is an isotropic body of solid, liquid or gas matter at constant and uniform temperature. The following considerations shortly summarize the reasoning introduced in [14]. Let us divide both sides of the Eq. (2) by $\mathrm{v}_o V$, being v_o an arbitrary velocity and V an arbitrary volume. So one finds

$$\mathrm{v}_x C = \Delta J_x, \qquad C = \frac{\Delta p_x}{\mathrm{v}_o V}, \qquad \Delta J_x = \frac{\Delta\varepsilon/c^2}{V}\mathrm{v}_x. \quad (4)$$

As C has physical dimensions $mass/volume$, it represents the average concentration of a mass m in the volume V, whereas ΔJ_x is the net change of the flux of particles moving at average rate v_x through V. So ΔJ_x, whose physical dimensions are $mass/(time \times surface)$, describes the net flux of matter entering in and leaving out two opposite surfaces delimiting V; the first Eq. (4) also implies that the functional dependence of any J_x within its uncertainty range ΔJ_x upon the corresponding local flux of m fits the classical definition $J_x = Cv_x$. Assuming that $\Delta\varepsilon/c^2$ is the energy equivalent of mass, the last equation inferred with the help of the Eq. (2) extends the definition of flux of the first equation to the change of energy density inside V. Write now $V = \Delta x^3$, which is certainly possible regardless of the particular geometric shape because both V and Δx are arbitrary; so any shape factor, e.g. $4\pi/3$ for spherical V, is inessential because it would still yield $V = \Delta x'^3$ once included in $\Delta x'$. Since $\Delta x^{-3} = -\partial\Delta x^{-2}/2\partial\Delta x$, one finds

$$\Delta J_x = \frac{\Delta p_x}{\Delta x^3} = -\frac{\Delta p_x}{2}\frac{\partial \Delta x^{-2}}{\partial \Delta x}.$$

Moreover $\Delta x^{-2} = \Delta p_x^2/(n\hbar)^2$, so that

$$\Delta J_x = -\frac{\Delta p_x^2}{(n\hbar)^2}\frac{\partial \Delta p_x}{\partial \Delta x} = -\frac{1}{3(n\hbar)^2}\frac{\partial \Delta p_x^3}{\partial \Delta x}$$

which yields in turn

$$\Delta J_x = -\frac{n\hbar}{3}\frac{\partial(1/\Delta x^3)}{\partial \Delta x} = -\frac{n\hbar}{3m}\frac{\partial(m/\Delta x^3)}{\partial \Delta x}. \quad (5)$$

The last equality holds under the reasonable assumption of constant mass m in the volume Δx^3: as both V and m are arbitrary, the former can be conveniently chosen in order to fulfil the requirement that the latter is simply redistributed within Δx^3 during an assigned diffusion time Δt related to ΔJ_x. Indeed the fact of having defined C as the average concentration of a constant amount of diffusing mass does not exclude the existence of a concentration gradient within V; in effect ΔJ_x results in the Eq. (5) as the concentration gradient driven mass flux at the boundary surfaces of V. Also note that $\hbar/m$ has the same physical dimensions, $length^2/time$, of a diffusion coefficient D; so, as shown in [14], it is possible to write $D = qn\hbar/m$ being q an appropriate numerical coefficient able to fit the experimental value of D of any species moving in any diffusion medium. Owing to the generality of the Eqs. (1), no specific hypothesis is necessary about whether the concerned diffusion process occurs in gas or liquid or solid phase or even in the vacuum; also, this holds at any temperature and value of C. So the last equation (5) reads

$$\Delta J_x = -D\frac{\partial C}{\partial \Delta X}, \quad C = \frac{m}{\Delta x^3}, \quad \Delta X = \frac{\Delta x}{q}, \quad D = \frac{qn\hbar}{m}. \quad (6)$$

Of course the inessential factor 3 has been included into q. Here C is related to the given amount of mass m redistributed within V; so it depends not only on m itself, but on the space extent through which this redistribution was allowed to occur. This result is nothing else but the well known first Fick gradient law, now straightforward consequence of the fundamental Eqs. (1). So far, for simplicity has been concerned the one-dimensional case, symbolized by the subscript x denoting the actual vector components of momentum and displacement velocity of m along an arbitrary x-axis. Yet it is useful to account explicitly for the vector nature of the equations above summarizing the Eqs. (4) and (6) as follows:

$$\Delta\mathbf{J} = C\mathbf{v} = -D\nabla C. \quad (7)$$

For the following purposes, it is interesting to extend these first results. Given an arbitrary function $f(x,t)$ of coordinate and time, express its null variation $\delta f(x,t) = 0$ as $(\partial f/\partial x)\delta x + (\partial f/\partial t)\delta t = 0$ that reads $v_x(\partial f/\partial x) + (\partial f/\partial t) = 0$ i.e. $\mathbf{v}\cdot\nabla f + \partial f/\partial t = 0$; this yields $\nabla\cdot(f\mathbf{v}) - f\nabla\cdot\mathbf{v} = -\partial f/\partial t$. It is convenient in the present context to specify this result putting $f = C$, in which case $f\mathbf{v} = \mathbf{J}$; thus

$$\nabla\cdot\Delta\mathbf{J} = -\nabla\cdot(D\nabla C) = -\frac{\partial C}{\partial t} + C\nabla\cdot\mathbf{v} \qquad C = C(x,y,z,t). \quad (8)$$

In the particular case where $\mathbf{v}$ is such that the second addend vanishes, one obtains a well known result, the second Fick equation subjected to the continuity boundary condition required by $\delta f = 0$ i.e.

$$\nabla\cdot\Delta\mathbf{J} = -\frac{\partial C}{\partial t} \qquad \nabla\cdot\mathbf{v} = 0. \quad (9)$$

The condition on $\mathbf{v}$ is satisfied if in particular:
(i) $\mathbf{v} = \mathbf{i}v_1(y,z,t) + \mathbf{j}v_2(x,z,t) + \mathbf{k}v_3(x,y,t)$ or (ii) $\mathbf{v} = \mathbf{v}(t)$ or (iii) $\mathbf{v} = const$.

Anyway, whatever the general analytical form of $\mathbf{v}$ might be, this condition means that the vector $\mathbf{v}$ is solenoidal, which classically excludes sinks or sources of matter in the volume Δx^3 enclosing m. Note however that since the boundaries of any uncertainty range are arbitrary and unknown, introducing the range $\Delta\mathbf{J} = \mathbf{J} - \mathbf{J}_0$ means implementing the actual $\mathbf{J}$ as change of the flux in progress with respect to a reference flux $\mathbf{J}_0$ appropriately defined. For instance $\mathbf{J}_0$ could be a constant initial value at an initial time t_0 of $\Delta t = t - t_0$ where the diffusion process begins, in which case $\mathbf{J}_0$ can be put equal to zero by definition; this means determining the initial boundary condition $\mathbf{J}_0 = 0$ at $t_0 = 0$. Yet more in general is remarkable the fact that, according to the Eq. (8), the usual classical form $\mathbf{J} = C\mathbf{v}$ is also obtained if $\mathbf{J}_0$ is regarded as a reference flux as a function of which is defined $\mathbf{J}$ that fulfils the condition

$$\nabla\cdot\mathbf{J} = -\frac{\partial C}{\partial t} \qquad \nabla\cdot\mathbf{J}_0 = -C\nabla\cdot\mathbf{v}. \quad (10)$$

The quantum chance of expressing the diffusion equations considering $\Delta\mathbf{J}$ instead of $\mathbf{J}$ emphasizes that the classical view point is a particular case of, and in fact compatible with, the Eqs. (1).

This section has shown that the usual Fick equation (8) written as a function of $\mathbf{J}$ and C does not hold necessarily in the absence of sinks or sources of matter only, it includes also the chance $\nabla \cdot \mathbf{v} \neq 0$ provided that the boundary condition about the reference flux gradient $\nabla \cdot \mathbf{J}_0$ is properly implemented. In this subsection it has been also shown that all this has a general quantum basis.

2.2 Diffusion and relativistic velocity addition rule

Let us consider the Eq. (7) $\Delta\mathbf{J} = C\mathbf{v}$ and express the change $\delta\Delta\mathbf{J}$ of $\Delta\mathbf{J}$ as a function of the variations of $\delta\mathbf{v}$ and δC

$$\delta\Delta\mathbf{J} = \mathbf{v}\delta C + C\delta\mathbf{v} \qquad \mathbf{v} = \mathbf{v}_x + \mathbf{v}_y + \mathbf{v}_z \qquad \mathbf{v} = \mathbf{v}(\Delta t) \quad (11)$$

to calculate the scalar product of $\delta\Delta\mathbf{J}$ by one component of $\mathbf{v}$, e.g. $\mathbf{v}_x$:

$$\mathbf{v}_x \cdot \delta\Delta\mathbf{J} = \mathbf{v}_x \cdot \mathbf{v}\delta C + C\mathbf{v}_x \cdot \delta\mathbf{v}. \quad (12)$$

It is interesting to define in particular $\delta\mathbf{v}$ orthogonal to this component $\mathbf{v}_x$ for reasons clarified below; hence

$$\mathbf{v}_x \cdot \delta\mathbf{v} = 0, \qquad \mathbf{v}_x = \delta\mathbf{v} - (\delta\mathbf{v})^2 \frac{\mathbf{v}_o}{\mathbf{v}_o \cdot \delta\mathbf{v}}. \quad (13)$$

The second equation shows the form of $\mathbf{v}_x$ that satisfies the former condition whatever the ancillary vector $\mathbf{v}_o$ might be. So, owing to the Eqs. (7) and (12), one finds

$$\mathbf{v}_x \cdot \delta\Delta\mathbf{J} = \mathbf{v}_x \cdot \mathbf{v}\delta C = \delta\Delta\mathbf{J} \cdot \delta\mathbf{v} - (\delta\mathbf{v})^2 \frac{\mathbf{v}_o \cdot \delta\Delta\mathbf{J}}{\mathbf{v}_o \cdot \delta\mathbf{v}}. \quad (14)$$

As concerns the second equality, eliminating $(\delta\mathbf{v})^2$ between the Eqs. (14) and (13) one finds

$$\mathbf{v}_x = \delta\mathbf{v} - \frac{(\delta\mathbf{v} - \mathbf{v}_x) \cdot \delta\Delta\mathbf{J}}{\mathbf{v}_o \cdot \delta\Delta\mathbf{J}}\mathbf{v}_o. \quad (15)$$

As concerns the first equality (14), it is possible to write

$$\mathbf{v}_x \cdot \delta\Delta\mathbf{J} = \pm \mathrm{v}_x \delta\Delta J_x,$$

$$\delta\Delta J_x = \pm \frac{\mathbf{v} \cdot \mathbf{v}_x \delta x}{\mathrm{v}_x} \frac{\delta C}{\delta x} = \pm(\mathrm{v}_x \delta x)\frac{\delta C}{\delta x}, \quad (16)$$

being $\delta\Delta J_x$ the modulus of the component of $\delta\Delta\mathbf{J}$ along $\mathbf{v}_x$. Note that $\mathbf{v} \cdot \mathbf{v}_x \delta x/\mathrm{v}_x = \mathbf{v} \cdot \mathbf{u}_x \delta x$, where $\mathbf{u}_x$ is a unit vector oriented along $\mathbf{v}_x$, has the physical dimensions of a diffusion coefficient D; so, being $|\mathbf{v}_x|$ arbitrary, the Eq. (16) reads

$$\delta\Delta J_x = \pm D\frac{\delta C}{\delta X}, \qquad D = q\mathrm{v}_x\delta x, \qquad \delta X = q\delta x, \quad (17)$$

with q again proportionality coefficient, as previously introduced. With the minus sign, the first equation fits the quantum result (6); this sign therefore is that to be retained. Also, this agreement supports the usefulness of the condition (13) and introduces a further result in the quantum frame of the present approach. Put $\mathbf{v}_x = \xi\mathbf{v}_o + \mathbf{v}_1$, being ξ an arbitrary constant and $\mathbf{v}_1$ another arbitrary vector; in this way $\mathbf{v}_x$ has been simply redefined through a linear combination of two vectors, as it is certainly possible. So the second Eq. (13) reads

$$\mathbf{v}_o = \frac{\delta\mathbf{v} - \mathbf{v}_1}{\xi - \dfrac{\xi(\delta\mathrm{v})^2}{\mathbf{v}_1 \cdot \delta\mathbf{v}}}.$$

Multiplying both sides of this equation by the unit vector $\mathbf{u}_z$ one finds

$$\mathrm{v}_{oz} = \frac{\delta\mathrm{v}_z}{\xi - \dfrac{\xi(\delta\mathrm{v})^2}{\mathbf{v}_1 \cdot \delta\mathbf{v}}}, \quad \mathrm{v}_{oz} = \mathbf{v}_o \cdot \mathbf{u}_z, \quad \delta\mathrm{v}_z = (\delta\mathbf{v} - \mathbf{v}_1) \cdot \mathbf{u}_z. \quad (18)$$

It is natural at this point to express the terms with physical dimensions of velocity and square velocity appearing in the last result as follows

$$\delta\mathrm{v}_z/\xi = u_a - u_b, \qquad (\delta\mathrm{v})^2 = u_a u_b, \qquad \mathbf{v}_1 \cdot \delta\mathbf{v} = c^2,$$

being u_a and u_b two arbitrary velocities; then one obtains

$$\mathrm{v}_{oz} = \frac{u_a - u_b}{1 - \dfrac{u_a u_b}{c^2}}. \quad (19)$$

The physical meaning of this result is acknowledged by reasoning "a posteriori", i.e. by assessing its implications. Trivial considerations show that, whatever the actual numerical value of c might be, if $u_a = u_b = c$ then $\mathrm{v}_{oz} = c$; also, the right hand side never exceeds c. Knowing that c is the upper value of velocity accessible to any particle [16], and so just for this reason invariant in different inertial reference systems in reciprocal motion [17], the Eq. (19) must have the physical meaning of addition velocity rule; the appropriate notation should be therefore $\mathrm{v}_{oz} = u'_a$ with u'_a corresponding to u_a in another reference system, which is possible because $\mathbf{v}_o$ has not been specifically defined. Also this conclusion is a corollary of the quantum principle of uncertainty, Eqs. (1), from which started the present reasoning.

Let us summarize the results achieved in this subsection. The Eqs. (6) and (7) introduce the laws of physics where the gradient of some non-equilibrium property, e.g. the non-uniform concentration of matter or charges and even temperature or pressure field gradients, generates the respective mass or charge or heat flows and related driving forces; this expresses the tendency of nature towards an equilibrium configuration corresponding to the maximum entropy [14]. Next the Eq. (12) enabled to infer the x-component of $\delta\Delta\mathbf{J}$ corresponding to that of the Eq. (6), thus emphasizing the connection of the present analysis with the straightforward quantum result. Eventually the orthogonality position of the Eq. (13) was also necessary to ensure that $\delta\mathbf{v}$ associated to $\delta\Delta\mathbf{J}$ does not imply the change of $\mathbf{v}_x$ to which is related D of the Eq. (17); so the Eq. (19) results pertinent to the Eq. (6) although obtained via $\delta\mathbf{v}$. This last result, Eq. (19), is a well known relativistic equation: the addition of the velocities, here expressed through

one velocity component along an arbitrary axis identified by $\mathbf{u}_z$, cannot overcome the limit speed c despite u_a or u_b or both are themselves equal to c. All of these results have been obtained via the first equation (13) only, which is straightforward consequence itself of the Eqs. (1). Besides the concrete importance of these results, however, the question arises at this point: what is the physical connection between the gradient laws of physics and the relativistic composition of the velocities? Otherwise stated: if the gradient law describes the tendency of physical systems towards the equilibrium state, why this result has been inferred contextually to the velocity addition rule of the special relativity? This question can be further extended also considering the dimensional properties of the flux of matter of the Eq. (7), whose time derivative obtained differentiating the Eq. (7) yields

$$\frac{\delta\Delta\mathbf{J}}{\delta\Delta t} = C\dot{\mathbf{v}} + \mathbf{v}\dot{C}, \qquad \dot{\mathbf{v}} = \frac{\delta\mathbf{v}}{\delta\Delta t}, \qquad \dot{C} = \frac{\delta C}{\delta\Delta t}; \quad (20)$$

as explained in [17], the derivatives are defined in the present model via the Eqs. (1) only, i.e. as ratios of the uncertainty ranges therein introduced. In the present context the ratio regards the change $\delta\Delta\mathbf{J}$ during $\delta\Delta t$. Being $C = mass/volume$ and noting that $\Delta\dot{\mathbf{J}}$ is $force/volume$, one infers that $\mathbf{F} \approx m\mathbf{a}$ in the case where $\mathbf{v}\dot{C}$ can be neglected with respect to the former addend. As it is known, force and acceleration are parallel vectors in the non-relativistic approximation only; since both C and $\mathbf{v}$ are arbitrary, in general they are expected to contribute at increasing $\mathbf{v}$ to the relativistic limit $|\mathbf{v}| \to c$ where reasonably the second addend becomes important. In effect is sensible the fact that $\mathbf{v}\dot{C}$ someway surrogates the relativistic consequences of the space-time deformation, recalling that $C = m/V$; writing $V = \Delta x^3$ and regarding the time derivative as that due to the change of V pertinent to a fixed amount m of mass, in agreement with the Eq. (5), one infers $\dot{C} = -3C\Delta\dot{x}/\Delta x$. In fact $\Delta\dot{x}/\Delta x$ is a deformation of the space-time uncertainty range Δx, being by definition $\Delta\dot{x} = \delta\Delta x/\delta\Delta t$; so, at least in principle, the involvement of relativistic concepts like the deformation of the space-time in the presence of the mass is understandable. In effect, is not accidental the fact that just this space-time deformation is the relativistic contribution to the Newtonian term $m\dot{\mathbf{v}}$.

In conclusion, the actual quantum origin of the diffusion equations stimulates the question about why relativistic implications, apparently dissimilar, have been contextually obtained without any "ad hoc" hypothesis. The only possible answer is that the mere context of the quantum uncertainty contains itself the intimate connection that underlies fundamental laws even of apparently different nature. All considerations have been carried out by elaborating the Eqs. (1), which are thus the common root of these results: so this conclusion is not surprising because, as shown in [17], even the basic statements of quantum mechanics and special and general relativity are obtained as corollaries of the Eqs. (1). Therefore further considerations are expectedly hidden in this kind of approach, even as concerns the field gradient driven forces.

2.3 Diffusion and driving forces

The second equality (7) reads $\mathbf{v} = -D\nabla\log(C)$ and suggests a reasonable link with the known expression of the chemical potential $\mu = k_BT\log(C)$; this hint yields

$$\mathbf{v} = -\frac{D}{k_BT}\nabla k_BT\log(C) \qquad \mathbf{F} = -\nabla k_BT\log(C); \quad (21)$$

then merging the thermodynamic definitions of μ and mobility β, i.e. $\mathbf{v} = \beta\mathbf{F}$, one finds contextually the force $\mathbf{F} = -\nabla\mu$ acting on the diffusing species and the Einstein equation $D = \beta k_BT$ linking mobility and diffusion coefficient. Note however that it is convenient to define μ as

$$\mu = k_BT\log(C/C_j) \qquad C_j = C_j(t) \quad (22)$$

which leaves unaffected $\mathbf{F}$ and $\mathbf{v}$ and is still consistent with the asymptotic limits $\mathbf{F} \to 0$ and $\mathbf{v} \to 0$ for $C \to const$: i.e. the driving force of the diffusion process vanishes when C evolves as a function of time to reach any constant concentration. This limit implies a gradient free distribution of matter attained for $C \to C_j$ evolving as well e.g. to fit the limit value of C. Further information is also inferred with the help of the Eq. (2); dividing both sides by Δt, this equation reads in vector form $\mathbf{F} = \Delta\mathbf{p}/\Delta t = (\Delta\varepsilon/c^2\Delta t)\mathbf{v}$, which yields with the help of the Eqs. (1)

$$\mathbf{F} = \frac{n\hbar(c\Delta t)\mathbf{v}}{(c\Delta t)^3} = \frac{n\hbar}{\delta x^3}\mathbf{v}\delta x, \quad \delta x = c\Delta t, \quad \beta = \frac{c^2\Delta t}{\Delta\varepsilon} = \frac{(c\Delta t)^2}{n\hbar}.$$

Calculate the component of $\mathbf{F}$ along the arbitrary direction of a unit vector $\mathbf{u}$; owing to the Eq. (17) the scalar $\mathbf{v}\cdot\mathbf{u}\delta x$ at right hand side defines the diffusion coefficient D, so

$$\frac{F_u}{D} = \frac{n\hbar}{V}, \qquad V = \delta x^3, \qquad D = \mathbf{v}\cdot\mathbf{u}\delta x. \quad (23)$$

Merging the last equation with the Eq. (6), one finds $\mathbf{v}\cdot\mathbf{u}\delta x = qn\hbar/m$, which reads $m\mathrm{v}_u\delta X = n\hbar$ and thus is just nothing else but the first equality (1). Implementing again the idea of expressing D via $n\hbar/m$ by dimensional reasons, see the Eqs. (6), the Eq. (23) reads

$$F_u = \frac{(n\hbar)^2}{mV}; \quad (24)$$

this step of the reasoning introduces diffusing mass and volume in the expression of the driving force of the macroscopic process whose diffusion coefficient is D. Interesting evidence about the importance of this result has been already emphasized in [16]; this point is so simple that it is worth being shortly summarized here for completeness.

The Eqs. (1) and (6) yield $qF_u/D = n\hbar/V$ and thus $qF_u/D = \Delta\varepsilon/\nu V$ having defined $\nu = \Delta t^{-1}$; so the right hand

side is an energy range per unit frequency and unit volume. Putting $\Delta\varepsilon = h\nu$ one finds thus $qF_u/D = nh/V$. Let now V be the volume of a cavity in a body filled with radiation in equilibrium with its internal walls, whose size is able to contain the longest wavelength $\lambda = c/\nu$ of the steady radiation field; of course λ is arbitrary. Then $V = (2c/\nu)^3$, where the factor 2 accounts for λ with nodes just at the boundaries of the cavity, whose size is thus one half wavelength. Hence $F_u/D = 8h(\nu/c)^3 n/q$. Is significant here the physical meaning of the ratio F_u/D, which has physical dimensions $h/volume$, regardless of the specific values of F_u and D separately; thus, being F_u/D the component of the vector $\mathbf{F}/D$ along the arbitrary direction defined by $\mathbf{u}$, regard this latter as a unit vector drawn outwards from the surface of the body at the centre of the cavity. As $\mathbf{u}$ represents any possible path of the radiation leaving the cavity, let q be defined in this case in agreement with $\int(F_u/D)d\Omega = \pi nh/V$. Actually F_u/D is taken out of the integral because it has no angular dependence, whereas the integral $\int d\Omega$ is carried out over the half plane above the surface of the cavity only, which yields 2π; a factor 1/2 is also necessary as this is the probability that one photon at the surface of the cavity really escapes outwards instead of being absorbed inwards within the cavity. So $\int(F_u/D)d\Omega = 8\pi h(\nu/c)^3 n$ yields the Planck black body formula once replacing the number n of states allowed to the radiation field with the factor $(\exp(h\nu/k_BT) - 1)^{-1}$ of the Bose distribution statistics of all oscillators: as an arbitrary number of particles is allowed in each state, n is also representative of any number of particles concerned by the statistical distribution.

Implement now the definition of mobility to write $\delta\mathbf{v} = \beta\delta\mathbf{F} + \mathbf{F}\delta\beta$; dividing both sides by $\delta\beta$ one finds $\delta\mathbf{v}/\delta\beta - \mathbf{F}' = \mathbf{F} = -\nabla\mu$, having put $\mathbf{F}' = \beta\delta\mathbf{F}/\delta\beta$. By analogy with $\mathbf{F}$, let us introduce the position $\mathbf{F}' = -\nabla Y$ with Y appropriate energy function related to $\delta\mathbf{F}$; thus the result is

$$\frac{\delta\mathbf{v}}{\delta\beta} = -\nabla(Y + \mu). \tag{25}$$

The physical meaning of this result is highlighted thinking that the physical dimensions of β are $time/mass$; considering in particular a volume V of matter where the mass is conserved and simply redistributed, exactly as assumed in the Eq. (5), $\delta\mathbf{v}/\delta\beta$ is proportional to $mass \times \delta\mathbf{v}/\delta t$, i.e. it is nothing else but the law of dynamics previously found via $\partial\mathbf{J}/\partial t$. The Eq. (25), which agrees with the additive character of the force vectors, could be also obtained via Euler's homogeneous function theorem. Here $\mathbf{F}'$ is regarded as if it would be a function of β, whereas it is usually implemented as a function of the position vector $\mathbf{r}$ defined in an appropriate reference system. To this purpose it is enough to put the modulus $r = a\beta$, being a a parameter that controls the local values of mobility as a function of r, to write $\mathbf{F}(a\beta) = a^k\mathbf{F}(\beta)$. So calculating $\partial\mathbf{F}(a\beta)/\partial a\beta = \beta\partial\mathbf{F}(a\beta)/\partial a = ka^{k-1}\mathbf{F}(\beta)$ and putting then in particular $a = 1$, as shown in standard textbooks, one finds $\beta\partial\mathbf{F}/\partial\beta = k\mathbf{F}(\beta)$; this is the essence of the Euler theorem. Eventually, once having inferred $\mathbf{F}' = \beta\delta\mathbf{F}/\delta\beta = a^k\mathbf{F}(\beta)$, similarly to $\mathbf{F} = -\nabla\mu$ one concludes $\mathbf{F}' = -\nabla Y$ too. An example to elucidate Y could be the familiar force $\nabla Y = -ze\nabla\phi$ to which is subjected an ion of charge ze under the electric potential gradient $\nabla\phi$, in which case $Y + \mu = ze\phi + \mu$ is the well known electro-chemical potential controlling the working conditions of a fuel cell. The result (25) is in fact possible because $\delta\mathbf{F} = \mathbf{F}_2 - \mathbf{F}_1$ is an arbitrary force; whatever $\mathbf{F}_2$ and $\mathbf{F}_1$ might be, their arbitrariness ensures the general physical meaning of $\mathbf{F}'$ and thus its ability to be specified according to some particular physical condition. Suppose known for instance C, solution of the Eq. (8) with or without the condition (9). This solution provides one with information about the momentum pertinent to the mass transfer involved by the diffusion process. Indeed $\Delta\mathbf{J}$ represents from the dimensional point of view the momentum change per unit volume related to the redistribution of the mass within V. Thus, collecting the Eqs. (2) and (7), one finds $\Delta\mathbf{J} = \Delta\mathbf{p}/V = \mathbf{v}\Delta\varepsilon/c^2V = C\mathbf{v}$ being $\Delta\varepsilon/c^2 = m$ and $mC = V$ by definition. Putting then $\Delta\mathbf{p} = \mathbf{p} - \mathbf{p}_o$, trivial manipulations with the help of the first Eq. (21) yield

$$\frac{\mathbf{p}}{m} = \frac{\mathbf{p}_o}{m} - D\nabla\log(C).$$

The ratios involve the velocities $\mathbf{v}$ and $\mathbf{v}_o$ in agreement with the Eqs. (21); for instance, the former is the rate with which occurs the redistribution of m in V, the latter is the initial velocity of the concerned species before the redistribution. In summary, this section has shown that the diffusion equations imply the transfer of matter, energy and momentum; moreover, the velocity addition rule shows that the particles responsible of the mass transfer move in agreement with the relativistic requirements under the condition (13). Eventually the fact of having inferred $\mathbf{F} \approx m\mathbf{a}$ without precluding, at least in principle, even its possible generalization to the relativity, suggests that the quantum basis of these preliminary results is appropriate to carry out further tasks to describe the fundamental interactions too.

3 Entropy and chemical potential

As concerns μ of the Eq. (22) it is known that [21]

$$\left(\frac{\partial\mu}{\partial T}\right)_{P,\mathrm{n}} = -\left(\frac{\partial S}{\partial \mathrm{n}}\right)_{T,P}, \tag{26}$$

being dS the entropy change calculated keeping constant the pressure and temperature during the time necessary to increase n by dn; here n is a dimensionless amount of the concerned substance, e.g. a number of atoms or molecules, whereas dn can be approximately treated as a differential for large n only. The following considerations aim to integrate the Eq. (26) with respect to dn with the help of the Eq. (22).

Let m consist of a cluster of n_m atoms or molecules randomly distributed over an arbitrary number of elementary volumes V_j forming V, i.e. such that $V = \sum_j V_j$: so the given

amount m of mass in the actual volume V is in fact distributed into several elementary volumes $V_j = V_j(t)$. Regard thus each V_j as a possible state allowed to one or more particles among the n_m available: if for instance V_j would be all equal, then each ratio $V_j/V = 1/\mathrm{n}_j$ would yield the probability $\Pi_j = 1/\mathrm{n}_j$ of each state accessible to m, being by definition $\sum_j \mathrm{n}_j^{-1} = 1$. Moreover the possible distributions of n_m objects into the various V_j are functions of time related to the corresponding number N_j of allowed quantum configurations: whatever N_j might be in general, depending on the kind of statistical distribution compliant with the possible spin of the n_m particles, V_j/V is in fact a parameter related to the degree of disorder characteristic of m in V. Hence integrating the Eq. (26) with respect to $d\mathrm{n}$ means summing over all of the probabilities n_j^{-1} consistent with all possible V_j compatible with V; this also means integrating over $d(V_j/V)$ while keeping constant the total number of particles n_m in V, as required at left hand side of the Eq. (26) and in agreement with the Eq. (5). Putting therefore $C_j = m/V_j$ by analogy with $C = m/V$, one infers $C/C_j = V_j/V$ and then

$$S_j = S_o - \int (\partial\mu_j/\partial T)_{P,\mathrm{n}} d\mathrm{n} = S_o - k_B \int \log(V_j/V) d(V_j/V) =$$

$$= S_o - k_B (V_j/V)\left(\log(V_j/V) - 1\right).$$

Clearly the reasoning about the j-th states in V can be repeated for the j'-th states pertinent to the ratios V'_j/V' concerning the volume V', which consists of related elementary volumes V'_j such that $\sum_{j'} V'_j/V' = 1$. The same holds also for a volume V'' defined as sum of elementary volumes V'' and so on; in this way it is possible to define the resulting extensive entropy collecting together all integrals on V_j/V plus that on V'_j/V' and V''_j/V'', with $V + V' + V'' + \cdot\cdot = V_{tot}$ and the respective masses $m + m' + m'' + \cdot\cdot = m_{tot}$ each one of which is that already concerned in the Eq. (5). Then since by definition $\sum_{j'} V'_j/V' = \sum_{j''} V''_j/V'' = 1$ and thus $\sum_j V_j/V + \sum_{j'} V'_j/V' + \sum_{j''} V''_j/V'' + \cdot\cdot = j_{tot}$, summing over all elementary volumes of which consist the total mass and volume of the body yields

$$S = (S_o + j_{tot} k_B) - k_B \sum_j \frac{V_j}{V} \log\left(\frac{V_j}{V}\right). \qquad (27)$$

The first addend is clearly a constant. This result defines an extensive function that collects all possible configurations N_j corresponding to all distributions of the various m in the respective volumes V_j compatible with each V where holds the Eq. (5). In principle V is arbitrary; yet it must be sufficiently large to be subdivided into V_j whose n_j allow considering $d\mathrm{n}_j$ as differentials. Note that the Eq. (27) has been early obtained in [14] elaborating directly the Eqs. (5). Appears clear the link between diffusion, regarded as the way through which the nature drives a thermodynamic system towards the equilibrium state, and entropy, $-\Sigma_j \pi_j \log \pi_j$, which measures the tendency towards states of progressively increasing disorder: this link is the underlying chemical potential μ, strictly connected with the concentration gradient of the diffusing species on the one side and with the related entropy change on the other side. If in the Eq. (26) $d\mu = 0$, which corresponds to $\mathbf{F} = -\nabla\mu = 0$ for uniform distribution of C, then $dS = 0$ reveals that the concerned system is in the state of maximum disorder. The diffusion of matter and energy is thus the driving force that puts into action the second law.

4 Diffusion and fundamental interactions

This is the central section of the paper. The fact of having inferred the results of the previous section from the fundamental Eqs. (1) along with relativistic implications, suggests that additional outcomes should be obtainable elaborating further the concepts hitherto introduced. For the following considerations it is useful to remark that the physical dimensions of $\mathbf{J}$ imply $flux/velocity = density = \rho$ and $flux \times velocity = energy\ density = \eta$. The interactions are thus described by a flux $\mathbf{J}$ of messenger particles, the respective boson vectors, displacing at rate $\mathbf{v}$ and characterized by mass and energy densities ρ and η. The starting point of this section is again the initial Eq. (9) identically rewritten as

$$\nabla \cdot \Delta\mathbf{J} + \frac{\partial C}{\partial t} = +\nabla \cdot \nabla \times \mathbf{U}_+,$$

which holds whatever the arbitrary vector $\mathbf{U}_+$ might be; indeed the last addend is anyway null. Let us rewrite this equation with the help of the position $\nabla \cdot \mathbf{U}_- = C$, which in turn yields

$$\nabla \cdot \left(\Delta\mathbf{J} + \frac{\partial \mathbf{U}_-}{\partial t} - \nabla \times \mathbf{U}_+\right) = 0. \qquad (28)$$

So the vector within parenthesis must be a constant or a function of time only; then in general

$$\Delta\mathbf{J} + \frac{\partial \mathbf{U}_-}{\partial t} - \nabla \times \mathbf{U}_+ = \mathbf{J}_w, \qquad \mathbf{J}_w = \mathbf{J}_w(t), \qquad \nabla \cdot \mathbf{U}_- = C. \qquad (29)$$

The physical dimensions of $\mathbf{U}_-$ and $\mathbf{U}_+$ are $mass \times surface^{-1}$ and $mass \times time^{-1} \times length^{-1}$, whence $\mathbf{U}_+ = \mathbf{U}_- c$ from dimensional point of view; c is the pertinent constant velocity. The homogeneous differential equation obtained from the Eq. (29) is

$$\Delta\mathbf{J} + \frac{\partial \mathbf{U}_-}{\partial t} - \nabla \times \mathbf{U}_+ = 0, \qquad \mathbf{J}_w = 0. \qquad (30)$$

Starting from this quantum groundwork, the next subsections aim to highlight the steps ahead toward the goal of inferring the four fundamental interactions of nature as contextual corollaries.

4.1 The Maxwell equations

This subsection summarizes the reasoning reported in [15]; it is emphasized in the next subsection 4.2 how to include also the weak interaction still in the frame of the same approach.

Consider first the homogeneous differential equation inferred from the Eq. (30)

$$\nabla \times \mathbf{U}_+ = \Delta\mathbf{J} + \frac{\partial \mathbf{U}_-}{\partial t}, \qquad \nabla \cdot \mathbf{U}_- = C. \tag{31}$$

The first equation (31) defines the vector $\mathbf{U}_+$ as a function of $\mathbf{U}_-$, the second one defines the vector $\mathbf{U}_-$ as a function of C. Putting $\Delta\mathbf{J} = \mathbf{J}_2 - \mathbf{J}_1$, it is reasonable to expect also $\mathbf{U}_- = \mathbf{U}_2 - \mathbf{U}_1$ and thus $C = C_2 - C_1$. Moreover, besides the dimensional link, appears now a preliminary reason to define $\mathbf{U}_+$ via the same vectors that implement $\mathbf{U}_-$: there is no compelling necessity to introduce further vectors additional to $\mathbf{U}_1$ and $\mathbf{U}_2$, about which specific hypotheses would be necessary to solve both Eqs. (31). This choice simply requires $\mathbf{U}_+ = (\mathbf{U}_2 + \mathbf{U}_1)\xi$, being ξ an appropriate proportionality factor. The vectors $\mathbf{U}_1$ and $\mathbf{U}_2$ just introduced are arbitrary, likewise the respective C_1 and C_2; for this reason both $\mathbf{U}_+$ and $\mathbf{U}_-$ have been defined with coefficients of the linear combinations of $\mathbf{U}_1$ and $\mathbf{U}_2$ equal to 1 without loss of generality. Hence, combining these definitions with the dimensional requirements, one finds

$$\mathbf{U}_+ = c(\mathbf{U}_2 + \mathbf{U}_1), \qquad \mathbf{U}_- = \mathbf{U}_2 - \mathbf{U}_1, \tag{32}$$

$$\mathbf{U}_2, \mathbf{U}_1 = mass/surface,$$

so that the second Eq. (31) yields

$$\nabla \cdot \mathbf{U}_2 = C_2, \qquad \nabla \cdot \mathbf{U}_1 = C_1, \tag{33}$$

whereas the first Eq. (31) takes the form

$$c\nabla \times \mathbf{U}_2 + c\nabla \times \mathbf{U}_1 - \mathbf{J}_2 + \mathbf{J}_1 - \frac{\partial \mathbf{U}_2}{\partial t} + \frac{\partial \mathbf{U}_1}{\partial t} = 0. \tag{34}$$

Now the problem arises about how could be rearranged the terms appearing in this equation. For instance the chance

$$c\nabla \times \mathbf{U}_2 - \mathbf{J}_2 - \frac{\partial \mathbf{U}_2}{\partial t} = \mathbf{J}' = -c\nabla \times \mathbf{U}_1 - \mathbf{J}_1 - \frac{\partial \mathbf{U}_1}{\partial t} \tag{35}$$

separates the quantities with subscript "2" from those with subscript "1"; the ancillary arbitrary vector $\mathbf{J}'$ that satisfies both equalities (35) can be in general different from zero. If so, then one obtains two equations

$$c\nabla \times \mathbf{U}_2 - \mathbf{J'}_2 - \frac{\partial \mathbf{U}_2}{\partial t} = 0, \quad -c\nabla \times \mathbf{U}_1 - \mathbf{J'}_1 - \frac{\partial \mathbf{U}_1}{\partial t} = 0,$$

$$\mathbf{J'}_2 = \mathbf{J}_2 + \mathbf{J}', \qquad \mathbf{J'}_1 = \mathbf{J}_1 + \mathbf{J}'. \tag{36}$$

Note that it is possible to change the physical meaning of the mass concentrations C_1 and C_2 of the Eqs. (33) simply multiplying both sides by q_m/m and q_e/m respectively; q_e is the total amount of electric charge possibly owned by the mass m, the physical meaning of q_m will be explained later in analogy with that of q_e. The multiplicative factors convert the mass density C_2 into the q_e charge density C_2^*, whereas C_1 turns into the q_m density C_1^*; analogously $\mathbf{U}_1$ and $\mathbf{U}_2$ turn into $\mathbf{U}_1^*$ and $\mathbf{U}_2^*$ in the Eqs. (33), whereas the same holds for $\mathbf{J'}_2$ and $\mathbf{J'}_1$ that turn respectively into charge and q_m flows $\mathbf{J}_2^*$ and $\mathbf{J}_1^*$ in the Eqs. (36). This means having converted $\mathbf{U}_1$ and $\mathbf{U}_2$ into quantities corresponding to the respective $\mathbf{J}_1^*$ and $\mathbf{J}_2^*$. Indeed the Eqs. (33) and the last two equations read

$$\nabla \cdot \mathbf{U}_1^* = C_1^*, \qquad \nabla \cdot \mathbf{U}_2^* = C_2^*,$$

$$C_1^* = C_1\frac{q_m}{m}, \qquad C_2^* = C_2\frac{q_e}{m}, \tag{37}$$

whence

$$c\nabla\times\mathbf{U}_2^* - \mathbf{J}_2^* - \frac{\partial \mathbf{U}_2^*}{\partial t} = 0, \qquad \mathbf{U}_2^* = \mathbf{U}_2\frac{q_e}{m}, \qquad \mathbf{J}_2^* = \mathbf{J'}_2\frac{q_e}{m}, \tag{38}$$

and

$$-c\nabla \times \mathbf{U}_1^* - \mathbf{J}_1^* - \frac{\partial \mathbf{U}_1^*}{\partial t} = 0$$

$$\mathbf{U}_1^* = \mathbf{U}_1\frac{q_m}{m}, \qquad \mathbf{J}_1^* = \mathbf{J'}_1\frac{q_m}{m}. \tag{39}$$

The Eqs. (38) and (39) have physical meaning different from that of the respective Eqs. (36); subtracting side by side these latter one of course finds again the initial Eq. (34), whereas the same does not hold for the Eqs. (38) and (39) that have been multiplied by the respective factors implemented in the Eqs. (37).

Exploit now the fact that the Eqs. (38) and (39) can be still merged together because anyway $c\nabla \times \mathbf{U}_2^* - \mathbf{J}_2^* - \partial\mathbf{U}_2^*/\partial t = -c\nabla \times \mathbf{U}_1^* - \mathbf{J}_1^* - \partial\mathbf{U}_1^*/\partial t$. Note however that the vectors $\mathbf{U}_1^*(\mathbf{J}_1^*)$ and $\mathbf{U}_2^*(\mathbf{J}_2^*)$ obtained solving separately the Eqs. (38) and (39) have scarce physical interest, because the boundaries of the initial uncertainty range $\Delta\mathbf{J}$ are arbitrary; whatever their form might be, they provide two independent solutions that are functions of their own flux vectors only. More interesting seems instead a general solution like $\mathbf{U}_1^*(\mathbf{J}_1^*, \mathbf{J}_2^*)$ and $\mathbf{U}_2^*(\mathbf{J}_1^*, \mathbf{J}_2^*)$, in fact also prospected by the initial Eqs. (35) themselves: this hint appears sensible because $\mathbf{U}_+$ and $\mathbf{U}_-$ consist by definition of the same vectors $\mathbf{U}_1$ and $\mathbf{U}_2$ in the Eq. (31). So rewrite the last result as

$$c\nabla \times \mathbf{U}_1^* - \mathbf{J}_2^* - \partial\mathbf{U}_2^*/\partial t = 0 = -c\nabla \times \mathbf{U}_2^* - \mathbf{J}_1^* - \partial\mathbf{U}_1^*/\partial t,$$

where we have simply exchanged the sides where appear the curl vectors. For simplicity of notation, but without loss of generality, has been omitted the new flux vector $\mathbf{J}''$ possibly shared by both equalities; indeed, as previously done with $\mathbf{J}'$ to infer the Eqs. (36) from the Eq. (35), $\mathbf{J}''$ would have been once more incorporated within $\mathbf{J}_2^*$ and $\mathbf{J}_1^*$. In conclusion one obtains from the Eqs. (37) to (39)

$$\nabla \cdot \mathbf{U}_1^* = C_1^*, \qquad \nabla \cdot \mathbf{U}_2^* = C_2^*, \tag{40}$$

$$c\nabla \times \mathbf{U}_1^* - \mathbf{J}_2^* - \frac{\partial \mathbf{U}_2^*}{\partial t} = 0, \qquad c\nabla \times \mathbf{U}_2^* + \mathbf{J}_1^* + \frac{\partial \mathbf{U}_1^*}{\partial t} = 0.$$

Despite the notations, mere consequence of the fact that the starting point to attain the Eqs. (40) were the diffusion equations of the section 2, is evident the conceptual equivalence of these equations with the well known ones

$$\nabla \cdot \mathbf{H} = 0, \qquad \nabla \cdot \mathbf{E} = \rho_{ch}, \tag{41}$$

$$\nabla \times \mathbf{H} - \frac{\partial \mathbf{E}}{\partial t} - \mathbf{J}_{ch} = 0, \qquad \nabla \times \mathbf{E} + \frac{\partial \mathbf{H}}{\partial t} = 0,$$

simply regarding $\mathbf{U}_2^* \equiv \mathbf{E}$ and $\mathbf{U}_1^* \equiv \mathbf{H}$ together with the charge density $C_2^* \equiv \rho_{ch}$ and $C_1^* = 0$. So, being $\mathbf{J}_2^*$ by definition identified with the charge current density $\mathbf{J}_{ch}$, the Eqs. (41) are nothing else but the Maxwell equations, usually written putting $C_1^* = \rho_{qm} = 0$ and $\mathbf{J}_1^* = \mathbf{J}_{qm} = 0$; these positions, due to $q_m = 0$, acknowledge the lack of experimental evidence of magnetic monopoles. Since these monopoles have not yet been observed experimentally, the correspondence has been emphasized as in the Eqs. (41), despite it would be very attracting and convincing to consider $q_m \neq 0$ too in the equations (41) by formal symmetry: it is worth emphasizing indeed that the reasoning hitherto carried out does not exclude at all the theoretical existence of the magnetic monopoles, rather this approach suggests explicitly them. The positions above that read now

$$\mathbf{U}_+^*/c = \mathbf{E} + \mathbf{H}, \qquad \mathbf{U}_-^* = \mathbf{E} - \mathbf{H},$$

entail four more reasons to validate the positions (32), according which $\mathbf{U}_-$ and $\mathbf{U}_+$ can be expressed through the same vectors they introduce:
(i) $\mathbf{U}_+^*/c + \mathbf{U}_-^* = 2\mathbf{H}$ and $\mathbf{U}_+^*/c - \mathbf{U}_-^* = 2\mathbf{E}$;
(ii) the same holds for the scalars $\mathbf{U}_+ \cdot \mathbf{U}_-/c = H^2 - E^2$ and $U_+^2/c^2 - U_-^2 = 4\mathbf{E} \cdot \mathbf{H}$;
(iii) $\mathbf{U}_- \times \mathbf{U}_+/c = 2\mathbf{E} \times \mathbf{H}$;
(iv) $U_+^2/c^2 + U_-^2 = 2(H^2 + E^2)$.

Once having specified in particular $\mathbf{H}$ and $\mathbf{E}$ as vectors proportional to magnetic and electric fields, then the proposed definitions of $\mathbf{U}_-$ and $\mathbf{U}_+$ entail the well known features: the scalars (ii) define two invariants with respect to Lorentz transformations, whereas the vector (iii) is proportional to the Poynting vector and defines the energy density flux; moreover the point (iv) defines a scalar proportional to the energy density of the electromagnetic field; finally, the integral $c^{-1} \int \mathbf{U}_+ \cdot \mathbf{U}_- dV$ over the volume previously introduced is proportional to the Lagrangian of a free field. As the only velocity that appears in these equations is c, one must conclude that the carriers of this kind of interaction are the photons. Despite these last considerations are well known, their mentioning here is not redundant: indeed these outcomes of the diffusion laws come from and complete the quantum frame of the Maxwell equations.

4.2 The weak interactions

The starting point of this subsection is the non-homogeneous Eq. (29) which concerns $\mathbf{J}_w \neq 0$. Of course even the results of the previous subsection hold when $\mathbf{J}_w \neq 0$ is negligible with respect to $\Delta\mathbf{J}$; so the content of this subsection is not to be regarded separately from the previous one, rather as its completion and generalization. Note that the Eq. (29) results formally similar to the Eqs. (35); the only difference is that $\mathbf{J}'$ is in general function of x, y, z, t, as no hypothesis has been necessary about it, whereas $\mathbf{J}_w$ is instead by definition function of time only in agreement with the Eq. (28). So this case can be formally handled as before, simply rewriting the Eq. (29) as

$$\Delta\mathbf{J}' + \frac{\partial \mathbf{U}_-}{\partial t} - \nabla \times \mathbf{U}_+ = 0, \quad \Delta\mathbf{J}' = \Delta\mathbf{J} - \mathbf{J}_w, \quad \mathbf{J}_w = \mathbf{J}_w(t). \tag{42}$$

Once replacing the previous change of flux $\Delta\mathbf{J} = \mathbf{J}_2 - \mathbf{J}_1$ with $\Delta\mathbf{J}' = \mathbf{J}_2 - \mathbf{J}_1 - \mathbf{J}_w$, is attracting the idea that in the present problem $\mathbf{J}_w$ describes a quantum time fluctuation of energy range $\Delta\varepsilon_w$ and time length Δt_w consistent with the uncertainty equations (1). To highlight the link between the flux modulus $J_w = |\mathbf{J}_w|$ and $\Delta\varepsilon_w$, let $\eta_w = \mathbf{v} \cdot \mathbf{J}_w$ be the energy density transient of time length $\Delta t_w = \hbar/\eta_w V$, being $V = \Delta x^3$ the volume within which is generated the mass density transient $\rho_w = m_w/V = J_w/\mathrm{v}$; of course $\mathrm{v} = |\mathbf{v}|$ is the modulus of the velocity with which the messenger particles propagate this kind of interaction, whereas $\Delta\varepsilon_w$ is the fluctuation energy change necessary to create messengers with lifetime Δt_w. It is possible to express the mass flux J_w of m_w as $\hbar/\Delta x_w^4$ by dimensional reasons; so $J_w = \xi\hbar/\Delta x_w^4$, being ξ a proportionality constant. Hence $\xi\hbar/\Delta x_w^4 = m_w \mathrm{v}/\Delta x_w^3$ yields

$$\zeta \frac{\hbar}{\Delta x_w} = m_w c, \qquad \mathrm{v} = \gamma c, \qquad \zeta = \frac{\xi}{\gamma};$$

so the range of this interaction force is $\Delta x_w = (\xi/\gamma)(\hbar c/m_w c^2)$. Let us estimate Δx_w putting preliminarily $\xi/\gamma \approx 1$, according to the reasonable idea that a proportionality constant correlating two quantities should be of the order of the unity; otherwise some further physical effect should be identified and implemented to justify $\xi/\gamma >> 1$. So one expects

$$\Delta x_w \approx \frac{\hbar c}{m_w c^2}, \quad \Delta x_w \approx 10^{-16}\mathrm{cm}, \quad m_w c^2 \approx 250\ \mathrm{GeV}. \tag{43}$$

The estimates have been guessed to exemplify the correlation between space range and energy scale; the figures are plausibly typical of the weak interactions. This preliminary estimate aimed merely to show that the positions $J_w \approx \hbar/\Delta x_w^4$ and $\rho_w \approx J_w/\mathrm{v}$ and mass m_w of the messenger particles are reasonable; this result must be however better assessed and more thoroughly justified.

The basic idea is that during the time transient described by $\mathbf{J}_w$, the range of the related interaction cannot be very wide; a long distance travel of messenger particles would require an extended time length, incompatible with the short-lasting transient Δt_w during which the classical energy conservation is temporarily replaced by the related quantum en-

ergy uncertainty $\Delta\varepsilon_w$. The next reasoning attempts to introduce a short range force mediated by massive particles created somewhere in the space-time by the energy fluctuation $\Delta\varepsilon_w$ and moving at rate $v_w < c$: once having waived in the Eqs. (1) the local time and space coordinates, it is possible to say that at an arbitrary time t_0 the quantum fluctuation nucleates at the arbitrary point x_0, y_0, z_0 the total mass m_w that flows along with $\mathbf{J}_w$ within a volume V with average density ρ_w.

To confirm the existence of massive particles describing this interaction, divide the Eqs. (1) by Δt so that $v_x \Delta p_x = \hbar/\Delta t = \Delta\varepsilon$ with $\Delta p_x \approx (m' - m)v_x$ according to the Eq. (3): hence the uncertainty prospects the chance of two kinds of vector bosons of different masses describing the interaction.

Consider first the carrier of mass m and implement the Eq. (24), noting that the volume V defining the density ρ_w can be written as $V = \Delta x^2 \delta x_u$ without loss of generality; introducing indeed V via an arbitrary coefficient ξ is actually irrelevant, because $\xi\Delta x^2\delta x_u$ would be handled exactly like $V = \Delta x^2 \delta x'_u$ simply rewriting $\delta x'_u = \xi\delta x_u$. So the actual geometric shape of V is waived because the sizes of Δx and δx_u are arbitrary in the conceptual frame based on the uncertainty Eqs. (1) only. Let us write the Eq. (24) as $\varepsilon_u = (n\hbar)^2/m\Delta x^2$ with $\varepsilon_u = F_u \delta x_u$ and then identify ε_u with the energy mc^2 necessary to create just the concerned rest mass m by virtue of the quantum energy fluctuation only; so one finds with $n = 1$ the reduced Compton length associated to m

$$\lambda\!\!\!^{-} = \Delta x, \qquad \lambda\!\!\!^{-} = \frac{\hbar}{mc}. \tag{44}$$

This expression holds for any particle free and neutral: the former condition assumes that m does not directly interact with m', the latter requires that no additional net charge is created during Δt_w because of the total charge conservation with respect to that early concerned by the Maxwell equations before the quantum fluctuation.

Analogous considerations hold for m', in particular as concerns the condition of charge conservation during the fluctuation time of $\mathbf{J}_w$. So m' either describes another neutral particle or it could actually consist of a couple of particles having equal mass and opposite charges; as in the latter case the charges interact to form an electromagnetic interaction driven Coulomb system with gain of energy, let therefore m' consist of two particles of equal reduced mass $m'_r = m'/2$. The energy ε_{em} and Bohr radius r_{em} of a hydrogenlike system are well known: considering the ground energy state with $n = 1$ only, they are $\varepsilon_{em} = -\alpha^2 m'_r c^2/2 = -e^2/2r_{em}$ with $r_{em} = \alpha^{-1}\hbar/m'_r c$; thus ε_{em} is defined by the diametric delocalization distance $2r_{em}$ only of the system of charges orbiting around their centre of mass [18]. Express r_{em} via the condition of steady circular waves $2\pi r_{em} = n_w \lambda_w$ early introduced to account for the stability of the old Bohr atom, whence $\varepsilon_{em} = -\pi e^2/n_w\lambda_w$ with $n_w \geq 1$ an arbitrary integer. Define then the new energy $\varepsilon_w = n_w\varepsilon_{em} = -\pi e^2/\lambda_w$. Clearly $n_w = 1$ still implies the electromagnetic energy $\varepsilon_w = \varepsilon_{em}$, whereas $n_w > 1$ implies $\varepsilon_w > \varepsilon_{em}$ since $\lambda_w < r_{em}$: this shows that actually ε_{em} and ε_w are both allowed and thus coexisting. On the one hand ε_w is hidden into and closely related to ε_{em}: having merely replaced r_{em} with the wavelengths λ_w allowed to the circular waves of charge, ε_w appears as a sort of short range high energy compatible with the electromagnetic interaction from which it differs for $n_w > 1$, rather than the energy of a separate form of interaction. On the other hand, if really the masses of all three particles correspond to the available energy ε_w, it should be true that $\varepsilon_w \approx 3m_w c^2$ for three equal masses m_w. In fact this expectation is compatible with $-\pi e^2/\lambda_w$ putting $m_w c^2 \approx e^2/\lambda_w$ while $\lambda_w \approx \lambda\!\!\!^{-} \approx \lambda\!\!\!^{-}'$; the replacement of r_{em} with the smaller λ_w accounts for the increase of energy necessary to create short range massive boson vectors, whereas the factor π replacing the expected factor 3 simply reveals that the masses of the neutral and charged boson vectors should actually be slightly different. Otherwise stated, regarding this result as $(m_0 + m_+ + m_-)c^2 = \pi e^2/\lambda_w$ with obvious meaning of symbols, one infers

$$m_0 c^2 + 2m_\pm c^2 = \pi\frac{e^2}{\lambda_w}, \qquad m_\pm c^2 = \frac{e^2}{\lambda_w},$$

$$m_0 c^2 = (\pi - 2)\frac{e^2}{\lambda_w}, \qquad m_+ = m_- = m_\pm. \tag{45}$$

Hence, it should be true that

$$m_0/(m_0 + m_+ + m_-) = (\pi - 2)/\pi,$$

$$m_\pm/(m_0 + m_+ + m_-) = 1/\pi.$$

Compare this last conclusion with the experimental data

$$m_{Z^0} = 91.19 \text{ GeV}, \qquad m_{W^\pm} = 80.39 \text{ GeV},$$

$$m_{tot} = m_{Z^0} + 2m_{W^\pm} = 251.97 \text{ GeV}.$$

Indeed $m_0/m_{tot} = 0.36$ and $m_\pm/m_{tot} = 0.32$ agree well with $(\pi - 2)/\pi = 0.363$ and $1/\pi = 0.318$; despite the non-relativistic approach, this agreement supports the idea that the energy gain ε_w due to the charge system accounts for the creation of its own mass plus a further neutral particle as well. The experimental energies support the idea that contracting λ_w from $2\pi r_{em}$ down to $2\pi r_{em}/n_w$ implies the chance of a new form of interaction correlated to and coexisting with the familiar electromagnetic interaction at increasing values of the quantum number n_w.

Let us put now

$$m'c^2 \approx \frac{\hbar}{\Delta t_w} \tag{46}$$

being Δt_w the characteristic lifetime of the vector bosons.

This result is reasonable, as m' is proportional to the characteristic energy $\hbar/\Delta t_w$. To calculate this expression, let us also assume $m' \propto \Delta t_w$: as any process in nature requires a

definite time to be completed, it is natural to expect that the amount of mass creatable during the fluctuation of $\mathbf{J}_w$ is proportional to the time length of this fluctuation. In other words: the longer the fluctuation, the greater the transient amount of energy and thus of mass that can be created. Putting then $m' = k_w \Delta t_w$, where k_w is an appropriate proportionality constant, there are two chances: either $k_w \approx 1$ or $k_w \neq 1$. In general the latter chance means that some physical effect is still hidden in k_w, whereas the former chance means that in fact k_w accounts for the concerned physical correlation without need of further considerations. Let us guess that $k_w \approx 1$ effectively represents the fluctuation lifetime; then, replacing into the Eq. (46), one finds

$$k_w (c\Delta t_w)^2 = \hbar, \qquad k_w \approx 1\mathrm{g/s}, \tag{47}$$

which yields $\Delta t_w \approx 10^{-24}$s. Note that the second Eqs. (45) reads $m_\pm c^2 = \hbar\alpha c/\lambda_w$, which suggests that αc is the actual displacement rate of the charged vector bosons having energy $\hbar \mathrm{v}/\lambda_w$ and that the same holds for the neutral boson. Assuming therefore that $\mathrm{v} = \alpha c$ is the actual displacement rate of the massive bosons, the characteristic range of this interaction should be of the order of $\Delta x_w \approx \alpha c \Delta t_w = 2 \times 10^{-16}$cm, whereas $\hbar c/\Delta x_w \approx 0.15$ erg $= 98$ GeV in agreement with the Eq. (43) previously found.

In conclusion we have introduced three particles of comparable mass, of the order of 90 GeV, two of which with opposite charges and the third neutral, that propagate the interaction within the sub-nuclear space range Δx_w during a characteristic time range Δt_w. These results are the fingerprint of the weak interaction, which has been inferred as a generalization of the Maxwell equations inherent the homogeneous diffusion equation (30) via the transient fluctuation term $\mathbf{J}_w(t)$ appearing in the more general Eq. (29). So this kind of interaction differs in principle from, but it is strictly related to, the electromagnetic interactions of the Maxwell equations; it is simply an extension of these latter to the transient formation of three further short range carriers consistent with the time flux function $\mathbf{J}_w$ additional to the electric and magnetic fields described by $\mathbf{J}_2^*$ and $\mathbf{J}_1^*$, consequences themselves of the early Fick diffusion equations. It is worth emphasizing once again that the existence of magnetic monopoles does not conflict with, rather comes directly from, all of these outcomes and their quantum origin.

4.3 The gravity force

Exploit the dimensional relationship

$$\pm \mathbf{J} \cdot \mathbf{v} = \frac{|\mathbf{F}|}{surface}; \tag{48}$$

of course $\mathbf{v}$ is the rate with which propagate the carriers of the force $\mathbf{F}$ at right hand side and $\mathbf{J}$ their flux. The double sign takes into account either chance of sign in principle possible at left hand side, being the modulus of force positive by definition. The gravitons are acknowledged to be the carriers of the gravity force at the light speed; anyway, whatever the actual physical nature of these boson vectors and their displacement rate might specifically be, is enough for the present purposes to introduce a one-dimensional reference system R to which will be referred the scalars of the Eq. (48). This assumption on R is consistent with the chance of describing the gravitational interaction between two masses placed arbitrarily apart along one coordinate. Imposing this condition and thus introducing an arbitrary x-axis, write $|\mathbf{F}| = \xi F_x$: the x-component of $\mathbf{F}$ has been related to its modulus $|\mathbf{F}|$ via the dimensionless proportionality factor ξ, which obviously is an unknown variable quantity. Moreover, being $J_x = \hbar/\Delta x^4$, it is possible to write in an analogous way $\mathbf{J} \cdot \mathbf{v} = \pm\zeta J_x \mathrm{v}_x = \pm\zeta\hbar c/\Delta x^4$: once more the dimensionless proportionality factor ζ relating the scalar $\mathbf{J} \cdot \mathbf{v}$ to its arbitrary component $J_x \mathrm{v}_x$ is an unknown variable quantity. In this way, whatever v_x and the interaction carriers might be, $J_x \mathrm{v}_x$ can be expressed via ζ as a function of the constant quantity $\hbar c$. Of course, even $surface$ reduces to Δx^2 in R. These positions are useful to rewrite the initial Eq. (48) as $\zeta\hbar c/\Delta x^4 = \pm\xi F_x/\Delta x^2$ and thus $\zeta m_o^2 G/\Delta x^4 = \pm\xi F_x/\Delta x^2$ in R, having put $\hbar c = G m_o^2$ by dimensional reasons; this is surely possible by defining appropriately the value of the constant mass m_o. Yet the specific value of m_o is not essential: the term $m_o^2\zeta/\xi$ yields indeed $m_1 m_2$, with $m_1 = m_o\zeta$ and $m_2 = m_o/\xi$ because of the arbitrary values of the proportionality factors ζ and ξ. In this way m_1 and m_2 are two arbitrary inputs defining F_x, which indeed owing to the Eq. (48) reads

$$F_x = \pm G \frac{m_1 m_2}{\Delta x^2}.$$

Note that the Δx^{-2} law could be directly inferred from the Eqs. (1), since in the present model the derivatives are defined as mere ratios of uncertainty ranges. Differentiating the Eqs. (1) at constant n yields $\delta\Delta p_x = -(n\hbar/\Delta x^2)\delta\Delta x$, then dividing both sides by $\delta\Delta t$ corresponding to $\delta\Delta x$ one finds $\delta\Delta p_x/\delta\Delta t = -n\hbar \mathrm{v}_x/\Delta x^2$ with $\mathrm{v}_x = \delta\Delta x/\delta\Delta t$: at left hand side appears the x-component of a force, at right hand side the concept of mass is hidden in the physical dimensions of the factor $\hbar \mathrm{v}_x$, which reveals its physical meaning of space-time deformation rate of $\delta\Delta x$ during $\delta\Delta t$. Of course v_x is positive or negative depending on whether $\delta\Delta x$ represents expansion or contraction of Δx.

This short note aims to emphasize that in the present model the concept of gravity force is still linked to that of space-time deformation; yet the force also explicitly follows from the diffusion equations. In conclusion, taking the minus sign, we have found the Newton gravity law. Note however three remarks:

(i) this result is not new, it has been inferred in different ways directly from the Eqs. (1) in [20, 23];

(ii) here even the anti-gravity with the plus sign is allowed, as it has been repeatedly found elsewhere [22, 23];

(iii) the Newton law is actually an approximation of a more general gravity law, as found previously when concerning $\mathbf{F} \approx m\mathbf{a}$.

In fact one could guess an expression of $surface$ like $\Delta x'^2 = \Delta x^2(1 + a_1\Delta x_o/\Delta x + a_2(\Delta x_o/\Delta x)^2 + \cdot\cdot)$; the series expansion is dimensionally compatible with the Eq. (48) and reduces to Δx^2 previously considered for $\Delta x \to \infty$ only, i.e. for weak gravity fields at large distances between the masses. This expansion defines a more general scalar component $\zeta J'_x \mathrm{v}_x = \pm\xi F'_x/\Delta x'^2$ defining a more complex force component $\pm F'_x$ that coincides, as a particular case, with that F_x previously found simply putting equal to zero the higher order coefficients $a_{j\geq 1}$ of the series expansion. Note that $F_x \to 0$ for $\Delta x \to \infty$. The present choice to express the series expansions of $surface$ has been purposely assumed in order that even the non-Newtonian $F'_x \to 0$ satisfies the same condition of the Newtonian F_x.

4.4 The strong interaction

The starting point and the subsequent reasoning are still that of the subsection 4.3. Note however that the dimensional equation (48) does not compel defining $force$ as purposely done before; as a subtle and possible alternative, nothing hinders defining in the one dimensional R the right hand side as

$$\pm\mathbf{J}\cdot\mathbf{v} = \frac{|\mathbf{F}|}{\Delta x^2} + \frac{energy}{\Delta x^3}. \tag{49}$$

Proceeding as before, we merge again $\mathbf{J}\cdot\mathbf{v}$ with the concerned force per unit surface at the right hand side of the Eq. (48); one finds $\pm\xi\hbar c/\Delta x^4 = F_x/\Delta x^2 + \varepsilon_o/\Delta x^3$ i.e. $F_x = \pm\xi\hbar c/\Delta x^2 - \varepsilon_o/\Delta x$, where ε_o is a constant. This force component is derivable from a potential energy U having the form

$$U = \pm\frac{\xi\hbar c}{\Delta x} + \varepsilon_o \log(\Delta x/\Delta x_o), \tag{50}$$

which in turn, putting $\Delta x = \Delta x_o \pm \delta x$, reads

$$U \approx \pm\left(\frac{a}{\Delta x} \pm b\delta x\right), \qquad \Delta x = \Delta x_o \pm \delta x,$$

$$a = \xi\hbar c, \qquad b = \frac{\varepsilon_o}{\Delta x_o}, \qquad \frac{\delta x}{\Delta x_o} << 1. \tag{51}$$

This is certainly possible because, being both Δx and Δx_o arbitrary, the necessary inequality can be actually verified at short distances $\Delta x \gtrsim \Delta x_o$ or $\Delta x \lesssim \Delta x_o$. This result with the minus sign at right hand side reads

$$U \approx -\frac{a}{\Delta x} + b\delta x,$$

i.e. it leads to the sought interaction energy of interest here.

It is however also interesting to note that attractive and repulsive strong forces are in principle allowed in this model.

The physical dimensions of the constants a and b are $energy \times length$ and $energy/length$, so that $ab = energy^2$ and $a/b = length^2$: write then $\hbar/\sqrt{ab} = \Delta t_s$ whence $\hbar c/\sqrt{ab} = \lambda_s = c\Delta t_s$. The chance of introducing the characteristic range λ_s directly via c agrees with the idea of massless vector bosons mediating this kind of interaction, which follows in turn from the lack of a compelling motivation to introduce a slower velocity of heavy particles. Thus, putting reasonably $\lambda_s = \sqrt{a/b}$ too, one finds

$$a = \hbar c, \qquad \xi = 1, \tag{52}$$

i.e. a sensible value of the proportionality constant ξ. Moreover holds also now the reasoning previously introduced about the proportionality between mass and characteristic lifetime of particles mediating the interaction. Let us repeat therefore an identical approach, concerning however the energy of the messengers instead of their mass to rewrite the proportionality condition $m \propto \Delta t$ as $\sqrt{ab}/c^2 \propto \Delta t_s$; introducing once more a proportionality constant k one finds $\sqrt{ab} = kc^2\Delta t_s$, which reads in turn $\sqrt{ab} = kc^2\hbar/\sqrt{ab}$ so that $ab = k\hbar c^2$. Hence, owing to the Eq. (52),

$$b = kc, \qquad k \approx 1\mathrm{g/s}. \tag{53}$$

The last position, coherent with that of the Eq. (47), is justified by the same hint of the previous section about the physical meaning of any proportionality constant correlating two physical amounts. The values of these constants are therefore

$$a = 3\times 10^{-17}\mathrm{erg\ cm} = 0.2\ \mathrm{GeV\ fm},$$

$$b \approx 10^{10}\mathrm{dyn} = 10^5\mathrm{N}. \tag{54}$$

These figures yield therefore the characteristic length Δx_o defined by $a/\Delta x_o = b\Delta x_o$ and the characteristic interaction time as a function of the characteristic energy $\sqrt{ab}$; one obtains

$$\Delta x_o = \sqrt{a/b} \approx 10^{-13}\mathrm{cm}, \qquad \Delta t_s = \hbar/\sqrt{ab} \approx 10^{-24}\mathrm{s},$$

$$\sqrt{ab} = \sqrt{k\hbar c^2} \approx 10^{-3}\mathrm{erg} = 0.6\mathrm{GeV}.$$

Note that $a/\Delta x$ reads $\hbar c/\Delta x_o = \alpha^{-1}e^2/\Delta x_o$, i.e. the strength of this kind of interaction is α^{-1} times greater than that of the electromagnetic interaction. The form of U in the Eq. (51) and these figures are fingerprints of the strong interaction.

5 Connection between gravity and electromagnetism

Note that in the cgs system $(charge/mass)^2$ has physical dimensions l^3/mt^2, i.e. the same as the gravity constant. Yet, what has to do the electromagnetism with the gravity force? The possible answer relies just on the hint suggested by the question itself, i.e. the link between $(e/m_G)^2$ and G. It is interesting the possibility of specifying m_G directly as follows

$$G = \frac{\hbar c}{m_G^2} = \frac{1}{\alpha}\left(\frac{e}{m_G}\right)^2,$$

which defines $m_G = 2.2 \times 10^{-5}$g as a function of the value of G assumed known; moreover, introducing m_G via its reduced Compton length $\lambda\!\!\!^{-}_G$, one finds

$$G = \frac{1}{\alpha}\left(\frac{e\lambda\!\!\!^{-}_G c}{\hbar}\right)^2 = \frac{e}{\alpha}\frac{e}{m_G^2}, \qquad \lambda\!\!\!^{-}_G = \frac{\hbar}{m_G c}. \tag{55}$$

It is interesting the fact that the gravity constant is linked: (i) to the electromagnetism via the electric charge, (ii) to the relativity via c and (iii) to the quantum theory via $\hbar$; also, $\lambda\!\!\!^{-}_G$ results to be of the order of the Planck length. However we acknowledge gravity and electromagnetism as two separate forces despite their common origin from the diffusion equations, whence the question: how and why does actually the nature split the electromagnetic and gravity forces? The starting point to answer this question is the Newton law itself previously found. Rewrite first the Newton law with the help of the Eq. (55) as

$$F = G\frac{m_1 m_2}{\Delta x^2} = \frac{e}{\alpha}\frac{e}{\Delta x^2}\frac{m_1}{m_G}\frac{m_2}{m_G}. \tag{56}$$

The only term of the second equality that does not depend neither upon Δx nor upon m_1 and m_2 is e/α. Let us split therefore this equation via a proportionality constant k as follows

$$G = k\frac{e}{\alpha}, \qquad \frac{m_1 m_2}{\Delta x^2} = \frac{F}{G} = \frac{1}{k}\frac{e}{\Delta x^2}\frac{m_1}{m_G}\frac{m_2}{m_G}. \tag{57}$$

Note now that the masses m_1 and m_2 appear in this equation as dimensionless ratios m_1/m_G and m_2/m_G; these pure numbers yield therefore

$$\frac{F}{G} = \frac{r_2}{k}\frac{Q_{e1}}{\Delta x^2} = \frac{1}{\alpha G}\frac{Q_{e2}Q_{e1}}{\Delta x^2}, \qquad Q_{e1} = r_1 e, \qquad Q_{e2} = r_2 e,$$
$$\frac{m_1}{m_G} = r_1, \qquad \frac{m_2}{m_G} = r_2. \tag{58}$$

In practice we have eliminated the concept of mass from the right hand side of F: the arbitrary variable r_1, which depends on the arbitrary value of m_1, converts the fixed charge e of the second equation (57) into the arbitrary total charge Q_{e1}. The ratio r_2/k involves an arbitrary number r_2 and a factor k that is reasonably related to the measure units of the modulus $Q_{e1}/\Delta x^2$ of a new quantity we call electric field strength due to the charge Q_{e1} at a distance Δx: hold indeed for Q_{e2} the same considerations highlighted for Q_{e1}, i.e. Q_{e2} is an arbitrary charge in the field of Q_{e1}. In fact the first Eq. (58) turns into

$$F = \frac{Q_{e2}}{\alpha}\frac{Q_{e1}}{\Delta x^2}. \tag{59}$$

From numerical and dimensional points of view, the factor α^{-1} is immaterial: since both Q_{e1} and Q_{e2} are arbitrary, one could identically write F as $Q'_{e2}Q_{e1}/\Delta x^2$ with $Q'_{e2} = Q_{e2}/\alpha$ without loss of generality. Conceptually, however, α^{-1} replaces in fact G: the latter describes the interaction between m_1 and m_2, the former that between Q_{e1} and Q_{e2}. This also shows that the analogous analytical form of the Coulomb and Newton laws is not at all accidental, as already shown in [23]. It is clear that the key step of this conclusion is the position $G = k(e/\alpha)$ of the Eq. (57). It is instructive to calculate e/α and compare it with the experimental values of G in the cgs and SI systems

$$G = 6.68 \times 10^{-8}\mathrm{cm^3 g^{-1} s^{-2}} = 6.68 \times 10^{-11}\mathrm{m^3 Kg^{-1} s^{-2}};$$

while being

$$e_{cgs} = 4.8 \times 10^{-10}\mathrm{esu}, \qquad e_{SI} = -1.6 \times 10^{-19}\mathrm{C}.$$

One finds

$$k_{cgs}\frac{e_{cgs}}{\alpha} = k_{cgs} 6.6 \times 10^{-8}\mathrm{cm^3 g^{-1} s^{-2}},$$

$$k_{SI}\frac{e_{SI}}{\alpha} = k_{SI} 2.1 \times 10^{-12}\mathrm{m^3 Kg^{-1} s^{-2}}.$$

Of course $k_{SI} \neq k_{cgs}$ for two reasons: (i) because of the different measure units and (ii) because in the cgs system the charge is directly defined via the electric force, in the SI the charge is defined in an independent way via the Ampere; thus k_{SI} requires an additional multiplicative factor k_0 to match G calculated simply changing the mass and length units of the proportionality constants k_{cgs} and k_{SI}. As the physical dimensions of k_{cgs} are $(length/mass)^{3/2}/time$, one expects $k_{SI} = (10^{3/2}k_{cgs})k_0$; the factor in parenthesis accounts for the different metric units only. Hence

$$G = k_{cgs} 6.6 \times 10^{-8}\mathrm{cm^3 g^{-1} s^{-2}},$$

$$G = k_{cgs}k_0 6.6 \times 10^{-11}\mathrm{m^3 Kg^{-1} s^{-2}}. \tag{60}$$

This result clearly shows that the actual value of the gravity constant is well described by the dimensionless proportionality constant $k_{cgs} \approx 1$ and that $k_{cgs}k_0 \approx 1$ is also true; actually $k_0 \approx 1$ is not surprising, it is consequence of having implemented e_{SI} by including the Coulomb factor in the second Eq. (60). As repeatedly stated, a proportionality factor of the order of the unity shows that the correlation between two quantities is physically correct; no hidden effect is to be expected. What is significant is that the dimensionless values $k_{cgs} \approx 1$ and $k_0 \approx 1$ fit the experimental values of G in both systems.

To conclude this section, it is worth noticing that the value of G had been correctly calculated in several ways as a function of the fundamental constants of nature in the previous paper [20]; moreover more details about the connection between gravity and electric forces have been emphasized in a recent paper [23].

6 Discussion

The idea of linking the diffusion laws to the fundamental interactions was suggested by their generality and by the various implications inherent their basic concepts. Regarding the formulae of the section 2 as strictly related to the mere displacement of chemical elements, thus with outcomes pertinent to the solid state physics only, is certainly reductive. Actually some concepts can be extrapolated beyond the plain domain of the materials science, e.g. as they concern even the fields. This aspect, evidenced by the first and last Eqs. (4), has been emphasized considering for instance that the heat transfer Fourier law has formal physical analogy with the displacement of matter [14]. The connection with the fundamental interactions appears thus natural once acknowledging that these latter consist of the exchange of messenger particles, the vector bosons, that propagate throughout the space-time.

Follow the idea that any body of matter is surrounded by a cloud of bosons randomly flowing towards another body with which it interacts, and that in general both bodies are moving by effect of the interaction itself; consequently transients of local concentration gradients of these carriers throughout the space-time are also allowed to form. If so, the ability of the carriers to mediate the pertinent interaction reduces basically to the diffusion laws governing the displacement of clusters of these carriers. It has been evidenced that the concept of particle flux is crucial in finding the correlation between density gradient of the carriers and strength and kind of interaction; as the flux related to the concept of diffusion concerns intrinsically a non-equilibrium situation, even the interactions fit the idea of dynamical universe evolving towards a thermodynamic steady state.

Obviously the results introduced here are not exhaustive in describing themselves all features of the fundamental forces of the nature; this detailed investigation about each form of interactions is not the actual purpose of the model, which instead aims merely to identify their common root only by merging diffusion laws and quantum uncertainty only. On the one hand, the present conclusions must be regarded having already in mind also previous results, obtained starting directly from the Eqs. (1) to explain the significant features of the various interactions [15]. On the other hand, the fact that the same results are also obtainable via the diffusion laws is informative of the physical mechanism upon which these latter rely: otherwise stated, all interactions are consequences of the second law, i.e. the vector bosons transfer the interaction moving likewise chemical elements of a non-equilibrium thermodynamic system to increase the global internal entropy of the system. Are significant in this respect the considerations of the section 3. A further implication of the present model relies on the possibility of demonstrating that the magnetic monopoles can in fact exist, being compatible with the basic ideas from which the interactions are inferred: at the present stage of development, the model does not prospect any reason to reject their existence. The isotropy of the space-time is essential to introduce the pertinent diffusion coefficient as a numerical value D without requiring instead a tensor matrix; even without excluding that actually this position could be an oversimplification only, the results indicate that the assumption is acceptable at least at the present level of development of the model. Moreover no necessity of extra-dimensions appears in this context, which however does not exclude that these latter might actually exist.

A short remark is useful to explain why the diffusion equations are the key to infer contextually and in a surprisingly simple way the basic aspects of the fundamental interactions. A partial answer is that the concept of uncertainty does not require hypotheses or information about the kind of diffusion medium, kind of vector bosons and strength and range of the interactions; as the Eqs. (1) have a primary significance regardless of any ancillary information, their consequences are expected to match different kinds of interaction just because of their generality. Yet a more comprehensive answer is that the quantum Eqs. (1) are inherently consistent with the general relativity [17], so any reasoning based on these equations leads consequently to relativistic conclusions as well; this explains why some valuable relativistic implications have been contextually found as side outcomes throughout the paper. Previous and present results demonstrate the validity of the theoretical model where uncertainty ranges replace the local values of the dynamical variables; ignoring these latter means accepting that the former only have true physical meaning. On the one hand, it is worth recalling the key role of the arbitrary boundaries of the uncertainty ranges to demonstrate that the quantum origin of the Maxwell equations and related consequences, e.g. the Gauss theorem and the Faraday law, rely on the concept of space-time ranges: **E** and **H** were contextually introduced implementing just both boundaries of ranges to express via the Eqs. (1) the flux of vector bosons that mediate the electromagnetic interaction between charged particles. On the other hand, the most interesting aspect of the formalism based on ranges concerns its conceptual meaning that merges quantum theory and relativity: so the usefulness of the results presently achievable is not the only support to their validity.

In the wave mechanics the dynamical variables of the classical formulae are replaced by operators that constitute the wave equations, whose solutions provides the eigenvalues of the observables; in the present model the dynamical variables are replaced by the respective uncertainty ranges, the eigenvalues are inferred by elementary manipulations of the classical formulae while the quantization is introduced via n. The present model reverts thus fundamental inputs and outcomes of the standard wave mechanics: the uncertainty is no longer consequence of the commutation rules of postulated quantum operators, it becomes instead the fundamental statement as a function of which the operator formalism is inferred by consequence of the range formalism. Several papers, e.g.

[18, 19] show that this way of thinking is a valid alternative to the standard wave mechanics: the expressions of the eigenvalues are identical in all cases where the wave equations can be solved analytically without the need of numerical procedures. The intriguing advantage of the present approach is thus that it not only agrees with the wave formalism, in fact inferable as a corollary so that the present model is in principle compliant with any quantum results today known, but contextually implies even the conceptual foundations of the special and general relativity [17]; so are not surprising the chance of having obtained the Eq. (19) and recognized the approximate character of the Netwton law $\mathbf{F} \approx m\mathbf{a}$, preliminarily obtainable as in the Eq. (20), without the relativistic correction involving the space-time deformation in the presence of mass.

The quantum space-time uncertainty has profound implications in relativity, whose formulae result indeed expressed themselves via uncertainty ranges; although the formulae are seemingly identical, however their physical meaning is definitely different. E.g., it has been emphasized that the Eq. (2) entails the functional dependence $p_x = \mathrm{v}_x\varepsilon/c^2$ of the local dynamical variables: the latter equation is well known, the former seems a redundant and pretextuous attempt to rewrite the standard relativistic result. Yet just in this way, introducing ranges that replace local variables, the relativity is made compliant with the quantum theory. The local dynamical variables are incompatible with the Heisenberg principle, the uncertainty ranges do by definition; so the usual formulae of the standard relativity are mere classical limit cases of range sizes tending to zero, in agreement with the classical character of the relativity itself.

In short, the present paper is a further contribution confirming that the Eqs. (1) represent the common root underlying quantum theory and relativity.

7 Conclusion

The necessity of skipping a detailed analysis about the specific features of all forms of interaction, outside of the scope of this paper, ranks the significance of the essential outcomes provided by the model; the value of results already known relies on the fact of being obtained contextually in the frame of a unique idea, which emphasizes the validity of the theoretical basis so far implemented. The approach proposed here suggests that an appropriate basic assumption about the displacement mechanism of the vector bosons has prioritary importance with respect to the detailed speculation about the single interactions themselves; moreover the scalar $\mathbf{J} \cdot \mathbf{v}$ was proven effective as a common basis to infer distinguishing information even without introducing explicit hypotheses on the pertinent vector bosons. The analytical form of the gravity force was inferred waiving the specific nature of the gravitons; the well known form (51) of the strong force has been inferred waiving the features of the gluons and their property of exchanging the colour force between quarks, whereas the electromagnetic interaction was found related to the photons as a particular case of a more general electro-weak interaction involving massive vector bosons. The weak interaction only required considering explicitly the displacement velocity of the carriers, which cannot travel at the light speed as their masses affect the characteristic space range and lifetime. Yet the basic features of all interactions depend primarily on the diffusion like behaviour of vector bosons described case by case through the form of the respective scalars $\mathbf{J} \cdot \mathbf{v}$. Although such theoretical approach is seemingly classical, indeed the section 2 exploits standard vector calculus, relativistic implications are anyway evident and occasionally even unexpected; this is because the Eqs. (1) contain an obvious quantum character that however encloses also relativistic implications, which therefore appear by consequence while implementing them. Considering the quantum origin of the diffusion laws, it is not surprising that the implications of the model are general enough to span not only the solid state physics but also the fundamental interaction physics.

Submitted on February 11, 2015 / Accepted on February 14, 2015

References

1. Weinberg S. Dreams of a Final Theory. Vintage Books, London, 1993.
2. Davies P. The Forces of Nature. Cambridge Univ. Press 2nd ed., 1996.
3. Braybant S., Giacomelly G., Spurio M. Particles and Fundamental Interactions. An Introduction to Particle Physics. Springer, Dordrecht, 2012.
4. Bjorken J.D., Drell S.D. Relativistic Quantum Mechanics. New York, McGraw-Hill, 1964.
5. Abers E.S., Lee B.W. Gauge teorie. *Physics Reports*, 1973, v. 9, 1–141.
6. Feynman R.P., Weinberg S. Elementary Particles and the Laws of Physics. Cambridge University Press, Cambridge, 1987.
7. Baak M. The Electroweak Fit of the Standard Model after the Discovery of a New Boson at the LHC. *The European Physical Journal C*, 2012, v. 72, no. 11, 1–2.
8. Kaku M. Introduction to Superstring and M-Theory. 2nd ed., Springer-Verlag, New York, USA, 1999.
9. Narlikar J.V. and Padnababhand T. Gravity, Gauge Theories and Cosmology. Reidel Publishing Company, Dordrecht, Holland, 1986.
10. Weinberg S. Quantum contribution to cosmological correlation. *Phys. Rev. D*, 2005, Vol 72, 4, 43514–43533.
11. Ross G. Grand Unified Theories. Westview Press, 1984.
12. Buras A.J., Ellis J., Gaillard M.K., Nanopoulos D.V. Aspects of the grand unification of strong, weak and electromagnetic interactions. *Nuclear Physics B*, 1978, v. 135(1), 66–92.
13. Wilczek F. Quantum field theory. *Reviews of Modern Physics*, 1999, v. 71, S83–S95.
14. Tosto S. Fundamentals of diffusion for optimized applications. *EAI*, 2012, no. 4–5, part 1, 94–107.
15. Tosto S. Quantum uncertainty and fundamental interactions. *Progress in Physics*, 2013, v. 2, 56–81.
16. Tosto S. Quantum Uncertainty and Relativity. *Progress in Physics*, 2012, v. 2, 58–81.
17. Tosto S. Quantum Uncertainty, Relativity and Cosmology. *International Journal of Physics and Astronomy*, 2014, v. 27, Issue 1, 1136–1157.

18. Tosto S. An analysis of the states in the phase space: the energy levels of quantum systems. *Il Nuovo Cimento B*, 1996, v. 111, no. 2, 193–215.

19. Tosto S. An analysis of the states in the phase space: the diatomic molecules. *Il Nuovo Cimento D*, 1996, v. 18, 1363–1394.

20. Tosto S. An analysis of states in the phase space: from quantum uncertainty to general relativity. arXiv gr-qc/0807.1011

21. Job G., Hermann F. Chemical potential - a quantity in search of recognition. *European Journal of Physics*, 2006, v. 27, 353–371.

22. Tosto S. Quantum standpoint for a more understandable universe. *American Journal of Space Science*, 2013, v. 1(1), 22–32.

23. Tosto S. Quantum approach to the gravitational waves. *Physics International*, 2013, v. 4(2), 135–151

Scaling of Moon Masses and Orbital Periods in the Systems of Saturn, Jupiter and Uranus

Hartmut Müller
Advanced Natural Research Institute in memoriam Leonhard Euler, Munich, Germany
E-mail: admin@anr-institute.com

The paper shows, that the sequence of sorted by value masses of the largest moons in the systems of Saturn, Jupiter and Uranus is connected by constant scaling exponents with the sequence of their sorted by value orbital periods.

1 Introduction

In [1] we have shown, that the connection between the body mass distribution and the distribution of orbital periods of planets and planetoids in the Solar System can be described by the scaling law:

$$M = \mu \cdot T^{\mathrm{D}}, \tag{1}$$

where M is a celestial body mass, T is a celestial body orbital period and μ and D are constants. We have shown, that for sorted by value couples of a body mass M and an orbital period T the exponent D is quite constant and is closed to the model value 3/2. Furthermore, for M in units of the proton rest mass $m_p \approx 1.67 \times 10^{-27}$ kg [2] and T in units of the proton oscillation period $\tau_p = \hbar/m_p c^2 \approx 7.02 \times 10^{-25}$ s, the constant $\mu = 1$.

In this paper we will show, that the scaling law (1) describes also the distribution of masses and orbital periods in the moon systems of Saturn, Jupiter and Uranus.

2 Methods

In [3] we have shown that the scaling exponent 3/2 arises as consequence of natural oscillations in chain systems of harmonic oscillators.

Within our fractal model [4] of matter as a chain system of oscillating protons and under the consideration of quantum oscillations as model mechanism of mass generation [5], we interpret the exponent D in (1) as a Hausdorff [6] fractal dimension of similarity (2):

$$\mathrm{D} = \frac{\ln M/m_p}{\ln T/\tau_p}. \tag{2}$$

The ratio M/m_p is the number of model protons, the ratio T/τ_p is the number of model proton oscillation cycles.

Already in the eighties the scaling exponent 3/2 was found in the distribution of particle masses [7]. Possibly, the model approximation of $\mathrm{D} \approx 3/2$ and $\mu = 1$ in (1) for proton units is a macroscopic quantum physical property, which is based on the baryon nature of normal matter, because $\mu = 1$ means that:

$$M/T^{\mathrm{D}} = m_p/\tau_p^{\mathrm{D}} \tag{3}$$

In [1] we have shown, that for planets and the most massive planetoids the average empiric value $\mathrm{D} \approx 1.527$ is a little bit larger then the model value 3/2. If we interpret the deviation of the empiric value $\mathrm{D} \approx 1.527$ in comparison with the model value 3/2 as a consequence of the fractality of the mass distribution in the system, then we can represent (1) in the form:

$$M^{\Delta}/T^2 = 1 \tag{4}$$

where $\Delta = 2/\mathrm{D}$ is the fractal dimension of the mass distribution, the constant of proportionality is 1 for proton units m_p and τ_p. The model value of Δ is 2/(3/2) = 4/3.

3 Results

The tables 1-3 contain properties of the largest moons of the Saturn, Juputer and Uranus systems. Always on the left side the moons are sorted by their masses, on the right side the moons are sorted by their orbital periods. The tables show, that within each moon system the fractal dimension Δ (4) is quite constant, but different from the average empiric value $\Delta = 2/D = 2/1.527 \approx 1.31$ for planets and planetoids [1]. This fact we interpret as criterion of different levels of fractality of the mass distribution in these systems. Furthermore, the tables show, that for the systems of Saturn and Uranus the fractal dimension Δ is nearly of the same average value, which is quite different of Δ for the system of Jupiter.

4 Resume

Within our fractal model [8], the scaling law (4) arises in chain systems of many harmonic oscillators and can be understood as fractal equivalent of the Hooke law. The scaling law (4) is valid for sorted by value couples of system properties. The Saturn system shows, that the scaling law (4) can be valid for one and the same body. The Jupiter and Uranus systems shows, that the scaling law (4) can be valid also for couples of different bodies. This may mean, that in general, the orbital period of each body does not depend only on its own mass, but depends on the body mass distribution in the system.

5 Acknowledgements

I'm thankful to my friend Victor Panchelyuga, my son Erwin and my partner Leili for the great experience to work with them, for the deep discussions and permanent support.

Submitted on February 15, 2015 / Accepted on February 17, 2015

Saturn moons, sorted by M	Body mass M, kg	$\ln(M/m_p)$	Δ	$\ln(T/\tau_p)$	Orbital period T, years	Saturn moons sorted by T
Mimas	3.7493×10^{19}	106.7277	1.2541	66.9235	0.9420	Mimas
Enceladus	1.0802×10^{20}	107.7858	1.2487	67.2983	1.3702	Enceladus
Tethys	6.1745×10^{20}	109.5291	1.2347	67.6187	1.8878	Tethys
Dione	1.0955×10^{21}	110.1024	1.2350	67.9901	2.7369	Dione
Iapetus	1.8056×10^{21}	110.6022	1.2385	68.4914	4.5182	Rhea
Rhea	2.3065×10^{21}	110.8470	1.2585	69.7524	15.9450	Titan
Titan	1.3452×10^{23}	114.9130	1.2419	71.3568	79.3215	Iapetus

Table 1: For sorted by value couples of a body mass M and an orbital period T the fractal dimension $\Delta(4)$ is quite constant within the Saturn moon system. The Saturn moon system average $\Delta = 1.2445$. Data comes from [9].

Jupiter moons, sorted by M	Body mass M, kg	$\ln(M/m_p)$	Δ	$\ln(T/\tau_p)$	Orbital period T, years	Jupiter moons sorted by T
Europa	4.7998×10^{22}	113.8824	1.1864	67.5538	1.7691	Io
Io	8.9319×10^{22}	114.5035	1.1921	68.2506	3.5512	Europa
Callisto	1.0759×10^{23}	114.6896	1.2024	68.9510	7.1546	Ganymede
Ganymede	1.4819×10^{23}	115.0098	1.2138	69.7980	16.6890	Callisto

Table 2: For sorted by value couples of a body mass M and an orbital period T the fractal dimension $\Delta(4)$ is quite constant within the Jupiter moon system. The Jupiter moon system average $\Delta = 1.1987$. Data comes from [12].

Uranus moons, sorted by M	Body mass M, kg	$\ln(M/m_p)$	Δ	$\ln(T/\tau_p)$	Orbital period T, years	Uranus moons sorted by T
Miranda	6.5900×10^{19}	107.2916	1.2551	67.3294	1.4135	Miranda
Umbriel	1.1720×10^{21}	110.1700	1.2328	67.9076	2.5200	Ariel
Ariel	1.3530×10^{21}	110.3136	1.2402	68.4050	4.1440	Umbriel
Oberon	3.0140×10^{21}	111.1145	1.2446	69.1473	8.7062	Titania
Titania	3.5270×10^{21}	111.2717	1.2507	69.5833	13.4632	Oberon

Table 3: For sorted by value couples of a body mass M and an orbital period T the fractal dimension $\Delta(4)$ is quite constant within the Uranus moon system. The Uranus moon system average $\Delta = 1.2447$. Data comes from [10, 11].

References

1. Müller H. Scaling of Body Masses and Orbital Periods in the Solar System. *Progress in Physics*, 2015, v. 2, 133–135.
2. Physical constants. Particle Data Group. www.pdg.lbl.gov
3. Müller H. Scaling Models of Natural Oscillations in Chain Systems and the Mass Distribution of Particles. *Progress in Physics*, 2010, v. 3, 61-66.
4. Müller H. Scaling models of Natural Oscillations in Chain Systems and the Mass Distribution of the Celestial Bodies in the Solar System. *Progress in Physics*, 2010, v. 1, 62–66.
5. Müller H. Emergence of Particle Masses in Fractal Scaling Models of Matter. *Progress in Physics*, 2012, v. 4, 44–47.
6. Hausdorff F. Dimension und äußeres Maß, 1919, v. 79.
7. Kolombet V. Macroscopic fluctuations, masses of particles and discrete space-time. *Biofizika*, 1992, v. 36, 492–499.
8. Müller H. Fractal scaling models of Resonant Oscillations in Chain systems of Harmonic Oscillators. *Progress in Physics*, 2009, v. 2, 72-76.
9. Bordi J., Jacobson R., Antreasian P. et al. The Gravity Field of the Saturnian System from Satellite Observations and Spacecraft Tracking Data. *Astronomical Journal*, 2006, v. 132, 2520–2526.
10. Uranus System Nomenclature Table Of Contents. Gazetteer of Planetary Nomenclature. USGS Astrogeology, 2009.
11. Taylor A., Synnott S., Jacobson R., Campbell J. The masses of Uranus and its major satellites from Voyager tracking data and Earth based Uranian satellite data. *Astronomical Journal*, 1992, v. 103, 2068–2078.
12. Malhotra R., Showman A. The Galilean Satellites. *Science*, 1999, v. 286, 77–84.

Birkeland Currents: A Force-Free Field-Aligned Model

Donald E. Scott

Department of Electrical Engineering (Retired), University of Massachusetts, Amherst, MA, USA.
e-mail: dascott3@cox.net

The fundamental vector calculus definition of a force-free, field-aligned current in space is expanded in cylindrical coordinates to directly obtain the Bessel partial differential equation that specifies the magnetic field created by such a current. This result is often called the Lundquist solution. A simple but detailed derivation is included here. The physical properties of the resulting intricate magnetic field structure are described. The cause of its characteristic counter-rotation and counter-flows are identified. The describing equations are put into state-variable form and a step-wise approximation is applied. This solution reveals the primary effect of the force-free parameter, α, as being a scale factor of radial distance. We show that: 1) both the axial and azimuthal magnetic and current density components cyclically reverse their directions with radial distance from the central axis of the current; 2) the magnetic field extends farther from the central axis within a force-free field than it would if produced by a current in a long straight conductor. The total magnetic field magnitude and current density are shown to vary inversely as the square root of r. For large r, outside the plasma, the azimuthal magnetic field is shown to vary as $1/r$. These results are shown to be consistent with laboratory and astronomical observations.

1 Introduction

After Kristian Birkeland [1] (1867-1917) suggested in 1908 that Earth's auroras were powered by corpuscular rays emanating from the Sun that become deflected into Earth's polar regions by the geomagnetic field, the existence of such magnetic field-aligned currents was strongly disputed based partially on the idea that currents could not cross the presumed "vacuum" of space [2, p. 181]. Birkeland's main problem, however, was that having made detailed measurements of Earth's geomagnetic field on the ground, he then wanted to extrapolate that knowledge into a description of the current-density distribution that caused those magnetic effects. This is not possible because a given magnetic field value can be produced by more than one distribution of current-density.

A level of interest did, however, develop regarding the Sun's photosphere and plasma properties of the solar corona. For example, a mathematical model of a force-free magnetic field was proposed as early as 1950 by Lundquist [3, 4]. He investigated whether magnetic fields could exist in an electrically conducting liquid and his results included presentation of the now well-known Bessel solution for force-free fields. Later in 1957, investigators such as Chandrasekhar and Kendall [5] applied a similar analysis to the spherical geometry of the Sun.

NASA scientists and many other investigators worked on Birkeland currents and flux rope observations since the mid-to-late 1960's [6–18], with substantial activity on this topic after the late 1980's [19–24]. A few researchers have sought cylindrical coordinate solutions [25] but almost always in reference to intricate quasi-cylindrical solar surface or coronal applications. Potemra [24] concluded that Birkeland currents and Alfvén waves are fundamental to an understanding of the Earth's plasma environment. It is now generally assumed that magnetic fields inside interplanetary magnetic clouds and flux ropes in the solar photosphere are force-free [26]. In 2009, space probe Themis discovered a flux rope pumping a 650,000 A current down into the arctic auroral region [27]. This strong observational evidence supports the existence of Birkeland Currents.

Consistent with this, the major goals of this paper are:

1. To present a simple, but complete derivation of Lundquist's equations that describe the magnetic field structure of a field-aligned current.
2. To fully describe the physical (not only magnetic, but also both the electrical and structural) consequences of those equations; to develop a model.
3. To demonstrate the correspondence between the properties of that model and observational evidence gathered from both plasma laboratories and astronomical images.

First we show that the basis of any model of a Birkeland current is what is called a force-free, field-aligned current.

2 Definition of a force-free field-aligned current

Consider a stream of moving charged particles (an electrical current) in a plasma that is not subject to any external forces. A useful mathematical idealization of such a physical cosmic current is a vector field of current density, $\boldsymbol{j}$, that, when viewed in a cylindrical coordinate system, creates an overall average current vector, $\boldsymbol{I}$, which, by definition determines the direction of the z-axis. The magnitude of $\boldsymbol{I}$ is assumed to be everywhere independent of the z coordinate. The coordinate system defines a point, p, represented by (r, θ, z), as illustrated in Figure 1.

The basic structure of such a cosmic magnetic field is controlled by the momentum equation of ideal magneto-hydrodynamics [25, 28–30],

$$(\nabla \times \boldsymbol{B}) \times \boldsymbol{B} = \mu_0 \nabla p \tag{1}$$

where μ_0 is the permeability of free-space.

The left hand side of this expression represents the compressive magnetic (Lorentz) force and the right side is the expansive force (pressure gradient multiplied by the permeability of the plasma). We distinguish between force-free fields with $\nabla p = 0$ and pressure balanced fields with $\nabla p \neq 0$. On the photosphere and within the lower chromosphere of the Sun the energy of the plasma motion dominates the magnetic energy and therefore the field is swept passively along with the plasma. This condition is characterized as a high-β plasma [31], where the parameter β is defined as the ratio between the plasma pressure p and the magnetic pressure,

$$\beta = 2\mu_0 \frac{p}{\boldsymbol{B}^2}. \tag{2}$$

Higher up in the corona, in interplanetary and in cosmic space, a lower pressure (lower ion and electron densities), low-β plasma often exists depending on local field pressure. Here the plasma can take on a force-free character [6,32,33]. However, care must be exercised in assuming low-β properties. For example, "*the extensive magnetosheath flow downstream of Earth's bow shock is a high-beta plasma. Along a radial cut of the plasma coming inward from the Sun near the dayside sub-solar point, the solar wind and magnetosheath flow is high-beta, the magnetopause and immediate (thin) plasma boundary provides a high to low beta transition, and immediately within the low-latitude boundary layer (within the outer magnetosphere) plasma is low-beta. Then with lower radial distance the plasma again becomes high-beta.*" [34]. We now present here a model that requires a low-β plasma environment.

The electromagnetic force experienced by each charge within such a plasma is given by,

$$\boldsymbol{F} = q(\boldsymbol{E} + \boldsymbol{v} \times \boldsymbol{B}). \tag{3}$$

The first term, $q\boldsymbol{E}$, is the *electric force* and the second term, $q(\boldsymbol{v} \times \boldsymbol{B})$, is called the *magnetic force*. The name *Lorentz force* is used to describe expression (3). The plasma region contains the cylindrical current stream. No initial assumptions are made about the distribution of the current density across the cross-section.

A flow of charge creates its own magnetic field through which the charge flows. The site at which each charged particle, q, in the stream is located is the point of origin of two local vectors: $\boldsymbol{j} = q\boldsymbol{v}$ (current density) and $\boldsymbol{B}$ (magnetic field). The current density vector $\boldsymbol{j}$ at each point inherently creates a *curl*($\boldsymbol{B}$) vector given by Maxwell [35]:

$$\nabla \times \boldsymbol{B} = \mu \left(\boldsymbol{j} + \epsilon \frac{\partial \boldsymbol{E}}{\partial t} \right). \tag{4}$$

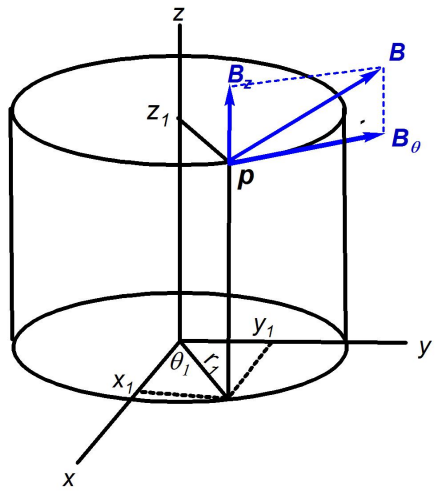

Fig. 1: Total magnetic field vector $\boldsymbol{B} = \boldsymbol{B}(r, \theta, z)$, and its two components B_z and B_θ at a particular location; $B_r = 0$. Note that at any point r, the pitch angle of the vector $\boldsymbol{B}$ measured upward from the horizontal plane is defined as the arctan $[B_z(r)/B_\theta(r)]$.

The derivative term in (4) which was added by Maxwell is called the displacement current. It is often considered to be zero valued, as we do here, when it can be assumed there are no time-varying electric fields in the region. Integrating the *curl*($\boldsymbol{B}$) vectors over a cross-section of the cylindrical stream (Stoke's theorem) yields,

$$\int_S \nabla \times \boldsymbol{B} \cdot d\boldsymbol{S} = \int_S \mu \boldsymbol{j} \cdot d\boldsymbol{S} = \oint_C \boldsymbol{B} \cdot d\boldsymbol{l} \tag{5}$$

where S is any cross-section of the plasma, and μ and ϵ are the permeability and permittivity respectively of the plasma medium. The second term in (5) is equivalently $\mu\boldsymbol{I}$ where $\boldsymbol{I}$ is the total current carried by the plasma. If the cross-section is circular with radius r, then the last term in (5) is $2\pi r\boldsymbol{B}$ where $\boldsymbol{B}$ is in the azimuthal, θ, direction, not aligned with $\boldsymbol{I}$ and the z-axis. Thus the $\boldsymbol{B}$ field produced by a cylindrical plasma at its outer boundary, $r = R$, is

$$\boldsymbol{B}_\theta = \frac{\mu \boldsymbol{I}}{2\pi R}. \tag{6}$$

Expression (4) is the *point form* and (5) is the *integral (macroscopic) form* of that Maxwell equation. Expression (4) is valid at any point. The integral forms given in (5) and (6) imply that $\boldsymbol{B}$ is a vector sum of the effects of all the $\boldsymbol{j}$ vectors on the surface $\boldsymbol{S}$ that is enclosed by C. $\boldsymbol{B}$ is not directly produced by any single $\boldsymbol{j}$. In (4) it is clear that $\boldsymbol{j}$, the current density at a point, creates only a single *curl*($\boldsymbol{B}$) vector, not a $\boldsymbol{B}$ vector. In general, there can be (and often is) a non-zero valued $\boldsymbol{B}$ vector at points at which $\boldsymbol{j} = \boldsymbol{0}$.

Prior to the time a cosmic current system, free of externally applied forces or fields, reaches a steady-state config-

uration, the $\boldsymbol{j}$ and $\boldsymbol{B}$ vectors are interacting – all the $\boldsymbol{j}$'s are creating *curl*($\boldsymbol{B}$) vectors that sum to form the local $\boldsymbol{B}$ vectors. At any point in the plasma where $\boldsymbol{j} \neq \boldsymbol{0}$ a force can exist between that current density vector and its local magnetic $\boldsymbol{B}$-field vector. This force is a magnetic *Lorentz force* given by the second term in (3). This vector cross product of a moving charge's velocity vector $\boldsymbol{v}$ and the local vector $\boldsymbol{B}$ implies that the scalar value (magnitude) of the resulting Lorentz force on each q is given by,

$$F_L = qvB\sin\varphi \tag{7}$$

where φ is the smallest angle between the vectors $\boldsymbol{v}$ and $\boldsymbol{B}$, with scalar values v and B. We call φ the Lorentz angle. If this angle is zero or 180 degrees, the magnetic Lorentz $\boldsymbol{v}\times\boldsymbol{B}$ force at that point is zero-valued.

The *magnetic intensity* (symbol $\boldsymbol{H}$) is often used to describe the macroscopic forcing function that creates a magnetic field,

$$H = \frac{B}{\mu} = \frac{NI}{l}. \tag{8}$$

The dimensions of $\boldsymbol{H}$ are A/m. (The number of turns, N, is dimensionless). $\boldsymbol{H}$ has also been called the *magnetic field strength*, and the *magnetizing force*.

The scalar magnitude, B, in (8) arises from the integral form (5). In that expression, B is shown to be the result of the total current, I. It follows that H is not a point form variable.

It may be shown that the energy density, W_B (Joules/m^3), stored in the magnetic field of such a current stream is given by,

$$W_B = \frac{\mu}{2}H^2. \tag{9}$$

Using (8) in (9), the total energy stored, ψ (Joules), in the magnetic field of a cosmic current is given by,

$$\psi = \frac{1}{2}\left(\frac{\mu N^2 A_c}{l}\right)I^2 \tag{10}$$

where A_c is the cross-sectional area and the *inductance* of the current stream is defined by the factor in parentheses. This shows that the only way to reduce the entire stored energy to zero is to completely cut off the current (set $I = 0$); in which case the entire cosmic current structure would cease to exist.

However, we assume that in unconstrained plasma in cosmic space, the current stream is free to move and distribute itself so as to minimize the internally stored potential energy due to the stresses resulting from magnetic Lorentz forces everywhere throughout the plasma. In fact space plasmas are uniquely situated to obey the *minimum total potential energy principle* [36], which asserts that a system or body shall deform or displace to a position and/or morphology that minimizes its total potential (stored) energy (a formalization of the idea that "water always flows downhill.").

The energy described in (10) is irreducible because it is caused by the fixed quantity, I. But the Lorentz energies can be eliminated because they do not depend on the value of I, only on the cross-products between local $\boldsymbol{B}$ and $\boldsymbol{j}$ vectors.

If and when the process of shedding the internal magnetic-force energy reaches a steady-state equilibrium, this structure is called a *force-free current* and is defined by the relation between the magnetic field vector, $\boldsymbol{B}$, and the current density vector, $\boldsymbol{j}$, at every location at which a charge, q, exists in the current stream:

$$q(\boldsymbol{v}\times\boldsymbol{B}) = \boldsymbol{j}\times\boldsymbol{B} = 0. \tag{11}$$

It follows from (11) that the Lorentz forces are everywhere equal to zero in a force-free current because every $\boldsymbol{j}$ is collinear with its corresponding $\boldsymbol{B}$. This arrangement is therefore also called a *field-aligned current* (FAC).

It follows directly from (4) and (11) that, if there is no time-varying electric field present, then (11) is equivalent to

$$(\nabla\times\boldsymbol{B})\times\boldsymbol{B} = 0 \tag{12}$$

which is identical to (1) with $\nabla p = 0$. This is the basic defining property of a force-free, field-aligned current.

Expression (4) implies that, if at any point in an otherwise field-aligned current, $\boldsymbol{j} = \boldsymbol{0}$, (12) is automatically fulfilled even if $\boldsymbol{B}$ is non-zero. The value of the magnitude and direction of $\boldsymbol{B}$ at any given point is generally not sufficient information to determine the magnitude, direction, or even the existence of $\boldsymbol{j}$ at that point. This is the problem that confronted Birkeland in his attempts to identify the currents responsible for the magnetic field variations he measured. However, from (4), knowledge of the direction and magnitude of the $\nabla\times\boldsymbol{B}$ vector at any given point does identically determine the value of $\mu\boldsymbol{j}$ there.

Field-aligned, force-free currents represent the lowest state of stored magnetic energy attainable in a cosmic current [31]. We seek an expression for the magnetic field, $\boldsymbol{B}(r,\theta,z)$, in such a current/field structure.

3 Quantitative model of a force-free field-aligned current

Equation (12) can be expanded into differential equation form using the cylindrical coordinate definition of curl and the 3-dimensional vector product determinant. However, this leads to an expression of little utility. Because (12) is satisfied if the current density, $\boldsymbol{j}$, has the same direction (except for sign) as $\boldsymbol{B}$ (and with no requirements on its magnitude), it was suggested (Lundquist [3, 4] and many others) that,

$$\nabla\times\boldsymbol{B} = \alpha\boldsymbol{B} \tag{13}$$

which from (4) is equivalently,

$$\mu\boldsymbol{j} = \alpha\boldsymbol{B} \tag{14}$$

where α is any non-zero valued scalar, which is equivalent to (12). This leads to a simple solution, but it is important

to note that accepting (14) as a substitute for (12) assumes *a priori* that, for any non-zero α, a non-zero valued $\boldsymbol{B}$ at any point requires the existence of a current density $\boldsymbol{j} \neq \boldsymbol{0}$ at that same point. This is in general, an unwarranted presumption. This is especially so in light of the well-known tendency of plasmas to form filaments (creating regions where $\boldsymbol{j} = \boldsymbol{0}$ but $\boldsymbol{B}$ is not). There are many examples in the study of electromagnetism, such as: Given that, in otherwise empty space, a current, $I_x = +1$ A exists in a straight, infinitely long conductor lying along the x-axis, find the value of the resulting magnetic field vector, $\boldsymbol{B}$, at the point $(x = y = 0, z = 1)$. The goal of this exercise is to find a value of $\boldsymbol{B}$ at a point where $\boldsymbol{j}$ is explicitly zero-valued. The answer is not zero.

However, most investigators start unhesitatingly with (13) and therefore (14) as givens. (This rules out applying the solution to a filamented plasma.) For example, Wiegelmann [37] does this and derives a vector Helmholtz equation which he states, can be solved by a separation *ansatz*, a Green's function method [8] or a Fourier method [18].

An *ansatz* is the establishment of the starting equation(s), the theorem(s), or the value(s) describing a mathematical or physical problem or solution. After an *ansatz* has been established (constituting nothing more than an assumption), the equations are solved for the general function of interest (constituting a confirmation of the assumption). That the mathematical solution accurately describes the physics is assumed.

In his 1950 paper Lundquist (after accepting the validity of (13)), without further explanation or derivation states that the solution of (14) with constant α is,

$$\begin{aligned} H_z &= A\, J_0(\alpha r) \\ H_\theta &= A\, J_1(\alpha r). \end{aligned} \tag{15}$$

Lundquist thus presents α as being a radial distance scale factor in the argument of his Bessel function solution. No evaluation of the coefficient A is offered. He also presents an image similar to Figure 6 below, but does not derive the current density or the physical consequences of these functions such as periodic reversals with increasing radius or counter-rotation and counter-flows of the plasma within the current structure.

Other investigators [45] start with (13) and then take its curl to obtain,

$$\begin{aligned} \nabla(\nabla\cdot\boldsymbol{B}) - \nabla^2\boldsymbol{B} &= \alpha(\nabla\times\boldsymbol{B}) \\ \nabla^2\boldsymbol{B} &= -\alpha(\nabla\times\boldsymbol{B}). \end{aligned} \tag{16}$$

They then also present the solution of (16) as being that given in (15). This agrees with Lundquist.

One of the most extensive reviews of force-free currents in a cylindrical geometry by Botha & Evangelidis [25] contains several references to similar studies. However, none of these investigators make the simplest assumptions: adopt a piece-wise linear approach, assume α to be any scalar value, and assume no variation of $\boldsymbol{j}$ or $\boldsymbol{B}$ in either the azimuthal or axial directions. Such simplifications may not be justified on the solar surface, but are in deep space. Therefore, we derive here a simple solution that follows from this and carefully note the effect of the parameter α on the resulting model.

Before beginning this derivation, we specify the dimensions of several involved quantities. Using (8),

$$[\mu] = \left[\frac{B}{H}\right] = \frac{\mathrm{Wb}}{\mathrm{m}^2}\frac{\mathrm{m}}{\mathrm{A}} = \frac{\mathrm{Wb}}{\mathrm{mA}}. \tag{17}$$

Using (4) the following units obtain,

$$[\nabla\times\boldsymbol{B}] = [\mu j] = \frac{\mathrm{Wb}}{\mathrm{mA}}\frac{\mathrm{A}}{\mathrm{m}^2} = \frac{\mathrm{Wb}}{\mathrm{m}^3}. \tag{18}$$

Using (13),

$$\frac{\mathrm{Wb}}{\mathrm{m}^3} = [\alpha]\frac{\mathrm{Wb}}{\mathrm{m}^2} \tag{19}$$

or

$$[\alpha] = 1/\mathrm{meter}. \tag{20}$$

Our derivation is as follows: The left side of (13) is expanded in cylindrical coordinates:

$$\begin{aligned} \nabla\times\boldsymbol{B} = \Bigg(&\frac{1}{r}\frac{\partial B_z}{\partial\theta} - \frac{\partial B_\theta}{\partial z}, \frac{\partial B_r}{\partial z} - \frac{\partial B_z}{\partial r}, \\ &\frac{1}{r}\frac{\partial}{\partial r}(rB_\theta) - \frac{1}{r}\frac{\partial B_r}{\partial\theta}\Bigg) \end{aligned} \tag{21}$$

and the right side of (13) is expressed as,

$$\alpha\boldsymbol{B} = (\alpha B_r, \alpha B_\theta, \alpha B_z). \tag{22}$$

In (21) and (22), all field components are functions of the position vector, $\boldsymbol{p}$. Given that there is no reason to assume any variation of current density $\boldsymbol{j}$ in the θ or z directions in cosmic space, (14) implies the same is true for $\boldsymbol{B}$.

It follows from the absence of any externally applied forces other than possibly a static axial electric field to maintain $\boldsymbol{I}$ (first term in (3)) and any time-varying electric fields, that all partial derivatives of $\boldsymbol{B}$ with respect to θ and z are zero and, therefore, what remains of (13) after these simplifications in (21) are the following three expressions: In the radial direction,

$$\alpha\boldsymbol{B}_r = 0. \tag{23}$$

There is no radial component of the $\boldsymbol{B}$ vector. This is consistent with Maxwell's $\nabla\cdot\boldsymbol{B} = 0$. In the azimuthal direction,

$$\frac{\partial B_z}{\partial r} = -\alpha B_\theta \tag{24}$$

and in the axial direction,

$$\frac{1}{r}\frac{\partial}{\partial r}(rB_\theta) = \alpha B_z. \tag{25}$$

This results in two non-trivial coupled differential equations in the two dependent variables B_z and B_θ as shown in (24) and (25). The independent variable in both is radial distance, r.

4 Solution in closed form

Combining (24) and (25) yields a single second-order differential equation in a single dependent variable,

$$r^2 \frac{\partial^2 B_z(r)}{\partial r^2} + r \frac{\partial B_z(r)}{\partial r} + \alpha^2 r^2 B_z(r) = 0. \tag{26}$$

The dependent variable $B_z(r)$ is the axial component of the force-free steady-state magnetic field. The component field $B_z(r)$ is allowed to extend as far as the differential equation (26) provides for. No boundary condition at any non-zero value of r is introduced. There will be, in all real currents in space, a natural limit, $r = R$, to the extent of the current density $\boldsymbol{j}(r)$.

Having now fully specified the differential equation (26), it is recognized as being identical to Bessel's equation of order zero, with scalar parameter α (the units of which are (see (20)) the reciprocal of the units of r). We thus have a closed-form solution for the dependent variable in that differential equation that results from expanding equation (13). Its solution is,

$$y = AJ_0(\alpha x) + CY_0(\alpha x). \tag{27}$$

$J_0(x)$ is the Bessel function of the first kind and zero$^{\text{th}}$ order, and $Y_0(x)$ is the Bessel function of the second kind (or sometimes called the Weber or Neumann function) of zero$^{\text{th}}$ order.

The function $J_0(\alpha x)$ has the value unity at the boundary $x = 0$, and the function $Y_0(\alpha x)$ has a singularity at this same boundary. Because reality dictates that the magnetic field remain finite-valued, the value of arbitrary coefficient C must be set equal to zero. Thus, the solution to (26) is given by,

$$B_z(r) = B_z(0) J_0(\alpha r). \tag{28}$$

This Bessel function of the first kind and of order zero is used to produce Bessel functions of the first kind and orders 1, 2, 3, ... by simple differentiation. The recursion relation for the first-order Bessel function is,

$$J_1(x) = -\frac{dJ_0(x)}{dx}. \tag{29}$$

Thus, from (24) and (29), we obtain,

$$B_\theta(r) = B_z(0) J_1(\alpha r). \tag{30}$$

Consequently, from (28) and (30), the scale of the size, r, of the magnetic field in the radial direction is determined by the parameter α. Allowing $\alpha = \alpha(r)$ would distort the radial axis used to plot $B_z(r)$ and $B_\theta(r)$.

These Bessel functions approach damped trigonometric functions for large r, but the amplitude decrease is unusually gradual – varying inversely as the *square root* of αr, which is a more gradual decay than the typical exponential, or $1/\alpha r$, or $1/(\alpha r)^2$ damping.

This decay behavior is seen from the asymptotic forms shown here in (31) below,

$$\begin{aligned} J_0(x) &= \sqrt{\frac{2}{\pi x}}\left[\cos\left(x - \frac{\pi}{4}\right) + O\left(\frac{1}{x}\right)\right] \\ J_1(x) &= \sqrt{\frac{2}{\pi x}}\left[\cos\left(x - \frac{3\pi}{4}\right) + O\left(\frac{1}{x}\right)\right]. \end{aligned} \tag{31}$$

Therefore, $B_r(r)$, $B_z(r)$ and $B_\theta(r)$ shown in (23), (28), and (30) together provide a complete description of the magnetic field that surrounds and pervades the final force-free, minimum-energy, steady-state, cylindrical current. In this state, all Lorentz forces have been reduced to zero. The physical implications of these expressions are fully described in Section 8, below.

5 Euler method of solution

Another approach to solving (26), one that does not require that it be recognized as a Bessel equation, is to use an iterative numerical method. One such method is based on a *state-variable representation* of the differential equation – in this case the pair (24) and (25). In order to describe those differential equations in state-variable form, the product rule for derivatives is first applied to (25) as follows:

$$\frac{\partial(rB_\theta)}{\partial r} = r\alpha B_z \tag{32}$$

$$r\frac{\partial B_\theta}{\partial r} + B_\theta = r\alpha B_z. \tag{33}$$

Two state-variables may be defined as follows:

$$x_1 = B_z \tag{34}$$

$$x_2 = B_\theta \tag{35}$$

so that rewriting (24) and (25) in state-variable form yields,

$$\frac{dx_1}{dr} = -\alpha x_2 \tag{36}$$

$$\frac{dx_2}{dr} = \alpha x_1 - \left(\frac{1}{r}\right) x_2. \tag{37}$$

An Euler/Runge-Kutta algorithm for obtaining an approximate step-wise solution to (36) and (37) was implemented. The results, presented in Figure 2, show, as expected, the familiar shapes of Bessel functions J_0 and J_1 as $B_z(r)$ the axial component, and $B_\theta(r)$ the azimuthal component. Also shown is the total magnetic field strength $|\boldsymbol{B}|$ (the square root of the sum of the squares of the two component scalar fields, B_z and B_θ). This total field strength magnitude is strongest at a minimum radial value r and decreases monotonically with increasing r.

Specifically, in Figure 2, *total magnetic field magnitude* is shown to decrease with increasing radial distance from the

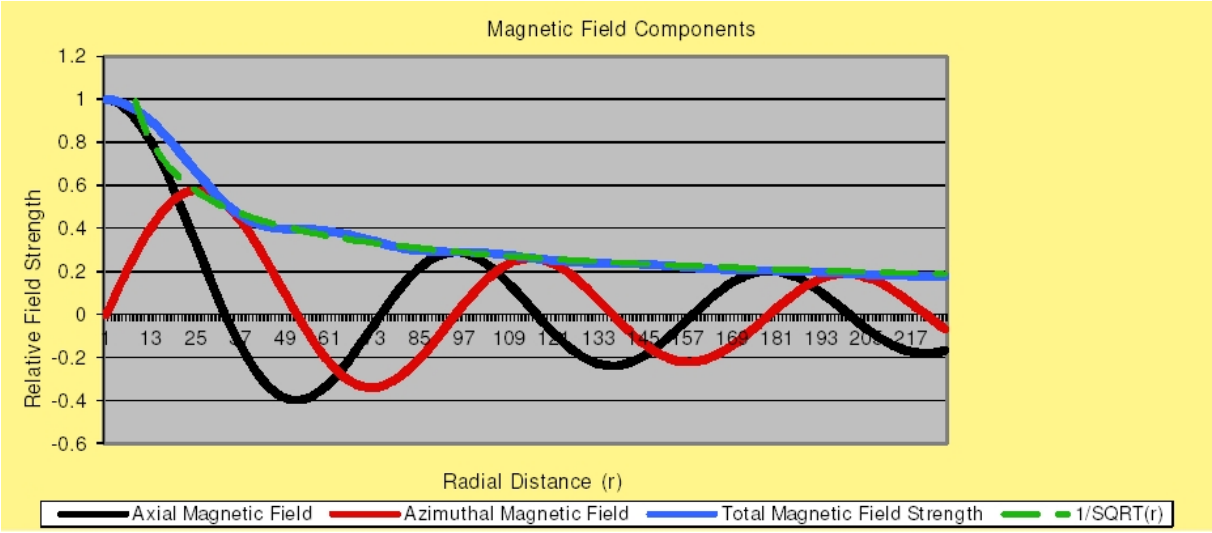

Fig. 2: Axial Magnetic Field component B_z, the Azimuthal Magnetic Field component B_θ, the magnitude of the Total Magnetic Field; and, for reference, a plot of $1/\sqrt{r}$ – all vs. radial distance quantized to integer multiples of the step-size h = 0.1. The value of α arbitrarily selected in (36) and (37) to achieve adequate resolution of the Bessel functions with this step-size is 0.075. The horizontal axis in this plot is the radius r-axis. Note in Table I that in every case (row) the inherently dimensionless Bessel function argument, $x = \alpha r$, thus demonstrating the scale factor utility of α. (e.g., $2.4048 = 0.075 \times 32$.)

central axis of the current as $(\alpha r)^{-1/2}$. This function is shown, for reference, as the fourth series plotted in Figure 2. This behavior was fully described in Section 4 (see (31)). Therefore, the magnetic fields within field-aligned cosmic currents clearly extend outward in space much farther and less diminished in strength than the magnetic field that would be generated by a simple straight-wire electric current (see (6)).

The parameter α appears as a scale factor operating on the radius variable, r. In the result shown in Figure 2, the value for that distance-scaling parameter was arbitrarily chosen to be $\alpha = 0.075$. The horizontal axis of Figure 2 is in units of actual radial distance, r. For example, the first zero of $J_0(x)$ is located at $x = 2.4048$. In Figure 2 it is shown to occur at $r = x/0.075 = 32$. This demonstrates the relationship between the non-dimensional argument of the Bessel functions, x, and the scaled variable, r: $x = \alpha r$. Nothing is inferred or implied about the current density vector field $\boldsymbol{j}$ at this stage.

The step-wise Euler method described here can also be used in the event the state-equations are nonlinear due to choosing an arbitrary $\alpha = \alpha(r)$.

6 General validity of solution

A question remains regarding the generality of the solutions (23), (28), and (30), for $B_r(r)$, $B_\theta(r)$, and $B_z(r)$ respectively. Directly or indirectly all three of these quantities result from solving the Bessel equation (26), which, itself, is derived from the substitute equation (13), not from the fundamental, definition of a *force-free current* (12). This substitute, (13), was posited as being a valid alternative to (12), the defining property. Expressions (12) and (13) impose similar but not identical requirements on the magnetic field $\boldsymbol{B}(r, \theta, z)$ and the current density field $\boldsymbol{j}(r, \theta, z)$. Therefore, it has not yet been demonstrated that the vector field solutions of (13) listed in (23), (28) and (30) are also valid solutions of the fundamental definition, (12).

Table 1: IMPORTANT VALUES FOR RADIAL MAGNETIC COMPONENTS

Radius Values $r = x/\alpha$	Zeros of $J_0(x)$ X	Zeros of $J_1(x)$ x	Description
0		0	B_z pos max, B_θ zero
32	2.4048		B_z zero, B_θ pos max
51		3.8317	B_z neg max, B_θ zero
74	5.5201		B_z zero, B_θ neg max
94		7.0156	B_z pos max, B_θ zero
116	8.6537		B_z zero, B_θ pos max
136		10.1735	B_z neg max, B_θ zero
158	11.7915		B_z zero, B_θ neg max
178		13.3237	B_z pos max, B_θ zero
199	14.9309		B_z zero, B_θ pos max

In order to demonstrate this, we insert those solutions back into (12) by writing the central three-dimensional cross product contained in that expression in determinant form:

$$(\nabla \times \boldsymbol{B}) \times \boldsymbol{B} = \begin{vmatrix} \hat{r} & \hat{\theta} & \hat{z} \\ (\nabla \times \boldsymbol{B}_r) & (\nabla \times \boldsymbol{B}_\theta) & (\nabla \times \boldsymbol{B}_z) \\ \boldsymbol{B}_r & \boldsymbol{B}_\theta & \boldsymbol{B}_z \end{vmatrix}. \quad (38)$$

Using the cylindrical curl expansion of (21),

$$\left|\mathrm{b}_{ij}\right| = (\nabla \times \boldsymbol{B}) \times \boldsymbol{B} = \begin{vmatrix} \hat{r} & \hat{\theta} & \hat{z} \\ 0 & -\frac{\partial B_z}{\partial r} & \frac{1}{r}\frac{\partial}{\partial r}(rB_\theta) \\ B_r & B_\theta & B_z \end{vmatrix}. \quad (39)$$

We use (23), (28) and (30). Then in (39) the element b_{22} becomes,

$$\begin{aligned} b_{22} &= -\frac{\partial}{\partial r}\left[B_z(0)\,J_0(\alpha r)\right] \\ &= \alpha B_z(0)\,J_1(\alpha r)\,. \end{aligned} \tag{40}$$

The element b_{23} becomes,

$$\begin{aligned} b_{23} &= \frac{1}{r}\left(r\frac{\partial B_\theta}{\partial r}+B_\theta\right) = \frac{\partial B_\theta}{\partial r}+\frac{1}{r}B_\theta \\ &= \alpha B_z(0)\left[\frac{\partial J_1(\alpha r)}{\partial r}+\frac{1}{\alpha r}J_1(\alpha r)\right]. \end{aligned} \tag{41}$$

Since

$$\frac{\partial J_1}{\partial x} = J_0 - \frac{1}{x}J_1, \tag{42}$$

(41) becomes,

$$\begin{aligned} b_{23} &= \alpha B_z(0)\left[J_0(\alpha r)-\frac{1}{\alpha r}J_1(\alpha r)+\frac{1}{\alpha r}J_1(\alpha r)\right] \\ &= \alpha B_z(0)\,J_0(\alpha r)\,. \end{aligned} \tag{43}$$

Using the above expressions together with (23), (28), and (30), in (39) and omitting functions' arguments for clarity,

$$(\nabla\times\boldsymbol{B})\times\boldsymbol{B} = \begin{vmatrix} \hat{r} & \hat{\theta} & \hat{z} \\ 0 & \alpha B_0 J_1 & \alpha B_0 J_0 \\ 0 & B_0 J_1 & B_0 J_0 \end{vmatrix} = \mathbf{0}. \tag{44}$$

(QED)

Thus, the components of $\boldsymbol{B}(r,\theta,z)$ given in (23), (28), and (30) are shown to be valid solutions of the original defining equation (12). That fact remains valid whether or not the alternative (13) had ever been suggested.

Regarding the practical evaluation of α when approximate observations of both $\boldsymbol{B}$ and $\nabla\times\boldsymbol{B}$ are available, we have [31, p.107],

$$\alpha = \frac{(\nabla\times\boldsymbol{B})\cdot\boldsymbol{B}}{B^2}. \tag{45}$$

Inserting the appropriate components from (23), (28), and (30) into (45) yields the identity,

$$\alpha = \alpha. \tag{46}$$

This indicates that the results presented here as (23), (28) and (30) are consistent with the formulation for α given in (45).

7 Current density of a field aligned current

Having accepted the postulated alternative definition (13) and (14) to determine the force-free magnetic-field solutions (28) and (30) (repeated below as (47) and (48)), it is then logically consistent to simply insert these into (14) to obtain the companion current-density relations (49) and (50):

$$B_z(r) = B_z(0)\,J_0(\alpha r) \tag{47}$$

$$B_\theta(r) = B_z(0)\,J_1(\alpha r) \tag{48}$$

$$j_z(r) = \frac{\alpha B_z(0)}{\mu}\,J_0(\alpha r) \tag{49}$$

$$j_\theta(r) = \frac{\alpha B_z(0)}{\mu}\,J_1(\alpha r)\,. \tag{50}$$

A dimensional analysis of (49) and/or (50) using (18) and (20) shows the units of the constant term $\alpha B_z(0)/\mu$ to be $\mathrm{A/m^2}$ as they must be.

In (49) and (50), it is clear that as the radial size of the model is increased (by decreasing the value of α), the magnitude of both current density components decrease proportionally.

Wiegelmann [37] ***defines*** α as being $\alpha(x,y) = \mu_0 j_0/B_0$ (see (49) and (50)). This definition also has units of 1/m (reciprocal of distance) (see (17)-(20)). Peratt [31, p.107] states that α is adjusted until reasonable agreement is obtained with observations (see (45) and (46)).

8 Consequences of the oscillatory nature of the Bessel (Lundquist) solution

Expressions (47)–(50) fully describe the structure of the model of a minimum (Lorentz force) energy, cylindrical, force-free, field-aligned current (FAC) under the assumption of equation (14). Thus:

1. There are no points within the plasma where $\boldsymbol{B}=\mathbf{0}$. A non-zero valued magnetic field exists at every point. In the first paragraph after (3) it was stated, nor are any assumptions made about the distribution of the current density across the cross-section. (49) and (50) now express that spatial distribution of $\boldsymbol{j}(\boldsymbol{p})$.
2. At every point in the plasma, $\boldsymbol{j}$ and $\boldsymbol{B}$ are collinear.
3. At every point in the plasma $\mu\boldsymbol{j} = \alpha\boldsymbol{B}$ (assumption, as discussed in Section 3).
4. The model expressions (47)–(50) remain valid only over the range $0 < r < R$. Farther out from the z-axis than $r = R$, $\boldsymbol{j}=\mathbf{0}$. From that point outward, the cylindrical plasma appears more and more like a single straight, isolated current-carrying wire. So beyond radius R, the magnetic field strength will decay approaching $1/r$. This is shown directly using (14): for $r > R$, $\boldsymbol{j}=\mathbf{0}$, $\alpha = 0$. Then using (32) and (33) yields:

$$B_\theta(r) = \frac{k_z}{r}. \tag{51}$$

This is consistent with (6).

Visualizing this field configuration with the aid of Figures 2, 3, and 5, reveals that, within the plasma, at increasing radial values, the magnetic field, together with its collinear current density, wrap the axis of the current stream with a continuously increasing helical pitch angle.

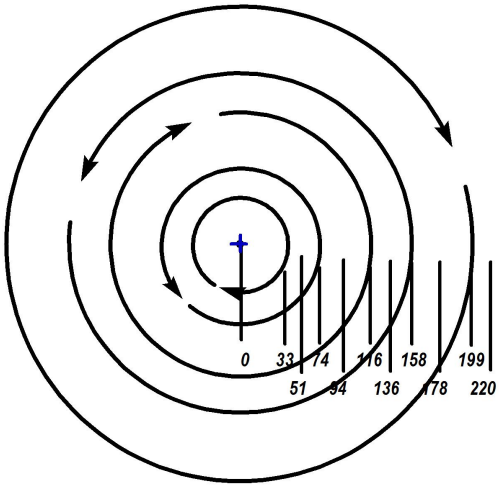

Fig. 3: Cross-section of a force-free current. In this view the reader is looking in the $+z$-direction, in the direction of main current flow. The radius values shown are plotted as values of $r = x/\alpha$ ($\alpha = 0.075$), which were used in the Euler iterative solution of (36) and (37). At the radius values shown, the axial $\boldsymbol{B}$-field is zero-valued so the total field is only azimuthal (either clockwise or counter-clockwise circles).

From (23), there is no outward radiation of the magnetic field (nor its collinear $\boldsymbol{j}$) from inside the plasma where $\alpha \neq 0$. There is no non-zero B_r or j_r component anywhere. Thus no matter escapes from the plasma. This preserves the structural integrity of the FAC over large axial distances.

Both solutions (closed-form and Euler) demonstrate repeated reversals in the directions of both the axial and the azimuthal magnetic field components with increasing radial distance. This implies the existence of a discrete set of virtual concentric cylindrical surfaces (see Figure 3). These surfaces are centered on the z-axis of the field-aligned current. At these discrete radial values, the axial field component, B_z is zero-valued and the azimuthal magnetic component, B_θ, is at alternatingly clockwise and counter-clockwise maxima. As a function of r the axial and azimuthal field strengths are observed to be in quadrature. For example in Figure 2, in a region such as that between radial distances 74 and 116, the axial field, B_z, is unidirectional (in the positive z-direction, attaining maximum strength at $r = 94$); whereas the azimuthal field reverses direction at $r = 94$, changing from the negative direction of θ to the positive direction. This results in a total magnetic field vector that wraps the current stream, its pitch angle rotating (with increasing r) in a clockwise direction when viewed looking inward in a radial direction, toward the central axis of the current (see Figure 5).

Thus, the axis of a cosmic, field-aligned current is wrapped with a compound helical magnetic field whose angle with respect to the $+z$-axis increases continuously with increasing radial distance, r. This gives rise to a structure suggestive of some ancient Roman fasces.

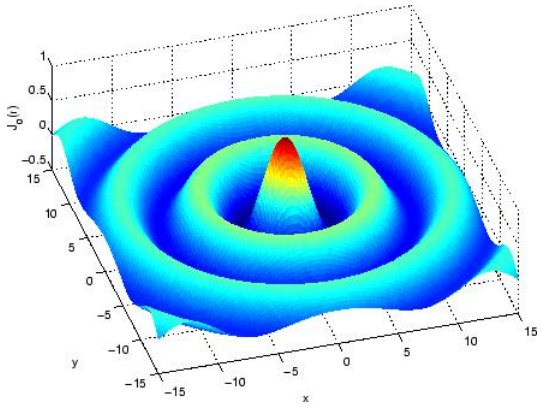

Fig. 4: Three-dimensional plot of the magnitude of the axial magnetic field component $B_z(r)$ and the current density $j_z(r)$. This demonstrates the relative strength of both those central (on-axis) fields. The magnitude scale of the horizontal axes used in this Figure are both x, the dimensionless arguments of the Bessel $J_0(x)$ and $J_1(x)$ functions.

In Figure 5, one cycle (0°–360°) of the pitch angle is shown. The cycle is sketched at eleven incrementally increasing sample values of radius. The shaded arrows show the total magnetic field direction at each value of radius, r, and the white arrows show the field direction at an increment just below each of those values of radius. At every point in a stable force-free, field-aligned current, the current density $\boldsymbol{j}$ is collinear with $\boldsymbol{B}$.

The Lundquist-Alfvén image shown in Figure 6, which is often used to describe the Birkeland current steady-state minimum-energy magnetic field, is in agreement with these results (47–50), but it only describes the morphology for small values of r. As r increases beyond what is shown in Figure 6, an uninterrupted rotation of the pitch angle of the magnetic/current helices continues (see Figure 5). The field rotation does not abruptly stop at 90° (where the total magnetic field is orthogonal to the direction of z) as might be inferred from Figure 6. The helical wrapping of the $\boldsymbol{j}$ and $\boldsymbol{B}$ fields continues with increasing radius values. This adds strength to the overall FAC structure. The tangent of the helical angle at any point, r, is the ratio (see Figure 1),

$$\frac{B_z(r)}{B_\theta(r)} = \frac{J_0(\alpha r)}{J_1(\alpha r)} = \frac{J_0(x)}{J_1(x)}. \tag{52}$$

Therefore if the value of the scale factor, $\alpha = x/r$ is, say, doubled, then that same pitch angle will occur at a value of r at half the original radius (x value unchanged). Thus the scale of the entire model will be halved (see Figure 6).

9 Effects of increased axial current

In a geomagnetic storm, a surge in the flux of charged particles (current increase) often temporarily alters Earth's magnetic field.

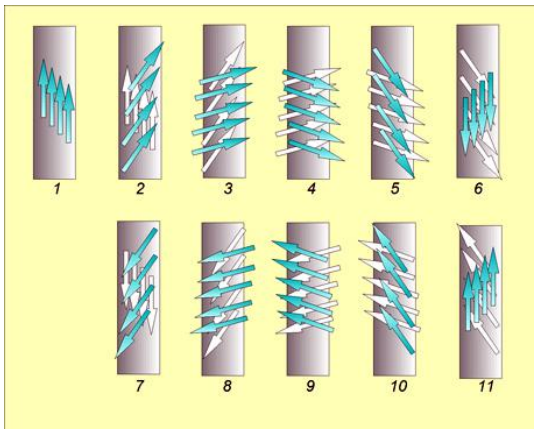

Fig. 5: The pitch angle of the helical total magnetic field, $\boldsymbol{B}$ vector, that encircles a field-aligned current changes continuously with increasing radial distance from the central axis of the current. There are no abrupt quantum jumps or breaks in this angle's change or in the field's magnitude. One cycle (0°–360°) of the pitch angle is shown. The cycle is sketched at eleven incrementally increasing sample values of radius. The shaded arrows show the total magnetic field direction at each value of radius, r, and the white arrows show the field direction at an increment just below each of those values of radius.

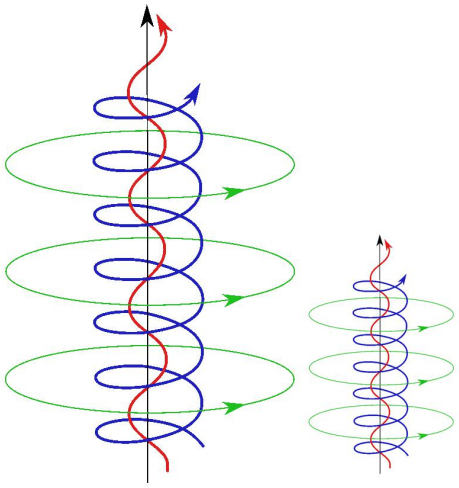

Fig. 6: Two different sized scale models of a FAC. These are both Lundquist-Alfvén-type images showing the helical structure of the collinear $\boldsymbol{j}$ and $\boldsymbol{B}$ vectors for small values of radius, r. (Left: Using $\alpha = \alpha_o$. Right: Using $\alpha = 2\alpha_o$.) This demonstrates why some investigators say that alpha controls the "tightness of twist". It only appears to do that as a secondary effect because it's primary effect is as a scale factor on the overall dimensional ***size*** (r, z) of the model's structure.

The entirety of this paper up to this point has been focused on the consequences of the reduction or possible elimination of the Lorentz $\boldsymbol{v}\times\boldsymbol{B}$ forces as defined in the second term of (3). But, the first term in that expression produces an independent, conduction component of the current density that may be added, via superposition, to the current density, $\boldsymbol{j}_z$, that has been derived above. This additional term is written as,

$$j_{cond} = q\boldsymbol{E}\left(\sum_k n_k \mu_{ions}^{(k)} + n_e \mu_e\right) \qquad (53)$$

where n_k is the ion density, with k = ionization number of the various ions, n_e is the electron density and $\mu_{ions}^{(k)}$ and μ_e are the respective mobilities of those ions and electrons in the plasma. Expression (53) is the point form of Ohm's Law. Another way that $\boldsymbol{j}_z$ might become increased is by narrowing the cross-sectional area of a Birkeland current as it squeezes down into a polar cusp in a geomagnetic field.

It is not known if any actual, observed cosmic currents are in the complete minimum (Lorentz force) energy, field-aligned state. Several apparently show evidence of near-force-free behavior [31]. In the steady-state minimum energy FAC configuration, all Lorentz forces have been eliminated and charge simply follows the magnetic field structure. For example, in Figure 3, any positively charged matter located at $r = 158$, has counter-clockwise motion.

The image shown in Figure 8 was obtained in a plasma laboratory. Neither this nor the image of Saturn's north pole in Figure 7 represent force-free currents because they both are images of collisions of such currents with material objects.

Figure 8 suggests what may occur if such an overall current density increase were to occur. The force-free structure would begin to undergo changes (if not be totally destroyed). Exactly what would happen is pure conjecture but if we start with Figure 3 and consider what might occur if and when a low intensity stream of positive charge begins to infuse the entire cross-section in a $+z$ direction (away from the reader), these additional positive charges would likely be deflected by Lorentz forces as follows (see Figure 3). At radii 33, 116, and 199 – deflection inward and clockwise. At radii 74, and 158 – deflection outward and counter-clockwise.

The two paths (inward and clockwise at $r = 116$ and the one at $r = 74$ moving outward and counter-clockwise) might appear to be a single path spiraling inward from $r = 116$ toward $r = 74$. Such pathways are suggested in Figure 8. Clearly in that state, the system is no longer at minimum energy – Lorentz forces are at work within the no-longer force-free plasma.

Another effect of an increase in the magnitude of the axial component of the current density, j_z, would be to add a small incremental vector in the $+z$-axis direction to each existing $\boldsymbol{j}_z$-vector. For example, consider sub-figures 2-5 in Figure 5. A small $+\boldsymbol{j}_z$ vector added to each of the shaded $\boldsymbol{j}$-vectors shown there would tend to twist them slightly counter-clockwise, away from being aligned with their corresponding $\boldsymbol{B}$-vector that remains fixed. The resulting Lorentz force ($\boldsymbol{j}\times\boldsymbol{B}$) would be directed inward (away from the viewer). However, if a similar small $+\boldsymbol{j}_z$ vector were to be added to each of the shaded $\boldsymbol{j}$-vectors shown in sub-figures 7-10 in Figure 5, this would

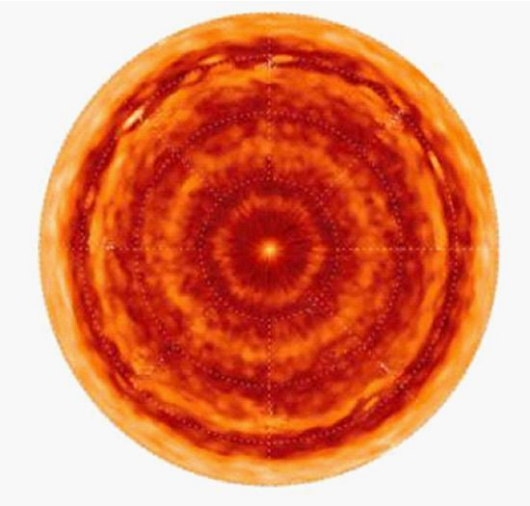

Fig. 7: Saturn's north pole, infrared Cassini image. Saturn is a gaseous planet composed mainly of hydrogen and helium. This image was obtained during the dark winter. The pole is encircled by a hexagonal feature in its atmosphere, which is thought to be caused by a planetary (atmospheric) wave. Image obtained using the infrared mapping spectrometer on board the Cassini Orbiter spacecraft. Courtesy of: NASA/JPL-Caltech/University of Arizona. The Cassini-Huygens mission is a cooperative project of NASA, the European Space Agency and the Italian Space Agency. Image Credit: NASA/JPL/GSFC/Oxford University/Science Photo Library [40].

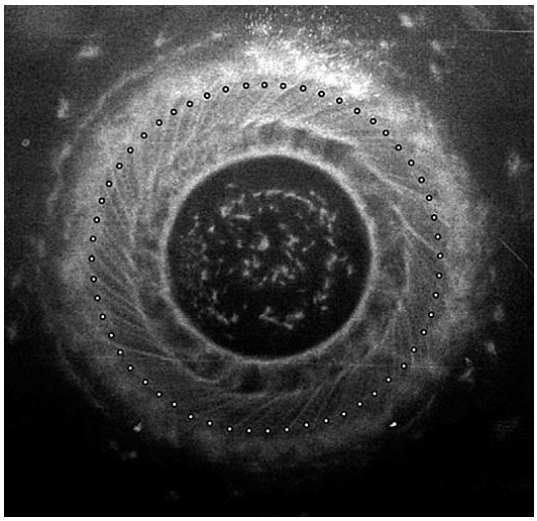

Fig. 8: Cross-section of a dense plasma focus Birkeland Current carrying $I = 174,000$ amperes. This image was captured by a witness plate placed in the discharge in a plasma lab. The spiral structure of the cross-section is visible. The 56-dot circular overlay shows the locations of the apparent spiral shaped paths of matter. Courtesy of A.L. Peratt, from Characteristics of a High-Current, Z-Pinch Aurora As Recorded in Antiquity, Part II Directionality and Source by Peratt, Directionality and Source. IEEE Transactions on Plasma Sci., August 2007 [41].

twist them slightly clockwise and the Lorentz force would, at those points, be directed outward (toward the viewer). Ions, then, will be pushed inward over radial ranges wherever azimuthal magnetic field, $\boldsymbol{B}_\theta$, is directed clockwise in Figure 3. Ions will be expelled outward wherever $\boldsymbol{B}_\theta$ is directed counter-clockwise in Figure 3. Matter (ions and neutral dust) will thus tend to congregate at intermediate radius values such as $r = 0, 94$, and 178. These are radii defined by the *odd zeros of* $J_1 = J_1(x) = J_1(\alpha r)$, $(x = 0, 7, 13, \dots)$ (see Figure 4 and column 3 of Table I for values). Electrons moving in the $-z$-direction will tend to be scavenged into the same r-regions. These are hollow cylindrical surfaces where $+\boldsymbol{j}_z$ dominates.

10 Comparison of results with observations

Images in Figures 7, 9, and 10 are obtained from actual astronomical observations. The image shown in Figure 7 is consistent with the hypothesis that Saturn is receiving a flow of electric charge via a Birkeland current directed into its north pole much as Earth is known to be experiencing. It is well known that currents in plasma drag un-ionized (as well as ionized) matter along in their path [42]. Figure 3 and the discussion at the end of Section 9, above, imply that clockwise and counter-clockwise counter-rotating current paths such as those at $r =$ 33 and 74 ought to exhibit such counter-rotation. But, for years it has been unknown whether the spiraling/circular paths appearing in Figures 7, 8 and 9 are really counter-rotating. It would require a video to reveal that relative motion.

It so happens that NASA has produced exactly such a video clearly showing counter-rotating (plasma) clouds within what appears to be the hexagonal shape at Saturn's north pole (see: [43] NASA video - Saturn's Hurricane). In this video, the term hurricane is used repeatedly by the narrator who expresses concern about the fact that the "storm" is fixed to the planet's north pole and that no water ocean exists below it to cause it to exist. He does not mention that actual hurricane winds do not counter-rotate as these do.

In that video, in shear regions between counter-rotating shells, what appear to be diocotron instabilities are visible (see Figure 9). Without NASA's video, the counter-rotational motions of these areas in the Saturnian surface would not be observed and therefore their existence would go undiscovered. This recent motion picture is crucial evidence of part of what is being presented here. Many other edited versions of the original NASA video exist that do not show counter-rotation taking place. The uncut original does.

11 Conclusions

It has been well-known for decades that the Lundquist solution (15) constitutes a simple model of a cylindrical force-free, field-aligned current. This model:

1. Dictates that the two vector fields $\boldsymbol{j}(r, \theta, z)$ and $\boldsymbol{B}(r, \theta, z)$ be everywhere collinear;

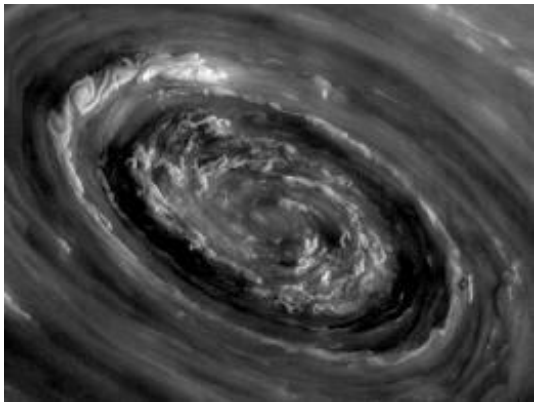

Fig. 9: Series of diocotron (shear) instabilities, especially obvious in the upper left of this image. This was taken from the NASA video [43] which clearly shows counter-rotation. From NASA Cassini mission video of Saturn's North Pole. Courtesy of: NASA/JPL-Caltech/University of Arizona. The Cassini-Huygens mission is a cooperative project of NASA, the European Space Agency and the Italian Space Agency. The imaging operations center is based at the Space Science Institute in Boulder, Colo. The Visual and Infrared Mapping Spectrometer team is based at the University of Arizona [43].

2. States that the overall solutions that specify the spatial dependence of those fields' magnitudes and directions are Bessel functions;
3. Assumes α is constant inside the plasma.

In this present paper we present a simple, but detailed derivation of this model of a force-free current and demonstrate, through straightforward mathematical analysis and strict adherence to the principles delineated in Maxwell's equations [35], a number of significant characterizations [44] of these field equations that are in strong agreement with reliable imagery obtained from both actual observations of phenomena in space and measurements in experiments in plasma laboratories. The most significant of those results are:

1. The complete mathematical model of a cylindrical, force-free FAC, including expressions for its current-density field is presented by (47)–(50), not just (15).
2. Magnetic fields produced by force-free currents stretch out radially from the central axis of the current stream much farther, and with greater effect, than previously thought. For radial distances, r, within the plasma ($r < R$) the amplitudes of those helical fields decay slowly *in inverse proportion to the square root of* r.
3. The fact that expression (23) requires that no component of the magnetic field, $\boldsymbol{B}$, can extend outward in the radial direction (and the fact that $\boldsymbol{B}$ and $\boldsymbol{j}$ are everywhere collinear) demonstrates that no dissipative currents or fields leave the cylindrical structure along its length. Birkeland's critics thought that the final, relaxed distribution would be an infinite dispersion, not a strong, tight cylinder (which it is).
4. The structural stability of the spiraling fasces-like wrapping of the magnetic field explains the observed enigmatic stability of Birkeland currents over long inter-planetary, inter-stellar, and inter-galactic distances. For example, the cosmic current "jet" emanating from galaxy M87 remains collimated over a distance exceeding 5000 light years [46]. The stability of the flux-rope connecting the Sun and Earth is now better understood (see Section 8).
5. The angle of pitch of the helix varies smoothly and continuously with increasing radial distance, r, from the central axis of the current out as far as the plasma's current-carrying charge density extends. This causes cyclical reversals of direction (counter-flows) in both the axial and azimuthal magnetic field and its collinear current density. The magnitude of both the $\boldsymbol{B}$ and $\boldsymbol{j}$-fields may be greater than zero for r values far beyond the first zero of $J_0(\alpha r)$ (which occurs at $r = 2.4048/\alpha$). Figure 6 is shown to be correct but incomplete, and thus potentially misleading.
6. Coupled with the new NASA video of Saturn's north polar region, this presentation strongly supports the hypothesis that a Birkeland current is feeding electric current into that region.
7. Parameter α controls the size of the resulting model in both the r and z dimensions (together – not separately). The value of α is arbitrary and is selected to enable the model to fit the size of the actual space-plasma being modeled.
8. The major difference between a field-aligned current (FAC) and a Birkeland current is that in a FAC the total current, $\boldsymbol{I}$, is a minimum. When the current density at any point, $\boldsymbol{j}$, increases for any reason above its minimal value, non-zero Lorentz forces begin to occur and the matter scavenging described in Section 9 takes place.
9. The mathematical procedure offered here is circumscribed to an extent not typical of other papers by caveats regarding the consequences of the universal unquestioning acceptance of the generality of the expression $\mu\boldsymbol{j} = \alpha\boldsymbol{B}$ (14). This is not applicable in filamented plasma.

The conclusions drawn from the analysis of the mathematical model derived in this paper have been tested against original motivating observations and measurements. Consistently strong agreement is found. Many otherwise enigmatic images stand witness to the potential benefits of considering possible electrical causation of other cosmic plasma phenomena.

The M2-9 Hourglass planetary nebula in Figure 10 is a prime case in point. We suggest that the narrowing of the

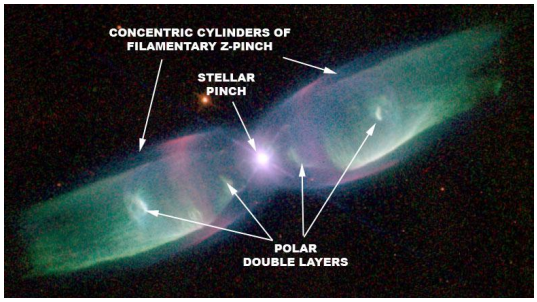

Fig. 10: The Hourglass (or Butterfly) planetary nebula, M2-9. In this image the separate hollow, cylindrical tubes of matter are clearly visible. The cross-sectional area of the structure diminishes near the center of the pinch. Since the total current is the same at every cross-section, this means regions near the central pinch have increased current density (A/m^2) and corresponding greater visual brightness. Courtesy of the Hubble Legacy Archive, NASA, ESA Processing *Judy Schmidt*. The Hubble Legacy Archive (HLA) is designed to optimize science from the Hubble Space Telescope by providing online, enhanced Hubble products and advanced browsing capabilities. The HLA is a joint project of the Space Telescope Science Institute (STScI), the Space Telescope European Coordinating Facility (ST-ECF), and the Canadian Astronomy Data Centre (CADC) [45].

plasma FAC channel due to the z-pinch creates an increased current density which causes a transition of the plasma from the dark mode into the visible glow and arc modes. The observed dual, concentric cylinders of excited plasma are consistent with the counter-rotation, matter scavenging, and reversing flows described in this paper.

Acknowledgements

The author wishes to express his sincere thanks to Dr. Jeremy Dunning-Davies for recognizing that the differential equation derived in this study is a Bessel Equation, whose solutions are given by the Bessel functions, J_0 and J_1. He also gave the author much appreciated encouragement and very much needed advice.

Dr. Timothy Eastman, Wyle senior scientist at NASA Goddard, Dr. Ron DeLyser, EE Department U. of Denver, Dr. C. J. Ransom of Vemasat Labs, Dr. W. A. Gardner, and Dr. Michael Clarage gave freely and graciously of their time, advice, and assistance to help in this effort.

Submitted on: January 27, 2015 / Accepted on: February 17, 2015
First published online on: February 20, 2015

References

1. Birkeland K. The Norwegian Polaris Expedition 1902–1903, Vol. 1, Sect. 1. Aschehoug, Oslo, Norway, 1908.
2. Lerner E. The Big Bang Never Happened. New York, 1991. p. 181.
3. Lundquist S. Magneto-hydrostatic fields. *Arch. Fys.*, 1950, v. 2, 361.
4. Lundquist S. On the stability of magneto-hydrostatic fields. *Phys. Rev.*, 1951, v. 83 (2), 307–311. Available online: http://link.aps.org/doi/10.1103/PhysRev.83.307.
5. Chandrasekhar S. and Kendall P. On force-free magnetic fields. *Astrophys. J.*, 1957, v. 12 (6), 457.
6. Gold T. AAS-NASA Symposium on Physics of Solar Flares. Hess W. N., ed., NASA SP–50, 1964, p. 389.
7. Alekseev I. and Shabansky V. A model of a magnetic field in the geomagnetosphere. *Planet. Space Sci.*, 1972, v. 20, 117.
8. Chiu Y. and Hilton H. Exact Green's function method of solar force-free magnetic-field computations with constant alpha. I. Theory and basic test cases. *Astrophys. J.*, 1977, v. 212, 873–885.
9. Cloutier P. and Anderson H. Observations of Birkeland currents. *Space Sci. Rev.*, 1975, v. 17, 563–587.
10. Alfvén H. Evolution of the solar system. Scientific and Technical Information Office National Aeronautics and Space Administration, Washington, D.C., 1976.
11. Hasegawa A. and Sato T. Generation of Field Aligned Current during Substorm in Dynamics of the Magnetosphere. Akasofu, S-I., ed., D. Reidel, Hingham, MA, 1979, p. 529.
12. Nakagawa J. and Raadu M. A. On practical representation of magnetic field. *Solar Phys.*, 1972, v. 25, 127.
13. Olson W. A model of distributed magnetospheric currents. *J. Geophys. Res.*, 1974, v. 79, 3731.
14. Rostoker G., Armstrong J. C., and Zmuda A. J. Field-aligned current flow associated with intrusion of the substorm-intensified westward electrojet into the evening sector. *J. Geophys. Res.*, 1975, v. 80, 3571–3579.
15. Zmuda A., Armstrong J. C., and Heuring F. Characteristics of transverse magnetic disturbances observed at 1100 kilometers in the auroral oval. *J. Geophys. Res.*, 1970, v. 75 (25), 4757–4762.
16. Dessler A. Corotating Birkeland currents in Jupiter's magnetosphere - An Io plasma-torus source. *Plan. Space Sci.*, 1980, v. 28, 781–788.
17. Harel M., Wolf R. A., Reiff P. H., Spiro R. W., Burke W. J., Rich F. J., and Smiddy M. Quantitative simulation of a magnetospheric substorm 1. Model logic and overview. *J. Geophys. Res.*, 1981, v. 86, 2217–2241.
18. Alissandrakis C. On the computation of constant alpha force-free magnetic field. *J. Astron. Astrophys.*, 1981, v. 100 (1), 197–200.
19. Burlaga L. Magnetic clouds and force-free fields with constant alpha. *J. Geophys. Res.: Space Phys.*, 1988, v. 93 (A7), 7217–7224.
20. Durrant C. J. Linear force-free magnetic fields and coronal models. *Aust. J. Phys.*, 1989, v. 42, 317–329.
21. Falthammer C. G. Magnetosphere-Ionosphere interaction. Near-Earth Manifestations of the plasma universe. *IEEE Trans. Plasma. Sci.*, 1986, v. 14 (6), 616–628,
22. Potemra T. Birkeland Currents I. The Earth's Magnetosphere (From a special issue dedicated to Hannes Alfvén on his 80th Birthday). *Astrophys. Space Sci.*, 1988, v. 144 (1–2), 155–169.
23. Potemra T. Observation of Birkeland currents with the TRIAD Satellite. *Astrophys. Space Sci.*, 1978, v. 58 (1), 207–226.
24. Potemra T. Alfvén Waves and Birkeland Currents. *Physica Scripta*, 1995, v. T60, 107–112.
25. Botha G. J. J. and Evangelidis E. A. Cylindrical linear force-free magnetic fields with toroidal flux surfaces. *Mon. Not. Roy. Astron. Soc.*, 2004, v. 350 (1), 375–384.
26. Romashets E. and Vandas M. Force-free magnetic field in a cylindrical flux rope without a constant alpha. *Adv. Space Res.*, 2005, v. 36 (12), 2268–2272.
27. Eastwood J. Flux ropes. NASA Goddard, 2009.
28. Goedbloed J. and Poedts S. Principles of Magnetohydrodynamics: With Applications to Laboratory and Astrophysical Plasmas. Cambridge University Press, Cambridge, UK, 2004.
29. Biskamp D. Nonlinear Magnetohydrodynamics. Cambridge University Press, Cambridge, UK, 1997.

30. Ferraro V. and Plumpton C. An Introduction of Magneto-Fluid Mechanisms. Clarendon Press, Oxford, 1966.

31. Peratt A. Physics of the Plasma Universe. Springer-Verlag, New York, 1992, p. 44. Republished ISBN 978-1-4614-7818-8, 2015, p. 406.

32. Titov V., Török T., Mikic Z., and Linker J. A. A method for embedding circular force-free ropes in potential magnetic fields. *Astrophys. J.*, 2014, v. 790 (2), 163.

33. Yang Y. Y., Shen C., Zhang Y. C., Rong Z. J., Li X., Dunlop M., Ma Y. H., Liu Z. X., Carr C. M., and Rème H. The force-free configuration of flux ropes in geomagnetotail: cluster observations. *J. Geophys. Res.: Space Phys.*, 2014, v. 119 (8), 6327–6341.

34. Eastman T. Wyle Senior Scientist at NASA Goddard, Personal communication, 5 February 2015.

35. Jackson J. Classical Electrodynamics, 2nd ed. John Wiley, New York, NY, 1975.

36. Callen H. Thermodynamics and an Introduction to Thermostatistics, 2nd ed. John Wiley, New York, NY, 1985.

37. Wiegelmann T. and Sakurai T. Solar force-free magnetic fields. *Living Rev. Solar Phys.*, 2012, v. 9 (5). Available online: http://solarphysics.livingreviews.org/Articles/lrsp-2012-5/.

38. Alfvén H. Cosmic Plasma. D. Reidel, Hingham, MA, 1981, p. 97.

39. Matlab, Bessel functions of the First and Second Kind. Available online: http://www.mhtlab.uwaterloo.ca/courses/me755/web_chap4.pdf.

40. Infrared image of Saturn's North pole. Available online: http://www.sciencephoto.com/media/326994/view, 4 February 2015.

41. Peratt A. Image: Penumbra from a dense plasma focus device. Available online: http://www.academia.edu/9156605/Neolithic_rock_art_associated_with_intense_auroral_currents, Figure 51, 4 February 2015.

42. Mehdipour H. and Foroutan G. The magnetized sheath of a dusty plasma with nanosize dust grains. *Phys. Plasmas*, 2010, v. 17, 083704.

43. NASA video of the Saturn hurricane. Available online: http://www.jpl.nasa.gov/video/details.php?id=1213, 4 February 2015.

44. Scott D. Real properties of electromagnetic fields and plasma in the cosmos. *IEEE Trans. Plasma Sci.*, 2007, v. 35 (4), 822–827.

45. High resolution NASA image of the Hour-Glass or Butterfly planetary nebula M2-9. Available online: http://apod.nasa.gov/apod/ap130915.html, 4 February 2015).

46. Messier 87 - SEDS catalog. Available online: http://messier.seds.org/m/m087.html.

LETTERS TO PROGRESS IN PHYSICS

An Eidetic Reflex and Moment of Breakthrough in Time and Scientific Creation: 10 Years of Progress in Physics, 100 Years of General Relativity, and the Zelmanov Cosmological Group

Indranu Suhendro

The Zelmanov Cosmological Group, Secretary of the Zelmanov Journal for General Relativity, Gravitation, and Cosmology

We celebrate the first 10-year momentous span of the solid body of critical scientific results and efforts delivered by the visionary editorial and founding team of the pioneering open new-millennium journal for advanced studies in theoretical and experimental physics, mathematics, astronomy, and cosmology, *Progress in Physics* (see the Editor-in-Chief's message: "Progress in Physics: 10 years in Print"), behind which is the core scientists and guardians of universal scientific creation, scientific revolution, and scientific-intellectual freedom and ethics: the few core scientists of the quintessential Zelmanov Cosmological Group, such as the founding editors and scientific creators Dmitri Rabounski and Larissa Borissova.

The Zelmanov Cosmological Group, which is also behind *The Abraham Zelmanov Journal* for General Relativity, gravitation, and cosmology, dedicates itself to the profound and extensive scope and depth of the works of the master theoretician "par excellence" of the Soviet-era general relativistic and cosmological school, Abraham Leonidovich Zelmanov, and to the most unique problems and possible extensions of General Relativity in general. Abraham Zelmanov's profundity "sine qua non" is reflected in the singular creation of the theories of chronometric, kinemetric, and orthometric (monad) formalism in General Relativity, the Infinite Relativity Principle, the Anthropic Principle, the extensive classification of all possible cosmological models in the space-time of General Relativity (the Zelmanov Classification, including the possibility of absolute reference frames in a deforming, rotating, gravitating closed finite Universe), and many others (see the website of *The Abraham Zelmanov Journal* for details, and in particular the 2012 foreword to the book *Particles Here and Beyond the Mirror*). So, Zelmanov's theoretical mastery singularly encompasses the general fully non-linear, anisotropic, inhomogeneous, anholonomic, non-simply-connected space-time structure (and sub-structure) of General Relativity and the fabric of the cosmos, achieving the unification of the underlying structure of space-time, reference frame systems, and the fundamental observer. Zelmanov's few students and theoretical inheritors — such as Dmitri Rabounski and Larissa Borissova — have thereby preserved and extended his scientific and philosophical ideals as a whole, comprehensive, unitive scientific legacy: a singular univocity — "Zelmanovian Universum" — in the form of an ideologically most unique and versatile platform for the most singular kind of meta-science and scientific creation, which is the embryo of the present Zelmanov Cosmological Group.

In the background of such unique origination, the general fundamental physics journal *Progress in Physics*, with a substantial portion of publications in General Relativity and differential geometry — in common with *The Abraham Zelmanov Journal*, is dedicated mostly to original, profound, critical, and challenging scientific works that potentially engage with the overall, far-reaching horizons and verizons of theoretical and experimental physics, mathematics, astronomy/cosmology, and of science as a whole, thereby expanding and synthesizing new scientific landscapes for both the present and the future. This is done mostly by identifying the pertinent objective quality and originality of the idea(s) in a submitted scientific work and the first and foremost crucial identification of the author as an essentially independent creative mind (whether specifically affiliated or not) and as a true person of integrity and clarity, therefore isolating the process of scientific judgement infinitely and decisively from the pervasively corruption-mongering, business-minded, pseudo-scientific (so, pseudo-objective) politics of typical modern academic practice and science administration (i.e., "big-wig scientism"). In specific cases where the editors and expert peer reviewers (who dare be non-anonymous) do not agree with the ideology and content of a submitted paper, a fidelity to pure scientific-intellectual freedom is still maintained as much as possible in the publication of the said work, as long as the basic technicality and competence (such as the mathematics and logical reasoning) is fulfilled. This is also true for some tremendous-looking extremely short papers that can subtly serve as an impetus for reflection and future scientific inspiration: they can be so short and still publishable in view of inspiring some pertinent new ideas in the future.

A word on a better peer-review system is at hand: above all, the journal categorically and distinctly promotes original thinkers and original scientific creators, along with fundamentally improving and transcending the largely deficient anonymous peer-review system, thus often allowing a work to be published with the potential for an on-going open peer-review (in the full critical vastness of time and space as regards judgement and validation): such as witnessed in the

forced, pioneering open peer-review case of Grisha Perelman's ground-breaking works on Ricci flow, manifold surgery, and the Poincaré conjecture. Thus, the journal employs a unique, more substantial form of peer-review system covering both immediate (pre-publication) and open-to-future-validation fully substantiated peer-review models. The journal does not welcome typical celebrity popularization and "celebrity fetishism/worship". Thus, it does not endorse exercising scientific judgement based on mere consensus and popularity, which is the maladious, rotten, decadent business of politics and pseudo-science arising from the fact that there are too many people nowadays claiming to be "career scientists" (while careerism and science are most certainly two different things by way of subtle logical discernment) while essentially they are at large socially, inter-subjectively active opportunists and imitators. Such is to be compared to Einstein's time when scientists were truly still a rare breed or species — or say, before World War II, a war that changed so many ways of doing things in science and life, in science especially with the hijacking of some old journals and institutions by a plethora of powerful pseudo-scientists and pervasive mediocrity: certainly Einstein would not have survived today's popularity-concocting, narrow-minded, overly pretentious, intrinsically and extrinsically flawed scientific administration laden with closed-minded and pathetically rigid apathy against fundamental scientific novelty, individuality, and originality.

The common board of *Progress in Physics* and *The Abraham Zelmanov Journal* therefore comprises and welcomes scientific pioneers, as ethically liberal-democratic and inter-disciplinarily universal as possible: this, while the said board consists mostly of theoreticians and scientific creators in General Relativity, cosmology, and differential geometry at the heart of the Zelmanov Cosmological Group. While the journal is hosted by the said general relativists and differential geometers, it does not oppose alternative views: it acknowledges the two kinds of "alternative" (not one): the categorically superior "alternative" and the simple (ordinary) "alternative" (which can be either inferior or relatively on-par at times). Consequently, it promotes the fully open discussion of categorically different (often opposing) scientific views and ontologies, thus covering both the substance and event of all possible ideological presentations and representations.

In conducting a superior, alternative form of scientific peer-review, the board is also helped a great deal in dealing with radical, paradoxical, universal, inter-disciplinary scientific submissions and reasoning by the Smarandache Neutrosophy Group that extends the content, expression, and scope of logic and dialectics. This then is meant to be a fundamental platform for the creation of new physics, new mathematics, new cosmology, new phenomenology, new ontology, and new epistemology.

In other words, the journal aims at the rapid and transparent publication of uniquely qualified original scientific ideas and impetuses: anything that is counter-productive, parasitic, and artificial to the true spirit of genuine scientific judgement (no matter how trendy), such as the extremely pernicious and popular trends and developments in the superficial politics of today's scientism, is not recognized by it. In addition to substantiating and upgrading peer-review, the journal also strives to help improve fully the genuine open-access system in all possible ways. This is the firmest future model for any true future science and scientific organization, where the quality of an individual original scientific work alone can reflect the journal's over-all stance as a whole, not simply the very superficial, idiotic, logically and semantically flawed concoction of "citation-only impact factor" (based merely on the number of citations) misused by so many "illiterate" (essentially quality-blind and quality-devoid) pretentious people in the typical administration nowadays. The journal philosophy as a whole serves in many ways as an absolute separator between real science and artificial politics, between originality and imitation, between profundity and superficiality, between integrity and hypocrisy. Any reader or any institution is absolutely free to download the materials (papers and books) published by both *Progress in Physics* and *The Abraham Zelmanov Journal*.

The year 2015 also marks the 100th anniversary of Einstein's geometric theory of space-time and gravitation, the General Theory of Relativity, since the final formulation of the generally covariant Einstein's field equations of gravitation in the last quarter of 1915 (during a very tragic and difficult time of World War I). It goes without saying that this was achieved by Einstein almost at the same time as Hilbert's final formulation of the field equations of gravitation, an axiomatic, lone, and colossal problem Hilbert rather spontaneously worked on upon witnessing Einstein's Göttingen lecture on the (at that time agonizingly stifled) progress of the formulation of the theory during the same year. It took well over 8 years of one of mankind's greatest intellectual (philosophical, physical, mathematical) struggles towards synthesis in history for the greatly isolated, independent, original, and visionary young scientific creator — Albert Einstein — to complete the task since 1907 when he first attempted the logical extension of the Special Theory of Relativity (born in 1905) to include gravitation and more general reference frames under the umbrella of differential geometry and general covariance (first with the help of Einstein's friend, Marcel Grossmann, who helped select and qualify Riemannian geometry for Einstein's new physics program, and also of Tulio Levi-Civita and Hermann Weyl upon the later publication of the final form of General Relativity). This was not so long after Poincarë and Minkowski (among Einstein's own teachers) proposed a basic four-dimensional space-time structure for the world, which later became incorporated into Special Relativity, and into particle physics and group theory via algebraic symmetry classification. Today, as per differential geometry and topology, both Riemannian and non-Riemannian

geometry (such as Finsler geometry) can be used in General Relativity to understand better its geometric-folitional structure (such as Riemannian sub-manifolds and singular spaces) as well as its extensions (most ontologically and epistemologically unique, though, would be General Relativity's orthometric extensions — not just any extension — as I have alluded to elsewhere).

Understood initially by very few in the world — and now genuinely and profoundly understood (truly in-depth, not merely in the popular and prevalent context) still by very few — General Relativity as such is a universal scientific construct and superstructure equivalent to a pure work of visual and musical art and a novel philosophical edifice of ontology and epistemology. I therefore would like to salute the truly small number of the world's most dedicated and original scientists (absolutely indifferent to mere popularity) whose field of work encompasses General Relativity, gravitation, cosmology, and the unified geometric theory of space-time and the physical fields (fundamental extension of Einstein's theory): those who singularly live Einstein's theory of General Relativity and generally the Einsteinian ideology of the geometrization of space-time, matter, and fields, i.e. those with real creative contributions to the field (excluding mere "toy models") and not simply those very many who opportunistically make a living out of it by hijacking Einstein's theory and name. Congratulations to the rarest and most universal kind of scientific creators in Einstein's name: those few scientific creators in possession of insight and ideation, originality and profundity, solitude and singularity, of new ideas in the unmistakable footsteps of Einstein himself.

Again, a disclaimer — a song of epistemic suffering and near-despair, arising from a saddest line and event of alienation in science — is immediately at hand also. It is a sad, tragic fact that Einstein's name today has been hijacked, misappropirated, and misused in the said way by the throngs of aggressively narrow-minded and self-promoting scientific imitators and popularizers (and "launderers" of shallow scientific outputs, opinions, and hypernarrations) the world over: they typically and consensually announce a plethora of trivial toy models of physics and the Universe and (by the blind forces of "status quo" consisting of greedy and petty power grabbers, false opinion manufacturers, and all their stooges) often force and entrench them as prevailing dogmas while hiding rather cowardly and manipulatively behind Einstein's stature. Such is a patently false misuse of power and a trivial, empty concoction of prestige, and an epitome of great prevalent hypocrisy, amounting to the greatest corruption done in the name of science: a categorical scientific abuse by way of mere opinion-making, large political and financial backing, and all sorts of flawed prestige and opinion manufacture absolutely without (and in contrast to) the first-principle ontic-epistemic determination of scientific profundity, quality, and reality with all its reflexively self-evident intrinsic logic, semantics, and syntax. It is clear that Einstein himself would never take the side of those professing such a dogmatic and popular position, let alone those who pathetically suffer from — what I always call — utter ontic-epistemic shallowness, solipsistic folly, sycophant opportunism, and hypernarration (see the previous scientific letter "Meta-Epistemic Determination of Quality and Reality in Scientific Creation" as to how to epistemically qualify real quality science as simply genuine science and to disqualify bad popular science and its politics as simply bad science). I and my colleagues disassociate ourselves forever, once and for all, from such people who are the latent enemies and cancers of science. We care solely about the subtle and sublime spirit of science and scientific creation, and of scientific-intellectual freedom, not all the flawed manufactures of politics and such contingency.

The above diseased situation, often fogged and misunderstood in popular venues, has to be clearly understood by not only those working fundamentally in Einstein's theory, but also those who have engendered a relative (or absolute) opposition to Einstein and General Relativity. The latter group of people with certain alternative views — which we certainly usually can tolerate as long as science is the objective — ought not to mistake the flawed-in-mind opportunistic hijackers of Einstein's name and theory for Einstein himself (and General Relativity), so as to very arbitrarily and shorthandedly fume out "war against Einstein". They have to at least understand the semantics and hermeneutics of Einstein and General Relativity a little better than usual: not from the said hijackers (who have no ontological, substantial relation to Einstein whatsoever), but from the solitary few who are real Einsteinian experts and inheritors. The Zelmanov Cosmological Group would welcome anyone who wants to understand Einstein and General Relativity better in a different way, as to disclose that great light in a solitary, often dark and hidden, true cosmic lane.

Finally, I salute once again the truly intellectually free — true scientists, minds symphonically swarthed with the cosmos and ideas, like true poets and artists — anywhere on this Earth and in the cosmos, on the most unique joint birthday occasion and resonance of Einstein's General Relativity and *Progress in Physics*.

Dedicated to Grisha Perelman and all the (few) truly free, corageous, revolutionary minds in the world of science. And to professors Brian Josephson and Sydney Brenner, and the late Joseph C. Hafele, from a silent observer on a distant but immediate star, as was Einstein unto Spinoza and as was Newton unto Copernicus: "... as this song of truth, this utter knowing — the poem — falls to the beautiful soul as dew to grass" (Pablo Neruda).

Submitted on February 25, 2015 / Accepted on February 26, 2015

Qualitative Prediction of Isotope Abundances with the Bipolar Model of Oscillations in a Chain System

Andreas Ries
Universidade Federal de Pernambuco (alumnus), Centro de Tecnologia e Geociências, Laboratório de Dispositivos e Nanoestruturas,
Rua Acadêmico Hélio Ramos s/n, 50740-330 Recife – PE, Brazil
E-mail: andreasries@yahoo.com

We analyzed the individual masses of non-radioactive isotopes of the chemical elements with an extended version of the bipolar model of oscillations in a chain system. When defining a small set of appropriate rules, the model is able to predict the isotope which possesses the highest abundance. This information can be read out from the continued fraction representations of the isotope masses. Isotopes with enhanced nuclear stability due to a magic number of neutrons in the nucleus were frequently found as exceptions from the model. The model is applicable to the di-, tri- and tetranuclidic chemical elements; it fails completely as soon as a chemical element is composed of 5 or more stable isotopes. From this we conclude that the bipolar model of oscillations in a chain system – in its present form – is not yet the final version; the model must still be extended.

1 Introduction

In a previous paper [1], the bipolar model of oscillations in a chain system was applied to the standard atomic weights of the chemical elements. The atomic weights of the 19 mononuclidic elements and Helium, which have the lowest standard deviations, were expressed in continuous fraction form without any outliers. This was the calibration (and determination oh the phase shift) of the model. It was then found that the vast majority of atomic weights of the polynuclidic elements could be reproduced through continued fractions as well.

The underlying mathematical formalism worked as follows: the mean atomic weights were transformed into a continued fraction according to the equations

$$\ln \frac{m}{m_{electron}} = p_e + S, \qquad \ln \frac{m}{m_{proton}} = p_p + S, \qquad (1)$$

where p is the phase shift (it must hold p_p = -p_e) and S is the continued fraction (e is Euler's number)

$$S = n_0 + \cfrac{e}{n_1 + \cfrac{e}{n_2 + \cfrac{e}{n_3 + ...}}}. \qquad (2)$$

Numerically (if $\neq 0$), p_p was found to be -1.7918229 for the calibrating (low standard deviation) data set.

In this article we extend this previously established version of the model and demonstrate how to predict with an adequate set of rules, which isotope of a given chemical element has the highest abundance.

2 Data sources and computational details

All masses and percentage abundances of isotopes were taken from the web-site of the National Institute of Standards (NIST). An isotope mass is understood as the mass of the neutral atom in its nuclear and electronic ground state.

As in previous articles, the continued fraction representation $p + S$ is abbreviated as $[p; n_0 \mid n_1, n_2, n_3, \dots]$, where the free link n_0 is allowed to be $0, \pm3, \pm6, \pm9, \pm12, \pm15\dots$ and all partial denominators n_i can take the values e+1, $-e$−1, ±6, ±9, ±12, ±15 ....

3 Results and discussion

3.1 Model extension

Within the originally presented form of the bipolar model (eq. 1) it is not possible to express all the nuclide masses through continued fractions within the accuracy of their standard deviations. Two adjustments are mandatory, one is related to the model itself, the other one to the data set.

First we introduce an additional phase shift δ, as it was already done in a previous article dealing with the electron density distribution in the Hydrogen atom [2]. We write

$$\ln \frac{m}{m_{electron}} = \delta_e + p_e + S, \qquad \ln \frac{m}{m_{proton}} = \delta_p + p_p + S. \quad (3)$$

In the same manner as holds p_p = -p_e, must consequently hold $\delta_p = -\delta_e$, which means the bipolarity is strictly conserved. The only difference between δ and p is the fact that δ is a small phase shift ($\neq 0$, with either positive or negative sign) applying to *all* isotope masses, while the phase shift p varies among the data points. Some of the masses are associated to the phase shift zero, others to its non-zero value.

Second, in order to be able to express (almost) all the nuclide masses through continued fractions, we have to split the data set of non-radioactive nuclide masses into groups:

Group zero is the set of 19 mononuclidic elements, which was already analyzed in a previous article. Here the phase shift p was determined (p_p = -1.7918229) and a δ parameter was not considered, which means $\delta_p = 0$.

Group 1 is the set of dinuclidic elements. We require that the phase shift p remains the same for all nuclides, so only δ

must be adjusted in such a way that ideally all isotopes can be expressed through a continued fraction.

Group 2 is composed of all stable isotopes of the set of the trinuclidic chemical elements.

Analogously the remaining chemical elements can be grouped. Every group of masses leads to the determination of a different numerical value of the parameter δ.

The first task (before making any abundance prediction) is the determination of δ, so that from the continued fraction representations (ideally) every isotope mass can be reproduced with a numerical error smaller than its standard deviation.

This means for every isotope mass we obtain 4 different continued fraction representations (eq. 3): two of them interpret the mass as a proton resonance and two others as electron resonances. In the case of no outliers, at least one of these continued fractions reproduces the mass value with an error smaller than its standard deviation.

3.2 Prediction rules

The following simple rules lead to a prediction of nature's preference for the one or the other isotope.

Rule 1:
The electrons contribute very little to the isotope mass, therefore the electron resonances are not decisive and we express the nuclide masses only as proton resonances, according to the equations

$$\ln \frac{m(nuclide)}{m_{proton}} = \delta_p + 0 + S_0$$

and

$$\ln \frac{m(nuclide)}{m_{proton}} = \delta_p + (-1.7918229) + S_p.$$

This means we calculate two continued fractions S_0 and S_p. In all the fractions below, the number -1.7918229 is abbreviated as p.

Rule 2:
It is obvious that now, due to the elimination of the electron resonances, many nuclide masses cannot be expressed anymore through a continued fraction with a numerical error smaller than the standard deviation. Consequently we ignore the standard deviation criterion and consider continued fractions leading to a numerical error up to 0.3 u as valid; whenever this error is greater, the result is interpreted as "no continued fraction found".

The choice of 0.3 u as the allowed numerical error is not fully arbitrary. It was adjusted in such a way to make it possible to express at least 95% of the masses through *valid continued fractions*. If the allowed error is too small, many masses fall out of the model, so the model automatically does not work for them. However, with increasing error also rises the probability that the continued fraction has no physical relation to the mass.

Rule 3:
The priority rule for continued fractions with different phase shifts: the fractions with phase shift zero have priority.

Rule 4:
Comparison rule: we can compare only continued fractions (of different masses) which were calculated considering the same phase shift.

Rule 5:
Abundant isotopes accumulate in nodes and sub-nodes with *high positive denominator*.

Rule 6:
A nuclide mass which cannot be expressed through a continued fraction is not abundant.

3.3 Model verification

These rules are now applied to the different groups of isotope masses. For simplicity, only the first four denominators of the fractions are given, which is sufficient for comparison purposes.

Group 1: dinuclidic chemical elements, $\delta_p = 0.002919$.

1. Hydrogen:
   ^{1}H: [0; 0 | **-1146**, e+1, -e-1, e+1], 99.9885%
   ^{2}D: [0; 0 | **e+1**, 12, 9, 6], 0.0115%
   Here we compare the first denominators: e+1 > -1146, so the model predicts that the isotope ^{2}D is more abundant than the isotope ^{1}H, which is not observed. The reason for the failure of the model is simply the fact that the isotope ^{1}H is directly linked to the proton, the reference mass of the model, always more abundant than any other nuclide mass.
2. Helium:
   ^{3}He: [p; 3 | **-24**, 12, -e-1, -9], 0.000134%
   ^{4}He: [p; 3 | **15**, e+1, -e-1, e+1], 99.999866%
   It is not possible to express the Helium isotope masses through continued fractions with phase shift zero. According to the priority rule for phase shifts we now consider the phase shifted fractions. As the first denominator (15) is higher than (-24), the isotope ^{4}He should be preferred by nature.
3. Lithium:
   ^{6}Li: [p; 3 | e+1, **e+1**, -e-1, e+1], 7.59%
   ^{7}Li: [p; 3 | e+1, **441**, -6, -e-1], 92.41%
   441 > e+1, therefore the isotope ^{7}Li should have the higher abundance, as observed. None of the Li isotope masses can be expressed via a continued fraction with phase shift zero.
4. Boron:
   ^{10}B: [0; 3 | -e-1, **-21**, 18, -15], 19.9%
   ^{11}B: [0; 3 | -e-1, **-e-1**, -150, 15], 80.1%
   -e-1 > -21, therefore preference to ^{11}B.

5. Carbon:
   ^{12}C: [0; 3 | -6, **e+1**, -6, -6], 98.93%
   ^{13}C: [0; 3 | -6, **-24**, -e-1, e+1], 1.07%
   e+1 > -24, therefore preference to ^{12}C.
6. Nitrogen:
   ^{14}N: [0; 3 | **-6**, -e-1, e+1, -e-1], 99.636%
   ^{15}N: [0; 3 | **-9**, 1137, -e-1, e+1], 0.364%
   -6 > -9, therefore preference to ^{14}N.
7. Chlorine:
   ^{35}Cl: [0; 3 | **6**, -e-1, e+1, -e-1], 75.76%
   ^{37}Cl: [0; 3 | **e+1**, e+1, -6, -e-1], 24.24%
   6 > e+1, therefore preference to ^{35}Cl.
8. Vanadium:
   ^{50}V: [0; 3 | e+1, -e-1, **-18**, e+1], 0.25%
   ^{51}V: [0; 3 | e+1, -e-1, **15**, e+1], 99.75%
   15 > -18, therefore preference to ^{51}V.
9. Copper:
   ^{63}Cu: [p; 6 | **-36**, 6, e+1, -e-1], 69.15%
   ^{65}Cu: [p; 6 | **-60**, -9, 9, e+1], 30.85%
   -36 > -60, therefore preference to ^{63}Cu.
10. Gallium:
    ^{69}Ga: [p; 6 | **186**, -e-1, 6, -6], 60.108%
    ^{71}Ga: [p; 6 | **63**, -15, 30, 6], 39.892%
    186 > 63, therefore preference to ^{69}Ga.
11. Bromine:
    ^{79}Br: [p; 6 | **18**, 24, -27, 21], 50.69%
    ^{81}Br: [p; 6 | **15**, 6, -e-1, 6], 49.31%
    18 > 15, therefore preference to ^{79}Br.
12. Rubidium:
    ^{85}Rb: [p; 6 | 12, **15**, 6, -e-1], 72.17%
    ^{87}Rb: [p; 6 | 12, **-e-1**, e+1, -e-1], 27.83%
    15 > -e-1, therefore preference to ^{85}Rb.
13. Silver:
    ^{107}Ag: [p; 6 | 6, **-375**, 12, e+1], 51.839%
    ^{109}Ag: [p; 6 | 6, **-12**, e+1, -9], 48.161%
    As -12 > -375, the model predicts the higher abundance for the isotope ^{109}Ag, which is not observed. So the element Silver is the first and only unexplained outlier where our model fails.
    It is completely impossible to express theses masses through continued fractions with $p = 0$.
14. Indium:
    ^{113}In: [p; 6 | 6, -e-1, **-6**, 54], 4.29%
    ^{115}In: [p; 6 | 6, -e-1, **6**, 18], 95.71%
    6 > -6, preference to ^{115}In, as observed.
15. Antimony:
    ^{121}Sb: [p; 6 | e+1, e+1, -e-1, **e+1**], 57.21%
    ^{123}Sb: [p; 6 | e+1, e+1, -e-1, **-e-1**], 42.79%
    e+1 > -e-1, preference to ^{121}Sb, as observed.
16. Lanthanum:
    ^{138}La: [p; 6 | e+1, **24**, -e-1, e+1], 0.09%
    ^{139}La: [p; 6 | e+1, **33**, 6, -e-1], 99.91%
    33 > 24, preference to ^{139}La, as observed.
17. Europium:
    ^{151}Eu: [0; 6 | -e-1, e+1, -e-1, **e+1**], 47.81%
    ^{153}Eu: [0; 6 | -e-1, e+1, -e-1, **6**], 52.19%
    6 > e+1, preference to ^{153}Eu, as observed.
18. Lutetium:
    ^{175}Lu: [0; 6 | -e-1, 6, **-e-1**, -e-1], 97.41%
    ^{176}Lu: [0; 6 | -e-1, 6, **-6**, e+1], 2.59%
    -e-1 > -6, preference to ^{175}Lu, as observed.
19. Tantalum:
    ^{180}Ta: [p; 6 | e+1, -e-1, e+1, **-9**], 0.012%
    ^{181}Ta: [p; 6 | e+1, -e-1, e+1, **-6**], 99.988%
    -6 > -9, preference to ^{181}Ta, as observed.
20. Rhenium:
    ^{185}Re: [0; 6 | -e-1, **9**, e+1, -9], 37.40%
    ^{187}Re: [0; 6 | -e-1, **12**, -15, e+1], 62.60%
    12 > 9, preference to ^{187}Re, as observed.
21. Iridium:
    ^{191}Ir: [0; 6 | -e-1, **21**, -6, e+1], 37.3%
    ^{193}Ir: [0; 6 | -e-1, **33**, -27, -e-1], 62.7%
    33 > 21, preference to ^{193}Ir, as observed.
22. Thallium:
    ^{203}Tl: [0; 6 | -e-1, **-15**, -396, -e-1], 29.52%
    ^{205}Tl: [0; 6 | -e-1, **-12**, 6, e+1], 70.48%
    -12 > -15, preference to ^{205}Tl, as observed.

Group 2: trinuclidic chemical elements, $\delta_p = -0.016544$.

Now we apply the same system to the set of 6 trinuclidic chemical elements. We see that (with one magic number exception) the model identifies the most abundant isotope.

1. Oxygen:
   ^{16}O: [0; 3 | **-12**, -6, -24, e+1], 99.757%
   ^{17}O: [0; 3 | **-18**, e+1, -36, -e-1], 0.038%
   ^{18}O: [0; 3 | **-27**, -33, -e-1, e+1], 0.205%
   -12 > (-18 or -27), preference to ^{16}O, as observed; however the model does not explain why the isotope ^{18}O is more abundant than ^{17}O.
2. Neon:
   ^{20}Ne: [0; 3 | **585**, -15, 18, 6], 90.48%
   ^{21}Ne: [0; 3 | **51**, -12, -e-1, 21], 0.27%
   ^{22}Ne: [0; 3 | **27**, 15, -e-1, e+1], 9.25%
   585 > (51 or 27), preference to ^{20}Ne, as observed.
3. Magnesium:
   ^{24}Mg: [0; 3 | **15**, -6, -18, -e-1], 78.99%
   ^{25}Mg: [0; 3 | **12**, -48, 12, -e-1], 10.00%
   ^{26}Mg: [0; 3 | **9**, e+1, -e-1, e+1], 11.01%
   15 > (12 or 9), preference to ^{24}Mg, as observed.
4. Silicon:
   ^{28}Si: [0; 3 | **9**, -e-1, e+1, -e-1], 92.223%

^{29}Si: no continued fraction found, 4.685%
^{30}Si: [0; 3 | **6**, e+1, 6, -e-1], 3.092%
9 > 6, preference to ^{28}Si, as observed.

5. Argon:
^{36}Ar: [0; 3 | e+1, **e+1**, -e-1, e+1], 0.3365%
^{38}Ar: [0; 3 | e+1, **6**, -6, 93], 0.0632%
^{40}Ar: [0; 3 | e+1, **15**, 39, 6], 99.6003%
15 > (6 or e+1), preference to ^{40}Ar, as observed.

6. Potassium:
^{39}K: [0; 3 | e+1, **9**, -e-1, -12], 93.2581%
^{40}K: [0; 3 | e+1, **15**, 30, e+1], 0.0117%
^{41}K: [0; 3 | e+1, **57**, e+1, -6], 6.7302%
57 > (9 or 15), preference expected to ^{41}K, which is against the experimental observations. Reason: Potassium is the element with atomic number 19. The isotope ^{39}K has 39 − 19 = 20 neutrons, which means a magic number of neutrons. This explains the increased abundance.

Group 3: tetranuclidic chemical elements, $\delta_p = 0.025770$.

1. Sulfur:
^{32}S: [0; 3 | 6, **9**, 12, -429], 94.99%
^{33}S: [0; 3 | 6, **-21**, -e-1, e+1], 0.75%
^{34}S: [0; 3 | 6, **-6**, 9, -e-1], 4.25%
^{36}S: [0; 3 | 6, **-e-1**, e+1, -e-1], 0.01%
9 is the highest denominator, preference to the isotope ^{32}S, which is indeed observed.

2. Chromium:
^{50}Cr: [0; 3 | e+1, -e-1, **-e-1**, -6], 4.345%
^{52}Cr: [0; 3 | e+1, -e-1, **24**, -15], 83.789%
^{53}Cr: [0; 3 | e+1, -e-1, **6**, e+1], 9.501%
^{54}Cr: [0; 3 | e+1, -e-1, **e+1**, e+1], 2.365%
24 is the highest denominator, therefore preference to the isotope ^{52}Cr, as observed.

3. Iron:
When considering the phase shift zero, for both isotopes, ^{57}Fe and ^{58}Fe, no continued fraction is found. This is the only case where two isotopes of a chemical element could not be expressed as proton resonance simultaneously. A better description is found for the phase shifted fractions, here only ^{54}Fe turns out to be an outlier. The model is correct when going down the priority hierarchy and analyze these phase shifted fractions:
^{54}Fe: no continued fraction found, 5.845%
^{56}Fe: [p; 6 | **-12**, -6, e+1, -6], 91.754%
^{57}Fe: [p; 6 | **-15**, e+1, -e-1, e+1], 2.119%
^{58}Fe: [p; 6 | **-15**, 48, 150, 12], 0.282%
-12 > -15, therefore ^{56}Fe has the highest abundance.

4. Strontium:
^{84}Sr: [p; 6 | **15**, -e-1, -e-1, e+1], 0.56%
^{86}Sr: [p; 6 | **12**, e+1, -6, -e-1], 9.86%
^{87}Sr: [p; 6 | **12**, 18, -9, -6], 7.00%
^{88}Sr: [p; 6 | **12**, -6, -12, 9], 82.58%
15 > 12, so the model predicts the highest abundance for the isotope ^{84}Sr, which is not observed. Reason: Strontium is the element with atomic number 38. The most abundant nuclide ^{88}Sr has 88 − 38 = 50, a magic number of neutrons, which explains the failure of our model.

5. Cerium:
^{136}Ce: [p; 6 | e+1, **9**, -e-1, e+1], 0.185%
^{138}Ce: [p; 6 | e+1, **12**, -e-1, e+1], 0.251%
^{140}Ce: [p; 6 | e+1, **15**, e+1, -e-1], 88.450%
^{142}Ce: [p; 6 | e+1, **30**, e+1, e+1], 11.114%
Our model predicts the highest abundance for the isotope ^{142}Ce. However, the most abundant isotope $^{140}_{58}$Ce has a magic number of 140 − 58 = 82 neutrons, so its abundance is increased.

6. Lead:
^{204}Pb: [0; 6 | -e-1, **-33**, 6, e+1], 1.4%
^{206}Pb: [0; 6 | -e-1, **-21**, e+1, -e-1], 24.1%
^{207}Pb: [0; 6 | -e-1, **-18**, e+1, -e-1], 22.1%
^{208}Pb: [0; 6 | -e-1, **-15**, e+1, 6], 52.4%
-15 is the highest denominator, the model predicts the highest abundance for ^{208}Pb, as observed.

Higher groups: unfortunately, the model fails completely when predicting the most abundant nuclide for all chemical elements consisting of more than four isotopes. Despite the fact that the grouping scheme still allows the expression of the nuclide masses through continued fractions (with few outliers), no correlation between the maximum abundance and the denominators is visible.

4 Conclusions

We have shown that a minor extension of the bipolar model of oscillations in a chain system allows a satisfactory prediction of the most abundant isotope for a given chemical element. Most outliers occur when one of the isotopes has a magic number of neutrons in the nucleus. From its total failure for elements with 5 ore more stable isotopes, we conclude that our model is still incomplete and must be extended.

Acknowledgments

The author greatly acknowledges the financial support from the Brazilian governmental funding agencies FACEPE and CNPq.

Submitted on March 2, 2015 / Accepted on March 3, 2015

References

1. Ries A. Atomic weights confirm bipolar model of oscillations in a chain system. *Progress in Physics*, 2013, v. 9(4), 63–67.
2. Ries A. The radial electron density in the Hydrogen atom and the model of oscillations in a chain system. *Progress in Physics*, 2012, v. 8(3), 29–34.

LETTERS TO PROGRESS IN PHYSICS

Addenda to My Paper "New Possible Physical Evidence of the Homogeneous Electromagnetic Vector Potential for Quantum Theory. Idea of a Test Based on a G. P. Thomson-like Arrangement"

Spiridon Dumitru

(Retired) Department of Physics, "Transilvania" University, B-dul Eroilor 29, 500036 Brasov, Romania
E-mail: s.dumitru42@unitbv.ro

This is addenda to my paper entitled "New Possible Physical Evidence of the Homogeneous Electromagnetic Vector Potential for Quantum Theory. Idea of a Test Based on a G. P. Thomson-like Arrangement", which was published in *Progress in Physics*, 2014, v. 10, Issue 3, 196–200.

1 On the special coil able to create a homogeneous vector potential $\boldsymbol{h} - \vec{A}$

Some experimenters potentially interested in evaluating the test suggested in my article communicated me comments like:

- *'It is practically difficult to realize with a desired level of geometrical accuracy the special annular coil designed in [1]. Then it arises the question if it is possible to imagine another system (of coils) able to create also a $\boldsymbol{h} - \vec{A}$ and which can be manufactured more easily and with a required precision'.*$\star$

Here we wish to note shortly that a system of alluded type can be devised in form of a set consisting in two parallel flat coils pictured below in Fig. 3b. Each such a coil has the aspect shown in Fig. 3a. Note that here we were indexing figures and equations by the consecutive numbers from [1].

In the case of coils system from Fig. 3b the expression of the $\boldsymbol{h} - \vec{A}$ in an interior point P is given by

$$A = A_z(P) = \mu_0 \cdot I \cdot n \cdot d \tag{11}$$

where n denote the number of conductors per unit length along the coil (in direction of Ox axis).

The expression (11) can be achieved through a set of several simple calculations and the reasoning done in the following sequence of items

- α: Taking into account the equation (6) and its motivation from [1] as starting elements;
- β: Imagining a scheme of infinitely long conductors, located in xOz plane and mutually parallel with the Oz axis. The conductors are crossed by currents of same value I;
- γ: Evaluation of the $\boldsymbol{h} - \vec{A}$ field generated by the respective currents in a point P situated on the Oy axis at some distance h of xOz plane;
- δ: The respective evaluation can be done by integration over the Ox-axis and using formula (2.733) from [2];

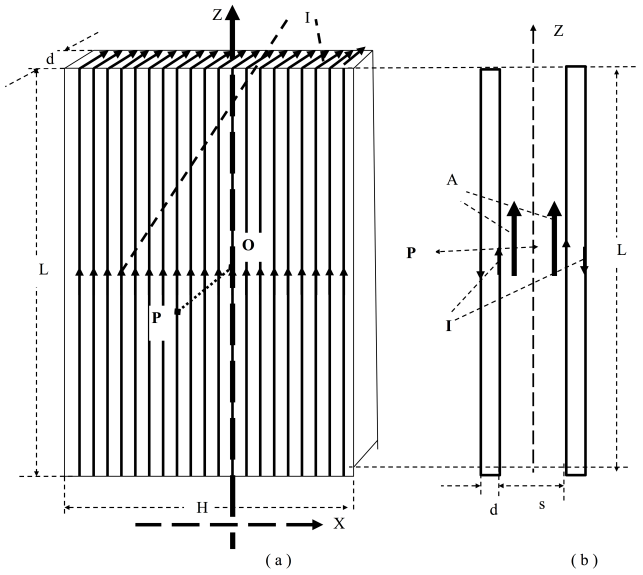

Fig. 3: Schemas with special flat coils. (a) Frontal image of a single coil. (b) Side view of a couple of coils

- η: Consideration in Fig. 3 that the quantities L and H are much larger than the dimensions d and s specific to the set of flat and finite coils from Fig. 3b. One requires also that the respective coils to satisfy the conditions specified in note "*From the ideal coil to a real one*" from [1];
- τ: Then, through some modest calculations, by using the evaluation mentioned in item δ one obtains the formula (11).

So, if one uses the coils-system from Fig. 3b, for evaluating the quantity $i_{eff}^{dB}(A)$ mentioned in relation (5) from [1], become of interest the result (11). This means that for the value of $\boldsymbol{h} - \vec{A}$ must be taken the value $A = \mathfrak{R} \cdot I$ with $\mathfrak{R} = \mu_0 \cdot n \cdot d$. Then instead of relation (5) from [1] the

test in question has to check the formula

$$\frac{1}{i_{eff}^{dB}(A)} = \frac{a\sqrt{2me}}{hD}\sqrt{U} + \frac{ae}{hD}A = \frac{a\sqrt{2me}}{hD}\sqrt{U} + \frac{ae\Re}{hD}I. \quad (12)$$

The last formula points out the fact that the quantity $(i_{eff}^{db})^{-1}$ (inverse of effective interfringe distance) shows linear dependence of the value of the $\boldsymbol{h} - \vec{A}$ (and of course of the current I which crosses the coils set). Such a fact can be significant in checking the plausibility of the proposed test.

2 On the G. P. Thomson-like arrangement

As instrument for testing the possible distinct physical signification of $\boldsymbol{h} - \vec{A}$ in [1] we suggested to use a G. P. Thomson-like arrangement. Such an arrangement can be designed and manufactured as a new apparatus specially dedicated to the concerned test. But one can appreciate that for such a device it is possible to use with sufficient confidence some scientific equipments already existent on the specialized market. As example of such an equipment can be taken into account the set "*Electron diffraction P2511300*" manufactured by the PHYWE company [3]. The main piece of the alluded set is in fact a G. P. Thomson-like device. In the respective device the role of diffraction grating (crystal lattice) mentioned in [1] is played by a graphite foil with interatomic spacing a and D as distance between crystalline foil and observational screen.

Usually [3] the respective device is used for measuring the diameter Q of the first (and eventually of second) smallest diffraction ring at different anode voltages U. Note that, in terms used by us in [1], the diameter Q of first such a ring is twofold of interfringe width i that is $Q = 2 \cdot i$. The interplanar spacing of graphite used in [3] is nothing but the interatomic spacing a in the crystal lattice (diffraction grating) mentioned in Fig.1 from [1]. Also a quantity D plays the role of distance between graphite foil and observational screen.

Notice: Putting into practice the test [1] by using the PHYWE-device can be performed by eluding the concrete values of a and D. Such a performance can be done as follows. In a first step is completed a measurement in absence of $\boldsymbol{h} - \vec{A}$ field (i.e. when in (12) $A = 0$ and $I = 0$). From the respective measurement is possible to evaluate a couple of values U_0 and $Q_{eff}^{dB}(0)$ for the quantities U and Q. So accordingly with (12) can be calculated device parameter

$$\Gamma = \frac{a}{hD} = \left[Q_{eff}^{dB}(0)\sqrt{\frac{meU_0}{2}} \right]^{-1}. \quad (13)$$

Take into account the fact that in the case of the PHYWE-device the values of quantities a, D and Γ as well as the permitted range for the voltages U_0 and U are predetermined by manufacturer. The respective fact must be considered when one operates with the alluded device and the set of numerical estimations from Section 4 of [1] are not important.

With the aid of parameter Γ the relation (12) can be transcribed as

$$\left[Q_{eff}^{dB}(A) \right]^{-1} = \Gamma\sqrt{\frac{meU}{2}} + \Gamma\frac{eA}{2} = \Gamma\sqrt{\frac{meU}{2}} + \Gamma\frac{e\Re}{2}I. \quad (14)$$

By using the above relations the mentioned PHYWE-device can be put in practice in order to check the proper evidence of the $\boldsymbol{h} - \vec{A}$ field.

Submitted on March 6, 2015 / Accepted on March 8, 2015

References

1. Dumitru S. New possible physical evidence of the homogeneous electromagnetic vector potential for quantum theory. Idea of a test based on a G. P. Thomson-like arrangement. *Progress in Physics*, 2014, v. 10, issue 3, 196–200.
2. Gradshteyn I.S., Ryzhik I.M. Table of Integrals, Series, and Products. Seventh Edition, Elsevier, 2007.
3. Electron diffraction P2511300, Physics University Experiments, Oct. 2013, PHYWE Systeme GmbH and Co. KG. http://www.phywe.com/index.php/fuseaction/download/lrn_file/TEP_2013_Final_low2.pdf

The de Broglie Relations Derived from the Electron and Proton Coupling to the Planck Vacuum State

William C. Daywitt

National Institute for Standards and Technology (retired), Boulder, Colorado. E-mail: wcdaywitt@me.com

This paper argues that the de Broglie relations for the electron and proton are the result of their coupling to the Planck vacuum state, the continuum nature of that state impressing a wave-like behavior onto the free-space-particle aspect of the two particles. Lorentz transforming the vanishing of their corresponding particle/vacuum coupling forces at their respective Compton radii, treated as Lorentz invariant constants, leads to their space-direction and time-direction de Broglie relations. Results: explain the peculiar form of the relativistic particle energy $\sqrt{m^2c^4 + c^2p^2}$; define the de Broglie waves for the electron and proton as periodic undulations within the Planck vacuum in the vicinity of the electron and proton cores; and easily explain the double-slit electron-diffraction thought experiment.

1 Force transformation

The electron and proton cores, $(-e_*, m_e)$ and (e_*, m_p), exert the two-term coupling forces [1]

$$\pm\left(\frac{e_*^2}{r^2} - \frac{mc^2}{r}\right) \tag{1}$$

on the Planck vacuum (PV) negating-energy continuum, where the plus and minus signs refer to the electron and proton respectively and mc^2 represents the rest energy of either particle. The bare charge e_* is assumed to be a massless point charge. The massive particle cores, however, possess a small spherical extension due to the zero-point formation of their derived masses [2].

The coupling force vanishes

$$\frac{e_*^2}{r_c^2} - \frac{mc^2}{r_c} = 0 \tag{2}$$

at the Compton radius $r_c\,(= e_*^2/mc^2)$ of either particle, leading to the Compton relations

$$r_c \cdot mc^2 = e_*^2 \qquad \longrightarrow \qquad r_e m_e c^2 = r_p m_p c^2 = e_*^2 \tag{3}$$

for the electron $(r_e m_e)$ and proton $(r_p m_p)$, and the (reduced) Planck constant $\hbar = e_*^2/c$. It is noted that (1) is a force acting between a free-space particle and the vacuum state – it is not a free-space/free-space force as are the Coulomb and Newton forces. The Compton relations and $\hbar = e_*^2/c$ are used throughout the following calculations.

The vanishing force (2) can be expressed as a tensor 4-force difference. In the primed rest frame of the particle where these static forces apply, this vanishing force difference $\Delta F'_\mu$ is $(\mu = 1, 2, 3, 4)$

$$\Delta F'_\mu = \left[\mathbf{0}, i\left(\frac{e_*^2}{r_c^2} - \frac{mc^2}{r_c}\right)\right] = [0, 0, 0, i\,0] \tag{4}$$

where $i = \sqrt{-1}$. Thus the vanishing of the component $\Delta F'_4 = 0$ in (4) can be thought of as the source of the Compton relations in (3).

The force difference in the laboratory frame (in which the rest frame travels at velocity v along the z-axis) [3]

$$\Delta F_\mu = a_{\mu\nu}\Delta F'_\nu = 0_\mu \tag{5}$$

follows from the tensor nature of (4) and the Lorentz transformation $x_\mu = a_{\mu\nu}\, x'_\nu$, where $x_\mu = (x, y, z, ict)$,

$$a_{\mu\nu} = \begin{pmatrix} 1 & 0 & 0 & 0 \\ 0 & 1 & 0 & 0 \\ 0 & 0 & \gamma & -i\beta\gamma \\ 0 & 0 & i\beta\gamma & \gamma \end{pmatrix} \tag{6}$$

and $\mu, \nu = (1, 2, 3, 4)$. Thus (5) yields

$$\begin{aligned} \Delta F_\mu &= \left[0, 0, \beta\gamma\left(\frac{e_*^2}{r_c^2} - \frac{mc^2}{r_c}\right), i\,\gamma\left(\frac{e_*^2}{r_c^2} - \frac{mc^2}{r_c}\right)\right] \\ &= \left[0, 0, \frac{1}{r_c}\left(\frac{e_*^2}{r_d} - c\cdot m\gamma v\right), \frac{i}{r_c}\left(\frac{e_*^2}{r_L} - c\cdot m\gamma c\right)\right] \\ &= [0, 0, 0, i\,0] \end{aligned} \tag{7}$$

where

$$r_d = \frac{r_c}{\beta\gamma} \qquad \text{and} \qquad r_L = \frac{r_c}{\gamma} \tag{8}$$

are the de Broglie radii for the space and time directions respectively; and where $\beta = v/c < 1$ and $\gamma = 1/\sqrt{1-\beta^2}$.

The force difference $\Delta F_3 = 0$ in (7) gives the de Broglie relation

$$r_d \cdot cp = e_*^2 \qquad \text{or} \qquad r_d = \frac{\hbar}{p} \tag{9}$$

in the space direction, where $p = m\gamma v$ is the relativistic particle momentum. The force difference $\Delta F_4 = 0$ gives the de Broglie relation

$$r_L \cdot E = e_*^2 \qquad \text{or} \qquad r_L = \frac{\hbar}{m\gamma c} \tag{10}$$

in the time direction, where $E = m\gamma c^2$ is the total relativistic particle energy.

The momentum and energy in equations (9) and (10) are derived from nothing more than the vanishing of the Lorentz transformation of (2), whose results can be taken a step further:

$$\begin{aligned} E &= \frac{e_*^2}{r_L} = \frac{e_*^2\gamma}{r_c} = mc^2\gamma \\ &= mc^2\left(1 + \frac{\beta^2}{1-\beta^2}\right)^{1/2} \\ &= \left(m^2c^4 + c^2p^2\right)^{1/2} \end{aligned} \tag{11}$$

showing that this well known equation has its source in the two-term particle/PV coupling force.

2 Conclusions and comments

The vast accumulation of electron diffraction data leaves no doubt that the electron and proton possess a wave nature. If the corresponding waves are roughly expressed in terms of planewaves, then it is reasonable to assign $2\pi r_d$ and $2\pi r_L$ as the wavelengths in the space and time directions respectively. As a first approximation then, the electron and proton de Broglie waves are planewaves propagating within the PV continuum.

The Synge primitive (or planewave) quantization of spacetime [4, p.106] is an independent calculation that parallels the ideas of the previous paragraph. That quantization divides the space and time axes of the Minkowski spacetime diagram into equal segments, where the space and time segments are r_d and r_L respectively (Synge actually multiplies these two segments by 2π which defines a phase space). The particle/PV coupling of the previous section provides the physical explanation for that quantization in terms of the coupling force (1).

Although the implied mathematics of the two previous paragraphs involves planewaves (which are global), the PV wave phenomenon must be a local property associated with the particle/PV interaction in the neighborhood of the particle cores $(-e_*, m_e)$ and (e_*, m_p), with characteristic (radian) frequencies defined by

$$\omega_c = \frac{e_*^2/r_c}{\hbar} = \frac{c}{r_c} \tag{12}$$

with

$$\omega_L = \frac{e_*^2/r_L}{\hbar} = \gamma\omega_c \quad \text{and} \quad \omega_d = \frac{e_*^2/r_d}{\hbar} = \beta\gamma\omega_c \tag{13}$$

for each particle. Then (11) yields

$$\omega_L^2 = \omega_c^2 + \omega_d^2\,. \tag{14}$$

The preceding results offer a simple explanation for the double-slit thought experiment [5, p.85]. Consider a collimated beam of monoenergetic electrons that is directed at an opaque wall containing two narrow, parallel, and closely spaced slits A and B, with a detection screen at some distance beyond the slits. Being a particle (although with a wave-like nature), the electron cannot go through both slits at the same time. Now consider the two experiments: (1) with slit A open and slit B closed; and (2) with both slits A and B open. Assume that the slits are narrower than one de Broglie wavelength ($2\pi r_d$) and that their separation distance is several wavelengths.

If the electrons are particle-like with no wave-like qualities, the screen would show a bell-shaped excitation curve in case (1) and two superimposed bell-shaped curves in case (2). But for case (2), however, the *overwhelming* diffraction evidence demands a well defined oscillatory excitation curve on the screen — because the particle exhibits a definite wave-particle nature. Since the electron must go through A or B, but not both, this result is difficult to understand [5, p.85] with present-day physics. But if the free-space particle is accompanied by a PV de Broglie wave, the diffraction of that wave through A and B, and its interaction with the particle core, easily explains the oscillatory curve on the detection screen.

Submitted on March 21, 2015 / Accepted on March 27, 2015

References

1. Daywitt W.C. The Strong and Weak Forces and their Relationship to the Dirac Particles and the Vacuum State. *Progress in Physics*, 2014, v. 11, 18. See also www.planckvacuum.com.
2. Daywitt W.C. Why the Proton is Smaller and Heavier than the Electron. *Progress in Physics*, 2014, v. 10, 175.
3. Jackson J.D. Classical Electrodynamics. John Wiley & Sons, Inc., 1st ed., 2nd printing, NY, 1962.
4. Synge J.L. Geometrical Mechanics and de Broglie Waves. Cambridge University Press, 1954.
5. Leighton R.B. Principles of Modern Physics. McGraw-Hill Book Co., New York, Toronto, London, 1959.

The Journal on Advanced Studies in Theoretical and Experimental Physics, including Related Themes from Mathematics

PROGRESS IN PHYSICS

A quarterly issue scientific journal, registered with the Library of Congress (DC, USA). This journal is peer reviewed and included in the abstracting and indexing coverage of: Mathematical Reviews and MathSciNet (AMS, USA), DOAJ of Lund University (Sweden), Zentralblatt MATH (Germany), Scientific Commons of the University of St. Gallen (Switzerland), Open-J-Gate (India), Referativnyi Zhurnal VINITI (Russia), etc.

Electronic version of this journal:
http://www.ptep-online.com

Postal Address

Department of Mathematics and Science,
University of New Mexico,
705 Gurley Ave., Gallup, NM 87301, USA

ISSN: 1555-5534 (print)
ISSN: 1555-5615 (online)

Standard Address Number: 297-5092
Printed in the United States of America

July 2015 **Vol. 11, Issue 3**

CONTENTS

Information for Authors and Subscribers

Progress in Physics has been created for publications on advanced studies in theoretical and experimental physics, including related themes from mathematics and astronomy. All submitted papers should be professional, in good English, containing a brief review of a problem and obtained results.

All submissions should be designed in LaTeX format using *Progress in Physics* template. This template can be downloaded from *Progress in Physics* home page http://www.ptep-online.com. Abstract and the necessary information about author(s) should be included into the papers. To submit a paper, mail the file(s) to the Editor-in-Chief.

All submitted papers should be as brief as possible. Short articles are preferable. Large papers can also be considered in exceptional cases. Letters related to the publications in the journal or to the events among the science community can be applied to the section *Letters to Progress in Physics*.

All that has been accepted for the online issue of *Progress in Physics* is printed in the paper version of the journal. To order printed issues, contact the Editors.

This journal is non-commercial, academic edition. It is printed from private donations. (Look for the current author fee in the online version of the journal.)

A New Understanding of Particles by $\overrightarrow{G}$-Flow Interpretation of Differential Equation

Linfan Mao
Chinese Academy of Mathematics and System Science, Beijing 100190, P. R. China.
E-mail: maolinfan@163.com

Applying mathematics to the understanding of particles classically with an assumption that if the variables t and x_1, x_2, x_3 hold with a system of dynamical equations (1.4), then they are a point (t, x_1, x_2, x_3) in $\mathbb{R}^4$. However, if we put off this assumption, how can we interpret the solution space of equations? And are these resultants important for understanding the world? Recently, the author extended Banach and Hilbert spaces on a topological graph to introduce $\overrightarrow{G}$-flows and showed that all such flows on a topological graph $\overrightarrow{G}$ also form a Banach or Hilbert space, which enables one to find the multiverse solution of these equations on $\overrightarrow{G}$. Applying this result, this paper discusses the $\overrightarrow{G}$-flow solutions on Schrödinger equation, Klein-Gordon equation and Dirac equation, i.e., the field equations of particles, bosons or fermions, answers previous questions by "yes", and establishes the many world interpretation of quantum mechanics of H. Everett by purely mathematics in logic, i.e., mathematical combinatorics.

1 Introduction

Matter consists of bosons with integer spin n and fermions with half-integer spin $n/2$, $n \equiv 1 \pmod 2$. The elementary particles consist of leptons and hadrons, i.e. mesons, baryons and their antiparticles, which are composed of quarks [16]. Thus, a hadron has an internal structure, which implies that all hadrons are not elementary but leptons are, viewed as point particles in elementary physics. Furthermore, there is also unmatter which is neither matter nor antimatter, but something in between [19-21]. For example, an atom of unmatter is formed either by electrons, protons, and antineutrons, or by antielectrons, antiprotons, and neutrons.

Usually, a particle is characterized by solutions of differential equation established on its wave function $\psi(t, x)$. In non-relativistic quantum mechanics, the wave function $\psi(t, x)$ of a particle of mass m obeys the Schrödinger equation

$$i\hbar \frac{\partial \psi}{\partial t} = -\frac{\hbar^2}{2m} \nabla^2 \psi + U, \tag{1.1}$$

where, $\hbar = 6.582 \times 10^{-22}$MeVs is the Planck constant, U is the potential energy of the particle in applied field and

$$\nabla = \left(\frac{\partial}{\partial x}, \frac{\partial}{\partial y}, \frac{\partial}{\partial z}\right) \text{ and } \nabla^2 = \frac{\partial^2}{\partial x^2} + \frac{\partial^2}{\partial y^2} + \frac{\partial^2}{\partial z^2}.$$

Consequently, a free boson $\psi(t, x)$ hold with the Klein-Gordon equation

$$\left(\frac{1}{c^2}\frac{\partial^2}{\partial t^2} - \nabla^2\right)\psi(x, t) + \left(\frac{mc}{\hbar}\right)^2 \psi(x, t) = 0 \tag{1.2}$$

and a free fermion $\psi(t, x)$ satisfies the Dirac equation

$$\left(i\gamma^\mu \partial_\mu - \frac{mc}{\hbar}\right)\psi(t, x) = 0 \tag{1.3}$$

in relativistic forms, where,

$$\begin{aligned} \gamma^\mu &= \left(\gamma^0, \gamma^1, \gamma^2, \gamma^3\right), \\ \partial_\mu &= \left(\frac{1}{c}\frac{\partial}{\partial t}, \frac{\partial}{\partial x_1}, \frac{\partial}{\partial x_2}, \frac{\partial}{\partial x_3}\right), \end{aligned}$$

c is the speed of light and

$$\gamma^0 = \begin{pmatrix} I_{2\times 2} & 0 \\ 0 & -I_{2\times 2} \end{pmatrix}, \ \gamma^i = \begin{pmatrix} 0 & \sigma_i \\ -\sigma_i & 0 \end{pmatrix}$$

with the usual Pauli matrices

$$\sigma_1 = \begin{pmatrix} 0 & 1 \\ 1 & 0 \end{pmatrix}, \ \sigma_2 = \begin{pmatrix} 0 & -i \\ i & 0 \end{pmatrix},$$

$$\sigma_3 = \begin{pmatrix} 1 & 0 \\ 0 & -1 \end{pmatrix}.$$

It is well known that the behavior of a particle is on superposition, i.e., in two or more possible states of being. But *how to interpret this phenomenon in accordance with (1.1)–(1.3)* ? The many worlds interpretation on wave function of (1.1) by H. Everett [2] in 1957 answered the question in machinery, i.e., viewed different worlds in different quantum mechanics and the superposition of a particle be liked those separate arms of a branching universe ([15], also see [1]). In fact, H. Everett's interpretation claimed that the state space of particle is a multiverse, or parallel universe ([23, 24]), an application of philosophical law that *the integral always consists of its parts*, or formally, the following.

Definition 1.1([6],[18]) *Let* $(\Sigma_1; \mathcal{R}_1)$, $(\Sigma_2; \mathcal{R}_2)$, $\cdots$, $(\Sigma_m; \mathcal{R}_m)$ *be m mathematical or physical systems, different two by two. A Smarandache multisystem* $\widetilde{\Sigma}$ *is a union* $\bigcup_{i=1}^{m} \Sigma_i$ *with rules* $\widetilde{\mathcal{R}} = \bigcup_{i=1}^{m} \mathcal{R}_i$ *on* $\widetilde{\Sigma}$*, denoted by* $\left(\widetilde{\Sigma}; \widetilde{\mathcal{R}}\right)$.

Furthermore, *things are inherently related, not isolated* in the world. Thus, every particle in nature is a union of elementary particles underlying a graph embedded in space, where, a graph G is said to be embeddable into a topological space $\mathscr{E}$ if there is a $1-1$ continuous mapping $f: G \to \mathscr{E}$ with $f(p) \neq f(q)$ if $p \neq q$ for $\forall p, q \in G$, i.e., edges only intersect at end vertices in $\mathscr{E}$. For example, a *planar graph* such as those shown in Fig. 1.

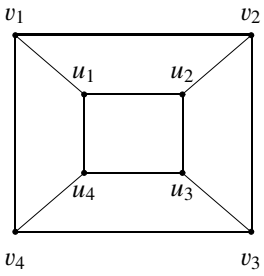

Fig. 1

Definition 1.2([6]) *For any integer $m \geq 1$, let $\left(\widetilde{\Sigma}; \widetilde{\mathcal{R}}\right)$ be a Smarandache multisystem consisting of mathematical systems $(\Sigma_1; \mathcal{R}_1), (\Sigma_2; \mathcal{R}_2), \cdots, (\Sigma_m; \mathcal{R}_m)$. An inherited topological structures $G^L\left[\widetilde{\Sigma}; \widetilde{\mathcal{R}}\right]$ on $\left(\widetilde{\Sigma}; \widetilde{\mathcal{R}}\right)$ is defined by*

$$V\left(G^L\left[\widetilde{\Sigma}; \widetilde{\mathcal{R}}\right]\right) = \{v_{\Sigma_1}, v_{\Sigma_2}, \cdots, v_{\Sigma_m}\},$$

$$E\left(G^L\left[\widetilde{\Sigma}; \widetilde{\mathcal{R}}\right]\right) = \{(v_{\Sigma_i}, v_{\Sigma_j}) | \Sigma_i \bigcap \Sigma_j \neq \emptyset,\ 1 \leq i \neq j \leq m\}$$

with a labeling $L: v_{\Sigma_i} \to L(v_{\Sigma_i}) = \Sigma_i$ and $L: (v_{\Sigma_i}, v_{\Sigma_j}) \to L(v_{\Sigma_i}, v_{\Sigma_j}) = \Sigma_i \bigcap \Sigma_j$, where $\Sigma_i \bigcap \Sigma_j$ denotes the intersection of spaces, or action between systems Σ_i with Σ_j for integers $1 \leq i \neq j \leq m$.

For example, let $\widetilde{\Sigma} = \bigcup_{i=1}^{4} \Sigma_i$ with $\Sigma_1 = \{a, b, c\}$, $\Sigma_2 = \{a, b\}$, $\Sigma_3 = \{b, c, d\}$, $\Sigma_4 = \{c, d\}$ and $\mathcal{R}_i = \emptyset$. Calculation shows that $\Sigma_1 \bigcap \Sigma_2 = \{a, b\}$, $\Sigma_1 \bigcap \Sigma_3 = \{b, c\}$, $\Sigma_1 \bigcap \Sigma_4 = \{c\}$, $\Sigma_2 \bigcap \Sigma_3 = \{b\}$, $\Sigma_2 \bigcap \Sigma_4 = \emptyset$, $\Sigma_3 \bigcap \Sigma_4 = \{c, d\}$. Such a graph $G^L\left[\widetilde{\Sigma}; \widetilde{\mathcal{R}}\right]$ is shown in Fig. 2.

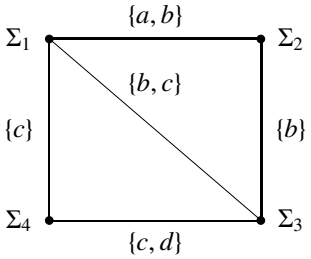

Fig. 2

Generally, a particle should be characterized by $\left(\widetilde{\Sigma}; \widetilde{\mathcal{R}}\right)$ in theory. However, we can only verify it by some of systems $(\Sigma_1; \mathcal{R}_1)$, $(\Sigma_2; \mathcal{R}_2)$, $\cdots$, $(\Sigma_m; \mathcal{R}_m)$ for the limitation of human beings because he is also a system in $\left(\widetilde{\Sigma}; \widetilde{\mathcal{R}}\right)$. Clearly, the underlying graph in H. Everett's interpretation on wave function is in fact a binary tree and there are many such traces in the developing of physics. For example, a baryon is predominantly formed from three quarks, and a meson is mainly composed of a quark and an antiquark in the models of Sakata, or Gell-Mann and Ne'eman on hadrons ([14]), such as those shown in Fig. 3, where, $q_i \in \{\mathbf{u}, \mathbf{d}, \mathbf{c}, \mathbf{s}, \mathbf{t}, \mathbf{b}\}$ denotes a quark for $i = 1, 2, 3$ and $\overline{q}_2 \in \left\{\overline{\mathbf{u}}, \overline{\mathbf{d}}, \overline{\mathbf{c}}, \overline{\mathbf{s}}, \overline{\mathbf{t}}, \overline{\mathbf{b}}\right\}$, an antiquark. Thus, the underlying graphs $\overrightarrow{G}$ of a meson, a baryon are respectively $\overrightarrow{K}_2$ and $\overrightarrow{K}_3$ with actions. In fact, a free quark was not found in experiments until today. So it is only a machinery model on hadrons. Even so, it characterizes well the known behavior of particles.

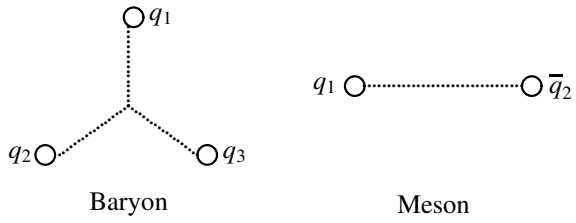

Fig. 3

It should be noted that the geometry on Definition 1.1–1.2 can be also used to characterize particles by combinatorial fields ([7]), and there is a priori assumption for discussion in physics, namely, *the dynamical equation of a subparticle of a particle is the same of that particle*. For example, the dynamical equation of quark is nothing else but the Dirac equation (1.3), a characterizing on quark from the macroscopic to the microscopic, the quantum level in physics. However, (1.3) cannot provide such a solution on the behaviors of 3 quarks. We can only interpret it similar to that of H. Everett, i.e., there are 3 parallel equations (1.3) in discussion, a seemly rational interpretation in physics, but not perfect for mathematics. Why this happens is because the interpretation of solution of equation. Usually, we identify a particle to the solution of its equation, i.e., if the variables t and x_1, x_2, x_3 hold with a system of dynamical equations

$$\mathscr{F}_i\left(t, x_1, x_2, x_3, u_t, u_{x_1}, \cdots, u_{x_1 x_2}, \cdots\right) = 0,$$

$$\text{with} \quad 1 \leq i \leq m, \tag{1.4}$$

the particle in $\mathbb{R} \times \mathbb{R}^3$ is a point (t, x_1, x_2, x_3), and if more than one points (t, x_1, x_2, x_3) hold with (1.4), the particle is nothing else but consisting of all such points. However, the solutions of (1.1)–(1.3) are all definite on time t. *Can this interpretation be used for particles in all times*? Certainly not because a particle can be always decomposed into elementary particles, and it is a little ambiguous which is a point, the particle itself or its one of elementary particles sometimes.

This speculation naturally leads to a question on mathematics, i.e., *what is the right interpretation on the solution of differential equation accompanying with particles*? Recently, the author extended Banach spaces on topological graphs $\overrightarrow{G}$ with operator actions in [13], and shown all of these extensions are also Banach space, particularly, the Hilbert space with unique correspondence in elements on linear continuous functionals, which enables one to solve linear functional equations in such extended space, particularly, solve differential equations on a topological graph, i.e., find multiverse solutions for equations. This scheme also enables us to interpret the superposition of particles in accordance with mathematics in logic.

The main purpose of this paper is to present an interpretation on superposition of particles by $\overrightarrow{G}$-flow solutions of (1.1)–(1.3) in accordance with mathematics. Certainly, the geometry on non-solvable differential equations discussed in [9]–[12] brings us another general way for holding behaviors of particles in mathematics. For terminologies and notations not mentioned here, we follow references [16] for elementary particles, [6] for geometry and topology, and [17]–[18] for Smarandache multi-spaces, and all equations are assumed to be solvable in this paper.

2 Extended Banach $\vec{G}$-flow space

2.1 Conservation laws

A conservation law, such as those on energy, mass, momentum, angular momentum and electric charge states that a particular measurable property of an isolated physical system does not change as the system evolves over time, or simply, constant of being. Usually, a local conservation law is expressed mathematically as a continuity equation, which states that the amount of conserved quantity at a point or within a volume can only change by the amount of the quantity which flows in or out of the volume. According to Definitions 1.1 and 1.2, a matter in the nature is nothing else but a Smarandache system $\left(\widetilde{\Sigma};\widetilde{\mathcal{R}}\right)$, or a topological graph $G^L\left[\left(\widetilde{\Sigma};\widetilde{\mathcal{R}}\right)\right]$ embedded in $\mathbb{R}^3$, hold with conservation laws

$$\sum_k \mathbf{F}(\mathbf{v})_k^- = \sum_l \mathbf{F}(\mathbf{v})_l^+$$

on $\forall v \in V\left(G^L\left[\left(\widetilde{\Sigma};\widetilde{\mathcal{R}}\right)\right]\right)$, where, $\mathbf{F}(\mathbf{v})_k^-$, $k \geq 1$ and $\mathbf{F}(\mathbf{v})_l^+$, $l \geq 1$ denote respectively the input or output amounts on a particle or a volume v.

2.2 $\vec{G}$-flow spaces

Classical operation systems can be easily extended on a graph $\overrightarrow{G}$ constraint on conditions for characterizing the unanimous behaviors of groups in the nature, particularly, go along with the physics. For this objective, let $\overrightarrow{G}$ be an oriented graph with vertex set $V(G)$ and arc set $X(G)$ embedded in $\mathbb{R}^3$ and let $(\mathscr{A};\circ)$ be an operation system in classical mathematics, i.e., for $\forall a, b \in \mathscr{A}$, $a \circ b \in \mathscr{A}$. Denoted by $\overrightarrow{G}^L_{\mathscr{A}}$ all of those labeled graphs $\overrightarrow{G}^L$ with labeling $L : X\left(\overrightarrow{G}\right) \to \mathscr{A}$. Then, we can extend operation $\circ$ on elements in $\overrightarrow{G}^{\mathscr{A}}$ by a ruler following:

R: *For* $\forall \overrightarrow{G}^{L_1}, \overrightarrow{G}^{L_2} \in \overrightarrow{G}^L_{\mathscr{A}}$, *define* $\overrightarrow{G}^{L_1} \circ \overrightarrow{G}^{L_2} = \overrightarrow{G}^{L_1 \circ L_2}$, *where* $L_1 \circ L_2 : e \to L_1(e) \circ L_2(e)$ *for* $\forall e \in X\left(\overrightarrow{G}\right)$.

For example, such an extension on graph $\overrightarrow{C}_4$ is shown in Fig. 4, where, $\mathbf{a_3}$=$\mathbf{a_1}\circ\mathbf{a_2}$, $\mathbf{b}_3$ =$\mathbf{b_1}\circ\mathbf{b_2}$, $\mathbf{c_3}$=$\mathbf{c_1}\circ\mathbf{c_2}$, $\mathbf{d}_3$ =$\mathbf{d_1}\circ\mathbf{d_2}$.

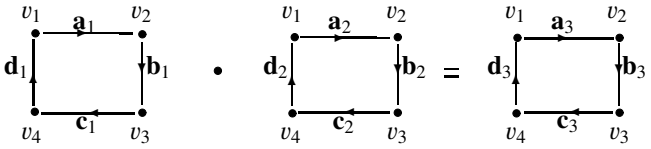

Fig. 4

Clearly, $\overrightarrow{G}^{L_1} \circ \overrightarrow{G}^{L_2} \in \overrightarrow{G}^L_{\mathscr{A}}$ by definition, i.e., $\overrightarrow{G}^L_{\mathscr{A}}$ is also an operation system under ruler **R**, and it is commutative if $(\mathscr{A},\circ)$ is commutative,

Furthermore, if $(\mathscr{A},\circ)$ is an algebraic group, $\overrightarrow{G}^L_{\mathscr{A}}$ is also an algebraic group because

(1) $\left(\overrightarrow{G}^{L_1} \circ \overrightarrow{G}^{L_2}\right) \circ \overrightarrow{G}^{L_3} = \overrightarrow{G}^{L_1} \circ \left(\overrightarrow{G}^{L_2} \circ \overrightarrow{G}^{L_3}\right)$ for $\forall \overrightarrow{G}^{L_1}, \overrightarrow{G}^{L_2}, \overrightarrow{G}^{L_3} \in \overrightarrow{G}^{\mathscr{A}}$ because

$$(L_1(e) \circ L_2(e)) \circ L_3(e) = L_1(e) \circ (L_2(e) \circ L_3(e))$$

for $e \in X\left(\overrightarrow{G}\right)$, i.e., $\overrightarrow{G}^{(L_1 \circ L_2) \circ L_3} = \overrightarrow{G}^{L_1 \circ (L_2 \circ L_3)}$.

(2) there is an identify $\overrightarrow{G}^{L_{1_{\mathscr{A}}}}$ in $\overrightarrow{G}^L_{\mathscr{A}}$, where $L_{1_{\mathscr{A}}} : e \to 1_{\mathscr{A}}$ for $\forall e \in X\left(\overrightarrow{G}\right)$;

(3) there is an uniquely element $\overrightarrow{G}^{L^{-1}}$ for $\forall \overrightarrow{G}^L \in \overrightarrow{G}^L_{\mathscr{A}}$.

However, for characterizing the unanimous behaviors of groups in the nature, the most useful one is the extension of vector space $(\mathscr{V};+,\cdot)$ over field $\mathcal{F}$ by defining the operations $+$ and $\cdot$ on elements in $\overrightarrow{G}^{\mathscr{V}}$ such as those shown in Fig. 5 on graph $\overrightarrow{C}_4$, where $\mathbf{a}$, $\mathbf{b}$, $\mathbf{c}$, $\mathbf{d}$, $\mathbf{a}_i$, $\mathbf{b}_i$, $\mathbf{c}_i$, $\mathbf{d}_i \in \mathscr{V}$ for $i = 1, 2, 3$, $\mathbf{x_3}$=$\mathbf{x_1}$+$\mathbf{x_2}$ for $\mathbf{x}$=$\mathbf{a}$, $\mathbf{b}$, $\mathbf{c}$ or $\mathbf{d}$ and $\alpha \in \mathcal{F}$.

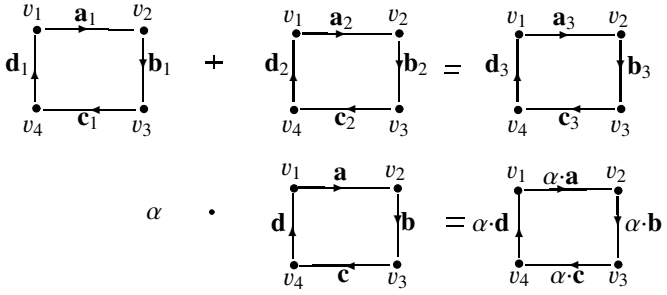

Fig. 5

A $\overrightarrow{G}$-*flow* on $\overrightarrow{G}$ is such an extension hold with $L(u,v) = -L(v,u)$ and conservation laws

$$\sum_{u\in N_G(v)} L(v,u) = \mathbf{0}$$

for $\forall v \in V\left(\overrightarrow{G}\right)$, where $\mathbf{0}$ is the zero-vector in $\mathscr{V}$. Thus, a $\overrightarrow{G}$-flow is a subfamily of $\overrightarrow{G}^L_{\mathscr{V}}$ limited by conservation laws. For example, if $\overrightarrow{G} = \overrightarrow{C}_4$, there must be $\mathbf{a}$=$\mathbf{b}$=$\mathbf{c}$=$\mathbf{d}$, $\mathbf{a}_i$=$\mathbf{b}_i$=$\mathbf{c}_i$=$\mathbf{d}_i$ for $i = 1, 2, 3$ in Fig. 5.

Clearly, all conservation $\overrightarrow{G}$-flows on $\overrightarrow{G}$ also form a vector space over $\mathcal{F}$ under operations + and $\cdot$ with zero vector $\mathbf{O} = \overrightarrow{G}^{L_{\mathbf{0}}}$, where $L_{\mathbf{0}}: e \to \mathbf{0}$ for $\forall e \in X\left(\overrightarrow{G}\right)$. Such an extended vector space on $\overrightarrow{G}$ is denoted by $\overrightarrow{G}^{\mathscr{V}}$.

Furthermore, if $(\mathscr{V}; +, \cdot)$ is a Banach or Hilbert space with inner product $\langle\cdot,\cdot\rangle$, we can also introduce the *norm* and *inner product* on $\overrightarrow{G}^{\mathscr{V}}$ by

$$\left\|\overrightarrow{G}^L\right\| = \sum_{(u,v)\in X\left(\overrightarrow{G}\right)} \|L(u,v)\|$$

or

$$\left\langle \overrightarrow{G}^{L_1}, \overrightarrow{G}^{L_2} \right\rangle = \sum_{(u,v)\in X\left(\overrightarrow{G}\right)} \langle L_1(u,v), L_2(u,v)\rangle$$

for $\forall \overrightarrow{G}^L, \overrightarrow{G}^{L_1}, \overrightarrow{G}^{L_2} \in \overrightarrow{G}^{\mathscr{V}}$, where $\|L(u,v)\|$ is the norm of $L(u,v)$ in $\mathscr{V}$. Then it can be verified that

(1) $\left\|\overrightarrow{G}^L\right\| \geq 0$ and $\left\|\overrightarrow{G}^L\right\| = 0$ if and only if $\overrightarrow{G}^L = \mathbf{O}$;

(2) $\left\|\overrightarrow{G}^{\xi L}\right\| = \xi\left\|\overrightarrow{G}^L\right\|$ for any scalar ξ;

(3) $\left\|\overrightarrow{G}^{L_1} + \overrightarrow{G}^{L_2}\right\| \leq \left\|\overrightarrow{G}^{L_1}\right\| + \left\|\overrightarrow{G}^{L_2}\right\|$;

(4) $\left\langle \overrightarrow{G}^L, \overrightarrow{G}^L \right\rangle = \sum_{(u,v)\in X\left(\overrightarrow{G}\right)} \langle L(u^v), L(u^v)\rangle \geq 0$ and $\left\langle \overrightarrow{G}^L, \overrightarrow{G}^L \right\rangle = 0$ if and only if $\overrightarrow{G}^L = \mathbf{O}$;

(5) $\left\langle \overrightarrow{G}^{L_1}, \overrightarrow{G}^{L_2} \right\rangle = \overline{\left\langle \overrightarrow{G}^{L_2}, \overrightarrow{G}^{L_1} \right\rangle}$ for $\forall \overrightarrow{G}^{L_1}, \overrightarrow{G}^{L_2} \in \overrightarrow{G}^{\mathscr{V}}$;

(6) For $\overrightarrow{G}^L, \overrightarrow{G}^{L_1}, \overrightarrow{G}^{L_2} \in \overrightarrow{G}^{\mathscr{V}}$ and $\lambda, \mu \in \mathcal{F}$,

$$\begin{aligned}&\left\langle \lambda\overrightarrow{G}^{L_1} + \mu\overrightarrow{G}^{L_2}, \overrightarrow{G}^L \right\rangle\\ &= \lambda\left\langle \overrightarrow{G}^{L_1}, \overrightarrow{G}^L \right\rangle + \mu\left\langle \overrightarrow{G}^{L_2}, \overrightarrow{G}^L \right\rangle.\end{aligned}$$

The following result is obtained by showing that Cauchy sequences in $\overrightarrow{G}^{\mathscr{V}}$ is converges hold with conservation laws.

Theorem 2.1([13]) *For any topological graph $\overrightarrow{G}$, $\overrightarrow{G}^{\mathscr{V}}$ is a Banach space, and furthermore, if $\mathscr{V}$ is a Hilbert space, $\overrightarrow{G}^{\mathscr{V}}$ is a Hilbert space also.*

According to Theorem 2.1, the operators action on Banach or Hilbert space $(\mathscr{V}; +, \cdot)$ can be extended on $\overrightarrow{G}^{\mathscr{V}}$, for example, the linear operator following.

Definition 2.2 *An operator $\mathbf{T}: \overrightarrow{G}^{\mathscr{V}} \to \overrightarrow{G}^{\mathscr{V}}$ is linear if*

$$\mathbf{T}\left(\lambda\overrightarrow{G}^{L_1} + \mu\overrightarrow{G}^{L_2}\right) = \lambda\mathbf{T}\left(\overrightarrow{G}^{L_1}\right) + \mu\mathbf{T}\left(\overrightarrow{G}^{L_2}\right)$$

for $\forall \overrightarrow{G}^{L_1}, \overrightarrow{G}^{L_2} \in \overrightarrow{G}^{\mathscr{V}}$ and $\lambda, \mu \in \mathscr{F}$, and is continuous at a $\overrightarrow{G}$-flow $\overrightarrow{G}^{L_0}$ if there always exist a number $\delta(\varepsilon)$ for $\forall \epsilon > 0$ such that

$$\left\|\mathbf{T}\left(\overrightarrow{G}^L\right) - \mathbf{T}\left(\overrightarrow{G}^{L_0}\right)\right\| < \varepsilon$$

if

$$\left\|\overrightarrow{G}^L - \overrightarrow{G}^{L_0}\right\| < \delta(\varepsilon).$$

The following interesting result generalizes the result of Fréchet and Riesz on linear continuous functionals, which opens us mind for applying $\overrightarrow{G}$-flows to hold on the nature.

Theorem 2.3([13]) *Let $\mathbf{T}: \overrightarrow{G}^{\mathscr{V}} \to \mathbb{C}$ be a linear continuous functional. Then there is a unique $\overrightarrow{G}^{\widehat{L}} \in \overrightarrow{G}^{\mathscr{V}}$ such that*

$$\mathbf{T}\left(\overrightarrow{G}^L\right) = \left\langle \overrightarrow{G}^L, \overrightarrow{G}^{\widehat{L}} \right\rangle$$

for $\forall \overrightarrow{G}^L \in \overrightarrow{G}^{\mathscr{V}}$.

Particularly, if all flows $L(u,v)$ on arcs (u,v) of $\overrightarrow{G}$ are state function, we extend the differential operator on $\overrightarrow{G}$-flows. In fact, a *differential operator* $\frac{\partial}{\partial t}$ or $\frac{\partial}{\partial x_i}: \overrightarrow{G}^{\mathscr{V}} \to \overrightarrow{G}^{\mathscr{V}}$ is defined by

$$\frac{\partial}{\partial t}: \overrightarrow{G}^L \to \overrightarrow{G}^{\frac{\partial L}{\partial t}}, \quad \frac{\partial}{\partial x_i}: \overrightarrow{G}^L \to \overrightarrow{G}^{\frac{\partial L}{\partial x_i}}$$

for integers $1 \leq i \leq 3$. Then, for $\forall \mu, \lambda \in \mathcal{F}$,

$$\begin{aligned}&\frac{\partial}{\partial t}\left(\lambda\overrightarrow{G}^{L_1} + \mu\overrightarrow{G}^{L_2}\right)\\ &= \frac{\partial}{\partial t}\left(\overrightarrow{G}^{\lambda L_1 + \mu L_2}\right) = \overrightarrow{G}^{\frac{\partial}{\partial t}(\lambda L_1 + \mu L_2)}\\ &= \overrightarrow{G}^{\frac{\partial}{\partial t}(\lambda L_1) + \frac{\partial}{\partial t}(\mu L_2)} = \overrightarrow{G}^{\frac{\partial}{\partial t}(\lambda L_1)} + \overrightarrow{G}^{\frac{\partial}{\partial t}(\mu L_2)}\\ &= \frac{\partial}{\partial t}\overrightarrow{G}^{(\lambda L_1)} + \frac{\partial}{\partial t}\overrightarrow{G}^{(\mu L_2)}\\ &= \lambda\frac{\partial}{\partial t}\overrightarrow{G}^{L_1} + \mu\frac{\partial}{\partial t}\overrightarrow{G}^{L_2},\end{aligned}$$

i.e.,

$$\frac{\partial}{\partial t}\left(\lambda\overrightarrow{G}^{L_1} + \mu\overrightarrow{G}^{L_2}\right) = \lambda\frac{\partial}{\partial t}\overrightarrow{G}^{L_1} + \mu\frac{\partial}{\partial t}\overrightarrow{G}^{L_2}.$$

Similarly, we know also that

$$\frac{\partial}{\partial x_i}\left(\lambda\overrightarrow{G}^{L_1} + \mu\overrightarrow{G}^{L_2}\right) = \lambda\frac{\partial}{\partial x_i}\overrightarrow{G}^{L_1} + \mu\frac{\partial}{\partial x_i}\overrightarrow{G}^{L_2}$$

for integers $1 \le i \le 3$. Thus, operators $\dfrac{\partial}{\partial t}$ and $\dfrac{\partial}{\partial x_i}$, $1 \le i \le 3$ are all linear on $\overrightarrow{G}^{\mathscr{V}}$.

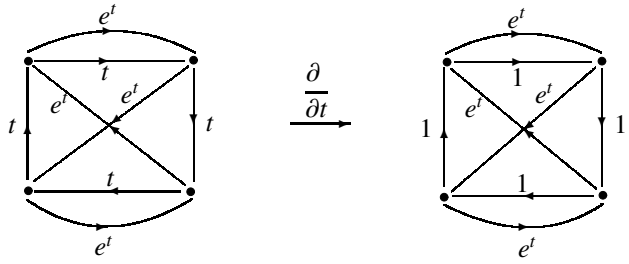

Fig. 6

Similarly, we introduce *integral operator* $\int : \overrightarrow{G}^{\mathscr{V}} \to \overrightarrow{G}^{\mathscr{V}}$ by

$$\int : \overrightarrow{G}^{L} \to \overrightarrow{G}^{\int L dt}, \quad \overrightarrow{G}^{L} \to \overrightarrow{G}^{\int L dx_i}$$

for integers $1 \le i \le 3$ and know that

$$\int \left(\mu \overrightarrow{G}^{L_1} + \lambda \overrightarrow{G}^{L_2}\right) = \mu \int \left(\overrightarrow{G}^{L_1}\right) + \lambda \int \left(\overrightarrow{G}^{L_2}\right)$$

for $\forall \mu, \lambda \in \mathcal{F}$,

$$\int \circ \left(\frac{\partial}{\partial t}\right) \text{ and } \int \circ \left(\frac{\partial}{\partial x_i}\right) : \overrightarrow{G}^{L} \to \overrightarrow{G}^{L} + \overrightarrow{G}^{L_c},$$

where L_c is such a labeling that $L_c(u, v)$ is constant for $\forall (u, v) \in X\left(\overrightarrow{G}\right)$.

3 Particle equations in $\vec{G}$-flow space

We are easily find particle equations with nonrelativistic or relativistic mechanics in $\overrightarrow{G}^{\mathscr{V}}$. Notice that

$$i\hbar \frac{\partial \psi}{\partial t} = E\psi, \qquad -i\hbar \nabla \psi = \overrightarrow{p}^2 \psi$$

and

$$E = \frac{1}{2m}\overrightarrow{p}^2 + U,$$

in classical mechanics, where ψ is the state function, $E, \overrightarrow{p}, U$ are respectively the energy, the momentum, the potential energy and m the mass of the particle. Whence,

$$\begin{aligned} \mathbf{O} &= \overrightarrow{G}^{(E - \frac{1}{2m}\overrightarrow{p}^2 - U)\psi} \\ &= \overrightarrow{G}^{E\psi} - \overrightarrow{G}^{\frac{1}{2m}\overrightarrow{p}^2 \psi} - \overrightarrow{G}^{U\psi} \\ &= \overrightarrow{G}^{i\hbar \frac{\partial \psi}{\partial t}} - \overrightarrow{G}^{-\frac{\hbar}{2m}\nabla^2 \psi} - \overrightarrow{G}^{U\psi} \\ &= i\hbar \frac{\partial \overrightarrow{G}^{L_\psi}}{\partial t} + \frac{\hbar}{2m}\nabla^2 \overrightarrow{G}^{L_\psi} - \overrightarrow{G}^{L_U}\overrightarrow{G}^{L_\psi}, \end{aligned}$$

where $L_\psi : e \to$ state function and $L_U : e \to$ potential energy on $e \in X\left(\overrightarrow{G}\right)$. According to the conservation law of energy, there must be $\overrightarrow{G}^{U} \in \overrightarrow{G}^{\mathscr{V}}$. We get the Schrödinger equation in $\overrightarrow{G}^{\mathscr{V}}$ following.

$$-i\hbar \frac{\partial \overrightarrow{G}^{L_\psi}}{\partial t} = \frac{\hbar}{2m}\nabla^2 \overrightarrow{G}^{L_\psi} - \widehat{U}\overrightarrow{G}^{L_\psi}, \tag{3.1}$$

where $\widehat{U} = \overrightarrow{G}^{L_U} \in \overrightarrow{G}^{\mathscr{V}}$. Similarly, by the relativistic energy-momentum relation

$$E^2 = c^2 \overrightarrow{p}^2 + m^2 c^4$$

for bosons and

$$E = c\alpha_k \overrightarrow{p}_k + \alpha_0 mc^2$$

for fermions, we get the Klein-Gordon equation and Dirac equation

$$\left(\frac{1}{c^2}\frac{\partial^2}{\partial t^2} - \nabla^2\right)\overrightarrow{G}^{L_\psi} + \left(\frac{cm}{\hbar}\right)\overrightarrow{G}^{L_\psi} = \mathbf{O} \tag{3.2}$$

and

$$\left(i\gamma^\mu \partial_\mu - \frac{mc}{\hbar}\right)\overrightarrow{G}^{L_\psi} = \mathbf{O}, \tag{3.3}$$

of particles in $\overrightarrow{G}^{\mathscr{V}}$ respectively. Particularly, let $\overrightarrow{G}$ be such a topological graph with one vertex but only with one arc. Then, (3.1)–(3.3) are nothing else but (1.1)–(1.3) respectively. However, (3.1)–(3.3) conclude that we can find $\overrightarrow{G}$-flow solutions on (1.1)–(1.3), which enables us to interpret mathematically the superposition of particles by multiverse.

4 $\vec{G}$-flows on particle equations

Formally, we can establish equations in $\overrightarrow{G}^{\mathscr{V}}$ by equations in Banach space $\mathscr{V}$ such as (3.1)–(3.3). However, the important thing is not just on such establishing but finding $\overrightarrow{G}$-flows on equations in $\mathscr{V}$ and then interpret the superposition of particles by $\overrightarrow{G}$-flows.

4.1 $\vec{G}$-flow solutions on equation

Theorem 2.3 concludes that there are $\overrightarrow{G}$-flow solutions for a linear equations in $\overrightarrow{G}^{\mathscr{V}}$ for Hilbert space $\mathscr{V}$ over field $\mathcal{F}$, including algebraic equations, linear differential or integral equations without considering the topological structure. For example, let $ax = b$. We are easily getting its $\overrightarrow{G}$-flow solution $x = \overrightarrow{G}^{a^{-1}L}$ if we view an element $b \in \mathscr{V}$ as $b = \overrightarrow{G}^{L}$, where $L(u, v) = b$ for $\forall (u, v) \in X\left(\overrightarrow{G}\right)$ and $0 \ne a \in \mathcal{F}$, such as those shown in Fig. 7 for $\overrightarrow{G} = \overrightarrow{C}_4$ and $a = 3$, $b = 5$.

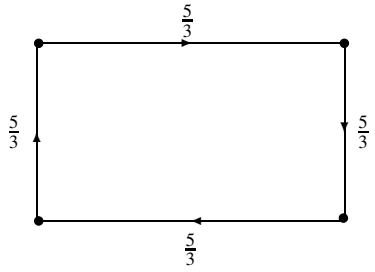

Fig. 7

Generally, we know the following result:

Theorem 4.1([13]) *A linear system of equations*

$$\begin{cases} a_{11}x_1 + a_{12}x_2 + \cdots + a_{1n}x_n = b_1 \\ a_{21}x_1 + a_{22}x_2 + \cdots + a_{2n}x_n = b_2 \\ \cdots\cdots\cdots\cdots\cdots\cdots\cdots\cdots \\ a_{m1}x_1 + a_{m2}x_2 + \cdots + a_{mn}x_n = b_m \end{cases}$$

with $a_{ij}, b_j \in \mathcal{F}$ for integers $1 \leq i \leq n, 1 \leq j \leq m$ holding with

$$\operatorname{rank}\left[a_{ij}\right]_{m\times n} = \operatorname{rank}\left[a_{ij}\right]^{+}_{m\times(n+1)}$$

has $\overrightarrow{G}$-flow solutions on infinitely many topological graphs $\overrightarrow{G}$, where

$$\left[a_{ij}\right]^{+}_{m\times(n+1)} = \begin{bmatrix} a_{11} & a_{12} & \cdots & a_{1n} & L_1 \\ a_{21} & a_{22} & \cdots & a_{2n} & L_2 \\ \cdots & \cdots & \cdots & \cdots & \cdots \\ a_{m1} & a_{m2} & \cdots & a_{mn} & L_m \end{bmatrix}.$$

We can also get $\overrightarrow{G}$-flow solutions for linear partial differential equations ([14]). For example, the Cauchy problems on differential equations

$$\frac{\partial X}{\partial t} = c^2 \sum_{i=1}^{n} \frac{\partial^2 X}{\partial x_i^2}$$

with initial value $X|_{t=t_0} = \overrightarrow{G}^{L'} \in \overrightarrow{G}^{\mathscr{V}}$ is also solvable in $\overrightarrow{G}^{\mathscr{V}}$ if $L'(u,v)$ is continuous and bou- nded in $\mathbb{R}^n$ for $\forall (u,v) \in X\left(\overrightarrow{G}\right)$ and $\forall \overrightarrow{G}^{L'} \in \overrightarrow{G}^{\mathscr{V}}$. In fact, $X = \overrightarrow{G}^{L_F}$ with $L_F : (u,v) \to F(u,v)$ for $\forall (u,c) \in X\left(\overrightarrow{G}\right)$, where

$$\begin{aligned} F(u,v) &= \frac{1}{(4\pi t)^{\frac{n}{2}}}\left(\int_{-\infty}^{+\infty} e^{-\frac{(x_1-y_1)^2+\cdots+(x_n-y_n)^2}{4t}}\right. \\ &\times \left. L'(u,v)(y_1,\cdots,y_n)dy_1\cdots dy_n\right) \end{aligned}$$

is such a solution.

Generally, if $\overrightarrow{G}$ can be decomposed into circuits $\overrightarrow{C}$, the next result concludes that we can always find $\overrightarrow{G}$-flow solutions on equations, no matter what the equation looks like, linear or non-linear ([13]).

Theorem 4.2 *If the topological graph $\overrightarrow{G}$ is strong-connected with circuit decomposition*

$$\overrightarrow{G} = \bigcup_{i=1}^{l} \overrightarrow{C}_i$$

such that $L(u,v) = L_i(\boldsymbol{x})$ for $\forall (u,v) \in X\left(\overrightarrow{C}_i\right)$, $1 \leq i \leq l$ and the Cauchy problem

$$\begin{cases} \mathscr{F}_i(\boldsymbol{x}, u, u_{x_1}, \cdots, u_{x_n}, u_{x_1x_2}, \cdots) = 0 \\ u|_{\boldsymbol{x}_0} = L_i(\boldsymbol{x}) \end{cases}$$

is solvable in a Hilbert space $\mathscr{V}$ on domain $\Delta \subset \mathbb{R}^n$ for integers $1 \leq i \leq l$, then the Cauchy problem

$$\begin{cases} \mathscr{F}_i(\boldsymbol{x}, X, X_{x_1}, \cdots, X_{x_n}, X_{x_1x_2}, \cdots) = 0 \\ X|_{\boldsymbol{x}_0} = \overrightarrow{G}^{L} \end{cases}$$

such that $L(u,v) = L_i(\boldsymbol{x})$ for $\forall (u,v) \in X\left(\overrightarrow{C}_i\right)$ is solvable for $X \in \overrightarrow{G}^{\mathscr{V}}$.

In fact, such a solution is constructed by $X = \overrightarrow{G}^{L_{u(\mathbf{x})}}$ with $L_{u(\mathbf{x})}(u,v) = u(\mathbf{x})$ for $(u,v) \in X\left(\overrightarrow{G}\right)$ by applying the input and the output at vertex v all being $u(\mathbf{x})$ on $\overrightarrow{C}$, which implies that all flows at vertex $v \in V\left(\overrightarrow{G}\right)$ is conserved.

4.2 $\vec{G}$-flows on particle equation

The existence of $\overrightarrow{G}$-flow solutions on particle equations (1.1)–(1.3) is clearly concluded by Theorem 4.2, also implied by (3.1)–(3.3) for any $\overrightarrow{G}$. However, the superposition of a particle P shows that there are $N \geq 2$ states of being associated with a particle P. Considering this fact, a convenient $\overrightarrow{G}$-flow model for elementary particle fermions, the lepton or quark P is by a bouquet $\overrightarrow{B}_N^{L_\psi}$, and an antiparticle $\overline{P}$ of P presented by $\overrightarrow{B}_N^{L_{\psi^{-1}}}$ with all inverse states on its loops, such as those shown in Fig. 8.

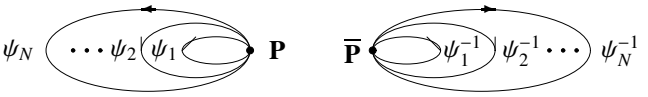

Particle Antiparticle

Fig. 8

An elementary unparticle is an intermediate form between an elementary particle and its antiparticle, which can be presented by $\overrightarrow{B}_N^{L_\psi^C}$, where $L_\psi^C : e \to L_{\psi^{-1}}(e)$ if $e \in C$ but $L_\psi^C : e \to L_\psi(e)$ if $e \in X\left(\overrightarrow{B}_N\right) \setminus C$ for a subset $C \subset X\left(\overrightarrow{B}_N\right)$, such as those shown in Fig. 9,

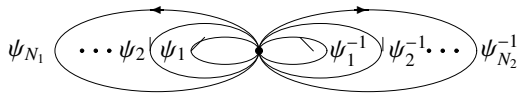

Fig. 9 Unparticle

where $N_1, N_2 \geq 1$ are integers. Thus, an elementary particle with its antiparticles maybe annihilate or appears in pair at a time, which consists in an elementary unparticle by combinations of these state functions with their inverses.

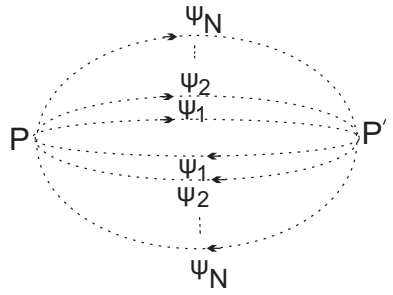

Fig. 10 $\overrightarrow{D^{\perp}}^{L_\psi}_{0,2N,0}$

For those of mediate interaction particle quanta, i.e., boson, which reflects interaction between particles. Thus, they are conveniently presented by dipole $\overrightarrow{D^{\perp}}^{L_\psi}_{0,2N,0}$ but with dotted lines, such as those in Fig. 10, in which the vertex P, P' denotes particles, and arcs with state functions $\psi_1, \psi_2, \cdots, \psi_N$ are the N states of P. Notice that $\overrightarrow{B}^{L_\psi}_N$ and $\overrightarrow{D^{\perp}}^{L_\psi}_{0,2N,0}$ both are a union of N circuits.

According to Theorem 4.2, we consequently get the following conclusion.

Theorem 4.3 *For an integer $N \geq 1$, there are indeed $\overrightarrow{D^{\perp}}^{L_\psi}_{0,2N,0}$ -flow solution on Klein-Gordon equation (*1.2*), and $\overrightarrow{B}^{L_\psi}_N$ -flow solution on Dirac equation (*1.3*).*

Generally, this model enables us to know that the $\overrightarrow{G}$-flow constituents of a particle also.

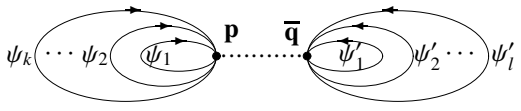

Fig. 11 Meson

Thus, if a particle $\widetilde{P}$ is consisted of l elementary particles $P_1, P_1, \cdots, P_l$ underlying a graph $\overrightarrow{G}\left[\widetilde{P}\right]$, its $\overrightarrow{G}$-flow is obtained by replace each vertex v by $\overrightarrow{B}^{L_{\psi v}}_{N_v}$ and each arc e by $\overrightarrow{D^{\perp}}^{L_{\psi e}}_{0,2N_e,0}$ in $\overrightarrow{G}\left[\widetilde{P}\right]$, denoted by $\overrightarrow{G}^{L_\psi}\left[\overrightarrow{B}_v, \overrightarrow{D}_e\right]$. For example, the model of Sakata, or Gell-Mann and Ne'eman on hadrons claims that the meson and the baryon are respectively the dipole $\overrightarrow{D^{\perp}}^{L_{\psi e}}_{k,2N,l}$-flow shown in Fig. 11 and the triplet $\overrightarrow{G}$-flow $\overrightarrow{C^{\perp}}^{L_\psi}_{k,l,s}$ shown in Fig. 12,

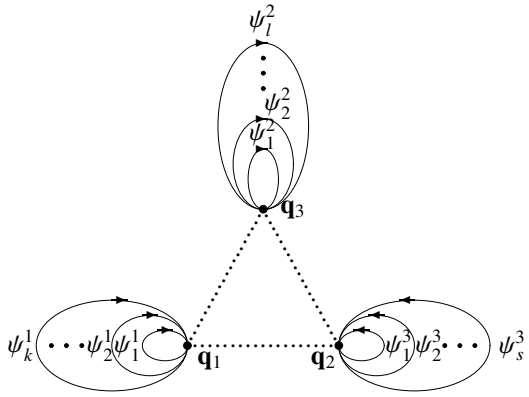

Fig. 12 Baryon

Theorem 4.4 *If $\widetilde{P}$ is a particle consisted of elementary particles $P_1, P_1, \cdots, P_l$ for an integer $l \geq 1$, then $\overrightarrow{G}^{L_\psi}\left[\overrightarrow{B}_v, \overrightarrow{D}_e\right]$ is a $\overrightarrow{G}$-flow solution on the Schrödinger equation (*1.1*) whenever λ_G is finite or infinite.*

Proof If λ_G is finite, the conclusion follows Theorem 4.2 immediately. We only consider the case of $\lambda_G \to \infty$. In fact, if $\lambda_G \to \infty$, calculation shows that

$$\begin{aligned} & i\hbar \lim_{\lambda_G\to\infty}\left(\frac{\partial}{\partial t}\left(\overrightarrow{G}^{L_\psi}\left[\overrightarrow{B}_v, \overrightarrow{D}_e\right]\right)\right) \\ &= \lim_{\lambda_G\to\infty}\left(i\hbar\frac{\partial}{\partial t}\left(\overrightarrow{G}^{L_\psi}\left[\overrightarrow{B}_v, \overrightarrow{D}_e\right]\right)\right) \\ &= \lim_{\lambda_G\to\infty}\left(-\frac{\hbar^2}{2m}\nabla^2\overrightarrow{G}^{L_\psi}\left[\overrightarrow{B}_v, \overrightarrow{D}_e\right] + \overrightarrow{G}^{L_U}\right) \\ &= -\frac{\hbar^2}{2m}\nabla^2 \lim_{\lambda_G\to\infty}\overrightarrow{G}^{L_\psi}\left[\overrightarrow{B}_v, \overrightarrow{D}_e\right] + \overrightarrow{G}^{L_U}, \end{aligned}$$

i.e.,

$$\begin{aligned} & i\hbar \lim_{\lambda_G\to\infty}\left(\frac{\partial}{\partial t}\left(\overrightarrow{G}^{L_\psi}\left[\overrightarrow{B}_v, \overrightarrow{D}_e\right]\right)\right) \\ &= -\frac{\hbar^2}{2m}\nabla^2 \lim_{\lambda_G\to\infty}\overrightarrow{G}^{L_\psi}\left[\overrightarrow{B}_v, \overrightarrow{D}_e\right] + \overrightarrow{G}^{L_U}. \end{aligned}$$

In particular,

$$i\hbar \lim_{N\to\infty}\left(\frac{\partial \overrightarrow{B}^{L_\psi}_N}{\partial t}\right) = -\frac{\hbar^2}{2m}\nabla^2 \lim_{N\to\infty}\overrightarrow{B}^{L_\psi}_N + \overrightarrow{G}^{L_U},$$

$$i\hbar \lim_{N\to\infty}\frac{\partial}{\partial t}\left(\overrightarrow{D^{\perp}}^{L_\psi}_{0,2N,0}\right) = -\frac{\hbar^2}{2m}\nabla^2 \lim_{N\to\infty}\overrightarrow{D^{\perp}}^{L_\psi}_{0,2N,0} + \overrightarrow{G}^{L_U}$$

for bouquets and dipoles. □

5 $\vec{G}$-flow interpretation on particle superposition

The superposition of a particle P is depicted by a Hilbert space $\mathscr{V}$ over complex field $\mathbb{C}$ with orthogonal basis $|1\rangle, |2\rangle, \cdots, |n\rangle, \cdots$ in quantum mechanics. In fact, the linearity of Schrödinger equation concludes that all states of particle P are in such a space. However, an observer can grasp only one state, which promoted H. Everett devised a multiverse consisting of states in splitting process, i.e., the quantum effects spawn countless branches of the universe with different events occurring in each, not influence one another, such as those shown in Fig. 13, and the observer selects by randomness, where the multiverse is $\bigcup\limits_{i\geq 1}\mathscr{V}_i$ with $\mathscr{V}_{kl}=\mathscr{V}$ for integers $k\geq 1,\ 1\leq l\leq 2^k$ but in different positions.

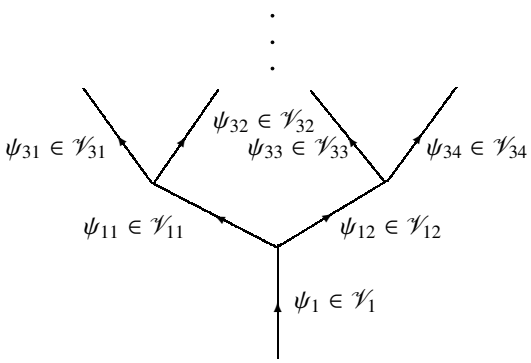

Fig. 13

Why it needs an interpretation on particle superposition in physics lies in that we characterize the behavior of particle by dynamic equation on state function and interpret it to be the solutions, and different quantum state holds with different solution of that equation. However, we can only get one solution by solving the equation with given initial datum once, and hold one state of the particle P, i.e., the solution correspondent only to one position but the particle is in superposition, which brought the H. Everett interpretation on superposition. It is only a biological mechanism by infinite parallel spaces $\mathscr{V}$ but loses of conservations on energy or matter in the nature, whose independently runs also overlook the existence of universal connection in things, a philosophical law.

Even so, it can not blot out the ideological contribution of H. Everett to sciences a shred because all of these mentions are produced by the interpretation on mathematical solutions with the reality of things, i.e., scanning on local, not the global. However, if we extend the Hilbert space $\mathscr{V}$ to $\overrightarrow{B}_N^{L_\psi}$, $\overrightarrow{D^{\perp}}_{0,2N,0}^{L_\psi}$ or $\overrightarrow{G}^{L_\psi}\left[\overrightarrow{B}_v,\overrightarrow{D}_e\right]$ in general, i.e., $\overrightarrow{G}$-flow space $\overrightarrow{G}^{\mathscr{V}}$, where $\overrightarrow{G}$ is the underling topological graph of P, the situation has been greatly changed because $\overrightarrow{G}^{\mathscr{V}}$ is itself a Hilbert space, and we can identify the $\overrightarrow{G}$-flow on $\overrightarrow{G}$ to particle P, i.e.,

$$P=\overrightarrow{G}^{L_\psi}\left[\overrightarrow{B}_v,\overrightarrow{D}_e\right] \tag{5.1}$$

for a globally understanding the behaviors of particle P whatever $\lambda_G\to\infty$ or not by Theorem 4.4. For example, let $P=\overrightarrow{B}_N^{L_\psi}$, i.e., a free particle such as those of electron e^-, muon μ^-, tauon τ^-, or their neutrinos ν_e,ν_μ,ν_τ. Then the superposition of P is displayed by state functions ψ on N loops in $\overrightarrow{B}_N$ hold on its each loop with

$$\text{input } \psi_i=\text{ ouput } \psi_i \text{ at vertex } P$$

for integers $1\leq i\leq N$. Consequently,

$$\text{input } \sum_{i\in I}\psi_i=\text{ ouput } \sum_{i\in I}\psi_i \text{ at vertex } P$$

for $\forall I\subset\{1,2,\cdots,N\}$, the conservation law on vertex P. Furthermore, such a $\overrightarrow{B}_N^{L_\psi}$ is not only a disguise on P in form but also a really mathematical element in Hilbert space $\overrightarrow{B}^{\mathscr{V}}$, and can be also used to characterize the behavior of particles such as those of the decays or collisions of particles by graph operations. For example, the β-decay $n\to p+e^-+\mu_e^-$ is transferred to a decomposition formula

$$\overrightarrow{C^{\perp}}_{k,l,s}^{L_{\psi_n}}=\overrightarrow{C^{\perp}}_{k_1,l_1,s_1}^{L_{\psi_p}}\bigcup\overrightarrow{B}_{N_1}^{L_{\psi_e}}\bigcup\overrightarrow{B}_{N_2}^{L_{\psi_\mu}},$$

on graph, where, $\overrightarrow{C^{\perp}}_{k_1,l_1,s_1}^{L_{\psi_p}}$, $\overrightarrow{B}_{N_1}^{L_{\psi_e}}$, $\overrightarrow{B}_{N_2}^{L_{\psi_\mu}}$ are all subgraphs of $\overrightarrow{C^{\perp}}_{k,l,s}^{L_{\psi_n}}$. Similarly, the β- collision $\nu_e+p\to n+e^+$ is transferred to an equality

$$\overrightarrow{B}_{N_1}^{L_{\psi_{\nu_e}}}\bigcup\overrightarrow{C^{\perp}}_{k_1,l_1,s_1}^{L_{\psi_p}}=\overrightarrow{C^{\perp}}_{k_2,l_2,s_2}^{L_{\psi_n}}\bigcup\overrightarrow{B}_{N_2}^{L_{\psi_e}}.$$

Even through the relation (5.1) is established on the linearity, it is in fact truly for the linear and non-liner cases because the underlying graph of $\overrightarrow{G}^{L_\psi}\left[\overrightarrow{B}_v,\overrightarrow{D}_e\right]$-flow can be decomposed into bouquets and dipoles, hold with conditions of Theorem 4.2. Thus, even if the dynamical equation of a particle P is non-linear, we can also adopt the presentation (5.1) to characterize the superposition and hold on the global behavior of P. Whence, it is a presentation on superposition of particles, both on linear and non-linear.

6 Further discussions

Usually, a dynamic equation on a particle characterizes its behaviors. But *is its solution the same as the particle*? Certainly not! Classically, a dynamic equation is established on characters of particles, and different characters result in different equations. Thus the superposition of a particle should be characterized by at least 2 differential equations. However, for a particle P, all these equations are the same one by

chance, i.e., one of the Schrödinger equation, Klein-Gordon equation or Dirac equation, which lead to the many world interpretation of H. Everett, i.e., put a same equation or Hilbert space on different place for different solutions in Fig. 12. As it is shown in Theorems 4.1 – 4.4, we can interpret the solution of (1.1)–(1.3) to be a $\overrightarrow{G}^{L_\psi}\left[\overrightarrow{B}_v, \overrightarrow{D}_e\right]$-flow, which properly characterizes the superposition behavior of particles by purely mathematics.

The $\overrightarrow{G}$-flow interpretation on differential equation opens a new way for understanding the behavior of nature, particularly on superposition of particles. Generally, the dynamic equations on different characters maybe different, which will brings about contradicts equations, i.e., non-solvable equations. For example, we characterize the behavior of meson or baryon by Dirac equation (1.3). However, we never know the dynamic equation on quark. Although we can say it obeying the Dirac equation but it is not a complete picture on quark. If we find its equation some day, they must be contradicts because it appear in different positions in space for a meson or a baryon at least. As a result, the $\overrightarrow{G}$-solutions on non-solvable differential equations discussed in [9]–[12] are valuable for understanding the reality of the nature with $\overrightarrow{G}$-flow solutions a special one on particles.

As it is well known for scientific community, any science possess the falsifiability but which depends on known scientific knowledge and technical means at that times. Accordingly, it is very difficult to claim a subject or topic with logical consistency is truth or false on the nature sometimes, for instance the multiverse or parallel universes because of the limitation of knowing things in the nature for human beings. In that case, a more appreciated approach is not denied or ignored but tolerant, extends classical sciences and developing those of well known technical means, and then get a better understanding on the nature because the pointless argument would not essentially promote the understanding of nature for human beings ([3,4,22]).

Submitted on April 8, 2015 / Accepted on April 15, 2015

References

1. Bousso R. and Susskind L. Multiverse interpretation of quantum mechanics. *Physical Review*, 2012, D85 (4), DOI:10.1103; *Phys. Rev.* D.85.045007.
2. Everett H. Relative state formulation of quantum mechanics. *Rev. Mod. Phys.*, 1957, v. 29, 454–462.
3. George E. Does the multiverse really exist? *Scientific American*, 2011, v. 305 (2), 38–43.
4. Kragh H. Contemporary history of cosmology and controversy over the multiverse. *Annals of Science*, 2009, v. 66 (4), 529.
5. Tian Ma. View Physics by Mathematics – Elementary Particles and Unified Field Theory (in Chinese). Science Press, Beijing, 2014.
6. Linfan Mao. Combinatorial Geometry with Applications to Field Theory. The Education Publisher, USA, 2011.
7. Linfan Mao. Combinatorial fields – an introduction. *International J. Math. Combin.*, 2009, v. 3, 1–22.
8. Linfan Mao. Relativity in combinatorial gravitational fields. *Progress in Physics*, 2010, v. 6 (3), 39–50.
9. Linfan Mao. Global stability of non-solvable ordinary differential equations with applications. *International J. Math. Combin.*, 2013, v. 1, 1–37.
10. Linfan Mao. Geometry on G^L-systems of homogenous polynomials. *International J. Contemp. Math. Sciences*, 2014, v. 9 (6), 287–308.
11. Linfan Mao. Non-solvable equation systems with graphs embedded in $\mathbf{R}^n$. in Proceedings of the First International Conference on Smarandache Multispace and Multistructure, The Education Publisher, July 2013.
12. Linfan Mao. Cauchy problem on non-solvable system of first order partial differential equations with applications. *Methods and Applications of Analysis*, (Accepted for publication).
13. Linfan Mao. Extended Banach $\overrightarrow{G}$-flow spaces on differential equations with applications. *Electronic J. Mathematical Analysis and Applications*, 2015, v. 3 (2), 59–91.
14. Nambu Y. Quarks: Frontiers in Elementary Particle Physics. World Scientific Publishing, 1985.
15. Byrne Peter The many worlds of Hugh Everett III. *Scientific American*, December 2007, 98–105.
16. Quang Ho-Kim and Pham Xuan Yem. Elementary Particles and Their Interactions. Springer-Verlag, Berlin-Heidelberg, 1998.
17. Smarandache F. *Paradoxist Geometry*, State Archives from Valcea, Rm. Valcea, Romania, 1969, and in Paradoxist Mathematics, Collected Papers (Vol. II), Kishinev University Press, Kishinev, 1997, 5–28.
18. Smarandache F. Multi-space and multi-structure, in Neutrosophy – Neutrosophic Logic, Set, Probability and Statistics, American Research Press, 1998.
19. Smarandache F. A new form of matter – unmatter, composed of particles and anti-particles. *Progress in Physics*, 2005, v. 1 (1), 9–11.
20. Smarandache F. Verifying unmatter by experiments, more types of unmatter. *Progress in Physics*, 2005, v. 1 (2), 113–116.
21. Smarandache F. and Rabounski D. Unmatter entities inside nuclei, predicted by the Brightsen nucleon cluster model. *Progress in Physics*, 2006, v. 2 (1), 14–18.
22. Steinhardt P. Theories of anything. http://www.edge.org/response-detail/25405, 2014.
23. Tegmark M. Parallel universes in Science and Ultimate Reality: From Quantum to Cosmos. in Barrow J. D., Davies P. C. W. and Harper C. L. (eds), Cambridge University Press, 2003.
24. Tegmark M. Our mathematical universe: My quest for the ultimate nature of reality. Knopf Doubleday Publishing Group, 2014.

Question of Planckian "Action" in Gravitational Wave Detection Experiments

Joseph F. Messina
Topical Group in Gravitation, American Physical Society, P.O. Box 130520,
The Woodlands, TX 77393, USA. E-mail: jfmessina77@yahoo.com

It is shown that in the absence of a *purely* gravitational measurement of Planck's constant one *cannot* at present rule out the possibility that the ripples in the curvature of the *fabric* of spacetime may be *scaled* by a more diminutive "action" whose detection requires sensitivities beyond the standard quantum limit. An experiment that could unequivocally test this possibility is suggested.

1 Introduction

The search for gravitational waves, one of the centerpieces of general relativity, has been a work in progress for over five decades. Two main forms of detectors are currently in use worldwide. The first, pioneered by Weber [1] in the 1960s, is based on the expectation that a passing gravitational wave will induce a mechanical oscillation in a cryogenically cooled cylindrical bar whose resonance can then be amplified and recorded. The second method, using lasers, is designed to measure spacetime geometry variations between mirrors suspended in vacuum using interferometry in a Michelson configuration.

Despite the ever increasing sensitivity of these detectors these ripples in the curvature of the fabric of spacetime have yet to be detected. After these many years of experimentation one may therefore be justified in questioning whether the failure to detect these perturbations is symptomatic of yet to be discovered physics beyond the standard quantum limit.

It should be observed that if we examine this question from a quantum mechanical perspective we are inevitably struck by the fact that the role of Planck's constant in gravitational wave phenomena has always been taken for granted without questions regarding the possible limits of its applicability being asked, which is somewhat perplexing since no *purely* gravitational measurement of Planck's constant exists. As will be shown in this paper, if pursued, this element of uncertainty gives rise to the possibility that gravitational quanta may not be *scaled* by Planck's constant.

2 Scaling of gravitational quanta

It should be emphasized from the outset that any discussion of this possibility has as its foundation the irrefutable fact that nature has made available *two* immutable elementary "actions" in the context of the framework of quantum mechanics. That is, Planck's familiar constant, h, which has been shown experimentally to play an indispensable role in the microphysical realm, and a second, more diminutive "action" formed from two of the fundamental constants of quantum mechanics, namely, e^2/c – the ratio of the square of the elementary charge to the velocity of light, which has the value 7.6957×10^{-37} J s.

In what follows I shall put forward an experimentally verifiable hypothesis in favor of a dynamical interpretation of the fabric of spacetime. That is, we shall allow for the possibility that this more diminutive "action" is an *intrinsic* property of the fabric of spacetime; the *size* of the gravitational quanta being always *scaled* in terms of e^2/c. Implicit in this conceptualization is the widely held expectation that spacetime should play a dynamic role in its own right, rather than being a passive observer.

3 Possible experimental test

Clearly, the most direct way of verifying if this hypothesis corresponds to reality is to measure the *vibrational* displacement induced in a resonant detector by a passing gravitational wave. To give an illustration, let us assume, using the "action" constant e^2/c, that a gravitational quantum of *angular* frequency ω has an energy

$$E = \left(\frac{e^2}{2\pi c}\right)\omega\,. \tag{1}$$

We can then profit from the fact that the *vibrational* energy induced in a *resonant* detector, by a gravitational wave, can be converted to the fractional change in *vibrational* displacement by making use of the relation between amplitude x_0, energy E and the total mass M for a harmonic oscillator, in the familiar form

$$E = \frac{1}{2}M\omega^2 x_0^2\,. \tag{2}$$

If we now take as an example Weber's seminal experiment, which used as an antenna a 1400 kg cylindrical aluminum bar that had a natural *resonance* frequency ν_0 of 1660 Hz, we can readily compute the *vibrational* displacement, x, caused by a *single* quantum of gravitational radiation of *angular* frequency $\omega = 2\pi\nu_0$, and energy $(e^2/2\pi c)\,\omega$. Combining Eqs. (1) and (2) and then substituting these values, we obtain

$$\begin{aligned} x &= \sqrt{\frac{2}{M\omega}\frac{e^2}{2\pi c}} \\ &\approx 1.3 \times 10^{-22}\ \text{m}. \end{aligned} \tag{3}$$

Needless to say, such extraordinarily small displacements could not be measured with the technology available in Weber's day. Indeed, even today such a feat remains out of reach since there are no resonant-mass antennas in operation that have the required sensitivity.

Fortunately, since Weber's pioneering work in the 1960s numerous projects have been undertaken in an effort to enhance detector sensitivity. One of the more innovative of these efforts has been the development of the Schenberg *spherical* resonant-mass telescope in Brazil [2], which has the advantage of being omnidirectional. When fully operational it will provide information regarding a wave's amplitude, polarization, and direction of source. The detector program, which we shall presently exploit, uses an 1150 kg spherical resonant-mass made of a copper-aluminum alloy, and has a *resonance* frequency ν_0 of 3200 Hz. The *vibrational* displacement caused by a *single* quantum of gravitational radiation of *angular* frequency $\omega = 2\pi\nu_0$ can easily be computed by direct substitution of these values in Eq. (3). We thus obtain

$$x \approx 1.0 \times 10^{-22} \text{ m}. \tag{4}$$

Verification of this result is contingent on the Schenberg surpassing the standard quantum limit by *squeezing* the signal, which should result in a ten-fold increase in sensitivity. Clearly, in the absence of a physical law that prohibits an elementary "action" smaller than Planck's this result must be taken seriously.

4 Summary

The possibility was raised that gravitational quanta may not be scaled by Planck's constant. It was shown that in the absence of a *purely* gravitational measurement of Planck's constant one *cannot* at present rule out the possibility that gravitational quanta may be *scaled* by the more diminutive of nature's two *elementary* "actions", namely, e^2/c, which was conjectured to be an *intrinsic* property of the fabric of spacetime. A possible experiment requiring sensitivities beyond the standard quantum limit was suggested.

Acknowledgments

I would like to thank Dr. Odylio Aguiar for his update on the status of the Schenberg detector, and his assessment of its potential. I also wish to thank Dr. Alexander Khalaidovski for his assessment of the potential of the squeezed light technique for reducing quantum noise.

Submitted on April 11, 2015 / Accepted on April 15, 2015

References

1. Weber J. Evidence for Discovery of Gravitational Radiation. *Phys. Rev. Lett.*, 1969, v. 22, 1320–1324.
2. Aguiar O. D. The Brazilian Spherical Detector: Progress and Plans. *Class. Quantum Grav.*, 2004, v. 21, 457–463.

Appendix

The recognition of the "action" e^2/c as an intrinsic property of the fabric of spacetime inevitably leads to quantum uncertainty at a more fundamental level than Planck's constant, in the analogous form

$$(\Delta x)(\Delta p) \approx \frac{e^2}{c} \tag{1}$$

where, as usual, x is uncertainty of position, and p the uncertainty in momentum. Its implication for the *temporal* events that make up the big bang can be simply illustrated in terms of the *sub-Planckian* unit of time, T_0, analogous to the Planck time $T_P = \sqrt{\hbar G/c^5}$, in the form

$$T_0 = \sqrt{\frac{e^2}{2\pi c}\frac{G}{c^5}} = 1.837 \times 10^{-45} \text{ s} \tag{2}$$

where $(e^2/2\pi c)$ is the reduced *sub-Planckian* "action" constant, G is the Newtonian gravitational constant, and c is the velocity of light. Unfortunately, because of the *sub-Planckian* uncertainty principle, Eq. (1), we are prevented from speculating on times shorter than 10^{-44} seconds after the big bang, which is an order of magnitude prior to the Planck era (10^{-43} seconds). The disparity in this temporal sequence of events is, needless to say, cosmologically significant since it implies that a *sub-Planckian* era *preceded* the Planck era in the nascent universe, which should be discernible from its gravitational signature.

Dynamical 3-Space: Anisotropic Brownian Motion Experiment

Reginald T. Cahill

School of Chemical and Physical Sciences, Flinders University, South Australia. E-mail: reg.cahill@flinders.edu.au

In 2014 Jiapei Dai reported evidence of anisotropic Brownian motion of a toluidine blue colloid solution in water. In 2015 Felix Scholkmann analysed the Dai data and detected a sidereal time dependence, indicative of a process driving the preferred Brownian motion diffusion direction to a star-based preferred direction. Here we further analyse the Dai data and extract the RA and Dec of that preferred direction, and relate the data to previous determinations from NASA Spacecraft Earth-flyby Doppler shift data, and other determinations.

1 Introduction

In 2014 Jiapei Dai [1] reported evidence of anisotropic Brownian motion, and in 2015 Felix Scholkmann [3] detected a sidereal time dependence, indicative of a process driving the preferred Brownian motion diffusion direction to a star-based preferred direction. Here we further analyse the Dai data and extract the RA and Dec of that preferred direction, and relate the data to previous determinations from NASA spacecraft Earth-flyby Doppler shift data, and other determinations [5]. It is shown that the anisotropic Brownian motion is an anisotropic "heating" generated by the dynamical 3-space [4].

2 Anisotropic Brownian motion

Dai in Wuhan City detected anisotropic Brownian motion by loading a small drop of toluidine blue solution into a container of water. The diffusion pattern was photographed starting within 30 sec of loading the water cell and then once every ten minutes until the end of observations [1]. The images were analysed using image analysis software. The observations were performed 24 times per day, and repeated from December 22, 2011 to March 23, 2013.

The image of the diffusion anisotropy is illustrated in Figure 1, with directions measured from East in a clockwise direction. Dai reported the preferred direction of diffusion from 15 days, plotted against Wuhan Solar Time. In Fig. 2 that data has been replotted against Local Sidereal Time for Wuhan City. We now analyse that data from the point of view of a preferred 3-space velocity, where the Right Ascension, RA, is defined by when the preferred diffusion direction is from S to N. The Declination is to be determined by the dynamic range of the diffusion direction over one day, as in Fig. 4. We report herein that the anisotropic Brownian motion data confirms various properties of the 3-space flow previously reported [5].

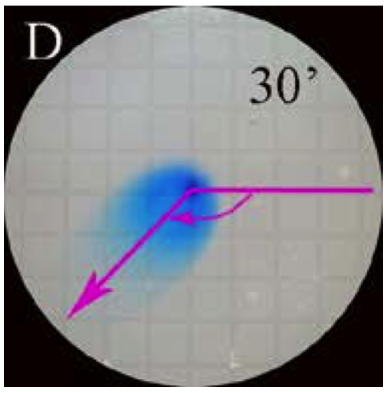

Fig. 1: Illustration of anisotropic diffusion of the toluidine blue solution in water, 30 min after inserting drop. The preferred direction is measured clockwise in degrees from East. Reproduced from [1].

3 Dynamical 3-space

The Schrödinger equation must be extended to include the dynamical space [6]

$$i\hbar\frac{\partial\psi(\mathbf{r},t)}{\partial t} = -\frac{\hbar^2}{2m}\nabla^2\psi(\mathbf{r},t) + V(\mathbf{r},t)\psi(\mathbf{r},t) - \\ -i\hbar\left(\mathbf{v}(\mathbf{r},t)\cdot\nabla + \frac{\mathbf{1}}{\mathbf{2}}\nabla\cdot\mathbf{v}(\mathbf{r},\mathbf{t})\right)\psi(\mathbf{r},t). \quad (1)$$

Here $\mathbf{v}(\mathbf{r},t)$ is the velocity field describing the dynamical space at a classical field level, [4], and the coordinates $\mathbf{r}$ give the relative location of $\psi(\mathbf{r},t)$ and $\mathbf{v}(\mathbf{r},t)$, relative to a Euclidean embedding space, and also used by an observer to locate structures. This is not an aether embedded in a non-dynamical space, but a dynamical space which induces an embedding space or coordinate system. This minimal generalisation of the original Schrödinger equation arises from the replacement $\partial/\partial t \to \partial/\partial t + \mathbf{v}.\nabla$, the Euler derivative, which ensures that the quantum system properties are determined by the dynamical space, and not by the embedding coordinate system. The extra $\nabla\cdot\mathbf{v}$ term in (1) is required to make the hamiltonian in (1) hermitian.

4 Analysing Brownian motion data

For a plane wave $\psi = e^{i\mathbf{k}\cdot\mathbf{r}-i\omega t}$, for water molecules, this results in an energy shift $E = \hbar\omega \to E + \hbar\mathbf{k}\cdot\mathbf{v}$. The Dai data in Fig. 2 reveals a complex behaviour, with not all data revealing a RA for the preferred flow. However this is explainable by two key observations. First the fluctuations in the 3-space

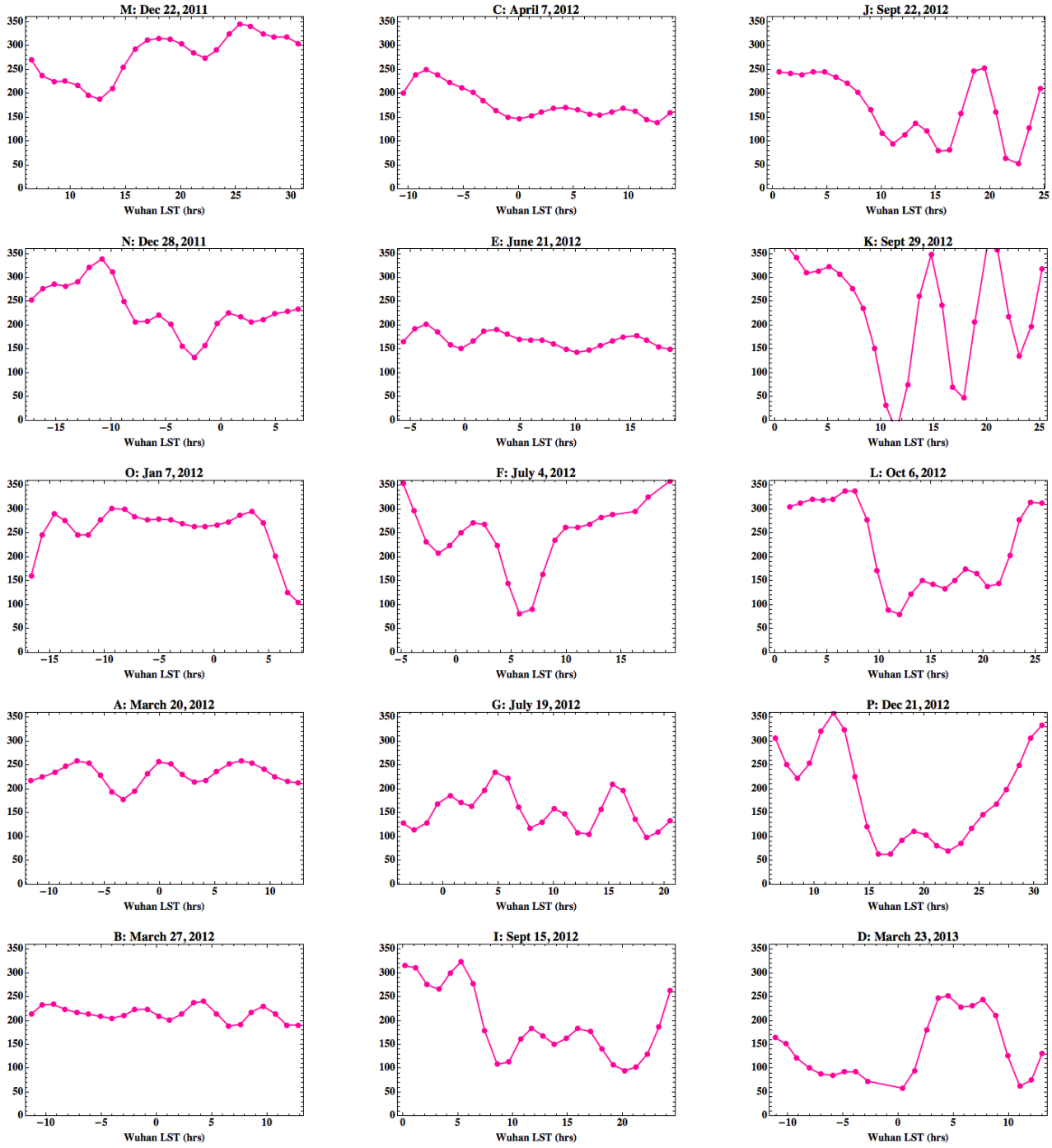

Fig. 2: Dai data [1], showing preferred direction of colloidal diffusion, plotted against Wuhan Local Sidereal Time (LST), for the various indicated days. The coding M, N, ... refers to the labelling in [1], which reported the data against Wuhan local solar time. The preferred direction of diffusion is measured as indicated in Fig. 1.

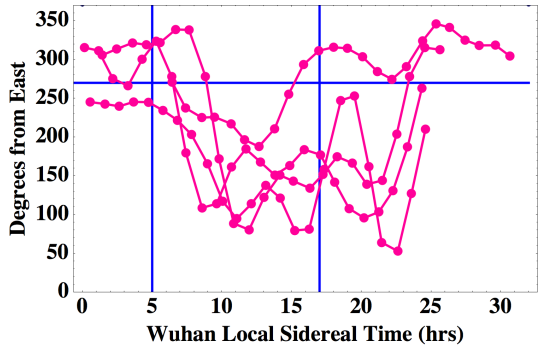

Fig. 3: Plot of the better data from Fig. 2: M, I, J, L. These days show trend of preferred direction to be from South to North (270°) at ~5 hrs LST. A similar trend might be expected for 17hrs LST, but is not seen in all days shown. This is because at this approximate LST the space flow passes more deeply through the Earth, see Fig. 5, which results in considerable increase in turbulence.

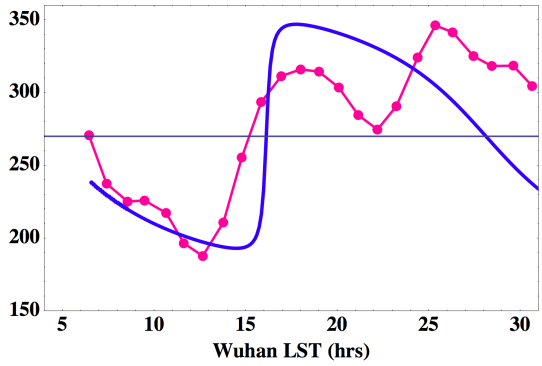

Fig. 4: Plot of Dai data vs Wuhan LST for Dec 22, 2011 (plot M in Fig. 2). Smooth curve (blue) is predicted form for RA=5hrs, Dec=60°S. The RA is defined by when dynamical 3-space flow direction is from S to N, here RA 5hrs and 17hrs. The Dec determines the variation in direction, here 270° ± 40°. Note the increased turbulence, manifesting as fluctuations in direction of the flow, when the flow is more deeply through the Earth. For Dec 8, 1992, the NASA Doppler shift data gave RA=5.23hrs, Dec=80°S, [5].

flow manifest as changes in both speed and direction. When the data for the better days is plotted, as in Fig. 3, we see that the RA cluster around 5hrs Local Sidereal Time. However we would also expect to see the data crossing the due N direction (270°) some 12 hours later. However the data in Fig. 3 shows much noisier variations. This second key observation is that this is also expected as during these times the 3-space flow has passed deeply into the earth, as shown in Fig. 5, and this results in increased turbulence in both speed and direction. One consequence of this is that future studies of anisotropic Brownian motion should be performed well into the southern hemisphere. Finally, from the 3-space turbulence, we expect the best quality data, being least affected by 3-space turbulence, would be for day M. That data is shown in Fig. 4, which gives an approximate RA=5hrs, Dec=60°S. This is consistent with the RA and Dec for December from the NASA Doppler shift data [5].

5 Conclusion

That the known characteristics of the 3-space flow agree with results from the anisotropy of the Brownian motion data suggests a simple mechanism, namely that the 3-space flow generates an energy shift in the water molecules; $E \to E + \hbar\mathbf{k}\cdot\mathbf{v}$, where $\mathbf{k}$ is the wavenumber vector for water molecules, and that this is largest for water molecules moving in the direction of $\mathbf{v}$. This results in water molecules moving in the direction of $\mathbf{v}$ having a greater kinetic energy, and imparting more momentum to the toluidine colloidal particles than water molecules moving in the opposite direction. So the $-i\hbar\mathbf{v}\cdot\nabla$ term gives rise to an enhanced Brownian diffusion in the direction of $\mathbf{v}$.

A similar effect was observed by Shnoll [7] in which the α decay rate of ^{239}Pu is directional dependent. This is also explained by the $-i\hbar\mathbf{v}\cdot\nabla$ term, as it causes the α kinetic energy to be different in different directions related to $\mathbf{v}$, and so affects the quantum tunnelling process, with more α emerging in the direction of $\mathbf{v}$.

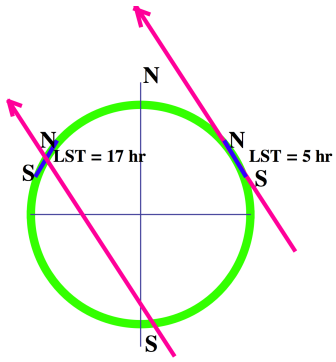

Fig. 5: Cross section of Earth showing Wuhan horizontal planes and the local N and S directions at Local Sidereal Times of 5 hr and 17 hr. Also shown is dynamical 3-space flow direction, with a Declination of -60°. At LST of ~17hr the flow passes most deeply into the Earth, resulting in significant turbulence, as revealed by the Brownian motion data in Figs. 3 and 4.

Submitted on April 2, 2015 / Revised on April 17, 2015
/ Accepted on April 20, 2015

References

1. Dai J. Macroscopic Anisotropic Brownian Motion is Related to the Directional Movement of a "Universe Field". *Natural Science*, 2014, v. 6 (2), 54–58.
2. Scholkmann F. Indications for a Diurnal and Annual Variation in the Anisotropy of Diffusion Patterns – A Reanalysis of Data Presented by J. Dai (2014, Nat. Sci.). *Progress in Physics*, 2014, v. 10 (4), 232–235.
3. Scholkmann F. Solar-Time or Sidereal-Time Dependent? The Diurnal Variation in the Anisotropy of Diffusion Patterns Observed by J. Dai (2014, Nat. Sci.). *Progress in Physics*, 2015, v. 11 (2), 137–138.

4. Cahill R. T. Discovery of Dynamical 3-Space: Theory, Experiments and Observations – A Review. *American Journal of Space Science*, 2013, v. 1 (2), 77–93.
5. Cahill R. T. Combining NASA/JPL One-Way Optical-Fiber Light-Speed Data with Spacecraft Earth-Flyby Doppler-Shift Data to Characterise 3-Space Flow. *Progress in Physics*, 2009, v. 5 (4), 50–64.
6. Cahill R. T. Dynamical Fractal 3-Space and the Generalised Schrödinger Equation: Equivalence Principle and Vorticity Effects. *Progress in Physics*, 2006, v. 2 (1), 27–34.
7. Shnoll S. E. Cosmophysical Factors in Stochastic Processes. American Research Press, Rehoboth, New Mexico, USA, 2012. http://www.ptep-online.com.

Beyond Quantum Fields: A Classical Fields Approach to QED

Clifford Chafin

Department of Physics, North Carolina State University, Raleigh, NC 27695. E-mail: cechafin@ncsu.edu

A classical field theory is introduced that is defined on a tower of dimensionally increasing spaces and is argued to be equivalent to QED. The domain of dependence is discussed to show how an equal times picture of the many coordinate space gives QED results as part of a well posed initial value formalism. Identical particle symmetries are not, a priori, required but when introduced are clearly propagated. This construction uses only classical fields to provide some explanation for why quantum fields and canonical commutation results have been successful. Some old and essential questions regarding causality of propagators are resolved. The problem of resummation, generally forbidden for conditionally convergent series, is discussed from the standpoint of particular truncations of the infinite tower of functions and a two step adiabatic turn on for scattering. As a result of this approach it is shown that the photon inherits its quantization $\hbar\omega$ from the free lagrangian of the Dirac electrons despite the fact that the free electromagnetic lagrangian has no $\hbar$ in it. This provides a possible explanation for the canonical commutation relations for quantum operators, $[\hat{P}, \hat{Q}] = i\hbar$, without ever needing to invoke such a quantum postulate. The form of the equal times conservation laws in this many particle field theory suggests a simplification of the radiation reaction process for fields that allows QED to arise from a sum of path integrals in the various particle time coordinates. A novel method of unifying this theory with gravity, but that has no obvious quantum field theoretic computational scheme, is introduced.

1 Introduction

Quantum field theory, in some ways, marks the ultimate state of our understanding of physics. In its computational exactness, it can be thrilling yet its conceptual grounding is very unsatisfactory. Field theory has its origins in the 1920's and 1930's when attempts to include particle creation and the quantization of the photon necessitated a larger mathematical structure [13, 17]. Fock space seemed to have sufficient features to encompass the intrinsic quantum and particle number variable features. The ladder operators of the harmonic oscillator could be formally modified to give an algebra that allowed these various particle number spaces to interact. Different attempts to generate an equation of motion and find transition rates led to various formal procedures. Classical lagrangians were varied in a formal manner with "second quantized" operators in approaches by Schwinger and Tomanaga and systematic procedures to handle the divergent terms were introduced [15, 17]. Feynman gave a very intuitive approach using path integrals that was put into a formal structure by Dyson. This approach has gained prominence due to its ease of organizing the terms of the expansion.

Quantum mechanics is the quantum theory of fixed particle number systems. Certain quasi-classical approaches made the treatment of radiative decay possible without QED at low energies. Nevertheless, even in this low energy domain, the theory had lingering conceptural problems. Measurement and the "collapse of the wavefunction" led to paradoxes that have spawned an enormous literature [7]. Decoherence is a popular "explanation" of these effects but these tend to rely on assumptions that are just pushed off to other parts of the analysis [16]. The Born interpretation, due to its simplicity and historical inertia, still dominates most treatments of classical-quantum interactions. Some may object that there are now ways to treat measurements independently of the Born interpretation to handle to new sorts of quantum nondemolition measurements [11] but these ultimately involve other ad hoc statistical assumptions. Quantum statistical mechanics has never found any solid conceptual footing despite the frequent success of its formalism in describing thermodynamic behavior and providing numerical results. This problem is often given a short comment in books on the subject and little progress has been made. Ultimately, an initial data formulation approach must resolve all of these issues in terms of the dynamical equations and provide evidence for the kinds of initial data that is physically relevant.

The quantum field theory approach to quantum mechanics is on a solid footing. Even though operators may change the particle number, it is always changed back at every order in the expansion. One may show [15] that this gives an exact isomorphism with the Schrödinger, Heisenberg and interaction picture versions of QM. This leads to the Feynman path integral approach to quantum mechanics which, while equivalent, generally gives absurdly difficult derivations of results compared to other means. In contrast, regularization of the path integral has never had a very solid mathematical foundation but applying the theory in a "standard" fashion gives correct results. The main uses of QFT is in relativistic physics, quasiparticle motions in condensed matter and in the "Wick rotated" form which converts temporal evolution

to a high temperature expansion of the thermodynamic potentials. The correspondence of QFT in the case of quasiparticle evolution to that of Schrödinger evolution is itself challenging [2]. Fundamentally, one must give a description of the many-body wavefunction's excited states to give such a correspondence. This has led to the popularity of Green's function methods in condensed matter physics since it sidesteps this difficult work and leads directly to calculations. The validity of the derivation of the Kubo formula [8] has been extensively criticized [9] but it has, nevertheless, proved to be of great use over a broader range of phenomena than should be expected.

Given that no true classical-quantum correspondence of objects is known, it is unclear when one should impose classical structures (like hydrodynamics) on the system and when to extract certain properties (like viscosity) by quantum means. This is of particular interest in the study of ultracold gas dynamics [5] and superfluid Helium. There are popular and sometimes successful approaches for doing this but it is never clear that they must follow from the true many body dynamical theory or that we have simply made enough assumptions to stumble on to the tail of a correct derivation, the first, and correct part of which is a mystery to us. The general vagueness and nonspecificity of the subject allows theorists great freedom to generate calculations that then can be compared with experimental or Monte-Carlo data for affirmation of which ones to keep. This very freedom should undermine our reasons for faith in our theory and intuition. Instead it, together with professional publication demands, seems to create a selective pressure in favor of optimism and credulity on the part of practitioners and an air of mystical prophecy of our physics fathers and those who derive experimentally matching results.

In relativistic field theory, where particle creation is important, there are additional problems. Renormalization is necessary because of the local interactions of particles and fields. Classical physics certainly has such a problem and the radiation reaction problem of classical electrodynamics still has unanswered questions [14]. The series derived from QFT in the relativistic and quasiparticle cases tend to be asymptotic series and conditionally converging. Nonetheless, it seems very important to resum these series over subsets of diagrams to get desired approximations and Green's functions that are analytically continued to give the propagator pole structure corresponding to masses and lifetimes of resonances. The path integral itself has too large a measure to give a rigorous derivation. Regularization procedures, like putting the integrals on a Euclidean lattice for computation, length scale cutoffs, Wilson momentum cutoffs, dimensional regularization and others, are introduced to get finite results [13]. Of the conceptual problems facing quantum theory, renormalization will be shown to be a rather modest one. Justifying the use of resummation will be much more serious.

The Schrödinger approach to quantum mechanics has a special place. Questions of causality and geometric intuition are most naturally discussed in a real space picture. The diffusive nature of this equation is problematic but vanishes in the relativistic limit of the Dirac equation. Unfortunately, this is exactly where particle creation effects become important. In relativistic classical field theory, all causality questions are resolvable systematically. The structure of the equations ensures that it is valid. Other advantages of classical fields are that they are deterministic, propagate constraints exactly, give clearly obeyed conservation laws and introduce a specificity that allows all philosophical questions and thought experiments to be resolved through examination of their own mathematically consistent structure. In some cases, like relativity, our intuition may need to be updated but how this is to be done is made clear through such examples. QFT clearly works at the level of computation for many problems. This makes one believe that maybe our precursory arguments and descriptions leading to those calculations are fine and merely need elaboration. Given the success of so many calculations, it comes as a great disappointment that almost any interacting field theory is inconsistent [6].

Beyond these problems, the use of one particle lagrangians and couplings that get promoted to many body interacting theory through canonical quantization or propagator methods lead to a kind of conceptual disconnect that makes the solid implications of classical field theory, e.g. Noether's theorem and conservation laws, unclear. These conservation laws can be formally defined by a correspondence of operators and checked but are no longer strict implications of the symmetries of a lagrangian. The symmetries of one-particle systems themselves require a more explicit definition in the many body case where multiple coordinate labels of the wavefunction Ψ can describe independent motions but the current state of theory does not present a solid enough foundation to show how and when to make this manifest as an important symmetry. The meaning of a "propagator" in classical theory is simple yet it is often not appreciated that the full reality described by a Klein-Gordon (KG) field is not necessarily contained in the support of ϕ in a given constant time slice due to its second order nature. This is often lost in confusing discussions in terms of positive and negative energy components. This will be resolved for both KG and Dirac equations in the classical and quantum cases and clear up any apparently acausal effects without reference to commutation relations and formal measurement.

It is an emotionally identical state to feel that something is wrong but unclear, lacking sufficient specificity, or that we simply don't understand. The formal character of quantum field theory has produced a useful computational tool but left enough vague and ill-defined that there is plenty to improve. It is interesting that it has been proved that no interacting quantum field theory is consistent [6]. People typically shrug this off as with the other conceptual troubles in quantum theory. At some point people have to generate work or do some-

thing else but eventually formal approaches are destined to lose productivity. Beyond that is the lack of satisfaction that one really understands what one is doing. It is very common in physics to find clever solutions or long derivations that turn out to be flawed. Classical systems exist as well posed initial value problems so that they can be tackled from many angles: perturbation theory, conservation laws, idealized systems, ... A well posed such problem that describes field theory would doubtlessly open some new doors.

The foregoing was to show that some new approach to the reality described by QFT is justified. In doing so, QFT's successes are the best guide to start. In the following we will seek a well-posed classical relativistic theory over a tower of spaces of increasing dimension that will have some loose correspondence with Fock space. This will not be guided by the computational convenience it affords but logical and mathematical consistency and specificity. Since we are taking the point of view that the fields are valid at all time (so implicitly have an "emergent measurement theory" at work) we don't need to think of "particles" as something more than a label for some axes in our higher dimensional space. It will turn out that we will need a larger encompassing structure than field theory on Fock space to describe the phenomenology of QFT adequately. From this we can derive QFT phenomenology in a suitable limit and use its rigid structure to answer conceptual questions in a more convincing fashion. Since this will strictly be a deterministic covering to QFT we consider for it a new name, *deterministic wave mechanics* (DWM). Its purpose is to elucidate an explanation of why quantum field theory works and give a framework for modifications, like the inclusion of gravity, that may have a well posed structure but not exist in the framework of QFT itself. In the following we will use QED as a particular case but the generalizations will be evident.

2 Overview

The goal here is to introduce set of many particle number spaces where energy, mass, charge, probability, stress, ... can travel between the spaces at two-body diagonals. This will necessitate we make sense of multiple time labels and have a well defined set of initial data and regions where interacting fields can consistently evolve in this high dimensional many-time structure. Because there will be no "field operators" there will be no need for a translationally invariant vacuum to build particles from. If we start with N electrons, the number of photons may increase and electron-positron pairs can appear but the net charge is the same in every space where nonzero amplitude exists. This eliminates the basis of Haag's theorem and its contradiction.

Firstly, we will introduce separate equations of motion and particle labels for electrons and positrons. The amplitude of each of these will be positive locally and interactions will not change this. Negative norm states exist but are never utilized by the system. This is due to a symmetry of the dynamical equations not a constraint akin to the Gupta-Bueler formalism. The photon fields will be described by both A and $\dot{A}$ labels so that, each "photon" will now have $4 \to 2 \times 4$ coordinate labels. An important distinction here with QFT is that there will be nonzero functions in the "tower" of fields that have zero norm. For example, in a one-electron zero-photon system, $\psi(x)$ has full norm while the function in the one-electron and Φ_{em} sector is nonzero. The norm of electromagnetic fields will not be a simple square of the function amplitude but a function of its amplitude and derivatives in such a way that only if there are imaginary parts will it contribute to the "norm." Thus our tower of functions will involve many nonzero ones that have no norm and the electromagnetic field can pick up some complex components. This suggests that our theory may have a larger configuration space than QFT. A explanation of QFT may arise from this by thinking of QFT tracking the flow of norm and other conserved quantities through the system while ignoring these higher nonzero functions and, in some gauges, treating them as constraints.

Once we have a suitable configuration space, equations of motion and reasonable sense of "future" we seek a mapping of QED into the space. The tools used to treat scattering in QFT involve "adiabatic turn on/off" of the interactions, regularization and renormalization. Typically we sum over special subsets of diagrams and adjust the "bare" parameters to get the right free behavior for these modifications. The regularization can be easily dealt with as in classical theory by assuming finite size effects. This is essential for the radiation reaction. It is still unclear how QFT can treat the radiation reaction adequately so this alone may introduce new physics. The sort of initial data with interactions already "on" requires we work with a truncated set of the total space on interactions. Implicit here is that the bare parameters be chosen to give the right momenta and other observable for the "free" particles (in the sense that they are ballistic not that interactions are turned off). The structure of the theory allows us to adjust couplings and interactions with far more freedom than QFT for perturbative purposes. Resummation has always been the most dubious aspect of QFT. Conditionally convergent series should not be rearranged so having a limiting method to make sense of this is an important improvement. In this paper we will not prove an isomorphism with QED, and, given the inconsistencies in the theory, this may be for the best. A foundation is laid with some arguments for its ability to generate QED results, but given the scope of the subject, much more work remains than can be done in this one paper.

Finally we will discuss a method of combining this with gravity by promoting the γ matrices themselves. This will require some extension of most fields to allow dual pairs so that the quadratic lagrangians become bilinear. Such a method is distinct from vierbein approaches and works on a flat background. Some important extensions of the notion of gauge freedom arise here and the "reality" of the particles can be

shown to move causally yet not be definable in any obvious fashion in terms of the fields.

3 The configuration space

3.1 Dirac fields

In the early days of the Dirac equation, interpretations have evolved from a proposed theory of electrons and protons to that of electrons and positrons with positrons as "holes" in an infinitely full electron"sea" to that of electrons with positrons as electrons moving "backwards in time." The first interpretation failed because the masses of the positive and negative parts are forced to be equal. The second was introduced out of fear that the negative energy solutions of the Dirac equations would allow a particle to fall to endlessly lower energies. The last was introduced as a computational tool. The negative mass solutions were to be reinterpreted as positive mass with negative charge. Necessary fixes to this idea are subtly introduced through the anticommutation relations and the algebraic properties of the vacuum ground state used in the field theory approach.* If we are going to seek a classical field theory approach to this problem we need another mechanism.

In a universe containing only electrons and positrons we require the fields Ψ_e, Ψ_p, Ψ_{ee}, $\Psi_{ep}\ldots$ where the number of spinor and coordinate labels is given by the number of particle type labels as in $\Psi_{ee} = \Psi^{ab}_{ee}(x^\mu, y^\nu)$. The lagrangian density must distinguish electrons and positron by their charge only. Since we have not included any photons yet and we have asserted that positive norm will be enforced on the initial data (and suggested it will be propagated even in the interacting case) these will have equations of motion that follow from the related one particle lagrangians

$$\begin{aligned}\mathcal{L}_e &= i\hbar\bar{\psi}_e\gamma^\mu\nabla_\mu\psi_e - m\bar{\psi}_e\psi_e\\ \mathcal{L}_p &= i\hbar\bar{\psi}_p\gamma^\mu\nabla_\mu\psi_p + m\bar{\psi}_p\psi_p.\end{aligned} \tag{1}$$

The sign of the charge will be discussed when the electromagnetic field is added but, at this point, could be chosen either $\pm q$. We confine ourselves to the Dirac representation and the positron lagrangian is chosen so that its rest positive energy contribution is in the v component of the spinor $\binom{u}{v}$ unlike the the electron case. We will only be interested in initial data with positive energy. Later we will see that this is consistent with the kinds of creation and annihilation operator couplings in QED that allows positrons to have positive energy. We still need a lagrangian for our many particle wavefunctions. In this noninteracting case, we consider this to be built of a sum of the one particle ones so that the lagrangian of the two electron field $\Psi_{ab}(x^\mu, y^\nu)$ is

$$\begin{aligned}\mathcal{L}_{ee} = {}& i\hbar\Psi^*_{af}\gamma^0_{ab}\gamma^\mu_{bc}\nabla_\mu\Psi_{cf} - m\Psi^*_{ab}\gamma^0_{ac}\Psi_{cb} +\\ &+ i\hbar\Psi^*_{fa}\gamma^0_{ab}\gamma^\nu_{bc}\nabla_\nu\Psi_{fc} - m\Psi^*_{ab}\gamma^0_{ac}\Psi_{cb}\end{aligned} \tag{2}$$

where we have explicitly written out the indices associated with spinor labels and coordinates and the summation convention is assumed for all repeated indices. The action is to be computed by integrating over a region in the 2-fold Lorentz space $\mathbb{R}^4\times\mathbb{R}^4$. Variation of the function can be done holding it constant along y and x respectively leading to the usual equations of motion along the separate time coordinates t^x, t^y for a product function $\Psi = \psi_1(x^\mu)\,\psi_2(y^\nu)$.

From a dynamical point of view, we are mostly interested in the cases where the fields are all evaluated at equal times. However we should ask what it even means to evaluate a function at two different times. When is this even meaningful? If we specify $\Psi(x^\mu_1, x^\nu_2)$ at $t_1 = t_2$ we desire to know into what region of this many-time future we should expect a solution. Further explanation of the equal time evolution is discussed in Sec. 3.4.

Considering free propagators we can evolve the data from (x_1, x_2) in the t_1 direction indefinitely and similarly for t_2. The domain of dependence is then the union of the two backwards light-cones $|x'_1 - x_1| < c\,(t_{1'} - t_1)$ and $|x'_2 - x_2| < c\,(t_{2'} - t_2)$. Interactions will allow free evolution for such a function except on 2-body diagonals $x^\mu = y^\nu$. When these cones intersect these regions sources and sinks with other particle number functions will arise. When these produce a net change in amplitude versus simply a potential force remains to be seen. Furthermore, it is still unclear that we can derive the static electromagnetic force effects from such a restricted local interaction. This will be explained later but first we investigate the case of free photons.

3.2 Photons

The classical electromagnetic field is a real vector field A^μ. For our many body generalization as $\Psi^\mu_a \sim \psi_a(x)\,A^\mu(y)$ we will have, generally nonseparable, combinations of electromagnetic and electron fields so making the assignment of which is "real" is ambiguous. We will find that phase differences between these fields on the many body diagonals give sources and sinks of amplitude from one particle number space to another. Firstly, let us consider the classical electromagnetic field which we can, loosely, think of as a single particle field.† The lagrangian of the electromagnetic field is

$$\mathcal{L}_A = -\frac{1}{4}F^{\mu\nu}F_{\mu\nu} \tag{3}$$

where $F_{\mu\nu} = \partial_{[\mu}A_{\nu]} = \partial_\mu A_\nu - \partial_\nu A_\mu$. For now consider only the "classical" field theory case where we have one field of each type on $\mathbb{R}^4$. The complex Klein-Gordon field has a norm conservation law induced by the global phase change $\phi \to \phi e^{i\gamma}$. In this case of a noninteracting electromagnetic field we have equations of motion $\Box A^\mu = 0$ and, allowing complex values, we have four independent global phase changes allowed in

*It is interesting to note that it is precisely the properties of this ground state that lead to the inconsistencies shown by Haag's theorem.

†Generally classical electromagnetic fields are considered as combinations of photon fields of all photon number.

addition to the usual $A_\mu \to A_\mu + \nabla\xi$ gauge freedom. We will revisit this shortly and reveal how photon quantization arises naturally from the lagrangian once coupling is introduced.

One important distinction of the electromagnetic fields versus the Dirac fields is that the equations are second order. These can be rendered into first order equations by introducing an auxiliary field $C^\mu = \dot{A}^\mu$ so that the equations of motion become

$$\begin{aligned} \partial_t A^\mu &= C^\mu \\ \partial_t C^\mu &= \partial_i \partial^i A^\mu. \end{aligned} \tag{4}$$

The extension to the many particle case leads to a proliferation of functions akin to the rapid number of increasing spin states for multiple Dirac fields. In each time direction of a two photon state $A^{\mu\nu}(x^\alpha, y^\beta)$ we need first and second order time derivatives. A complete set of first order initial data is then A, $C_x = \partial_{t^x} A$, $C_y = \partial_{t^y} A$, and $C_{x,y} = \partial_{t^x,t^y} A$ with equations of motion

$$\begin{aligned} \partial_{t^x} A^{\mu\nu} &= C_x^{\mu\nu} \\ \partial_{t^y} A^{\mu\nu} &= C_y^{\mu\nu} \\ \partial_{t^x} C_x^{\mu\nu} &= \partial_i \partial^i A^{\mu\nu} \\ \partial_{t^y} C_y^{\mu\nu} &= \partial_j \partial^j A^{\mu\nu} \\ \partial_{t^x} C_y^{\mu\nu} &= \partial_{t^y} C_x^{\mu\nu} = C_{x,y}^{\mu\nu} = C_{y,x}^{\mu\nu} \\ \partial_{t^x} C_{x,y}^{\mu\nu} &= \partial_i \partial^i C_y^{\mu\nu} \\ \partial_{t^y} C_{x,y}^{\mu\nu} &= \partial_j \partial^j C_x^{\mu\nu} \end{aligned} \tag{5}$$

where the roman indices are spatial indices related to the corresponding spacetime indices as $(t^x, x^i) = x^\mu, (t^y, y^j) = y^\nu$, etc. We can see that the number of first order fields for a source free N-photon system is $4 \cdot 2^N$ analogous to the number of spin subspaces for an N-electron system. A convenient notation for this is (P, Q) where P, Q can be 0 or 1 and the pair indicates how many derivatives of A with respect to x and y are taken. This notation gives (suppressing spacetime indices)

$$\begin{aligned} A &= C_{00} \\ C_x &= C_{10} \\ C_y &= C_{01} \\ C_{x,y} &= C_{11} \end{aligned} \tag{6}$$

which will be convenient for later generalization.

3.3 Interactions

The presence of interactions is what makes dynamics interesting. The mixing of gauge freedom means that any notion of "reality" of an electron now involves a photon field as is illustrated through the Aharonov-Bohm (A-B) effect. This is seen in the definition of a gauge invariant electron current in its explicit use of A. In the many body case we need a set of interaction terms tailored for our, now distinct, equations of motion for electrons and positrons. It also radically constrains our domain of dependence in this many time coordinate space.

Let us begin with the classical or "one body" case. The interaction terms tailored for electrons and positrons are respectively:

$$\begin{aligned} \Lambda_{eA} &= -q\bar{\psi}_a^{(e)} \gamma_{ab}^\mu A_\mu \psi_b^{(e)} \\ \Lambda_{pA} &= -q\bar{\psi}_a^{(p)} \gamma_{ab}^\mu A_\mu \psi_b^{(p)}. \end{aligned} \tag{7}$$

The free Dirac equation does not require such extra terms but we will include them from now on to make the interaction terms nicer. The sign stays the same here because of the sign flip in the charge induced by the γ^0 factor in the Dirac representation where we assume the amplitude for the resting positron is chosen in the "v" component of the spinor $\psi = \binom{u}{v}$. We previously changed the sign of the mass term in $\mathcal{L}_p$ so that the energy of this field is positive.

Including the interaction term $\mathcal{L}_e$, variation of the action yields the equations of motion

$$\begin{aligned} \tfrac{\partial F_{\mu\nu}}{\partial x^\nu} &= q j_\mu = q\bar{\psi}\gamma\psi \\ i\hbar\gamma\psi + qA^\mu\gamma_\mu\psi - m\psi &= 0. \end{aligned} \tag{8}$$

These are not all dynamic. Since the first is a second order equation of motion, the equations of motion must have two time derivatives. In this case we have the constraint $\nabla \cdot E = q\rho = q j_0$ which is propagated by the equations of motion. This is induced by the conservation law we derive from the sources, $\partial_\mu j^\mu = 0$ which shows that only three of these equations are now dynamical. We can rewrite this as a set of first order equations by the definition $C_\mu = \partial_t A_\mu$. Choosing the Lorentz gauge, $\partial_\mu A^\mu = -C_t + \partial_i A^i = 0$, we obtain $\Box A^\mu = q j^\mu$ in a form that automatically generates compatibility with the conservation of charge and is propagated for all time.

Interactions for the many body case, QED, involves two ways of coupling electrons and positrons to the electromagnetic field: a lone electron can couple to a lone electron and a photon or a photon can couple to an electron and a positron. We are not interested in any of the common "backwards in time" mnemonics or procedures here since this is an initial value approach. Firstly we should give a picture of the "tower" of states that need to be coupled.

$$\begin{aligned} &\alpha \\ &\Psi^\mu_{(A),Q}(x), \Psi^{\mu\nu}_{(AA),QR}(x,y)\dots \\ &\Psi_{(e),a}(x), \Psi^\mu_{(eA),aQ}(x,y), \Psi^{\mu\nu}_{(eAA),aQR}(x,y,z)\dots \\ &\Psi_{(p),a}(x), \Psi^\mu_{(pA),aQ}(x,y), \Psi^{\mu\nu}_{(pAA),aQR}(x,y,z)\dots \\ &\Psi_{(ep),ab}(x,y), \Psi^\mu_{(epA),abQ}(x,y,z), \\ &\qquad\qquad , \Psi^{\mu\nu}_{(epAA),abQR}(x,y,z,w)\dots \\ &\dots \end{aligned} \tag{9}$$

The first line holds a complex value α that indicates occupancy of the "vacuum" state. The next line gives the pure photon states. The N photon state has $4 \cdot 2^N$ degrees of freedom (dof) in the free case if we have not imposed any gauge constraints. Below this are the one electron states with the 1, 2, ... photon states to the right. Below are the one positron states with the various photon number states then the electron and positron states with corresponding photon number cases. The action to describe these as free fields is given by a collection of independent actions

$$\begin{aligned} S_{(e)} &= \int \left(i\hbar \Psi^*_a \gamma^\mu_{ab} \partial_\mu \Psi_b - m \Psi^*_a \Psi_a \right) dx \\ S_{(ee),1} &= \iint \left(i\hbar \Psi^*_{ba} \gamma^0_{bc} \gamma^\mu_{cd} \partial_\mu \Psi_{da} - m \Psi^*_{ba} \gamma^0_{bc} \Psi_{ca} \right) dxdy \\ S_{(ee),2} &= \iint \left(i\hbar \Psi^*_{ab} \gamma^0_{bc} \gamma^\nu_{cd} \partial_\nu \Psi_{ad} - m \Psi^*_{ab} \gamma^0_{bc} \Psi_{ac} \right) dxdy \\ &\dots \end{aligned} \tag{10}$$

The action for a single particle photon field is

$$\begin{aligned} S_{(A)} &= -\int \tfrac{1}{4} F^{\mu\nu} F_{\mu\nu} \, dx \\ &= -\tfrac{1}{4} \int \left(\partial^{[\mu} \Psi^{*\nu]}_{(A)} \right) \left(\partial_{[\mu} \Psi^{(A)}_{\nu]} \right) dx \end{aligned} \tag{11}$$

where we have included a complex conjugation. This seems unnecessary since we generally consider the electromagnetic field to be real. When we consider the functions that correlate electron and photon fields we will see that we cannot neglect it. The two photon actions are*

$$\begin{aligned} S_{(AA),1} =& -\tfrac{1}{4} \int \left(\partial^{[\mu}_{(x)} \Psi^{*\nu]\alpha}_{(AA)}(x^{\cdot}, y^{\cdot}) \right) \\ & \left(\partial^{(x)}_{[\mu} \Psi^{(AA)}_{\nu]\alpha}(x^{\cdot}, y^{\cdot}) \right) dxdy \\ S_{(AA),2} =& -\tfrac{1}{4} \int \left(\partial^{[\mu}_{(y)} \Psi^{*\nu\alpha]}_{(AA)}(x^{\cdot}, y^{\cdot}) \right) \\ & \left(\partial^{(y)}_{[\mu} \Psi^{(AA)}_{\nu\alpha]}(x^{\cdot}, y^{\cdot}) \right) dxdy \\ S_{(AC),1} =& -\tfrac{1}{4} \int \left(\partial^{[\mu}_{(x)} \Psi^{*\nu]\alpha}_{(AC)}(x^{\cdot}, y^{\cdot}) \right) \\ & \left(\partial^{(x)}_{[\mu} \Psi^{(AC)}_{\nu]\alpha}(x^{\cdot}, y^{\cdot}) \right) dxdy \\ S_{(CA),2} =& -\tfrac{1}{4} \int \left(\partial^{[\mu}_{(y)} \Psi^{*\nu\alpha]}_{(CA)}(x^{\cdot}, y^{\cdot}) \right) \\ & \left(\partial^{(y)}_{[\mu} \Psi^{(CA)}_{\nu\alpha]}(x^{\cdot}, y^{\cdot}) \right) dxdy \end{aligned} \tag{12}$$

where the $1, 2, \dots$ subscripts on the actions indicate the respective coordinate label $x^{\cdot}, y^{\cdot} \dots$ where the derivatives are being taken. The previous notation we used to distinguish coordinate order for the Dirac fields is not available here because of the more complicated index structure and we replace A and C as field labels with $\Psi_{(A)}$ and $\Psi_{(C)}$ for the sake of a uniform notation when both electrons and photons are present. Here we explicitly include the coordinates and label the first coordinate, $x^{\cdot}$, in the derivative operator $\partial^\mu_{(x)}$ and order the indices in $\Psi^{\mu\nu}$ to correspond to $x^{\cdot}$ and $y^{\cdot}$ respectively. The square backets, [ ], indicate antisymmetry over the two indices immediately to their open sides. The first order time derivative data from the "inactive" coordinates, those not being dynamically evolved by the particular lagrangian, are included with the C labels to get a full set of first order initial data. Variation of these lagrangians, through a combination of explicit and implicit expressions, gives the four functions $\Psi^{\mu\nu}_{(C_{PQ})}$ and eight linear Equations of Motion (EoM) for each function in each of the two time directions t^x, t^y.

The (noninteracting) mixed one-electron one-photon actions on $\Psi(x^{\cdot}, y^{\cdot})$ to generate EoM in each time label are

$$\begin{aligned} S_{(eA),1} =& \int \left(i\hbar \Psi^{*,\nu}_{(eA),a} \gamma^\mu_{ab} \partial^{(x)}_\mu \Psi_{(eA),b\nu} - \right. \\ & \left. - m \Psi^{*\nu}_{(eA),a} \Psi^{(eA)}_{a\nu} \right) dx \\ S_{(eA),2} =& -\tfrac{1}{4} \int \left(\partial^{[\mu}_{(y)} \Psi^{*\nu]}_{(eA),a} \right) \left(\partial^{(y)}_{[\mu} \Psi^{(eA)}_{a\nu]} \right) dx. \end{aligned} \tag{13}$$

Generalizations to higher particle numbers from here are evident but rapidly become onerous. Symmetries among identical particle types are not required by these actions but it is not hard to see that imposing them as initial data lets them be propagated.

To give an interesting theory there must be interactions. The vacuum u is strictly formal and does not couple to anything. We know that electrons and positrons can annihilate and electrons/positrons can scatter and produce a photon. The couplings must be "local" in some sense that we enforce, with inspiration from QED, as

$$\begin{aligned} S_{(e)} =& \int \left(i\hbar \bar{\Psi}^*_a \gamma^\mu_{ab} \partial_\mu \Psi_b - m \bar{\Psi}^*_a \Psi_a \right) dx \\ & + \Lambda_{(e-eA)} \\ S_{(eA),1} =& \int \left(i\hbar \bar{\Psi}^{*,\nu}_{(eA),a} \gamma^\mu_{ab} \partial^{(x)}_\mu \Psi_{(eA),b\nu} - \right. \\ & \left. - m \bar{\Psi}^{*\nu}_{(eA),a} \Psi^{(eA)}_{a\nu} \right) dx + \Lambda_{(eA-eAA)} \\ S_{(eA),2} =& -\tfrac{1}{4} \int \left(\partial^{[\mu}_{(y)} \Psi^{*\nu]}_{(eA),a} \right) \left(\partial^{(y)}_{[\mu} \Psi^{(eA)}_{a\nu]} \right) dx + \\ & + \Lambda_{(e-eA)} + \Lambda_{(eep-eA)} \\ &\dots \end{aligned} \tag{14}$$

where the "bar" action over the Ψ is hiding a γ^0 considered to be contracted on the active spinor indices. Here we see that the one-electron field $\psi = \Psi_{(e)}$ feels the electromagnetic field from $\Psi_{(eA)}$ as we evolve in its time coordinate direction $t^{(e)}$. The notion of locality for this interaction is chosen so that ψ feels the field of $\Psi_{(eA)}$ when all three spacetime coordinates agree. In this case, this gives only a self energy contribution but will give the usual two body static interaction for two charges. Conversely, the field $\Psi_{(eA)}$ feels the influence of ψ as a source where all three coordinates agree when we evolve in the time direction $t^{(eA)}_2$, the second time label corresponding

*The "upper" or "lower" state of the particle type labels (AA), (AC), (eA) etc. have no meaning but are chosen to make the expression as uncluttered as possible. Summation conventions are in effect for spacetime and spinor indices.

to A. For an electron-positron pair production or annihilation amplitude we give a similar definition of locality.

Explicitly, the couplings are

$$\begin{aligned}\Lambda_{e-eA} &= -q\int \bar{\Psi}^{(e)}_{a}(x^{\cdot})\gamma^{\mu}_{ab}\Psi^{(eA)}_{\mu,b}(y^{\cdot},z^{\cdot})\delta(x^{\cdot}-y^{\cdot})\\ &\quad \delta(x^{\cdot}-z^{\cdot})\,dxdydz\\ \Lambda_{p-pA} &= -q\int \bar{\Psi}^{(p)}_{a}(x^{\cdot})\gamma^{\mu}_{ab}\Psi^{(pA)}_{\mu,b}(y^{\cdot},z^{\cdot})\delta(x^{\cdot}-y^{\cdot})\\ &\quad \delta(x^{\cdot}-z^{\cdot})\,dxdydz\\ \Lambda_{ep-A} &= \pm q\int \Psi^{(ep)*}_{ab}(x^{\cdot},y^{\cdot})\gamma^{0}_{ac}\gamma^{\mu}_{cb}\Psi^{(A)}_{\mu}(z^{\cdot})\delta(x^{\cdot}-y^{\cdot})\\ &\quad \delta(x^{\cdot}-z^{\cdot})\,dxdydz.\end{aligned} \tag{15}$$

The sign of the pair production term is not clearly constrained here and neither is our choice of where to place the complex conjugations. Comparison with QED suggests that the sign be chosen negative and these be the correct choices of conjugation and contraction with γ^0 factors. The evolution of the free equations ensures conservation of the stress-energy, charge and particle number. These coupling terms can introduce relative phase differences at these many-body diagonals so can act as source and sink terms for amplitude. The complexity of the quantum version of the photon is important in generating these sources and in creating a norm conservation law that governs the flow of "norm-flux" between these spaces. Interestingly the conservation of charge and norm arise from the same global phase symmetry. The electron-positron field has no net charge yet will have a well defined norm from the phase symmetry $\Psi_{ab}\rightarrow e^{i\theta}\Psi_{ab}$ in the free lagrangians

$$\begin{aligned}S_{(ep),1} &= \iint\left(i\hbar\Psi^{*}_{ba}\gamma^{0}_{bc}\gamma^{\mu}_{cd}\partial^{(x)}_{\mu}\Psi_{da}-\right.\\ &\quad \left.-m\Psi^{*}_{ba}\gamma^{0}_{bc}\Psi_{ca}\right)dxdy\\ S_{(ep),2} &= \iint\left(i\hbar\Psi^{*}_{ab}\gamma^{0}_{bc}\gamma^{\nu}_{cd}\partial^{(y)}_{\nu}\Psi_{ad}+\right.\\ &\quad \left.+m\Psi^{*}_{ab}\gamma^{0}_{bc}\Psi_{ac}\right)dxdy.\end{aligned} \tag{16}$$

There is an obvious extension of these interactions to the tower of fields. We need to discuss why the equal times slice of the evolution* here is most related to what we see and experience. Before we do this let us consider the electrostatic interaction between two electrons. It has always seemed a little ad hoc that we impose the two point interaction $\frac{q}{4\pi}|x_1^2-x_2^2|^{-1}$ for a function $\Psi(x,y)$ in quantum mechanics. Certainly we can write down a one body wavefunction $\psi(x)$ and vector potential A^{μ} and impose a classical 4D lagrangian. We find an electrostatically driven self spreading distribution where the density of the norm gives the charge density. This is not at all what we see for the two charge quantum system. No such self-force is manifested beyond the usual quantum pressure.

*Specifically, for any many body point of any function of the tower, we choose all the times corresponding to the spatial coordinates equal: $t^1=t^2=t^3\ldots$.

Given the fields $\Psi^{(ee)}_{ab}(x^{\cdot},y^{\cdot})$ and $\Psi^{(eeA),\mu}_{ab}(x^{\cdot},y^{\cdot},z^{\cdot})$, we see that when we impose the Coulomb gauge that

$$\Psi^{(eeA),t}_{ab}=\Psi^{(ee)}_{ab}(x,y)\,\frac{q}{4\pi}\left(|\vec{x}^{\,2}-\vec{z}^{\,2}|^{-1}+|\vec{y}^{\,2}-\vec{z}^{\,2}|^{-1}\right). \tag{17}$$

The nature of the self-energy for such a theory seems more opaque than in the classical case where we can consider it in terms of finitely sized objects [14]. Locality and causality here are not so forgiving with such a construction and a constituent based approach would likely require an infinite number of fields of vanishing mass and charge that bind to a state of finite extent with the center-of-mass coordinates appearing as the x^{μ},y^{ν} coordinates in our $\Psi^{(ee)}_{ab}$. We will not discuss this point further but should be aware of the complication in managing self field contributions that affect both the energy and momenta of particles. Shortly we will see that even though $\Psi^{(eeA),t}_{ab}$ is nonzero it contains zero norm and that there is an infinite tower of such nonzero fields above it. This is not so evident in QFT which we may think of as tracking the nonzero norm of the fields through the tower. Now would be a good time to emphasize that these are all classical fields in a tower of spaces of growing dimensionality. There are no Grassmann variables, q-numbers or field operators and their associated commutation relations. These have always been conceptually dubious or ad hoc constructions on which field theory is built and the goal of our construction is to show why (and when) they work.

3.4 Diagonal time evolution

The relationship between the quantum and classical worlds is an enduring problem. It is not just explaining quantum measurement that is troublesome. Encoding the classical world in a quantum description is a challenge to do correctly. Naive approaches have led to such useful results as band theory and the Kubo relations but ultimately lead to inconsistencies. One approach is to assume the classical world is a very restricted subset of localized many body wavefunctions that are sparsely distributed in the total Fock space. The usual quantum statistics then follow trivially along with an arrow of time [1, 3]. The new problem is justifying such initial data. In this many time description we have the further challenge of justifying why we, as observers, seem to observe the universe of "equal times" and not the vast regions of unequal space and time locations where the many body quality of the description is more evident.

Possible explanations for this is that interactions occur at many body diagonals. Since our observations require interactions this is the part of the universe we see. In general, many body wavefunctions do not act in a form similar to discrete state machines which seem to underlie our notions of memory and consciousness. The special cases do seem to define our classical world. We will show that the equal times evolution defines the motion everywhere so all the other regions are

defined by them and so give no other possible observations of the world.

As an example, consider the evolution of the two photon field $A^{\mu\nu}(x^\alpha, y^\beta)$ along the $t^x = t^y$ axis with respect to $t = t^x + t^y$

$$\begin{aligned}
\partial_t A^{\mu\nu} &= C_x^{\mu\nu} + C_y^{\mu\nu} \\
\partial_t C_x^{\mu\nu} &= \partial_i \partial^i A^{\mu\nu} + C_{x,y}^{\mu\nu} \\
\partial_t C_y^{\mu\nu} &= \partial_j \partial^j A^{\mu\nu} + C_{x,y}^{\mu\nu} \\
\partial_t C_{x,y}^{\mu\nu} &= \partial_i \partial^i C_y^{\mu\nu} + \partial_j \partial^j C_x^{\mu\nu}.
\end{aligned} \tag{18}$$

It is unclear if this is particularly useful but it does illustrate how the evolution along the equal times axis is locally determined in the equal time coordinate t. However, we still need to evolve spatially in a neighborhood of this diagonal so the many body and many time propagator approach seems hard to avoid.

3.5 Quantization of the photon

Here we show that the quantization of the photon inherits its norm from the purely electron part of the lagrangians. This is the photon analog to the way that the "reality" of the Schrödinger electron picks up a contribution from A in the current $j^k = \frac{\hbar}{m}\nabla^k\phi - eA^k$.* This explains how the photon quantization condition can be a function of $\hbar$ despite having no such factor in its own lagrangian. It is quantized in the sense that if all the amplitude (normalized to 1) is initially in the lepton fields then it is all converted to a photon then the factor $\hbar\omega$ gives the magnitude of the photon norm. Up to this point we have been using units where $c = \mu_0 = \epsilon_0 = 1$ but left $\hbar$ general. In this section, we revert to full SI units to emphasize this connection more clearly.

In the free field cases, the usual definitions of momentum, energy... follow from the stress tensors for the classical Dirac and electromagnetic fields regardless of whether they are real or complex. The one additional conserved quantity that Dirac fields have is "norm" associated with the complex global phase freedom. The fields in the tower possess a U(1) symmetry in the sense that $\Psi \to \Psi e^{i\theta}$ and similar transformations for every function in the tower leaves the set of lagrangians invariant. When a fermion and photon field interact the coupling terms act as complex source terms resulting in, for example, a complex $\Psi^{(eA)}$ functions as the amplitude of $\Psi^{(e)}$ decreases. Since this is not generally a separable function, we cannot say whether the photon or electron part is complex individually but can predict the phase difference between the function pair and derive a many body conserved norm.

Firstly, we can modify the photon lagragian to allow complex fields as

$$\mathcal{L}_A = \frac{1}{4\mu_0}\left(\partial_\mu A^*_\nu \partial^\mu A^\nu + \partial_\mu A_\nu \partial^\mu A^{\nu^*}\right) \tag{19}$$

*We have neglected the "spin current" fraction here for simplicity.

This is essentially the massless Klein-Gordon field. The conserved current is

$$j_\mu = \frac{i}{4\mu_0}\left(\partial_\mu A_\nu \cdot A^{*\nu} - A_\nu \cdot \partial_\mu A^{*\nu}\right) \tag{20}$$

Consider the case of a complex plane wave solution $A_y(x,t) = \mathcal{A}e^{i(kx-\omega t)}$. If this was a real (classical) field there would be no current and norm would equal zero. For the complex case, $\rho = j_0 = \mathcal{A}^2\omega/2\mu_0$ and $j_x = -\mathcal{A}^2 k/2\mu_0$. In computing the norm for $\Psi^{(eA)}$ we need to use this $j^0_{(A)}$ and evaluate

$$\begin{aligned}
\hat{\mathcal{N}}(\Psi_{(eA)}) = \tfrac{i}{2\mu_0}\iint \Big(&\partial_t^{(A)}\Psi^{(eA)}_{a\nu}\Psi^{*\nu}_{(eA),a} - \\
&-\Psi^{(eA)}_{a\nu}\partial_t^{(A)}\Psi^{*\nu}_{(eA),a}\Big)\,dx^3dy^3 \\
= \tfrac{i}{2\mu_0}\iint \Big(&\Psi^{(eC)}_{a\nu}\Psi^{*\nu}_{(eA),a} - \\
&-\Psi^{(eA)}_{a\nu}\Psi^{*\nu}_{(eC),a}\Big)\,dx^3dy^3
\end{aligned} \tag{21}$$

where $\hat{\mathcal{N}}$ is the norm operator defined by j^0 for the argument function. A Dirac field gives a conserved $\int \psi^*\psi$ so this clearly gives the correct electron-photon conserved current in the noninteracting case so this is the quantity that is conserved along the equal times diagonal. Let the volume of the space be $V = 1$. Now let us investigate the implications of simultaneous conservation of energy and norm in a radiative decay process.

Suppose we start with an excited positronium state $\Psi^*_{(ep)}$ that radiates with frequency ω into the state $\{\Psi_{(epA)}, \Psi_{(epC)}\}^\dagger$ and possibly higher photon number ones. The resulting photon must have the same frequency ω since this is the frequency at which the source term oscillates. The initial norm for the states is $\hat{\mathcal{N}}\Psi_{(ep)} = 1$ and $\hat{\mathcal{N}}\Psi_{(epA)} = 0$. Our goal is to find the resulting norms after the transfer is completed, in these units. This will tell us the ratio of energy to norm transferred, which we construe as the meaning of photon quantization.

Assume the resulting function is $\Psi_{(epx)} = \Psi'_{(ep)}\mathcal{A}e^{i(kx-\omega t)}$ where $\hat{\mathcal{N}}(\Psi'_{(ep)}) = 1$. Since these lagrangians are coupled the coefficients they define a relative size for them which are respectively $\hbar$ at $t = 0$ (from the factor in the kinetic term in the electron and positron lagrangians) and

$$\hat{\mathcal{N}}\Psi_{(epA)} = \hat{\mathcal{N}}\Psi_{(A)} = \mathcal{A}^2\omega/2\mu_0 \tag{22}$$

at $t = t_f$. Since these must be equal we obtain the amplitude of the wave as $\mathcal{A} = (2\mu_0\hbar/\omega)^{1/2}$. The final energy of the system must be the same with the electron and positron in a new state with $\Delta E_{(ep)} = \Delta E_{(epA)}$. The photon contribution is given by $E_{(A)} = \int \frac{1}{2\mu_0}C^2 dx = \frac{1}{2\mu_0}\mathcal{A}^2\omega^2 = \hbar\omega$. This shows that to radiate any more energy an additional photon would need to be generated.

†Note that the notation $\{,\}$ does not denote anticommutation here. These are functions and the braces here just indicate a set.

In quantum mechanics and quantum field theory this is one of the assumptions that is hidden in the formalism. Since we are constructing an explicit classical field theory we do not have such a liberty. It was not, a priori, necessary that a transfer of energy, $\hbar\omega$, from a decay between two eigenstates give a unit norm transfer. We might have had a partial occupancy of the $\Psi_{(epA)}$ state and not completely emptied the $\Psi_{(ep)}$ one or had to resort to higher $\Psi_{(epAA\ldots)}$ states to contain all the norm that was generated by the event. This is the first actual derivation of the "quantization" of the photon. In this model, the statement of photon quantization is more precisely stated that the ratio of energy flux to norm flux between different photon number states is $j_E/j_n = \hbar\omega$, at least for the case where the frequency of the radiation is monochromatic. It is interesting that the photon "norm" depends on $\hbar$ even though the only lagrangian with such a factor is that of the fermions. The coupling has done several things. It introduces a constraint on one of the components of the electromagnetic field from the current conservation of the charges. It mixes the "reality" of the A and ψ fields to give the electron current. Here we see that it also induces the proportionality constant in the norm flux of the photon between different particle number spaces. This relationship between norm and energy flux may be what underlies the success of the formal commutation relations for field operators $[\hat{P}, \hat{Q}] = i\hbar$ [4].

4 Dynamics

We have not firmly established an isomorphism with QED for a precise subset of initial data. Ideally, imposing the usual particle symmetries on such data and evolving will match the usual scattering amplitudes. We have several barriers to doing this. Firstly is renormalization and the singularity of the coupling terms. The dimensionality of the space is so enormous and the number of nonzero yet norm free subspaces is infinitely large so finding an economical and compact manner to even start the problem is unclear if possible at all. Even finding the suitable "dressed" particles to scatter is not yet accomplished. The largest hurdle to overcome is probably the fact that no interacting field theory is well defined by Haag's theorem. This has been solved here so it might be unfair to even ask for an isomorphism between the theories. However, QED has a record of impressive calculations and the most reasonable notion of "isomorphism" may be to reproduce these. The foundational aspects of QED were designed after the fact on the tail of a process of refining procedures to obtain useful calculations so the inconsistency of these foundations may not be so important. Let us begin with a process of restricting the subspaces in a fashion that gives observable particles with enough of the interactions necessary for good approximations. Given the expanse of QED we cannot do all the work necessary to make a convincing case for this theory in a single paper. Some of this section is meant to be suggestive of more essential work ahead, not an exhaustive argument or thorough calculation to this end.

4.1 Scattering and adiabatic coupling changes

One of the most frustrating aspects of QFT is that the interim state of the system is clouded in the language of "virtual particles" and it seems to be not well defined at every time. Our measurements are confined to in and out states once the interactions are over. This is a formulaic extension to bound states where the interaction persists but this does not solve this problem. The current formulation shows that there is a well defined state at every time. Ironically, the in and out state picture has more problems at $t = \pm\infty$! This is because the interactions have been "turned off" here so the "virtual cloud" of many particle states that must always accompany a particle are no longer there. By adjusting the bare mass parameter slowly we can make an association with such states of the same net mass and momentum.

This is already formally discussed in many books. Here we will make some small changes that don't affect the results but make the process a bit more logical. Firstly, notice that the equations of motion above have been selected to give the usual propagators in the single time coordinate functions and the couplings to model those of QED. The role of the many photon coordinate spaces has been suppressed by the QED formalism and we see that there are many more spaces to consider than in the usual treatment. Once we impose the Coulomb gauge, we see that many of the constraints described by the "longitudinal photons" are just nonzero zero-norm functions in the tower.

If we consider the case of scattering of two particles, say an electron and a positron, we should properly "dress" them first. This suggests we partition our tower into a set of higher photon and electron-positron pair spaces that only couple to these particles separately. By turning on the interaction parameters slowly enough we can force the net mass and momentum of these waves to be the same without inducing any unwanted reflection. Since we typically work with plane waves of infinite extent instead of wave packets, we don't have a natural way to let spatial separation of packets prevent them from interacting but we can now use a second adiabatic turn on that lets these towers now interact and couple to the set of higher photon and electron-positron pair spaces that include both of these in more interesting ways. The more flowery aspects of QED such as "the positron is an electron moving backwards in time" is removed by our positive mass independent equation for the positron and superluminal virtual particles are now to be understood as a feature of evolving propagators in separate time spaces to arrive at the equal times result. We will now show that the apparent superluminal contributions to the Feynman propagator is actually a constraint on consistent initial data not faster than light effects that are cancelled by a measurement ansatz.

4.2 Causality considerations

The divergences we see in field theory with interactions are directly related to the singular nature of the δ-function coupling in the lagrangian. This is usually phrased in the loose semi-classical language of quantum theory as the "particles are point-like". We already expressed that our opinion was that finer nonsingular structure existed at a level we cannot yet probe. The oldest method of handling such a situation is with "cutoffs". Naively done, these are intrinsically nonrelativistic for reasons of their small nonlocality. We can make them as mild a problem as possible by choosing them in the local frame defined by the two body currents at the interaction diagonal. Specifically, it is here we need to couple two fields such as $\Psi_{(e)}$ and $\Psi_{(eA)}$ so that the electron field of $\Psi_{(e)}$ generates the electromagnetic field in $\Psi_{(eA)}$ as a source at the $x_e = x_A$ diagonal. The current $j^\mu(\Psi_{(e)})$ defines a velocity $v = j/\rho$. This specifies a local frame to construct a spherical region of radius r_0. We can then modify the electromagnetic source interaction term as $\bar{\Psi}_{(e)}\gamma^\mu\Psi_{(eA);a\mu}\delta(x_{(e),1} - x_{(e),2})\delta(x_{(e)} - x_{(A)}) \to \bar{\Psi}_{(e)}\gamma^\mu\Psi_{(eA);a\mu}\delta(x_{(e),1} - x_{(e),2})f(v, x_{(e)}, \Theta(r_0 - |x_{(e)} - x_{(A)}|))$ where f gives a boost distortion to the r_0 sphere in the rest frame defined by the current. As long as the oscillations we consider are much longer than r_0 this has little contribution to nonlocal and nonrelativistic errors for a long time. It does create a recursive (hence nonlinear) definition. We only expect cutoffs to be useful when the details of the cutoff are not important in the result. It is expected that this extension of the usual cutoff procedure will give new radiation reaction contributions not present in QED although it is possible that other regularization procedures to cut off integrals may effectively do this implicitly. The small range of the boost dependent shape of the cutoff has effects only for field gradients that can probe it, however, this is exactly the case in the radiation reaction problem. There is considerable belief that the radiation reaction force and rate of particle creation is not captured by standard QED and that all such approaches are plagued with the pre-acceleration problems standard in the classical case [14] but some useful limits have been derived [10].

The perturbative schemes generally built on the interaction representation yields a time ordered exponential [13, 17] of terms ordered by the number of discrete interactions in the terms. The details of this construction allow S_F to be pieced together from forwards and backwards propagators in a spacelike slice. This results in a propagator that lives outside the light cone. Usual arguments [13] tell us that the vanishing of the commutator of the field operators outside the light cone is sufficient for causality, an explanation that sounds excessively hopeful and reaching but all too familiar to students of QFT. For our initial data formalism there is no such analog. Firstly let us argue that this unconfined behavior of $S(x - y)$ at $t^x = t^y = 0$ is not an expression of acausal behavior just a statement that the "reality" the initial data has not been localized to start with. How can this be? We could start with a classical delta function source and evolve with this and arrive at a true solution that evolves past the light cone. The usual answer to this is obscured by the usual cloudy use of positive and negative energy states in QFT. Here we have distinct equations of motion or electrons and positrons so the "negative energy" components are a reality to contend with and not to be "reinterpreted" through some measurement ansatz.

To address this consider the case of the classical (massive) KG equation

$$\nabla^2\phi - \partial_t^2\phi = \frac{m^2}{\hbar^2}\phi \tag{23}$$

where the propagator has the same problem. Here the initial data is ϕ and $\dot{\phi}$. Localizing ϕ as a delta function gives

$$\begin{aligned} \phi &= \sum e^{i(px-\omega t)} \\ \dot{\phi} &= -i\sum E_p e^{i(px-\omega t)} \end{aligned} \tag{24}$$

where $E_p = \omega(p) = \sqrt{p^2 + m^2/\hbar^2}$. This shows that whatever reality is associated with the KG field ϕ is not localized even though ϕ itself is. Interestingly, if we force localization of $\dot{\phi}$ then $\phi = i(2\pi)^3\sum E_p^{-1}e^{i(px-\omega t)} = i(2\pi)^3 G_p(x)$ so it embodies the delocalized initial data we complain about in the propagator. We can produce a localization of ϕ and $\dot{\phi}$ by setting $\phi(x) = \delta(x)$ and $\dot{\phi} = 0$ as the particular linear combination

$$\phi(x, t = 0) = \frac{1}{2\pi}\int_0^\infty dk\left(ae^{ikx+i\omega(k)t} + be^{-ikx-i\omega(k)t}\right)|_{t=0} \tag{25}$$

with $a + b = 1$ and $a - b = 0$ so $a = b = \frac{1}{4}$ but this will turn out not to be the interesting solution for coupling of KG to a positive energy Dirac field.

Our inability to constrain the total reality (charge, energy, mass, ...) of the particle to a point indicates that we have a constraint on our physical initial data not a measure of the incompleteness of our basis or a causality problem with our propagators. It should now not be surprising that a similar situation arises for the Dirac fields. For a spin up, positive energy state, localization of all components is inconsistent with the equations of motion. In coupling the Dirac field to the KG (or electromagnetic) field we cannot couple a delocalized Dirac packet to a localized one and the use of the propagator G_p to build the interaction now is more reasonable that the solution given by (25) since it follows directly from the Fourier transforms of the couplings Λ_{e-eA}, Λ_{ee-eeA}, etc.

4.3 Subspace restrictions and resummation

The problems of finding initial data and evolving in an infinite tower of spaces is daunting. The perturbative solutions embodied in the path integral approach are a way of working around this without stating it in these terms. The problems of field theory are often such that a finite perturbative approach is inadequate. Superconductivity is a canonical example of

this where this "nonperturbative" behavior delayed an explanation for half a century. Summing over the same diagrammatic sequence such as with "ladder diagrams" lets us capture some small slice of the infinite character of the space and derive new effective propagators where effective mass terms arise. The number of terms in the total perturbative expansion grow exponentially so it is unclear if such a sum actually has any meaning to which we are attempting convergence. We now know that such series are generally asymptotic so that there is no meaning to them in this limit. However, these particularly abbreviated series have been very valuable and are often capturing essential parts of the physics.

In this article, we are seeking a higher standard of conceptual justification for such sums. Even though we cannot hope to complete this task in a single article, let us seek a foundation for such calculations based on the data set and coupling provided. The self energies have been addressed through a relativistically valid, if slightly nonlocal, approach through cutoffs. Consider a single particle of mass parameter m and momentum p. This should be thought of as including $\Psi_{(e)}, \Psi_{(eA)}, \Psi_{(eAA)}, \ldots$ (and associated C_{PQ} fields) with all amplitude in the bottom state but constraints holding in the upper level functions but no other space couplings. This can be exactly and easily solved with the Coulomb gauge imposed at each level. Turning up the other interactions through the pair creation states $\Psi_{(eep)}, \Psi_{(eepA)}, \ldots$ can be done independently since the couplings between all function pairs, labelled by q, can be controlled separately. These states acquire little contribution in dressing a lone charge because they add so much energy to the system although the effects can be larger during deep scattering events with other charges.

In order to evolve such a system with a gradually changing interaction term while preserving the net norm, mass, and charge (observed from a distance) we can control the m and q parameters and an overall multiplicative constant, β, of the system. The final observed mass is the net energy of the system in the rest frame. We assert that the observed charge is determined by the electric flux that we can observe through large spheres in the A-coordinate subspaces in $\Psi_{(eA)}, \Psi_{(epA)}, \Psi_{(eAA)}, \ldots$. When a large "classical" body interacts with such a particle we assume it is broadly and uniformly distributed through a large variation in photon number spaces. This may seem ad hoc but for such a body to affect a lone dressed charge it must act in all the photon number spaces available or it leads to spectroscopic filtering of charge subspace components as they move in its field. Since this is not observed and we don't have a clear understanding of how classical bodies are represented with a quantum description, this seems like a reasonable supposition. These ideas lead to a prescription to modify the m, q, and β as we turn up the interaction. We need to be careful here as we now implicitly have multiple q's! This has been obscured by our choice of labeling them the same in our tower of interactions. There is the value q_{eA} that gives the self energy coupling in the towers of strictly photon number increasing states e.g. $\Psi_{(eA)}, \Psi_{(eAA)}, \Psi_{(eAAA)}, \ldots$ and the value q_{eep} that gives the couplings to the towers of electron positron pair increase $\Psi_{(e)}$, $\Psi_{(eep)}$, $\Psi_{(eeepp)}, \ldots$. Ultimately we want these parameters to be both the same. This seems to be a nontrivial process and it is somewhat impressive that the usual QED adiabatic turn on gets this to work by starting with a completely undressed charge and a single parameter.

Once we have dressed up lone charges on a subset of the towers deemed to be sufficiently rich to describe the dynamics of the process of interest, the interactions between them must be turned up. Given the states Ψ_{e_1A} and Ψ_{e_2A} we expect an antisymmetrized product of the two to give a first approximation to $\Psi_{e_1e_2A}$ and evolve these new "crossing" interaction parameters $q_{1,2}$ gradually and then hold it steady for a much longer period of time followed by a turn off of the interactions. If these adiabatic processes can be done in a way that leaves momenta of scattered waves unchanged then we can infer the actual scattering rates and angles for dressed particles. To this author, this is the simplest possible way to arrive at the scattering results from a well-posed initial value formalism. Ultimately, we must try other less restrictive subspace restrictions to show that our assumption that they made a small contribution was valid. There is reason to believe this actually works and gives the usual QED results and will be a subject of a followup work.

5 Conclusions

The need for establishing a well-defined space and set of dynamical equations for the reality described by QED, and QFT in general, has been discussed and presented in the form of a tower of spaces of continuum functions. Subsets of the dimensional labels of these spaces give meaning to the notion of "particle" and symmetries in the couplings and initial data define "identicality" of them. There have been a number of subtle issues to confront. Not the least of these is how to give meaning to the many time labels that arise in such a construction and why we, as observers built from the fields, should observe only one time. Such a construction has a number of advantages. It removes the ad hoc character of the construction and the need for the notion of "quantum fields." The inconsistencies described by Haag's theorem are resolved by a partitioning of the tower space into subsets of fixed lepton number that never couple to the ground state. Most importantly we have given an explanation for the quantization of the photon and an indication of the origin of the quantization conditions for quantum operators and the appearance of $\hbar$ in them.

The biggest downside of this construction is that of computability. QED was built from computations and arose out of many ad hoc attempts to make sense of observed dynamics on the part of many stellar physicists. The actual foundations of the subject are almost a necessary afterthought. Of course, no

class is taught this way and the foundations must come first regardless of how flimsy they are. A cynic might worry that field theory courses are filtering students based on their levels of credulity or lack of concern with consistency, a possible advantage in a field driven by extreme publication pressures.

The work here is still hardly complete and it is still to be shown that such construction can validate the successful results of QED for scattering. The subject of bound state corrections has been untouched here and an important topic that needs attention. There is good reason to believe that, ultimately, this theory will have corrections that are not found in QED and therefore be inequivalent at some level of accuracy. The subject of the radiation reaction and QED is still disputed. Given that the classical radiation reaction is resolved by keeping track of the self fields that traverse the extent of a finite body, one might worry that the renormalization procedure to handle self energy might be too simplistic and miss the asymmetric forces that must arise to give the back reaction. A primary motivation for this construction is the incorporation of gravity in a consistent fashion with the quantum world and other fundamental forces. A recent construction by the author in a classical direction relies on a greatly expanded gauge group and a flat background construction. Here couplings mock up the "geometric" effects of general relativity to observers and provides a new avenue for this problem as discussed briefly in the appendix.

A Gravity

Recently the author has presented a treatment of classical GR, electromagnetism and the Dirac field on a flat background that retains the apparently geometric features of GR and yet puts the fields on a similar footing [3]. The motivation for this is in promoting the Dirac γ^μ matrices to dynamic fields without imposing the vierbein approach. This has a number of consistency challenges to work out that will not be reproduced here. One of the essential features is that the γ^0 that is hidden in the $\bar{\Psi}$ has to go. We must replace all the $\bar{\Psi}$'s with new independent fields Φ's that implicitly do the work of them. The quadratic nature of the equations then become bilinear and, while the fields may not evolve causally, it can be shown that the gauge invariant reality of them do. Promoting the γ^μ_{ab} matrices to dynamical fields necessitates that we reinterpret them as vectors in the μ index and scalars in the a, b indices. This seems at odds with the usual SU(2) representation theory. This can be resolved by keeping track of the gauge invariant quantities and allowing new rules to actively boost fields in the space. The various details surrounding this are discussed in Chafin [1].

The metric and its inverse can be defined in terms of these fields as

$$\begin{aligned} g^{\mu\nu} &= -4^{-1}\mathrm{Tr}_{ac}\gamma^{(\mu}_{ab}\gamma^{\nu)}_{bc} \\ g_{\mu\nu} &= \mathrm{Inv}(-4^{-1}\mathrm{Tr}_{ac}\gamma^{(\mu}_{ab}\gamma^{\nu)}_{bc}), \end{aligned} \tag{26}$$

however the complexity of the inverse definition makes it more convenient to define an auxiliary field λ^μ and define the γ matrix with its index down

$$\begin{aligned} g^{\mu\nu}\delta_{ac} &= -2^{-1}\{\lambda^\mu, \lambda^\nu\} = -\lambda^{(\mu}, \lambda^{\nu)} \\ g_{\mu\nu}\delta_{ac} &= -2^{-1}\{\gamma_\mu, \gamma_\nu\} = -\gamma_{(\mu}, \gamma_{\nu)}. \end{aligned} \tag{27}$$

Some dynamic interaction terms will then lead to these forcing of the inverse matrix relation for the trace of these at low enough energy e.g. through the "Higgs-ish" coupling in the action

$$S_c = M\,|g_{\mu\nu}(\gamma)g^{\nu\rho}(\lambda) - \delta^\rho_\mu|^2 \tag{28}$$

for a large "mass" parameter M.

In our many body tower of functions we need to ask how the couplings with such a gravity field γ^μ_{ab} would work. Modeling it on the electromagnetic field by introducing γ and λ labels to Ψ as in $\Psi^\nu_{(eA\gamma),\mu,abc}(x, y, z)$ has some appeal in thinking of gravitons as correlated with other particles but is problematic in the details. When we look at the modified Dirac lagrangian we find that there is always an extra μ index to accommodate:

$$\mathcal{L} = i(\phi_a\gamma^\mu_{ab}\partial_\mu\psi_b - \partial_\mu\phi_a\gamma^\mu_{ab}\psi_b) - 2m\phi_a\psi_a \tag{29}$$

Furthermore the γ function will need to span the full coordinate set of the function it is evolving. For example, when we wish to evolve $\Psi_{(eA)}(x, y)$ in the t^e direction we must multiply by a function $\gamma^\mu_{ab}(x, y)$ so that the $x^{(A)} = y$ coordinate must still be present even if it is only in a passive role. For these reasons it seems important to include not just a dual field $\Phi_{(eA)}$ to go with $\Psi_{(eA)}$ but an independent $\gamma^\mu_{(eA)}(x, y)$ field to contract with the derivative operator $\partial^{(e)}_x$. Note that we have labeled the gravity function γ^μ_{ab} with the electron and photon coordinate labels not some new graviton coordinate and it has only one μ and two a, b indices. This will persist regardless of how many coordinate functions are embedded in it. Thus the tower of functions of electron, positron and photon fields (and their Φ associated fields) has an associated tower

$$\begin{aligned} &\gamma^\mu_{(A),Q}(x), \gamma^\mu_{(AA),abQR}(x, y)\ldots \\ &\gamma^\mu_{(e),ab}(x), \gamma^\mu_{(eA),abQ}(x, y), \gamma^\mu_{(eAA),abQR}(x, y, z)\ldots \\ &\gamma^\mu_{(p),ab}(x), \gamma^\mu_{(pA),abQ}(x, y), \gamma^\mu_{(pAA),abQR}(x, y, z)\ldots \\ &\gamma^\mu_{(ep),ab}(x, y), \gamma^\mu_{(epA),abQ}(x, y, z), \\ &\qquad\qquad , \gamma^\mu_{(epAA),abQR}(x, y, z, w)\ldots \\ &\ldots \end{aligned} \tag{30}$$

This allows these functions to be straightforwardly coupled into the electron, positron and photon lagrangians using the mapping $g^{\mu\nu} = -8^{-1}\mathrm{Tr}\{\lambda^\mu, \lambda^\nu\}$.

The problem now is reduced to giving an evolution equation for these various γ^μ_{ab} functions in each of the implicit time directions. The Einstein-Hilbert action $S_{EH} = \int R\sqrt{g_{..}}$

suggests a start. The measure can be extracted from $g_{\mu\nu} = -8^{-1}\mathrm{Tr}\{\gamma^\mu, \gamma^\nu\}$. The geometric meaning of these terms is not clear but it is not necessarily required. We know that we want GR to arise in some, probably uncorrelated classical limit of particles over the energy scales we currently observe but beyond that we only require that we have a well defined set of evolution equations. Define the Riemann operator $\hat{R}_{(e)_i}$ to be the Riemann function of the connections $\Gamma(\lambda, \gamma)$ in terms of the two associated gravity fields where all the derivatives are taken with respect to the $x^{(e)_i}$ coordinate label, ith electron label, in the $\gamma_{(eee...ppp...AAA...)}$ function. The interactions are provided by the remaining classical lagrangians that now needs no delta function to localize the interaction.

The global gauge freedom we associate with norm $\Psi \rightarrow \Psi e^{i\theta}$ and $\Phi \rightarrow \Phi e^{-i\theta}$ does not involve the γ functions so it seems to not acquire or lose amplitude in the fashion of particle creation so exists as a new kind of field entity that makes gravity seem fundamentally different than the other fields even though the geometric nature of the theory is subverted in favor of a flat background formalism. It seems that any generalization of this theory needs three fields (with various particle label sets). It would be interesting to see if there is some high energy unification which treats them in a more symmetric fashion.

Submitted on April 17, 2015 / Accepted on April 23, 2015

References

1. Chafin C. The Quantum State of Classical Matter I: Solids and Measurements. arXiv: quant-ph/1308.2305.
2. Chafin C. The Quantum State of Classical Matter II: Thermodynamic Equilibrium and Hydrodynamics. arXiv: quant-ph/1309.1111.
3. Chafin C. The Slicing Theory of Quantum Measurement: Derivation of Transient Many Worlds Behavior, *Progress in Physics*, v. 11 (3), 221–230. arXiv: quant-ph/1410.8238.
4. Dirac P. A. M. The Principles of Quantum Mechanics, 4$^{\text{th}}$ed. Oxford University Press, New York, 1986.
5. Dalfovo F., Giorgini S., Pitaevskii L. P., Stringari S. Theory of Bose-Einstein condensation in trapped gases. *Rev. Mod. Phys.*, 1999, v. 71 (3), 463.
6. Haag R. On quantum field theories. *Kong. Dan. Vidensk. Sels., Mat. Fys. Medd.*, 1955, v. 29 (12), 1–37.
7. Jammer M. The Philosophy of Quantum Mechanics; the Interpretations of Quantum Mechanics in Historical Perspective. Wiley, New York, 1974.
8. Kubo R. Statistical-Mechanical Theory of Irreversible Processes I. *J. Phys. Soc. Japan*, 1957, v. 12, 570–586.
9. van Kampen N. The Case Against Linear Response Theory. *Phys. Norv.*, 1971, v. 5, 279–284.
10. Ilderton A., Torgrimsson G. Radiation reaction in strong field QED. *Phys Lett. B*, 2013, v. 725, 481–486.
11. Louisell W. H. Quantum Statistical Properties of Radiation. Wiley, New York, 1973.
12. Misner C. W., Thorne K. S., Wheeler J. A. Gravitation. W. H. Freeman and Company, San Francisco, 1973.
13. Peskin M. E., Schroeder D. V. An Introduction to Quantum Field Theory. Westview Press, Boulder, 1995.
14. Rohrlich F. Classical Charged Particles. World Scientific, Reading, MA, 2007.
15. Schweber S. S. An Introduction to Relativistic Quantum Field Theory. Harper and Row, New York, 1962.
16. Schlosshauer M. Decoherence, the measurement problem, and interpretations of quantum mechanics. *Rev. Mod. Phys.*, 2004, v. 76, 1267–1305.
17. Weinberg S. The Quantum Theory of Fields, Vol. I & II. Cambridge University Press, Cambridge, 1995.

The Slicing Theory of Quantum Measurement: Derivation of Transient Many Worlds Behavior

Clifford Chafin

Department of Physics, North Carolina State University, Raleigh, NC 27695. E-mail: cechafin@ncsu.edu

An emergent theory of quantum measurement arises directly by considering the particular subset of many body wavefunctions that can be associated with classical condensed matter and its interaction with delocalized wavefunctions. This transfers questions of the "strangeness" of quantum mechanics from the wavefunction to the macroscopic material itself. An effectively many-worlds picture of measurement results for long times and induces a natural arrow of time. The challenging part is then justifying why our macroscopic world is dominated by such far-from-eigenstate matter. Condensing cold mesoscopic clusters provide a pathway to a partitioning of a highly correlated many body wavefunction to long lasting islands composed of classical-like bodies widely separated in Fock space. Low mass rapidly delocalizing matter that recombines with the solids "slice" the system into a set of nearby yet very weakly interacting subsystems weighted according to the Born statistics and yields a kind of many worlds picture but with the possibility of revived phase interference on iterative particle desorption, delocalization and readsorption. A proliferation of low energy photons competes with such a possibility. Causality problems associated with correlated quantum measurement are resolved and conserved quantities are preserved for the overall many body function despite their failure in each observer's bifurcating "slice-path". The necessity of such a state for a two state logic and reliable discrete state machine suggests that later stages of the universe's evolution will destroy the physical underpinnings required for consciousness and the arrow of time even without heat-death or atomic destruction. Some exotic possibilities outside the domain of usual quantum measurement are considered such as measurement with delocalized devices and revival of information from past measurements.

1 Introduction

The interpretation of quantum measurement has been a confounding topic since the early days of quantum mechanics. Approaches have ranged from very formulaic as in the Copenhagen interpretation to the many worlds view and decoherence [7, 9, 15, 16]. The statistics derived from these are typically excellent. Their accuracy for some systems that have some mix of classical and quantum character is still debated. Questions about locality and causality regularly arise in the case of correlations [1]. The purpose of this article is to show that a unification of classical and quantum worlds under the same description is easy given the right set of questions and that quantum statistics arise naturally from the dynamical equations of motion (and conservation laws). Specifically, the sorts of states that lead to observed classical matter arise in a natural way from a primordial delocalized and nonclassical gas due to contraction and the relative cheapness of creating low energy photons. The photon induced interactions of the induced clusters and massive proliferation of photons, hence increasing dimensionality of the space, will then lead to a kind of "slicing" of the space into many classical subspaces in the overall Fock space. The independence of these are long lasting when their particle numbers are modestly large and slow delocalization is "resliced" regularly by the interactions of delocalizing particles with the condensed matter portions of the system. The small particles that are capable of delocalizing on small time scales are mediators for further partitioning of the space with the probabilities given the square of the amplitude of its wavefunction*.

Any emergent discussion of measurement invariably runs into the need for the many body wavefunction. This is a high dimensional object and we typically have small particles with delocalization to measure that then interact and produce "collapse". This implies some separability in the net wavefunction. Any such explanation of quantum measurement must explain the following

1. The kinds of wavefunctions that correspond to classical matter and their origin;
2. The separability of the classical world from the isolated evolving quantum one;
3. The statistics of the interaction of the two.

One point often overlooked is that measurements occur at particular times and this is measurable. A delocalized packet of

*Here we are referring to the one body wavefunction, $\psi(x)$, that arises from ejection of a localized particle from classical-like matter which will produce a near product function $\Psi_N \approx \Psi_{N-1}\psi(x)$ up to symmetrizations. The framework here will help us extend measurement theory for the collapse of correlated delocalized particles in a causal manner.

an atom incident on a surface will give both a location and a time. Invariably this leads to some vague discussion involving the uncertainty relations, $\Delta x \Delta p \geq \hbar/2$ and $\Delta E \Delta t \geq \hbar/2$, however our concern is how the duration of a position measurement relates to the localization in any one slice. Our goal here is to produce a theory that has no operators or such relations as fundamentals to it. Rather we seek initial data and an evolution that deterministically arrives at the statistics and evolution we see and, ultimately, gives an explanation for the rather special subsets of wavefunctions that correspond to classical objects and the classical world.

This article will unfold as follows. First we discuss a delocalized cooling gas with proliferating photons and how these influence condensing clusters to produce islands of classical behavior for the condensed matter in the many body wavefunction. These are long lived and promote an arrow of time until the system recontracts and becomes relatively photon poor. To achieve this we need a description of matter with photon fields of varying number. Recently it has become possible to subsume the dynamics of QED in a many coordinate and many time classical field theory formalism where the observers perceive a world with *equal times* only [5]. This formalism and its associated many body conservation laws will be utilized to provide qualitative wavefunction descriptions of measurement as well as quantitative statistics. Next we discuss how the usual measurement statistics follow for such a system through "slicing" over delocalized particle coordinates with such condensed matter states. A nonlinearity, hidden while using the usual operator formalism, arises in the generation of radiation fields that removes some of the paradoxes in equilibration for purely linear operators on a Hilbert space. Finally, we use these structures to investigate some paradoxes in quantum mechanics, place some bounds on violation of Born statistics and suggest experiments to reveal such behavior.

2 Classical genesis: a first look

The primordial state of the universe is expected to be a gas that cools and condenses into stars and dust. If the photon number is zero and there are N particles, we expect a single wavefunction Ψ to describe this state*. It is clear, that a general such function is not describable by some mapping to hydrodynamics as a commutative mapping of $\Psi(X) \rightarrow (\rho(x), v(x))$ where the left hand side is governed by the Schrödinger equation and the right by Navier-Stokes. The states on the left are just too large. Instead of making an argument that the system should settle down to such a state we accept that this may never arise. It is the author's opinion that classical behavior arises from condensed matter and the proliferation of photons and that it is then induced on gases so we continue our story with nucleation.

*We ignore the role of virtual particles to this approximation.

Nucleation theory is still in a theoretically very unsatisfactory state and errors in nucleation rates are measured in orders of magnitude. However, this is fortunately not a complication to the relevant parts of our discussion. When the atoms of a gas condense into a cluster, a large number of photons are released. This means that we have now both increased the mean photon number and occupied a large region of Fock space. The ground state of a cluster of N-particles is nearly spherical (through some polygonal approximation) and rotationally invariant. This seems initially paradoxical. No discrete crystal has rotational invariance. The resolution follows from the fact that these are $3N$ dimensional wavefunctions. The translation is given by three of these and the rotational freedom by two more. Rotation always requires radial excitation, as we see from the case of the Hydrogen atom. In the case of a large cluster, this radial excitation is a centrifugal distortion. The rotationally invariant ground state has no well defined atom location, even if the structure is crystalline in that we cannot find peaks at locations r_i so that $\Psi \sim \prod_S (x_i - r_j)$. The states where such arises, as in the physical states we observe, must then be manifested by the cluster being in a mixture of high rotational eigenstates (even if having net angular momentum zero).

A surprising complication is that any classical body is in such a mixture of states so, even at "$T = 0$" it is far from its own ground state. The kinds of condensed matter we encounter have well defined shape, orientation, etc. They define a "classicality" that is very specific, three dimensional and Newtonian, and far-from-eigenstates. A solid can be specifically described and phonons given as excitations of the localized cores along particular many body diagonals and are eigenstate-like despite the ultimately transient nature of the classicality on which their description depends [4]. We now are compelled to ask how such apparently omnipresent states can arise.

Consider a pair of irregularly shaped bodies, A and B, that are spatially separated, but suffering delocalization about their centers of mass, and are bathed in a sea of photons. Let these be in their ground states initially. A photon that travels from far away and casts a shadow from body B onto A gets absorbed and produces a localized excitation on them. In the case of absorption by A the surface builds up a history through local heating or chemical changes. After many such photon events the body A has a record of the shape of body B in this shadow. Of course, some fraction of the amplitude of each photon gets absorbed by B or flies past without interaction. If the bodies A and B had localized atomic constituents, then their boundaries would be well defined and the shadows sharp. Since this is not the case we have to ask what happens. We can consider each to be a superposition of states that are in various angular orientations. This is reasonable since the centrifugal forces of these many angular states are small and make little deformation of the bodies. Each such case produces shadows that are well defined so we have a

macroscopic superposition of all the configurations with well defined orientations and atomic locations. The crucial part is how this then evolves.

Given a superposition of nearly overlapping macroscopic bodies in a space with no photons the energy change is huge. Atoms cannot sit on top of each other without inducing large repulsive forces from their electronic structure. However, for a system with a huge variation in the photon number states, such slight changes can easily have different photon numbers so be, ostensibly, at the same location but in different photon number spaces. This allows an apparent overlap with no energy cost. Specific details of this rely on an initial value (rather than operator based) description of low energy QED described in [5] and summarized below. Since the delocalization rate of large N objects is very small, such states can then evolve for long periods of time with essentially no interaction between them. Ultimately, we are such objects. Our very consciousness and memory depends on our being reliable discrete state machines. Once the expanding and cooling universe is so partitioned we have a set of "many worlds" that are sufficiently separated in Fock space to be insulated from each other. Of course, this is not expected to persist. In a gravitational contraction or long term stagnation, these worlds will come back together and the "information" made up by these separated worlds will be lost. This is an appealing way for the arrow of time to arise naturally despite the time reversal symmetry of the equations of motion. To be fair, this is a very vague and qualitative discussion. Now let us try for a more specific, but less general case in an attempt to justify this partitioning of the many body wavefunction.

3 Classical genesis: cluster collisions and photons

Here we give a justification for the "sparse worlds" state that we claim is a set of many-body wavefunctions that correspond to classical condensed matter objects (plus gas and a few delocalized particles). By this we mean that the solid and liquid objects have well defined boundaries, shapes and orientations as 3D objects but encoded in the N-body space of atoms where these atoms have well defined locations to within some localization distance determined by the electronic bonds between them. Of course, such a state is not an eigenstate. Each body will tend to delocalize both radially and in location. Such a state is an unfathomably complicated mix of eigenstates of the true system yet it makes some sense to think of the excitations of the bodies in terms of collective phonon modes as eigenstates in such clumps of matter.

Matter begins in the universe as a gas that collapses into stars and explodes to create the clusters that condense into dust that eventually coalesces into planets and other rocky objects. The gas undoubtably begins as delocalized and "correlated" in the sense that the particles have no well defined 3D locations so the many body Ψ cannot be represented as some symmetrized N-fold product. The implications of this are rarely considered. How does classical hydrodynamics arise in such a system and lead to stars of well defined location much less the larger scale density structures we observe? Is this classical localization a result of some product of our consciousness in creating a "measurement". This is pretty unpalatable to most scientists. The alternative is that such condensing occurs but the resulting stars have no well defined location, particle number, boundary and orientation relative to one another. Such a universe is a truly many body object and how it would "look" to an observer injected into it is not clear. Later we will see that the consciousness required for observation may be incompatible with such a universe.

The resolution we suggest is that this is the true state of the early universe and it is the presence of condensed matter that "slices" the space into a well defined collection of stars of well defined locations and velocities. The collapse picture implies that only one such state is selected and exists. In this picture, the the coordinates of the observer contain copies of the "observer $\otimes$ system" that cease to be the same for all values of the system coordinates. This divides the wavefunction of the many body space into a collection of independently evolving states of well defined 3D structure with long lasting independence and duration. We can then think of quantum measurement as the "auto-fibration" of the macroscopic world over the coordinates of the measured particle.

Consider a classical-like block of matter floating in space. A superposition of a star at two locations shining on such a block creates a superposition of the block in the star's coordinates. If we view the block as a measurement device that is recording observations in the changes in its surface under the influence of photons from the star, then it "observes" its own history to have the star at one continuously connected path of locations. It now has a double life as two blocks with different histories even though the number of coordinates has not changed. Its classicality has been compromised (albeit in a very minimal way) by the influence of the delocalized star even though the star and the block are widely separated and the net mass and energy transferred by the photons is typically miniscule. The "measurement device" has not forced a change in the larger system. Rather, the larger system has induced a change in the measurement device so it now follow separate paths in the many body space. This is possible, in part, due to the massive size of the many body space and its capacity to hold many classical world alternatives as distinct for long times. Note that the size of the block compared to the superimposed object is irrelevant in producing this effect.

The problem then amounts to the creation of such a set of classical-like bodies distributed in a set of sparse worlds embedded in the many body space. As a prototype world consider a collection of dust of different sizes, shapes, orientations, internal excitation, positions and velocities. These begin as a highly correlated system that has no classical meaning despite having formed solid matter. Let us start with an idealized simple system to discuss the mechanism. Consider

two solid balls of radius r but nonspecific location and velocity in many body space described by a cube of length L. Ignoring internal degrees of freedom, we can consider the system to be a 6D wavefunction in an L^6 cube with excluded volume given by the 2 body cylindrical projection of the interior of the sphere. At higher energies the wavefunction will tend to have oscillations much smaller than the radius $\lambda \ll r$. The state of the system in terms of eigenstates is assumed to be of a broad energy distribution $\Delta E \gtrsim <E>$ and have random phases or have evolved for a long but random length of time. Such a condition is necessary to have fluctuations in the many body current $\mathcal{J}$. The energy density and fluctuations then tend to uniformly fill the box and we have a soup of high frequency and highly varied oscillations bound by the excluded volume.

So far we have said nothing about photons. Let us assume there are none to start with. Currents induced by the fluctuations in the wavefunction produce flux on the boundaries of the excluded volume. Classically this corresponds to the collision of two spheres with velocities given by the two velocities

$$v_1, v_2 = \frac{\mathcal{J}}{\mathcal{P}}$$

given by the 6D current $\mathcal{J}$ and density $\mathcal{P}$ at the coordinate $X = (x_1, x_2)$. Depending on the angle and relative speed of the collision, a certain number of photons are created in the event. Photons are exceedingly inexpensive at low energies. This has led to the infrared divergence problem in QED where an unbounded number of low energy photons get created. Our finite box regularizes this to some degree but for short enough collision times no such problem arises since they cannot traverse the box during their creation.

A small change in the location of the collision creates a different number and set of photons. Thus one location can generate a large occupancy in the tower of spaces Ψ_{bb}, Ψ_{bbA}, Ψ_{bbAA}, Ψ_{bbAAA}, Ψ_{bbAAAA} ... where b indicates the coordinates of each ball and A are the photon coordinate labels. In a short time, the current flux at that location can be very different and generate a very different occupancy the the ball-photon wavefunction tower (Fock space). Once each small current fluctuation is completed, the higher photons spaces have acquired an occupancy of localized spatial position in the b-coordinates (defined by the length of time of the local fluctuation in current) and a broad number of photon waves moving away from it in the A-coordinates. The long time limit we argue is of a sum of such states distributed among the tower with almost all the amplitude having left the Ψ_{bb} state. These can now evolve with no quantum interference of other states (since all b and A coordinates would have to match up in one of the towers for this to happen). By "long time" we mean long enough for the currents in the Ψ_{bb} state to have had time to have all reached the excluded volume surface and hence pushed amplitude up the photon tower, $\tau \gtrsim L/\mathrm{Min}(v_1, v_2)$, but not so long as to cause delocalization of the amplitude in each n-photon space so these begin to interact and interfere.

The actual process "in vivo" of the universe is of course more organic and occurs while the dust is forming. It must create the orientation of the dust as well as select these subslices to have well defined atom number in each. It seems that the cheap and plentiful photon along with dust formation is what drives the formation of these "classical worlds" as isolated long lasting packets in the many body space. Quantum mechanics then arises for each of these universes by the action of condensed matter as discrete state machines. Clearly this process cannot persist forever. The universes will delocalize, meet, possibly gravitationally collapse and get driven to a density where the full correlated structure of the universe matters.

4 Measurement

Part of the formalism of quantum mechanics has been to use Hilbert space and eigenfunctions of operators to give measurement results.

These Hamiltonians are often effective Hamiltonians of subspaces created by the kinds of localized "classical" states described above. This introduces a kind of metastable feature to the evolution that is connected with the duration of the classical nature of the external world. One has to wonder what the role of the eigenstates are in arriving at measurements, specifically how one collection of matter indicates one particular operator and spectrum. In the case of position measurements, we see from above that the system has partitioned itself so that measurement of particle location is inherited by the special independently evolving nature of the classical states. In this case we say the system has been "sliced" in a manner that gives it its classical character but not into a subset of eigenstates of the net or any obvious subset of the Hamiltonian. We assert that momentum, energy and other measurements are universally inferred from position data e.g. a local color change in a material or spatial measurements at different times. It has already been long debated how general a measurement can be made from an arbitrary linear self adjoint operator (LCAO) and it is this author's opinion that position and time measurements are the fundamental sort that arise and all others are derivative.

Note that our "measurement" process has nothing to do with consciousness of an observer but of a specific property of condensed matter in a photon rich environment. In fact, photon production at low energies is so cheap that it is hard to conceive of a measurement that didn't produce copious numbers of them. Let us now consider temporal effects and measurements. It is inevitable that temporal effects arise. Wavepackets can be delocalized and measurement devices can move. This makes it clear that the measurement operator $\hat{x}$ is going to have some insufficiencies. Furthermore, measurement devices have finite spatial extent. Screens are essentially 2D so they are typically only picking up a tiny

fraction of a wavefunction's motion at any time.

To illustrate these points consider a narrow single particle packet incident on a screen with a couple of adsorption sites as in Fig. 1. We can simplify this by breaking it up into a set of disjoint regions of support as in Fig. 2. The duration of an adsorption event is not related to the length of a packet but the radiation time for the electronic decay that produces binding. For simplicity let the binding action be mediated by the release of a single photon of energy E so the radiative process has a time scale $\tau \sim \hbar/\Delta E$. Let the parcels be roughly monochromatic so they have a well defined velocity $v = j/\rho$ and the parcel widths $w \approx v\tau$. A parcel separation of nw lets the adsorption events be well separated.

When a subparcel reaches the site at x_0 it adsorbs and creates a photon so that some amplitude flows from $\psi(x)\Psi_N$, the photon free wavefunction of the system, to $\Psi_{N+1,A}$, the single photon and N+1 particle wavefunction with a radiation field flowing away from it. The operator formalism obscures some features of this problem so we invoke an equivalent formalization of low energy QED by using a many time approach where one body equations of motion hold for each time coordinate in the many body tower [5]:

$$\begin{array}{l} \vdots \\ \Psi_{N,AAA} \\ \Psi_{N,AA} \\ \Psi_{N,A} \\ \Psi_N \end{array} \tag{1}$$

We call this theory "deterministic wave mechanics" (DWM) in contrast with the formal operator and path integral formulation of the theory. A basis of states in each photon number space is given by $\Psi^{(m)}_N \mathcal{A}_m$ where $\mathcal{A}_m$ is a stationary state in the space spanned by $A^{i_1} \otimes A^{i_2} \otimes \ldots \otimes A^{i_m}$ of complex 3-vectors fields for photons*. The net norm and energy are conserved in such approach when they are defined as

$$\begin{aligned} \hat{\mathcal{N}}(\Psi_{N,n}) = & \int dx_s^{i_1} \ldots dx_s^{i_N} \bar{\Psi}_N \Psi_N \\ & + \tfrac{1}{4\mu_0} \int dx_s^{i_1} \ldots dx_s^{i_N} \int dx_A^{i_1} \ldots dx_A^{i_n} \\ & \textstyle\sum_{k=1}^{n} \left(\bar{\Psi}^{i_1 \ldots i_n} \partial_{t_A^{i_k}} \Psi_{i_1 \ldots i_n} - \partial_{t_A^{i_k}} \bar{\Psi}^{i_1 \ldots i_n} \Psi_{i_1 \ldots i_n} \right) \\ = & \int dx_s^{i_1} \ldots dx_s^{i_N} \bar{\Psi}_N \Psi_N \\ & + \tfrac{1}{4\mu_0} \int dx_s^{i_1} \ldots dx_s^{i_N} \int dx_A^{i_1} \ldots dx_A^{i_n} \\ & \textstyle\sum_{k=1}^{n} \left(\bar{\Psi}^{i_1 \ldots i_n} \hat{\mathcal{N}}^A_k \Psi_{i_1 \ldots i_n} \right). \end{aligned} \tag{2}$$

$$\begin{aligned} E_{N,k} = \bar{\Psi}_{N,k} \Big(& \textstyle\sum_{i=1}^{N} \hat{E}_{s_i} \hat{\mathcal{N}}_{1 \ldots \hat{i} \ldots N} \hat{\mathcal{N}}^A_{1 \ldots k} + \\ & + \textstyle\sum_{j=1}^{k} \hat{E}_{A_j} \hat{\mathcal{N}}_{1 \ldots N} \hat{\mathcal{N}}^A_{1 \ldots \hat{j} \ldots k} \Big) \Psi_{N,k} \end{aligned} \tag{3}$$

and we evaluate on the equal time slices $t \doteq t_{net} = t_s^{i_1} = t_s^{i_2} = \ldots = t_A^{i_1} = t_A^{i_2} = \ldots$. The operators $\hat{\mathcal{N}}_s$ and $\hat{\mathcal{N}}_A$ are the one body norm operators for massive and photon fields respectively. The operators $\hat{E}_s$ and $\hat{E}_A$ are similarly the one body energy operators. The many body versions are simply concatenations of these where the "hatted" indices are excluded. The definition of $\bar{\Psi}$ for Dirac fields is to apply γ^0's to all the spinor indices of Ψ (which have been suppressed here). Here we are interested in atomic center-of-mass wavefunctions. For these we simply require the transpose conjugate.

Using this picture we can derive the long time states of the system. The radiative decay occurs at frequency ω with an envelope of duration τ as in Fig. 6. The atom binds a location x_0 with a mean width of d so that it may be represented by a peaked function $\delta_d(x - x_0)$ akin to a delta function of finite width d. Assume the first peak arrives as time $t = 0$ and that there are only two equal pulses that contain all the amplitude of ψ. Initial data at $t \lesssim 0$ is

$$\begin{aligned} \Psi_{N+1} &= \Psi_N \psi(x, 0) \\ &= \tfrac{1}{\sqrt{2}} \Psi_N (\delta_w(x - x_0) + \delta_w(x - x_0 - wn)) \\ \Psi_{N+1,A} &= 0 \\ &\vdots \end{aligned} \tag{4}$$

The final wavefunction for $t > t' = 2\tau + n\tau$ is

$$\begin{aligned} \Psi_{N+1} &= 0 \\ \Psi_{N+1,A} &\approx \tfrac{1}{\sqrt{2}} \Psi_N \delta_d(x - x_0) \Big(\tfrac{1}{r} e^{i(kr - \omega t)} h(r - ct) \\ &\quad + \tfrac{1}{r} e^{i(kr - \omega(t - t'))} h(r - c(t - t')) \Big) e^{i\phi(t)} \hat{\epsilon}_\kappa \\ \Psi_{N,AA} &= 0 \\ \Psi_{N,AAA} &= 0 \\ &\vdots \end{aligned} \tag{5}$$

We have implicity assumed the block is essentially transparent and the radiation flies unobstructed into infinite space. (The orientation of the radiation field $\hat{\epsilon}_\kappa$ is determined by the direction of the dipole produced by the radiation. This may be a superposition of such solutions and a function of the local geometry of the solid. For now we neglect its details.) The meaning of this solution is that the wavefuction support has exactly partitioned into two parts. The "reality" of a classical field can have some surprising subtleties† [3]. In this

*Coulomb gauge is assumed for every coordinate label so that the $\Psi^{\mu=0}_{N,1}$, $\Psi^{\nu,\mu=0}_{N,2}$, etc. components are fixed by constraint.

†We can consider this as the "Schrödinger" and "first quantized" analog to usual QFT formalism in terms of field operators.

case the support and its values there contain all the meaning there is to the system. We see that we have two bound states that occurred at times $t = 0$ and $t = t'$. The packet is flying away from the location $X \approx x_0 \otimes X(0)$ at c in the x direction when viewed in the equal times coordinate t. The motion in the material coordinates is essentially static unless some other dynamics were present to start with. If we consider the block to contain a discrete state machine as in Fig. 3 that has internal dynamics that makes a record of when the event occurs, then each one exists in a kind of parallel universe with a record of a different time. Unless these photon coordinate portions of the packet are reflected or forced to interfere, this situation continues in perpetuity and each evolves according to their own record of their particular past. Should they generate their own delocalized particles and repeat this experiment they will find the Born-like $\psi^*\psi$ probabilities for when the measurement occurs. This is a direct consequence of the above norm conservation law. Ultimately the delocalization can only go on so long before the "classicality" of the system fails. The consequences of this we will soon consider.

Let us now consider a broad packet that intercepts the screen at the same time as in Fig. 4. Analogously to above, let us consider this to be broken into two parts with the width of the measurement centers and less than $w = v\tau$ as in Fig. 5. Here a similar analysis yields a resulting pair of packets radiating outwards from the two centers at the same time. Our system now seems to be split into two spatially distinct parts as indicated by the outer product in Fig. 7 where the radiative field shells have been suppressed. These shells are no longer disjoint but contain a finite volume fraction of overlap. For farther apart centers this is of order $w/R(t)$ where $R(t) = ct$. To the extent this overlap remains negligible, these solutions remain disjoint and evolve as separate worlds.

This is a good point to pause and reflect on what overlap of these systems means for evolution. The emphasis on linear operators and Hamiltonians leads one to believe that any superimposed world is equivalent to each world evolving separately. As such, when one decomposition evolves it is hard to see how anything interesting can really happen. However, there is a hidden nonlinearity in our problem. The classical radiation reaction problem holds a nonlinearly due to current acceleration which is best thought of in terms of finite sizes of radiators and crossing times [11]. Our radiation fields can be thought of in a similar fashion with a small unknown structure involving many hidden internal coordinates. The "radiation reaction" now must transfer both four momentum *and* particle norm at the interacting two-body diagonals that connect the states in the Fock space tower. The implications of this is that overlapping of states in the Fock space do not simply superimpose so there are no true eigenstates when photon interactions are included. This is to be expected. If we superimpose the eigenstates ψ_{2p} and ψ_{1s} of the Hydrogen atom then it is the presence of the current that drives amplitude from ψ_H to $\psi_{H,A}$. In the low energy limit the Hydrogenic states are stationary but the overlap drives the transition to higher photon levels. This is an intrinsic nonlinearity that is obscured by the formal operator description of quantum field theory. It is unclear if this is adequately accounted for in quantum field theory through its operator calculus.

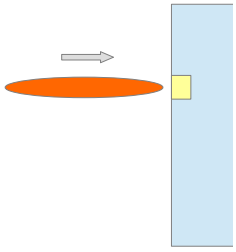

Fig. 1: A long narrow packet illustrates the measurement of event time at a particular location and how these can lead to a persistent slicing of the space (up to the delocalization time of the device) in an infinite space.

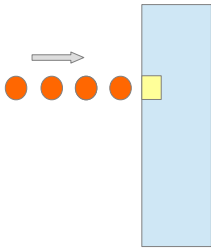

Fig. 2: An idealized sequence of packets of a *single* incident particle.

5 Slice memory and revival of measurement history

One of the unpleasant features of the many worlds interpretation is that the size of the universe seems to grow. In this and all "interpretations" of quantum mechanics, the role of the measurement device and how and when it acts lacks specificity. The action of the "observable" associated with each such device is not clearly determined by the microstructure of the device. The DWM theory here addresses each of these and lets us ask some new questions that may take us outside the bounds of traditional quantum theoretical problems. One of the obvious questions is to what extent is the measurement a complete destructive event (at least from the perspective of the observers). Can we somehow undo measurement and recover some of the delocalization and phase information from before? Now that we can nanoengineer systems and create extremely cold ones, highly decoupled from the external world, other quantum domains can be probed. A molecular two-slit experiment was recently realized [10]. In the measurement direction what happens when a measurement device itself has a mass comparable to the delocalized system it measures? Is there a measurable "back reaction" to

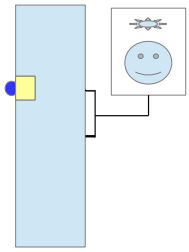

Fig. 3: A measurement device with a coupled observer or programmable device to respond to observations.

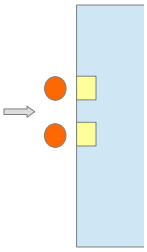

Fig. 5: An idealization of the narrow one-particle packet into localized subparcels.

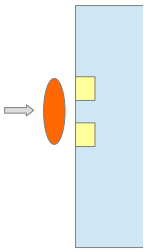

Fig. 4: A narrow one-particle packet incident on a detector surface.

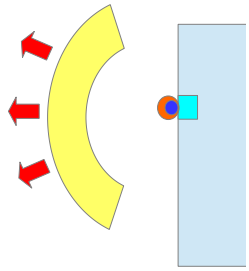

Fig. 6: The absorption of a particle at a site is correlated with radiation field moving away from the selected location.

the measurement event? If a measurement device is partially delocalized itself how does this affect the measurement once we then slice the measurement device so it is back in the fully classical domain of our experience?

5.1 Wavefunction revival: inverse measurement

On the topic of slicing of the space into independently evolving subspaces we have introduced the restriction on the form of macroscopic matter that gives a classical limit for dynamics. This was far more restrictive than the rather naive Ehrenfest-limit defined by large mass and moving packets [12]. The continuing lack of overlap given by large mass induced slow spreading and the rapid motion of light speed packets in the A-coordinate directions into an empty space help preserve this "many-worlds" picture for long times. Constraints on the space that photons can move about in leads to greater overlap possibilities and opportunities for such slices to interact through radiation absorption and production however, since low energy photons are so prolific this kind of interference may be difficult to engineer in practice. Nevertheless, we should investigate the possible bounds on slice independence.

Consider the example system given in Fig. 5. Generally, there are going to be internal motions and radiation fields that exist in any such large body. Let the incident atom be distinct from those of the device so that it is unconstrained by symmetry and the binding to the surface can be much less than that of the device particles to each other. We can imagine a situation where we heat the block and the atom ejects and delocalizes then is pulled back to the surface by an external field such that this process is iterated. The CM of the device gradually delocalizes (at a much increased rate) from this process. If this system is closed then the photon number will gradually increase as the battery driving the process loses energy. This tells us that the system is undergoing important changes and so reejecting the particles may not create a system that interferes with previous slice histories. On the other hand, if the system is in a finite volume, the radiation fields can all be contained in this finite space so that past slices eventually can interfere if the photon number does not grow much faster than the number of iterations.

It is simpler to consider the case of a photon that is absorbed at a pair of sites and then ejected as in the process $\Psi_{N,1} \rightarrow \Psi_{N,0} \rightarrow \Psi_{N,1}$. The release times for the two slices may vary over a large range but, if we restrict ourselves to looking at the fraction of amplitude that occur at the same time (e.g. by use of a beam chopper on the input and ejected flux), then the phases of the resulting two components of the single photon may be compared. After absorption, the system is a photon free wavefunction consisting of a superposition of two different internally excited states that evolves according to the net mass-energy in it. The relative phase of each space is fixed by the phase difference of the original photon at the time it was absorbed by the two sites $\Delta\phi = \phi(x_1, t = 0) - \phi(x_2, t = 0)$. Restricting our measurements to the case where the frequency of the emitted photons are the same, this phase difference should be preserved in the $T = 0$ limit. Thermal fluctuations in phase between the two points will produce

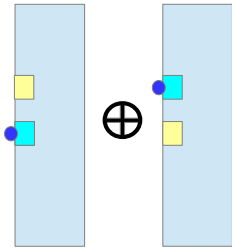

Fig. 7: The two possible configurations of a broad packet measurement (with suppressed radiative fields) exist as a kind of direct sum indexed by the coordinate label of the original incident particle.

a shift in this value. This procedure gives a measure of the regional phase fluctuations and isolation of the system.

5.2 Measurement back reaction

The subject of back reaction has been around for some time [8]. If one believes in a collapse picture then one can readily see that center of mass motion is not conserved in a position measurement. This means either it is truly not conserved or there is an unspecified back reaction on the system. In DWM we see that conservation laws only hold for the totality of slices not for individual "observer-paths". Therefore no back reaction is expected. We can utilize a pair of ultracold traps to give a specific test of this. Given a delocalized large mass molecule in a pair of widely separated traps we can send an atom through two paths to make contact with each of these. If a collapse produces a net conservation of all the usual conserved quantities then the center of mass shift will be proportional to the separation of the traps so can be made as large as desired and easily detected by florescent behavior of the molecule.

5.3 Nested and fuzzy measurement

The meaning of superposition of macroscopic objects has been debated at least as long as the famous Schrödinger's cat paradox [2, 13]. By our judicious selection of initial data we see that this is resolvable. The overlap of such states is explained by the proper consideration of correlations of photon fields in partitioning the system under such a slicing event as above. The nature of macroscopic superposition does however beg some interesting questions when the measuring device is also delocalized. For example, if the incident ψ has positive and negative regions that are shared equally over the same site due to delocalization then the net norm of ψ at that site may be zero. Does this mean there is no probability of adsorption at the site and the amplitude there is reflected? Furthermore, we can ask if the order of a meta-observer's action on the system in measuring the measurement device before it acts on the ψ or after makes any difference in the resulting statistics. These two scenarios can be classified as "fuzzy measurements" and "nested measurements".

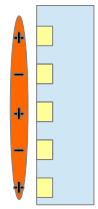

Fig. 8: A broad narrow packet incident on a screen. There is a relatively slow phase oscillation component parallel to the surface that matches the possible adsorption sites.

Firstly, consider a "device" that is a pair of separated, localized and slowly spreading heavy atoms or molecules in a trap. This allows for the possibility of the larger bodies capturing a small atom then moving the bound bodies around before ejecting the light atom from them. If the atoms are initially well localized and remain so for the duration of the experiment then the resulting phases on revival will be determined by the amplitude emission time and rate from each source atom. Note that this situation depends on the particles and what is moving them. If they are isolated like a gas then this is certainly true. If, however, the particles are being localized and moved by macroscopic classical matter or radiation that then is absorbed by it then the interactions with the external world may produce a slicing of the system. There may be no "meta-observer" or other unsliced mechanism to eject the light atoms and produce a spreading in its coordinate direction that causes the system to be seen as a wavefunction with some stored phase history and an external world. We can apply a radiation field to eject the light atom but have no way to know that our counterparts in the other slices have chosen to do the same.

Let us now extend the above case of the heavy atoms to the case of a measurement device i.e. a screen, as in Fig. 4. Here let us utilized a nearly monochromatic (wavelength λ) packet moving towards the screen but with a slow additional phase oscillation ($\lambda_{\|} \ll \lambda$) parallel to the screen surface. Let the screen have five adsorption sites and have separation equal to half this long wavelength oscillation $D = \lambda_{\|}/2$ as in Fig. 8. Now let the measurement device be delocalized in the vertical direction by a vertical shift D. We consider this to be in the form of two narrow packets of equal amplitude akin to the case of the incident wave in Fig. 5. The resulting initial state is described by the sum of configurations in Fig. 9.

Upon interaction the sites on the screen now feel both a positive and negative amplitude component of the wave. This is our first case of a correlated two body system. The system slices into a set of $4 + 5 = 9$ cases where the first four correspond to a screen that is upwardly displaced by D and the other five do not. For an "observer" living in the screen body itself, one of these cases appears to represent his initial data for the evolving future for all the initial data he has available to him. If somehow these slices are brought together in his future and the photon fields radiated from the adsorption

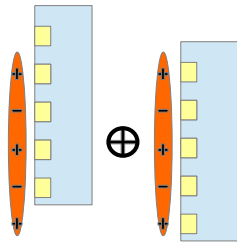

Fig. 9: A superimposed case of a measurement device with vertical delocalization and an incident wave packet.

events are confined with the system, the neighboring slices can interfere and this would seem to be a statistical aberration that flows from an unknown source. Now let us consider the situation from the "meta-observer" outside the system. This person can interact with the screen before or after the screen interacts with the packet. The bifurcation of amplitude gives the same results in both cases so there is nothing "fuzzy" about the measurement from the delocalized device and the measurement operations commute.

6 Conclusions

One alternate title to this article could have been: "The Cheap Photon and the Classical Limit: The Origin of Discrete State Machines, the Apparently 3D World, Quantum Measurement, the Arrow of Time and Why You Have Any Memory at All". It is impressive that such disparate topics should all be connected to mapping the classical world properly into quantum mechanics. A sister document on the dynamic process of thermalization and time dependent fluctuations has also been recently completed by this author [4]. The many body wavefunction of a system is a complicated high dimensional object. By including the photons a large number of degrees of freedom appear that allows condensing matter to sparsely occupy subdomains corresponding to very similar objects that retain independent existence for long periods of time. This provides a subset of wavefunctions that correspond to classical bodies that can withstand many quantum slicing events without producing significant overlap. The release of low mass particles from a condensed matter "classical" body leads to a product function state where the low mass component spreads rapidly and, when reabsorbed, creates a bifurcated class of such classical states with probabilities given by the Copenhagen interpretation defining a set of measurement events. These are locations and times specified by the atomic granularity scale of our condensed matter and a temporal granularity scale by the photon decay process associated with binding times. This resolves the paradoxes of quantum measurement and introduces an arrow of time in a rather simple fashion. We have argued that the genesis of such a state follows naturally from early universe conditions assuming condensation of small clusters of very low internal energy have time to interact and produce the localized classicality that partition the wavefunction into Newtonian-like parts.

One of the more unclear features yet to be resolved here is in the behavior of gases. Gases are made of light particles that have rapid delocalization so the persistent localization property we have argued for solids is not applicable. Collisions with solids surfaces of a container produce some localization by the slicing process but low diffusion rates suggest that this does not propagate well into the bulk of the gas. Hydrodynamic and thermodynamic behavior either requires some regular interaction with condensed matter by collision or possibly by photons or by some other process. We know that such gases have the power of producing quantum like measurement paths in cloud chambers (though clouds by definition involve condensed droplets). These are not pointlike but linelike events. This introduces an interesting direction to further investigate this model. Ultracold gas dynamics has become a very popular probe of quantum limits on viscosity [6, 14]. It is not clear that at such low temperatures for gases bound by fields and so not in contact with condensed matter, that hydrodynamics and thermodynamics are valid limiting behaviors on any timescale. These macroscopic formal models are often justified by vague scaling arguments. It is hard to argue against them because we have lacked a proper quantum description of gases in its "classical" limit. If this can be found, we may have a framework to see how well such a description can hold in the ultracold case and if such parameters like temperature and viscosity can have any relevant meaning for them.

Submitted on April 17, 2015 / Accepted on April 23, 2015

References

1. Bell J. S. On the problem of hidden variables in quantum mechanics. *Rev. Mod. Phys.*, 1966, v. 38, 447–452.
2. Carpenter R. H. S., Anderson A. J. The death of Schrödinger's cat and of consciousness-based wave-function collapse. *Annales de la Fondation Louis de Broglie*, 2006, v. 31 (1), 45–52.
3. Chafin C. Gauge freedom and relativity: A unified treatment of electromagnetism, gravity and the Dirac field. *Prog. in Phys.*, 2015, v. 11 (1), 25–37. arXiv: quant-ph/1410.8238.
4. Chafin C. Thermalization in quantum systems: an emergent approach. arXiv: quant-ph/1412.1347.
5. Chafin C. Beyond quantum fields: a classical fields approach to QED. *Progress in Physics*, 2015, v. 11 (3), 208–220.
6. Dalfovo F., Giorgini S., Pitaevskii L. P., Stringari S. Theory of Bose-Einstein condensation in trapped gases. *Rev. Mod. Phys.*, 1999, v. 71 (3), 463.
7. Everett H. "Relative state" formulation of quantum mechanics. *Rev. Mod. Phys.*, 1957, v. 29, 454–462.
8. Holland P. Hamiltonian theory of wave and particle in quantum mechanics II: Hamilton-Jacobi theory and particle back-reaction. *Nuovo Cimento B*, 2001, v. 116, 1143-1172.
9. Jammer Max. The Philosophy of Quantum Mechanics; the Interpretations of Quantum Mechanics in Historical Perspective. Wiley, New York, 1974.
10. Kreidi K et al. Interference in the collective electron momentum in double photoionization of H_2. *Phys. Rev. Lett.*, 2008, v. 100 (13), 133005.

11. Rohrlich F. Classical Charged Particles. World Scientific, Reading, MA, 2007.
12. Sakurai J. J. Modern Quantum Mechanics, 2nd ed. Addison Wesley, New York, 1993.
13. Schrödinger E. Die gegenwärtige Situation in der Quantenmechanik. *Naturwissenschaften*, 1935, v. 23, 49.
14. Son D. T. and Starinets A. O. Viscosity, black holes, and quantum field theory. *Ann. Rev. Nucl. Part. Sci.*, 2007, v. 57 (95), 95–118. arXiv: hep-th/0704.0240.
15. Schlosshauer M. Decoherence, the measurement problem, and interpretations of quantum mechanics. *Rev. Mod. Phys.*, 2004, v. 76, 1267–1305.
16. von Neumann J. Mathematical Foundations of Quantum Mechanics. Princeton University Press, Princeton, 1955.

Synchronous Changes of the Shape of Histograms Constructed from the Results of Measurements of ^{90}Sr β-Decay and ^{239}Pu α-Decay Observed in More than 3000 km Distant Laboratories

E. Y. Filin, A. V. Repkov, V. V. Voronov, A. A. Tolokonnikova[1], S. E. Shnoll[1,2]

[1]Institute of Theoretical and Experimental Biophysics, Russian Academy of Sciences.
[2]Department of Physics, Moscow State University, Russia.
E-mail: shnoll@mail.ru

It was discovered many years ago that histograms constructed from the results of measurements of various natural processes are not random. The histogram shape was demonstrated to be determined by the diurnal rotation and circumsolar movement of the Earth and to be independent of the nature of the process considered [1-17]. The results of those works change our basic views about stochasticity of natural processes. When the time series of physical measurements, which are traditionally considered stochastic, are transformed into the series of histograms constructed for an *optimally small number* of the results (i.e., *optimally short segment* of the time series), one can see regular changes in the histogram shape. The paper illustrates the main manifestations of this phenomenon by comparing the results of ^{90}Sr β-radioactivity and ^{239}Pu α-decay measurements, with the distance between the laboratories in which the data were collected being about 3000 km.

1 Introduction

The material for our research were results of long-term measurements of ^{239}Pu α-radioactivity in Pushchino (at the latitude of 54° north and longitude of 37°38' east) and ^{90}Sr β-radioactivity in Novosibirsk (at the latitude of 55°02'13" north and longitude of 82°54'05" east). The data were collected with a 1-second interval for many days. With the aid of Edwin Pozharsky's computer program GM [3], non-overlapping 60-point segments of 1-second time series were transformed into series of 1-minute histograms. The same program was used for a visual comparison of the histograms – after the procedures of smoothing, stretching, squeezing and mirror transformation, necessary to achieve the maximal similarity (for details, see [1]).

2 Experimental details

α-Radioactivity of a ^{239}Pu preparation was measured using low-voltage semiconductor detectors with collimators [10]. β-Radioactivity was measured using CTC-6 Geiger counters fixed in a metal case in a horizontal position, with their longitudinal axis directed along the azimuth of NN-SSW NNW-SSO (~320°). The source of β-radiation (^{90}Sr–^{90}Y, a flat disk of 20 mm diameter) was fixed 10 cm above the counter, with its radiating surface directed downwards to the counter.

3 Results

Fig. 1 shows a time series: the results of ^{90}Sr β-activity measurements. According to all fitting criteria, it is a purely stochastic process obeying the Poisson statistics.

As seen from Fig. 2, the results of measurements shown in Fig. 1 ideally correspond to the Poisson-Gauss statistics. That is why radioactive decay is considered an ideal example of the stochastic process. In Fig. 3, however, the same material of Fig. 1 is shown without smoothing, in the form of cumulative layers, where every next layer adds 3000 measurement points to the previous layer.

This figure demonstrates that contrary to the law of large numbers (the total number of measurements is 259200), the fine structure of the layered lines is not smoothed when the number of measurements is increased – it becomes even sharper. This paradox has a general character and can be observed in the measurements of any "stochastic" physical

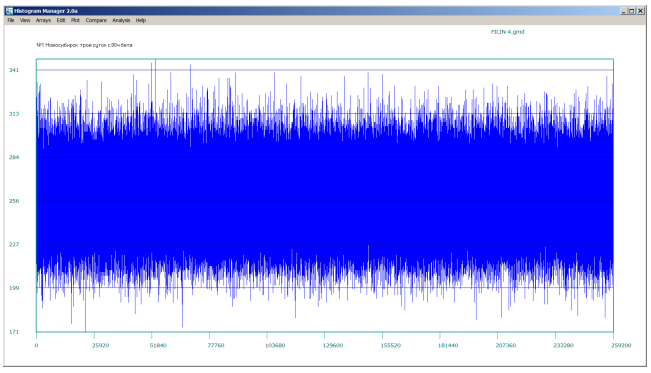

Fig. 1: A time series – the results of 1-second ^{90}Sr β-activity measurements for a period of 3 days (from 00:00 of June 19, 2013 to 23:59 of June 21, 2013). Novosibirsk local time (UTC + 7). X-axis: time, seconds. Y-axis: number of β-decays per second.

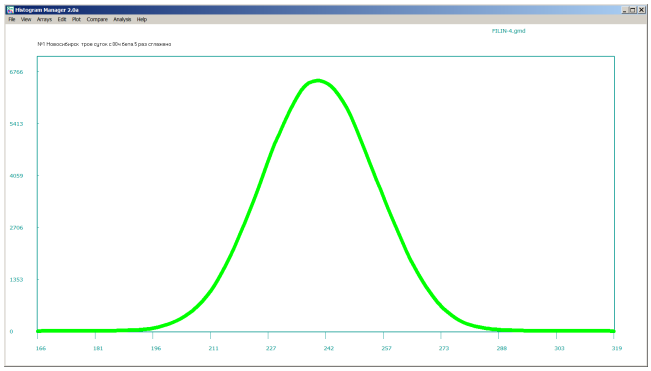

Fig. 2: Distribution of the results of measurements shown in Fig. 1. An ideal Poisson-Gauss distribution. X-axis: radioactivity, counts per second. Y-axis: number of results with the corresponding radioactivity value.

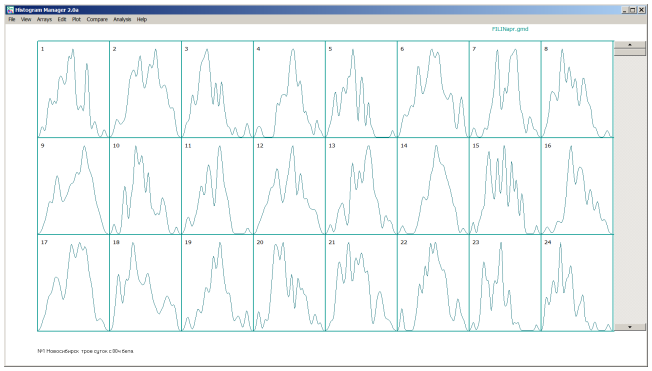

Fig. 4: Measurements of ^{90}Sr β-radioactivity. Transformation of a time series (Fig. 1) into a sequence of 60-point histograms smoothed 5 times. The figure shows the first 24 histograms from the total set of 4320 histograms.

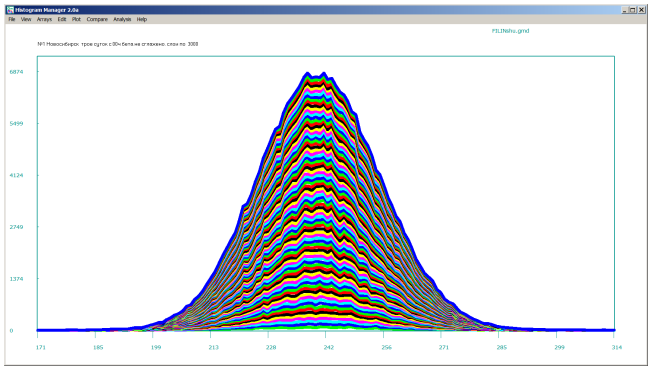

Fig. 3: Non-smoothed layered distribution of the results shown in Fig. 1. Every layer adds 3000 measurement points to the neighbor layer below. The axes are as in Fig. 2.

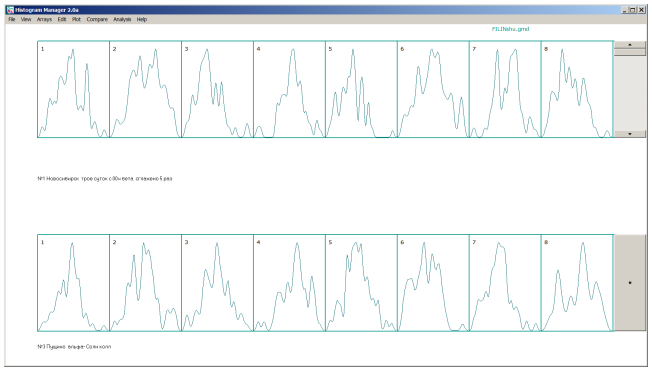

Fig. 5: A screenshot demonstrating comparison of two histogram sequences. Top band: measurements of ^{90}Sr β-radioactivity; bottom band: measurements of ^{239}Pu α-radioactivity. For each step, both bands shift forward by one number, and the new histograms, appearing at the right, are compared: the new top with all the bottom ones and the new bottom with all the top ones – this being repeated 360 times to build a distribution of the number of similar histogram pairs over the interval between these histograms (see Fig. 7 and hereinafter).

process [1].

In the paper, though, we consider histograms constructed for an *optimally small* number of measurements. It is transformation of time series into sequences of such *inconsistent* histograms, revealing well-reproducible cosmo-physical regularities, indicating nonrandomness of "stochastic" physical processes [1]. In the paper, this is demonstrated through synchronous measurements of ^{90}Sr β-radioactivity in Novosibirsk and ^{239}Pu α-radioactivity in Pushchino; the distance between these laboratories is about 3000 km.

The subject of this paper – as that of our previous works [1-17] – is the demonstration of regularities in the change of the shape of histograms constructed from an optimally small (30–60) number of results. Such a transformation of time series of the results of measurements into the sequences of histograms reveals the nonrandom character of these time series.

Fig. 4 shows some histograms constructed for the segments of the time series represented in Fig. 1. Each segment contains 60 ^{90}Sr β-radioactivity measurement points; the histograms were smoothed 5 times.

The fact that changes of the shape of such histograms in time are not random follows from a number of regularities found in our previous studies [1-17]. Even a careful examination of Fig. 4 would indicate this nonrandomness. It can, however, be estimated quantitatively. A quantitative measure of nonrandomness of the shape of inconsistent histograms is the results of their thorough comparison. The histograms can be compared either by a human expert, with the aid of Edwin Pozharsky's program, or by application of completely automated algorithms written by V. Gruzdev [19] and V.V. Strelkov et al. [18, 20–22].

Fig. 5 illustrates the procedure of pairwise histogram comparison, showing histograms constructed from the results of synchronous measurements of ^{90}Sr β-radioactivity in No-

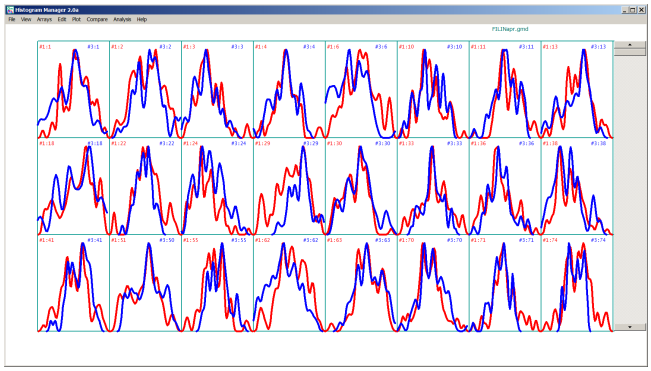

Fig. 6: A fragment of the computer journal (archive). Pairs of histograms considered similar by an expert.

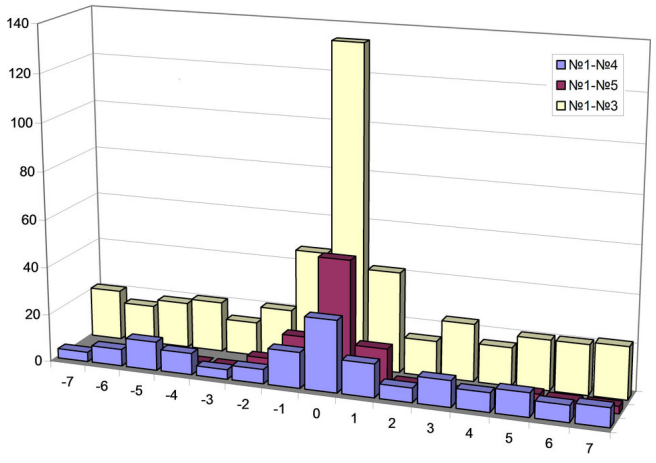

Fig. 7: Distribution of the number of pairs of similar histograms over the interval between them. Measurements of ^{90}Sr β-radioactivity in Novosibirsk and ^{239}Pu α-radioactivity in Pushchino with the collimators directed to the Sun (no. 3), Polar star (no. 4) or west (no. 5). Pairs no. 1-3; 1-4; 1-5. X-axis: intervals between similar histograms (min). Y-axis: number of similar histograms per 360 compared pairs.

vosibirsk (top band) and ^{239}Pu α-radioactivity in Pushchino (bottom band). Each band contained 360 numbers. In total, about 20,000 histogram pairs were compared, and the results are given in Figs. 6 and 7.

Fig. 6 shows an example of the histogram pairs that an expert deemed similar upon visual comparison.

Fig. 7 demonstrates the results of histogram comparison in the synchronous measurements of ^{90}Sr β-radioactivity in Novosibirsk and ^{239}Pu α-radioactivity in Pushchino in 3 variants of experimental setup: with the collimator aimed at the Polar star (no. 4); with the collimator constantly aimed at the Sun (no. 3) (on a rotating platform compensating for the diurnal rotation of the Earth); with the collimator directed west (no. 5). These results are represented as a dependence of the number of similar histogram pairs on the interval between the histograms.

As seen in Fig. 7, when the collimator in Pushchino is aimed at the Polar star, there is no synchronism in the change of histogram shape in Novosibirsk and Pushchino. When the collimator in Pushchino is directed west, synchronism is not very apparent but statistically significant ($P < 10^{-3}$). When the collimator is aimed at the Sun, synchronism is evident ($P < 10^{-7}$).

We shall not discuss now why the extent of synchronism depends on the direction of collimators in Pushchino (for details, see [1]). What is important is that with other conditions being equal, these differences in the experimental setup make the effects observed statistically significant. Therefore, the shape of histograms constructed from the results of measurements of β- and α-radioactivity at the distance between the laboratories ~3000 km does not depend on the nature of the process measured and the method of measurement. This agrees with the conclusion that the shape of histograms and its changes are determined by the orbital movement and diurnal rotation of the Earth and other cosmo-physical factors [1, 10–17].

This conclusion is confirmed by demonstration of the effects that are traditional for our works. The first effect is the

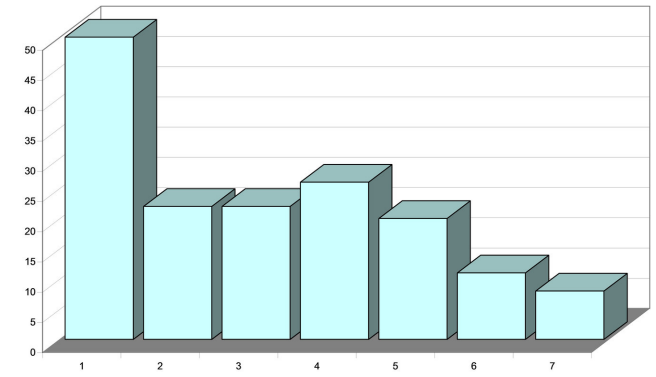

Fig. 8: Measurements of ^{90}Sr β-activity. The "effect of near zone", a higher probability of neighbor histograms (interval = 1) to be similar comparatively to the histograms separated by larger intervals. X-axis is time interval in minutes, Y-axis is number of similar histograms per 360 compared pairs.

"effect of near zone". It means that the neighbour histograms are much more probable to be similar, and Fig. 8 shows how it looks for the β-activity measurements.

Since histograms are constructed for non-overlapping segments of time series, the effect of near zone is the first sign of histogram shape to be determined by an external factor [1]. The second traditional effect, indicating cosmo-physical conditionality of the shape of histograms, is the existence of two clearly resolvable near-daily periods: sidereal and solar [1]. Fig. 9 shows these near-daily periods revealed in the measurements of ^{90}Sr β-activity in Novosibirsk (no. 1) and ^{239}Pu α-activity in Pushchino (no. 3–5)

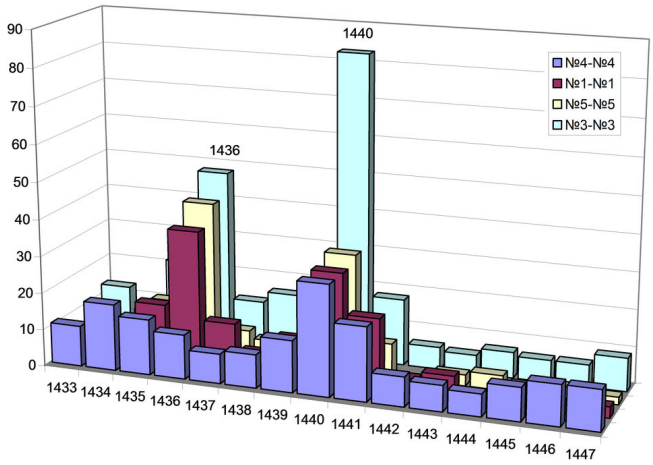

Fig. 9: Sidereal (1436 min) and solar (1440 min) daily periods in the appearance of similar histograms in the measurements of ^{90}Sr β-activity in Novosibirsk (no. 1) and ^{239}Pu α-activity in Pushchino (no. 3, 4, 5). Collimator is aimed at the Sun – no. 3; collimator is aimed at the Polar star – no. 4; collimator is directed west – no. 5. X-axis is time interval in minutes, Y-axis is number of similar histograms per 360 compared pairs.

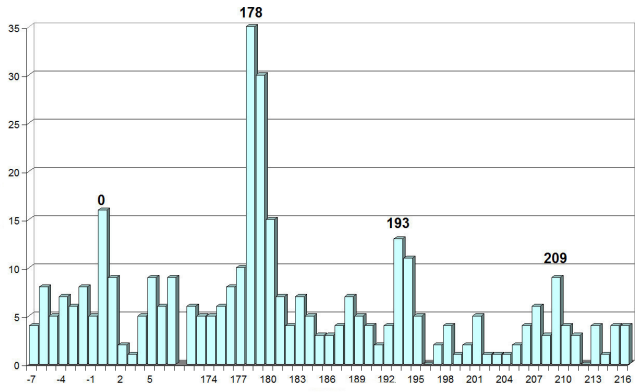

Fig. 10: Effect of synchronism by local time revealed upon comparison of the histograms constructed for the measurements of ^{90}Sr β-activity in Novosibirsk and ^{239}Pu α-activity in Pushchino with a collimator directed west. X-axis is time interval in minutes, Y-axis is number of similar histograms per 360 compared pairs.

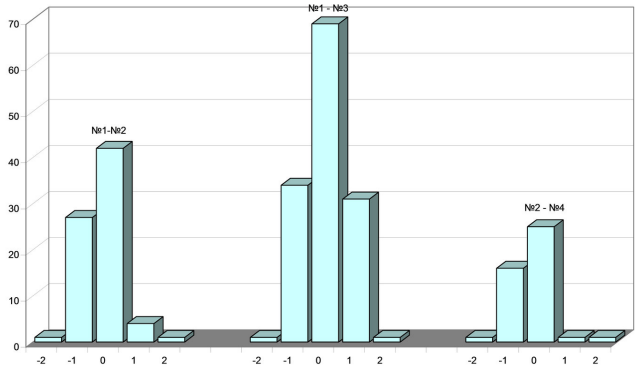

Fig. 11: Measurements of ^{90}Sr β-activity. The "palindrome effect" revealed upon comparison of a daytime histogram sequence (no. 1; from 6:00 to 18:00 by accurate local time) to the non-inverse (no. 2) and inverse (no. 3) nighttime sequences (from 18:00 to 6:00 of the next day) and the next daytime sequence (no. 4). X-axis is time interval in minutes, Y-axis is number of similar histograms per 360 compared pairs.

The existence of well-resolvable sidereal and solar daily periods means a sharp anisotropy of the effects observed. The difference between the direction at the immobile stars (sidereal daily period) and the Sun (solar daily period) is about 1 degree. As seen in Fig. 9, these periods are 4 minutes apart, i.e., they are resolved with the accuracy of 15 angular minutes. We also observe spatial anisotropy in the effects of synchronism by the absolute and local time [1, 11].

One can see the effect of spatial anisotropy in Fig. 10, which demonstrates local-time synchronism in the change of the shape of histograms constructed for the measurements of ^{90}Sr β-activity in Novosibirsk (no. 1) and ^{239}Pu α-activity in Pushchino with a west-directed collimator. The calculated difference in local time is equal to 179–180 min. As seen in Fig. 10, there is a sharp extremum – evidence of the effect – at 178^{th} minute (peak height, 134 similar pairs). Other extrema, corresponding to the moments of absolute-time synchronism (at 0^{th}, 193^{rd} and 209^{th} minutes), are substantially lower (peak height, 16 similar pairs and less).

Thus, the measurements of ^{90}Sr β-activity performed in Novosibirsk give us another confirmation of universality of the effects described earlier.

As the last illustration, we shall consider the "effect of palindrome", which indicates a dependence of the histogram shape on the spatial relation between the directions of the Earth diurnal rotation and its movement along the circumsolar orbit [8, 9]. The effect consists in the reverse change of the histogram sequences at the moments when the relation between the directions alternates its sign. According to the previously published works, it occurs at 6:00 and 18:00 by accurate (longitudinal) local time. In the course of its diurnal rotation, the Earth starts moving against its orbital translocation at 6:00. At 18:00, the directions of both movements become the same. The effect manifests itself in a dramatic difference in the similarity of consecutive histograms when a "daytime" histogram sequence (from 6:00 to 18:00) is compared to either inverse or non-inverse "nighttime" sequence (from 18:00 to 6:00 of the next day). This effect is illustrated in Fig. 11.

The effect of palindrome is clearly seen in Fig. 11. After inversion of one half of a day (in the points of palindrome), the number of similar histogram pairs doubles.

4 Discussion

The objective of this paper was to check if the results of ^{90}Sr β-activity measurements conducted by E.Y. Filin can be compared with the results of other measurements obtained within the research on "cosmo-physical fluctuations". As follows from the presented data, all the expected effects were reproduced with these experiments. Since β-particles run a distance of a few meters in the air (in contrast to α-particles, which run only a few centimeters), these measurements can be a valuable tool for a study of the spatial anisotropy of the observed effects.

Acknowledgements

The authors are grateful to M.E. Astashev and V.A. Kolombet for their help in measuring α-activity and data processing, as well as for participation in the discussion of the results.

Submitted on March 31, 2015 / Accepted on April 29, 2015

References

1. Shnoll S.E. Cosmo-physical factors in stochastic processes. Svenska Fysikarkivet, Stockholm, 2009.
2. Shnoll S.E., Kolombet V.A., Pozharsky E.V., Zenchenko T.A., Zvereva I.M., Konradov A.A. Realization of discrete states in the course of fluctuations of macroscopic processes. *Uspekhi Fiz. Nauk*, 1998, v. 168(10), 1129–1140 (in Russian).
3. Shnoll S.E., Kolombet V.A., Pozharsky E.V., Zenchenko T.A., Zvereva I.M., Kondradov A.A. Cosmo-physical causation of "macroscopic fluctuations". *Biofizika*, 1998, v. 43(5), 909–915 (in Russian).
4. Shnoll S.E., Zenchenko T.A., Zenchenko K.I., Pozharsky E.V., Kolombet V.A., Konradov A.A. Regular changes in the fine structure of statistical distributions as a consequence of cosmo-physical causes. *Uspekhi Fiz. Nauk*, 2000, v. 170(2), 214–218 (in Russian).
5. Shnoll S.E. Changes in fine structure of stochastic distributions as a consequence of space-time fluctuations. *Progress in Physics*, 2006, v. 2, 39–45.
6. Shnoll S.E. Fine structure of statistical distributions as a reflection of spatial and gravitational anisotropy of our world. *Russian Chem. J.* (Journal of D.I. Mendeleev's Russian Chemical Society), 2007, v. 51(1), 150–157 (in Russian).
7. Shnoll S.E. A cosmo-physical nature of the "idea of shape" of histograms constructed from the results of measurements of processes of diverse nature. In "Metaphysics. XXI Century", 2007, issue 2 (Y.S. Vladimirov, ed.) Binomial C Press, 284–319 (in Russian).
8. Shnoll S.E., Panchelyuga V.A., Shnoll S.E. The palindrome effect. *Progress in Physics*, 2008, v. 2, 151–153.
9. Shnoll S.E. The "scattering of the results of measurements" of processes of diverse nature is determined by the Earth's motion in the inhomogeneous space-time continuum. The effect of "half-year palindromes". *Progress in Physics*, 2009, v. 1, 3–7.
10. Shnoll S.E. and Rubinstein I.A. Regular changes in the fine structure of histograms revealed in the experiments with collimators which isolate beams of alpha-particles flying at certain directions. *Progress in Physics*, 2009, v. 2, 83–95.
11. Shnoll S.E., Rubinstein I.A., Vedenkin N.N. "The arrow of time" in the experiments in which alpha-activity was measured using collimators directed east and west. *Progress in Physics*, 2010, v. 1, 26–29.
12. Kaminsky A.V. and Shnoll S.E. Cosmophysical factors in the fluctuation amplitude spectrum of Brownian motion. *Progress in Physics*, 2010, v. 3, 25–30.
13. Shnoll S.E., Astahev M.E., Rubinshtein I.A., Kolombet V.A., Shapovalov S.N., Bokalenko B.I., Andreeva A.A., Kharakoz D.P., Melnikov I.A. Synchronous measurements of alpha-decay of ^{239}Pu carried out at North pole, Antarctic, and in Pushchino confirm that the shapes of the respective histograms depend on the diurnal rotation of the Earth and on the direction of the alpha-particle beam. *Progress in Physics*, 2012, v. 3, 11–16.
14. Rubinshtein I.A., Shnoll S.E., Kaminsky A.V., Kolombet V.A., Astashev M.E., Shapovalov S.N., Bokalenko B.I., Andreeva A.A., Kharakoz D.P. Dependence of changes of histogram shapes from time and space direction is the same when intensities of fluctuations of both of light-diode provided light flux and ^{239}Pu alpha-activity are measured. *Progress in Physics*, 2012, v. 3, 17–24.
15. Shnoll S.E., Kaminsky A.V., Rubinstein I.A., Shapovalov S.N., Kharakoz D.P. Fine structure of the fluctuation-amplitude spectra constructed for the results of measurements of processes of diverse nature as a characteristic of inhomogeneities (anisotropy) of space-time. In "Metaphysics. XXI Century", 2012, issue 3 (Y.S. Vladimirov, ed.), Binomial C Press, 36–66 (in Russian).
16. Shnoll S.E. Fractality, "coastline of the Universe", movement of the Earth and macroscopic fluctuations. *Biofizika*, 2013, v. 58(2), 357–376 (in Russian).
17. Rubinstein I.A., Kaminsky A.V., Tolokonnikova A.A., Kolombet V.A., Shnoll S.E. Basic phenomena of "macroscopic fluctuations" are repeated on light beams generated by lasers or light-emitting diodes. *Biophysics* (transl. from *Biofizika*, in Russian), 2014, v. 59, issue 3, 492–502.
18. Kaminsky A.V., Rubinstein I.A., Shapovalov S.N., Tolokonnikova A.A., Kolombet V.A. and Shnoll S.E. "Macroscopic fluctuations" of light beams as a novel tool for astrophysical studies. *Astrophys. Space Sci.*, 2015, v. 355, 9–21.
19. Strelkov V.V. A new measure for histogram comparison in time series analysis. *Pattern Recognition Letters*, 2008, v. 29, 1768–1774.
20. Gruzdev A. Algorithmization of histogram comparing process. Calculation of correlations after deduction of normal distribution curves. *Progress in Physics*, 2012, v. 3, 25–28.
21. Khmaladze E.V. Martingal limit theorems for separate statistics. *Probability Theory and Its Applications*, 1983, v. 28(3), 504 (in Russian).
22. Udaltsova N.V., Urinov I.K. Estimation of the probability of observed extrema in the histograms constructed from small samples. In the Proceedings of the 3rd All-Union Conference "Perspective Methods of Planning and Analysis" (Grodno), 1988, p. 155–156 (in Russian).
23. Bodrova N.B. Udaltsova N.V., Ivanov P.S., Shnoll S.E. On the non-randomness of the shape of inconsistent histograms. SCBR Preprint, Pushchino, 1989.

Polarized Light from the Sun: Unification of the Corona and Analysis of the Second Solar Spectrum – Further Implications of a Liquid Metallic Hydrogen Solar Model

Pierre-Marie Robitaille[1] and Dmitri Rabounski[2]

[1]Department of Radiology, The Ohio State University, 395 W. 12th Ave, Columbus, Ohio 43210, USA
E-mails: robitaille.1@osu.edu[1], rabounski@ptep-online.com[2]

In order to account for the slight polarization of the continuum towards the limb, proponents of the Standard Solar Model (SSM) must have recourse to electron or hydrogen-based scattering of light, as no other mechanism is possible in a gaseous Sun. Conversely, acceptance that the solar body is comprised of condensed matter opens up new avenues in the analysis of this problem, even if the photospheric surface itself is viewed as incapable of emitting polarized light. Thus, the increased disk polarization, from the center to the limb, can be explained by invoking the scattering of light by the atmosphere above the photosphere. The former is reminiscent of mechanisms which are known to account for the polarization of sunlight in the atmosphere of the Earth. Within the context of the Liquid Metallic Hydrogen Solar Model (LMHSM), molecules and small particles, not electrons or hydrogen atoms as required by the SSM, would primarily act as scattering agents in regions also partially comprised of condensed hydrogen structures (CHS). In addition, the well-known polarization which characterizes the K-corona would become a sign of emission polarization from an anisotropic source, without the need for scattering. In the LMHSM, the K, F, and T-coronas can be viewed as emissive and reflective manifestations of a single coronal entity adopting a radially anisotropic structure, while slowly cooling with altitude above the photosphere. The presence of "dust particles", advanced by proponents of the SSM, would no longer be required to explain the F and T-corona, as a single cooling structure would account for the properties of the K, F, and T coronas. At the same time, the polarized "Second Solar Spectrum", characterized by the dominance of certain elemental or ionic spectral lines and an abundance of molecular lines, could be explained in the LMHSM, by first invoking interface polarization and coordination of these species with condensed matter in the chromosphere. The prevalence of polarized signals from the Rare Earth metals, a chemically unique group of the periodic table, provides powerful evidence, based on the "Second Solar Spectrum", that chemical reactions and coordination are taking place in the atmosphere of the Sun. This concept is also supported by the polarized signal from lithium, an element previously hypothesized to assist in stabilizing metallic hydrogen structures. The possibility that some atoms are coordinated with CHS implies that the relative abundance of elements cannot be simply ascertained through the analysis of emission or absorption lines in the solar atmosphere.

... it follows that a body, which absorbs more rays from one plane of polarization than from another, sends out in the same ratio more rays from the first plane of polarization than from the second.

Gustav Kirchhoff, 1860 [1]

1 Introduction

Recently, considerable doubt has been raised [2–4] relative to Kirchhoff's formulation of his law of thermal emission [1]. In this regard, the equivalence between emitted and absorbed radiation under conditions of thermal equilibrium, properly known as Stewart's law [5], has not been questioned. However, the German scientist's claim that the radiation within an arbitrary cavity will always be independent of the nature of the walls, while subject only to the temperature and the frequency of observation, has never been demonstrated experimentally and is unsupported by mathematical derivation [2–4]. Regrettably, even the proof of Kirchhoff's law of thermal emission, as advanced by Max Planck, has been found to be physically unsound [2].* As such, beyond the restatement of Stewart's law [5], it would appear that little can be preserved from Kirchhoff's classic paper [1].

Yet, there is an experimental aspect of Kirchhoff's work which can never be discounted, namely that a tourmaline plate can absorb radiation more favorably in one plane than in the other [1, § 16]:

*Since mathematics is the language of physics, this is a serious problem for all those who adhere to the validity of Kirchhoff's claims [2].

> *"A tourmaline plate, cut parallel to the optic axis, absorbs, at ordinary temperatures, more of the rays which strike it normally, if the plane of polarization of these is parallel to the axis than when it is perpendicular to it. Assuming that the tourmaline plate retains this property when it is at a glowing heat, it must give out rays in a direction normal to it, which are partially polarized in the plane passing through the optic axis and which is the plane perpendicular to that which is called the plane of polarization of tourmaline. I have proved this striking deduction from theory by experiment and it confirmed the same."*

With this observation, Kirchhoff was emphasizing that certain objects, especially when highly anisotropic in their crystal structure, could emit polarized light [6, p. 604]. Kirchhoff's finding, that the light emitted by a heated tourmaline plate was polarized in the same plane as that which preferentially absorbed light, had also been noted by Balfour Stewart [7, § 68]. P. P. Feofilov addressed this aspect of nature in his classic text on *The Physical Basis of Polarized Emission* [8, p. 33–34]:

> *"... in order that the polarization should appear in the radiation due to a macroscopic system, it is necessary that the mutual orientation of the elementary radiating systems should not be random. A random aggregate of anisotropic elementary radiators, gives, clearly, a completely unpolarized radiation. A regular orientation of the separate elements of a macroscopic system may be due to the properties of the system itself, and this is the case, for example, in anisotropic crystals, or it may be induced from outside by electric and magnetic fields, by mechanical action, or finally, by light incident from outside the system, since a light ray, because of its nature, is always anisotropic ... In the case of regular crystals, the orientation of the emitting centers may be complete, and the emitted light may be practically totally polarized ... "*

In the case of tourmaline, the degree of polarization can approach 40% [9, p. 112].

Beyond crystals, it is not generally known that incandescent metals can often be a source of strongly polarized light [9, p. 110 & 138]. This effect does not occur when observing metals perpendicular to the surface, but polarization can approach 90% when the angle of observation departs substantially from the normal, in studying a clean metal [9, p. 110 & 138]. Thin metal wires exhibit polarized emission [10, 11] and the heat radiation, from small but long cylindrical objects, can also be highly polarized [12]. More recently, polarized light emission has been noted from individual carbon nanotubes, their fibers, bundles, and arrays (see [13, 14] and references therein). Importantly, within these carbon-based bundles, the light emission maintained a blackbody spectral appearance [13].

Fig. 1: An anisotropic tourmaline crystal (National Mining Hall of Fame and Museum — Leadville, CO; 3/18/2015; Photo by PMR).

Still, Kirchhoff's observation relative to tourmaline [1], these others [6–14], and many more, which highlight the importance of anisotropy relative to the emission of polarized light, have been discounted by astronomy. Clearly, since the Standard Solar Model (SSM) advocates that the Sun is gaseous in nature, there is little room in modern astrophysics for condensed matter.* The stars are thought to be devoid of solids and liquids. Rather, most astronomers believe that these objects are composed either of gaseous plasmas or highly degenerate matter, in accordance with the stellar type involved and the dictates of mathematical models. Nonetheless, ample evidence exists that the Sun itself is comprised of condensed matter or, more specifically, of metallic hydrogen [15]. Thus, it is fitting to reconsider the lessons of the tourmaline plate [1] in order to obtain a new perspective with respect to the emission of polarized light by the Sun and the stars.

2 Polarized light in the corona

Knowledge that the solar corona emitted polarized light was first gained at the eclipse of 1868 [16, p. 44]. Schuster provided a mathematical treatment of the problem as early as 1879 [17]. But it was not until R. K. Young analyzed photographic plates of the eclipses of 1901, 1905, and 1908 with a Hartmann microphotometer, that the extent of polarization could be properly quantified [18]. Young discovered that polarization increased gradually, with increasing elevation above the photosphere, to a value of ~37% before slowly starting to decrease. He also noted [18] that the corona was

*With the exception perhaps of some planets, meteors, asteroids, etc.

> *"...formed from matter which has been projected from the Sun"* and that *"The distribution of matter in the corona is dependent on high inverse powers of the distance from the Sun's center, probably the sixth or eighth or a combination of the two."*

Young also believed that the polarization was due to the scattering of photospheric light by small particles. As a consequence of such early studies, it was established that the light arising from the K-corona was radially polarized [18].

With the advent of the Lyot coronograph in 1930, the study of the solar corona outside of total eclipses became possible [19]. That same year, Minnaert published his work on the nature of the continuous coronal light and its polarization [20]. Minnaert considered the idea that the corona was self-luminous [20]. Sixty years earlier, William Harkness had viewed a total eclipse from Iowa and had also concluded that the corona was *"...a highly rarefied self-luminous atmosphere surrounding the Sun"* [21, p. 199].

However, the concept that the corona could be self-luminous has been largely abandoned by astronomy. In part, this dates back to the days of Schuster and his analysis of the polarization question. The British scientist had treated a luminous sphere surrounded by small particles which could scatter the light, thereby producing the desired polarization [17]. Schuster noted that [17]:

> *"In reality the polarisation rapidly diminishes and very soon a point is reached at which no polarisation can be observed; the corona must therefore contain some matter which is either self-luminous or too large to polarise the light while scattering it ...The rapid decrease of polarisation with increasing distances from the Sun, as well as the comparatively small amount of observed polarization, shows that a large part of the light is not due to scattering particles. This light may either be produced by incandescence, or by particles which are too large to polarise the light in the act of scattering it."*

Like Schuster, Minnaert also left open the possibility that the corona was capable of both scattering photospheric light and self-emission [20]. For his presentation, Minnaert considered that the scattering, leading to polarization, was taking place through the action of free electrons.

Within the context of the SSM, K-coronal polarization is thought to be produced by relativistic electrons which scatter photospheric light such that most Fraunhofer lines can no longer be observed [16, p. 4-5 & 135].

At the same time, streamers are known to constitute the most polarized portion of the corona, with values ranging from 30-60% [16, p. 136–138]. Such findings, along with Young's discovery that the degree of polarization could first increase and then decrease with elevation above the photosphere [18], provide strong evidence that the cause of polarization must involve structure and not simply the presence of relativistic free electrons.

In this respect, given the degree of ionized atoms in the E-corona [16, p. 4–5 & 135], it is doubtful that the determinations of electron density from polarization measurements could be accurate [16]. Furthermore, such calculations discount the notion that condensed matter may well be present in this region of the Sun [22]. It has been proposed that the metallic hydrogen which makes up the corona is electron starved and this, in turn, not MK temperatures, leads to the presence of the highly ionized atoms which characterize the E-corona [23, 24]. The Liquid Metallic Hydrogen Solar Model (LMHSM) [15, 22–24] leaves little possibility for the presence of substantial numbers of free electrons, in the upper coronal atmosphere of the Sun. In order that a star can remain stable, it must work to salvage both its hydrogen [25–27] and its electrons [22–24]. Such an idea has only been advanced within the context of the LMHSM [15, 22–27].*

3 Unifying the K-, F-, and T-coronas in the LMHSM

Throughout much of the solar atmosphere, K-coronal polarized light is mixed with F-coronal radiation. The F-corona is characterized by the presence of Fraunhofer lines and, in the SSM, is believed to be produced by dust particles which act to scatter photospheric light without polarization [16, p. 4–5 & 135]. Indeed, polarization has been utilized as a basis of discriminating between the K- and F-coronas, as F-coronal light was initially thought to be unpolarized [32–34]. However, it soon became clear that the polarization of the F-corona beyond $5R_\odot$ could not be ignored [35].† Using the degree of polarization, attempts to excise a K-coronal signal has been

*One of the authors (PMR) recently became aware that Professor J.E. Hirsch proposed, in 1989, that sunspots might be composed of metallic hydrogen based on the presence of strong magnetic fields in these regions: *"Sunspots are characterized by having a lower temperature than their environment, and very strong magnetic fields. It is natural to conclude that metallic hydrogen develops large spin polarization in these regions"* [28]. Since no lattice structure was specified to account for the emission of sunspots, Professor Hirsch appears to have adopted the accepted view from the SSM that the lower emissivities from these structures are associated with decreased temperatures [28] and not due to changes in emissivity as a result of increased metallic character [15]. Unlike Robitaille, who has promoted the idea that sunspots reflect slightly higher densities relative to the photosphere [15], Professor Hirsch speaks of a lower density inside sunspots [28]. At the same time, Hirsch makes a compelling case for the importance of metallic hydrogen throughout astronomy, as a universal cause of magnetism. On a related question, based on solar densities of $\sim 150 g/cm^3$ associated with the SSM, Professor Setsuo Ichimaru has advanced that the solar core might be comprised of metallic hydrogen [29–31]. Conversely, while Robitaille recognizes the presence of a solar core, he has advocated that the Sun possesses a nearly uniform density of $\sim 1 g/cm^3$ (see [15] and references cited therein). This is because a density of $150 g/cm^3$ in the core, as proposed by Ichimaru [29–31], would leave little material to build condensed structures on the photosphere. Further, Robitaille's position is in keeping with the idea that liquids are essentially incompressible.

†Coronal polarization has been measured out to an amazing 10 solar radii [36, p. 187].

used to compute electron densities in this region [32–35]. The problem rests in that electron densities calculated in this manner are dictated by the very mechanism proposed for the polarization, without any independent confirmation that polarization was in fact produced by electrons. In addition, it is evident that there should be a strong decrease in free electron density as a function of distance from the Sun (e.g. [36, p. 188]). It is difficult to justify distant polarization with relativistic electrons.

Relative to the nature of the "dust" which is believed to constitute F-coronal matter in the SSM, Mukai et al. [37] advocated, in 1974, that graphite grains were the most likely candidate. They envisioned that the grains would sublime, as the distance to the solar surface was decreased, hence accounting for the known reduction in the F-coronal contribution in this direction [37]. A T-corona has also been hypothesized to exist, in order to account for the increased reddening of coronal light with increasing altitude above the photosphere [16, p. 4–5 & 135]. This reddening had been noted long ago by Allen [38]:

> *"microphotograms for solar distances varying from $R = 1.2\,s$ to $R = 2.6\,s$ show that the coronal radiation reddens slightly as the distance from the Sun is increased."*

Pondering on all of these fragmented pieces of information, there is a need to arrive at a unifying principle relative to the corona of the Sun.*

Rather than speak of the K-, F-, and T- coronas as separate entities [16, p. 4–5 & 135], the idea should be entertained that the corona is composed of condensed matter which is manifesting spatially variable emissive, reflective, and structural properties. It is logical to postulate that condensed coronal matter is based on photospheric Type-1 metallic hydrogen which has been ejected from the solar surface [22–24]. Since photospheric matter produces unpolarized radiation, it is reasonable that, in the lower solar atmosphere, coronal material will also lack the ability to significantly polarize light. Nonetheless, it will remain capable of self-emission. With elevation above the solar surface, the ejected photosheric material, which now constitutes the corona, begins to adopt a radially anisotropic structure, as manifested by streamers, for instance. Such structural anisotropy thereby enables the emission of polarized light from incandescent radially aligned coronal material [8]. This explains the presence of the K-coronal signals. No Fraunhofer lines are present, because the coronal matter is self-luminous and positioned above the elevation where intense absorption by free atoms or ions is possible. With increased elevation above the photosphere, coronal material begins to cool, loosing incandescence. In response to decreased temperatures, emissivity decreases and reflectivity increases, much like the iron rod placed in a forge. With increased reflectivity, coronal material becomes less able to emit polarized light in the visible range. Rather, it now increasingly reflects photospheric light. That is why the Fraunhofer lines become visible in the F-coronal spectrum. At the same time, since coronal material is cooling, it begins to emit its light, not in the visible, but in the infrared. Hence, the production of the T-coronal spectrum.

With this new proposal, the K-, F-, and T- coronas simply become manifestations of the same coronal material. A streamer can be viewed as a real structure whose emissive and reflective behavior is characterized by both temperature and structural changes within the *same* entity. A streamer is unlikely to be comprised of an assembly of isolated gaseous ions or atoms, as currently held by the SSM, as the simplest explanation for such structure rests upon condensed matter.

As for the E-corona [39], it is being produced, not by the presence of MK temperatures in the corona, but rather through the removal of atomic and ionic electrons by condensed coronal material [15,22–24]. With increased elevation above the photoshere, the coronal metallic hydrogen, which acts to channel electrons back onto the solar surface, can be viewed as becoming increasingly electron starved. As a result, any ion or atom which comes into contact with such material will be likely to be stripped of electrons, since the Sun is working to maintain neutrality [22–24]. Electron affinities, not extreme temperatures, govern the production of highly ionized elements in the corona.

4 Polarization at the solar limb

In 1946, Chandrashekhar, through mathematical consideration of Thomson scattering by electrons [40, p. 249], first advanced that the body of the stars could emit a continuous spectrum, characterized by polarization, concluding that [41]

> *"the degree of polarization must vary from zero at the center of the disk to 11 per cent at the limb"*

Using similar approaches, Sobolev confirmed Chandrashekhar's finding [42] and the problem has been extensively reviewed [43, p. 119–203].

According to Dolginov, Gnedin and Silant'ev [43, p. 120], stellar polarization can be attributed to three major factors:

> *"a) nonsphericity of stellar shape, b) the eclipses of a hot star within a binary system, c) scattering in a nonspherical circumstellar envelope by gas flux."*

They argue that even a spherical star can have mechanisms for changes in luminosity across its surface, the most important of which might be temperature variations [43, p. 121]. The scattering of light by electrons has continued to play an

*The idea that the F-corona was produced by interplanetary dust particles was initially adopted in accounting for the behavior of the corona, even within the context of the LMHSM [22–24]. However, upon further reflection, it is clear that the SSM explanation for the presence of the F-corona should not be salvaged.

important role, relative to accounting for the production of polarized light in the context of gaseous stars and the SSM.

In the final analysis, the need to account for the production of polarized light in a gaseous object requires a suspension of objective reality. For instance, Chandrashekhar's analysis depends on the generation of polarized light from a gaseous star [41]. Yet, at the same time, the SSM views the Sun and the stars as a nearly ideal blackbody emitters [44–46]. It is well-known that blackbodies are incapable of emitting polarized light, by definition (see [47, p. 450], and [48, §5 &107]). Hence, it should have been difficult for proponents of the SSM to accept Chandrashekhar's claim that a gaseous star could emit up to 11.7% polarized light at the limb, a number which was actually very large [41]. In order to reconcile Chandrashekhar's findings with the SSM and blackbody behavior, a gaseous Sun must be divided into that opacity region which produces the thermal spectrum and an upper layer responsible for polarization [49,50]. The reality remains that, since the Sun sustains convection currents and conduction, it makes for a very poor example of a blackbody [15], as highlighted by Max Planck himself [48, § 51]. Moreover, because Thomson scattering by an electron is frequency independent [51, p. 69] and the polarization of the continuous solar spectrum is frequency dependent, Rayleigh scattering by neutral hydrogen had to be introduced to reconcile theory [40–43] with solar observations [49, 50].

In order to account for the slight degree of frequency-dependent polarization in the continuous spectrum towards the solar limb, it is more prudent to postulate that the body of the Sun emits unpolarized light. A single photon can be considered which leaves the photosphere at the center of the solar disk. That photon, if it escapes at an angle far from the normal, could then travel in the direction of the limb. Along its path, it will encounter molecules and small particles which could cause scattering in the direction of the Earth. In this manner, photons experiencing a 90° scatter towards the Earth could then be polarized.* It does not depend on the electron and does not necessitate that the body of the Sun itself emit polarized light, as theoreticians have proposed [41–43]. The only requirement rests in acceptance that both polarizing molecules and various forms of condensed matter† exist above the photosphere of the Sun, a concept supported by ample evidence, including both spectroscopy and coronal seismology [15].

5 Polarization and second solar spectrum

Beyond the frequency dependent polarization of the continuous solar spectrum [49, 50], the Sun also emits polarized light from numerous individual spectral lines. In combination, these two findings lead to the "Second Solar Spectrum" [49,50,56–67]. Brief historical accounts of this problem have been presented [58, 61] and the major features of the Second Solar Spectrum are as follows:

1. Relative to the Fraunhofer spectrum, these signals are extremely weak, rarely exceeding a Q/I level of 10^{-3} in the visible range [57, 58].

2. The most important atomic lines in the Second Solar Spectrum are produced from Ti I and Cr I [58]. These two elements possess ground state electronic configurations of $[Ar]3d^24s^2$ and $[Ar]3d^54s^1$, respectively.‡

3. The phase of the emission lines relative to the continuum can be highly variable [61]. Therefore, spectroscopic lines are said to either add to (i.e. polarize [61]) or subtract from (i.e. depolarize [62]) the continuum polarization. It is also said that the lines appear, either in emission or absorption, for the same reason [50], but that the strongest lines tend to be depolarizing [57].

4. The strongest polarizing lines include the following: H I , Na I, Mg I, Ca I, Ca II (6.11 eV), Ti I, Ti II (6.83 eV), V I, V II (6.75 eV), Cr I, Mn I, Fe I, Co I, Ni I, Cu I, Sr I, Sr II (5.69 eV), Zr I, Zr II (6.63 eV), Nb II (6.76 eV), Ru I, Pb I, Ba I, and Ba II (5.21 eV) [61].§

5. The spectrum is particularly rich in molecular lines, including, most notably, lines from MgH, C_2, and CN [56,57, 63–65]. The intensity of this polarization increases towards the solar limb.

6. The spectrum contains an amazing array of lines from the Rare Earth elements: Sc II (6.56 eV), Y I, Y II (6.22 eV), La II (5.58 eV), Ce II (5.54 eV), Nd II (5.53 eV), Sm II (5.64 eV), Eu II (5.67 eV), Gd II (6.15 eV), Dy II (5.94 eV), and Yb I [61].

7. Lithium, Li, is barely detectable in the regular solar spectrum of the photosphere [70], but its doublet at 6708 Å appears at the $\sim 10^{-4}$ level in the polarized spectrum [57, 67]. This constitutes a tremendous increase in relative detectability for this element.

5.1 The second solar spectrum and the standard solar model

Adherence to the SSM brings many difficulties when studying the Second Solar Spectrum. A means must first be found to excite these atoms or molecules, such that they can later emit the required line spectrum. The only reasonable mechanism available, in the context of a gaseous Sun, involves

*The phenomenon parallels that which occurs daily with sunlight in the atmosphere of the Earth [9, 47, 52–54].

†Atomic clusters are known to be polarizable [55, p. 64–85]. Thus, it might be appropriate to consider that small hydrogen based atomic clusters might also be present in the solar chromosphere and corona.

‡The calculated, or experimentally determined, static electric dipole polarizabilities, α_D, of neutral atoms in their ground state are readily available (see e.g. [68, p. 11] and [69, § 10; 188–189]). However, these values are of limited interest for this problem, as the polarizability of the excited atoms or ions may be more appropriate to consider, but are not easily ascertained.

§The elements followed by a Roman numeral I are neutral and said to be in spectroscopic state I. Elements in the +1 oxidation state are in the second spectroscopic state (i.e. state II). The ionization energy for each element involved in producing its state II ion is provided in brackets [69, § 10;197–198].

direct excitation through photon absorption and subsequent re-emission. Thus, a random process is invoked. Chemical reactions are never considered, despite the fact that the chemically similar Rare Earth elements produce prominent signals. Furthermore, all ionic strongly polarizing lines present were produced by the removal of a single electron from atoms, requiring ~6 eV of energy, as can be ascertained by examining the ionization potentials listed in 4 and 6 above.

In the SSM, a polarization mechanism must also be advanced, namely anisotropic radiation. Thus, in order to polarize the emitting species, proponents of the SSM must also have recourse to anisotropic light as follows [57]:

> *"The polarization arises because the incident radiation, being anisotropic, induces a net dipole moment in the scattering particle. If the particle does not suffer a collision before it re-radiates, the phase relations between the vector components of the dipole moment ... are preserved and become imprinted on the scattered radiation."*

Such arguments bring further complications, as a cause for anisotropic radiation in the atmosphere of a fully gaseous Sun must now also be advanced. In the end, the center-to-limb variation (CLV) in solar intensity is adopted, to account for the anisotropic light [49, 50, 57]. However, at the level where these lines are being produced, such a mechanism is unlikely to be valid. Thus, it is also advanced that *"... local inhomogeneities on the Sun will produce scattering polarization all over the solar disk ..."* [57]. But, in the SSM, there can be no local cause of inhomogeneities. The magnetic fields, so often advanced to explain such inhomogeneities, cannot be reasonably generated in the context of a gaseous Sun [15].

Finally, since many of the lines appear to *depolarize* the continuum polarization, some means of accounting for this effect must be brought forward. In this regards, three mechanisms have been hypothesized [61]: 1) Hanle depolarization produced by random magnetic fields [57, 71], 2) collisional depolarizations produced by hydrogen atoms (see [72] and references cited therein) and 3) radiation transfer effects (see [72] and references cited therein). Consequently, magnetic fields must be applied in the SSM, both to produce the anisotropic light required for polarization and as a means of depolarization. At the same time, collisional depolarization using the hydrogen atom contradicts one of the tenets of the gaseous Sun, namely that collisional processes are not significant in the gaseous solar atmosphere associated with the SSM: *"Collisional processes of excitation and de-excitation occur so seldom that they are of no importance"* [73, p. 10]. This is because, within this model, the chromosphere and corona exist as tremendous vacuums, essentially devoid of material and with inferred densities of less than 10^{-12} g/cm^3 (see references within [15]). While computations of collisional and radiation transfer effects might be reasonably applied to a few lines, the problem becomes daunting, when considering an entire spectrum, especially given that *"... our knowledge of the collisional rates is still very limited"* and *"... there are many physical processes that are involved in the generation and modification of the polarization"* [61].

The dilemmas faced in the context of the SSM relative to accounting for the Second Solar Spectrum has been outlined [61]:

> *"... probably one of the most important questions concerning the whole Second Solar Spectrum, that still waits for an answer, is why only particular lines, of certain elements, produce strong polarizing signals. For instance, one can wonder why some elements are particularly present with their lines in the Second Solar Spectrum, whereas other elements of comparable abundance are totally absent."*

5.2 The second solar spectrum and the LMHSM

Novel insight can be gained, with respect to the Second Solar Spectrum, if the findings are interpreted within the context of a model wherein condensed matter participates in the generation of spectroscopic lines.

5.2.1 Excitation and relaxation in the LMHSM

Contrary to the SSM which advocates that emitting species must first be excited through the interaction with light, followed by re-emission disconnected from chemical processes, the LMHSM proposes that all emission lines are inherently linked to chemical or electrical processes in the Sun [23–27]. In the corona, the interaction between free atoms or ions with condensed matter results in the production of highly ionized species, like FeXXV [23, 24], since condensed matter has the ability to maintain a higher electron affinity than a free atom. It is this affinity, not the presence of extreme temperatures, which is hypothesized to be responsible for the production of such highly ionized atoms in the corona [23, 24]. In this manner, the body of the Sun can recapture lost electrons, by stripping coronal atoms or ions and channeling the resulting harvest back down to the photosphere. Consequently, the emission lines observed in the corona are associated with the capture of electrons from free atoms or ions by condensed matter. Such processes should be exothermic in nature, hence their association with light emission [23, 24]. Electron capture is thus associated with the activation of a highly ionized species which then emits the well known coronal lines. Unlike the SSM, light need not be invoked to excite these highly ionized species. Collisional relaxation processes are not important in this region of the Sun. Any excited ion achieves the ground state through the emission of light.

As for the chromosphere, it has been viewed as the site of proton and hydrogen recapture [25–27]. The hypothesized condensation reactions take advantage of hydrogen's tremen-

dous ability to form hydrides. These are then used to deposit hydrogen atoms onto condensed hydrogen structures, CHS [25–27]. Such a model can account for the presence of both He I and He II emission lines in the chromospheric spectrum [27]. In this case, line emission becomes associated with exothermic hydrogen based condensation reactions [25–27]. Collisional processes of excited atoms or ions back to the ground state is not necessary either for further excitation or relaxation back to the ground state.

In combination, the mechanisms advanced in the corona and chromosphere act to reclaim both protons and electrons in the outer solar atmosphere and, thereby, help to maintain mass and charge balance in the LMHSM. Such means of preserving the integrity of the Sun are absent in the SSM.

As mentioned above, in order to account for the behavior of several ions in the Second Solar Spectrum, collisional depolarization mechanisms have been invoked (see [72] and references cited therein). Yet, such random processes are unlikely to be of true significance in governing the behavior of emission lines in this spectrum, as definite lineshapes must depend on repeatable processes, not chance occurrence. Moreover, the densities for the chromosphere proposed in the SSM of 10^{-12} g/cm^3 (see references within [15]), leave little room for such processes. Lineshapes are inherently linked to the environment in the vicinity of the emitter itself. It is this microenvironment which must be considered, not the presence of macroscopic phenomena, as will be addressed in the next section.

In the LMHSM, the presence of condensed matter and elevated chromospheric densities, well-beyond the densities of the Earth's atmosphere, are entirely compatible with a condensed solar photosphere. Unlike the setting proposed by the SSM, collisional processes can be invoked in the LMHSM. Such processes do not need to play any role in understanding the emission lines of the chromosphere and corona. But they can provide an important relaxation mechanism for the Fraunhofer lines, as the atoms involved in photon absorption, must relax again prior to repeating the process. It is here that collisional relaxation mechanisms can play an important function, beyond simple scattering, in the context of the LMHSM. This is because, the LMHSM does not insist that the chromosphere of the Sun possesses a density which is vacuum-like and greatly inferior to that in the Earth's atmosphere. This is another important advantage of the LMHSM over the SSM.

5.2.2 Chemical reactions and the second solar spectrum

Rather than speak of polarizing (or emission) and depolarizing (or absorption) signals, it is best to consider all the lines in the Second Solar Spectrum as inherently polarized, but with an emission phase which can either add to or subtract from the polarized continuum. Thus, lineshape becomes a question of phase, as with any other spectroscopic process.

If a species is to have a net phase, then it must be relative to a common framework. In nuclear magnetic resonance (NMR), phase is determined relative to receiver channels placed in quadrature, with respect to one another, as dictated by a master oscillator. In NMR, lineshapes reflect specific nuclear environments and populations at the local level. These same principles can guide lineshape analysis in the Sun, with phase being determined by electronic orbital orientation relative to a polarizing interface. Since emission lines are being observed, then chemical activation of the emitting species can once again be invoked, but this time within the context of coordination of the emitting species.

As noted in introduction to section 5, the Second Solar Spectrum is characterized by many powerful lines from molecules and the Rare Earth elements [74]. Rare Earth metals are actually relatively abundant in the Earth's crust [74] and they are likely to be similarly abundant in the Sun with respect to the other metals, as polarization studies suggest. These elements share a common outer electron configuration often with a single electron in an outer d-shell and two electrons in the immediately inferior s-shell. In this regard, the Lanthanide series is slowly filling the 4f-shell, while maintaining a ($6s^25d^1$) outer configuration. The latter is similar to the Group IIIB elements of scandium (Sc), Yttrium (Y), and Lanthanum (La), which have outer electronic configurations of $4s^23d^1$, $5s^24d^1$, and $6s^25d^1$, respectively. Generally speaking, atoms with a single unpaired electron are easiest to polarize.

The presence of the Rare Earth elements in the Second Solar Spectrum strongly suggests that *a similar chemical reaction is responsible for all of these lines*. It is likely that these reactions involve the condensation of hydrogen onto CHS, a process which has been inherently tied to the function of the chromosphere in the LMHSM [25–27].

Consequently, Rare Earth metal hydrides could interact with CHS in the chromosphere. Upon release of their hydrogen atom, the resulting activated Rare Earth metal would be interface polarized by the adjacent CHS with which it would remain at least partially interacting. In this way, atomic orbitals always maintain the same orientation, relative to the surface and relative to all other ions or atoms involved in similar interactions with CHS, while maintaining coordination. As a result, the relative phase of all atoms involved in such processes would be dictated by coordination with the charged interface. Upon relaxation through emission, these atoms would then be released in association with the delivery of hydrogen.

The ability to deliver hydrogen and the exact strength and nature of the associated coordination would depend on the atomic species involved. Some atoms, like He for instance, may well participate in condensation reactions [27], but given their nobel gas electronic configurations, might be difficult to polarize and might remain uncoordinated during emission. Others, like the nobel gases below helium in group VIIIA of

the periodic table, would not be expected to interact at all with hydrogen. Hence, given their inability to participate in condensation reactions, they should be devoid of neutral atom chromospheric emission lines.

Thus, within the context of the LMHSM, it is reasonable to conceive that structures comprised of condensed matter exist in the chromosphere. Such condensed hydrogen structures, CHS, could possess a surface electric charge polarizing any atom brought in its proximity through interface polarization mechanisms. Each atomic species involved in condensation reactions would have a preferred means of being coordinated with the surface, in a manner dependent on their atomic orbitals. In such a way, it is possible to explain why a given line would adopt a consistent and at times complex appearance in the Second Solar Spectrum.

Support for the idea that chemical reactions are involved can be gained by appreciating not only the prevalence of the chemically similar Rare Earth metals, but also from the fact that all of the most polarizing lines from ions arise from elements with a first ionization potential of ~ 6 eV [61]. This cannot be coincidental, but strongly supports the contention that chemistry, and not random processes, are involved.

The same is true for the presence of molecular lines. Note that the three most important molecular species observed, namely CN, MgH, and C2, all have the potential of delivering hydrogen to CHS structures, through species such as HCN, MgH_2, HC_2, and HCCH.

Note also that, at first glance, none of the elements from Group IVA, VA, VIA, and VIIA (with the exception of Pb at the bottom of group IVA), appear to participate in generating the Second Solar Spectrum. Since these atoms are increasingly electronegative towards the upper right of the periodic table, they may share a lack of ability to enter into condensation reactions that involve the delivery of a hydrogen atom.

Finally, the presence of a doublet signal from Li in the polarized spectrum provides another important clue that chemical processes are involved [57, 67]. Signals from this element are weak or non-existent in other spectra (Fraunhofer, chromospheric, or coronal), leading proponents of the SSM to advocate depletion of Li in the Sun and the stars, despite its abundance in meteors [70]. Conversely, within the LMHSM, the paucity of detectable lithium has been linked to the ability of this element to stabilize metallic hydrogen, a proposal first advanced by Zurek et al. [75]. Coordination within the solar interior, not depletion, appears to be a more reasonable answer, especially given meteoric abundances [70]. This idea is also in keeping with the proposal that atoms, which are involved in condensation reactions, can be interface polarized in the excited state prior to emission. This helps to account for the presence of lithium in the Second Solar Spectrum. It also provides powerful evidence that interface polarization, not random processes and anisotropic radiation, is responsible for the production of the Second Solar Spectrum.

6 Conclusion

The study of solar and stellar polarimetry is one of the most fascinating aspects of astronomy, as the associated observations hold a treasure of clues, relative to the structure and functioning of the Sun, the stars, and the galaxies [76, 77]. At every turn, polarization studies also add tremendous support to the concept that the Sun is comprised of condensed matter [15]. In this regard, the LMHSM provides a strong platform to account for the polarization of the K-corona, enabling polarized self-emission from an anisotropic structure. At the same time, the model elegantly unifies the K-, F-, and T-coronas into a single entity, with variable emissivity based on cooling with elevation and increasingly radial anisotropy. The idea that the chromosphere and the corona act to recapture hydrogen and electrons which have escaped from the solar body has no equivalent in the SSM [23–27].

Given the evidence, it is more reasonable to postulate that the Second Solar Spectrum results from interface polarization and associated condensation reactions, rather than calling for anisotropic radiation, Hanle depolarization, and collisional depolarization.

Ample proof exists that the Second Solar Spectrum is inherently tied to chemistry, as the presence of Rare Earth elements, relevant ionization potentials, molecular lines, and phase sensitive lineshapes suggest. In the end, the Second Solar Spectrum is perhaps the most significant of all spectroscopic signals obtained from the Sun, as in its lines, the scientist can find compelling evidence for the presence of chemical reactions within the solar atmosphere.

Dedication

This work is dedicated to our friend, Larissa Borissova.

Submitted on: May 1, 2015 / Accepted on: May 11, 2015
First published online on: May 13, 2015

References

1. Kirchhoff G.R. Über das Verhältnis zwischen dem Emissionsvermögen und dem Absorptionsvermogen. der Körper fur Wärme und Licht. *Poggendorfs Annalen der Physik und Chemie*, 1860, v. 109, 275–301. (English translation by F. Guthrie: Kirchhoff G. On the relation between the radiating and the absorbing powers of different bodies for light and heat. *Phil. Mag.*, 1860, ser. 4, v. 20, 1–21; also found in Harper's Scientific Memoirs, edited by J. S. Ames: The Laws of Radiation and Absorption: Memoirs of Prévost, Stewart, Kirchhoff, and Kirchhoff and Bunsen, translated and edited by D. B. Brace, American Book Company, New York, 1901, 74–97, also available online).
2. Robitaille P.-M. and Crothers S.J. "The Theory of Heat Radiation" revisited: A commentary on the validity of Kirchhoff's law of thermal emission and Max Planck's claim of universality. *Progr. Phys.*, 2015, v. 11, no. 2, 120–132.
3. Robitaille P.-M. Blackbody radiation and the carbon particle. *Progr. Phys.*, 2008, v. 3, 36–55.
4. Robitaille P.-M. Kirchhoff's Law of thermal emission: 150 Years. *Progr. Phys.*, 2009, v. 4, 3–13.
5. Stewart B. An account of some experiments on radiant heat, involving an extension of Prévost's theory of exchanges. *Trans. Royal Soc.*

Edinburgh, 1858, v. 22, no. 1, 1–20 (also found in Harper's Scientific Memoirs, edited by J. S. Ames: The Laws of Radiation and Absorption: Memoirs of Prévost, Stewart, Kirchhoff, and Kirchhoff and Bunsen, translated and edited by D. B. Brace, American Book Company, New York, 1901, 21–50).

6. Wood R.W. Physical Optics (2nd Edition), The MacMillan Company, New York, N.Y., 1911.
7. Tait P.G. Sketch of Thermodynamics, Edmonston and Douglas, Edinburgh, 1868.
8. Feofilov P.P. The Physical Basis of Polarized Emission. Consultants Bureau, New York, N.Y., 1961.
9. Können G.P. Polarized Light in Nature (Translated by G.A. Beerling), Cambridge University Press, Cambridge, U.K., 1985.
10. Öhman Y. Polarized thermal emission from narrow tungsten filaments. *Nature*, 1961, v. 192, 254.
11. Bimonte G., Cappellin L., Carugno G., Ruoso G., Saadeh D. Polarized thermal emission by thin metal wires. *New J. Phys.*, 2009, v. 11, 033014.
12. Golyk V.A., Krüger M., Kardar M. Heat radiation from long cylindrical objects. *Phys. Rev. E*, 2012, v. 85, 046603.
13. Li P., Jiang K., Liu M., Li Q., Fan S. and Sun J. Polarized incandescent light emission from carbon nanotubes. *Appl. Phys. Lett.*, 2003, v. 82, 1763.
14. Singer S.B, Mecklenburg M., White E.R., and Regan B.C. Polarized light emission from individual incandescent carbon nanotubes. *Phys. Rev. B*, 2011, v. 83, 233404.
15. Robitaille P.-M. Forty lines of evidence for condensed matter – The Sun on trial: Liquid metallic hydrogen as a solar building block. *Progr. Phys.*, 2013, v. 4, 90–142.
16. Golub L. and Pasachoff J.M. The Solar Corona, Cambridge University Press, Cambridge, U.K., 1997.
17. Schuster A. On the polarization of the solar corona. *Mon. Not. Roy. Astron. Soc.*, 1879, v. 40, 35–56.
18. Young R.K. Polarization of the light in the solar corona. *Lick Observatory Bulletin*, 1910–1911, v. 6, no. 205, 166-181; summary in: *Publ. Astron. Soc. Pacific*, 1912, v. 24, no. 141, 123–125.
19. Lyot B. La couronne solaire étudiée en dehors des éclipses. *Comptes Rendus*, 1930, v. 191, 834–837.
20. Minnaert M. On the continuous spectrum of the corona and its polarisation. *Zeitschrift für Astrophysik*, 1930, v. 1, 209–236.
21. Dick S. Sky and Ocean Joined: The U.S. Naval Observatory 1830–2000. Cambridge University Press, Cambridge, 2003, p. 196–205.
22. Robitaille P.M. The Liquid Metallic Hydrogen Model of the Sun and the Solar Atmosphere II. Continuous Emission and Condensed Matter Within the Corona. *Progr. Phys.*, 2013, v. 3, L8–L10.
23. Robitaille P.M. The Liquid Metallic Hydrogen Model of the Sun and the Solar Atmosphere V. On the Nature of the Corona. *Progr. Phys.*, 2013, v. 3, L22–L25.
24. Robitaille P.M. The Liquid Metallic Hydrogen Model of the Sun and the Solar Atmosphere VII. Further Insights into the Chromosphere and Corona. *Progr. Phys.*, 2013, v. 3, L30–L36.
25. Robitaille P.M. The Liquid Metallic Hydrogen Model of the Sun and the Solar Atmosphere I. Continuous Emission and Condensed Matter Within the Chromosphere. *Progr. Phys.*, 2013, v. 3, L5–L7.
26. Robitaille P.M.The Liquid Metallic Hydrogen Model of the Sun and the Solar Atmosphere IV. On the Nature of the Chromosphere. *Progr. Phys.*, 2013, v. 3, L15–L21.
27. Robitaille P.M. The Liquid Metallic Hydrogen Model of the Sun and the Solar Atmosphere VI. Helium in the Chromosphere. *Progr. Phys.*, 2013, v. 3, L26–L29.
28. Hirsch J.E. Ferromagnetism in metallic hydrogen. *Phys. Letters A*, 1989, v. 141, 191–195.
29. Ichimaru S. Statistical Plasma Physics – Volume II: Condensed Plasmas, Addison-Westly, Redwood, CA, 1991 (reprinted by Westview Press, Boulder, CO, 2004).
30. Ichimaru S. and Kitamura H. Pycnonuclear reactions in dense astrophysical and fusion plasmas. *Phys. Plasmas*, 1999, v. 6, no. 7, 2649–2671.
31. Ichimaru S. Radiative proton-capture of high-Z nuclei in the sun and in liquid metallic hydrogen. *Phys. Letters A*, 2000, v. 266, 167–172.
32. van de Hulst H.C. The electron density of the solar corona. *Bull. Astron. Soc. Netherlands*, 1950, v. 11, no. 410, 135–149.
33. van de Hulst H.C. On the polar rays of the corona. *Bull. Astron. Soc. Netherlands*, 1950, v. 11, no. 410, 150–159.
34. Schmidt M. Brightness, polarization and electron density of streamers in the solar corona. *Bull. Astron. Soc. Netherlands*, 1953, v. 12, no. 447, 61–67.
35. Hayes A.P., Vorlidas A. and Howard R.A. Deriving the electron density of the solar corona from the inversion of total brightness measurements. *Astrophys. J.*, 2001, v. 548, 1081–1086.
36. Zirin H. The Solar Atmosphere. Blaisdell Publishing Company, Waltham, M.A., 1966.
37. Mukai T., Yamamoto T., Hasegawa H., Fujiwara A. and Koike C. On circumsolar grain materials. *Publ. Astron. Soc. Japan*, 1974, v. 26, 445–458.
38. Allen C.W. The spectrum of the corona at the eclipse of 1940 October1. *Mon. Not. Roy. Astron. Soc.*, 1946, v. 106, 137–150.
39. Phillips K.J.H, Feldman U. and Landi E. Ultraviolet and X-Ray Spectroscopy of the Solar Atmosphere. Cambridge University Press, Cambridge (U.K.), 2008.
40. Chandrasekhar S. Radiative Transfer. Dover Publications, Inc., New York, N.Y., 1960.
41. Chandrasekhar S. On the radiative equilibrium of a stellar atmosphere X. *Astrophys. J.*, 1946, v. 103, 351–370.
42. Sobolev V.V. A Treatise on Radiative Transfer (Translated by S.I. Gaposchkin), D. Van Nostrand Company, Inc., Princeton, N.J. 1963.
43. Dolginov A.Z., Gnedin Yu.N., and Silant'ev N.A. Propagation and Polarization of Radiation in Cosmic Media. Gordon and Breach Publishers, Basel, Switzerland, 1995.
44. Eddington A.S. The Internal Constitution of the Stars. Cambridge University Press, Cambridge, U.K., 1926.
45. Reddish V.C. The Physics of Stellar Interiors: An Introduction. Edinburgh University Press, Edinburgh, U.K., 1974.
46. Kippenhahn R. and Weigert A. Stellar Structure and Evolution. Springer-Verlag, Berlin, 1990.
47. Jenkins F.A. and White H.E. Fundamentals of Optics (4th Edition), McGraw-Hill, Inc, New York, 1976.
48. Planck M. The theory of heat radiation. P. Blakiston's Son & Co., Philadelphia, PA, 1914, http://gutenberg.org/ebooks/40030.
49. Fluri D.M. and Stenflo J.O. Continuum polarization in the solar spectrum. *Astron. Astrophys.*, 1999, v. 341, 902–911.
50. Stenflo J.O. Polarization of the Sun's continuous spectrum. *Astron. Astrophys.*, 2005, v. 429, 713–730.
51. van de Hulst H.C. Light Scattering by Small Particles, Dover Publications, New York, 1957.
52. Tenquist D.W., Whittle R.M., and Yarwood J. University Optics, Vol. II, Gordon and Breach Science Publishers, New York, 1970, p. 96–97.
53. Smith G.S. The polarization of skylight: An example from nature. *Am. J. Phys.*, 2007, v. 75, no. 1, 25–35.

54. Liu Y. and Voss K. Polarized radiance distribution measurement of skylight II. Experiment and data. *Applied Optics*, 1997, v. 36, no. 33, 8753–8764.
55. Bonin K.D. and Kresin V.V. Electric-Dipole Polarizabilities of Atoms, Molecules, and Clusters. World Scientific, Singapore, 1997.
56. Stenflo J.O. and Keller C.U. New window for spectroscopy. *Nature*, 1996, v. 382, 588.
57. Stenflo J.O. and Keller C.U. The Second Solar Spectrum: A new window for diagnostics of the Sun. *Astron. Astrophys.*, 1997, v. 321, 927–934.
58. Gandorfer A. A high resolution atlas of the Second Solar Spectrum.*APS Conference Series*, 2001, v. 236, 109–116.
59. Gandorfer A. The Second Solar Spectrum: A High Spectral Resolution Polarimetric Survey of Scattering Polarization at the Solar Limb in Graphical Representation, Vol. I: 4625Å to 6995Å, Hochschulverlag, AG an der ETH Zurich, 2000; Gandorfer A. The Second Solar Spectrum: A High Spectral Resolution Polarimetric Survey of Scattering Polarization at the Solar Limb in Graphical Representation, Vol. II: 3910Å to 4630Å, Hochschulverlag, AG an der ETH Zurich, 2002; Gandorfer A. The Second Solar Spectrum: A High Spectral Resolution Polarimetric Survey of Scattering Polarization at the Solar Limb in Graphical Representation, Vol. III: 3160Å to 3915Å, Hochschulverlag, AG an der ETH Zurich, 2005.
60. Nagendra K.N. and Stenflo J.O. Solar Polarization, Kluwer Academic Publishers, Dordrecht, Germany, 1999.
61. Belluzzi L. and Landi Degl'Innocenti E. A spectroscopic analysis of the most polarizing atomic lines in the Second Solar Spectrum. *Astron. Astrophys.*, 2009, v. 495, 577–586.
62. Fluri D.M. and Stenflo J.O. Depolarizing lines in the Sun's spectrum. *Astron. Astrophys.*, 2003, v. 398, 763–773.
63. Milić I. and Faurobert M. Modeling scattering polarization in molecular solar lines in spherical geometry. *Astron. Astrophys.*, 2012, v. 539, A10.
64. Landi Degl'Innocenti E. Polarization properties of resonance scattering in molecular bands.: The intermediate (a-b) coupling regime. *Astron. Astrophys.*, 2007, v. 461, 1–10.
65. Ramos A.A. and Bueno J.T. Evidence for collisional depolarization in MgH lines of the Second Solar Spectrum. *Astrophys. J.*, v. 635, L109–L112.
66. Manso Sainz R., Landi Degl'Innocenti E., and Bueno J.T. A qualitative interpretation of the Second Solar Spectrum of Ce II. *Astron. Astrophys.*, 2006, v. 447, 1125–1129.
67. Belluzzi L., Landi Degl'Innocenti E., and Bueno J.T. The physical origin and the diagnostic potential of the scattering polarization in the Li I resonance doublet at 6708Å. *Astrophys. J.*, 2009, v. 705, 218–225.
68. Maroulis G. Atoms, Molecules and Clusters in Electric Fields: Theoretical Approaches to the Calculation of Electric Polarizability. Imperial College Press, London, U.K., 2006.
69. CRC Handbook of Chemistry and Physics, 95th Edition (Internet Edition, W.M. Haynes, T.J. Bruno, D.R. Lide, Eds), Boca Raton, Fl, 2014–2015.
70. Robitaille P.M. Commentary on the Liquid Metallic Hydrogen Model of the Sun III. Insight into Solar Lithium Abundances. *Progr. Phys.*, 2013, v. 2, L12–L13.
71. Stenflo J.O. Limitations and Opportunities for diagnostics of solar and stellar magnetic fields in "Magnetic Fields across the Hertzsprung-Russell Diagram" (G. Mathys, S.K. Solanki, and D.T. Wickramasinghe, Eds.), APS Conference Series, 2001, v. 248, 639–650.
72. Derouich M., Sahal-Bréchot S. and Barklem P.S. Collisional depolarization and transfer rates of spectral lines by atomic hydrogen. IV. Application to ionized ions. *Astron. Astrophys.*, 2004, v. 426, 707–715.
73. Athay R.G. Radiation Transport in Spectral Lines. D. Reidel Publishing Company, Dordrocht, Hollarnd, 1972.
74. Barrett S.D. and Dhesi S.S. The Structure of Rare-Earth Metal Surfaces, Imperial College Press, London, 2001.
75. Zurek E., Hoffmann R., Ashcroft N.W., Oganov A.R., Lyakhov A.O. A little bit of lithium does a lot for hydrogen. *Proc. Nat. Acad. Sci. USA*, 2009, v. 106, no. 42, 17640–17643.
76. Clarke D. Stellar Polarimetry. Wiley-VCH Verlag GmbH & Co., Weinheim, Germany, 2010.
77. Dufay J. Galactic Nebulae and Interstellar Matter. Dover Publications, Inc., N.Y., N.Y., 1968.

LETTERS TO PROGRESS IN PHYSICS

Unmatter Plasma Discovered

Florentin Smarandache
University of New Mexico, Gallup, NM 87301, USA
E-mail: smarand@unm.edu

The electron-positron beam plasma was generated in the laboratory in the beginning of 2015. This experimental fact shows that unmatter, a new form of matter that is formed by matter and antimatter bind together (mathematically predicted a decade ago) really exists. That is the electron-positron plasma experiment of 2015 is the experimentum crucis verifying the mathematically predicted unmatter.

Unmmatter Plasma is a novel form of plasma, exclusively made of matter and its antimatter counterpart. It was first generated in the 2015 experiment [1, 2] based on the 2004 considerations [3].

There are four fundamental states of matter: solid, liquid, gas, and plasma. Plasma consists of positive ions and free electrons (negative particles), typically at low pressures, and it is overall almost neutral. Plasma is an ionized gas (as in fluorescent neon, in lightning, in stars, in nuclear reactors). An ion is a positive or negative charged particle. A positive ion is called cation, while a negative ion is called anion. If the ion is an atom, then it may contain less electrons than needed for being neutrally charged (hence one has a cation), or more electrons than needed for being neutrally charged (hence one has an anion). Similarly if the ion is a molecule or a group (of atoms or molecules). The process of forming ions is called ionization. The degree of ionization depends on the proportion of atoms that have lost or gained electrons. By applying a strong electromagnetic field to a gas, or by heating a gas, one obtains plasma.

Unmatter as theoretically predicted in the framework of the neutrosophic logic and statistics [4–6] is considered as a combination of matter and antimatter that bound together, or a long-range mixture of matter and antimatter forming a weakly-coupled phase. For example, the electron-positron pair is a type of unmatter. We coined the word *unmatter* that means neither matter nor antimatter, but something in between. Besides matter and antimatter there may exist unmatter (as a new form of matter) in accordance with the neutrosophy theory that between an entity and its opposite there exist intermediate entities.

The 2015 experiment [1, 2] on matter-antimatter plasma (*unmatter plasma*, in terms of the neutrosophic logic and statistics) was recently successful in the Astra Gemini laser facility of the Rutherford Appleton Laboratory in Oxford, United Kingdom. The 2015 experiment has produced electron-positron plasma. The positron is the antimatter of the electron, having an opposite charge of the electron, but the other properties are the same.

Also, the meson is a clear example of unmatter whose configuration includes a pair quark-antiquark. Unmatter is mostly expected to emerge in exotic states outside the boundaries of the Standard Model for particle physics (for example in the Dark Matter sector) and in the regime of high-energy astrophysical objects [7].

"It is definitely a jet of unmatter, because a plasma consisting of the electrons and the positrons is neither matter nor antimatter in the same time. This experiment is the truly verification of unmatter as the theoretical achievements of neutrosophic logic and statistics. This experiment is a milestone of both experimental physics and pure mathematics" [8].

Submitted on May 24, 2015 / Accepted on May 26, 2015

References

1. Sarri G., Poder K., Cole J., et al. Generation of neutral and high-density electron–positron pair plasmas in the laboratory. *Nature Communications*, 23 April 2015, 6:6747.
2. Feuerstein B. A matter-antimatter plasma. *Innovations Report*, 4 May 2015. Accessed from http://www.innovations-report.com/html/reports/physics-astronomy/a-matter-antimatter-plasma.html
3. Surko C.M. and Greaves R.G. Emerging science and technology of antimatter plasmas and trap-based beams. *Physics of Plasmas*, 2004, v.11, no. 5, 2333–2348.
4. Smarandache F. A new form of matter — unmatter, formed by particles and anti-particles. *Bull. of Pure and Appl. Sciences*, 2004, v. 23D, no. 2, 173–177.
5. Smarandache F. Matter, antimatter and unmatter. *Infinite Energy*, 2005, v.11, issue 62, 50–51.
6. Smarandache F. A new form of matter — unmatter, formed by particles and anti-particles. CERN CDS, EXT-2004-182, 2004.
7. Goldfain E. Private communication with the author. May, 2015.
8. Rabounski D. Private communication with the author. May, 2015.

Unexplained Oscillations in Deflection Angle Fluctuations of a Novel Type of Torsion Balance

Felix Scholkmann[1] and Alexander F. Pugach[2]

[1]Bellariarain 10, 8038 Zürich, Switzerland
[2]Main Astronomical Observatory of National Academy of Sciences, 27 Akademika Zabolotnoho St., 03680 Kiev, Ukraine
E-mails: felix.scholkmann@gmail.com, pugach@yandex.ru

For more than four years, fluctuations in the deflection angle $\theta(t)$ of novel type of torsion balance have been monitored at the Main Astronomical Observatory of National Academy of Sciences in Kiev, Ukraine. During this all-year recording, unpredictable spontaneous high-frequency oscillations were observed occasionally. The aim of the present paper was to investigate four of these high-frequency oscillatory events by performing a detailed time-frequency analysis. From the overall available $\theta(t)$ signal, we selected four 24-hour long segments containing a clearly visible oscillations observed on 20 and 21 November 2009 (data segments 1 and 2) and on 24 and 25 December 2012 (data segments 3 and 4). High-resolution time-frequency analysis was performed for each of the four data segments using the generalized S-transform with a hyperbolic window. The oscillation of $\theta(t)$ present in data segment 1 shows clearly an increase in frequency, starting at 0.0002205 Hz (period length $T = 75.59$ min) and ending at 0.0002325 Hz ($T = 71.68$ min). The oscillation of $\theta(t)$ present in data segment 2 has instead a stable frequency of $f = 0.000243$ Hz ($T = 68.59$ min). Both high frequency oscillations of $\theta(t)$ of data segment 3 and 4 show an increase in frequency, starting at 0.006179 Hz ($T = 161.84$ s) and ending at 0.006859 Hz ($T = 145.79$ s) for data segment 3, and starting at 0.005379 Hz ($T = 185.91$ s) and ending at 0.005939 Hz ($T = 168.38$ s) for data segment 4, respectively. In addition, the oscillation present in data segment 3 is periodically amplitude-modulated with a period length of $T = 57 \pm 4.2$ min. Regarding the origin of the observed high frequency oscillation we discuss possible technical or natural factors that could be related to these oscillations.

1 Introduction

At the Main Astronomical Observatory of National Academy of Sciences in Kiev, Ukraine, a high-sensitive torsion balance with a new design (termed "torsind", refering to the device's function as a *tors*ion *ind*icator) has been quasi-continuously measuring fluctuations of its angular deflection since 2009.

The specific design of the device (i.e. replacement of the linear light beam by a light disc of non-magnetic material and the free suspension of the disk with a specific type of monofilament) makes it insensitive to changes in the gravitational potential so that gravitational (tidal) influences from any directions are excluded in the measurements. In addition, since the device is sealed into a container, variations of temperature, pressure, humidity and environmental electric field strength do not influence the reading [1]. Also changes in the excitation of the ionosphere over the place of observation were shown not to influence the measured values of the device [1].

Based on the long-term measurement of the tosind's disc rotations, different types of non-random fluctuations in the time-dependent deflection angle $\theta(t)$ were observed.

The main oscillatory component in the variability is an (amplitude-modulated) diurnal oscillation (i.e. an increase in d/dt($\theta(t)$) at sunrise, a decrease at sunset and a maximum deflection at noon) [1, 2], having a period length of 1440.24 ± 2.60 min [2], indicating that it is related to solar and not sidereal time (length of sidereal day: 1436 min, solar day: 1440 min). Such a diurnal oscillation was also observed in other experiments where torsion or vertical pendulums were used [3–6].

The fluctuations of $\theta(t)$ measured by the torsind seem also to be related to cosmophysical processes and events since significant changes in $\theta(t)$ were observed during solar and lunar eclipses [1, 7–9], the transit of Venus across the Sun's disk [1], and even specific astronomical configurations [10]. Remarkably, it was observed that the torsind responds to a solar eclipse occurring on the opposite side of the globe [7, 10] or when the measurement is performed underground at a depth of 40 meters [8].

During the all-long recording as a whole, unpredictable spontaneous high-frequency (period length: $T < 24$ h) oscillations were observed occasionally.

The aim of the present paper was to investigate four of these high-frequency oscillatory events by performing a detailed time-frequency analysis.

The motivation to perform this kind of analysis was based on the first author's (FS) previous work on the analysis of unexplained oscillations in electrochemical reactions [11] and diffusion processes [12, 13].

2 Materials and Methods

2.1 Measurement Setup

As described in detail in [1], the torsind device resembles a classical torsion balance but has a very light aluminium disc (diameter: 120 mm, weight: approx. 100 mg) instead of a linear beam. The disc is suspended by a monofilament (diameter: 20 μm) made from natural silk, which has the advantage of not having a reverse torque when twisted. The disc rotation is monitored by a webcam and the image live-stream is processed automatically by custom-made software that determines the angular deflection θ every minute with a standard error of each measurement of $\pm$ 0.157° (determined under stable space weather conditions on 13 February 2013) [2].

The device is housed in a quartz glass cylinder (having a high of 240 mm and a wall thickness of 2 mm) with two round glass plates covering the top and bottom. Various efforts were made to isolate the torsind device from environmental changes [1]. To reduce electrostatic influences, the inner wall and the bottom of the glass cylinder are surrounded by a grounded aluminium foil. To ensure that environmental changes in humidity and pressure are not influencing the device, the edges of the quartz-glass housing are sealed with a silicon joint sealant material. The sealing also improves the thermal stabilization.

Measurements were made with the torsind in isolated, shaded room with tightly closed doors and windows at the Main Astronomical Observatory of National Academy of Sciences in Kiev. The place of measurement was selected to ensure that no technical electrical or mechanical processes were happening within a radius of 50 m that could influence the measurement (i.e. no electrical devices, no electromagnetic wireless data-transfer devices, no devices that cause mechanical vibrations).

Concerning the sensitivity of the torsind to detect (extremely) weak forces, the torque (M) of the minimal acceleration value that could be recorded by the device was estimated to be $M \approx 6.5 \times 10^{-12}$ Nm) [1].

2.2 Data

For the analysis presented in this paper, we selected four 24-hour-long signal segments from the overall available signal that contain a clearly visible oscillation. Two of the data segments show a long-lasting fast oscillation with multiple maxima during the 24-hour interval (recording dates: 20 November 2009 [data segment 1], 21 November 2009 [data segment 2]). The other two segments contain a brief, very fast oscillation (recording dates: 24 December 2012 [data segment 3], 25 December 2012 [data segment 4]). Thus, the two distinct oscillatory phenomena investigated in the present study occurred in November 2009 and December 2012. All signals were recorded with respect to Universal Time (UT1) which is the same everywhere on Earth due to its proportionality to the Earth's rotation angle with respect to the International Celestial Reference Frame.

2.3 Time-Frequency Analysis

High-resolution time-frequency analysis was performed for each of the four data segments, applying a specific type of Stockwell (S)-transform, the generalized S-transform (GST) with a hyperbolic window according to the approach developed by Pinnegar and Mansinha [14].

3 Results

3.1 Data Segments 1 and 2

Data segments 1 and 2 contain both a clearly visible oscillation of $\theta(t)$ (see subfigures a1–3 of Fig. 1).

The oscillation of $\theta(t)$ present in data segment 1 clearly shows a frequency increase, starting at 0.0002205 Hz (T = 75.59 min) and ending at 0.0002325 Hz (T = 71.68 min) (see subfigures b1 and c1 of Fig. 1). This is not the case for the oscillation of $\theta(t)$ present in data segment 2 which exhibits a stable frequency of f = 0.000243 Hz (T = 68.59 min) (see subfigures b2 and c2 of Fig. 1).

Subfigures b3 and c3 of Fig. 1 show the time-frequency spectrum of the combined signal (data segment 1 + data segment 2) with the increasing frequency on day one (20 November 2009) and the stable frequency on day two (21 November 2009).

3.2 Data Segments 3 and 4

A very high frequency oscillation is present in data segments 3 and 4.

The high frequency oscillation in data segment 3 started at 746 min and ended at 969 min (total duration: 223 min), whereas the start of the high frequency oscillation of data segment 4 started at 347 min and ended at 549 min (total duration: 202 min) (see subfigures a1 and b1, as well as a2 and b2 of Fig. 2). Thus, both periods of high-frequency activity are of similar duration.

Both high frequency oscillations of $\theta(t)$ of data segment 3 and 4 show an increase in frequency, starting at 0.006179 Hz (T = 161.84 s) and ending at 0.006859 Hz (T = 145.79 s) for data segment 3, and starting at 0.005379 Hz (T = 185.91 s) and ending at 0.005939 Hz (T = 168.38 s) for data segment 4. What distinguishes these two oscillatory events is that the oscillation present in data segment 3 is periodically amplitude-modulated (see subfigure c1 of Fig. 2) whereas such a periodic modulation is not obvious in the oscillation of data segment 4. Three peaks in the variability of the power can be distinguished that correspond to an amplitude-modulation with a period length of $T = 57 \pm 4.2$ min.

Besides the high frequency oscillations, both data segments contain strong shifts of $\theta(t)$. For data segment 3, two significant shifts can be identified within the time frame 318-376 min ($\theta(t)_{start} = 232.5°$, $\theta(t)_{end} = 774.7°$, resulting in $\Delta\theta(t)$

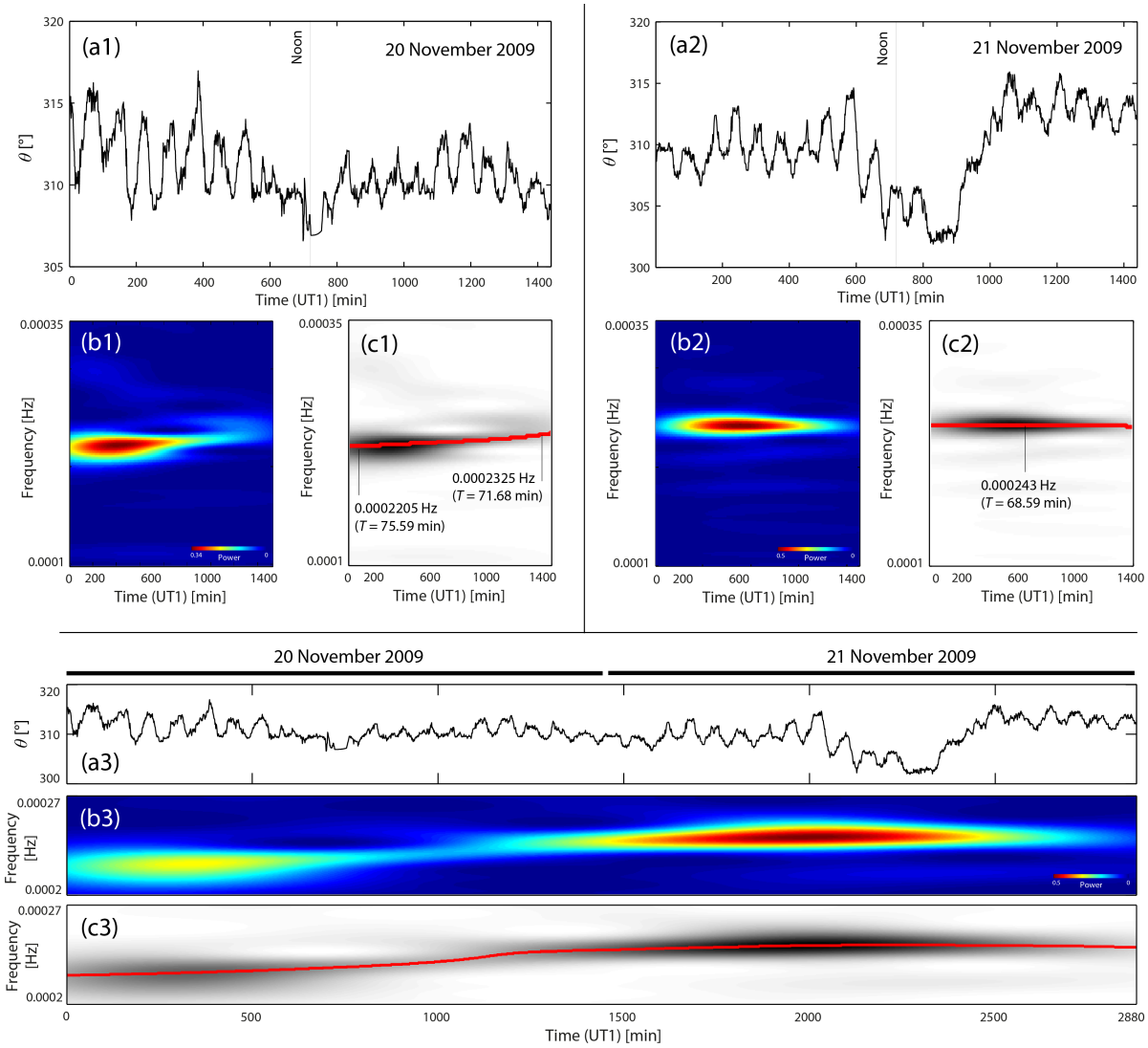

Fig. 1: (a1-a3) Time series of $\theta(t)$ recorded on 20 and 21 November 2009, as well as the stitched time series covering both dates. (b1-b3) Spectrogram showing the time-frequency changes of the oscillation. The power is color-coded. (c1-c3) Spectrogram with red line indicating the maximum power depending on frequency and time.

= 542.2°), and the time frame 1396–1402 min ($\theta(t)_{start}$ = 703.4°, $\theta(t)_{end}$ = 566.9°, resulting in $\Delta\theta(t)$ = 136.5°). In data segment 4, one strong shift is present, occurring in the time frame 1250–1273 min ($\theta(t)_{start}$ = 550.5°, $\theta(t)_{end}$ = 192.3°, $\Delta\theta(t)$ = 358.2°). These kind of shifts (also termed "spikes" [2]) correspond to moments when a strong rotational momentum is acting on the torsind.

4 Discussion and Conclusion

The analysis performed revealed that the fast variations observed in the four days of data segments exhibit oscillations with clearly defined frequencies. The fast oscillations starting at 20 and ending at 21 November 2009 are characterized by an increase in frequency. This characteristic of frequency increase is also observed in the very fast oscillations present in the data from 24 and 25 December 2012.

In the following we will briefly discuss the possibility that these oscillations could be artefacts caused by technical or natural processes, or effects from well-known factors associated with geophysical processes.

Artefacts caused by technical or natural processes. Torsion balance measurements can be generally influenced by changes in the local environmental parameters like temperature, humidity, pressure or electromagnetic fields. The influence of these factors was actively minimized during the measurement with the torsind by applying proper shielding and the effectiveness of the shielding was evaluated experimentally. For this reason, we conclude that it is unlikely that the observed oscillations are simply artifacts due to technical or

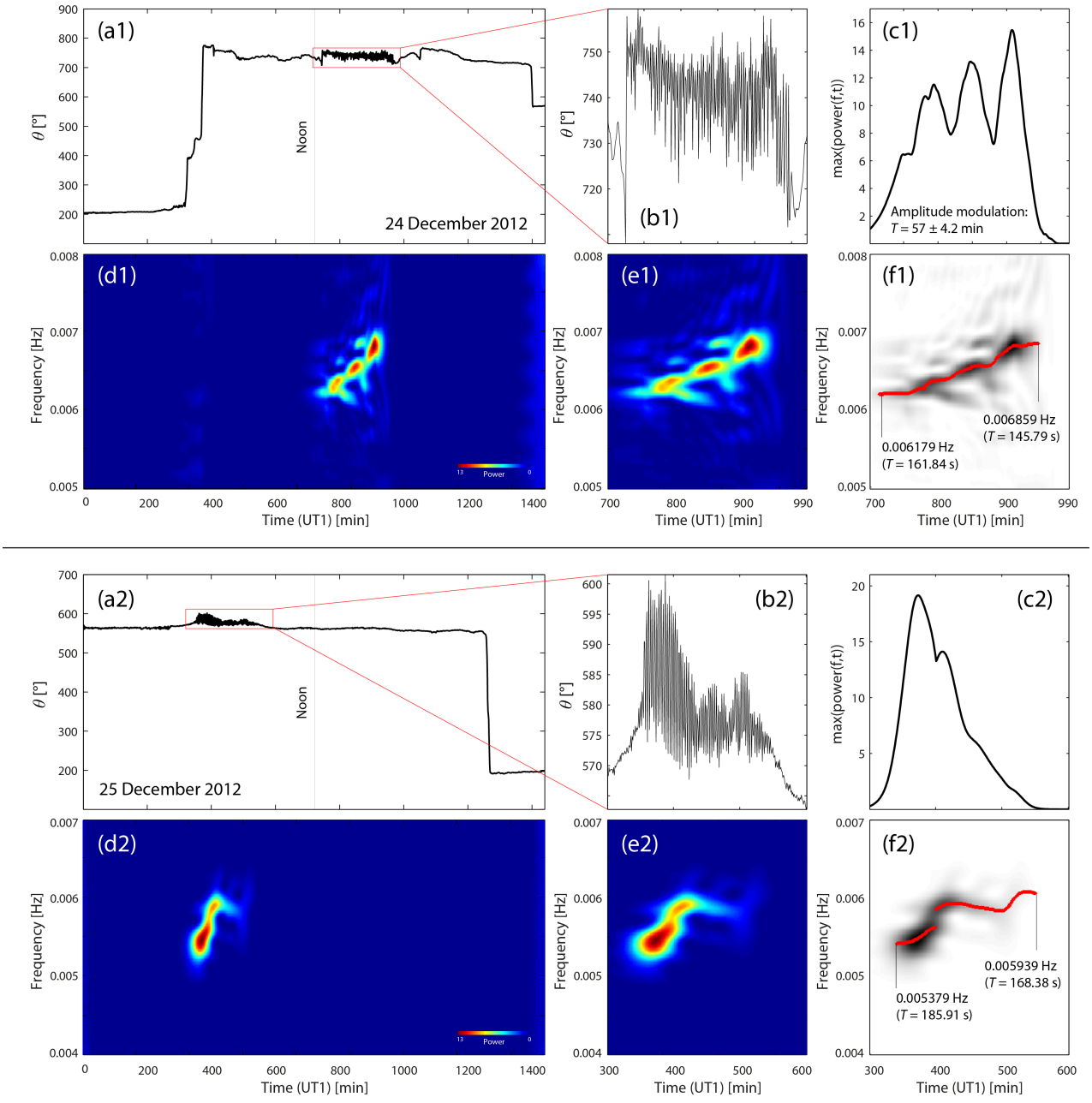

Fig. 2: (a1, a2) Time series of $\theta(t)$ recorded on 24 and 25 December 2012. (b1, b2) Zoom into the intervals with fast oscillations. (c1, c2) Time series of the maximum power depending on the frequency, showing a periodic (c1) and a unimodal (c2) amplitude modulation. (d1, d2) Spectrograms of the entire time series. The power is color-coded. (e1, e2) Spectrograms of the zoomed-in parts of the time series. (f1, f2) Spectrograms with red lines indicating the maximum power depending on frequency and time.

natural processes happening in the local environment of the measurement.

Effects from geophysical processes. What geophysical or astrophysical phenomena exhibit a frequency of approx. 0.002 Hz (as observed in data segments 1 and 2) or approx. 0.006–0.007 Hz (as observed in data segments 3 and 4)? It is known that the geomagnetic field can exhibit periodic fluctuations, termed "geomagnetic pulsations" [15, 16].

Those geomagnetic pulsations in the frequency range of 0.002–0.006 Hz ($T = 166.67 - 500$s), termed "Pc5 pulsations", overlap with the oscillation in $\theta(t)$ found in the present study. Geomagnetic pulsations are the result of solar wind disturbances (caused by increased solar activity) perturbing the magnetosphere and causing disturbances/modulations of the geomagnetic field. We checked whether there were any significant disturbances in the geomagnetic field on the dates of the data segments investigated (20–21 November 2009 and 24–25 December 2012) by analysing the hourly Dcx index (http://dcx.oulu.fi), i.e. the corrected Dst index [17, 18]. Geomagnetic disturbances are seen as negative deflections of the Dcx (and Dst) index, associated with an enhanced westward directed electric current during the geomagnetic storm. During the two periods (20–21 November 2009 and 24–25 December 2012) no geomagnetic storms or significant disturbances occurred. The observed oscillations in $\theta(t)$ can therefore to be regarded as most likely not caused by Pc5 geomagnetic pulsations.

Another principal possibility is low-frequency microseismic oscillations or "long-period seismic noise" [19]. However, it is known that in the range of 0.002–0.02 Hz microseismic activity is the lowest compared to the frequency ranges off approx. < 0.002 Hz and > 0.02 Hz [20, 21]. Also, these kinds of microseismic fluctuations in general do not exhibit the clear frequency stability and do not occur for such a long time span as observed in the $\theta(t)$ oscillations analysed in the present paper. Therefore, we believe microseismicity is unlikely to be responsible for the fast $\theta(t)$ oscillations.

Future experimental work involving measurements with the torsind and data analysis is needed to identify the mechanism causing the non-random fluctuations in $\theta(t)$ measured by the torsind device. Further data analysis is ongoing and will be reported in the near future.

Submitted on May 13, 2015 / Accepted on May 27, 2015

References

1. Pugach A. F. The torsind — A device based on a new principle for non-conventional astronomical observations. *International Journal of Astronomy and Astrophysics*, 2013, v. 3, 33–38.
2. Pugach A. F. Diurnal variations and spikes by the torsind registered and their impact on the accuracy of G measurement. *International Journal of Astronomy and Astrophysics*, v. 5 (1), 28–37.
3. Saxl E. J., Allen M. 1970 solar eclipse as "seen" by a torsion pendulum. *Physical Review D*, v. 3 (4), 823–825.
4. Neumann L., Kalenda P. Static vertical pendulum-apparatus for in-situ relative stress measurement. In F. Xie (Ed.), *Rock Stress and Earthquakes* (pp. 255–261). London: Taylor and Francis Group.
5. Bagley C. H., Luther G. G. Preliminary results of a determination of the Newtonian constant of gravitation: a test of the Kuroda hypothesis. *Physical Review Letters*, 1997, v. 78 (16), 3047–3050.
6. Stoyko N. Sur la variation jouralière de la mache des pendules et de la deviation de la verticale [On the diurnal variation of pendulum motion and of plumb line deflection]. *Comptes Rendus de l'Académie des Sciences*, 1947, v. 224 (20), 1440–1441.
7. Pugach A. F. Observations of the astronomical phenomena by torsion balance. *Physics of Consciousness and Life, Cosmology and Astrophysics*, v. 9 (2), 30–51.
8. Olenici D., Pugach A. F. Precise underground observations of the partial solar eclipse of 1 June 2011 using a Foucault pendulum and a very light torsion balance. *International Journal of Astronomy and Astrophysics*, 2012, v. 2 (4), 204–209.
9. Pugach A. F., Olenici D. Observations of correlated behavior of two light torsion balances and a paraconical pendulum in separate locations during the solar eclipse of January 26th, 2009. *Advances in Astronomy*, 2012, Article ID 263818.
10. Olenici D., Pugach A. F., Cosovanu I., Lesanu C., Deloly J.-B., Vorobyov D., Delets A., Olenici-Craciunescu S.-B. (2014). Syzygy effects studies performed simultaneously with Foucault pendulums and torsinds during the solar eclipses of 13 November 2012 and 10 May 2013. *International Journal of Astronomy and Astrophysics*, v. 4 (1), 39–53.
11. Scholkmann F., Muzuno T., Nagel D. J. Statistical analysis of unexpected daily variations in an electrochemical transmutation experiment. *Journal of Condensed Matter Nuclear Science*, 2012, v. 8 (3), 37–48.
12. Scholkmann F. Indications for a diurnal and annual variation in the anisotropy of diffusion patterns — A reanalysis of data presented by J. Dai (2014, Nat. Sci.). Progress in Physics, 2014, v. 10 (4), 232–235.
13. Scholkmann F. Solar-Time or sidereal-time dependent? The diurnal variation in the anisotropy of diffusion patterns observed by J. Dai (2014, Nat. Sci.). *Progress in Physics*, 2015, v. 11 (2), 137–138.
14. Pinnegar C. R., Mansinha L. The S-transform with windows of arbitrary and varying shape. *Geophysics*, v. 68 (1), 381–385.
15. Schott J. J., Kleimenova N. G., Bitterly J., Kozyreva O. V. The strong Pc5 geomagnetic pulsations in the initial phase of the great magnetic storm of March 24, 1991. *Earth, Planets and Space*, v. 50 (2), 101–106.
16. Saito T. Geomagnetic pulsations. *Sapce Science Reviews*, 1969, v. 10 (3), 319–412.
17. Marsular K., Karinen A. Explaining and correcting the excessive semiannual variation in the Dst index. *Geophysical Research Letters*, 2005, v. 32v. (14), L14107.
18. Karinen A., Marsula K. Correcting the Dst index: Consequences for absolute level and correlations. *Journal of Geophysical Research: Space Physics*, 2006, v. 111 (A8), A08207.
19. Tanimoto, T. Excitation of normal modes by atmospheric turbulence: source of long-period seismic noise. *Geophysical Journal International*, v. 136 (2), 395–402.
20. Nishida K., Kobayashi N., Fukao Y. Origin of Earth's ground noise from 2 to 20 mHz. *Geophysical Research Letters*, 2002, v. 29 (10), 51–54.
21. Agnew D. C., Berger J. Vertical seismic noise at very low frequencies. *Journal of Geophysical Research: Solid Earth*, 1978, v. 83 (B11), 5420–5424.

Analytical Study of the Van der Pol Equation in the Autonomous Regime

Hafeez Y. Hafeez [1], Chifu E. Ndikilar [2] and Sabo Isyaku [3]

Physics Department, Federal University Dutse, P.M.B. 7156, Jigawa State, Nigeria.
[1] Email: hafeezyusufhafeez@gmail.com
[2] Email: ebenechifu@yahoo.com
[3] Email: saboisyaku@gmail.com

The Van der Pol differential equation was constructed for an autonomous regime using link's law. The Van der Pol equation was studied analytically to determine fixed points, stability criteria, existence of limit cycles and solved numerically. The graphs of the equation are drawn for different values of damping coefficient μ.

1 Introduction

Balthazar Van der Pol (1899-1959) was a Dutch electrical engineer who initiated experimental dynamics in the laboratory during the 1920's and 1930's. He first introduced his (now famous) equation in order to describe triode oscillations in electric circuits, in 1927.

Van der Pol found stable oscillations, now known as limit cycles, in electrical circuits employing vacuum tubes. When these circuits are driven near the limit cycle they become entrained, i.e. the driving signal pulls the current along with it. The mathematical model for the system is a well known second order ordinary differential equation with cubic non linearity: the Van der Pol equation. The Van der Pol equation has a long history of being used in both the physical and biological sciences. For instance, Fitzhugh [1] and Nagumo [2] used the equation in a planer field as a model for action potential of neurons. The equation has also been utilized in seismology to model the plates in a geological fault [3].

During the first half of the twentieth century, Balthazar Van der Pol pioneered the field of radio telecommunication [4–9]. The Van der pol equation with large value of nonlinearity parameter has been studied by Cartwright and Littlewood in 1945 [10]; they showed that the singular solution exists. Also analytically, Lavinson [11] in 1949, analyzed the Van der Pol equation by substituting the cubic non linearity for piecewise linear version and showed that the equation has singular solution also. Also, the Van der Pol Equation for Nonlinear Plasma Oscillations has been studied by Hafeez and Chifu in 2014 [12]; they showed that the Van der pol equation depends on the damping co-efficient μ which has varying behaviour. In this article, the analytical study of the Van der Pol equation in the autonomous regime is studied.

2 Description of the Van der Pol oscillator

The Van der Pol oscillator is a self-maintained electrical circuit made up of an Inductor (L), a capacitor initially charged with a capacitance (C) and a non-linear resistance (R); all of them connected in series as indicated in Fig. 1 below. This oscillator was invented by Van der Pol while he was trying to find out a new way to model the oscillations of a self-maintained electrical circuit. The characteristic intensity-tension U_R of the nonlinear resistance (R) is given as:

$$U_R = -R_0\, i_0 \left[\frac{i}{i_0} - \frac{1}{3}\left(\frac{i}{i_0}\right)^3\right] \tag{1}$$

where i_0 and R_0 are the current and the resistance of the normalization respectively. This non linear resistance can be obtained by using the operational amplifier (op-amp). By applying the link's law to Fig. 1 below,

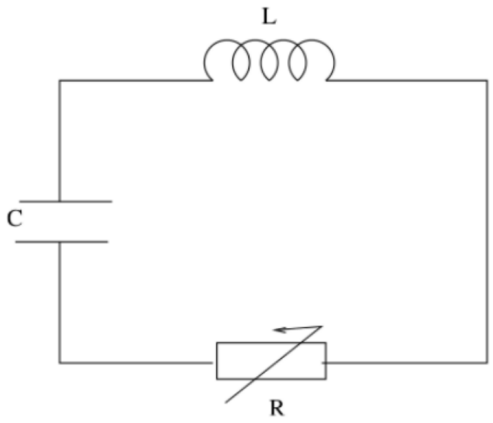

Fig. 1: Electric circuit modelizing the Van der Pol oscillator in an autonomous regime.

we have:

$$U_L + U_R + U_C = 0 \tag{2}$$

where U_L and U_C are the tension to the limits of the inductor and capacitor respectively and are defined as

$$U_L = L\frac{di}{d\tau} \tag{3}$$

$$U_C = \frac{1}{C}\int i d\tau. \tag{4}$$

Substituting (1), (3) and (4) in (2), we have:

$$L\frac{di}{d\tau} - R_0\, i_0 \left[\frac{i}{i_0} - \frac{1}{3}\left(\frac{i}{i_0}\right)^3\right] + \frac{1}{C}\int i d\tau = 0. \tag{5}$$

Differentiating (5) with respect to τ, we have

$$L\frac{d^2i}{d\tau^2} - R_0\left[1 - \frac{i^2}{i_0^2}\right]\frac{di}{d\tau} + \frac{i}{C} = 0. \tag{6}$$

Setting

$$x = \frac{i}{i_0} \tag{7}$$

and

$$t = \omega_e\tau \tag{8}$$

where $\omega_e = \frac{1}{\sqrt{LC}}$ is an electric pulsation, we have:

$$\frac{d}{d\tau} = \omega_e\frac{d}{dt} \tag{9}$$

$$\frac{d^2}{d\tau^2} = \omega_e^2\frac{d^2}{dt^2}. \tag{10}$$

Substituting (9) and (10) in (6), yields

$$\frac{d^2x}{dt^2} - R_0\sqrt{\frac{C}{L}}\left(1 - x^2\right)\frac{dx}{dt} + x = 0. \tag{11}$$

By setting $\mu = R_0\sqrt{\frac{C}{L}}$ Eq. (11) takes dimensional form as follows

$$\ddot{x} - \mu\left(1 - x^2\right)\dot{x} + x = 0 \tag{12}$$

where μ is the scalar parameter indicating the strength of the nonlinear damping, and (12) is called the Van der Pol equation in the autonomous regime.

3 Analytical study

3.1 Fixed points and stability

Transforming the higher order ODE (12) into a system of simultaneous ODE's i.e. let $x_1 = x$ and $x_2 = \dot{x}$

$$\begin{bmatrix} \dot{x_1} \\ \dot{x_2} \end{bmatrix} = \begin{bmatrix} x_2 \\ -x_1 + \mu\left(1 - x_1^2\right)x_2 \end{bmatrix}. \tag{13}$$

Introducing the standard transformation

$$y = x \tag{14}$$

$$z = \dot{x} - \mu\left(x - \frac{x^3}{3}\right) \tag{15}$$

and letting

$$F(x) = \mu\left(\frac{x^3}{3} - x\right), \tag{16}$$

now

$$\dot{y} = \dot{x}. \tag{17}$$

Using (15) we have,

$$\dot{y} = z + \mu\left(y - \frac{y^3}{3}\right) \tag{18}$$

and

$$\dot{z} = \ddot{x} - \mu\dot{x}\left(1 - x^2\right)$$

$$\dot{z} = -\mu\left(y^2 - 1\right)\dot{x} - x - \mu\left(1 - y^2\right)\dot{x} = -x = -y. \tag{19}$$

This transformation puts the equation into the form:

$$\begin{bmatrix} \dot{y} \\ \dot{z} \end{bmatrix} = \begin{bmatrix} z - \mu\left(\frac{y^3}{3} - y\right) \\ -y \end{bmatrix}. \tag{20}$$

Eq. (20) is the particular case of Lienard's Equation

$$\begin{bmatrix} \dot{y} \\ \dot{z} \end{bmatrix} = \begin{bmatrix} z - f(y) \\ -y \end{bmatrix} \tag{21}$$

where $f(y) = \mu\left(\frac{y^3}{3} - y\right)$. Linearizing (20) around the origin i.e. fixed point (0,0), we have

$$\begin{bmatrix} \dot{y} \\ \dot{z} \end{bmatrix} = \begin{bmatrix} \mu & 1 \\ -1 & 0 \end{bmatrix}\begin{bmatrix} y \\ z \end{bmatrix}. \tag{22}$$

The characteristic equation of (22) is given as

$$\lambda^2 - \mu\lambda + 1 = 0 \tag{23}$$

with eigenvalues of

$$\lambda_\pm = \frac{\mu \pm \sqrt{\mu^2 - 4}}{2} \tag{24}$$

and eigenvectors of

$$\vec{e}_+ = \begin{bmatrix} \frac{-2}{\mu - \sqrt{(\mu^2-4)}} \\ 1 \end{bmatrix}, \quad \vec{e}_- = \begin{bmatrix} \frac{-2}{\mu + \sqrt{(\mu^2-4)}} \\ 1 \end{bmatrix}. \tag{25}$$

The stability of this fixed point depends on the signs of the eigenvalues of the Jacobian matrix (22).

3.2 Existence of the limit cycles

Let us now analytically study the amplitude of the limit cycle by using the average method [13]. Considering the following transformations

$$x(t) = A(t)\cos\left(t + \varphi(t)\right) = A\cos\psi \tag{26}$$

$$\dot{x}(t) = -A(t)\sin\left(t + \varphi(t)\right) = -A\sin\psi \tag{27}$$

where $A(t)$ is the amplitude, $\varphi(t)$ being the phase and with $\psi(t) = \varphi(t) + t$. Supposing the amplitude and phase feebly vary during a period $T = 2\pi$, we have the fundamental equations of the average method as follows:

$$\dot{A}(t) = -\frac{\mu}{2\pi}\int_0^{2\pi} f(A\cos\psi, -A\sin\psi)\sin\psi\,\mathrm{d}\psi \tag{28}$$

$$\dot{\varphi}(t) = -\frac{\mu}{2\pi}\int_0^{2\pi} f(A\cos\psi, -A\sin\psi)\sin\psi\,\mathrm{d}\psi \tag{29}$$

Eqs. (28) and (29) help to determine the amplitude $A(t)$ and phase $\varphi(t)$ of the oscillator. Applying this method to (12) for which

$$f(x, \dot{x}, t) = (1 - x^2)\,\dot{x}$$

then, we have

$$f(A, \psi) = -A \sin\psi + A^3 \sin\psi \cos^2\psi. \tag{30}$$

Substituting (30) into (28) and (29), we get

$$\dot{A}(t) = -\frac{\mu}{2\pi}\int_0^{2\pi}\left(-A\sin^2\psi + A^3\sin^2\psi\cos^2\psi\right)\mathrm{d}\psi \tag{31}$$

$$\dot{\varphi}(t) = -\frac{\mu}{2\pi}\int_0^{2\pi}\left(-A\sin\psi\cos\psi + A^3\sin\psi\cos^3\psi\right)\mathrm{d}\psi. \tag{32}$$

Integration of (31) and (32) gives the evolution equation of the amplitude $A(t)$ and the phase $\varphi(t)$:

$$\dot{A}(t) = -\frac{\mu A(t)}{2}\left(1 - \frac{A^2(t)}{4}\right) \tag{33}$$

$$\dot{\varphi}(t) = 0. \tag{34}$$

The average method states that the amplitude and the phase feebly vary during a period. Therefore $\dot{A}(t) = 0$, and the amplitude is eventually $A(t) = 2$.

4 Numerical solution

The numerical solution to the Van der Pol equation for various values of μ are presented in Figs. 2 to 4.

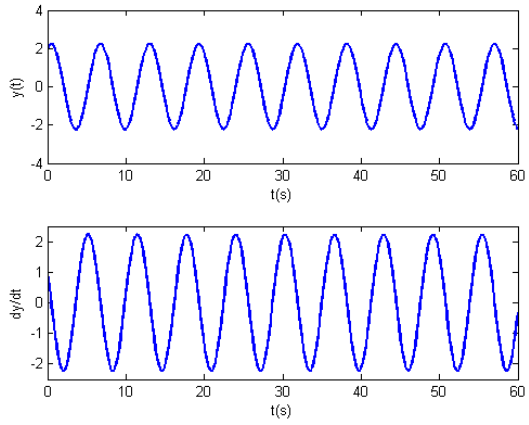

Fig. 2: Plot of $y(t)$ and dy/dt against $t(s)$ for $\mu = 0$.

5 Discussion

The classical Van der Pol equation (12) depends on the damping coefficient μ and the following varying behaviors were obtained. When $\mu < 0$, the system will be damped and the limit $\lim_{t\to\infty} \to 0$. From Fig. 2, where $\mu = 0$, there is no damping and we have a simple harmonic oscillator. From Figs. 3 and 4, where $\mu \geq 0$, the system will enter a limit cycle, with continuous energy to be conserved. The wave generated by this oscillator is periodic with sinusoidal form for $\mu \ll 1$ and relaxation for large value of μ [14] with fix amplitude equal to 2. Also when $-\infty < \mu \leq 0$ and $\lambda_\pm$ is $\mathrm{Re}(\lambda_\pm) < 0$, the point is stable; if $\mu = 0$ and $\lambda_\pm = \pm i$, the point is marginally stable and unstable; if $0 \leq \mu < \infty$ and $\lambda_\pm$ is $\mathrm{Re}(\lambda_\pm) > 0$, the origin is unstable. If $0 \leq \mu \leq 2$ and $\lambda_\pm$ is $\mathrm{Im}(\lambda_\pm) \neq 0$, then the fixed point (0,0) is an unstable center. If $2 < \mu < \infty$ and $\lambda_\pm$ is $\mathrm{Im}(\lambda_\pm) = 0$, then the fixed point (0,0) is still unstable.

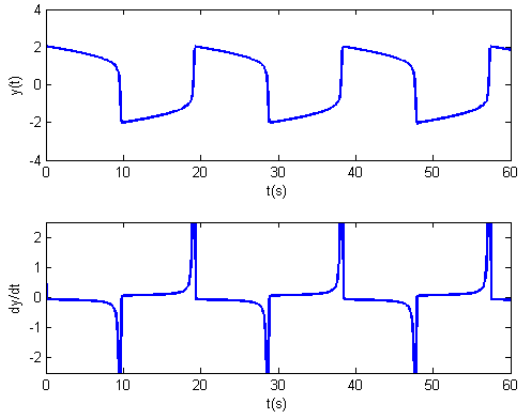

Fig. 3: Plot of $y(t)$ and dy/dt against $t(s)$ for $\mu = 10$.

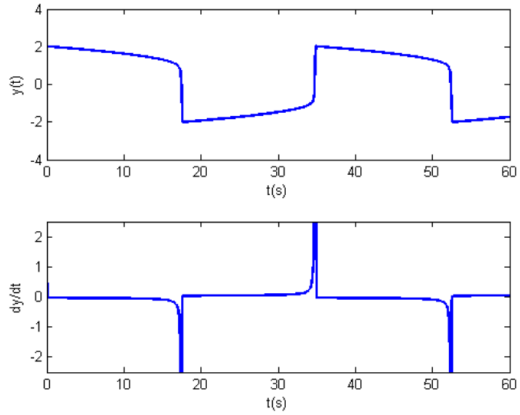

Fig. 4: Plot of $y(t)$ and dy/dt against $t(s)$ for $\mu = 20$.

6 Conclusion

In the above analysis, a class of analytical study of the Van der Pol equation in the autonomous regime is presented. Analytically, we conclude that the fixed point (0,0) is unstable whatever the value of the damping coefficient μ and the system enters a limit cycle with amplitude $A(t)$ of the Van der Pol oscillator limit cycle equal to 2. We showed that there exists a unique limit cycle.

Acknowledgement

The authors wish to thank Prof. J. Chabi Orou of African University of Science and Technology, Abuja for his time, useful discussions and help in the analytical study of this problem.

Submitted on April 19, 2015 / Accepted on May 11, 2015

References

1. Fitzhugh R. Impulse and physiological state in theoretical models of nerve membranes. *Biophys. J.*, 1961, v. 1, 444–466.
2. Nagumo J., Arimoto, S., and Yoshizawa S. An active pulse transmission line simulating nerve axons. *Proc. IRL*, 1960, v. 50, 2061–2070.
3. Cartwright J., Eguiluz V., Hernendez-Garcia E. and Piro O. Dynamic of elastic excitable media. *Internat. J. Bifur. Chaos Appl. Sci. Eng.*, 1999, v. 9, 2197–2202.
4. Cartwright M. L. Balthazar Van der Pol. *J. London Math. Soc.*, 1960, v. 35, 367–376.
5. Cartwright M. Van der Pol equation for relaxation oscillation. In Contribution to the theory of nonlinear oscillation II. Princeton Ann., Math. Stud. 2, Princeton University Press, Princeton, NJ, 1952, pp. 3–18.
6. Van der Pol B. A Theory of amplitude of force and force triode vibration. *Radio Review*, 1920, v. 1, 701–710, 754–762.
7. Van der Pol B. Relaxation Oscillations I. *Phil. Mag.*, 1926, v. 2, 978–992.
8. Van der Pol B. The nonlinear theory of electric oscillations. *Proc. IRE*, 1934, v. 22, 1051–1086.
9. Van der Pol B. and Van der Mark J. Frequency of demultiplication. *Nature*, 1927, v. 120, 363–364.
10. Cartwright M. L. and Littlewood J. E. *J. London Math. Soc.*, 1945, v. 20, 180.
11. Levinson N. A second order differential equation with singular solutions. *The Annals of Mathematics,* 2^{nd} *ser.*, 1949, v. 50 (1), 127–153.
12. Hafeez H. Y. and Chifu, E. N. Van der Pol Equation for Nonlinear Plasma Oscillations. *J. Adv. Phys.*, 2014, v. 3 (4), 278–281.
13. Nayfeh Ali Hassan. Introduction to perturbation techniques. Wiley-Vch, 2004, pp. 164–166.
14. Van der Pol B. *Phil. Mag.*, 1927, v. 3, 64

Shape Transition in the Even-Even Cerium Isotopes

Benyoucef Mohammed-Azizi[1], Abderrachid Helmaoui[2], and Djamal-Eddine Medjadi[3]

[1]University of Bechar, Bechar, Algeria. E-mail: aziziyoucef@voila.fr
[2]University of Bechar, Bechar, Algeria. E-mail: helmaouiabderrachid@yahoo.fr
[3]École Normale Supérieure, Vieux Kouba, Algiers, Algeria. E-mail: medjadide@voila.fr

The deformation energy of the even-even nuclei of the Cerium isotopic chain is investigated by means of the Macroscopic-Microscopic method with a semiclassical shell correction. We consider axially symmetric shapes. Binding energy and two neutron separation energy are also evaluated. For the sake of clarity several important details of the calculations are also given. It turns out that all these nuclei have prolate equilibrium shape. The regions of maximum deformation are obtained around $N = 64$ and $N = 102$. There is no critical-point of quantum phase transition in this isotopic chain.

1 Introduction

Nowadays it is well established that the majority of nuclei possess a nonzero intrinsic electric quadrupole moment (IE QM). This feature means that the charge distribution inside the nucleus deviates from the spherical symmetry. In other words, apart from very few nuclei, the surface of the nucleus is generally not spherical in its ground state. The intrinsic quadrupole electric moments (or equivalently the nuclear deformation) can be deduced from two types of measurements:

- The reduced electric quadrupole transition probability, $B(E2)$ [1];
- The static electric quadrupole moments of ground and excited states, Q [2].

It turns out that in a number of cases, the two methods of measurement do not systematically lead to the same values. Important discrepancies occur for several nuclei. This is essentially due to the fact that not only different experimental techniques are used but above all, because different models can be implemented to deduce the nuclear deformation for the both cases.

In [3] it is stated that deformations deduced from $B(E2)$ have a "more general character". In other words, "$B(E2)$-type" data reflect not only static nuclear deformation (permanent deviation of the nuclear shape from sphericity), but also dynamic deformation. Furthermore, $B(E2)$ measurements are model independent and thus are generally more reliable. This is corroborated by the fact that the only systematic compilation in which the deformation of the ground state is given explicitly is based on $B(E2; 0^+ \rightarrow 2^+)$ and has been published in [1]. In the present work, experimental values refer to these ones.

Theoretical approaches to the deformation energy can be divided into two categories; Dynamic calculations to find the shape of the ground state (or even of excited states) and static calculations by determining the absolute minimum (ground state) or multiple minima (shape isomers) in the potential energy surface (PES) for a given nucleus.

Thus, on the one hand, we have the so-called collective models, which themselves are subdivided into two groups: The "Geometric Collective Model" also called the "Collective Bohr Hamiltonian" (CBH and its variants) and the "Algebraic Model", well known under the name of the "Interacting Boson Model" (IBM and its variants) [4]. On the other hand, "particle models" consider the nucleus as a collection of interacting nucleons (fermions).

In practice, the classical N-body problem can be approximately solved by the usual approximation of the mean field with eventually residual interactions. In this respect, the "best" mean field is deduced after applying a variational principle in the Hartree-Fock-Bogoliubov method (HFB). In this model, the determination of the potential energy surface (PE S) of the nucleus amounts to perform constrained Hartree-Fock-Bogoliubov (CHFB) calculations [5]. We will not address very complicated methods "beyond the mean field" such as the Quasiparticle Random Phase Approximation (QRP A) or the Generator-Coordinate-Method (GCM) methods which are unsuitable in practice for large scale calculations.

Because of CHFB calculations are time consumers, especially in large studies, Microscopic-Macroscopic method (Mic-Mac) constitutes a good alternative which, is up to now, implemented [6]. In the present work, we use an improved variant of this method. The word "improved" means that we use semi-classical method to avoid the well-known drawbacks (spurious dependence on two mathematical parameters) of the standard Strutinsky shell correction (see text below).

The present study is devoted to the deformation energy, equilibrium nuclear shapes and binding energy of the ground state of the even-even cerium isotopes. There are many reasons to this choice. One of them is to re-test our previous calculations. In effect, similar calculations have been already performed by us in the xenon, barium, and cerium region [7]. However because the phenomenological mean potential varies smoothly with N and Z, we have made, in the past, a rough approximation by choosing the same set of parameters for the phenomenological mean potential, for the all treated

nuclei. Originally, this approximation was done only for simplifying the calculations.

Here, contrarily to that study, each nucleus has its "own" mean potential with a specific set of parameters. In this way it is possible to evaluate in a rigorous way the uncertainty introduced in the previous calculations. Apart from this remark, there are several main other reasons which could justify this choice: (i) First, it should be interesting to see how the deformation energy and binding energy vary with the neutron number (N) for this isotopic chain. (ii) Second, the present study extends the previous calculations to all cerium isotopes up to the drip lines (34 versus 13 nuclei). (iii) Third, we also will attempt to deduce, from potential energy surface (PES) curves, the shape transition from spherical to axially deformed nuclei, looking for the so-called $X(5)$ critical-point between U(5) and SU(3) symmetry limits of the IBM [8, 9].

It is worth to recall briefly some information deduced from the literature for the cerium isotopes. In the past, a number of experimental as well as theoretical studies have been done for the cerium isotopes. Among the numerous studies, we only cite some of them.

In 2005 Smith et al [10] have studied excited states of ^{122}Ce up to spin $14\hbar$ deducing a probable quadrupole deformation of about $\beta \approx 0.35$. The deformed nucleus ^{130}Ce has been studied in 1985, using the techniques of in-beam gamma -ray spectroscopy [11]. The corresponding data have been interpreted in terms of the cranking model by assuming a prolate deformation with $\varepsilon_2 \approx 0.25$ ($\beta \approx 0.27$).

High-spin states in ^{132}Ce have been also studied by A.J. Kirwan et al [12]. They found a superdeformed band with deformation $\beta \approx 0.4$ much more larger that the ground state deformation ($\beta \approx 0.2$). E. Michelakakis et al [13] by evaluating $\gamma-$ray transitions in ^{142}Ce and ^{144}Ce conclude that in cerium isotopes (near the beta-stable line) the onset of nuclear deformation occur between $N = 86$ and $N = 88$. "Pure" theoretical calculations have been performed in [14] and [15] with projected shell model (PSM) and Hartree-Bogoliubov ansatz in the valence space respectively for ^{122}Ce and $^{124-132}$Ce for low lying yrast spectra. Good values of energy levels and reduced transition probabilities $B(E2, 0^+ \rightarrow 2^+)$ have been obtained respectively in these two papers.

Other approaches for the rich-neutron cerium isotopes have been made in [16]. A study of the shape transition from spherical to axially deformed nuclei in the even Ce isotopes has been done in [17] using the nucleon-pair approximation of the shell model. The result of a such study is that the transition has been found too rapid. Relativistic Hartree-Fock-Bogoliubov theory has been used to predict ordinary halo for ^{186}Ce,^{188} Ce,^{190} Ce, and giant halo for ^{192}Ce,^{194} Ce,^{196} Ce, and ^{198}Ce near the neutron drip line.

Systematic studies about nuclear deformations and masses of the ground state can be found in [18–21] with respectively, the Finite-Range Droplet-Model (FRDM), Hartree-Fock-Bogoliubov (HFB), HFB+5-dimensional collective quadrupole Hamiltonian and Relativistic Mean Field (RMF) models.

2 The Macroscopic–Microscopic method

2.1 Liquid drop model and microscopic corrections

This method combines the so-called semi-empirical mass formula (or liquid drop model) with shell and pairing corrections deduced from microscopic model. Thus the binding energy is given as a function of nucleon numbers and deformation parameter (referred to as β) by mean of the usual symbols:

$$B(A, Z, \beta) = E_{LDM}(\beta) - \delta B_{micro}(\beta). \tag{1}$$

δB_{micro} contains the shell and pairing correction (see text below). The minus sign before δB_{micro} is consistent with the convention that the binding energy is defined as positive here.

For the liquid drop model we take the old version of Myers and Swiatecki [28] (because of its simplicity compared to more recent formulae). Here, there is no need to look for very high accuracy in binding energy, because this is not the purpose of the present work.

$$\begin{aligned} E_{LDM}(\beta) = C_V A - C_S A^{2/3} B_S(\beta) - C_C Z^2 A^{-1/3} B_C(\beta) + \\ + \varepsilon a_{pair} A^{-1/2} + C_d Z^2 A^{-1}. \end{aligned} \tag{2}$$

In (2), we have the usual contributions of volume, surface and coulomb energies.

The different constants of Myers and Swiatecki are given in Appendix A. The shape dependence (β) of the surface and coulomb energies are contained in $B_S(\beta)$ and $B_C(\beta)$. They are normalized to the unity for a spherical nuclear surface. The latter is symbolized by $\beta = 0$. The two last terms in (2) are respectively due to the smooth part of the pairing energy and the correction of the Coulomb energy to account for the diffuseness of the nucleus surface. The different constants will be fixed later.

The potential energy surface (PES without zero point energy correction) is defined as follows:

$$\begin{aligned} E_{PES}(\beta) &= E_{LDM}(0) - B(A, Z, \beta) \\ &= \Delta E_{LDM}(\beta) + \delta B_{micro}(\beta) \end{aligned} \tag{3}$$

in which

$$\begin{aligned} \Delta E_{LDM}(\beta) &= E_{LDM}(0) - E_{LDM}(\beta) \\ &= C_S A^{2/3} \left[B_S(\beta) - B_S(0) \right] + \\ &+ C_C Z^2 A^{-1/3} \left[B_C(\beta) - B_C(0) \right]. \end{aligned} \tag{4}$$

Constants C_V and C_S are expressed by means of three other constants a_V, a_S, and κ. For spherical shape, as said before, the normalization is expressed by: $B_S(0) = B_C(0) = 1$. As it can be easily seen, the potential energy surface is related only to two macroscopic constants C_S (which depends actually on

a_S and κ) and C_C. To calculate microscopic shell an pairing corrections contained in δB_{micro}, we have to proceed in two steps. The first consists in solving the Schrödinger equation and the second in deducing the shell and pairing corrections in an appropriate way, as explained in the following.

2.2 Microscopic model

We briefly present the microscopic model which is based on the Schrödinger equation of the deformed independent particle model:

$$\hat{H}(\beta) \mid \Psi_i(\beta)\rangle = \varepsilon_i(\beta) \mid \Psi_i(\beta)\rangle \tag{5}$$

where $|\Psi_i\rangle$ and ε_i are respectively the eigenfunctions and the associated eigenvalues of nucleons. Hamiltonian $\hat{H}$ contains four contributions which are: (i) kinetic energy, (ii) central deformed mean field, (iii) spin-orbit and (iv) Coulomb interactions.

We perform analogous calculations as in Nilsson model but our deformed mean potential is of Woods-Saxon type and therefore is "more realistic". Although calculations are not self consistent, they are microscopic. It is to be noted that our Schrödinger equation has a form which is very close to the one of the Skyrme-Hartree-Fock method. Eq. (5) is solved by our FORTRAN program described in details in [22] and improved in two successive versions [23] and [24].

2.3 Microscopic corrections

Microscopic corrections are defined as the sum of shell and pairing corrections which themselves are calculated separately for each kind of nucleons:

$$\begin{aligned}\delta B_{micro}(\beta) = \delta E_{shell}(N,\beta) + \delta E_{shell}(Z,\beta) + \\ + \delta P_{pairing}(N,\beta) + \delta P_{pairing}(Z,\beta).\end{aligned} \tag{6}$$

In this formula the shell correction is defined by the usual Strutinsky prescription, i.e. as the difference between the sum of the single particle energies (which contains the shell effects) and an averaged (or smoothed) sum (which is free from shell effects)

$$\delta E_{shell}(N \text{ or } Z) = \sum_{i=1}^{N\text{or}Z} \varepsilon_i(\beta) - \overline{\sum_{i=1} \varepsilon_i(\beta)}. \tag{7}$$

Energies $\varepsilon_i(\beta)$ are deduced from (5). In our procedure, the second sum is found by means of a semi-classical way instead a Strutinsky smoothing procedure, see [27]. This avoids the well-known weakness of the standard shell correction method, namely, the dependence on two unphysical parameters which are the "smoothing" parameter and the order of the curvature correction.

Moreover, it has been clearly shown that Strutinsky level density method is only an approximation of that of the semi-classical theory [26]. The "pure" pairing correlation energy is defined by:

$$P(\beta) = \sum_{i=1}^{\infty} 2\varepsilon_i(\beta)\upsilon_i^2 - \sum_{i=1}^{N/2\text{or}Z/2} 2\varepsilon_i(\beta) - \frac{\Delta^2}{G} \tag{8}$$

where υ_i^2, Δ and λ are the usual occupation probabilities, gap and Fermi energy of the BCS approximation (the factor "2" is simply due to the Kramers degeneracy). Since the smooth part of pairing correlations is already contained in the liquid drop model, we have to add only the one due to the shell oscillations of the level density. This contribution is defined by means of a formula similar to (7)

$$\delta P_{pairing}(N \text{ or } Z,\ \beta) = P(\beta) - \overline{P(\beta)} \tag{9}$$

where the averaged pairing is defined as

$$\overline{P(\beta)} = \frac{1}{2}\, g_{semicl.}(\lambda)\, \overline{\Delta}^2.$$

We use a simple BCS method to account for pairing correlations. To calculate (7) and (9) we follow the method detailed in [27] with its FORTRAN code. The treatment of the pairing has also been explained in [7] and references quoted therein.

2.4 Numerical constants and prescriptions

2.4.1 Constants of the microscopic model

For each kind of particles the mean central and the mean spin-orbit field are written as [22]:

$$\begin{aligned}V(\beta) &= \frac{V_0}{1 + \exp(R_V L_V(\beta)/a_0)} \\ V_{SO}(\beta) &= \lambda\left(\frac{\hbar}{2Mc}\right)\frac{V_0}{1 + \exp(R_{SO} L_{SO}(\beta)/a_0)}\end{aligned} \tag{10}$$

where $L_V(\beta)$ and $L_{SO}(\beta)$ contain the information on the deformation. In fact, these functions contain 9 constants: V_{0neut}, V_{0prot}, R_{Vneut}, R_{Vprot}, $R_{SO-neut}$, $R_{SO-prot}$, a_0, λ_{neut}, λ_{prot}. These quantities are taken from the "universal" parameters [29] (see Appendix B) which is an optimized set. The Coulomb mean field is approximated by a uniform charge distribution inside a deformed surface. The volume conservation is therefore $Vol = (4/3)\pi R_{ch}^3$ with the simple assumption $R_{ch} = R_{Vprot}$.

2.4.2 Constants of the liquid drop model

As already stated, we have chosen the parameters of Myers and Swiatecki (see Table 1) because this set contains a reduced number of parameters with respect to more modern formulae. All the constants are needed in the binding energy whereas only a_S, C_C, κ play a role in the potential energy surface.

	a_V	a_S	C_C	κ	C_d	a_{pair}
Myers and Swiatecki	15.67 MeV	18.56 MeV	0.72 MeV	1.79	1.21 MeV	11 MeV

Table 1: Parameters of the liquid drop model in the Myers and Swiatecki version [28].

2.4.3 Nuclear mass excesses

Nuclear masses are deduced as mass excesses:

$$M_{excess}(A,Z) = ZM_H + (A-Z)M_n - B(A,Z)$$

where $M_H = 7.289034$ MeV is the hydrogen mass excess and $M_n = 8.071431$ MeV the neutron mass excess. This makes comparisons with experimental values easiest.

3 Results

In our previous paper [7] calculations for isotopes $^{116-130}$Ce showed that the equilibrium deformations ($\beta \approx 0.25 - 0.30$) have always been obtained for symmetric prolate shapes ($\gamma = 0°$). Results obtained in [32] with a similar approach for the nuclei $^{116-130}Ce$, corroborate this fact. For these reasons, we think that it is needless to account for the axial asymmetry in a "pure" static study of the equilibrium deformation. However, we have to consider prolate ($\gamma = 0°$) as well as oblate ($\gamma = 60°$) nuclear shapes. In this regard, it is worth remembering that oblate shape given by ($\beta > 0, \gamma = 60°$) is equivalent to the set ($\beta < 0, \gamma = 0°$).

3.1 Comparison between the different contributions entering in the potential energy surface

It could be useful to compare the importance of the different terms entering in the right hand side of (6). In this respect, we have drawn in Fig.1 for axially prolate shape, the four microscopic contributions

$$\delta E_{shell}(N,\beta), \delta E_{shell}(Z,\beta), \delta P_{pairing}(N,\beta), \delta P_{pairing}(Z,\beta)$$

for the case of ^{160}Ce as functions of β. Following the cited order, we can say that the difference between the highest and lowest values in the interval $\beta \in [0.0, 0.7]$ are respectively about 11.0 MeV, 10.5 MeV, 5.7 MeV, 3.5 MeV for the four corrections.

Thus, these variations show that the shell corrections

$$\delta E_{shell}(N,\beta), \delta E_{shell}(Z,\beta)$$

are more important than

$$\delta P_{pairing}(N,\beta), \delta P_{pairing}(Z,\beta)$$

and have a clear minimum at respectively $\beta = 0.35$ and $\beta = 0.30$. It is well known that for each kind of nucleon the shell correction is in opposite phase with respect to the pairing correction (this means for that when $\delta E_{shell}(N,\beta)$ increases with β, $\delta P_{pairing}(N,\beta)$ decreases and vice versa).

Contrarily to these curves, the liquid drop model is strictly increasing with β, and its minimum occurs always at the beginning $\beta = 0.0$ (spherical shape). When all the contributions are added, the minimum of the potential energy surface of the nucleus is reached at about $\beta = 0.3$ and is mainly due to the shell corrections. When β becomes more and more, larger the contribution of the liquid drop energy becomes preponderant so that the equilibrium deformation occurs generally between $\beta = 0$ and $\beta = 0.4$. Because of the convention of the sign stated before, δB_{micro} defined in (1) must be negative in order to increase the binding energy of the nucleus. Since the shell corrections (for protons and neutrons) play a major role in δB_{micro}, it is naturally expected that negative (but absolute large) values of shell correction contribute to increase the binding energy of the nucleus.

In this respect, it is well known that the shell correction is essentially determined by the distribution of single-particle levels in the vicinity of the sharp Fermi level (defined here as midway between the last occupied level and the first empty level). Following [31], we can state that "the nuclear ground state, as well as any other relatively stable state, should correspond to the lowest possible degeneracy, or, in other words, the lowest density of state near the Fermi level". This is illustrated in Fig. 2 where the single-particle levels are drawn as function of the deformation β (γ being fixed at $\gamma = 0°$). To this end we have used the FORTRAN code of [22] and [24]. The area where the single-particle level density is low near the Fermi level (black stars) is indicated by a circle. Thus, it is not so surprising that, it is in this region where the neutron shell correction becomes the most important, involving a minimum in the PES of the nucleus.

3.2 Equilibrium deformations

Equilibrium deformations are given in Table (2) for prolate as well as oblate shapes (see table legend for details). The minima of PES for the corresponding wells are denoted *minpro* and *minobl*. The deformation energy is defined as the difference $E_{def} = E_{PES}(0) - E^{\min}_{PES}(\beta)$, i.e. the difference between the potential energy surface for a spherical shape and the one corresponding to the absolute minimum of PES. Permanent deformations will be in principle characterized by large values of E_{def} and are responsible of rotational spectra.

From this table, some remarks may be drawn:
(i) Two regions of prolate deformation are found. They occur around $N = 64$ and $N = 102$ with maximum deformation about $\beta \approx 0.30$. The deformation energy (between spherical and deformed shape) is about 6.70 MeV for $N = 64$ and

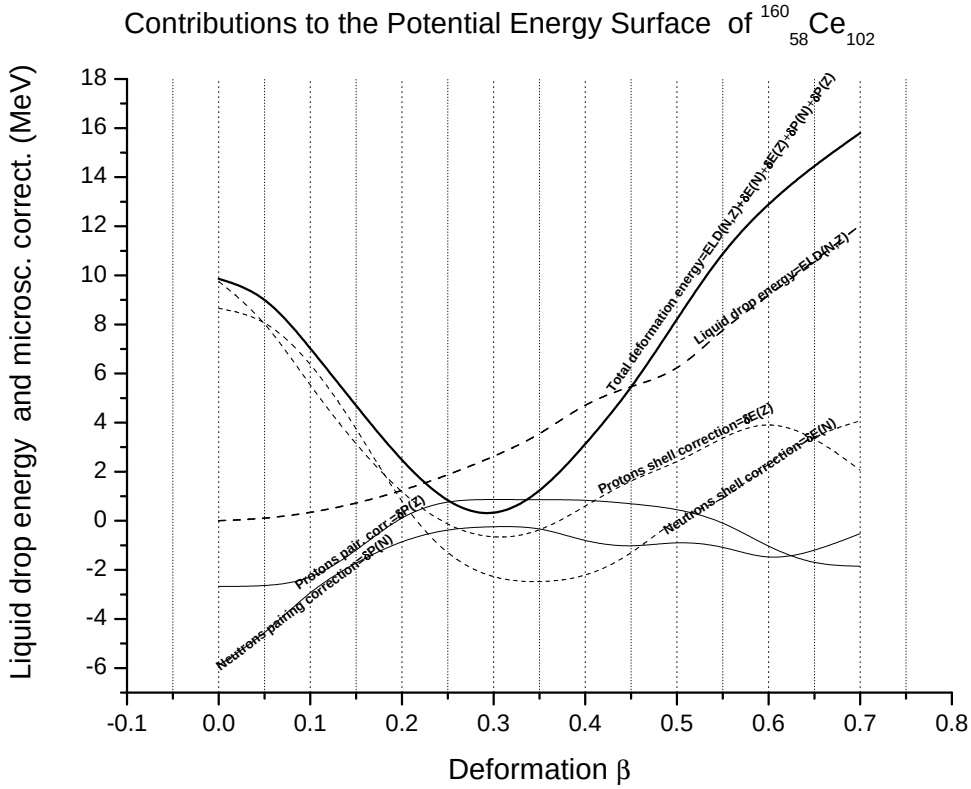

Fig. 1: Contributions of the shell and pairing corrections for the two kind of nucleons and the one of the liquid drop model to the total potential energy surface of the nucleus ^{160}Ce.

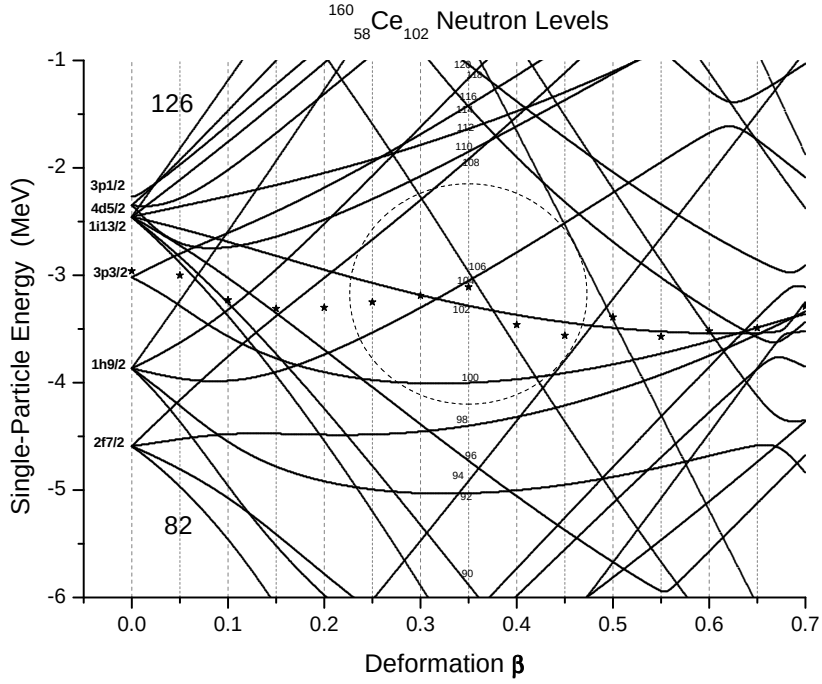

Fig. 2: Single-particle energies of the microscopic model as function of deformation for prolate shapes ($\beta > 0$) for the nucleus ^{160}Ce. Spherical spectroscopic notation is given for spherical deformation ($\beta = 0$) .The circle in dotted line indicates the area of lowest level density.

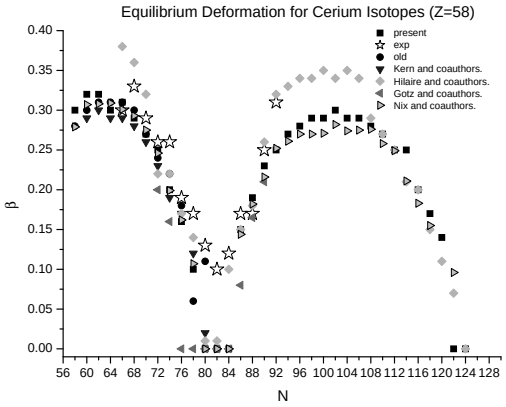

Fig. 3: Theoretical equilibrium deformations for even-even cerium isotopes evaluated by different or similar approaches.

9.30 MeV for $N = 102$ and decreases from either side from these two nuclei.
(ii) Spherical deformation occur at and near the (magic) numbers $N = 82$ and $N = 128$ (not shown).
(iii) The deformation energy decreases from $N = 64$ (maximum) to $N = 82$ (minimum) and reincreases again to $N = 102$ (maximum). We have found graphically that the first inflexion point occurs between $N = 72$ and $N = 74$ and a second inflexion point is found between $N = 90$ and $N = 92$. One can consider (somewhat arbitrarily) that spherical shapes occur approximately between these two limits.
(iv) The minima of prolate equilibrium deformations are, by far, always deeper compared to the ones of the oblate minima ($minpro \ll minobl$). In other words cerium isotopes prefer, by far, prolate shapes. In other words, the deformation energy increases in average with the asymmetry γ. This justifies a posteriori that, in a static study of the equilibrium deformation, it is needless to account for axial asymmetry. It is worth to remember that most of nuclei of the chart have prolate shape (see [25]).
(v) Even though the experimental deformations are known only in absolute value from $B(E2)$, a good agreement is obtained if one excepts the three "nearly magic" nuclei $^{138-142}$Ce

In Fig. (3) are displayed the present equilibrium deformations, experimental values [1] , our "old" calculations [7] and other studies performed by different authors which are: Kern et al. [32], Hilaire and Girod [34], Gotz et al. [33] and Nix et al. [18]. All calculations are based on Macro-Micro method (with different mean fields or different parameters). Except the one of [34] which uses Hartree-Fock-Bogoliubov model with Gogny force.
(i) Near magic number ($N = 82$) all calculations give spherical equilibrium deformation whereas experimental results are always slightly deformed (even for $N = 82$). It seems difficult to overcome this defect with a pure static approach which neglects the role of the mass parameters.
(ii) The overall tendency of these calculations is the same except the fact that HFB calculations differ significantly from the others with higher values in some regions.
(iii) Apart from HFB calculations, theoretical values are generally quite close from each others.
(iv) Our old and new calculations give very close results (see Table 3). Thus, even if it is better to choose a proper set of mean-field parameters for each nucleus, we do not commit a significant error by taking the same set of parameters for nuclei that do not differ strongly by the number of neutrons (N).

3.3 Mass excesses

We list from a FORTRAN file (see Fig. 4) the results of our theoretical calculations of the binding energies and mass excesses (m-excess) for the even-even cerium isotopic chain. For the sake of completeness, experimental mass excesses and the ones of the FRDM model (see [18]) are also given. We must keep in mind that only 6 parameters are used in the liquid drop model whereas 16 parameters are necessary in the FRDM model. This explains the "better quality" of the FRDM model. However, we have checked that the variations of binding energy or mass excesses from one isotope to the nearest is practically the same in our model and the one of FRDM (the deviations are about ±0.35 MeV). For this reason, the calculation of the two neutron separation energies (see the following subsection 3.4) will almost be probably the same for the two approaches even though our model is not so accurate.

3.4 Transitional regions in cerium isotopes

In Fig. 5 is shown the gradual transition in the potential energy surface from spherical vibrator to the axially deformed rotor when the number of neutrons (N) increases from 76 to 92. One signature of $X(5)$ symmetry which is a critical-point of phase/shape transitions (quantum phase transition between spherical and axial symmetries) should be a long flatness of the potential energy surface with eventually a weak barrier from prolate to oblate shapes. In this figure, for $N > 82$, the width of the flatness increases as one moves away from $N = 82$ but at the same time the difference between oblate and prolate minima and barrier between oblate and prolate shapes also increase. For example the differences between oblate and prolate energy minima and barriers for isotopes with $N = 88, 90, 92$ are respectively about 1.5 MeV, 2.5 MeV and 3.3 MeV with energy barrier about 2 MeV, 4 MeV and 5.5 MeV respectively. The wideness of the bottom of the well must be relativized with the height of the barrier. Thus for the case of $N = 92$ the width is important, i.e. about $\Delta\beta \approx \beta_{pro} - \beta_{obl} \approx 0.26 - (-0.20) \approx 0.46$ but the barrier is about 5.5 MeV and therefore seems too high. The case $N = 90$ gives a width of $\Delta\beta \approx 0.3$ with a barrier of about 4 MeV. For $N < 82$, the case $N = 76$ seems to be rela-

N	A	β_{pro}	$minpro$ (MeV)	β_{obl}	$minobl$ (MeV)	E_{def} (MeV)	$\lvert\beta_{\exp}\rvert$	N	A	β_{pro}	$minpro$ (MeV)	β_{obl}	$minobl$ (MeV)	E_{def} (MeV)	$\lvert\beta_{\exp}\rvert$
58	116	0.30	0.90	−0.21	3.62	4.80		92	150	0.25	1.23	−0.17	4.45	5.12	0.31
60	118	0.32	0.88	−0.23	4.07	5.87		94	152	0.27	1.21	−0.19	5.05	6.40	
62	120	0.32	1.03	−0.23	4.33	6.19		96	154	0.28	0.64	−0.21	4.94	7.47	
64	122	0.31	1.16	−0.23	4.23	6.68		98	156	0.29	0.66	−0.22	5.13	8.44	
66	124	0.30	1.47	−0.21	4.15	6.17	0.30	100	158	0.29	0.71	−0.22	5.14	9.08	
68	126	0.29	1.75	−0.21	3.87	5.43	0.33	102	160	0.30	0.32	−0.22	4.52	9.27	
70	128	0.27	1.82	−0.21	3.48	4.67	0.29	104	162	0.29	0.71	−0.22	4.42	9.08	
72	130	0.25	2.02	−0.2	3.27	3.34	0.26	106	164	0.29	1.00	−0.23	4.23	8.44	
74	132	0.20	1.90	−0.17	2.60	1.97	0.26	108	166	0.28	1.16	−0.23	3.92	7.57	
76	134	0.16	1.28	−0.14	1.63	0.93	0.19	110	168	0.27	1.46	−0.21	3.84	6.39	
78	136	0.10	0.04	−0.07	0.18	0.19	0.17	112	170	0.25	1.68	−0.20	3.55	5.33	
80	138	0.00	−1.93	0.00	−1.93	0.00	0.13	114	172	0.25	1.97	−0.19	3.20	4.19	
82	140	0.00	−3.96	0.00	−3.96	0.00	0.10	116	174	0.2	1.93	−0.17	2.79	2.95	
84	142	0.00	−2.07	0.00	−2.07	0.00	0.12	118	176	0.17	1.71	−0.16	2.17	1.68	
86	144	0.15	0.02	−0.06	0.53	0.50	0.17	120	178	0.14	1.39	−0.14	1.60	0.55	
88	146	0.19	0.73	−0.11	2.43	1.99	0.17	122	180	0.0	0.3	0.00	0.30	−0.15	
90	148	0.23	1.15	−0.14	3.76	3.15	0.25	124	182	0.0	−1.08	0.00	−1.08	−0.08	

Table 2: Equilibrium deformations as well as deformation energies for the cerium isotopic chain. The columns give successively the number of neutrons (N), the mass number (A), the prolate equilibrium deformation (β_{pro}), the minimum of the prolate well ($minpro$), the oblate equilibrium deformation (β_{obl}), the minimum of the oblate well ($minobl$), the deformation energy (E_{def},see text), the experimental equilibrium deformation ($\beta_{\exp}$). Note: The deformation energy is always given for the prolate equilibrium shape because no absolute minimum is obtained for oblate shape.

Cerium ($Z = 58$)	$N = 58$	60	62	64	66	68	70	72	74	76	78	80	82
Present β	+0.30	+0.32	+0.32	+0.31	+0.30	+0.29	+0.27	+0.25	+0.20	+0.16	+0.10	+0.00	+0.00
Old β	+0.28	+0.30	+0.31	+0.31	+0.31	+0.30	+0.27	+0.24	+0.22	+0.18	+0.06	+0.11	+0.00
Present $E_{def}(MeV)$	4.80	5.87	6.19	6.68	6.17	5.43	4.67	3.34	1.97	0.93	0.19	0.00	0.00
Old $E_{def}(MeV)$	4.82	5.77	6.03	6.31	7.08	5.36	4.41	3.35	2.13	0.77	0.00	0.24	0.00

Table 3: New equilibrium deformations and deformations energies vs old [7].

tively equivalent to $N = 90$ with a slightly smaller width and a lower height barrier. Thus it is difficult to determine clearly the existence of a $X(5)$ critical-point. Thus, everything seems to indicate a continuous transition.

In Fig. 6 is displayed the two-neutron separation energy (TSN) as function of the neutron number N. A clear jump is seen from $N = 82$ to $N = 84$, i.e. from one major shell to the following. Just before $N = 82$ and just after $N = 84$ the TSN varies more slowly. Far for the "jump" the curve becomes quasi-linear. Once again, no special behavior is noted around $N = 90$ which from [35] and [36] should constitute with $Z \approx 62$ the first order shape transition ($X(5)$ critical-point) in the rare earth region. In [37], it has been pointed out that "Empirical evidence of transitional symmetry at the $X(5)$ critical-point has been observed in ^{150}Nd, ^{152}Sm, ^{154}Gd, and ^{156}Dy". One of the most important signatures of the phase transition is given by a sudden jump in the value of the energy ratio $R_{4/2} = 4_1^+/2_1^+$ from one nucleus to the next. We found it useful to compare the experimental values of this ratio (see Fig. 7) in the cases of the isotopic chains of Ce and Sm (The experimental values of the considered levels have been deduced from the adopted level of $ENSDF$ site [38]). The figure shows clearly two facts. First, the important variation of $R_{4/2}$ near of the magic number $N = 82$ for both isotopic chains and then, the important difference between the behavior the two isotopic chain from $N = 88$ to $N = 90$. In effect

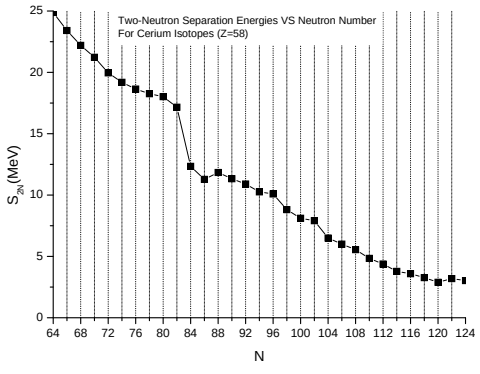

Fig. 6: Two-neutron separation energies (S_{2N}) along the cerium isotopic chain. This quantity is defined as $S_{2N}(A,Z,N) = Bind(A,Z,N) - Bind(A-2,Z,N-2)$ where the binding energy $Bind(A,Z,N)$ is given by (1). Note that in our approache the neutron drip line (where $S_{2N} \approx 0$) can be extrapolated around $N = 128$ for Cerium isotopes.

N	58	A	116.	Z	58	bind	914.85	m-excess	-23.94	exp	*********	frdm	-29.21
N	60	A	118.	Z	58	bind	942.64	m-excess	-35.59	exp	*********	frdm	-40.57
N	62	A	120.	Z	58	bind	968.86	m-excess	-45.66	exp	*********	frdm	-50.01
N	64	A	122.	Z	58	bind	993.74	m-excess	-54.40	exp	*********	frdm	-57.99
N	66	A	124.	Z	58	bind	1017.15	m-excess	-61.67	exp	*********	frdm	-64.93
N	68	A	126.	Z	58	bind	1039.35	m-excess	-67.73	exp	*********	frdm	-70.82
N	70	A	128.	Z	58	bind	1060.58	m-excess	-72.81	exp	*********	frdm	-75.54
N	72	A	130.	Z	58	bind	1080.54	m-excess	-76.63	exp	*********	frdm	-79.17
N	74	A	132.	Z	58	bind	1099.73	m-excess	-79.68	exp	*********	frdm	-81.89
N	76	A	134.	Z	58	bind	1118.37	m-excess	-82.18	exp	-84.750	frdm	-84.02
N	78	A	136.	Z	58	bind	1136.63	m-excess	-84.30	exp	-86.500	frdm	-85.67
N	80	A	138.	Z	58	bind	1154.66	m-excess	-86.18	exp	-87.570	frdm	-87.62
N	82	A	140.	Z	58	bind	1171.81	m-excess	-87.19	exp	-88.090	frdm	-88.68
N	84	A	142.	Z	58	bind	1184.16	m-excess	-83.39	exp	-84.540	frdm	-84.78
N	86	A	144.	Z	58	bind	1195.44	m-excess	-78.53	exp	-80.440	frdm	-80.23
N	88	A	146.	Z	58	bind	1207.28	m-excess	-74.23	exp	-75.720	frdm	-76.00
N	90	A	148.	Z	58	bind	1218.60	m-excess	-69.41	exp	-70.430	frdm	-70.83
N	92	A	150.	Z	58	bind	1229.50	m-excess	-64.17	exp	-64.990	frdm	-65.80
N	94	A	152.	Z	58	bind	1239.76	m-excess	-58.28	exp	*********	frdm	-59.78
N	96	A	154.	Z	58	bind	1249.85	m-excess	-52.23	exp	*********	frdm	-52.90
N	98	A	156.	Z	58	bind	1258.66	m-excess	-44.90	exp	*********	frdm	-45.40
N	100	A	158.	Z	58	bind	1266.78	m-excess	-36.87	exp	*********	frdm	-37.29
N	102	A	160.	Z	58	bind	1274.68	m-excess	-28.63	exp	*********	frdm	-28.70
N	104	A	162.	Z	58	bind	1281.19	m-excess	-19.00	exp	*********	frdm	-19.01
N	106	A	164.	Z	58	bind	1287.19	m-excess	-8.86	exp	*********	frdm	-8.62
N	108	A	166.	Z	58	bind	1292.74	m-excess	1.74	exp	*********	frdm	2.23
N	110	A	168.	Z	58	bind	1297.58	m-excess	13.04	exp	*********	frdm	13.43
N	112	A	170.	Z	58	bind	1301.96	m-excess	24.81	exp	*********	frdm	25.00
N	114	A	172.	Z	58	bind	1305.73	m-excess	37.17	exp	*********	frdm	36.82
N	116	A	174.	Z	58	bind	1309.33	m-excess	49.72	exp	*********	frdm	49.07
N	118	A	176.	Z	58	bind	1312.60	m-excess	62.59	exp	*********	frdm	61.53
N	120	A	178.	Z	58	bind	1315.49	m-excess	75.84	exp	*********	frdm	74.94
N	122	A	180.	Z	58	bind	1318.69	m-excess	88.79	exp	*********	frdm	87.48
N	124	A	182.	Z	58	bind	1321.72	m-excess	101.90	exp	*********	frdm	99.94

Fig. 4: Theoretical binding energies and mass excesses of the present approach compared to the experimental mass excesses and the ones given by the FRDM model of [18]. All energies are expressed in MeV. The experimental data as well as the frdm results have been entered manually in the code. Asterics mean that no experimental data is available for the corresponding nucleus.

in the case of Samarium, there is a sudden increase of this ratio whereas this is not the case for the Cerium isotopes. This has been attributed to the $X(5)$ critical-point symmetry of the nucleus ^{152}Sm. Thus the present study confirms that cerium isotopic chain is characterized by a continuous shape/phase transition.

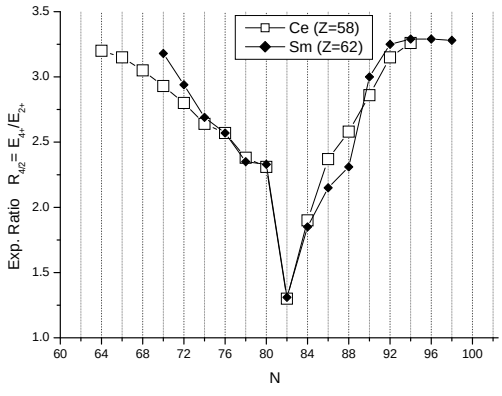

Fig. 7: $R_{4/2}$ energy ratio as function of neutron number for Cerium and Samarium isotopes. Sudden variations are associated with magic closure shells for the both chains (at $N = 82$) and with $X(5)$ critical point which occurs only for Sm (at $N = 90$).

4 Conclusion

Potential energy surfaces have been drawn for the cerium isotopic chain. All even-even nuclei between the two drip lines have been considered. To this end, we have used the microscopic–macroscopic method in which the quantum corrections have been evaluated by a semi-classical procedure. The microscopic model is based on a "realistic" Schrödinger equation including a mean field of a Woods-Saxon type. The macroscopic part of the energy is evaluated from the liquid drop model using the version of Myers and Swiatecki. The following points must be remembered:

(i) All equilibrium deformations have been found prolate with an important deformation energy compared to oblate shapes.

(ii) The maximum deformations are of order $\beta \approx 0.3$ and are located around $N = 64$ and $N = 102$ with deformation energy about 6 MeV and 9 MeV respectively. The equilibrium deformations decrease as one moves away from these two nuclei.

(iii) Spherical shapes are found in the neighborhood of $N = 82$.

(iv) Good agreement is obtained between theoretical and experimental values if one excepts the area of the shell closure $N = 82$ where the latter are slightly larger.

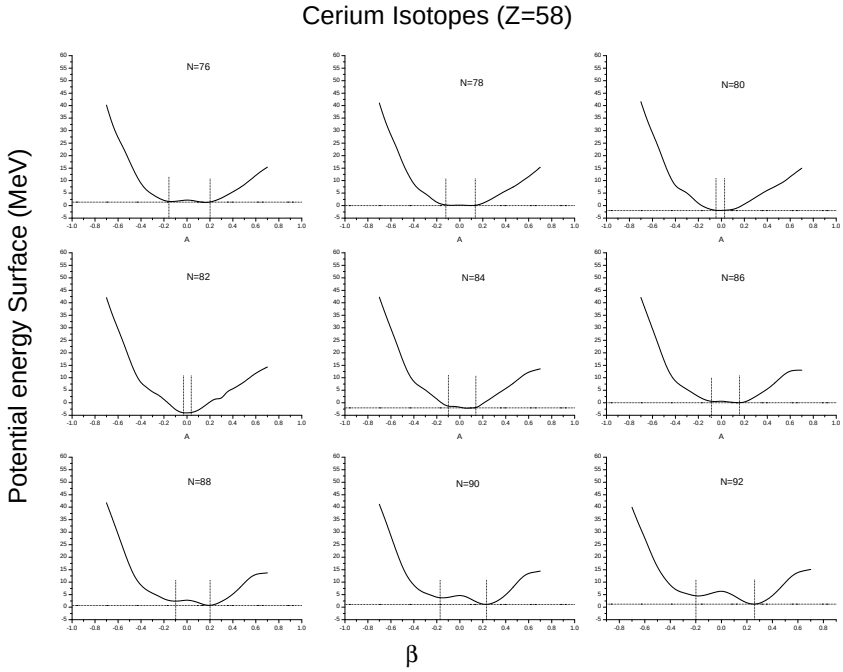

Fig. 5: Shape evolution for cerium isotopes from $N = 78$ to $N = 92$.

(v) This isotopic chain possesses a continuous shape/phase transition from spherical shapes toward the axially symmetric ones.

Submitted on May 2, 2015 / Accepted on May 22, 2015

References

1. Raman S., Nestor C. W. Jr. and Tikkanen P. *At. Data Nucl. Data Tables*, 2001, v. 78, 1.
2. Stone N. J., *At.Data Nucl.Data Tables*, 2005, v. 90, 75.
3. Boboshin I., Ishkhanov B., Komarov S., Orlin V., Peskov N., and Varlamov V. ND 2007 – International Conference on Nuclear Data for Science and Technology. Nice, France, April 22–27 2007.
4. Iachello F. and Arima, A. The Interacting Boson Model. Cambridge University Press, Cambridge, 1987.
5. Bayram T. *Rom. Journ. Phys.*, 2013, v. 58 (7–8), 931–938.
6. Bhagwat A., Viñas X., Centelles M., Schuck P., and Wyss R. *Phys. Rev. C*, 2010, v. 81, 044321.
7. Mohammed-Azizi B. and Medjadi D. E. *J. Phys. G : Nucl. Part. Phys.*, 2008, v. 35, 035101.
8. Cejna P., Jolie J., Casten R. F. *Rev. Mod. Phy.*, 2010, v. 82, 2155–2212.
9. Khalaf A. M., Gaballah N., Elgabry M. F. and Ghanim H. A. *Progress in Physics*, 2015, v. 11(2), 141–145.
10. Smith J. F. et al. *Phys. Lett.*, 2005, v. B625, 203.
11. Todd D. M. et al. *J. Phys. G. Nucl. Phys.*, 1984, v. 10, 1407.
12. Kirwan A. J., Ball G. C., Bishop E. J., Godfrey M. J., Nolan P. J., Thornley D. J., Love D. J. G. and Nelson A. H. *Phys. Rev. Lett.*, 1987, v. 58, 467.
13. Michelakakis E. et al. 4.International Conference on Nuclei Far From Stability, Helsingør, Denmark, 7–13 Jun 1981. In European Organization for Nuclear Research, Geneva, Switzerland, (20 Jul 1981), pp. 581–588.
14. Devi R., Sehgal B. D. and Khosa S. K. *Pramana Journal of Physics*, 2006, v. 67 (3), 467–475.
15. Bhat R. K., Devi R., and Khosa S. K. *Brazilian Journal of Physics*, 2003, v. 33 (2), 340–345.
16. Long Wen Hui, Ring Peter, Meng Jie, Giai Nguyen Van, and Bertulani Carlos A. *Phys. Rev. C*, 2010, v. 81, 031302.
17. Pittel S., Lei Y., Fu G. J. and Zhao Y. M. *Journal of Physics: Conference Series*, 2013, v. 445, 012031.
18. Moller P., Nix J. R., Myers W. D. and Swiatecki W. J. *At. Data Nucl. Data Tables*, 1995, v. 59, 185.
19. Goriely S., Samyn M., Bender M. and Pearson J. M. *Phys. Rev. C*, 2003, v. 68, 054325.
20. Delaroche J.-P., Girod M., Libert J., Goutte H., Hilaire S., Péru S., Pillet N., and Bertsch G. F. *Phys. Rev. C*,2010, v. 81, 014303.
21. Geng L., Toki H. and Meng J. *Progress of Theoretical Physics*, 2005, v. 113 (4), 785–800.
22. Mohammed-Azizi B. and Medjadi D. E. *Comput. Phys. Commun.*, 2004, v. 156, 241–282.
23. Mohammed-Azizi B. and Medjadi D. E. *Comput. Phys. Commun.*, 2007, v. 176, 634–635.
24. Mohammed-Azizi B. and Medjadi D. E. *Comput. Phys. Commun.*, 2014, v. 185, 3067–3068.
25. Stránský P., Frank A. and Bijker R. *Journal of Physics: Conference Series*, 2011, v. 322, 012018.
26. Mohammed-Azizi B. and Medjadi D. E. *Phys. Rev. C*, 2006, v. 74, 054302.
27. Mohammed-Azizi B. *Intern. Journal of Modern Physics C*, 2010, v. 21 (5), 681–694.
28. Myers W. D. and Swiatecki W. J. *Nucl. Phys. A*, 1966, v. 81, 1.
29. Cwiok S., Dudek J., Nazarewicz W. and Werner T. *Comput. Phys. Commun.*, 1987, v. 46, 379.
30. Pauli H. C. *Phys. Lett. C*, 1973, v. 7, 35.

31. Brack M., Damgaard L., Jensen A. S., Pauli H. C., Strutinsky V. M. and Wong C. Y. *Rev. Mod. Phys.*, 1972, v. 44, 320–405.
32. Kern B. D. et al. *Phys. Rev. C*, 1987, v. 36, 1514.
33. Gotz U., Pauli H. C., and Adler K. *Nucl. Phys. A*, 1971, v. 175, 481.
34. Hilaire S., Girod M. http://www-phynu.cea.fr/science_en_ligne/carte_potentiels_microscopiques/carte_potentiel_nucleaire.htm, Jan. 2015.
35. Casten R. F., Cakirli R. B. *Acta Physica Polonica B*, 2009, v. 40 (3), 493–502.
36. Anghel S., Danil G. C., Zamfir N. V., *Romanian Journ. Phys.*, 2009, v. 54 (3–4), 301–319.
37. Sarriguren P., Rodrıguez-Guzman R. R., Robledo L. M. *Journal of Physics: Conference Series*, 2010, v. 205, 012024.
38. http://www.nndc.bnl.gov/ensdf/, January 2015.

A Constants of the binding energy of the liquid drop model

The constants of (1) are defined as follows:

$$C_V = a_V \left[1 - \kappa I^2\right] \text{ (in the volume term)}$$

$$C_S = a_S \left[1 - \kappa I^2\right] \text{ (in the surface term)}$$

$$I = \frac{N - Z}{N + Z} \text{ (relative neutron excess)}$$

$$\varepsilon = +1 \text{ (even} - \text{even) (in the pairing term),}$$
$$0 \text{ (odd),}$$
$$-1 \text{ (odd} - \text{odd)}$$

$$C_C = \frac{3}{5}\frac{e^2}{r_0} \text{ (in the Coulomb term)}$$

$$C_d = \frac{\pi^2}{2}\left(\frac{a_0}{r_0}\right)^2 \frac{e^2}{r_0} \text{ (diffuseness correction)}$$

The last correction to the Coulomb energy takes into account that the liquid drop has not a sharp but a diffuse surface of the Woods-Saxon type. The diffuseness parameter is a_0 and the charge radius "contains" r_0 ($R_{ch} = r_0 A^{1/3}$).

B Constants of the Woods-Saxon mean potential

"Universal parameters" of the Woods-Saxon central and Spin-orbit potentials entering in (10).

Neutrons	
V_{0neut}=49.6(1-0.86I)	depth of cmf (MeV)
R_{Vneut}=1.347$A^{1/3}$	radius of cmf (fm)
λ=35.0 (dimensionless)	spin-orb. coupling strength
$R_{SO-neut}$=1.310$A^{1/3}$	Radius of somf (fm)
a_0=0.70	diffuseness of cmf (fm)
a_0=0.70	diffuseness of somf (fm)
Protons	
V_{0prot}=49.6(1+0.86I)	depth of cmf (MeV)
R_{Vprot}=1.275$A^{1/3}$	radius of cmf (fm)
λ=36.0 (dimensionless)	spin-orb. coupling strength
$R_{SO-nprot}$=1.200$A^{1/3}$	radius of somf (fm)
a_0=0.70	diffuseness of cmf (fm)
a_0=0.70	diffuseness of somf (fm)

cmf = central mean field
somf = spin-orbit mean field

Other Earths: Search for Life and the Constant Curvature

Megan M. Khoshyaran

Economics Traffic Clinic-ETC, 34 Avenue des champs Elyses, 75008 Paris, France
E-mail: megan.khoshyaran@wanadoo.fr

The objective of this paper is to propose a search methodology for finding other exactly similar earth like planets (or sister earths). The theory is based on space consisting of Riemann curves or highways. A mathematical model based on constant curvature, a moving frame bundle, and gravitational dynamics is introduced.

1 Introduction

The objective of this paper is to propose a search methodology that could show the way to finding other exactly similar earth like planets (or sister earths). The main idea in this paper lies behind the theory that space contains of what is called highways. The term highway refers to a path with no obstructions. Examples of obstructions are black holes and stars or any celestial objects with significant masses and gravitational forces. Paths are non-linear graphs.

Space is composed of these highways, on which there is at least one sister earth. Topologically highways are made up of constant Riemann curvatures, [1]. It is posited that sister earths are located at the points of constant curvature; more accurately, these are the points where two oppositely directed highways (or paths) with identical constant curvatures share a moving tangent frame where the coordinate frame is the derivative of their gravitational tensors with respect to the (x) coordinate.

A sister earth comes with its satellite (or a moon) just as earth has its satellite, the moon. A satellite is found at the point of intersection of two oppositely directed highways. The earth's moon provides a parallel highway to the earth's highway. So far the methods of detecting earth like exoplanets consist of observation through Hubble space telescope of extrasolar giant planets and their gravitational influence on parent stars, [2,3,4]. Transit method, [5], orbital brightness modulations, [6], timing variations, [7], gravitational microlensing, [8], direct imaging, [9], and polarimetry, [10], are among methods currently used for the detection of earth like exoplanets. In all these methods the main element of study is observation of light and gravitational changes as it distorts light around planets.

The advantage of the current theory proposed in this paper is that it provides an analytical approach based on Riemannian curvature, and the dynamics of gravitation mathematically represented by differential gravity calculations around the points of constant curvature. The important first step is to find pathways (or space highways) with constant curvatures. One Riemann path or space highway with constant curvature is known, and that is the Riemann path of the earth. The Riemann path of the moon is another known pathway or space highway that is parallel to the earth's Riemann path. Other Riemann paths can be traced out parallel to the earth's and the moon's Riemann paths or space highways. A path to a sister earth can be traced out assuming that it has the same curvature with different gravitational tensor described in the following section.

2 Space highways

Space highways are paths that extend to infinity. The word infinity is used to imply very long distances. These paths can be considered as Riemannian curves with constant curvatures. Riemann paths with constant curvatures contain no obstacles. Here, obstructions are mainly black holes, and massive stars, or any significant electrostatic system, moving with a certain velocity (v) corresponding to an electromagnetic momentum, (H).

In other words, any significant mass with inertia, momentum, and thus velocity that produces gravitational and electromagnetic forces. Vector $(\mathbf{H})$ represents the electromagnetic direction and magnitude. The electromagnetic momentum can be expressed as the multiplication of the vector $(\mathbf{H})$ by the velocity $(\mathbf{v})$, as $(\mathbf{H} \cdot \mathbf{v})$. The assumption of Riemann paths in dark regions of space is fundamental to the structure of the model to be introduced.

The earth's Riemann path with constant curvature can be constructed given the coordinates of the sun and the earth. Let's assume that the earth is in a stationary system $(\mathbf{K})$, where $[\mathbf{x}_\tau = (x, y, z, t) \in \mathbf{K}]$ denotes the coordinates and the system $(\mathbf{K})$ holds a homogeneous gravitational field, and gravitational acceleration equal to $[\gamma = (\gamma_x, \gamma_y, \gamma_z)]$. In system $(\mathbf{K})$, Newtonian laws hold in their most basic form, the same basic laws equally hold with respect to any other coordinate system moving in uniform translation with respect to $(\mathbf{K})$.

Let system $(\mathbf{K})$ represent the sun system. It is assumed that the coordinates of the sun are $(0, 0, 0, 0)$, meaning that the sun is considered to be the first solar system of its kind. Let's assume that earth is located in a second coordinate system $(\mathbf{K}')$, where $[\mathbf{x}_\sigma = (x', y', z', t') \in \mathbf{K}']$ signifies the coordinates in this system. It is also assumed that for any other coordinate system outside of the two systems $(\mathbf{K})$ and $(\mathbf{K}')$, the laws of general relativity hold with respect to the two coordinate systems.

By this it is meant that the velocity of light (c) in vacuum

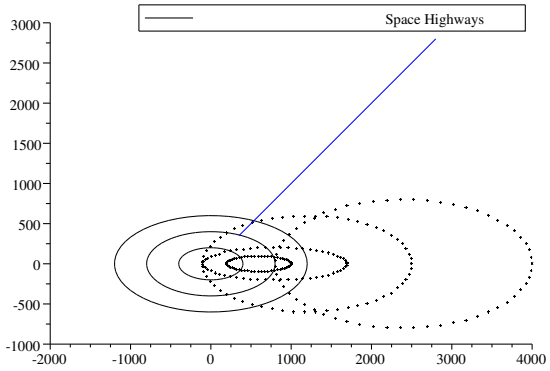

Fig. 1: A graphical representation of Riemann Paths.

is constant, [11], and in combination with the principles of relativity, follows the relativity of simultaneity, the Lorentz transformation rules, and the related laws indicating the behaviour of bodies in motion. The laws of geometry are taken directly as laws relating to relative positions of mass at rest. The laws of kinematics are to be taken as laws which describe the relation of a solid body with respect to another in terms of their distance from each other in definite length independent of the location and the orientation of the two bodies in time. An example of space highways is given in Fig. 1.

Let's consider the earth as an event point in system ($\mathbf{K}'$) in a uniform constant rotation in a finite space with respect to system ($\mathbf{K}$). The curvature from the event point to the stationary system ($\mathbf{K}$) is given by (1):

$$ds^2 = \sum_{\sigma\tau} G_{\sigma\tau} dx_\sigma dx_\tau. \tag{1}$$

(dx_σ) corresponds to differentials in system ($\mathbf{K}'$), (σ) represents the (x', y', z', t') coordinate system in ($\mathbf{K}'$), and (dx_τ) corresponds to differentials in system ($\mathbf{K}$), where τ represents the (x, y, z, t) coordinate system. ($G_{\sigma\tau}$) is the gravitation tensor, signifying the gravitational forces exerted mutually between systems ($\mathbf{K}$) and ($\mathbf{K}'$) multiplied by the differential of the electromagnetic force ($d\mathbf{H}$).

The gravitation tensor ($G_{\sigma\tau}$) is a matrix obtained by multiplying matrix ($g_{\sigma\tau}$), the matrix of the differentials of the gravitational force, given as:

$$g_{\sigma\tau} = \begin{pmatrix} \frac{\partial x'}{\partial x} & \frac{\partial x'}{\partial y} & \frac{\partial x'}{\partial z} & \frac{\partial x'}{\partial t} \\ \frac{\partial y'}{\partial x} & \frac{\partial y'}{\partial y} & \frac{\partial y'}{\partial z} & \frac{\partial y'}{\partial t} \\ \frac{\partial z'}{\partial x} & \frac{\partial z'}{\partial y} & \frac{\partial z'}{\partial z} & \frac{\partial z'}{\partial t} \\ \frac{\partial t'}{\partial x} & \frac{\partial t'}{\partial y} & \frac{\partial t'}{\partial z} & \frac{\partial t'}{\partial t} \end{pmatrix}$$

with matrix ($d\mathbf{H}$), the matrix of the differentials of the electromagnetic force or the matrix of the curl of ($\mathbf{H}$) given by (2):

$$G_{\sigma\tau} = g_{\sigma\tau} \times d\mathbf{H}. \tag{2}$$

The matrix of the curl of ($\mathbf{H}$), the electromagnetic force is given as:

$$d\mathbf{H} = \begin{pmatrix} \left(\frac{\partial H_{x'}}{\partial z} - \frac{\partial H_{z'}}{\partial x}\right) & 0 & 0 & 0 \\ 0 & \left(\frac{\partial H_{y'}}{\partial x} - \frac{\partial H_{x'}}{\partial y}\right) & 0 & 0 \\ 0 & 0 & \left(\frac{\partial H_{z'}}{\partial y} - \frac{\partial H_{y'}}{\partial z}\right) & 0 \\ 0 & 0 & 0 & 1 \end{pmatrix}.$$

In the presence of significant mass, and the electromagnetic momentum ($\mathbf{H} \cdot \mathbf{v}$), the diagonal entries of the curl of ($\mathbf{H}$) are given in (3)–(5) as:

$$\left(\frac{\partial H_{x'}}{\partial z} - \frac{\partial H_{z'}}{\partial x}\right) = \frac{1}{c} \times \rho \times v_{x'} \tag{3}$$

$$\left(\frac{\partial H_{y'}}{\partial x} - \frac{\partial H_{x'}}{\partial y}\right) = \frac{1}{c} \times \rho \times v_{y'} \tag{4}$$

$$\left(\frac{\partial H_{z'}}{\partial y} - \frac{\partial H_{y'}}{\partial z}\right) = \frac{1}{c} \times \rho \times v_{z'}. \tag{5}$$

In (3)–(5), (c) is the velocity of light, (ρ) is the volume-density charge of a mass, and the vector ($\mathbf{v}$) is the velocity of the electromagnetic momentum where $\mathbf{v} = (\mathbf{v_{x'}}, \mathbf{v_{y'}}, \mathbf{v_{z'}})$.

The curvature of the system ($\mathbf{K}$)-($\mathbf{K}'$) in a finite region between an event-point in system ($\mathbf{K}'$), and a stationary point in system ($\mathbf{K}$) such as the earth and the sun is well-known to be an ellipsoid in the form expressed by (6) as:

$$S = G_{\sigma\tau} \times \left(\frac{(\mathbf{x}_\sigma - \mathbf{x}_\tau)^2}{\mathbf{a^2}}\right). \tag{6}$$

($\mathbf{x}_\sigma$) is the vector of coordinates in the ($\mathbf{K}'$) system, where $\mathbf{x}_\sigma = (\mathbf{x}', \mathbf{y}', \mathbf{z}', \mathbf{t}')$, and ($\mathbf{x}_\tau$) is the vector of coordinates in the ($\mathbf{K}$) system, where $\mathbf{x}_\sigma = (\mathbf{x}, \mathbf{y}, \mathbf{z}, \mathbf{t})$. Equation (6) can be rewritten with respect to the coordinates given in (7):

$$\begin{aligned} S = A_1 \times \left(\frac{(x - x')^2}{{a_1}^2}\right) + A_2 \times \left(\frac{(y - y')^2}{{a_2}^2}\right) + \\ + A_3 \times \left(\frac{(z - z')^2}{{a_3}^2}\right) + A_4 \times \left(\frac{(t - t')^2}{{a_4}^2}\right). \end{aligned} \tag{7}$$

The coefficients ($\mathbf{A}$) are the columns of ($G_{\sigma\tau}$), the gravitation tensor. The denominators in (7), (a_1, a_2, a_3, a_4) are constants less than 1, and the coefficients ($\mathbf{A} = (\mathbf{A_1}, \mathbf{A_2}, \mathbf{A_3}, \mathbf{A_4})$) are given at the top of the next page.

The time (t) in the ($\mathbf{K}$) system is formulated in a relativistic sense as in (8):

$$t = \frac{\left(1 - \frac{v}{c}\right) \times t'}{\sqrt{1 - \frac{v^2}{c^2}}}. \tag{8}$$

$$\mathbf{A} = \begin{pmatrix} \frac{\partial x'}{\partial x} \times \left(\frac{\partial H_{x'}}{\partial z} - \frac{\partial H_{z'}}{\partial x}\right) & 0 & 0 & 0 \\ 0 & \frac{\partial y'}{\partial y} \times \left(\frac{\partial H_{y'}}{\partial x} - \frac{\partial H_{x'}}{\partial y}\right) & 0 & 0 \\ 0 & 0 & \frac{\partial z'}{\partial z} \times \left(\frac{\partial H_{z'}}{\partial y} - \frac{\partial H_{y'}}{\partial z}\right) & 0 \\ 0 & 0 & 0 & \frac{\partial t'}{\partial t} \times 1 \end{pmatrix}$$

The elements of the coefficient matrix (**A**) are:

$$A_{11} = \frac{\partial x'}{\partial x} \times \left(\frac{\partial H_{x'}}{\partial z} - \frac{\partial H_{z'}}{\partial x}\right) = \frac{1}{c} \times \rho \times \gamma_{x'} \tag{9}$$

$$A_{22} = \frac{\partial y'}{\partial y} \times \left(\frac{\partial H_{y'}}{\partial x} - \frac{\partial H_{x'}}{\partial y}\right) = \frac{1}{c} \times \rho \times \gamma_{y'} \tag{10}$$

$$A_{33} = \frac{\partial z'}{\partial z} \times \left(\frac{\partial H_{z'}}{\partial y} - \frac{\partial H_{y'}}{\partial z}\right) = \frac{1}{c} \times \rho \times \gamma_{z'} \tag{11}$$

and

$$A_{44} = \frac{\partial t'}{\partial t} = \frac{\left(\sqrt{1 - \frac{v_{x'}{}^2}{c^2}}\right)}{\left(1 - \frac{v_{x'}}{c}\right)} \times (t' - t)\,. \tag{12}$$

In (9–11), the vector (γ) is the vector of acceleration of the electromagnetic momentum ($\mathbf{H} \cdot \mathbf{v}$), where $\gamma = (\gamma_{\mathbf{x}'}, \gamma_{\mathbf{y}'}, \gamma_{\mathbf{z}'})$. The assumption is that the curvatures of Riemann paths or space highways should be formulated in exactly the same manner as the curvature formulated for the system (**K**)-(**K**′). This assumption can be justified since any event point (earth like planet) on a Riemann curve of constant curvature should exhibit the same characteristics as the event-point earth.

An important element to consider, is how to find the coordinates of an event point (earth like planet) with respect to the coordinate system (**K**). These coordinates are arbitrary since the only point of reference is the system (**K**). All the same, let's assign coordinates to an event point (earth like planet) as ($\mathbf{x}_\nu$) where [$\mathbf{x}_\nu = (\mathbf{x}'', \mathbf{y}'', \mathbf{z}'', \mathbf{t}'') \in \mathbf{K}''$] denotes the coordinate system in (**K**′′). The coordinates of the event point (earth like planet) can be determined given that the event point is in the finite region from the sun. The event point (earth like planet) in the dark region is chosen assuming that it is on an ellipsoid parallel to the ellipsoid that contains the coordinate system (**K**), with coordinates $\mathbf{x}_\tau = (\mathbf{x}, \mathbf{y}, \mathbf{z}, \mathbf{t})$, in other words the sun.

The curvature can be formulated in (9) as:

$$ds'^2 = \sum_{\nu\sigma} g^{\nu\sigma} \times G_{\sigma\tau} \times (dx_\sigma dx_\tau)\, dx_\nu. \tag{13}$$

The tensor ($g^{\nu\sigma}$) represents the gravitational force exerted between the two coordinate systems (**K**) and (**K**′′). Given that the coordinate system (**K**′′) is in a finite region with respect to the coordinate system (**K**), the tensor ($g^{\nu\sigma}$) takes on values equal to the Lorentz factor as is given in the first matrix at the top of the next page.

The Lorentz factor gives length contraction and time dilation. As the function of velocity (v), the Lorentz factor starts at value (1) at ($v = 0$), and approaches infinity as ($v \to c$), the velocity of a particle approaches the speed of light (c). The solution to differential equation (9) is an ellipsoid similar to the one given in (6), and its extended form similar to (7) is given in (10) as:

$$S' = \mathbf{B} \times \left(\frac{(\mathbf{x}_\nu - \mathbf{x}_\tau)^2}{\mathbf{b}^2}\right) \tag{14}$$

$$\begin{aligned} S = B_1 \times \left(\frac{(x'' - x)^2}{{b_1}^2}\right) + B_2 \times \left(\frac{(y'' - y)^2}{{b_2}^2}\right) + \\ + B_3 \times \left(\frac{(z'' - z)^2}{{b_3}^2}\right) + B_4 \times \left(\frac{(t'' - t)^2}{{b_4}^2}\right) = 1. \end{aligned} \tag{15}$$

The denominators in (11), (b_1, b_2, b_3, b_4) are constants less than 1, and the coefficients $\mathbf{B} = (\mathbf{B_1}, \mathbf{B_2}, \mathbf{B_3}, \mathbf{B_4})$ are given in the second matrix at the top of the next page.

The elements of the coefficient matrix (**B**) are:

$$\begin{aligned} B_{11} &= -\left(\frac{\partial x''}{\partial x} \times \frac{1}{\sqrt{1 - \frac{v^2_{x''}}{c^2}}}\right) \\ &= -\left(\frac{1}{\sqrt{1 - \frac{v^2_{x''}}{c^2}}}\right) \times |\, x'' - x\,| \end{aligned} \tag{16}$$

$$\begin{aligned} B_{22} &= -\left(\frac{\partial x''}{\partial x} \times \frac{1}{\sqrt{1 - \frac{v^2_{x''}}{c^2}}}\right) \\ &= -\left(\frac{1}{\sqrt{1 - \frac{v^2_{x''}}{c^2}}}\right) \times |\, y'' - y\,| \end{aligned} \tag{17}$$

$$\begin{aligned} B_{33} &= -\left(\frac{\partial x''}{\partial x} \times \frac{1}{\sqrt{1 - \frac{v^2_{x''}}{c^2}}}\right) \\ &= -\left(\frac{1}{\sqrt{1 - \frac{v^2_{x''}}{c^2}}}\right) \times |\, z'' - z\,| \end{aligned} \tag{18}$$

$$g^{\nu\sigma} = \begin{pmatrix} -\frac{1}{\sqrt{1-\frac{v^2_{x''}}{c^2}}} & 0 & 0 & 0 \\ 0 & -\frac{1}{\sqrt{1-\frac{v^2_{y''}}{c^2}}} & 0 & 0 \\ 0 & 0 & -\frac{1}{\sqrt{1-\frac{v^2_{z''}}{c^2}}} & 0 \\ 0 & 0 & 0 & \frac{\partial t''}{\partial t} \times \frac{1}{\sqrt{1-\frac{v^2_{x''}}{c^2}}} \end{pmatrix}$$

$$\mathbf{B} = \begin{pmatrix} -\frac{\partial x''}{\partial x} \times \frac{1}{\sqrt{1-\frac{v^2_{x''}}{c^2}}} & 0 & 0 & 0 \\ 0 & -\frac{\partial y''}{\partial y} \times \frac{1}{\sqrt{1-\frac{v^2_{y''}}{c^2}}} & 0 & 0 \\ 0 & 0 & -\frac{\partial z''}{\partial z} \times \frac{1}{\sqrt{1-\frac{v^2_{z''}}{c^2}}} & 0 \\ 0 & 0 & 0 & -\frac{\partial t''}{\partial t} \times \frac{1}{\sqrt{1-\frac{v^2_{x''}}{c^2}}} \end{pmatrix}$$

and

$$B_{44} = \frac{\partial t''}{\partial t} \times \left(\frac{1}{\sqrt{1-\frac{v^2_{x''}}{c^2}}} \right) = \left(\frac{1}{1-\frac{v_{x''}}{c}} \right) \times (t'' - t) \tag{19}$$

where $(\mid x'' - x \mid)$ is the absolute distance.

Any event point in the dark regions of space that does not violate the Lorentz factor impact of the gravitational force between the two coordinate systems (**K**) and (**K**″) can be considered to be on the constant curvature. The event point earth like planet should be found on such a constant curvature. Any other significant mass such as a black hole or a star would create discontinuity and thus disrupts the Riemann path.

Fig. 2 provides a graphical representation of an ellipsoidal curve with an event point (earth). Fig. 2 depicts the rotation of the earth around the sun scaled down to (100^{-3}) of the actual size. Fig. 3 demonstrates a Riemann path with respect to the sun system. Fig. 4 demonstrates Riemann paths with respect to the sun system.

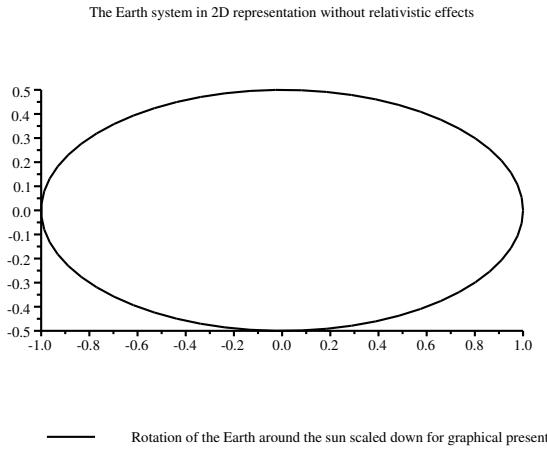

Fig. 2: A graphical representation of the rotation of the earth around the sun (the earth system).

3 Other earths

An event point (earth), is located at the point of constant curvature of two opposing Riemann paths or space highways, where the two curves share common points. Let (S') be the Riemann path of constant curvature of an ellipsoidal form given in (13). Let (S_{c_2}) be a Riemann path with a singular event point earth. The event point on (S_{c_2}) has a mass (M), and a density (ρ), and a velocity (v), equal to that of the earth. The values of mass, density, and velocity of the event point earth of the space highway (S_{c_2}) is independent of it's coordinates. Assuming that this condition holds, then the Riemann path (S_{c_2}) is in such a region of space where (S_{c_2}) is of constant curvature, and thus assumes an ellipsoidal form of type given in (13). The event point earth conserves its momentum and energy. The curvature (s_{c_2}) can be written as in (12).

The coordinates of this solar system are the same as the earth's solar system with the exception that the new sun's coordinates are that of our sun added the distance between the

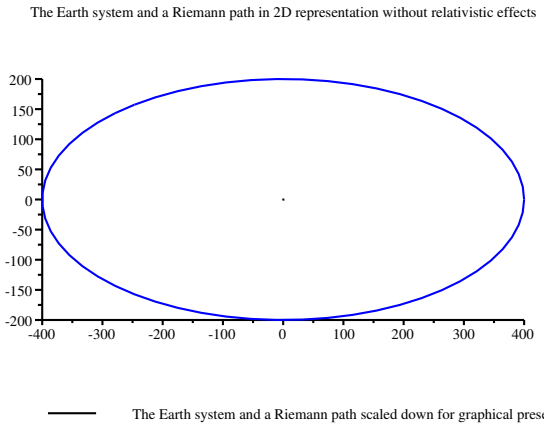

Fig. 3: A graphical representation of a Riemann path with respect to the sun system.

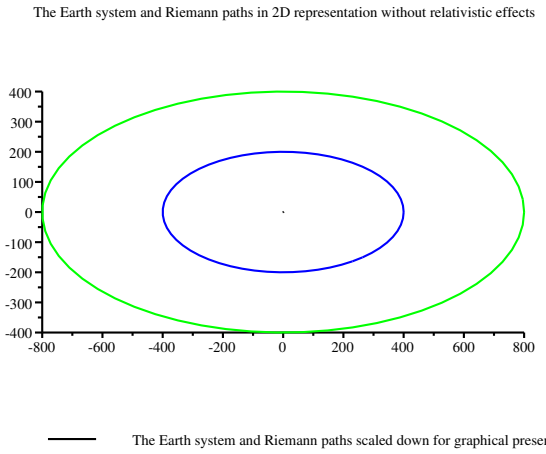

Fig. 4: A graphical representation of Riemann paths with respect to the sun system.

two stars. The coordinates of the new sun are

$$\mathbf{x}_{\tau'} = [(\mathbf{x}_{\tau'} + \Xi), \mathbf{y}_{\tau'}, \mathbf{z}_{\tau'}, \mathbf{t}_{\tau'}]$$

where (Ξ) is the distance between the two stars. The coordinates of the event point earth are

$$(\mathbf{x}_{\mathbf{c}_2}\eta) = [(\mathbf{x}_{\mathbf{c}_2} + \mathbf{\Gamma}), \mathbf{y}_{\mathbf{c}_2}, \mathbf{z}_{\mathbf{c}_2}, \mathbf{t}_{\mathbf{c}_2}]$$

where (Γ) is the distance from the sun to the point of constant curvature where the two Riemann paths meet.

The ellipsoidal form of the Riemann path (S_{c_2}) is given in (13) as:

$$ds^2_{c_2} = \sum_{\tau'\eta} G^{\tau'\eta}_{c_2} dx_{\tau'} dx^{\eta}_{c_2} \tag{20}$$

$$S_{c_2} = -\mathbf{G}^{\tau'\eta}_{\mathbf{c}_2} \times \frac{\left(\mathbf{x}_{\tau'} - \mathbf{x}^{\eta}_{\mathbf{c}_2}\right)^2}{\mathbf{b}^2_{\mathbf{c}_2}}. \tag{21}$$

The denominators in (13),

$$\left(\mathbf{b}_{\mathbf{c}_2} = \mathbf{b}^{\mathbf{c}_2}_{\mathbf{1}}, \mathbf{b}^{\mathbf{c}_2}_{\mathbf{2}}, \mathbf{b}^{\mathbf{c}_2}_{\mathbf{3}}, \mathbf{b}^{\mathbf{c}_2}_{\mathbf{4}}\right)$$

are constants less than 1, and the coefficients

$$-\mathbf{G}^{\tau'\eta}_{\mathbf{c}_2} = (-A^{c_2}_1, -A^{c_2}_2, -A^{c_2}_3, A^{c_2}_4)$$

are given at the top of the next page.

The elements of the coefficient matrix $(-\mathbf{G}^{\tau'\eta}_{\mathbf{c}_2})$ are:

$$-A^{c_2}_{11} = -\frac{\partial x^{\eta}_{c_2}}{\partial x_{\tau'}} \times \left(\frac{\partial H_{x^{\eta}_{c_2}}}{\partial z_{\tau'}} - \frac{\partial H_{z^{\eta}_{c_2}}}{\partial x_{\tau'}}\right) = \frac{1}{c} \times \rho \times -\gamma_{x^{\eta}_{c_2}} \tag{22}$$

$$-A^{c_2}_{22} = -\frac{\partial y^{\eta}_{c_2}}{\partial y_{\tau'}} \times \left(\frac{\partial H_{y^{\eta}_{c_2}}}{\partial x_{\tau'}} - \frac{\partial H_{x^{\eta}_{c_2}}}{\partial y_{\tau'}}\right) = \frac{1}{c} \times \rho \times -\gamma_{y^{\eta}_{c_2}} \tag{23}$$

$$-A^{c_2}_{33} = -\frac{\partial z^{\eta}_{c_2}}{\partial z_{\tau'}} \times \left(\frac{\partial H_{z^{\eta}_{c_2}}}{\partial y_{\tau'}} - \frac{\partial H_{y^{\eta}_{c_2}}}{\partial z_{\tau'}}\right) = \frac{1}{c} \times \rho \times -\gamma_{z^{\eta}_{c_2}} \tag{24}$$

and

$$A_{44} = \frac{\partial t''}{\partial t} = \frac{\sqrt{1 - \frac{\left(v_{x^{\eta}_{c_2}}\right)^2}{c^2}}}{\left(1 - \frac{v_{x^{\eta}_{c_2}}}{c}\right)} \times (t'' - t). \tag{25}$$

$(-\gamma_{x^{\eta}_{c_2}})$ states that the acceleration on the Riemann path (S_{c_2}) should be opposite of the acceleration on the (S') curve. In the above matrix the (x_{c_2}) coordinate should be taken equal to $(x_{c_2} + \Gamma)$.

The event point earth is located where

$$\frac{-\partial \mathbf{G}^{\nu\eta}_{\mathbf{c}_2}}{\partial x^{\eta}_{c_2}} = \frac{\partial \mathbf{B}_{\mathbf{x}_\nu}}{\partial x_\nu}$$

the derivative of the gravitational tensor $(-\mathbf{G}^{\tau'\eta}_{\mathbf{c}_2})$ belonging to the (c_2) Riemann path with respect to the coordinates of the (c_2) solar system, is equal to the derivative of the gravitational tensor of the (S') Riemann path with respect to its coordinate system. In Fig. 5, the event point earth can be found where the green ellipse Riemann path (S') and the Riemann path (c_2) (the red ellipse) meet. Fig. 6 depicts the tangent vector at the event point earth.

It should be stated that the magnitude of the electromagnetic force of the event point earth $(\mathbf{H}_{\mathbf{x}^{\eta}_{\mathbf{c}_2}})$ is equal to the magnitude of the electromagnetic force of the solar system's earth, $(\mathbf{H})$,

$$|\, \mathbf{H}_{\mathbf{x}^{\eta}_{\mathbf{c}_2}} \,| = |\, \mathbf{H} \,|\, .$$

Consequently, the curl of $(\mathbf{H}_{\mathbf{x}^{\eta}_{\mathbf{c}_2}})$, and the curl of $(\mathbf{H})$ should be equal. Thus the density, the volume-density charge of the mass, and the velocity of the event point earth are equal to that of the solar system's earth.

Let (T) be the set of all frames at all points of Riemann path (c_2). Let $[(U_\alpha, X^\alpha)_{\alpha\in c_2}]$, represent all pairs where (U_α)

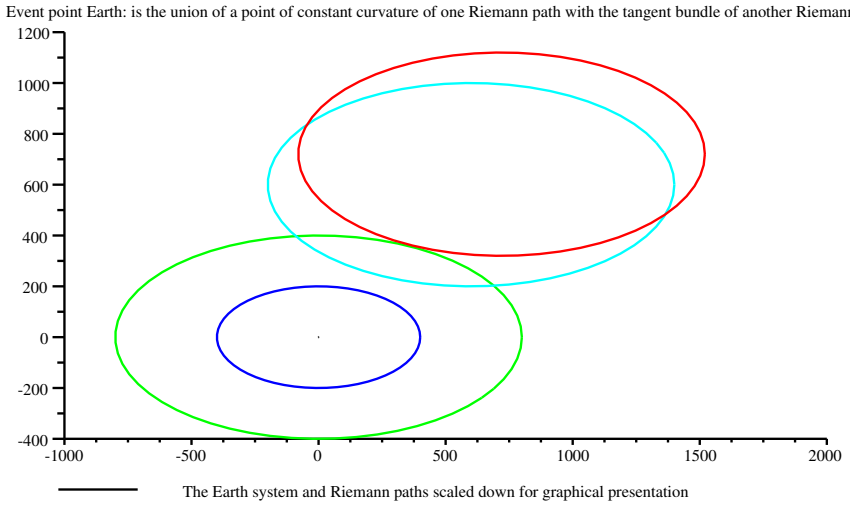

Fig. 5: A graphical representation of the event point earth.

$$-\mathbf{G}_{\mathbf{c_2}}^{\tau'\eta} = \begin{pmatrix} -\frac{\partial x_{c_2}^{\eta}}{\partial x_{\tau'}} \times \left(\frac{\partial H_{x_{c_2}^{\eta}}}{\partial z_{\tau'}} - \frac{\partial H_{z_{c_2}^{\eta}}}{\partial x_{\tau'}} \right) & 0 & 0 & 0 \\ 0 & -\frac{\partial y_{c_2}^{\eta}}{\partial y_{\tau'}} \times \left(\frac{\partial H_{y_{c_2}^{\eta}}}{\partial x_{\tau'}} - \frac{\partial H_{x_{c_2}^{\eta}}}{\partial y_{\tau'}} \right) & 0 & 0 \\ 0 & 0 & -\frac{\partial z_{c_2}^{\eta}}{\partial z_{\tau'}} \times \left(\frac{\partial H_{z_{c_2}^{\eta}}}{\partial y_{\tau'}} - \frac{\partial H_{y_{c_2}^{\eta}}}{\partial z_{\tau'}} \right) & 0 \\ 0 & 0 & 0 & \frac{\partial t_{c_2}^{\eta}}{\partial t_{\tau'}} \times 1 \end{pmatrix}$$

is an open subset of (T), and $(X^{\alpha} = (X_1^{\alpha}, ..., X_n^{\alpha}))$ is a moving frame on (U_{α}), then

$$\left(U, \frac{-\partial \mathbf{G}_{\mathbf{c_2}}^{\nu\eta}}{\partial X^{\alpha}} = \frac{\partial \mathbf{B}_{\mathbf{x}_{\nu}}}{\partial X^{\beta}} \right) \in (U_{\alpha}, X^{\alpha})_{\alpha \in c_2},$$

where $(X^{\beta} = (X_1^{\beta}, ..., X_n^{\beta}))$ is a moving frame on (S'). This gives the following set of differential equations for each $(\alpha \in c_2)$, and $(\beta \in S')$:

$$\begin{aligned} &\frac{\partial}{\partial X^{\alpha}} \left(\frac{\partial X^{\alpha}}{\partial x_{\tau'}} \times \left(\frac{\partial H_{X^{\alpha}}}{\partial z'_{\tau}} - \frac{\partial H_{X^{\alpha}}}{\partial x'_{\tau}} \right) \right) \\ &= -\frac{\partial}{\partial X^{\beta}} \left(\frac{\partial X^{\beta}}{\partial x''} \times \frac{1}{\sqrt{1 - \frac{v_{x''}^2}{c^2}}} \right) \end{aligned} \tag{26}$$

and

$$\frac{\partial}{\partial X^{\alpha}} \left(\frac{\partial t_{c_2}^{\eta}}{\partial t_{\nu}} \times 1 \right) = -\frac{\partial}{\partial X^{\beta}} \left(\frac{\partial t'}{\partial t} \times \frac{1}{\sqrt{1 - \frac{v_{x''}^2}{c^2}}} \right). \tag{27}$$

The equalities in (26) and (27) mean that the moving frame contains an open set of points $(X^{\alpha} = X^{\beta})$ where accelerations on the two Riemann paths (c_2) and (S') are equal. For (26) and (27) to hold a condition is imposed. The condition is that (26) and (27) must respect the linear translation $(L_{n\times n}, \Re)$, where (n) is the dimension of a matrix. If (M) was a (2×2) matrix , then the Jacobian of (M) would be equal to 1, $([M] = 1)$. This implies that the tangent bundle forms an isomorphic group to $(\Re^1)$. Matrix (M) is given at the top of the next page. $[M]$ is given by (28) below:

$$\begin{aligned} [M] = &\frac{\partial}{\partial X^{\alpha}} \left(\frac{\partial X^{\alpha}}{\partial x_{\tau'}} \times \left(\frac{\partial H_{X^{\alpha}}}{\partial z'_{\tau}} - \frac{\partial H_{X^{\alpha}}}{\partial x'_{\tau}} \right) \right) \times \\ &\times \left(-\frac{\partial}{\partial X^{\beta}} \left(\frac{\partial t'}{\partial t} \times \frac{1}{\sqrt{1 - \frac{v_{x''}^2}{c^2}}} \right) \right) \\ &- \frac{\partial}{\partial X^{\alpha}} \left(\frac{\partial t_{c_2}^{\eta}}{\partial t_{\nu}} \times 1 \right) \times \left(-\frac{\partial}{\partial X^{\beta}} \left(\frac{\partial X^{\beta}}{\partial x''} \times \frac{1}{\sqrt{1 - \frac{v_{x''}^2}{c^2}}} \right) \right) \\ &= 1. \end{aligned} \tag{28}$$

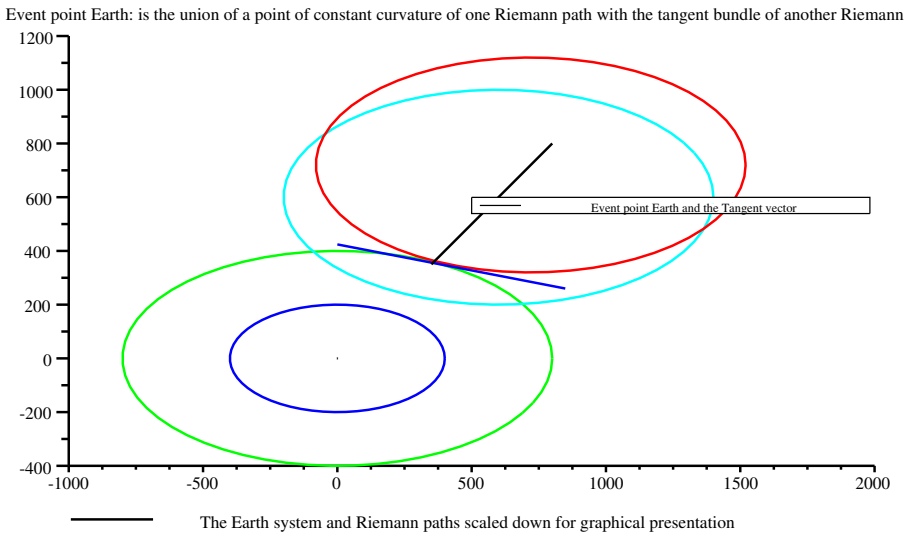

Fig. 6: Tangent vector at the event point earth.

$$M = \begin{pmatrix} \frac{\partial}{\partial X^\alpha}\left(\frac{\partial X^\alpha}{\partial x_{\tau'}} \times \left(\frac{\partial H_{X^\alpha}}{\partial z'_\tau} - \frac{\partial H_{X^\alpha}}{\partial x'_\tau}\right)\right) & \frac{\partial}{\partial X^\alpha}\left(\frac{\partial t^\eta_{c_2}}{\partial t_\nu} \times 1\right) \\ -\frac{\partial}{\partial X^\beta}\left(\frac{\partial X^\beta}{\partial x''} \times \frac{1}{\sqrt{1-\frac{v^2_{x''}}{c^2}}}\right) & -\frac{\partial}{\partial X^\beta}\left(\frac{\partial t'}{\partial t} \times \frac{1}{\sqrt{1-\frac{v^2_{x''}}{c^2}}}\right) \end{pmatrix}$$

(M) is the representation of $(\Re^1)$ in the (2×2) matrix form, thus is an invertible linear transformation of the tangent bundle. Given that the Riemann path is of constant curvature, then the implication is that the tangent bundle is invariant with respect to space-time. This condition would give the point on the (S_{c_2}) path that touches the (S') Riemann path. Therefore, it traces out the movement of the event point earth.

4 Conclusion

In this paper a new methodology is introduced that gives a mathematical approach to finding other exactly similar earth like planets. The mathematical model is based on finding what is called "space highways" or "Riemann paths". The characteristic of these highways is that they are found in the dark regions or non-deformed by gravitational forces regions of space, where there are no stars, or black holes, or planets. Riemann paths are considered as paths of constant curvature. Space highways are modelled as ellipsoidal forms with coefficients as columns of a gravitational tensor.

It is assumed that the coordinates of the sun are $(0, 0, 0, 0)$, meaning that the sun is considered to be the first solar system of its kind. This assumption is justified, since there is no evidence to the contrary to this day.

Space highways or Riemann paths are parallel to each other if they are in the same direction. The location of the event point earth (or exactly similar earth type planet) is where a Riemann path or space highway intersects at points of constant curvature with another space highway coming from an opposite direction. The movement of the event point earth is traced out where the two Riemann paths share the same tangent bundle. It is hoped that the search methodology introduced in this paper opens up a new possibility of finding planets that harbor life as we know it.

Acknowledgements

This research has made use of the Exoplanet Orbit Database and the Exoplanet Data Explorer at exoplanets.org.

Submitted on May 27, 2015 / Accepted on May 28, 2015

References

1. Wolfe J. A. Spaces of Constant Curvature. AMS Chelsea Publishing, Providence, 2000.
2. Eunkyu H., Wang S. X., Wright J. T., Feng Y. K., Zhao M., Fakhouri O., Brown J. I., Hancock C. Exoplanet Orbit Database. II. Updates to Exoplanets.org. *Publications of the Astronomical Society of the Pacific*, 2014, v. 126 (943), 827–837. California Planet Survey. http://exoplanets.org/, 14 October 2014.

3. Extrasolar Planet Search Programme at Haute-Provence Observatory. http://obswww.unige.ch/ udry/planet/elodie.html, 14 October 2014.
4. The Extrasolar Planets Encyclopaedia. http://exoplanet.eu, 14 October 2014.
5. Deming D., Seager S., Richardson J. Infrared radiation from an extrasolar planet. *Nature*, 2005, v. 434, 740–743.
6. Jenkin J. M., Doyle L. R. Detecting reflected light from close-in giant planets using space-based photometers. *Astrophysical Journal*, 2003, v. 595, 429–445.
7. Beaulieu J. P. Discovery of a cool planet of 5.5 Earth masses through gravitational microlensing. *Nature*, 2005, v. 439, 437–440.
8. Janson M., Brandener W., Henning T., Zinnecker H. Early come on + adaptive optics observations of GQ Lupi and its sub stellar companion. *Astronomy and Astrophysics*, 2006, v. 453 (2), 609–614.
9. Einstein A. On the Influence of Gravitation on the Propagation of Light. *Annalen der Physik*, 1911, v. 35, 898–908.

On the Possible Mechanism of Interaction of High-Energy Particles with Nuclei

Mirzajan A. Asimov and Takhir R. Akhmedov

333 S. Webster Ave., Suite 4, Norman, OK 73069, USA. E-mail: TakhirAkhmedov@yandex.ru

Based on an analysis of classical views stating that a charged particle creates certain magnetic field around its trajectory, we draw a conclusion about possible polarization of target nuclei within the magnetic field of approaching charged particle.

1 Introduction

While studying of scattering of electrons and neutrons by nuclei Mott [1] and J. Schwinger [2] suggested the mechanism of interaction of the scattering particle's magnetic moment with Coulomb field of a nucleus. Such scattering has been known as Mott-Schwinger interaction. Polarization of scattered particles is considered within the framework of this interaction [3].

In the present study, the interaction of the magnetic field of the scattering charged particles with the magnetic moment of nuclei is investigated.

It was demonstrated earlier that within the framework of this interaction the nucleus is also polarized. Spin of the nucleus interacting with the fast-moving (primary) charged particle orient itself in the plane perpendicular to the direction of the primary particle's momentum.

2 Magnetic field of the charged particle

The charged particle moving with the velocity v induces magnetic field H wrapped around its path. H depends on the distance from the charged particle as follows [4]:

$$H = \frac{e\,v\sin\theta}{r^2}\,, \tag{1}$$

where e is the charge of the scattered particle, r is the distance from the particle, and θ is the angle between the direction of the particle's velocity and r. Using this expression, one can calculate the intensity of the magnetic field H as a function of r and the speed of the particle with $\beta \sim 1$. It is assumed that laws of electromagnetism apply for small distances down to 10^{-13} cm. The calculations are presented in Table 1.

The numbers in the Table 1 indicate that pretty strong fields still not achieved by any experimental instrument. As it is known the magnetic field of a single charged particle has rotational characteristics.

3 Interaction of the magnetic field of the charged particle with the magnetic field of the nucleus

Magnetic charge of the scattering particle functions as an external magnetic field in respect to the nucleus. However, specific characteristic of the rotational magnetic field must be accounted for. Magnetic intensity lines are in the plane that is perpendicular to the direction of the particle's velocity. At the same time the vector of the magnetic field H at any arbitrary point on that plane at the distance r from the path of the particle is tangential to the circle of the radius r, and the direction of H is determined by the right-hand screw rule.

Let's consider that the nucleus is not exactly in the center of such a circle, but instead at some distance r from it. One can estimate the energy of interaction of the magnetic moment of the nucleus, μ, and the field H at distance r:

$$U = \mu H\,. \tag{2}$$

One has to take into consideration that magnetic moment acts like a top, and, in non-relativistic case, precession of the nucleus is simple Larmor precession. Relativistic case was described by Bargman et al [5].

Following Bargman, one can consider the case when the angle between the spin of the nucleus and magnetic field H is close to $\frac{\pi}{2}$. The spin will start precessing around the magnetic field H with the frequency

$$\Omega = \omega L\left(\frac{g}{2} - 1\right), \tag{3}$$

where $\omega L = \frac{e}{m\gamma} H$ is the frequency of Larmor precession, g is gyromagnetic ratio, and $\gamma = (1–\beta^2)–2$. It follows that

$$\Omega = \frac{eH}{m\gamma}\left(\frac{g}{2} - 1\right). \tag{4}$$

As Ω can be expressed as $\Omega = \frac{2\pi}{t}$ and for those nuclei whose spin satisfies the condition of $\frac{g}{2} \neq 1$ the spin of the target nucleus will precess in the magnetic field of the incoming particle. Forced polarization appears while turning the direction of the spin by $\frac{\pi}{2}$.

Time necessary for the turn is determined by

$$t = \frac{m\pi\gamma}{eH}\,(g-2)\,, \tag{5}$$

where m is the mass of the nucleus. For $\gamma = 10$, $m = 50$ a.m.u., we have $(g-2) \sim 1$, and $\mu = 1$ (nuclear magneton). Other examples in Table 2 demonstrate some interesting faces of the interaction.

Figures in Table 2 demonstrate that during the interaction of a fast moving charged particle with a nucleus (at $r \sim 10^{-12}$ cm) the orientation of the spin of the target nucleus takes as little time as $\sim 10^{-26}$ seconds. During this time interval the fast moving charged particle covers only 3×10^{-16} cm. This allows drawing a conclusion that right at the beginning of the interaction the nucleus target has time to orient its spin and further interaction takes place with the already polarized nucleus.

r, cm	10^{-13}	10^{-12}	10^{-11}	10^{-10}	10^{-9}	10^{-8}
H, Ersted	4.8×10^{16}	4.8×10^{14}	4.8×10^{12}	4.8×10^{10}	4.8×10^{8}	4.8×10^{6}

Table 1: The magnetic field intensity H as a function of r and the speed of the particle with $\beta \sim 1$.

r, cm	10^{-13}	10^{-12}	10^{-11}	10^{-10}	10^{-9}	10^{-8}
T, sec	10^{-28}	10^{-26}	10^{-24}	10^{-22}	10^{-20}	10^{-18}
$l = ts$, cm	3×10^{-18}	3×10^{-16}	3×10^{-14}	3×10^{-12}	3×10^{-10}	3×10^{-8}
$U = \mu H$, eV	1.5×10^{5}	1.5×10^{3}	15	0.15	1.5×10^{-3}	1.5×10^{-5}

Table 2: During the interaction of a fast moving charged particle with a nucleus (at $r \sim 10^{-12}$ cm), the orientation of the spin of the target nucleus takes as little time as $\sim 10^{-26}$ seconds.

4 Evaluation of energy required to change orientation of the nuclear spin within the external magnetic field

In known experiments of Dr. Wu et al [6], Co-60 nuclei were polarized at $T \sim 0.003$ K and the parity conservation was tested. Low temperatures were achieved by adiabatic demagnetization of Cerous Magnesium Nitrate. The energy of the effect can be estimated to be < 2.5 eV. Energy of the interaction of Co-60 nucleus magnetic moment with the outside magnetic field of a few hundred oersteds is negligible.

Therefore, the condition $\mu H \gg \kappa T$ is satisfied entirely (see Table 2): $\mu H \sim 10^3$, $\kappa T \sim 10^{-2}$.

Submitted on May 26, 2015 / Accepted on May 28, 2015

References

1. Mott N.F., Massey H.S.W. The Theory of Atomic Collisions. Oxford University Press, Oxford, 1965.
2. Schwinger J. On the polarization of fast neutrons. *Phys. Rev.*, 1948, v. 73, 407.
3. Tolhoek H.A. Electron polarization, theory and experiment. *Rev. Mod. Phys.*, 1956, v. 28, 277.
4. Landau L.D., Lifshitz E.M. The Classical Theory of Fields. 3rd edition, Butterworth-Heinemann, 2002.
5. Bargmann V., Michel L., and Telegdi V.L. Precession of the polarization of particles moving in a homogeneous electromagnetic field. *Phys. Rev. Lett.*, 1959, v. 2, 435.
6. Wu C.S., Ambler E., Hayward R.W., Hoppes D.D., and Hudson R.P. Experimental test of parity conservation in beta decay. *Phys. Rev.*, 1957, v. 105, 1413.

A Review on Natural Reality with Physical Equations

Linfan Mao
Chinese Academy of Mathematics and System Science, Beijing 100190, P. R. China
E-mail: maolinfan@163.com

A natural behavior is used to characterize by differential equation established on human observations, which is assumed to be on one particle or one field complied with reproducibility. However, the multilateral property of a particle P and the mathematical consistence determine that such an understanding is only local, not the whole reality on P, which leads to a central thesis for knowing the nature, i.e. *how to establish a physical equation with a proper interpretation on a thing*. As it is well-known, a thing consists of parts. Reviewing on observations, we classify them into two categories, i.e. *out-observation* and *in-observation* for discussion. The former is such an observation that the observer is out of the particle or the field P, which is in fact a macroscopic observation and its dynamic equation characterizes the coherent behavior of all parts in P, but the later is asked into the particle or the field by arranging observers simultaneously on different subparticles or subfields in P and respectively establishing physical equations, which are contradictory and given up in classical because there are not applicable conclusions on contradictory systems in mathematics. However, the existence naturally implies the necessity of the nature. Applying a combinatorial notion, i.e. G^L-solutions on non-solvable equations, a new notion for holding on the reality of nature is suggested in this paper, which makes it clear that the knowing on the nature by solvable equations is macro, only holding on these coherent behaviors of particles, but the non-coherent naturally induces non-solvable equations, which implies that the knowing by G^L-solution of equations is the effective, includes the classical characterizing as a special case by solvable equations, i.e. mathematical combinatorics.

1 Introduction

An observation on a physical phenomenon, or characters of a thing in the nature is the received information via hearing, sight, smell, taste or touch, i.e. sensory organs of the observer himself, little by little for human beings fulfilled with the reproducibility. However, it is difficult to hold the true face of a thing for human beings because he is analogous to a blind man in "*the blind men with an elephant*", a famous fable for knowing the nature. For example, let $\mu_1, \mu_2, \cdots, \mu_n$ be all observed and $\nu_i, i \geq 1$ unobserved characters on a particle P at time t. Then, P should be understood by

$$P = \left(\bigcup_{i=1}^{n}\{\mu_i\}\right)\bigcup\left(\bigcup_{k\geq 1}\{\nu_k\}\right) \tag{1.1}$$

in logic with an approximation $P^\circ = \bigcup_{i=1}^{n}\{\mu_i\}$ for P at time t. All of them are nothing else but Smarandache multispaces ([17]). Thus, $P \approx P^\circ$ is only an approximation for its true face of P, and it will never be ended in this way for knowing P as Lao Zi claimed "*Name named is not the eternal Name*" in the first chapter of his *TAO TEH KING* ([3]), a famous Chinese book.

A physical phenomenon of particle P is usually characterized by differential equation

$$\mathscr{F}\left(t, x_1, x_2, x_3, \psi_t, \psi_{x_1}, \psi_{x_2}, \cdots, \psi_{x_1x_2}, \cdots\right) = 0 \tag{1.2}$$

in physics established on observed characters of $\mu_1, \mu_2, \cdots, \mu_n$ for its state function $\psi(t, x)$ in $\mathbb{R}^4$. Usually, these physical phenomenons of a thing is complex, and hybrid with other things. *Is the reality of particle P all solutions of* (1.2) *in general?* Certainly not because (1.2) only characterizes the behavior of P on some characters of $\mu_1, \mu_2, \cdots, \mu_n$ at time t abstractly, not the whole in philosophy. For example, the behavior of a particle is characterized by the Schrödinger equation

$$i\hbar\frac{\partial\psi}{\partial t} = -\frac{\hbar^2}{2m}\nabla^2\psi + U\psi \tag{1.3}$$

in quantum mechanics but observation shows it in two or more possible states of being, i.e. superposition. We can not even say which solution of the Schrödinger equation (1.3) is the particle because each solution is only for one determined state. Even so, the understanding of all things is inexhaustible by (1.1).

Furthermore, *can we conclude* (1.2) *is absolutely right for a particle P?* Certainly not also because the dynamic equation (1.2) is always established with an additional assumption, i.e. the geometry on a particle P is a point in classical mechanics or a field in quantum mechanics and dependent on the observer is out or in the particle. For example, a water molecule H_2O consists of 2 Hydrogen atoms and 1 Oxygen atom such as those shown in Fig. 1. If an observer receives information on the behaviors of Hydrogen or Oxygen atom but stands out of the water molecule H_2O by viewing it a geometrical point, then such an observation is an out-observation because it only receives such coherent information on atoms H and O with the water molecule H_2O.

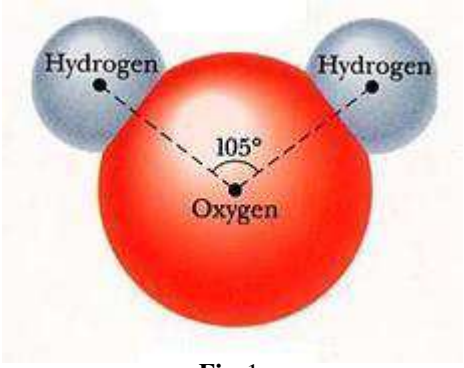

Fig. 1

If an observer is out the water molecule H_2O, his all observations on the Hydrogen atom H and Oxygen atom O are the same, but if he enters the interior of the molecule, he will view a different sceneries for atom H and atom O, which are respectively called *out-observation* and *in-observation*, and establishes 1 or 3 dynamic equations on the water molecule H_2O.

The main purpose of this paper is to clarify the natural reality of a particle with that of differential equations, and conclude that a solvable one characterizes only the reality of elementary particles but non-solvable system of differential equations essentially describe particles, such as those of baryons or mesons in the nature.

For terminologies and notations not mentioned here, we follow references [1] for mechanics, [5] for combinatorial geometry, [15] for elementary particles, and [17] for Smarandache systems and multispaces, and all phenomenons discussed in this paper are assumed to be true in the nature.

2 Out-observations

An *out-observation* observes on the external, i.e. these macro but not the internal behaviors of a particle P by human senses or via instrumental, includes the size, magnitudes or eigenvalues of states, ..., etc.

Certainly, the out-observation is the fundamental for quantitative research on matters of human beings. Usually, a dynamic equation (1.2) on a particle P is established by the principle of stationary action $\delta S = 0$ with

$$S = \int_{t_1}^{t_2} dt\, L(q(t), \dot{q}(t)) \tag{2.1}$$

in classical mechanics, where $q(t), \dot{q}(t)$ are respectively the generalized coordinates, the velocities and $L(q(t), \dot{q}(t))$ the *Lagrange function* on the particle, and

$$S = \int_{\tau_2}^{\tau_1} d^4x \mathcal{L}(\phi, \partial_\mu \psi) \tag{2.2}$$

in field theory, where ψ is the state function and $\mathcal{L}$ the *Lagrangian density* with τ_1, τ_2 the limiting surfaces of integration by viewed P an independent system of dynamics or a field. The principle of stationary action $\delta S = 0$ respectively induced the *Euler-Lagrange equations*

$$\frac{\partial L}{\partial q} - \frac{d}{dt}\frac{\partial L}{\partial \dot{q}} = 0 \quad \text{and} \quad \frac{\partial \mathcal{L}}{\partial \psi} - \partial_\mu \frac{\partial \mathcal{L}}{\partial(\partial_\mu \psi)} = 0 \tag{2.3}$$

in classical mechanics and field theory, which enables one to find the dynamic equations of particles by proper choice of L or $\mathcal{L}$. For examples, let

$$\mathcal{L}_S = \frac{i\hbar}{2}\left(\frac{\partial \psi}{\partial t}\overline{\psi} - \frac{\partial \overline{\psi}}{\partial t}\psi\right) - \frac{1}{2}\left(\frac{\hbar^2}{2m}|\nabla\psi|^2 + V|\psi|^2\right),$$
$$\mathcal{L}_D = \overline{\psi}\left(i\gamma^\mu \partial_\mu - \frac{mc}{\hbar}\right)\psi,$$
$$\mathcal{L}_{KG} = \frac{1}{2}\left(\partial_\mu \psi \partial^\mu \psi - \left(\frac{mc}{\hbar}\right)^2 \psi^2\right).$$

Then we respectively get the Schrödinger equation (1.3) or the Dirac equation

$$\left(i\gamma^\mu \partial_\mu - \frac{mc}{\hbar}\right)\psi(t, x) = 0 \tag{2.4}$$

for a free fermion $\psi(t, x)$ and the Klein-Gordon equation

$$\left(\frac{1}{c^2}\frac{\partial^2}{\partial t^2} - \nabla^2\right)\psi(x, t) + \left(\frac{mc}{\hbar}\right)^2 \psi(x, t) = 0 \tag{2.5}$$

for a free boson $\psi(t, x)$ hold in relativistic forms by (2.3), where $\hbar = 6.582 \times 10^{-22}$MeV s is the Planck constant, c is the speed of light,

$$\nabla = \left(\frac{\partial}{\partial x}, \frac{\partial}{\partial y}, \frac{\partial}{\partial z}\right), \qquad \nabla^2 = \frac{\partial^2}{\partial x^2} + \frac{\partial^2}{\partial y^2} + \frac{\partial^2}{\partial z^2},$$
$$\partial_\mu = \left(\frac{1}{c}\frac{\partial}{\partial t}, \frac{\partial}{\partial x_1}, \frac{\partial}{\partial x_2}, \frac{\partial}{\partial x_3}\right),$$
$$\partial^\mu = \left(\frac{1}{c}\frac{\partial}{\partial t}, -\frac{\partial}{\partial x_1}, -\frac{\partial}{\partial x_2}, -\frac{\partial}{\partial x_3}\right)$$

and $\gamma^\mu = \left(\gamma^0, \gamma^1, \gamma^2, \gamma^3\right)$ with

$$\gamma^0 = \begin{pmatrix} I_{2\times 2} & 0 \\ 0 & -I_{2\times 2} \end{pmatrix}, \quad \gamma^i = \begin{pmatrix} 0 & \sigma_i \\ -\sigma_i & 0 \end{pmatrix}$$

with the usual Pauli matrices

$$\sigma_1 = \begin{pmatrix} 0 & 1 \\ 1 & 0 \end{pmatrix}, \ \sigma_2 = \begin{pmatrix} 0 & -i \\ i & 0 \end{pmatrix}, \ \sigma_3 = \begin{pmatrix} 1 & 0 \\ 0 & -1 \end{pmatrix}.$$

Furthermore, let $\mathcal{L} = \sqrt{-g}R$, where $R = g^{\mu\nu}R_{\mu\nu}$, the Ricci scalar curvature on the gravitational field. The equation (2.3) then induces the vacuum Einstein gravitational field equation

$$R_{\mu\nu} - \frac{1}{2}g_{\mu\nu}R = 0. \tag{2.6}$$

Usually, the equation established on the out-observations only characterizes those of coherent behaviors of all parts in a particle P. For example, a water molecule H_2O obeys the Schrödinger equation (1.3), we assume its Hydrogen atom H and oxygen atom O also obey the Schrödinger equation (1.3) as a matter of course. However, the divisibility of matter initiates human beings to search elementary constituting cells of matter, i.e. elementary particles such as those of quarks, leptons with interaction quanta including photons and other particles of mediated interactions, also with those of their antiparticles at present ([14]), and unmatters between a matter and its antimatter which is partially consisted of matter but others antimatter ([8-19]). For example, a baryon is predominantly formed from three quarks, and a meson is mainly composed of a quark and an antiquark in the models of Sakata, or Gell-Mann and Ne'eman on hadron and meson, such as those shown in Fig. 2, where, $q_i \in \{\mathbf{u}, \mathbf{d}, \mathbf{c}, \mathbf{s}, \mathbf{t}, \mathbf{b}\}$ denotes a quark for $i = 1, 2, 3$ and $\overline{q}_2 \in \left\{\overline{\mathbf{u}}, \overline{\mathbf{d}}, \overline{\mathbf{c}}, \overline{\mathbf{s}}, \overline{\mathbf{t}}, \overline{\mathbf{b}}\right\}$, an antiquark. But a free quark was never found in experiments. We can not even conclude the Schrödinger equation (1.3) is the right equation (1.2) for quarks because it is established on an independent particle, can not be divided again in mathematics.

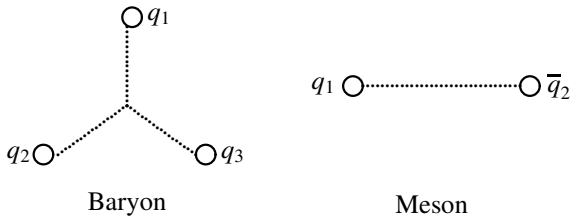

Fig. 2

Then, *why is it believed without a shadow of doubt that the dynamical equations of elementary particles such as those of quarks, leptons with interaction quanta are (*1.3*) in physics?* It is because that all our observations come from a macro viewpoint, the human beings, not the particle itself, which rationally leads to H. Everett's multiverse interpretation on the superposition by letting parallel equations for the wave functions $\psi(t, x)$ on positions of a particle in 1957 ([2]). We only hold coherent behaviors of elementary particles, such as those of quarks, leptons with interaction quanta and their antiparticles by (1.3), not the individual, and it is only an equation on those of particles viewed abstractly to be a geometrical point or an independent field from a macroscopic point, which leads physicists to assume the internal structures mechanically for hold the behaviors of particles such as those shown in Fig. 2 on hadrons. However, such an assumption is a little ambiguous in logic, i.e. we can not even conclude which is the point or the independent field, the hadron or its subparticle, the quark.

In fact, a point is non-divisible in geometry. Even so, the assumption on the internal structure of particles by physicists was mathematically verified by extending Banach spaces to extended Banach spaces on topological graphs $\overrightarrow{G}$ in [12]:

Let $(\mathscr{V}; +, \cdot)$ be a Banach space over a field $\mathscr{F}$ and $\overrightarrow{G}$ a strong-connected topological graph with vertex set V and arc set X. A vector labeling $\overrightarrow{G}^L$ on $\overrightarrow{G}$ is a $1-1$ mapping $L: \overrightarrow{G} \to \mathscr{V}$ such that $L: (u, v) \to L(u, v) \in \mathscr{V}$ for $\forall (u, v) \in X\left(\overrightarrow{G}\right)$ and it is a $\overrightarrow{G}$-flow if it holds with

$$L(u, v) = -L(v, u) \quad \text{and} \quad \sum_{u \in N_G(v)} L(v^u) = \mathbf{0}$$

for $\forall (u, v) \in X\left(\overrightarrow{G}\right)$, $\forall v \in V(\overrightarrow{G})$, where $\mathbf{0}$ is the zero-vector in $\mathscr{V}$.

For $\overrightarrow{G}$-flows $\overrightarrow{G}^L$, $\overrightarrow{G}^{L_1}$, $\overrightarrow{G}^{L_2}$ on a topological graph $\overrightarrow{G}$ and $\xi \in \mathscr{F}$ a scalar, it is clear that $\overrightarrow{G}^{L_1} + \overrightarrow{G}^{L_2}$ and $\xi \cdot \overrightarrow{G}^L$ are also $\overrightarrow{G}$-flows, which implies that all $\overrightarrow{G}$-flows on $\overrightarrow{G}$ form a linear space over $\mathscr{F}$ with unit $\mathbf{O}$ under operations + and $\cdot$, denoted by $\overrightarrow{G}^{\mathscr{V}}$, where $\mathbf{O}$ is such a $\overrightarrow{G}$-flow with vector $\mathbf{0}$ on (u, v) for $\forall (u, v) \in X\left(\overrightarrow{G}\right)$. Then, it was shown that $\overrightarrow{G}^{\mathscr{V}}$ is a Banach space, and furthermore a Hilbert space if introduce

$$\begin{aligned} \left\|\overrightarrow{G}^L\right\| &= \sum_{(u,v) \in X\left(\overrightarrow{G}\right)} \|L(u, v)\|, \\ \left\langle \overrightarrow{G}^{L_1}, \overrightarrow{G}^{L_2} \right\rangle &= \sum_{(u,v) \in X\left(\overrightarrow{G}\right)} \langle L_1(u, v), L_2(u, v) \rangle \end{aligned}$$

for $\forall \overrightarrow{G}^L, \overrightarrow{G}^{L_1}, \overrightarrow{G}^{L_2} \in \overrightarrow{G}^{\mathscr{V}}$, where $\|L(u, v)\|$ is the norm of $L(u, v)$ and $\langle \cdot, \cdot \rangle$ the inner product in $\mathscr{V}$ if it is an inner space. The following result generalizes the representation theorem of Fréchet and Riesz on linear continuous functionals on $\overrightarrow{G}$-flow space $\overrightarrow{G}^{\mathscr{V}}$, which enables us to find $\overrightarrow{G}$-flow solutions on linear equations (1.2).

Theorem 2.1([12]) *Let* $\mathbf{T}: \overrightarrow{G}^{\mathscr{V}} \to \mathbb{C}$ *be a linear continuous functional. Then there is a unique* $\overrightarrow{G}^{\widehat{L}} \in \overrightarrow{G}^{\mathscr{V}}$ *such that*

$$\mathbf{T}\left(\overrightarrow{G}^L\right) = \left\langle \overrightarrow{G}^L, \overrightarrow{G}^{\widehat{L}} \right\rangle$$

for $\forall \overrightarrow{G}^L \in \overrightarrow{G}^{\mathscr{V}}$.

For non-linear equations (1.2), we can also get $\overrightarrow{G}$-flow solutions on them if $\overrightarrow{G}$ can be decomposed into circuits.

Theorem 2.2([12]) *If the topological graph* $\overrightarrow{G}$ *is strong-connected with circuit decomposition*

$$\overrightarrow{G} = \bigcup_{i=1}^{l} \overrightarrow{C}_i$$

such that $L(u^v) = L_i(\mathbf{x})$ *for* $\forall (u,v) \in X\left(\overrightarrow{C}_i\right)$, $1 \le i \le l$ *and the Cauchy problem*

$$\begin{cases} \mathscr{F}_i(\mathbf{x}, u, u_{x_1}, \cdots, u_{x_n}, u_{x_1x_2}, \cdots) = 0 \\ u|_{\mathbf{x}_0} = L_i(\mathbf{x}) \end{cases}$$

is solvable in a Hilbert space $\mathscr{V}$ *on domain* $\Delta \subset \mathbb{R}^n$ *for integers* $1 \le i \le l$, *then the Cauchy problem*

$$\begin{cases} \mathscr{F}_i(\mathbf{x}, X, X_{x_1}, \cdots, X_{x_n}, X_{x_1x_2}, \cdots) = 0 \\ X|_{\mathbf{x}_0} = \overrightarrow{G}^L \end{cases}$$

such that $L(u^v) = L_i(\mathbf{x})$ *for* $\forall (u,v) \in X\left(\overrightarrow{C}_i\right)$ *is solvable for* $X \in \overrightarrow{G}^{\mathscr{V}}$.

Theorems 2.1 – 2.2 conclude the existence of $\overrightarrow{G}$-flow solution on linear or non-linear differential equations for a topological graph $\overrightarrow{G}$, such as those of the Schrödinger equation (1.3), Dirac equation (2.4) and the Klein-Gordon equation (2.5), which all implies the rightness of physicists assuming the internal structures for hold the behaviors of particles because there are infinite many such graphs $\overrightarrow{G}$ satisfying conditions of Theorem 2.1 – 2.2, particularly, the bouquet $\overrightarrow{B}_N^{L_\psi}$, the dipoles $\overrightarrow{D^{\perp}}_{0,2N,0}^{L_\psi}$ for elementary particles in [13].

3 In-observations

An *in-observation* observes on the internal behaviors of a particle, particularly, a composed particle P. Let P be composed by particles $P_1, P_2, \cdots, P_m$. Different from out-observation from a macro viewing, in-observation requires the observer holding the respective behaviors of particles $P_1, P_2, \cdots, P_m$ in P, for instance an observer enters a water molecule H_2O receiving information on the Hydrogen or Oxygen atoms H, O.

For such an observation, there are 2 observing ways:

(1) there is an apparatus such that an observer can simultaneously observe behaviors of particles $P_1, P_2, \cdots, P_m$, i.e. $P_1, P_2, \cdots, P_m$ can be observed independently as particles at the same time for the observer;

(2) there are m observers $O_1, O_2, \cdots, O_m$ simultaneously observe particles $P_1, P_2, \cdots, P_m$, i.e. the observer O_i only observes the behavior of particle P_i for $1 \le i \le m$, called *parallel observing*, such as those shown in Fig. 3 for the water molecule H_2O with $m = 3$.

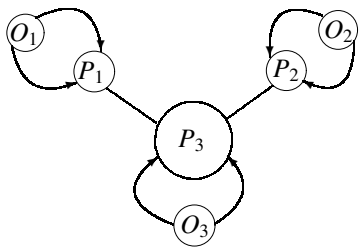

Fig. 3

Certainly, each of these observing views a particle in P to be an independent particle, which enables us to establish the dynamic equation (1.2) by Euler-Lagrange equation (2.3) for P_i, $1 \le i \le m$, respectively, and then we can apply the system of differential equations

$$\begin{cases} \dfrac{\partial L_1}{\partial \mathbf{q}} - \dfrac{d}{dt}\dfrac{\partial L_1}{\partial \dot{\mathbf{q}}} = 0 \\ \dfrac{\partial L_2}{\partial \mathbf{q}} - \dfrac{d}{dt}\dfrac{\partial L_2}{\partial \dot{\mathbf{q}}} = 0 \\ \cdots \\ \dfrac{\partial L_m}{\partial \mathbf{q}} - \dfrac{d}{dt}\dfrac{\partial L_m}{\partial \dot{\mathbf{q}}} = 0 \\ \mathbf{q}(t_0) = \mathbf{q}_0, \dot{\mathbf{q}}(t_0) = \dot{\mathbf{q}}_0 \end{cases} \tag{3.1}$$

for characterizing particle P in classical mechanics, or

$$\begin{cases} \dfrac{\partial \mathcal{L}_1}{\partial \psi} - \partial_\mu \dfrac{\partial \mathcal{L}_1}{\partial(\partial_\mu \psi)} = 0 \\ \dfrac{\partial \mathcal{L}_2}{\partial \psi} - \partial_\mu \dfrac{\partial \mathcal{L}_2}{\partial(\partial_\mu \psi)} = 0 \\ \cdots \\ \dfrac{\partial \mathcal{L}_m}{\partial \psi} - \partial_\mu \dfrac{\partial \mathcal{L}_m}{\partial(\partial_\mu \psi)} = 0 \\ \psi(t_0) = \psi_0 \end{cases} \tag{3.2}$$

for characterizing particle P in field theory, where the i^{th} equation is the dynamic equation of particle P_i with initial data $\mathbf{q}_0, \dot{\mathbf{q}}_0$ or ψ_0.

We discuss the solvability of systems (3.1) and (3.2). Let

$$S_{\mathbf{q}_i} = \left\{ (x_i, y_i, z_i)(\mathbf{q}_i, t) \in \mathbb{R}^3 \,\middle|\, \frac{\partial L_1}{\partial \mathbf{q}_i} - \frac{d}{dt}\frac{\partial L_1}{\partial \dot{\mathbf{q}}_i} = 0, \ \mathbf{q}_i(t_0) = \mathbf{q}_0, \dot{\mathbf{q}}_i(t_0) = \dot{\mathbf{q}}_0 \right\}$$

for integers $1 \le i \le m$. Then, the system (3.1) of equations is solvable if and only if

$$\mathscr{D}(\mathbf{q}) = \bigcap_{i=1}^{m} S_{\mathbf{q}_i} \neq \emptyset. \tag{3.3}$$

Otherwise, the system (3.1) is non-solvable. For example, let particles P_1, P_2 of masses M, m be hanged on a fixed pulley, such as those shown in Fig. 4.

Then, the dynamic equations on P_1 and P_2 are respectively

$$P_1 : \ \ddot{x} = g, \ x(t_0) = x_0 \text{ and } P_2 : ddotx = -g, \ x(t_0) = x_0$$

but the system

$$\begin{cases} \ddot{x} = g \\ \ddot{x} = -g, \ x(t_0) = x_0 \end{cases}$$

is contradictory, i.e. non-solvable.

Similarly, let $\psi_i(x,t)$ be the state function of particle P_i, i.e. the solution of

$$\begin{cases} \dfrac{\partial \mathcal{L}_i}{\partial \psi_i} - \partial_\mu \dfrac{\partial \mathcal{L}_i}{\partial(\partial_\mu \psi_i)} = 0 \\ \psi(t_0) = \psi_0. \end{cases}$$

Then, the system (3.2) is solvable if and only if there is a state function $\psi(x,t)$ on P hold with each equation of system (3.2), i.e.

$$\psi(x,t) = \psi_1(x,t) = \cdots = \psi_m(x,t), \quad x \in \mathbb{R}^3,$$

which is impossible because if all state functions $\psi_i(x,t)$, $1 \le i \le m$ are the same, the particles $P_1, P_2, \cdots, P_m$ are nothing else but just one particle. Whence, the system (3.2) is non-solvable if $m \ge 2$, which implies we can not characterize the behavior of particle P by classical solutions of differential equations.

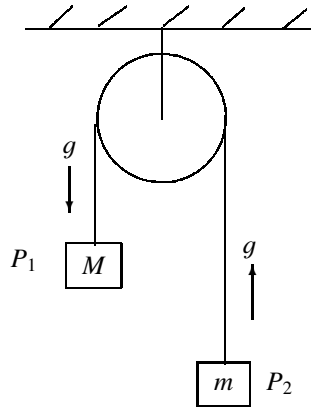

Fig. 4

For example, if the state function $\psi_O(x,t) = \psi_{H_1}(x,t) = \psi_{H_2}(x,t)$ in the water molecule H_2O for $x \in \mathbb{R}^3$ hold with

$$\begin{cases} -i\hbar \dfrac{\partial \psi_O}{\partial t} = \dfrac{\hbar^2}{2m_O}\nabla^2\psi_O - V(x)\psi_O \\ -i\hbar \dfrac{\partial \psi_{H_1}}{\partial t} = \dfrac{\hbar^2}{2m_{H_1}}\nabla^2\psi_{H_1} - V(x)\psi_{H_1} \\ -i\hbar \dfrac{\partial \psi_{H_2}}{\partial t} = \dfrac{\hbar^2}{2m_{H_2}}\nabla^2\psi_{H_2} - V(x)\psi_{H_2} \end{cases}$$

Then $\psi_O(x,t) = \psi_{H_1}(x,t) = \psi_{H_2}(x,t)$ concludes that

$$A_O e^{-\frac{i}{\hbar}(E_O t - \mathbf{p}_O x)} = A_{H_1} e^{-\frac{i}{\hbar}(E_{H_1} t - \mathbf{p}_{H_1} x)} = A_{H_2} e^{-\frac{i}{\hbar}(E_{H_2} t - \mathbf{p}_{H_2} x)}$$

for $\forall x \in \mathbb{R}^3$ and $t \in \mathbb{R}$, which implies that

$$A_O = A_{H_1} = A_{H_2},\ E_O = E_{H_1} = E_{H_2} \text{ and } \mathbf{p}_O = \mathbf{p}_{H_1} = \mathbf{p}_{H_2},$$

a contradiction.

Notice that each equation in systems (3.1) and (3.2) is solvable but the system itself is non-solvable in general, and they are real in the nature. Even if the system (3.1) holds with condition (3.3), i.e. it is solvable, we can not apply the solution of (3.1) to characterize the behavior of particle P because such a solution only describes the coherent behavior of particles $P_1, P_2, \cdots, P_m$. Thus, we can not characterize the behavior of particle P by the solvability of systems (3.1) or (3.2). We should search new method to characterize systems (3.1) or (3.2).

Philosophically, the formula (1.1) is the understanding of particle P and all of these particles $P_1, P_2, \cdots, P_m$ are inherently related, not isolated, which implies that P naturally inherits a topological structure $G^L[P]$ in space of the nature, which is a vertex-edge labeled topological graph determined by:

$$V\left(G^L[P]\right) = \{P_1, P_2, \cdots, P_m\},$$
$$E\left(G^L[P]\right) = \{(P_i, P_j) | P_i \bigcap P_j \neq \emptyset,\ 1 \le i \neq j \le m\}$$

with labeling

$$L:\ P_i \to L(P_i) = P_i \quad \text{and}$$
$$L:\ (P_i, P_j) \to L(P_i, P_j) = P_i \bigcap P_j$$

for integers $1 \le i \neq j \le m$. For example, the topological graphs $G^L[P]$ of water molecule H_2O, meson and baryon in the quark model of Gell-Mann and Ne'eman are respectively shown in Fig. 5,

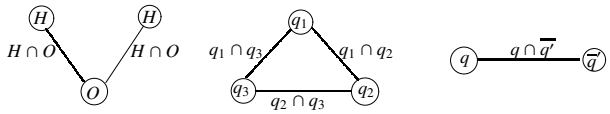

H_2O Baryon Meson

Fig. 5

where $O, H, q, \overline{q'}$ and $q_i, 1 \le i \le 3$ obey the Dirac equation but $O \cap H, q \cap \overline{q'}, q_k \cap q_l, 1 \le k, l \le 3$ comply with the Klein-Gordon equation.

Such a vertex-edge labeled topological graph $G^L[P]$ is called G^L-*solution* of systems (3.1)–(3.2). Clearly, the global behaviors of particle P are determined by particles $P_1, P_2, \cdots, P_m$. We can hold them on G^L-solution of systems (3.1) or (3.2). For example, let $u^{[v]}$ be the solution of equation at vertex $v \in V\left(G^L[P]\right)$ with initial value $u_0^{[v]}$ and $G^{L_0}[P]$ the initial G^L-solution, i.e. labeled with $u_0^{[v]}$ at vertex v. Then, a G^L-solution of systems (3.1) or (3.2) is *sum-stable* if for any number $\varepsilon > 0$ there exists $\delta_v > 0$, $v \in V(G^{L_0}[P])$ such that each $G^{L'}$-solution with

$$\left|u'^{[v]}_0 - u^{[v]}_0\right| < \delta_v, \qquad \forall v \in V(G^{L_0}[P])$$

exists for all $t \ge 0$ and with the inequality

$$\left| \sum_{v \in V(G^{L'}[P])} u'^{[v]} - \sum_{v \in V(G^L[P])} u^{[v]} \right| < \varepsilon$$

holds, denoted by $G^L[P] \overset{\Sigma}{\sim} G^{L_0}[P]$. Furthermore, if there exists a number $\beta_v > 0$ for $\forall v \in V(G^{L_0}[P])$ such that every $G^{L'}[P]$-solution with

$$\left|u'^{[v]}_0 - u^{[v]}_0\right| < \beta_v, \qquad \forall v \in V(G^{L_0}[P])$$

satisfies

$$\lim_{t\to\infty}\left|\sum_{v\in V(G^{L'}[P])} u'^{[v]} - \sum_{v\in V(G^{L}[P])} u^{[v]}\right| = 0,$$

then the $G^L[P]$-solution is called asymptotically stable, denoted by $G^L[P] \overset{\Sigma}{\to} G^{L_0}[P]$. Similarly, the energy integral of G^L-solution is determined by

$$E(G^L[P]) = \sum_{G\le G^{L_0}[P]} (-1)^{|G|+1} \int_{\mathscr{O}_G} \left(\frac{\partial u^G}{\partial t}\right)^2 dx_1 dx_2 \cdots dx_{n-1},$$

where u^G is the $\mathbb{C}^2$ solution of system

$$\left.\begin{array}{l} \dfrac{\partial u}{\partial t} = H_v(t, x_1, \cdots, x_{n-1}, p_1, \cdots, p_{n-1}) \\ u|_{t=t_0} = u^{[v]}_0(x_1, x_2, \cdots, x_{n-1}) \end{array}\right\} v \in V(G)$$

and $\mathscr{O}_G = \bigcap\limits_{v\in V(G)} \mathscr{O}_v$ with $\mathscr{O}_v \subset \mathbb{R}^n$ determined by the vth equation

$$\left\{\begin{array}{l} \dfrac{\partial u}{\partial t} = H_v(t, x_1, \cdots, x_{n-1}, p_1, \cdots, p_{n-1}) \\ u|_{t=t_0} = u^{[v]}_0(x_1, x_2, \cdots, x_{n-1}). \end{array}\right.$$

All of these global properties were extensively discussed in [7–11], which provides us to hold behaviors of a composed particle P by its constitutions $P_1, P_2, \cdots, P_m$.

4 Reality

Generally, the reality is the state characters (1.1) of existed, existing or will exist things whether or not they are observable or comprehensible by human beings, and the observing objective is on the state of particles, which then enables us to find the reality of a particle. However, an observation is dependent on the perception of the observer by his organs or through by instruments at the observing time, which concludes that to hold the reality of a particle P can be only little by little, and determines local reality of P from a macro observation at a time t, no matter what P is, a macro or micro thing. Why is this happening because we always observe by one observer on one particle assumed to be a point in space, and then establish a solvable equation (1.2) on coherent, not individual behaviors of P. Otherwise, we get non-solvable equations on P contradicts to the law of contradiction, the foundation of classical mathematics which results in discussions following:

4.1 States of particles are multiverse

A particle P understood by formula (1.1) is in fact a multiverse consisting of known characters $\mu_1, \mu_2, \cdots, \mu_n$ and unknown characters $\nu_k, k \ge 1$, i.e. different characters characterize different states of particle P. This fact also implies that the multiverse exist everywhere if we understand a particle P with in-observation, not only those levels of $I - IV$ of Max Tegmark in [24]. In fact, the infinite divisibility of a matter M in philosophy alludes nothing else but a multiverse observed on M by its individual submatters. Thus, the nature of a particle P is multiple in front of human beings, with unity character appeared only in specified situations.

4.2 Reality only characterized by non-compatible system

Although the dynamical equations (1.2) established on unilateral characters are individually compatible but they must be globally contradictory with these individual features unless all characters are the same one. It can not be avoided by the nature of a particle P. Whence, the non-compatible system, particularly, non-solvable systems consisting of solvable differential equations are suitable tools for holding the reality of particles P in the world, which also partially explains a complaint of Einstein on mathematics, i.e. *as far as the laws of mathematics refer to reality, they are not certain; and as far as they are certain, they do not refer to reality* because the multiple nature of all things.

4.3 Reality really needs mathematics on graph

As we know, there always exists a universal connection between things in a family in philosophy. Thus, a family $\mathscr{F}$ of things naturally inherits a topological graph $G^L[\mathscr{F}]$ in space and we therefore conclude that

$$\mathscr{F} = G^L[\mathscr{F}] \tag{4.1}$$

in that space. Particularly, if all things in $\mathscr{F}$ are nothing else but manifolds $M_T(x_1, x_2, x_3; t)$ of particles P determined by equation

$$f_T(x_1, x_2, x_3; t) = 0, \qquad T \in \mathscr{F} \tag{4.2}$$

in $\mathbb{R}^3 \times \mathbb{R}$, we get a geometrical figure $\bigcup\limits_{T\in\mathscr{F}} M_T(x_1, x_2, x_3; t)$, a combinatorial field ([6]) for $\mathscr{F}$. Clearly, the graph $G^L[\mathscr{F}]$ characterizes the behavior of $\mathscr{F}$ no matter whether the system (4.2) is solvable or not. Calculation shows that the system (4.2) of equations is non-solvable or not dependent on

$$\bigcap_{T\in\mathscr{F}} M_T(x_1, x_2, x_3; t) = \emptyset \ \text{ or not.}$$

Particularly, if $\bigcap\limits_{T\in\mathscr{F}} M_T(x_1, x_2, x_3; t) = \emptyset$, the system (4.2) is non-solvable and we can not just characterize the behavior of $\mathscr{F}$ by the solvability of system (4.2). We must turn the contradictory system (4.2) to a compatible one, such as those

shown in [10] and have to extend mathematical systems on graph $G^L[\mathscr{F}]$ ([12]) for holding the reality of $\mathscr{F}$.

Notice that there is a conjecture for developing mathematics in [4] called *CC conjecture* which claims that *any mathematical science can be reconstructed from or turned into combinatorization*. Such a conjecture is in fact a combinatorial notion for developing mathematics on topological graphs, i.e. finds the combinatorial structure to reconstruct or generalize classical mathematics, or combines different mathematical sciences and establishes a new enveloping theory on topological graphs for hold the reality of things $\mathscr{F}$.

5 Conclusion

Reality of a thing is hold on observation with level dependent on the observer standing out or in that thing, particularly, a particle classified to out- or in-observation, or parallel observing from a macro or micro view and characterized by solvable or non-solvable differential equations, consistent with the universality principle of contradiction in philosophy. For holding on the reality of things, the out-observation is basic but the in-observation is cardinal. Correspondingly, the solvable equation is individual but the non-solvable equations are universal. Accompanying with the establishment of compatible systems, we are also needed to characterize those of contradictory systems, particularly, non-solvable differential equations on particles and establish mathematics on topological graphs, i.e. *mathematical combinatorics*, and only which is the appropriate way for understanding the nature because all things are in contradiction.

Submitted on June 18, 2015 / Accepted on June 20, 2015

References

1. Abraham R. and Marsden J. E. Foundation of Mechanics, 2nd ed. Addison-Wesley, Reading, MA, 1978.
2. Everett H. Relative state formulation of quantum mechanics. *Rev.Mod.Phys.*, 1957, v. 29, 454–462.
3. Lu J. C. Fangfo Analyzing LAO ZHI – Explaining TAO TEH KING by TAI JI (in Chinese). Tuan Jie Publisher, Beijing, 2004.
4. Linfan Mao. Combinatorial speculation and combinatorial conjecture for mathematics. *International J.Math. Combin.*, 2007, v. 1 (1), 1–19.
5. Linfan Mao. Combinatorial Geometry with Applications to Field Theory. The Education Publisher Inc., USA, 2011.
6. Linfan Mao. Combinatorial fields – an introduction. *International J. Math.Combin.*, 2009, v. 3, 1–22.
7. Linfan Mao. Global stability of non-solvable ordinary differential equations with applications. *International J.Math. Combin.*, 2013, v. 1, 1–37.
8. Linfan Mao. Non-solvable equation systems with graphs embedded in $\mathbf{R}^n$. in Proceedings of the First International Conference on Smarandache Multispace and Multistructure, The Education Publisher Inc., July 2013.
9. Linfan Mao. Geometry on G^L-systems of homogenous polynomials. *International J.Contemp. Math. Sciences*, 2014, v. 9 (6), 287–308.
10. Linfan Mao. Mathematics on non-mathematics – A combinatorial contribution. *International J.Math. Combin.*, 2014, v. 3, 1–34.
11. Linfan Mao. Cauchy problem on non-solvable system of first order partial differential equations with applications. *Methods and Applications of Analysis*, 2015, v. 22 (2), 171–200.
12. Linfan Mao. Extended Banach $\vec{G}$-flow spaces on differential equations with applications. *Electronic J.Mathematical Analysis and Applications*, 2015, v. 3 (2), 59–91.
13. Linfan Mao. A new understanding of particles by $\vec{G}$-flow interpretation of differential equation, *Progress in Physics*, 2015, v. 11, 39–50.
14. Nambu Y. Quarks: Frontiers in Elementary Particle Physics. World Scientific Publishing, 1985.
15. Quang Ho-Kim and Pham Xuan Yem. Elementary Particles and Their Interactions. Springer-Verlag, Berlin Heidelberg, 1998.
16. Reid T. An inquiry into the human mind on the principles of common sense. in Brookes D., ed., Edinburgh University Press, 1997.
17. Smarandache F. Paradoxist Geometry. State Archives from Valcea, Rm. Valcea, Romania, 1969, and in Paradoxist Mathematics. Collected Papers (Vol. II). Kishinev University Press, Kishinev, 1997, pp. 5–28.
18. Smarandache F. A new form of matter – unmatter, composed of particles and anti-particles. *Progress in Physics*, 2005, v 1, 9–11.
19. Smarandache F. and Rabounski D. Unmatter entities inside nuclei, predicted by the Brightsen nucleon cluster model. *Progress in Physics*, 2006, v. 2, 14–18.
20. Tegmark M. Parallel universes. in Barrow J. D., Davies P. C. W. and Harper C. L., eds. Science and Ultimate Reality: From Quantum to Cosmos. Cambridge University Press, 2003.

LETTERS TO PROGRESS IN PHYSICS

Abraham I. Fet (1924–2007). In Memory of the 90th Anniversary

Abraham I. Fet (1924–2007) belonged to a particular "species of human" that is becoming extinct today: he could be rather a man of Renaissance in late Medieval Italy or Enlightenment in France in the 18th century, or a bright representative of intelligentsia in Russia of the 19th century.

A. Fet got his basic university education in mathematics and submitted a brilliant candidate (PhD) thesis at Moscow University being barely 24 years old. The mathematical results of his doctoral (DSc) thesis, presented later at the same University, still remain unsurpassed. He mainly published papers in mathematics, but he was also enrolled to research in physics that he started in collaboration with Yuriy B. Rumer, the famous Russian theoretical physicist. The results of their joint work were published in two co-authored books *Theory of Unitary Symmetry* (1970) and *Group Theory and Quantum Fields* (1977). Then there followed *Symmetry Group of Chemical Elements*, a book written by Fet alone, which presented a new physical perspective of the System of Chemical Elements and has become classics.

His research interests, however, were not limited to mathematics and physics. He remarkably explored many sciences and humanities, among which biology, economics, history, philosophy, sociology, psychology, and even literature, music, and arts. Moreover, being an encyclopedic scientist, he was not just an "erudite": with his powerful intellect, he built up a solid worldview from seemingly dispersed lines of knowledge.

First and utmost, Abraham Fet was a thinker, and his thinking was a blend of intellect, passion and concern. His major concern was about the fate of Mankind; he felt himself an active and responsible protagonist rather than being an observer "heeding to good and evil with equanimity, knowing neither pity nor ire".

A. Fet thought a lot on the human society, on the biological and cultural nature of man, on religious beliefs and ideals, and on the social mission of the intelligentsia, which he saw primarily in enlightening. He summarized his ideas in numerous essays and several books: *Pythagoras and the Ape* (1987), *Letters from Russia* (1989–1991), *Delusions of Capitalism, or the Fatal Conceit of Professor Hayek* (1996), and finally *Instinct and Social Behavior* (2005). The latter became his main work, where he investigated the history of culture in terms of ethology, with the aim to "reveal the impact of the social instinct on the human society, to describe the conditions frustrating its manifestations and to explain the effects of various attempts to suppress this invincible instinct". That

Abraham Ilych Fet

was his discovery and first study of a social instinct unique to humans, which he called "the instinct of intraspecific solidarity". With comprehensive historic examples, he has convincingly demonstrated how the morals and love for our neighbors originated from tribal solidarity within a minor kindred group and how the mark of kinship spread progressively to ever larger communities, as far as the entire mankind.

Two previously published books, together with a wealth of unpublished manuscripts, are now coming to the public with his *Collected Works* in seven volumes*.

With his excellent command of seven European languages, Abraham Fet not only had an extremely broad range of reading but also chose some important books and translated them for his friends and broad public. It was especially valuable in the conditions of harsh censorship in the Soviet times, when many books, for instance on psychology, were forbidden. Thus he translated Eric Berne, Erich Fromm, Karen Horney, Gregory Bateson, and many others. Being himself fascinated with the works of Konrad Lorenz, Fet was the first to introduce Lorenz's main books to the Russian readers. Namely,

*The publicaiton is just in Russian; an English volunteer translator is wanted. Ask Ludmila Petrova aifet@academ.org, for detail.

he translated *Das sogennannte Böse* ("The So-Called Evil"), *Die acht Todsünden der zivilisierten Menschheit* ("Civilized Man's Eight Deadly Sins"), *Die Rückseite des Spiegels* ("Behind the Mirror"), which were then published twice in post-Soviet Russia.

Abraham Fet was an ardent opponent to tyranny. Although being more a thinker than an active public person, he signed the "*Letter of 46*" in spring 1968 in defense of imprisoned dissidents. That lost him his job, both at the research institute and the university, and left him unemployed for years, to survive from occasional earns. Another reason of his dismissal, though, besides the very fact of signing the letter, was rather his spirit of independence and straight speaking. He called things the way he saw them, were they professional or personal characteristics of his fellows, or intrigues of functionaries or the privileges in science. A moral maximalist, Abraham Fet despised those who "lived as the others do" and called this lifestyle "the life of insects".

Beginning with the mid-1970s, Fet closely followed the events which took place in Poland. He perceived the revolt of 1980–1981 as the start of collapse of the so-called socialist camp. His book *The Polish Revolution* written in the wake of the events was anonymously published in 1985 in Munich and London. He not only provided deep review of the Polish events but also disclosed their historic prerequisites, demonstrated the outstanding role of the Polish intellectuals and foretold the further historic paths of the country.

Making retrospective of Fet's life and works, we can definitely put his name along with the most outstanding scientists and thinkers of the 20th century. He was among those who rarely get recognition during their lifetime. Rather than being in line with the "spirit of epoch", his ideas were against the mainstream. However, these are the ideas that are worth the most as they blaze truly trails to the science of the future and appeal to the future Mankind. Let his memory live for ever!

A. V. Gladky, L. P. Petrova, R. G. Khlebopros

The Journal on Advanced Studies in Theoretical and Experimental Physics, including Related Themes from Mathematics

PROGRESS IN PHYSICS

A quarterly issue scientific journal, registered with the Library of Congress (DC, USA). This journal is peer reviewed and included in the abstracting and indexing coverage of: Mathematical Reviews and MathSciNet (AMS, USA), DOAJ of Lund University (Sweden), Zentralblatt MATH (Germany), Scientific Commons of the University of St. Gallen (Switzerland), Open-J-Gate (India), Referativnyi Zhurnal VINITI (Russia), etc.

Electronic version of this journal:
http://www.ptep-online.com

Postal Address

Department of Mathematics and Science,
University of New Mexico,
705 Gurley Ave., Gallup, NM 87301, USA

ISSN: 1555-5534 (print)
ISSN: 1555-5615 (online)

Standard Address Number: 297-5092
Printed in the United States of America

October 2015 **Vol. 11, Issue 4**

CONTENTS

Information for Authors and Subscribers

Progress in Physics has been created for publications on advanced studies in theoretical and experimental physics, including related themes from mathematics and astronomy. All submitted papers should be professional, in good English, containing a brief review of a problem and obtained results.

All submissions should be designed in LaTeX format using *Progress in Physics* template. This template can be downloaded from *Progress in Physics* home page http://www.ptep-online.com. Abstract and the necessary information about author(s) should be included into the papers. To submit a paper, mail the file(s) to the Editor-in-Chief.

All submitted papers should be as brief as possible. Short articles are preferable. Large papers can also be considered in exceptional cases. Letters related to the publications in the journal or to the events among the science community can be applied to the section *Letters to Progress in Physics*.

All that has been accepted for the online issue of *Progress in Physics* is printed in the paper version of the journal. To order printed issues, contact the Editors.

This journal is non-commercial, academic edition. It is printed from private donations. (Look for the current author fee in the online version of the journal.)

Dislocations in the Spacetime Continuum: Framework for Quantum Physics

Pierre A. Millette

PierreAMillette@alumni.uottawa.ca, Ottawa, Canada

This paper provides a framework for the physical description of physical processes at the quantum level based on dislocations in the spacetime continuum within STCED (Spacetime Continuum Elastodynamics). In this framework, photon and particle self-energies and interactions are mediated by the strain energy density of the dislocations, replacing the role played by virtual particles in QED. We postulate that the spacetime continuum has a granularity characterized by a length b_0 corresponding to the smallest *STC* elementary Burgers dislocation-displacement vector. Screw dislocations corresponding to transverse displacements are identified with photons, and edge dislocations corresponding to longitudinal displacements are identified with particles. Mixed dislocations give rise to wave-particle duality. The strain energy density of the dislocations are calculated and proposed to explain the QED problem of mass renormalization.

1 Introduction

In a previous paper [1], the deformable medium properties of the spacetime continuum *(STC)* led us to expect dislocations, disclinations and other defects to be present in the *STC*. The effects of such defects would be expected to manifest themselves mostly at the microscopic level. In this paper, we present a framework to show that dislocations in the spacetime continuum are the basis of quantum physics. This paper lays the framework to develop a theory of the physical processes that underlie Quantum Electrodynamics (QED). The theory does not result in the same formalism as QED, but rather results in an alternative formulation that provides a physical description of physical processes at the quantum level. This framework allows the theory to be fleshed out in subsequent investigations.

1.1 Elastodynamics of the Spacetime Continuum

As shown in a previous paper [1], General Relativity leads us to consider the spacetime continuum as a deformable continuum, which allows for the application of continuum mechanical methods and results to the analysis of its deformations. The Elastodynamics of the Spacetime Continuum (*STCED*) [1–7] is based on analyzing the spacetime continuum within a continuum mechanical and general relativistic framework.

The combination of all spacetime continuum deformations results in the geometry of the *STC*. The geometry of the spacetime continuum of General Relativity resulting from the energy-momentum stress tensor can thus be seen to be a representation of the deformation of the spacetime continuum resulting from the strains generated by the energy-momentum stress tensor.

As shown in [1], for an isotropic and homogeneous spacetime continuum, the *STC* is characterized by the stress-strain relation

$$2\bar{\mu}_0\varepsilon^{\mu\nu} + \bar{\lambda}_0 g^{\mu\nu}\varepsilon = T^{\mu\nu} \tag{1}$$

where $T^{\mu\nu}$ is the energy-momentum stress tensor, $\varepsilon^{\mu\nu}$ is the resulting strain tensor, and

$$\varepsilon = \varepsilon^{\alpha}{}_{\alpha} \tag{2}$$

is the trace of the strain tensor obtained by contraction. The volume dilatation ε is defined as the change in volume per original volume [8, see pp. 149–152] and is an invariant of the strain tensor. $\bar{\lambda}_0$ and $\bar{\mu}_0$ are the Lamé elastic constants of the spacetime continuum: $\bar{\mu}_0$ is the shear modulus and $\bar{\lambda}_0$ is expressed in terms of $\bar{\kappa}_0$, the bulk modulus:

$$\bar{\lambda}_0 = \bar{\kappa}_0 - \bar{\mu}_0/2 \tag{3}$$

in a four-dimensional continuum.

As shown in [1], energy propagates in the spacetime continuum as wave-like deformations which can be decomposed into *dilatations* and *distortions*. *Dilatations* involve an invariant change in volume of the spacetime continuum which is the source of the associated rest-mass energy density of the deformation. On the other hand, *distortions* correspond to a change of shape of the spacetime continuum without a change in volume and are thus massless. Thus deformations propagate in the spacetime continuum by longitudinal (*dilatation*) and transverse (*distortion*) wave displacements.

This provides a natural explanation for wave-particle duality, with the transverse mode corresponding to the wave aspects of the deformation and the longitudinal mode corresponding to the particle aspects of the deformation [7]. The rest-mass energy density of the longitudinal mode is given by [1, see Eq.(32)]

$$\rho c^2 = 4\bar{\kappa}_0\varepsilon \tag{4}$$

where ρ is the rest-mass density, c is the speed of light, $\bar{\kappa}_0$ is the bulk modulus of the *STC* (the resistance of the spacetime continuum to *dilatations*), and ε is the volume dilatation.

This equation demonstrates that rest-mass energy density arises from the volume dilatation of the spacetime continuum.

The rest-mass energy is equivalent to the energy required to dilate the volume of the spacetime continuum. It is a measure of the energy stored in the spacetime continuum as mass. The volume dilatation is an invariant, as is the rest-mass energy density.

This is an important result as it demonstrates that mass is not independent of the spacetime continuum, but rather mass is part of the spacetime continuum fabric itself. Mass results from the dilatation of the *STC* in the longitudinal propagation of energy-momentum in the spacetime continuum. Matter does not warp spacetime, but rather, matter *is* warped spacetime (i.e. dilated spacetime). The universe consists of the spacetime continuum and energy-momentum that propagates in it by deformation of its (*STC*) structure.

Note that in this paper, we denote the *STCED* spacetime continuum constants $\bar{\kappa}_0, \bar{\lambda}_0, \bar{\mu}_0, \bar{\rho}_0$ with a diacritical mark over the symbols to differentiate them from similar symbols used in other fields of Physics. This allows us to retain existing symbols such as μ_0 for the electromagnetic permeability of free space, compared to the Lamé elastic constant $\bar{\mu}_0$ used to denote the spacetime continuum shear modulus.

1.2 Defects in the Spacetime Continuum

As discussed in [1], given that the spacetime continuum behaves as a deformable medium, there is no reason not to expect dislocations, disclinations and other defects to be present in the *STC*. Dislocations in the spacetime continuum represent the fundamental displacement processes that occur in its structure. These fundamental displacement processes should thus correspond to basic quantum phenomena and provide a framework for the description of quantum physics in *STCED*.

Defect theory has been the subject of investigation since the first half of the XX$^{\text{th}}$ century and is a well-developed discipline in continuum mechanics [9–14]. The recent formulation of defects in solids in based on gauge theory [15, 16].

The last quarter of the XX$^{\text{th}}$ century has seen the investigation of spacetime defects in the context of string theory, particularly cosmic strings [17, 18], and cosmic expansion [20, 21]. Teleparallel spacetime with defects [18, 22, 23] has resulted in a differential geometry of defects, which can be folded into the Einstein-Cartan Theory (ECT) of gravitation, an extension of Einstein's theory of gravitation that includes torsion [19, 20]. Recently, the phenomenology of spacetime defects has been considered in the context of quantum gravity [24–26].

In this paper, we investigate dislocations in the spacetime continuum in the context of *STCED*. The approach followed till now by investigators has been to use Einstein-Cartan differential geometry, with dislocations (translational deformations) impacting curvature and disclinations (rotational deformations) impacting torsion. The dislocation itself is modelled via the line element ds^2 [17]. In this paper, we investigate spacetime continuum dislocations using the underlying displacements u^ν and the energy-momentum stress tensor. We thus work from the RHS of the general relativistic equation (the stress tensor side) rather than the LHS (the geometric tensor side). It should be noted that the general relativistic equation used can be the standard Einstein equation or a suitably modified version, as in Einstein-Cartan or Teleparallel formulations.

In Section 2 of this paper, we review the basic physical characteristics and dynamics of dislocations in the spacetime continuum. The energy-momentum stress tensor is considered in Section 2.2. This is followed by a detailed review of stationary and moving screw and edge dislocations in Sections 3, 4 and 5, along with their strain energy density as calculated from *STCED*. The framework of quantum physics, based on dislocations in the spacetime continuum is covered in Section 6. Screw dislocations in quantum physics are considered in Section 6.2 and edge dislocations are covered in Section 6.3. Section 7 covers dislocation interactions in quantum physics, and Section 8 provides physical explanations of QED phenomena provided by dislocations in the *STC*. Section 9 summarizes the framework presented in this paper for the development of a physical description of physical processes at the quantum level, based on dislocations in the spacetime continuum within the theory of the Elastodynamics of the Spacetime Continuum (*STCED*).

2 Dislocations in the Spacetime Continuum

A dislocation is characterized by its dislocation-displacement vector, known as the *Burgers vector*, b^μ in a four-dimensional continuum, defined positive in the direction of a vector ξ^μ tangent to the dislocation line in the spacetime continuum [14, see pp.17–24].

A *Burgers circuit* encloses the dislocation. A similar reference circuit can be drawn to enclose a region free of dislocation (see Fig. 1). The Burgers vector is the vector required to make the Burgers circuit equivalent to the reference circuit (see Fig. 2). It is a measure of the displacement between the initial and final points of the circuit due to the dislocation.

It is important to note that there are two conventions used to define the Burgers vector. In this paper, we use the convention used by Hirth [14] referred to as the local Burgers vector. The local Burgers vector is equivalently given by the line integral

$$b^\mu = \oint_C \frac{\partial u^\mu}{\partial s} ds \tag{5}$$

taken in a right-handed sense relative to ξ^μ, where u^μ is the displacement vector.

A dislocation is thus characterized by a line direction ξ^μ and a Burgers vector b^μ. There are two types of dislocations: an *edge dislocation* for which $b^\mu \xi_\mu = 0$ and a *screw dislocation* which can be right-handed for which $b^\mu \xi_\mu = b$, or left-handed for which $b^\mu \xi_\mu = -b$, where b is the magnitude of the Burgers vector. Arbitrary mixed dislocations can be decom-

Fig. 1: A reference circuit in a region free of dislocation, S: start, F: finish

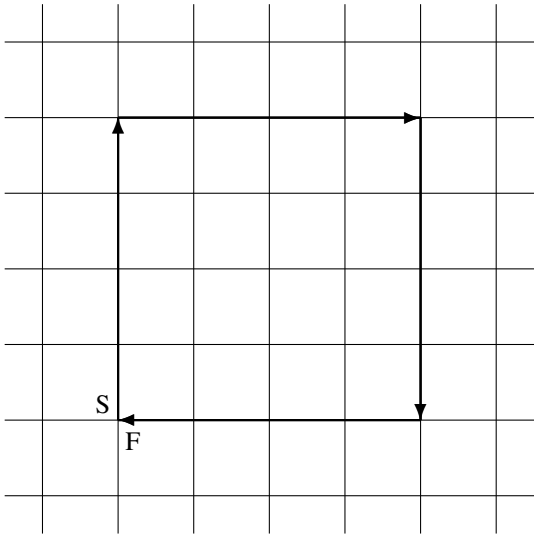

Fig. 2: A dislocation showing the Burgers vector b^μ, direction vector ξ^μ which points into the paper and the Burgers circuit, S: start, F: finish

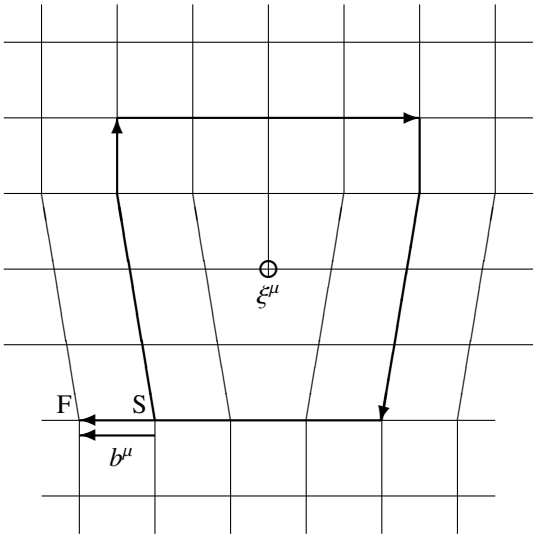

posed into a screw component, along vector ξ^μ, and an edge component, perpendicular to vector ξ^μ.

The edge dislocation was first proposed by Orowan [27], Polanyi [28] and Taylor [29] in 1934, while the screw dislocation was proposed by Burgers [30] in 1939. In this paper, we extend the concept of dislocations to the elastodynamics of the spacetime continuum. Edge dislocations correspond to *dilatations* (longitudinal displacements) and hence have an associated rest-mass energy, while screw dislocations correspond to *distortions* (transverse displacements) and are massless [1].

2.1 Dislocation dynamics

In three-dimensional space, the dynamic equation is written as [31, see pp. 88–89],

$$T^{ij}{}_{,j} = -X^i + \bar{\rho}_0 \ddot{u}^i \tag{6}$$

where $\bar{\rho}_0$ is the spacetime continuum density, X^i is the volume (or body) force, the comma (,) represents differentiation and $\dot{u}$ denotes the derivative with respect to time. Substituting for $\varepsilon^{\mu\nu} = \frac{1}{2}(u^{\mu;\nu} + u^{\nu;\mu})$ in (1), using (2) and $u^\mu{}_{;\mu} = \varepsilon^\mu{}_\mu = \varepsilon$ in this equation, we obtain

$$\bar{\mu}_0 \overrightarrow{\nabla}^2 u^i + (\bar{\mu}_0 + \bar{\lambda}_0)\varepsilon^{;i} = -X^i + \bar{\rho}_0 \ddot{u}^i \tag{7}$$

which, upon converting the time derivative to indicial notation and rearranging, is written as

$$\bar{\mu}_0 \overrightarrow{\nabla}^2 u^i - \bar{\rho}_0 c^2 u^i{}_{,00} + (\bar{\mu}_0 + \bar{\lambda}_0)\varepsilon^{;i} = -X^i. \tag{8}$$

We use the arrow above the nabla symbol to indicate the 3-dimensional gradient whereas the 4-dimensional gradient is written with no arrow. Using the relation [1]

$$c = \sqrt{\frac{\bar{\mu}_0}{\bar{\rho}_0}} \tag{9}$$

in the above, (8) becomes

$$\bar{\mu}_0(\overrightarrow{\nabla}^2 u^i - u^i{}_{,00}) + (\bar{\mu}_0 + \bar{\lambda}_0)\varepsilon^{;i} = -X^i \tag{10}$$

and, combining the space and time derivatives, we obtain

$$\bar{\mu}_0 \nabla^2 u^i + (\bar{\mu}_0 + \bar{\lambda}_0)\varepsilon^{;i} = -X^i. \tag{11}$$

This equation is the space portion of the *STCED displacement wave equation* (51) of [1]

$$\bar{\mu}_0 \nabla^2 u^\nu + (\bar{\mu}_0 + \bar{\lambda}_0)\varepsilon^{;\nu} = -X^\nu. \tag{12}$$

Hence the dynamics of the spacetime continuum is described by the dynamic equation (12), which includes the accelerations from the applied forces.

In this analysis, we consider the simpler problem of dislocations moving in an isotropic continuum with no volume force. Then (12) becomes

$$\bar{\mu}_0 \nabla^2 u^\nu + (\bar{\mu}_0 + \bar{\lambda}_0)\varepsilon^{;\nu} = 0, \tag{13}$$

where ∇^2 is the four-dimensional operator and the semi-colon (;) represents covariant differentiation.

Separating u^ν into its longitudinal (irrotational) component $u^\nu_\parallel$ and its transverse (solenoidal) component $u^\nu_\perp$ using the Helmholtz theorem in four dimensions [32] according to

$$u^\nu = u^\nu_\parallel + u^\nu_\perp, \tag{14}$$

(12) can be separated into a screw dislocation displacement (transverse) equation

$$\bar{\mu}_0 \nabla^2 u^\nu_\perp = 0 \tag{15}$$

and an edge dislocation displacement (longitudinal) equation

$$\nabla^2 u^\nu_\parallel = -\frac{\bar{\mu}_0 + \bar{\lambda}_0}{\bar{\mu}_0} \varepsilon^{,\nu}. \tag{16}$$

2.2 The energy-momentum stress tensor

The components of the energy-momentum stress tensor are given by [33]:

$$\begin{aligned} T^{00} &= H \\ T^{0j} &= s^j \\ T^{i0} &= g^i \\ T^{ij} &= \sigma^{ij} \end{aligned} \tag{17}$$

where H is the total energy density, s^j is the energy flux vector, g^i is the momentum density vector, and σ^{ij} is the Cauchy stress tensor which is the i^{th} component of force per unit area at x^j.

From the stress tensor $T^{\mu\nu}$, we can calculate the strain tensor $\varepsilon^{\mu\nu}$ and then calculate the strain energy density of the dislocations. As shown in [3], for a general anisotropic continuum in four dimensions, the spacetime continuum is approximated by a deformable linear elastic medium that obeys Hooke's law [31, see pp. 50–53]

$$E^{\mu\nu\alpha\beta}\varepsilon_{\alpha\beta} = T^{\mu\nu} \tag{18}$$

where $E^{\mu\nu\alpha\beta}$ is the elastic moduli tensor. For an isotropic and homogeneous medium, the elastic moduli tensor simplifies to [31]:

$$E^{\mu\nu\alpha\beta} = \bar{\lambda}_0 \left(g^{\mu\nu} g^{\alpha\beta}\right) + \bar{\mu}_0 \left(g^{\mu\alpha} g^{\nu\beta} + g^{\mu\beta} g^{\nu\alpha}\right). \tag{19}$$

For the metric tensor $g_{\mu\nu}$, we use the flat spacetime diagonal metric $\eta_{\mu\nu}$ with signature $(-+++)$ as the *STC* is locally flat at the microscopic level. Substituting for (19) into (18) and expanding, we obtain

$$\begin{aligned} T^{00} &= (\bar{\lambda}_0 + 2\bar{\mu}_0)\,\varepsilon^{00} - \bar{\lambda}_0\,\varepsilon^{11} - \bar{\lambda}_0\,\varepsilon^{22} - \bar{\lambda}_0\,\varepsilon^{33} \\ T^{11} &= -\bar{\lambda}_0\,\varepsilon^{00} + (\bar{\lambda}_0 + 2\bar{\mu}_0)\,\varepsilon^{11} + \bar{\lambda}_0\,\varepsilon^{22} + \bar{\lambda}_0\,\varepsilon^{33} \\ T^{22} &= -\bar{\lambda}_0\,\varepsilon^{00} + \bar{\lambda}_0\,\varepsilon^{11} + (\bar{\lambda}_0 + 2\bar{\mu}_0)\,\varepsilon^{22} + \bar{\lambda}_0\,\varepsilon^{33} \\ T^{33} &= -\bar{\lambda}_0\,\varepsilon^{00} + \bar{\lambda}_0\,\varepsilon^{11} + \bar{\lambda}_0\,\varepsilon^{22} + (\bar{\lambda}_0 + 2\bar{\mu}_0)\,\varepsilon^{33} \\ T^{\mu\nu} &= 2\bar{\mu}_0\,\varepsilon^{\mu\nu}, \quad \mu \neq \nu. \end{aligned} \tag{20}$$

In terms of the stress tensor, the inverse of (20) is given by

$$\begin{aligned} \varepsilon^{00} &= \frac{1}{4\bar{\mu}_0(2\bar{\lambda}_0 + \bar{\mu}_0)} \Big[(3\bar{\lambda}_0 + 2\bar{\mu}_0)\,T^{00} + \\ &\quad + \bar{\lambda}_0\,(T^{11} + T^{22} + T^{33})\Big] \\ \varepsilon^{11} &= \frac{1}{4\bar{\mu}_0(2\bar{\lambda}_0 + \bar{\mu}_0)} \Big[(3\bar{\lambda}_0 + 2\bar{\mu}_0)\,T^{11} + \\ &\quad + \bar{\lambda}_0\,(T^{00} - T^{22} - T^{33})\Big] \\ \varepsilon^{22} &= \frac{1}{4\bar{\mu}_0(2\bar{\lambda}_0 + \bar{\mu}_0)} \Big[(3\bar{\lambda}_0 + 2\bar{\mu}_0)\,T^{22} + \\ &\quad + \bar{\lambda}_0\,(T^{00} - T^{11} - T^{33})\Big] \\ \varepsilon^{33} &= \frac{1}{4\bar{\mu}_0(2\bar{\lambda}_0 + \bar{\mu}_0)} \Big[(3\bar{\lambda}_0 + 2\bar{\mu}_0)\,T^{33} + \\ &\quad + \bar{\lambda}_0\,(T^{00} - T^{11} - T^{22})\Big] \\ \varepsilon^{\mu\nu} &= \frac{1}{2\bar{\mu}_0}\,T^{\mu\nu}, \quad \mu \neq \nu. \end{aligned} \tag{21}$$

where $T^{ij} = \sigma^{ij}$. We calculate $\varepsilon = \varepsilon^\alpha{}_\alpha$ from the values of (21). Using $\eta_{\mu\nu}$, (3) and $T^\alpha{}_\alpha = \rho c^2$ from [2], we obtain (4) as required. This confirms the validity of the strain tensor in terms of the energy-momentum stress tensor as given by (21).

Eshelby [34–36] introduced an elastic field energy-momentum tensor for continuous media to deal with cases where defects (such as dislocations) lead to changes in configuration. The displacements u^ν are considered to correspond to a field defined at points x^μ of the spacetime continuum. This tensor was first derived by Morse and Feshback [37] for an isotropic elastic medium, using dyadics. The energy flux vector s_j and the field momentum density vector g_i are then given by [34, 37]:

$$\begin{aligned} s_j &= -\dot{u}_k\,\sigma_{kj} \\ g_i &= \bar{\rho}_0\,u_{k,i}\,\dot{u}_k \\ b_{ij} &= L\,\delta_{ij} - u_{k,i}\,\sigma_{kj} \end{aligned} \tag{22}$$

where $\bar{\rho}_0$ is the density of the medium, in this case the spacetime continuum, L is the Lagrangian equal to $K - W$ where W is the strain energy density and K is the kinetic energy density ($H = K + W$), and b_{ij} is known as the Eshelby stress tensor [38, see p. 27]. If the energy-momentum stress tensor is symmetric, then $g^i = s^i$. In this paper, we consider the case where there are no changes in configuration, and use the energy-momentum stress tensor given by (17) and (20).

Fig. 3: A stationary screw dislocation in cartesian (x, y, z) and cylindrical polar (r, θ, z) coordinates [14, see p. 60].

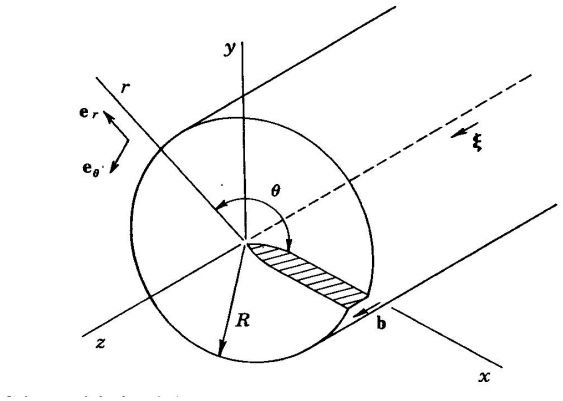

3 Screw dislocation

3.1 Stationary screw dislocation

We consider a stationary screw dislocation in the spacetime continuum, with cylindrical polar coordinates (r, θ, z), with the dislocation line along the z-axis (see Fig. 3). Then the Burgers vector is along the z-axis and is given by $b_r = b_\theta = 0$, $b_z = b$, the magnitude of the Burgers vector. The only non-zero component of the deformations is given by [14, see pp. 60–61] [13, see p. 51]

$$u_z = \frac{b}{2\pi}\,\theta = \frac{b}{2\pi}\,\tan^{-1}\frac{y}{x}. \tag{23}$$

This solution satisfies the screw dislocation displacement equation (15).

Similarly, the only non-zero components of the stress and strain tensors are given by

$$\begin{aligned} \sigma_{\theta z} &= \frac{b}{2\pi}\,\frac{\bar{\mu}_0}{r} \\ \varepsilon_{\theta z} &= \frac{b}{4\pi}\,\frac{1}{r} \end{aligned} \tag{24}$$

respectively.

3.2 Moving screw dislocation

We now consider the previous screw dislocation, moving along the x-axis, parallel to the dislocation, at a constant speed $v_x = v$. Equation (13) then simplifies to the wave equation for massless transverse shear waves for the displacements u_z along the z-axis, with speed $c_t = c$ given by (9), where c_t is the speed of the transverse waves corresponding to c the speed of light.

If coordinate system (x', y', z', t') is attached to the uniformly moving screw dislocation, then the transformation between the stationary and the moving screw dislocation is given by [14]

$$\begin{aligned} x' &= \frac{x - vt}{(1 - v^2/c^2)^{1/2}} \\ y' &= y \\ z' &= z \\ t' &= \frac{t - vx/c^2}{(1 - v^2/c^2)^{1/2}}. \end{aligned} \tag{25}$$

which is the special relativistic transformation.

The only non-zero component of the deformation in cartesian coordinates is given by [14, see pp. 184–185]

$$u_z = \frac{b}{2\pi}\,\tan^{-1}\frac{\gamma y}{x - vt}, \tag{26}$$

where

$$\gamma = \sqrt{1 - \frac{v^2}{c^2}}. \tag{27}$$

This solution also satisfies the screw dislocation displacement equation (15). It simplifies to the case of the stationary screw dislocation when the speed $v = 0$.

Similarly, the only non-zero components of the stress tensor in cartesian coordinates are given by [14]

$$\begin{aligned} \sigma_{xz} &= -\frac{b\bar{\mu}_0}{2\pi}\,\frac{\gamma y}{(x - vt)^2 + \gamma^2 y^2} \\ \sigma_{yz} &= \frac{b\bar{\mu}_0}{2\pi}\,\frac{\gamma(x - vt)}{(x - vt)^2 + \gamma^2 y^2}. \end{aligned} \tag{28}$$

The only non-zero components of the strain tensor in cartesian coordinates are derived from $\varepsilon^{\mu\nu} = \frac{1}{2}(u^{\mu;\nu} + u^{\nu;\mu})$ [1, see Eq.(41)]:

$$\begin{aligned} \varepsilon_{xz} &= -\frac{b}{4\pi}\,\frac{\gamma y}{(x - vt)^2 + \gamma^2 y^2} \\ \varepsilon_{yz} &= \frac{b}{4\pi}\,\frac{\gamma(x - vt)}{(x - vt)^2 + \gamma^2 y^2}, \end{aligned} \tag{29}$$

in an isotropic continuum.

Non-zero components involving time are given by

$$\begin{aligned} \varepsilon_{tz} = \varepsilon_{zt} &= \frac{1}{2}\left(\frac{\partial u_z}{\partial(ct)} + \frac{\partial u_t}{\partial z}\right) \\ \varepsilon_{tz} &= \frac{b}{4\pi}\,\frac{v}{c}\,\frac{\gamma y}{(x - vt)^2 + \gamma^2 y^2} \end{aligned} \tag{30}$$

where $u_t = 0$ has been used. This assumes that the screw dislocation is fully formed and moving with velocity v as described. Using (20), the non-zero stress components involving time are given by

$$\sigma_{tz} = \sigma_{zt} = \frac{b\bar{\mu}_0}{2\pi}\,\frac{v}{c}\,\frac{\gamma y}{(x - vt)^2 + \gamma^2 y^2}. \tag{31}$$

Screw dislocations are thus found to be Lorentz invariant.

3.3 Screw dislocation strain energy density

We consider the stationary screw dislocation in the spacetime continuum of Section 3.1, with cylindrical polar coordinates (r, θ, z), with the dislocation line along the z-axis and the Burgers vector along the z-axis $b_z = b$.

Then the strain energy density of the screw dislocation is given by the transverse distortion energy density [1, see Eq. (74)]

$$\mathcal{E}_\perp = \bar{\mu}_0 \, e^{\alpha\beta} e_{\alpha\beta} \tag{32}$$

where from [1, see Eq. (33)],

$$e^{\alpha\beta} = \varepsilon^{\alpha\beta} - e_s g^{\alpha\beta} \tag{33}$$

where $e_s = \frac{1}{4}\varepsilon^\alpha{}_\alpha$ is the dilatation which for a screw dislocation is equal to 0. The screw dislocation is thus massless ($\mathcal{E}_\parallel = 0$).

The non-zero components of the strain tensor are as defined in (24). Hence

$$\mathcal{E}_\perp = \bar{\mu}_0 \left({\varepsilon_{\theta z}}^2 + {\varepsilon_{z\theta}}^2 \right). \tag{34}$$

Substituting from (24),

$$\mathcal{E}_\perp = \frac{\bar{\mu}_0 \, b^2}{8\pi^2} \, \frac{1}{r^2} = \mathcal{E}. \tag{35}$$

We now consider the more general case of the moving screw dislocation in the spacetime continuum of Section 3.2, with cartesian coordinates (x, y, z). The non-zero components of the strain tensor are as defined in (29) and (30). Substituting in (32), the equation becomes [1, see Eqs.(114–115)]

$$\mathcal{E}_\perp = 2\bar{\mu}_0 \left(-{\varepsilon_{tz}}^2 + {\varepsilon_{xz}}^2 + {\varepsilon_{yz}}^2 \right). \tag{36}$$

Substituting from (29) and (30) into (36), the screw dislocation strain energy density becomes

$$\mathcal{E}_\perp = \frac{\bar{\mu}_0 \, b^2}{8\pi^2} \, \frac{\gamma^2}{(x - vt)^2 + \gamma^2 y^2} = \mathcal{E}. \tag{37}$$

This equation simplifies to (35) in the case where $v = 0$, as expected. In addition, the energy density (which is quadratic in energy as per [1, see Eq.(76)]) is multiplied by the special relativistic γ factor.

4 Edge dislocation

4.1 Stationary edge dislocation

We consider a stationary edge dislocation in the spacetime continuum in cartesian coordinates (x, y, z), with the dislocation line along the z-axis and the Burgers vector $b_x = b, b_y = b_z = 0$ (see Fig. 4). Then the non-zero components of the deformations are given in cartesian coordinates by [14, see p. 78]

Fig. 4: A stationary edge dislocation in cartesian (x, y, z) and cylindrical polar (r, θ, z) coordinates [14, see p. 74].

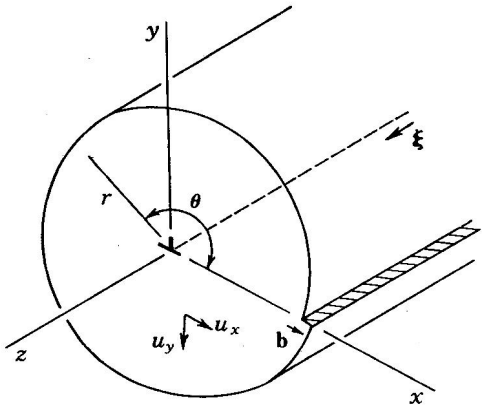

$$\begin{aligned} u_x &= \frac{b}{2\pi} \left(\tan^{-1} \frac{y}{x} + \frac{\bar{\mu}_0 + \bar{\lambda}_0}{2\bar{\mu}_0 + \bar{\lambda}_0} \, \frac{xy}{x^2 + y^2} \right) \\ u_y &= -\frac{b}{2\pi} \left(\frac{1}{2} \, \frac{\bar{\mu}_0}{2\bar{\mu}_0 + \bar{\lambda}_0} \, \log(x^2 + y^2) + \right. \\ &\quad \left. + \frac{1}{2} \, \frac{\bar{\mu}_0 + \bar{\lambda}_0}{2\bar{\mu}_0 + \bar{\lambda}_0} \, \frac{x^2 - y^2}{x^2 + y^2} \right). \end{aligned} \tag{38}$$

This solution results in a non-zero R.H.S. of the edge dislocation displacement equation (16) as required. Equation (16) can be evaluated to give a value of ε in agreement with the results of Section 4.3 as shown in that section.

The cylindrical polar coordinate description of the edge dislocation is more complex than the cartesian coordinate description. We thus use cartesian coordinates in the following sections, transforming to polar coordinate expressions as warranted. The non-zero components of the stress tensor in cartesian coordinates are given by [14, see p. 76]

$$\begin{aligned} \sigma_{xx} &= -\frac{b\bar{\mu}_0}{\pi} \, \frac{\bar{\mu}_0 + \bar{\lambda}_0}{2\bar{\mu}_0 + \bar{\lambda}_0} \, \frac{y(3x^2 + y^2)}{(x^2 + y^2)^2} \\ \sigma_{yy} &= \frac{b\bar{\mu}_0}{\pi} \, \frac{\bar{\mu}_0 + \bar{\lambda}_0}{2\bar{\mu}_0 + \bar{\lambda}_0} \, \frac{y(x^2 - y^2)}{(x^2 + y^2)^2} \\ \sigma_{zz} &= \frac{1}{2} \, \frac{\bar{\lambda}_0}{\bar{\mu}_0 + \bar{\lambda}_0} \left(\sigma_{xx} + \sigma_{yy} \right) \\ &= -\frac{b\bar{\mu}_0}{\pi} \, \frac{\bar{\lambda}_0}{2\bar{\mu}_0 + \bar{\lambda}_0} \, \frac{y}{x^2 + y^2} \\ \sigma_{xy} &= \frac{b\bar{\mu}_0}{\pi} \, \frac{\bar{\mu}_0 + \bar{\lambda}_0}{2\bar{\mu}_0 + \bar{\lambda}_0} \, \frac{x(x^2 - y^2)}{(x^2 + y^2)^2}. \end{aligned} \tag{39}$$

The non-zero components of the strain tensor in cartesian coordinates are derived from $\varepsilon^{\mu\nu} = \frac{1}{2}(u^{\mu;\nu} + u^{\nu;\mu})$ [1, see

Eq.(41)]:

$$\begin{aligned}
\varepsilon_{xx} &= -\frac{b}{2\pi}\,\frac{y}{x^2+y^2}\left(1+\frac{\bar{\mu}_0+\bar{\lambda}_0}{2\bar{\mu}_0+\bar{\lambda}_0}\,\frac{x^2-y^2}{x^2+y^2}\right)\\
&= -\frac{by}{2\pi}\,\frac{(3\bar{\mu}_0+2\bar{\lambda}_0)x^2+\bar{\mu}_0y^2}{(2\bar{\mu}_0+\bar{\lambda}_0)\,(x^2+y^2)^2}\\
\varepsilon_{yy} &= -\frac{b}{2\pi}\,\frac{\bar{\mu}_0}{2\bar{\mu}_0+\bar{\lambda}_0}\,\frac{y}{x^2+y^2}\left(1-\frac{\bar{\mu}_0+\bar{\lambda}_0}{\bar{\mu}_0}\,\frac{2x^2}{x^2+y^2}\right)\\
&= \frac{by}{2\pi}\,\frac{(\bar{\mu}_0+2\bar{\lambda}_0)x^2-\bar{\mu}_0y^2}{(2\bar{\mu}_0+\bar{\lambda}_0)\,(x^2+y^2)^2}\\
\varepsilon_{xy} &= \frac{b}{2\pi}\,\frac{\bar{\mu}_0+\bar{\lambda}_0}{2\bar{\mu}_0+\bar{\lambda}_0}\,\frac{x(x^2-y^2)}{(x^2+y^2)^2}
\end{aligned} \tag{40}$$

in an isotropic continuum.

4.2 Moving edge dislocation

We now consider the previous edge dislocation, moving along the x-axis, parallel to the z-axis, along the slip plane x–z, at a constant speed $v_x = v$. The solutions of (13) for the moving edge dislocation then include both longitudinal and transverse components. The only non-zero components of the deformations in cartesian coordinates are given by [11, see pp. 39–40] [39, see pp. 218–219]

$$\begin{aligned}
u_x &= \frac{bc^2}{\pi v^2}\left(\tan^{-1}\frac{\gamma_l y}{x-vt}-\alpha^2\,\tan^{-1}\frac{\gamma y}{x-vt}\right)\\
u_y &= \frac{bc^2}{2\pi v^2}\left(\gamma_l\log\left[(x-vt)^2+\gamma_l^2y^2\right]-\right.\\
&\quad\left.-\frac{\alpha^2}{\gamma}\,\log\left[(x-vt)^2+\gamma^2y^2\right]\right),
\end{aligned} \tag{41}$$

where

$$\alpha = \sqrt{1-\frac{v^2}{2c^2}}, \tag{42}$$

$$\gamma_l = \sqrt{1-\frac{v^2}{c_l^2}} \tag{43}$$

and c_l is the speed of longitudinal deformations given by

$$c_l = \sqrt{\frac{2\bar{\mu}_0+\bar{\lambda}_0}{\bar{\rho}_0}}. \tag{44}$$

This solution again results in a non-zero R.H.S. of the edge dislocation displacement equation (16) as required, and (16) can be evaluated to give a value of ε as in Section 4.3. This solution simplifies to the case of the stationary edge dislocation when the speed $v = 0$.

The non-zero components of the stress tensor in cartesian coordinates are given by [14, see pp. 189–190] [11, see pp. 39–40]

$$\begin{aligned}
\sigma_{xx} &= \frac{bc^2y}{\pi v^2}\left(\frac{\bar{\lambda}_0\gamma_l^3-(2\bar{\mu}_0+\bar{\lambda}_0)\gamma_l}{(x-vt)^2+\gamma_l^2y^2}+\right.\\
&\quad\left.+\frac{2\bar{\mu}_0\alpha^2\gamma}{(x-vt)^2+\gamma^2y^2}\right)\\
\sigma_{yy} &= \frac{bc^2y}{\pi v^2}\left(\frac{(2\bar{\mu}_0+\bar{\lambda}_0)\gamma_l^3-\bar{\lambda}_0\gamma_l}{(x-vt)^2+\gamma_l^2y^2}-\right.\\
&\quad\left.-\frac{2\bar{\mu}_0\alpha^2\gamma}{(x-vt)^2+\gamma^2y^2}\right)\\
\sigma_{zz} &= \frac{1}{2}\,\frac{\bar{\lambda}_0}{\bar{\mu}_0+\bar{\lambda}_0}\left(\sigma_{xx}+\sigma_{yy}\right)\\
&= \frac{\bar{\lambda}_0 b}{\pi}\,\frac{c^2}{c_l^2}\,\frac{-\gamma_l y}{(x-vt)^2+\gamma_l^2y^2}\\
&= \frac{b}{\pi}\,\frac{\bar{\lambda}_0\bar{\mu}_0}{2\bar{\mu}_0+\bar{\lambda}_0}\,\frac{-\gamma_l y}{(x-vt)^2+\gamma_l^2y^2}\\
\sigma_{xy} &= \frac{\bar{\mu}_0 bc^2(x-vt)}{\pi v^2}\left(\frac{2\gamma_l}{(x-vt)^2+\gamma_l^2y^2}-\right.\\
&\quad\left.-\frac{\alpha^2(\gamma+1/\gamma)}{(x-vt)^2+\gamma^2y^2}\right).
\end{aligned} \tag{45}$$

It is important to note that for a screw dislocation, the stress on the plane $x - vt = 0$ becomes infinite at $v = c$. This sets an upper limit on the speed of screw dislocations in the spacetime continuum, and provides an explanation for the speed of light limit. This upper limit also applies to edge dislocations, as the shear stress becomes infinite everywhere at $v = c$, even though the speed of longitudinal deformations c_l is greater than that of transverse deformations c [14, see p. 191] [11, see p. 40].

The non-zero components of the strain tensor in cartesian coordinates are derived from $\varepsilon^{\mu\nu} = \frac{1}{2}(u^{\mu;\nu}+u^{\nu;\mu})$ [1, see Eq.(41)]:

$$\begin{aligned}
\varepsilon_{xx} &= \frac{bc^2y}{\pi v^2}\left(\frac{-\gamma_l}{(x-vt)^2+(\gamma_l y)^2}+\frac{\alpha^2\gamma}{(x-vt)^2+(\gamma y)^2}\right)\\
\varepsilon_{yy} &= \frac{bc^2y}{\pi v^2}\left(\frac{\gamma_l^3}{(x-vt)^2+(\gamma_l y)^2}-\frac{\alpha^2\gamma}{(x-vt)^2+(\gamma y)^2}\right)\\
\varepsilon_{xy} &= \frac{bc^2(x-vt)}{2\pi v^2}\left(\frac{2\gamma_l}{(x-vt)^2+(\gamma_l y)^2}-\right.\\
&\quad\left.-\frac{\alpha^2(\gamma+1/\gamma)}{(x-vt)^2+(\gamma y)^2}\right)
\end{aligned} \tag{46}$$

in an isotropic continuum.

Non-zero components involving time are given by

$$\begin{aligned}
\varepsilon_{tx} &= \varepsilon_{xt} = \frac{1}{2}\left(\frac{\partial u_x}{\partial(ct)} + \frac{\partial u_t}{\partial x}\right)\\
\varepsilon_{ty} &= \varepsilon_{yt} = \frac{1}{2}\left(\frac{\partial u_y}{\partial(ct)} + \frac{\partial u_t}{\partial y}\right)\\
\varepsilon_{tx} &= \frac{b}{2\pi}\,\frac{c}{v}\left(\frac{\gamma_l y}{(x-vt)^2+\gamma_l^2 y^2} - \right.\\
&\quad \left. - \alpha^2\,\frac{\gamma y}{(x-vt)^2+\gamma^2 y^2}\right)\\
\varepsilon_{ty} &= -\frac{b}{2\pi}\,\frac{c}{v}\left(\frac{\gamma_l (x-vt)}{(x-vt)^2+\gamma_l^2 y^2} - \right.\\
&\quad \left. - \frac{\alpha^2}{\gamma^2}\,\frac{\gamma(x-vt)}{(x-vt)^2+\gamma^2 y^2}\right)
\end{aligned} \tag{47}$$

where $u_t = 0$ has been used. This assumes that the edge dislocation is fully formed and moving with velocity v as described. Using (20), the non-zero stress components involving time are given by

$$\begin{aligned}
\sigma_{tx} &= \frac{b\bar{\mu}_0}{\pi}\,\frac{c}{v}\left(\frac{\gamma_l y}{(x-vt)^2+\gamma_l^2 y^2} - \right.\\
&\quad \left. - \alpha^2\,\frac{\gamma y}{(x-vt)^2+\gamma^2 y^2}\right)\\
\sigma_{ty} &= -\frac{b\bar{\mu}_0}{\pi}\,\frac{c}{v}\left(\frac{\gamma_l (x-vt)}{(x-vt)^2+\gamma_l^2 y^2} - \right.\\
&\quad \left. - \frac{\alpha^2}{\gamma^2}\,\frac{\gamma(x-vt)}{(x-vt)^2+\gamma^2 y^2}\right).
\end{aligned} \tag{48}$$

4.3 Edge dislocation strain energy density

As we have seen in Section 3.3, the screw dislocation is massless as $\varepsilon = 0$ and hence $\mathcal{E}_{\|} = 0$ for the screw dislocation: it is a pure distortion, with no dilatation. In this section, we evaluate the strain energy density of the edge dislocation.

As seen in [1, see Section 8.1], the strain energy density of the spacetime continuum is separated into two terms: the first one expresses the dilatation energy density (the mass longitudinal term) while the second one expresses the distortion energy density (the massless transverse term):

$$\mathcal{E} = \mathcal{E}_{\|} + \mathcal{E}_{\perp} \tag{49}$$

where

$$\mathcal{E}_{\|} = \frac{1}{2}\,\bar{\kappa}_0\varepsilon^2 \equiv \frac{1}{32\bar{\kappa}_0}\left(\rho c^2\right)^2 \equiv \frac{1}{2\bar{\kappa}_0}\,t_s^2 \tag{50}$$

where ε is the volume dilatation and ρ is the mass energy density of the edge dislocation, and

$$\mathcal{E}_{\perp} = \bar{\mu}_0 e^{\alpha\beta}e_{\alpha\beta} \equiv \frac{1}{4\bar{\mu}_0}\,t^{\alpha\beta}t_{\alpha\beta}. \tag{51}$$

where from [1, see Eq. (36)] the energy-momentum stress tensor $T^{\alpha\beta}$ is decomposed into a stress deviation tensor $t^{\alpha\beta}$ and a scalar t_s, according to

$$t^{\alpha\beta} = T^{\alpha\beta} - t_s g^{\alpha\beta} \tag{52}$$

where $t_s = \frac{1}{4}T^{\alpha}{}_{\alpha}$. Then the dilatation strain energy density of the edge dislocation is given by the (massive) longitudinal dilatation energy density (50) and the distortion (massless) strain energy density of the edge dislocation is given by the transverse distortion energy density (51).

4.3.1 Stationary edge dislocation energy density

We first consider the case of the stationary edge dislocation of Section 4.1. The volume dilatation ε for the stationary edge dislocation is given by

$$\varepsilon = \varepsilon^{\alpha}{}_{\alpha} = \varepsilon_{xx} + \varepsilon_{yy} \tag{53}$$

where the non-zero diagonal elements of the strain tensor are obtained from (40). Substituting for ε_{xx} and ε_{yy} from (40), we obtain

$$\varepsilon = -\frac{b}{\pi}\,\frac{\bar{\mu}_0}{2\bar{\mu}_0+\bar{\lambda}_0}\,\frac{y}{x^2+y^2}. \tag{54}$$

In cylindrical polar coordinates, (54) is expressed as

$$\varepsilon = -\frac{b}{\pi}\,\frac{\bar{\mu}_0}{2\bar{\mu}_0+\bar{\lambda}_0}\,\frac{\sin\theta}{r}. \tag{55}$$

We can disregard the negative sign in (54) and (55) as it can be eliminated by using the **FS**/*RH* convention instead of the **SF**/*RH* convention for the Burgers vector [14, see p. 22]).

As mentioned in Section 4.1, the volume dilatation ε can be calculated from the edge dislocation displacement (longitudinal) equation (16), viz.

$$\nabla^2 u_{\|}^{\nu} = -\frac{\bar{\mu}_0+\bar{\lambda}_0}{\bar{\mu}_0}\varepsilon^{,\nu}.$$

For the x-component, this equation gives

$$\nabla^2 u_x = \frac{\partial^2 u_x}{\partial x^2} + \frac{\partial^2 u_x}{\partial y^2} = -\frac{\bar{\mu}_0+\bar{\lambda}_0}{\bar{\mu}_0}\varepsilon_{,x}. \tag{56}$$

Substituting for u_x from (38), we obtain

$$\nabla^2 u_x = -\frac{2b}{\pi}\,\frac{\bar{\mu}_0+\bar{\lambda}_0}{2\bar{\mu}_0+\bar{\lambda}_0}\,\frac{xy}{(x^2+y^2)^2} = -\frac{\bar{\mu}_0+\bar{\lambda}_0}{\bar{\mu}_0}\varepsilon_{,x}. \tag{57}$$

Hence

$$\varepsilon_{,x} = \frac{2b}{\pi}\,\frac{\bar{\mu}_0}{2\bar{\mu}_0+\bar{\lambda}_0}\,\frac{xy}{(x^2+y^2)^2} \tag{58}$$

and

$$\varepsilon = \frac{2b}{\pi}\,\frac{\bar{\mu}_0}{2\bar{\mu}_0+\bar{\lambda}_0}\int \frac{xy}{(x^2+y^2)^2}\,dx. \tag{59}$$

Evaluating the integral [40], we obtain

$$\varepsilon = -\frac{b}{\pi}\,\frac{\bar{\mu}_0}{2\bar{\mu}_0+\bar{\lambda}_0}\,\frac{y}{x^2+y^2} \tag{60}$$

in agreement with (54).

Similarly for the y-component, substituting for u_y from (38), the equation

$$\nabla^2 u_y = \frac{\partial^2 u_y}{\partial x^2} + \frac{\partial^2 u_y}{\partial y^2} = -\frac{\bar{\mu}_0+\bar{\lambda}_0}{\bar{\mu}_0}\varepsilon_{,y} \tag{61}$$

gives

$$\varepsilon_{,y} = -\frac{b}{\pi}\,\frac{\bar{\mu}_0}{2\bar{\mu}_0+\bar{\lambda}_0}\,\frac{x^2-y^2}{(x^2+y^2)^2}. \tag{62}$$

Evaluating the integral [40]

$$\varepsilon = -\frac{b}{\pi}\,\frac{\bar{\mu}_0}{2\bar{\mu}_0+\bar{\lambda}_0}\int \frac{x^2-y^2}{(x^2+y^2)^2}\,dy, \tag{63}$$

we obtain

$$\varepsilon = -\frac{b}{\pi}\,\frac{\bar{\mu}_0}{2\bar{\mu}_0+\bar{\lambda}_0}\,\frac{y}{x^2+y^2} \tag{64}$$

again in agreement with (54).

The mass energy density is calculated from (4)

$$\rho c^2 = 4\bar{\kappa}_0\,\varepsilon = 2(2\bar{\lambda}_0+\bar{\mu}_0)\,\varepsilon \tag{65}$$

where (3) has been used. Substituting for ε from (54), the mass energy density of the stationary edge dislocation is given by

$$\rho c^2 = \frac{4b}{\pi}\,\frac{\bar{\kappa}_0\bar{\mu}_0}{2\bar{\mu}_0+\bar{\lambda}_0}\,\frac{y}{x^2+y^2}. \tag{66}$$

In cylindrical polar coordinates, (66) is expressed as

$$\rho c^2 = \frac{4b}{\pi}\,\frac{\bar{\kappa}_0\bar{\mu}_0}{2\bar{\mu}_0+\bar{\lambda}_0}\,\frac{\sin\theta}{r}. \tag{67}$$

Using (54) in (50), the stationary edge dislocation longitudinal dilatation strain energy density is then given by

$$\mathcal{E}_{\parallel} = \frac{b^2}{2\pi^2}\,\frac{\bar{\kappa}_0\,\bar{\mu}_0^2}{(2\bar{\mu}_0+\bar{\lambda}_0)^2}\,\frac{y^2}{(x^2+y^2)^2}. \tag{68}$$

In cylindrical polar coordinates, (68) is expressed as

$$\mathcal{E}_{\parallel} = \frac{b^2}{2\pi^2}\,\frac{\bar{\kappa}_0\,\bar{\mu}_0^2}{(2\bar{\mu}_0+\bar{\lambda}_0)^2}\,\frac{\sin^2\theta}{r^2}. \tag{69}$$

The distortion strain energy density is calculated from (51). The expression is expanded using the non-zero elements of the strain tensor (40) to give

$$\mathcal{E}_{\perp} = \bar{\mu}_0\left({e_{xx}}^2 + {e_{yy}}^2 + {e_{xy}}^2 + {e_{yx}}^2\right). \tag{70}$$

As seen previously in (33),

$$e^{\alpha\beta} = \varepsilon^{\alpha\beta} - e_s g^{\alpha\beta} \tag{71}$$

where $e_s = \frac{1}{4}\varepsilon$ is the volume dilatation calculated in (54) and

$$e^{\alpha\beta}e_{\alpha\beta} = \left(\varepsilon^{\alpha\beta} - \frac{1}{4}\varepsilon g^{\alpha\beta}\right)\left(\varepsilon_{\alpha\beta} - \frac{1}{4}\varepsilon g_{\alpha\beta}\right). \tag{72}$$

For $g^{\alpha\beta} = \eta^{\alpha\beta}$, the off-diagonal elements of the metric tensor are 0, the diagonal elements are 1 and (70) becomes

$$\mathcal{E}_{\perp} = \bar{\mu}_0\left[\left(\varepsilon_{xx} - \frac{1}{4}\varepsilon\right)^2 + \left(\varepsilon_{yy} - \frac{1}{4}\varepsilon\right)^2 + 2\varepsilon_{xy}^2\right]. \tag{73}$$

Expanding the quadratic terms and making use of (53), (73) becomes

$$\mathcal{E}_{\perp} = \bar{\mu}_0\left(\varepsilon_{xx}^2 + \varepsilon_{yy}^2 - \frac{3}{8}\varepsilon^2 + 2\varepsilon_{xy}^2\right) \tag{74}$$

and finally

$$\mathcal{E}_{\perp} = \bar{\mu}_0\left(\frac{5}{8}\varepsilon^2 - 2\varepsilon_{xx}\varepsilon_{yy} + 2\varepsilon_{xy}^2\right). \tag{75}$$

Substituting from (40) and (54) in the above,

$$\begin{aligned}\mathcal{E}_{\perp} = {}& \frac{5}{8}\,\frac{b^2\bar{\mu}_0}{\pi^2}\left(\frac{\bar{\mu}_0}{2\bar{\mu}_0+\bar{\lambda}_0}\right)^2\frac{y^2}{(x^2+y^2)^2} + \frac{b^2\bar{\mu}_0}{2\pi^2}\\ & \frac{y^2\left[(3\bar{\mu}_0+2\bar{\lambda}_0)(\bar{\mu}_0+2\bar{\lambda}_0)x^4 - 2\bar{\mu}_0^2x^2y^2 - \bar{\mu}_0^2y^4\right]}{(2\bar{\mu}_0+\bar{\lambda}_0)^2(x^2+y^2)^4} +\\ & + \frac{b^2\bar{\mu}_0}{2\pi^2}\left(\frac{\bar{\mu}_0+\bar{\lambda}_0}{2\bar{\mu}_0+\bar{\lambda}_0}\right)^2\frac{x^2(x^2-y^2)^2}{(x^2+y^2)^4}.\end{aligned} \tag{76}$$

which becomes

$$\begin{aligned}\mathcal{E}_{\perp} = {}& \frac{b^2}{2\pi^2}\,\frac{\bar{\mu}_0}{(2\bar{\mu}_0+\bar{\lambda}_0)^2}\,\frac{1}{(x^2+y^2)^4}\\ & \left\{\frac{5}{4}\,\bar{\mu}_0^2\,y^2\,(x^2+y^2)^2 - \right.\\ & -y^2\left[(3\bar{\mu}_0+2\bar{\lambda}_0)(\bar{\mu}_0+2\bar{\lambda}_0)x^4 - 2\bar{\mu}_0^2\,x^2y^2 - \bar{\mu}_0^2\,y^4\right] +\\ & \left. + (\bar{\mu}_0+\bar{\lambda}_0)^2\,x^2(x^2-y^2)^2\right\}.\end{aligned} \tag{77}$$

In cylindrical polar coordinates, (77) is expressed as

$$\begin{aligned}\mathcal{E}_{\perp} = {}& \frac{b^2}{2\pi^2}\,\frac{\bar{\mu}_0}{(2\bar{\mu}_0+\bar{\lambda}_0)^2}\left\{\frac{5}{4}\,\bar{\mu}_0^2\,\frac{\sin^2\theta}{r^2} - \frac{\sin^2\theta}{r^2}\right.\\ & \left[(3\bar{\mu}_0+2\bar{\lambda}_0)(\bar{\mu}_0+2\bar{\lambda}_0)\cos^4\theta - \right.\\ & \left. -2\bar{\mu}_0^2\,\cos^2\theta\sin^2\theta - \bar{\mu}_0^2\,\sin^4\theta\right] +\\ & \left. + (\bar{\mu}_0+\bar{\lambda}_0)^2\,\frac{\cos^2\theta}{r^2}\,\left(\cos^2\theta - \sin^2\theta\right)^2\right\}\end{aligned} \tag{78}$$

or

$$\mathcal{E}_\perp = \frac{b^2}{2\pi^2}\frac{\bar{\mu}_0}{(2\bar{\mu}_0+\bar{\lambda}_0)^2}\left\{\frac{5}{4}\bar{\mu}_0^2\frac{\sin^2\theta}{r^2}-\right.$$
$$-\Big[(3\bar{\mu}_0+2\bar{\lambda}_0)(\bar{\mu}_0+2\bar{\lambda}_0)\cos^4\theta\frac{\sin^2\theta}{r^2}-$$
$$-2\bar{\mu}_0^2\cos^2\theta\frac{\sin^4\theta}{r^2}-\bar{\mu}_0^2\frac{\sin^6\theta}{r^2}\Big]+ \quad (79)$$
$$\left.+(\bar{\mu}_0+\bar{\lambda}_0)^2\cos^2 2\theta\frac{\cos^2\theta}{r^2}\right\}.$$

4.3.2 Moving edge dislocation energy density

We next consider the general case of the moving edge dislocation in the spacetime continuum of Section 4.2, with cartesian coordinates (x, y, z). We first evaluate the volume dilatation ε for the moving edge dislocation. The volume dilatation is given by

$$\varepsilon = \varepsilon^\alpha{}_\alpha = \varepsilon_{xx} + \varepsilon_{yy} \quad (80)$$

where the non-zero diagonal elements of the strain tensor are obtained from (46). Substituting for ε_{xx} and ε_{yy} from (46) in (80), we notice that the transverse terms cancel out, and we are left with the following longitudinal term:

$$\varepsilon = \frac{bc^2y}{\pi v^2}\frac{\gamma_l^3-\gamma_l}{(x-vt)^2+\gamma_l^2y^2} \quad (81)$$

This equation can be further reduced to

$$\varepsilon = \frac{bc^2}{\pi v^2}\frac{v^2}{{c_l}^2}\frac{\gamma_l y}{(x-vt)^2+\gamma_l^2y^2} \quad (82)$$

and finally, using $c^2/{c_l}^2 = \bar{\mu}_0/(2\bar{\mu}_0+\bar{\lambda}_0)$ (see (9) and (44)),

$$\varepsilon(x_i,t) = \frac{b}{2\pi}\frac{2\bar{\mu}_0}{2\bar{\mu}_0+\bar{\lambda}_0}\frac{\gamma_l y}{(x-vt)^2+\gamma_l^2y^2}. \quad (83)$$

As seen previously, the mass energy density is calculated from (65):

$$\rho c^2 = 4\bar{\kappa}_0\,\varepsilon = 2(2\bar{\lambda}_0+\bar{\mu}_0)\,\varepsilon. \quad (84)$$

Substituting for ε from (83), the mass energy density of an edge dislocation is given by

$$\rho(x_i,t)\,c^2 = \frac{b}{2\pi}\frac{8\bar{\kappa}_0\bar{\mu}_0}{2\bar{\mu}_0+\bar{\lambda}_0}\frac{\gamma_l y}{(x-vt)^2+\gamma_l^2y^2}. \quad (85)$$

Using (83) in (50), the edge dislocation longitudinal dilatation strain energy density is then given by

$$\mathcal{E}_\parallel = \frac{1}{2}\bar{\kappa}_0\left(\frac{b}{2\pi}\frac{2\bar{\mu}_0}{2\bar{\mu}_0+\bar{\lambda}_0}\frac{\gamma_l y}{(x-vt)^2+\gamma_l^2y^2}\right)^2. \quad (86)$$

The distortion strain energy density is calculated from (51). The expression is expanded using the non-zero elements of the strain tensor (46) and (47) and, from (71) and (72), we obtain [1, see Eqs.(114–115)])

$$\mathcal{E}_\perp = \bar{\mu}_0\left[\left(\varepsilon_{xx}-\frac{1}{4}\varepsilon\right)^2+\left(\varepsilon_{yy}-\frac{1}{4}\varepsilon\right)^2\right.$$
$$\left.-2{\varepsilon_{tx}}^2-2{\varepsilon_{ty}}^2+2\varepsilon_{xy}^2\right]. \quad (87)$$

Expanding the quadratic terms and making use of (53) as in (74), (87) becomes

$$\mathcal{E}_\perp = \bar{\mu}_0\left(\varepsilon_{xx}^2+\varepsilon_{yy}^2-\frac{3}{8}\varepsilon^2-2{\varepsilon_{tx}}^2-2{\varepsilon_{ty}}^2+2\varepsilon_{xy}^2\right). \quad (88)$$

Substituting from (46), (47) and (82),

$$\mathcal{E}_\perp = \bar{\mu}_0\left(\frac{b}{2\pi}\frac{c^2}{v^2}\right)^2\left\{-\frac{3}{8}\left(2\frac{v^2}{{c_l}^2}\frac{\gamma_l y}{(x-vt)^2+\gamma_l^2y^2}\right)^2+\right.$$
$$+4\left(\frac{-\gamma_l y}{(x-vt)^2+\gamma_l^2y^2}+\frac{\alpha^2\gamma y}{(x-vt)^2+\gamma^2y^2}\right)^2+$$
$$+4\left(\frac{\gamma_l^3 y}{(x-vt)^2+\gamma_l^2y^2}-\frac{\alpha^2\gamma y}{(x-vt)^2+\gamma^2y^2}\right)^2-$$
$$-2\frac{v^2}{c^2}\left(\frac{\gamma_l y}{(x-vt)^2+\gamma_l^2y^2}-\alpha^2\frac{\gamma y}{(x-vt)^2+\gamma^2y^2}\right)^2- \quad (89)$$
$$-2\frac{v^2}{c^2}\left(\frac{-\gamma_l(x-vt)}{(x-vt)^2+\gamma_l^2y^2}+\frac{\alpha^2}{\gamma^2}\frac{\gamma(x-vt)}{(x-vt)^2+\gamma^2y^2}\right)^2+$$
$$\left.+2\left(\frac{2\gamma_l(x-vt)}{(x-vt)^2+\gamma_l^2y^2}-\frac{\alpha^2(\gamma+1/\gamma)(x-vt)}{(x-vt)^2+\gamma^2y^2}\right)^2\right\}$$

which simplifies to

$$\mathcal{E}_\perp = \bar{\mu}_0\frac{b^2}{2\pi^2}\frac{c^4}{v^4}\left\{\frac{\alpha^4(3+\gamma^2)}{(x-vt)^2+\gamma^2y^2}-\right.$$
$$-2\alpha^2\frac{\left(3+\frac{1}{\gamma^2}\right)\gamma_l\gamma(x-vt)^2+\left(2\gamma_l^2-\frac{v^2}{c^2}\right)\gamma_l\gamma y^2}{\left((x-vt)^2+\gamma_l^2y^2\right)\left((x-vt)^2+\gamma^2y^2\right)}+ \quad (90)$$
$$\left.+\frac{(3+\gamma^2)\gamma_l^2(x-vt)^2+2\left(\alpha^2+\gamma_l^4-\frac{3}{8}\frac{v^4}{c_l^4}\right)\gamma_l^2y^2}{\left((x-vt)^2+\gamma_l^2y^2\right)^2}\right\}.$$

We consider the above equations for the moving edge dislocation in the limit as $v \to 0$. Then the terms

$$\frac{\gamma y}{(x-vt)^2+\gamma^2y^2} \to \frac{\sin\theta}{r} \quad (91)$$

and

$$\frac{x-vt}{(x-vt)^2+\gamma^2y^2} \to \frac{\cos\theta}{r} \quad (92)$$

in cylindrical polar coordinates. Similarly for the same terms with γ_l instead of γ.

The volume dilatation obtained from (83) is then given in cylindrical polar coordinates (r, θ, z) by

$$\varepsilon \to \frac{b}{2\pi} \frac{2\bar{\mu}_0}{2\bar{\mu}_0 + \bar{\lambda}_0} \frac{\sin\theta}{r}. \tag{93}$$

The mass energy density is obtained from (85) to give

$$\rho c^2 \to \frac{b}{2\pi} \frac{8\bar{\kappa}_0\bar{\mu}_0}{2\bar{\mu}_0 + \bar{\lambda}_0} \frac{\sin\theta}{r}. \tag{94}$$

From (86), the edge dislocation dilatation strain energy density is then given by

$$\mathcal{E}_{\parallel} \to \frac{b^2}{2\pi^2} \frac{\bar{\kappa}_0\bar{\mu}_0^2}{(2\bar{\mu}_0 + \bar{\lambda}_0)^2} \frac{\sin^2\theta}{r^2}. \tag{95}$$

These equations are in agreement with (55), (67) and (69) respectively.

The edge dislocation distortion strain energy density in the limit as $v \to 0$ is obtained from (89) by making use of (91) and (92) as follows:

$$\begin{aligned}
\mathcal{E}_{\perp} \to \bar{\mu}_0 \frac{b^2}{4\pi^2}\frac{c^4}{v^4}\Bigg\{ &-\frac{3}{2}\frac{v^4}{c_l{}^4}\frac{\sin^2\theta}{r^2}+ \\
&+4\left(-\frac{\sin\theta}{r}+\alpha^2\frac{\sin\theta}{r}\right)^2+4\left(\gamma_l^2\frac{\sin\theta}{r}-\alpha^2\frac{\sin\theta}{r}\right)^2- \\
&-2\frac{v^2}{c^2}\left(\frac{\sin\theta}{r}-\alpha^2\frac{\sin\theta}{r}\right)^2- \\
&-2\frac{v^2}{c^2}\left(-\gamma_l\frac{\cos\theta}{r}+\frac{\alpha^2}{\gamma}\frac{\cos\theta}{r}\right)^2+ \\
&+2\left(2\gamma_l\frac{\cos\theta}{r}-\alpha^2\left(\gamma+\frac{1}{\gamma}\right)\frac{\cos\theta}{r}\right)^2\Bigg\}.
\end{aligned} \tag{96}$$

Simplifying,

$$\begin{aligned}
\mathcal{E}_{\perp} \to \bar{\mu}_0 \frac{b^2}{4\pi^2}\frac{c^4}{v^4}\Bigg\{ &-\frac{3}{2}\frac{v^4}{c_l{}^4}\frac{\sin^2\theta}{r^2}+ \\
&+4\left(-1+\alpha^2\right)^2\frac{\sin^2\theta}{r^2}+4\left(\gamma_l^2-\alpha^2\right)^2\frac{\sin^2\theta}{r^2}- \\
&-2\frac{v^2}{c^2}\left(1-\alpha^2\right)^2\frac{\sin^2\theta}{r^2}- \\
&-2\frac{v^2}{c^2}\left(-\gamma_l+\frac{\alpha^2}{\gamma}\right)^2\frac{\cos^2\theta}{r^2}+ \\
&+2\left(2\gamma_l-\alpha^2\left(\gamma+\frac{1}{\gamma}\right)\right)^2\frac{\cos^2\theta}{r^2}\Bigg\}.
\end{aligned} \tag{97}$$

Using the definitions of γ^2, γ_l^2 and α^2 from (27), (42) and (43) respectively, using the first term of the Taylor expansion for γ and γ_l as $v \to 0$, and neglecting the terms multiplied by $-2v^2/c^2$ in (97) as they are of order v^6/c^6, (97) becomes

$$\begin{aligned}
\mathcal{E}_{\perp} \to \bar{\mu}_0 \frac{b^2}{4\pi^2}\frac{c^4}{v^4}\Bigg\{\Bigg[&-\frac{3}{2}\frac{v^4}{c_l{}^4}+\frac{v^4}{c^4}+ \\
&+4\left(1-\frac{v^2}{c_l^2}-1+\frac{v^2}{2c^2}\right)^2\Bigg]\frac{\sin^2\theta}{r^2}+ \\
&+4\left[1-\frac{1}{2}\frac{v^2}{c_l^2}-1+\frac{v^2}{2c^2}\right]^2\frac{\cos^2\theta}{r^2}\Bigg\}.
\end{aligned} \tag{98}$$

Squaring and simplifying, we obtain

$$\begin{aligned}
\mathcal{E}_{\perp} \to \bar{\mu}_0 \frac{b^2}{4\pi^2}\frac{c^4}{v^4}\Bigg\{ &\left(\frac{5}{2}\frac{v^4}{c_l{}^4}+2\frac{v^4}{c^4}+4\frac{v^4}{c_l^2c^2}\right)\frac{\sin^2\theta}{r^2}+ \\
&+\left(\frac{v^4}{c_l{}^4}+\frac{v^4}{c^4}-2\frac{v^4}{c_l^2c^2}\right)\frac{\cos^2\theta}{r^2}\Bigg\}
\end{aligned} \tag{99}$$

and further

$$\begin{aligned}
\mathcal{E}_{\perp} \to \bar{\mu}_0 \frac{b^2}{2\pi^2}\Bigg\{ &\left(1+2\frac{c^2}{c_l^2}+\frac{5}{4}\frac{c^4}{c_l{}^4}\right)\frac{\sin^2\theta}{r^2}+ \\
&+\frac{1}{2}\left(1-2\frac{c^2}{c_l^2}+\frac{c^4}{c_l{}^4}\right)\frac{\cos^2\theta}{r^2}\Bigg\}.
\end{aligned} \tag{100}$$

Using $c^2/c_l{}^2 = \bar{\mu}_0/(2\bar{\mu}_0 + \bar{\lambda}_0)$ (see (9) and (44)), (100) becomes

$$\begin{aligned}
\mathcal{E}_{\perp} \to \bar{\mu}_0 \frac{b^2}{2\pi^2}\Bigg\{\Bigg(&1+\frac{2\bar{\mu}_0}{2\bar{\mu}_0+\bar{\lambda}_0}+ \\
&+\frac{5}{4}\frac{\bar{\mu}_0^2}{(2\bar{\mu}_0+\bar{\lambda}_0)^2}\Bigg)\frac{\sin^2\theta}{r^2}+\frac{1}{2}\Bigg(1- \\
&-\frac{2\bar{\mu}_0}{2\bar{\mu}_0+\bar{\lambda}_0}+\frac{\bar{\mu}_0^2}{(2\bar{\mu}_0+\bar{\lambda}_0)^2}\Bigg)\frac{\cos^2\theta}{r^2}\Bigg\}.
\end{aligned} \tag{101}$$

This equation represents the impact of the time terms included in the calculation of (87) and the limit operation $v \to 0$ used in (89).

5 Curved dislocations

In this section, we consider the equations for generally curved dislocations generated by infinitesimal elements of a dislocation. These allow us to handle complex dislocations that are encountered in the spacetime continuum.

5.1 The Burgers displacement equation

The Burgers displacement equation for an infinitesimal element of a dislocation $d\mathbf{l} = \boldsymbol{\xi} dl$ in vector notation is given by [14, see p. 102]

$$\begin{aligned}
\mathbf{u}(\mathbf{r}) = &\frac{\mathbf{b}}{4\pi}\int_A \frac{\hat{\mathbf{R}}\cdot d\mathbf{A}}{R^2} - \frac{1}{4\pi}\oint_C \frac{\mathbf{b}\times d\mathbf{l}'}{R}+ \\
&+\frac{1}{4\pi}\frac{\bar{\mu}_0+\bar{\lambda}_0}{2\bar{\mu}_0+\bar{\lambda}_0}\nabla\left[\oint_C \frac{(\mathbf{b}\times\mathbf{R})\cdot d\mathbf{l}'}{R}\right]
\end{aligned} \tag{102}$$

where $\mathbf{u}$ is the displacement vector, $\mathbf{r}$ is the vector to the displaced point, $\mathbf{r}'$ is the vector to the dislocation infinitesimal element $d\mathbf{l}'$, $\mathbf{R} = \mathbf{r}' - \mathbf{r}$, $\mathbf{b}$ is the Burgers vector, and closed loop C bounds the area A.

In tensor notation, (102) is given by

$$\begin{aligned} u_\mu(r^\nu) = &-\frac{1}{8\pi}\int_A b_\mu \frac{\partial}{\partial x'^\alpha}\left(\nabla'^2 R\right) dA^\alpha - \\ &-\frac{1}{8\pi}\oint_C b^\beta \epsilon_{\mu\beta\gamma}\nabla'^2 R\, dx'^\gamma - \\ &-\frac{1}{4\pi}\frac{\bar\mu_0+\bar\lambda_0}{2\bar\mu_0+\bar\lambda_0}\oint_C b_\beta \epsilon^{\beta\alpha\gamma}\frac{\partial^2 R}{\partial x'^\mu\,\partial x'^\alpha}\, dx'_\gamma \end{aligned} \tag{103}$$

where $\epsilon^{\alpha\beta\gamma}$ is the permutation symbol, equal to 1 for cyclic permutations, -1 for anti-cyclic permutations, and 0 for permutations involving repeated indices. As noted by Hirth [14, see p. 103], the first term of this equation gives a discontinuity $\Delta\mathbf{u} = \mathbf{b}$ over the surface A, while the two other terms are continuous except at the dislocation line. This equation is used to calculate the displacement produced at a point $\mathbf{r}$ by an arbitrary curved dislocation by integration over the dislocation line.

5.2 The Peach and Koehler stress equation

The Peach and Koehler stress equation for an infinitesimal element of a dislocation is derived by differentiation of (103) and substitution of the result in (20) [14, see p. 103–106]. In this equation, the dislocation is defined continuous except at the dislocation core, removing the discontinuity over the surface A and allowing to express the stresses in terms of line integrals alone.

$$\begin{aligned} \sigma_{\mu\nu} = &-\frac{\bar\mu_0}{8\pi}\oint_C b^\alpha \epsilon_{\beta\alpha\mu}\frac{\partial}{\partial x'^\beta}\left(\nabla'^2 R\right) dx'_\nu - \\ &-\frac{\bar\mu_0}{8\pi}\oint_C b^\alpha \epsilon_{\beta\alpha\nu}\frac{\partial}{\partial x'^\beta}\left(\nabla'^2 R\right) dx'_\mu - \\ &-\frac{\bar\mu_0}{4\pi}\frac{\bar\mu_0+\bar\lambda_0}{2\bar\mu_0+\bar\lambda_0}\oint_C b_\alpha \epsilon^{\beta\alpha\gamma} \\ &\left(\frac{\partial^3 R}{\partial x'^\beta\,\partial x'^\mu\partial x'^\nu} - \delta_{\mu\nu}\frac{\partial}{\partial x'^\beta}\left(\nabla'^2 R\right)\right) dx'_\gamma. \end{aligned} \tag{104}$$

This equation is used to calculate the stress field of an arbitrary curved dislocation by line integration.

6 Framework for quantum physics

In a solid, dislocations represent the fundamental displacement processes that occur in its atomic structure. A solid viewed in electron microscopy or other microscopic imaging techniques is a tangle of screw and edge dislocations [10, see p. 35 and accompanying pages]. Similarly, dislocations in the spacetime continuum are taken to represent the fundamental displacement processes that occur in its structure. These fundamental displacement processes should thus correspond to basic quantum phenomena and provide a framework for the description of quantum physics in *STCED*.

We find that dislocations have fundamental properties that reflect those of particles at the quantum level. These include self-energy and interactions mediated by the strain energy density of the dislocations. The role played by virtual particles in Quantum Electrodynamics is replaced by the interaction of the energy density of the dislocations. This theory is not perturbative as in QED, but rather calculated from analytical expressions. The analytical equations can become very complicated, and in some cases, perturbative techniques are used to simplify the calculations, but the availability of analytical expressions permit a better understanding of the fundamental processes involved.

Although the existence of virtual particles in QED is generally accepted, there are physicists who still question this interpretation of QED perturbation expansions. Weingard [41] "argues that if certain elements of the orthodox interpretation of states in QM are applicable to QED, then it must be concluded that virtual particles cannot exist. This follows from the fact that the transition amplitudes correspond to superpositions in which virtual particle type and number are not sharp. Weingard argues further that analysis of the role of measurement in resolving the superposition strengthens this conclusion. He then demonstrates in detail how in the path integral formulation of field theory no creation and annihilation operators need appear, yet virtual particles are still present. This analysis shows that the question of the existence of virtual particles is really the question of how to interpret the propagators which appear in the perturbation expansion of vacuum expectation values (scattering amplitudes)." [42]

The basic Feynman diagrams can be seen to represent screw dislocations as photons, edge dislocations as particles, and their interactions. The exchange of virtual particles in interactions can be taken as the forces resulting from the overlap of the dislocations' strain energy density, with suitably modified diagrams. The perturbative expansions are also replaced by finite analytical expressions.

6.1 Quantization

The Burgers vector as defined by expression (5) has similarities to the Bohr-Sommerfeld quantization rule

$$\oint_C p\, dq = nh \tag{105}$$

where q is the position canonical coordinate, p is the momentum canonical coordinate and h is Planck's constant. This leads us to consider the following quantization rule for the *STC*: at the quantum level, we assume that the spacetime continuum has a granularity characterized by a length b_0 corresponding to the smallest elementary Burgers dislocation-displacement vector possible in the *STC*. The idea that the existence of a shortest length in nature would lead to a natural cut-off to generate finite integrals in QED has been raised

before [43]. The smallest elementary Burgers dislocation-displacement vector introduced here provides a lower bound as shown in the next section. Then the magnitude of a Burgers vector can be expressed as a multiple of the elementary Burgers vector:

$$b = nb_0. \tag{106}$$

We find that b is usually divided by 2π in dislocation equations, and hence we define

$$\hbar = \frac{b}{2\pi}, \tag{107}$$

and similarly for the elementary Burgers dislocation-displacement vector b_0,

$$\hbar_0 = \frac{b_0}{2\pi}. \tag{108}$$

6.2 Screw dislocations in quantum physics

Screw dislocations in the spacetime continuum are identified with massless, transverse deformations, specifically photons. Consider the displacement of a stationary screw dislocation as derived in Section 3.1:

$$u_z = \frac{b}{2\pi}\,\theta = \hbar\,\theta. \tag{109}$$

Taking the derivative with respect to time, we obtain

$$\dot{u}_z = v_z = \frac{b}{2\pi}\,\dot{\theta} = \frac{b}{2\pi}\,\omega. \tag{110}$$

The speed of the transverse displacement is c, the speed of light. Substituting for $\omega = 2\pi\nu$, (110) becomes

$$c = b\,\nu. \tag{111}$$

Hence

$$b = \lambda, \tag{112}$$

the wavelength of the screw dislocation. This result is illustrated in Fig. 5. It is important to note that this relation applies only to screw dislocations.

The strain energy density of the screw dislocation is given by the transverse distortion energy density derived in Section 3.3. For a stationary screw dislocation, substituting (107) into (35),

$$\mathcal{E}_\perp = \frac{\bar{\mu}_0\,\hbar^2}{2}\,\frac{1}{r^2}. \tag{113}$$

The total strain energy of the screw dislocation is then given by

$$W_\perp = \int_V \mathcal{E}_\perp\,\mathrm{d}V \tag{114}$$

where the volume element $\mathrm{d}V$ in cylindrical polar coordinates is given by $r\mathrm{d}r\,\mathrm{d}\theta\,\mathrm{d}z$. Substituting for $\mathcal{E}_\perp$ from (113), (114) becomes

$$W_\perp = \int_V \frac{\bar{\mu}_0\,\hbar^2}{2r^2}\,r\mathrm{d}r\,\mathrm{d}\theta\,\mathrm{d}z. \tag{115}$$

Fig. 5: A wavelength of a screw dislocation.

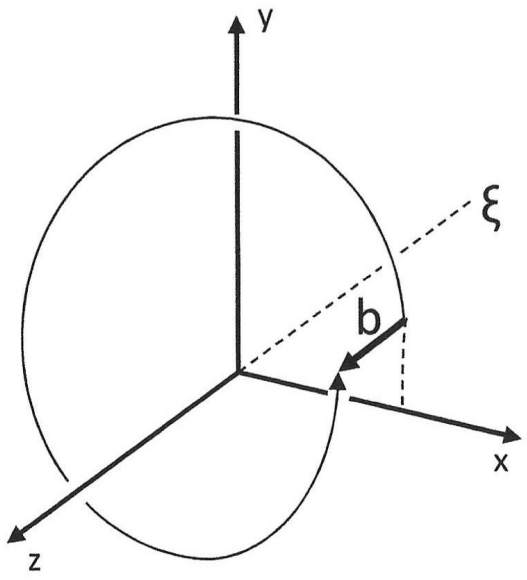

From (106), $\hbar$ can be taken out of the integral to give

$$W_\perp = \frac{\bar{\mu}_0\,\hbar^2}{2}\int_b^\Lambda \frac{1}{r}\mathrm{d}r\int_\theta \mathrm{d}\theta\int_z \mathrm{d}z \tag{116}$$

where Λ is a cut-off parameter corresponding to the radial extent of the dislocation, limited by the average distance to its nearest neighbours.

The strain energy per wavelength is then given by

$$\frac{W_\perp}{\lambda} = \frac{\bar{\mu}_0\,\hbar^2}{2}\log\frac{\Lambda}{b}\int_0^{2\pi}\mathrm{d}\theta \tag{117}$$

and finally

$$\frac{W_\perp}{\lambda} = \frac{\bar{\mu}_0\,b^2}{4\pi}\log\frac{\Lambda}{b}. \tag{118}$$

The implications of the total strain energy of the screw dislocation are discussed further in comparison to Quantum Electrodynamics (QED) in Section 7.

6.3 Edge dislocations in quantum physics

The strain energy density of the edge dislocation is derived in Section 4.3. The dilatation (massive) strain energy density of the edge dislocation is given by the longitudinal strain energy density (50) and the distortion (massless) strain energy density of the edge dislocation is given by the transverse strain energy density (51).

For the stationary edge dislocation of (79), using (107)

into (79), we have

$$\mathcal{E}_\perp = \frac{2\mathfrak{b}^2\bar{\mu}_0}{(2\bar{\mu}_0+\bar{\lambda}_0)^2}\left\{\frac{5}{4}\bar{\mu}_0^2\,\frac{\sin^2\theta}{r^2} - \right.$$
$$-\Big[(3\bar{\mu}_0+2\bar{\lambda}_0)(\bar{\mu}_0+2\bar{\lambda}_0)\,\cos^4\theta\,\frac{\sin^2\theta}{r^2} -$$
$$-2\bar{\mu}_0^2\,\cos^2\theta\,\frac{\sin^4\theta}{r^2} - \bar{\mu}_0^2\,\frac{\sin^6\theta}{r^2}\Big] + \tag{119}$$
$$\left. +(\bar{\mu}_0+\bar{\lambda}_0)^2\,\cos^2 2\theta\,\frac{\cos^2\theta}{r^2}\right\}.$$

The distortion strain energy of the edge dislocation is then given by

$$W_\perp = \int_V \mathcal{E}_\perp\,\mathrm{d}V \tag{120}$$

where the volume element $\mathrm{d}V$ in cylindrical polar coordinates is given by $r\mathrm{d}r\,\mathrm{d}\theta\,\mathrm{d}z$. Substituting for $\mathcal{E}_\perp$ from (119) and taking $\mathfrak{b}$ out of the integral, (120) becomes

$$W_\perp = \frac{2\mathfrak{b}^2\bar{\mu}_0}{(2\bar{\mu}_0+\bar{\lambda}_0)^2}\int_z\int_\theta\int_{b_0}^{\Lambda}\left\{\frac{5}{4}\bar{\mu}_0^2\,\frac{\sin^2\theta}{r^2} - \right.$$
$$-\Big[(3\bar{\mu}_0+2\bar{\lambda}_0)(\bar{\mu}_0+2\bar{\lambda}_0)\,\cos^4\theta\,\frac{\sin^2\theta}{r^2} -$$
$$-2\bar{\mu}_0^2\,\cos^2\theta\,\frac{\sin^4\theta}{r^2} - \bar{\mu}_0^2\,\frac{\sin^6\theta}{r^2}\Big] + \tag{121}$$
$$\left. +(\bar{\mu}_0+\bar{\lambda}_0)^2\,\cos^2 2\theta\,\frac{\cos^2\theta}{r^2}\right\} r\mathrm{d}r\,\mathrm{d}\theta\,\mathrm{d}z$$

where again Λ is a cut-off parameter corresponding to the radial extent of the dislocation, limited by the average distance to its nearest neighbours.

Evaluating the integral over r,

$$W_\perp = \frac{2\mathfrak{b}^2\bar{\mu}_0}{(2\bar{\mu}_0+\bar{\lambda}_0)^2}\,\log\frac{\Lambda}{b_0}\int_z\int_0^{2\pi}\left\{\frac{5}{4}\bar{\mu}_0^2\,\sin^2\theta - \right.$$
$$-\Big[(3\bar{\mu}_0+2\bar{\lambda}_0)(\bar{\mu}_0+2\bar{\lambda}_0)\,\cos^4\theta\,\sin^2\theta -$$
$$-2\bar{\mu}_0^2\,\cos^2\theta\,\sin^4\theta - \bar{\mu}_0^2\,\sin^6\theta\Big] + \tag{122}$$
$$\left. +(\bar{\mu}_0+\bar{\lambda}_0)^2\,\cos^2 2\theta\,\cos^2\theta\right\}\mathrm{d}\theta\,\mathrm{d}z.$$

Evaluating the integral over θ [40], we obtain (123) at the top of the next page. Applying the limits of the integration, both the coefficients of $\bar{\lambda}_0^2$ and $\bar{\mu}_0\bar{\lambda}_0$ are equal to 0 and only the coefficient of $\bar{\mu}_0^2$ is non-zero. Equation (123) then becomes

$$W_\perp = \frac{2\mathfrak{b}^2\bar{\mu}_0}{(2\bar{\mu}_0+\bar{\lambda}_0)^2}\,\log\frac{\Lambda}{b_0}\int_0^\ell\frac{9\pi}{4}\bar{\mu}_0^2\,\mathrm{d}z. \tag{124}$$

where ℓ is the length of the edge dislocation.

Evaluating the integral over z, we obtain the stationary edge dislocation transverse strain energy per unit length

$$\frac{W_\perp}{\ell} = \frac{9\pi}{2}\,\mathfrak{b}^2\bar{\mu}_0\left(\frac{\bar{\mu}_0}{2\bar{\mu}_0+\bar{\lambda}_0}\right)^2\log\frac{\Lambda}{b_0}. \tag{125}$$

We find that the stationary edge dislocation transverse strain energy per unit length (where we have added the label E)

$$\frac{W_\perp^E}{\ell} = \frac{9}{8\pi}\,b^2\bar{\mu}_0\left(\frac{\bar{\mu}_0}{2\bar{\mu}_0+\bar{\lambda}_0}\right)^2\log\frac{\Lambda}{b_0} \tag{126}$$

is similar to the stationary screw dislocation transverse strain energy per unit length

$$\frac{W_\perp^S}{\ell} = \frac{1}{4\pi}b^2\bar{\mu}_0\,\log\frac{\Lambda}{b_0} \tag{127}$$

except for the proportionality constant.

Similarly, the longitudinal strain energy of the stationary edge dislocation is given by

$$W_\parallel^E = \int_V \mathcal{E}_\parallel\,\mathrm{d}V. \tag{128}$$

Substituting for $\mathcal{E}_\parallel$ from (69), this equation becomes

$$W_\parallel^E = \int_V \frac{b^2}{2\pi^2}\,\frac{\bar{\kappa}_0\bar{\mu}_0^2}{(2\bar{\mu}_0+\bar{\lambda}_0)^2}\,\frac{\sin^2\theta}{r^2}\,\mathrm{d}V. \tag{129}$$

Similarly to the previous derivation, this integral gives

$$\frac{W_\parallel^E}{\ell} = \frac{1}{2\pi}b^2\,\bar{\kappa}_0\left(\frac{\bar{\mu}_0}{2\bar{\mu}_0+\bar{\lambda}_0}\right)^2\log\frac{\Lambda}{b_0}. \tag{130}$$

The total strain energy of the stationary screw and edge dislocations have similar functional forms, with the difference residing in the proportionality constants. This is due to the simpler nature of the stationary dislocations and their cylindrical polar symmetry. This similarity is not present for the general case of moving dislocations as evidenced in equations (37), (86) and (90).

For the moving edge dislocation in the limit as $v \to 0$, subsituting for (101) in (120) and using (107), we have

$$W_\perp^E \to 2\mathfrak{b}^2\bar{\mu}_0\int_z\int_\theta\int_{b_0}^{\Lambda} r\mathrm{d}r\,\mathrm{d}\theta\,\mathrm{d}z$$
$$\left\{\left(1+\frac{2\bar{\mu}_0}{2\bar{\mu}_0+\bar{\lambda}_0}+\frac{5}{4}\,\frac{\bar{\mu}_0^2}{(2\bar{\mu}_0+\bar{\lambda}_0)^2}\right)\frac{\sin^2\theta}{r^2} + \right. \tag{131}$$
$$\left. +\frac{1}{2}\left(1-\frac{2\bar{\mu}_0}{2\bar{\mu}_0+\bar{\lambda}_0}+\frac{\bar{\mu}_0^2}{(2\bar{\mu}_0+\bar{\lambda}_0)^2}\right)\frac{\cos^2\theta}{r^2}\right\}$$

where again Λ is a cut-off parameter corresponding to the radial extent of the dislocation, limited by the average distance to its nearest neighbours.

$$W_\perp = \frac{2\bar{b}^2\bar{\mu}_0}{(2\bar{\mu}_0+\bar{\lambda}_0)^2}\log\frac{\Lambda}{b_0}\int_z\left[\frac{5}{4}\bar{\mu}_0^2\left(\frac{\theta}{2}-\frac{1}{4}\sin 2\theta\right)-\right.$$
$$-(3\bar{\mu}_0+2\bar{\lambda}_0)(\bar{\mu}_0+2\bar{\lambda}_0)\left(\frac{\theta}{16}+\frac{1}{64}\sin 2\theta-\frac{1}{64}\sin 4\theta-\frac{1}{192}\sin 6\theta\right)+$$
$$+2\bar{\mu}_0^2\left(\frac{\theta}{16}-\frac{1}{64}\sin 2\theta-\frac{1}{64}\sin 4\theta+\frac{1}{192}\sin 6\theta\right)+ \quad (123)$$
$$+\bar{\mu}_0^2\left(\frac{5\theta}{16}-\frac{15}{64}\sin 2\theta+\frac{3}{64}\sin 4\theta-\frac{1}{192}\sin 6\theta\right)+$$
$$\left.+(\bar{\mu}_0+\bar{\lambda}_0)^2\left(\frac{\theta}{4}+\frac{3}{16}\sin 2\theta+\frac{1}{16}\sin 4\theta+\frac{1}{48}\sin 6\theta\right)\right]_0^{2\pi}\mathrm{d}z$$

Evaluating the integral over r,

$$W_\perp^E \to 2\bar{b}^2\bar{\mu}_0\log\frac{\Lambda}{b_0}\int_z\int_0^{2\pi}\mathrm{d}\theta\,\mathrm{d}z$$
$$\left\{\left(1+\frac{2\bar{\mu}_0}{2\bar{\mu}_0+\bar{\lambda}_0}+\frac{5}{4}\frac{\bar{\mu}_0^2}{(2\bar{\mu}_0+\bar{\lambda}_0)^2}\right)\sin^2\theta+\right. \quad (132)$$
$$\left.+\frac{1}{2}\left(1-\frac{2\bar{\mu}_0}{2\bar{\mu}_0+\bar{\lambda}_0}+\frac{\bar{\mu}_0^2}{(2\bar{\mu}_0+\bar{\lambda}_0)^2}\right)\cos^2\theta\right\}.$$

Evaluating the integral over θ [40] and applying the limits of the integration, we obtain

$$W_\perp^E \to 2\bar{b}^2\bar{\mu}_0\log\frac{\Lambda}{b_0}\int_0^\ell\mathrm{d}z$$
$$\left\{\left(1+\frac{2\bar{\mu}_0}{2\bar{\mu}_0+\bar{\lambda}_0}+\frac{5}{4}\frac{\bar{\mu}_0^2}{(2\bar{\mu}_0+\bar{\lambda}_0)^2}\right)(\pi)+\right. \quad (133)$$
$$\left.+\frac{1}{2}\left(1-\frac{2\bar{\mu}_0}{2\bar{\mu}_0+\bar{\lambda}_0}+\frac{\bar{\mu}_0^2}{(2\bar{\mu}_0+\bar{\lambda}_0)^2}\right)(\pi)\right\}$$

and evaluating the integral over z, we obtain the moving edge dislocation transverse strain energy per unit length in the limit as $v\to 0$

$$\frac{W_\perp^E}{\ell}\to\frac{3}{4\pi}b^2\bar{\mu}_0\left(1+\frac{2}{3}\frac{\bar{\mu}_0}{2\bar{\mu}_0+\bar{\lambda}_0}+\right.$$
$$\left.+\frac{7}{6}\frac{\bar{\mu}_0^2}{(2\bar{\mu}_0+\bar{\lambda}_0)^2}\right)\log\frac{\Lambda}{b_0} \quad (134)$$

where ℓ is the length of the edge dislocation.

6.4 Strain energy of moving dislocations

In the general case of moving dislocations, the derivation of the screw dislocation transverse strain energy and the edge dislocation transverse and longitudinal strain energies is more difficult. In this section, we provide an overview discussion of the topic.

6.4.1 Screw dislocation transverse strain energy

The transverse strain energy of a moving screw dislocation, which also corresponds to its total strain energy, is given by

$$W_\perp^S = \int_V \mathcal{E}_\perp^S\,\mathrm{d}V \quad (135)$$

where the strain energy density $\mathcal{E}_\perp^S$ is given by (113), viz.

$$\mathcal{E}_\perp^S = \frac{1}{2}\bar{b}^2\bar{\mu}_0\frac{\gamma^2}{(x-vt)^2+\gamma^2y^2} \quad (136)$$

and V is the 4-dimensional volume of the screw dislocation. The volume element $\mathrm{d}V$ in cartesian coordinates is given by $\mathrm{d}x\,\mathrm{d}y\,\mathrm{d}z\,\mathrm{d}(ct)$.

Substituting for $\mathcal{E}_\perp^S$, (135) becomes

$$W_\perp^S = \int_V\frac{1}{2}\bar{b}^2\bar{\mu}_0\frac{\gamma^2}{(x-vt)^2+\gamma^2y^2}\,\mathrm{d}x\,\mathrm{d}y\,\mathrm{d}z\,\mathrm{d}(ct). \quad (137)$$

As before, $\bar{b}$ is taken out of the integral from (106), and the integral over z is handled by considering the strain energy per unit length of the dislocation:

$$\frac{W_\perp^S}{\ell} = \frac{\bar{b}^2\bar{\mu}_0}{2}\int_{ct}\int_y\int_x\frac{\gamma^2}{(x-vt)^2+\gamma^2y^2}\,\mathrm{d}x\,\mathrm{d}y\,\mathrm{d}(ct) \quad (138)$$
$$b^2\le x^2+y^2\le\Lambda^2$$

where ℓ is the length of the dislocation and as before, Λ is a cut-off parameter corresponding to the radial extent of the dislocation, limited by the average distance to its nearest neighbours.

Evaluating the integral over x [40],

$$\frac{W_\perp^S}{\ell} = \frac{\bar{b}^2\bar{\mu}_0}{2}\gamma^2\int_{ct}\int_y\mathrm{d}y\,\mathrm{d}(ct)$$
$$\left[\frac{1}{\gamma y}\arctan\left(\frac{x-vt}{\gamma y}\right)\right]_{\sqrt{y^2-b^2}}^{\sqrt{\Lambda^2-y^2}} \quad (139)$$

where the limits corresponding to the maximum cut-off parameter Λ and minimum cut-off parameter b are stated explicitly. Applying the limits of the integration, we obtain

$$\frac{W^S_\perp}{\ell} = \frac{\bar{b}^2\,\bar{\mu}_0}{2}\,\gamma^2 \int_{ct}\int_y \mathrm{d}y\,\mathrm{d}(ct) \left\{\frac{1}{\gamma y}\,\arctan\left(\frac{\sqrt{\Lambda^2-y^2}-vt}{\gamma y}\right)- -\frac{1}{\gamma y}\,\arctan\left(\frac{\sqrt{y^2-b^2}-vt}{\gamma y}\right)\right\}. \tag{140}$$

This integration over y is not elementary and likely does not lead to a closed analytical form. If we consider the following simpler integral, the solution is given by

$$\int_y \frac{1}{\gamma y}\,\arctan\left(\frac{x-vt}{\gamma y}\right)\mathrm{d}y = -\frac{i}{2}\left[\mathrm{Li}_2\left(-i\,\frac{x-vt}{\gamma y}\right)-\mathrm{Li}_2\left(i\,\frac{x-vt}{\gamma y}\right)\right] \tag{141}$$

where $\mathrm{Li}_n(x)$ is the polylogarithm function. As pointed out in [44], "[t]he polylogarithm arises in Feynman diagram integrals (and, in particular, in the computation of quantum electrodynamics corrections to the electrons gyromagnetic ratio), and the special cases $n = 2$ and $n = 3$ are called the dilogarithm and the trilogarithm, respectively." This is a further indication that the interaction of strain energies are the physical source of quantum interaction phenomena described by Feynman diagrams as will be seen in Section 7.

6.4.2 Edge dislocation longitudinal strain energy

The longitudinal strain energy of a moving edge dislocation is given by

$$W^E_\parallel = \int_V \mathcal{E}^E_\parallel\,\mathrm{d}V \tag{142}$$

where the strain energy density $\mathcal{E}^E_\perp$ is given by (86), viz.

$$\mathcal{E}^E_\parallel = \frac{1}{2}\,\bar{\kappa}_0\,\bar{b}^2\left(\frac{2\bar{\mu}_0}{2\bar{\mu}_0+\bar{\lambda}_0}\,\frac{\gamma_l y}{(x-vt)^2+\gamma_l^2 y^2}\right)^2 \tag{143}$$

and V is the 4-dimensional volume of the edge dislocation. The volume element $\mathrm{d}V$ in cartesian coordinates is given by $\mathrm{d}x\,\mathrm{d}y\,\mathrm{d}z\,\mathrm{d}(ct)$.

Substituting for $\mathcal{E}^E_\parallel$, (142) becomes

$$W^E_\parallel = \int_V \frac{1}{2}\,\bar{\kappa}_0\,\bar{b}^2\left(\frac{2\bar{\mu}_0}{2\bar{\mu}_0+\bar{\lambda}_0}\,\frac{\gamma_l y}{(x-vt)^2+\gamma_l^2 y^2}\right)^2 \mathrm{d}x\,\mathrm{d}y\,\mathrm{d}z\,\mathrm{d}(ct). \tag{144}$$

As before, $\bar{b}$ is taken out of the integral from (106), and the integral over z is handled by considering the strain energy per unit length of the dislocation:

$$\frac{W^E_\parallel}{\ell} = 2\,\bar{\kappa}_0\,\bar{b}^2\,\frac{\bar{\mu}_0^2}{(2\bar{\mu}_0+\bar{\lambda}_0)^2} \int_{ct}\int_y\int_x \frac{(\gamma_l y)^2}{\left((x-vt)^2+\gamma_l^2 y^2\right)^2}\,\mathrm{d}x\,\mathrm{d}y\,\mathrm{d}(ct) \quad {\scriptstyle b^2\le x^2+y^2\le\Lambda^2} \tag{145}$$

where ℓ is the length of the dislocation and as before, Λ is a cut-off parameter corresponding to the radial extent of the dislocation, limited by the average distance to its nearest neighbours.

The integrand has a functional form similar to that of (138), and a similar solution behaviour is expected. Evaluating the integral over x [40],

$$\frac{W^E_\parallel}{\ell} = 2\,\bar{\kappa}_0\,\bar{b}^2\,\frac{\bar{\mu}_0^2}{(2\bar{\mu}_0+\bar{\lambda}_0)^2}\int_{ct}\int_y \mathrm{d}y\,\mathrm{d}(ct) \left[\frac{1}{2}\,\frac{x-vt}{(x-vt)^2+(\gamma_l y)^2}+ +\frac{1}{2\gamma_l y}\,\arctan\left(\frac{x-vt}{\gamma_l y}\right)\right]_{\sqrt{y^2-b^2}}^{\sqrt{\Lambda^2-y^2}} \tag{146}$$

where the limits corresponding to the maximum cut-off parameter Λ and minimum cut-off parameter b are stated explicitly. Applying the limits of the integration, we obtain

$$\frac{W^E_\parallel}{\ell} = 2\,\bar{\kappa}_0\,\bar{b}^2\,\frac{\bar{\mu}_0^2}{(2\bar{\mu}_0+\bar{\lambda}_0)^2}\int_{ct}\int_y \mathrm{d}y\,\mathrm{d}(ct) \left\{\frac{1}{2}\,\frac{\sqrt{\Lambda^2-y^2}-vt}{(\sqrt{\Lambda^2-y^2}-vt)^2+(\gamma_l y)^2}- -\frac{1}{2}\,\frac{\sqrt{y^2-b^2}-vt}{(\sqrt{y^2-b^2}-vt)^2+(\gamma_l y)^2}+ +\frac{1}{2\gamma_l y}\,\arctan\left(\frac{\sqrt{\Lambda^2-y^2}-vt}{\gamma_l y}\right)- -\frac{1}{2\gamma_l y}\,\arctan\left(\frac{\sqrt{y^2-b^2}-vt}{\gamma_l y}\right)\right\}. \tag{147}$$

This integration over y is again found to be intractable, including that of (140), and likely does not lead to a closed analytical form. In the $\arctan\Lambda$ integral of (140) and (147), we can make the approximation $\sqrt{\Lambda^2-y^2}\simeq\Lambda$ and evaluate this term as seen in (141):

$$\int_y \frac{1}{\gamma_l y}\,\arctan\left(\frac{\Lambda-vt}{\gamma_l y}\right)\mathrm{d}y = -\frac{i}{2}\left[\mathrm{Li}_2\left(-i\,\frac{\Lambda-vt}{\gamma_l y}\right)-\mathrm{Li}_2\left(i\,\frac{\Lambda-vt}{\gamma_l y}\right)\right] \tag{148}$$

where $\mathrm{Li}_n(x)$ is the polylogarithm function as seen previously.

6.4.3 Edge dislocation transverse strain energy

The transverse strain energy of a moving edge dislocation is given by

$$W_{\perp}^{E} = \int_{V} \mathcal{E}_{\perp}^{E}\, \mathrm{d}V \tag{149}$$

where the strain energy density $\mathcal{E}_{\perp}^{E}$ is given by (90), viz.

$$\begin{aligned}\mathcal{E}_{\perp}^{E} = 2\bar{\mu}_0\, \bar{b}^2 \frac{c^4}{v^4}\Bigg\{ & \frac{\alpha^4\,(3+\gamma^2)}{(x-vt)^2+\gamma^2 y^2} - \\ -2\alpha^2 & \frac{\left(3+\frac{1}{\gamma^2}\right)\gamma_l\,\gamma\,(x-vt)^2 + \left(2\gamma_l^2 - \frac{v^2}{c^2}\right)\gamma_l\,\gamma\,y^2}{\left((x-vt)^2+\gamma_l^2 y^2\right)\left((x-vt)^2+\gamma^2 y^2\right)} + \\ + & \frac{(3+\gamma^2)\gamma_l^2(x-vt)^2 + 2\left(\alpha^2+\gamma_l^4 - \frac{3}{8}\frac{v^4}{c_l^4}\right)\gamma_l^2 y^2}{\left((x-vt)^2+\gamma_l^2 y^2\right)^2}\Bigg\}\end{aligned} \tag{150}$$

and V is the 4-dimensional volume of the edge dislocation. The volume element $\mathrm{d}V$ in cartesian coordinates is given by $\mathrm{d}x\,\mathrm{d}y\,\mathrm{d}z\,\mathrm{d}(ct)$.

Substituting for $\mathcal{E}_{\perp}^{E}$ as before, taking $\bar{b}$ out of the integral from (106), and handling the integral over z by considering the strain energy per unit length of the dislocation, (149) becomes

$$\begin{aligned}\frac{W_{\perp}^{E}}{\ell} = 2\bar{\mu}_0\, \bar{b}^2 \frac{c^4}{v^4} & \int_{ct}\int_{y}\int_{x}_{b^2\le x^2+y^2\le\Lambda^2} \mathrm{d}x\,\mathrm{d}y\,\mathrm{d}(ct) \\ \Bigg\{ & \frac{\alpha^4\,(3+\gamma^2)}{(x-vt)^2+\gamma^2 y^2} - \\ -2\alpha^2 & \frac{\left(3+\frac{1}{\gamma^2}\right)\gamma_l\,\gamma\,(x-vt)^2 + \left(2\gamma_l^2 - \frac{v^2}{c^2}\right)\gamma_l\,\gamma\,y^2}{\left((x-vt)^2+\gamma_l^2 y^2\right)\left((x-vt)^2+\gamma^2 y^2\right)} + \\ + & \frac{(3+\gamma^2)\gamma_l^2(x-vt)^2 + 2\left(\alpha^2+\gamma_l^4 - \frac{3}{8}\frac{v^4}{c_l^4}\right)\gamma_l^2 y^2}{\left((x-vt)^2+\gamma_l^2 y^2\right)^2}\Bigg\}\end{aligned} \tag{151}$$

where ℓ is the length of the dislocation and as before, Λ is a cut-off parameter corresponding to the radial extent of the dislocation, limited by the average distance to its nearest neighbours.

Again, the integrand has functional forms similar to that of (138) and (145). A similar, but more complex, solution behaviour is expected, due to the additional complexity of (151).

7 Dislocation interactions in quantum physics

As mentioned is Section 6, the basic Feynman diagrams can be seen to represent screw dislocations as photons, edge dislocations as particles, and their interactions. More specifically, the external legs of Feynman diagrams that are on mass-shell representing real particles correspond to dislocations, while the virtual off mass-shell particles are replaced by the interaction of the strain energy densities. The exchange of virtual particles in QED interactions can be taken as the perturbation expansion representation of the forces resulting from the overlap of the strain energy density of the dislocations. The Feynman diagram propagators are replaced by the dislocation strain energy density interaction expressions.

The properties of Burgers vectors and dislocations [14, see pp. 25-26] have rules similar to those of Feynman diagrams, but not equivalent as virtual particles are replaced by dislocation strain energy density interactions. A Burgers vector is invariant along a dislocation line. Two Burgers circuits are equivalent if one can be deformed into the other without crossing dislocation lines. The resultant Burgers vector within equivalent Burgers circuits is the same.

Dislocation nodes are points where multiple dislocations meet. If all the dislocation vectors ξ_i are taken to be positive away from a node, then

$$\sum_{i=1}^{N} \boldsymbol{\xi}_i = 0 \tag{152}$$

for the N dislocations meeting at the node. Burgers vectors are conserved at dislocation nodes.

In this section, we consider the interactions of dislocations which are seen to result from the force resulting from the overlap of their strain energy density in the *STC* [14, see p. 112].

7.1 Parallel dislocation interactions

From Hirth [14, see pp. 117-118], the energy of interaction per unit length between parallel dislocations (including screw and edge dislocation components) is given by

$$\begin{aligned}\frac{W_{12}}{\ell} = & -\frac{\bar{\mu}_0}{2\pi}\,(\mathbf{b_1}\cdot\boldsymbol{\xi})\,(\mathbf{b_2}\cdot\boldsymbol{\xi})\,\log\frac{R}{R_\Lambda} - \\ & -\frac{\bar{\mu}_0}{\pi}\,\frac{\bar{\mu}_0+\bar{\lambda}_0}{2\bar{\mu}_0+\bar{\lambda}_0}\,(\mathbf{b_1}\times\boldsymbol{\xi})\cdot(\mathbf{b_2}\times\boldsymbol{\xi})\,\log\frac{R}{R_\Lambda} - \\ & -\frac{\bar{\mu}_0}{\pi}\,\frac{\bar{\mu}_0+\bar{\lambda}_0}{2\bar{\mu}_0+\bar{\lambda}_0}\,\frac{[(\mathbf{b_1}\times\boldsymbol{\xi})\cdot\mathbf{R}]\,[(\mathbf{b_2}\times\boldsymbol{\xi})\cdot\mathbf{R}]}{R^2}\end{aligned} \tag{153}$$

where ξ is parallel to the z axis, $(\mathbf{b_i}\cdot\boldsymbol{\xi})$ are the screw components, $(\mathbf{b_i}\times\boldsymbol{\xi})$ are the edge components, R is the separation between the dislocations, and R_Λ is the distance from which the dislocations are brought together, resulting in the decrease in energy of the "system".

The components of the interaction force per unit length between the parallel dislocations are obtained by differentiation:

$$\begin{aligned}\frac{F_R}{\ell} &= -\frac{\partial(W_{12}/\ell)}{\partial R} \\ \frac{F_\theta}{\ell} &= -\frac{1}{R}\,\frac{\partial(W_{12}/\ell)}{\partial\theta}.\end{aligned} \tag{154}$$

Substituting from (153), (154) becomes

$$\frac{F_R}{\ell} = \frac{\bar{\mu}_0}{2\pi R}(\mathbf{b_1}\cdot\boldsymbol{\xi})(\mathbf{b_2}\cdot\boldsymbol{\xi}) + \\ + \frac{\bar{\mu}_0}{\pi R}\frac{\bar{\mu}_0+\bar{\lambda}_0}{2\bar{\mu}_0+\bar{\lambda}_0}(\mathbf{b_1}\times\boldsymbol{\xi})\cdot(\mathbf{b_2}\times\boldsymbol{\xi}) \\ \frac{F_\theta}{\ell} = \frac{\bar{\mu}_0}{\pi R^3}\frac{\bar{\mu}_0+\bar{\lambda}_0}{2\bar{\mu}_0+\bar{\lambda}_0}[(\mathbf{b_1}\cdot\mathbf{R})[(\mathbf{b_2}\times\mathbf{R})\cdot\boldsymbol{\xi}] + \\ + (\mathbf{b_2}\cdot\mathbf{R})[(\mathbf{b_1}\times\mathbf{R})\cdot\boldsymbol{\xi}]]. \tag{155}$$

7.2 Curved dislocation interactions

In this section, we extend the investigation of curved dislocations initiated in Section 5, to the interaction energy and interaction force between curved dislocations [14, see pp. 106-110]. The derivation considers the interaction between two dislocation loops, but has much more extensive applications, being extendable to the interaction energy between two arbitrarily positioned segments of dislocation lines.

If a dislocation loop 1 is brought in the vicinity of another dislocation loop 2, the stresses originating from loop 2 do work $-W_{12}$ on loop 1 where W_{12} is the interaction energy between the two dislocation loops. The work done on loop 1 represents a decrease in the strain energy of the total system. In that case, if W_{12} is negative, the energy of the system decreases and an attractive force exists between the loops [14, see p. 106].

The interaction energy between the two dislocation loops is given by [14, see p. 108]

$$W_{12} = -\frac{\bar{\mu}_0}{2\pi}\oint_{C_1}\oint_{C_2}\frac{(\mathbf{b_1}\times\mathbf{b_2})\cdot(d\mathbf{l_1}\times d\mathbf{l_2})}{R} + \\ + \frac{\bar{\mu}_0}{4\pi}\oint_{C_1}\oint_{C_2}\frac{(\mathbf{b_1}\cdot d\mathbf{l_1})(\mathbf{b_2}\cdot d\mathbf{l_2})}{R} + \\ + \frac{\bar{\mu}_0}{2\pi}\frac{\bar{\mu}_0+\bar{\lambda}_0}{2\bar{\mu}_0+\bar{\lambda}_0}\oint_{C_1}\oint_{C_2}\frac{(\mathbf{b_1}\times d\mathbf{l_1})\cdot\mathbf{T}\cdot(\mathbf{b_2}\times d\mathbf{l_2})}{R} \tag{156}$$

where $\mathbf{T}$ is given by

$$T_{ij} = \frac{\partial^2 R}{\partial x_i \partial x_j}. \tag{157}$$

The force produced by an external stress acting on a dislocation loop is given by [14, see p. 109]

$$d\mathbf{F} = (\mathbf{b}\cdot\boldsymbol{\sigma})\times d\mathbf{l} \tag{158}$$

where $\boldsymbol{\sigma}$ is the stress tensor in the medium, $\mathbf{b}$ is the Burgers vector, and $d\mathbf{l}$ is the dislocation element. This equation can be used with (104) to determine the interaction force between dislocation segments.

As each element $d\mathbf{l}$ of a dislocation loop is acted upon by the forces caused by the stress of the other elements of the dislocation loop, the work done against these corresponds to the self-energy of the dislocation loop. The self-energy of a dislocation loop can be calculated from (156) to give [14, see p. 110]

$$W_{self} = \frac{\bar{\mu}_0}{8\pi}\oint_{C_1=C}\oint_{C_2=C}\frac{(\mathbf{b}\cdot d\mathbf{l_1})(\mathbf{b}\cdot d\mathbf{l_2})}{R} + \\ + \frac{\bar{\mu}_0}{4\pi}\frac{\bar{\mu}_0+\bar{\lambda}_0}{2\bar{\mu}_0+\bar{\lambda}_0}\oint_{C_1=C}\oint_{C_2=C}\frac{(\mathbf{b}\times d\mathbf{l_1})\cdot\mathbf{T}\cdot(\mathbf{b}\times d\mathbf{l_2})}{R} \tag{159}$$

where $\mathbf{T}$ is as defined in (157).

More complicated expressions can be obtained for interactions between two non-parallel straight dislocations [14, see pp. 121-123] and between a straight segment of a dislocation and a differential element of another dislocation [14, see pp. 124-131]. This latter derivation can be used for more arbitrary dislocation interactions.

7.3 Physical application of dislocation interactions

In Quantum Electrodynamics, these correspond to particle-particle and particle-photon interactions, which are taken to be mediated by virtual particles. This is in keeping with the QED picture, but as shown above, particle-particle and particle-photon interactions physically result from the overlap of their strain energy density which results in an interaction force. Again, this improved understanding of the physical nature of dislocation interactions demonstrates that the interactions do not need to be represented by virtual particle exchange as discussed in Section 6.

This theory provides a straightforward physical explanation of particle-particle and particle-photon interactions that is not based on perturbation theory, but rather on a direct evaluation of the interactions.

7.4 Photons and screw dislocation interactions

Screw dislocations interact via the force resulting from the overlap of the strain energy density of the dislocations in the *STC* [14, see p. 112].

As seen in Section 6.2, screw dislocations in the spacetime continuum are identified with the massless, transverse deformations, photons. As pointed out in [45], it has been known since the 1960s that photons can interact with each other in atomic media much like massive particles do. A review of collective effects in photon-photon interactions is given in [46].

In QED, photon-photon interactions are known as photon-photon scattering, which is thought to be mediated by virtual particles. This is in keeping with the QED picture, but as shown in this work, photon-photon interactions physically result from the overlap of their strain energy density. This improved understanding of the physical nature of photon-photon interactions demonstrates that the interaction does not need to

be represented by virtual particle exchanges, in that the nature of the physical processes involved is now understood.

From (153), the energy of interaction per unit length between parallel screw dislocations (photons) is given by

$$\frac{W_{12}^{ss}}{\ell} = -\frac{\bar{\mu}_0}{2\pi}\,(\mathbf{b_1}\cdot\boldsymbol{\xi})\,(\mathbf{b_2}\cdot\boldsymbol{\xi})\,\log\frac{R}{R_\Lambda} \tag{160}$$

where ξ is parallel to the z axis, $(\mathbf{b_i}\cdot\boldsymbol{\xi})$ are the screw components, R is the separation between the dislocations, and R_Λ is the distance from which the dislocations are brought together, resulting in the reduction in the energy of the 2-photon "system".

From (155), the components of the interaction force per unit length between the parallel screw dislocations are given by:

$$\begin{aligned}\frac{F_R^{ss}}{\ell} &= \frac{\bar{\mu}_0}{2\pi R}\,(\mathbf{b_1}\cdot\boldsymbol{\xi})\,(\mathbf{b_2}\cdot\boldsymbol{\xi})\\ \frac{F_\theta^{ss}}{\ell} &= 0.\end{aligned} \tag{161}$$

The interaction force is radial in nature, independent of the angle θ, as expected.

8 Physical explanations of QED phenomena

As we have seen in previous sections, spacetime continuum dislocations have fundamental properties that reflect those of phenomena at the quantum level. In particular, the improved understanding of the physical nature of interactions mediated by the strain energy density of the dislocations. The role played by virtual particles in Quantum Electrodynamics is replaced by the work done by the forces resulting from the dislocation stresses, and the resulting interaction of the strain energy density of the dislocations. In this section, we examine the physical explanation of QED phenomena provided by this theory, including self-energy and mass renormalization.

8.1 Dislocation self-energy and QED self energies

Dislocation self energies are found to be similar in structure to Quantum Electrodynamics self energies. They are also divergent if integrated over all of spacetime, with the divergence being logarithmic in nature. However, contrary to QED, dislocation self energies are bounded by the density of dislocations present in the spacetime continuum, which results in an upperbound to the integral of half the average distance between dislocations. As mentioned by Hirth [14], this has little impact on the accuracy of the results due to the logarithmic dependence.

The dislocation self-energy is related to the dislocation self-force. The dislocation self-force arises from the force on an element in a dislocation caused by other segments of the *same* dislocation line. This process provides an explanation for the QED self-energies without the need to resort to the emission/absorption of virtual particles. It can be understood, and is particular to, dislocation dynamics as dislocations are defects that extend in the spacetime continuum [14, see p. 131]. Self-energy of a straight-dislocation segment of length L is given by [14, see p. 161]:

$$\begin{aligned}W_{self} = \frac{\bar{\mu}_0}{4\pi}&\left((\mathbf{b}\cdot\boldsymbol{\xi})^2 + \frac{\bar{\mu}_0+\bar{\lambda}_0}{2\bar{\mu}_0+\bar{\lambda}_0}\,|(\mathbf{b}\times\boldsymbol{\xi})|^2\right)\\ &L\left(\log\frac{L}{b} - 1\right),\end{aligned} \tag{162}$$

where there is no interaction between two elements of the segment when they are within $\pm b$, or equivalently

$$\begin{aligned}W_{self} = \frac{\bar{\mu}_0}{4\pi}&\left((\mathbf{b}\cdot\boldsymbol{\xi})^2 + \frac{\bar{\mu}_0+\bar{\lambda}_0}{2\bar{\mu}_0+\bar{\lambda}_0}\,|(\mathbf{b}\times\boldsymbol{\xi})|^2\right)\\ &L\,\log\frac{L}{eb},\end{aligned} \tag{163}$$

where $e = 2.71828\ldots$. These equations provide analytic expressions for the non-perturbative calculation of quantum self energies and interaction energies, and eliminate the need for the virtual particle interpretation.

In particular, the pure screw (photon) self-energy

$$W_{self}^{S} = \frac{\bar{\mu}_0}{4\pi}\,(\mathbf{b}\cdot\boldsymbol{\xi})^2\,L\,\log\frac{L}{eb} \tag{164}$$

and the pure edge (particle) self-energy

$$W_{self}^{E} = \frac{\bar{\mu}_0}{4\pi}\,\frac{\bar{\mu}_0+\bar{\lambda}_0}{2\bar{\mu}_0+\bar{\lambda}_0}\,|(\mathbf{b}\times\boldsymbol{\xi})|^2\,L\,\log\frac{L}{eb} \tag{165}$$

are obtained from (163), while (163) is also the appropriate equation to use for the dual wave-particle "system".

8.2 Dislocation strain energy and QED mass renormalization

This approach also resolves and eliminates the mass renormalization problem. This problem arises in QED due to the incomplete description of particle energies at the quantum level. This paper shows that the strain energy density of an edge dislocation, which corresponds to a particle, consists of a longitudinal dilatation mass density term and a transverse distortion energy density term, as shown in (49), (50), and (51).

QED, in its formulation, only uses the transverse distortion strain energy density in its calculations. This is referred to as the bare mass m_0. However, there is no dilatation mass density term used in QED, and hence no possibility of properly deriving the mass. The bare mass m_0 is thus renormalized by replacing it with the actual experimental mass m. Using the longitudinal dilatation mass density term as in this paper will provide the correct mass m and eliminate the need for mass renormalization.

9 Discussion and conclusion

This paper provides a framework for the physical description of physical processes at the quantum level based on dislocations in the spacetime continuum within the theory of the Elastodynamics of the Spacetime Continuum (*STCED*).

We postulate that the spacetime continuum has a granularity characterized by a length b_0 corresponding to the smallest elementary Burgers dislocation-displacement vector possible. One inference that comes out of this paper is that the basic structure of spacetime consists of a lattice of cells of size b_0, rather than the "quantum foam" currently preferred in the literature. The "quantum foam" view may well be a representation of the disturbances and fragmentation of the b_0 lattice due to dislocations and other defects in the spacetime continuum.

There are two types of dislocations: Edge dislocations correspond to dilatations (longitudinal displacements) which have an associated rest-mass energy, and are identified with particles. Screw dislocations correspond to distortions (transverse displacements) which are massless and are identified with photons when not associated with an edge dislocation. Arbitrary mixed dislocations can be decomposed into a screw component and an edge component, giving rise to wave-particle duality.

We consider both stationary and moving dislocations, and find that stationary dislocations are simpler to work with due to their cylindrical polar symmetry, but are of limited applicability. Moving screw dislocations are found to be Lorentz invariant. Moving edge dislocations involve both the speed of light corresponding to transverse displacements and the speed of longitudinal displacements c_l. However, the speed of light c upper limit also applies to edge dislocations, as the shear stress becomes infinite everywhere at $v = c$, even though the speed of longitudinal deformations c_l is greater than that of transverse deformations c.

We calculate the strain energy density of both stationary and moving screw and edge dislocations. The strain energy density of the screw dislocation is given by the transverse distortion energy density, and does not have a mass component. On the other hand, the dilatation strain energy density of the edge dislocation is given by the (massive) longitudinal dilatation energy density, and the distortion (massless) strain energy density of the edge dislocation is given by the transverse distortion energy density. This provides a solution to the mass renormalization problem in QED. Quantum Electrodynamics only uses the equivalent of the transverse distortion strain energy density in its calculations, and hence has no possibility of properly deriving the mass, which is in the longitudinal dilatation massive strain energy density term that is not used in QED.

The theory provides an alternative model for Quantum Electrodynamics processes, without the mathematical formalism of QED. In this framework, self-energies and interactions are mediated by the strain energy density of the dislocations. The role played by virtual particles in Quantum Electrodynamics is replaced by the interaction of the strain energy densities of the dislocations. This theory is not perturbative as in QED, but rather calculated from analytical expressions. The analytical equations can become very complicated, and in some cases, perturbative techniques will need to be used to simplify the calculations, but the availability of analytical expressions permits a better understanding of the fundamental physical processes involved.

We provide examples of dislocation-dislocation interactions, applicable to photon-photon, photon-particle, and particle-particle interactions, and of dislocation self-energy calculations, applicable to photons and particles. These equations provide analytical expressions for the non-perturbative calculation of quantum self energies and interaction energies, and provides a physical process replacement for the virtual particle interpretation used in QED.

The theory proposed in this paper is formulated in a formalism based on Continuum Mechanics and General Relativity. This formalism is different from that used in Quantum Mechanics and Quantum Electrodynamics, and is currently absent of quantum states and uncertainties as is commonplace in quantum physics. Both formalisms are believed to be equivalent representations of the same physical phenomena. It may well be that as the theory is developed further, the formalism of orthonormal basis function sets in Hilbert spaces will be introduced to facilitate the solution of problems.

As shown in [47], it is a characteristic of Quantum Mechanics that conjugate variables are Fourier transform pairs of variables. The Heisenberg Uncertainty Principle thus arises because the momentum p of a particle is proportional to its de Broglie wave number k. Consequently, we need to differentiate between the measurement limitations that arise from the properties of Fourier transform pairs of conjugate variables, and any inherent limitations that may or may not exist at the quantum level, independently of the measurement process. Quantum theory currently assumes that the inherent limitations are the same as the measurement limitations. As shown in [47], quantum measurement limitations affect our perception of the quantum environment only, and are not inherent limitations of the quantum level, i.e. there exists a physical world, independently of an observer or a measurement, as seen here. See also the comments in [48, pp. 3–15].

This framework lays the foundation to develop a theory of the physical description of physical processes at the quantum level, based on dislocations in the spacetime continuum, within the theory of the Elastodynamics of the Spacetime Continuum. The basis of this framework is given in this initial paper. This framework allows the theory to be fleshed out in subsequent investigations. Disclinations in the spacetime continuum are expected to introduce new physical processes at the quantum level, to be worked out in future investigations. Additional spacetime continuum fundamental

processes based on ongoing physical defect theory investigations will emerge as they are applied to *STCED*, and will lead to further explanation of current quantum physics challenges.

Submitted on June 30, 2015 / Accepted on July 1, 2015

References

1. Millette P. A. Elastodynamics of the Spacetime Continuum. *The Abraham Zelmanov Journal*, 2012, v. 5, 221–277.
2. Millette P. A. On the Decomposition of the Spacetime Metric Tensor and of Tensor Fields in Strained Spacetime. *Progress in Physics*, 2012, v. 8 (4), 5–8.
3. Millette P. A. The Elastodynamics of the Spacetime Continuum as a Framework for Strained Spacetime. *Progress in Physics*, 2013, v. 9 (1), 55–59.
4. Millette P. A. Derivation of Electromagnetism from the Elastodynamics of the Spacetime Continuum. *Progress in Physics*, 2013, v. 9 (2), 12–15.
5. Millette P. A. Strain Energy Density in the Elastodynamics of the Spacetime Continuum and the Electromagnetic Field. *Progress in Physics*, 2013, v. 9 (2), 82–86.
6. Millette P. A. Dilatation–Distortion Decomposition of the Ricci Tensor. *Progress in Physics*, 2013, v. 9 (4), 32–33.
7. Millette P. A. Wave-Particle Duality in the Elastodynamics of the Spacetime Continuum (STCED). *Progress in Physics*, 2014, v. 10 (4), 255–258.
8. Segel L. A. Mathematics Applied to Continuum Mechanics. Dover Publications, New York, 1987.
9. Landau L. D., Lifshitz E. M., Kosevich A. M. and Pitaevskii L. P. Theory of Elasticity, 3rd ed., revised and enlarged. Butterworth-Heinemann, Oxford, 1986, pp. 108–132.
10. Hull D. and Bacon D. J. Introduction to Dislocations, 5th ed. Elsevier Ltd., Amsterdam, 2011.
11. Weertman J. and Weertman J. R. Elementary Dislocation Theory. Oxford University Press, Oxford, 1992.
12. Nabarro F. R. N., ed. Dislocations in Solids, Volume I, The Elastic Theory. North-Holland Publishing Co., New York, 1979.
13. Kosevich A. M. Crystal Dislocations and the Theory of Elasticity. in Nabarro F. R. N., ed. Dislocations in Solids, Volume I, The Elastic Theory. North-Holland Publishing Co., New York, 1979, pp. 33–141.
14. Hirth R. M. and Lothe J. Theory of Dislocations, 2nd ed. Krieger Publishing Co., Florida, 1982.
15. Edelen, D. G. B. and Lagoudas D. C. Gauge Theory and Defects in Solids. North-Holland Publishing, Amsterdam, 1988.
16. Kleinert H. Gauge Fields in Condensed Matter, Vol. II Stresses and Defects. World Scientific Publishing, Singapore, 1989.
17. Puntigam R. A., Soleng, H. H. Volterra Distortions, Spinning Strings, and Cosmic Defects. *Class. Quantum Grav.*, 1997, v. 14, 1129–1149. arXiv: gr-qc/9604057.
18. Maluf J. W., Goya, A. Space-Time Defects and Teleparallelism. arXiv: gr-qc/0110107.
19. Sabbata V. de, Sivaram C. Spin and Torsion in Gravitation. World Scientific, Singapore, 1994.
20. Rugiero M. L., Tartaglia A. Einstein-Cartan theory as a theory of defects in space-time. arXiv: gr-qc/0306029.
21. Tartaglia A. Defects in Four-Dimensional Continua: a Paradigm for the Expansion of the Universe? arXiv: gr-qc/0808.3216.
22. Unzicker A. Teleparallel Space-Time with Defects yields Geometrization of Electrodynamics with quantized Charges. arXiv: gr-qc/9612061.
23. Unzicker A. What can Physics learn from Continuum Mechanics?. arXiv: gr-qc/0011064.
24. Hossenfelder S. Phenomenology of Space-time Imperfection I: Nonlocal Defects. arXiv: hep-ph/1309.0311.
25. Hossenfelder S. Phenomenology of Space-time Imperfection II: Local Defects. arXiv: hep-ph/1309.0314.
26. Hossenfelder S. Theory and Phenomenology of Spacetime Defects. arXiv: hep-ph/1401.0276.
27. Orowan E. *Z. Phys.*, 1934, v. 89, 605, 634.
28. Polanyi M. *Z. Phys.*, 1934, v. 89, 660.
29. Taylor G. I. *Proc. Roy. Soc.*, 1934, v. A145, 362.
30. Burgers J. M. *Proc. Kon. Ned. Akad. Wetenschap.*, 1939, v. 42, 293, 378.
31. Flügge W. Tensor Analysis and Continuum Mechanics. Springer-Verlag, New York, 1972.
32. Woodside D.A. Uniqueness theorems for classical four-vector fields in Euclidean and Minkowski spaces. *Journal of Mathematical Physics*, 1999, v. 40, 4911—4943.
33. Misner C. W., Thorne K. S., Wheeler J. A. (1973). *Gravitation*, W. H. Freeman and Co., San Francisco, pp.137–138.
34. Eshelby J. D. Energy Relations and the Energy-Momentum Tensor in Continuum Mechanics. in Kanninen M. F., Adler W. F., Rosenfield A. R. and Jaffee R. I., eds. Inelastic Behavior of Solids. McGraw-Hill, New York, 1970, pp. 77–115.
35. Eshelby J. D. The Elastic Energy-Momentum Tensor. *Journal of Elasticity*, 1975, v. 5, 321–335.
36. Eshelby J. D. The Energy-Momentum Tensor of Complex Continua. in Kröner, E. and Anthony K.-H., eds. Continuum Models of Discrete Systems. University of Waterloo Press, Waterloo, 1980, pp. 651–665.
37. Morse M. M., Feshback H. (1953, 1981). *Methods of Theoretical Physics, Part I*. Feshback Publishing, Minneapolis, pp.322–323.
38. Maugin G. Material Inhomogeneities in Elasticity. Chapman & Hall / CRC, Boca Raton, 1993.
39. Eshelby J. D. Aspects of the Theory of Dislocations. in Hopkins H. G. and Sewell M. J., eds. Mechanics of Solids – The Rodney Hill 60th Anniversary Volume.Pergamon Press, Oxford, 1982, pp. 185–225.
40. Wolfram Mathematica Online Integrator. integrals.wolfram.com, June 2015.
41. Weingard R. Virtual Particles and the Interpretation of Quantum Field Theory. in Brown H. R. and Harré R. Philosophical Foundations of Quantum Field Theory. Clarendon Press, Oxford, 1988, pp. 43–58.
42. Brown H. R. and Harré R. Philosophical Foundations of Quantum Field Theory. Clarendon Press, Oxford, 1988, p. 3.
43. Hansson J. On the Origin of Elementary Particle Masses. *Progress in Physics*, 2014, v. 10, 45–47.
44. Wolfram MathWorld Polylogarithm. mathworld.wolfram.com/Polylogarithm.html, June 2015.
45. Lukin M. D. Nonlinear Optics and Quantum Entanglement of Ultra-Slow Single Photons. arXiv: quant-ph/9910094.
46. Marklund M., Shukla P. K. Nonlinear Collective Effects in Photon–Photon and Photon–Plasma Interactions. *Rev. Mod. Phys.*, 2006, v. 78, 591–637. arXiv: hep-ph/0602123.
47. Millette P. A. The Heisenberg Uncertainty Principle and the Nyquist-Shannon Sampling Theorem. *Progress in Physics*, 2013, v. 9 (3), 9–14. arXiv: quant-ph/1108.3135.
48. Auyang S. Y. How is Quantum Field Theory Possible? Oxford University Press, Oxford, 1995.

A Planck Vacuum Pilot Model for Inelastic Electron-Proton Scattering

William C. Daywitt

National Institute for Standards and Technology (retired), Boulder, Colorado. E-mail: wcdaywitt@me.com

This paper describes the scattering of an incident electron from a proton initially at rest, under the assumptions: that the structureless electron interacts directly with the proton and its structure; that the energy and "size" of the electron are determined by its de Broglie radii; and that the shape of the inelastic scattering curve depends upon how deeply the electron core penetrates the proton structure. Deep inelastic scattering ends when the electron is small enough (energetic enough) to penetrate and destroy the proton core and its derived mass.

1 Introduction

The current theory describing electron-proton (e-p) scattering is the Standard Model theory, where the incident electron interacts with the proton via the exchange of a single virtual photon [1, p. 160]. The present paper offers an alternative theory that is based on the emerging Planck vacuum (PV) theory, where the electron interacts directly with the proton [2–5].

In the PV theory both the electron and proton particles are assumed to possess an invisible (vacuum) substructure, while in addition the proton possesses a visible free-space structure due to its positive charge acting on the degenerate PV quasi-continuum (Appendix A). The particle / PV forces and potentials, and their corresponding Compton and de Broglie radii, are associated with this vacuum substructure. The term "structure" by itself refers in what follows exclusively to the free-space proton structure.

2 Electron energy and size

The electron core $(-e_*, m_e)$ exerts the two-term coupling force

$$\frac{(-e_*)(-e_*)}{r^2} - \frac{m_e c^2}{r} \tag{1}$$

on the PV state, where the first $(-e_*)$ belongs to the electron and the second $(-e_*)$ to the separate Planck particles making up the PV continuum. This force difference vanishes

$$\frac{e_*^2}{r_e^2} - \frac{m_e c^2}{r_e} = 0 \tag{2}$$

at the electron Compton radius r_e $(= e_*^2/m_e c^2)$. Treating this vanishing force as a Lorentz invariant constant then leads to the important Compton-(de Broglie) relations for the electron [6]

$$r_e \cdot m_e c^2 = r_d \cdot cp = r_L \cdot E = e_*^2 \qquad (= c\hbar) \tag{3}$$

where p $(= m_e \gamma v)$ and E $(= m_e \gamma c^2)$ are the relativistic momentum and energy of the electron, and e_* is the massless bare charge. The radii r_d $(= r_e/\beta\gamma)$ and r_L $(= r_e/\gamma)$ are the electron de Broglie radii in the space and time directions on the Minkowski space-time diagram, where $\beta = v/c < 1$ and $\gamma = 1/\sqrt{1-\beta^2}$.

From (3) the size of the electron is taken to be the de Broglie radii

$$r_d = \frac{r_e}{\beta\gamma} \approx \frac{r_e}{\gamma} = r_L \tag{4}$$

where the approximation applies to the high energy $(\beta \approx 1)$ calculations of the present paper. With (4) inserted into (3),

$$cp = \frac{e_*^2}{r_d} \approx \frac{e_*^2}{r_L} = E \tag{5}$$

leading to

$$E = cp = \frac{e_*^2}{r_d}\,. \tag{6}$$

Thus to reduce the electron size to the proton Compton radius $(r_d = r_p)$ requires an electron energy equal to $E = e_*^2/r_p$.

The comparisons to follow utilize

$$E = \frac{e_*^2}{r_d} = \frac{e_*^2}{r_p}\frac{r_p}{r_d} = m_p c^2 \frac{r_p}{r_d} \tag{7}$$

to convert electron energies to r_d/r_p ratios. The Lorentz invariance of (2) ensures that equations (3) and (7) apply in any inertial reference frame.

3 Proton structure

The proton substructure arises from the two-term coupling force [7]

$$\frac{(e_*)(-e_*)}{r^2} + \frac{m_p c^2}{r} \tag{8}$$

the proton core (e_*, m_p) exerts on the PV state, where the force vanishes at the proton Compton radius r_p $(= e_*^2/m_p c^2)$.

The proton also possesses a free-space structure (in contradistinction to the electron) in the form of a spherical rest-frame "collar" surrounding the proton core (Appendix A). This collar may affect the formation of the proton de Broglie radii; if, indeed, these radii even exist for the proton. Either way, the following scattering calculations employ only the proton Compton radius from the vanishing of (8).

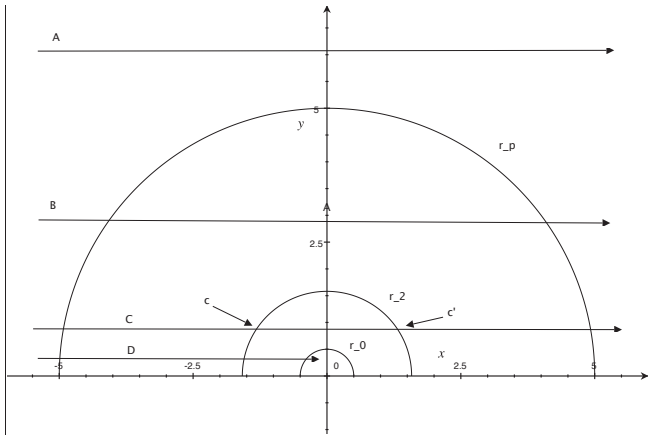

Fig. 1: A highly schematic cross section of the proton structure and four electron-core "trajectories". The radii r_p and $r_2\,(=\,r_p/3.15)$ represent respectively the proton Compton radius of the substructure and the outer radius of the free-space proton structure.

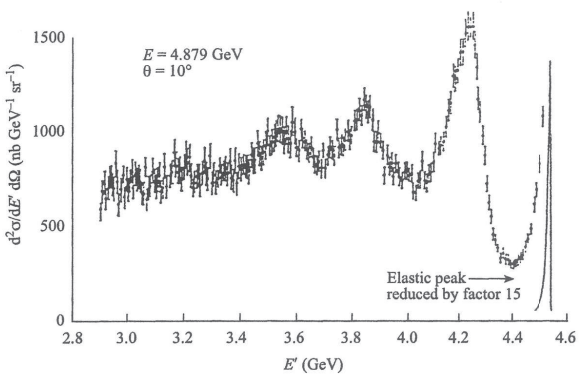

Fig. 2: Elastic and inelastic electron scattering from protons, where E' represents the energy of the scattered electron [9, p. 14] [10]. The scattering angle is 10°. Electron loss increases from right to left.

4 e-p scattering

A highly schematic diagram of the proton cross section is presented in Fig. 1, where r_p is the substructure Compton radius for reference, $r_2\,(=\,r_p/3.15)$ is the outer radius of the proton structure on whose surface resides the apparent charge e of the proton, and r_0 is the radius of the proton core. The latter radius is assumed to be no larger than $r_p/39000$ [7]. Also shown are four electron-core "trajectories" A, B, C, and D, where A and B are propagating in free space and thus represent two elastic e-p scatterings.

Trajectory C ($r_0 < r_d < r_2$) goes through the proton structure, where the electron continuously looses energy (due to excitations of that structure) between its entry and exit points c and c'. Furthermore, since the electron possesses a de Broglie radius (with a corresponding de Broglie wavelength $2\pi r_d$), it exhibits a wave-like nature throughout the trajectory. This wave-like nature, and the finite length (c-c') of the traversed section, produce a resonance within the measured scattering data.

Finally, when the electron energy is great enough ($r_d \ll r_0$) to allow the electron core to penetrate the proton core, this highly energized electron destroys the proton core, leading to the destruction of the proton mass and Compton radius, with a resulting hadron debris field (see Fig. 8.13 in [1, p. 199]).

Fig. 2 shows the experimental scattering data for a beam of 4.879 GeV electrons ($r_d = r_p/5.2$ in (7)) from a proton at rest. The elastic peak at the far right of the figure is represented by B in Fig. 1 with $r_d = r_2$. (This elastic peak is shifted down from the incident electron energy 4.879 GeV to approximately 4.55 GeV ($r_d = r_p/4.9$) by recoil effects.) From the far right to approximately 2.9 GeV on the left the scattering is represented by C in Fig. 1, where the destruction of the proton core has not yet taken place. The three inelastic resonance peaks from left to right in the figure correspond to $r_d \approx r_p/(3.8, 4.1, 4.5)$ from (7).

Fig. 3 shows a repetition of Fig. 2 in a different format, for various scattering angles of the electron. Once more, the destruction of the proton core has not taken place, but the idea of the resonance scattering in the second and fourth paragraphs above is reinforced by the set of five three-peaked curves in the figure. The curves become monotonic when the trajectory between c and c' is deep enough to prevent constructive and destructive interference between reflections at c and c'. Furthermore, when the trajectory is deeper still, D ($r_d \le r_0$), the electron core will scatter off the proton core.

Again, the proton core is destroyed when $E \gg m_p c^2$ ($r_d \ll r_0$). In this case the incident electron energy is sufficient to overcome the loss sustained in crossing the structure interval ($r_2 - r_0 \approx r_2$) to penetrate the proton core.

Appendix A: Structure

This appendix is a brief review of why the proton is structured and the electron is not [7].

The electron and proton are assumed to exert the two coupling forces

$$F(r) = \pm\left(\frac{e_*^2}{r^2} - \frac{mc^2}{r}\right) \tag{A1}$$

on the PV state, where the plus and minus signs refer to the electron and proton respectively. In effect the negative charge of the electron core $(-e_*, m_e)$ in (1) repels the negative PV charges $(-e_*)$ away from this core; while the positive charge in the proton core (e_*, m_p) attracts the PV charges. These oppositely charged Coulomb forces (the first terms in (A1)), close to their respective cores, are the fundamental cause of the structureless electron and the structured proton.

The potential energies associated with (A1) are defined by [7]

$$V(r) - V_0 = \int_{0^+}^{r} F(r')\,dr' \quad \text{with} \quad V(r_c) = 0 \tag{A2}$$

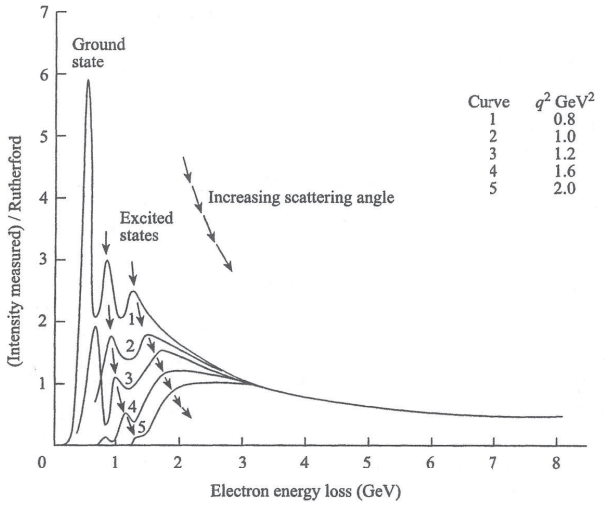

Fig. 3: Inelastic e-p scattering as a function of electron scattering angle [9, p. 17] [11]. Electron loss increases from left to right

where $r_c\,(= e_*^2/mc^2)$ is the Compton radius of either particle and the 0^+ accounts for the finite (but small) size of the cores. This definition leads to

$$V_p(r) \geq 0 \quad \text{and} \quad V_e(r) \leq 0 \tag{A3}$$

where V_p and V_e are the proton/ and electron/PV coupling potentials.

It is shown in the Klein paradox [8, p. 127] that a sufficiently strong positive potential acting on the vacuum state can force a portion of that state into free space, where that part of the vacuum can then be attacked by free-space particles. Thus the positive and negative potentials in (A3) imply that the proton core, but not the electron core, forces a small spherical (in the core's rest frame) portion of the vacuum into the free space around the proton core. *This free-space vacuum "collar" is identified in the PV theory as the proton structure.* Furthermore, this structure leads to an apparent spread in the charge e_* of the proton core (Appendix B).

Appendix B: Charge spread

The polarization of the proton structure by the proton core leads to an apparent spread of the proton charge that is roughly expressed in the proton electric field as

$$E_p(r) = \frac{e(r)}{r^2} \tag{B1}$$

where the spread is

$$e(r) = \begin{cases} e_* & , r < r_0 \\ < e_* & , r_0 < r < r_2 \\ e = \alpha^{1/2} e_* & , r_2 \leq r \end{cases} \tag{B2}$$

$r_2 = r_p/3.15$, and $\alpha\,(\approx 1/137)$ is the fine structure constant. The radius r_2 defines the outer extent of the proton structure.

An important characteristic of this result is the large charge gradient

$$\frac{\Delta e}{\Delta r} = \frac{e - e_*}{r_2 - r_0} \approx -\frac{e_*(1 - \sqrt{\alpha})}{r_2} \approx -\frac{0.92 e_*}{r_2} \tag{B3}$$

between the core charge e_* and the observed proton charge e at r_2. This result explains a similar gradient in the QED spread depicted in Fig. 11.6 of [9, p. 319].

Submitted on June 11, 2015 / Accepted on July 2, 2015

References

1. Thomson M. Modern Particle Physics. McGraw-Hill Book Company, U.S.A., 2013.
2. Daywitt W. C. The Planck Vacuum. *Progress in Physics*, 2009, v. 5 (1), 20. See also www.planckvacuum.com.
3. Daywitt W. C. The Source of the Quantum Vacuum. *Progress in Physics*, 2009, v. 5 (1), 27.
4. Daywitt W. C. The Electron and Proton Planck-Vacuum Coupling Forces and the Dirac Equation. *Progress in Physics*, 2014, v. 10, 114.
5. Daywitt W. C. The Strong and Weak Forces and their Relationship to the Dirac Particles and the Vacuum State. *Progress in Physics*, 2015, v. 11, 18.
6. Daywitt W. C. The de Broglie Relations Derived from the Electron and Proton Coupling to the Planck Vacuum State. *Progress in Physics*, 2015, v. 11 (2), 189.
7. Daywitt W. C. The Structured Proton and the Structureless Electron as Viewed in the Planck Vacuum Theory. *Progress in Physics*, 2015, v. 11 (2), 117.
8. Gingrich D. M. Practical Quantum Electrodynamics. CRC, The Taylor & Francis Group, Boca Raton, 2006.
9. Aitchison I. J. R., Hey A. J. G. Gauge Theories in Particle Physics, Vol. 1. Taylor & Francis, New York, London, 2003.
10. Bartel W. B. *et al*. Electroproduction of Pions Near the Δ1236 Isobar and the Form Factor $G_M^*(q^2)$ of the $(\gamma N\Delta)$-Vertex. *Phys. Lett.*, 1968, v. 28B, 148.
11. Perkins D. Introduction to High Energy Physics, 1st ed. Addison Wesley Publishing , 1972.

Antiparticles and Charge Conjugation in the Planck Vacuum Theory

William C. Daywitt

National Institute for Standards and Technology (retired), Boulder, Colorado. E-mail: wcdaywitt@me.com

This short paper defines charge conjugation in terms of the Planck vacuum substructure rather than the particle equation of motion. As such, the corresponding operator applies to the proton as well as the electron. Results show that, like their electron and proton counterparts, the positron is structureless while the antiproton possesses a structure consisting of a small vacuum "collar" surrounding its charged core.

1 Introduction

At present the Planck vacuum (PV) theory includes a model for both the electron and proton and the PV state to which these two particles are coupled [1]. But there is a problem: while the theory suggests a source for the negative bare charge $(-e_*)$ of the electron (the current PV state itself), it is mute when it comes to the positive bare charge (e_*) of the proton. What follows assumes a bifurcated vacuum state that includes both negative and positive bare charges $(\mp e_*)$. This bifurcated state is understood to mean that at each point in free space there exists a PV subspace consisting of a charge doublet $(\mp e_*)$, to either branch of which a free particle charge can be coupled.

The charge conjugation operator C from the quantum theory is an operator that changes particles into antiparticles, and visa versa [2, p. 118]. An analogous operator is defined below to expand the PV model to include the particle-antiparticle symmetries and a source for the proton charge (e_*).

2 Charge conjugation

The electron and proton cores, $(-e_*, m_e)$ and (e_*, m_p) respectively, exert the two particle/PV coupling forces

$$\pm\left(\frac{e_*^2}{r^2}-\frac{mc^2}{r}\right) \tag{1}$$

on the PV state, where the plus and minus signs in (1) refer to the electron and proton respectively. At their respective Compton radii these forces reduce to

$$F_e=\frac{(-e_*)(-e_*)}{r_e^2}-\frac{m_ec^2}{r_e}=\frac{e_*^2}{r_e^2}-\frac{m_ec^2}{r_e}=0 \tag{2}$$

and

$$F_p=\frac{(e_*)(-e_*)}{r_p^2}+\frac{m_pc^2}{r_p}=-\left(\frac{e_*^2}{r_p^2}-\frac{m_pc^2}{r_p}\right)=0 \tag{3}$$

where $r_e\,(=e_*^2/m_ec^2)$ and $r_p\,(=e_*^2/m_pc^2)$ are the electron and proton Compton radii. The first $(-e_*)$ and second $(-e_*)$ in (2) belong to the electron core and PV charges respectively. The charge (e_*) in (3) belongs to the proton core. The vanishing forces F_e and F_p are Lorentz invariant constants; and the two forces on the right side of (2) are the "weak" forces, while the two on the right side of (3) are the "strong" forces.

If it is assumed that the charge conjugation operator C' applies only to free-particle charges, then from (2) and (3)

$$C'F_e=\frac{(e_*)(-e_*)}{r_e^2}-\frac{m_ec^2}{r_e}=-\left(\frac{e_*^2}{r_e^2}+\frac{m_ec^2}{r_e}\right)\neq 0 \tag{4}$$

and

$$C'F_p=\frac{(-e_*)(-e_*)}{r_p^2}+\frac{m_pc^2}{r_p}=\frac{e_*^2}{r_p^2}+\frac{m_pc^2}{r_p}\neq 0 \tag{5}$$

both of which destroy the electron and proton Compton radii because the equations are nonvanishing. Since the corresponding antiparticles should possess a Compton radius like their particle counterparts, the C' operator is not a valid charge conjugation operator.

If it is assumed, however, that the charge conjugation operator C applies to both the free-space particle charge and the PV charge doublet, then (2) and (3) yield

$$CF_e=\frac{(e_*)(e_*)}{r_e^2}-\frac{m_ec^2}{r_e}=\frac{e_*^2}{r_e^2}-\frac{m_ec^2}{r_e}=0 \tag{6}$$

and

$$CF_p=\frac{(-e_*)(e_*)}{r_p^2}+\frac{m_pc^2}{r_p}=-\left(\frac{e_*^2}{r_p^2}-\frac{m_pc^2}{r_p}\right)=0 \tag{7}$$

where both the electron and proton Compton radii are preserved in their antiparticles. Equations (6) and (7) imply that the equations in (1) are also the antiparticle/PV coupling forces. It is clear from the first charges in (6) and (7), (e_*) and $(-e_*)$, that the positron is positively charged and that the antiproton carries a negative charge.

3 Comments

The second charges $(-e_*)$ in the first terms of (2) and (3), and the second charges (e_*) in the first terms of (6) and (7), suggest that free particles and their antiparticles exist in two separate spaces, corresponding respectively to the negative and positive branches of the PV charge doublet.

In addition to the C operator preserving electron and proton Compton radii, the form of the first terms in (6) and (7)

imply that the positron is structureless and that the antiproton has structure [1, App. A]. This mirrors those same qualities in the electron and proton, the first terms in (2) and (3).

As an aside, it is interesting to apply C to the electron equation of motion. The Dirac equation for the electron can be expressed as [2, p. 74]

$$ic\hbar\left(\frac{\partial}{c\partial t}+\boldsymbol{\alpha}\cdot\nabla\right)\psi = m_e c^2\beta\psi \tag{8}$$

or, using $c\hbar = e_*^2$,

$$\left[i(-e_*)(-e_*)\left(\frac{\partial}{c\partial t}+\boldsymbol{\alpha}\cdot\nabla\right)-m_e c^2\beta\right]\psi = 0 \tag{9}$$

where the first $(-e_*)$ belongs to the electron and the second to the negative branch of the PV charge doublet. The corresponding positron equation of motion is then obtained from the charge conjugation of (9)

$$\begin{aligned} &C\left[i(-e_*)(-e_*)\left(\frac{\partial}{c\partial t}+\boldsymbol{\alpha}\cdot\nabla\right)-m_e c^2\beta\right]\psi \\ &=\left[i(e_*)(e_*)\left(\frac{\partial}{c\partial t}+\boldsymbol{\alpha}\cdot\nabla\right)-m_e c^2\beta\right]\psi_c = 0 \end{aligned} \tag{10}$$

where ψ_c is the positron spinor that obeys the same equation (9) as the electron spinor ψ. Due to the second (e_*) in (10), it is clear that the positron belongs in the positive branch of the PV doublet.

The same calculations in (8)–(10) are not applicable to the proton particle because, due to the vacuum "collar" (of radius $r_p/3.15$) surrounding the proton core (e_*, m_p), the proton does not obey a Dirac equation of motion. In effect, the proton cannot be modeled as a point charge because of this "collar", even though its core (e_*, m_p) is orders-of-magnitude smaller than its Compton radius r_p.

Submitted on July 5, 2015 / Accepted on July 13, 2015

References

1. Daywitt W.C. A Planck Vacuum Pilot Model for Inelastic Electron-Proton Scattering. *Progress in Physics*, v. 11 (4), 308, 2015.
2. Gingrich D.M. *Practical Quantum Electrodynamics*. CRC, The Taylor & Francis Group, Boca Raton, 2006.

The Burgers Spacetime Dislocation Constant b_0 and the Derivation of Planck's Constant

Pierre A. Millette

PierreAMillette@alumni.uottawa.ca, Ottawa, Canada

In a previous paper, a framework for the physical description of physical processes at the quantum level based on dislocations in the spacetime continuum within STCED (Spacetime Continuum Elastodynamics) was proposed and it was postulated that the spacetime continuum has a granularity characterized by a length b_0 corresponding to the smallest elementary Burgers dislocation vector possible. Based on the identification of screw dislocations in the spacetime continuum with photons, the relation between the Burgers constant b_0 and Planck's constant h is determined. Planck's constant is expressed in terms of the spacetime continuum constants. The calculated value of b_0 is found to be equivalent to the Planck length within the approximations of the derivation. Numerical values of the spacetime constants $\bar{\kappa}_0$, $\bar{\mu}_0$ and $\bar{\rho}_0$ are derived. A consistent set of the spacetime constants is proposed based on the Burgers spacetime dislocation constant b_0 being equivalent to the Planck length ℓ_P.

1 Introduction

A previous paper [1] provided a framework for the physical description of physical processes at the quantum level based on dislocations in the spacetime continuum within the theory of the Elastodynamics of the Spacetime Continuum (*STCED*). Dislocations in the spacetime continuum represent the fundamental displacement processes that occur in its structure, corresponding to basic quantum phenomena and quantum physics in *STCED*.

Spacetime Continuum Elastodynamics (*STCED*) [2–5] is based on analyzing the spacetime continuum within a continuum mechanical and general relativistic framework. As shown in [2], for an isotropic and homogeneous spacetime continuum, the *STC* is characterized by the stress-strain relation

$$2\bar{\mu}_0\varepsilon^{\mu\nu} + \bar{\lambda}_0 g^{\mu\nu}\varepsilon = T^{\mu\nu} \tag{1}$$

where $T^{\mu\nu}$ is the energy-momentum stress tensor, $\varepsilon^{\mu\nu}$ is the resulting strain tensor, and

$$\varepsilon = \varepsilon^{\alpha}{}_{\alpha} \tag{2}$$

is the trace of the strain tensor obtained by contraction. $\bar{\lambda}_0$ and $\bar{\mu}_0$ are the Lamé elastic constants of the spacetime continuum: $\bar{\mu}_0$ is the shear modulus and $\bar{\lambda}_0$ is expressed in terms of $\bar{\kappa}_0$, the bulk modulus:

$$\bar{\lambda}_0 = \bar{\kappa}_0 - \bar{\mu}_0/2 \tag{3}$$

in a four-dimensional continuum.

A dislocation is characterized by its dislocation vector, known as the *Burgers vector*, b^μ in a four-dimensional continuum, defined positive in the direction of a vector ξ^μ tangent to the dislocation line in the spacetime continuum [6, pp. 17–24].

As discussed in [1], the spacetime continuum, at the quantum level, is assumed to have a granularity characterized by a length b_0 corresponding to the smallest elementary Burgers dislocation vector possible in the *STC*. Then the magnitude of a Burgers vector can be expressed as a multiple of the elementary Burgers vector:

$$b = nb_0. \tag{4}$$

We find that b is often divided by 2π in dislocation equations, and hence the constant

$$\hbar = \frac{b}{2\pi}, \tag{5}$$

is also defined.

In this paper, we explore the relation between the spacetime Burgers dislocation constant b_0 and Planck's constant, and derive the value of the spacetime continuum constants.

2 Screw dislocations in quantum physics

There are two types of dislocations [1]: 1) Edge dislocations corresponding to dilatations, longitudinal displacements with an associated rest-mass energy, are identified with particles, and 2) screw dislocations corresponding to distortions, transverse displacements which are massless, are identified with photons. Arbitrary mixed dislocations can be decomposed into a screw component and an edge component, giving rise to wave-particle duality [5].

Hence screw dislocations in the spacetime continuum are massless, transverse deformations, and are identified specifically with photons. As shown in [1], the screw dislocation Burgers vector is equal to the wavelength of the screw dislocation

$$b = \lambda. \tag{6}$$

This result is illustrated in Fig. 1.

If we consider a stationary screw dislocation in the spacetime continuum, with cylindrical polar coordinates (r, θ, z),

Fig. 1: A wavelength of a screw dislocation.

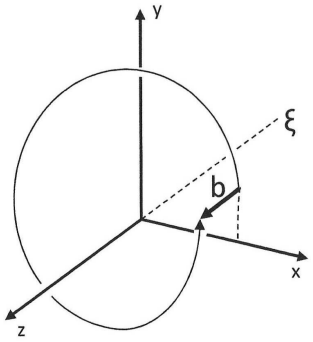

with the dislocation line along the z-axis (see Fig. 2), then the Burgers vector is along the z-axis and is given by $b_r = b_\theta = 0$, $b_z = b$, the magnitude of the Burgers vector.

The only non-zero component of the deformation is given by [6, pp. 60–61]

$$u_z = \frac{b}{2\pi}\,\theta = \text{ƀ}\,\tan^{-1}\frac{y}{x}. \tag{7}$$

Similarly, the only non-zero components of the stress and strain tensors are given by

$$\begin{aligned}\sigma_{\theta z} &= \frac{b}{2\pi}\,\frac{\bar{\mu}_0}{r}\\ \varepsilon_{\theta z} &= \frac{b}{4\pi}\,\frac{1}{r}\end{aligned} \tag{8}$$

respectively.

The strain energy density of the screw dislocation is given by the transverse distortion energy density [2, Eq. (74)]. The non-zero components of the strain tensor are as defined in (8). Hence

$$\mathcal{E}_\perp = \bar{\mu}_0\left({\varepsilon_{\theta z}}^2 + {\varepsilon_{z\theta}}^2\right). \tag{9}$$

Substituting from (8),

$$\mathcal{E}_\perp = \frac{\bar{\mu}_0\, b^2}{8\pi^2}\,\frac{1}{r^2} = \mathcal{E}. \tag{10}$$

3 Planck's constant

Based on our identification of screw dislocations in the space-time continuum with photons, we can determine the relation between the Burgers constant b_0 and Planck's constant h.

Even though the photon is massless, its energy is given by the strain energy density of the screw dislocation, equivalent to the transverse distortion energy density. As shown in [2, Eq. (147)],

$$\hat{p}^2c^2 = 32\bar{\kappa}_0\,\mathcal{E}_\perp, \tag{11}$$

where $\hat{p}$ is the momentum density. For a screw dislocation, substituting for $\mathcal{E}_\perp$ from (10) in (11), we obtain

$$\hat{p}^2c^2 = 32\bar{\kappa}_0\,\frac{\bar{\mu}_0\, b^2}{8\pi^2}\,\frac{1}{r^2}. \tag{12}$$

The kinetic energy density $\hat{p}c$ has to be equivalent to the wave energy density $\widehat{h\nu}$ for the screw dislocation (photon):

$$\hat{p}c = \widehat{h\nu}. \tag{13}$$

The photon's energy is given by

$$h\nu = \int_V \widehat{h\nu}\,\mathrm{d}V = \widehat{h\nu}\,V \tag{14}$$

where V is the volume of the screw dislocation. We consider the smallest Burgers dislocation vector possible and replace b with the elementary Burgers dislocation vector b_0 and V with the smallest volume V_0 to derive Planck's constant. Combining (14), (13) and (12), (14) becomes

$$h = \sqrt{\frac{16\bar{\kappa}_0\,\bar{\mu}_0\,{b_0}^2}{(2\pi r)^2}}\,\frac{V_0}{\nu}. \tag{15}$$

Using (6), the frequency $\nu = c/\lambda$ becomes $\nu = c/b_0$ for the smallest Burgers dislocation vector considered. Substituting into (15), the equation becomes

$$h = \frac{4\sqrt{\bar{\kappa}_0\,\bar{\mu}_0}\,b_0}{2\pi r}\,\frac{V_0 b_0}{c}. \tag{16}$$

The volume of one wavelength of the screw dislocation can be approximated by a cylinder and, using (6), written as

$$V = \pi r^2\lambda = \pi r^2 b, \tag{17}$$

which in the limit as $b \to b_0$, becomes

$$V_0 = \pi r^2 b_0. \tag{18}$$

Substituting for V_0 into (16), the equation becomes

$$h = \frac{4\sqrt{\bar{\kappa}_0\,\bar{\mu}_0}\,b_0}{2\pi r}\,\frac{\pi r^2 b_0^2}{c}. \tag{19}$$

Fig. 2: A stationary screw dislocation in cylindrical polar coordinates (r, θ, z) [6, p. 60].

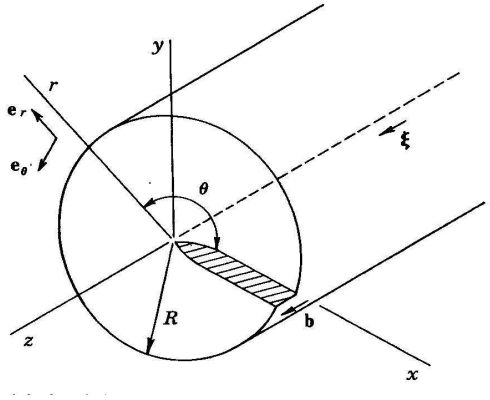

Simplifying,

$$h = \frac{2\sqrt{\bar{\kappa}_0\,\bar{\mu}_0}}{c}\, r b_0^3, \tag{20}$$

and in the limit as r approaches b_0, becomes

$$h = 2\frac{\sqrt{\bar{\kappa}_0\,\bar{\mu}_0}\, b_0^4}{c} \tag{21}$$

where the units of h are J-s as expected. This is the basic definition of Planck's constant h in terms of the Lamé spacetime constants and the Burgers spacetime dislocation constant b_0.

This relation can be further simplified using $\bar{\mu}_0 = 32\bar{\kappa}_0$ from [2, Eq. (150)]. Then

$$h = 8\sqrt{2}\,\frac{\bar{\kappa}_0\, {b_0}^4}{c} = \frac{1}{2\sqrt{2}}\,\frac{\bar{\mu}_0\, {b_0}^4}{c}. \tag{22}$$

Numerically,

$$\bar{\mu}_0\, {b_0}^4 = 2\sqrt{2}\, hc = 5.8\times 10^{-25}\,\mathrm{J\,m}. \tag{23}$$

The value of the spacetime shear modulus $\bar{\mu}_0$ is not a known physical constant, neither is the value of the spacetime bulk modulus $\bar{\kappa}_0$. However, Macken [8] has derived a value of $\bar{\kappa}_0 = 4.6\times 10^{113}\,\mathrm{J/m^3}$ which as we will see in Section 4 is expected to be a valid estimate. Using $\bar{\mu}_0 = 32\bar{\kappa}_0$ from Millette [2, Eq. (150)], this yields a value of

$$\bar{\mu}_0 = 1.5\times 10^{115}\,\mathrm{J/m^3}. \tag{24}$$

Note that the units can be expressed equivalently as $\mathrm{N/m^2}$ or $\mathrm{J/m^3}$. Substituting for $\bar{\mu}_0$ in (23), we obtain the value of the elementary Burgers vector

$$b_0 = 1.4\times 10^{-35}\,\mathrm{m}. \tag{25}$$

This value compares very favorably with the Planck length 1.6×10^{-35} m. Given the approximations used in its derivation, this suggests that the elementary Burgers vector b_0 and the Planck length are equivalent.

With these constants, we are now in a position to calculate the remaining unknown spacetime constant, the density of the spacetime continuum $\bar{\rho}_0$. Using the relation [2]

$$c = \sqrt{\frac{\bar{\mu}_0}{\bar{\rho}_0}}, \tag{26}$$

the density of the spacetime continuum is

$$\bar{\rho}_0 = 1.7\times 10^{98}\,\mathrm{kg/m^3}. \tag{27}$$

4 Analytic form of constants b_0 and $\bar{\kappa}_0$

Blair [7, p. 3–4] writes Einstein's field equation as

$$\mathbf{T} = \frac{c^4}{8\pi G}\mathbf{G},$$

where $\mathbf{T}$ is the stress energy tensor, $\mathbf{G}$ is the Einstein curvature tensor and G is the universal gravitational constant. He notes the very large value of the proportionality constant. This leads him to point out that spacetime is an elastic medium that can support waves, but its extremely high stiffness means that extremely small amplitude waves have a very high energy density. He notes that the coupling constant $c^4/8\pi G$ can be considered as a modulus of elasticity for spacetime, and identifies the quantity c^3/G with the characteristic impedance of spacetime [7, p. 45].

From this, Macken [8] derives an "interactive bulk modulus of spacetime", which we identify with the spacetime continuum bulk modulus, given by

$$\bar{\kappa}_0 = \frac{c^7}{\hbar G^2}. \tag{28}$$

The result obtained for the numerical value of b_0 and its close correspondance to the Planck length suggests that the value of $\bar{\kappa}_0$ proposed in [8] is correct. From Millette [2, Eq. (150)] we then have

$$\bar{\mu}_0 = 32\frac{c^7}{\hbar G^2}. \tag{29}$$

From (23), we can write

$${b_0}^4 = 2\sqrt{2}\,\frac{hc}{\bar{\mu}_0}. \tag{30}$$

Substituting from (29), this relation becomes

$${b_0}^4 = \frac{\sqrt{2}\pi}{8}\,\frac{\hbar^2 G^2}{c^6} \tag{31}$$

and finally

$$b_0 = \left(\frac{\pi}{4\sqrt{2}}\right)^{\frac{1}{4}}\sqrt{\frac{\hbar G}{c^3}} = 0.86\,\ell_P \tag{32}$$

where ℓ_P is Planck's length, defined as [9]

$$\ell_P = \sqrt{\frac{\hbar G}{c^3}}. \tag{33}$$

Hence, as mentioned in Section 3, this suggests that the elementary Burgers dislocation vector b_0 and the Planck length ℓ_P are equivalent within the approximations of the derivation.

5 Recommended constants

Starting from the statement that the Burgers spacetime dislocation constant b_0 is equivalent to the Planck length ℓ_P, we derive the constant of proportionality of (21). We thus set

$$h = k\,\frac{\sqrt{\bar{\kappa}_0\,\bar{\mu}_0}\, b_0^4}{c} \tag{34}$$

where k is the improved constant of proportionality for the relation. Substituting for $\bar{\kappa}_0$ from (28), for $\bar{\mu}_0$ from (29), and setting $b_0 = \ell_P$ from (33), the equation becomes

$$h = k\ \sqrt{32}\ \frac{c^7}{\hbar G^2}\ \frac{1}{c}\ \frac{\hbar^2 G^2}{c^6} \tag{35}$$

from which we obtain

$$k = \frac{\pi}{2\sqrt{2}}. \tag{36}$$

Hence, with the Burgers spacetime dislocation constant b_0 equivalent to the Planck length ℓ_P, the basic definition of Planck's constant h in terms of the Lamé spacetime constants and the Burgers spacetime dislocation constant b_0 is given by

$$h = \frac{\pi}{2\sqrt{2}}\ \frac{\sqrt{\bar{\kappa}_0\,\bar{\mu}_0}\,b_0^4}{c}. \tag{37}$$

In terms of $\bar{\kappa}_0$, we have

$$h = 2\pi\ \frac{\bar{\kappa}_0\,b_0^4}{c} \tag{38}$$

or

$$\hbar = \frac{\bar{\kappa}_0\,b_0^4}{c} \tag{39}$$

and in terms of $\bar{\mu}_0$, we have

$$h = \frac{\pi}{16}\ \frac{\bar{\mu}_0\,b_0^4}{c}. \tag{40}$$

As stated, the Burgers spacetime dislocation constant b_0 is given by

$$b_0 = \ell_P = \sqrt{\frac{\hbar G}{c^3}} \tag{41}$$

and the spacetime continuum Lamé constants are as per (28) and (29):

$$\begin{aligned} \bar{\kappa}_0 &= \frac{c^7}{\hbar G^2} \\ \bar{\mu}_0 &= 32\frac{c^7}{\hbar G^2}. \end{aligned} \tag{42}$$

It is recommended that the relations in this section be retained as the official definition of these constants.

6 Discussion and conclusion

We have expressed Planck's constant in terms of the spacetime continuum constants $\bar{\kappa}_0$, $\bar{\mu}_0$, b_0, and the speed of light c. The calculated value of b_0 compares very favorably with the Planck length and suggests that the elementary Burgers vector b_0 and the Planck length are equivalent within the approximations of the derivation. An estimate of the numerical values of the spacetime constants $\bar{\kappa}_0$, $\bar{\mu}_0$ and $\bar{\rho}_0$ is also obtained, based on Macken's [8] derived value of $\bar{\kappa}_0$ which is found to be a valid estimate, given the agreement between b_0 and the Planck length ℓ_P.

A consistent set of recommended spacetime constants is obtained based on setting the Burgers spacetime dislocation constant b_0 equivalent to the Planck length ℓ_P.

Submitted on July 15, 2015 / Accepted on July 18, 2015

References

1. Millette P. A. Dislocations in the Spacetime Continuum: Framework for Quantum Physics. *Progress in Physics*, 2015, v. 11 (4), 287–307.
2. Millette P. A. Elastodynamics of the Spacetime Continuum. *The Abraham Zelmanov Journal*, 2012, v. 5, 221–277.
3. Millette P. A. The Elastodynamics of the Spacetime Continuum as a Framework for Strained Spacetime. *Progress in Physics*, 2013, v. 9 (1), 55–59.
4. Millette P. A. Strain Energy Density in the Elastodynamics of the Spacetime Continuum and the Electromagnetic Field. *Progress in Physics*, 2013, v. 9 (2), 82–86.
5. Millette P. A. Wave-Particle Duality in the Elastodynamics of the Spacetime Continuum (STCED). *Progress in Physics*, 2014, v. 10 (4), 255–258.
6. Hirth R. M. and Lothe J. Theory of Dislocations, 2nd ed. Krieger Publishing Co., Florida, 1982.
7. Blair D. G., ed. The Detection of Gravitational Waves. Cambridge University Press, Cambridge, 1991.
8. Macken J. A. The Universe is Only Spacetime, Rev. 7.1. Self-published, Santa Rosa, CA, 2013, p. 4-24.
9. Kaku M. Quantum Field Theory, A Modern Introduction. Oxford University Press, Oxford, 1993, p. 10.

Quantum Gravity Experiments

Reginald T. Cahill

School of Chemical and Physical Sciences, Flinders University. E-mail: reg.cahill@flinders.edu.au

A new quantum gravity experiment is reported with the data confirming the generalisation of the Schrödinger equation to include the interaction of the wave function with dynamical space. Dynamical space turbulence, via this interaction process, raises and lowers the energy of the electron wave function, which is detected by observing consequent variations in the electron quantum barrier tunnelling rate in reverse-biased Zener diodes. This process has previously been reported and enabled the measurement of the speed of the dynamical space flow, which is consistent with numerous other detection experiments. The interaction process is dependent on the angle between the dynamical space flow velocity and the direction of the electron flow in the diode, and this dependence is experimentally demonstrated. This interaction process explains gravity as an emergent quantum process, so unifying quantum phenomena and gravity. Gravitational waves are easily detected.

1 Introduction

The quantum theory of gravity explains the gravitational acceleration of matter as caused by the refraction of quantum waves by the time dependence and spatial inhomogeneities of the dynamical space flow [1]. This has been tested against numerous experimental gravitational phenomena [2]: bore hole g anomalies, flat spiral galaxy rotation curves, black hole systematics and star orbit data [3], lensing of light by stars and galaxies, expanding universe supernova redshift-brightness data without need for dark matter or dark energy [4], anisotropic Brownian motion [5], directional dependence of nuclear decay rates [6]. The key initial experiments detected the dynamical space using light speed anisotropy gas-mode Michelson optical interferometers and EM speed anisotropy in RF coaxial cables. More recently quantum detectors have been discovered that directly detected the space flow [7, 8]. All these different experimental techniques reveal a turbulent space flow speed from direction RA $\sim$ 4.5hrs, Dec=80°S, with a speed of $\sim$500 km/s. These velocities are moderated over a year by the orbital motion of the Earth.

The dynamical space quantum detectors, which use reverse biased Zener Diodes, Fig. 1 and Fig. 2, have given rise to a new critical test of the quantum theory of gravity, reported herein, namely an orientation dependent effect, which directly tests the modified Schrödinger equation which includes the effects of the dynamical space. This uses collocated quantum detectors which are either in parallel configuration or anti-parallel configuration, Fig. 3.

2 Quantum gravity

Dynamical space is a phenomenon repeatedly detected by a variety of experimental techniques [2]. The Schrödinger equation must be extended to include the dynamical space by using the Euler time derivative $\partial/\partial t \to \partial/\partial t + \mathbf{v}(\mathbf{r},t)\cdot\nabla$, where $\mathbf{v}(\mathbf{r},t)$ is the classical field description of the dynamical space

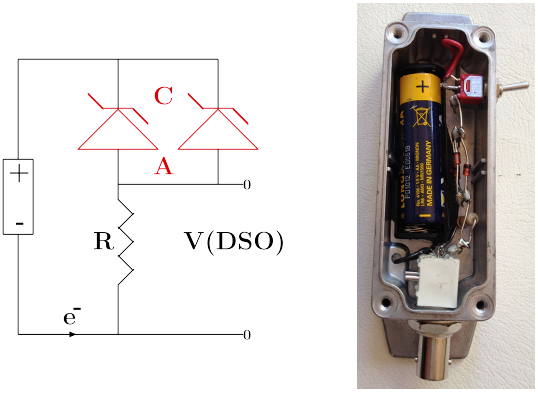

Fig. 1: Left: Circuit of Zener Diode Space Flow Detector, showing 1.5 V AA battery, two 1N4728A zener diodes operating in reverse bias mode, and having a Zener voltage of 3.3 V, and resistor R= 10 KΩ. Voltage V across resistor is measured and used to determine the turbulent space flow driven fluctuating tunnelling current through the Zener diodes. Correlated currents from two collocated detectors are shown in Fig. 4. Right: Photo of detector with 5 Zener diodes in parallel.

velocity:

$$i\hbar\frac{\partial\psi(\mathbf{r},t)}{\partial t} = -\frac{\hbar^2}{2m}\nabla^2\psi(\mathbf{r},t) + V(\mathbf{r},t)\psi(\mathbf{r},t) \\ -i\hbar\mathbf{v}(\mathbf{r},t)\cdot\nabla\psi(\mathbf{r},\mathbf{t})\,. \tag{1}$$

Here $\mathbf{v}(\mathbf{r},t)$ is the velocity field describing the dynamical space at a classical field level, and the coordinates $\mathbf{r}$ give the relative location of $\psi(\mathbf{r},t)$ and $\mathbf{v}(\mathbf{r},t)$, relative to a Euclidean embedding space, and also used by an observer to locate structures. This is not an aether embedded in a non-dynamical space, but a dynamical space which induces an

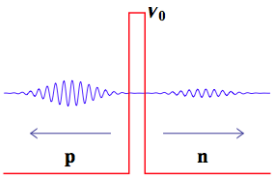

Fig. 2: Electron wave function after barrier quantum transmission and reflection from the LHS, with p and n denoting semiconductor type, showing partially transmitted component and partially reflected component, when the diode is operated in reverse-bias mode, as shown in Fig. 1. Space flow fluctuations raise and lower the energy of the incident wave function, which changes the relative magnitude of these two components.

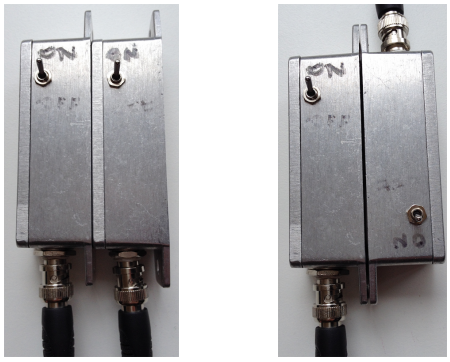

Fig. 3: Left: Two collocated detectors in parallel configuration, Right: anti-parallel configuration. The corresponding data is shown in Fig. 4. The data in Fig. 5 was obtained with one of the detectors in the parallel configuration shifted by 1cm, and together aligned with the Earth's spin axis.

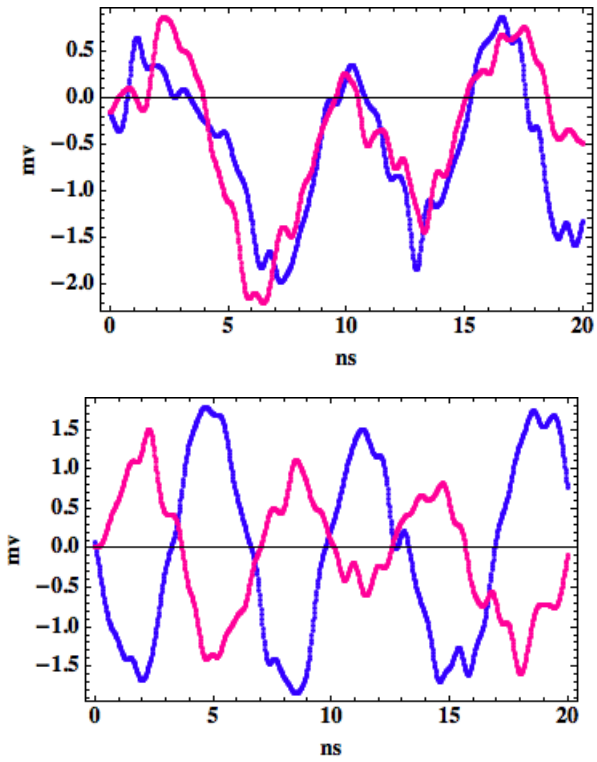

Fig. 4: Correlated current fluctuations, as indicated by voltage across resistor R, and with DSO operated with 1 MΩ AC input, and no filters. Top: From two collocated parallel detectors, as shown in Fig. 1. Bottom: Anti-correlated current fluctuations from the two collocated but anti-parallel detectors, also shown in Fig. 1. This data confirms the dynamical consequences of the $-i\hbar\mathbf{v}\cdot\nabla\psi$ term in the new Schrödinger equation. This term is the origin of the quantum gravity.

embedding space or coordinate system. The Euler derivative was first introduced by Euler in 1757 when beginning the study of fluids, and ensures that fluid dynamics are relative to the fluid, and not fixed relative to an observer. Hertz in 1890 introduced this Euler derivative into Maxwell's EM theory, but was unaware of the meaning of $\mathbf{v}(\mathbf{r},t)$. The detection of the dynamical space then mandates the use of the Euler derivative in the Schrödinger equation [1].

A significant effect follows from (1), namely the emergence of gravity as a quantum effect: an Ehrenfest wave-packet analysis reveals the classical limit and shows that the acceleration of a localised wave packet, due to the space terms alone, when $V(\mathbf{r},t)=0$, given by $\mathbf{g}=\mathrm{d}^2<\mathbf{r}>/\mathrm{d}t^2$, gives [1]

$$g(\mathbf{r},t)=\frac{\partial\mathbf{v}}{\partial t}+(\mathbf{v}\cdot\nabla)\mathbf{v} \tag{2}$$

That derivation showed that the acceleration is independent of the mass m: whence we have the derivation of the Weak Equivalence Principle, discovered experimentally by Galileo.

Note that the emergent quantum-theoretic matter acceleration in (2), is also, and independently, the constituent acceleration $\mathbf{a}(\mathbf{r},t)$ of the space flow velocity field,

$$\begin{aligned}\mathbf{a}(\mathbf{r},t)&=\lim_{\Delta t\to 0}\frac{\mathbf{v}(\mathbf{r}+\mathbf{v}(\mathbf{r},t)\Delta t,t+\Delta t)-\mathbf{v}(\mathbf{r},t)}{\Delta t}\\&=\frac{\partial\mathbf{v}}{\partial t}+(\mathbf{v}\cdot\nabla)\mathbf{v}\,.\end{aligned} \tag{3}$$

which describes the acceleration of a constituent element of space by tracking its change in velocity. This means that space has a structure that permits its velocity to be defined and detected, which experimentally has been done. This then suggests, from (2) and (3), that the simplest dynamical equation for $\mathbf{v}(\mathbf{r},t)$ is

$$\nabla\cdot\left(\frac{\partial\mathbf{v}}{\partial t}+(\mathbf{v}\cdot\nabla)\mathbf{v}\right)=-4\pi G\rho(\mathbf{r},t);\quad\nabla\times\mathbf{v}=\mathbf{0} \tag{4}$$

because it then gives $\nabla.\mathbf{g}=-4\pi G\rho(\mathbf{r},t)$, $\nabla\times\mathbf{g}=\mathbf{0}$, which is Newton's inverse square law of gravity in differential form. Hence the fundamental insight is that Newton's gravitational acceleration field $\mathbf{g}(\mathbf{r},t)$ for matter is really the acceleration

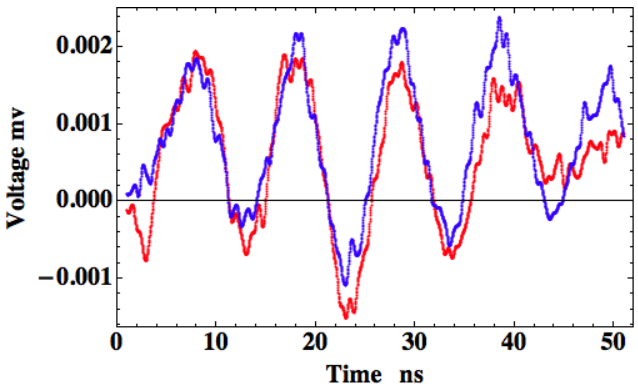

Fig. 5: Correlated current fluctuations, as indicated by voltage across resistor R, and with DSO operated with 1 MΩ AC input, and no filters. Detectors in parallel configuration, and orientated parallel to Earth axis , but offset by 1 cm, and plotted with a time offset of 20 ns, implying a speed of 500 km/s.

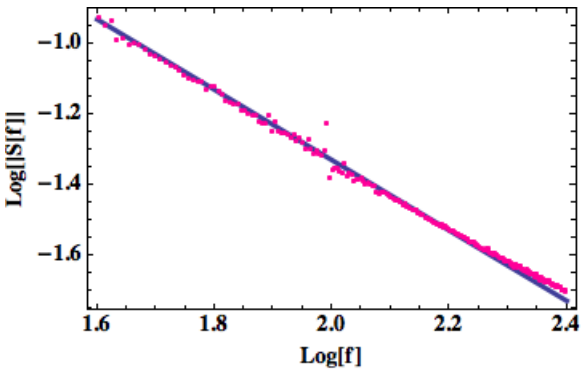

Fig. 6: Typical frequency spectrum data, showing $Log[S[f]]$ plotted against $Log[f]$ from the current fluctuation data, showing slope of −1.0, as the solid plot, revealing a $1/f$ spectrum, typical of Johnson 1/f electronic systems "noise", and so explaining the origin of Johnson noise [10] , and also demonstrating again the fractal structure of the dynamical space.

field $\mathbf{a}(\mathbf{r}, t)$ of the structured dynamical space and that quantum matter acquires that acceleration because it is fundamentally a wave effect, and the wave is refracted by the accelerations of space. While (4) is the simplest 3-space dynamical equation, this derivation permits further terms which maintain Newton's inverse square law external to a spherical mass, but which otherwise leads to new observed aspects of gravity, which have previously been ascribed to "dark matter", but which are now revealed to be a dynamical aspect of space.

3 Quantum gravity directional experiment

The presence of the $-i\hbar\mathbf{v}\cdot\nabla$ dynamical space term provides a critical test of the emergent quantum gravity theory. For plane wave electrons, $\psi \sim e^{(i\mathbf{k}\cdot\mathbf{r}-i\omega t)}$, the space interaction term changes the energy of the electrons, for uniform $\mathbf{v}$,

$$E = \hbar\omega \rightarrow \hbar\omega + \hbar\mathbf{k}\cdot\mathbf{v} \qquad (5)$$

This space induced energy shift changes the potential energy barrier electron quantum tunnelling amplitudes in a reverse-biased Zener diode, Fig. 2. This effect is easily measured by means of the circuit in Fig. 1. A critical implication is that the electron tunnelling current must depend on the angle θ between $\mathbf{k}$ and $\mathbf{v}$, as in in $\mathbf{k}\cdot\mathbf{v} = kv\cos\theta$. To test this effect two collocated detectors were arranged as in Fig. 3, with parallel and anti-parallel configurations. The resulting currents are shown in Fig. 4, and confirm this angle dependence effect.

As well if one of the detectors in the parallel configuration is moved by 1 cm, then a time delay effect of 20 ns is detected, as in Fig. 5. This corresponds to a spatial speed of ~500 km/s from a S direction, as detected in numerous other experiments.

Most electronic devices exhibit Johnson noise [10], where the electron current has a characteristic $1/f$ spectrum. The origin of this noise has never been explained until now. The frequency spectrum for one of the current fluctuations in Fig. 4 is shown in Fig. 6, and exhibits a $1/f$ spectrum. This implies that Johnson noise is a consequence of the fractal structure of the space flow.

4 Conclusions

The experimental detection of dynamical space required generalisation of Maxwell's EM Theory, Schrödinger's Quantum Theory and a corresponding generalisation of the Dirac Quantum Theory [9], and the determination of a dynamical theory for space. As a consequence it has been discovered that gravity is an emergent quantum effect. Here we have reported new key tests of this quantum theory of gravity by detecting predicted angle dependencies of quantum barrier electron tunnelling currents. The fluctuating electron currents amount to the detection of wave effects of the dynamical space: gravitational waves [11].

Submitted on August 6, 2015 / Accepted on August 10, 2015

References

1. Cahill R. T. Dynamical Fractal 3-Space and the Generalised Schrödinger Equation: Equivalence Principle and Vorticity Effects, *Progress in Physics*, 2006, v. 1, 27–34.
2. Cahill R. T. Discovery of Dynamical 3-Space: Theory, Experiments and Observations - A Review, *A. J. Spac. Sci.*, 2013, v. 1 (2), 77–93.
3. Cahill R. T. and Kerrigan D. Dynamical Space: Supermassive Black Holes and Cosmic Filaments, *Progress in Physics*, 2011, v. 4, 79–82.
4. Cahill R. T. and Rothall D. Discovery of Uniformly Expanding Universe, *Progress in Physics*, 2012, v. 1, 63–68.
5. Cahill R. T. Dynamical 3-Space: Anisotropic Brownian Motion Experiment, *Progress in Physics*, 2015, v. 11 (3), 204–207.

6. Shnoll S. E., Cosmophysical Factors in Stochastic Processes, American Research Press, Rehoboth, NM, 2012. http://www.ptep-online.com.
7. Cahill R. T. Nanotechnology Quantum Detectors for Gravitational Waves: Adelaide to London Correlations Observed, *Progress in Physics*, 2013, v. 4, 57–62.
8. Cahill R. T. Gravitational Wave Experiments with Zener Diode Quantum Detectors: Fractal Dynamical Space and Universe Expansion with Inflation Epoch, *Progress in Physics*, 2014, v. 10 (3), 131–138.
9. Cahill R. T. Dynamical 3-Space: Neo-Lorentz Relativity, *Physics International*, 2013, v. 4 (1), 60–72.
10. Johnson J. B. The Schottky Effect in Low Frequency Circuits, *Phys. Rev.*, 1925, v. 26, 71–85.
11. Cahill R. T. Review of Gravitational Wave Detections: Dynamical Space, *Physics International*, 2014, v. 5 (1), 49–86.

Dispelling Black Hole Pathologies Through Theory and Observation

Robin James Spivey

Biological Sciences, Bangor University, Brambell, Deiniol Road, Bangor, Gwynedd, Great Britain
E-mail: y.gofod@gmail.com

Astrophysical black holes are by now routinely identified with metrics representing eternal black holes obtained as exact mathematical solutions of Einstein's field equations. However, the mere existence and discovery of stationary solutions is no guarantee that they can be attained through dynamical processes. If a straightforward physical caveat is respected throughout a spacetime manifold then the ingress of matter across an event horizon is prohibited, in accordance with Einstein's expectation. As black hole formation and growth would be inhibited, the various pathological traits of black holes such as information loss, closed timelike curves and singularities of infinite mass density would be obviated. Gravitational collapse would not terminate with the formation of black holes possessing event horizons but asymptotically slow as the maximal time dilation between any pair of worldlines tends towards infinity. The remnants might be better described as dark holes, often indistinguishable from black holes except in certain astrophysically important cases. The absence of trapped surfaces circumvents topological censorship, with potentially observable consequences for astronomy, as exemplified by the remarkable electromagnetic characteristics, extreme energetics and abrupt extinction of quasars within low redshift galaxies.

1 Introduction

Quasars are exceptionally luminous objects located at cosmological distances [1]. Rapid fluctuations in their emissions arguably provide the most compelling hints that black holes of some description exist in nature. The empirically determined "M-sigma relation" points to a causal kinematic connection between black hole growth and galactic evolution, with motions of nearby gas and stars providing irrefutable evidence that $10^6 \sim 10^9\ M_\odot$ black hole candidates are present [2]. This has led many researchers to conclude that the universe is home to a multitude of black holes conforming to one of the stationary, asymptotically flat, black hole metrics – in accordance with the claim of a leading relativist that the "black holes of nature are the most perfect macroscopic objects that are in the universe" [3].

Potentially pre-dating the earliest stars, quasars may have fostered galaxy formation [4]. However, the question of how their central engines operate remains clouded in considerable uncertainty. Furthermore, astronomical observations have not been satisfactorily reconciled with theory. For instance, the abrupt cessation of quasar activity during the early universe calls for some efficient shutdown mechanism [5]. It is now generally believed that virtually all galactic nuclei harbour a supermassive black hole, most galaxies have undergone a period of quasar activity in the past, black holes have at present scarcely lost any mass through Hawking radiation and a healthy fraction of galaxies are still rich in gas. It is therefore puzzling that the temporary revival of quasar activity is not occasionally observed, especially within gas-rich galaxy clusters. A glaring inconsistency arises with the currently in vogue gas-starvation model of quasar extinction.

Karl Schwarzschild provided the first solution to the field equations of general relativity (GR), obtaining a spherically symmetric metric describing an eternal black hole* with an event horizon [6]. After lengthy deliberation, Einstein remained dismissive of the notion that objects with an event horizon might actually exist in nature, pointing out that a clock arriving at an event horizon would totally cease to advance compared to more remotely situated clocks [7]. The more interesting case of dynamic gravitational collapse within GR, abandoning the assumption of stationary geometry, was tackled analytically that same year by Oppenheimer & Snyder [8]. The mathematical results, as valid now as they ever were [9], establish that from the perspective of a distant observer the implosion initially accelerates until the contraction becomes relativistic, whereupon the implosion rate declines – ultimately halting just as the critical radius is approached. From this vantage, an event horizon only forms in an asymptotic sense, after the infinite passage of time.

Oppenheimer & Snyder also commented on their results from the perspective of the infalling matter. They found that as external time approaches infinity, the proper time along the worldline of an infalling particle tends towards some finite value. They then considered what might happen at later proper times of the infalling particle, apparently without pausing to consider whether time could physically continue to advance for the infalling particle: "after this time an observer comoving with the matter would not be able to send a light signal from the star". It is currently fashionable to ignore Einstein's objection regarding infinite time dilation. But is

*The term "black hole" was not coined until some years after Einstein's departure, the alternative "frozen star" had previously been widely used.

that wise? The field of black hole physics is by now plagued by a variety of serious difficulties. Closed timelike curves seem to be unavoidable within rotating black hole spacetimes, with potentially disturbing connotations for causality and hence physics at its most fundamental level. The notion that information might be captured and destroyed by black holes has also troubled theoretical physicists for decades [10, 11]. This "information paradox" recently led to the suggestion that black holes only possess apparent horizons [12] as opposed to genuine event horizons: features traditionally regarded as the defining hallmarks of true black holes [13].

There is also a widespread expectation that naturally occurring black holes lack "hair" and comply with the principle of topological censorship [14], rapidly settling down either to a Kerr-Newman or, more realistically, a Kerr geometry corresponding to an electrically uncharged, rotating black hole. As will be discussed, astronomical observations cast significant doubt on the reliability of this common assumption. Moreover, due to the generality of results obtained in dynamical collapse scenarios such as Oppenheimer & Snyder considered, there is a suspicion that Einstein was right: it may be difficult or impossible to produce stationary black holes through physically realistic processes.

The goal of this work is to argue that these various conceptual problems can vanish, without departing from Einstein's gravitational theory, if a straightforward physical consideration is respected throughout a spacetime manifold. This caveat does not impinge upon general covariance and the mathematical apparatus of general relativity is unchanged. A discussion then follows of why quasar observations support the contention that black holes lack event horizons and might be better described as *dark holes*.

2 The Schwarzschild black hole

The Schwarzschild metric represents a non-rotating eternal black hole with the spherically symmetric spacetime

$$ds^2 = \left(1-\frac{r_s}{r}\right)c^2dt^2 - \left(1-\frac{r_s}{r}\right)^{-1}dr^2 - r^2(d\theta^2+\sin^2\theta d\phi^2) \quad (1)$$

where ds is the spacetime interval, t represents the proper time of a stationary clock at spatial infinity, $(r,\, \theta,\, \phi)$ are the usual spherical coordinates ($2\pi r$ being the circumference of a circle at radius r). The event horizon is located at $r = r_s = 2Gm/c^2$, known as the Schwarzschild radius of a black hole. The gravitating mass of the black hole, m, is concentrated at the origin.

As is well-known, if the metric is expressed in this way it has a coordinate singularity at $r = r_s$, the (critical) radius of the event horizon, despite the lack of matter there (the spacetime itself is only singular at $r = 0$). The exterior solution, $r > r_s$, accurately approximates the spacetime outside a spherically symmetric star [15]. This region is well-behaved and suffices for the present discussion.

For a particle following a timelike worldline, $ds^2 \equiv c^2d\tau^2$ where τ is the proper time of the particle and $d\tau \equiv 0$ for null particles (light rays). Therefore, along the worldline of any particle, $ds^2 \geqslant 0$, and the following inequality must hold:

$$\left(1-\frac{r_s}{r}\right)c^2dt^2 \geqslant \left(1-\frac{r_s}{r}\right)^{-1}dr^2 + r^2(d\theta^2+\sin^2\theta d\phi^2). \quad (2)$$

It is convenient to rearrange this expression to obtain

$$\frac{1}{(1-\frac{r_s}{r})^2}\left(\frac{dr}{dt}\right)^2 + \frac{r^2}{1-\frac{r_s}{r}}\left(\frac{d\theta}{dt}\right)^2 + \frac{r^2\sin^2\theta}{1-\frac{r_s}{r}}\left(\frac{d\phi}{dt}\right)^2 \leqslant c^2. \quad (3)$$

The Schwarzschild metric is asymptotically flat and, for regions far outside the event horizon, $r \gg r_s$, the effects of gravitational time dilation are negligible. One then finds that $(dr/dt)^2 + r^2\ (d\theta/dt)^2 + r^2\sin^2\theta\ (d\phi/dt)^2 \leqslant c^2$ which, considering the spherical coordinate system, confirms the expectation that the speed of light is insurmountable in special relativity, with the possible exception of tachyonic particles.

3 Spacetime coherency

Spacetime is a four-dimensional continuum, a differentiable and connected Lorentzian manifold. In general relativity it is dynamically acted upon by gravitation so as to alter the geodesics of motion. General relativity is a global theory: the presence of mass-energy does not merely influence the local spacetime, but the entire spacetime manifold. Thus, gravity's range is limited only by the size of the universe. General relativity abides by the principle of general covariance allowing its physical laws to be expressed independently of coordinates.

The order in which events occur is observer-dependent in both special and general relativity. Nevertheless, the *relative rate at which time elapses along two worldlines* (i.e. time dilation/contraction) can be uniquely defined whether the separation between the worldlines is timelike, null or spacelike. Time dilation is a non-local, coordinate-independent quantity encoding genuine physics which is necessary for global consistency. For an arbitrary number n of distinct test particles with proper times $\tau_1, \tau_2 \ldots \tau_n$, it must hold that

$$\frac{d\tau_1}{d\tau_n} \times \prod_{i=1}^{n-1}\frac{d\tau_{i+1}}{d\tau_i} = 1. \quad (4)$$

If general relativity is applied to the universe then the proper elapsed time, τ, along any worldline cannot exceed the time since the big bang, even if the universe is spatially infinite. Hence, along any worldline, the proper time $\tau < \infty$ and the proper distance $\ell < \infty$. Recognising that proper time τ is an affine parameter along the worldline $x^\alpha(\tau)$, for a specified spacetime manifold the demand of finite proper time along all worldlines within the universe can be formally stated as

$$\forall\ \ x^\alpha(\tau) : \tau < \infty. \quad (5)$$

It should be self-evident that this constraint will be satisfied by any physically realistic spacetime manifold. Non-compliance, as would occur once the advancement of proper times along any pair of worldlines could not proceed in tandem, would break the global coherency and connectedness of the spacetime continuum. Such a basic physical requirement must have priority over all "philosophical" concerns, an issue returned to in the discussion. Spacetime is not merely a local union of space and time but a global one. Failure to appreciate that localised physics can have wider implications for a spacetime manifold may be at the root of some persistent confusions in current black hole research.

4 Time dilation between arbitrary particles

For lightlike particles, the Schwarzschild metric provides a relationship involving two time coordinates t and τ

$$\left(\frac{d\tau}{dt}\right)^2 = \alpha c^2 - \frac{1}{\alpha}\left(\frac{dr}{dt}\right)^2 - r^2\left(\frac{d\theta}{dt}\right)^2 - r^2\sin^2\theta\left(\frac{d\phi}{dt}\right)^2. \quad (6)$$

The parameter α is defined as $\alpha \equiv 1 - r_s/r$ for the range $r > r_s$ so that α is strictly positive with $0 < \alpha \leqslant 1$. This expression allows the time dilation relative to Schwarzschild time t, a coordinate independent physical quantity, to be determined for an arbitrarily moving test particle located anywhere outside the event horizon.

Although particles travelling at the speed of light experience no passage of proper time ($d\tau = 0$), photons travelling radially towards the event horizon are eventually brought to a halt since the original metric then reduces to $(dr/dt)^2 = \alpha^2 c^2$ and, in the limit as $r \to r_s$, one sees that $\alpha \to 0$. This represents a worst case scenario since, for non-radial motion of the photon, $(dr/dt)^2 < \alpha^2 c^2$. For a purely radial ingoing photon, $dr/dt = -\alpha c$ and so the minimum Schwarzschild time, $\Delta t_{\min}$, required for a photon to travel from an initial radius r_0 to a final radius r_*, with $r_0 > r_* > r_s$, is given by

$$\Delta t_{\min} = t_* - t_0 = \int_{r_0}^{r_*}\left(\frac{dt}{dr}\right)dr = \int_{r_*}^{r_0}\frac{dr}{\alpha c}$$
$$= \frac{1}{c}\int_{r_*}^{r_0}\frac{r\,dr}{r - r_s} = \frac{r_0 - r_*}{c} + \frac{r_s}{c}\ln\left(\frac{r_0 - r_s}{r_* - r_s}\right). \quad (7)$$

Due to the denominator in the logarithm term, as $r_* \to r_s$, this time interval grows without limit. Hence, regardless of the location at which photons are emitted outside the black hole, gravitational time dilation prohibits them reaching the event horizon in finite time according to the clock of a Schwarzschild observer.

In order to broaden this result, a quantity v is now defined such that

$$v^2 = \frac{1}{\alpha^2}\left(\frac{dr}{dt}\right)^2 + \frac{r^2}{\alpha}\left(\frac{d\theta}{dt}\right)^2 + \frac{r^2\sin^2\theta}{\alpha}\left(\frac{d\phi}{dt}\right)^2. \quad (8)$$

With reference to (3), it is apparent that one can write $v^2 \leqslant c^2$. This is consistent with v representing a physical velocity whose magnitude, corrected for relative motion and gravitational time dilation, remains bounded by the speed of light. It can then be seen from (6) that

$$(d\tau/dt)^2 = \alpha(c^2 - v^2)$$

and consequently $0 \leqslant (d\tau/dt)^2 \leqslant 1$. The time dilation relation between two arbitrary worldlines with proper times τ_1 and τ_2 exploring the exterior Schwarzschild geometry can therefore be obtained from formula (9) where $\alpha_1 = 1 - r_s/r_1$ and $\alpha_2 = 1 - r_s/r_2$ with subscripts referring to worldlines 1 and 2 respectively. Thus, α_1 and α_2 have the same range as α such that consideration is strictly restricted to the region external to the event horizon. Since $v_1^2 \leqslant c^2$ and $v_2^2 \leqslant c^2$, neither the numerator nor denominator of (9) can be negative under any circumstances.

If a timelike particle following worldline 2 approaches the event horizon, $r_2 \to r_s$, then $\alpha_2 \to 0$ with the numerator of (9) remaining positive. For a timelike observer moving along worldline 1 sufficiently distant from the event horizon that $\alpha_1 \gg \alpha_2$ it is then apparent that $d\tau_2/d\tau_1 \to 0$, meaning that proper time ceases to advance along worldline 2. Noting that timelike particles take longer to approach the event horizon than light rays and that $d\tau_1/dt$ remains finite for any timelike observer comfortably outside the event horizon, one may conclude that

> *According to any external observer following a timelike worldline, light rays and timelike particles require infinite proper time to reach the event horizon of a Schwarzschild black hole.*

Because (5) must be respected it follows that

> *Since infalling particles cannot experience the passage of time beyond that corresponding to infinite proper time along all other worldlines, they are incapable of penetrating the event horizon of a Schwarzschild black hole.*

These statements are completely independent of the (arbitrary) choice of coordinate system. Furthermore, they do not require that observers be either stationary or infinitely remote. Indeed, observers could be relatively close to the event horizon without violating the assumption that $\alpha_1 \gg \alpha_2$. There is no optical illusion at play associated with the time of flight of photons – the conclusion holds for inanimate clocks lacking the faculty of vision just as well as it does for conventional observers.

Note also that there is no need for any special synchronisation procedure between the two particles: infinite time dilation prevents the ingress of matter across an event horizon as long as external clocks continue to mark time. If $\tau_2 = 0$ at the commencement of worldline 2 and the event horizon is approached as $\tau_2 \to \tau_h$, a finite proper time, then regardless of where and when worldline 1 commences it is still true that

$$\left(\frac{d\tau_2}{d\tau_1}\right)^2 = \left(\frac{d\tau_2}{dt}\right)^2 \div \left(\frac{d\tau_1}{dt}\right)^2 = \frac{\alpha_2 c^2 - \frac{1}{\alpha_2}\left(\frac{dr_2}{dt}\right)^2 - r_2^2\left(\frac{d\theta_2}{dt}\right)^2 - r_2^2 \sin^2\theta_2 \left(\frac{d\phi_2}{dt}\right)^2}{\alpha_1 c^2 - \frac{1}{\alpha_1}\left(\frac{dr_1}{dt}\right)^2 - r_1^2\left(\frac{d\theta_1}{dt}\right)^2 - r_1^2 \sin^2\theta_1 \left(\frac{d\phi_1}{dt}\right)^2} = \frac{\alpha_2\,(c^2 - v_2^2)}{\alpha_1\,(c^2 - v_1^2)}. \tag{9}$$

$\tau_1 \to \infty$ as $\tau_2 \to \tau_h$. This is manifestly so because

$$\begin{aligned}\tau_1(\tau_2 \to \tau_h) &= \int_0^{\tau_h} \left(\frac{d\tau_1}{d\tau_2}\right) d\tau_2 \\ &= \int_0^{\tau_h} \left(\frac{d\tau_2}{d\tau_1}\right)^{-1} d\tau_2 \to \infty.\end{aligned} \tag{10}$$

Proper times separating events along worldlines are invariant quantities, as are infinitesimal proper times. Thus, the same can be said of the ratio of the rate of passage of proper times along distinct worldlines. If the previous calculation were to be repeated using so-called horizon-penetrating coordinates (e.g. Lemaître, Novikov, Gullstrand-Painlevé, Kruskal-Szekeres, ingoing Eddington-Finkelstein [16]) the same results would of course be obtained by virtue of general covariance. The fact that the time dilation approaches infinity as $r_2 \to r_s$ has nothing to do with the Schwarzschild coordinate singularity at r_s, the coordinates being regular and well-behaved for all $r > r_s$, a range that was entirely adequate for the purposes of this analysis.

Therefore, contrary to some common assertions, an astronaut could not fall into a black hole without incident. Although τ_2 would remain finite in such circumstances, τ_1 would approach infinity as $\tau_2 \to \tau_h$. The astronaut encounters no immediate physical impediment at the event horizon but, due to the demand of global coherency and the need for proper times along worldlines to remain finite in (5), the condition $\tau_2 \leqslant \tau_h$ must be respected. Thus, the worldline of the astronaut would terminate as $\tau_2 \to \tau_h$, *corresponding to a situation in which the spacetime manifold totally ceases to evolve*. The astronaut simply would not experience proper times later than τ_h which, in effect, would be the moment when his or her worldline reaches future timelike infinity within the Schwarzschild spacetime. Times $\tau_2 > \tau_h$ would necessarily be fictitious and unphysical due to violation of (5).

For all $\tau_2 < \tau_h$, there is no consistency problem. One is not obliged to make an *either or* selection, exclusively choosing between the infalling or remote observer perspectives – they are mutually compatible projections of a globally coherent spacetime manifold. However, if one insists on abandoning coherency to consider the physically impossible case $\tau_2 > \tau_h$, a choice is then mandatory but the results are physically meaningless. That infalling matter indefinitely hovers above the horizon from the perspective of a distant Schwarzschild observer is a well-established result [15, 17]. In order to further clarify matters, it has been extended here to arbitrarily situated and potentially moving external observers who may be in quite close proximity to the event horizon.

The impermeability of the event horizon due to time dilation effects has in recent years been highlighted in the context of the black hole information paradox [18]. Furthermore, several core arguments promulgating that belief that event horizons are traversable have been dispelled [19]. While it is well-known that nothing can escape from a black hole, this analysis suggests that event horizons cannot be traversed in *any* direction whilst offering a readily comprehensible explanation as to why that is. Although angular momentum has been ignored here for simplicity, one would not expect its influence to alter the conclusions. Rotation would only represent an additional barrier, further hindering the arrival of particles at the event horizon of a Kerr black hole.

5 Dynamically formed black holes

A classic general relativity textbook originally published four decades ago argued that eternal black holes provide an excellent approximation to the outcome of gravitational collapse [15]. This advice may have been taken a tad too literally. Clearly, if event horizons are bidirectionally impermeable then the black hole information paradox would be trivially resolved. The interior geometry of the Schwarzschild metric may satisfy the field equations, but the constraint (5) suggests it cannot be arrived at through gravitational collapse, it is merely a hypothetical arrangement. Spacetime coherency issues aside, the equivalent rest mass energy of the Schwarzschild singularity goes no way towards counterbalancing its gravitational potential energy which, by any realistic assessment, is infinitely negative. Therefore, a Schwarzschild black hole and a collapsing star of the same mass forming a dark hole frozen in time have vastly different energies and are hence inequivalent on energy conservation grounds.

If the proper time for an infalling particle is advanced without regard for physics elsewhere then the spacetime can decouple and become non-connected, leading to a host of conceptual difficulties. For physically realistic gravitational collapse, however, it is not that infalling matter would hover in suspension above an event horizon – but that an event horizon would never form, in keeping with the external observer perspective of Oppenheimer & Snyder's analysis. However, in the unlikely event that the universe were host to fully-formed eternal black holes, their event horizons would behave as impenetrable barriers to infalling matter. Due to time-reversal symmetry, the geometry of spacetime in general relativity is as much a function of the future distribution of mass and energy as the past distribution, endowing the theory with a teleological quality. Thus, the event horizons of such hypo-

thetical black holes could in principle expand in anticipation of infalling matter so that time dilation halts the ingress of matter sooner than it might otherwise do. Notice that such expansion need not involve any increase in the gravitational potential of infalling matter since the potential near the event horizon is independent of black hole mass.

Hawking radiation arises due to separation of virtual particle pairs in the vicinity of a black hole event horizon [20], causing eternal black holes to evaporate with a perfect thermal spectrum, devoid of information content. Conversely, frozen stars with their rich, history-dependent structure, are able to radiate in the regular black body manner – thus avoiding information loss [21]. However, this issue is of lesser importance to the present discussion than the need for spacetime to remain coherent and connected. Black hole research has not led to many testable predictions but this consideration can have readily observable astronomical implications.

6 Topological admissibility

Trapped surfaces are defined as surfaces from which light rays initially pointing outwards are obliged to converge inwardly. The existence of a trapped surface is a precondition of several well-known theorems in general relativity. The event horizon of a Schwarzschild black hole is a null surface inside which surfaces equidistant from the horizon are all trapped. According to the Penrose-Hawking singularity theorems [22–24], a trapped surface inevitably leads to a geodesically incomplete spacetime manifold, implying the imminent formation of a singularity. However, if time dilation and global spacetime considerations prohibit the formation of event horizons then trapped surfaces cannot naturally arise and the singularity theorems have no physical relevance. By the same logic, the closed timelike curves of rotating eternal black holes would be avoided. Speculations concerning the physics internal to an event horizon are invulnerable to falsification and hence, strictly speaking, outside the scope of empirical science. However, although the presence of event horizons cannot be directly verified [13], evidence of their non-existence could in principle be obtained.

Like the singularity theorems, the principle of topological censorship [14] assumes the presence of a trapped surface. Therefore, if time dilation guards against event horizon formation, the gravitational collapse of a rapidly spinning cloud of gas would be capable of forming an axisymmetric structure of toroidal topology. Due to its dynamic nature, this scenario also falls outside the scope of earlier constraints on black hole topology [25, 26]. If physically realistic astrophysical black holes can be toroidal, the astronomical implications could be observable from afar.

Amongst the most energetic phenomena of the universe, quasars outshine galaxies by as many as three orders of magnitude. They were most abundant at redshifts of $z \sim 2$ when the universe was less than 20% its present age and are significantly more scarce by now [27]. They create bipolar outflows [28], axially aligned relativistic jets penetrating intergalactic space and ultimately forming gigantic radio lobes as their energy is dissipated. Often chaotically turbulent, the jets are comprised of electrically charged particles which can form knots via magnetohydrodynamic processes. The orientation of the jets exhibits long-term stability, hinting at a direct dependency on the angular momentum vector of a supermassive black hole as opposed to that of an accretion disk of relatively low mass which is vulnerable to significant disruption by the assimilation of roving stars. This is another weakness of models seeking to account for jet formation in terms of a magnetised accretion disk.

The discovery of various metrics describing stationary spacetimes in which black holes are completely described by mass, angular momentum and electromagnetic charge alone led to the "no-hair conjecture". Though the Schwarzschild and Kerr-Newman metrics are lacking in "follicles", it is very natural to expect macroscopic departures from these metrics during realistic collapse scenarios. Furthermore, since the formation of trapped surfaces would violate spacetime coherency (5), crucial assumptions underpinning the singularity theorems and the principle of topological censorship may not apply.

Providing its assumptions are satisfied, topological censorship requires the central aperture of a toroidal black hole to seal up so rapidly that a ray of light lacks sufficient time to traverse it. Numerical simulations have provided some support for this [29]. However, computational approaches almost invariably adopt horizon-penetrating coordinates and fail to enforce the physical requirement (5). Instead, event horizons are located retrospectively after simulations terminate, without global consistency checks.

Theoretically, metrics describing black holes with toroidal event horizons have been obtained for anti-de Sitter backgrounds with a negatively valued cosmological constant. In such situations, Λ can be arbitrarily small [30]. Thus, toroidal event horizons are only marginally prohibited when considering eternal black holes in asymptotically flat spacetimes. However, if trapped surfaces cannot realistically form during gravitational collapse then topological censorship is bypassed entirely, leaving the toroidal dark hole (TDH) a viable possibility. Most stars capable of undergoing core collapse are massive, hence rapidly reaching the ends of their lifecycles. They are likely to retain sufficient angular momentum from their formation that during implosion their cores will adopt a toroidal geometry, if only transiently. A toroidal core can be supported by degeneracy (electron/neutron) pressure but, for very massive and rapidly rotating stars, direct collapse to a TDH is conceivable. Any of these eventualities could have potentially explosive consequences, scattering ejecta deep into space [31].

The angular momentum of a Kerr black hole is bounded by $|J| \leqslant GM^2/c$. In the field of black hole thermodynam-

ics, the temperature at which the event horizon radiates is proportional to its surface gravity. This vanishes for an extremal black hole, implying extremality is unattainable by the third law of black hole thermodynamics. However, for a TDH lacking an event horizon, angular momentum should approximately scale with the major radius of the torus. Thus, the Kerr bounds, $-GM^2/c < J < GM^2/c$, could easily be exceeded. Accumulation of angular momentum beyond the Kerr limit may buffer TDH topology, even if accretion is erratic. Evidence has recently emerged of a supermassive black hole within a galactic nucleus rotating at a near extremal rate [32].

Nature possesses only two long range forces and, of the two, electromagnetism is far stronger than gravity. Furthermore, gravity is purely attractive, making it ill-suited as a mechanism for launching relativistic jets of charged particles flowing directly away from a supermassive black hole. Therefore, it is virtually certain that electromagnetism is primarily responsible for jet production. There are no magnetic monopoles in nature but electrically charged particles make up all atoms. That ultrarelativistic jets of charged particles can be sustained for millions of years strongly suggests that the central black hole must itself be electrically charged.

Traditional models have nevertheless taken black holes to be electrically neutral due to common assumptions regarding their topology and the fact that plasma of a surrounding accretion disk can swiftly neutralise any electrical charge accumulating on a spheroidal black hole. A charged (Kerr-Newman) black hole would necessarily possess a magnetosphere due to its rotation but its flux lines would lead directly to the event horizon: oppositely charged particles would be strongly attracted to it, spiralling along the lines of magnetic flux to swiftly neutralise the black hole. Hence, theorists have struggled to explain the extreme energetics of quasars. The popular Blandford-Znajek mechanism [33] appeals to a strongly magnetised accretion disk whose flux lines thread the event horizon of an electrically neutral, Kerr black hole, enabling some coupling to its rotational energy. However, the model has been criticised because one would not expect an accretion disk to become strongly magnetised and the degree of magnetisation required seems infeasibly large [34].

The difficulty is overcome in the TDH case, a strong candidate for the central engine of quasars [31]. It has been previously proposed that a toroidal black hole might be stabilised by quantum gravitational effects [35] but in the present work there is no need for any departure from classical general relativity. If a TDH amasses an electrical charge, e.g. via the proton-electron charge/mass ratio disparity, neutralisation processes involving ambient plasma particles will be suppressed due to topological considerations. Flux lines of the induced dipolar magnetosphere along which charged particles tend to spiral would not lead towards the TDH. Instead, they would locally run parallel to its surface, as depicted in figure 1. Plasma from an orbiting accretion disk would be channelled along the flux lines towards the central aperture,

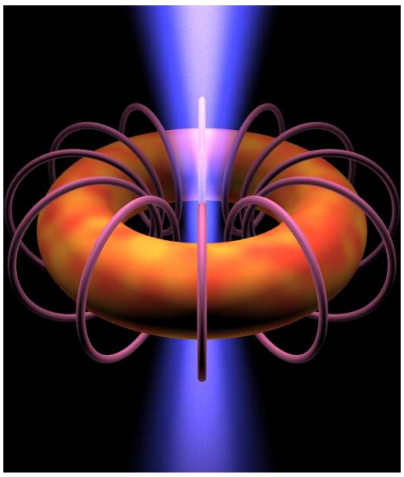

Fig. 1: A rotating toroidal black hole with a non-zero electrical charge generates a magnetic field whose flux lines are capable of resisting a neutralising flow of charged particles from the plasma of an orbiting accretion disk or imploding star. Flux lines point away from the black hole along the rotation axis where, due to extraction of the black hole's rotational energy, biaxial jets may be launched from the central aperture.

the region where the magnetic flux density is highest: the only location where the flux lines lead directly away from the TDH. Conditions for particle ejection are likely to be most favourable at a small displacement along the rotation axis either side of the symmetry plane. There, the magnetic field remains strong and aligned with the observed jets – but gravitational time dilation is less pronounced [31]. The relatively gentle decline in flux with axial displacement can be seen, for example, by considering the magnetic field strength, $B(z)$, of a current, I, flowing along a circular path of radius r at a distance z along the axis from the centre of symmetry:

$$B(z) = \frac{\mu_0 I r^2}{2(z^2 + r^2)^{3/2}} \approx \frac{\mu_0 I}{r(2 + 3z^2/r^2)} \quad \text{for} \quad z \ll r. \quad (11)$$

For a current loop spread over a toroidal surface, the flux density within the central aperture, B_{ap}, whose radius is a can, due to the conservation of charge on the torus and the integrated flux threading the aperture, be approximated by $B_{ap} \approx (r/a)^2 B(0) \approx \mu_0 I r/2a^2$. Thus, the magnetic field would be strongly amplified when the torus approaches pinch-off, $a \ll r$. Plasma magnetically siphoned into the aperture from the surrounding accretion disk could interact directly with the TDH via this magnetosphere. Furthermore, the lack of an actual event horizon would not preclude an ergoregion [36]. Hence, energy extraction via the Penrose process [37] may also contribute somewhat towards jet production. With lower mass electrons being preferentially ejected, a net charge on the TDH could be reliably maintained, thereby supporting the black hole's magnetosphere. Emitted particles would tend to

emerge in cones around the rotation axis, their convergence assisted by magnetohydrodynamic focusing. A population of neutral atoms and free neutrons in the accretion flow could feed TDH growth and support its long-term rotation against angular momentum losses.

Additional support for this model comes from the observed dichotomy between active and quiescent galaxies and the curious fact that quasars have distinctly finite lifetimes. Given that many galaxies still have ample reserves of gas to sustain accretion disks around supermassive black holes, and that the masses of these black holes cannot have decreased appreciably with time, it is puzzling that quasar activity is in such steep decline in the low redshift universe. One would expect nearby supermassive black holes, in particular those present in galaxy clusters, to at least feast upon stray matter sporadically. Only $\sim$10% of the primordial gas in galaxy clusters has so far been utilised by star formation. For comparison, the figure for the Milky Way is closer to 90%. Nearly all galaxies harbour supermassive black holes so one wonders where are the vestigial traces of radio lobes caused by fleeting flares? Observational data suggests that once a quasar becomes quiescent there is little or no prospect of activity being revived: the galactic nucleus not only seems dormant, but utterly defunct. With regards to this finite lifetime riddle and the apparent lack of even temporary revival of quasar activity in quiescent galaxies, a topological transition offers a very natural and appealing hysteresis mechanism [31, 38, 39]. It has long been appreciated that this is a difficulty for more conventional models [40].

Once a dark hole grows too large, even a steadily supplied accretion disc cannot maintain sufficient influx of angular momentum to sustain the geometry. In addition, the angular momentum of the TDH is continually being sapped by jet generation. Closure of the central aperture is not easily reversed, especially as the ensuing charge neutralisation is rapid when flux lines lead directly to the dark hole. A potential explanation can also be found here for the gamma-ray burst phenomenon, relatively short-lived affairs compared to most supernovae. Such events may correspond to the temporary formation of a TDH/toroidal neutron degenerate structure during the core collapse of a massive spinning star.

7 Discussion

The development of general relativity was one of the greatest triumphs not only of theoretical physics but of all science, providing a description of gravitation compatible with the notion that space and time are part of a unified four dimensional continuum with experimentally verifiable implications. However, as with any intrinsically mathematical theory of physics, its interpretation must be guided by physical considerations and one should not lose sight of the scientific method. Indeed, some existing solutions in general relativity are already widely regarded as unphysical. Examples include the Tipler cylinder and the Gödel metric, which exhibits closed timelike curves threading all events within its spacetime. It is possible that Einstein's intuition was correct and that all metrics describing eternal black holes should be similarly regarded with a healthy degree of scepticism and replaced with a new dark hole paradigm.

The present work has attempted to reconcile astronomically observed characteristics of quasars, which have inspired suggestions that their central engines may not abide by topological censorship, with a theoretical understanding of why that might be. A global constraint has been highlighted which, if respected everywhere within a spacetime manifold, holds considerable promise for resolving other long-standing problems in black hole research. It requires merely that the advancement of proper time along any worldline never necessitates the physically impossible advancement of proper time along any other worldline. In many circumstances this is trivially satisfied, but the situation changes radically within a spacetime containing pairs of timelike worldlines for which the relative time dilation grows without limit. Some particle worldlines will then reach future timelike infinity in finite proper time, much as light rays/photons do. Worldlines of timelike particles can thereby be truncated. In the case of particles approaching the event horizon of an eternal black hole, this is a consequence of their asymptotically approached apparent velocity – particles moving at the speed of light experience no passage of time. On the other hand, if a spacetime manifold is initially free of event horizons or singularities, it will always remain free of them. A picture emerges of general relativity as a remarkably benign theory of gravitation gracefully accommodating all eventualities. Analytical solutions to the field equations of general relativity are confined to highly idealised situations. More complex and realistic scenarios can only be studied numerically. Nevertheless, the basic conclusions drawn here concerning the non-formation of event horizons for spherically symmetric situations are likely to carry through to more general circumstances.

The present proposal differs significantly from the *gravastar* model [41] which invokes new physics, replacing the interior black hole region with a de Sitter spacetime blending into the exterior Schwarzschild geometry via a carefully-tailored transition layer [42]. It is also distinct from the *eternally collapsing object* (ECO) scenario [43, 44] in that gravitational collapse can be stabilised without recourse to radiation pressure. Furthermore, there is no need to invoke the presence of some "firewall" or exotic new physics at or near the horizon in order to overcome the information paradox [45].

For several decades now, black holes with event horizons have been seriously entertained despite the lack of a single mathematical example of an event horizon forming in finite universal time and their dismissal by the architect of general relativity. There is a deep-seated expectation amongst relativists that all observers should enjoy equal status but one

must not overlook the fact that general relativity is a theory in which global relationships exist between observers. By tracing the progress of an infalling observer beyond the event horizon, as Oppenheimer & Snyder did, one forsakes concern for external observers. In such situations, the worldlines of external observers must magically transcend what is, for them, future timelike infinity – and indeed, therefore, future timelike infinity for the entire spacetime manifold. Thus, the original notion of a "democracy" amongst observers is naïve if one interprets it in a purely local manner, eschewing the original spirit of relativity.

The proper times along all worldlines should remain finite in any physically realistic spacetime manifold. Whilst self-evidently true, this has profound repercussions for gravitational collapse. Global relationships within a spacetime manifold override local considerations. This can arrest dynamical collapse, prohibiting both the initial formation of event horizons and the ingestion of matter across pre-existing event horizons. Hence, any theorems reliant on the presence of trapped surfaces may have no physical bearing. Prevailing expectations that gravitational collapse inevitably leads to singularities and event horizons appear to be in error and fears that black holes destroy information misplaced. Furthermore, if topological censorship is circumvented, then electrically-charged toroidal dark holes could form the central engines of quasars, consistent with astronomical observations. Thus, quasars may already provide intriguing hints that nature's black holes lack event horizons, and that various physically disturbing pathologies associated with traditional black hole models are obviated in realistic situations – without need for any adjustment to Einstein's theory of gravitation.

Submitted on August 23, 2015 / Accepted on August 25, 2015

References

1. Schmidt M. 3C 273: a star-like object with large red-shift. *Nature*, 1963, v. 197 (4872), 1040.
2. Ferrarese L. and Merritt D. A fundamental relation between supermassive black holes and their host galaxies. *ApJ*, 2000, v. 539 (1), L9.
3. Chandrasekhar S. The mathematical theory of black holes. 1983. Oxford University Press (International Series of Monographs on Physics. Volume 69), 663.
4. Silk J. and Rees M. J. Quasars and galaxy formation. *Astron. Astrophys*, 1998, v. 331, L1.
5. Hopkins P. F. and Hernquist L. Quasars are not light bulbs: testing models of quasar lifetimes with the observed Eddington ratio distribution. *ApJ*, 2009, v. 698 (2), 1550.
6. Schwarzschild K. On the gravitational field of a mass point according to Einstein's theory, 1916. (Translation by Antoci S. and Loinger A. arXiv:physics/9905030v1).
7. Einstein A. On a stationary system with spherical symmetry consisting of many gravitating masses. *Annals of Mathematics*, 1939, v. 40, 4.
8. Oppenheimer J. R. and Snyder H. On continued gravitational contraction. *Phys. Rev.*, 1939, v. 56 (5), 455.
9. Novikov I.D. and Frolov V.P. Black holes in the universe. *Physics-Uspekhi*, 2001, v. 44 (3), 291.
10. Preskill J. Do black holes destroy information? 1992, arXiv: hep-th/9209058.
11. Hawking S. W. Information loss in black holes. *Phys. Rev. D*, 2005, v. 72 (8), 084013.
12. Hawking S. W. Black holes and the information paradox. Proceedings 17th Int. Conf. Dublin, 2004, *Gen. Rel. & Grav.*, doi:10.1142/9789812701688_0006; arXiv: 1401.5761 (2014); doi:10.1038/nature.2014.14583.
13. Abramowicz M. A., Kluzniak W. and Lasota J. P., No observational proof of the black-hole event-horizon, *Astron. Astrophys,* 2002, v. 396, L31.
14. Friedman J. L., Schleich K. and Witt D. M. Topological censorship. *Phys. Rev. Lett.*, 1993, v. 71 (10), 1486.
15. Misner C. W., Thorne K. S. and Wheeler J. A. Gravitation. Macmillan. 1973.
16. Finkelstein D. Past-future asymmetry of the gravitational field of a point particle. *Phys. Rev.*, 1958, v. 110 (4), 965.
17. Landau L. D. and Lifshitz E. M. The classical theory of fields (Vol. 2), 1975, Butterworth-Heinemann.
18. Vachaspati T., Stojkovic D. and Krauss L. M. Observation of incipient black holes and the information loss problem. *Phys. Rev. D*, 2007, v. 76 (2), 024005.
19. Weller D. Five fallacies used to link black holes to Einstein's relativistic space-time. *Progress in Physics*, 2011, v. 1, 93.
20. Hawking S. W. Black hole explosions. *Nature*, 1974, v. 248 (5443), 30.
21. Chafin C. E. Globally causal solutions for gravitational collapse. 2014. arXiv :1402.1524v1
22. Penrose R. Gravitational collapse and space-time singularities. *Phys. Rev. Lett.*, 1965, v. 14 (3), 57.
23. Hawking S. W. The occurrence of singularities in cosmology. III. Causality and singularities. *Proc. Roy. Soc. A*, 1967, v. 300 (1461), 187.
24. Hawking S. W. and Penrose R. The singularities of gravitational collapse and cosmology. *Proc. Roy. Soc. A*, 1970, v. 314 (1519), 529.
25. Hawking S. W. Gravitational radiation from colliding black holes. *Phys. Rev. Lett.*, 1971, v. 26, 1344.
26. Hawking S. W. Black holes in general relativity. *Commun. Math. Phys.*, 1972, v. 25, 152.
27. Shaver P. A., Wall J. V., Kellermann K. I., Jackson C. A. and Hawkins M. R. S. Decrease in the space density of quasars at high redshift. *Nature*, 1996, v. 384, 439.
28. Ganguly R. and Brotherton M. S. On the fraction of quasars with outflows. *ApJ*, 2008, v. 672 (1), 102.
29. Shapiro S. L., Teukolsky S. A. and Winicour J. Toroidal black holes and topological censorship. *Phys. Rev. D*, 1995, v. 52 (12), 6982.
30. Galloway G. J., Schleich K., Witt D. M. and Woolgar E. Topological censorship and higher genus black holes. *Phys. Rev. D*, 1999, v. 60 (10), 104039.
31. Spivey R. J. (2000). Quasars: a supermassive rotating toroidal black hole interpretation. *MNRAS*, 2000, v. 316 (4), 856.
32. Risaliti G., Harrison F. A., Madsen K. K., Walton D. J., Boggs S. E., Christensen F. E., ... and Zhang W. W. A rapidly spinning supermassive black hole at the centre of NGC 1365. *Nature*, 2013, v. 494 (7438), 449.
33. Blandford R. D. and Znajek R. L. Electromagnetic extraction of energy from Kerr black holes. *MNRAS*, 1977, v. 179 (3), 433.
34. Ghosh P. and Abramowicz M. A. Electromagnetic extraction of rotational energy from disc-fed black holes: the strength of the Blandford-Znajek process. *MNRAS* 1997, v. 292 (4), 887.

35. Bambi C. and Modesto L. Can an astrophysical black hole have a topologically non-trivial event horizon? *Phys. Lett. B*, 2011, v. 706 (1), 13.

36. Butterworth E. M. and Ipser J. R. On the structure and stability of rapidly rotating fluid bodies in general relativity. *ApJ*, 1976, v. 204, 200.

37. Penrose R. and Floyd R.M. Extraction of rotational energy from a black hole. *Nature*, 1971, v. 229 (6), 177.

38. Pompilio F., Harun-or-Rashid S. M. and Roos M. A toroidal black hole for the AGN phenomenon. arXiv: astro-ph/0008475; *Astron. & Astrophys.*, 2000, v. 362, 885.

39. Harun-or-Rashid S. M. Cosmological parameters and black holes, Univ. Helsinki PhD thesis, 2002, arXiv: astro-ph/0210253.

40. Hopkins P. F., Hernquist L., Martini P., Cox T. J., Robertson B., Di Matteo T. and Springel v. A physical model for the origin of quasar lifetimes. *ApJ Lett.*, 2005, v. 625 (2), L71.

41. Mazur P. O. and Mottola E., Gravitational vacuum condensate stars, *Proc. Nat. Acad. Sci.*, 2004, v. 101, 9545.

42. Martin-Moruno P., Garcia N. M., Lobo F. S. and Visser M. Generic thin-shell gravastars. *JCAP*, 2012, v. 3, 034.

43. Mitra A. Radiation pressure supported stars in Einstein gravity: eternally collapsing objects. *MNRAS*, 2006, v. 369 (1), 492.

44. Mitra A. and Glendenning N. K. Likely formation of general relativistic radiation pressure supported stars or "eternally collapsing objects". *MNRAS Lett.*, 2010, v. 404 (1), L50.

45. Almheiri A., Marolf D., Polchinski J. and Sully J. Black holes: complementarity or firewalls? *JHEP*, 2013 v. 2, 1.

LETTERS TO PROGRESS IN PHYSICS

Reservations on Cahill's Quantum Gravity Experiment

Anton L. Vrba

Ryde, Isle of Wight, Great Britain. E-mail: vrba@iow.onl

Cahill reports in *Progr. Phys.*, 2015, v.11(4), 317–320 [1] on the correlations of the random noise generated by two Zener diodes, when they are linearly displaced or differently orientated. His conclusions that this could be a detection, and evidence, of quantum gravity variations are exciting, however in my opinion premature.

Semiconductor diodes have provided means for generating noise [2] used in a variety of applications including cryptography, signal jamming, sound masking, and instrument calibration. The diode noise is usually amplified by factors greater than 100 [3] to obtain a signals around the −50 dBm levels, which are of same order magnitude that Cahill reports.

Referring to Cahill's Figure 1, we can observe the internal arrangement of the apparatus consisting of a parallel connected array of five diodes, which are serially connected to the sensing resistor, switch and battery — these components, in that particular arrangement, form an EM-sensing loop having a substantial cross-section. There is no local amplification, and buffering, of the noise signal contrary to Zener-diode based noise generators. Figure 3, presumably, depicts the experimental configurations. In my Fig. 1 (guided by Cahill's Figure 3 right hand side) I reconstructed the experimental electrical circuit diagrams of the inverted arrangement on a common plane formed by the electrical loops defined by the battery, Zener diode and resistor. From this figure it is evident that any EM-induced currents, marked Im, would induce signals, marked Vm. These are of opposite polarity in the inverted apparatus, as Cahill observed.

In my opinion, the experiment needs to be performed with apparatus that reduce the effects of EM-induced interference to a minimum, achieved by a symmetrical arrangement of the diode array around the sensing resistor, as well as a soft steel enclosure to ensure magnetic and electrical shielding. For those wishing to duplicate the experiment, I propose arranging the components as sketched in Fig. 2, with the edition of a decoupling filter, comprising of a resister R1 and the four capacitors marked C, that reduces the effect of induced EM interference in the electrical loop formed by the battery circuit. The noise-signal, generated by the four Zener diodes Z1–4, is detected over R2. All components should be nicely, and compactly, sandwiched between two printed circuit boards to ensure symmetry around the longitudinal axis of R2. An EM-induced current in, say, the loop Z1-C-R2 would be of the same magnitude as induced in R2-C-Z2 and thus canceling across R2.

Submitted on August 23, 2015 / Accepted on August 26, 2015

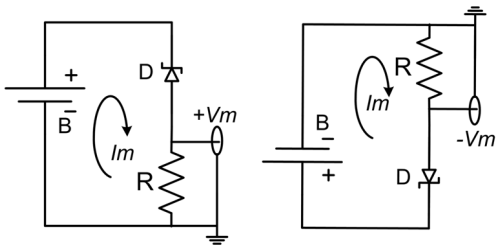

Fig. 1: Inverted Experimental Configuration

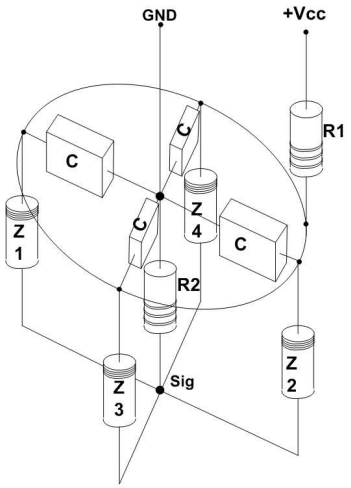

Fig. 2: Proposed Component Arrangement

References

1. Cahill R. T. Quantum gravity experiments. *Progress in Physics*, 2015, v. 11(4), 317–320.
2. Somlo P. I. Zener-diode noise generators. *Electronic Letters*, 1975, v. 11(14), 290.
http://users.cosylab.com/~msekoranja/tmp/04236738.pdf
3. Appl. Note 3469 "Building a Low-Cost White-Noise Generator", Maxim Integrated Products, Inc.
http://www.maximintegrated.com/an3469 accessed 8/25/2015

A Model of Dust-like Spherically Symmetric Gravitational Collapse without Event Horizon Formation

Miquel Piñol

Unidad de Medicina Intensiva, Hospital La Fe, 46026, Valencia, Spain. E-mail: miquel.pinyol@gmail.com

Some dynamical aspects of gravitational collapse are explored in this paper. A time-dependent spherically symmetric metric is proposed and the corresponding Einstein field equations are derived. An ultrarelativistic dust-like stress-momentum tensor is considered to obtain analytical solutions of these equations, with the perfect fluid consisting of two purely radial fluxes — the inwards flux of collapsing matter and the outwards flux of thermally emitted radiation. Thermal emission is calculated by means of a simplistic but illustrative model of uninteracting collapsing shells. Our results show an asymptotic approach to a maximal space-time deformation without the formation of event horizons. The size of the body is slightly larger than the Schwarzschild radius during most of its lifetime, so that there is no contradiction with either observations or previous theorems on black holes. The relation of the latter with our results is scrutinized in detail.

1 Introduction

The aim of this paper is to discuss several open problems of conceptual interest concerning black holes and, in particular, to elaborate a simple model of dust-like spherically symmetric gravitational collapse with account of both the inwards flux of the collapsing matter and the outwards flux of emitted thermal radiation. We illustrate how the latter may avoid the formation of event horizons. The metric considered in this work is time-dependent, unlike the Schwarzschild one. Spherical polar coordinates will be used and there will be no need for analytical extensions (such as the one given by the Kruskal-Szekeres chart) because the occurrence of an event horizon at the Schwarzschild radius will be avoided.

In Sec. 2 the main historical events concerning the development of the well-known concept of black hole are reviewed and its precise significance is shortly but precisely detailed. In Sec. 3 some open problems of the common black hole model are pointed out and their relationship with the corresponding historical findings is emphasized. Section 4 deals with the development of the metric of the present model: First of all, in subsec. 4.1 a time-dependent spherically symmetric metric in spherical polar coordinates is presented and the corresponding Einstein field equations are specified. Secondly, a dust-like energy momentum tensor for a purely radial motion with account of an ultrarelativistic collapsing matter and thermally emitted radiation is obtained in subsec. 4.2. Temporal evolution of the metric components is studied in subsec. 4.3, with the absence of emitted thermal radiation being detailed as a particular case. Fourthly, in subsec. 4.4 it is shown that there should exist a limit where the inwards flux of collapsing matter and the outwards flux of thermal radiation become *compensated*. It is also shown the asymptotic character of the approximation to this limit. Some additional considerations about the total mass and the edge of the collapsing body will be made in subsec. 4.5. Finally, our results are discussed in Sec. 5, paying a special attention to the plausibility of the different hypothesis and the implications of their alternatives.

2 Important historical results concerning black holes

Several historical results in General Relativity led to the concept of black hole. The following list includes some of the most important ones:

1. K. Schwarzschild found in 1916 an exact solution of the Einstein field equations describing the field created by a point particle [1]. (According to Birkhoff's theorem, this solution is also valid for any spherically symmetric body at a distance larger than its radius [2].)
2. J. R. Oppenheimer and G. M. Volkoff discovered in 1939 the existence of upper limit for the mass of neutron stars, above which gravitational collapse could not be avoided [3].
3. In 1967 J. Wheeler used the term "black hole" to name a "gravitationally completely collapsed star" [5].
4. S. Hawking and R. Penrose proved in 1970 that, under certain circumstances, singularities could not be avoided. This is known as the Hawking-Penrose theorem of singularity [6].

   All these results concerning black holes arise basically from Einstein's General Relativity. On the other hand, there exist two important features in the description of black holes which require from both Thermodynamics and Quantum Field Theory (QFT):
5. J. Bekenstein defined the entropy of black holes in 1972 and, based on thermodynamic grounds, deduced the need for black-hole radiation [7].
6. In 1974 S. Hawking justified Bekenstein's speculations about the existence of black-hole radiation from the

point of view of QFT. Hawking model implies the creation of particles of negative mass near the event horizon of black holes. The conservation of information is not clearly ensured by this model [8].

3 Some open problems in gravitational collapse

In this section we discuss if the previous historical results genuinely imply the actual existence of black holes as physical objects. It is widely believed that these findings prove the existence of black holes. The argument supporting black hole formation is the following:

1. There exist stars which are massive enough to exceed the Oppenheimer-Volkoff limit at the end of their "vital cycle". Those stars must finally enter collapse.
2. According to the Hawking-Penrose theorem of singularity, all the mass inside an event horizon must reach a single central point, that is, form a singularity.
3. The solution of the Einstein field equations for the metric of a "point mass" is the Schwarzschild metric, that describes a black hole.

Entering collapse, however, does not immediately lead to the formation of an event horizon and, while the event horizon is not formed, the Hawking-Penrose theorem of singularity is not properly applicable (notice that one of its conditions of application is equivalent either to the existence of an event horizon, or to an expanding Universe taken as a whole). Hence, *a priori* entering collapse must not necessarily lead to a complete collapse.

Certainly, the period of time involved in the process of collapse may be proven to be infinite from the point of view of any external observer (that is, from our perspective on Earth). On the other hand, a "free falling observer" would measure a finite period of time for the collapse, at least if nothing destroys it before reaching its goal [4, 10]. A well-known feature of General Relativity is that space and time are relative but events are absolute. Consequently, it is necessary to reconcile the observations from both reference frames.

It is usually assumed that the free falling observer actually reaches the singularity in a finite time, and the infinite-lasting collapse measured by the external observer is justified in the following way: the free falling body has already reached the central singularity, but as the light emitted from the body inside the black hole never escapes from it, we cannot see it falling; furthermore, the light emitted near the event horizon of the black hole comes to us with a great delay, making us believe that it is still falling.

In fact, there are compelling reasons that make us doubt about the previous explanation: The Schwarzschild metric is symmetric under temporal inversion, which suggests that trajectories in the corresponding space-time should be also reversible, in contrast to the most common interpretation of black holes and their event horizon. Furthermore, General Relativity is not only intended to explain what an observer "sees" in a given reference frame, but what truly "occurs" in there. Additionally, S. Hawking defended the incompatibility of event horizons with Quantum Mechanics [9].

Solution of this apparent paradox requires a careful analysis of what an external observer would exactly see when looking at a body free falling towards a black hole. On the one hand, it would see the free-falling body approaching asymptotically to the event horizon of the black hole, without ever crossing it. On the other hand, according to Hawking's law of black hole radiation, the observer should also see the whole black hole evaporating in a very large, but finite period of time. The evaporation of the whole mass of the black hole must logically include that of the free-falling body as well. Were it not to be like this, that is, if the crossing of the event horizon had to be accomplished before the emission of thermal radiation, it would never emit thermal radiation and the laws of Thermodynamics would be infringed. As the temporal order of causally-related events is always the same for all reference frames, we must conclude that the free falling observer should also observe its own complete evaporation before having reached the event horizon. If it had reached the singularity in a finite period of time, its complete evaporation must have occurred in a finite and *lesser* period of time.

Not only should these considerations be valid for the free-falling body approaching a black hole, but also for the process of collapse itself [28]. Consequently, collapsing bodies should never becomes black holes. On the contrary, they should asymptotically tend to form an event horizon until the time at which they become completely emitted in the form of radiation. An equivalent thesis has already been defended by Mitra [14–18], Robertson and Leiter [19–21], Vachaspati *et al.* [11, 12], and by Piñol and López-Aylagas [13]. In addition, there exist some calculations in string theory which point towards the same direction [22].

Thus, the metric of a collapsing body shall never be in a strict sense Schwarzschild's one (as it never completely collapses) but a time-dependent metric. In the next section, we solve the Einstein field equations of a time-dependent spherically symmetric metric. Several simplifications are considered to make calculations plausible, but the essential Physics of the problem is respected.

4 Deduction of a metric for gravitational collapse

4.1 Einstein field equations

As we have already pointed out, our goal in this paper is to study the temporal evolution of a spherically symmetric gravitational collapse. Rotations and local inhomogeneities are beyond the scope of the present work. Therefore, the starting point shall be a time-dependent spherically symmetric metric, which in spherical polar coordinates is given by the expression

$$d\tau^2 = e^{\nu}dt^2 - e^{\lambda}dr^2 - r^2 d\Omega^2, \qquad (1)$$

where $\nu = \nu(r,t)$ and $\lambda = \lambda(r,t)$. Notice that geometrized units have been used ($G = 1, c = 1$). The corresponding Einstein field equations for such metric are the following [23]:

$$8\pi T_0^0 = -e^{-\lambda}\left(\frac{1}{r^2} - \frac{\lambda'}{r}\right) + \frac{1}{r^2}\,, \tag{2}$$

$$8\pi T_1^1 = -e^{-\lambda}\left(\frac{\nu'}{r} + \frac{1}{r^2}\right) + \frac{1}{r^2}\,, \tag{3}$$

$$8\pi T_2^2 = -\frac{1}{2}\,e^{-\lambda}\left(\nu'' + \frac{\nu'^2}{2} + \frac{\nu' - \lambda'}{r} + \frac{\nu'\lambda'}{2}\right) + \\ + \frac{1}{2}\,e^{-\nu}\left(\ddot{\lambda}\,\frac{\dot{\lambda}^2}{2} \;-\; \frac{\dot{\lambda}\,\dot{\nu}}{2}\right), \tag{4}$$

$$8\pi T_3^3 = 8\pi T_2^2\,, \tag{5}$$

$$8\pi T_0^1 = -e^{-\lambda}\frac{\dot{\lambda}}{r}\,. \tag{6}$$

Subtraction of 3 from 2 yields the identity

$$8\pi\left(T_0^0 - T_1^1\right) = \frac{e^{-\lambda}}{r}\left(\nu' + \lambda'\right). \tag{7}$$

It will be useful to define a function $\phi(r,t)$

$$-2\phi \equiv \nu + \lambda \tag{8}$$

so that

$$\nu = -\lambda - 2\phi\,, \qquad 8\pi\left(T_0^0 - T_1^1\right) = \frac{e^{-\lambda}}{r}\left(-2\phi'\right). \tag{9}$$

A mathematical structure for the stress-momentum tensor must be specified in order to solve the previous equations, which will be discussed in next subsection.

4.2 A dust-like stress-momentum tensor of ultrarelativistic particles

The stress-momentum tensor of a perfect fluid may be written in terms of the energy density ρ, the pressure p and the four-velocity u^α as:

$$T_\beta^\alpha = g_{\beta\delta}\,(\rho + p)\,u^\alpha u^\delta - \,\eta_\beta^\alpha\,p\,. \tag{10}$$

If the pressure appears to be very small compared to the energy density, in the limit $p \to 0$ one obtains the stress-momentum tensor of dust:

$$T_\beta^\alpha = \,g_{\beta\delta}\,\rho\,u^\alpha\,u^\delta. \tag{11}$$

In our model we deal with a dust-like stress-momentum tensor. For the sake of simplicity, we shall consider the perfect fluid splitting into two perfectly radial fluxes: a flux of ingoing collapsing matter and a second flux of outgoing thermal radiation. Both the ingoing collapsing matter and the outgoing thermal radiation are going to be dealt as ultrarelativistic particles. It has been already established that the matter in a process of gravitational collapse reaches celerities near the speed of light [24]. It is also a well-known fact that, despite photons being "massless", a photon gas may be assimilated to a gas of ultrarelativistic particles with an effective mass density [25].

It could be expected that the relation between pressure and mass-energy density should be given by the identity $p = \frac{\rho}{3}$ due to the particles being ultrarelativitic. A closer insight into this points out that the above identity would only be properly applicable to an *isotropic* gas and not to the higly *directed* movement considered in the present work. The consideration of two purely "radial" fluxes shall simplify calculations and it is in this sense that a "dust-like" stress-momentum tensor may be used. A similar approach has been already adopted by Borkar and Dhongle [26].

With account of the metric 1 the coefficients of the dust energy-momentum tensor 11 become

$$T_0^0 \;=\; e^{-2\phi}\,e^{-\lambda}\,\rho\left(u^0\right)^2, \tag{12}$$

$$T_1^1 \;=\; -\,e^{\lambda}\,\rho\,\left(u^1\right)^2, \tag{13}$$

$$T_0^1 \;=\; e^{-2\phi}\,e^{-\lambda}\,\rho\,u^0\,u^1. \tag{14}$$

For a purely radial movement (characterized by $d\Omega = 0$) Eq. 1 leads to the relation

$$d\tau^2 = e^{-2\phi}e^{-\lambda}dt^2 - e^{\lambda}dr^2 \tag{15}$$

which, with account of the identities $\frac{dt}{d\tau} \equiv u^0$ and $\frac{dr}{d\tau} \equiv u^1$, becomes

$$1 = e^{-2\phi}e^{-\lambda}\left(u^0\right)^2 - e^{\lambda}\left(u^1\right)^2. \tag{16}$$

Isolating $\left|u^1\right| = \sqrt{(u^1)^2}$, we obtain

$$\left|u^1\right| = e^{-\phi}e^{-\lambda}u^0\left[1 - \frac{e^{2\phi}e^{\lambda}}{(u^0)^2}\right]^{\frac{1}{2}}. \tag{17}$$

In the ultrarelativistic limit $u^0 \to \infty$ ($u^0 \gg e^{2\phi}e^{\lambda}$) the component u^1 of the four-velocity becomes

$$\left|u^1\right| = e^{-\phi}e^{-\lambda}u^0. \tag{18}$$

Notice that this same relation could have been obtained by imposing the identity $d\tau \sim 0$ in Eq. 15.

Concerning the sign of u^1, it is clear that $u^1 < 0$ for ingoing matter and $u^1 < 0$ for outgoing thermal radiation, i.e.

$$u^1_{in} = -e^{-\phi}\,e^{-\lambda}\,u^0, \tag{19}$$

$$u^1_{out} = e^{-\phi}\,e^{-\lambda}\,u^0. \tag{20}$$

4.2.1 Stress-momentum tensor of the ingoing matter

If we denote the energy density of the infalling matter by ρ_{in}, according to Eqs. 12, 13, 14 and 19 we have

$$T^0_{0,in} = e^{-2\phi}\, e^{-\lambda}\, \rho_{in}\, \left(u^0\right)^2 , \quad (21)$$

$$T^1_{1,in} = -e^{-2\phi}\, e^{-\lambda}\, \rho_{in}\, \left(u^0\right)^2 = -T^0_{0,in} , \quad (22)$$

$$T^1_{0,in} = -e^{-3\phi}\, e^{-2\lambda}\, \rho_{in}\, \left(u^0\right)^2 = -e^{-\phi}\, e^{-\lambda}\, T^0_{0,in} . \quad (23)$$

4.2.2 Stress-momentum tensor of the outgoing thermal radiation

Denoting the energy density of the outgoing thermal radiation by ρ_{out}, according to Eqs. 12, 13, 14 and 20 we obtain

$$T^0_{0,out} = e^{-2\phi}\, e^{-\lambda}\, \rho_{out}\, \left(u^0\right)^2 , \quad (24)$$

$$T^1_{1,out} = -e^{-2\phi}\, e^{-\lambda}\, \rho_{out}\, \left(u^0\right)^2 = -T^0_{0,out} , \quad (25)$$

$$T^1_{0,out} = e^{-3\phi}\, e^{-2\lambda}\, \rho_{out}\, \left(u^0\right)^2 = e^{-\phi}\, e^{-\lambda}\, T^0_{0,out} . \quad (26)$$

4.2.3 Total stress-momentum tensor of the collapsing body

Addition of the stress-momentum tensors of both the infalling matter and the outgoing thermal radiation leads to the total stress-momentum tensor of the collapsing body, which is given by the expressions

$$T^0_0 = e^{-2\phi}\, e^{-\lambda}\, (\rho_{in} + \rho_{out})\, \left(u^0\right)^2 , \quad (27)$$

$$T^1_1 = -e^{-2\phi}\, e^{-\lambda}\, (\rho_{in} + \rho_{out})\, \left(u^0\right)^2 = -T^0_0 , \quad (28)$$

$$T^1_0 = -e^{-3\phi}\, e^{-2\lambda}\, (\rho_{in} - \rho_{out})\, \left(u^0\right)^2 \quad (29)$$

$$= -e^{-\phi}\, e^{-\lambda}\, \left(\frac{\rho_{in} - \rho_{out}}{\rho_{in} + \rho_{out}}\right) T^0_0 .$$

Once the mathematical structure of the stress-momentum tensor of the collapsing body is established, we are able to study the temporal evolution of the collapse by solving the Einstein field equations 2-6.

4.3 Temporal evolution of collapse

Substitution of T^1_0 by Eq. 27 in Eq. 6 leads to the following equation:

$$-e^{-\phi}\, e^{-\lambda}\, \left(\frac{\rho_{in} - \rho_{out}}{\rho_{in} + \rho_{out}}\right) 8\pi T^0_0 = -e^{-\lambda}\, \frac{\dot{\lambda}}{r} . \quad (30)$$

From this an expression for the temporal evolution of λ may be isolated:

$$\dot{\lambda} = e^{-\phi} \left(\frac{\rho_{in} - \rho_{out}}{\rho_{in} + \rho_{out}}\right) 8\pi r T^0_0 . \quad (31)$$

Initially it is expected that $\rho_{in} \gg \rho_{out}$, as the amount of energy emitted in the form of thermal radiation should reasonably correspond to a very small proportion of the total energy of the collapsing body. In that case, $\left(\frac{\rho_{in} - \rho_{out}}{\rho_{in} + \rho_{out}}\right) \sim 1$ and $\dot{\lambda} \sim e^{-\phi} \left(8\pi r T^0_0\right)$, so that λ shall be a strictly increasing function with time and it is expected to acquire considerably large values. In any case, for $\lambda \gg 1$ we have the asymptotic expression

$$8\pi T^0_0 = \frac{1}{r^2} + O(e^{-\lambda}) , \quad (32)$$

and therefore,

$$\dot{\lambda} = e^{-\phi} \left(\frac{\rho_{in} - \rho_{out}}{\rho_{in} + \rho_{out}}\right) \frac{1}{r} + O(e^{-\lambda}) . \quad (33)$$

On the other hand, we need to estimate as well the value of ϕ. From Eqs. 9 and 28 we obtain

$$\phi' = -\frac{1}{2}\, e^{\lambda}\, 8\pi r\, \left(T^0_0 - T^1_1\right) = -e^{\lambda}\, \left(8\pi r T^0_0\right) , \quad (34)$$

which combined with Eq. 32 yields

$$\phi' = -\frac{e^{\lambda}}{r} + \left(\frac{1}{r} - \lambda'\right) \sim -\frac{e^{\lambda}}{r} . \quad (35)$$

According to Birkhoff's theorem, outside the radius R of the collapsing body the space-time geometry will be exactly Schwarzschild-like, so that $\phi = 0$ for $r > R$. Inside the collapsing body $T^0_0 > 0$ and consequently $\phi' < 0$. This yields $\phi > 0$ for $r < R$ and $\phi(R, t) = 0$ because of the analytic character of this function.

Equations 33 and 35 are not trivial to resolve analytically. For any time t, however, Eq. 33 and the fact that $\phi > 0$ for any $r < R$ lead to the following inequality:

$$\lambda(t, r) < \lambda(0, r) + \frac{t}{r} . \quad (36)$$

4.4 Asymptotic approach to a pseudo-stability phase

According to the results obtained in the previous section, for any given time t the function $\lambda(r, t)$ is analytic on the domain $r > 0$. Nonetheless, as Eq. 36 is an inequality, no specific values for this function have been provided.

It has been discussed that the ingoing flux of infalling matter is initially expected to be much larger than the outgoing flux of thermal radiation. Despite this, as λ becomes larger, according to Eq. 35 $|\phi'|$ must also increase. On the other hand, as $\phi \geqslant 0$ the ingoing flux must decrease according to Eq. 23.

As the values of $T^1_{0,in}$ may become as small as wanted, if λ and ϕ were not upper bounded it would not be unreasonable to think that the ingoing flux of infalling matter may eventually become *compensated* by the outgoing flux of thermal radiation. It could be discussed as well that, according to Eq. 26, the flux of outgoing thermal radiation may also become

arbitrarily small, but we proceed first to analyse the details concerning the compesation of fluxes and the consequences of this hypothesis.

The condition for the compensation of both fluxes is naturally given by the equation

$$T^1_{0,in,s} + T^1_{0,out,s} = 0\,. \tag{37}$$

It must not be misunderstood as a transgression of Oppenheimer-Volkoff's theorem. The star *is not* in equilibrium. It is actually collapsing, as nothing prevents the infalling matter of keeping in collapse. There would simply be an additional flux (arguable in the basis of thermodynamic grounds, and justifiable by the conversion of a portion of the collapsing matter into thermal radiation due to the interaction of their respective fields) that would compensate the energy interchange across a given surface of $r-$radius.

In that hypothetical state of "stability", from Eqs. 23 and 26 a relation between the energy densities ρ_{in} and ρ_{out} can be derived

$$\rho_{in,s} = \rho_{out,s} = \frac{1}{2}\,\rho_s\,, \tag{38}$$

where the subindex s stands for "stability" (notice that the aforementioned relations are specific of that hypothetical phase). Several considerations concerning the emission of thermal radiation due to collapsing bodies must be made in order to proceed further with the theoretical development.

4.4.1 A model of Hawking-like radiation

According to Hawking [8], the temperature of a black hole is proportional to the inverse of its Schwarzschild radius (R_S) and the thermal radiation emission rate is proportional to the inverse of the square of R_S:

$$\dot{M}_H = -\frac{k}{R_S^2}\,. \tag{39}$$

We have denoted the thermal emission by $\dot{M}_H$ as it implies a loss in the total mass of the black hole.

In what follows, both the approach and the nomenclature adopted in the study of the mass and its mathematical relation with the components of the stress-momentum tensor and with the functions $\nu(r,t)$ and $\lambda(r,t)$ of the metric 1 are the ones given in Ref. [23]. The total mass of a spherically symmetric body of radius R is given by the following expression:

$$M = \int_0^R 4\pi r^2 T^0_0(r,t)dr. \tag{40}$$

Analogously, the mass contained inside a surface of radius r (concentric to the spherically symmetric body of interest) is given by

$$m(r,t) = \int_0^r 4\pi \tilde{r}^2 T^0_0(\tilde{r},t)\,d\tilde{r}. \tag{41}$$

Comparing Eqs. 2 and 41, the following relation can be set between $m(r,t)$ and $\lambda(r,t)$:

$$e^{-\lambda(r,t)} = 1 - \frac{2m(r,t)}{r}\,, \tag{42}$$

and therefore we have $-e^{-\lambda}\dot{\lambda} = -\frac{2\dot{m}}{r}$ or, equivalently,

$$\dot{\lambda} = \frac{2\dot{m}}{r}\,e^{\lambda}. \tag{43}$$

Despite the fact that there is solely "one" function $\lambda(r,t)$, it is useful to split $\dot{\lambda}$ into the sum of $\dot{\lambda}_{in}$ (due to the ingoing flux $\dot{m}_{in}$ of collapsing matter) and $\dot{\lambda}_{out}$ (due to the outgoing flux $\dot{m}_{out}$ of thermal radiation). In so doing we obtain

$$\dot{\lambda} = \dot{\lambda}_{in} + \dot{\lambda}_{out} \tag{44}$$

with

$$\dot{\lambda}_{in} = \frac{2\dot{m}_{in}}{r}\,e^{\lambda}, \qquad \dot{\lambda}_{out} = \frac{2\dot{m}_{out}}{r}\,e^{\lambda}. \tag{45}$$

As pointed out before, the thermal emission of black holes $\dot{m}_H$ is given by Eq. 39. On the other hand, Vachaspati *et al.* showed that the thermal emission of a collapsing shell approaching the Schwarzschild's radius of a black hole would follow a law of the same style [11]: according to their calculations, the temperature of the collapsing shell turns out to be proportional to the Hawking's one ($T_V \sim 2.4T_H$, where T_V stands for Vachaspati's temperature and T_H for Hawking's temperature).

With account of Eq. 42 the metric 1 becomes

$$\begin{aligned} d\tau^2 = \left(1 - \frac{2m(r,t)}{r}\right) e^{-2\phi(r,t)}\,dt^2 - \\ - \left(1 - \frac{2m(r,t)}{r}\right)^{-1} dr^2 \;-\; r^2\,d\Omega^2, \end{aligned} \tag{46}$$

where the resemblance with Schwarzschild's metric results evident. Certainly, there exist two main differences between Eq. 46 and the Schwarzschild's metric: 1) the mass is not a constant, but a function of the radius. 2) there is an additional factor $e^{-2\phi(r,t)}$ in the coefficient g_{00}.

However, if we 1) deal with motions whose variation in the r-coordinate is small enough and 2) assume a temporal proximity to the hypothetical stationary case that we postulated (i.e., $\dot{m}(r,t) \sim 0$ and $\dot{\phi}(r,t) \sim 0$), then the metric 46 may be *locally* transformed into the Scwarzschild's one.

In fact, in the *vicinity* of a given radius R_a, where $m(r,t) \sim M_a$ and $\phi(r,t) \sim \Phi_a$, we have

$$d\tau^2 \sim \left(1 - \frac{2M_a}{r}\right) d\tilde{t}^2 - \left(1 - \frac{2M_a}{r}\right)^{-1} dr^2 - r^2 d\Omega^2, \tag{47}$$

with

$$d\tilde{t} \equiv e^{-\Phi_a} dt. \tag{48}$$

At this point it is time to introduce our Hawking-like radiation model. We will conceptually split the collapsing body

into a sequence of concentric spherical shells, each of which asymptotically approaches its corresponding radius $r = 2M_a$ in the coordinate system given by the metric 47. We assume that these collapsing shells do not interact with each other. Along the lines of Ref. [12] it can be deduced that the radiation law obtained for a spherical shell asymptotically approaching in time t the event horizon of a black hole is also valid for any of the concentric shells asymptotically approaching in time $\tilde{t}$ its corresponding $r = 2M_a$ radius in our model. Consequently,

$$\frac{dm_{out}}{d\tilde{t}} = -\frac{k}{r^2} \tag{49}$$

and so

$$\dot{m}_{out} \equiv \frac{dm_{out}}{dt} = \frac{d\tilde{t}}{dt}\frac{dm_{out}}{d\tilde{t}} = -e^{-\phi}\frac{k}{r^2}\,. \tag{50}$$

From this, we straightforwardly obtain the identity

$$\dot{\lambda}_{out} = \frac{2e^{\lambda}}{r}\left(\frac{-e^{-\phi}k}{r^2}\right) = -e^{-\phi}\,\frac{2k\,e^{\lambda}}{r^3}\,. \tag{51}$$

On the other hand, according to Eqs. 6 and 23 an equivalent expression for $\dot{\lambda}_{in}$ is given by

$$\dot{\lambda}_{in} = e^{-\phi}\left(8\pi r T^0_{0,in}\right)\,. \tag{52}$$

From Eqs. 12, 21 and 32 we conclude that, asymptotically,

$$8\pi T^0_{0,in} = \frac{\rho_{in}}{\rho_{in}+\rho_{out}}\,\frac{1}{r^2} + O(e^{-\lambda}) \tag{53}$$

and therefore, with account of Eq. 38, we obtain

$$\dot{\lambda_{in}} = e^{-\phi}\left(\frac{\rho_{in}}{\rho_{in}+\rho_{out}}\right)\frac{1}{r} \simeq e^{-\phi}\frac{1}{2r}\,. \tag{54}$$

The stability phase is naturally defined by the condition

$$\dot{\lambda}_s = 0 \tag{55}$$

and therefore, from Eqs. 44, 51, 54 and 55 we obtain the relation

$$-e^{-\phi_s}\frac{2k\,e^{\lambda_s}}{r^3} + e^{-\phi_s}\frac{1}{2r} = 0. \tag{56}$$

Equivalently,

$$e^{\lambda_s} = \frac{1}{4k}\,r^2, \tag{57}$$

from which a functional dependence of λ on r is obtained for the stability phase

$$\lambda_s(r) = -\ln(4k) + \ln\left(r^2\right). \tag{58}$$

Taking into account Eq. 35, from the previous equation we easily obtain an expression for ϕ_s:

$$\phi_s' = -\frac{e^{\lambda_s}}{r} = -\frac{r}{4k}. \tag{59}$$

Integration over r with account of the contour condition $\phi(R,t) = 0\ \forall t$ discussed in the previous section yields the identity

$$\phi_s(r) = \int_R^r \phi_s'(\tilde{r})\,d\tilde{r} = \frac{1}{8k}\left(R^2 - r^2\right), \tag{60}$$

and thus

$$e^{-\phi_s(r)} = e^{\frac{-1}{8k}\left(R^2-r^2\right)}. \tag{61}$$

It must be noticed that the existence of the postulated stability phase is self-consistent and that it may be clearly derived from equations 45: both $\left|\dot{\lambda}_{in}\right|$ and $\left|\dot{\lambda}_{out}\right|$ decrease as $\phi(r,t)$ increases by a factor $e^{-\phi(r,t)}$, but only $\left|\dot{\lambda}_{out}\right|$ increases as $\lambda(r,t)$ increases (by a factor $e^{\lambda(r,t)}$). Consequently, even when initially $\left|\dot{\lambda}_{out}\right| \ll \left|\dot{\lambda}_{in}\right|$ at large enough times both quantities should become of the same magnitude.

Nonetheless, a significant issue concerning the behaviour of $\lambda(r,t)$ for small values of r must be remarked. We are going to deal it with detail in the following subsection.

4.4.2 Corrections to the equation of λ_s for small radii

From Eq. 42, as $m(r,t) \geqslant 0\ \forall r,t$, it becomes evident that also $\lambda(r,t)$ must be $\geqslant 0\ \forall r,t$. However, in Eq. 58, it can be checked that it yields $\lambda_s = 0$ at $r = 2\sqrt{k}$ and $\lambda_s < 0$ for $r < 2\sqrt{k}$. Consequently, the mentioned expression cannot be valid for small radii.

As it has been clearly established in subsec. 4.3, if no outwards flux of thermal radiation is taken into account the values of $\lambda(r,t)$ would grow in an unlimited way. Thus, at large times, it would become great enough to imply the T^0_0 component of the stress-momentum tensor to approach the asymptotic expression given in Eq. 32. By contrast, in the previous subsection we have actually taken into account the emission of thermal radiation, and it has been performed with the Hawking-like law specified in Eq. 39, which entails a most prominent emission rate for inner shells. As a consequence, λ_s values decrease at small radii (or, what is the same, it results to be a strictly increasing function with r).

For radii $r \gg 2\sqrt{k}$, all the calculations which have been deduced after Eq. 32 are completely justified. Fortunately, that corresponds to most values of r, since $k \ll 1$ (certainly, the thermal evaporation process takes place at a considerably slow rhythm).

Thus, the steps which we have followed in order to determine $\lambda_s(r)$ must be reviewed in order to obtain a valid expression for small radii. A suitable analytical solution to the problem is far from being straightforward, but we are going to analyse it a bit more of care in the following lines.

Firstly, the complete identity of T^0_0 in Eq. 2 must be used instead of Eq. 32. Therefore, the expression for λ_{in}, instead of the one specified in Eq. 54, according to 52 will be

$$\dot{\lambda}_{in} = e^{-\phi}\frac{1}{2r}\left(1 - e^{-\lambda}\left(1 - r\lambda'\right)\right). \tag{62}$$

From this, keeping the same radiation law of Eq. 39 and the expression for λ_{out} of Eq. 51, it is not hard to follow that the stability condition in Eq. 55 entails

$$e^{\lambda_s} = \frac{r^2}{4k}\left(1 - e^{-\lambda_s}\left(1 - r\lambda_s'\right)\right). \tag{63}$$

When $\lambda_s \gg 1$, Eq. 57 is recovered. As we had already signalled, its resolution in the regions where the mentioned limit ceases to be valid is far from being trivial. Nonetheless, a possibility could consist in the application of an iterative method. Instead of making $e^{\lambda_s} \to 0$, in the right side of the equation we may use as a first approximation (well, actually as a *second* approximation) the expression for λ_s obtained in Eq. 58 (being its derivative $\lambda_s' = 2/r$):

$$e^{*\lambda_s} \sim \frac{r^2}{4k}\left(1 - \frac{4k}{r^2}\left(1 - r\frac{2}{r}\right)\right) = \frac{r^2}{4k} + 1, \tag{64}$$

where the asterisk (*) stands for "iterated".

Thus,

$$\lambda_s* \sim \ln\left(\frac{r^2}{4k} + 1\right), \tag{65}$$

which can be assimilated to Eq. 58 for large values, but that has the advantage of accomplishing the necessary condition $\lambda(r,t) \geqslant 0\ \forall r, t$.

In the next subsection, we are not going to have longer into account the corrections for small radii, but we will focus onto temporal variations of $\lambda(r,t)$ when approaching the stability phase described by 58 (only valid for $r > 2\sqrt{k}$).

4.4.3 Small variations of $\lambda_{(r,t)}$ before the stability phase

According to Eqs. 44, 51 and 54 we have

$$\dot{\lambda}(r,t) = e^{-\phi}\left(\frac{1}{2r} - \frac{2ke^{\lambda}}{r^3}\right). \tag{66}$$

In the stability phase, defined by Eq. 55, the functional dependence of λ is given by Eq. 57. Now we proceed to study small variations of $\lambda(r,t)$ before it acquires the stability value, that is,

$$\lambda(r,t) = \lambda_s(r) - \lambda_\Delta(r,t)\,. \tag{67}$$

Notice that, by definition, $\dot{\lambda}_s(r) = 0$. This fact implies

$$\dot{\lambda}(r,t) = -\dot{\lambda}_\Delta(r,t)\,. \tag{68}$$

Furthermore, because of the inequality $\lambda_\Delta \ll \lambda$, we will consider $\phi \simeq \phi_s$. Therefore, from Eqs. 57, 66, 67 and 68 we obtain the expression

$$\dot{\lambda}_\Delta = -\frac{e^{-\phi_s}}{2r}\left(1 - e^{-\lambda_\Delta}\right). \tag{69}$$

In the limit $\lambda_\Delta \ll 1$ we can approximate $1 - e^{-\lambda_\Delta} \sim \lambda_\Delta$, so that

$$\dot{\lambda}_\Delta = -\frac{e^{-\phi_s}}{2r}\,\lambda_\Delta + O\left(\lambda_\Delta^2\right), \tag{70}$$

whose integration over t leads to the following solution

$$\lambda_\Delta = A(r)\exp\left(-\frac{e^{-\phi_s}}{2r}t\right) = A(r)\exp\left(-e^{\frac{-1}{8k}\left(R^2 - r^2\right)}\frac{t}{2r}\right), \tag{71}$$

where $A(r)$ is an arbitrary positive defined function depending on the initial conditions of the problem.

Therefore, according to the hypothesis of the model, $\lambda_{(r,t)}$ asymptotically approaches its stability value:

$$\lambda(r,t) = -\ln(4k) + \ln\left(r^2\right) - A(r)\exp\left(-e^{\frac{-1}{8k}\left(R^2 - r^2\right)}\frac{t}{2r}\right). \tag{72}$$

4.5 Some considerations about the mass and the edge of the collapsing body

From Eq. 19 the infalling velocity $\dot{r}_{in}$ of any collapsing shell in the present model is given by

$$\dot{r}_{in} \equiv \frac{dr}{dt} = \frac{dr}{d\tau}\frac{d\tau}{dt} = \frac{u^1_{in}}{u^0} = -e^{-\phi}e^{-\lambda}. \tag{73}$$

According to Eqs. 42 and 73 and with account of the contour condition $\phi(R,t) = 0\ \forall t$, the motion of the edge R of a collapsing body of mass M must be given by the expression

$$\dot{R} = -\left(1 - \frac{2M}{R}\right), \tag{74}$$

whose solution for large enough times is

$$R = 2M + \Delta R_0 e^{\frac{-t}{2M}} \tag{75}$$

with ΔR_0 being a constant depending on the initial conditions of the collapse.

An important detail must be pointed out. In the previous equations we have dealt with the total mass M of the collapsing body as if it was a constant. It may be actually considered constant in practice for long periods of time but, in fact, it slowly diminishes due to the emission of thermal radiation, unless the surrounding background presents a greater CMB temperature or news amounts of infalling mass are provided. Thus, having into account that $R_S = 2M$, from Eq. 39,

$$\dot{M} = \frac{-k}{R_S^2} = \frac{-k}{4M^2}\,. \tag{76}$$

Therefore,

$$M(t) = \left(M_0^3 - \frac{3kt}{4}\right)^{\frac{1}{3}}, \tag{77}$$

from which the evaporation time t_v may be isolated:

$$t_v = \frac{4M_0^3}{3k}\,. \tag{78}$$

5 Discussion

The model of gravitational collapse presented in this paper contains an important number of simplifications which have allowed us to find analytical solutions of the coefficients of the metric all over the space at any given time (for small radius values, we have seen that some special considerations must be taken into account, but no essential contradiction is risen). The results obtained are self-consistent and do not lead to the formation of an event horizon, what would provide a simpler interpretation of the information loss problem: if no event horizon is formed, thermal radiation should be directly emitted by the collapsing body. Hence, there is no need for postulating a special mechanism of radiation such the one that S. Hawking proposed *ad hoc* for black holes. Let us now analyse more carefully the hypothesis that we have made, their implications and the consequences that would have been derived from making slightly different considerations.

Our starting point has been a time-dependent spherically symmetric metric. It is a well-known fact that spherical symmetry is an almost universal *approximate* characteristic of any celestial body. Two kind of phenomena certainly prevents it from being *perfect*: the first one is rotation (which implies the modification from spherical surfaces to ellipsoidal ones), while the second one consists of the local inhomogeneities of any *real* system.

Concerning rotation, it constitutes *per se* a very interesting but mathematically complex problem. To deal properly with a rotating process of gravitational collapse, a kind of modified time dependent Kerr metric should be formulated (in the same way that in this paper a kind of "time-dependent Schwarzschild metric" has been proposed). From an intuitive point of view, however, one would expect that rotation should lead to a genuinely *slower* collapsing process (due to the "centrifugal" effect of angular momentum). Concerning local inhomogeneities, a detailed study of the effect of small perturbations on the metric could constitute another *per se* attractive problem, but *a priori* it is not unreasonable to assume that the emission of gravitational waves should tend to diminish these effects with time. This is a consequence of the "no hair" theorem for black holes (even when we have found no black hole in the mathematical development of this article).

About the temporal dependence of the metric coefficients, it appears to be a strict logical requirement of the problem. The displacement of the infalling matter along the collapsing process must necessarily imply a temporal change in the metric coefficients. In this sense, Schwarzschild metric -a good solution for the stationary "punctual mass" problem- is not the best choice for the question of collapse itself. In words of J. A. Wheeler, "matter tells spacetime how to curve, and curved spacetime tells matter how to move". With our choice of time-dependent metric, Kruskal-Szekeres coordinates are not needed because the ordinary polar spherical coordinates cover the entire spacetime manifold and the functions $\lambda(r,t)$ and $\nu(r,t)$ are analytic all over the space.

With respect to the choice of stress-momentum tensor, its dust-like nature has been greatly aimed for the sake of simplicity. As it has been already emphasized in the pertinent section, it seems paradoxal to consider simultaneously the features of "dust-like" and "ultrarelativistic" because the relation between pressure and energy density in an ultrarelativistic *gas* turns out to be $p = \frac{1}{3}\rho$. Nonetheless, two subtle points should be raised here: First of all, the concept of "ultrarelativistic dust" is not as strange as it appears to be, since a privileged direction of motion has been considered (the ultrarelativistic motion is highly "directed" towards purely radial lines). Secondly, even if a relation of proportionality between p and ρ would have been chosen, that would not have changed the fact that all the other stress-momentum tensor components could be expressed as a product of certain factors and T^0_0. It is straightforward to check that changing the aforementioned factors would not alter drastically the subsequent mathematical development. As a matter of fact, the "linearity" between T^1_0 and T^0_0 has allowed us to set a temporal dependence for λ. In fact, as $\dot{\lambda}$ turns out to be proportional to T^0_0, the function λ would only diverge if T^0_0 became infinite too. Nevertheless, when λ increases T^0_0 does not diverge but tends to $\frac{1}{8\pi r^2}$. In a similar way, it may be proved that ν, or $\phi = -\frac{1}{2}(\nu + \lambda)$, is also a well-behaved function despite [reasonable] modifications in the stress-momentum tensor.

Thus, whether we consider thermal radiation or not, the study of the temporal evolution of a spherically symmetric gravitational collapse in spherical polar coordinates does not lead to incoherences, but constitutes a sensible alternative to the usual black hole model. In addition, when thermal radiation is considered, very high (but finite) values of λ are obtained at any given r. Definitely, the radiation law proposed in this paper has been deduced in a rather "heuristic" way by assuming the extensibility of the calculations detailed in Ref. [12] to a model of *scarcely interacting* collapsing shells. Certainly, in the original paper by Vachaspati *et al.* the emission of radiation was calculated from a spherical Nambu-Goto domain wall using the functional Schrödinger formalism, with vacuum close to the wall. Therefore, our *analytical* extension of their results to "inner shells" may be cautiously considered, but it is a reasonable hypothesis, specially having into account Birkhoff theorem (according to which, in a system with spherical symmetry, the gravity in a surface is basically determined by the mass of the matter contained in the inner, not outer, shells). As a matter of fact, it is a much more consistent assumption than some of those that may be found in the published works, as the use of a *strictu sensu* Hawking radiation in a *process* of gravitational collapse (as, for instance, in Ref. [28]), as Hawking radiation implies (essentialy, not just formally) a transition from vacuum, and in truth a collapsing star is not void.

On the other hand, even if the genuine radiation law ap-

peared to be completely different, it would still be true that an asymptotic approach to a "stationary" phase (where the value of λ would stop increasing) should happen. In fact, this phase should be always reached just by assuming the reasonable hypothesis that the outgoing flux of thermal radiation should not diminish with time (the temperature of the collapsing body should be expected to rise with the progression of collapse), while the ingoing flux of collapsing matter should become smaller as the spacetime deformation becomes larger.

In summary, even when several of the assumptions of the model of gravitational collapse proposed in this paper may be considered excessively "idealistic", it provides an illustrative description of how a time-dependent metric should be the most logical choice for the study of gravitational collapse and that the polar spherical coordinates of an asymptotic observer (a scientific on the Earth, not an astronaut falling into a black hole) are sufficient to cover the whole collapsing process. The supposed completion of the collapsing process in a finite proper time for a co-mobile observer would never be truly accomplished due to the invariance of causal order for any relativistic system (in a finite and lesser proper time, the co-mobile observer would be fully evaporated by the emission of thermal radiation). The astronomic objects already *identified* as "black holes" could equally correspond to "asymptotically collapsing bodies". Empirically, few differences would be expected. From a theoretical point of view, the latter ones may be obtained in a very natural way from the Einstein field equations and avoid many of the paradoxes and illogical aspects of the former ones. Thus, according to Occam's razor, asymptotic collapse should be preferred to black holes.

Acknowledgements

The author acknowledges very specially the help and support of I. López-Aylagas, as well as D. Jou and R. Zarzuela for their encouragement, sensible advices and careful review of the whole work.

Submitted on September 8, 2015 / Accepted on September 11, 2015

References

1. Schwarzschild K. Über das gravitationsfeld eines massenpunktes nach der einsteinschen theorie. *Sitzungsberichte der Königlich Preußischen Akademie der Wissenschaften (Berlin)*, 1916, v. 1 Seite 189–196.
2. Birkhoff G. D., Langer R. E. Relativity and modern physics. Cambridge MA: Harvard University Press, 1924.
3. Oppenheimer J. R., Volkoff G. M. On massive neutron cores. *Physical Review*, 1939, v. 55 (4), 374.
4. Oppenheimer J. R., Snyder H. On continued gravitational contraction. *Physical Review*, 1939, v. 56 (5), 455.
5. Wheeler J. A., Ford K. W. Geons, black holes, and quantum foam: a life in physics. Norton and Company, New York, 1998.
6. Hawking S. W., Ellis G. F. R. The large scale structure of space-time (Vol. 1). Cambridge university press, 1973.
7. Bekenstein J. D. Black holes and entropy. *Physical Review D*, 1973, v. 7 (8), 2333.
8. Hawking S. W. Black hole explosions? *Nature*, 1974, v. 248 (5443),30–31.
9. Hawking S. W. Information preservation and weather forecasting for black holes. arXiv:1401. 5761, 2014.
10. Penrose R. Gravitational collapse: the role of general relativity. Birkbeck College, London, 1969.
11. Vachaspati T., Stojkovic D., Krauss L.M. Observation of incipient black holes and the information loss problem. *Physical Review D*, 2007, v. 76 (2), 024005.
12. Vachaspati T., Stojkovic D., Krauss L.M. Quantum radiation from quantum gravitational collapse. *Physics Letters B*, 2008, v. 663 (1), 107–110.
13. Piñol M., Aylagas I. L. Transition from Established Stationary Vision of Black Holes to Never-Stationary Gravitational Collapse. arXiv: 1007.2734.
14. Mitra A. The Mass of the Oppenheimer-Snyder black hole. arXiv: astro-ph/9904163.
15. Mitra A. Non-occurrence of trapped surfaces and black holes in spherical gravitational collapse. *Foundations of Physics Letters*, 2000, v. 13 (6), 543–579.
16. Mitra A. Why gravitational contraction must be accompanied by emission of radiation in both Newtonian and Einstein gravity. *Physical Review D*, 2006, v. 74 (2), 024010.
17. Mitra A. Radiation pressure supported stars in Einstein gravity: eternally collapsing objects. *Monthly Notices of the Royal Astronomical Society*, 2006, v. 369 (1), 492–496.
18. Mitra A. The fallacy of Oppenheimer Snyder collapse: no general relativistic collapse at all, no black hole, no physical singularity. *Astrophysics and Space Science*, 2011, v. 332 (1), 43–48.
19. Robertson, S. L., Leiter, D. J. Evidence for intrinsic magnetic moments in black hole candidates. *The Astrophysical Journal*, 2002, v. 565 (1), 447.
20. Robertson S. L., Leiter D. J. On intrinsic magnetic moments in black hole candidates. *The Astrophysical Journal Letters*, 2003, v. 596 (2), L203.
21. Robertson S. L., Leiter D. J. The magnetospheric eternally collapsing object (MECO) model of galactic black hole candidates and active galactic nuclei. arXiv: astro-ph/0602453.
22. Karczmarek J. L., Maldacena J., Strominger A. Black hole non-formation in the matrix model. *Journal of High Energy Physics*, 2006, v. 2006 (01), 039.
23. Landau L. D., Lifshitz E. M. The classical theory of fields (Volume 2). University of Minnesota, 1987.
24. Lu Y. Black Hole Radiation and Energy-Momentum Tensor. Diploma Thesis for Theoretical Physics in Utrecht University. Netherlands, 2010.
25. Hazlehurst J., Sargent W. L. W. Hydrodynamics in a Radiation Field-A Covariant Treatment. *The Astrophysical Journal*, 1959, v. 130 276.
26. Borkar M. S., Dhongle P. R. Pre–Hawking Radiating Gravitational Collapse in Stationary Space-Time. *International Journal of Theoretical and Applied Sciences*, 2013, v. 5 (2), 27–31.
27. Delsate T., Rocha J. V., Santarelli R. Collapsing thin shells with rotation. *Physical Review D*, 2014, v. 89 (12), 121501.Sc.
28. Mersini-Houghton L. Backreaction of Hawking radiation on a gravitationally collapsing star I: Black holes? *Physics Letters B*, 2014, v. 738 61–67.

LETTERS TO PROGRESS IN PHYSICS

The *c*-global Revival in Physics

Otto E. Rossler

Division of Theoretical Chemistry, University of Tübingen, Auf der Morgenstelle 18, 72076 Tübingen, Germany
E-mail: oeross00@yahoo.com

A return is proposed to the 6-years-long period before Einstein gave up on the global constancy of the speed of light c in the vacuum. *c-global* remains implicit in Maxwell's equations and in quantum electrodynamics. Reluctantly, Einstein abandoned *c-global* in 1911 after a $3\frac{1}{2}$ years long silence kept on gravitation during which he had tried in vain to avoid the conclusion that c is only an everywhere locally but not a globally valid constant of nature. It is shown that Einstein just overlooked a *corollary* to his own finding of an optically reduced speed of an horizontal light ray downstairs in his constantly accelerating long rocketship in outer space. The new corollary reads: *slantedness relative to the tip* of the locally horizontal light ray. Hence Einstein's famous gravitational redshift — the increase in wavelength compared to above of a *vertically* emitted light ray — is accompanied by a proportional enlargement of space. The new horizontal size increase is masked from above by the upwards slant valid relative to the tip. Einstein's *gravitational time dilation* thus goes hand in hand with an equal *gravitational space dilation*. Surprisingly, Quantum Mechanics enforces the same conclusion independently: the reduced energy of the locally normal-appearing photons downstairs generates (via Quantum Mechanics' creation and annihilation operators) atoms of a proportionally reduced mass and hence proportionally enlarged size. Two disappointing implications follow: *c-global rules out* both cosmological space expansion and black hole evaporation. The uplifting third implication is: *c-global* makes the equivalence principle compatible with Quantum Mechanics for the first time. This new compatibility predictably extends to the implied "*c-global*-rescaled General Relativity". Hence the "holy grail of physics" is bound to exist. The *cgr-GR* only waits to be written down.

1 Foreword

The following text seems to represent a footnote on the early prehistory of General Relativity, dealing only with long overhauled ways of thinking and of groping in the dark, because since 1915 we have the indubitable final reality of the theory of space and time in the large. The purpose of the present note is to show that this is not so. In the very foundations of the grandiose recipe, there is hidden a tiny minor oversight. It has little influence on most implications, but it nonetheless allows one to improve the theory eventually by at last putting straight an element that belongs into it since 1915: the nonglobality of c.

Many specialists will strongly disagree with the view that it could pay to return to the most early stage of this beautiful superhuman theory to find a little oversight in it and repair it. But this is exactly the purpose and aim of the following text. As the reader will see, the consequences — if this friendly detour into a long-gone stage of science is followed for the fun of it for a short stretch since everything is maximally simple on that level — are maximally far-reaching and rewarding.

Admittedly, such "nostalgic physics" à la Yul Brynner in the movie "Westworld" is an unusual approach. It looks like History of Science and has a dusty smell to it. But IF it unearths something that was really and actually overlooked, it has an important role to play. So with this Foreword, which owes its existence to a spirited written dialogue with the Editor-in-Chief, the present note belongs into a twilight category of theoretical physics. But it is the fruits that make results recognizable eventually. So if the result derived below, a so far overlooked gravitational-redshift-proportional size increase in gravitation, is correct — as is shown on the limited level of knowledge available in 1907 below, aided only by an independent development in physics that did not exist at the time, quantum electrodynamics —, then a major progress in today's thinking occurs. So the paper which follows after this acutely added preface is perhaps indeed worth the scrutiny of the specialists.

It is rare that such a naive but rigorous spatial thinking is used in theoretical physics. It reminds its author of the early phase in chaos theory when "absurdly simple" geometric ideas, like overlaying two transparencies with an expanding spiral drawn on each and defining straight threshold lines of transitions between them, sufficed to catapult chaos theory into the applied sciences. In that latter case, the specialists arrived at the same trick called "singular perturbation" eventually. In the present case, a similar "canonization" is hoped for.

2 Introduction

Einstein's biggest early discovery was an intuitive understanding of Maxwell's *c-global*: he saw in his mind that a light flash can expand as a sphere with the *same* speed c around each of two observers who are passing by each other at a high speed while the flash goes off at their feet at that moment.

This logical impossibility (one expects *two* light spheres around the two mutually fast receding observers) becomes a logical truth if the *simultaneities* valid for the two runners which coincide at the encounter, are *mutually slanted* as two equal-rights cuts through the same light cone. This fact Einstein was able to picture in his mind after a long nightly discussion with his by a few years older friend Michele Besso. On the next morning, he excitedly returned to Besso's front door to tell him: "*Thanks to you*, I have solved the problem!" This event Einstein reported to a Japanese audience 17 years later when he had just received the news of his Nobel Prize. His rare German phrase "Dank Dir" (thanks to you) got confounded with the conventional German phrase "danke Dir" (thank you) in the ensuing translation — so the co-authorship of Einstein's lifelong friend Besso never became public.

The miracle of the individualized global constancy of c fell in doubt with Einstein himself $2\frac{1}{2}$ years later, in December of 1907 [1], to be abandoned for good in mid-1911 [2]. By serendipity, *c-global* was retrieved a century later in 2007 as an allowed formal implication of the Schwarzschild metric of General Relativity [3, 4]. Subsequently, *c-global* was also discovered in the equivalence principle of Special Relativity [5], the very theory in which it had become questionable in late 1907 and been abandoned in 1911.

3 Motivation

The return of *c-global* into the foundations is important because a "facelift of physics" is implicit. For instance, the long-accepted paradigm of the *Big Bang* ceases to be tenable since it implies that two sufficiently distant objects on the expanding "balloon" recede from each other at a *superluminal* speed. As a second implication, black holes can now no longer "evaporate" since the well-known infinite *temporal distance* of their surface (called horizon) from the outside world is, by virtue of the global c, accompanied by an equally large *spatial distance*. Hence there can be no "tunneling" to the horizon anymore and thence no *Hawking radiation*. Thirdly, metrology acquires a whole new face [5].

What is the best way to convince the reader that *c-global* holds true again after a century? The answer lies in a return to the early Einstein. In 1905, he had described two radically new implications of *c-global*: the *twins paradox* (one twin ageing faster as if in a *Grimm Brothers*' fairy tale) and the *transversal Doppler effect*, which had both been overlooked by his great predecessors in the developing discovery of Special Relativity, Lorentz and Poincaré.

4 Genealogy

The drama with *c-global* began in 1907 with the last step in the discovery of the equivalence principle. The latter principle [1, 6] had just yielded the absolutely incredible but in retrospect true prediction of the *gravitational redshift*: inside a constantly accelerating long rocketship in outer space described by Special Relativity, a light pulse ascending with a finite c from the bottom reaches the tip only when the latter has picked up a fixed relative speed away from the original emission point. The GPS satellites confirm this absurdly daring insight of "gravitational time dilation" downstairs every minute.

Einstein's look at a *vertically* emitted light ray was then followed by his also having a look at a locally *horizontal* light ray that hugs the flat bottom of the ignited rocketship. This led him to his final discovery in the equivalence principle: a horizontal light pulse automatically *looks slowed* by the gravitational redshift factor when watched from above [1] (see the last unnumbered equation on the last-but-second page).

5 Main result

The second revolutionary finding of Einstein regarding gravitation is again absolutely correct notwithstanding its absurdity from a common-sense point of view. However, it happens to admit of a final touch. The latter takes the first Einstein result (the fact that the bottom is in constant recession relative to the tip) into account in the second (the apparent transversal slowdown of c). The synthesis is that the locally *horizontal* light ray hugging the floor is necessarily at the same time *slanted-upwards* relative to the tip at every point due to the continual falling-back of the bottom. Note that when the light from the neighboring spatial cell downstairs reaches the next, the latter is a bit faster already, etc. Owing to this new *relative slant*, the horizontal reduction of c discovered by Einstein becomes a mere *projection effect*: the new upwards slant restores *c-global*.

It is worth pointing out here that *c-global* formally underlies the equivalence principle from the outset since the latter is exclusively based on Special Relativity with its built-in global c. This fact was not sufficient, however, to directly rule out the conclusion that c is locally reduced. The lack of confidence shown has to do with the fact that the rocketship paradigm is so impossibly hard to think-through in every respect [6].

The newly retrieved global speed of light c downstairs in the equivalence principle now has its consequences: all *transversal lengths* downstairs which at first sight look unchanged from above are actually increased by the gravitational redshift factor relative to the tip. They only look optically compressed towards the original length by virtue of the slant. The only readily visible consequence upstairs is the seemingly reduced transversal speed of light c' downstairs, discovered by Einstein [1].

6 Consistency

The new found *transversal size increase downstairs matches* the increase in wavelength of all light emitted downstairs. Moreover, these lower-energy photons emitted downstairs remain, with their locally unchanged-appearing frequencies, *locally interconvertible* with particles of matter (as in positronium creation and annihilation) as a consequence of the much later discovered quantum electrodynamics. Hence *all* local atoms have a mass that is lower by the redshift factor valid relative to above. This *mass reduction*, in turn, entails a proportional size increase of these atoms via the Bohr radius formula of Quantum Mechanics. Therefore, space is enlarged downstairs, *both* by the *c-global* of Special Relativity and by virtue of Quantum Mechanics, in an identical fashion. The two theories confirm each other independently. The optically unchanged-appearing horizontal distances downstairs with their creeping c' seen by Einstein do therefore indeed mask a *size increase* proportional to the gravitational redshift.

Note that the thus doubly confirmed *new Einstein effect* of "gravitational space dilation" exactly matches the *old Einstein effect* of "gravitational time dilation" (implying *c-global*). The equivalence principle thus becomes even more powerful by the fact that the size change derived geometrically in it via the laws of Special Relativity gets independently confirmed by the creation and annihilation operators of quantum electrodynamics.

Thus, the original interpretation of Einstein's creeping effect (as a reduction in c [1, 2]) can be given up for good to date. However, it is important to realize that in the days *before* the advent of quantum electrodynamics with its creation and annihilation operators, the double-tiered consistency obtained above was *inaccessible*. Hence the above-described fractal-like *relative local slant*, which saves *c-global* on the part of Special Relativity downstairs, was in the absence of Quantum Mechanics' own rest-mass-dependent size increase impossible to spot. Einstein's giving *c-global* up for good in 1911 after more than 3 years of trying to preserve it was therefore preprogrammed.

The *new Einstein effect* of "gravitational space dilation," when added to the *old Einstein effect* of "gravitational time dilation" (so that c remains a global constant of nature), has mind-boggling consequences like the two already mentioned (no Big Bang and no Hawking evaporation). The second implication is especially important in view of the fact that it renders the most hoped-for success of a currently running experiment — generation of miniature black holes down on earth — undetectable by virtue of the absence of their generally expected Hawking signature. Any unrecognized success at CERN will then grow exponentially inside earth [3]. So the return to *c-global* implies "tangible consequences" for an experiment rated innocuous in its last — still pre-*c-global* — safety report LSAG of 2008. Einstein's results are notorious for entailing existential consequences.

7 Discussion

It is a good idea to "return to the mothers" from time to time, poet Goethe advised. In the present case, a trip back to the *pioneer phase* of relativistic gravitation theory was offered. The retrieved crumb from Einstein's table — *c-global* — is still big enough to revolutionize cosmology and metrology.

All of this is only possible because in 1907, a young outsider dared think clearly in three dimensions with an almost superhuman exactitude including motion effects and their entailed delays — much as a computer-games freak of today would do with the aid of modern simulation tools, cf. [7]. Composing the computer game "*Einstein Rocket*" and putting it on the web will greatly aid physics. In this way, a modern young Einstein may be enabled to let the only "to some extent accessible" [6] thought experiment of the younger Einstein reveal its most important if presently still unfathomable secret.

To conclude, a *revolution in physics* based on Einstein's early work was described. A *corollary* to his optically manifest reduced speed of light c' downstairs in gravitation was pointed out — a gravitational-redshift proportional *size increase* downstairs in gravity that is masked from above. The *new space dilation* is proportional to the *old time dilation* and thus restores *c-global* in accordance with the special-relativistic nature of the equivalence principle of Einstein. Consistency of the equivalence principle with Quantum Mechanics arises for the first time (the previous absence of this feature had gone unnoticed). As a bonus, the new size dilation predictably enables the long-missed unification of General Relativity with Quantum Mechanics — "the holy grail of physics" [8].

Acknowledgments

I thank Wolfgang Rindler for decades of correspondence and Christophe Letellier and Valérie Messager for early discussions. For J.O.R.

Submitted on September 27, 2015 / Accepted on September 28, 2015

References

1. Einstein A. On the relativity principle and the conclusions drawn from it (in German). *Jahrbuch der Radioaktivität*, 1907, Bd. 4, 411–462 (ref. to p. 458).
2. Einstein A. On the influence of gravitation on the propagation of light (in German). *Annalen der Physik*, 1911, Bd. 35, 898–908 (ref. to p. 906).
3. Rossler O. E. Abraham solution to Schwarzschild metric implies that CERN miniblack holes pose a planetary risk. *Vernetzte Wissenschaften — Crosslinks in Natural and Social Sciences* (P. J. Plath and E. C. Hass, eds.), Logos Verlag, Berlin, 2008, pp. 263–270. [Correction: the phrase "infinite proper in-falling time" must read "finite proper in-falling time"].
4. Rossler O. E. Abraham-like return to constant c in general relativity: Gothic-R theorem demonstrated in Schwarzschild metric. *Fractal Spacetime and Noncommutative Geometry in Quantum and High Energy Physics*, 2012, v. 2, 1–14.

5. Rossler O. E. Einstein's equivalence principle has three further implications besides affecting time: T-L-M-Ch theorem ("Telemach"). *African Journal of Mathematics and Computer Science Research*, 2012, v. 5, 44–47.

6. The essential phrase in Einstein's paper on the equivalence principle [1], p. 454 (p. 302 of the English translation) reads as follows: "[. . .] in the discussion that follows, we shall therefore assume the complete physical *equivalence* of a gravitational [field] and a corresponding acceleration of the reference system. This assumption extends the principle of relativity to the uniformly accelerated translational motion of the reference system. The heuristic value of this assumption rests on the fact that it permits the replacement of a homogeneous gravitational field by a uniformly accelerated reference system, the latter case being *to some extent accessible* to theoretical treatment." (Emphases added.)

7. Rossler O. E. Bye-bye Big Bang due to the analogical thinking of the young Einstein. In: *Das Numen* (Julian Charriere, Andreas Greiner, Markus Hoffmann and Felix Kiessling, eds.), pp. 59–75. Distanz Verlag GmbH & Institut für Raumexperimente, Berlin, 2015.

8. The remaining task is to write down the "*c-global*-rescaled (cgr) general relativity". Hereby, the Einstein field equations must be condensed into a "global-*c* skeleton". Before this job has been finished, "experimentation in the dark" is discouraged. Once the "global-*c* spacetime theory" is found, the deeper meaning of the retrieved "Maxwell-Einstein miracle of *c-global*" can start to be addressed.

Progress in Physics is an American scientific journal on advanced studies in physics, registered with the Library of Congress (DC, USA): ISSN 1555-5534 (print version) and ISSN 1555-5615 (online version). The journal is peer reviewed and listed in the abstracting and indexing coverage of: Mathematical Reviews of the AMS (USA), DOAJ of Lund University (Sweden), Zentralblatt MATH (Germany), Scientific Commons of the University of St.Gallen (Switzerland), Open-J-Gate (India), Referential Journal of VINITI (Russia), etc. Progress in Physics is an open-access journal published and distributed in accordance with the Budapest Open Initiative: this means that the electronic copies of both full-size version of the journal and the individual papers published therein will always be acessed for reading, download, and copying for any user free of charge. The journal is issued quarterly (four volumes per year).

Electronic version of this journal: http://www.ptep-online.com

Postal address:
Department of Mathematics and Science, University of New Mexico,
705 Gurley Avenue, Gallup, NM 87301, USA